THE JOURNAL
OF
CHEMICAL PHYSICS

VOLUME 34, NUMBER 5 MAY, 1961

Thermodynamic Theory of the Pair Correlation Function

EDWARD W. HART

General Electric Research Laboratory, Schenectady, New York

(Received October 13, 1960)

The thermodynamic description of inhomogeneous systems is adapted to a determination of the pair correlation function. The method is most effective for describing the correlation behavior near a critical point. The critical-point behavior is investigated for a simple model fluid of the van der Waal's type. A novel optical scattering phenomenon is predicted for the interface between two equilibrium phases for temperatures below but very near to the critical temperature. The effect of inclusions on critical point phenomena is noted.

I. INTRODUCTION

A SELF-CONSISTENT thermodynamic methodology that is capable of describing the inhomogeneous states of a system is readily adapted to the description of the density correlations in such a system. Such a methodology has been developed by Cahn and Hilliard[1] and by myself.[2] In the present paper I propose to develop the application to the determination of the pair correlation function for a simple system.

As a practical matter, the method to be described here is not well suited to accurate determination of the pair correlation function for distances comparable to the molecular spacing even though, in principle, self-consistency is maintained. The reason for this is that the particular form of the phenomenology employed here for simplicity is a good representation of the energetics of inhomogeneities only if the inhomogeneities are neither too large nor too abrupt. The methods of this paper are best suited then to a discussion of the correlations of a simple fluid near its critical temperature and composition or for the treatment of a fluid whose intermolecular forces have a range greater than the mean intermolecular spacing. The present discussion will be restricted to the behavior of a single component fluid near its critical point.

The point of view that will be adopted here is that for a fluid in which quantum effects are negligible the pair correlation function can be easily deduced from the equilibrium singlet number density distribution produced by holding one molecule of the same species fixed at some point in an otherwise average sample of the fluid. More precisely, the difference of the equilibrium density distributions (singlet distribution functions) will be evaluated between a large homogeneous sample of the fluid and the inhomogeneous state of same sample brought about by holding one of its molecules stationary at a fixed point in the sample. This difference will, in fact, be the pair correlation function. A similar consideration has been used in the work of Reiss, Frisch, and Lebowitz[3] in the treatment of the hard-sphere fluid. They specified the surrounding distribution, however, in microscopic terms whereas a thermodynamic model is employed in the present work. The present computation will be carried out according to the thermodynamic description of inhomogeneous systems mentioned above; in particular, I shall use the formulation that I have developed in two previous papers.[2] In that formulation the free-energy density is considered to be a point function of the gradients and higher space derivatives of the singlet density n as well as a function of the density itself and of a strain dilatation variable e. In the present treatment it will be assumed that the main dependence on inhomogeneity is determined by the Laplacian of the density $\nabla^2 n$ and this variable will be called λ. In the previous work it has been shown that the total Helmholtz free energy F is given in terms of the free-energy density f (ignoring external boundary effects) by

$$F=\int dv f$$

$$f=\mu n+\nu\lambda-p,$$

[1] J. W. Cahn and J. E. Hilliard, J. Chem. Phys. **28**, 258 (1958).
[2] Edward W. Hart, Phys. Rev. **113**, 412 (1959); **114**, 27 (1959).
[3] H. Reiss, H. L. Frisch, and J. L. Lebowitz, J. Chem. Phys. **31**, 369 (1959).

Copyright © 1961 by the American Institute of Physics

where

$$\mu \equiv (\partial f/\partial n)_{T,\lambda,e}$$

$$\nu \equiv (\partial f/\partial \lambda)_{T,n,e}$$

$$p \equiv -(\partial fe/\partial e)_{T,en,e\lambda}.$$

Landau and Lifschitz[4] have used a similar but somewhat more restricted model to describe the critical point density fluctuations. Their method is adapted only to what I term below the linear approximation.

II. GENERAL FORMULATION

The pair correlation function can be defined by the relationship

$$g(r) = (\langle n \rangle)^{-1} \langle \xi(r)\xi(0) \rangle - \delta(r), \tag{1}$$

where

$$\xi(r) \equiv n(r) - \langle n \rangle,$$

the angular brackets denote configuration average and, since we are considering a system that is homogeneous on the average, the point of origin $r=0$ is indifferent. I shall call $\xi(r)$ the *density derivation* at r. The pair correlation function can be interpreted as the mean density deviation at a distance from another molecule. An alternative interpretation is that $g(r)$ is the mean density deviation at the spatial point r *when there is a molecule at* $r=0$. It is this latter formulation that enables us to compute $g(r)$ directly as equal to the real equilibrium density deviation $\xi^{(1)}(r)$ that is obtained when one molecule is fixed at the origin. The fixed molecule is not counted as one of the molecules in the distribution $\xi^{(1)}(r)$.

In order to specify this distribution in equilibrium we shall specify that the Helmholtz free energy F be an extremum subject to the conditions that the total number of molecules N be fixed, and that $n(0)$ be fixed at some arbitrary value. The free-energy density, as noted above, will be assumed for simplicity to depend only on n and λ. We may ignore explicit boundary dependence in this treatment.

The conditions are, in greater detail, that for

$$F = \int dv(\mu n + \nu\lambda - p), \tag{2}$$

we require that

$$\delta F = 0 \tag{3}$$

$$\delta N \equiv \delta \int dv n = 0 \tag{4}$$

$$\delta n(0) \equiv \delta \int dv n \delta(r) = 0. \tag{5}$$

We choose Lagrange multipliers for the two subsidiary constraints and formulate the combined extremal,

$$\delta[F - \mu_0 N - \theta n(0)] = 0. \tag{6}$$

From this we see immediately that θ is a new general thermodynamic force, characteristic of the system, and satisfying the relationship

$$\theta = [\partial F/\partial n(0)]_{T,V,N}. \tag{7}$$

The intrinsic form of Eq. (6) is

$$0 = \int dv[(\mu - \mu_0)\delta n + \nu\delta\lambda - \theta\delta(r)\delta n]$$

$$= \int dv[\mu - \mu_0 + \nabla^2\nu - \theta\delta(r)]\delta n, \tag{6a}$$

where any suitable boundary conditions take care of the surface integral that has been dropped in Eq. (6a). The *chemical equilibrium equation* is now

$$\mu - \mu_0 + \nabla^2\nu = \theta\delta(r). \tag{8}$$

The boundary conditions on this equation are such that would yield a homogeneous solution for $n(r)$ when $\theta=0$. If the value of the density for that solution is $n^{(0)}$, then Eq. (8) will be simply an equation to determine $\xi(r) = n(r) - n^{(0)}$ for some given value of θ.

Equation (8) is most simply considered in a linear expansion in ξ and its derivatives. We obtain this *linear approximation* as follows:

$$\mu - \mu_0 \cong (\partial\mu/\partial n)\xi + (\partial\mu/\partial\lambda)\lambda = (\partial\mu/\partial n)\xi + (\partial\mu/\partial\lambda)\nabla^2\xi$$

$$\nabla^2\nu \cong \nabla^2[(\partial\nu/\partial\lambda)\lambda + (\partial\nu/\partial n)\xi]$$

$$= (\partial\nu/\partial\lambda)\nabla^4\xi + (\partial\nu/\partial n)\nabla^2\xi.$$

The derivatives are all evaluated at $\xi=\lambda=0$. By noting that $(\partial\mu/\partial\lambda) = (\partial\nu/\partial n)$, we may finally write the linear approximation to Eq. (8),

$$(\partial\nu/\partial\lambda)\nabla^4\xi + 2(\partial\nu/\partial n)\nabla^2\xi + (\partial\mu/\partial n)\xi = \theta\delta(r). \tag{9}$$

In a later section we shall substitute some typical coefficients to investigate the behavior of a fluid near a critical point. The equation is exhibited at this place to give more concrete form to Eq. (8).

To return to a general consideration of Eq. (8), we note that any value of the force θ results in a solution $\xi(r)$ that depends on the value of θ. Now, if the force θ is that exerted by a molecule of the same species, fixed at the origin, then $\xi(r) = \xi^{(1)}(r) = g(r)$. We can compute the appropriate value of θ since we know the integral of $\xi^{(1)}(r)$ over the volume V of the system;

$$\int dv\xi^{(1)}(r) = \int dv g(r)$$

$$= [\langle \Xi^2 \rangle / V\langle n \rangle] - 1,$$

where $\Xi \equiv \int dv\xi(r)$. It is well known[5] that

$$\langle \Xi^2 \rangle = VkT/(\partial\mu/\partial n)_{T,V}$$

[4] L. D. Landau and E. M. Lifshitz, *Statistical Physics* (Addison-Wesley Publishing Company, Inc., Reading, Massachusetts, 1958), p. 366 ff.

[5] J. W. Gibbs, *Collected Works* (Longman's, Green and Company, Inc., New York, 1928), Vol. II, pp. 201, 202.

and so

$$\int dv\xi^{(1)}(r)=[(kT/n)-(\partial\mu/\partial n)]/(\partial\mu/\partial n). \quad (10)$$

The correct value of θ is then the one for which the resultant $\xi^{(1)}(r)$ satisfies the condition stated in Eq. (10). Clearly, this procedure for determining θ can be applied only where $(\partial\mu/\partial n)>0$.

III. CRITICAL-POINT BEHAVIOR

The model and the method treated here are not capable of giving good detail of $g(r)$ for distances r comparable to the molecular spacing. Near the critical point, however, the range of correlation is large compared to molecular spacing, and the model gives a fair asymptotic representation of a real fluid.

We shall consider as an example a fluid whose homogeneous behavior will be taken to be that of a van der Waal's gas and whose free-energy dependence on λ will be prescribed. Let the subscript h on a quantity denote that it is the quantity characteristic of the fluid when $\lambda=0$. Then we shall write the free-energy density and derived quantities as follows:

$$f=f_h+\alpha n\lambda+\tfrac{1}{2}\beta\lambda^2$$
$$\mu=\mu_h+\alpha\lambda$$
$$\nu=\alpha n+\beta\lambda$$
$$p=p_h-\alpha n\lambda-\tfrac{1}{2}\beta\lambda^2.$$

Let the mean density be the critical density n_c and so μ_0 will be the chemical potential appropriate to n_c at the temperature of observation. We assume in our model that the temperature dependence of α and β is unimportant. Noting that $\nabla^2 n=\nabla^2\xi$,

$$\mu-\mu_0=(27/4)bR(T-T_c)\xi+(3\cdot 27/8)b^3RT\xi^3+\alpha\nabla^2\xi,$$
$$\nabla^2\nu=\beta\nabla^4\xi+\alpha\nabla^2\xi.$$

We shall ignore the nonlinear term in $\mu-\mu_0$ and write the equivalent of Eq. (9),

$$\beta\nabla^4\xi+2\alpha\nabla^2\xi+(27/4)bR(T-T_c)\xi=\theta\delta(r), \quad (11)$$

or, if we write $c\equiv(27/4)bR(T-T_c)$,

$$\beta\nabla^4\xi+2\alpha\nabla^2\xi+c\xi=\theta\delta(r). \quad (11a)$$

Now stability requires that $\beta>0$ and a crude estimate shows that $\alpha<0$ for substances whose molecules have attractive interactions, and, of course, the sign of c is the same as the sign of $T-T_c$. There are two general types of solution for Eq. (11a) near the critical temperature. They are

$$\xi(r)=\xi(0)(e^{-\kappa r}-e^{-\eta r})/(\eta-\kappa)r \quad (12)$$

for

$$T>T_c$$

and

$$\xi(r)=\xi(0)(\cos\kappa r-e^{-\eta r})/\eta r \quad (13)$$

for

$$T<T_c,$$

where (approximating for T close to T_c),

$$\kappa^2=-(\alpha/\beta)\,|\{1-[1-(\beta c/\alpha^2)\,|^{\frac{1}{2}}\}\,|\cong-\tfrac{1}{2}(\,|c\,|/\alpha), \quad (14)$$

and

$$\eta^2=-(\alpha/\beta)\{1+[1-(\beta c/\alpha^2)]^{\frac{1}{2}}\}\cong-2(\alpha/\beta). \quad (15)$$

A rough estimate determines α to be of the order of $-b^{\frac{1}{3}}a$, where a is the familiar van der Waal's measure of the attractive interaction, equal to $-(27/8)bRT_c$, and b is equal to one-third the volume per molecule at the critical density. Then near the critical point

$$\kappa^2\cong b^{-\frac{1}{3}}\,|T-T_c\,|/T_c,$$

and the principal correlation distance is

$$\kappa^{-1}\cong b^{\frac{1}{3}}(T_c/\,|T-T_c\,|)^{\frac{1}{2}}.$$

For a substance with a critical temperature about 500°K, κ^{-1} is 10^3 atom spacings when $|T-T_c|$ is 1 mdeg. The same number crudely measures the thickness of the boundary between the two phases when $T<T_c$. The number η is, in general, much larger than κ and is relatively temperature independent. In our example it plays a practical role of keeping $\xi(0)$ finite in a consistent way without appealing to the nonlinearity of Eq. (8).

Now let us examine $\xi(0)$ for $T>T_c$,

$$\xi(0)=-\theta[4\pi(\partial\nu/\partial\lambda)(\kappa+\eta)]^{-1}.$$

If we let $\xi(r)$ be $\xi^{(1)}(r)$, which is the same as $g(r)$, we can compute the value of θ appropriate to a molecule at the origin by Eq. (10). From Eq. (12) we have

$$\int dv\xi^{(1)}(r)=4\pi(\kappa+\eta)\xi^{(1)}(0)/\kappa^2\eta^2. \quad (16)$$

And so, combining Eqs. (10) and (16), and noting that

$$\kappa^2\eta^2=(\partial\mu/\partial\eta)/(\partial\nu/\partial\lambda),$$

we obtain the result,

$$\theta^{(1)}=(\partial\mu/\partial n)-(kT/n). \quad (17)$$

The value of $\theta^{(1)}$ determined in this way has no exceptional behavior near $T=T_c$, and so we may take the value determined by Eq. (17) to hold below the critical temperature as well.

IV. DISCUSSION

The form of the correlation function that we have deduced for $T>T_c$ is, from Eq. (12),

$$g(r)=g(0)[e^{-\kappa r}-e^{-\eta r}]/(\eta-\kappa)r. \quad (18)$$

There is nothing special about the form of Eq. (18) except for the finite value of $g(r)$ when $r=0$. In the present model that feature is obtained in a thermo-

dynamic manner. For $r \gg \eta^{-1}$, $g(r)$ is the same as the result obtained by Ornstein and Zernike in their classical study[6] and subsequently by most investigators. The one special characteristic of the present treatment is that Eq. (18) is obtained as the result of a completely thermodynamic description of an equilibrium configuration. I feel, therefore, that this result may be considered as a demonstration of the generality of such an asymptotic correlation behavior. In principle, the short-range part of $g(r)$ could be obtained with high accuracy if the dependence of f on higher derivatives of n was known. In that case it would also be advisable to replace the condition of Eq. (5) by an additive term in f that was equal to the potential energy density of the fluid in the vicinity of the fixed molecule at $r=0$. There is little to be gained with that refinement, however, in the cruder model treated here.

This brings us to a consideration of the correlation behavior expressed in Eq. (13). The asymptotic form of this correlation may be written

$$g(r) = g(0)\,(\cos\kappa r)/\eta r. \tag{18}$$

Now, clearly, such a correlation function would lead to divergent fluctuations. This is simply indicative of the fact that there is no stable bulk phase at the critical density for $T<T_c$. There can exist, however, a stable region of density equal to the critical density in the interface between the two phases that are in equilibrium at $T<T_c$. Since in such a region the average singlet density is not homogeneous, the pair correlation function depends explicitly on the points 0 and r rather than only on the distance between them as in our computation above. In fact $g(0, r)$ is no longer symmetric in 0 and r, and a slightly different expression from Eq. (1) must be used for its definition.

The change in density at $\mathbf{r}$ when there is a molecule at $\mathbf{r}_0$ will be written $g(\mathbf{r}_0, \mathbf{r})$ and is given by

$$g(\mathbf{r}_0, \mathbf{r}) = \langle \xi(\mathbf{r})\xi(\mathbf{r}_0)\rangle / \langle n(\mathbf{r}_0)\rangle - \delta(\mathbf{r}-\mathbf{r}_0). \tag{19}$$

It will therefore be represented, as before, by an equilibrium density deviation $\xi^{(1)}(\mathbf{r}_0, \mathbf{r})$ that is the solution of an equation similar to Eq. (8) but has the slightly modified form

$$\mu-\mu_0+\nabla^2\nu=\theta\delta(\mathbf{r}-\mathbf{r}_0), \tag{8'}$$

and the even more modified boundary conditions that, when $\theta=0$, the solution $n^{(0)}(\mathbf{r})$ describes a mixture of two phases separated by a planar interfacial region. If the z axis is taken normal to the interface, and if $n^{(0)}(\mathbf{r})=n_c$ when $z=0$, the solution $n^{(0)}(\mathbf{r})$ will be a function only of z and will have the values characteristic of one of the stable phases when $z=-\infty$ and of the other phase when $z=+\infty$. We shall continue to consider $\xi^{(1)}$ as a small change in the density and so Eq. (8') can be converted into an equation that is linear in $\xi^{(1)}$ and its derivatives and that resembles Eq. (9). Thus

$$(\partial\nu/\partial\lambda)\nabla^4\xi+2(\partial\nu/\partial n)\nabla^2\xi+(\partial\mu/\partial n)\xi=\theta\delta(\mathbf{r}-\mathbf{r}_0), \tag{9'}$$

where the coefficients are now functions of z instead of constants as before. The most important variation will occur in the coefficient $\partial\mu/\partial n$ since it will be negative when $\mathbf{r}$ is well within the interface and positive when $\mathbf{r}$ is in the region of the stable phases. An actual solution for a system like this is somewhat complicated, and so I shall adopt a model for it instead. The model will represent the principal effect to be noticed without placing undue emphasis on the special details of the solution.

For the interface model I shall assume that the interface is a region of thickness τ and of uniform density n_c. The adjacent stable phases are at their bulk densities n_1 and n_2. The result is easily seen to be

$$g(\mathbf{r}_0, \mathbf{r}) = g_0(\cos\kappa\,|\mathbf{r}-\mathbf{r}_0|)/|\mathbf{r}-\mathbf{r}_0|, \tag{18'}$$

when both $\mathbf{r}_0$ and $\mathbf{r}$ are in the interface, and, for all practical purposes, $g(\mathbf{r}_0, \mathbf{r})=0$ when $\mathbf{r}_0$ or $\mathbf{r}$ are in either stable phase. Again only the asymptotic form has been written. This can be simplified still further in order to compute the light scattering associated with this correlation behavior. As will appear below, the contributions to the scattering by the first couple of oscillations of $g(\mathbf{r}_0, \mathbf{r})$ is small compared to the remainder. It is allowable, therefore, to replace $|\mathbf{r}-\mathbf{r}_0|$ by the projection of $\mathbf{r}-\mathbf{r}_0$ on the plane of the interface. If that projection is called ρ, and if z and z_0 are the z components of $\mathbf{r}$ and $\mathbf{r}_0$, respectively, then

$$g(\mathbf{r}_0, \mathbf{r}) = g_0F(z)\,F(z_0)\,(\cos\kappa\rho)/\rho, \tag{20}$$

where

$$F(z)=1, \quad \text{for} \quad -\tfrac{1}{2}\tau\leq z\leq\tfrac{1}{2}\tau,$$
$$=0, \quad \text{otherwise.}$$

Although $g(\mathbf{r}_0, \mathbf{r})$ as derived here is an asymptotic form it should be noted that the detailed behavior of g at atomic spacings can modify the asymptotic form by introducing a phase shift in the argument of the cosine. There is no reliable way of evaluating such a phase shift by the present methods, and so I shall ignore it.

Now this correlation function leads to the prediction of rather striking light scattering properties of the interface. If the incident beam has wave vector $\mathbf{k}_0$, and one looks at the scattered light of the wave vector $\mathbf{k}$ it is readily seen that the ratio R of scattered intensity to incident intensity due to scattering by the density fluctuations is

$$R=|f|^2\int d^3r\int d^3r'\,\langle\xi(\mathbf{r})\xi(\mathbf{r}')\rangle\exp[i\mathbf{q}\cdot(\mathbf{r}-\mathbf{r}')],$$

where $\mathbf{q}=\mathbf{k}-\mathbf{k}_0$, and f is the usual molecular scattering factor. Ignoring the coherent scattering, and employing

[6] L. S. Ornstein and F. Zernike, Proc. Roy. Acad. Amst. **17**, 793 (1914).

the form of g given by Eq. (20), we quickly reach the intermediate result

$$R=|f|^2 n_c A\tau^2 g_0(\sin\tfrac{1}{2}q_z\tau/\tfrac{1}{2}q_z\tau)^2\int_0^{2\pi}d\phi\int_0^{\infty}d\rho\,\cos\kappa\rho\,\cos K\rho,$$

where A is the area of the interface, q_z is the projection of $\mathbf{q}$ on the z axis, ϕ is the azimuth angle about the z axis of the radius vector ρ measured from the planar component $\mathbf{q}_p$ of $\mathbf{q}$, and $K\equiv q_p\cos\phi$. Finally,

$$R=2\pi|f|^2 n_c A\tau^2 g_0(\sin\tfrac{1}{2}q_z\tau/\tfrac{1}{2}q_z\tau)^2/(q_p^2-\kappa^2)^{\frac{1}{2}} \quad (21)$$

for $q_p>\kappa$, and

$$R=0$$

for $q_p<\kappa$.

The distinctive part of this scattering behavior is represented entirely by the denominator of Eq. (21). In fact, the pre-factors are not to be taken too seriously and are included mainly for completeness. The factor that depends on q_z is a thickness form factor and is characteristic of the special model I have employed. To illustrate the main features of this diffraction scattering I shall discuss the case for light that is incident normal to the interface only as it depends on the denominator.

If $\mathbf{k}_0$ is parallel to the z axis and θ is the angle between $\mathbf{k}$ and $\mathbf{k}_0$, $q_p=k\sin\theta$, and

$$R\sim(k^2\sin^2\theta-\kappa^2)^{-\frac{1}{2}}.$$

The scattering is symmetrical about $\theta=\frac{1}{2}\pi$. Clearly there is no scattering at all for $k<\kappa$, and, furthermore, for $k>\kappa$ there is no scattering for $\theta<\theta_1$, where $k\sin\theta_1=\kappa$. The scattering is brightest at $\theta=\theta_1$ and falls off to a minimum at $\theta=\frac{1}{2}\pi$. Even though the differences between my model and the correct solution for a real fluid may cause some broadening of this pattern, I expect that the distinctive feature of the forward and back zones of extinction should still be observable.

The response of the interface to white light illumination is also distinctive. If k_1 and k_2 are the lower and upper limits of the visible spectrum, respectively, it should be observed that for $\kappa>k_2$ there is no anomalous scattering and so the interface is visible only through usual refraction phenomena. But, when κ becomes smaller than the wave vectors characteristic of the visible spectrum, the interface should become strongly scattering and should appear bright. There is some qualitative evidence that an abrupt, anomalous brilliance of the interface is in fact observed as a two-phase sample is heated up to its critical temperature.[7]

There is another consequence of the extensive correlation behavior near T_c that is of some importance in considering the experimental phenomena in the vicinity of T_c. I am referring to the possibility of anomalous disturbances that can be produced by the presence of suspended foreign matter in the sample fluids. Most chemical purefaction processes allow very fine inclusions that are relatively chemically inert to remain. Under ordinary circumstances these particles have negligible effect on the properties of the fluid, but near the critical point their effect may extend over hundreds and thousands of atom distances. I believe that inclusions may be responsible for persistence of the meniscus above T_c since the inclusions may segregate in one of the phases or in the interface. In fact it may be that the kinetics in the vicinity of T_c are strongly controlled by the influence of inclusions.

V. CONCLUSIONS

I have demonstrated a thermodynamic theory for the asymptotic behavior of the pair correlation function. The results support the general conclusions of the Ornstein-Zernike theory for $T>T_c$. A novel correlation behavior and its experimental consequences are predicted for $T<T_c$. Finally, I have noted that finely divided inclusions can affect observations near the critical point.

[7] J. E. Mayer (private communication).

On the Theory of Raman Intensities*

ANDREAS C. ALBRECHT

Department of Chemistry, Cornell University, Ithaca, New York

(Received September 6, 1960)

The Herzberg-Teller development for vibronic transition moments is introduced into the Kramers-Heisenberg dispersion equation. It is shown how "forbidden" character (vibrationally induced intensity) in *allowed* electronic transitions is responsible for the Raman intensities of fundamentals. This suggests a direct link between certain vibronic spectroscopic observations and Raman intensities. The development is carried to the first order in nuclear displacements only—the higher terms give rise to Raman intensities of combinations and overtones. An equation for the polarizability components is obtained which leads directly to the Raman selection rules and in addition provides interesting predictions concerning the Raman and the resonance Raman effect in relation to excited electronic states. Rules are worked out governing the participation of excited electronic states in the Raman effect and these are employed to demonstrate a separability of σ and π contributions to the scattering of totally symmetric modes. The polarizability expression obtained here is compared with that of the semiclassical theory of Shorygin and an interesting resemblance is found. Finally it is shown how, depending on details of the electronic structure, the predicted form of the frequency dependence of scattered intensity ranges between the two expressions that have been commonly used to interpret observations.

I. INTRODUCTION

THE formal theory which underlies Rayleigh scattering and the Raman effect has been in the literature now for many years. At its heart lies the Kramers-Heisenberg dispersion equation. In 1929 Van Vleck[1] carried out an important expansion of the dispersion equation and was able to demonstrate rigorously certain Raman selection rules. At the same time his work, which embodies a modified quantum-mechanical sum rule, provides the formal basis for any future applications. In effect, the sum over all virtual vibronic states that appears in the dispersion theory is reduced to a sum over electronic states. Even with this simplification the possibility of computing polarizabilities from basic electronic structure or, alternatively, of interpreting scattering data in terms of electronic structure appeared remote. In 1934 Placzek[2] presented a comprehensive outline and elaboration of the theory of Rayleigh and Raman scattering. At the same time another approach to the problem was discussed in which the ground-state polarizability components are developed in a Taylor's series expansion in nuclear displacements. The components of the polarizabilities responsible for scattering consist of the matrix elements of the polarizability with respect to the initial and final state functions. Since no reference to virtual states is necessary, the role of excited electronic states in contributing to the polarizability is obscured. It is shown how Rayleigh intensity derives largely from the polarizability tensor consisting of the zeroth-order terms of the expansion, while Raman intensities of fundamentals are related to the so-called derived polarizability tensor whose elements consist of the first derivatives with respect to nuclear displacement—the coefficients of the first-order terms in the expansion. Most of the developments since have occurred within the framework of this theory—known as Placzek's polarizability theory. Recently, however, interest has arisen in resonance or near-resonance scattering, in particular the resonance Raman effect. Here incident light of a frequency approaching that of a virtual transition is used, and the role of low-lying electronic (virtual) states is greatly emphasized. This has encouraged a return to the context of the dispersion theory, which contains explicit reference to excited electronic states, and which, in modified form, is valid under resonance conditions, unlike the polarizability theory.[2]

In 1956 Behringer and Brandmüller[3] published an extensive article containing a review of the basic theory, a valuable critique of the attempts made to simplify it, and an organized presentation of experimental results to illustrate some points theoretically anticipated. Special emphasis is given to the semiclassical theory of Shorygin[4] and other Russian work especially in relation to the resonance Raman effect. The theory of Shorygin, which combines the polarizability theory with the dispersion equation, permits a correlation between Raman intensity and certain parameters relating to the shape of the potential-energy surface cross sections of the virtual states. The theory has met at least with qualitative success although it departs from the correct theory through certain very drastic approximations. More recently Behringer[5] has elaborated upon the correct quantum-mechanical approach outlined by Van Vleck and Placzek and is able to employ Franck-Con-

* This investigation was supported by the National Science Foundation.

[1] J. H. Van Vleck, Proc. Natl. Acad. Sci. U. S. **15**, 754 (1929).

[2] G. Placzek, *Handbuch der Radiologie*, edited by E. Marx (*Akademische Verlagsgesellschaft*, Leipzig, 1934), Vol. VI, part 2, p. 205.

[3] J. Behringer and J. Brandmüller, Z. Elektrochem. **60**, 643 (1956).

[4] See footnotes 3 and 5 for details and further references.

[5] J. Behringer, Z. Elektrochem. **62**, 906 (1958).

don-principle arguments to provide some insight into Raman and resonance Raman intensities. Two most recent examples[6,7] of experimental studies in resonance Raman spectroscopy illustrate strikingly its potential usefulness in the understanding of electronic properties.

At the same time, there has been considerable activity in the field of vibronic spectroscopy—primarily theoretical. Work on vibrationally induced intensities in forbidden electronic transitions has received special attention. However, another study has just been completed[8] where vibrationally induced intensities in allowed electronic transitions are investigated. It is now found that, in the first approximation, it is exactly this "forbidden" (vibrationally induced) character in allowed transitions that is responsible for Raman intensities. In particular in the resonance Raman effect it is the "forbidden" character in the allowed electronic band near resonance that determines the resonance Raman intensities. When the results of the vibronic theory are introduced directly into the dispersion theory expression for the components of the polarizability, an equation is recovered which gives the selection rules directly and in addition provides a framework for studying a variety of properties such as intensities, additivity effects, σ–π separation, depolarization ratios, and especially the properties of the contributing electronic states. As will be seen, one important prediction is that even in the resonance Raman case the low-lying electronic state is not the only important state and that at least one other state must contribute in an important manner.

The theory is now outlined for the Raman and resonance Raman effects. This is followed by a general discussion of the selection rules and by a preliminary exploration of some of the consequences of the theory. A comparison is made with Shorygin's theory but specific applications will be reported in future work.

II. THEORY

A. General

Suppose a molecule, initially in a vibronic state m, is perturbed by plane-polarized incident light of frequency ν_0 (not near resonance) and intensity I_0, in a manner causing it to pass into a vibronic state n while scattering light of frequency $\nu_0 + \nu_{mn}$ ($\nu_{mn} = \nu_m - \nu_n$). The total intensity of scattered light (4π solid angle), after averaging over all orientations of the molecule, is given by[9]

$$I_{mn}=\frac{2^7\pi^5}{3^2c^4}I_0(\nu_0+\nu_{mn})^4\sum_{\rho,\sigma}|(\alpha_{\rho\sigma})_{mn}|^2, \tag{1}$$

where c is the velocity of light and the sum goes over $\rho=x, y, z$ and $\sigma=x, y, z$ which independently refer to the molecule fixed coordinate system. According to the dispersion theory, the $\rho\sigma$th matrix element of the polarizability tensor for transition $m\rightarrow n$, $(\alpha_{\rho\sigma})_{mn}$, is given by

$$(\alpha_{\rho\sigma})_{mn}=\frac{1}{h}\sum_r\left(\frac{(M_\rho)_{rn}(M_\sigma)_{mr}}{\nu_{rm}-\nu_0}+\frac{(M_\rho)_{mr}(M_\sigma)_{rn}}{\nu_{rn}+\nu_0}\right), \tag{2}$$

where h is Planck's constant and the sum goes over the vibronic states of the molecules. Here $(M_\rho)_{rn}$, $(M_\sigma)_{mr}$, etc., refer to the amplitudes (scalars) of the corresponding transition moments. Thus for example $(M_\rho)_{mr}$ represents the amplitude of the transition moment,

$$(\mathbf{M}_\rho)_{mr}=\int\Psi_r^*\mathbf{m}_\rho\Psi_m d\tau, \tag{3}$$

where Ψ_r and Ψ_m are the vibronic wave functions and $\mathbf{m}_\rho$ is the ρth component of the electric moment operator. The frequencies ν_{rm} and ν_{rn} are obtained from the energy differences of the vibronic states.

The zeroth-order Born-Oppenheimer approximation will be introduced. A given vibronic state must now be identified according to electronic and vibrational states and therefore requires two labels. Thus let $m=gi$ (electronic state g and vibrational state i), $r=ev$, and $n=gj$ where g will always represent the ground electronic state. The vibronic-state function Ψ_m reads

$$\Psi_m=\Theta_g(\xi, Q)\phi_j^g(Q),$$

where $\Theta_g(\xi, Q)$ is the electronic wave function for state g and $\phi_j^g(Q)$ is the jth vibrational state function of the ground electronic state. The symbols ξ and Q represent the complete set of internal coordinates locating, respectively, the electrons and the nuclei. Equation (2) now reads

$$(\alpha_{\rho\sigma})_{gi,gj}=\frac{1}{h}\sum_{ev}\left(\frac{(M_\rho)_{ev,gj}(M_\sigma)_{gi,ev}}{\nu_{ev,gi}-\nu_0}+\frac{(M_\rho)_{gi,ev}(M_\sigma)_{ev,gj}}{\nu_{ev,gj}+\nu_0}\right) \tag{4}$$

and Eq. (3) reads

$$(\mathbf{M}_\rho)_{gi,ev}=\int(\Theta_e\phi_v^e)^*\mathbf{m}_\rho(\Theta_g\phi_i^g)d\xi dQ. \tag{5}$$

The sum in Eq. (4) may exclude the ground electronic state with negligible error.[1] A formal integration over electron coordinates in Eq. (5) yields

$$(\mathbf{M}_\rho)_{gi,ev}=\int(\phi_v^e)^*(\mathfrak{M}_\rho(Q))_{g,e}(\phi_i^g)dQ, \tag{6}$$

where

$$[\mathfrak{M}_\rho(Q)]_{g,e}=\int\Theta_e^*\mathbf{m}_\rho\Theta_g d\xi. \tag{7}$$

[6] W. Maier and F. Dörr, Appl. Spectroscopy **14**, 1 (1960).
[7] D. G. Rea, J. Mol. Spectroscopy **4**, 499 (1960).
[8] A. C. Albrecht, J. Chem. Phys. **33**, 156 (1960).
[9] See, for example, footnote 3 for details and further references.

Equation (7) is the expression for the electronic transition moment at nuclear configuration Q. To carry out the integration over the space of the nuclei (Eq. 6) an explicit form of the Q dependence of the electronic transition moment is required. At this point in scattering theory it is customary[1,2,5] to expand the $[\mathfrak{M}_\rho(Q)]_{g,e}$ in a Taylor's series in nuclear displacements with coefficients that are not further analyzed. The same path has been followed in those vibronic investigations having their basis in the early Herzberg-Teller theory of vibronic transitions. However, in these studies the first-order coefficients have been explicitly formulated within the framework of first-order perturbation theory.[10] Thus

$$\mathfrak{M}_{g,e}=\mathfrak{M}_{g,e}{}^0+\sum_s \lambda_{es}(Q)\,\mathfrak{M}_{g,s}{}^0, \tag{8}$$

where to first order in Q

$$\lambda_{es}(Q)=(\sum_a h_{es}{}^a Q_a)\,(\Delta E_{es}{}^0)^{-1} \tag{9}$$

is derived from first-order perturbation theory. The sum in Eq. (8) extends over all excited electronic states except state e, and $\mathfrak{M}_{g,s}{}^0$ is the electronic transition moment to state s evaluated for the ground-state equilibrium configuration. In Eq. (9) the sum is over all normal modes where Q_a is the displacement of the ath normal mode, $h_{es}{}^a$ is a perturbation energy per unit displacement of the ath normal mode due to the mixing of ground-state equilibrium configuration electronic states $\Theta_s{}^0$ and $\Theta_e{}^0$ under vibrational perturbation. (If $\mathfrak{H}$ is the electronic Hamiltonian, $(\partial\mathfrak{H}/\partial Q_a)_0 Q_a$ is the perturbing operator and $\Delta E_{es}{}^0=E_e{}^0-E_s{}^0$ appears as the resonance denominator.

With Eq. (9) and the ρth component of Eq. (8), Eq. (6) becomes

$$(\mathbf{M}_\rho)_{gi,ev}=(\mathfrak{M}_\rho)_{g,e}{}^0(ev\,|\,gi)+\sum_{s,a} h_{es}{}^a(\Delta E_{es}{}^0)^{-1}(\mathfrak{M}_\rho)_{g,s}{}^0(ev\,|\,Q_a\,|\,gi), \tag{10}$$

where a simplified notation is used for the integration over nuclear coordinates. Similar expressions may be obtained for the remaining transition moments. Without serious loss of generality we shall assume that the wave functions are real ($\mathfrak{H}$ is taken as real) so that, for example, $(\mathfrak{M}_\rho)_{e,g}{}^0=(\mathfrak{M}_\rho)_{g,e}{}^0$ for all ρ. With the appropriate substitutions Eq. (4) now reads to first order in Q_a

$$(\alpha_{\rho\sigma})_{gi,gj}=A+B+C, \tag{11}$$

where

$$A=\frac{1}{h}\sum_{ev}\left(\frac{1}{\nu_{ev,gi}-\nu_0}+\frac{1}{\nu_{ev,gj}+\nu_0}\right)[(\mathfrak{M}_\rho)_{g,e}{}^0(\mathfrak{M}_\sigma)_{g,e}{}^0(gi\,|\,ev)\,(ev\,|\,gj)\,], \tag{11a}$$

$$B=\frac{1}{h}\sum_{ev}\left(\frac{1}{\nu_{ev,gi}-\nu_0}\right)\sum_{s,a}\frac{h_{es}{}^a}{\Delta E_{es}{}^0}\{(\mathfrak{M}_\rho)_{g,e}{}^0(\mathfrak{M}_\sigma)_{g,s}{}^0(gj\,|\,ev)\,(ev\,|\,Q_a\,|\,gi)+(\mathfrak{M}_\sigma)_{g,e}{}^0(\mathfrak{M}_\rho)_{g,s}{}^0(gi\,|\,ev)\,(ev\,|\,Q_a\,|\,gj)\}, \tag{11b}$$

and

$$C=\frac{1}{h}\sum_{ev}\left(\frac{1}{\nu_{ev,gj}+\nu_0}\right)\sum_{s,a}\frac{h_{es}{}^a}{\Delta E_{es}{}^0}\{(\mathfrak{M}_\rho)^0{}_{g,e}(\mathfrak{M}_\sigma)_{g,s}{}^0(gi\,|\,ev)\,(ev\,|\,Q_a\,|\,gj)+(\mathfrak{M}_\sigma)_{g,e}{}^0(\mathfrak{M}_\rho)_{g,s}{}^0(gj\,|\,ev)\,(ev\,|\,Q_a\,|\,gi)\}. \tag{11c}$$

It is now necessary to distinguish between the ordinary Raman effect where $\nu_{ev,gi}\gg\nu_0$ and the resonance Raman effect where ν_0 approaches $\nu_{ev,gi}$.

B. Raman Effect

1. Theory

With $\nu_{ev,gi}\gg\nu_0$ it is possible without serious error to replace $\nu_{ev,gi}$ by

$$\nu_{e,g}=(1/h)\,(E_e{}^0-E_g{}^0)=\nu_e.$$

This permits the sum over v for a given e in Eq. (11) to apply to the integrals over nuclear space only.[11] The approximate[8] quantum-mechanical sum rule first developed by Van Vleck[1] is introduced to obtain

$$\sum_v (gi\,|\,ev)\,(ev\,|\,gj)=(gi\,|\,gj)=\delta_{ij}$$

$$\sum_v (gi\,|\,ev)\,(ev\,|\,Q_a\,|\,gj)=\sum_v (gj\,|\,ev)\,(ev\,|\,Q_a\,|\,gi)=(gi\,|\,Q_a\,|\,gj)=\begin{cases}0, & \text{if } v_a{}^j\neq v_a{}^i\pm 1\\ [(v_a{}^i+1)/2\gamma_a]^{\frac{1}{2}}, & \text{if } v_a{}^j=v_a{}^i+1\\ (v_a{}^i/2\gamma_a)^{\frac{1}{2}}, & \text{if } v_a{}^j=v_a{}^i-1,\end{cases} \tag{12}$$

[10] A discussion and reference to earlier work may be found in footnote 8. [Correction for a sign mistake therein (Eq. 10) is incorporated in the present Eq. (9).]

[11] This step already represents a specialization of the formal development given by Van Vleck. However for nonresonance conditions the latter development in effect reduces to this approximation.

where the values for the nonvanishing integrals are taken for harmonic oscillator wave functions. Here v_a^i, for example, represents the number of quanta in normal mode a of the ith vibrational state. (All other modes in states i and j must be identically excited.) Also, $\gamma_a=(4\pi^2\nu_a/h)$ where ν_a is the characteristic frequency of the ath normal mode. Introducing these results into Eq. (11) and writing $\Delta E_{es}^0=-h(\nu_s-\nu_e)$ we obtain

$$(\alpha_{\rho\sigma})_{gi,gj}=A'+B', \tag{13}$$

where

$$A'=\frac{1}{h}\sum_e\left(\frac{2\gamma_e}{\nu_e^2-\nu_0^2}\right)(\mathfrak{M}_\rho)_{g,e}^0(\mathfrak{M}_\sigma)_{g,e}^0(gi\,|\,gj) \tag{13a}$$

and

$$B'=\frac{-1}{h^2}\sum_{\substack{e,s\\ e\neq s}}\sum_a\frac{2h_{es}{}^a\nu_e}{(\nu_s-\nu_e)(\nu_e^2-\nu_0^2)}((\mathfrak{M}_\rho)_{g,e}^0(\mathfrak{M}_\sigma)_{g,s}^0+(\mathfrak{M}_\rho)_{g,s}^0(\mathfrak{M}_\sigma)_{g,e}^0)(gi\,|\,Q_a\,|\,gj). \tag{13b}$$

The terms of the sum over electronic state e and s in Eq. (13b) may be conveniently paired into terms that are negatively equal exclusive of the factor $\nu_e/(\nu_e^2-\nu_0^2)$. Compare for example the es term with the term $e's'$ where $e'=s$ and $s'=e$. The term $e's'$ may be obtained by simply interchanging labels, e and s, in the es term. Thus $\nu_e/(\nu_e^2-\nu_0^2)\rightarrow\nu_s/(\nu_s^2-\nu_0^2)$, $h_{es}{}^a\rightarrow h_{se}{}^a=h_{es}{}^a$ (for real wave functions), and $(\nu_s-\nu_e)\rightarrow(\nu_e-\nu_s)=-(\nu_s-\nu_e)$. The factor containing the transition amplitudes remains unchanged. Thus by combining these pairs and rearranging one obtains

$$(\alpha_{\rho\sigma})_{gi,gj}=A''+B'', \tag{14}$$

where

$$A''=A' \tag{14a}$$

from [Eq. (13a)] and

$$B''=\frac{-2}{h^2}\sum_{\substack{e,s\\ s>e}}\sum_a\frac{(\nu_e\nu_s+\nu_0^2)h_{es}{}^a}{(\nu_e^2-\nu_0^2)(\nu_s^2-\nu_0^2)}((\mathfrak{M}_\rho)_{g,e}^0(\mathfrak{M}_\sigma)_{g,s}^0+(\mathfrak{M}_\rho)_{g,s}^0(\mathfrak{M}_\sigma)_{g,e}^0)(gi\,|\,Q_a\,|\,gj). \tag{14b}$$

A discussion of selection rules based on these results will be of interest.

Implicit in what follows is an assumed practical validity of the approximate sum rule employed above. Should experience reveal instances of the failure of the sum rule then in those cases a number of the following arguments will lose some of their precision.

2. *Selection Rules and Discussion*

According to Eqs. (12) it is seen that A' [Eq. (13a)] vanishes when $i\neq j$ and is therefore responsible for undisplaced, or Rayleigh scattering. At the same time the expression B'' [Eq. (14b)] is uniquely responsible for displaced scattering of fundamentals—the major part of the Raman effect—since it vanishes unless $v_a{}^j=v_a{}^i\pm1$. Scattering of combinations and overtones is derived from terms of higher order.

The condition that $v_a{}^j=v_a{}^i\pm1$ is necessary but not sufficient for B'' not to vanish. It is further required that neither $h_{es}{}^a$ nor appropriate components of $\mathfrak{M}_{g,e}{}^0$ and $\mathfrak{M}_{g,s}{}^0$ vanish. Thus the electronic states e and s must both be upper states in allowed electronic transitions. For a totally symmetric ground state this means that the symmetry species, Γ_s and Γ_e, of these electronic states must correspond separately to Γ_ρ the species of at least one of the translations.[12] At the same time the direct product $\Gamma_e\times\Gamma_{\mathfrak{IC}'}\times\Gamma_s$ must contain the totally symmetric representation in order for $h_{es}{}^a$ not to vanish. Here $\Gamma_{\mathfrak{IC}'}$ is the species symbol for the irreducible representation for which $(\partial\mathfrak{IC}/\partial Q_a)_0$ is a basis. Now Q_a, in the configuration space of the nuclei, is a basis for the same representation that $(\partial\mathfrak{IC}/\partial Q_a)_0$ is in electron space. Thus if Γ_a is the species symbol for the ath normal mode and $\Gamma_e=\Gamma_\rho$ and $\Gamma_s=\Gamma_{\rho'}$ the requirement is that $\Gamma_a\times\Gamma_\rho\times\Gamma_{\rho'}$ contain the totally symmetric species. Thus Γ_a must correspond to at least one of the species contained in the direct product $\Gamma_\rho\times\Gamma_{\rho'}$ (namely, Γ_{x^2}, Γ_{xy}, Γ_{xz}, Γ_{y^2}, Γ_{yz}, Γ_{z^2}). These are well-known selection rules for the Raman effect.

Apart from these formal selection rules the expression for B'' yields additional qualitative conditions for Raman activity. *Those normal modes which are most responsible for "forbidden" intensity in allowed transitions should show the greatest activity in Raman scattering.* The one qualification must be with regard to possible interference effects entering when summing over states

[12] A subscript ρ in this paper will always refer to an arbitrary molecule fixed coordinate (or corresponding translation). The symbol σ has been similarly used but later will acquire different meanings. Thus whenever reference to two arbitrary coordinates is necessary, the symbols ρ and ρ' will be used in cases where confusion might otherwise arise.

s and e. In the resonance Raman effect (see below) this qualification is unnecessary. It has been shown[8] how "forbidden" character in allowed transitions leads to mixed polarization of absorption in a given electronic band when the mixing is through a non-totally symmetry mode. When mixing is through a totally symmetric mode mixed polarization cannot result. Thus in at least the former case the $|h_{es}{}^{a}|$ may be determined experimentally by polarized absorption spectroscopy. If good zeroth-order functions are available they may be obtained theoretically.

In any case it will be possible to make some general statements concerning the vanishing or nonvanishing of $h_{es}{}^{a}$, but first the resonance Raman condition will be discussed.

C. Resonance-Raman Effect

When ν_0 approaches $\nu_{ev,gi}$ Eq. (2) is no longer valid. However, when a dampling correction is made Eq. (2) is modified only through an additional term in the frequency denominators. Without elaboration we shall adopt the modified form of Eq. (4) given by Behringer,[5] namely (in our notation)

$$(\alpha_{\rho\sigma})_{gi,gj}=\frac{1}{h}\sum_{ev}\left\{\frac{(M_\rho)_{ev,gj}(M_\sigma)_{gi,ev}}{\nu_{ev,gi}-\nu_0+i\gamma_e{}'}+\frac{(M_\rho)_{gi,ev}(M_\sigma)_{ev,gj}}{\nu_{ev,gj}+\nu_0+i\gamma_e{}'}\right\}, \quad (4a)$$

where $\gamma_e{}'$ is the damping constant for electronic state e. For the resonance or near-resonance conditions the second part of Eq. (4a) may be ignored and only the lowest excited state e need be considered in the sum. After introducing the expressions for the transition amplitudes as above, one obtains to first order in nuclear displacement

$$(\alpha_{\rho\sigma})_{gi,gj}=A'''+B''', \quad (15)$$

where

$$A'''=\frac{1}{h}\sum_{v}\left(\frac{(\mathfrak{M}_\rho)_{g,e}{}^{0}(\mathfrak{M}_\sigma)_{g,e}{}^{0}(gi|ev)(ev|gj)}{\nu_{ev,gi}-\nu_0+i\gamma_e{}'}\right) \quad (15a)$$

and

$$B'''=\frac{-1}{h^2}\sum_{v}\sum_{s}\sum_{a}h_{es}{}^{a}\left(\frac{(\mathfrak{M}_\rho)_{g,e}{}^{0}(\mathfrak{M}_\sigma)_{g,s}{}^{0}(gj|ev)(ev|Q_a|gi)+(\mathfrak{M}_\sigma)_{g,e}{}^{0}(\mathfrak{M}_\rho)_{g,s}{}^{0}(gi|ev)(ev|Q_a|gj)}{(\nu_{ev,gi}-\nu_0+i\gamma_e{}')(\nu_s-\nu_e)}\right); \quad (15b)$$

e refers to the electronic state near resonance. It is not possible to perform the sum over vibrations previously carried out because the frequency denominator is now sensitive to this sum. The sum rule previously employed is no longer helpful.

Qualitative consideration of Eqs. (15) reveals interesting differences from, say, Eqs. (14). First it is seen that whenever the vibrational wave functions of electronic state e and those of the ground state are not solutions to the same Schrödinger equation (which is generally the case), then the "Rayleigh" term A''' can be responsible for Raman scattering. Thus with $i\neq j$, $(gi|ev)(ev|gj)$ need not vanish. Further, the contribution from A''' to Raman intensity depends in no way on vibronic mixing of state e with other states. Similarly Rayleigh intensity may derive in part from the B''' term since neither $(gi|Q_a|ev)(ev|gj)$ nor $(gi|ev)(ev|Q_a|gj)$ need vanish when $i=j$. The same arguments of course could be applied to Eqs. (11), however, after employing the sum rule (Eqs. 12) these effects appear to cancel. In any case it would seem that qualitatively at least $(gi|ev)(ev|gj)$ must be small when $i\neq j$ while either $(gi|Q_a|ev)(ev|gj)$ or $(gi|ev)(ev|Q_a|gj)$ can be large especially when $v_a{}^{j}=v_a{}^{i}\pm 1$. It is reasonable to expect that B''' is still responsible for most of the Raman effect while A''' leads primarily to Rayleigh scattering.

In contrast to the term B'' [Eq. (14b)] in the ordinary Raman effect, the term B''' uniquely emphasizes the role of the lowest allowed electronic transition (near resonance) and the lowest-lying allowed transition (to state s) from which intensity is stolen through vibrational mixing. For example, B'' contains no factor such as $1/(\nu_s-\nu_e)$ which tends to select the lowest favorable s. While the formal selection rules remain the same, it is clear that B''' can favor different vibrations than B'' does. In general one can expect the distribution of intensities in a Raman spectrum to change as resonance is approached. This point of course is not new. However the present approach permits more detailed comment. Suppose the lowest allowed transition is x polarized and the next transition from which the first acquires "forbidden" intensity is y polarized. Then as resonance is approached the intensity of the very vibration that is mixing the two electronic states should increase relative to all other Raman lines. Thus knowledge gained from vibronic spectroscopy permits one to anticipate not only the symmetry of the enhanced vibration but also which particular mode of that symmetry it must be. Conversely if enhancement of a particular normal mode is noticed in the Raman spectrum when approaching resonance then its identity can lead to predictions concerning the polarizations of the combining electronic transitions.

These points become the more valid the nearer state s lies to state e. When however state e is well separated from other states, then several states s may more or less equally exert their influence. Thus instead of only α_{xy} being enhanced, α_{xz} and α_{xx} may also contribute. Still α_{yy} or α_{yz} are excluded.

These considerations permit a further general remark. Near resonance, depolarization ratios for totally symmetric vibrations must reach a maximum since a minimum number (only one for a nondegenerate case) of diagonal terms of the polarizability tensor is enhanced through resonance. This point has been made very recently and verified qualitatively by Rea[7] whose discussion is based on Shorygin's equation.

It seems clear that resonance Raman investigations will be extremely fruitful in providing information regarding electronic-state properties. At the same time vibronic spectroscopic investigations such as theoretical calculations of "forbidden" intensities in allowed transitions (for totally symmetric modes as well as non-totally symmetric modes) and detailed polarization studies acquire additional importance. They should be very useful for the understanding of the resonance Raman effect (and more remotely the Raman effect itself).

Before concluding this section it will be worthwhile to carry Eq. (15b) to the extreme of assuming identical Schrödinger equations for states e and s. This, at least, will reveal the limiting form for $(\alpha_{\rho\sigma})_{gi,gj}$ as this idealized condition is approached. Under these conditions the sum over v in Eq. (15b) yields only two nonvanishing terms, namely $v=j$, and $v=i$ [because $(gi|ev)=\delta_{iv}$ and $(gj|ev)=\delta_{jv}$]. When $v=j$ the first part of B''' enters while when $v=i$ the second part contributes. For a nondegenerate case where, say, $(\mathfrak{M}_\rho)_{g,e}{}^0\neq 0$ the term with $v=j$ contributes to $\alpha_{\rho\sigma}$ while the term with $v=i$ contributes to $\alpha_{\sigma\rho}$. Both contribute simultaneously to $\alpha_{\rho\rho}$. Thus with $ev=gj$ (and $ev=gi$) and Eqs. (12) (for $v_a{}^j=v_a{}^i+1$) with Eq. (15b) we obtain

$$(\alpha_{\rho\sigma})_{gi,gj}=\frac{-1}{h^2}\sum_{s,a}\frac{h_{es}{}^a(\mathfrak{M}_\rho)_{g,e}{}^0(\mathfrak{M}_\sigma)_{g,s}{}^0[(v_a{}^i+1)/2\gamma_a]^{\frac{1}{2}}}{(\nu_s-\nu_e)(\nu_e-\nu_0+\nu_a+i\gamma_e')}, \tag{16}$$

$$(\alpha_{\sigma\rho})_{gi,gj}=\frac{-1}{h^2}\sum_{s,a}\frac{h_{es}{}^a(\mathfrak{M}_\rho)_{g,e}{}^0(\mathfrak{M}_\sigma)_{g,s}{}^0[(v_a{}^i+1)/2\gamma_a]^{\frac{1}{2}}}{(\nu_s-\nu_e)(\nu_e-\nu_0+i\gamma_e')}, \tag{16a}$$

and

$$(\alpha_{\rho\rho})_{gi,gj}=\frac{-1}{h^2}\sum_{s,a}\frac{h_{es}{}^a}{(\nu_s-\nu_e)}\left(\frac{1}{\nu_e-\nu_0+\nu_a+i\gamma_e'}+\frac{1}{\nu_e-\nu_0+i\gamma_e'}\right)(\mathfrak{M}_\rho)_{g,e}{}^0(\mathfrak{M}_\rho)_{g,s}{}^0\left(\frac{v_a{}^i+1}{2\gamma_a}\right)^{\frac{1}{2}}. \tag{16b}$$

These are the limiting forms for the Stokes resonance Raman polarizability components (first order in Q) on assuming harmonic oscillator wave functions.

III. GENERAL DISCUSSION

A. Rules Governing the Electronic Contributions to Raman Intensities

A principal result of the present formulation is that Raman intensity has its origin in "forbidden" intensities in allowed electronic transitions. All virtual pure electronic states which participate in allowed transitions are active in Rayleigh scattering, but only those pairs of these states which interact under vibrational perturbation can give rise to Raman scattering. The question arises whether or not some general rules (valid to first order in Q) can be discerned regarding the Raman activity of a given pair of states. Since it is difficult to anticipate interference effects among contributing pairs of states (except in the resonance Raman case where there is probably almost no interference), it is appropriate to outline conditions for which a given pair of states has a vanishing contribution. Already the first rule can be stated.

Rule 1. A given pair of pure electronic states, e and s, cannot contribute to Raman intensity if a dipole transition to either or both is pure-electronically forbidden [that is if either $\mathfrak{M}_{g,e}{}^0$ or $\mathfrak{M}_{g,s}{}^0$ (or both) vanishes].

Given that states e and s participate in allowed transitions then it remains to discover the conditions causing $h_{es}{}^a$ to vanish. The operator $(\partial\mathcal{H}/\partial Q_a)_0$ which mixes the electronic states, is a one-electron operator since the only part of the electronic Hamiltonian that depends on nuclear position is the Coulomb potential between electrons and nuclei. Thus

$$(\partial\mathcal{H}/\partial Q_a)_0=-e\sum_i\left[\sum_\sigma\left(\frac{\partial(Z_\sigma/r_{i\sigma})}{\partial Q_a}\right)_0\right], \tag{17}$$

where e is the electronic charge, Z_σ the charge of nucleus σ, and $r_{i\sigma}$ the distance separating electron i and nucleus σ. The sums go over all electrons and nuclei. In such a case it is useful to turn to the transition density formalism introduced by Longuet-Higgins[13] and applied by Murrell and Pople[14] to the vibronic problem. The operator whose expectation value is the chance of finding particle i at a point defined by a vector r is just the Dirac delta function, $\delta(r-r_i)$, which has the property illustrated through the equation

$$\int f(\mathbf{r})\,\delta(\mathbf{r}-\mathbf{r}')\,d\mathbf{r}'=f(\mathbf{r}').$$

The electric density operator, excluding the contribu-

[13] H. C. Longuet-Higgins, Proc. Roy. Soc. (London) **A235**, 537 (1956).

[14] J. N. Murrell and J. A. Pople, Proc. Phys. Soc. (London) **A69**, 245 (1956).

tion of the nuclei, is

$$-e\sum_i \delta(\mathbf{r}-\mathbf{r}_i)=\rho(\mathbf{r}). \tag{18}$$

Now consider any one-electron operator

$$G=-e\sum_i G(\mathbf{r}_i).$$

It can be seen that

$$G=\int G(\mathbf{r})\rho(\mathbf{r})d\mathbf{r}. \tag{19}$$

The matrix element of this operator linking electronic states k and l reads

$$(k|G|l)=\left(k\left|\int G(\mathbf{r})\rho(\mathbf{r})d\mathbf{r}\right|l\right)$$

$$=\int (k|\rho(\mathbf{r})|l)G(\mathbf{r})d\mathbf{r}, \tag{20}$$

where

$$(k|\rho(\mathbf{r})|l)=\int \Theta_k^0(-e\sum_i \delta(\mathbf{r}-\mathbf{r}_i))\Theta_l^0(\Pi d\mathbf{r}_i) \tag{21}$$

is known as the transition density since the dipole moment of this charge distribution is just the electron transition moment. In the present case G is given by Eq. (17) and the interaction energy corresponds to the interaction of the transition density (Eq. 21) with a set of dipoles each centered at a nucleus with direction and amplitude fixed by the normal coordinate involved and the effective nuclear charge. Clearly if the transition density vanishes there can be no question of states k and l interacting and thereby contributing to Raman intensities.

Consider the electronic wave functions to be ASMO functions with CI (configurational interaction), where the MO are obtained from an SCF (self-consistent-field) calculation for a closed-shell ground state.[15] The MO are orthonormal and the excited configurations are constructed by promoting electron(s) from the closed-shell ground state into unfilled MO. When highly excited configurations are required (for Rydberg transitions, for example), and additional MO's are needed, we shall assume that these, too, are orthonormal (with respect to the whole set). Since the electric density operator $\rho(\mathbf{r})$ is also a one-electron operator, the integral in Eq. (21) must vanish whenever two configurations differ in the MO occupation of more than one electron. That is, only those configurations can interact which are related by a shift of no more than one electron. Thus a second rule may be formulated.

Rule 2. A pair of configurations which differ in MO *occupancy by more than one electron cannot mix (under the vibrational perturbation) and as a pair cannot contribute to the Raman intensity.* To the extent that excited states are approximated by single configurations this rule applies to any pair of states.

[Incidentally, since the transition moment operator $\mathbf{m}$ is also a one-electron operator $(-e\sum\mathbf{r}_i)$ then according to rule 1 and our assumption of a closed-shell ground state, only the singly excited configuration contributions to state functions need be considered; these alone can combine with the ground state to give allowed transitions.]

A third important rule within the approximation of this development may be formulated. Suppose two configurations differ by the occupancy of only one electron; the integration in Eq. (21) will vanish for every term in $\rho(\mathbf{r})$ except the one referring to the unmatched electron. For this term integration over all other electrons is straightforward giving unity when all but the one are perfectly matched. The remaining integration over the space of the electron in the unmatched MO gives a transition density which is large or small depending on the extent to which the two different MO occupy the same regions of space. Thus:

Rule 3. When the two MO *which distinguish two mixing configurations can be said to occupy different regions of the molecule, then the contribution of this pair of configurations to the Raman intensity must be small, if not vanishing.* Again, to the extent that two states are represented by single configurations then rule 3 applies directly to the mixing of the two states.

The rules just outlined can be useful for discussing problems such as chromophore additivity in Raman intensities, depolarization ratios, the relative importance of pairs of certain types of electronic states (n, π states, charge-transfer states, Rydberg states, etc.) and the question of additivity of "σ" and "π" polarizability. As an example, the question of σ, π separation in the Raman effect shall be considered.

B. Additivity of σ and π Contributions to the Polarizability

A single bond can be said to have a local symmetry of $D_{\infty h}$ or $C_{\infty h}$. In such a case, orbitals may be classified according to their angular momentum about the symmetry axis as σ, π, δ, etc. orbitals. Further, in groups where there exists a plane of symmetry normal to the symmetry axis a σ, π distinction is commonly made according to the symmetric (σ) or antisymmetric (π) behavior with respect to reflection through this plane. Where distinction is meaningful, the closed-shell ground state for many molecules contains σ and π orbitals. Within the framework of Placzek's polarizability theory, which explicitly refers to ground-state properties, one may speak of the σ contributions and the π contributions to the derived polarizability.

[15] C. C. J. Roothaan, Revs. Modern Phys. **23**, 69 (1951).

Recently Yoshino and Bernstein[16] have reported examples of an apparent additivity of the derived polarizability in the σ and π parts of a multiple bond for totally symmetric modes. And, incidentally, the total contribution appears to be proportional to the bond order. On the other hand an equality of the σ and π contributions does not seem to be found in a study of totally symmetric modes in oxyanions by Chantry and Plane.[17] Still the concept of the separation of σ and π contributions is retained. It appears that it is possible to provide a degree of formal support for this useful concept when dealing with totally symmetric normal modes.

Suppose excited electron configurations are separated into two classes. One class, the σ class, will include all those configurations which are constructed by promoting an electron from a ground-state σ orbital (into any other orbital) and the other class, the π class, will consist of those configurations which involve excitation from a ground-state π orbital. (Doubly excited configurations need not be considered.) Of all members of each class we need consider only those configurations which combine with the ground state through the electric moment operator (rule 1). The question remains whether the configurations, thus selected, of one class can interact with those of the other class through vibrational perturbation. Now rule 2 demands that interacting configurations differ by no more than one orbital. The configurations in our two classes already differ *at least* by one orbital, namely, the σ and π orbitals of the ground state. For those configurations that might interact, let j symbolize the common excited orbital. For a totally symmetric mode, interacting states must have the same polarization. Can two configurations, one in each class, have a common singly occupied orbital j and at the same time combine with the ground state with the same polarization? Group-theoretically the question is reduced to determining whether or not the direct products $\Gamma_\sigma \times \Gamma_j$ and $\Gamma_\pi \times \Gamma_j$ contain simultaneously $\Gamma_\rho(\rho = x, y, \text{or } z)$. To ask that these two direct products contain a common representation is equivalent to asking that $\Gamma_\sigma \times \Gamma_\pi$ contain the totally symmetric representation. Since this cannot be the case it is seen that for totally symmetric modes, configurations from the two classes cannot interact. The electronic states e and s [Eq. (14b)] are not in general single configurations. However, by the same argument just presented no one-electron operator can mix relevant configurations (for totally symmetric modes) coming from the two classes, since the two singly occupied MO of one must differ from the two singly occupied MO of the other. The electron repulsion operator, however, can bring about mixing. To the extent that intra-class CI is dominant over inter-class CI—and it is likely that the former dominates—then to that extent can excited electronic states be assigned to one or the other of the two classes. The sum over e and s in Eq. (14b) may be divided into two parts one referring exclusively to electronic states of the σ class and the other to electronic states of the π class. Thus

$$\sum_{e,s} = \sum_{e_\sigma, s_\sigma} + \sum_{e_\pi, s_\pi} \qquad (s > e),$$

where the first term may be regarded as related to the derived polarizability of the ground-state σ orbitals and the second term to the derived polarizability of the ground-state π orbitals for a given *totally symmetric normal mode*. For non-totally symmetric modes this separation is not possible. Here $\Gamma_{\rho'} \times \Gamma_\sigma$ and $\Gamma_\rho \times \Gamma_\pi (\rho' \neq \rho)$ can contain a common Γ_j. (Configurations in different classes can interact through one-electron operators if the polarizations are different.)

C. Preliminary Comments Regarding Ethylene, Acetylene, and Benzene

A preliminary analysis of ethylene, acetylene, and benzene has been carried out. Common to these three molecules (excluding σ class configurations) is one, intense allowed sub-Rydberg transition ($N \rightarrow V$; degenerate in the case of acetylene and benzene). In addition, there are a great number of Rydberg transitions. Since at least two pure electronic states are required to contribute to the Raman effect, evidently the $N \rightarrow V$ transitions can be active only through vibronic interaction with the Rydberg states. It is possible that this interaction may be weak according to rule 3 although this is by no means certain. In any case it is quite likely that the π contribution to the derived polarizability is governed to a large extent by the Rydberg states and their vibronic interactions. This is probably also true for the σ contributions as well, although to understand how σ and π contributions (per bond order) are approximately equal[16] is still difficult to see. It is hoped that later more detailed comment will be possible regarding this and regarding depolarization ratios in these molecules.

D. Intensity Dependence on Frequency and Comparison with the Equation of Shorygin

When the frequency of the incident light is very much smaller than the frequency of the virtual transitions and yet at the same time is much larger than the Raman displacement, then the intensity of the displaced line is proportional to ν_0^4. Thus Eqs. (2) and (1) with $\nu_{rm}, \nu_{rn} \gg \nu_0 \gg \nu_{mn}$ give $I_{mn} \propto \nu_0^4$. As the frequency of the incident light approaches that of the virtual transitions, deviation from this proportionality must occur. The nature of this deviation can constitute a test of theoretical predictions. It appears that the semiclassical theory of Shorygin has been quite suc-

[16] T. Yoshino and H. J. Bernstein, *Petroleum Institute Conference on Molecular Spectroscopy* (Pergamon Press, New York, 1958), p. 141.

[17] G. W. Chantry and R. A. Plane, J. Chem. Phys. **32**, 319 (1960).

cessful[3] with regard to this point. It will prove interesting to examine the predictions made on the basis of Eq. (14b) and also to compare this equation with that of Shorygin. The latter equation is obtained by setting $\rho=\sigma$ and $m=n=k$ in Eq. (2) [giving an expression for $(\alpha_{\rho\rho})_{kk}$] and then taking a derivative with respect to normal coordinate Q_a. Thus

$$\partial(\alpha_{\rho\rho})_{kk}/\partial Q_a = A+B, \tag{22}$$

where

$$A=\frac{1}{h}\sum_r\left(\frac{2\nu_{rk}}{(\nu_{rk}^2-\nu_0^2)}\frac{\partial|(M_\rho)_{rk}|^2}{\partial Q_a}\right) \tag{22a}$$

and

$$B=\frac{-2}{h}\sum_r\frac{\nu_{rk}^2+\nu_0^2}{(\nu_{rk}^2-\nu_0^2)^2}|(M_\rho)_{rk}|^2\frac{\partial\nu_{rk}}{\partial Q_a}, \tag{22b}$$

where r is a virtual state. When ν_0 approaches ν_{rk} the second term, B dominates. This expression [Eq. (22b)] bears an interesting gross resemblance to Eq. (14b) of our theory. The present h_{es}^a can be related to $(\partial h\nu_{rk}/(\partial Q_a)$, since, loosely speaking, both represent a change in electronic energy of state $e(r)$ per displacement of normal mode a. (However, h_{es}^a, is only that part of this due to mixing with state s.) When Eqs. (22) are inserted into Placzek's polarizability theory the same amplitude integral appears namely, $(gi|Q_a|gj)$—that is found in Eq. (14b). The transition amplitude factors and the frequency-dependent factors are also similar. Equation (22b) for near-resonance conditions, where the sum over r is dropped, leads to the following expression for the intensity,

$$I\propto\nu_0^4[(\nu_{rk}^2+\nu_0^2)^2/(\nu_{rk}^2-\nu_0^2)^4. \tag{23}$$

This is the form that has proven to be relatively successful,[3] in predicting the ν_0 dependence of I. Usually ν_{rk} is taken as a representative excitation frequency between the ground state and the active virtual excited electronic state. Compare now the predictions made by Eq. (14b). On making similar assumptions for the near-resonance condition it is seen that

$$I\propto\nu_0^4\{(\nu_e\nu_s+\nu_0^2)^2/[(\nu_e^2-\nu_0^2)(\nu_s^2-\nu_0^2)]^2\}. \tag{24}$$

When $\nu_s\rightarrow\nu_e$ (very close-lying vibronically mixing states), Eq. (24) reduces to Eq. (23) and the two theories predict the same ν_0 dependence. When, however, $\nu_s\gg\nu_e$, Eq. (24) resembles more the form

$$I\propto\nu_0^4/(\nu_s^2-\nu_0^2)^2, \tag{25}$$

which has been found to be relatively less successful,[3] than Eq. (23). Evidently the present theory can express a range of behavior depending on the relative location of the electronic states e and s. As one recedes from resonance conditions the distinction between ν_e and ν_s becomes less important and the ν_0 dependence of Eq. (14b) will resemble more and more that of Eq. (22b). However, it is just under such circumstances that Eq. (22a) dominates in the Shorygin theory. Thus, in fact, the two theories diverge. In view of the serious assumptions involved in the semiclassical theory[3,5] it may be that the success of Eq. (22b) lies in its resemblance to Eq. (14b). The present discussion has not dealt with the very near resonance condition. Here the ν_0 dependence must be examined within the framework of Eqs. (15) or possibly Eqs. (16).

It would seem that the present theory would be subject to relatively straightforward experimental testing. This will receive more direct attention in future investigations.

ACKNOWLEDGMENTS

The author thanks Professor R. Plane and Dr. G. Chantry for a number of informative discussions and Dr. A. D. Liehr for his criticism.

Statistical Mechanics of Isotope Effects on the Thermodynamic Properties of Condensed Systems*

JACOB BIGELEISEN

Chemistry Department, Brookhaven National Laboratory, Upton, New York

(Received August 26, 1960)

Evidence for the role of molecular structure on the difference in the thermodynamic properties of isotopic molecules in the liquid and solid states is summarized. The properties considered are vapor pressure, heats of vaporization, molal volume, and transition temperatures. It is shown that the molecular structure must be taken into consideration even for small quantum effects. In the approximation of the first quantum correction the difference in thermodynamic properties of isotopic molecules in the condensed state depends upon the atomic masses and an energy parameter associated with each atom in the molecule. The results are extended to higher-order quantum corrections for a harmonic potential. The rules of the mean are obtained directly. Various frequency distributions for the lattice modes are considered. For the case where the internal frequencies in the condensed phase are similar to the free molecule, the ordered quantum corrections can be used for $T > (h\nu_{max}/12(2)^{\frac{1}{2}}k)_{mol}$; $T > (h\nu_{lattice}/2\pi k)$. The role of the gas imperfection and the molal volume of the condensed phase is discussed for equilibria between gaseous and condensed phases. It is shown that the difference in molal volumes of isotopic molecules is a second-order effect. The difference in molal volumes of isotopic molecules is evaluated by an extension of Gruneisen's equation of state to molecular lattices. The results are in good agreement with available experimental data.

I. INTRODUCTION

THE problem of the effect of isotopic substitution on the vapor pressure of a condensed phase is an old one. The first theoretical treatment of the subject was given about 40 years ago by Lord Cherwell[1] for a monatomic Debye solid. A similar derivation was given independently some years later by Otto Stern.[2] Both Stern and Lindemann recognized the role of the zero-point energy of the lattice vibrations and treated the case of a monatomic Debye solid in equilibrium with an ideal gas. Their treatment was extended by Scott *et al.*[3] to include gas imperfection and the difference between the Gibbs and Helmholtz free energies for an incompressible solid. They then showed that good agreement was obtained between theoretical calculations using the calorimetrically determined Debye θ's and their experimental measurements on the difference in vapor pressures of solid H_2 and D_2.

The theory of the effect of isotopic substitution on the vapor pressure of liquids is necessarily in a much rougher status than that of the solid. This is simply another manifestation of the current inadequacies of the theory of quantum corrections to the liquid partition function. Herzfeld and Teller[4] published an important paper on the theory of the effect of isotopic substitution on the vapor pressures of liquids. By the use of the Wigner quantum correction to the Boltzmann distributions,[5] they developed the partition function of the liquid in terms of the classical partition function. From this development one can easily show that, in a first approximation, the logarithm of the ratio of vapor pressures should be a linear function of the reciprocal of the square of the absolute temperature. This development is not applicable to the case of He^3 and He^4, even apart from the question of the difference in statistics, because of the large quantum correction. From the Herzfeld-Teller expansion it is obvious that the light isotope should always have the higher vapor pressure. Yet numerous cases are known where the light isotope has the higher vapor pressure at the low temperature, but the heavy isotope has the higher vapor pressure at the high temperature. This cross-over phenomenon was discussed originally by Topley and Eyring[6] in terms of the shift of an internal frequency on condensation. Such shifts are well established by spectroscopic data, and will contribute a subtractive term of the form B/T to the logarithm of the vapor-pressure ratio if ϵ/kT for the vibration is of the order of 2π or greater. This is one effect which contributes to the cross-over phenomenon. In addition, Bailey and Topley[7] called attention to the effect of isotopic substitution on the molar polarizabilities. No rigorous quantitative treatment of this problem has been given to date, but the work of Bailey and Topley and the discussion of Herzfeld and Teller suffice to show that this effect, as well as the difference in molar volumes of isotopic liquids, both contribute to the cross-over phenomenon. Unfortunately more recent discussions of the cross-over phenomenon have overlooked these considerations and are in general erroneous.

More recently de Boer[8] has developed a semiempirical approach to the theory of quantum corrections to the reduced thermodynamic properties of liquids. The method has been remarkably successful in predicting the thermodynamic properties of He^3 by the use of the

* Research performed under the auspices of the U. S. Atomic Energy Commission.

[1] F. A. Lindemann, Phil. Mag. **38**, 173 (1919).

[2] Quoted by W. H. Keesom and H. van Dijk, Proc. Acad. Sci. Amsterdam **34**, 42 (1931).

[3] R. B. Scott, F. G. Brickwedde, H. C. Urey, and M. H. Wahl, J. Chem. Phys. **2**, 454 (1934).

[4] K. F. Herzfeld and E. Teller, Phys. Rev. **54**, 912 (1938).

[5] E. Wigner, Phys. Rev. **40**, 749 (1932).

[6] B. Topley and H. Eyring, J. Chem. Phys. **2**, 217 (1934).

[7] C. R. Bailey and B. Topley, J. Chem. Soc. **1936**, 921.

[8] J. de Boer, Physica **14**, 139 (1948).

quantum mechanical parameter $\Lambda^*=h/\sigma(m\epsilon)^{\frac{1}{2}}$.[9] It is to be noted that according to de Boer's definition of Λ^*, ϵ is the depth of the intermolecular potential, σ is the range of the force, and m is the molecular weight. Whereas the de Boer method has much to recommend it in the treatment of rare gases, it fails for the case of the isotopic liquid hydrogens. Two types of failure are to be noted. In the symmetrical molecules, D_2 and T_2, the thermodynamic properties calculated[10,11] by interpolation of the reduced properties of protium (H_2) and neon are not in agreement with experiment.[11,12] This failure results from the fact that the form of the intermolecular potential in hydrogen is different from that of the rare gases and a simple interpolation in terms of Λ^* is therefore inadequate. The second type of failure of the de Boer method as applied to hydrogen, has been recognized only recently.[13,14] It is the failure of any theory which relates the thermodynamic properties of isotopic species to the molecular weight to predict the well-known rule of the geometric mean, i.e., $P_{HD}=(P_{H_2}P_{D_2})^{\frac{1}{2}}$. Since the semiempirical theories of Friedman, White, and Johnston,[12] and Libby and Barter[15] are also in terms of the molecular weight, they are also subject to a similar objection. Theories which relate the vapor-pressure difference to the molecular weight also fail to explain the fact that the vapor pressures of the isotopic CO molecules[16] fall in the sequence $C^{12}O^{16}>C^{12}O^{18}>C^{13}O^{16}$, etc. Of course there is also the well-known fact that isomers of the type CH_3OD and CH_2DOH do not have the same vapor pressures. It is thus apparent that any theory of isotopic substitution on the equation of state of a condensed phase must take account of the structure of the molecule.

A structural effect arises from the mass asymmetry of a molecule and its change with isotopic substitution. The centers of force describing the interaction of a pair or cluster of asymmetric molecules will not, in general, coincide with the centers of gravity. Thus, even if the molecular motion can be described approximately as a restricted translation and hindered rotation, there will be a coupling between the translation and rotation. The degree of coupling will be changed by isotopic substitution, since this substitution will change the center of gravity and moments of inertia. In some cases where there is no such asymmetry, isotopic substitution may introduce one, e.g., H_2 vs HD. A treatment of this translational-rotational coupling effect by the method of perturbation theory has been given recently by Babloyantz.[17] Wave functions appropriate for a cell model were used by Babloyantz for the unperturbed system.

In the present paper we shall treat the effect of isotopic substitution on the vapor pressure for systems with small quantum corrections in the harmonic approximation, after correction for the molal volume effect. The method implicitly accounts for all types of coupling such as between optical and accoustical modes and translation and rotation. As such, we obtain, therefore, the high-temperature limiting correction to the classical behavior, subject only to the harmonic approximation. It will be shown that the first quantum correction in the harmonic approximation leads to deviations from the rigid-sphere model and provides an explanation for the structural effects discussed previously and the rule of the geometric mean.

II. STATISTICAL THERMODYNAMIC CONSIDERATIONS

In this section we relate the vapor-pressure ratio of isotopic substances to the partition functions for the gas and condensed phases. For the condensed phase the Gibbs free energy is

$$G_c=-kT\ln Q+PV. \tag{2.1}$$

In Eq. (2.1) all extensive properties are molar quantities and the partition function, Q, is for an assembly of N molecules. We now define an average molecular partition function $\bar{Q}$,

$$\bar{Q}=Q^{1/N}, \tag{2.2}$$

and the free-energy equation for the condensed phase becomes

$$G_c=-RT\ln\bar{Q}+PV. \tag{2.3}$$

The gas imperfection makes a significant contribution to the vapor-pressure ratio. We write the equation of state of the gas in the form

$$PV/RT=1+B_0P+C_0P^2. \tag{2.4}$$

The Gibbs free energy for the real gas is then

$$G_r/RT=\ln P-\tfrac{3}{2}\ln M-\tfrac{5}{2}\ln T-\ln Q_i+(B_0P+\tfrac{1}{2}C_0P^2)+K_{ST}, \tag{2.5}$$

where K_{ST} is the Sackur-Tetrode constant, M is the molecular weight, and Q_i includes the rotational and internal partition functions. The equilibrium condition $G_c=G_r$ gives

$$\ln P=\ln(Q_iM^{\frac{3}{2}}/\bar{Q})+\tfrac{5}{2}\ln T+(PV/RT)-(B_0P+\tfrac{1}{2}C_0P^2)-K_{ST}. \tag{2.6}$$

[9] See Chap. 6 by J. de Boer and R. B. Bird in J. O. Hirschfelder, C. F. Curtiss, and R. B. Bird, *Molecular Theory of Gases and Liquids* (John Wiley & Sons, Inc., New York, 1954).

[10] E. F. Hammel, J. Chem. Phys. **18**, 228 (1950).

[11] E. R. Grilly, J. Am. Chem. Soc. **73**, 843 (1951).

[12] A. S. Friedman, D. White, and H. L. Johnston, J. Chem. Phys. **19**, 126 (1951).

[13] J. Bigeleisen, BNL 2190 and Phys. Rev. **99**, 638(A) (1955).

[14] J. Bigeleisen and E. C. Kerr, J. Chem. Phys. **23**, 2442 (1955).

[15] W. F. Libby and C. A. Barter, J. Chem. Phys. **10**, 184 (1942).

[16] T. F. Johns, *Proceedings of the International Symposium on Isotope Separation*, edited by J. Kistemaker, J. Bigeleisen, and A. O. C. Nier (North-Holland Publishing Company, Amsterdam, 1958), pp. 74–101.

[17] A. Babloyantz, J. Mol. Phys. **2**, 39 (1959).

The vapor-pressure ratio for a pair of isotopic molecules at the temperature T is

$$\ln P'/P=\ln(Q_i'M'^{\frac{3}{2}}\bar{Q}/Q_iM^{\frac{3}{2}}\bar{Q}')+(RT)^{-1}(P'V'-PV)-(B_0P+\tfrac{1}{2}C_0P^2)'+(B_0P+\tfrac{1}{2}C_0P^2). \quad (2.7)$$

We note that

$$Q_i'M'^{\frac{3}{2}}/Q_iM^{\frac{3}{2}}=Q'/Q, \quad (2.8)$$

where Q and Q' are the complete quantum-mechanical partition functions for the isotopic ideal-gas molecules when P equals P'. We recall the definition[18] of the reduced partition function ratio of a pair of isotopic molecules

$$s/s'f=(s/s')(Q/Q')\prod_i^n(m_i'/m_i)^{\frac{3}{2}}, \quad (2.9)$$

where the product runs over the n atoms in the molecule and m_i is the mass of the ith atom. The molecular symmetry appears as the symmetry number ratio s/s'. We combine Eqs. (2.7), (2.8), and (2.9) to give

$$\ln P'/P=\ln\frac{(\bar{Q}/\bar{Q}')}{(s'/s)\prod_i^n(m_i/m_i')^{\frac{3}{2}}}-\ln s/s'f+(RT)^{-1}(P'V'-PV)-(B_0P+\tfrac{1}{2}C_0P^2)'+(B_0P+\tfrac{1}{2}C_0P^2). \quad (2.10)$$

The average molecular partition function $\bar{Q}$ is a function of T, V, and m_i. It may be convenient to compare the isotopic systems at the same molal volume. For this purpose we write

$$\ln\bar{Q}'(T,V',m')=\ln\bar{Q}'(T,V,m')+\int_V^{V'}(\partial\ln\bar{Q}'/\partial V)dV. \quad (2.11)$$

But

$$(\partial\ln\bar{Q}'/\partial V)_T=P'/RT, \quad (2.12)$$

and Eq. (2.10) becomes

$$\ln P'/P=\ln\frac{\bar{Q}(T,V,m)/\bar{Q}'(T,V,m')}{(s'/s)\prod_i(m_i/m_i')^{\frac{3}{2}}}-(RT)^{-1}\int_V^{V'}P'dV-\ln s/s'f+(RT)^{-1}(P'V'-PV)-(B_0P+\tfrac{1}{2}C_0P^2)'+(B_0P+\tfrac{1}{2}C_0P^2). \quad (2.13)$$

We now consider the analogous classical systems at the molar volume V. If we assume that the potential energy of the system is invariant with respect to isotopic substitution, then

$$[\bar{Q}(T,V,m)/\bar{Q}'(T,V,m')]_{cl}=s'/s\prod_i^n(m_i/m_i')^{\frac{3}{2}}, \quad (2.14)$$

where $[\bar{Q}(T,V,m)/\bar{Q}'(T,V,m')]_{cl}$ is the ratio of the partition functions of the condensed phases for classical systems. In the classical limit $B_0=B_0'$, $V=V'$, and the vapor pressures of isotopic molecules are the same. We now define

$$s/s'(f_c)_V=\frac{\bar{Q}(T,V,m)/\bar{Q}'(T,V,m')}{[\bar{Q}(T,V,m)/\bar{Q}'(T,V,m')]_{cl}} \quad (2.15)$$

and obtain

$$\ln P'/P=\ln s/s'(f_c)_V-\ln s/s'f-(RT)^{-1}\int_V^{V'}P'dV+(RT)^{-1}(P'V'-PV)-(B_0P+\tfrac{1}{2}C_0P^2)'+(B_0P+\tfrac{1}{2}C_0P^2). \quad (2.16)$$

If $\ln P'/P$ is small and $B_0'\simeq B_0$, $V'\simeq V$, then after neglecting terms of the order C_0P^2, the corrections to the vapor-pressure equation for the finite pressure of the gas can be written as

$$(\ln P'/P)[1+P(B_0-V/RT)]=\ln s/s'(f_c)_V-\ln s/s'f-(RT)^{-1}\int_V^{V'}P'dV. \quad (2.17)$$

There is a simple physical interpretation to the various terms, in Eq. (2.16), which contribute to the vapor-pressure difference of isotopes. The term $\ln s/s'f_c-\ln s/sf$ is the difference in the quantum effects in the condensed and gaseous states. It is the vapor-pressure difference that would be observed if the two isotopes had the same molar volume in the condensed phase and if the gases were infinitely dilute. The terms

$$1/RT(P'V'-PV)-(B_0P+\tfrac{1}{2}C_0P^2)'+(B_0P+\tfrac{1}{2}C_0P^2),$$

represent the change in the vapor pressure when the condensed phase is subject to a pressure change from P to P' and the nonideal gases are compressed to P and P', respectively. The quantum effects on the equation of state of the gas appear by virtue of the fact that B_0' and C_0' are different from B_0 and C_0, respectively. Finally the work integral $\int PdV$ after multiplication by $1/RT$, corrects $\ln s/s'f_c$ for the fact that the molar volumes of the condensed phases are not the same.

III. THE HARMONIC APPROXIMATION

We shall show in Sec. IV that the correction of the vapor-pressure ratio for the molal volume of the condensed phase is a second-order effect, and that there is, in fact, little difference between Eqs. (2.10) and (2.16). At present we are interested in the vapor-pressure ratio with the condensed phases in equilibrium with their respective vapors. We, therefore, return to Eq. (2.10) and write

$$\ln P'/P=\ln s/s'f_c-\ln s/s'f+(RT)^{-1}(P'V'-PV)-(B_0P+\tfrac{1}{2}C_0P^2)'+(B_0P+\tfrac{1}{2}C_0P^2), \quad (3.1)$$

[18] J. Bigeleisen and M. G. Mayer, J. Chem. Phys. **15**, 261 (1947).

where

$$s/s'f_c=\frac{\bar{Q}(T,V,m)/\bar{Q}'(T,V',m')}{[\bar{Q}(T,V,m)/\bar{Q}'(T,V',m')]_{cl}}. \quad (3.2)$$

In the harmonic approximation

$$\ln s/s'f_c = N^{-1}\left\{\frac{hc}{2kT}\sum_{i=1}^{3nN}(\nu_i'-\nu_i)+\sum_{i=1}^{3nN}\ln\frac{u_i[1-\exp(-u_i')]}{u_i'[1-\exp(-u_i)]}\right\}_c \quad (3.3)$$

and $\ln s/s'f$ can be written

$$\ln s/s'f=N^{-1}\left\{\frac{hc}{2kT}\sum_{i=1}^{3N(n-2)}(\nu_i'-\nu_i)+\sum_{i=1}^{3N(n-2)}\ln\frac{u_i[1-\exp(-u_i')]}{u_i'[1-\exp(-u_i)]}\right\}_g+G(\sigma,\sigma')_g, \quad (3.4)$$

where $u_i\equiv hc\nu_i/kT$ and $G(\sigma,\sigma')$ is a correction for nonclassical rotation in the gas. Since $(\nu_i'-\nu_i)$ and $\ln u_i[1-\exp(-u_i')]/u_i'[1-\exp(-u_i)]$ are each zero when $\nu_i'=\nu_i=0$, we can include the six zero frequencies of translation and rotation in the gas in the sums in Eq. (3.4). The sum can now be extended to

$$\sum_{i=1}^{3nN},$$

and Eq. (3.1) for the vapor-pressure ratio becomes

$$\ln P'/P=N^{-1}\left\{\frac{hc}{2kT}\sum_{i=1}^{3nN}(\nu_i'-\nu_i)_c-(\nu_i'-\nu_i)_g+\sum_{i=1}^{3nN}\ln(u_i/u_i')_c(u_i'/u_i)_g\left[\frac{1-\exp(-u_i')}{1-\exp(-u_i)}\right]_c\times\left[\frac{1-\exp(-u_i)}{1-\exp(-u_i')}\right]_g\right\}$$
$$-G(\sigma,\sigma')_g+(RT)^{-1}(P'V'-PV)-(B_0P+\tfrac{1}{2}C_0P^2)'+(B_0P+\tfrac{1}{2}C_0P^2). \quad (3.5)$$

Equation (3.5) can be developed in terms of two kinds of frequency shifts: (1) the conventional isotopic shift, where $\Delta\nu_i=\nu_i'-\nu_i$, and $\delta\lambda_i^n=\lambda_i'^n-\lambda_i^n$, and (2) a phase-frequency shift where $\mathfrak{d}\nu_i'=\nu_{ic}'-\nu_{ig}'$, $\mathfrak{d}\nu_i=\nu_{ic}-\nu_{ig}$, and $\mathfrak{d}\lambda_i^n=\lambda_{ic}^n-\lambda_{ig}^n$. When the development is in terms of the isotopic-frequency shift, wecan utilize the various forms in which $\ln s/s'f$ and the related thermal functions have been developed.[18–24] When Δu_i is small, one finds[21] through terms in $(\Delta u_i)^2$,

$$\ln s/s'f=\sum G(u_i)[1+S(u_i)\Delta u_i/2u_iG(u_i)]\Delta u_i \quad (3.6)$$

$$\ln s/s'f=\sum_i[G(u_i)-S(u_i)]\Delta u_i+S(u_i)\delta u_i^2/2u_i, \quad (3.7)$$

where $G(u_i)=[\frac{1}{2}-u_i^{-1}+(e^{u_i}-1)^{-1}]$ and $S(u_i)=\{u_i^{-1}-u_ie^{u_i}/(e^{u_i}-1)^2\}$. In addition, when $u_i'_{\max}$ is less than 2π, there is the expansion[21] in powers of u and u'

$$\ln s/s'f=N^{-1}\sum_{i=1}^{3nN}\sum_{j=1}^{\infty}(-1)^{j+1}(B_{2j-1}\delta u_i^{2j}/2j(2j)!) \quad (u_i'_{\max}<2\pi). \quad (3.8)$$

The B's are the Bernoulli numbers ($B_1=\frac{1}{6}$, $B_3=1/30$, $B_5=1/42$, etc.). In the development in powers of δu_i^{2j}, one can use the various order sum rules[20,22] in

$$\sum^{3nN}\lambda_i'^j-\lambda_i^j.$$

Entirely analogous developments can be given in terms of $\mathfrak{d}u_i$ for $(\nu_{ic}-\nu_{ig})$ small, and for the case $u_i'_{\max}<2\pi$. We define

$$\ln\mathfrak{D}=(hc/2kT)\sum_{i=1}^{3nN}(\nu_{ic}-\nu_{ig})+\sum_{i=1}^{3nN}\ln(u_{ig}(1-e^{-u_i})_c/u_{ic}(1-e^{-u_i})_g). \quad (3.9)$$

Corresponding to Eqs. (3.6) and (3.8), there are the relationships

$$\ln\mathfrak{D}'=N^{-1}\sum_{i=1}^{3nN}G(u_i')[1+S(u_i')\Delta u_i'/2u_i'G(u_i')]\mathfrak{d}u_i' \quad (\mathfrak{d}u_i'\ll 1) \quad (3.10)$$

$$\ln\mathfrak{D}'=N^{-1}\sum_{i=1}^{3nN}\sum_{j=1}^{\infty}(-1)^{j+1}(B_{2j-1}\mathfrak{d}u_i'^{2j}/2j(2j)!) \quad (u_i'_{\max}<2\pi). \quad (3.11)$$

Equations (3.10) and (3.11) are useful when the vibrational motion of the condensed phased is expressed in terms of $\mathfrak{d}\nu_i$ or $\mathfrak{d}\lambda_i^n$ and ν_{ig} or λ_{ig}, respectively. The sum rules are not applicable directly to Eq. (3.11), since

$$\sum_{i=1}^{3nN}\mathfrak{d}\lambda_i'=\sum_{i=1}^{3nN}\mu_i'(a_{iic}-a_{iig}), \quad (3.12)$$

where $\mu_i'=1/m_i'$ and the a_{ii}'s are Cartesian force constants for the displacement of the ith atom. However, they can be applied to $\ln\mathfrak{D}'/\mathfrak{D}$.

We now consider the vapor pressure Eq. (3.1) with $\ln s/s'f$ as given by Eq. (3.8). The expansion (3.8) is not applicable to simple polyatomic gases at temperatures below 100°K. For these gases, the characteristic temperatures of the internal vibrations are greater than 1000°K and $u_{i\max}'$ is one or two orders of magnitude greater than 2π. The expansion is, nevertheless, applicable to a wide range of substances and would

[19] J. Bigeleisen, J. Chem. Phys. **21**, 1333 (1953).
[20] J. Bigeleisen, J. Chem. Phys. **23**, 2264 (1955).
[21] J. Bigeleisen, *Proceedings of the Amsterdam Symposium on Isotope Separation*, edited by J. Kistemaker, J. Bigeleisen, and A. O. C. Nier (North-Holland Publishing Company, Inc., Amsterdam, 1958), pp. 121–157.
[22] J. Bigeleisen, J. Chem. Phys. **28**, 694 (1958).
[23] J. Bigeleisen, *Proceedings of the Second United Nations International Conference on the Peaceful Uses of Atomic Energy* (United Nations, Geneva, 1958), Vol. 4, pp. 480–484.
[24] J. Bigeleisen, *Isotope Separation*, edited by H. London (George Newnes, Ltd., London, in press), Chap. 5.

describe the high-temperature asymptotic behavior of all substances in the harmonic approximation. The sum

$$\sum^{3nN}\lambda_i$$

can be written explicitly in terms of atomic masses and force constants and the vapor pressure equation becomes

$$\ln P'/P=(24N)^{-1}(\hbar/kT)^2\sum_{i=1}^{3nN}(\mu_i'-\mu_i)(a_{ii}-b_{ii})$$
$$+0(\hbar^4T^{-4})+\cdots, \quad (3.13)$$

where a_{ii} and b_{ii} are the Cartesian force constants for the ith atom in the condensed and gaseous phases, respectively. Just as in the case of gaseous exchange equilibria,[20] the term in $(\hbar/kT)^2$, which is the dominant one, leads to the rule of the geometric mean in the vapor pressure. Deviations from the rule are contributed by the higher-order terms, the corrections for gas imperfectation, and the PV/RT terms. The first-order term,

$$(1/24N)(\hbar/kT)^2\sum_{i=1}^{3nN}(\mu_i'-\mu_i)(a_{ii}-b_{ii})$$

leads to the prediction of a structural effect, since the vapor-pressure ratio depends in first approximation on the reciprocal mass of the atom multiplied by a force parameter for the particular atom. In this approximation, one is led to anticipate a difference in vapor pressure between $C^{14}O^{16}$ and $C^{12}O^{18}$, HT and D_2[14], and $N^{14}N^{15}O$ and $N^{15}N^{14}O$. *In fact, all of the theorems derived for isotopic gaseous exchange equilibria have an exact analog in the vapor-pressure ratio.* If one restricts oneself to terms of the order of $(\hbar/kT)^2$, the harmonic approximation, which has been used here, can be avoided by the use of Mayer and Band's[25] reformulation of the Wigner distribution function.

Systems with Specific Frequency Distribution

We have seen that, subject to certain restrictions, the correlation of the vapor pressures of related isotopic molecules can be carried out without knowledge of the frequency distribution function. The calculation of the absolute value of the vapor-pressure ratio of a particular isotopic pair does require a knowledge of the frequency distribution. In the thermodynamics of crystal lattices it is convenient to utilize the method of moments. We shall, therefore, transform the vapor-pressure equation, so that the method of moments becomes directly applicable to the ratio of vapor pressure of isotopes.

We divide the $3nN$ frequencies in the condensed phase into two groups. The first group of $3N(n-2)$ vibrations ν_{ic}^{g} are those vibrations which are related to the internal vibrations in the gaseous molecule and the second group of $6N$ vibrations ν_{ic}^{0} are zero translational and rotational frequencies in the gas. (It is understood that when n is equal to unity that $3N(n-2)$ is zero and $6N$ is really $3N$.) The sum $\ln\mathfrak{D}'$ can be written

$$\ln\mathfrak{D}'=N^{-1}\sum\nu_{ic}^{0\prime}\sum_{j=1}^{\infty}(-1)^{j+1}\frac{B_{2j-1}(\hbar/kT)^{2j}(\lambda_{ic}^{0\prime})^{2j}}{2j(2j!)}$$
$$+N^{-1}\sum\nu_{ig}'\left\{(hc/2kT)(\nu_{ic}^{g\prime}-\nu_{ig}')\right.$$
$$\left.+\ln\frac{u_{ig}'[1-\exp(-u_{ic}^{g\prime})]}{u_{ic}^{g\prime}[1-\exp(-u_{ig}')]}\right\}$$
$$[(\hbar\lambda_{ic}^{0\,\frac{1}{2}}/kT)_{\max}<2\pi]. \quad (3.14)$$

The lattice moments can be utilized only if the matrix form of the secular equation can be factored into two matrices, one of which has eigenvalues $\lambda_{ic}^{0\prime}$ and the other $\lambda_{ic}^{g\prime}$. This would imply no coupling of the internal motion with the lattice modes. If the secular equation can be factored in this way, then

$$(4\pi^2N)^{-1}\sum\nu_{ic}^{0\prime}(\lambda_{ic}^{0\prime})^j=(3,6)\mu_{2j}'$$
$$=(3,6)I(2j)(\nu_m')^{2j}, \quad (3.15)$$

where μ_{2j}' is the $2j$th moment of the lattice vibrations, ν_m' is the maximum frequency of the spectrum of lattice vibrations and the factor 3 is used for monatomic lattices. We define

$$\ln\mathfrak{D}_g'=N^{-1}\sum\nu_{ig}'\left\{(hc/2kT)(\nu_{ic}^{g\prime}-\nu_{ig}')\right.$$
$$\left.+\ln\frac{u_{ig}'[1-\exp(-u_{ic}^{g\prime})]}{u_{ic}^{g\prime}[1-\exp(-u_{ig}')]}\right\}. \quad (3.16)$$

The vapor-pressure equation then becomes

$$\ln P'/P=\sum_{j=1}^{\infty}(-1)^{j+1}\frac{B_{2j-1}(h/kT)^{2j}(3,6)(\mu_{2j}'-\mu_{2j})}{2j(2j)!}$$
$$+\ln(\mathfrak{D}_g'/\mathfrak{D}_g)+(1/RT)(P'V'-PV)-(B_0P+\tfrac{1}{2}C_0P^2)'$$
$$+(B_0P+\tfrac{1}{2}C_0P^2)-G(\sigma,\sigma')_g. \quad (3.17)$$

We now divide the $3N(n-2)$ vibrations summed in $\ln\mathfrak{D}_g'$ into two groups. The first have u_{ig}' and $u_{ic}^{g\prime}$ less than 2π. Their contribution to $\ln\mathfrak{D}_g'$ is given individually by an expansion in powers of $\delta u_i'^{2j}$ as set forth in Eq. (3.11). For those vibrations with u_i' greater than 2π we proceed as follows. When $u_i'>2\pi$ the excitation of the higher vibrational levels is negligible and the ratio $[1-\exp(-u_{ic}^{g\prime}]/[1-\exp(-u_{ig}')]$ is unity to a very high approximation. We introduce the plausible assumption, which is sufficiently accurate for the present purposes, that

$$u_{ig}'/u_{ic}^{g\prime}\cong u_{ig}/u_{ic}^{g}.$$

[25] J. E. Mayer and W. Band, J. Chem. Phys. **15**, 141 (1947).

Under these assumptions $\ln\mathfrak{D}_g'/\mathfrak{D}_g$ can be positive, negative, or zero and the present development is applicable to systems which show the cross-over phenomenon. We can now write

$$N\ln\mathfrak{D}_g'/\mathfrak{D}_g=\sum_{\nu_a}\sum_{j=1}^{\infty}(-1)^{j+1}\frac{B_{2j-1}(\delta u_i'^{2j}-\delta u_i^{2j})}{2j(2j)!}$$
$$+\tfrac{1}{2}\sum_{\nu_b}(\delta u_i'-\delta u_i)\qquad[u_{ia}'<2\pi,\ u_{ib}>2\pi]. \tag{3.18}$$

We now develop $\delta u_i'$ and δu_i in terms of a characteristic parameter of the molecule, to be defined presently;

$$\delta u_i/2=\tfrac{1}{24}(u_{ic}^2-u_{ig}^2)/\bar{u}/6, \tag{3.19}$$

where $2\bar{u}=u_{ic}+u_{ig}$. Let $\bar{u}/6$ equal y. We adopt a procedure developed by Bigeleisen and Goldstein[26] and expand y in a Taylor series about a dimensionless quantity y_0;

$$(y^2/y_0^2)^{\frac{1}{2}}=x^{\frac{1}{2}}=\tfrac{1}{2}+\tfrac{1}{2}x+\sum_{n=2}^{\infty}(-1)^{n+1}\frac{(2n-2)!(x-1)^n}{2^{2n-1}(n-1)!n!} \tag{3.20}$$
$$[|x-1|\leqq 1].$$

We limit the expansion to the first two terms, $\frac{1}{2}+\frac{1}{2}x+\cdots$, for the present and

$$y=\tfrac{1}{2}y_0[1+(y^2/y_0^2)+\cdots]. \tag{3.21}$$

We choose $y_0=2$ and

$$y=1+\tfrac{1}{4}y^2+\cdots. \tag{3.22}$$

The convergence condition of the series (3.20) and the *a fortiori* choice of the coefficient 1/24 in (3.19) restricts the application to $2\pi\leqq\bar{u}\leqq 12(2)^{\frac{1}{2}}$. The lower bound is set by Eq. (3.18). Note that Eq. (3.22) is exact when $\bar{u}$ equals 12. The approximation is in error by 20% when $\bar{u}$ is close to the lower bound of 2π. However, this manifests itself by higher-order terms in y, with which we are not presently concerned. With this expansion, one obtains

$$\delta u_i/2\cong\tfrac{1}{24}(u_{ic}^2-u_{ig}^2)+\cdots[2\pi\leqq u_i\leqq 12(2)^{\frac{1}{2}}] \tag{3.23}$$

up to terms in u^4. Thus

$$\ln\mathfrak{D}_g'/\mathfrak{D}_g=(24N)^{-1}\sum\nu_{ig}(\delta u_i'^2-\delta u_i^2)+\cdots 0(u_i'^4,u_i^4)$$
$$[u_i'<12(2)^{\frac{1}{2}}] \tag{3.24}$$

and the vapor-pressure equation becomes

$$\ln P'/P=(24N)^{-1}\sum^{3nN}(\delta u_i'^2-\delta u_i^2)+0(u_i'^4,u_i^4)$$
$$+(RT)^{-1}(P'V'-PV)-(B_0P+\tfrac{1}{2}C_0P^2)'$$
$$+(B_0P+\tfrac{1}{2}C_0P^2)-G(\sigma,\sigma')_g$$
$$[u_i'\leqq 12(2)^{\frac{1}{2}}], \tag{3.25}$$

which is the same as Eq. (3.13), but now valid over three times the range of u_i. With the present range of u_i, the conclusions from the sum rule (i.e., rule of the mean, correlation of double labeled molecules, etc.) become applicable to the isotope effect on vapor pressures and other thermodynamic properties involving phase equilibria for all substances above room temperature. The results are also directly applicable to most of the permanent gases.

We now call attention to those substances for which $\ln\mathfrak{D}_g'/\mathfrak{D}_g$ is zero. Cases of this type may be found with molecules with no dipole moment and with very small bond moments. For such substances we obtain Eq. (3.13) with the restriction that $(u_{ic}')_{\max}<2\pi$.

For a Debye spectrum, the moments are

$$\mu_{2j}=3(k\theta_D/h)^{2j}/(2j+3). \tag{3.26}$$

If $(P'V'-PV)$ is negligible with respect to RT, Eq. (3.17) reduces to the Stern-Lindemann formula for a monatomic solid in equilibrium with an ideal gas.

In the Debye model, the lattice consists of point masses and rotations are not accounted for. Due account of these modes must be taken, and one obtains the following modification of the simpler Stern-Lindemann formula

$$\ln P'/P=\sum_{j=1}^{\infty}\frac{(-1)^{j+1}B_{2j-1}}{(2j)(2j)!}$$
$$\times\{[9/(2j+3)][(\theta'/T)^{2j}-(\theta/T)^{2j}]$$
$$+3(h/kT)^{2j}(\mu_{2j}'-\mu_{2j})_r\}$$
$$+\ln(\mathfrak{D}_g'/\mathfrak{D}_g)+(RT)^{-1}(P'V'-PV)-(B_0P+\tfrac{1}{2}C_0P^2)'$$
$$+(B_0P+\tfrac{1}{2}C_0P^2)$$
$$-G(\sigma,\sigma')_g[\theta'/T,\ (h\nu_m'/kT)_r<2\pi], \tag{3.27}$$

where $(\mu_{2j}')_r$ is the $2j$th moment of the rotational oscillations in the lattice. For an Einstein lattice, the factor $(9/2j+3)$ in Eq. (3.27) is replaced by 3. There is in Eq. (3.27) the implication that the secular equation for the lattice vibrations can be factored into one corresponding to hindered translation and one corresponding to hindered rotation.

IV. MOLAL VOLUME EFFECTS

We have shown in Sec. II, Eqs. (2.10), (2.12), and (2.16), that if one wishes to compare the vapor-pressure ratio at the same molal volume of the condensed phase, there is a correction

$$(1/RT)\int_V^{V'}PdV$$

to the partition function. We shall now evaluate this integral for the case where β', the compressibility, is independent of pressure. The equation of state is

$$P=P'+(1/\beta')\ln(V'/V), \tag{4.1}$$

where P and P' are the pressures on the system when the molal volumes are V and V', respectively. After

[26] J. Bigeleisen and P. Goldstein (unpublished).

integration and expansion of $\ln(V'/V)$ through terms in $(V'-V)^2/V^2$, one obtains

$$-(RT)^{-1}\int_V^{V'} PdV$$

$$\cong -(RT)^{-1}\left[P'(V'-V)+\frac{(V'-V)^2}{2\beta' V}\right]. \quad (4.2)$$

The vapor-pressure equation at constant molal volume is then

$$\ln P'/P=\ln s/s'(f_c)_V-\ln s/s'f$$
$$+(RT)^{-1}(P'-P)V-[(V'-V)^2/2\beta' VRT]$$
$$-(B_0P+\tfrac{1}{2}C_0P^2)'+(B_0P+\tfrac{1}{2}C_0P^2). \quad (4.3)$$

We shall now proceed to develop a relationship between $(V'-V)^2/2\beta' VRT$ and $\ln P'/P$. From the calculus of partial differentiation

$$(\partial V/\partial m)_{P,T}=\beta V(\partial P/\partial m)_{T,V}, \quad (4.4)$$

where m is the mass of the atom in the molecule which is varied by isotopic substitution. We introduce the variable E_c^0, defined as

$$E_c^0=\phi(V)+kT\sum_j^{6N} x_j f'(x_j), \quad (4.5)$$

where $x_j=hc\nu_{jc}^0/kT$ and $f'(x_j)$ is the partial derivative with respect to the argument x_j of some function of x_j. We replace $(\partial P/\partial m)_{T,V}$ by $(\partial P/\partial E_c^0)_{T,V}(\partial E_c^0/\partial m)_{T,V}$ and Eq. (4.4) is

$$(\partial V/\partial m)_{P,T}=\beta V(\partial P/\partial E_c^0)_{T,V}(\partial E_c^0/\partial m)_{T,V}. \quad (4.6)$$

The evaluation of $(\partial P/\partial E_c^0)_{T,V}$ follows by an extension of London's method[27] to molecular lattices and avoids the assumption of harmonic oscillators. The Helmholtz free energy of the condensed phase is taken as

$$F=\phi(V)+kT\sum f(x_j)+kT\sum f(y_j), \quad (4.7)$$

where $y_j=hc\nu_{ic}^g/kT$ and $f(y_j)$ is summed over $3(n-2)N$ oscillators. The pressure and total energy of the system are, respectively,

$$P=-(\partial F/\partial V)_T=-\phi'(V)-kT\sum(\partial x_j/\partial V)_T f'(x_j)$$
$$-kT\sum(\partial y_j/\partial V)_T f'(y_j) \quad (4.8)$$

$$E=-T^2[\partial(F/T)/\partial T]_V=E_c^0+kT\sum y_j f'(y_j). \quad (4.9)$$

We now assume

$$(\partial x_j/\partial V)_T=-\gamma(x_j/V) \quad (4.10)$$

and

$$(\partial y_j/\partial V)_T=0. \quad (4.11)$$

These assumptions are analogous to the Grüneisen equation of state for monatomic lattices. The assumption $(\partial y_j/\partial V)_T=0$ is supported by the experimental finding that there are but small differences between the internal frequencies of a molecule in the gas and a condensed phase. The molal volume of a gas is about 10^3 times that of the condensed phase. We thus obtain

$$(\partial P/\partial E_c^0)_{T,V}=\gamma/V \quad (4.12)$$

and

$$(\partial V/\partial m)_{T,P}=\beta\gamma(\partial E_c/\partial m)_{T,V}. \quad (4.13)$$

The integration of Eq. (4.13) with respect to m is carried out under the assumption that β and γ are constant to give

$$V'-V=\beta\gamma(E_c'^0-E_c^0)_{T,V}. \quad (4.14)$$

The energy term, $E_c'^0-E_c^0$, can be obtained to first order by differentiating Eq. (3.17) with respect to the temperature and subsequent multiplication by RT^2. We note that $\ln(Q'/Q)_{el}$ is independent of temperature. Then

$$E_c'^0-E_c^0=RT^2(\partial/\partial T)[\ln(P/P')_{V,V'}$$
$$+\ln\mathfrak{T}_g'/\mathfrak{T}_g+b(T,P)_{V,V'}], \quad (4.15)$$

where

$$b(T,p)=(RT)^{-1}(P'V'-PV)-(B_0P+\tfrac{1}{2}C_0P^2)'$$
$$+(B_0P+\tfrac{1}{2}C_0P^2)-G(\sigma,\sigma')_g. \quad (4.16)$$

If $\ln P'/P$ can be expressed in the form AT^{-n}, then

$$RT^2\frac{\partial \ln P/P'}{\partial T}=nRT\ln P'/P.$$

Since $b(T,p)$ appears as a correction to $\ln P'/P$ in Eq. (4.15), we shall take the temperature derivative of b with the assumption that B_0 and C_0 are temperature independent. The change of pressure with the temperature for the saturated vapor can be approximated by the Clausius-Clapeyron equation

$$dP/dT\cong PL/RT^2,$$

where L is the molar heat of sublimation or vaporization. With these approximations

$$RT^2[\partial b(T,P)/\partial T]_{V,V'}$$
$$\simeq -RT^2[\partial G(\sigma,\sigma')/\partial T]$$
$$+P'[(L'V'/RT)-V'-B_0'L'-C_0'P'L']$$
$$-P[(LV/RT)-V-B_0L-C_0PL)] \quad (4.17)$$

$$\simeq -RT^2\frac{\partial G(\sigma,\sigma')}{\partial T}+P'L'[(V'/RT)-B_0']$$
$$-PL[(V/RT)-B_0]. \quad (4.18)$$

We neglect differences between L and L', V and V', and B_0 and B_0', respectively, in Eq. (4.18) and write

$$RT^2[\partial b(T,P)/\partial T]_{V,V'}\simeq -RT^2[\partial G(\sigma,\sigma')/\partial T]$$
$$+L[(V/RT)-B_0](P'-P). \quad (4.19)$$

[27] H. London, Z. physik. Chem., Neue Folge **16**, Simon Gedenkheft, 302 (1958).

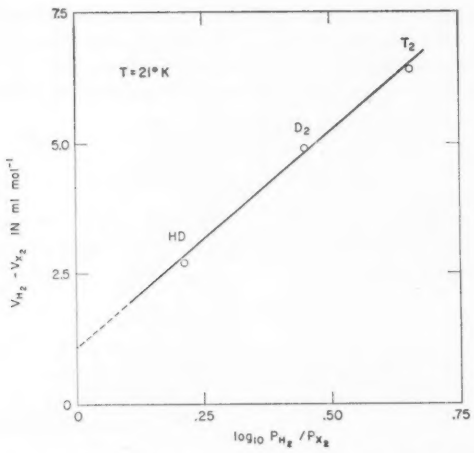

FIG. 1. Correlation of molal volumes of the liquid hydrogens with vapor pressures according to Eq. (4.21).

When $P'-P$ is small, the quantity

$$L[(V/RT)-B_0](P'-P)$$

can be written

$$L[(V/RT)-B_0](P'-P)=LP[(V/RT)-B_0]\ln P'/P, \qquad \Delta P/P \ll 1. \quad (4.20)$$

Finally

$$V'-V \cong n\beta\gamma RT\ln P'/P+\beta\gamma L[(V/RT)-B_0](P'-P) + RT^2\frac{\partial \ln \mathfrak{D}_g'/\mathfrak{D}_g}{\partial T}-RT^2\frac{\partial G(\sigma,\sigma')}{\partial T} \quad (4.21)$$

and

$$V'-V \cong \beta\gamma \ln(P'/P)\left[nRT+LP\left(\frac{V}{RT}-B_0\right)\right] + RT^2\frac{\partial \ln \mathfrak{D}_g'/\mathfrak{D}_g}{\partial T}-RT^2\frac{\partial G(\sigma,\sigma')}{\partial T} \quad (4.22)$$

when $\Delta P/P$ is small.

Before we compute $(V'-V)^2/2\beta' VRT$ from either Eq. (4.21) or (4.22), we shall compare these equations with experiment. In most cases we can neglect $RT^2(\partial/\partial T)(\ln \mathfrak{D}_g'/\mathfrak{D}_g)-G(\sigma,\sigma')$. The term $\ln \mathfrak{D}_g'/\mathfrak{D}_g$ follows a T^{-1} dependence, whereas $\ln P/P'$ follows a T^{-n} dependence, where n is between 1 and 2 and closer to the latter. This term will be of importance for systems which show the cross-over phenomenon. In this case the assumption (4.11), $(\partial y_j/\partial V)_T=0$, will not be valid. We should, therefore, not expect Eq. (4.21) to hold near the cross-over temperature. Here $G(\sigma,\sigma')$ either follows a T^{-1} dependence or must be considered in detail. In most cases, it can also be neglected. The difference in molal volumes is a linear function of the logarithm of the vapor-pressure ratio. If there is an intercept in a plot of $(V'-V)$ against $\ln P'/P$, as in Eq. (4.21), it is to a good approximation isotope invariant. For, when $\Delta P/P$ is of the order of unity, the intercept is approximately $\beta\gamma L[(V/RT)-B_0]P'$. The difference in molal volumes is thus predicted to behave in a fashion similar to the logarithm of the vapor-pressure ratio. Such behavior has been noted previously by de Boer[8] by his correlation of each of these quantities with Λ^*. In view of Sec. III we no longer expect $V'-V$ to depend on the difference in molecular weight, as given by de Boer's theory. We expect a structure effect on the molal volume just as the vapor pressure ratio.

The experimental data on molal volumes of isotopes is scant. London[27] has used Eq. (4.14) to compute the difference in molal volumes of Li^6 and Li^7 metal and Li^6F and Li^7F. His calculations are in reasonable agreement with experiment. A correlation of the difference in molal volume with the vapor-pressure ratio is at present restricted to the data on the isotopes of hydrogen and helium. For He^3-He^4 and $H_2-HD-D_2-T_2$ second-order terms in $V'-V$ cannot be neglected. Nevertheless, Eq. (4.21) does predict the large differences in molal volumes of these systems within a factor of 1.5, with a reasonable choice of γ. Equation (4.21) gives an excellent correlation of the difference in molal volumes of the isotopic liquid hydrogens. In Fig. 1 we plot $V_{H_2}-V_{X_2}$ vs $\log P_{H_2}/P_{X_2}$ at 21°K. The points almost fall on a straight line. From the slope we get $\beta\gamma=1.1\times10^{-3}$ while the intercept gives 1.2×10^{-3}. If we use the compressibility of liquid D_2 as the average β, we obtain 1.1 and 1.2, respectively, for γ. This value may be compared with a value of γ calculated from the relationship $\gamma=\alpha V/\beta C_v$, where α is the compressibility. Evaluation of γ for liquid D_2 gives 2.2. The discrepancy arises from the fact that the assumption that $(\partial x_j/\partial V)_T$ equals $-\gamma x_j/V$ does not hold. In the next approximation one might introduce two γ's, one associated with the translational modes and one associated with rotation. Further, the second-order terms, neglected in the present treatment, will make a significant correction to Eq. (4.21) for such large differences in molal volumes.

To obtain the effect of the molal volume on the vapor-pressure ratio, we make the further approximation

$$V'-V \simeq n\beta\gamma RT\ln P'/P. \quad (4.23)$$

We introduce the thermodynamic relationship

$$C_p-C_v=\alpha^2VT/\beta \quad (4.24)$$

and obtain

$$(V'-V)^2/2\beta' VRT \simeq [n^2R(C_p-C_v)/2C_v^2] \times(\ln P'/P)^2. \quad (4.25)$$

Since the coefficient of $(\ln P'/P)^2$ in (4.25) is less than unity, we find that when $\ln P'/P$ is small, the correction to the vapor-pressure ratio for the difference in molal volume is a second-order effect. An evaluation of Eq. (4.25) for the neon isotopes, Ne^{20} and Ne^{22}, gives

$(V'-V)^2/2\beta' VRT$ of the order of 5×10^{-4} between 18–24°K. In this temperature range the volume effect is thus $7\times10^{-3}\ln P'/P$.

V. TRANSITION TEMPERATURES

The vapor pressure of a condensed phase with small quantum corrections can be written, as a consequence of Eq. (3.13), in the form

$$\ln p=\alpha(T)+B\sum\nu_i^2/T^2. \tag{5.1}$$

The functional dependence of $\alpha(T)$ on the temperature depends on the phase but is independent of isotopic substitution. The coefficient B is a natural constant. The equilibrium condition for the coexistence of two phases, $\ln p_1=\ln p_2$, gives

$$T_{tr}^2=B\frac{\sum\nu_i^2(1)-\nu_i^2(2)}{\alpha(2)_{Tr}-\alpha(1)_{Tr}}. \tag{5.2}$$

It is immediately apparent that a rule of the mean in T_r^2 can be obtained, if $\alpha(2)-\alpha(1)$ does not change when the transition temperature changes on isotopic substitution. Similarly, there will be a structure effect on the transition temperature. The order of magnitude of $\alpha(2)-\alpha(1)$, at the transition temperature, T, is L/RT, where L is the latent heat associated with the phase change. Therefore, as long as the difference in transition temperature effected by substitution of one isotope is small compared with the absolute temperature, $\alpha(2)-\alpha(1)$ can be taken as a constant. It follows then directly that

$$T_{tr}^2MY_2+T_{tr}^2MY_2'=2T_{tr}^2MYY', \tag{5.3}$$

when the summation in (5.2) runs over all degrees of freedom.

If the transition temperatures of the molecules MY_n and $MY_{n-1}Y'$ differ by an amount small compared to T, then one obtains from Eq. (5.3) the result that the transition temperature will vary in a linear manner with successive isotopic substitution. This result will also be obtained if the vapor-pressure equation is of the form given by Eq. (3.17). If the dominant contribution to the vapor-pressure ratio is $\ln\mathfrak{D}_0'/\mathfrak{D}_0$ and $\mu_{i0}>2\pi$, then one will again find that the transition temperature will vary in a linear manner in the homologous series MY_n, $MY_{n-1}Y'\cdots MY_n'$. The latter result is a consequence of the approximate sum rule[20] in ν_i. Again one requires the assumption of $\Delta T_{tr}\ll T_{tr}$. Under these circumstances the heavy isotope will have the lower triple point. It is apparent, therefore, that a linear rule in the transition temperature will be found for any system in which $\Delta T_{tr}\ll T_{tr}$. This is the behavior found by Armstrong, Brickwedde, and Scott[28] for the triple points of the deuteromethanes. We note that Clusius and Bühler[29] found the triple-point pressure of $C^{13}H_4$ to be 0.04 mm lower than that of $C^{12}H_4$, whereas the triple-point pressure of $C^{12}H_3D$ is 3.2 mm lower than that of $C^{12}H_4$. The results are in agreement with the present treatment of structural effects.

VI. HEATS OF VAPORIZATION

The difference in heats of vaporization of isotopic molecules can serve as a useful check on the interpretation of the vapor-pressure ratio. The latter is usually measured over a limited temperature range and the experimental data may be fitted equally well by various temperature functions. The difference in heats of vaporization is given by

$$\begin{aligned}(L'-L)/RT=&[(\partial\ln\bar{Q}/\bar{Q}')/\partial\ln T]_V\\&-[(H_i-H_i')_0/RT]+[(PV-P'V')/RT]\\&+(H_r-H_i)'/RT-(H_r-H_i)/RT,\end{aligned} \tag{6.1}$$

where H_i-H_i' is the enthalpy difference of the ideal gases and $(H_r-H_i)'$ and (H_r-H_i) are the respective corrections to the enthalpy of the gas for nonideality. Here H_i-H_i' depends solely on the molecular vibrations.[19] We now consider the case where the vapor-pressure ratio is given by Eq (3.25). The difference in heats of vaporization is then

$$\begin{aligned}(L'-L)/RT=&-2\ln P'/P+(P'V'-PV)/RT\\&-(F_r-F_i)'/RT+(F_r-F_i)/RT\\&+(S_r-S_i)'/R-(S_r-S_i)/R.\end{aligned} \tag{6.2}$$

Equation (6.2) has two significant results: (1) the difference in heats of vaporization behaves similar to the logarithm of the vapor-pressure ratio and (2) the magnitude of the difference in heats of vaporization serves as a sensitive criterion of the temperature dependence of the vapor-pressure ratio. A test of these relationships has been given recently for the isotopic NO molecules.[30]

---

[28] G. T. Armstrong, F. G. Brickwedde, and R. B. Scott, J. Research Natl. Bur. Standards **55**, 1 (1955).

[29] K. Clusius and H. Bühler, Z. Naturforsch. **9a**, 775 (1954).

[30] J. Bigeleisen, J. Chem. Phys. **33**, 1775 (1960).

Competitive Reaction Rates of Hydrogen Atoms with HCl and Cl_2. Entropy Considerations of the HCl_2 Transition State* †

FRITZ S. KLEIN AND MAX WOLFSBERG‡

Isotope Department, Weizmann Institute of Science, Rehovoth, Israel, and

Chemistry Department, Brookhaven National Laboratory, Upton, Long Island, New York

(Received August 5, 1960)

The relative rates of the reactions

$$H+HCl \xrightarrow{k_3} H_2+Cl$$

and

$$H+Cl_2 \xrightarrow{k_6} HCl+Cl,$$

were determined in the temperature range of 0° to 62°C and found to be given by

$$k_3/k_6 = (0.143\pm0.033)\ \exp-(1540\pm130/RT).$$

The temperature-independent factor in the above expression is interpreted in terms of the structure and the vibrational frequencies of the HCl_2 transition state. The doubly degenerate bending frequency of this transition state is found to have a value of about 105 cm^{-1}.

INTRODUCTION

In connection with recent measurements[1,2] of the reaction of Cl atoms with isotopically substituted hydrogen molecules, there arose the problem of the relative rates of the fast reaction step $H+Cl_2$ compared to the back reaction H+HCl. It was shown in a preliminary experiment,[1] that this ratio is sufficiently large so that the back reaction does not affect the measured H_2/HD isotope effect to any appreciable extent. The present work was undertaken to obtain a more precise value for this ratio of competitive rates.

Pre-exponential factors in the Arrhenius-type expression for rate constants may be used to yield information about the structure and the vibrational frequencies of the transition state.[3,4] Since considerable information exists now [1-3] about the H_2Cl transition state, the present study can be used as a starting point for the exploration of the HCl_2 transition state.

EXPERIMENTAL PRINCIPLE

The rate of appearance of isotopically substituted hydrogen in the photochemically induced reaction of protium with chlorine in the presence of isotopically labeled hydrogen chloride constitutes a measure for the reaction type $H+HCl \rightarrow H_2+Cl$. The total decrease in hydrogen may be used to measure the fast $H+Cl_2 \rightarrow HCl+Cl$ reaction step. The above statement embodies the basic principle of the present experiment. Further elaborations will now be given.

Tank hydrogen was made to react with a mixture of dry chlorine and tritium-labeled hydrogen chloride. The following reaction steps are to be considered:

$$H_2+Cl \rightarrow HCl+H \quad (1)$$

$$HT+Cl \rightarrow TCl+H \quad (2a)$$

$$HT+Cl \rightarrow HCl+T \quad (2b)$$

$$HCl+H \rightarrow H_2+Cl \quad (3)$$

$$TCl+H \rightarrow HT+Cl \quad (4)$$

$$HCl+T \rightarrow HT+Cl \quad (5)$$

$$Cl_2+H \rightarrow HCl+Cl \quad (6)$$

$$Cl_2+T \rightarrow TCl+Cl \quad (7)$$

$$HT+H \rightarrow H_2+T \quad (8)$$

$$H_2+T \rightarrow HT+H \quad (9)$$

$$TCl+H \rightarrow HCl+T \quad (10)$$

$$HCl+T \rightarrow TCl+H. \quad (11)$$

The chain-initiating step and the chain-terminating steps have been omitted, as well as wall reactions in

* The experimental aspects of this paper are the work of F.S.K., the theoretical aspects the joint endeavors of both authors.

† Research at Brookhaven National Laboratory carried out under the auspices of the U. S. Atomic Energy Commission.

‡ Most of this work was carried out while M.W. was a visitor at the Weizmann Institute. He is very grateful to the Institute for its hospitality.

[1] J. Bigeleisen, F. Klein, R. E. Weston, and M. Wolfsberg, J. Chem. Phys. **30**, 1340 (1959).

[2] W. M. Jones, J. Chem. Phys. **19**, 78 (1951).

[3] K. S. Pitzer, J. Am. Chem. Soc. **79**, 1804 (1957).

[4] D. R. Herschbach, H. S. Johnston, K. S. Pitzer, and R. E. Powell, J. Chem. Phys. **25**, 736 (1956).

general.[5] Also neglected are molecule-molecule reactions, under the given experimental temperature conditions[6] and reactions which involve two tritiums at the trace tritium concentrations of the present experiment.

The time rate of change of r, the ratio of the HT concentration to the H_2 concentration, is given by

$$dr/dt=[1/(H_2)]\cdot[d(HT)/dt]-[r/(H_2)]\cdot[d(H_2)/dt]. \quad (12a)$$

Now

$$d(HT)/dt=k_5(HCl)(T)+k_9(H_2)(T)+k_4(TCl)(H)-(k_{2a}+k_{2b})(HT)(Cl)-k_8(HT)(H), \quad (12b)$$

and

$$-(d(H_2)/dt=k_1(H_2)(Cl)+k_9(H_2)(T)-k_3(HCl)(H)-k_8(HT)(H). \quad (12c)$$

The following expressions are obtained for the steady-state concentrations of H and T,

$$(H)=\frac{k_1(H_2)(Cl)+k_{2a}(HT)(Cl)+k_9(H_2)(T)+k_{11}(HCl)(T)}{k_3(HCl)+k_4(TCl)+k_6(Cl_2)+k_8(HT)+k_{10}(TCl)}=\frac{k_1(H_2)(Cl)}{k_6(Cl_2)} \quad (12d)$$

and

$$(T)=\frac{k_{2b}(HT)(Cl)+k_8(HT)(H)+k_{10}(TCl)(H)}{k_5(HCl)+k_7(Cl_2)+k_9(H_2)+k_{11}(HCl)}=\frac{k_{2b}(HT)(Cl)+k_{10}k_1(H_2)(TCl)(Cl)/k_6(Cl_2)}{k_7(Cl_2)}. \quad (12e)$$

In the simplification of Eqs. (12d) and (12e), use has been made of the knowledge of the experimental conditions, especially of the fact that tritium is present only in tracer concentrations and that $(HT)\ll(TCl)$. Use has also been made of a knowledge of some of the rate constants and of isotope effects on these (e.g., k_9, $k_8\ll k_1$[7]). Moreover, k_3/k_6 has been taken to be self-consistently of the order of 10^{-2}. Since $(HT)\ll(TCl)$ and k_{10}, $k_{11}\ll k_7$,[8] (T) is so small that the first two terms on the right-hand side of Eq. (12b) make a negligible contribution compared to the third term. The expressions for (H) and (T) are substituted into Eqs. (12b) and (12c) and the resulting expressions for $d(HT)/dt$ and $d(H_2)/dt$ are themselves again simplified in the same manner as Eqs. (12d) and (12e). One then obtains

$$d(HT)/dt=k_4k_1(H_2)(TCl)(Cl)/k_6(Cl_2)-(k_{2a}+k_{2b})(HT)(Cl) \quad (12f)$$

$$-d(H_2)/dt=k_1(H_2)(Cl). \quad (12g)$$

The substitution of Eqs. (12f) and (12g) into Eq. (12a) gives[9]

$$dr/k_1(Cl)dt=r(1-R^{-1})+(k_4/k_6)[(TCl^0)/(Cl_2)]$$

or

$$dr/dg=-g^{-1}\{r(1-R^{-1})+(k_4/k_6)[(TCl^0)/(Cl_2)]\}, \quad (13)$$

where g is the fraction of hydrogen which finally remains unreacted, $R=k_1/(k_{2a}+k_{2b})$ and the superscript 0 designates initial concentration. Use has been made of the fact that the TCl concentration changes little during the course of the experiment.

Equation (13) is a linear differential equation of the first order which can be easily solved by introducing an

[5] In the course of the experiments the inner surface of the reaction vessel became covered by a thin film of mercurous chloride. No difference in results, within experimental error, was found between a fresh Pyrex surface, a surface coated with HgCl and the same after flaming from the outside.

[6] M. Steiner and E. K. Rideal, Proc. Roy. Soc. (London) **A173**, 503 (1939).

[7] K. H. Geib and P. Harteck, Z physik. Chem. Bodenstein Festband, 849 (1931); P. G. Ashmore and J. Chanmugan, Trans. Faraday Soc. **49**, 254 (1953).

[8] M. Steiner and E. K. Rideal, Proc. Roy. Soc. (London) **A173**, 503 (1939), P. A. Leighton and P. C. Cross, J. Chem. Phys. **6**, 345 (1938), and S. Glasstone, K. J. Laidler, and H. Eyring, *The Theory of Rate Processes* (McGraw-Hill Book Company, Inc., New York, 1941), pp. 226–229. The high temperature result $k_5\gg k_{11}$ (with D instead of T) has been interpreted by Steiner and Rideal in terms of a very low transmission coefficient for reaction type 11 compared to reaction 5 and consequently reaction 7. The activation energies for reactions 10 and 11 are expected to be larger than that for reaction 7.

[9] Where possible, calculations were carried out without the various simplifications and it was determined that the error made in the determination of the ratio k_3/k_6 would be less than the order of 1%.

TABLE I. Experimental data.
(For all experiments $\rho_0 = 1.185 \times 10^6$.)

Temperature °C	p	g	HCl^0/H_2^0	Cl_2^0/H_2^0	$k_3/k_6 \times 10^6$
0.2	7.434	0.7755	1.402	3.229	8.14
	11.39	0.7081	1.358	2.767	7.85
	39.00	0.4261	1.370	2.873	8.51
	16.62	0.6680	1.992	3.906	9.17
25.2	18.24	0.7522	2.846	4.141	9.40
	11.81	0.7989	1.138	2.764	13.13
	36.84	0.5148	2.028	4.530	10.60
	12.21	0.7729	1.658	3.683	10.75
	33.02	0.5261	1.656	3.684	9.74
	58.07	0.4080	1.510	3.400	10.94
62.2	199.9	0.1884	1.192	3.276	14.17
	139.5	0.3144	1.806	3.929	14.59
	146.8	0.2982	1.294	2.830	13.79
25.2	0.5	0.9970	1.226	3.015	...

integrating factor.[10] We find then

$$k_3/k_6 = (r/s) \frac{g^{[(1-(1/R)]}}{\frac{(HCl^0)}{(H_2^0)} E \int_g^1 dg \Big/ \left[g^{1/R} \left(\frac{(Cl_2^0)}{(H_2^0)} - 1 + g \right) \right]}. \quad (14)$$

Here, we have immediately written the expression for the ratio of interest by inserting the factor E defined as k_4/k_3; s is the initial ratio of TCl concentration to HCl concentration. The hydrogen specific activity ρ is found directly. The initial hydrogen chloride is converted to hydrogen and the specific activity of this hydrogen is designated as ρ_0. Then $r/s = 2\rho/\rho_0$. The integral in Eq. (14) is evaluated numerically. We can derive E in the following way. We know[2] the ratio of rates of the reactions (1) and (2a) which are the inverse of reactions (3) and (4), respectively. This knowledge of k_1/k_{2a} involves the previously discussed[1] equality of k_{2a} and k_{2b}. One finds then

$$E = k_4/k_3 = f_{HT}/f_{TCl}(2R)^{-1}; \quad (15)$$

f is the deviation of the ratio of the relevant isotopic partition functions from the classical ratio, as defined by Bigeleisen and Mayer.[11]

EXPERIMENTAL PROCEDURE

The experimental apparatus was essentially the same as described in the work cited in footnote 1 except that an additional storage vessel for tritium-labeled hydrogen chloride was attached to the line next to the chlorine vessel. The experiment was carried out in a similar manner as described previously.[1] Measured quantities of dry chlorine gas followed by hydrogen chloride were frozen into the reaction vessel and a measured volume of pure tank hydrogen was then added. The reaction was run and the residual hydrogen was measured as before. A hydrogen sample was taken for radioassay. The tritium specific activity ρ was measured in a conventional Geiger gas counter. The initial specific activity $\rho_0/2$ of hydrogen chloride was measured by the same method after converson of the hydrogen chloride to pure hydrogen gas (specific activity ρ_0) on zinc amalgam and suitable dilution with tank hydrogen. The tritium-labeled hydrogen chloride was prepared by the distillation of tritiated water onto phosphorus pentachloride. The resulting hydrogen chloride was carefully dried by passage through an efficient multiple freeze-out trap cooled in a dry ice-acetone mixture.

EXPERIMENTAL RESULTS

The experimental results, calculated according to Eq. (14), are given in Table I. The last experiment in Table I is a dark run to check the efficiency of the separation of the hydrogen from the reaction mixture. Table II gives the relevant values of R taken from Jones[2] and the values of E^{-1} calculated as described above. By least-squares method we determined the constants of the Arrhenius-type equation for k_3/k_6 and found

$$k_3/k_6 = 0.143(\pm 0.033) \exp[-(1540 \pm 130)/RT]. \quad (16)$$

These results again prove the correctness of the assumption made in the work cited in footnote 1, that the back reaction (3), (H+HCl), to reaction (1), (H_2+Cl), does not significantly affect the isotope effect considerations in that work. The above results may be compared with the value indirectly deduced by Morris and Pease,[12]

$$k_3/k_6 = 0.1 \exp(-|>1400|/RT).$$

In a preliminary set of experiments by the method outlined in the work cited in footnote 1, a mixture of equal parts of 99.6% deuterium gas and tank hydrogen was reacted with chlorine at room temperature. The remaining unreacted hydrogen was analyzed on a CEC Model 21-401 mass spectrometer for the formation of HD in the sample. The accuracy was impaired by equilibration of D_2 with H_2 in the mass spectrometer.

TABLE II. Values of $E^{-1} = k_3/k_4$ and of R.

Temperature °C	R	E^{-1}
0.2	3.73	8.19
25.2	3.43	6.85
62.2	3.09	5.53

[10] See, for instance, A. Cohen, *An Elementary Treatise on Differential Equations* (D. C. Heath and Company, Boston, Massachusetts, 1933), p. 30.

[11] J. Bigeleisen and M. G. Mayer, J. Chem. Phys. **15**, 261 (1947).

[12] J. C. Morris and R. N. Pease, J. Chem. Phys. **3**, 796 (1935).

The experiments permitted only the setting of an upper limit of 0.05 to the ratio k_3/k_6.

DISCUSSION

The interpretation of the rate ratio will be undertaken within the framework of the transition state theory. The configurations of both the H_2Cl and HCl_2 transition states will be assumed to be linear. The ratio k_3/k_6 is then given by[13]

$$k_3(H_2Cl)/k_6(HCl_2)=(\kappa_3/\kappa_6)(m_{H_2Cl}/m_H m_{HCl})^{\frac{1}{2}} \times(m_H m_{Cl_2}/m_{HCl_2})^{\frac{1}{2}}(I_{Cl_2}/I_{HCl})(I_{H_2Cl}/I_{HCl_2}) (s_{HCl}s_{HCl_2}/s_{Cl_2}s_{H_2Cl})\alpha\exp(-A/T), \quad (17)$$

where

$$\alpha=[1-\exp(-u_{HCl})/\prod_3(1-\exp(-u_{H_2Cl})] \times[\prod_3(1-\exp(-u_{HCl_2})/(1-\exp(-u_{Cl_2})].$$

Here A is the difference (in degrees) in the activation energies (zero point of reactants to zero point of transition state) for the two reactions; κ_3 and κ_6 are transmission coefficients, assumed to be equal; the m, I, and s factors are defined in the usual way with $s_{HCl}=s_{HCl_2}=s_{H_2Cl}=1$, $s_{Cl_2}=2$; and $u=h\nu/kT$. The products run over the three vibrational frequencies of the respective transition states.

It has been possible to express the experimental results for k_3/k_6 in the temperature range in question in the form $k_3/k_6=Ce^{-D/T}$ [see Eq. (16)]. Equation (17) is already in the form $k_3/k_6=C'\alpha e^{-A/T}$. If one assumes that the individual factors of α, namely, $(1-e^{-u})^{-1}$, can be expressed as $ae^{b/T}$ (both a and b being temperature independent) one finds: $\ln a=(\partial/\partial T)[T\ln(1-e^{-u})^{-1}]$. The derivative is evaluated at some average temperature in the region of interest.

An actual attempt at least-squares fitting of $\ln(1-e^{-u})^{-1}$ by means of a straight line over the temperature range of interest has led to very similar values for $\ln a$ as those from the derivative expression above. The derivative expression is of course recognized as the vibrational entropy of an harmonic oscillator (except for the gas constant R) and the proper combination of the factors $\ln a$ becomes just as expected, the difference between the vibrational entropies of activation of the two reactions (again except for the gas constant R). Similarly then C (calculated) is the anti ln of R^{-1} times the difference between the total entropies of activation of the two reactions.

The factor D which does yield information about the total relative energies of the respective transition states will not be pursued further here.

Attention will be focused on the factor C which depends on the structure and on the vibrational frequencies of the transition states and the reactants. The necessary knowledge for the diatomic molecules is readily available in the literature.[14] Considerable information about the H_2Cl transition state has been obtained both from entropy of activation considerations of the hydrogen-chlorine reaction[3] and from the study of the isotope effects in this reaction.[1]

The unknowns contributing to the factor C, depend then only on the moments of inertia of HCl_2 and upon its doubly degenerate bending frequency ν_ϕ. The stretching frequency of the HCl_2 transition state is assumed sufficiently large so that it makes little contribution to the entropy. Since one can make reasonable assumptions on the moments of inertia, the present experimental data then serve to give information about the doubly degenerate bending frequency of HCl_2.

In his entropy considerations with respect to the H_2+Cl reaction, Pitzer[3] had to estimate H–H and H–Cl distances in the H_2Cl transition state. He used $d_{H-H}=0.9$ A and $d_{H-Cl}=1.5$ A. Proceeding similarly for HCl_2 we choose $d_{H-Cl}=1.5$ A and $d_{Cl-Cl}=2.2$ A. With these distance values one finds

$$(I_{Cl_2}/I_{HCl})(I_{H_2Cl}/I_{HCl_2})=3.6.$$

If one permits independent or combined increases of 0.2 A for any of the above estimated bond distances of the HCl_2 transition state, this ratio can increase by 35% or decrease by 15%. Using the above value of 3.6 one obtains for C' of Eq. (17): $C'=1.85$.

The stretching frequency of H_2Cl which is about 1340 cm^{-1} [1] makes no contribution to α in the temperature range in question. It is also assumed that the stretching frequency of HCl_2 makes no contribution, as mentioned above. A stretching frequency for the HCl_2 transition state larger than the Cl_2 frequency is plausible on the basis of the findings with respect to the H_2Cl transition state, where the most reasonable model appears to be one with a large H–Cl force constant. This postulate will be tested by the measurement of the isotope effect in this reaction, now in progress. If this frequency were as low as 500 cm^{-1}, α would increase by about 40%. Our later analysis shows that such an increase has little effect on the final value of the bending frequency.

The following values are used in the calculation of the contributions of the Cl_2 and H_2Cl frequencies to α,

$$\nu_{Cl_2}=565\ cm^{-1}, \qquad \nu_{\phi H_2Cl}=540\ cm^{-1},$$

where ν_ϕ refers to the doubly degenerate bending frequency of the linear triatomic molecule. An average temperature of 304°K is employed. Using the experimental value of $C=0.143$, one finds then that

$$\{(\partial/\partial T)\,T\ln[1-\exp(-u_{\phi HCl_2})]^{-1}\}=1.711,$$

[13] S. Glasstone, K. J. Laidler, and H. Eyring, *The Theory of Rate Processes* (McGraw-Hill Book Company, Inc., New York, 1941).

[14] G. Herzberg, *Molecular Spectra and Molecular Structure I. Spectra of Diatomic Molecules* (D. Van Nostrand Corporation, Inc., Princeton, New Jersey, 1950).

which means that[15]

$$\nu_{\phi HCl_2}=105\ cm^{-1}.$$

The experimental error of ± 0.033 in C leads to an error of ± 12 cm^{-1} in the bending frequency.[16] On the other hand the uncertainty in the moment of inertia ratio leads to an uncertainty of ± 13 cm^{-1} in the estimated frequency. Thus the bending frequency $\nu_{\phi HCl_2}$ is not expected to deviate by more than 20 cm^{-1} from the value of 105 cm^{-1}. It may be mentioned that the raising of Pitzer's frequency $\nu_{\phi H_2Cl}$ has a negligible effect on the present result, whereas a considerable lowering of that frequency would only produce a comparatively small lowering of the present value of $\nu_{\phi HCl_2}$. The comparison of $\nu_{\phi H_2Cl}$ and $\nu_{\phi HCl_2}$ leads to a value of the relative bending force constants[14] $k\delta_{HCl_2}/k\delta_{H_2Cl}=0.345$.

The experiment has thus served to give us our first insight into the potential energy surface of the HCl_2 transition state. Isotope effect studies will give us further information. As has been noted before,[1] however, they will not yield further data with regard to $\nu_{\phi HCl_2}$.

ACKNOWLEDGMENTS

We are thankful to Mrs. B. Man for performing the radioassays. We are also thankful to Dr. J. Bigeleisen for reading and commenting on this manuscript.

[15] J. B. Mayer and M. G. Mayer, *Statistical Mechanics* (John Wiley & Sons, Inc., New York, 1940), Table AIX 4.

[16] A least-squares calculation has been carried out to fit by $C\exp(-D/T)$ the values of k_3/k_5 given by Eq. (17) at the three temperatures of the experiment with the known molecular parameters (including $\nu_{\phi HCl_2}=105$ cm^{-1}) and with a value of A chosen to give the correct magnitude of k_3/k_5. The result of this calculation was $C=0.144\pm 0.0004$. This result justifies our procedure and indicates that the error introduced by the temperature variation of a is small compared to the experimental error.

Evidence of Trapped N Atoms in X-Ray Irradiated NaN_3

G. J. KING, F. F. CARLSON, B. S. MILLER, AND R. C. MCMILLAN

U. S. Army Engineer Research and Development Laboratories, Fort Belvoir, Virginia

(Received November 25, 1960)

Sodium azide irradiated with x rays at liquid-nitrogen temperature displays a power sensitive ESR spectrum of three equal lines of separation 6.2 oe. This spectrum is interpreted as N^{14} trapped in the crystal lattice.

ELECTRON spin resonance (ESR) experiments on x-ray irradiated sodium azide (NaN_3) show, in addition to other resonances, a separate three-line absorption (Fig. 1) which has the essential character of the resonance attributed[1,2] to trapped N^{14}. The separation from the previously reported *F*-center resonance[3] is accomplished by taking advantage of the large difference in microwave power saturation properties of the two resonances.

The irradiation and electron spin resonance measurements were performed at liquid-nitrogen temperature, since the signal decays at slightly higher temperatures. The x rays used were supplied by a General Electric Industrial x-ray generator with a tungsten tube and had an energy corresponding to 220 kv. The sodium azide, both powders and crystals, was sealed in evacuated Pyrex or quartz tubes to guard against contamination. The strong electron spin resonances produced by x rays in some quartz and Pyrex tubes were carefully avoided by shielding the parts of the tubes later to be placed in the cavity with heavy lead shields during the x-ray irradiation.

The tubes were approximately one-fourth filled with the sample and it was possible to shake the sample into the unshielded end of the tube for irradiation and later into the lead-shielded end for the spin resonance measurements. Blank runs on the shielded ends of the tubes showed no resonances. A Varian X-band EPR spectrometer and high-resolution NMR magnet were used for these experiments and both microwave frequencies and proton resonance magnetometer frequencies were measured by a 540B Hewlett Packard frequency counter system. In addition, the location of the center of the three-lined spectrum was also checked by using a sodium colloid marker[4] which fortuitously appears close to the center of the spectrum.

Computer analysis of the ESR spectrum (Fig. 1) shows that the resonance can be fitted by three equal Lorentzian lines having equal spacing about a central g value of 2.0021 ± 0.0001. The lines are separated by 6.2 oe. The equality of the absorption lines and the ease of resolution in the powdered sample indicates that the resonance is basically isotropic in nature. Experiments with single crystals show that the structure does not change with orientation of the crystal.

This information and the negative g-value shift from the free-electron value indicate that the structure responsible for the resonance is not a *V* center. Since triplet line structure is produced by the nuclear magnetic hyperfine field of the $2I+1=3$ states of the N^{14} nucleus, we assume the resonance is strongly centered on a single N^{14} atom and is, in fact, the resonance of N^{14} trapped in the NaN_3 lattice.

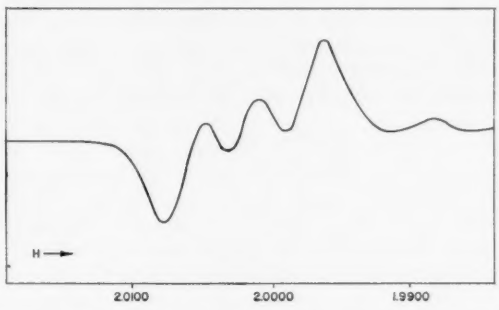

FIG. 1. Derivative of the electron spin resonance absorption $d\chi''/dH$ of N^{14} atoms trapped in the lattice of x-ray irradiated NaN_3 at 77°K. The small peak on the right is part of the *F*-center resonance which is still visible at low power. A scale of g values is shown beneath the curve.

The character of the trapped N^{14} atom in various matrices is well known.[5] The three-line ESR resonance structure is ascribed to the magnetic transitions in the $^4S_{\frac{3}{2}}$ ground state of N^{14}. The four allowed magnetic states are split into three lines each by the nuclear hyperfine fields, but selection rules allow only nine transitions which coalesce to give three triply degenerate absorption lines.

Comparison with the available data on N trapped by various other methods strengthens the evidence for identification of this resonance with trapped N. Nitrogen trapped at very low temperatures in matrices of

[1] T. Cole, J. T. Harding, J. R. Pellam, and D. M. Yost, J. Chem. Phys. **27**, 593 (1957).
[2] S. N. Foner, C. K. Jen, E. L. Cochran, and V. A. Bowers, J. Chem. Phys. **28**, 351 (1958); Phys. Rev. **112**, 1169 (1958).
[3] F. F. Carlson, G. J. King, and B. S. Miller, J. Chem. Phys. **33**, 1266 (1960).
[4] B. S. Miller, J. Chem. Phys. **33**, 889 (1960).
[5] C. K. Jen in *Formation and Trapping of Free Radicals*, edited by Arnold M. Bass and H. P. Broida (Academic Press, Inc., New York, 1960), Chap. 7.

TABLE I. Comparison of the electron spin resonance properties of N trapped in different matrices.[a]

Matrix	g_J	Approximate line separation (oes)
Free	2.00215(3)	...
H_2	2.00202(8)	4.1
N_2	2.00200(8)	4.3
CH_4	2.00203(8)	4.8
NaN_3	2.0021(1)	6.2

[a] Numbers in the parentheses indicate experimental and/or conversion errors in the last figures of the associated values.

frozen gases always shows three main lines which are sensitive to the matrix material as far as splitting of the lines is concerned, but shows a central-line g value which is nearly unshifted. For purposes of comparison, the data from Foner, Jen, Cochran, and Bowers[2] are partially repeated in Table I. Our data show a linewidth slightly larger than that found in other investigations which were performed at liquid-helium temperature. Since the rigid matrix here is crystalline, one expects dipolar and other forms of broadening to be stronger than for N trapped in condensed gas matrices. The deviation of A, the hyperfine coupling constant, from the free gas value is positive, which is typical of the N behavior but not for some other trapped radicals.[5]

The deviation is sensitive to environment and is larger than that encountered in other matrices which reflects the rigidity of the matrix and the relatively high temperature.

The thermal properties of the N^{14} resonance are similar to those of the F center. Both the F-center and N^{14} atom spin resonances are fairly stable at liquid-nitrogen temperature but bleach very rapidly at dry-ice temperature. A faint blue glow from the NaN_3 is observed by eye when a sample containing F centers and trapped N is suddenly warmed from liquid nitrogen to room temperature. Whether this is associated with the N-atom recombination or the F-center decay, or both, is not known at present.

The thermal stability of N atoms in the NaN_3 lattice is at first glance, somewhat surprising. These experiments, however, are similar to the experiments of Livingstone *et al.*, in which atomic H was stabilized in frozen acid at 77°K for several months.[6]

The production of atomic N may result from the x-ray photoreaction $N_3^- + h\nu \rightarrow N_2 + N + \epsilon$ in which the participants may be in an excited state to accommodate correlation rules. Another interaction may also occur according to the formula $N_3^- + h\nu \rightarrow N_2 + N^+ + 2\epsilon$.

In this case the N^+ is ejected from the anion lattice site to an interstitial site where it captures an electron and is trapped.

[6] R. Livingston, H. Zeldes, and E. H. Taylor, Phys. Rev. **94**, 725 (1954).

THE JOURNAL OF CHEMICAL PHYSICS VOLUME 34, NUMBER 5 MAY, 1961

Nuclear Relaxation Processes of a Nonequivalent Two-Spin System

HIROSHI SHIMIZU

Faculty of Pharmaceutical Sciences, The University of Tokyo, Hongo, Tokyo, Japan

AND

SHIZUO FUJIWARA

Department of Chemistry, Faculty of Science, The University of Tokyo, Tokyo, Japan

(Received August 1, 1960)

Nuclear magnetic relaxation of a two-spin system is discussed using Redfield's semiclassical formulation of the relaxation processes. Time dependences of longitudinal magnetizations are given as a function of the ratio $J/\delta\nu_0$. An expression for the nuclear induction signal is given, from which the expected shape of multiplet lines and their behaviors upon saturation under various origins of the relaxation are discussed in detail. The discussion leads to the conclusion that the mechanism of nuclear relaxation can be determined by carefully analyzing the spin multiplet lines on the basis of the theory. Finally, it is shown that there is a possibility of finding the absolute sign of the spin-spin coupling constant in a two-spin system using the multiple resonance method.

1. INTRODUCTION

THE spin relaxation process for the nuclear spin system, composed of the interacting two spins of $I=\frac{1}{2}$, has been studied by several workers. Bloembergen, Purcell, and Pound[1] discussed the case of identical nuclear spins which underwent completely random motions. Solomon[2,3] and Bloembergen[3] treated the case of nonidentical spins which showed no resolved fine structure in the liquid state. Then, using the density matrix of the spin system, Bloembergen[4] discussed identical spins in the solid state, where motion of the two spins around one axis was present.

A system of nonequivalent two nuclei with spin $\frac{1}{2}$ and independent dipole relaxations, was discussed by Bloch in his general theory of the nuclear induction.[5]

In this paper, which is an extension of Bloembergen's treatment to the liquid state, the relaxation of the generalized nonequivalent two-spin system is discussed. The system may or may not show fine structures. The treatment considers also the relaxation effect for each component of the fine structures obtained by high-resolution nuclear magnetic resonance apparatus.

The experimental requirements for the magnetic saturation of the components of the fine structures may require an accuracy of the order of $\sim 10^{-9}$ for the case of a proton pair.[6] Fortunately, the recent remarkable development of the high-resolution apparatus has made it possible to satisfy this requirement, hence, discussions in this paper now have a practical importance.

As pointed out by Bloch,[5,7,8] the BPP theory of the relaxation has some internal inconsistencies, that is, the omission of the Boltzmann factor for the nuclear spin population of each Zeeman level at thermal equilibrium, and the lack of quantum-mechanical generalization in the treatment of the random motions in the external bath. These inconsistencies were avoided in the approaches by Bloch[5,7,8] and Wangsness,[7] where the dynamics of the relaxation processes were quantum-mechanically formulated. In the present paper, we use the general treatment for the relaxation process given by Redfield,[9] which is the semiclassical reformulation of the Bloch theory, omitting the term referring to the external bath system from the total Hamiltonian.

If the density matrix σ of the spin system is once obtained in its time dependence, the time-dependent behavior of the expectation value $\langle \mathbf{Q} \rangle$ of any physical quantity $\mathbf{Q}$ of the spin system is then given by the equation

$$\langle \mathbf{Q} \rangle(t) = \mathrm{Tr}\{\mathbf{Q}\sigma(t)\}, \tag{1.1}$$

where $\mathrm{Tr}\{\mathbf{A}\}$ refers to the trace of any matrix $\mathbf{A}$. Therefore, the greater part of the determination of the relaxation effect is to obtain the density matrix of the spin system and then solve this matrix under various conditions. The matrix $\mathbf{A}^-$ represents the transpose of matrix $\mathbf{A}$.

2. THEORY OF THE RELAXATION

When a pair of nuclear spins A and B, magnetically well isolated from the other nuclear or electric spins in the same or other molecules, is placed in a strong static magnetic field H_0, the quantum-mechanical Hamiltonian $\mathcal{H}(t)$ which describes the spin system in

[1] N. Bloembergen, E. M. Purcell, and R. V. Pound, Phys. Rev. **73**, 679 (1948).
[2] I. Solomon, Phys. Rev. **99**, 559 (1955).
[3] I. Solomon and N. Bloembergen, J. Chem. Phys. **25**, 261 (1955).
[4] N. Bloembergen, Phys. Rev. **104**, 1542 (1956).
[5] F. Bloch, Phys. Rev. **102**, 104 (1956).
[6] Each component of the spectrum showing the fine structure is saturated successively by fixing the radiation frequency at the component frequency. Detailed conditions of this procedure are discussed in Sec. III.
[7] R. K. Wangsness and F. Bloch, Phys. Rev. **89**, 728 (1953).
[8] F. Bloch, Phys. Rev. **105**, 1206 (1957).
[9] A. G. Redfield, IBM J. Research Develop. **1**, 19 (1957).

TABLE I. Eigenfunctions and eigenvalues for a two-spin system AB.

n	Eigenfunction	Eigenvalue
3	$\beta\beta$	$\omega_A+\omega_B+\frac{1}{4}J$
$2'$	$\alpha\beta\sin\theta+\beta\alpha\cos\theta$	$-\frac{1}{4}J+C$[a]
2	$\alpha\beta\cos\theta-\beta\alpha\sin\theta$	$-\frac{1}{4}J-C$
1	$\alpha\alpha$	$-\omega_A-\omega_B+\frac{1}{4}J$

[a] $C=\frac{1}{2}[(\delta\nu_0)^2+J^2]^{\frac{1}{2}}$.

the laboratory coordinate system may be written as follows:

$$\mathcal{H}=\hbar\mathbf{E}_m+\hbar\mathbf{E}_J+\hbar\mathbf{E}_d+\hbar\mathbf{E}_\epsilon \tag{2.1}$$

$$\mathbf{E}_m=-\sum_i\gamma_i I_{Zi}H_{0i}=-(\gamma_A I_{ZA}H_{0A}+\gamma_B I_{ZB}H_{0B}) \tag{2.2}$$

$$\mathbf{E}_J=\sum_{i>j}J_{ij}\mathbf{I}_i\cdot\mathbf{I}_j=J\mathbf{I}_A\cdot\mathbf{I}_B \tag{2.3}$$

$$\mathbf{E}_d=\hbar\sum_{i>j}\gamma_i\gamma_j r_{ij}^{-3}[\mathbf{I}_i\cdot\mathbf{I}_j-3(\mathbf{I}_i\cdot\mathbf{r}_{ij})(\mathbf{I}_j\cdot\mathbf{r}_{ij})r_{ij}^{-2}]$$
$$=\hbar\gamma_A\gamma_B\mathbf{b}^{-3}[\mathbf{I}_A\cdot\mathbf{I}_B-3(\mathbf{I}_A\cdot\mathbf{b})(\mathbf{I}_B\cdot\mathbf{b})b^{-2}] \tag{2.4}$$

$$\mathbf{E}_\epsilon=\sum_i\gamma_i\mathbf{I}_i\cdot\boldsymbol{\epsilon}_i'\mathbf{H}_0=(\gamma_A\mathbf{I}_A\cdot\boldsymbol{\epsilon}_A'+\gamma_B\mathbf{I}_B\cdot\boldsymbol{\epsilon}_B')\mathbf{H}_0, \tag{2.5}$$

where $\mathbf{E}_m$ is the Zeeman energy of the system. In Eq. (2.2), the magnetic shielding effect due to the diamagnetic circulation of electrons[10] is included in H_{0i} as

$$\mathbf{H}_{0i}=\mathbf{H}_0(1-\langle\boldsymbol{\epsilon}_i\rangle_{Av}),$$

where $\boldsymbol{\epsilon}_i$ is the magnetic shielding tensor of the ith nucleus and $\langle\ \rangle_{Av}$ the average over all orientations. The term $\mathbf{E}_J$ refers to the electron-coupled spin-spin interaction.[11,12] This interaction may be taken to be independent of time in the ordinary case, but in the case when the spin exchange effect is dominant, it becomes a time-dependent perturbation[3] and the discrepancy between the experimental results and those predicted by the BPP theory becomes appreciable with regard to the ratio of the longitudinal and the transverse relaxation times,[13] that is, $T_1/T_2=1$. However, in the present treatment, we regard it to be time independent and treat it as a part of the time-independent zeroth order Hamiltonian. Here $\mathbf{E}_d$ refers to the direct dipolar interaction, where $\mathbf{b}$ is a vector from the nucleus A to B. Although its length is constant,[14] the orientation is assumed to be varied randomly with the rotational Brownian motion of the molecule. This randomness is responsible for the relaxation effect. Another origin of the random perturbation is $\mathbf{E}_\epsilon$, the interaction of the spins with the anisotropic shielding fields, which was discussed by Gutowsky and Woessner[15] and McConnell and Holm.[16] In Eq. (2.5) $\boldsymbol{\epsilon}_i'$ is the anisotropic shielding tensor, $\boldsymbol{\epsilon}_i'=\boldsymbol{\epsilon}_i-\langle\boldsymbol{\epsilon}_i\rangle_{Av}$. Hence, the shielding is not isotropic with respect to the secondary magnetic field which is caused by the circulation of the electrons. This secondary magnetic field has nonzero components which fluctuate in the $x-y$ plane as a result of the random motions of the molecules. The contribution of the anisotropic term may be larger in the case of F^{19} or P^{31} resonances than in the case of proton; the former have nonspherically symmetric distributions of the electronic clouds around the nuclei. In general, the indirect spin-spin coupling may be anisotropic,[12] but we omit this contribution from the Hamiltonian (2.1) for the sake of simplicity since it will be smaller than the anisotropic shielding effect. For convenience in the following discussion, we classify $\mathcal{H}$ into two parts, one is the time-independent zeroth order energy of the spin system $\hbar\mathbf{E}_0$, and the other, $\hbar\mathbf{G}$, the time-dependent coupling between the spin and bath systems, which is assumed to be a time-dependent perturbation to $\hbar\mathbf{E}_0$, that is,

$$\mathbf{E}_0=\mathbf{E}_m+\mathbf{E}_J \tag{2.6}$$

$$\mathbf{G}(t)=\mathbf{E}_d+\mathbf{E}_\epsilon. \tag{2.7}$$

The eigenvalues and eigenfunctions of $\hbar\mathbf{E}_0$, were concisely given by Bernstein, Pople, and Schneider[17] as shown in Table I. In this table, the Zeeman energies for the nuclei A and B, $\frac{1}{2}\omega_A$ and $\frac{1}{2}\omega_B$, are given as

$$\omega_A=\gamma_A H_{0A}/2\pi$$

and

$$\omega_B=\gamma_B H_{0B}/2\pi,$$

where the unit of energy is given in cycles per second. The positive quantity C and the angle θ $(0\leq\theta\leq\pi)$ are defined by

$$2C\cos2\theta=[\omega_A-\omega_B]\equiv\delta\nu_0 \tag{2.8a}$$

$$2C\sin2\theta=\mathrm{J}, \tag{2.8b}$$

thus

$$C=\tfrac{1}{2}[(\delta\nu_0)^2+J^2]^{\frac{1}{2}}. \tag{2.9}$$

The general appearance of the spectrum depends only on the absolute value of the ratio $J/\delta\nu_0$, the ratio of the spin coupling constant to the chemical shift, and is independent of the sign of J and $\delta\nu_0$.

As there are four nondegenerate eigenfunctions which describe the transitions, the density matrix of the spin system σ will, in general, be expressed as a four-by-four

[10] N. F. Ramsey, Phys. Rev. **78**, 699 (1950).
[11] N. F. Ramsey and E. M. Purcell, Phys. Rev. **85**, 143 (1952).
[12] N. F. Ramsey, Phys. Rev. **91**, 303 (1953).
[13] N. Bloembergen, J. Chem. Phys. **27**, 572 (1957).
[14] We have omitted the effect of the translational diffusion discussed by H. C. Torrey [Phys. Rev. **92**, 962 (1953)], since both spins are equally affected, provided that the diffusion is isotropic. However it will be briefly discussed in Sec. V.
[15] H. S. Gutowsky and D. E. Woessner, Phys. Rev. **104**, 843 (1956).
[16] H. M. McConnell and C. H. Holm, J. Chem. Phys. **25**, 1285 (1957).
[17] J. A. Pople, W. G. Schneider, and H. J. Bernstein, Can. J. Chem. **35**, 65 (1957).

matrix, whose motion is given by the equation[18]

$$d\sigma/dt=-i[\mathcal{H},\sigma]. \tag{2.10}$$

In Eq. (2.10), σ is successively perturbed by $\mathbf{G}$, where the magnitude of $\mathbf{G}$ is not only random in time, but also different for each member of the ensemble. Therefore, the perturbed σ will be connected with the correlation matrix of $\mathbf{G}$ by

$$\mathbf{P}(\tau)=\langle\mathbf{G}^{\dagger}(t)\mathbf{G}(t-\tau)\rangle, \tag{2.11}$$

where the dagger denotes the complex conjugate. By starting from Eq. (2.10) and retaining the terms up to the second order in $\mathbf{G}$, the equation of motion for each element of the density matrix is given as[9]

$$d\sigma_{\alpha\alpha'}/dt=-i\omega_{\alpha\alpha'}\sigma_{\alpha\alpha'}+\sum_{\beta\beta'}R_{\alpha\alpha'\beta\beta'}(\sigma_{\beta\beta'}-\sigma_{\beta\beta'}{}^{(T)}). \tag{2.12}$$

In Eq. (2.12), the first term of the right side expresses the unperturbed motion of the system, and the second is the relaxation term given by the second-order perturbation with respect to $\mathbf{G}$. The relaxation matrix $\mathbf{R}$ has been evaluated from the correlation matrix $\mathbf{P}$ by

$$R_{\alpha\alpha'\beta\beta'}=\tfrac{1}{2}\int_{-\infty}^{\infty}\{[\exp(i\omega_{\alpha'\beta'}\tau)+\exp(i\omega_{\alpha\beta}\tau)]P_{\alpha\beta\alpha'\beta'}$$
$$-\sum_{\gamma}[\delta_{\alpha'\beta'}\exp(i\omega_{\gamma\beta}\tau)P_{\gamma\beta\gamma\alpha}+\delta_{\alpha\beta}\exp(i\omega_{\gamma\beta'}\tau)P_{\gamma\alpha'\gamma\beta'}]\}d\tau. \tag{2.13}$$

Moreover Eq. (2.12) has been derived under the additional assumptions:

(1) The correlation matrix is symmetrical with respect to time, that is, $\mathbf{P}(\tau)=\mathbf{P}(-\tau)$, and we can define a correlation time which has the property: $\mathbf{P}(\tau)=0$, if $\tau\gg\tau_c$.

(2) The spin system approaches thermal equilibrium with the external bath at the bath temperature T by giving thermal energy to the bath system. The density matrix at equilibrium is then given by the Boltzmann distribution

$$\sigma_{\alpha\alpha'}{}^{(T)}=\delta_{\alpha\alpha'}\exp(-\omega_\alpha/kT)/\sum_\beta\exp(-\omega_\beta/kT). \tag{2.14}$$

(3) The correlation time is so short that the condition

$$R_{\alpha\alpha'\beta\beta'}\tau_c\ll 1 \tag{2.15}$$

is satisfied.

Equation (2.12) can be further simplified by omitting the elements of $\mathbf{R}$ which do not satisfy the relation

$$\omega_\alpha-\omega_\beta-\omega_{\alpha'}+\omega_{\beta'}=0 \tag{2.16}$$

or, more rigorously speaking, the relation

$$|\omega_\alpha-\omega_\beta-\omega_{\alpha'}+\omega_{\beta'}|\ll R_{\alpha\alpha'\beta\beta'}. \tag{2.17}$$

Such elements of $\mathbf{R}$ are ineffective in the relaxation of the spin system, for if this condition is not satisfied, the fluctuating field has no effective component which rotates in the $x-y$ plane with the angular frequency of the Larmor precessional motion of the magnetic moment vector $\mathbf{M}$. Thus such elements of $\mathbf{R}$ constitute merely a nonsecular perturbation to the spin system and it gives rise to varying oscillatory components in the density matrix. Unless there is an overlapping of the resonance lines,[19] the diagonal and the off-diagonal elements of the density matrix can be independent of the off-diagonal elements, and each of the off-diagonal elements relaxes independently of the diagonal elements and the other off-diagonal elements.

The equation of motion for the diagonal elements can be concisely written in matrix notation,

$$d\mathfrak{d}/dt=\mathbf{R}_d(\mathfrak{d}-\mathfrak{d}^{(T)}), \tag{2.18}$$

where $\mathbf{R}_d$ is the four-by-four relaxation matrix

$$\mathbf{R}_d=\begin{vmatrix} R_{1111} & R_{1122} & R_{112'2'} & R_{1133} \\ R_{2211} & R_{2222} & R_{222'2'} & R_{2233} \\ R_{2'2'11} & R_{2'2'22} & R_{2'2'2'2'} & R_{2'2'33} \\ R_{3311} & R_{3322} & R_{332'2'} & R_{3333} \end{vmatrix}, \tag{2.19}$$

and the transposes of the other matrices are denoted by

$$\mathfrak{d}^{-}=(\sigma_{11}\sigma_{22}\sigma_{2'2'}\sigma_{33}) \tag{2.20}$$

$$\mathfrak{d}^{(T)-}=(\sigma_{11}{}^{(T)}\sigma_{22}{}^{(T)}\sigma_{2'2'}{}^{(T)}\sigma_{33}{}^{(T)}) \tag{2.21}$$

$$d\mathfrak{d}^{-}/dt=(d\sigma_{11}/dt\ d\sigma_{22}/dt\ d\sigma_{2'2'}/dt\ d\sigma_{33}/dt). \tag{2.22}$$

The matrix element $R_{\alpha\alpha\beta\beta}$ in Eq. (2.19) refers to the probability of transition from state β to α.

The time dependences of the diagonal elements of the density matrix σ_{ii} are obtained from Eqs. (2.18)–(2.22). The order of Eq. (2.18) is reduced by the conditions

$$\sum_i d\sigma_{ii}/dt=0 \tag{2.23a}$$

and

$$\sum_i(\sigma_{ii}-\sigma_{ii}{}^{(T)})=0, \tag{2.24a}$$

where the relation (2.23a) is easily proved by summing the right-hand side of Eq. (2.18) and making use of the relation $R_{iiii}=-\Sigma'_j R_{iiij}=-\Sigma'_j R_{jjii}$; relation (2.24a) is evident from the definition of the normalization

$$\sum_i\sigma_{ii}=\sum_i\sigma_{ii}{}^{(T)}=1.$$

[18] U. Fano, Revs. Modern Phys. **29**, 74 (1957). The quantum mechanical description of states by the density matrix method is discussed.

[19] N. Bloembergen, S. Shapiro, P. S. Pershan, and J. O. Artman, Phys. Rev. **114**, 445 (1959).

We consider, for simplicity's sake, a case of the relaxation process caused by dipolar interactions. By using the relaxation matrix which will be given in Sec. IV and the transformed variables,

$$u=\sigma_{11}+\sigma_{33}-\sigma_{11}^{(T)}-\sigma_{33}^{(T)}$$
$$v=\sigma_{22}+\sigma_{2'2'}-\sigma_{22}^{(T)}-\sigma_{2'2'}^{(T)}$$
$$w=\sigma_{23}-\sigma_{2'3'}-\sigma_{23}^{(T)}+\sigma_{2'3'}^{(T)}$$
$$x=\sigma_{11}-\sigma_{33}-\sigma_{11}^{(T)}+\sigma_{33}^{(T)}. \tag{2.25}$$

Equation (2.18) is separated into the following two sets of simultaneous differential equations

$$du/dt=\tfrac{3}{10}\tau_c g^2(-u+v-\sin2\theta\cdot w)$$
$$dv/dt=\tfrac{3}{10}\tau_c g^2(u-v+\sin2\theta\cdot w)$$
$$dw/dt=\tfrac{3}{10}\tau_c g^2\{-\sin2\theta\cdot u+\sin2\theta\cdot v$$
$$-[(5-2\sin^2 2\theta)/3]\cdot w\} \tag{2.26a}$$

and

$$dx/dt=-\tfrac{3}{2}\tau_c g^2 x. \tag{2.27}$$

The relations (2.23a) and (2.24a) are rewritten in terms of the new set of variables as

$$du/dt+dv/dt=0, \tag{2.23b}$$

and

$$u+v=0, \tag{2.24b}$$

respectively. By these relations, Eqs. (2.26a) are further reduced to

$$-(10/\tau_c g^2)(du/dt)=6u+3\sin2\theta\cdot w$$
$$-(10/\tau_c g^2)(dw/dt)=6\sin2\theta\cdot u+(5-2\sin^2 2\theta)w. \tag{2.26b}$$

The solution of Eq. (2.27) is

$$x=X_0\exp(-\tfrac{3}{2}\tau), \tag{2.28}$$

where $\tau=\tau_c g^2 t$. The general solutions of Eqs. (2.26b) are obtained by substituting $u=U_0\exp[-(\lambda/10)\tau]$ and $w=W_0\exp[-(\lambda/10)\tau]$ into Eq. (2.26b), which gives the secular equation

$$\begin{vmatrix} 6-\lambda & 3\sin2\theta \\ 6\sin2\theta & (5-2\sin^2 2\theta)-\lambda \end{vmatrix}=0,$$

whose solutions are

$$\lambda_{1,2}=\tfrac{1}{2}[9+2\cos^2 2\theta\pm(4\cos^4 2\theta-84\cos^2 2\theta+81)^{\frac{1}{2}}].$$

With these solutions and Eq. (2.26), we obtain the relations

$$W_{01}=[(6-\lambda_1)/3\sin2\theta]u_{01}\equiv a(\theta)U_{01}$$
$$U_{02}=(5-2\sin^2 2\theta-\lambda_2)/6\sin2\theta=W_{02}\equiv b(\theta)W_{02}. \tag{2.29}$$

Although the coefficients $a(\theta)$ and $b(\theta)$ are mathematically indefinite at $\theta=0$, we assume that they are zero, that is,

$$a(0)=b(0)=0,$$

in order to satisfy the physical meaning of Eq. (2.29).

Deviation of the longitudinal magnetization from the equilibrium values is denoted by p_{ij}, whose suffixes i and j mean that the polarization p occurs between the Zeeman levels i and j.

If we write the initial value of p_{ij} as p_{ij}^0 the constants U_{01}, W_{02}, and X_0 are given in terms of p_{ij}, and hence, from Eqs. (2.24b), (2.25), and (2.29) the polarizations are

$$p_{12}=\tfrac{1}{8}[(1-ab)^{-1}(2+a)\{(1-2b)(p_{12}^0-p_{23}^0)$$
$$+(1+2b)(p_{12'}^0-p_{2'3}^0)\}\exp[-(\lambda_1/10)\tau]$$
$$-(1-ab)^{-1}(2b+1)\{(a-2)(p_{12}^0-p_{23}^0)$$
$$+(a+2)(p_{12'}^0-p_{2'3}^0)\}\exp[-(\lambda_2/10)\tau]$$
$$+4(p_{12}^0+p_{23}^0)\exp(-\tfrac{3}{2}\tau)]$$
$$p_{12'}=\tfrac{1}{8}[(1-ab)^{-1}(2-a)\{(1-2b)](p_{12}^0-p_{23}^0)$$
$$+(1+2b)(p_{12'}^0+p_{2'3}^0)\}\exp[-(\lambda_1/10)\tau]$$
$$-(1-ab)^{-1}(2b-1)\{(a-b)(p_{12}^0-p_{23}^0)+(a+2)$$
$$\times(p_{12'}^0-p_{2'3}^0)\}\exp[-(\lambda_2/10)\tau]$$
$$+4(p_{12'}^0+p_{2'3}^0)\exp(-\tfrac{3}{2}\tau)]$$
$$p_{23}=(p_{12}^0+p_{23}^0)\exp(-\tfrac{3}{2}\tau)-p_{12}$$
$$p_{2'3}=(p_{12'}^0+p_{2'3}^0)\exp(-\tfrac{3}{2}\tau)-p_{12'}. \tag{2.30}$$

As an example of the treatment, we consider the longitudinal relaxation processes when the nuclear polarization is given by a pulse rf field $H_1(\omega_{12'})$.[20] The initial polarizations may be given as $p_{12}=-\frac{1}{2}p_0$, $p_{12'}=-p_0$, $p_{23}=0$, and $p_{2'3}=\frac{1}{2}p_0$. The time-dependent p' are obtained by substituting these values into Eq. (2.30). The time-dependent behavior of the p is shown in Fig. 1, where the ordinates are the magnitudes of polarization and the abscissae the time $\tau=\tau_c g^2 t$. In Fig. 1(a) for $J\ll\delta\nu_0$, all lines except that of p_{23} approach monotonically to the equilibrium value; the line p_{12} shows the most rapid damping, whereas the lines $p_{12'}$ and $p_{2'3}$ decay more slowly. However, the line p_{23} deviates initially from equilibrium to the positive side due to the positive Overhauser effect, takes a small *negative* value in the range of $\tau\gtrsim 7.0$, and then approaches gradually to the equilibrium value again.

Since Fig. 1(b), for $J=\delta\nu_0$, and Fig. 1(c), for $J\gg\delta\nu_0$, are much alike, the relaxation processes in both cases will not be very different. The differences in the relaxation processes in these three cases may be conveniently shown by the effective relaxation times ob-

[20] We assume here, for convenience, that the sign of the coupling constant J is positive. The pulse $H_1(\omega_{12'})$ for the case of positive J is equivalent to the pulse $H_1(\omega_{23})$ for negative J.

tained graphically from Fig. 1 by measuring the time τ_r which corresponds to the value of the initial polarization multiplied by e^{-1}. The numerical values thus obtained are summarized in Table II, where the contributions from p_{23} are omitted. The definition of its effective relaxation time is difficult, as its initial value $p_{23}^0=0$. It should be noticed that these effective relaxation times depend on which line is polarized by the pulse.

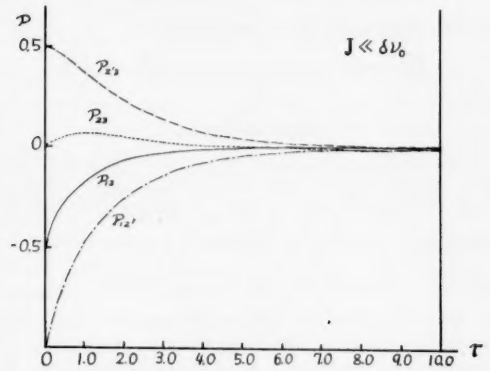

FIG. 1(a). Time-dependent behavior of the longitudinal polarization p in a two-spin system where $J/\delta\nu_0 \ll 1$.

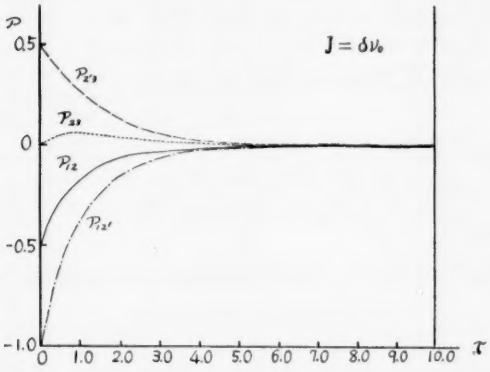

FIG. 1(b). Time-dependent behavior of the longitudinal polarization p in a two-spin system where $J/\delta\nu_0=0$.

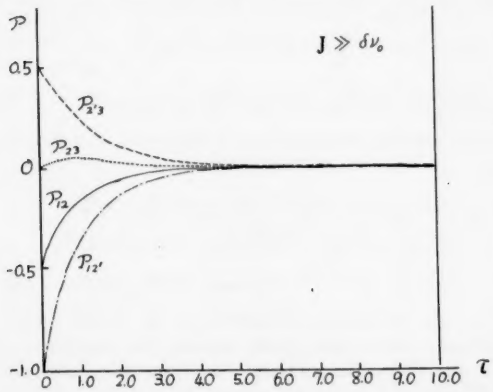

FIG. 1(c). Time-dependent behavior of the longitudinal polarization p in a two-spin system where $J/\delta\nu_0 \gg 1$.

TABLE II. Effective characteristic time τ_r of an AB system observed by the pulse method; $\tau=t/\tau_c g^2$.

$J/\delta\nu_0$	p_{12}	$p_{12'}$	p_{23}	$p_{2'3}$
$J \ll \delta\nu_0$	0.97	1.40	...	2.45
$J \sim \delta\nu_0$	0.95	1.06	...	1.57
$J \gg \delta\nu_0$	0.87	0.98	...	1.38

From the condition (2.16) the equation of motion of every off-diagonal density matrix element is given by the following equation, provided that all $\omega_{\alpha\beta}$ are different from each other in the sense of the condition (2.17):

$$d\sigma_{\alpha\beta}/dt=(R_{\alpha\beta\alpha\beta}-i\omega_{\alpha\beta})\sigma_{\alpha\beta}, \qquad (\alpha\neq\beta). \quad (2.31)$$

Thus, the relaxation of the transverse component is characterized by a single time constant which is related to the relaxation matrix as

$$T_{2\alpha\beta}=-1/R_{\alpha\beta\alpha\beta}. \quad (2.32)$$

Therefore, the decay of the transverse component is given as

$$M_{\alpha\beta}=M_{\alpha\beta}^0 \exp\{-t/T_{2\alpha\beta}\}. \quad (2.33)$$

From Eqs. (2.30) and (2.33), it is clear that the relaxations of the longutudinal and the transverse magnetizations have, in general, nonequivalent relaxation times. Moreover, the relaxation time of one transverse component is not always equal to that of another transverse component. The relaxational motions of the longitudinal magnetization, given by Eq. (2.30), may be interpreted as follows. The relaxation process is determined by the combination of four modes: the ith mode represents mainly the mode of the condition of the energy, initially given to the ith component of the diagonal density matrix. Hence, the local energy at any Zeeman level can affect other levels, and the longitudinal relaxation becomes a mechanism to smooth out the (total and the local) energy imbalances of the spin system.

In contrast to this situation, it may be thought from the form of Eq. (2.33), that the transverse relaxation is not affected by other levels which are not directly concerned with the transition under consideration. However, the relaxation matrix can be decomposed, as shown by Eq. (2.34), where the effects of other levels are included in the second terms of the right-hand side,

$$R_{\alpha\beta\alpha\beta}=2P_{\alpha\alpha\beta\beta}-\tfrac{1}{2}\sum_{\gamma}(R_{\alpha\alpha\gamma\gamma}+R_{\gamma\gamma\beta\beta}). \quad (2.34)$$

The significance of this feature is most clearly seen when the Zeeman levels are composed of only two levels, say

TABLE III. Coefficients $U_{\alpha\beta,\gamma\delta}\tau_c g^2$ of the transformation $\sigma_{\alpha\alpha}-\sigma_{\beta\beta}\rightarrow \Sigma I_m\{D_{\beta\alpha}{}^{+}\sigma_{\alpha\beta}\}$. In this table the symbol s indicates $\sin\theta$, and each value is divided by $\tau_c g^2$.

$\alpha\beta$ \ $\gamma\delta$	12	12′	23	2′3
12	$\frac{9-7s}{2(1-s)}$	$\frac{7}{2}$	$-\frac{19-13s}{6(1-s)}$	$-\frac{13}{5}$
12′	$\frac{7}{2}$	$\frac{9+7s}{2(1+s)}$	$-\frac{13}{6}$	$-\frac{19+13s}{6(1+s)}$
23	$-\frac{19-13s}{6(1-s)}$	$-\frac{13}{6}$	$\frac{9-7s}{2(1-s)}$	$\frac{7}{2}$
2′3	$-\frac{13}{6}$	$-\frac{19+13s}{6(1+s)}$	$\frac{7}{2}$	$\frac{9+7s}{2(1+s)}$

α and β, where we can put $\gamma=0$ in Eq. (2.34) and thus obtain the relation,

$$R_{\alpha\beta\alpha\beta}=R_{\alpha\alpha\beta\beta}. \tag{2.35}$$

In such cases, Bloembergen's assumption, $T_1=T_2$ for liquids, is valid.

3. EFFECTS OF rf FIELD

All phenomena produced by the rf field can be included by introducing explicitly into the Hamiltonian, a term $\hbar\mathbf{E}_{\rm rf}$, the interaction of the spin system with the rf field. This results in an equation of motion for the density matrix

$$d\sigma_{\alpha\alpha'}/dt=-i[E_0+E_{\rm rf},\sigma]_{\alpha\alpha'}+\sum_{\beta\beta'}R_{\alpha\alpha'\beta\beta'}(\sigma_{\beta\beta'}-\sigma_{\beta\beta'}{}^{(T)}), \tag{3.1}$$

where

$$E_{\rm rf}=-\tfrac{1}{2}\sum_{\alpha,\beta}H_1(\omega_{\alpha\beta}')[(\gamma_A I_A{}^{\pm}+I_B{}^{\pm})\exp(\pm i\omega_{\alpha\beta}'t)] \tag{3.2}$$

and $H_1(\omega_{\alpha\beta}')$ in Eq. (3.2) refers to the intensity of the rf field whose angular frequency $\omega_{\alpha\beta}'$ is near the resonance frequency, $\omega_{\alpha\beta}$. The symbol $\sum$ in Eq. (3.2) is used in order to indicate that the present treatment may include a multiple resonance. Equation (3.1) will give correct results whenever $\mathbf{E}_{\rm rf}$ is so small that the higher-order contributions can be neglected; that is, when the "weak field" condition

$$\gamma H_1(\omega_{ij}')\ll|\omega_{ij}-\omega_{kl}|\ll\omega_{ij} \tag{3.3}$$

is satisfied.

Because of this condition, the effect of the rf field is appreciable only when ω' is near to ω. On retaining only the effective terms in Eq. (3.1) and denoting the periodic part of the density matrix explicitly as

$$\sigma_{\alpha\beta}=\sigma_{\alpha\beta}{}^{*}\exp(i\omega_{\alpha\beta}'t), \tag{3.4}$$

the stationary-state equation for $\sigma_{\alpha\alpha'}{}^{*}$, where $\alpha'=\alpha-1$, is obtained

$$(iR_{\alpha\alpha'\alpha\alpha'}-\Delta_{\alpha\alpha'})\sigma_{\alpha\alpha'}{}^{*}+D_{\alpha\alpha'}{}^{-}(\sigma_{\alpha'\alpha'}-\sigma_{\alpha\alpha})+[D_{\alpha,\alpha+1}{}^{-}\sigma_{\alpha+1,\alpha-1}{}^{*}-D_{\alpha-2,\alpha-1}{}^{-}\sigma_{\alpha,\alpha-2}{}^{*}]=0. \tag{3.5}$$

Here we have used the abbreviations

$$D_{\alpha\beta}{}^{\pm}\equiv\tfrac{1}{2}(\alpha|\gamma_A I_A{}^{\pm}+\gamma_B I_B{}^{\pm}|\beta)H_1(\omega_{\alpha\beta}'),$$

and

$$\Delta_{\alpha\beta}\equiv\omega_{\alpha\beta}'-\omega_{\alpha\beta}.$$

Since the matrix elements in the bracket in Eq. (3.5) are assumed to be zero or, at best, very small, the terms in this bracket will be neglected. However, if by any reason such terms are appreciable, an interesting phenomenon will be observed as discussed in Sec. V. We note that the element $\sigma_{\alpha\alpha'}$ gives a nuclear magnetization in the $x-y$ plane at the resonance $\alpha'\leftrightarrow\alpha$. At first glance, a saturation term would not appear to be contained in Eq. (3.5); it is however implicitly included through the term $\sigma_{\alpha'\alpha'}-\sigma_{\alpha\alpha}$.

The dependence of the diagonal elements on the magnitude of the rf field is shown by substituting the off-diagonal elements for them. Thus the stationary-state equation for the diagonal element $\sigma_{\alpha\alpha}$ is

$$d\sigma_{\alpha\alpha}/dt=\sum R_{\alpha\alpha\beta\beta}(\sigma_{\beta\beta}-\sigma_{\beta\beta}{}^{(T)})+2\mathcal{I}_m\{D_{\alpha,\alpha+1}{}^{-}\sigma_{\alpha+1,\alpha}{}^{*}\}-2\mathcal{I}_m\{D_{\alpha-1,\alpha}{}^{-}\sigma_{\alpha,\alpha-1}{}^{*}\}=0, \tag{3.6}$$

where the relation $\sigma_{\beta\alpha}{}^{*}=\sigma_{\alpha\beta}{}^{*\dagger}$ is used. Elimination of the diagonal elements from Eqs. (3.5) and (3.6) results in a pair of equations for the off-diagonal elements only,

$$[\Delta_{\alpha\alpha'}{}^{2}+R_{\alpha\alpha'\alpha\alpha'}{}^{2}]\mathcal{I}_m\{\sigma_{\alpha\alpha'}{}^{*}\}+\mathcal{I}_m\{(\Delta_{\alpha\alpha'}+iR_{\alpha\alpha'\alpha\alpha'})D_{\alpha\alpha'}{}^{+}\}\times\sum_{\beta\beta'}U_{\alpha\alpha'\beta\beta'}\mathcal{I}_m\{D_{\beta\beta'}{}^{-}\sigma_{\beta\beta'}{}^{*}\}=\mathcal{I}_m\{(\Delta_{\alpha\alpha'}+iR_{\alpha\alpha'\alpha\alpha'})D_{\alpha\alpha'}{}^{+}\}(\sigma_{\alpha'\alpha'}{}^{(T)}-\sigma_{\alpha\alpha}{}^{(T)}), \tag{3.7a}$$

and

$$[\Delta_{\alpha\alpha'}{}^{2}+R_{\alpha\alpha'\alpha\alpha'}{}^{2}]\mathrm{Re}\{\sigma_{\alpha\alpha'}{}^{*}\}+\mathrm{Re}\{(\Delta_{\alpha\alpha'}+iR_{\alpha\alpha'\alpha\alpha'})D_{\alpha\alpha'}{}^{+}\}\times\sum_{\beta\beta'}U_{\alpha\alpha'\beta\beta'}\mathcal{I}_m\{D_{\beta\beta'}{}^{-}\sigma_{\beta\beta'}{}^{*}\}=\mathrm{Re}\{(\Delta_{\alpha\alpha'}+iR_{\alpha\alpha'\alpha\alpha'})D_{\alpha\alpha'}{}^{+}\}(\sigma_{\alpha'\alpha'}{}^{(T)}-\sigma_{\alpha\alpha}{}^{(T)}), \tag{3.7b}$$

where we used coefficients of a transformation defined as

$$\sigma_{\alpha'\alpha'}-\sigma_{\alpha\alpha}-\sigma_{\alpha'\alpha'}{}^{(T)}+\sigma_{\alpha\alpha}{}^{(T)}=U_{\alpha\alpha'21}\mathcal{I}_m\{D_{12}{}^{-}\sigma_{21}{}^{*}\}+U_{\alpha\alpha'2'1}\mathcal{I}_m\{D_{12'}{}^{-}\sigma_{2'1}{}^{*}\}+U_{\alpha\alpha'32}\mathcal{I}_m\{D_{23}{}^{-}\sigma_{32}{}^{*}\}+U_{\alpha\alpha'32'}\mathcal{I}_m\{D_{2'3}{}^{-}\sigma_{32'}{}^{*}\}. \tag{3.8}$$

When the relaxation is assumed to be caused by the spin-spin interaction which satisfies the condition of the "short" correlation time, $\omega\tau_c\ll1$, the transformation coefficients $U_{\alpha\alpha'\beta\beta'}$ are estimated as shown in the Table III. From the Eqs. (3.7a) and (3.7b), we obtain

the off-diagonal elements for the case of a single resonance,

$$\sigma_{\alpha\alpha'}=\tfrac{1}{2}(\sigma_{\alpha'\alpha'}{}^{(T)}-\sigma_{\alpha\alpha}{}^{(T)})$$

$$\times\frac{(\Delta_{\alpha\alpha'}+iR_{\alpha\alpha'\alpha\alpha'})\mathfrak{I}_{\alpha\alpha'}H_1(\omega_{\alpha\alpha'})}{\Delta_{\alpha\alpha'}{}^2+R_{\alpha\alpha'\alpha\alpha'}{}^2-\frac{1}{4}R_{\alpha\alpha'\alpha\alpha'}U_{\alpha\alpha'\alpha\alpha'}\mathfrak{I}_{\alpha\alpha'}H_1{}^2(\omega_{\alpha\alpha'})},\quad(3.9)$$

where $\mathfrak{I}_{\alpha\alpha'}$ is the relative intensity of the resonance $\alpha'\leftrightarrow\alpha$, which in this case is given by $\mathfrak{I}_{\alpha\alpha'}=1-\sin2\theta$ for the outer lines; $\mathfrak{I}_{\alpha\alpha'}=1+\sin2\theta$ for the central lines. In Fig. 2, the spectrum of the two-spin system is shown for $\gamma_A=\gamma_B$. If we define the effective relaxation times for the line $\alpha'\leftrightarrow\alpha$ as

$$T_{1\alpha\alpha'}=\tfrac{1}{4}\mathfrak{I}_{\alpha\alpha'}U_{\alpha\alpha'\alpha\alpha'}\quad(3.10a)$$

$$T_{2\alpha\alpha'}=-R_{\alpha\alpha'\alpha\alpha'}{}^{-1},\quad(3.10b)$$

Eq. (3.9) will assume a form equivalent with the phenomenological equation derived by Bloch.[5,21] The effective longitudinal relaxation times in any multiplet lines of the nuclear magnetic resonance spectrum is strongly dependent on the ratio $J/\delta\nu_0$ and, when the $U_{\alpha\alpha'\alpha\alpha'}$ are assumed to be equivalent over all component lines, $T_{1\alpha\alpha'}$ is proportional to the relative intensity $\mathfrak{I}_{\alpha\alpha'}$; this is quite understandable in view of the fact that the transition probability of the induced transition depends on this ratio.

4. EVALUATION OF THE RELAXATION MATRIX

Using an interaction operator of the form

$$\mathbf{G}(t)=\sum_\mu\mathbf{F}^{-\mu}(t)\mathbf{K}^\mu,\quad(4.1)$$

Redfield[9] gave the relaxation matrix as

$$R_{\alpha\alpha'\beta\beta'}=j_{\alpha\beta'\alpha'\beta'}(\omega_{\alpha'\beta'})+j_{\alpha\beta\alpha'\beta'}(\omega_{\alpha\beta})-\delta_{\alpha'\beta'}\sum_\gamma j_{\gamma\beta\gamma\alpha}(\omega_{\gamma\beta})$$
$$-\delta_{\alpha\beta}\sum_\gamma j_{\gamma\alpha'\gamma\beta'}(\omega_{\gamma\beta'}),\quad(4.2)$$

where $\mathbf{K}^\mu$ is a spin operator associated with the μ-quantum flip and $\mathbf{F}^{-\mu}$ is the corresponding operator of the external bath system. The matrix elements $j_{\alpha\alpha'\beta\beta'}(\omega)$ were given by

$$j_{\alpha\alpha'\beta\beta'}(\omega)=\sum_\mu K_{\alpha\alpha'}{}^\mu K_{\beta\beta'}{}^\mu k_\mu(\omega),\quad(4.3)$$

where $k_\mu(\omega)$ is the spectral density

$$\tfrac{1}{2}\int_{-\infty}^{\infty}\langle F^{-\mu\dagger}(t)F^{-\mu}(t-\tau)\rangle\exp(i\omega t)\,d\tau.\quad(4.4)$$

By assuming that the integrand in integral (4.4) may be expressed

$$\langle F^{-\mu\dagger}(t)F^{-\mu}(t-\tau)\rangle=\langle\langle|F^{-\mu}(0)|^2\rangle\rangle$$
$$\times\exp(-|\tau|/\tau_c),\quad(4.5)$$

[21] F. Bloch, Phys. Rev. **70**, 460 (1946).

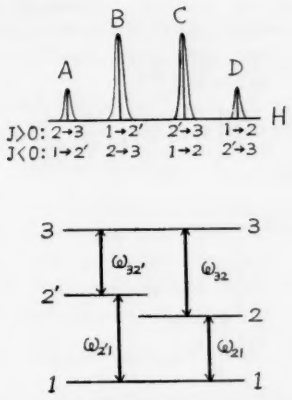

FIG. 2. The spectrum and the energy level diagram of a two-spin system.

(4.4) is evaluated as

$$k_\mu(\omega)=\langle\langle|F^{-\mu}(0)|^2\rangle\rangle[\tau_c/(1+\omega^2\tau_c{}^2)].\quad(4.6)$$

For the dipolar interaction $\hbar\mathbf{E}_d$, the product form of Eq. (4.1) was given by Bloembergen[1] as

$$\mathbf{E}_d=A+B+C+D+E+F,\quad(4.7)$$

where

$$A=I_{ZA}I_{ZB}\cdot g[1-3n^2(t)]$$

$$B=\tfrac{1}{4}(I_{+A}I_{-B}+I_{-A}I_{+B})\cdot g[1-3n^2(t)]$$

$$C=(I_{ZA}I_{+B}+I_{+A}I_{ZB})\cdot g[-\tfrac{3}{2}n(t)\{l(t)+im(t)\}]$$

$$D=(I_{ZA}I_{-B}+I_{-A}I_{ZB})\cdot g[-\tfrac{3}{2}n(t)\{l(t)-im(t)\}]$$

$$E=I_{+A}I_{+B}\cdot g[-\tfrac{3}{4}\{l(t)+im(t)\}^2]$$

$$F=I_{-A}I_{-B}\cdot g[-\tfrac{3}{4}\{l(t)-im(t)\}^2],$$

and

$$g=\hbar\gamma_A\gamma_B/b^3.$$

Also,

$$\langle\langle|F^0(0)|^2\rangle\rangle=\tfrac{4}{5}g^2$$

$$\langle\langle|F^{\pm1}(0)|^2\rangle\rangle=\tfrac{3}{10}g^2$$

$$\langle\langle|F^{\pm2}(0)|^2\rangle\rangle=\tfrac{3}{10}g^2.$$

Another contribution from the second term of Eq. (2.7) is evaluated by considering, at first, the property of the shielding tensor $\boldsymbol{\epsilon}^s$. With Eq. (2.7), we can easily obtain the equation

$$\mathbf{E}_\epsilon=\tfrac{1}{2}\gamma_AH_0\{2I_{ZA}\epsilon_A{}^0(t)+I_{+A}\epsilon_A{}^-(t)+I_{-A}\epsilon_A{}^+(t)\}$$
$$+\tfrac{1}{2}\gamma_BH_0\{2I_{ZB}\epsilon_B{}^0(t)+I_{+B}\epsilon_B{}^-(t)+I_{-B}\epsilon_B{}^+(t)\},\quad(4.8)$$

where, if we denote the anisotropic tensor which is expressed in a space-fixed (Cartesian) coordinate

TABLE IV. Relaxation matrix of a two-spin system AB.

$$R_{\alpha\alpha\beta\beta'}=R_{\beta\beta\alpha\alpha'}=\frac{3}{20}\frac{\tau_c\gamma_\beta^2}{1+\tau_c^2\omega_{\alpha\beta}^2}\mathfrak{J}_{\alpha\beta}$$

$$R_{\alpha\beta\alpha\beta'}=R_{\beta\alpha\beta\alpha'}=-\frac{\tau_c\gamma_\beta^2}{40}\left[14+\left\{13+\frac{4}{1+\tau_c^2\omega_{\alpha\beta}^2}\right\}\mathfrak{J}_{\alpha\beta}\right]$$

for $\alpha=\beta-1$,

$$R_{1133'}=R_{3311'}=\frac{3}{5}\frac{\tau_c\gamma_2^2}{1+\tau_c^2\omega_{31}^2}$$

$$R_{1313'}=R_{3131'}=-\frac{\tau_c\gamma_2^2}{10}\left[10-\frac{1}{1+\tau_c^2\omega_{31}^2}\right]$$

$$R_{2'22'2}=R_{22'2'2'}=\frac{1}{10}\frac{\tau_c\gamma_2^2\cos^2 2\theta}{1+\tau_c^2\omega_{22'}^2}$$

$$R_{22'22'}=R_{2'22'2'}=-\frac{\tau_c\gamma_2^2}{10}\left[5-\frac{1}{1+\tau_c^2\omega_{22'}^2}\right]$$

$$R_{\alpha\alpha\alpha\alpha'}=-\sum_\gamma{}'{}^{a}R_{\alpha\alpha\gamma\gamma'}\qquad(\gamma\neq\alpha)$$

$$R_{\alpha\alpha\beta\beta}''=R_{\beta\beta\alpha\alpha}''=\frac{\tau_c H_0^2}{1+\tau_c^2\omega_{\alpha\beta}^2}[(1\mp\cos 2\theta)\langle\langle|\epsilon_A{}^+|^2\rangle\rangle+(1\pm\cos 2\theta)\langle\langle|\epsilon_B{}^+|^2\rangle\rangle]$$

$$R_{\alpha\beta\alpha\beta}''=R_{\beta\alpha\beta\alpha}''=-\frac{\tau_c}{4}H_0^2[(1\mp\cos 2\theta)^2\langle\langle|\epsilon_A{}^0|^2\rangle\rangle+(1\pm\cos 2\theta)^2\langle\langle|\epsilon_B{}^0|^2\rangle\rangle]-\tfrac{1}{2}\sum_\gamma{}'(R_{\alpha\alpha\gamma\gamma}''+R_{\beta\beta\gamma\gamma}'')$$

where the upper signs are used for $\alpha\beta=12$ and $2'3$ and the lower signs are used for $\alpha\beta=12'$ and 23

$$R_{1133}''=R_{3311}''=R_{222'2'}''=R_{2'2'22}''=0$$

$$R_{1313}''=R_{3131}''=-\tfrac{1}{2}\sum_\gamma{}'(R_{11\gamma\gamma}''+R_{22\gamma\gamma}'')$$

$$R_{22'22'}''=R_{2'22'2}''=-\tau_c H_0^2[\langle\langle|\epsilon_A{}^0|^2\rangle\rangle+\langle\langle|\epsilon_B{}^0|^2\rangle\rangle]-\tfrac{1}{2}\sum_\gamma{}'(R_{22\gamma\gamma}''+R_{2'2'\gamma\gamma}).$$

[a] The prime symbol used on Σ indicates that the terms $R_{\alpha\alpha\alpha\alpha}$ and $R_{\beta\beta\beta\beta}$ etc. are omitted from the summation.

system $\mathbf{q}(x, y, z)$ as $\mathfrak{e}^s$, the operators ϵ^0, ϵ^+, and ϵ^- are given as

$$\epsilon^0=\epsilon_{zz}{}^s$$

$$\epsilon^\pm=\epsilon_{xz}{}^s\pm\varepsilon i_{yz}{}^s \tag{4.9}$$

From the assumption of the random fluctuation of ϵ^0 and $\epsilon^\pm$, with (4.5) and (4.4), we obtain the operator $\mathbf{j}$ which has been given by Eq. (4.3) as

$$j_{\alpha\alpha'\beta\beta'}(\omega)=H_0^2\frac{\tau_c}{1+\omega^2\tau_c^2}\sum_\mu\sum_{i=A}^{B}\langle\langle|\epsilon_i{}^{-\mu}(0)|^2\rangle\rangle I_{\alpha\alpha'i}{}^\mu I_{\beta\beta'i}{}^\mu. \tag{4.10}$$

In order to evaluate the mean value $\langle\langle|\epsilon_i{}^{-\mu}(0)|^2\rangle\rangle$, the shielding tensor $\mathfrak{e}^s$ must be given in terms of the molecular fixed coordinate system $Q(X, Y, Z)$ which diagonalizes the tensor $\mathfrak{e}^m$,[22] whose principal values are ϵ_X, ϵ_Y, and ϵ_Z.

If we define a matrix $\mathbf{L}$ by the transformation

$$\mathbf{q}=\mathbf{L}\mathbf{Q}, \tag{4.11}$$

[22] We assume here that the two tensors ϵ_A' and ϵ_B' are mutually so far separated that we can treat them independently.

$\mathfrak{e}^s$ will be expressed in terms of $\mathfrak{e}^m$ as

$$\mathfrak{e}^s=\mathbf{L}\mathfrak{e}^m\mathbf{L}^-. \tag{4.12}$$

The elements of the matrix $\mathbf{L}$ are given by

$$\mathbf{L}=\begin{vmatrix} l_X & l_Y & l_Z \\ m_X & m_Y & m_Z \\ n_X & n_Y & n_Z \end{vmatrix}, \tag{4.13}$$

where $l_X, l_Y, \cdots, n_Y$, and n_Z are the direction cosines of the x, y, and z axes to the X, Y, and Z axes. The matrix $\mathbf{L}$ has randomly fluctuating elements, and therefore, the mean of ϵ^μ will be conveniently evaluated by the use of Eulerian angles. Thus one obtains

$$\langle\langle|\epsilon^0(0)|^2\rangle\rangle$$
$$=\tfrac{1}{8}\{\tfrac{9}{8}(\epsilon_X{}^2+\epsilon_Y{}^2)+3\epsilon_Z{}^2+\tfrac{3}{4}\epsilon_X\epsilon_Y+(\epsilon_Y\epsilon_Z+\epsilon_Z\epsilon_X)\} \tag{4.14a}$$

and

$$\langle\langle|\epsilon^+(0)|^2\rangle\rangle=\langle\langle|\epsilon^-(0)|^2\rangle\rangle$$
$$=\tfrac{1}{8}\{\tfrac{7}{8}(\epsilon_X{}^2+\epsilon_Y{}^2)+\epsilon_Z{}^2-\tfrac{3}{4}\epsilon_X\epsilon_Y-(\epsilon_Y\epsilon_Z+\epsilon_Z\epsilon_X)\}. \tag{4.14b}$$

If $\mathfrak{e}^m$ is axially symmetric and its principal values, parallel and perpendicular to the symmetry axis, are

denoted by $\epsilon_{||}$ and $\epsilon_{\perp}$, respectively, the relations (4.14a) and (4.14b) are further reduced to

$$\langle\langle|\epsilon^0(0)|^2\rangle\rangle=\tfrac{1}{8}\{(\epsilon_{\perp}+\epsilon_{||})^2+(\epsilon_{\perp}^2+\epsilon_{||}^2)\}, \quad (4.15a)$$

and

$$\langle\langle|\epsilon^+(0)|^2\rangle\rangle=\langle\langle|\epsilon^-(0)|^2\rangle\rangle=\tfrac{1}{8}(\epsilon_{\perp}-\epsilon_{||})^2. \quad (4.15b)$$

Thus the relaxation matrix $\mathbf{R}$ is given by

$$\mathbf{R}=\mathbf{R}'+\mathbf{R}'', \quad (4.16)$$

where $\mathbf{R}'$ and $\mathbf{R}''$ are the contributions from $\mathbf{E}_d$ and $\mathbf{E}_\epsilon$, respectively. The elements of $\mathbf{R}'$ and $\mathbf{R}''$ are summarized in Table IV.

5. DISCUSSION

A. On the Mechanism of the Relaxation

From the point of view of the origin, the nuclear spin relaxation may be classified into two types; the first type of relaxation occurs by nuclear spin-nuclear spin interactions within a molecule or a system, and the second one by interactions with a local magnetic field around a system, including nuclear spin-nuclear spin interactions with other molecules. The former was discussed in detail in the preceding sections and therefore is not further explained here. In the latter case, the local fields may be of intra-and extramolecular origins. In diamagnetic substances, the largest contribution to the intramolecular local field will come from a secondary magnetic field induced by the surrounding electrons, that is, the anisotropic shielding effect, which may be roughly estimated by the magnitude of the paramagnetic term in the shielding tensor $\boldsymbol{\varepsilon}$ as $10^{-5}\sim10^{-6}$ of the external magnetic field for the case of proton resonance. The intermolecular spin-spin interactions will be the most effective cause of the extramolecular local field, often even larger than the intramolecular spin-spin interactions.[23] There are other possible causes of the local fields. A secondary field may arise due to a diamagnetic circulation of electrons in aromatic substances[24] or due to the deformation of the orbitals of surrounding electrons caused by electrostatic or van der Waals' interactions. Complex formations with neighboring molecules, etc., may account for the secondary field. Such effects may be, at best, comparable to that of the anisotropic shielding discussed above.

The aforementioned classification may be taken as a convenient and superficial concept to show that the spin-relaxation depends in different ways on the ratio $J/\delta\nu_0$, and, hence, the shapes of multiplet lines depend on the type of relaxation. Therefore, we can obtain information about the origin of the relaxation by analyzing the shape of NMR multiplets.[25]

To show this procedure explicitly, the signal intensity

$$S_{\alpha\alpha'}=\hbar N(d/dt)\mathrm{Tr}\{\sum_i\gamma_i I_{+i}\sigma_{\alpha\alpha'}(t)\}$$

$$=i\hbar N\omega_{\alpha\alpha'}\mathfrak{J}_{\alpha\alpha'}{}^{\frac{1}{2}}\sigma_{\alpha\alpha'} \quad (5.1)$$

is obtained, where N is the number of nuclear spins per unit volume. If H_1 is sufficiently small so that the term proportional to H_1^2 in the denominator of (3.9) can be neglected, the maximum height of the signal, $S_{\alpha\alpha'}{}^0$ may be expressed, using Eqs. (3.9) and (5.1) ,by

$$S_{\alpha\alpha'}{}^0=\mathfrak{J}_{\alpha\alpha'}\cdot T_{2\alpha\alpha'}(\sigma_{\alpha'\alpha}{}^{(T)}-\sigma_{\alpha\alpha}{}^{(T)})H_1. \quad (5.2)$$

The height $S_{\alpha\alpha'}{}^0$ will be proportional to the theoretical relative intensity of the line, provided that the effective transverse relaxation times of all component lines are equivalent. From Eqs. (3.10a), (3.10b), and Table IV, one obtains

$$T_{2\alpha\alpha'}{}'=40/\tau_c g^2(14+17\mathfrak{J}_{\alpha\alpha'}) \quad (5.3a)$$

for the spin-spin type relaxation and

$$T_{2\alpha\alpha'}{}''=2/\tau_c[(1+\cos^2 2\theta)\langle\langle|H_z'|^2\rangle\rangle+\langle\langle|H_+'|^2\rangle\rangle] \quad (5.3b)$$

for the local-field type relaxation, where the local fields H' at nuclei A and B are assumed to be equivalent, and H_+', the anisotropy of the local field, is $H_z'-H_{x-y}'$. Since this assumption is physically justified[26] except in special cases, we will confine ourselves to the consideration of equivalent local fields in the following discussion.

Since $T_{2\alpha\alpha'}{}'$ is a function of $\mathfrak{J}_{\alpha\alpha'}$ whereas $T_{2\alpha\alpha'}{}''$ is not, we can determine the relaxation type by comparing $S_{\alpha\alpha'}{}^0$ with $\mathfrak{J}_{\alpha\alpha'}$. The relations (5.1), (5.2), (5.3a), and (5.3b) result in the relation

$$S_{\mathrm{out}}{}^0/S_{\mathrm{cent}}{}^0\geqq\mathfrak{J}_{\mathrm{out}}/\mathfrak{J}_{\mathrm{cent}}. \quad (5.4)$$

The suffixes "out" and "cent" indicate the outer line and the central line, respectively, and the equality is satisfied when $T_2'\ll T_2''$ or $J/\delta\nu_0\ll1$, where $S_{\alpha\alpha'}{}^0$ is used in place of $\mathfrak{J}_{\alpha\alpha'}$. The effective longitudinal relaxation times $T_{1\alpha\alpha'}{}'$ and $T_{1\alpha\alpha'}{}''$ are dependent on $\mathfrak{J}_{\alpha\alpha'}$;

$$T_{1\alpha\alpha'}{}'=(2+7\mathfrak{J}_{\alpha\alpha'})/2\tau_c g^2 \quad (5.5a)$$

and

$$T_{1\alpha\alpha'}{}''=\mathfrak{J}_{\alpha\alpha'}/4\tau_c\langle\langle|H_+'|^2\rangle\rangle. \quad (5.5b)$$

By analogy to the phenomenological Bloch equation,[21] the saturation parameter is given by

$$\mathfrak{S}_{\alpha\alpha'}=T_{1\alpha\alpha'}\cdot T_{2\alpha\alpha'}\cdot H_1^2(\omega_{\alpha\alpha'}) \quad (5.6a)$$

[23] G. W. Nederbragt and C. A. Reilly, J. Chem. Phys. **24**, 1110 (1956).
[24] J. A. Pople, J. Chem. Phys. **24**, 1111 (1956).
[25] In the following discussion we assume that the two-spin system is composed of the nuclei belonging to the same species.
[26] W. A. Anderson, Phys. Rev. **104**, 850 (1956).

from which at resonance,

$$\mathfrak{S}_{\alpha\alpha'}=\frac{140H_1^2}{17\tau_c^2g^2}\left\{1-\frac{64}{7(14+17\mathfrak{J}_{\alpha\alpha'})}\right\} \qquad (5.6b)$$

and

$$\mathfrak{S}_{\alpha\alpha'}''=\frac{\gamma^2H_1^2\mathfrak{J}_{\alpha\alpha'}}{2\tau_c^2\langle\langle|H_+'|^2\rangle\rangle\{(1+\cos^2 2\theta)\langle\langle|H_Z'|^2\rangle\rangle+\langle\langle|H_+'|^2\rangle\rangle\}} \qquad (5.6c)$$

for the spin-spin type and the local field type relaxation, respectively. Here, $\mathfrak{S}_{\alpha\alpha'}''$ is more sharply dependent on $\mathfrak{J}_{\alpha\alpha'}$ than $\mathfrak{S}_{\alpha\alpha'}$.

There has been no experiment giving the relation between $\mathfrak{J}_{\alpha\alpha'}$ and $T_{2\alpha\alpha'}$ in the system of $J/\nu\delta_0\sim1$. Furthermore, the experimental results of the two-spin system of chloro-bromothiophene was explained only in terms of $\mathbf{R}''$.[26] The question of whether the condition $\mathbf{R}'<\mathbf{R}''$ is really satisfied or not in many solutions can be resolved by measuring a sample magnetically diluted with an indifferent solvent such as CS_2.

B. The Sign Determination of Spin-Coupling Constant

The nuclear magnetic resonance spectrum of a two-spin system is not affected by the sign of the spin-coupling constant, although the energy levels are affected as shown by Table I. Therefore, one can not determine the sign of the spin-coupling constant J by simply analyzing the spectrum obtained under ordinary conditions. In Fig. 2, the outer lines A and D correspond, respectively, to the transitions $2\rightarrow3$ and $1\rightarrow2$, and the central lines B and C to $1\rightarrow2'$ and $2'\rightarrow3$, if J is positive; if J is negative, A, D, B, and C correspond to $1\rightarrow2'$, $2'\rightarrow3$, $2\rightarrow3$, and $1\rightarrow2$, respectively. From Table I, one sees that the relation $E_2<E_{2'}$ is satisfied independent of the sign of J. Thus, the determination of the sign of J is effectively equivalent to identifying the energy level constructions (a) and (b) in Fig. 3.

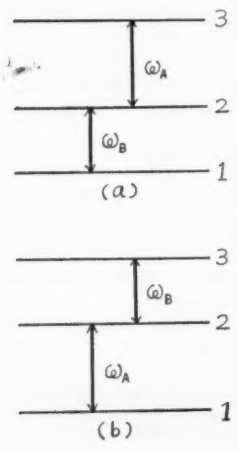

FIG. 3. The two nonequivalent constructions of the energy levels of systems which give identical spectra.

A first possible method is to study resonance at a very low temperature. Under such conditions one can expect that $\mathfrak{J}_{\alpha,\alpha-1}=\mathfrak{J}_{\alpha+1,\alpha}$ will no longer hold as it is does under ordinary conditions, but that the relation $\mathfrak{J}_{\alpha,\alpha-1}>\mathfrak{J}_{\alpha+1,\alpha}$ will be satisfied. In practice, however, this method is severely limited by the difficulty in holding a sample in the liquid state at such a low temperature.

The second possible method arises in the case of multiple resonance. Here one utilizes the relations in the bracket in Eq. (3.5). These terms appearing in the bracket were already discussed by Anderson[27] and interpreted in terms of Raman-like processes. The effects of the process $E_{\rm rf}(\omega_{\alpha,\alpha-1}')\sigma_{\alpha+1,\alpha-1}$ on $\sigma_{\alpha+1,\alpha}$ and $\mathbf{E}_{\rm rf}(\omega_{\alpha+1,\alpha}')\sigma_{\alpha+1,\alpha-1}$ on $\sigma_{\alpha,\alpha-1}$ are not equivalent, but inverted in action. If $\sigma_{\alpha+1,\alpha-1}$ is positive, $\mathbf{E}_{\rm rf}(\omega_{\alpha,\alpha-1}')\sigma_{\alpha+1,\alpha-1}$ weakens $\sigma_{\alpha+1,\alpha}$ whereas $\mathbf{E}_{\rm rf}(\omega_{\alpha+1,\alpha}')\sigma_{\alpha+1,\alpha-1}$ enhances $\sigma_{\alpha,\alpha-1}$, however, if $\sigma_{\alpha+1,\alpha-1}$ is negative, the effects of these processes are reversed. Using this phenomenon, one can identify the case (a) and (b); in the case of (a), where $\sigma_{\alpha+1,\alpha+1}>0$, $\mathbf{E}_{\rm rf}(\omega_a')$ weakens the resonance at ω_b and $\mathbf{E}_{\rm rf}(\omega_b')$ enhances the resonance at ω_a, whereas in the case (b), the situation is reversed.

The conditions required to determine the sign of J are thus, to have a nonzero element $\sigma_{\alpha+1,\alpha-1}$ and then to know its sign. The matrix element $\sigma_{\alpha+1,\alpha-1}$ represents a correlation induced between the phases of the states of $\Delta m=\pm2$. In an ordinary resonance, $\sigma_{\alpha+1,\alpha-1}$ will be zero or very small. We can, however, enhance it by means of a double resonance or a double quantum transition induced by a strong rf field at $\omega=\frac{1}{2}(\omega_{\alpha+1,\alpha}+\omega_{\alpha,\alpha-1})$.

When two rf fields $\mathbf{E}_{\rm rf}(\omega_{\alpha+1,\alpha})$ and $\mathbf{E}_{\rm rf}(\omega_{\alpha,\alpha-1})$ are applied for the stationary state, the equation of motion of $\sigma_{\alpha+1,\alpha-1}$ is

$$(\Delta_{\alpha+1,\alpha-1}-iR_{\alpha+1,\alpha-1,\alpha+1,\alpha-1})\sigma_{\alpha+1,\alpha-1}=D_{\alpha+1,\alpha}{}^{+}D_{\alpha,\alpha-1}{}^{+}(2\sigma_{\alpha\alpha}-\sigma_{\alpha-1,\alpha-1}-\sigma_{\alpha+1,\alpha+1}). \qquad (5.7)$$

The lack of information regarding the sign of $\sigma_{\alpha+1,\alpha-1}$ can be avoided, provided that we use a double quantum transition $\alpha-1\leftrightarrow\alpha+1$ induced by a third strong rf field

$$\mathbf{E}_\omega=-\mathfrak{D}[\exp(i\omega t)(\gamma_AI_{A+}+\gamma_BI_{B+})+\exp(i\omega t)(\gamma_AI_{A-}+\gamma_BI_{B-})]$$

at the angular frequency $\omega=\frac{1}{2}(\omega_A+\omega_B)$. Yatsiv[28] gave an expression for the general case which in our case has the following form:

$$\sigma_{\alpha+1,\alpha-1}{}^{*}=\frac{(\sigma_{\alpha-1,\alpha-1}{}^{(T)}-\sigma_{\alpha+1,\alpha+1}{}^{(T)})W(\Delta-iR)}{\Delta^2+R^2+RU|W^2|} \qquad (5.8)$$

[27] P. W. Anderson, J. Appl. Phys. **28**, 1049 (1957).
[28] S. Yatsiv, Phys. Rev. **113**, 1522 (1959).

for a two-spin system of equivalent nuclear species, where

$$W=(\mathfrak{D}^2/C^2)[(1+\sin\theta)^{-1}\times\{(1+2C\cos^2\theta)^{\frac{1}{2}}+(1-2C\cos^2\theta)^{\frac{1}{2}}\}-(1-\cos\theta)^{-1}\{(1+2C\cos^2\theta)^{\frac{1}{2}}-(1-2C\cos^2\theta)^{\frac{1}{2}}\}],$$

and

$$\mathfrak{D}=\tfrac{1}{4}\gamma H_1(\omega).$$

One must note here that, unlike Eq. (5.7), $\sigma_{\alpha\alpha}$ does not appear in Eq. (5.8), and that the strong rf field affects the component lines $\alpha-1\rightarrow\alpha$ and $\alpha\rightarrow\alpha+1$ in an identical manner. In practice, a better result can be expected, provided that the pair of outer lines is observed, since this pair is less affected by the saturation produced by the rf field than the pair of central lines.

ACKNOWLEDGMENTS

The authors want to express their gratitude to Professor Kenjiro Kambe of the University of Electro-Communications for reading the manuscript and making valuable suggestions for improvement. It is a pleasure also to thank Professor Tyunoshin Ukita and Professor Yonezo Morino for their constant encouragement in the development of this work.

THE JOURNAL OF CHEMICAL PHYSICS VOLUME 34, NUMBER 5 MAY, 1961

Calculation of Pressure Shifts of Optical Absorption Spectra from Solvent Data

W. W. ROBERTSON AND A. D. KING, JR.

Department of Physics, The University of Texas, Austin, Texas

(Received September 26, 1960)

Frequency shifts in the absorption spectra of both polar and nonpolar absorbers have been observed at atmospheric pressure in a range of polar and nonpolar solvents and in pentane and ethanol under hydrostatic pressures up to 5000 atm. McRae's equation representing frequency shifts in terms of solvent refractive index and dielectric constant can be modified by the use of the Debye equation to represent frequency shifts in terms of solvent density. If it is assumed that the volume of the cavity occupied by the absorber remains constant with solvent density, frequency shifts resulting from an increase in hydrostatic pressure can be calculated almost to within the limit of experimental error from solvent shift data.

INTRODUCTION

THE effects of solvents on the frequencies of electronic absorption bands bands have been of interest for many years, and although difficult to express quantitatively, are now well understood in principle.[1-3] In general, the characterizing macroscopic solvent properties are its dielectric constant and index of refraction.

Frequency shifts resulting from an increase in hydrostatic pressure upon an absorbing solution have also been investigated[4] and in principle the effects may be said also to be well understood.[5] Although pressure shifts are usually represented as a sum of pair-wise interactions between an absorber and a solvent molecule,[4,6,7] they have also been correlated with the change in solvent refractive index with pressure, using the Bayliss relation[3] and the density dependence of the solvent index.[8]

A correspondence between solvent frequency shifts and pressure frequency shifts is thus suggested, since each can be represented in terms of the same macroscopic properties of the solvent. This paper investigates this correspondence by calculating pressure shifts from solvent shift data and comparing the results to the experimentally observed pressure shifts.

EXPERIMENTAL

The weak ^1L_b transition of napthalene and the strong ^1B_b transitions of napthacene and azulene were recorded first in five normal hydrocarbons and then in five normal alcohols. Each spectrum was then taken in pentane and in ethanol as the hydrostatic pressure on the solution was increased to 5000 atm. The resulting frequency shift data thus represent both weak and strong transitions of polar and nonpolar absorbers in polar and nonpolar solvents.

The naphthalene, naphthacene, and azulene used in this work were spectroscopically pure in comparison

[1] E. G. McRae, J. Phys. Chem. **61**, 562 (1957).
[2] Y. Ooshika, J. Phys. Soc. Japan **9**, 594 (1954).
[3] N. S. Bayliss, J. Chem. Phys. **18**, 292 (1950).
[4] W. W. Robertson, O. E. Weigang, Jr., and F. A. Matsen, J. Mol. Spectroscopy **1**, 1 (1957).
[5] H. Margenau and W. W. Watson, Revs. Modern Phys. **8**, 22 (1936).
[6] W. W. Robertson and A. D. King, Jr., J. Chem. Phys. **31**, 473 (1959).
[7] S. E. Babb, Jr., J. M. Robinson, and W. W. Robertson, J. Chem. Phys. **30**, 427 (1959).
[8] W. W. Robertson, S. E. Babb, Jr., and O. E. Weigang, Jr., *Proprietés Optiques et Acoustiques des Fluides Comprimes* (Centre National de la Recherche Scientifique, Paris, 1959), p. 293.

with published spectra.[9,10] The hydrocarbons used were Phillips Petroleum Company Research Grade. The alcohols were Eastman White Label or the equivalent.

The short wavelength ^1B_b bands were recorded with sufficient accuracy on a Beckman model DU quartz spectrometer. The ^1L_b bands were recorded photographically on a 3-m grating and the absorption maxima were located on microphotometer tracings of the plates.

The pressure data were obtained using a previously described pressure system[11] in conjunction with either the Beckman DU or the 3-meter grating. The densities of the pentane and ethanol solvents at the various hydrostatic pressures were taken from Danforth.[12]

RESULTS AND DISCUSSION

McRae's[1] investigation of the effects of electric dipole interactions on electronic transition frequencies of solution absorption spectra led to the following simplified equation,

$$\Delta\nu=(AL+B)\left[\frac{n^2-1}{2n^2+1}\right]+C\left[\frac{D-1}{D+2}-\frac{n^2-1}{n^2+2}\right]+F\left[\frac{D-1}{D+2}-\frac{n^2-1}{n^2+2}\right]^2, \quad (1)$$

where A, B, C, and F are constants characteristic of a particular transition of a given light absorber, n is the index of refraction of the solvent, and D its dielectric constant. The first term with the constant A and the "weighted mean wavelength" L represents the induced dipole-induced dipole interaction, the second term with B the solute dipole-solvent induced dipole interaction, the third term the dipole-dipole, and the last term the solvent dipole-solute induced dipole interaction. The solvents used here were straight-chain saturated hydrocarbons and alcohols, chosen for the following reasons. First, the weighted mean wavelength L is approximately the same for the saturated hydrocarbons and alcohols and thus the term $(AL+B)$ will be the same for all of the solvents used for each particular transition. Second, only the normal saturated compounds were used because they gave a smaller scatter of data points from the calculated shifts of Eq. (1) than did the branched chain, cyclic, or unsaturated solvents.

For the hydrocarbon solvents, the third and fourth terms of Eq. (1) are zero, and the constant $K=AL+B$ was determined as the least-squares slope of the curve $\Delta\nu$ vs$[(n^2-1)/(2n^2+1)]$ for each of the transitions. In the alcohol solvents the nonpolar naphthalene and naphthacene would also experience solvent dipole-solute induced dipole interactions and, using the value of K previously determined, a least-squares value of F could be found. The polar azulene in addition experiences dipole-dipole interaction, and thus the constants C and F both had to be determined from the frequency shifts observed in alcohol solvents.

Equation (1) with the experimentally determined constants reproduces the observed frequency shifts with a standard deviation of only a few wave numbers for each of the transitions. The hydrogen bonding of the alcohol solvents makes the interpretation of the last two terms of Eq. (1) somewhat doubtful, but for the present purpose it is sufficient to consider the equation as an empirical representation of the solvent frequency shifts in terms of the parameters n and D.

A combination of the Debye and Lorenz-Lorentz[13] equations allows the solvent density to be introduced into Eq. (1). That is,

$$[(D-1)/(D+2)]-(n^2-1)/(n^2+2)]=\rho\{\tfrac{4}{3}(\pi N/M)[\alpha_a+(\mu^2/3kT)]\}. \quad (2)$$

At constant temperature, the bracketed term in Eq. (2) is practically constant with pressure and may be taken as a constant here.[12,14] Thus Eq. (1) may be rewritten as

$$\Delta\nu=(K'/a^3)[(n^2-1)/(2n^2+1)]+(C'/a^3)\rho+(F'/a^6)\rho^2, \quad (3)$$

where the cavity radius "a" that was included in the constants A, B, C, and F of Eq. (1) has been separately expressed. Since the Lorenz-Lorentz expression can be used to obtain the index of refraction of the solvent at any density ρ from the known value at atmospheric pressure, Eq. (3) with constants from Eq. (1) should predict frequency shifts with solvent density providing the effects of density upon the cavity radius "a" are known. It has seemed reasonable to assume that the volume of the cavity varies inversely with the solvent density, and in nonpolar solvents the frequency shift with density of nonpolar solutes has been found to be represented by the Bayliss relation in the following form,[8]

$$\Delta\nu=(\text{const.})\rho[(n^2-1)/(2n^2+1)]. \quad (4)$$

If this is so, then Eq. (3) should be modified to read

$$\Delta\nu=K''\rho[(n^2-1)/(2n^2+1)]+C''\rho^2+F''\rho^4. \quad (5)$$

Considering the comparatively small range of densities obtained by compressing liquids, together with the inaccuracies inherent in frequency measurements on broad bands, the correctness of Eq. (4) as determined from the linearity of the resulting curve must be considered doubtful. However, with the slope of the curve of $\Delta\nu$ vs$[(n^2-1)(2n^2+1)]$ already determined from

[9] R. A. Friedel and M. Orchin, *Ultraviolet Spectra of Aromatic Compounds* (John Wiley & Sons, Inc., New York, 1951).

[10] D. E. Mann, J. R. Platt, and H. B. Klevens, J. Chem. Phys. **17**, 481 (1949).

[11] D. S. Hughes and W. W. Robertson, J. Opt. Soc. Am. **46**, 557 (1956).

[12] W. E. Danforth, Jr., Phys. Rev. **38**, 1224 (1931).

[13] C. J. F. Bottcher, *Theory of Electric Polarization* (Elsevier Publishing Company, Inc., New York, 1952), p. 184.

[14] A. Michels, *et al.*, Physica **2**, 753 (1935); **1**, 627 (1934); **6**, 596 (1939); **19**, 1011 (1953).

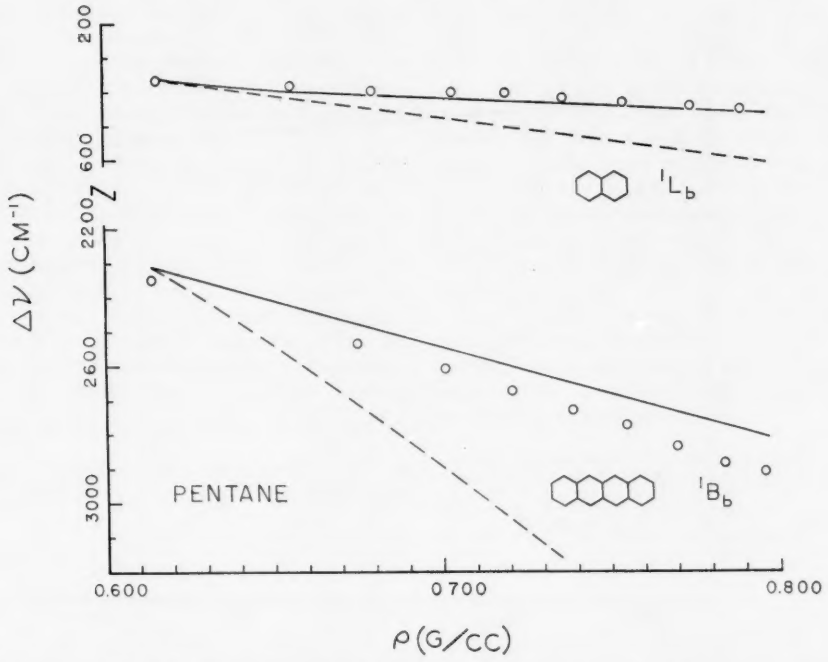

FIG. 1. The frequency shifts of the ^1L_b transition of naphthalene and the ^1B_b transition of naphthacene are shown as functions of the *n*-pentane solvent density. Using the Bayliss relation, the solid curves assume a constant cavity volume for the absorber, the dashed curves a cavity volume that varies inversely as the density ρ. The constants K and K^* are determined from solvent frequency shifts. Circles represent the experimental pressure data. Frequency shifts ($\Delta\nu$) are referred to the vapor absorption frequencies.

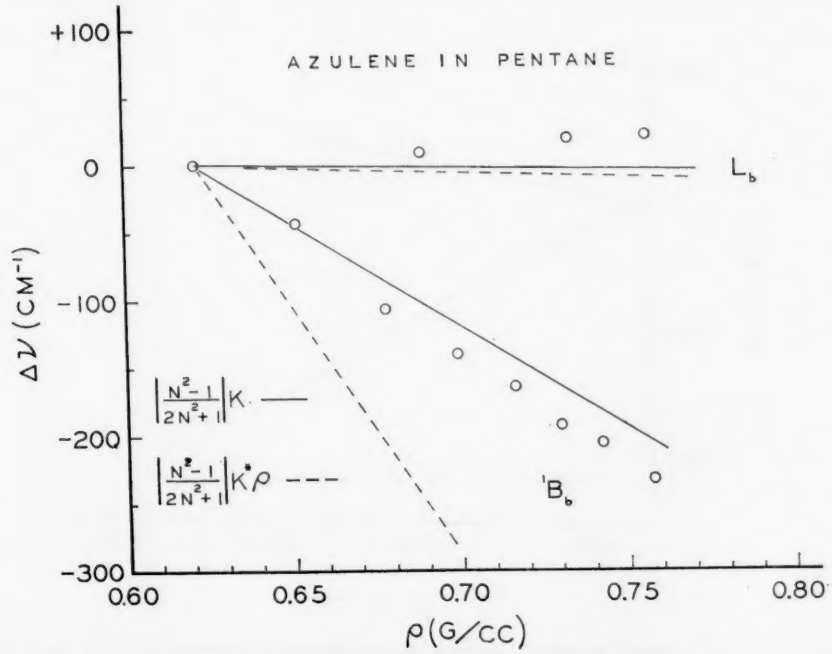

FIG. 2. As in Fig. 1, but for the polar azulene in *n*-pentane, and with the frequency shifts ($\Delta\nu$) being measured from the solution absorption frequencies.

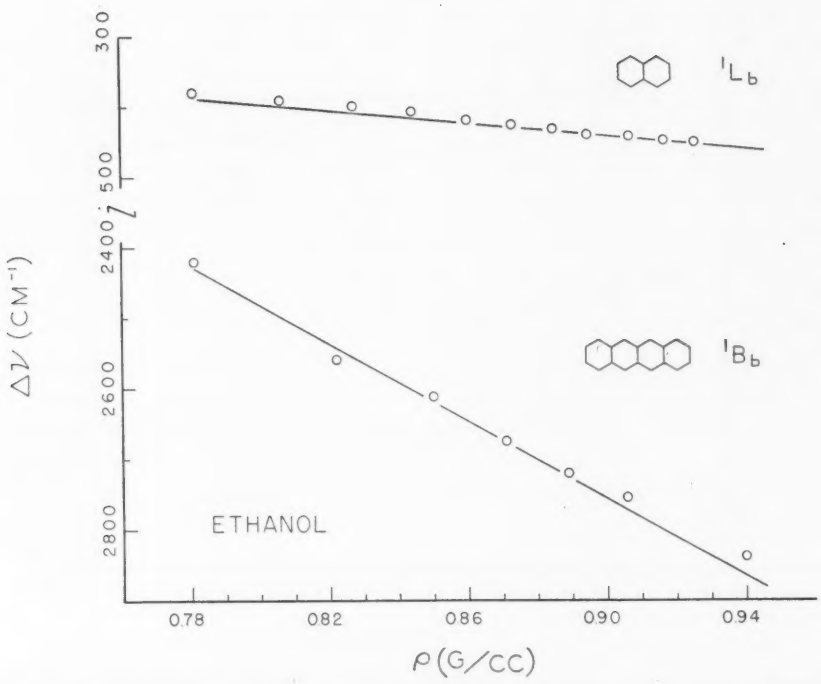

FIG. 3. The pressure frequency shifts calculated from solvent shift data are compared to the experimental pressure data for non-polar absorbers in a polar solvent.

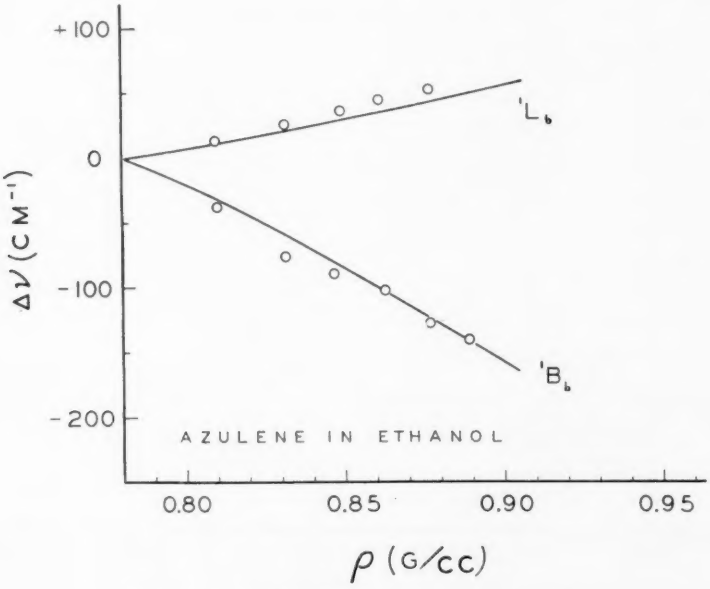

FIG. 4. As in Fig. 3, but for a polar absorber in a polar solvent.

measurements in nonpolar solvents, it can be decided easily enough whether the same equation with the same constant will represent the frequency shift when the variation in refractive index is obtained from compression, or if the density must be included to account for the change in cavity volume.

Figures 1 and 2 show the results of plotting $\Delta\nu = K^*\rho[(n^2-1)(2n^2+1)]$ (dashed curve) and $\Delta\nu = K[(n^2-1)(2n^2+1)]$ (solid curve) for a range of solvent densities ρ. Here $K = K^*\rho_0$, where ρ_0 is the solvent density at atmospheric pressure and K is the constant determined from solvent frequency shifts. The two sets of curves are widely different and the experimental points are found to lie close to the curve where the cavity radius is assumed to be constant with density.

Equation (5) should thus be modified to read

$$\Delta\nu = K[(n^2-1)(2n^2+1)] + C^*\rho + F^*\rho^2, \qquad (6)$$

where C^* and F^* are the solvent shift constants C and F of Eq. (1) modified by a constant in the introduction of the density from Eq. (2). How well this equation will represent pressure shifts of polar or nonpolar light absorbers in polar solvents is shown in Figs. 3 and 4. It is seen that the results of increasing hydrostatic pressure could be predicted almost within the limit of experimental error from solvent shift data. The apparent constancy of the cavity occupied by the absorber is in keeping with the concept of an increase in the population of the various coordination shells of the absorber with increasing solvent density without a decrease in the shell radius, which is a concept well established at least for gases.[15]

It is tempting to suggest that the results of Figs. 1 and 2 indicate a small change of cavity volume with solvent density and that the better results of Figs. 3 and 4 are due to the more rigid structure of the hydrogen-bonding ethanol solvent.

[15] J. O. Hirschfelder, C. F. Curtiss, and R. B. Bird, *Molecular Theory of Gases and Liquids* (John Wiley & Sons, Inc., New York, 1954), p. 323.

Microwave Spectrum of Isobutylene. Dipole Moment, Internal Barrier, Equilibrium Conformation, and Structure

VICTOR W. LAURIE*

National Bureau of Standards, Washington, D. C., and Department of Chemistry, University of California, Berkeley, California

(Received November 21, 1960)

The microwave spectra of isobutylene and isobutylene-*d*-3 have been studied in the region 17–36 kMc. Observed rotational constants (Mc) for isobutylene are $a_0=9133.32$, $b_0=8381.75$, $c_0=4615.99$; for *sym*-isobutylene-*d*-3, $a_0=9132.59$, $b_0=7788.98$, $c_0=4431.05$; for *asym*-isobutylene-*d*-3, $a_0=8819.46$, $b_0=7981.08$, $c_0=4469.59$. The most likely structure compatible with these data is $r_{c-c}=1.50_7$ A, $r_{c=c}=1.34$ A, r_{CH}(methyl) $=1.08_5$ A, r_{CH}(ethylenic) $=1.08_6$ A, $<$Me$-$C$-$Me$=115.9°$, $<$HCH(methyl)$=108°$, $<$HCH(ethylenic)$=117.5°$. Measurements of the Stark effect show that the dipole moment $\mu=0.503\pm0.009$ *D*. Fine structure leads to a barrier height hindering internal rotation of the methyl groups of 2.21 kcal/mole. The equilibrium conformation is C_{2v} with two methyl hydrogens in the plane of the carbon atoms and the CH bonds pointing away from the symmetry axis. It is concluded that although CC single bonds are shortened when adjacent to a double bond, the double bond length is probably not much affected by the presence of an adjacent CH_3 group.

DESPITE ethylene's fundamental place in theories of chemical bonding, electron diffraction,[1] infrared,[2] and Raman[3] studies have only recently arrived at reasonably consistent results for its structural parameters. Further, there are only a few of the simpler derivatives of ethylene whose structures are well determined. At the same time, there is considerable debate about the extent of the usefulness of many of the theoretical concepts commonly used in discussing bonding.[4] Because of its relationship to ethylene, a knowledge of the structure and dipole moment of isobutylene should help in clarifying some of these questions.

Additional interest in isobutylene follows from the information which can be obtained from a study of the internal rotations of its methyl groups. Few molecules with two internal rotors have been investigated and the interactions are not understood at present. Also, the internal rotation of propylene and some ot its simpler derivatives has been studied[5] and it is of interest to compare isobutylene with these similar molecules.

EXPERIMENTAL

The sample of ordinary $(CH_3)_2C=CH_2$ was obtained from the Matheson Company. The monodeuterated species, $CH_2DCH_3C=CH_2$, was prepared by Merck Company, Ltd. of Canada. The spectrograph was the Stark modulation apparatus which has been described elsewhere.[6]

The spectra were rather dense, with moderately intense absorption. Lines were generally quite narrow except when broadened by unresolved internal rotation effects. Measurements of frequency are estimated to be accurate to ±0.05 Mc, except where unresolved Stark components or internal rotation structure interfered. Stark fields of the order of 2–3 kv/cm were usually necessary for proper modulation. Some of the lines with higher J values required even larger fields.

SPECTRA AND ROTATIONAL CONSTANTS

The spectra of isobutylene and isobutylene-*d*-3 were studied in the region 17–36 kMc. In both cases *b*-type transitions were observed. Since the molecule is moderately heavy, a number of families of *Q*-branch transitions fall into the region studied, giving a rather rich spectrum. Many of these lines and several *R*-branch transitions have been measured; frequencies are given in Tables I and II. Most of the identified transitions were essentially unaffected by the internal rotations and the effective rigid-rotor constants of Table III give a good fit. Some of the lines with large values of J deviate somewhat because of centrifugal distortion, but the lines with the lower values are not appreciably affected and no detailed analysis of centrifugal distortion has been carried out. For those transitions with internal rotation splittings, the listed frequencies are values corrected for internal rotation.

The rotational spectrum of the isobutylene-*d*-3 contains transitions of a pair of distinct species. The two are distinguished by the position of the deuterium on the methyl group. In one (*sym*) the deuterium is in the plane of the carbon atoms. In the other (*asym*) the deuterium is out of the plane of the carbon atoms, and this species has a statistical weight twice that of the other form.

DIPOLE MOMENT

Quantitative measurements were made of the Stark effect of the $1_{10}\rightarrow2_{21}$ and $2_{02}\rightarrow3_{13}$ transitions. Observed

* National Research Council-National Bureau of Standards Research Associate 1958–1959; National Science Foundation Postdoctoral Fellow 1959–1960. Present address: Chemistry Department, Stanford University, Stanford, California.

[1] L. S. Bartell and R. A. Bonham, J. Chem. Phys. **31**, 400 (1959).

[2] H. C. Allen and E. K. Plyler, J. Am. Chem. Soc. **80**, 2673 (1958).

[3] J. M. Dowling and B. P. Stoicheff, Can. J. Phys. **37**, 703 (1959).

[4] For example, see R. S. Mulliken, Tetrahedron **6**, 68 (1959).

[5] For references, see C. C. Lin and J. D. Swalen, Revs. Modern Phys. **31**, 841 (1959).

[6] D. R. Lide, D. E. Mann, and R. M. Fristrom, J. Chem. Phys. **26**, 734 (1957).

TABLE I. Transitions of isobutylene.

Transition	Obs. ν(Mc)	Calc. ν-obs. ν
$1_{11}\rightarrow 2_{02}$	22 128.05	0.00
$1_{01}\rightarrow 2_{12}$	22 981.28	0.00
$1_{10}\rightarrow 2_{21}$	32 015.95	0.00
$2_{12}\rightarrow 3_{03}$	31 768.96	0.05
$2_{02}\rightarrow 3_{13}$	31 879.31	0.08
$3_{03}\rightarrow 3_{12}$	20 279.79	−0.23
$3_{13}\rightarrow 3_{22}$	20 767.71	−0.21
$4_{13}\rightarrow 4_{22}$	19 669.25	−0.11
$4_{22}\rightarrow 4_{32}$	21 026.60	0.18
$4_{04}\rightarrow 4_{13}$	28 771.06	0.02
$4_{14}\rightarrow 4_{23}$	28 830.61	0.06
$5_{42}\rightarrow 5_{51}$	18 358.45	1.44
$5_{23}\rightarrow 5_{32}$	18 703.70	0.91
$5_{33}\rightarrow 5_{42}$	21 519.40	0.74
$5_{14}\rightarrow 5_{23}$	28 557.28	0.91
$6_{52}\rightarrow 6_{61}$	20 766.70	2.56
$6_{43}\rightarrow 6_{52}$	22 320.86	1.23
$6_{24}\rightarrow 6_{33}$	28 121.48	2.10
$6_{24}\rightarrow 6_{42}$	28 775.67	1.53
$7_{61}\rightarrow 7_{70}$	19 736.70	2.47
$7_{53}\rightarrow 7_{62}$	23 490.64	1.64
$7_{62}\rightarrow 7_{71}$	23 524.94	4.06
$7_{44}\rightarrow 7_{53}$	28 851.31	2.44
$8_{71}\rightarrow 8_{80}$	23 994.84	4.40
$8_{54}\rightarrow 8_{63}$	29 089.07	3.19
$9_{72}\rightarrow 9_{81}$	18 747.34	−2.03
$9_{54}\rightarrow 9_{63}$	24 638.80	7.57
$9_{81}\rightarrow 9_{90}$	28 220.48	7.03
$10_{64}\rightarrow 10_{73}$	22 976.59	9.0
$11_{83}\rightarrow 11_{92}$	18 473.09	−5.1
$12_{93}\rightarrow 12_{10,2}$	21 449.36	−10.1
$14_{11,3}\rightarrow 14_{12,2}$	29 909.89	−18.5

Stark coefficients are given in Table IV. Experimental field strengths were calculated from the Stark effect[7] of the OCS line at 24 325.92 Mc. The calculated dipole moment of 0.503±0.009 D is in good agreement with the value 0.49 determined from gas-phase dielectric measurements.[8]

[7] S. A. Marshall and J. Weber, Phys. Rev. **105,** 1502 (1957).
[8] H. E. Watson, G. P. Kane, and K. L. Ramaswamy, Proc. Roy. Soc. (London) **A156,** 144 (1936).

TABLE II. Transitions of isobutylene-d-3.

Transition	Obs. ν(Mc)	Calc. ν-Obs. ν
	sym	
$1_{11}\rightarrow 2_{02}$	20 752.87	0.00
$1_{01}\rightarrow 2_{12}$	22 425.74	0.00
$1_{10}\rightarrow 2_{21}$	31 828.82	0.00
$2_{12}\rightarrow 3_{03}$	30 377.99	0.05
$2_{02}\rightarrow 3_{13}$	30 759.55	0.05
$3_{03}\rightarrow 3_{12}$	18 852.70	0.01
$3_{13}\rightarrow 3_{22}$	20 334.26	0.00
	asym	
$1_{11}\rightarrow 2_{02}$	21 256.85	0.00
$1_{01}\rightarrow 2_{12}$	22 228.22	0.00
$1_{10}\rightarrow 2_{21}$	30 927.96	0.00
$2_{12}\rightarrow 3_{03}$	30 657.22	0.16
$2_{02}\rightarrow 3_{13}$	30 803.61	0.15
$3_{13}\rightarrow 3_{22}$	19 730.99	−0.15
$4_{13}\rightarrow 4_{22}$	18 347.00	0.09
$4_{23}\rightarrow 4_{33}$	20 065.05	0.41

INTERNAL BARRIER AND CONFORMATION OF THE METHYL GROUPS

The theory of the rotational spectra of molecules of the isobutylene type has been discussed,[9,10] and it has been shown that tunneling of the methyl groups can split lines into triplets or quartets. These splittings can then be used to calculate the barrier hindering the internal rotations.

In isobutylene the barrier is high enough so that the internal rotation splittings could not be resolved for most of the identified transitions. Some of them, however, occurred as closely spaced symmetrical triplets. A few quartets were also observed but it was not possible

TABLE III. Rotational constants (Mc) and moments of inertia (amu A²).

	$(CH_3)_2CCH_2$	s-$CH_2DCH_2CCH_2$	a-$CH_2DCH_3CCH_2$
a_0	9133.32	9132.59	8819.46
b_0	8381.75	7788.98	7981.08
c_0	4615.99	4431.05	4469.59
I_a	55.3502	55.3546	57.3200
I_b	60.3133	64.9034	63.3412
I_c	109.517$_4$	114.088$_3$	113.104$_6$

[9] J. D. Swalen and C. C. Costain, J. Chem. Phys. **31,** 1562 (1959).
[10] R. J. Myers and E. B. Wilson, Jr., J. Chem. Phys. **33,** 186 (1960).

TABLE IV. Stark coefficients[a] and dipole moment of isobutylene.

Transition	M	$\Delta\nu/E^2$	μ (debyes)
$1_{10}\rightarrow 2_{21}$	1	-3.14×10^{-6}	0.506
$2_{02}\rightarrow 3_{13}$	1	2.05×10^{-7}	0.504
$2_{02}\rightarrow 3_{13}$	2	8.56×10^{-7}	0.498
			Av 0.503 ± 0.009

[a] Mc/(v/cm)^2.

to identify these. It is probable that they came from molecules in excited torsional states. Those identified transitions for which accurate measurements of the splittings could be made are given in Table V. From each of the splittings a value for the barrier has been calculated. In the calculation the structural parameters of Table VI were used. The physical model which is the basis for the calculation assumes that interactions between the two methyl groups are relatively small and that a threefold cosine potential is sufficient. The perturbation treatment was carried out only to second order. The average value obtained for the barrier was 2.21 kcal/mole, in good agreement with the thermodynamic determination[11] of 2.35 kcal/mole.

Since the observed splittings are small, experimental error is more important than in the usual microwave determination. Also it is likely that higher order terms in the perturbation treatment contribute somewhat to the observed splittings. These considerations and the uncertainties in the structural parameters lead to an estimate of about 10% for the limits of error.

The equilibrium conformation of the two methyl groups is established to be C_{2v} by the rotational constants of the two forms of isobutylene-*d*-3. These data show that each methyl group has one CH bond in the plane of the carbons and that these two bonds are directed away from each other. The coordinates of the H atoms are given in Table VII. An end-on view of the isobutylene molecule is shown in Fig. 1. The location of the methyl group with reference to the double bond is the same as previously found for propylene[12] and acetaldehyde.[13]

TABLE V. Internal rotation splittings[a] in isobutylene.

Transition	Splittings (Mc)	V_3 (kcal/mole)
$6_{52}\rightarrow 6_{61}$	0.49, 0.53	2.16
$7_{62}\rightarrow 7_{71}$	0.64, 0.64	2.16
$7_{61}\rightarrow 7_{70}$	0.70, b	2.18
$8_{71}\rightarrow 8_{80}$	0.66, b	2.25
$9_{72}\rightarrow 9_{81}$	0.72, 0.72	2.20
$9_{81}\rightarrow 9_{90}$	0.69, b	2.28
$11_{83}\rightarrow 11_{92}$	b, 0.64	2.20
$12_{93}\rightarrow 12_{10,2}$	0.78, 0.75	2.23
$14_{11,3}\rightarrow 14_{12,2}$	1.13, 1.09	2.26
		Av 2.21

[a] These lines are all triplets. Low-frequency splitting is given first.
[b] Stark components interfere with measurements.

TABLE VI. Parameters[a] used in barrier calculation for isobutylene.

$F=171.6$ kMc	$\lambda_a I_a/I_a=0.04837$
$I_a=3.120$ amu A^2	$\lambda_b I_a/I_b=0.02792$

[a] For notation, see work cited in footnote 9.

There are several aspects of the isobutylene results which have bearing on the general problem of hindered internal rotation. Not only is the conformation the same as in propylene, but also the barrier itself is little changed from the 1.98 kcal/mole of propylene.[14] This would seem to imply that methyl-methyl interactions are a relatively minor factor in the barrier. A similar situation has also been found in dimethylsilane[15] and propane.[16] On the other hand, the barrier of 2.72 kcal/mole of dimethyl ether[17] is much larger than the methanol[18] barrier of 1.07 kcal/mole. Likewise, the barrier in dimethyl sulfide[19] of 2.13 kcal/mole is considerably larger than the value 1.27 kcal/mole of methyl mercaptan.[20] These large changes are not presently understood although there is some suggestion that lone-pair electrons have a role.

It may be noted that the barrier in isobutylene is slightly higher than in propylene whereas the barrier in acetone[9] of 0.76 kcal/mole is considerably lower than the acetaldehyde[13] value of 1.15 kcal/mole. This same

TABLE VII. Coordinates (A) of methyl H atoms in principal axes[a] system of isobutylene.

	In-plane	Out-of-plane
x	2.1535	1.3144
y	0	0.8734
z	0.0904	1.3603

[a] The xz plane is the plane of the carbon atoms and the z axis is the symmetry axis.

[11] J. E. Kilpatrick and K. S. Pitzer, J. Research Natl. Bur. Standards **37**, 163 (1946).

[12] D. R. Herschbach and L. C. Krisher, J. Chem. Phys. **28**, 728 (1958).
[13] R. W. Kilb, C. C. Lin, and E. B. Wilson, J. Chem. Phys. **26**, 1695 (1957).
[14] D. R. Lide, Jr., and D. E. Mann, J. Chem. Phys. **27**, 868 (1957).
[15] L. Pierce, J. Chem. Phys. **31**, 547 (1959).
[16] D. R. Lide, Jr., J. Chem. Phys. **33**, 1514, 1519 (1960).
[17] P. Kasai and R. J. Myers, J. Chem. Phys. **30**, 1096 (1959).
[18] E. V. Ivash and D. M. Dennison, J. Chem. Phys. **23**, 1814 (1955).
[19] L. Pierce (to be published).
[20] T. Kojima and T. Nishikawa, J. Phys. Soc. Japan **10**, 240 (1955).

trend is found in the only other case where analagous derivatives of acetaldehyde and propylene can be compared. Acetyl fluoride [21] has a barrier of 1.08 kcal/mole, lower than acetaldehyde, and 2-fluoropropene[22] has a barrier of 2.42 kcal/mole, higher than propylene. However, acetyl chloride [23] (1.35 kcal/mole) is higher than acetaldehyde and it is very probable that 2-chloropropene is also higher than propylene.

STRUCTURE

Although the available rotational constants are not sufficient for a complete structural determination, several conclusions of interest may be made. From the isobutylene-*d*-3 data the coordinates of the methyl H atoms in the principal axis system of isobutylene can be obtained. Then if the reasonable assumption is made that the bond and angle involving the ethylenic H atoms have the same values as in ethylene[2] and propylene,[24] information about the skeletal carbon parameters can be obtained from the isobutylene data. What is considered to be the best structure consistent with the microwave data is given in Table VIII. The electron diffraction results of Bartell and Bonham[25] are included for comparison.

If the isobutylene-*d*-3 data are taken literally, the out-of-plane and in-plane H atoms must be considered as nonequivalent. However, the apparent differences are of the same order as zero-point effects and for the present purposes a symmetrical methyl group has been assumed. This procedure is admittedly arbitrary, but it is convenient and has a negligible effect on the conclusions about the carbon parameters.

The microwave results for the methyl CH length are distinctly shorter than those of the electron diffraction study. The same situation has been found in comparing microwave and electron diffraction studies of the saturated hydrocarbons.[16] Calculations have shown that differences ~0.02 A between microwave and electron diffraction results are to be expected, however, because of the different nature of the measured quantities. Also, the <Me—C—Me is distinctly larger than the reported electron-diffraction result. However, as pointed out by Bartell and Bonham,[25] their accuracy was limited by the unfavorable geometry. The microwave value of 1.507 A for the C—C single bond is in good agreement with the electron diffraction value and may be compared with the microwave propylene[24] value of 1.501 A. Unfortunately, the double bond length cannot be very well determined from the microwave data, but the most likely value is ~1.34 A. This may be compared with the propylene[24] value of 1.336 A and agrees within experimental uncertainties with the electron-diffraction results.

The C—C single-bond length is considerably shorter than corresponding bond lengths in saturated compounds and is in accord with the large amount of already existing data which shows that C—C single bonds are shortened when adjacent to multiple bonds. On the other hand, the effect of methyl groups on the double bond length seems to be relatively minor; within the present experimental uncertainties, the double bond lengths in ethylene, propylene, and isobutylene are essentially the same.

TABLE VIII. Structure of isobutylene.

	Microwave[a]	Electron diffraction[b]
CH (Me)	1.08_5	1.113
∠HCH (Me)	108°	108.5°
CC	1.50_7	1.505
C=C	1.34	1.331
CH (ethylene)	1.085	1.084
∠HCH (ethylene)	117.5°	115.5°
∠Me−C−Me	115.9°	112°

[a] The methyl H parameters are an average of the in-plane and out-of-plane values. The ethylenic H parameters are assumed.
[b] See work cited in footnote 25 of the text.

FIG. 1. End-on view of the isobutylene molecule showing the equilibrium conformation of the methyl groups. Lines represent CH bonds. Circles indicate carbon atoms. For clarity of illustration the perspective is somewhat distorted. In the actual molecule the inner CH bonds would point almost directly at the observer.

ACKNOWLEDGMENTS

The author would like to thank Professor L. S. Bartell for communications on the electron diffraction study of isobutylene and Dr. D. R. Lide for unpublished microwave results on propylene.

[21] L. Pierce and L. C. Krisher, J. Chem. Phys. **31**, 875 (1959).
[22] L. Pierce and J. M. O'Reilly, J. Mol. Spectroscopy **3**, 536 (1959).
[23] K. M. Sinnott, Bull. Am. Phys. Soc. Ser. II, **1**, 198 (1956).
[24] D. R. Lide, Jr., and D. Christensen (private communication).
[25] L. S. Bartell and R. A. Bonham, J. Chem. Phys. **32**, 824 (1960).

Half-Crystal Energy Constants

HARTLAND H. SCHMIDT

Division of Physical Sciences, University of California, Riverside, California

(Received September 6, 1960)

Tables of the summation constants required for the calculation of surface energies of perfect half-crystals with Lennard-Jones types of inverse-power pair potential functions have been calculated using an IBM 709 computer. The tables cover simple cubic, face-centered cubic, body-centered cubic, simple hexagonal, and hexagonal close-packed structures with face plane orientations having Miller indices up to 5 in some cases. The inverse powers included in the tabulation extend from 5 (the lowest power for which these sums converge) to 13. The applications of these results to the calculation of grain boundary energy and spacing and to the estimation of surface distortion in half-crystals according to methods previously developed by the author are pointed out. The energies of hcp and fcc close-packed surfaces are compared as an example.

INTRODUCTION

IN connection with methods developed by G. Jura and the author[1,2] for the calculation of the energies of various surface configuration models and grain boundary energies in atomic crystals, certain summation constants of inverse-power pair interaction potentials over the half-crystal are required. These summation constants in the potential energy expression for the excess surface energy have been computed for three faces of the fcc half-crystal by Shuttleworth[3] who used them for a discussion of the distortion of the equilibrium half-crystal normal to the face, but tabulations over a wider range of crystal structures and faces seemed desirable for the extension of these methods to more general problems of crystallite interfaces. Such tabulations would supplement those of Lennard-Jones and Ingham[4] for infinite crystals.

From a pair potential energy function of the form

$$\phi = \sum_p \pm \lambda_p / r^p, \tag{1}$$

and the assumption of pair-wise additivity of potential energy, it can be shown[3] that the excess surface energy of a half-crystal of particles obeying (1) is

$$E_s(h,k,l) = \tfrac{1}{2} w \sum_p \mp B_p(h,k,l) h_p / (a_0)^{p+2}, \tag{2}$$

where w is the density of the surface plane in atoms per square lattice unit (a_0^2) and $B_p(h,k,l)$ is a constant characteristic of the crystal structure and the face orientation (h,k,l). The most general expression for $B_p(h,k,l)$ is[3]

$$B_p(h,k,l) = \sum_L \sum_{n_1'} \sum_{n_2'} \sum_{n_3'} \sum_i (n_L / |\mathbf{r}(n_1', n_2', n_3', i, L)|^p), \tag{3}$$

where L is the distance in lattice units between a plane parallel to the face in the half-crystal and a virtual plane parallel to the face in the virtual lattice projected above the half-crystal. The numerator n_L is the number of such plane-virtual plane pairs separated by the distance L. The integers n_1', n_2', n_3' are unit cell indices in the virtual lattice relative to an atom site in the half-crystal. These indices are chosen to include all of the virtual lattice unit cells in the plane at the current value of the distance (L) between the plane of the lattice atom and the virtual lattice plane. The index i denotes the ith atom in the n_1', n_2', n_3' unit cell.

Analytical expansions for summations of the type

$$\sum_0^\infty{}_{n1} \sum_{-\infty}^\infty{}_{n2} \sum_{-\infty}^\infty{}_{n3} [1/|\mathbf{r}(n_1^2+n_2^2+n_3^2)|^p], \tag{4}$$

have been devised[5,6] which are much more rapidly converging than the untransformed summations for cubic systems. These can be modified to include the numerator of (3), the proper summation limits, and, by appropriate coordinate transformations, other crystal systems. However, the transformations necessary are in most cases awkward, and for surface planes of low densities, the convergences are still quite slow. The availability of a high speed computer, the IBM 709 at the Western Data Processing Center, University of California at Los Angeles, prejudiced us toward the less elegant direct summations of (3) to fairly large values of the denominator and the addition of integral approximations to the sum at larger values of the pair distance.

COMPUTATION

Expressions for evaluating the numerator and denominator of Eq. (3) are given in Table I. Choices of axes for the calculations are indicated in that table and in Figs. 1 and 2. Conversions of Miller indices for the fcc structure between the primitive system used in computations and the cubic system used for tabulation as well as the conversions to obtain orthogonal axes for

[1] H. Schmidt and G. Jura, J. Phys. Chem. Solids **16,** 60 (1961).
[2] H. Schmidt and G. Jura, J. Phys. Chem. Solids **16,** 67 (1961).
[3] R. Shuttleworth, Proc. Phys. Soc. (London) **62A,** 167 (1949).
[4] J. E. Lennard-Jones and A. E. Ingham, Proc. Roy. Soc. (London) **A107,** 636 (1925).
[5] J. Hove and J. A. Krumhansl, Phys. Rev. **92,** 569 (1953).
[6] G. C. Benson and H. P. Schreiber, Can. J. Phys. **33,** 529 (1955).

TABLE I. Functions used in the computation of $B_p(h, k, l)$.

Array	Unit dist. a_0	Miller ind. (hkl) system	Atom posit. x, y, z	$\mid \mathbf{r}(n_1+x,\ n_2+y,\ n_3+z) \mid^2$ [a] a_0 units	Numerator[b] of (3), n_L
Face-centered cubic	cube edge	Rhom.	0, 0, 0	$0.5(n_1^2+n_2^2+n_3^2+n_1n_2+n_1n_3+n_2n_3)$	N
Simple cubic	cube edge	Cubic	0, 0, 0	$n_1^2+n_2^2+n_3^2$	N
Cubic centers	cube edge	Cubic	$\frac{1}{2}, \frac{1}{2}, \frac{1}{2}$	$n_1^2+n_2^2+n_3^2+.75(n_1+n_2+n_3)$	$2(N+K)-1$
Simple hexagonal	nearest neighbor	Hex.	0, 0, 0	$n_1^2+n_2^2-n_1n_2+(8/3)n_3^2$	N
Internal hexagonal	nearest neighbor	Hex.	A. $\frac{1}{3}, \frac{2}{3}, \frac{1}{2}$	$n_1^2+n_2^2-n_1n_2+n_2+(8/3)(n_3^2+n_3)+1$	$(N+K$ with A denom.$)+(N+K-1)$ with B denom.)
			B. $\frac{2}{3}, \frac{1}{3}, \frac{1}{2}$	$n_1^2+n_2^2-n_1n_2+n_1+(8/3)(n_3^2+n_3)+1$	$(N+K-1$ with A denom.$)+(N+K$ with B denom.)

[a] Only positive nonzero radii enter the sum.

[b] $N=n_1h+n_2k+n_3l$ and if $M=n_1x+n_2y+n_3z$ then: $K=M$ if M is integral; $K=$ integral part of M if M is nonintegral positive; $K=$ (integral part of M)$+1$ if M is nonintegral negative. Only those terms for which $n_L>0$ are included in the sums in order to give the proper boundary condition at the surface.

distance calculations are described in standard reference works.[7]

The integral approximations to the sum at large $\mathbf{r}$ were derived in a manner similar to that of Shuttleworth[3] yielding the following additive corrections

$$[\pi\rho/d(p-4)R_0^{(p-4)}]-[d\pi\rho/4(p-2)R_0^{(p-2)}], \quad (5a)$$

for the primitive lattices and

$$\frac{2\pi\rho}{d(p-4)R_0^{(p-4)}}+\frac{2\pi\rho(1-2d'/d)}{(p-3)R_0^{(p-3)}}+\frac{\pi\rho[d^2/2-2dd'+2(d')^2]}{d(p-2)R_0^{(p-2)}}, \quad (5b)$$

for the internal atom lattices, where ρ is the density of the primitive lattice in atoms per unit cell, d is the interplanar distance normal to the surface in the primitive lattice, and d' is the distance between the surface and second planes in the complete lattice. The smoothed density hemispherical radius R_0 is an approximation to the effective limit of the summation terms when a maximum is placed upon the denominator of Eq. (3) and is given by

$$R_0=[\tfrac{3}{2}N/\rho\pi]^{\frac{1}{3}} \qquad N=\text{No. of terms summed.} \quad (6)$$

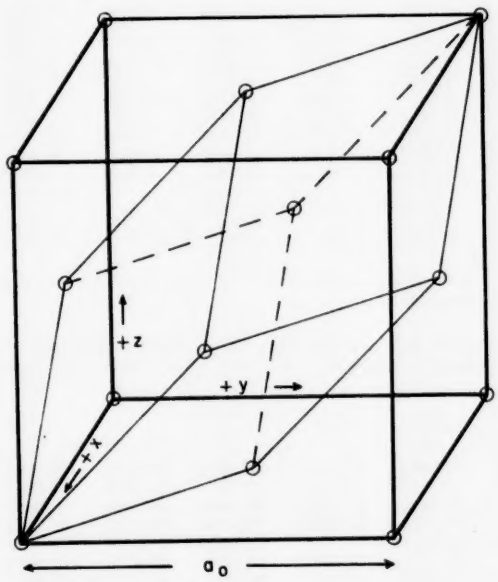

FIG. 1. Face-centered cubic unit cell. —— Reference system for Miller indices and distance calculations. —— Reference system for running indices n_1', n_2', n_3'.

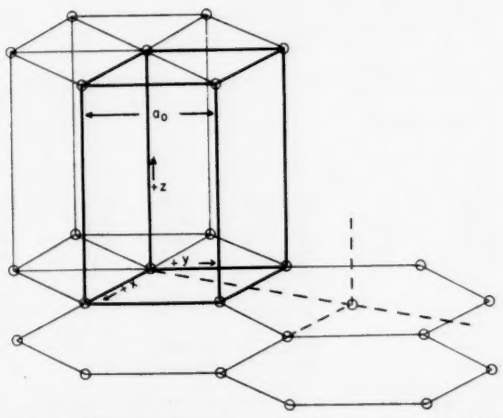

FIG. 2. Hexagonal unit cell. —— Reference system for Miller indices and running indices n_1', n_2', n_3'. —— Reference system for distance calculations.

[7] International Union of Crystallography, *International Tables for X-Ray Crystallography* (Kynoch Press, Birmingham, England, 1952), Vol. I.

TABLE II. Cubic close-packed half-crystal constants $B_p(h, k, l)$, unit length (a_0): unit cube edge, Miller indices: cubic system.

Exponent p		5	6	7	8	9	10	11	12	13
Face planes[a]	$(w/4)^{-2}$ (atoms/a_0^2)$^{-2}$									
(111)	3	40.006	36.217	42.576	54.855	73.679	101.1006	140.3782	196.2588	275.5217
(111)[b]			36.220	42.578	54.856	73.682	101.101	140.380	196.256	
(100)	4	48.469	45.232	54.252	70.858	96.077	132.7048	185.1130	259.6428	365.3403
(100)[b]			45.235	54.255	70.861	96.077	132.71	185.113	259.641	
(110)	8	71.137	67.395	81.337	106.484	144.474	199.5390	278.2475	390.1199	548.7286
(110)[b]			67.405	81.340	106.486	144.476	199.54	278.247	390.119	
(311)	11	83.614	79.136	95.358	124.671	168.974	233.2030	325.0177	455.5253	640.5602
(210)	20	115.321	110.541	134.234	176.366	239.809	331.6652	462.9020	649.3955	913.7730
(211)	24	122.459	114.994	137.780	179.453	242.617	334.2843	465.3860	651.7786	916.0790
(221)	36	148.806	139.059	166.141	216.015	291.732	401.6835	558.9707	782.6178	1099.7598
(310)	40	162.543	155.347	188.292	247.124	335.830	464.3385	647.9962	909.0276	1279.1064
(320)	52	185.781	177.734	215.491	282.811	384.265	531.1945	741.1449	1039.5126	1462.5003
(321)	56	190.753	181.059	218.292	285.360	386.667	533.5015	743.3842	1041.7022	1464.6518
(322)	68	201.845	187.299	222.899	289.151	389.970	536.4841	746.1423	1044.2964	1467.1225
Est. prob. error		6	5	4	2	1	5	4	3	2
Approx. no. of terms summed ($\times 10^{-3}$)		14.2	13.0	8.2	4.7	2.4	1.6	1.0	0.57	0.30

[a] By symmetry, all permutations and sign combinations of the indices (h, k, l) give identical sums.
[b] Calculations of R. Shuttleworth, Proc. Phys. Soc. (London) **62A**, 167 (1949).

TABLE III. Simple cubic half-crystal constants $B_p(h, k, l)$, unit distance (a_0): unit cube edge, Miller indices: cubic system.

Exponent p		5	6	7	8	9	10	11	12	13
Face planes[a]	w^{-2} (atoms/a_0^2)$^{-2}$									
(100)	1	3.5727	2.0596	1.5790	1.3527	1.2269	1.1505	1.1018	1.0697	1.0481
(110)	2	5.6614	3.5128	2.8295	2.5074	2.3279	2.2186	2.1485	2.1021	2.0707
(111)	3	7.3369	4.7357	3.9260	3.5538	3.3514	3.2309	3.1551	3.1057	3.0727
(210)	5	8.9623	5.5052	4.3861	3.8518	3.5515	3.3678	3.2498	3.1716	3.1188
(211)	6	10.3525	6.6161	5.4274	4.8688	4.5590	4.3712	4.2513	4.1723	4.1191
(310)	10	12.4565	7.5515	5.9621	5.2037	4.7782	4.5183	4.3515	4.2413	4.1669
(221)	9	12.7636	8.1875	6.7342	6.0529	5.6759	5.4481	5.3030	5.2075	5.1434
(311)	11	13.7372	8.6323	6.9931	6.2169	5.7842	5.5211	5.3529	5.2419	5.1672
(321)	14	15.8242	10.0809	8.2406	7.3702	6.8844	6.5888	6.3994	6.2742	6.1898
(322)	17	17.6202	11.3390	9.3500	8.4216	7.9102	7.6020	7.4064	7.2780	7.1919
Est. prob. error		5	2	1	0	0	0	0	0	0
Approx. no. of terms summed ($\times 10^{-3}$)		16.4	13.2	10.4	8.0	6.0	4.3	3.0	2.0	1.2

[a] By symmetry, all permutations and sign combinations of the indices (h, k, l) give identical sums.

TABLE IV. Cubic centers half-crystal constants $B_p'(h, k, l)$, unit distance (a_0): unit cube edge, Miller indices: cubic system.

Exponent p	5	6	7	8	9	10	11	12	13
Face planes[a]									
(100)	13.0024	11.2499	11.7982	13.0931	14.8490	16.9999	19.5474	22.5239	25.9807
(110)	9.2790	6.4828	6.2781	6.7389	7.5291	8.5589	9.8078	11.2819	13.0021
(111)	20.6308	17.3074	17.9136	19.7583	22.3416	25.5397	29.3447	33.8000	38.9795
(210)	27.0237	22.8601	23.7663	26.2755	29.7478	34.0282	39.1114	45.0576	51.9672
(211)	20.2737	15.3634	15.3371	16.6696	18.7277	21.3443	24.4890	28.1871	32.4949
(310)	29.6715	23.6311	24.0917	26.4351	29.8323	34.0750	39.1380	45.0731	51.9762
(221)	34.8946	29.0310	29.9446	32.9769	37.2618	42.5809	48.9164	56.3384	64.9687
(311)	40.2709	34.1721	35.5861	39.3768	44.6001	51.0295	58.6594	67.5818	77.9480
(321)	34.6163	27.1072	27.3749	29.8914	33.6490	38.3860	44.0609	50.7255	58.4842
(322)	48.4006	40.4537	41.8233	46.1127	52.1346	59.5945	68.4718	78.8670	90.9523
Est. prob. error	3	2	1	0	0	0	0	0	0
Approx. no. of terms summed ($\times 10^{-3}$)	24	24	20	16	12	9	6	4.1	2.6

[a] By symmetry, all permutations and sign combinations of the indices (h, k, l) give identical sums.

TABLE V. Simple hexagonal half-crystal constants $B_p(h, k, l)$, unit distance (a_0): nearest-neighbor distance, Miller indices: hexagonal.

Exponent p		5	6	7	8	9	10	11	12	13
face planes[a]	$2w^{-2}$ (atoms/a_0^2)$^{-2}$									
(001)	3/8	.9157	.30704	.13557	.06642	.034309	.018301	.009978	.005529	.003104
(010)	4/3	3.689	2.5500	2.2362	2.1130	2.0571	2.0298	2.0159	2.0086	2.0047
(011)	41/24	3.989	2.6706	2.2970	2.1460	2.0757	2.0405	2.0221	2.0122	2.0069
(012)	17/6	4.666	2.9230	2.4157	2.2066	2.1079	2.0580	2.0318	2.0176	2.0099
(110)	4	6.936	4.9536	4.4073	4.1934	4.0970	4.0503	4.0266	4.0143	4.0078
(111)	35/8	7.119	5.0295	4.4470	4.2158	4.1101	4.0581	4.0313	4.0171	4.0095
(013)	113/24	5.485	3.2131	2.5474	2.2720	2.1419	2.0762	2.0417	2.0232	2.0130
(11$\bar{2}$)	11/2	7.589	5.2102	4.5346	4.2618	4.1352	4.0720	4.0392	4.0216	4.0121
(1$\bar{2}$2)	11/2	7.589	5.2102	4.5346	4.2618	4.1352	4.0720	4.0392	4.0216	4.0121
(021)	137/24	7.626	5.2124	4.5314	4.2585	4.1326	4.0702	4.0380	4.0208	4.0116
(113)	59/8	8.252	5.4571	4.6510	4.3215	4.1670	4.0894	4.0488	4.0270	4.0151
(12$\bar{0}$)	28/3	10.535	7.4853	6.6385	6.3048	6.1536	6.0799	6.0424	6.0229	6.0125
(1$\bar{3}$1)	233/24	10.673	7.5480	6.6733	6.3253	6.0229	6.0874	6.0470	6.0257	6.0142
(121)	233/24	10.673	7.5480	6.6733	6.3253	6.1659	6.0874	6.0470	6.0257	6.0142
(122)	65/6	11.003	7.6770	6.7371	6.3595	6.1850	6.0983	6.0533	6.0293	6.0163
(031)	99/8	11.302	7.7613	6.7676	6.3715	6.1897	6.1000	6.0539	6.0294	6.0163
(131)	425/24	14.315	10.0901	8.9076	8.4377	8.2228	8.1171	8.0629	8.0343	8.0189
Est. prob. error		1	3	1	0	0	0	0	0	0
Approx. no. of terms summed ($\times 10^{-3}$)		8.4	7.2	5.5	4.1	3.0	2.0	1.4	0.9	0.5

[a] By symmetry, $B_p(h, k, l) = B_p(h, k, \bar{l})$ and $B_p(0, k, l) = B_p(0, \bar{k}, l)$.

TABLE VI. Internal hexagonal half-crystal constants $B_p'(h, k, l)$, unit distance (a_0): nearest-neighbor distance, Miller indices: hexagonal.

Exponent p	5	6	7	8	9	10	11	12	13
Face planes[a]									
(001)	5.245	3.9141	3.4930	3.2966	3.1884	3.1234	3.0826	3.0559	3.0382
(010)[b]	6.340	3.8049	2.9843	2.5947	2.3782	2.2479	2.1656	2.1121	2.0766
[c]	8.248	5.6992	4.8894	4.5168	4.3171	4.2012	4.1306	4.0861	4.0576
(011)	7.599	4.8224	3.9584	3.5631	3.3504	3.2255	3.1485	3.0993	3.0671
	10.054	7.1107	6.1505	5.6945	5.4415	5.2892	5.1932	5.1308	5.0894
(012)	11.719	8.2135	7.1485	6.6705	6.4160	6.2677	6.1763	6.1180	6.0799
	12.102	8.4743	7.3294	6.7970	6.5050	6.3305	6.2206	6.1493	6.1021
(110)	8.052	4.3068	3.1956	2.6972	2.4316	2.2766	2.1814	2.1210	2.0817
(111)	12.667	8.1118	6.6611	5.9856	5.6173	5.3992	5.2638	5.1767	5.1198
(013)	16.380	11.8917	10.5255	9.9058	9.5712	9.3727	9.2485	9.1681	9.1149
	16.677	12.0538	10.6161	9.9571	9.6004	9.3895	9.2581	9.1737	9.1180
(11$\bar{2}$)	11.050	6.6512	5.3627	4.7919	4.4900	4.3147	4.2070	4.1384	4.0936
(1$\bar{2}$2)	14.383	9.3640	7.7888	7.0616	6.6662	6.4322	6.2864	6.1926	6.1310
	16.582	11.4641	9.8417	9.0903	8.6822	8.4412	8.2916	8.1956	8.1325
(021)	13.794	8.5945	6.9327	6.1544	5.7274	5.4730	5.3139	5.2113	5.1437
	15.695	10.4861	8.8369	8.0761	7.6661	7.4263	7.2789	7.1854	7.1247
(113)	18.502	12.7572	10.9804	10.1694	9.7322	9.4746	9.3144	9.2115	9.1437
(12$\bar{0}$)	17.380	10.6766	8.5184	7.5033	6.9456	6.6136	6.4063	6.2729	6.1852
	19.060	12.4398	10.3469	9.3805	8.8581	8.5515	8.3622	8.2417	8.1631
(1$\bar{3}$1)	18.342	11.5863	9.4413	8.4449	7.9030	7.5829	7.3844	7.2573	7.1741
	18.738	11.8530	9.6250	8.5729	7.9927	7.6460	7.4289	7.2887	7.1964
(121)	18.342	11.5863	9.4411	8.4448	7.9030	7.5829	7.3844	7.2573	7.1741
	18.738	11.8528	9.6250	8.5728	7.9926	7.6460	7.4289	7.2887	7.1964
(122)	19.926	12.8142	10.5632	9.5195	8.9501	8.6159	8.4072	8.2732	8.1853
	20.048	13.8830	10.6032	9.5427	8.9653	8.6239	8.4118	8.2759	8.1869
(031)	20.104	12.3960	9.9168	8.7490	8.1056	7.7210	7.4796	7.3234	7.2203
	21.938	14.2644	11.8122	10.6676	10.0432	9.6738	9.4444	9.2975	9.2013
(131)	24.539	15.3547	12.4130	11.0347	10.2792	9.8300	9.5497	9.3692	9.2507
	26.315	17.1761	14.2767	12.9330	12.2045	11.7753	11.5101	11.3407	11.2302
Est. prob. error	1	4	2	1	0	0	0	0	0
Approx. no. of terms summed ($\times 10^{-3}$)	16.6	16.6	14.3	10.8	8.3	6.0	4.2	2.6	1.7

[a] By symmetry, $B_p'(h, k, l) = B_p'(h, k, \bar{l}) = B_p'(k, h, l)$ except for interchanges of "closer" and "further" plane pair surface cleavage values. Similarly,

$$B_p'(0, k, l) = B_p'(0, \bar{k}, l).$$

[b] Where there are two sets of values for a given face plane, the first represents a surface cleavage between a "further" pair of adjacent planes.

[c] The second set of values represents a cleavage between a "closer" set of adjacent planes and involves a higher surface energy.

Values of d were determined from the length of the reciprocal lattice vector which was computed by the machine from the face indices, and values of d' were related by general expressions to x, y, z, h, k, and l. Limits for the running integers n_1', n_2', n_3' were determined analytically such that for a chosen maximum radius $|\mathbf{r}_m|$ no terms were omitted within that radius. The maximum radius was modified according to the current value of the inverse power p so that fewer terms were considered in the more rapidly converging series. Even with making the program as efficient as possible for the computation, the machine time was between 1 and 2 hr per table computed.

Limits of error on the individual $B_p(h, k, l)$ values were estimated by making several additional runs at different summation–integration limits and determining the rate of approach to an asymptotic limit of $B_p(h, k, l)$ with increasing R_0. The regularity of this approach to the asymptotic value made it possible to estimate an additive correction to the last significant figure for the column $p=5$ in the final longest runs.

RESULTS

The results of the computations are given in Tables II through VI. Values from these tables can be used directly in expressions of the form in Eq. (2) for the cases of the primitive lattices fcc (tabulated using the primitive rhombohedral unit cell), sc, and sh. In the case of nonprimitive lattices, e.g., bcc and hcp, account must be taken of the interactions among internal atom planes in addition to the interactions between primitive lattice planes and internal atom planes covered in the tables as the constants $B_p'(h, k, l)$. Thus we have

$$B_p(h, k, l)\,\mathrm{bcc} = 2B_p(h, k, l)\ \text{simple cubic} + B_p'(h, k, l)\ \text{cubic centers}, \quad (7a)$$

and

$$B_p(h, k, l)\,\mathrm{hcp} = 2B_p(h, k, l)\ \text{simple hexagonal} + B_p'(h, k, l)\ \text{internal hexagonal}, \quad (7b)$$

while the surface density factor w which is proper in all cases, is that of the *primitive* cell even in the cases where the internal atom and the corner atom of the unit cell are coplanar in the surface plane. The expressions (7a) and (7b) take care of all the additional interactions due to internal atoms. It will be noted that because of the lack of certain symmetry elements in the hcp structure, many of the possible face plane orientations allow for two different surface energies depending upon whether the face cleavage separates a "closer" or "further" pair of adjacent planes parallel to the surface plane. The cleavage representing separation of the "further" pair would, of course, give lower surface energy and would therefore be the more stable.

DISCUSSION

With the results of the works cited in footnotes 1 and 2, and the tables of this paper, it is now possible to discuss the surface excess free energies at 0°K, the equilibrium distortion normal to the surface, the possibility of equilibrium distortion parallel to the plane of the surface, and the excess energy and equilibrium spacing of grain boundaries for lattices involving pair-wise additive inverse-power potential functions with a wide variety of structures and orientations. Similar treatments can be made with ionic crystals involving varying degrees of surface polarization by extending treatments given by workers referred to in the previous papers. However, the usual problems of very slow or conditional convergence in ionic crystals enter here.

It is interesting to note that although the minimization of the classical lattice energy of an inert gas type of crystal with a Lennard-Jones potential function predicts that the hcp structure would be slightly more stable than the fcc structure for an infinite crystal, the converse is true with respect to surface energy of the close-packed plane where the constants are:

$$B_6(1, 1, 1)\,\mathrm{fcc} = 36.217 \text{ (cube edge units)}$$

$$B_{12}(1, 1, 1)\,\mathrm{fcc} = 196.2588 \text{ (cube edge units)}$$

$$B_6(0, 0, 1)\,\mathrm{hcp} = 2B_6(0, 0, 1)\,\mathrm{sh} + B_6'(0, 0, 1)\ \mathrm{Int.H} = 36.226 \text{ (cube edge units)}$$

$$B_{12}(0, 0, 1)\,\mathrm{hcp} = 2B_{12}(0, 0, 1)\,\mathrm{sh} + B_{12}'(0, 0, 1)\,\mathrm{Int.H} = 196.288 \text{ (cube edge units)}.$$

These constants with the argon parameters[1]

$$a_0 = 5.32\ \mathrm{A}, \qquad \lambda_6 = 1.107\times10^{-10}\ \mathrm{erg\ A^6/atom},$$

$$\lambda_{12} = 1.859\times10^{-7}\ \mathrm{erg\ A^{12}/atom},$$

indicate very slightly lower (0.02%) surface energy for the fcc lowest energy surface.

ACKNOWLEDGMENTS

The author wishes to acknowledge the assistance of Charles Carlson in working out some of the transformation matrices involved in setting up this problem and of the Western Data Processing Center at the University of California, Los Angeles, for the use of their facilities and the assistance of Gordon Ashby of their staff.

Scattering of High-Velocity Neutral Particles. XI. Further Study of the He-He Potential*

I. AMDUR, J. E. JORDAN, AND S. O. COLGATE†

Department of Chemistry, Massachusetts Institute of Technology, Cambridge, Massachusetts

(Received November 14, 1960)

Results are presented for two studies of the scattering by room-temperature helium of beams of helium atoms with controlled energies in the approximate range 150–1500 ev. The interaction potential derived from the two sets of measurements is represented by

$$\phi(r)=5.56\times10^{-12}/r^{8.03}\ \text{erg} \qquad (0.97\ \text{A}<r<1.48\ \text{A}).$$

Where there are common ranges of the interaction distance r this potential is in reasonable agreement with He-He potentials previously determined from scattering experiments. In its specified range of validity, it is somewhat lower than most of the corresponding values calculated quantum mechanically.

TWO sets of experimental results have been published for the He-He intermolecular potential $\phi(r)$ as determined from the scattering of high-velocity helium atoms in room-temperature helium.[1,2] The potential energy functions have been represented by

$$\phi(r)=4.62\times10^{-12}/r^{1.79}\ \text{erg} \quad (0.52\ \text{A}<r<1.02\ \text{A}) \quad (1)$$

$$\phi(r)=7.55\times10^{-12}/r^{5.94}\ \text{erg} \quad (1.27\ \text{A}<r<1.59\ \text{A}). \quad (2)$$

The first set of results, Eq. (1), was based on measurements made in 1939–40 with the first molecular-beam apparatus which one of the authors (I.A.) had built to study the elastic scattering of high-velocity neutral particles.[3,4] The second set, Eq. (2), was based on measurements made in 1950 in a different apparatus which contained a number of improved features.[5]

Since the publication of the second experimental potential function, a number of quantum-mechanical calculations of the He-He interaction have appeared[6–10] which are in reasonably good agreement with Eq. (2) and with Eq. (1) near 1 A, but which, in general, predict values of $\phi(r)$ considerably larger than those of Eq. (1) near 0.5 A. Since it is of fundamental importance to find out whether the early scattering results or the recent theoretical calculations are correct at the smaller internuclear distances, additional results are presented here of He-He scattering in a third molecular-beam apparatus which is a major modification of the first beam apparatus. Two separate investigations are reported,[11,12] one completed in 1958 (J.E.J.), the other in 1959 (S.O.C.), with results which relate to the earlier work in the following manner:

(1) The valid range of interaction distance for the values of $\phi(r)$ derived from the present experiments covers the hitherto unexplored gap between the ranges associated with Eqs. (1) and (2). Thus, an experimental interpolation has been obtained for estimating directly the accuracy of the $\phi(r)$ curve from Eq. (1) near 1.02 A, and of the $\phi(r)$ curve from Eq. (2) near 1.27 A. In addition, the new experimental information can be compared directly with theoretical calculations.

(2) The range also includes that of Eq. (2) and thereby serves to check results obtained from two different apparatuses in three separate investigations.

(3) Since the present results indicate that Eq. (1) is reasonably correct near 1 A, a redetermination of $\phi(r)$ near 0.5 A should answer the question of whether the original experimental values given by Eq. (1) or the theoretical calculations of recent years (or, to some extent, both) are in error. Even in the absence of discrepancies between theory and experiment, a reinvestigation of the potential between 0.5 A and 1 A would be indicated since the apparatus which led to the results of Eq. (1) was, by present standards, primitive, and the accuracy of the measurements made in it considerably poorer than those made more recently. This experimental redetermination, in a slightly modified form of the present apparatus, is now in progress.

EXPERIMENTAL

The important features of the present apparatus are shown in Fig. 1. Positive ions are produced when electrons from the grounded filament 1 pass through helium, at 0.05 to 0.3-mm pressure, on their way to the copper anode 2 which is at a positive potential of 30–40 v. A copper cathode 3 at a negative potential between 0 and 100 v, serves to confine the low-voltage arc and to

* This research was supported in part by the U. S. Office of Naval Research.

† Present address: Department of Chemistry, University of Florida, Gainesville, Florida.

[1] I. Amdur, J. Chem. Phys. **17,** 844 (1949).
[2] I. Amdur and A. L. Harkness, J. Chem. Phys. **22,** 664 (1954).
[3] I. Amdur and H. Pearlman, J. Chem. Phys. **8,** 7 (1940).
[4] I. Amdur and H. Pearlman, J. Chem. Phys. **9,** 503 (1941).
[5] I. Amdur, C. F. Glick, and H. Pearlman, Proc. Am. Acad. Arts Sci. **76,** 101 (1948).
[6] V. Griffing and J. F. Wehner, J. Chem. Phys. **23,** 1024 (1955).
[7] M. Sakamoto and E. Ishiguro, Progr. Theoret. Phys. (Kyoto) **15,** 37 (1956).
[8] N. Lynn, Proc. Phys. Soc. (London) **72,** 201 (1958).
[9] T. Hashino and S. Huzinaga, Progr. Theoret. Phys. (Kyoto) **20,** 631 (1958).
[10] N. Moore, J. Chem. Phys. **33,** 471 (1960).
[11] J. E. Jordan, Ph.D. thesis, Massachusetts Institute of Technology, 1958.
[12] S. O. Colgate, Ph.D. thesis, Massachusetts Institute of Technology, 1959.

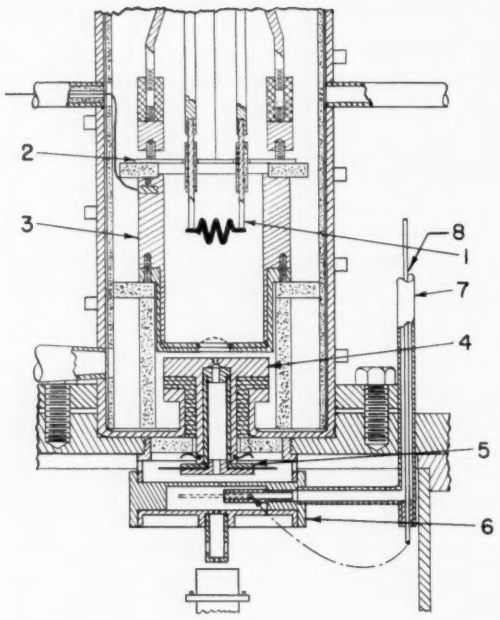

FIG. 1. Details of apparatus.

withdraw positive ions from the region between the filament and anode. Ions which enter the hole in the bottom of the cathode are focused by a nickel hemispherical screen onto an aluminum accelerating electrode, the atom gun 4 whose negative potential may be varied between 150 and 1500 v. Some of the positive ions which pass through the 0.508-mm diam hole in the atom gun are converted to high-velocity neutrals by charge transfer and the balance are deflected by a potential difference of about 1000 v across the plates of a condenser 5 mounted below the atom gun. Vycor is used to insulate the anode from the cathode and to support the cathode above the atom gun, while a lava bushing is used to insulate the atom gun from the metal flange which supports it. The condenser plates are insulated from the atom gun with Mycalex inserts. A 4-in. metal diffusion pump is connected to the rest of the metal appratus through a water-cooled baffle.

One of the important features of the present apparatus is the insertion of a narrow scattering chamber 51.98 mm below the top of the atom gun and coaxial with it, to localize the scattering gas and to facilitate calculation of the effective aperture of the beam-detector system. The advantages of this arrangement have been discussed previously.[5] The neutral beam enters the scattering chamber through a 0.521-mm hole in a fixed upper plate which is 0.79 mm thick, and leaves through a 0.96-mm hole in a removable plate, also 0.79 mm thick, after traversing a distance of 8.86 mm between the two plates. The entrance and exit holes of the scattering chamber are relieved with a 60° countersink from their bottom sides to reduce flow resistance. A cylindrical nozzle, attached to the bottom of the removable plate, supports a vane which is used to intercept the beam, and serves as a visual aid in positioning the detector in the beam axis.

A $\frac{1}{4}$-in. copper tube (7) connects the scattering chamber through a valve to the diffusion pump, or, when the valve is shut, to a special McLeod gauge which reads the pressure of the scattering gas. Gas is introduced into the scattering chamber through a $\frac{1}{16}$-in. copper tube (8) which is suspended coaxially in the $\frac{1}{4}$-in. tube. Inside the scattering chamber the $\frac{1}{16}$-in. tube is bent into a circular loop whose end is plugged. A number of small holes in the outer periphery of the loop feed gas uniformly into the scattering chamber.

In the 1958 measurements(hereafter referred to as series I) a thermocouple gauge, thermostatted at 0°C, and calibrated against the McLeod gauge, was eventually substituted for the McLeod gauge in order to reduce the time required for a reading of the scattering pressure. Input heater current and output voltage of the gauge were read potentiometrically. In the 1959 measurements(hereafter referred to as series II) a new bottom plate was used in the scattering chamber. This plate contained a compensated Pirani gauge of fine platinum wire for rapid measurement of the actual pressure in the scattering chamber, since dynamic and static comparison calibrations of the Pirani gauge showed that pressure gradients of several percent could exist between the scattering chamber and an external point at which a thermocouple or McLeod gauge was inserted. All scattering pressure measurements which were made with the McLeod gauge or thermocouple gauge were corrected for the effect of these gradients.

Thermal detectors were used to measure beam intensities in both sets of measurements. In series I two such detectors were used, a 40-junction bismuth-antimony thermopile with a sensitivity of 0.415 v/w[13] and a single-junction constantan-Chromel P thermocouple with a sensitivity of 4.96 v/w. In series II this latter single-junction detector was used initially but was replaced by a similar detector with a sensitivity of 1.06 v/w. The detectors, in brass shielding cases, were mounted so that their active surfaces were 18.12 mm below the bottom of the scattering chamber. In all cases the active detector area was defined by a mask with a hole 0.762 mm in diam directly above the detector surface.

McLeod gauges were used to measure pressures in the arc region and in the region surrounding the scattering chamber. Provision was also made for monitoring these pressures with a thermocouple gauge and an ionization gauge, respectively.

[13] L. Harris, J. Opt. Soc. Am. **36**, 597 (1946).

RESULTS

The total collision cross section S is computed from the relation

$$S = \ln(I_0/I)/n\Delta x(1+\alpha), \qquad (3)$$

where I_0 is the unscattered axis beam intensity, I the corresponding intensity when gas at molecular density n is in the scattering chamber, Δx the effective length of the scattering path, and $1+\alpha$ a correction for scattering in background regions outside the scattering chamber. The magnitude of α, which is a function of the increase in background pressure when gas is introduced into the scattering chamber, depends upon the size and shape of the entrance and exit holes in the scattering chamber and upon the size of the annular leakage space around the bottom removable plate of the scattering chamber. For series I the value of α was 0.063 and for series II (in which a different removable plate, containing the compensated Pirani gauge, was in the scattering chamber), α was 0.020. The effective scattering distance Δx is given by

$$\Delta x = \Delta x_{sc} + \sum_i \Delta x_i P_i / P_{sc}, \qquad (4)$$

where Δx_{sc} is the distance 8.86 mm inside the scattering chamber where there is a uniform pressure P_{sc} and Δx_i is the length of scattering path in other regions where the average pressure is P_i. These regions include the frustrum-shaped entrance and exit holes in the scattering chamber and the gas clouds that form outside these holes.[5] The value of Δx for series I was 9.96 mm, and for series II, 10.05 mm.

The experimental results are shown graphically in Fig. 2. For series I (open circles) each experimental point represents at least six individual determinations, with an average of eight determinations per point for the entire curve. For series II (closed circles) each point represents at least eight determinations, with an average of 11 determinations per point for the entire curve. The average deviation of the individual cross sections from the values represented by the points in Fig. 2 was 1.7% and 2.6% for the open and closed circles, respectively.

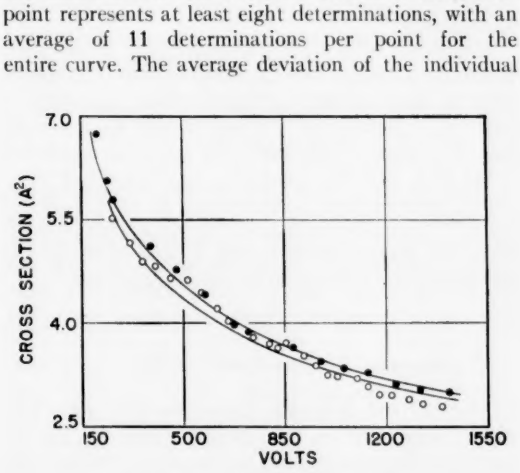

FIG. 2. Total collision cross sections.

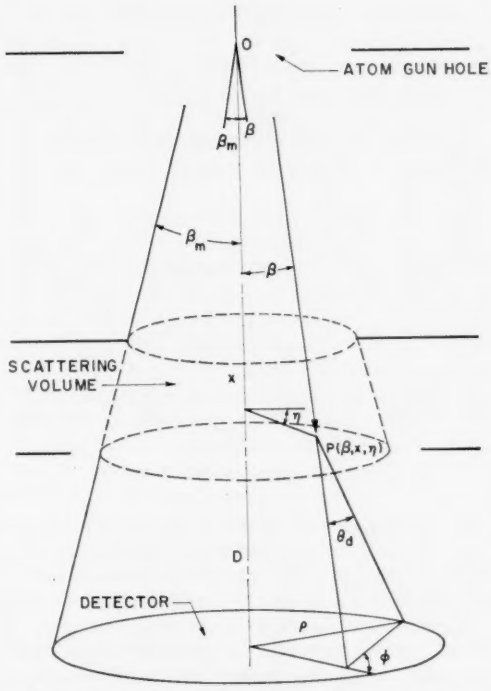

FIG. 3. Coordinate system for beam-detector geometry.

For an empirical potential function of the form $\phi(r) = K/r^s$, classical theory gives the following relation, in laboratory coordinates, for the total elastic cross section as measured with a detector having a small effective angular aperture θ_{eff}[14,15]

$$S = \pi(KC/E)^{2/s}[\langle\theta^{-2/s}\rangle - \langle\theta^{1-2/s}\rangle(m_1+m_2)/m_2C], \qquad (5)$$

where C is a constant, $\pi^{\frac{1}{2}}\Gamma(s/2+\frac{1}{2})/\Gamma(s/2)$; E the initial kinetic energy of the beam particle; $\langle\theta^{-2/s}\rangle$ and $\langle\theta^{1-2/s}\rangle$, quantities defined below which may be related to θ_{eff}; m_1 and m_2, the masses of the beam and scattering particles, respectively.

The use of classical scattering theory in deriving Eq. (5) is a well-justified approximation to quantum scattering theory if the fractional uncertainty in the momentum and in the change of momentum of the scattering system during a collision are both very much less than unity.[16] For both series of measurements shown in Fig. 2, these fractional uncertainties are of the order of 10^{-3} (momentum) and 10^{-2} (change in momentum).

[14] M. C. Kells, J. Chem. Phys. **16**, 1174 (1948).
[15] E. H. Kennard, *Kinetic Theory of Gases* (McGraw-Hill Book Company, Inc., New York, 1938), p. 115 ff.
[16] I. Amdur, J. Chem. Phys. **28**, 987 (1958).

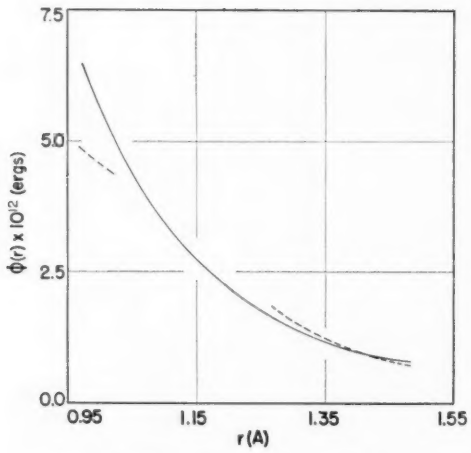

FIG. 4. He-He interaction potential.

The quantities θ_{eff}, $\langle\theta^{-2/s}\rangle$, and $\langle\theta^{1-2/s}\rangle$ are defined with reference to the coordinate system in Fig. 3 where, for mathematical facility, the beam is shown as originating at a point in the center of the hole in the atom gun and travelling in divergent straight lines toward the detector. For the geometry of the present apparatus, it can be shown that such a divergent beam leads to the same values of θ_{eff}, $\langle\theta^{-2/s}\rangle$, and $\langle\theta^{1-2/s}\rangle$ as a nondivergent beam travelling in straight lines parallel to the beam axis. Accordingly, a point $P(\beta, x, \eta)$ in the scattering volume is located by the "conical" coordinates β, x, η, where β is a polar angle measured from the beam axis, x is the vertical distance from the origin O to the plane in which P is located, and η is an azimuthal angle specifying the rotation of P from some reference direction. The scattering volume, in the scattering chamber, is specified by the maximum value of β, β_m, at the edge of the detector mask, and by the values of x, x_1 and x_2, at the top and bottom of the scattering chamber. The radius of the circular aperture in the detector mask is ρ, and the distance of the detector surface from the origin is D.

When a beam particle undergoes a collision in the scattering volume at P, θ_d is the minimum angular deflection required to miss the aperture in the detector mask; in general, θ_d is a function of $P(\beta, x, \eta)$ and of ϕ, an azimuthal angle defining the rotation of the plane containing the beam particle trajectory about a reference direction on the detector surface.

In terms of the coordinates and parameters in Fig. 3,

$$\langle\theta^{-2/s}\rangle=(2\pi V)^{-1}\int_0^{2\pi}\int_V \theta_d^{-2/s}dVd\phi \tag{6}$$

$$\langle\theta^{1-2/s}\rangle=(2\pi V)^{-1}\int_0^{2\pi}\int_V \theta_d^{1-2/s}dVd\phi, \tag{7}$$

where $dV=x^2\beta d\beta dx d\eta$ and

$$\theta_d=\{\rho/(D-x)\}\{-(\beta D/\rho)\cos\phi+[1-(\beta D/\rho)^2\times\sin^2\phi]^{\frac{1}{2}}\}. \tag{8}$$

In the present case, the expressions for $\langle\theta^{-2/s}\rangle$ and $\langle\theta^{1-2/s}\rangle$ have not been averaged over an intensity distribution since the intensity in the central portion of the beam which was intercepted by the aperture in the detector mask appeared to be essentially constant.

Equations (6) and (7) may be integrated to yield

$$\langle\theta^{-2/s}\rangle=XYZ; \qquad \langle\theta^{1-2/s}\rangle=X'Y'Z', \tag{9}$$

where

$$X=\pi^{\frac{1}{2}}\Gamma(\tfrac{3}{2}-1/s)/\Gamma(2-1/s);$$

$$X'=\pi^{\frac{1}{2}}\Gamma(2-1/s)/\Gamma(\tfrac{5}{2}-1/s)$$

$$Y=\frac{y_1^{3+2/s}-y_2^{3+2/s}}{3+2/s}-2D\frac{y_1^{2+2/s}-y_2^{2+2/s}}{2+2/s}+D^2\frac{y_1^{1+2/s}-y_2^{1+2/s}}{1+2/s};$$

$$Y'=\frac{y_1^{2+2/s}-y_2^{2+2/s}}{2+2/s}-2D\frac{y_1^{1+2/s}-y_2^{1+2/s}}{1+2/s}+D^2\frac{y_1^{2/s}-y_2^{2/s}}{2/s}$$

$$Z=\frac{6}{\pi(1-2/s)}\frac{(2\rho)^{-2/s}}{x_2^3-x_1^3};$$

$$Z'=\frac{12}{\pi(2-2/s)}\frac{(2\rho)^{1-2/s}}{x_2^3-x_1^3}, \tag{10}$$

after setting $V=\pi\beta_m^2(x_2^3-x_1^3)/3$, $D-x_1=y_1$, and $D-x_2=y_2$. The effective angular aperture θ_{eff}, which does not appear as such in the theoretical expression for S, is defined as $\theta_{eff}=\langle\theta^{-2/s}\rangle^{-s/2}$ and may be thought of as the average angle through which a beam particle must be deflected in order to miss the aperture in the detector mask. It is θ_{eff} rather than the simple geometric angular aperture θ which is the significant apparatus parameter in the present type of scattering experiments.

If $\phi(r)=K/r^s$ is a valid representation of the intermolecular potential over the range of r which is significant in the scattering collisions, then, according to Eq. (5), a plot of $\log S$ vs $\log E$ should be a straight line. The slope of the line $-2/s$ gives the numerical value of s, and the intercept, $\log\pi(KC)^{2/s}[\langle\theta^{-2/s}\rangle-\langle\theta^{1-2/s}\rangle(m_1+m_2)/m_2C]$, the value of K, since C, $\langle\theta^{-2/s}\rangle$ and $\langle\theta^{1-2/s}\rangle$ can be evaluated when s is known. Accordingly, the results shown in Fig. 2 were fitted, by the method of least squares, to obtain the functions

$$\text{(series I)} \quad \log S=-2.9442-0.3939\log E \tag{11}$$

$$\text{(series II)} \quad \log S=-2.9979-0.4019\log E, \tag{12}$$

for S in A^2 and E in ergs. Equations (11) and (12), which correspond to the smooth curves in Fig. 2, reproduce the experimental values of S with average absolute deviations of 3.1% and 1.5%, respectively,

and lead to the following relations for $\phi(r)$,
(series I)

$$\phi(r)=5.30\times10^{-12}/r^{5.08}\text{ erg}\quad(0.97\text{ A}<r<1.35\text{ A})\quad(13)$$

(series II)

$$\phi(r)=5.83\times10^{-12}/r^{4.98}\text{ erg}\quad(0.98\text{ A}<r<1.48\text{ A}).\quad(14)$$

The ranges of r for which Eqs. (13) and (14) are valid are obtained by finding the minimum and maximum values of the distance of closest approach r_0 from values of S calculated from Eqs. (11) and (12) using the smallest and largest experimental values of E. For this purpose Eq. (5) is rewritten as

$$S=\pi(KC/E)^{2/s}\langle\theta^{-2/s}\rangle[1-2\langle\theta^{1-2/s}\rangle/(C\langle\theta^{-2/s}\rangle)]$$
$$=\pi r_0^2[1-2\langle\theta^{1-2/s}\rangle/(C\langle\theta^{-2/s}\rangle)],\quad(15)$$

where the term $1-2\langle\theta^{1-2/s}\rangle/(C\langle\theta^{-2/s}\rangle)$ has a value of 0.985 for both series I and series II.

If Eq. (15) is solved for the potential parameter K the result may be written

$$K=(E/C)(S/0.985\pi)^{s/2}\langle\theta^{-2/s}\rangle^{-s/2}.\quad(16)$$

It is interesting to compare the values of the effective angular aperture $\theta_{\text{eff}}=\langle\theta^{-2/s}\rangle^{-s/2}$ with the simple average geometric aperture θ to demonstrate the magnitude of the error which can be made in evaluating potential parameters with improper analysis of the beam-detector geometry. In laboratory coordinates, θ_{eff} is 7.44×10^{-3} rad for series I and 7.55×10^{-3} rad for series II, whereas θ for both series is more than twofold larger, 1.62×10^{-2} rad.

Values of $\phi(r)$ from Eq. (14) average 10.5% greater than those from Eq. (13) in the common range of validity, 0.97 A to 1.48 A, and 10.7% greater over the maximum valid range for both series. Since there is no *a priori* reason for preferring one set of values to the other, the geometric mean of the two functions will be used to represent the best relation derivable from the two sets of measurements, namely,

$$\phi(r)=5.56\times10^{-12}/r^{5.03}\text{ erg}\quad(0.97\text{ A}<r<1.48\text{ A}).\quad(17)$$

DISCUSSION

The potential calculated from Eq. (17) is shown as the solid curve in Fig. 4 which also shows, as dashed curves, those portions of the potentials calculated from Eqs. (1) and (2) which fall within the range of Eq. (17). The portion of Eq. (1) near 1 A averages about 18% lower (with a maximum deviation of 25%) than the corresponding portion of Eq. (17). The portion of Eq. (2) between 1.27 A and 1.48 A intersects Eq. (17), showing an average absolute deviation of about 4.5% and a maximum deviation of 9%. It is therefore concluded that in the range of common validity Eqs. (1), (2), and (17) are in reasonable agreement. It may also be assumed that the potential between 1.02 A and 1.27 A has been confirmed since Eq. (17) represents quite well any possible interpolation between the ranges of validity of Eqs. (1) and (2). No appraisal of the reliability of Eq. (1) at distances smaller than 0.97 A is made at this time since, as mentioned previously, a redetermination of the intermolecular potential in this region of close distance interaction is in progress.

Although the scattering cross section at a given energy depends, effectively, upon the values of $\phi(r)$ over a narrow but finite range of r near r_0, the distance of closest approach during a collision, the limits of the range of validity of a given potential energy function are conventionally taken as those values of r_0 which correspond to the extreme values of S in the appropriate series of measurements. For this reason, and because a single empirical function, such as $\phi(r)=K/r^s$, can be used only as an approximate representation of the potential over a restricted range of r, intermolecular potentials determined from scattering experiments generally show marked discontinuities in slope where results from different investigations overlap. A typical example of this is shown in Fig. 4 near 1 A, and an exception to the general behavior is shown in the same figure near 1.5 A. In the latter case the unusually good concordance may result, in part, from the use of beam apparatuses which were much improved over that used to obtain the results of Eq. (1), and in part from the large range of overlap of Eqs. (2) and (17).

In view of the above considerations, it should be emphasized that, in general, *extrapolations of potential functions beyond their ranges of validity are not justified.* On the contrary, it is probably desirable to adopt a conservative approach which takes as the useful range of validity one that is slightly smaller than that which is conventionally defined, and which relies upon suitable direct measurements to obtain experimental potential energy functions whose ranges of validity, whenever possible, considerably overlap functions obtained in other investigations.

Since it is not feasible in a single investigation to obtain potential energy information over an extended range of interaction distance, and since the blending of separate potential energy functions in regions of overlap is somewhat subjective, it is interesting to examine the correlation of Buckingham[17] who obtained an analytical function for the He-He potential for r between 0 and 2.6 A. The general form of his function, which has the proper theoretical behavior in the limits of very small r and very large r is

$$\phi(r)=(Z_1Z_2/r)\,p(r)\,\exp(-ar),\quad(18)$$

where $p(r)=1+p_1r+p_2r^2+p_3r^3+p_4r^4$ and Z_1, Z_2 are the nuclear charges of the interacting particles. Buckingham has used the electronic energy of the "united

[17] R. A. Buckingham, Trans. Faraday Soc. **54**, 453 (1958).

atom," at $r=0$, the position of the zero of $\phi(r)$ (at $r=2.6$ A), and available scattering results, to evaluate the constants a, p_1, p_2, p_3, and p_4. For the He-He system the result is

$$\phi(r)=(92.3/r)\exp(-4.68r)[1+0.501r-8.64r^2+17.66r^3-5.56r^4]\times10^{-12}, \quad (19)$$

where $\phi(r)$ is in ergs and r is in A.

Between 0.97A and 1.48 A, values of $\phi(r)$ from Eq. (19) show an average absolute deviation of about 11% with respect to values calculated from Eq. (17). At 0.97 A the ratio of $\phi(r)$ from Eq. (19) to that from Eq. (17) is 0.72 and the corresponding ratio at 1.48 A is 1.06. Between 1.02 A and 1.27 A, the region for which scattering results were previously unavailable, Buckingham's equation and the present results agree within an average of about 9%.

It is the opinion of the authors that in the range 0.97 A to 1.48 A, the values of $\phi(r)$ from Eq. (17) are correct to 20%. This estimate takes into account concordance of the results of series I and series II as summarized in Eqs. (13) and (14), agreement of the present results with portions of earlier work as summarized in Eqs. (1) and (2), possible sources of error in the experimental determination of the scattering cross sections, and the values of the potential at somewhat larger distances as derived from measurements of transport properties and second virial coefficients of helium at relatively high temperatures. In view of this it would appear that most of the more recent quantum mechanical calculations of $\phi(r)$ are somewhat high in the region where results derived from scattering experiments were hitherto unavailable, namely, 1.02 A to 1.27 A. For example, at 1.058 A and 1.164 A values obtained by Sakamoto and Ishiguro[7] are about 38% higher than those from Eq. (17); at 1.097 A the value calculated by Moore[10] is 40% higher, while at 1.254 A the value of Griffing and Wehner[6] is 41% higher, that of Hashino and Huzinaga,[9] 30% higher. These deviations are not in themselves very serious, but in terms of a trend which may lead to more serious deviations at still smaller distances, the discrepancies may be significant. It is interesting to observe that the calculations of Lynn[8] are an exception to the observed trend. At 1.254 A he reports two values which are 0.6% lower, and 5.6% higher than that from Eq. (17), where his second value is obtained by using a parameter which is adjusted in accordance with Buckingham's equation Eq. (19) to obtain agreement at very much smaller values of r.

ACKNOWLEDGMENTS

The authors wish to thank Professor James W. Beatty, Jr., Professor William G. Sly, and Anthony P. Malinauskas for their help with calculations involved in this investigation. They also wish to express their appreciation to the M.I.T. Computation Center, Cambridge, Massachusetts, where part of the computational work was done.

Probability of Initial Ring Closure in the Restricted Random-Walk Model of a Macromolecule

B. J. HILEY AND M. F. SYKES*

Wheatstone Physics Laboratory, King's College, London, England

(Received August 22, 1960)

The probability of initial ring closure in the restricted random-walk model of a macromolecule is investigated. From a study of the known exact numbers of polygons on the simple quadratic lattice up to 18 sides and on the triangular lattice up to 16 sides, it is concluded that the probability of initial ring closure in two-dimensions of large ring size k varies inversely as $k^{1.83-\theta}$, where $0\leqslant\theta\leqslant 0.05$, and this is significantly higher than the dependence on the inverse square of k found by Wall's statistical investigation. It is found that the mean area of initial ring closures in a plane varies as k^1.

1. INTRODUCTION

In a recent series of papers Wall and his collaborators[1] have studied the mean dimensions of a macromolecule by a statistical investigation of restricted random walks on a lattice. A restricted random walk is a random walk subject to the condition that no site on the lattice is passed through more than once and the exact determination of the effect of this "excluded volume" is a matter of great mathematical difficulty. Wall[2] investigated the mean square end-to-end separation $\langle r_n^2\rangle_{Av}$ of a restricted walk of n steps statistically by Monte Carlo methods and employed a high-speed digital computor to generate the walks. The primary object of the investigation was to characterize the behavior of $\langle r_n^2\rangle_{Av}/n$ for large values of n by numerical procedures. If a restricted random walk of n steps on a lattice of coordination number q is continued in any of the $(q-1)$ possible directions it may fail owing to a self-intersection or "ring closure." The probability p of a failure at the $(n+1)$th step is the sum of the probabilities of ring closures of all possible sizes,

$$p=\sum_k p_k, \tag{1}$$

where p_k is the probability of failure due to a loop of k steps. Wall, Hiller, and Atchison[3] were able to establish a quasi-empirical difference equation between the successive $\langle r_n^2\rangle_{Av}$ which related these to the function $\sum_k kp_k$. From an examination of numerical data they noted that the probability of closing a loop of k steps at the origin $(k=n)$ was greater than that of closing a loop of an equal number of steps but not ending at the origin $(k<n)$. They therefore distinguished between the probability of initial ring closure (p_k^0) and the limiting ring closure probability (p_k). They concluded that for large k the behavior of these probabilities was approximately represented by expressions of the type

$$p_k^0=c^0/k^2, \tag{2a}$$

$$p_k=c/k^2, \tag{2b}$$

the constants c^0 and c depending on the particular lattice but the index of k being comparatively insensitive to changes of structure and indicated for both two and three-dimensional lattices. It is tempting to conclude that the results (2a) and (2b) are exact in the limit $k\to\infty$, and it is the object of this paper to investigate this point more closely.

The Monte Carlo methods employed by Wall provide a large sample of walks of n steps (for values of n between 1 and 800) from which satisfactory data on such properties as end-to-end length can be obtained. For the investigation of ring closures, samples with values of n up to 50 were employed. The probability p_k^0 is, however, particularly difficult to sample in this way since for large k the probability that a walk will fail at the origin becomes very small and this substantially reduces the accuracy of the statistical data.[4] It seems probable that the asymptotic behavior of p_k^0 could be deduced by extrapolation of the behavior of the values for small k if a sufficient number of terms in the sequence p_k^0 could be obtained. An attempt has been made to do this by Fisher and Sykes,[5] but owing to the inadequacy of the data they were unable to obtain accurate estimates of the asymptotic behavior. Their predictions for the behavior of p_k^0 and p_k can be summarized as

$$p_k^0=c^0/k^{1.80\pm 0.10} \text{ for three-dimensional lattices} \tag{3a}$$

and

$$p_k^0=c^0/k^{1.75\pm 0.10} \text{ for two-dimensional lattices,} \tag{3b}$$

and these are not in agreement with those of Wall.

* Imperial Chemical Industries Research Fellow, University of London.

[1] F. T. Wall, L. A. Hiller, Jr., and W. F. Atchison, J. Chem. Phys. **23**, 2314 (1955); **26**, 1742 (1957); F. T. Wall, R. J. Rubin, and L. M. Isaacson, *ibid.* **27**, 186 (1957).

[2] F. T. Wall, L. A. Hiller, Jr., and D. J. Wheeler, J. Chem. Phys. **22**, 1036 (1954).

[3] F. T. Wall, L. A. Hiller, Jr., and W. F. Atchison, J. Chem. Phys. **23**, 913 (1955).

[4] F. T. Wall (private communication).

[5] M. E. Fisher and M. F. Sykes, Phys. Rev. **114**, 45 (1959).

Type	Number on lattice of N sites	Area	Contribution to u_8
(a)	N	4	16
(b)	$2N$	3	32
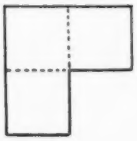 (c)	$4N$	3	64

FIG. 1. The three space types of p_8 on the simple quadratic lattice.

As an alternative to the direct examination of p_k^0 we shall study the related quantities c_n (the total number of n step restricted walks) and u_n (the total number of random walks that close on the last step). We then have

$$p_k^0 = u_k/(q-1)c_{k-1}. \tag{4}$$

We shall examine the data available and conclude that we may write for large n

$$c_n \sim n^g \mu^n \tag{5a}$$

$$u_n \sim n^h \nu^n. \tag{5b}$$

The asymptotic forms (5a) and (5b) have been previously proposed by Fisher and Sykes,[5] Rushbrooke and Eve,[6] and, apart from the factors n^g, n^h, by Wall.[1] In (5a) and (5b) μ and ν are constants for a given lattice. That $c_n \sim \mu^n$ has been proved rigorously by Hammersley.[7] We shall conclude that $\mu = \nu$ and this again has been suggested by the authors quoted above.[1,5,6] With this last result we have from (4) and (5a) and (5b)

$$p_k^0 \sim n^{h-g}. \tag{6}$$

As might be expected, the c_n assume a smooth behavior for smaller values of n than the corresponding u_n and the asymptotic behavior of the c_n can be inferred from the data already available.[5] Our task is therefore to investigate the u_n. (For most lattices more data is available for the u_n than for the c_n and extrapolation of the p_k^0 is then wasteful of this data.) We shall pay special attention to the two-dimensional problem since in this case additional data can be obtained by special methods.[8] We shall seek to show that the u_n do assume a smooth behavior for values of n not very much in excess of those required for smooth behavior of the walks c_n. Since as a by product of their derivation we have obtained the areas of all the two-dimensional polygons, we shall investigate the mean area of the closed walks in this case and show that the concept of area provides an alternative method of performing the extrapolation.

2. METHOD OF EXACT ENUMERATION

The first 18 coefficients of the chain-generating function defined[5] by

$$C(x) = \sum_{n=0}^{\infty} c_n x^n, \qquad c_0 = 1; \tag{7}$$

have been obtained by using a counting theorem which greatly reduces the labor of enumeration.[9] In the same way the corresponding expansions for the triangular and simple cubic lattices have been derived up to the term in x^{11} and we quote these series in the Appendix. (These data represent two further coefficients for the simple quadratic and simple cubic lattices and one for the triangular lattice compared with that used by Fisher and Sykes[5]). It will be part of our task to use these series to obtain estimates of μ, and they will be examined in the next section.

By using special methods based on the existence of a dual lattice,[8] the number of polygons with up to 18 sides on the simple quadratic lattice has been obtained. If p_n is the number of polygons per site, each individual polygon can be described from each vertex in two directions, and therefore $u_n = 2np_n$. On defining a generating function

$$U(x) = \sum_{n=0}^{\infty} u_n x^n, \qquad u_0 = 1, \tag{8}$$

we find

$$U(x) = 1 + 8x^4 + 24x^6 + 112x^8 + 560x^{10} + 2976x^{12} + 16\,464x^{14} + 94\,016x^{16} + 549\,648x^{18} + \cdots. \tag{9}$$

Each coefficient in (9) is made up from contributions from polygons with an equal number of sides but possibly differing in area. For example the term $112x^8$

[6] G. S. Rushbrooke and J. Eve, J. Chem. Phys. **31**, 1333 (1959).

[7] J. M. Hammersley, Proc. Cambridge Phil. Soc. **53**, 642 (1957).

[8] C. Domb, Advances in Phys. (April and June, 1960), review article.

[9] M. F. Sykes (to be published). (a) For a more detailed introductory treatment, the reader is referred to the work cited in footnote 8. (b) For the triangular lattice we shall use the power of y to denote the area expressed as multiples of the equilateral triangles from which the lattice is composed.

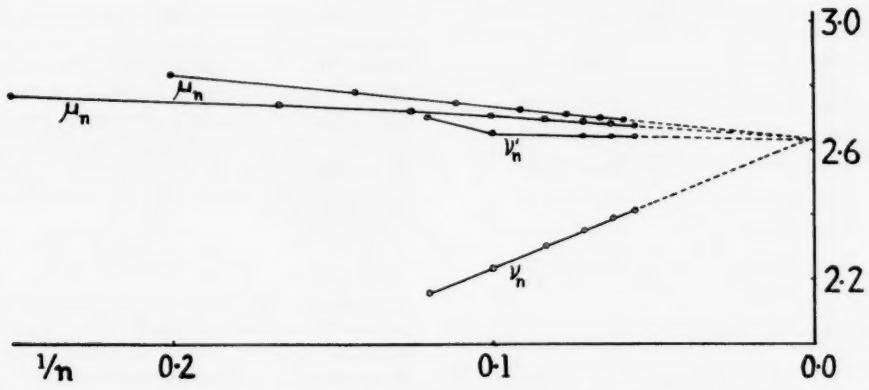

FIG. 2. Values of μ_n, ν_n, and ν_n' for the simple quadratic lattice against $1/n$.

results from three possible space-types[9a] of polygon which we illustrate in Fig. 1. We shall later show that an examination of the areas of polygonal paths provides a method of extrapolating the behavior of u_n, and we shall therefore include this information in the generating function by defining a dummy variable y, and denote a closed path of area a by y^a. Thus referring to Fig. 1. we shall write

$$u_8(y)=16y^4+96y^3, \tag{10}$$

the numerical value of u_8 being obtained by setting $y=1$. The definition (8) now becomes

$$U(x,y)=\sum_{n=0}^{\infty}u_n(y)x^n. \tag{11}$$

We give the expansion of $U(x,y)$ for the simple quadratic lattice in the Appendix together with the corresponding expansion[9b] for the triangular lattice which we have been able to extend as far as the term in x^{16}. The expansion of $U(x)$ for the simple cubic lattice has been obtained by Rushbrooke and Eve[8] up to the term in x^{14} by the enumeration of all the possible types on an electronic computor. (This series is also quoted in the Appendix).

For a plane lattice the total area enclosed by all the paths contributing to $u_n(y)$ will be $u_n'(1)$, the prime denoting differentiation with respect to y. We shall denote the mean area of all such paths by $\langle A_n\rangle_{Av}$ and we have

$$\langle A_n\rangle_{Av}=u_n'(1)/u_n(1). \tag{12}$$

Following Fisher and Sykes we shall introduce the ratios

$$c_n/c_{n-1}=\mu_n \tag{13a}$$

$$u_n(1)/u_{n-1}(1)=u_n/u_{n-1}=\nu_n \tag{13b}$$

[in the case of a loose-packed lattice we shall write $\nu_{2n}=(u_{2n}/u_{2n-2})^{\frac{1}{2}}$], and we shall also examine the ratios

$$u_n'(1)/u_{n-1}'(1)=\nu_n'. \tag{13c}$$

The values of μ_n, ν_n, and ν_n' for the simple quadratic lattice have been plotted against $1/n$ in Fig. 2. Their behavior suggests a proportionality to $1/n$ with increasing n and a common limit close to 2.64. It was for this reason that the asymptotic expressions (5a) and (5b) for c_n and u_n were first proposed, and we shall now introduce a similar asymptotic expression for u_n', namely,

$$u_n'(1)\sim n^{h'}\nu'^n. \tag{14}$$

We shall henceforth assume in all our treatment that for the lattices we shall study $\mu=\nu$ (although a rigorous proof of this has not been given) and that $\nu=\nu'$. It is quite easy to see in a nonrigorous manner that the ratios ν_n and ν_n' will have a common limit. The area of a polygon with n sides cannot increase slower than n or faster than n^2, and we should therefore expect the mean area to behave for large n like n^r, where $1\leq r\leq 2$ and $u_n(1)$ and $u_n'(1)$ would then only differ by a factor of order n^r. In Sec. 5 we will attempt to estimate the actual value of r by extrapolation.

3. ESTIMATION OF μ FROM THE SERIES $C(x)$

To estimate μ for the simple quadratic lattice we shall examine the ratios μ_n derived from the series $C(x)$. It is clear from Fig. 2 that there is a marked alternation between "odd" and "even" values. We therefore calculate the linear projections of alternate pairs of points in Fig. 2. at the line $n=\infty$, following the technique of Domb and Sykes,[10] as

$$B_n=\tfrac{1}{2}(n\mu_n-(n-2)\mu_{n-2}), \tag{15}$$

and the values of this quantity are given in Table I. They fall quite naturally into an odd and even series, and for values of $n>9$ a steady behavior is establishing itself and one may suppose that the limit lies between the two columns in Table I, or

$$2.635<\mu<2.643,$$

[10] C. Domb and M. F. Sykes, Proc. Roy. Soc. (London) **A240,** 214 (1957).

TABLE I. Values of B_n for the simple quadratic lattice.

Even series	Odd series
$B_6=2.68388$	$B_7=2.64615$
$B_8=2.65559$	$B_9=2.62809$
$B_{10}=2.65919$	$B_{11}=2.62817$
$B_{12}=2.65295$	$B_{13}=2.63128$
$B_{14}=2.64832$	$B_{15}=2.63399$
$B_{16}=2.64543$	$B_{17}=2.63515$
$B_{18}=2.64390$	

the two extremes, corresponding to $n=17$ and $n=18$, being separated by only 0.33%. To make an estimate of the limit we form the average sequence $B_n^*=\frac{1}{2}(B_n+B_{n-1})$ for even values of n (the corresponding odd series being slightly higher but also declining) and obtain

$$B_{10}^*=2.64364$$
$$B_{12}^*=2.64056$$
$$B_{14}^*=2.63980$$
$$B_{16}^*=2.63971$$
$$B_{18}^*=2.63952.$$

The behavior is not quite regular, but we estimate that the true value of μ is not far below 2.6395 and take as a first choice 2.6390. With this approximation we evaluate the successive g_n defined by

$$\mu_n=\mu(1+g_n/n) \tag{16}$$

and find, by repeating the same procedure for these quantities that we have used for the μ_n, that the corresponding average sequence which we denote by G_n^* is

$$G_{10}^*=0.31423$$
$$G_{12}^*=0.32425$$
$$G_{14}^*=0.33198$$
$$G_{16}^*=0.33215$$
$$G_{18}^*=0.33167.$$

From this we conclude that probably $0.33<g<0.34$, and since the estimated value of μ if in error will probably be too high and lead to too low a slope, we may suppose that g could very well be exactly $\frac{1}{3}$ as suggested by Fisher and Sykes.[5]

An approximate value of the slope having been obtained in this way we now attempt to obtain an improved value for μ by observing that if g is the correct slope the quantity $d_n=n\mu_n/(n+g)$ tends to μ as $n\to\infty$ with no slope on the $1/n$ plot. If we employ a value of g that is only approximately correct, the limit will be unaffected but there will be a small residual slope proportional to the error in g. The quantity d_n is a function of one ratio only and it is found that the successive values are more regular than the corresponding linear projections, the device of linear projection tending to magnify small irregularities in the data. In Fig. 3 we plot the d_n against $1/n$ (curves I_a, I_b) together with the means for even values (curve II) as well as B_n^* (curve III). It will be seen that curve II is very smooth and we estimate finally that

$$\mu=2.6390\pm0.0005. \tag{17}$$

We observe that (17) is in very good agreement with the latest estimate of Wall[11] of $\mu=2.6395\pm0.0015$. Wall's estimate is based on a Monte Carlo method in which very long walks of the order $n=800$ were sampled. Since his method does not take account of the slope, it has been suggested[12] that Wall's estimate should be reduced by a factor of about $(1-1/2400)$ when it becomes $\mu=2.6385\pm0.0015$. The very close agreement of these two estimates, obtained by independent methods, is striking confirmation of the proposed limit and also of the asymptotic behavior on which the estimate from $C(x)$ is based.

The series $C(x)$ for the triangular lattice was also examined by Fisher and Sykes[5] and as we have added only one further coefficient c_{11} we shall only remark that proceeding in an analogous way we have confirmed

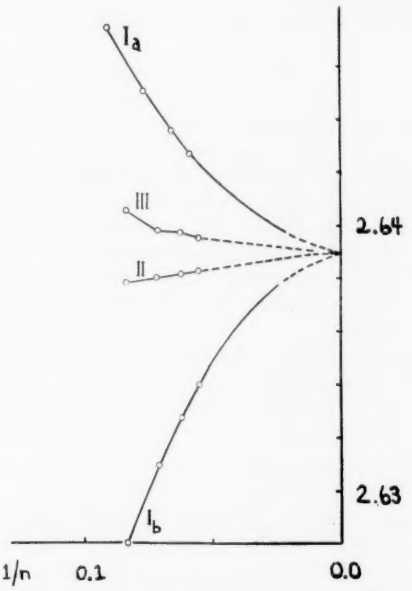

FIG. 3. Simple quadratic lattice. Estimation of μ. Curves I_a, I_b: $d_n=n\mu_n/(n+\frac{1}{3})$; curve II: mean of curves I_a, I_b; curve III: B_n^*.

[11] F. T. Wall and J. J. Erpenbeck, J. Chem. Phys. **30**, 634 (1959).
[12] M. E. Fisher (private communication).

their estimate within closer limits as

$$\mu = 4.152 \pm 0.003. \tag{18}$$

Although the coefficients are larger than the corresponding coefficients on the simple quadratic lattice and the odd-even oscillation is absent, it is difficult to make a more precise estimate as only the last four coefficients suggest a steady behavior. In view of the importance of an accurate estimate for μ in estimating limiting slopes it would be advisable to have further terms of this sequence and we are developing methods by which these might be obtained. On evaluating the g_n we find as successive estimates for g the slopes $g_7=0.3221$, $g_8=0.3237$, $g_9=0.3244$, $g_{10}=0.3250$, $g_{11}=0.3256$, and a limiting slope of $\frac{1}{3}$ could be applicable in this case also. This value has been taken, and the quantity $n\mu_n/(n+\frac{1}{3})$ used to estimate (18) is plotted against $1/n$ in Fig. 5, curve I.

TABLE II. Values of h_n and h_n' for the simple quadratic lattice.

$h_{10}=-1.5268$	$h_{10}'=+0.0581$
$h_{12}=-1.5175$	$h_{12}'=+0.0529$
$h_{14}=-1.5222$	$h_{14}'=+0.0294$
$h_{16}=-1.5118$	$h_{16}'=+0.0283$
$h_{18}=-1.5080$	$h_{18}'=+0.0246$

4. RING CLOSURE ON THE SIMPLE QUADRATIC LATTICE

On using the value $\mu=2.6390$ estimated in the previous section we calculate the successive slopes of the u_n from

$$\nu_n=\mu(1+h_n/n), \tag{19}$$

and these together with the corresponding h_n' for $u_n'(1)$ are given in Table II. The values are not very regular and we may suppose that a smooth behavior for the u_n is not yet established, and this conclusion is what might be expected in view of the relatively few polygons for small values of n. By a graphical extrapolation against $1/n$ we estimate that $h_n\to-1.5+\theta$ and $h_n'\to\theta'$ with $0\leq\theta\leq0.05$ and $0\leq\theta'\leq0.025$. It has been remarked by Wall[2] that it would not be unreasonable to expect the powers that occur in these problems to be simple numbers like $\frac{3}{2}$, 2, $\frac{5}{2}$, etc., and while the best objective choice for h is perhaps -1.46, the evidence is not strong enough to disprove the conjecture that h is exactly $-\frac{3}{2}$ which is appealing on the grounds of simplicity. (Simple fractions do occur in certain closely related problems that arise in the theory of the Ising model.) In support of this latter conjecture we would observe that the very small slope of $u_n'(1)$ suggests a logarithmic singularity or $h_n'\to0$, and we shall advance evidence in the next section that $h'-h=\frac{3}{2}$. For the probability of initial ring closure to be inversely proportional to the square of the ring size we would require $g-h=2$; the evidence that g is close to $\frac{1}{3}$ is strong and this would imply a value of h as low as -1.66. We think Table II is evidence that this cannot be correct, but we would not expect Wall's estimate to be far wrong in view of the good agreement already found with his estimate for μ.

Because of the somewhat irregular behaviour of the u_n for small values of n, we have derived further terms for the plane triangular lattice. Before examining these we shall take up the study of the area of a polygonal closure on a plane lattice.

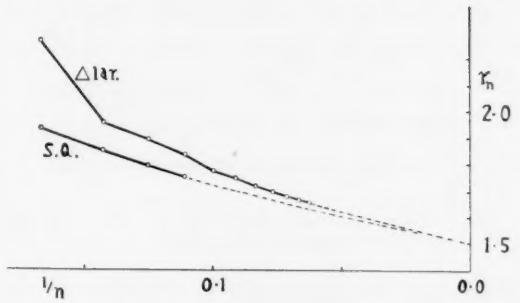

FIG. 4. Estimation of asymptotic behavior of the mean area of a polygonal closure on simple quadratic and triangular lattices.

5. MEAN AREA OF A POLYGONAL CLOSURE

One of the difficulties in estimating limiting slopes is the uncertainty of the value of μ. We shall now investigate the mean area of a polygonal closure and as we have remarked earlier this is independent of any choice of μ.

We shall find that $\langle A_n\rangle_{Av}\sim n^r$, and on this basis we consider successive values of r_n defined by

$$\langle A_n\rangle_{Av}/\langle A_{n-1}\rangle_{Av}=1+r_n/n. \tag{20}$$

In Fig. 4 we plot these r_n for the triangular and simple quadratic lattices against $1/n$. (For the simple quadratic lattice on which polygons only occur for even values of n we have modified (20) to $\langle A_{2n}\rangle_{Av}/\langle A_{2n-2}\rangle_{Av}=1+r_n/n$). So far as can be judged the r_n for these two lattices would appear to have a common limit about 1.50 ± 0.04 which we shall take to be $\frac{3}{2}$. This result

TABLE III. Triangular lattice. Data for $\mu=4.152$.

n	h_n	h_n'	ν_n'	$n\nu_n/(n-1.5)$
10	−1.46469	0.04876	4.17224	4.16925
11	−1.46374	0.05081	4.17118	4.16785
12	−1.45450	0.05498	4.17102	4.17000
13	−1.45641	0.05131	4.16839	4.16774
14	−1.45546	0.05050	4.16698	4.16679
15	−1.45610	0.04825	4.16535	4.16550
16	−1.45701	0.04564	4.16384	4.16431

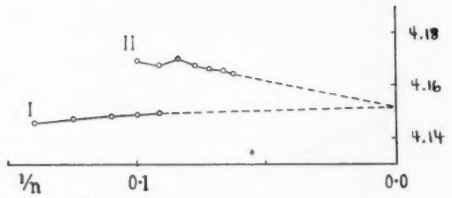

FIG. 5. Triangular lattice. Estimation of μ. Curve I: $n\mu_n/(n+\frac{1}{3})$; curve II: $n\nu_n/(n-\frac{3}{2})$.

implies that for a plane lattice

$$h'-h=\tfrac{3}{2}. \tag{21}$$

6. RING CLOSURE ON THE TRIANGULAR LATTICE

We give in Table III the values of h_n and h_n' for the triangular lattice calculated for $\mu=4.152$, together with the values of ν_n' and $n\nu_n/(n-1.5)$.

From the first two columns and the result (21) we conclude that $h_n\to-1.5+\theta$, $h_n'\to\theta$, and $0\leq\theta\leq0.05$, and the third and fourth columns confirm the conclusion of the preceding section that the slopes of $u_n(1)$ and $u_n'(1)$ differ by $\frac{3}{2}$, since the successive values in these columns are approaching equality. In Fig. 5 we have plotted $n\nu_n/(n-1.5)$ against $1/n$ together with $n\mu_n/(n+\frac{1}{3})$. It will be seen that these quantities are apparently converging to a limit not far from 4.152 and this provides confirmation of (18). (A graphical extrapolation of h_n against $1/n$ suggests $h_n\to-1.46$ in remarkable agreement with the corresponding result for the simple quadratic lattice.)

7. RING CLOSURE ON THE SIMPLE CUBIC LATTICE

The problem of ring closure on the simple cubic lattice has recently been studied by Rushbrooke and Eve.[6] Since it seems that more reliable values of μ can be obtained from the series $C(x)$ we have added two more coefficients to the data employed by Fisher and Sykes.[5] By using these, together with the extra polygon (p_{14}) quoted by Rushbrooke and Eve,[6] we have carried out an examination analogous to that employed in this paper for the simple quadratic lattice. The estimates divide again into an odd and even sequence the last pair, corresponding to μ_{10} and μ_{11}, indicating that $4.676<\mu<4.694$, the limits being separated by only 0.38%. While these are closer than the corresponding limits for the simple quadratic lattice a steady behavior has only just been established and a few more terms would seem desirable. The estimate we shall adopt is 4.680, and this leads to a probable value of g of 0.17 ± 0.03, and the following estimates for h:

$$h_8=-1.9454$$

$$h_{10}=-1.8452$$

$$h_{12}=-1.8085$$

$$h_{14}=-1.8008.$$

This sequence is not very regular but we may suppose that $h\to-1.75\pm0.05$.

8. CONCLUSIONS

We have found that the quantity c_n, the number of self-avoiding walks of n steps, assumes a steady behavior for quite small values of n (of order $n>9$) for the simple quadratic and triangular lattices. From an examination of further data we have confirmed the original conclusions of Fisher and Sykes that we may write for both these lattices

$$c_n\sim n^{\frac{1}{3}}\mu^n,$$

and we have estimated $\mu=2.6390\pm0.0005$ for the simple quadratic lattice and $\mu=4.152\pm0.003$ for the triangular lattice. By using these estimates in conjunction with the quantity u_n, the number of nonself-intersecting returns to the origin of n steps, which we have been able to derive together with data on the area enclosed by such returns, we have estimated that

$$u_n\sim n^{-1.50+\theta}\mu^n,$$

where $0\leq\theta\leq0.05$ for both the simple quadratic and triangular lattices. While we have advanced the hope that $\theta=0$, we have not found the data conclusive on this point. In the light of the evidence we have examined we conclude therefore that the probability of initial ring closure will behave for large n as

$$n^{-1.833+\theta}, \qquad 0\leq\theta\leq0.05. \tag{22}$$

Even in the extreme case of $\theta=0$ this is significantly greater than the n^{-2} suggested by Wall. We would therefore suggest that this latter conclusion results from the difficulty of obtaining an adequate sample of p_k^0 for large k by Monte Carlo methods.

For the simple cubic lattice we have estimated that

$$c_n\sim n^{0.17\pm0.03}\mu^n$$

$$u_n\sim n^{-1.75\pm0.05}\mu^n,$$

and very similar conclusions can be drawn from an examination of data on the face-centered cubic lattice. We thus estimate that for a three-dimensional lattice

$$p_k^0\sim n^{-1.92\pm0.08}. \tag{23}$$

While we have found that the slope of the functions $C(x)$ and $U(x)$ appears to be determined principally by the dimensionality of the lattice, it would seem from (22) and (23) that the probability of initial ring closure is not very sensitive to dimensionality. In this last respect our conclusions are in agreement with those of Wall.

We are continuing our study of this problem and of the closely related problem of the behavior of the limiting ring closure probability p_k which can also be extrapolated by our methods.

ACKNOWLEDGMENTS

The authors are indebted to Professor C. Domb and Dr. M. E. Fisher for helpful discussions and for criticism of the first draft of this paper. One of us (B.J.H.) would like to express gratitude to the Department of Scientific and Industrial Research for a research grant and the other (M.F.S.) to the University of London for the award of an I.C.I. fellowship.

APPENDIX

Expansions for $C(x)$

Simple Quadratic Lattice

$$C(x)=1+4x+12x^2+36x^3+100x^4+284x^5+780x^6+2172x^7+5916x^8+16\,268x^9+44\,100x^{10}+120\,292x^{11}+324\,932x^{12}+881\,500x^{13}+2\,374\,444x^{14}+6\,416\,596x^{15}+17\,245\,332x^{16}+46\,466\,676x^{17}+124\,658\,732x^{18}+\cdots.$$

Triangular Lattice

$$C(x)=1+6x+30x^2+138x^3+618x^4+2730x^5+11\,946x^6+51\,882x^7+224\,130x^8+964\,134x^9+4\,133\,166x^{10}+17\,668\,938x^{11}+\cdots.$$

Simple Cubic Lattice

$$C(x)=1+6x+30x^2+150x^3+726x^4+3534x^5+16\,926x^6+81\,390x^7+387\,966x^8+1\,853\,886x^9+8\,809\,878x^{10}+41\,933\,286x^{11}+\cdots.$$

Expansions for $U(x, y)$

Simple Quadratic Lattice

$$U(x,y)=1+8yx^4+24y^2x^6+16(6y^3+y^4)x^8+20(18y^4+8y^5+2y^6)x^{10}+24(55y^5+40y^6+22y^7+6y^8+y^9)x^{12}+28(174y^6+168y^7+134y^8+72y^9+30y^{10}+8y^{11}+2y^{12})x^{14}+32(566y^7+676y^8+656y^9+482y^{10}+310y^{11}+151y^{12}+68y^{13}+22y^{14}+6y^{15}+y^{16})x^{16}+36(1868y^8+2\,672y^9+2992y^{10}+2592y^{11}+2086y^{12}+1392y^{13}+864y^{14}+456y^{15}+218y^{16}+88y^{17}+30y^{18}+8y^{19}+2y^{20})x^{18}+\cdots.$$

Triangular Lattice

$$U(x,y)=1+12yx^3+24y^2x^4+60y^3x^5+12(14y^4+y^6)x^6+14(36y^5+6y^7)x^7+16(93y^6+27y^8+3y^{10})x^8+18(244y^7+110y^9+24y^{11}+2y^{13})x^9+20(648y^8+399y^{10}+135y^{12}+27y^{14}+3y^{16})x^{10}+22(1722y^9+1362y^{11}+636y^{13}+198y^{15}+42y^{17}+6y^{19})x^{11}+24(4603y^{10}+4460y^{12}+2631y^{14}+1113y^{16}+356y^{18}+87y^{20}+14y^{22}+y^{24})x^{12}+26(12\,360y^{11}+14\,136y^{13}+10\,032y^{15}+5340y^{17}+2244y^{19}+774y^{21}+210y^{23}+42y^{25}+6y^{27})x^{13}+28(33\,306y^{12}+43\,899y^{14}+36\,153y^{16}+22\,893y^{18}+11\,838y^{20}+5187y^{22}+1917y^{24}+585y^{26}+147y^{28}+27y^{30}+3y^{32})x^{14}+30(90\,128y^{13}+134\,336y^{15}+124\,992y^{17}+90\,926y^{19}+55\,202y^{21}+28\,992y^{23}+13\,296y^{25}+5290y^{27}+1836y^{29}+538y^{31}+128y^{33}+24y^{35}+2y^{37})x^{15}+32(244\,755y^{14}+406\,608y^{16}+419\,913y^{18}+341\,796y^{20}+235\,662y^{22}+142\,737y^{24}+77\,076y^{26}+37\,086y^{28}+16\,017y^{30}+6156y^{32}+2079y^{34}+609y^{36}+147y^{38}+27y^{40}+3y^{42})x^{16}+\cdots.$$

Simple Cubic Lattice

$$U(x)=1+24x^4+264x^6+3312x^8+48\,240x^{10}+762\,096x^{12}+12\,673\,920x^{14}+\cdots.$$

Statistical Mechanics of Monatomic Systems in an External Periodic Potential Field. I. Introduction, Virial Expansion, and Classical Second Virial Coefficient*

TERRELL L. HILL AND SAMUEL GREENSCHLAG

Department of Chemistry, University of Oregon, Eugene, Oregon

(Received September 13, 1960)

In the first section a general research program is outlined which is concerned with the behavior of an equilibrium macroscopic system (gas, liquid, or solid) of monatomic molecules in an external periodic potential field. The problems of particular interest are: condensation theory; crystalline state and theory of fusion; ideal degenerate gases; distribution functions; virial expansion for a gas; and the very dilute gas. In the second section the virial expansion is discussed and the classical second virial coefficient for an adsorbed monolayer on a crystal surface is calculated as an illustration. This computation is compared with results obtained from the two conventional cases which are limiting forms of the present treatment: mobile and localized adsorption. The differences are considerable.

I. INTRODUCTION

IN this section (by T. L. H.) we outline briefly a general research program in which the present paper is the first contribution. The next section (by S. G. and T. L. H.) deals with a particular topic within the program: the virial expansion and the classical second vibral coefficient. The second paper of the series (also in this issue) treats the theory of distribution functions for a fluid.

The general problem we consider is the behavior of an equilibrium, macroscopic system (gas, liquid, or solid) of monatomic molecules in an external periodic (in space, not time) potential field which is fixed (i.e., not varied) and unperturbed by the presence of molecules of the system in the field. The periodicity of the field exists in at least one and usually, but not necessarily, all of the dimensions of the system. The wavelength of the external potential field (Fig. 1) is of the order of molecular dimensions. This proves to be an essential point. We shall be concerned primarily but not entirely with *classical* systems in a periodic potential field with a *finite* potential barrier (Fig. 1) between neighboring potential minima (e.g., a cosine potential).

The most obvious real system to which the present model is a reasonable approximation is a monatomic monolayer physically adsorbed on the surface of a perfect crystal. In this case the crystal surface furnishes the periodic external potential field and we make the approximation that the molecules of the crystal are frozen in their equilibrium positions and that these positions are unaltered by the adsorbed monolayer. The molecules of the monolayer form the thermodynamic system under examination.

We are interested in the subject of this series primarily as a general problem in statistical mechanics and not as a problem in adsorption theory. We shall therefore consider one- and three-dimensional as well as two-dimensional cases. There are real one-dimensional systems involving polymers[1] or adsorption on polymers or polyelectrolytes which are close to our model. Some of these are of significance in physical biochemistry. In three dimensions, the system of electrons in a metal is a very special case (because of the extreme quantum degeneracy and long-range Coulombic forces) which we shall not consider. Another example in three dimensions is hydrogen absorbed in metals such as palladium and platinum. In general, though, impurity atoms in a three-dimensional crystal do not form a "system" which fits our model well because of the perturbation of the crystal structure (which provides the external field) by the impurity atoms.

We shall have some occasion (in paper II, for example) to discuss systems in general external potential fields (not necessarily periodic) for comparative purposes.

All of the methods, problems, and questions which arise in the statistical mechanics of monatomic systems (gas, liquid, solid, solutions, etc.) in the usual case in which no external field is present ($w_0=0$ in Fig. 1) can be extended to the periodic potential situation. Also, the well-known Ising model or lattice gas is closely related (see below) to systems of molecules in a periodic potential field. We shall list next, as illustrations, some of the problems, for a periodic field, which seem interesting and worthy of investigation. This will serve to clarify the motivation for this work and as a general introduction to later more detailed discussions.

(1) *Condensation theory.* The periodic potential field problem provides a continuous bridge between the two best known condensation theory problems of statistical mechanics, namely, (a) the usual gas-liquid condensation and (b) the lattice gas or Ising condensation. Let ϵ be the depth of the intermolecular pair potential and let w_0 be the potential barrier for a two- or three-dimensional system with an external potential periodic in all dimensions. In any case the critical temperature T_c for condensation will be related to ϵ by $kT_c=O(\epsilon)$.

* Supported by research grants to T. L. H. from the Heart Institute, Public Health Service and the Alfred P. Sloan Foundation.

[1] A. Peterlin, J. Chem. Phys. (to be published).

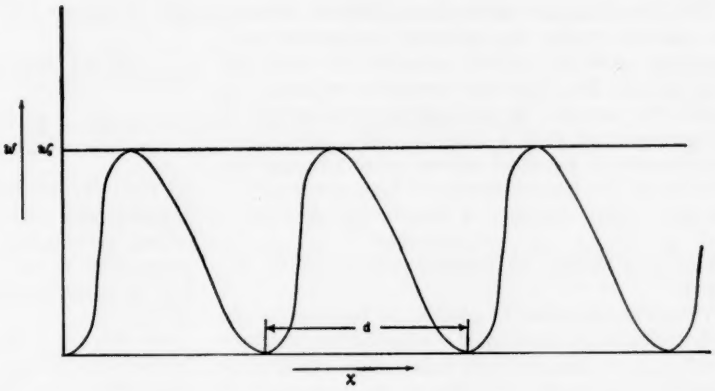

FIG. 1. Periodic external potential field in x direction. The wavelength is d and the potential barrier is w_0.

If ϵ, $kT_c \gg w_0$, we will have essentially an ordinary gas-liquid condensation since the molecules of the system [when $T=O(T_c)$] will be only slightly perturbed by the external field. If, on the other hand ϵ, $kT_c \ll w_0$, the molecules will be confined to potential minima (Fig. 1) thus forming a "lattice gas." We will have the usual Ising model if the intermolecular pair potential is such that only one molecule can occupy a given potential minimum owing to short-range intermolecular repulsion and if only interactions between molecules in nearest-neighbor sites (minima) need be taken into account. We can make the transition from one problem to the other by varying our choice of w_0/ϵ. Approximate methods will obviously be called for here since even the two extreme cases, (a) and (b), are very difficult and not completely solved.

(2) *Crystalline state and theory of fusion.* Consider a one- two- or three-dimensional system with $w_0=0$ and in the crystalline state. The periodicity of the crystal is determined by the intermolecular pair potential. Let r^* be the intermolecular distance corresponding to the minimum in the pair potential. Then the "wavelength" or lattice spacing of the crystal will be approximately r^* (this spacing will depend somewhat on p and T). Now imagine that the system is placed in a series of external periodic fields all with the same wavelength d (appreciably different from r^*) but with gradually increasing values of w_0. When w_0 is small and the temperature is such that the theory of small vibrations is adequate, the effect of w_0 on thermodynamic properties can be expressed in terms of the alteration of the normal vibrational frequency distribution. As w_0 is increased, the molecules of the system will be subject to competing forces favoring two different wavelengths, d and r^*. Eventually, with large enough w_0, the crystal will melt to form a "lattice liquid" (or sublime to form a "lattice gas"). An alternative but equivalent statement is that the melting point T_m of the crystal (at a given pressure) will be a function of w_0. Ordinarily T_m will decrease with increasing w_0 since the external field is a disrupting force on the crystal when $d \neq r^*$. Incidentally, when $d > r^*$, the "lattice liquid" formed on melting of the crystal will have all sites (potential minima) filled and still other molecules to be accomodated in energetically less favorable positions between sites. In a real two-dimensional system (adsorbed gas), second and possibly higher adsorbed layers would become involved in this case, but we shall not include this complication.

One might partially summarize (1) and (2) above by the following question: how does the phase diagram in the p, T plane depend on the values of w_0/ϵ and d/r^* for a given form of periodic potential (say cosine)?

(3) *Ideal degenerate gases.* The well-known problems of N identical, noninteracting Bose-Einstein or Fermi-Dirac particles in a box of one, two or three dimensions are also of interest with a periodic potential. In fact, the Fermi-Dirac case is related to the theory of metals and is not new. The Bose-Einstein case has a practical application in two dimensions: an adsorbed monolayer of helium on a solid surface. A question of particular interest is: what happens to the Bose-Einstein condensation when w_0 is increased from zero holding d constant (say, for a cosine potential)? A quantum-mechanical problem prerequisite to the above statistical problems is to find the density of energy levels (or its equivalent) for a single particle in a macroscopic box with a periodic potential. This is a well-known problem in the theory of metals.

(4) *Distribution function method.* In paper II we shall define distribution functions for a classical system in a periodic field, relate the distribution functions to thermodynamic functions, derive integral equations for the distribution functions, etc. Some new features arise which are not encountered in the absence of an external field.

(5) *Virial expansion for a gas.* The grand partition function method can be employed to obtain the virial expansion for an imperfect gas in an external periodic field. The transition from a lattice gas at low temperatures to an ordinary gas (free translation) at high temperatures can be followed. See Sec. II.

(6) *Very dilute gas.* In the limit of infinite dilution, the equation of state of a quantum system with intermolecular forces in a periodic potential field will be the ideal gas law. But some other properties will not be so simple. For example, the heat capacity as a function of temperature will show a quasi-transition from vibrational motion in potential minima at low temperatures (lattice gas) to free translation at high temperatures. An approximate treatment of this problem has already been given.[2] An exact analysis requires use of the energy-level density distribution referred to in (3) above.

There are, of course, in addition to the above equilibrium problems a number of nonequilibrium problems which suggest themselves for this system. An obvious example is the gradual transition in the mechanism of self-diffusion in a dilute gas when w_0 is increased starting from zero.

II. VIRIAL EXPANSION FOR AN IMPERFECT GAS

Consider a monatomic gas in an external periodic potential field. The basic thermodynamic equations for the system are the same as in the absence of the field since (a) the external field is not to be varied and (b) the pressure of the gas, as measured macroscopically by a piston, is the same in all directions (see paper II). An equivalent statement is that the Helmholtz free energy A is a function of N, T, and V, and is independent of the shape of the system. This is true only when the wavelength of the periodic potential is of molecular dimensions. We use three-dimensional notation at the outset; the external potential may then be periodic in one, two or three dimensions.

Let Q_N be the canonical ensemble partition function for N molecules in a volume V at T, and let $\lambda=\exp(\mu/kT)$, where μ=chemical potential. Then the grand partition function Ξ is related to pV/kT by

$$\ln\Xi=pV/kT=\ln\sum_{N\geq 0}Q_N\lambda^N. \tag{1}$$

We can obtain the virial coefficients by manipulating this equation in the usual way.[3]

We restrict ourselves in the remainder of this section to a *classical* gas. In this case

$$Q_N=Z_N/N!\Lambda^{3N}, \tag{2}$$

where

$$\Lambda=h/(2\pi mkT)^{\frac{1}{2}}$$

and

$$Z_N=\int_V \exp[-(U+W)/kT]d\mathbf{r}_1\cdots d\mathbf{r}_N \tag{3}$$

$$U=\sum_{1\leq i<j\leq N}u(r_{ij}), \qquad W=\sum_i w(\mathbf{r}_i). \tag{4}$$

In Eqs. (4) we assume pair-wise additivity in the intermolecular potential energy U and additivity of the external potential energy W. The quantity $w(\mathbf{r}_i)$ is the potential energy of molecule i in the external periodic field. In particular, we have

$$Z_1=\int_V \exp[-w(\mathbf{r}_1)/kT]d\mathbf{r}_1 \tag{5}$$

and

$$Z_2=\int_V \exp[-(u_{12}+w_1+w_2)/kT]d\mathbf{r}_1 d\mathbf{r}_2, \tag{6}$$

where w_i means $w(\mathbf{r}_i)$ and u_{ij} means $u(r_{ij})$. Note that Z_1 is not just V, as is the case in the absence of a field.

For a very dilute system ($\lambda\to 0$),

$$\ln\Xi=pV/kT=Q_1\lambda,$$

$$\bar{N}=\lambda(\partial\ln\Xi/\partial\lambda)_{V,T}=Q_1\lambda=pV/kT. \tag{7}$$

We define an activity z, proportional to λ, so that $z\to\rho$ ($\equiv\bar{N}/V$) as $\rho\to 0$,

$$z\equiv Q_1\lambda/V=Z_1\lambda/\Lambda^3 V. \tag{7'}$$

When we replace λ by z and Q_N by Z_N, Eq. (1) becomes

$$\ln\Xi=pV/kT=\ln\sum_{N\geq 0}(Z_N{}^*z^N/N!), \tag{8}$$

where

$$Z_N{}^*=Z_N/(Z_1/V)^N. \tag{9}$$

The point of defining $Z_N{}^*$ is to put Eq. (8) in "standard" form.[3] For now we can take over, without modification, well-known equations in imperfect gas theory:

$$p/kT=\sum_{j\geq 1}b_j(T)z^j, \qquad \rho=\sum_{j\geq 1}jb_j(T)z^j \tag{10}$$

$$p/kT=\rho+\sum_{n\geq 2}B_n(T)\rho^n, \tag{11}$$

where

$$B_2=-b_2, \qquad B_3=4b_2{}^2-2b_3, \qquad \text{etc.}, \tag{12}$$

and

$$1!Vb_1=Z_1{}^*=V, \qquad b_1=1 \tag{13}$$

$$2!Vb_2=Z_2{}^*-Z_1{}^{*2}, \tag{14}$$

[2] T. L. Hill, J. Chem. Phys. **14**, 441 (1946). See also T. L. Hill, *Statistical Thermodynamics* (Addison-Wesley Publishing Company, Inc., Reading, Massachusetts, 1960), pp. 172–175.

[3] See T. L. Hill, *Statistical Mechanics* (McGraw-Hill Book Company, Inc., New York, 1956), pp. 134–136, 143–144.

etc. Equation (11) is the desired virial expansion. The second virial coefficient, from Eqs. (5), (6), (9), (12), and (14), is

$$B_2=-b_2=-\tfrac{1}{2}V[(Z_2-Z_1^2)/Z_1^2]$$

$$=-\tfrac{1}{2}V\frac{\int_V[\exp(-u_{12}/kT)-1]\exp(-w_1/kT)\exp(-w_2/kT)d\mathbf{r}_1d\mathbf{r}_2}{\left(\int_V\exp(-w_1/kT)d\mathbf{r}_1\right)^2}. \tag{15}$$

A similar expression can be written for B_3, etc.

The rest of the section is devoted to a particular illustration of Eq. (15) for B_2. More will be said about Eq. (15) in general in paper II. Consider an adsorbed monolayer on the surface of a crystal which furnishes, for each adsorbed molecule, an external periodic potential with simple square symmetry. We approximate the potential by a sum of cosine functions,

$$w(\mathbf{r})=\tfrac{1}{2}w_0\left(1-\cos\frac{2\pi x}{d}\right)+\tfrac{1}{2}w_0\left(1-\cos\frac{2\pi y}{d}\right). \tag{16}$$

The wavelength is d, the potential barrier in either x or y direction is w_0, and the zero of potential energy is at the minima in $w(\mathbf{r})$ (for example, $x=y=0$). For two dimensional notation we shall use

$$\sigma=\bar{N}/\mathfrak{A},\qquad \mathfrak{A}=L^2,\qquad \phi/kT=\sigma+\sum_{n\geq 2}B_n\sigma^n,$$

$$Q_N=Z_N/N!\Lambda^{2N},$$

where $\mathfrak{A}$=area, L=length of a side, σ=surface concentration, and ϕ=surface pressure. Then

$$B_2=-\tfrac{1}{2}\mathfrak{A}\frac{\int_{\mathfrak{A}}[\exp(-u_{12}/kT)-1]\exp(-w_1/kT)\exp(-w_2/kT)dx_1dy_1dx_2dy_2}{\left(\int_{\mathfrak{A}}\exp(-w_1/kT)dx_1dy_1\right)^2}. \tag{17}$$

Before proceeding further with Eqs. (16) and (17), we note two limiting cases which are the usual ones employed as approximations in adsorption theory. If $w_0/kT\to 0$, that is, if the "structure" of the surface can be or is ignored (mobile adsorption)

$$B_2\to-(1/2\mathfrak{A})\int_{\mathfrak{A}}[\exp(-u_{12}/kT)-1]dx_1dy_1dx_2dy_2$$

$$=-\pi\int_0^\infty\{\exp[-u(r)/kT]-1\}rdr\qquad(w_0/kT\to 0). \tag{18}$$

If, on the other hand, $w_0/kT\to\infty$, we have a lattice gas with molecules confined to sites and executing small vibrations about the potential minima (localized adsorption). Let n_i be the number of ith neighbor sites to a given site, and let d_i be the distance to these sites. For a simple square lattice: $n_0=1$, $n_1=4$, $n_2=4$, $n_3=4$, $n_4=8$, etc.; $d_0=0$, $d_1=d$, $d_2=2^{\frac{1}{2}}d$, $d_3=4^{\frac{1}{2}}d$, $d_4=5^{\frac{1}{2}}d$, etc. In Eq. (17), the integral in the numerator reduces to

$$(\mathfrak{A}/d^2)\left(\int_{\text{site}}\exp(-w_1/kT)dx_1dy_1\right)^2\sum_{i\geq 0}n_i\{\exp[-u(d_i)/kT]-1\}$$

and the integral in the denominator to

$$(\mathfrak{A}/d^2)\int_{\text{site}}\exp(-w_1/kT)dx_1dy_1,$$

where the "site" integrals are simple harmonic oscillator configuration integrals about a single minimum [w in Eq. (16) can be expanded about $x=y=0$ to the quadratic terms to obtain an explicit expression]. Then

$$B_2\to-(d^2/2)\sum_{i\geq 0}n_i\{\exp[-u(d_i)/kT]-1\}\qquad(w_0/kT\to\infty). \tag{19}$$

We return now to Eqs. (16) and (17). The integral in the denominator of Eq. (17) is

$$Z_1=\int_{\mathcal{A}}\exp(-w_1/kT)\,dx_1dy_1=\left\{\int_0^L\exp\left[-(w_0/2kT)\left(1-\cos\frac{2\pi x_1}{d}\right)\right]dx_1\right\}^2$$

$$=\mathcal{A}\exp(-w_0/kT)\,I_0^2(w_0/2kT), \tag{20}$$

where I_0 is a modified Bessel function of the first kind. In the numerator of (17) we use the Lennard-Jones intermolecular potential

$$u(r)=4\epsilon[(r_0/r)^{12}-(r_0/r)^6].$$

The minimum in $u(r)$ occurs at $r^*=2^{1/6}r_0$. We change variables in the integral from x_1, y_1, x_2, y_2 to

$$x=\tfrac{1}{2}(x_1+x_2),\qquad y=\tfrac{1}{2}(y_1+y_2),\qquad s=(x_2-x_1)/r_0,\qquad t=(y_2-y_1)/r_0$$

$$dx_1dy_1dx_2dy_2=r_0^2dxdydsdt.$$

Then the integral becomes

$$Z_2-Z_1^2=r_0^2\int_{-\infty}^{+\infty}\int\{\exp[-u(s,t)/kT]-1\}dsdt\int_0^L\int\exp(-2w_0/kT)$$

$$\times\exp\{(w_0/kT)[\cos(\pi r_0s/d)\cos(2\pi x/d)+\cos(\pi r_0t/d)\cos(2\pi y/d)]\}dxdy. \tag{21}$$

After integration over x and y and substitution of Eqs. (20) and (21) back into Eq. (17), we have the final result

$$B_2/r_0^2=-\frac{\displaystyle\int_{-\infty}^{+\infty}\int\{\exp[-u(s,t)/kT]-1\}I_0[(w^*/T^*)\cos(\pi s/d^*)]I_0[(w^*/T^*)\cos(\pi t/d^*)]dsdt}{2I_0^4(w^*/2T^*)}, \tag{22}$$

where

$$u(s,t)/kT=(4/T^*)\{[(s^2+t^2)^6]^{-1}-[(s^2+t^2)^3]^{-1}\}$$

and

$$T^*=kT/\epsilon,\qquad w^*=w_0/\epsilon,\qquad d^*=d/r_0.$$

Equation (22) is in "corresponding states" form. We see that B_2/r_0^2 is a function of the reduced variable T^* and the reduced parameters w^* and d^*. In the limiting form (18), B_2/r_0^2 is a function of T^* only, as in the usual law of corresponding states, while in the limit (19), B_2/r_0^2 is a function of T^* and d^*.

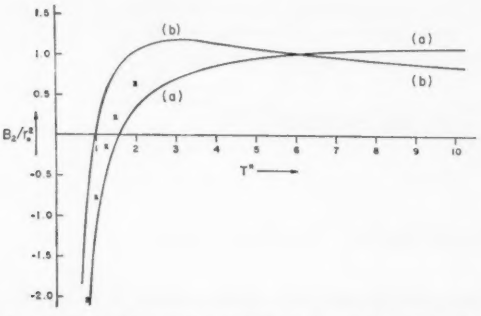

FIG. 2. Reduced second virial coefficient as a function of reduced temperature. Curve (a) = mobile adsorption, Eq. (18). Curve (b) = localized adsorption, Eq. (19) with $d^*=0.9184$. Points (crosses) = periodic potential, Eq. (22) with $d^*=0.9184$ and $w^*=0.732$.

Finally, we present a numerical example. Curve (a) in Fig. 2 shows B_2/r_0^2 as a function of T^*, calculated from Eq. (18). This is the second virial coefficient for mobile adsorption. The method of calculation is essentially to expand the factor $\exp[(4/T^*)(r_0/r)^6]$ in the integrand and integrate term by term.[4] In order to compute B_2/r_0^2 from Eq. (19) (localized adsorption) or Eq. (22) (general), we have to make a specific choice of parameters. Our selection is based on the system: argon on KCl. We take[5] $r_0=3.418$ A, $d=3.139$ A, $w_0=180$ cal mole^{-1} and $\epsilon=246$ cal mole^{-1}. Then $d^*=0.9184$ and $w^*=0.732$. Curve (b) in Fig. 2 gives B_2/r_0^2 for localized adsorption, calculated by direct summation of Eq. (19). The five points shown between curves (a) and (b) were calculated from Eq. (22) by a very tedious double numerical integration.[4] This example suffices to show that the two conventional limiting

[4] For further details, see the thesis of S. G. (University of Oregon, in preparation).

[5] The values of r_0 and ϵ were obtained from the following source: J. Hirschfelder, C. Curtiss, and R. Bird, *Molecular Theory of Gases* (John Wiley & Sons, Inc., New York, 1952), p. 1110. The value for d was found in: R. W. G. Wyckoff, *Crystal Structures* (Interscience Publishers, Inc., New York, 1958), Chap. III, table, page 11. The value for w_0 was calculated from data given in: W. J. C. Orr, Trans. Faraday Soc. **35,** 1247 (1939).

approximations (mobile or localized adsorption) lead to second virial coefficients which differ significantly at intermediate temperatures from the more general and realistic Eq. (22). Of course curve (a) is approached by Eq. (22) at high temperatures and curve (b) at low temperatures, but neither (a) nor (b) is suitable over the entire temperature range.

Equation (22) is based on classical statistical mechanics. But actually this equation should be a good approximation at all temperatures to the corresponding quantum statistical expressions (Bose-Einstein or Fermi-Dirac), which we have not attempted to derive here. This follows because: (1) at intermediate and high temperatures both forms of quantum statistics approach the classical expression (22); and (2) at low temperatures, both forms of quantum statistics [as well as Eq. (22)] reduce to Eq. (19) for B_2 provided that (as is the case with real molecules) $u(r)$ has a repulsive core which allows only one molecule per site (irrespective of statistics).

THE JOURNAL OF CHEMICAL PHYSICS VOLUME 34, NUMBER 5 MAY, 1961

Statistical Mechanics of Monatomic Systems in an External Periodic Potential Field. II. Distribution Function Theory for Fluids*

TERRELL L. HILL AND NOBUHIKO SAITÔ†

Department of Chemistry, University of Oregon, Eugene, Oregon

(Received September 20, 1960)

The theory of distribution functions for monatomic systems in an external periodic potential field is outlined. Particular attention is given to the equation of state, the second virial coefficient, and the Kirkwood and Born-Green-Yvon integral equations for the distribution functions. A brief discussion of a nonperiodic external field is given in an Appendix.

I. INTRODUCTION

THE first paper of this series[1] (referred to hereafter as I), which readers of the present paper should refer to, contains an introduction to the general problem of monatomic systems in an external periodic potential field. The purpose of this second paper is to consider the theory of distribution functions for classical fluids in such a field. We shall not attempt an exhaustive treatment but rather confine ourselves to an outline of some of the more important points. A brief discussion of the external *non*periodic field problem is given in Appendix A.

As a preface, some comments on the definition of a *fluid* in an external periodic field are in order. Consider a three-dimensional system in a triply periodic external field. Let us divide up the volume of the system into the smallest repeating units *of the external field*—which we call "cells." We restrict ourselves to cells with molecular dimensions. Now even an infinitely dilute gas in such an external field will have, for example, a triply periodic density: the periodicity will be that of the external field and the mean density over a cell will be the same for all cells. In fact, we can use generalizations of these statements as our definition of a fluid: any equilibrium molecular property which is periodic has the periodicity of the external field; hence, all cells in a fluid are equivalent. A crystal in an external periodic field will have periodic properties but the periodicity will in general be different from that of the field—the periodicity will usually be determined primarily by the intermolecular forces between the molecules of the system themselves (with the external field acting as a perturbation). In this case all cells will not be equivalent: properties (such as density) averaged over a cell will not have the same value for all cells; there will be a periodicity in the cell averages themselves.

For a fluid, then, since all cells are equivalent and of molecular dimensions, any alteration of the shape of the system (i.e., rearrangement of large blocks of cells) at constant volume will leave all of the thermodynamic functions of the system unchanged. Thus, for example, the Helmholtz free energy A is a function of N, V, and T only.

If, in three dimensions, the external field is periodic in two dimensions (x, y) but is constant in the third (z), we take as a three dimensional cell the smallest repeating unit of the external field in the xy plane with an infinitesimal extension dz in the z direction. If all such cells are equivalent in the sense used above, the system is a fluid. For a singly periodic field (x direction), the cell is the smallest repeating length (λ) in the x direction with extensions dy and dz in the other directions. Again equivalence of cells is the criterion for a fluid.

* Supported by research grants (to T.L.H.) from the Heart Institute, Public Health Service and the Alfred P. Sloan Foundation.

† On leave from the Department of Applied Physics, Waseda University, Tokyo, Japan.

[1] T. L. Hill and S. Greenschlag, J. Chem. Phys. **34**, 1538 (1961).

II. THERMODYNAMIC FUNCTIONS

We shall work primarily with canonical ensemble distribution functions and we begin with their definition.[2]

The classical canonical ensemble partition function for a three-dimensional system of N particles is

$$Q=(2\pi mkT/h^2)^{3N/2}(Z/N!)=Z/\Lambda^{3N}N!,$$

where

$$Z=\int_V \exp[-(U+W)/kT]d\mathbf{r}_1\cdots d\mathbf{r}_N \tag{1}$$

and

$$U=\sum_{1\leq i<j\leq N} u(r_{ij}) \qquad W=\sum_{i=1}^{N} w(\mathbf{r}_i). \tag{2}$$

U is the intermolecular potential energy and W the external potential energy. It follows[2] that if we define the distribution function $\rho^{(n)}$ by

$$\rho^{(n)}(\mathbf{r}_1,\cdots,\mathbf{r}_n)$$

$$=\frac{N!}{(N-n)!}\frac{\int_V \exp[-(U+W)/kT]d\mathbf{r}_{n+1}\cdots d\mathbf{r}_N}{Z} \tag{3}$$

then $\rho^{(n)}d\mathbf{r}_1\cdots d\mathbf{r}_n$ is the probability that any molecule of the system is in $d\mathbf{r}_1$, any other in $d\mathbf{r}_2$, etc. The normalization equation for $\rho^{(n)}$ is

$$\int_V \rho^{(n)}d\mathbf{r}_1\cdots d\mathbf{r}_n=N!/(N-n)!. \tag{4}$$

Except for negligible terms, the right-hand side can be replaced by N^n for small n.

The singlet distribution function $\rho^{(1)}(\mathbf{r})$ is of course just the local or point number density (a function of $\mathbf{r}$). This function has the periodicity of $w(\mathbf{r})$ in a fluid, by definition.

We give without proof (see the work cited in footnote 2, p. 202) the rather obvious limiting normalized forms for $\rho^{(1)}$ and $\rho^{(2)}$ at low density ($\rho=N/V\to 0$):

$$\rho^{(1)}(\mathbf{r}_1)=N\exp[-w(\mathbf{r}_1)/kT]/Z_1, \tag{5}$$

$$\rho^{(2)}(\mathbf{r}_1,\mathbf{r}_2)=(N^2/Z_1^2)\exp(-w_1/kT)\exp(-w_2/kT)$$
$$\times\exp(-u_{12}/kT), \tag{6}$$

where Z_1 is the configuration integral for one molecule,

$$Z_1=\int_V \exp[-w(\mathbf{r})/kT]d\mathbf{r}. \tag{7}$$

The potential of mean force $w^{(n)}$ and the correlation function $g^{(n)}$ may be defined[2] by

$$\exp[-w^{(n)}/kT]=V^n(N-n)!\rho^{(n)}/N!, \tag{8}$$

and

$$g^{(n)}=\rho^{(n)}/\rho^{(1)}(\mathbf{r}_1)\cdots\rho^{(1)}(\mathbf{r}_n). \tag{9}$$

The pair correlation function $g^{(2)}$ does not have radial symmetry here because of the periodicity of the external field.

Finally, we will need the unsymmetrical distribution function

$$\rho^{[n]}(\mathbf{r}_1,\cdots,\mathbf{r}_n)=\rho^{(n)}(\mathbf{r}_1,\cdots,\mathbf{r}_n)/\rho^{(n-1)}(\mathbf{r}_1,\cdots,\mathbf{r}_{n-1}). \tag{10}$$

The physical significance of $\rho^{[n]}$ is that $\rho^{[n]}d\mathbf{r}_n$ is the probability that any molecule of the system is in $d\mathbf{r}_n$ if molecules 1, 2, $\cdots$, $n-1$ are fixed in position at $\mathbf{r}_1$, $\cdots$, $\mathbf{r}_{n-1}$, respectively.

Energy

From

$$E=kT^2(\partial \ln Q/\partial T)_{N,V},$$

we find

$$E=\tfrac{3}{2}NkT+\bar{U}+\bar{W}, \tag{11}$$

where

$$\bar{U}=\int_V \exp[-(U+W)/kT]Ud\mathbf{r}_1\cdots d\mathbf{r}_N/Z$$

$$=\frac{N(N-1)}{2Z}\int_V \exp[-(U+W)/kT]u(r_{12})d\mathbf{r}_1\cdots d\mathbf{r}_N$$

$$=\tfrac{1}{2}\int_V u(r_{12})\rho^{(2)}(\mathbf{r}_1,\mathbf{r}_2)d\mathbf{r}_1d\mathbf{r}_2, \tag{12}$$

[2] See T. L. Hill, *Statistical Mechanics* (McGraw-Hill Book Company, Inc., New York, 1956), Chap. 6.

and, similarly,

$$\bar{W}=(N/Z)\int_V \exp[-(U+W)/kT]w(\mathbf{r}_1)d\mathbf{r}_1\cdots d\mathbf{r}_N$$

$$=\int_V w(\mathbf{r}_1)\rho^{(1)}(\mathbf{r}_1)d\mathbf{r}_1. \qquad (13)$$

This result for E is obvious intuitively.

Chemical Potential

For brevity, we use a simple type of argument exploited elsewhere.[3] For a very dilute gas, we have from Eq. (I–7)

$$N/V=\rho=(Z_1/\Lambda^3V)\exp(\mu/kT),$$

or

$$\mu=kT\ln\rho+kT\ln[\Lambda^3/(Z_1/V)]. \qquad (14)$$

Also, in the limit $\rho\to 0$, Eqs. (5) and (14) give

$$\mu=kT\ln\rho^{(1)}(\mathbf{r}_1)+kT\ln\Lambda^3+w(\mathbf{r}_1). \qquad (15)$$

The right-hand side is the local or point chemical potential at $\mathbf{r}_1$, a quantity which has the same value at all points at equilibrium, namely, the value of the macroscopic chemical potential μ.

When the fluid is not infinitely dilute we must correct Eqs. (14) and (15) for intermolecular forces. Consider a molecule fixed at $\mathbf{r}_1$ with its intermolecular interactions coupled to other molecules of the system to the degree (fraction) ξ_1. If ξ_1 is increased by $d\xi_1$, the work required in this "charging" process, on account of interactions with molecules in $d\mathbf{r}_2$, is

$$u(r_{12})d\xi_1\rho^{[2]}(\mathbf{r}_1,\mathbf{r}_2,\xi_1)d\mathbf{r}_2, \qquad (16)$$

where the notation for $\rho^{[2]}$ refers to the distribution of molecules when molecule 1 is coupled to the extent ξ_1. The total work, against intermolecular forces, required to add a new molecule at $\mathbf{r}_1$ is then

$$\int_0^1\int_V u(r_{12})\rho^{[2]}(\mathbf{r}_1,\mathbf{r}_2,\xi_1)d\mathbf{r}_2d\xi_1. \qquad (17)$$

Hence the equation expressing the constancy of the point chemical potential becomes

$$\mu=kT\ln\rho^{(1)}(\mathbf{r}_1)+kT\ln\Lambda^3+w(\mathbf{r}_1)+\int_0^1\int_V u(r_{12})\rho^{[2]}(\mathbf{r}_1,\mathbf{r}_2,\xi_1)d\mathbf{r}_2d\xi_1. \qquad (18)$$

For the macroscopic chemical potential, we must first average (16) over all locations $\mathbf{r}_1$ using the weight $\rho^{(1)}(\mathbf{r}_1)d\mathbf{r}_1$ and then integrate over $\mathbf{r}_2$ and ξ_1 as in (17). This gives the average work necessary to add one molecule to the system:

$$\frac{\int_0^1\int_V u(r_{12})\rho^{[2]}(\mathbf{r}_1,\mathbf{r}_2,\xi_1)\rho^{(1)}(\mathbf{r}_1)d\mathbf{r}_1d\mathbf{r}_2d\xi_1}{\int_V\rho^{(1)}(\mathbf{r}_1)d\mathbf{r}_1}.$$

Hence Eq. (14) becomes

$$\mu=kT\ln\rho+kT\ln\frac{\Lambda^3}{(Z_1/V)}+N^{-1}\int_0^1\int_V u(r_{12})\rho^{(2)}(\mathbf{r}_1,\mathbf{r}_2,\xi_1)d\mathbf{r}_1d\mathbf{r}_2d\xi_1. \qquad (19)$$

If the right-hand sides of Eqs. (18) and (19) are set equal to each other and the resulting equation solved for $kT\ln\rho^{(1)}$, we obtain the Kirkwood integral equation for $\ln\rho^{(1)}$ [compare Eq. (32.13) of the work cited in footnote 2]. This is a special case of Eq. (33) to be derived below.

Equation (5) gives the first term in the expansion of $\rho^{(1)}$ in powers of ρ. By use of the Kirkwood integral equation for $\ln\rho^{(1)}$, just referred to, we can easily find the ρ^2 term. To do this, we use the limiting ($\rho\to 0$) expressions (5) and (6) for $\rho^{(2)}$ and $\rho^{[2]}$ in the integrands of Eqs. (18) and (19) (note that u_{12} is replaced by ξ_1u_{12}), integrate over ξ_1, and obtain

$$\rho^{(1)}(\mathbf{r}_1)=\frac{\rho\exp(-w_1/kT)}{(Z_1/V)}\left\{1-\frac{\rho V}{Z_1^2}\left[\int_V\exp(-w_1/kT)\exp(-w_2/kT)[\exp(-u_{12}/kT)-1]d\mathbf{r}_1d\mathbf{r}_2-Z_1\int_V\exp(-w_2/kT)[\exp(-u_{12}/kT)-1]d\mathbf{r}_2\right]+\cdots\right\}. \qquad (20)$$

[3] T. L. Hill, *Introduction to Statistical Thermodynamics* (Addison-Wesley Publishing Company, Inc., Reading, Massachusetts, 1960), Chap. 17.

It is easy to verify, incidentally, that this expression satisfies the normalization condition (4) and has the periodicity of $w(\mathbf{r}_1)$ (as required by our definition of a fluid). Also, $\rho^{(1)}=\rho$ (a constant) if $w\equiv 0$.

Pressure

We first use Green's method. We take V as a cube of edge L and write

$$Z=V^N\int_0^1 \exp[-(U+W)/kT]dx_1'\cdots dz_N',$$

where $x_i=x_i'V^{1/3}$, etc. Then

$$Z^{-1}(\partial Z/\partial V)_{N,T}=p/kT=N/V-\frac{V^N}{ZkT}\int_0^1 \exp[-(U+W)/kT]\frac{\partial(U+W)}{\partial V}dx_1'\cdots dz_N' \tag{21}$$

in which

$$(\partial U/\partial V)_{\mathbf{r}'}=\sum_{1\le i<j\le N}(r_{ij}/3V)[du(r_{ij})/dr_{ij}]$$

$$(\partial W/\partial V)_{\mathbf{r}'}=\sum_i(\partial w_i/\partial x_i)(\partial x_i/\partial V)_{x_i'}+\text{terms in } y_i \text{ and } z_i$$

$$=(1/3V)\sum_i \mathbf{r}_i\cdot\nabla w_i.$$

Equation (21) then simplifies to

$$p/kT=\rho-(6VkT)^{-1}\int_V \rho^{(2)}(\mathbf{r}_1,\mathbf{r}_2)r_{12}[du(r_{12})/dr_{12}]d\mathbf{r}_1d\mathbf{r}_2-(3VkT)^{-1}\int_V \rho^{(1)}(\mathbf{r}_1)\mathbf{r}_1\cdot\nabla w_1 d\mathbf{r}_1. \tag{22}$$

The term in $\rho^{(2)}$ has the same formal appearance ($\rho^{(2)}$ is of course different) as in the absence of a field, but the term in $\rho^{(1)}$ is new. An obvious physical significance which can be attached to the contribution of the $\rho^{(1)}$ term to the pressure is that it is the statistically averaged value of the quantity $-(\partial W/\partial V)_{\mathbf{r}'}$ (i.e., the volume is increased holding the *relative* positions of all molecules constant). Similarly, the $\rho^{(2)}$ contribution to the pressure is the statistical average of $-(\partial U/\partial V)_{\mathbf{r}'}$.

Equation (22) also follows immediately from the virial theorem:

Mean kinetic energy = total virial $=-\frac{1}{2}\sum_i\langle\mathbf{r}_i\cdot\mathbf{F}_i\rangle_{\text{Av}}$

= virial of wall forces + virial of intermolecular forces + virial of external field forces

or

$$\tfrac{3}{2}NkT=\tfrac{3}{2}pV+\tfrac{1}{4}\int_V \rho^{(2)}r_{12}(du_{12}/dr_{12})d\mathbf{r}_1d\mathbf{r}_2+\tfrac{1}{2}\int_V \rho^{(1)}\mathbf{r}_1\cdot\nabla w_1 d\mathbf{r}_1. \tag{23}$$

Although we shall not give the proof, which is rather lengthy, the $\rho^{(2)}$ term in Eq. (22) can be derived as the averaged force per unit area which the molecules on one side of an infinitesimal surface element exert on the molecules on the other side. The force is different for different locations $\mathbf{r}$ of the surface element (as we should expect because of periodicity) and must be averaged over a cell to give the final result. This averaging is clearly appropriate because of the macroscopic nature of the thermodynamic pressure, in contrast with the molecular dimensions of a cell.

Equation (22) becomes a virial expansion if $\rho^{(1)}$ and $\rho^{(2)}$ are written as power series in ρ. The leading term in the expansion of $\rho^{(1)}$ in powers of ρ is the linear term while for $\rho^{(2)}$ it is the quadratic term [see Eqs. (5) and (6)]. Now we know from Eq. (I-7) that the equation of state is $p/kT=\rho$ in the limit $\rho\to 0$. Hence our first task is to verify that the integral in Eq. (22) of the $\rho^{(1)}$ linear term vanishes (otherwise $p/kT\neq\rho$ as $\rho\to 0$). We put Eq. (5) into the last term in Eq. (22) and obtain the integral (omitting constants)

$$\int_V \exp(-w_1/kT)[x_1(\partial w_1/\partial x_1)+y_1(\partial w_1/\partial y_1)+z_1(\partial w_1/\partial z_1)]dx_1dy_1dz_1.$$

We have to show, then, that, say,

$$\int_0^L \exp(-w_1/kT)x_1(\partial w_1/\partial x_1)dx_1=0. \tag{24}$$

An integration by parts gives

$$\int_0^L \exp(-w_1/kT)x_1(\partial w_1/\partial x_1)dx_1 = -kT\left| x_1\exp(-w_1/kT)\right|_0^L + kT\int_0^L \exp(-w_1/kT)dx_1$$

$$= -kTL\left[\exp(-w_1/kT)\right]_{x_1=L} + kT\int_0^L \exp(-w_1/kT)dx_1. \tag{25}$$

The *macroscopic* value of x_1, $x_1=L$, is equally consistent with any value of x_1 over a wavelength λ_x (the repeat distance in w_1 in the x direction). Hence we must take an average:

$$\left[\exp(-w_1/kT)\right]_{x_1=L} = \lambda_x^{-1}\int_L^{L+\lambda_x} \exp(-w_1/kT)dx_1 = L^{-1}\int_0^L \exp(-w_1/kT)dx_1.$$

Use of this evaluation in Eq. (25) gives the desired result, Eq. (24).

Insertion of the $\rho^{(1)}$ and $\rho^{(2)}$ quadratic terms in ρ into Eq. (22) gives an expression for the second virial coefficient B_2. These terms are available from Eqs. (6) and (20). We get [making use of Eq. (24)]

$$B_2 = -\frac{V}{6Z_1^2kT}\left[\int_V \exp(-w_1/kT)\exp(-w_2/kT)\exp(-u_{12}/kT)r_{12}(du_{12}/dr_{12})d\mathbf{r}_1d\mathbf{r}_2\right.$$

$$\left. +2\int_V \exp(-w_1/kT)\exp(-w_2/kT)\left[\exp(-u_{12}/kT)-1\right]\mathbf{r}_1\cdot\nabla w_1 d\mathbf{r}_1 d\mathbf{r}_2\right]. \tag{26}$$

On the other hand, we found in I from the grand partition function (the same result can be deduced from the canonical ensemble partition function) that

$$B_2 = -\frac{V}{2Z_1^2}\int_V \exp(-w_1/kT)\exp(-w_2/kT)\left[\exp(-u_{12}/kT)-1\right]d\mathbf{r}_1d\mathbf{r}_2. \tag{27}$$

To prove the equivalence of Eqs. (26) and (27), we start with the integral in Eq. (27) in the form

$$\int_0^L f(x_1)dx_1,$$

where

$$f(x_1) = \int_0^L \exp(-w_1/kT)dy_1dz_1\int_V \exp(-w_2/kT)\left[\exp(-u_{12}/kT)-1\right]d\mathbf{r}_2 \tag{28}$$

and integrate by parts:

$$\int_0^L f(x_1)dx_1 = \left| f(x_1)x_1\right|_0^L - \int_0^L x_1(df/dx_1)dx_1. \tag{29}$$

The first term on the right-hand side is equal to $L\langle f(L)\rangle_N$ where $\langle f(L)\rangle_N$ is the average of $f(L)$ over a wavelength λ_x. Now we note from Eq. (28) that $f(L)$ receives contributions from only those values of x_2 near $x_1=L$ [because of $\exp(u_{12}/kT)-1$] and with $x_2\leq x_1$ (because $\mathbf{r}_2$ ranges over V only). On the other hand, for x_1 not near zero or L, $f(x_1)$ receives contributions from those values of x_2 near x_1 but with both $x_2<x_1$ and $x_2>x_1$. Hence the average value of $f(L)$ over a wavelength is one-half of the average of $f(x_1)$ over a wavelength:

$$\bar{f} \equiv \lambda_x^{-1}\int_{x_1'}^{x_1'+\lambda_x} f(x_1)dx_1 = L^{-1}\int_0^L f(x_1)dx_1 = 2\langle f(L)\rangle_N.$$

Therefore Eq. (29) becomes

$$L\bar{f} = \tfrac{1}{2}L\bar{f} - \int_0^L x_1(df/dx_1)dx_1$$

or

$$B_2 = -(VL\bar{f}/2Z_1^2) = (V/Z_1^2)\int_0^L x_1(df/dx_1)dx_1. \tag{30}$$

We now examine the integral in Eq. (30). From Eq. (28),

$$df/dx_1 = -(1/kT)\int_0^L \exp(-w_1/kT)(\partial w_1/\partial x_1)dy_1dz_1\int_V \exp(-w_2/kT)[\exp(-u_{12}/kT)-1]d\mathbf{r}_2$$

$$-(1/kT)\int_0^L \exp(-w_1/kT)dy_1dz_1\int_V \exp(-w_2/kT)\exp(-u_{12}/kT)(\partial u_{12}/\partial x_1)d\mathbf{r}_2,$$

in which

$$\partial u_{12}/\partial x_1 = (du_{12}/dr_{12})[(x_1-x_2)/r_{12}].$$

On putting these expressions back in Eq. (30), we obtain

$$B_2 = -\frac{V}{Z_1^2kT}\left[\tfrac{1}{2}\int_V \exp(-w_1/kT)\exp(-w_2/kT)\exp(-u_{12}/kT)[(x_1-x_2)^2/r_{12}][du_{12}/dr_{12})d\mathbf{r}_1d\mathbf{r}_2\right.$$

$$\left.+\int_V \exp(-w_1/kT)\exp(-w_2/kT)[\exp(-u_{12}/kT)-1]x_1(\partial w_1/\partial x_1)d\mathbf{r}_1d\mathbf{r}_2\right]. \quad (31)$$

In the first integral in Eq. (31) we have used the fact that $x_1^2-x_1x_2$ is equivalent in the integrand to $x_2^2-x_1x_2$, by symmetry. Finally, we observe that Eq. (31) could have been derived with y_1 or z_1 in place of x_1 as a special variable; hence Eq. (26) follows immediately from Eq. (31).

The two expressions, (26) and (27), for B_2 are compared in a special case in Appendix B.

Compressibility

Distribution functions can be defined for an open system (grand ensemble) in the usual way[2] and related to thermodynamic functions. For example, the well known compressibility equation [see Eq. (37.19) of the work cited in footnote 2] is obtained without formal change.

III. INTEGRAL EQUATIONS FOR THE DISTRIBUTION FUNCTIONS

A short derivation[3] of the Kirkwood integral equation for $\rho^{(n)}$ follows by analogy with Eq. (18). We write down the local chemical potential at $\mathbf{r}_1$ when molecules are fixed at $\mathbf{r}_2, \cdots, \mathbf{r}_n$. The number density at $\mathbf{r}_1$ is [see Eq. (10)] $\rho^{(n)}(\mathbf{r}_1, \cdots \mathbf{r}_n)/\rho^{(n-1)}(\mathbf{r}_2, \cdots, \mathbf{r}_n)$. Then

$$\mu = kT\ln\frac{\rho^{(n)}(\mathbf{r}_1, \cdots, \mathbf{r}_n)}{\rho^{(n-1)}(\mathbf{r}_2, \cdots, \mathbf{r}_n)} + kT\ln\Lambda^3 + w(\mathbf{r}_1) + u_{12} + \cdots + u_{1n} + \text{work}. \quad (32)$$

The w and u terms are potential energy contributions to μ associated with the external field and the fixed molecules 2, $\cdots$, n. The work term is the work required against intermolecular forces (all molecules other than 2, $\cdots$, n) to add a molecule to the system at $\mathbf{r}_1$:

$$\text{work} = \int_0^1\int_V u(r_{1,n+1})\rho^{[n+1]}(\mathbf{r}_1, \cdots, \mathbf{r}_{n+1}, \xi_1)d\mathbf{r}_{n+1}d\xi_1.$$

We now equate the right-hand sides of Eqs. (19) and (32) to obtain

$$kT\ln\rho^{(n)}(\mathbf{r}_1, \cdots, \mathbf{r}_n) = kT\ln\left[\frac{\rho\exp(-w_1/kT)}{(Z_1/V)}\right] + kT\ln\rho^{(n-1)}(\mathbf{r}_2, \cdots, \mathbf{r}_n)$$

$$-u_{12}-\cdots-u_{1n}+N^{-1}\int_0^1\int_V u(r_{12})\rho^{(2)}(\mathbf{r}_1, \mathbf{r}_2, \xi_1)d\mathbf{r}_1d\mathbf{r}_2d\xi_1$$

$$-\int_0^1\int_V u(r_{1,n+1})\rho^{[n+1]}(\mathbf{r}_1, \cdots, \mathbf{r}_{n+1}, \xi_1)d\mathbf{r}_{n+1}d\xi_1. \quad (33)$$

We have already derived and used the $\ln\rho^{(1)}$ integral equation to deduce Eq. (20). As another application, let us use the $\ln\rho^{(2)}$ integral equation to obtain the expansion of $\rho^{(2)}$ to the cubic term in ρ [Eq. (6) gives the quadratic

term]. We take $n=2$ in Eq. (33) and on the right-hand side substitute (a) Eq. (20) for $\rho^{(1)}(\mathbf{r}_2)$, (b) Eq. (6) with $\xi_1 u_{12}$ in place of u_{12} for $\rho^{(2)}(\mathbf{r}_1, \mathbf{r}_2, \xi_1)$ and (c)

$$(N^3/Z_1^3)\exp(-w_1/kT)\exp(-w_2/kT)\exp(-w_3/kT)\exp(-\xi_1 u_{12}/kT)\exp(-\xi_1 u_{13}/kT)\exp(-u_{23}/kT)$$

for $\rho^{(3)}(\mathbf{r}_1, \mathbf{r}_2, \mathbf{r}_3, \xi_1)$. After integration with respect to ξ_1, we find

$$\rho^{(2)}(\mathbf{r}_1, \mathbf{r}_2) = \frac{\rho^2 \exp(-w_1/kT)\exp(-w_2/kT)\exp(-u_{12}/kT)}{(Z_1/V)^2}$$

$$\times\left\{1-(\rho V/Z_1^2)\left[2\int_V \exp(-w_1/kT)\exp(-w_2/kT)\,[\exp(-u_{12}/kT)-1]d\mathbf{r}_1 d\mathbf{r}_2\right.\right.$$

$$\left.\left.-Z_1\int_V \exp(-w_3/kT)\,[\exp(-u_{13}/kT)\exp(-u_{23}/kT)-1]d\mathbf{r}_3\right]+\cdots\right\}. \quad (34)$$

It is not difficult to verify that this expression satisfies the normalization condition (4).

From Eqs. (9), (20), and (34), we have for the pair correlation function

$$g^{(2)}(\mathbf{r}_1, \mathbf{r}_2) = \rho^{(2)}(\mathbf{r}_1, \mathbf{r}_2)/\rho^{(1)}(\mathbf{r}_1)\rho^{(1)}(\mathbf{r}_2)$$

$$=\exp(-u_{12}/kT)\left[1+(\rho V/Z_1)\int_V \exp(-w_3/kT)\,[\exp(-u_{13}/kT)-1]\,[\exp(-u_{22}/kT)-1]d\mathbf{r}_3+\cdots\right]. \quad (35)$$

Note that $g^{(2)}\to 1$ as $r_{12}\to\infty$.

We consider next the potential of mean force and the Born-Green-Yvon integral equation. Equations (3) and (8) define the function $\exp(-w^{(n)}/kT)$ for a set of molecules at $\mathbf{r}_1, \cdots, \mathbf{r}_n$. In the defining equation for $\exp(-w^{(n)}/kT)$, we take the gradient with respect to one of $\mathbf{r}_1, \cdots, \mathbf{r}_n$, say $\mathbf{r}_\alpha$:

$$\nabla_\alpha w^{(n)} = \nabla w_\alpha + \langle \nabla_\alpha U \rangle_{Nv}^{(n)}, \quad (36)$$

where

$$\langle \nabla_\alpha U \rangle_{Nv}^{(n)} = \frac{\int_V \exp[-(U+W)/kT]\nabla_\alpha U d\mathbf{r}_{n+1}\cdots d\mathbf{r}_N}{\int_V \exp[-(U+W)/kT]d\mathbf{r}_{n+1}\cdots d\mathbf{r}_N}. \quad (37)$$

The quantity $-\nabla w_\alpha$ is the force exerted on molecule α by the external field and $-\langle \nabla_\alpha U \rangle_{Nv}^{(n)}$ is the force exerted on molecule α by all other molecules in the system, averaged over all configurations of molecules other than the fixed set $1, \cdots, n$. Therefore $-\nabla_\alpha w^{(n)}$ is the mean total force on molecule α, $\langle \mathbf{F}_\alpha \rangle_{Nv}^{(n)}$, and $w^{(n)}$ is the potential of the mean force. Also, from Eq. (8),

$$kT\nabla_\alpha \ln\rho^{(n)} = -\nabla_\alpha w^{(n)} = \langle \mathbf{F}_\alpha \rangle_{Nv}^{(n)}. \quad (38)$$

If we use the first of Eqs. (2) in Eq. (37) we can easily derive the Born-Green-Yvon equation (with $\alpha=1$):

$$-\langle \mathbf{F}_1 \rangle_{Nv}^{(n)} = -kT\nabla_1 \ln\rho^{(n)}(\mathbf{r}_1, \cdots, \mathbf{r}_n)$$

$$=\nabla w_1 + \sum_{i=2}^{n}\nabla_1 u(r_{1i}) + \int_V \nabla_1 u(r_{1,n+1})\rho^{[n+1]}(\mathbf{r}_1, \cdots, \mathbf{r}_{n+1})d\mathbf{r}_{n+1}. \quad (39)$$

The right-hand side gives the sum of all the (negative) forces on molecule 1: external field; fixed molecules 2 to n; and all other molecules in the system.

If we put $n=1$, we obtain the force $\langle \mathbf{F}_1 \rangle_{Nv}^{(1)}$ on molecule 1 at $\mathbf{r}_1$, no other molecules being fixed. This is the case of most direct physical significance. The x component of this force is

$$[kT/\rho^{(1)}(\mathbf{r}_1)][\partial\rho^{(1)}(\mathbf{r}_1)/\partial x_1] = -(\partial w_1/\partial x_1) - \int_V (\partial u_{12}/\partial x_1)\rho^{[2]}(\mathbf{r}_1, \mathbf{r}_2)d\mathbf{r}_2. \quad (40)$$

For a dilute system, these terms can be deduced easily from Eqs. (6) and (20). Now if we multiply Eq. (40) by $\rho^{(1)}(\mathbf{r}_1)d\mathbf{r}_1$ and integrate over V, we get the total x component of force, due to the external field and intermolecular interactions, acting on the system:

$$kT\int_0^L dy_1dz_1\int_0^L(\partial\rho^{(1)}/\partial x_1)dx_1=-\int_V\rho^{(1)}(\partial w_1/\partial x_1)d\mathbf{r}_1-\int_V(\partial u_{12}/\partial x_1)\rho^{(2)}(\mathbf{r}_1,\mathbf{r}_2)d\mathbf{r}_1d\mathbf{r}_2. \tag{41}$$

The integral over x_1 on the left is zero since $\rho^{(1)}$ has the same average value over a wavelength λ_x at $x_1=0$ and $x_1=L$. Hence the total x (or y, z) component of force on the system is zero, as we might expect. On the right, the second integral is the total x component of intermolecular force on molecules of the system. If we use for $\rho^{(2)}$ the "interior" or "bulk" expression, unperturbed near the walls $x=0$ and $x=L$, we are in effect treating the walls as made up of the same material as the system itself. The $\rho^{(2)}$ integral then includes the x component of intermolecular forces of the "walls" on the system as well as all intermolecular forces within the system itself. The x components of the wall forces are equal and opposite at $x=0$ and $x=L$, and cancel. The total x component of the intermolecular forces within the system is zero (for each configuration of the system, even before statistical averaging) by Newton's third law. We can conclude, then, that the first term on the right, which is the total x component of force exerted by the periodic field on the system, is also zero.

If we put $n=1$ in Eq. (39), multiply by $d\mathbf{r}_1\rho^{(1)}(\mathbf{r}_1)\mathbf{r}_1\cdot$, and integrate, we obtain

$$-kT\int_V\rho^{(1)}\mathbf{r}_1\cdot\nabla\ln\rho^{(1)}d\mathbf{r}_1=-\int_V\rho^{(1)}\mathbf{r}_1\cdot\langle\mathbf{F}_1\rangle_w^{(1)}d\mathbf{r}_1$$

$$=\int_V\rho^{(1)}\mathbf{r}_1\cdot\nabla w_1d\mathbf{r}_1+\tfrac{1}{2}\int_V\rho^{(2)}\mathbf{r}_{12}(du_{12}/dr_{12})d\mathbf{r}_1d\mathbf{r}_2. \tag{42}$$

According to Eq. (23), this is twice the virial of the periodic and intermolecular forces and is equal to $3NkT-3pV$. Thus the equation of state can be written in the alternative form

$$p/kT=\rho+(3V)^{-1}\int_V\mathbf{r}_1\cdot\nabla\rho^{(1)}d\mathbf{r}_1. \tag{43}$$

As an illustration, if we substitute Eq. (20) for $\rho^{(1)}$ in Eq. (43), we find

$$p/kT=\rho+B_2\rho^2+\cdots,$$

with B_2 given by Eq. (26).

Since $\rho^{(1)}$ is a constant, equal to ρ, for a fluid with $w\equiv0$, we should read Eq. (43) as

$$\lim_{w_0\to0}\int_V$$

in this special case, where w_0 is the amplitude of the periodic potential. This leads to the conventional (no external field) equation of state [Eq. (22) with the last term omitted]. Equation (43) is appropriate as it stands for a crystal with $w\equiv0$ under a hydrostatic pressure p.

APPENDIX A

Nonperiodic External Field

We touch on only a few points here under this general title. Consider a classical monatomic system of N molecules in a container of cross sectional area (xy plane) $\mathcal{A}$ which extends from $z=L_1$ to $z=L_2(L_2>L_1)$. Thus the volume is $V=\mathcal{A}(L_2-L_1)$. There is an external potential field $w(z)$, a function of z only. The basic thermodynamic equation is

$$dA=-SdT-\phi d\mathcal{A}-p(L_2)\mathcal{A}dL_2+p(L_1)\mathcal{A}dL_1+\mu dN.$$

We shall be concerned with the special case $\mathcal{A}=$constant, $L_1=$constant$=0$, $L_2=L$:

$$dA=-SdT-p(L)\mathcal{A}dL+\mu dN.$$

Equations (1)–(20) are applicable here, essentially without change. Green's method for the pressure at L yields

$$p(L)/kT=\rho-(2VkT)^{-1}\int_0^L\rho^{(2)}(\mathbf{r}_1,\mathbf{r}_2)[(z_1-z_2)^2/r_{12}](du_{12}/dr_{12})d\mathbf{r}_1d\mathbf{r}_2-(LkT)^{-1}\int_0^L\rho^{(1)}(z_1)z_1(dw_1/dz_1)dz_1. \tag{44}$$

Note that $\rho=N/V$ is the *mean* number density between $z=0$ and $z=L$ [see Eq. (4)]:

$$L^{-1}\int_0^L\rho^{(1)}(z_1)dz_1=\rho.$$

Unlike Eq. (22) for a periodic potential, the last term in Eq. (44) contributes to the linear term in ρ. In the limit $\rho\to0$, we have from Eq. (5)

$$p(L)/kT=\rho-(N/LkTZ_1)\int_0^L\exp[-w(z_1)/kT]z_1(dw_1/dz_1)dz_1.$$

An integration by parts yields

$$p(L)/kT = N \exp[-w(L)/kT] \Big/ \mathcal{A}\int_0^L \exp[-w(z_1)/kT]dz_1 = \rho^{(1)}(L), \tag{45}$$

as we should expect.

The pressure at any z, $0 \leq z \leq L$, is obviously

$$p(z)/kT = z^{-1}\int_0^z \rho^{(1)}(z_1)dz_1 - (2\mathcal{A}zkT)^{-1}\int_0^z \rho^{(2)}(\mathbf{r}_1, \mathbf{r}_2)[(z_1-z_2)^2/r_{12}](du_{12}/dr_{12})d\mathbf{r}_1 d\mathbf{r}_2$$

$$-(zkT)^{-1}\int_0^z \rho^{(1)}(z_1)z_1(dw_1/dz_1)dz_1. \tag{46}$$

An expansion of $p(z)$ or $p(L)$ in powers of ρ is not at all natural in this problem, since ρ is an average quantity. A more obvious expansion variable is an activity, for example $\lambda = \exp(\mu/kT)$, which has the same value for all z (see the example below).

The Born-Green-Yvon equation for the z component of force on molecule 1 at z_1 is

$$\langle F_z \rangle_{\mathrm{av}}^{(1)} = \frac{kT}{\rho^{(1)}(z_1)}\frac{d\rho^{(1)}}{dz_1} = -\frac{dw_1}{dz_1} - \int_V \frac{du_{12}}{dz_1}\rho^{[2]}(\mathbf{r}_1, \mathbf{r}_2)d\mathbf{r}_2, \tag{47}$$

If we multiply by $\mathcal{A}\rho^{(1)}(z_1)dz_1$ and integrate over $0 \leq z_1 \leq L$, we obtain the total z component of external and intermolecular force acting on the system:

$$\mathcal{A}kT\int_0^L \frac{d\rho^{(1)}}{dz_1}dz_1 = \mathcal{A}kT[\rho^{(1)}(L) - \rho^{(1)}(0)]$$

$$= -\mathcal{A}\int_0^L \rho^{(1)}(z_1)\frac{dw_1}{dz_1}dz_1$$

$$-\int_V \frac{z_1 - z_2}{r_{12}}\frac{du_{12}}{dr_{12}}\rho^{(2)}(\mathbf{r}_1, \mathbf{r}_2)d\mathbf{r}_1 d\mathbf{r}_2. \tag{48}$$

If we use a $\rho^{(2)}$ "unperturbed" at the walls [see the discussion of Eq. (41)], the last term in Eq. (48) has three contributions: intermolecular forces between molecules of the system, which add up to zero by Newton's third law; the intermolecular force exerted by the "wall" at $z = L$ on the molecules of the system, $-p_U(L)\mathcal{A}$, where $p_U(L)$ is the intermolecular force contribution to $p(L)$; and $p_U(0)\mathcal{A}$ at $z = 0$. Then we can write Eq. (48) as

$$\mathcal{A}kT[\rho^{(1)}(L) - \rho^{(1)}(0)] = F_z^{\mathrm{ext}} - p_U(L)\mathcal{A} + p_U(0)\mathcal{A}$$

or

$$F_z^{\mathrm{ext}} - p(L)\mathcal{A} + p(0)\mathcal{A} = 0 \tag{49}$$

since $p = \rho^{(1)}kT + p_U$. Equation (49) expresses the mechanical equilibrium of the system.

Finally, we illustrate some of the above equations in a simple case: a slightly imperfect gas in an external field which varies slowly relative to molecular distances. In the limit $\rho \to 0$, Eq. (15) gives

$$\rho^{(1)}(z) = \Lambda^{-3}\exp(\mu/kT)\exp[-w(z)/kT].$$

Therefore we define activities $\mathfrak{z}$ and $\mathfrak{z}_0$ (for any ρ) by

$$\mathfrak{z}(z) = \Lambda^{-3}\exp(\mu/kT)\exp[-w(z)/kT],$$

$$\mathfrak{z}_0 = \Lambda^{-3}\exp(\mu/kT).$$

The activity $\mathfrak{z}_0$ has the same value for all z (unlike $\mathfrak{z}$). From imperfect gas theory we know that

$$\rho^{(1)}(z) = \mathfrak{z}(z) - 2B_2(T)\mathfrak{z}(z)^2 + \cdots$$

$$= \mathfrak{z}_0\exp[-w(z)/kT] - 2B_2\mathfrak{z}_0^2\exp[-2w(z)/kT]$$

$$+ \cdots. \tag{50}$$

This is the expansion of $\rho^{(1)}(z)$ in powers of $\mathfrak{z}_0$.

In Eq. (47), the term on the left is then

$$\langle F_z \rangle_{\mathrm{av}}^{(1)} = -(dw_1/dz_1)\{1 - 2B_2\mathfrak{z}_0\exp[-w(z_1)/kT]$$

$$+ \cdots\}.$$

Hence the last term in Eq. (47), the net z component of intermolecular force on a molecule at z_1, should be

$$2B_2(dw_1/dz_1)\mathfrak{z}_0\exp[-w(z_1)/kT]. \tag{51}$$

We now verify this by a direct calculation. In the limit $\mathfrak{z}_0 \to 0$,

$$\rho^{[2]} = \rho^{(2)}/\rho^{(1)} = \mathfrak{z}_0\exp(-u_{12}/kT)\exp[-w(z_2)/kT].$$

We expand $\exp[-w(z_2)kT]$ about $z = z_1$:

$$\exp[-w(z_2)/kT] = \exp[-w(z_1)/kT] - (1/kT)(dw_1/dz_1)\exp[-w(z_1)/kT](z_2 - z_1) + \cdots. \tag{52}$$

Then

$$-\int_V (du_{12}/dz_1)\rho^{[2]}d\mathbf{r}_2 = -Z_0\int_V [(z_1 - z_2)/r_{12}](du_{12}/dr_{12})\exp(-u_{12}/kT)\exp[-w(z_2)/kT]d\mathbf{r}_{12},$$

where $\mathbf{r}_{12}=\mathbf{r}_2-\mathbf{r}_1$. If we insert the series (52), the leading term makes no contribution to the integral and the second term gives

$$-(\mathfrak{Z}_0/kT)(dw_1/dz_1)\exp[-w(z_1)/kT]\int_V[(z_1-z_2)^2/r_{12}](du_{12}/dr_{12})\exp[-u_{12}/kT]d\mathbf{r}_{12}.$$

This is the same as (51).

By integration of the above terms in (47) we find that Eq. (48) is satisfied, with $\rho^{(1)}(L)$ and $\rho^{(1)}(0)$ given as in Eq. (50), and

$$\begin{aligned}\not{p}_U(0 \text{ or } L)&=B_2kT\mathfrak{z}_0^2\exp[-2w(0 \text{ or } L)/kT]+\cdots\\&=B_2kT[\rho^{(1)}(0 \text{ or } L)]^2+\cdots,\end{aligned}\tag{53}$$

as expected.

Finally, we compute the terms on the right in the equation of state, (44). From Eq. (50), the first term is

$$\rho=L^{-1}\int_0^L\rho^{(1)}dz=(\mathfrak{z}_0/L)\int_0^L\exp(-w/kT)dz-(2B_2\mathfrak{z}_0^2/L)\int_0^L\exp(-2w/kT)dz+\cdots,\tag{54}$$

and the third term

$$\begin{aligned}-(LkT)^{-1}\int_0^L\rho^{(1)}z(dw/dz)dz=\mathfrak{z}_0\Big[&\exp[-w(L)/kT]-L^{-1}\int_0^L\exp(-w/kT)dz\Big]\\&+B_2\mathfrak{z}_0^2\Big[-\exp[-2w(L)/kT]+L^{-1}\int_0^L\exp(-2w/kT)dz\Big]+\cdots.\end{aligned}$$

The second term is

$$\begin{aligned}-(2VkT)^{-1}&\int_0^L\rho^{(2)}\frac{(z_1-z_2)^2}{r_{12}}\frac{du_{12}}{dr_{12}}d\mathbf{r}_1d\mathbf{r}_2\\&=-\mathfrak{z}_0^2\Big[\alpha\Big(\int_0^L\exp(-2w/kT)dz\Big)\Big/2VkT\Big]\int_V\exp(-u_{12}/kT)\frac{(z_1-z_2)^2}{r_{12}}\frac{du_{12}}{dr_{12}}d\mathbf{r}_{12}+\cdots\\&=(\mathfrak{z}_0^2B_2/L)\int_0^L\exp(-2w/kT)dz+\cdots.\end{aligned}$$

Therefore

$$\not{p}(L)/kT=\mathfrak{z}_0\exp[-w(L)/kT]-B_2\mathfrak{z}_0^2\exp[-2w(L)/kT]+\cdots\tag{55}$$

$$=\rho^{(1)}(L)+B_2[\rho^{(1)}(L)]^2+\cdots\tag{56}$$

$$\begin{aligned}=&\Big[L\exp[-w(L)/kT]\Big/\int_0^L\exp(-w/kT)dz\Big]\rho+\Big[B_2L^2\exp[-w(L)/kT]\Big/\Big(\int_0^L\exp(-w/kT)dz\Big)^2\Big]\\&\times\Big\{\Big[2\int_0^L\exp(-2w/kT)dz\Big/\int_0^L\exp(-w/kT)dz\Big]-\exp[-w(L)/kT]\Big\}\rho^2+\cdots.\end{aligned}\tag{57}$$

APPENDIX B

One-Dimensional Special Case

In a one-dimensional system we find from Green's equation (22) that the second virial coefficient is (G=Green)

$$B_2^G=B_2^{(2)}+B_2^{(1)},\tag{58}$$

where

$$B_2^{(2)}=-(L/2Z_1^2kT)\int_0^L \exp(-w_1/kT)\exp(-w_2/kT)\exp(-u_{12}/kT)x_{12}(du_{12}/dx_{12})dx_1dx_2, \tag{59}$$

$$B_2^{(1)}=-(L/Z_1^2kT)\int_0^L \exp(-w_1/kT)\exp(-w_2/kT)[\exp(-u_{12}/kT)-1]x_1(dw_1/dx_1)dx_1dx_2, \tag{60}$$

$$Z_1=\int_0^L \exp(-w_1/kT)dx_1.$$

From the grand or canonical partition function, we have

$$B_2^{PF}=-(L/2Z_1^2)\int_0^L \exp(-w_1/kT)\exp(-w_2/kT)[\exp(-u_{12}/kT)-1]dx_1dx_2. \tag{61}$$

Now consider the special case of hard "spheres"

$$u_{12}=+\infty \qquad x_{12}\leq a$$
$$=0 \qquad x_{12}>a$$

in a "square" periodic potential with $w=w_0$ in, say, even intervals of length a and $w=0$ in odd intervals of length a:

$$w=w_0, \qquad na<x<(n+1)a, \qquad n=0, 2, 4, \cdots$$
$$w=0, \qquad ma<x<(m+1)a, \qquad m=1, 3, 5, \cdots.$$

We have immediately that

$$Z_1=(L/2)[1+\exp(-w_0/kT)],$$
$$B_2^{PF}=a. \tag{62}$$

The second virial coefficient is thus independent of w_0. This is consistent with the fact that $B_2=a$ when $w_0=0$ (ordinary one dimensional hard-sphere gas) or $w_0=+\infty$ (ideal lattice gas).

To compute $B_2^{(2)}$ and $B_2^{(1)}$ we need the following property of the δ function: if

$$h(x)=\alpha \qquad x<x_0$$
$$=\beta \qquad x>x_0$$

then

$$dh/dx=(\beta-\alpha)\delta(x-x_0).$$

We then find easily that

$$B_2^{(2)}=4a\exp(-w_0/kT)/[1+\exp(-w_0/kT)]^2.$$

In the integral in Eq. (60) for $B_2^{(1)}$ we integrate first over x_1 and second over x_2. There are two contributions to the integral. The first, over the range $a\leq x_2\leq L-a$, is

$$-(LkTa/2)[\exp(-w_0/kT)-1]^2.$$

The second comes from the interval $L-a\leq x_2\leq L$, and must be averaged over a wave length. The result is

$$(LkTa/4)[\exp(-w_0/kT)-1]^2.$$

The contribution from $0\leq x_2\leq a$ is of negligible order. Hence

$$B_2^{(1)}=a[\exp(-w_0/kT)-1]^2/[1+\exp(-w_0/kT)]^2,$$

and

$$B_2^{G}=a, \tag{63}$$

in agreement with Eq. (62).

Infrared Spectra of Methanol and Deuterated Methanols in Gas, Liquid, and Solid Phases*

M. FALK† AND E. WHALLEY

Division of Applied Chemistry, National Research Council, Ottawa, Canada

(Received September 2, 1960)

The infrared spectra of CH_3OH, CH_3OD, CD_3OH, and CD_3OD in the five phases gas, liquid, vitreous solid, α-crystal, and (except perhaps for CD_3OH and CD_3OD for which the solid-solid transitions have not been studied) β-crystal have been recorded in the range 4000 to 300 cm^{-1}. The Raman spectrum of liquid CD_3OH has been recorded. A complete assignment of the internal modes is given, which differs somewhat from previous assignments for the CH_3 bending and rocking vibrations. No significant difference in spectrum occurred between the α-crystal and β-crystal phases. Under the full symmetry of the β-phase determined by x-ray diffraction only one OH out-of-plane bending band should occur. Two bands are observed, and it is concluded that the carbon and oxygen atoms in one chain are not coplanar, as is required by the symmetry determined by x-ray diffraction [K. J. Tauer and W. N. Lipscomb, Acta Cryst. **5**, 606 (1952)], but that the chains are puckered and the x-ray symmetry arises because the puckered chains are irregularly distributed, a structure that had been previously suggested by Tauer and Lipscomb tentatively on the basis of high apparent thermal amplitudes. Bands occur in the crystal spectra near 500 cm^{-1} and 340 cm^{-1} at −180°C. These are interpreted as lattice modes, probably the two infrared-active modes that involve translations of the molecules.

1. INTRODUCTION

IN connection with a study of the intermolecular forces in CH_3OH and CH_3OD, a vibrational assignment was needed for the vapors and crystals at 0°K. The following previous investigations of the vibrational spectra of methanol and the deuterated methanols have been reported: CH_3OH: vapor infrared,[1–7] liquid infrared,[8–12] liquid Raman,[13–26] vapor Raman[21]; CH_3OD: vapor infrared,[3,4,7,8,27] liquid infrared,[7] liquid Raman;[15,17,19] CD_3OH and CD_3OD: vapor infrared[3,4]; CD_3OD: liquid Raman.[3,22] No work on the solids has been reported, except for a very brief statement about the 3-μ region of solid CH_3OH.[28,29] There were a number of uncertainties in the assignment of the vapor frequencies. We have, therefore, recorded the infrared spectra of the four methanols CH_3OH, CH_3OD, CD_3OH, and CD_3OD, in five phases, viz., gas, liquid, vitreous solid, α-crystal, and, except perhaps for CD_3OH and CD_3OD for which solid-solid transitions have not been studied, β-crystal.

2. EXPERIMENTAL

2.1 Materials

Reagent-grade methanol was dehydrated twice by treatment with magnesium turnings and distilled through a 19-in. Vigreux fractionating column, the middle third of the constant-boiling fraction being collected. The spectrum after purification differed in no way from that of the original alcohol, and vapor chromatographic analysis showed no impurities greater than 0.1%.

The deuterated methanols were purchased from the Merck Chemical Company, Montreal. Vapor-chromatographic analysis showed them to be free from impurities within 0.1% except for a trace of xylene, which was easily removed by a simple vacuum distillation. All four alcohols were anhydrous, as indicated by the absence in the vapor and solid spectra of the strong H_2O absorption band at 1640 cm^{-1} or the corresponding D_2O absorption band at 1220 cm^{-1}. However, a trace of atmospheric moisture was often introduced into the liquid samples, which were handled with a pipette. The CD_3 groups in CD_3OH and CD_3OD were over 99% deu-

* N.R.C. No. 6200.

† N.R.C. Postdoctorate Fellow 1958–60. Present address: Spectroscopy Laboratory, Massachusetts Institute of Technology, Cambridge, Massachusetts.

[1] E. L. Kinsey and J. W. Ellis, J. Chem. Phys. **5**, 399 (1937).
[2] A. Borden and E. F. Barker, J. Chem. Phys. **6**, 553 (1938).
[3] H. D. Noether, J. Chem. Phys. **10**, 693 (1942).
[4] B. I. Stepanov, J. Phys. Chem. (U.S.S.R.) **19**, 497 (1945).
[5] E. K. Plyler, J. Research Natl. Bur. Standards **48**, 281 (1952).
[6] A. V. Stuart and G. B. B. M. Sutherland, J. Chem. Phys. **24**, 559 (1956).
[7] P. Tarte and R. Deponthière, Bull. soc. chim. Belges **66**, 525 (1957).
[8] J. R. Quinan and S. E. Wiberley, J. Chem. Phys. **21**, 1896 (1953); Anal. Chem. **26**, 1762 (1954).
[9] A. M. Buswell, V. Deitz, and W. H. Rodebush, J. Chem. Phys. **5**, 501 (1937).
[10] D. R. McMillan, Jr., Phys. Rev. **57**, 941 (1940).
[11] M. Davies, J. Chem. Phys. **16**, 267 (1948).
[12] F. A. Smith and E. C. Creitz, J. Research Natl. Bur. Standards **46**, 145 (1951).
[13] S. Venkateswaran, Phil. Mag. **15**, 263 (1933).
[14] B. Trumpy, Kgl. Norske Videnskab. Selskabs Skrifter **1**, (1934).
[15] E. Bartholomé and H. Sachsse, Z. physik. Chem. **B30**, 40 (1935).
[16] R. G. Loyarte and J. S. Fernández, Contrib. estud. cienc. fis. y mat. (La Plata) **1**, 3 (1935).
[17] S. Mizushima, Y. Morino, and G. Okamoto, Bull. Chem. Soc. Japan **11**, 698 (1936).
[18] J. R. Bates, L. C. Anderson, and J. O. Halford, J. Chem. Phys. **4**, 535 (1936).
[19] J. O. Halford, L. C. Anderson, and G. H. Kissin, J. Chem. Phys. **5**, 927 (1937).
[20] J. Wagner, Z. physik. Chem. **B40**, 36 (1938).
[21] J. R. Nielsen and N. E. Ward, J. Chem. Phys. **10**, 81 (1942).
[22] M. de Hemptinne and T. Doehaerd, Bull. Acad. roy. Belg. Ser. 5, **30**, 189 (1944).
[23] A. L. S. Rao, J. Indian Chem. Soc. **22**, 260 (1945).
[24] P. K. Narayanaswamy, Proc. Indian Acad. Sci. **A26**, 121 (1947).
[25] W. G. Braun, D. F. Spooner, and M. R. Fenske, Anal. Chem. **22**, 1074 (1950).
[26] H. Nakamura and I. Obata, Busseiron Kenkyu **85**, 36 (1955); Chem. Abstr. **50**, 5406 (1956).
[27] E. F. Barker and G. Bosschieter, J. Chem. Phys. **6**, 563 (1938).
[28] M. van Thiel, E. D. Becker, and G. C. Pimentel, J. Chem. Phys. **27**, 95 (1957).
[29] G. C. Pimentel, in *Hydrogen Bonding* (Ljubljana Symposium, 1957, edited by D. Hadži, Pergamon Press, New York 1959), p. 107.

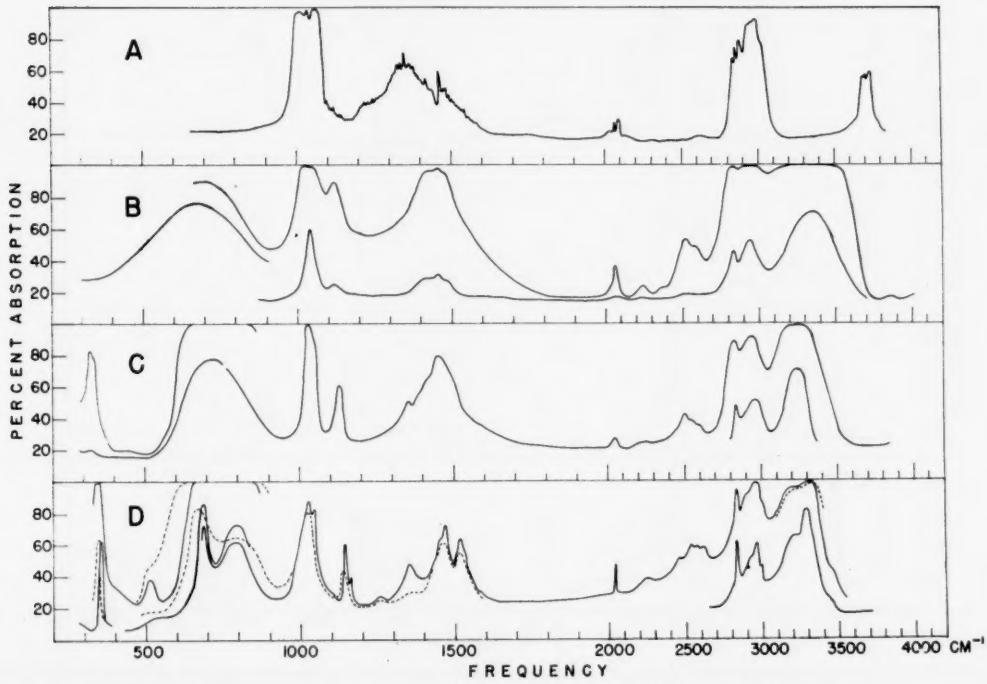

FIG. 1. Infrared absorption spectrum of CH_3OH. A—Vapor, 10-cm path-length, 80 mm Hg pressure, room temperature B—Liquid, room temperature. Two sample thicknesses are shown, approximately 5 and 50 μ. C—Vitreous solid, −180°C. D—Crystalline solid, −180°C (full line) and −108°C (broken line, shown only where the spectrum differs appreciably from that at −180°C). Several film thicknesses are shown.

terated, as shown by an almost complete lack of absorption in the CH stretching region. The OD groups in CH_3OD were about 95% deuterated.

2.2 Spectra

The vapor spectra were recorded using a standard 10-cm gas cell filled to about 80 mm Hg methanol pressure at room temperature. The liquid films were formed by squeezing a small drop between two flat silver-chloride or cesium-bromide disks. The solid samples were prepared by condensing small amounts of vapor onto a cesium-bromide disk mounted in a silver holder in a conventional low-temperature infrared cell. The disk was pressed tightly against the holder by a spring to ensure good thermal contact. The temperature was measured to about 2°C by a copper-constantan thermocouple embedded in the cesium-bromide disk; about −180°C was normally registered with liquid nitrogen in the coolant reservoir, and the temperature registered when films of CH_3OH melted was -97 ± 5°C, compared with the true melting point of −98°C.

The infrared spectra were recorded on a Perkin-Elmer model-21 double-beam spectrophotometer equipped with sodium-chloride and calcium-fluoride prisms, and on a Beckman IR-4 double-beam spectrophotometer equipped with cesium-bromide and, for some spectra, lithium-fluoride prisms. The instruments were regularly calibrated using the spectrum of water vapor and of thin polyethylene films. The Raman spectrum of liquid CD_3OH was recorded on a Cary model-81 Raman Spectrophotometer and the polarization of the bands was determined by the Edsal and Wilson technique.

3. RESULTS

Composite tracings of the infrared spectra of all four methanols in the gas and liquid phases at room temperature, the vitreous solid (see below) at −180°C, and the crystalline phases at −180°C and −108°C, are shown in Figs. 1–4. They were obtained by dividing the transmission of the cell containing the methanol sample by the transmission of the empty cell, except where the background was low and flat, when this procedure was not needed. The background noise was serious only below 350 cm^{-1}; it was smoothed out in replotting the spectra.

The observed frequencies and rough relative intensities are listed in Tables I–IV. They are usually the means of several measurements. The accuracy of the frequencies of sharp bands above 2000 cm^{-1} is at least ±4 cm^{-1}, below 2000 cm^{-1} at least ±2 cm^{-1}, and below 500 cm^{-1} at least ±1 cm^{-1}. The centers of broad bands are measured much less accurately. The intensities of the bands below 650

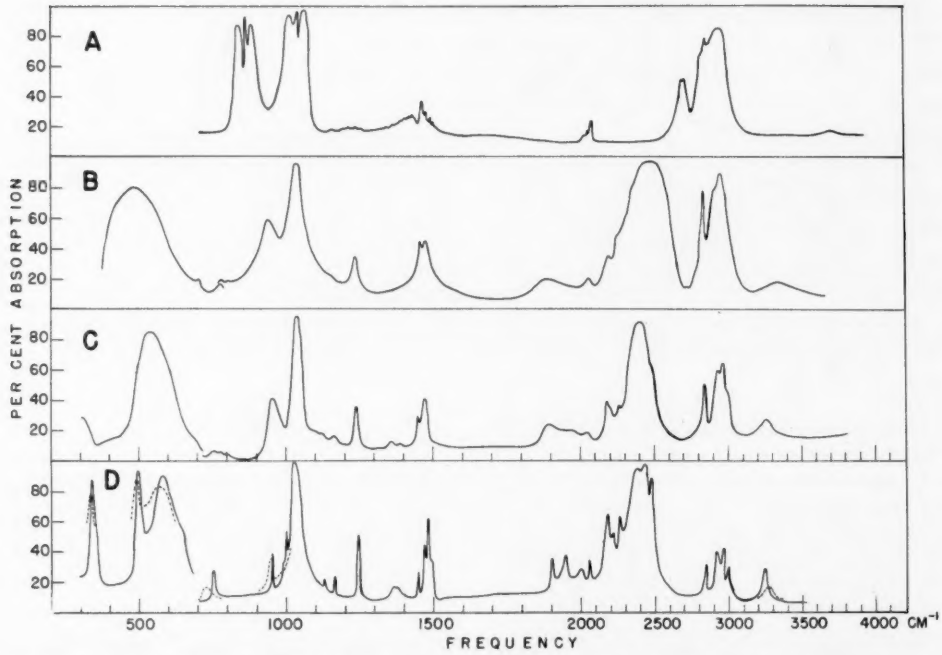

FIG. 2. Infrared absorption spectrum of CH_3OD. A—Vapor, 10-cm path-length, 80 mm Hg pressure, room temperature. B—Liquid, room temperature. C—Vitreous solid, −180°C. D—Crystalline solid, −180°C (full line) and −108°C (broken line, shown only where the spectrum differs appreciably from that at −180°C).

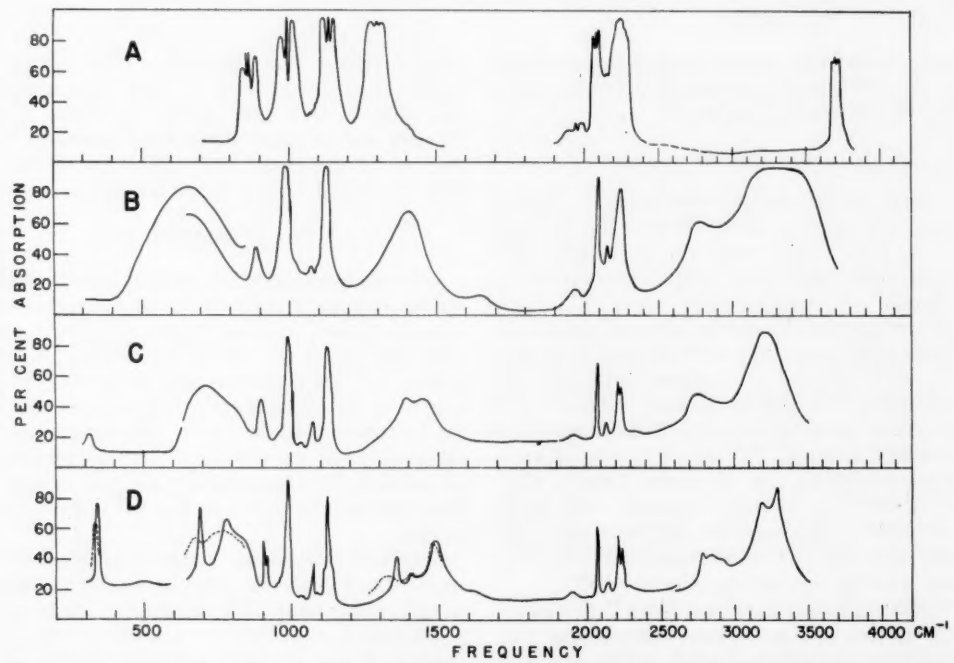

FIG. 3. Infrared absorption spectrum of CD_3OH. A—Vapor, 10-cm path-length, 80 mm Hg pressure, room temperature. B—Liquid, room temperature. C—Vitreous solid, −180°C. D—Crystalline solid, −180°C (full line) and −108°C (broken line, shown only where the spectrum differs appreciably from that at −180°C).

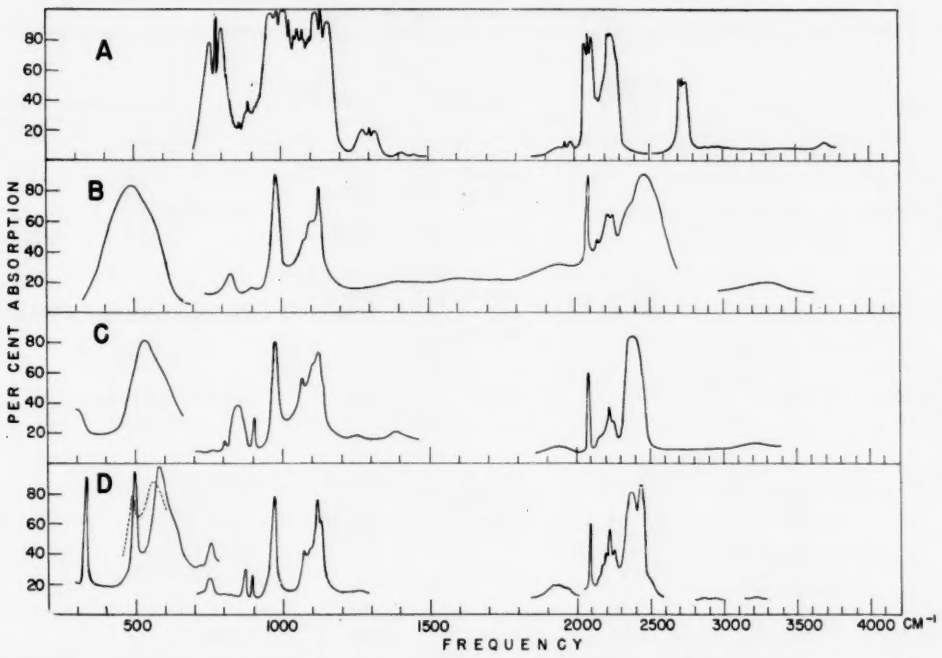

FIG. 4. Infrared absorption spectrum of CD_3OD. A—Vapor, 10-cm path-length, 80 mm Hg pressure, room temperature. B—Liquid, room temperature. C—Vitreous solid, −180°C. D—Crystalline solid, −180°C (full line) and −108°C (broken line, shown only where the spectrum differs appreciably from that at −180°C).

cm^{-1} are not comparable with those in other parts of the spectrum.

The Raman spectrum of CD_3OH is shown in Fig. 5, and the frequencies, estimated accuracy of the frequencies, polarizations, and rough relative intensities, are listed in Table V, together with the average Raman frequencies of the other methanols reported by previous authors.

3.1 Vapor Spectra

Infrared spectra of CH_3OH and CH_3OD have been obtained by Borden and Barker[2] and Barker and Bosschieter[27] under higher resolution than ours and their frequencies, which we list in Tables I and II in brackets, are to be preferred to ours. Our resolution is about the same as Plyler's[5] and our spectrum of CH_3OH vapor is

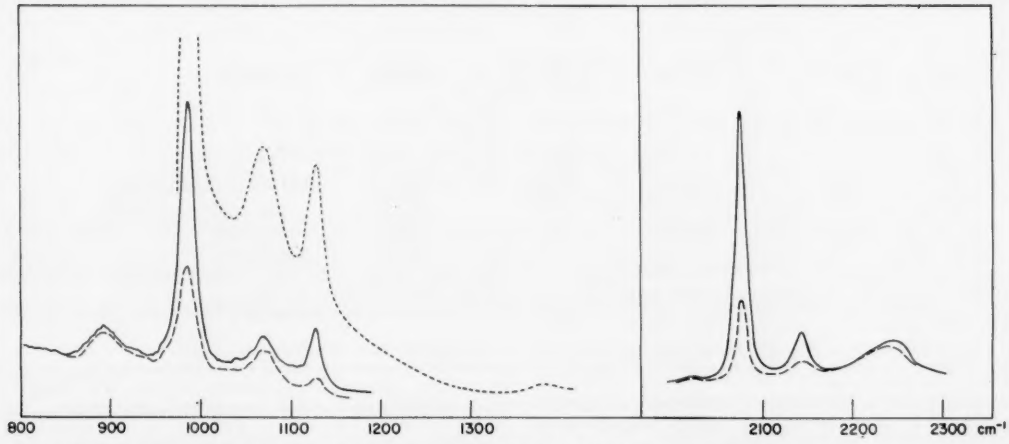

FIG. 5. Raman spectrum of liquid CD_3OH. Full line=exciting light polarized perpendicular to the scattered beam. Broken line=exciting light polarized parallel to the scattered beam. Short-dashed line: exciting light not polarized.

TABLE I. Infrared spectrum of CH_3OH.[a]

Vapor[b]	Liquid	Vitreous −180°C	Crystal −180°C	Crystal −108°C	Assignment[c]
			3443 sh		(?)
R 3713 *Q* 3687 s(3682) *P* 3673	3337 vs, br	3235 vs	3284 vs 3187 s	3297 vs 3193 s	OH stretching a'
		2982 sh, w	2982 m	2980 m	
2973 vs(2977)	2934 vs	2951 vs	2955 s 2912 sh, m	2954 s	CH_3 asym. stretching a' and a''[d]
R 2869 *Q* 2845 s(2844) *P* 2826	2822 s	2828 s	2829 s	2831 s	CH_3 sym. stretching a'
~2600 vw		2607 m	2617 m	2613 m	1346+1233[e](?)
	2571 w		2562 m	—	1415+1116(?)
	2502 w	2537 m	2538 m	~2540 m	1346+1116(?)
		2488 w	2457 w	2455 w	2×1233(?)
	2340 vw				1233+1116
	2232 vw	2230 w			2×1116
R 2078 *Q* 2056 w(2053) *P* 2035	2053 w	~2040 w	~2040 w	~2040 w	2×1034
			~1545 sh, vw	—	2×790
1477 m(1477)	1480 sh		1458 sh	~1459 sh	CH_3 asym. bending a'
1455 m(1455)	1455 m	1452 m	~1445 sh, m	—	CH_3 sym. bending a'
1415 w[1430?]	~1420[f]	1415 sh	1426 sh	1420	CH_3 asym. bending a''
1346 s(1340)	~1420 m, br	~1450 m	1514 m 1470 m	1506 m 1460 m	OH in-plane bending a'
		1350 w[g]	1345 m	~1370 w, br ~1300 w, br	2×685
1233 w[1260]	absent	~1256 w	1256 w	1257 w	CH_3 rocking a''
1116 w[1209]	1114 w	1124 w	1162 vw 1142 w	1142 w	CH_3 rocking a'
R 1060 *Q* 1034 vs(1034) *P* 1012	1029 vs	1032 vs	1046 w 1029 vs	1030 vs	CO stretching a'
			~1011 vw		$C^{13}O$ stretching
	655 s	730 s	790 s 685 m	765 s 675 m	OH out-of-plane bending
			520 w	~520 sh, w	lattice mode (or overtone)
		~320 m	357 m	346 m	lattice mode

[a] All frequencies are in cm^{-1}. vs=very strong, s=strong, m=medium, w=weak, vw=very weak, sh=shoulder, br=broad.

[b] Data in parentheses are those of Borden and Barker (see the work cited in footnote 2) and those in square brackets are those of Noether (see the work cited in footnote 3).

[c] Species of vibrations apply to vapor only. "Sym." and "asym." refer to the internal symmetry of the methyl group.

[d] Fermi resonance in the solid occurs between one of the CH_3 asymmetric stretching modes and an overtone or combination of the CH_3 bending modes, giving the extreme frequencies in this group.

[e] Frequencies proposed for the components of overtone bands are those of the vapor, or those of the solid at −180°K if not observed in the vapor.

[f] Overrun by the OH in-plane bending band.

[g] Probably due to partly crystallized material.

TABLE II. Infrared spectrum of CH_3OD.[a]

Vapor[b]	Liquid	Crystal: Vitreous −180°C	Crystal: −180°C	Crystal: −108°C	Assignment[c]
	3340 w, br	3225 m	3233 m	3258 m	OH stretching (CH_3OH)
	2990 sh, w	2985 sh, w	2993 w	2990 w	
2965 vs (2964)	2940 vs	2957 s	2962 s	2958 s	CH_3 asym. stretching a' and a''[d]
	2910 sh, s	2917 s	2917 s	2918 s	
R 2872 *Q* 2840 s (2850) *P* 2825	2825 s	2835 s	2838 s	2938 s	CH_3 sym. stretching a'
		2465 sh, m	2475 m	2475 sh, m	2×1228[e]
R 2745 *Q* 2720 m (2720) *P* 2705	2485 vs, br	2400 vs, br	2431 vs 2372 vs	2440 vs 2376 vs	OD stretching
	2260 sh, vw	2256 w	2252 w	2252 w	1041+1228
	2190 w	2200 vw	2215 vw	2215 vw	1228+998 (?)
		2175 w	2175 w	2177 w	1228+949
R 2082 *Q* 2062 w (2065) *P* 2043	2050 w	2051 w	2049 w	2050 w	2×1041
			1997 w	1985 w	2×998
		~1967 vw, br	1942 m	1935 m	1027+949
	1885 m, br	1885 w, br	1897 w–m	1889 w–m	2×945; 2×949
1500 (1480)	1472 m	1470 m	1486 w 1476 m	1475 m	CH_3 asym. bending a'
1458 m (1459)			1465 w	~1465 sh, w	CH_3 sym. bending a'
1427 (1427)	1452 m	1444 w			
1348 vvw			1443 w	~1443 w	CH_3 asym. bending a''
		1376 vw	1375 w	1375 w	1040+344 (?)
		1352 w	1362 w	1362 w	1027+344 (?)
1228 w [1232]	1235 m	1233 m	1238 m	1236 m	CH_3 rocking a''
1160 vw [1207]	1155 sh, vw	1158 w	1163 w	1162 w	CH_3 rocking a'
		1123 vw	1130 vw	1128 vw	CH_3 rocking a' (CH_3OH)
R 1061 *Q* 1041 vs (1040) *P* 1015	1038 vs	1032 vs	1040 sh, m 1027 vs	~1040 sh, w 1027 vs	CO stretching a'
R 885 *Q* 867 s (863) *P* 846	[942 s	945 m, br	998 w 985 sh, vw 949 m	980 sh, vw 943 m, br	OD in-plane bending a'
			750 m	725 m, br	OH out-of-plane bending (CH_3OH)
			640 sh, w	~640 sh, vw	2×344 (?)
	475 s	535 s	577 s 495 s	565 s 490 s	OD out-of-plane bending
		~290 br	344 s	333 s	lattice mode

[a] Abbreviations are given in Table I.

[b] Data in parentheses are from Barker and Bosschieter (see the work cited in footnote 27), and those in square brackets are from Noether (see the work cited in footnote 3).

[c], [d], [e] See Table I.

essentially identical with his. Our frequencies of CD_3OH and CD_3OD vapor are more accurate than Noether's because his resolution was lower and he has impurities in his deuterated methanols.

The present assignments for the four methanols are the same as Noether's,[3] Herzberg's,[30] and Plyler's[6] except for the bending and rocking vibrations of the CH_3 and CD_3 groups, which we shall now discuss in detail.

CH_3 *Bending Modes*

Three CH_3 bending modes are expected, viz., an a' internally symmetrical mode which has an approximately parallel band envelope, and two internally asymmetrical modes of species a' and a'' which have approximately perpendicular band envelopes. It seems likely that the sharp peak at 1455 cm^{-1} in CH_3OH is the Q branch of an approximately parallel band and so is probably due to the a' symmetrical bending mode.[2] The bands with centers at 1415 and 1477 cm^{-1}, both of which appear to be approximately perpendicular, may be the a' and a'' CH_3 internally asymmetrical bending modes. The a' mode is somewhat arbitrarily assigned to the higher frequency. In CH_3OD the bands are a good deal clearer owing to the absence of the OH bending mode. The sharp peak at 1458 cm^{-1} is clearly the Q branch of the approximately parallel band due to the CH_3 internally symmetrical bending mode, and the central gaps of the

[30] G. Herzberg, *Infrared and Raman Spectra of Polyatomic Molecules* (D. Van Nostrand Company, Inc., Princeton, New Jersey, 1945), p. 334.

TABLE III. Infrared spectrum of CD_3OH.[a]

Vapor[b]	Liquid	Vitreous −180°C	Crystal −180°C	Crystal −108°C	Assignment[c]
R 3708 *Q* 3690 *P* 3675 } s(~3680)	3310 vs, br	3195 vs, br	3285 vs 3175 s	3297 vs 3197 s	OH stretching *a'*
	2752 m, br	2760 m, br	2920 w 2830 w 2772 m	2920 w 2830 w ~2770 m	2×1488[e] 1488+1405 2×1405
2235 vs(2232)	2232 vs	2235 m 2213 s	2250 sh, w 2236 m 2214 s	2236 m ~2214 s	CD_3 asym. stretching *a'* and *a''*[d]
2147 vw	2145 w	2135 w	2138 w	~2138 w	2×1075
R 2098 *Q* 2077 *P* 2059 } s(2094)	2078 s	2075 s	2075 s	~2074 s	CD_3 sym. stretching *a'*
		~2020 vw	~2020 vw	~2020 vw	2×1047
R 1983 *Q* 1966 *P* 1947 } w(1975)	1962 w	1957 w	1969 sh, vw 1949 w	1947 w	2×988
R 1310 *Q* 1297 *P* 1274 } vs(1289)	1391 br	1445 s	1488 vs 1405 w	1479 vs 1404 w	OH in-plane bending *a'*[f]
		1389 s	1354 s	1320 br, m	2×685[f]
R 1145 *Q* 1134 *P* 1112 } vs(1123)	1122 vs	1122 vs	1131 sh, w 1121 vs	1118 vs	CD_3 sym. bending *a'*
		~1106 sh	1106 vw	1104 sh, vw	$C^{13}D_3$ sym. bending
1075 w(1080?)	1090 sh, vw 1069 w	1066 m	1083 sh, w 1069 m	~1086 sh, w 1069 m	CD_3 asym. bending *a''*
1047 (1055?)	1020 sh, vw	1026 w	1031 w 1023 w	1029 w 1023 w	CD_3 asym. bending *a'*
R 1007 *Q* 988 *P* 966 } vs(990)	982 vs	983 vs	987 sh, w 980 vs	~987 sh, w 981 vs	CO stretching *a'*
877 m(879)		950 sh, vw	953 vw 947 vw	953 vw 947 vw	CD_3 rocking *a''*
858 m(856)	882	895	912 w 902 m	909 vw 900 vw	CD_3 rocking *a'*
			823 sh, m		510+339(?)
	665 s, br	708 br	776 s, br 685 s	741 s, br 670 s	OH out-of-plane bending
		~314 w	~510 w, br 339 s	~490 w, br 332 m	lattice mode (or overtone) lattice mode

[a] Abbreviations are given in Table I.
[b] Data in parentheses are those of Noether (see the work cited in footnote 3).
[c], [d], [e] See Table I.
[f] Rather weak Fermi resonance seems to occur between 2×685 and one of the OH in-plane bending modes.

bands due to the internally asymmetrical modes are probably at 1500 and 1427 cm^{-1}. In the Raman spectra of the liquids the three bands are incompletely resolved. In crystalline CH_3OH the corresponding bands are overrun by the OH bending mode, but in crystalline CH_3OD the three bands due to the three CH_3 bending modes are clearly seen.

There are strong, approximately parallel bands in the vapor spectra of CD_3OH and CD_3OD with *Q* branches at 1134 and 1135 cm^{-1}, respectively, which are clearly due to the *a'* CD_3 internally symmetrical bending mode. In confirmation of this the corresponding Raman band in CD_3OH at 1127 cm^{-1} is polarized. There are two weak bands at somewhat lower frequencies, those in CD_3OD having their central gaps at 1080 cm^{-1} and 1035 cm^{-1} and those in CD_3OH being somewhat weaker and less well resolved at 1075 cm^{-1} and 1047 cm^{-1}. These are probably the two CD_3 internally asymmetrical bending bands. The assignment of the higher frequency to the *a''* mode is again rather arbitrary, but gives somewhat better agreement with the product rule. The two bands are not resolved in the Raman spectrum, only one maximum, which is depolarized, occurring at 1070 cm^{-1}. There are two bands in the infrared spectra of solid CH_3OH and CD_3OD, though possible contributions from one of the CD_3 rocking modes (see below) render interpretation uncertain.

The three CH_3 bending bands are not in the same order of frequency as the three CD_3 bending bands. Thus, in CH_3OH and CH_3OD the frequency of the CH_3

TABLE IV. Infrared spectrum of CD_3OD.[a]

Vapor[b]	Liquid	Crystal: Vitreous −180°C	Crystal: −180°C	Crystal: −108°C	Assignment[c]
3684 w(~3680)	3310 w, br	3195 w, br	3193 w	3216	OH stretching (CD_3OH)
2976			2975		CH stretching (CD_2HOD and CDH_2OD)
2953 vw			2925 vw		
2933					
2871 vw			2825 vw		CH stretching (CD_2HOD and CDH_2OD)
R 2746					
Q 2724 s(2725)	2474 vs, br	2384 s, br	2432 s	2432 s	OD stretching *a'*
P 2708			2361 s	2361 s	
	(2365 sh)				(?)
2242	2250 m	2240 w	2240 m	2248 m	CD_3 asym. stretching *a'* and *a''* [d]
2228 vs(2227)	2225 m	2213 m	2212 s	2223 s	
2215	2215 sh, vw	2190 sh, w	2189 m–w		
2140 vw	2145 w		2150 sh, vw		2×1060 or 2×1080[e]
			2130 sh, vw		
R 2100					
Q 2080 vs(2081)	2082 s	2075 s	2075 s	~2075 s	CD_3 sym. stretching *a'*
P 2063					
			1980 sh, w		1116+862(?)
R 1977					
Q 1959 w(1966)	~1940 br	1925 w	1935 w	~1920 w	2×983
P 1943			1920 w		
R 1310					
Q 1297 m(1290?)	~1380 vw, br	1382 w	1420 w	1422 w	OH bending (CD_3OH)[f]
P 1273			1395 w	1395 w	
		1256 vw	1248 vw	~1255 vw	CD_2H rocking (?)
R 1155					
Q 1135 vs(1121)	1124 vs	1117 vs	1116 vs	1116 vs	CD_3 sym. bending *a'*
P 1117					
1080±10 w(1075?)	1097 s	~1100 sh, w	~1080 sh, vw	~1085 sh, vw	CD_3 asym. bending *a''*
~1060 w(1045?)	1068 sh, m	1062 m	1064 w	1064 w	CD_3 asym. bending *a'*
~1024±10 w(?)	~1080(?)	~1125(?)	1131 w		CD_3 rocking and OD in-plane bending *a'*
R 1001					
Q 983 vs(987)	979 vs	975 vs	968 vs	969 vs	CO stretching *a'*
P 962					
892 w(?)					(?)
856 w(?)	898 w	896 m	895 m	892 m	CD_3 rocking *a''*
R 797					
Q 776 s(775)	818 m	831 m, br	862 m	857 w	CD_3 rocking and OD in-plane bending *a'*
P 753					
		800 w			(?)
		~730 vw	745 w	~755 sh, vw	OH out-of-plane bending (CD_3OH)
			~630	~630	2×336(?)
	483 s, br	533 s	578 s	556 s	OD out-of-plane bending
			495 s	487 s	
		~300(?)	336 vs	325.5 s	lattice mode

[a] Abbreviations given in Table I.
[b] Data in parentheses are those of Noether (see the work cited in footnote 3).
[c], [d], [e] See Table I.
[f] Doubling in the crystal is probably due to Fermi resonance with 2×705 cm^{-1}.

internally symmetrical bending mode appears to be between those of the two asymmetrical bending modes, whereas in CD_3OH and CD_3OD it appears to be a good deal higher. This is probably caused by interaction of the CH_3 internally symmetrical bending motion with the CO stretching motion. The CO stretching frequency drops from 1034 cm^{-1} in CH_3OH and 1041 cm^{-1} in CH_3OD to 988 cm^{-1} in CD_3OH and 983 cm^{-1} in CD_3OD, and at the same time the deuteration shift of the CH_3 internally symmetrical bending frequency is only 1.28 instead of the expected 1.36. The isotope shifts are shown diagrammatically in Fig. 6. The apparent inversion of the order of frequency for the two CH_3 and CD_3 internally asymmetrical bending modes is quite uncertain.

CH_3 *Rocking Modes*

There are two CH_3 rocking modes, of species *a'* and *a''*. In the absence of interaction of the motions with the motions of other atoms the frequencies are expected to be close together. However, we note that the shift of the OH bending frequency on deuteration is high, being

TABLE V. Raman frequencies of liquid CH_3OH, CH_3OD, CD_3OH, and CD_3OD.[a]

CH_3OH[b]	CH_3OD[c]	CD_3OH[d]	CD_3OD[e]	Assignment
3390±50 br, w	2490±50 br, m	3350±100 br, w	2500±60	OH stretching a'
2989 m	2990 m–s	2245±5 p, m	2247	CH_3 asym. stretching a' and a'' [f]
2943 p? s	2945 vs	2230±5 dp, m		
2910 m	2909 m	2213±8 p vw	2216	
		2141±1 p m	2147 m	2×(asym. CH_3 bending a'')
2835 p vs	2835 vs	2074±1 p vs	2076 s	CH_3 sym. stretching a'
		2020±3 dp? vw		2×(asym. CH_3 bending a')
1448 dp m	{... ...}	1127±2 p m	1130 vw	CH_3 sym. bending a'
1468 dp m	1464 br, s	1072±2 dp m	1069 vw	{CH_3 asym. bending a'' / CH_3 asym. bending a'}
1363 p? br, w	948	1360±10 br, w	...	OH bending a'
1160 vw	1226 w	894±5 dp m	824 vw	CH_3 rocking a''
1109 dp? w	1165 w			CH_3 rocking a'
1033 p s	1031 s	986±1 p vs	989 s	CO stretching a'

[a] p=polarized, dp=depolarized, other abbreviations are as in Table I.
[b] Average values from the works cited in footnotes 13, 14, 15, 16, 17, 19, 20, 22, 23, 24, 25. Polarization data are from the works cited in footnotes 13, 14, 25.
[c] Average values from the works cited in footnotes 15, 17, 18, 19. There are no polarization data.
[d] This work.
[e] Average values from the work cited in footnotes 3 and 22. There are no polarization data.
[f] Fermi resonance occurs between the a' asymmetric stretching mode and an overtone or combination of the CH_3 symmetric bending mode giving the extreme frequencies in this group.

1.55 for CH_3OH–CH_3OD, 1.67 for CD_3OH–CD_3OD, and 1.53 for CD_3OH–CH_3OD. Also, the OH bending frequency in CH_3OH and CD_3OH is 1346 and 1297 cm^{-1}. There is evidently considerable coupling in at least three of the methanols between the OH bending motion and the motions of other atoms. The a' CH_3 rocking motion is a likely candidate for coupling with the OH bending motion and so we may expect that in some of the methanols the a' and a'' rocking frequencies will be quite widely separated.

In CD_3OH there are two bands at 858 and 877 cm^{-1} which are almost certainly the CD_3 rocking bands. The bands are close together, and it seems likely that there is relatively little interaction with the OH bending motion,

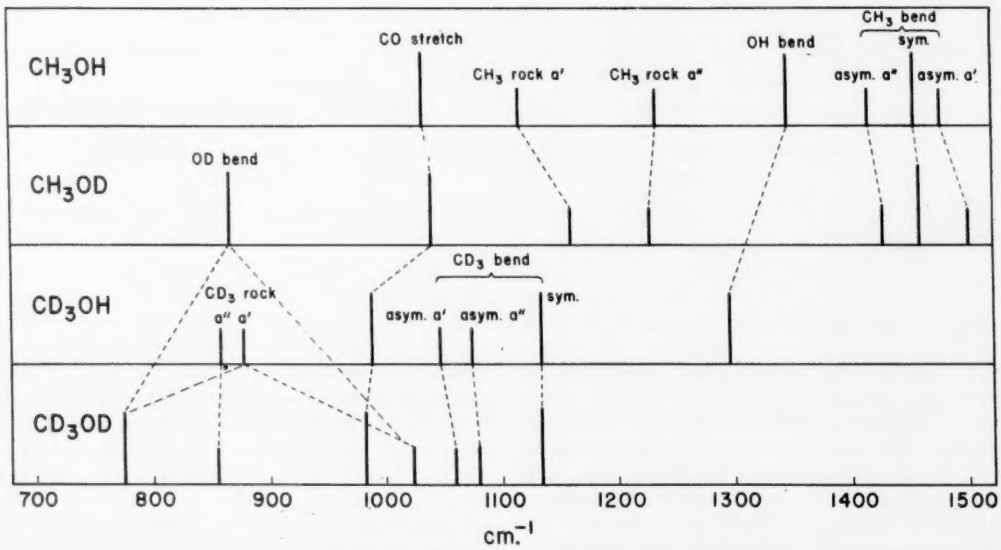

FIG. 6. Vapor-phase fundamental frequencies of the four isotopic methanols in the 700-to-1500-cm^{-1} region. Strong coupling occurs between OH bending and a' CH_3 rocking in CH_3OH; between OD bending and a' CD_3 rocking in CD_3OD; and between CO stretching and CD_3 symmetrical bending in CD_3OH and CD_3OD. There is also some coupling between OD bending and a' CH_3 rocking in CH_3OD.

TABLE VI. Fundamental frequencies of isotopic methanols in vapor-phase and product-rule ratios.

		CH_3OH	CH_3OD	CD_3OH	CD_3OD
a'	OH stretching	3687	2720	3690	2724
	CH_3 asym. stretching	2973	2965	2235	2228
	CH_3 sym. stretching	2845	2840	2077	2080
	CH_3 sym. bending	1455	1458	1134	1135
	CH_3 asym. bending	1477	1500	1047	1060
	OH bending	1346	867	1297	776
	CO stretching	1034	1041	988	983
	CH_3 rocking	1116	1160	877	1024
a''	CH_3 asym. stretching	2973	2965	2235	2228
	CH_3 asym. bending	1415	1427	1075	1080
	CH_3 rocking	1233	1228	858	856
	Molecular weight	32.04	33.05	35.06	36.07
	$10^{40} I_z$	35.32	38.20	43.58	46.80
	$10^{80} I_y I_z$	224.1	274.8	503.8	577.5
	$10^{40} I_{\text{internal rotation}}$	1.009	1.621	1.116	1.912
	a' ratio observed		0.504	0.210	0.114
	a' ratio calculated		0.536	0.216	0.115
	a'' ratio observed		1.002	0.415	0.397
	a'' ratio calculated		1.009	0.414	0.416

whose frequency, 1297 cm^{-1}, is relatively far away. In CH_3OH there are two broad bands with very complicated structure with centres near 1116 and 1233 cm^{-1} and it seems likely that these are the methyl rocking bands. These bands were observed, but not assigned, by Plyler[5] who suggested tentatively that the complicated structure in these regions may be due to combinations of the internal rotation with the CO stretching and CH_3 rocking modes. This does not appear to be entirely correct because the two vapor bands are clearly also present in the solid and are relatively little shifted. It would be surprising if combination bands of the kind suggested did not shift very considerably on condensation due to shifts in the internal rotation. In CH_3OD the CH_3 rocking bands are almost certainly at 1160 and 1228 cm^{-1}. It seems likely that the 1233-cm^{-1} band of CH_3OH and the 1228-cm^{-1} band of CH_3OD are due to the relatively uncoupled a'' CH_3 rocking modes, and that in CH_3OH the a' CH_3 rocking and the a' OH bending vibrations are coupled to give the 1116-cm^{-1} and 1346-cm^{-1} bands. The uncoupled a' OH bending frequency is presumably near the value of 1297 cm^{-1} that it has in CD_3OH, and in CH_3OH coupling with the a' CH_3 rocking vibration causes it to move upwards to 1346 cm^{-1}. In CH_3OD the a' CH_3 rocking and the a' OD bending modes are slightly coupled to give the 1160-cm^{-1} and 867-cm^{-1} bands. The relation between these frequencies is shown diagrammatically in Fig. 6.

A similar interaction occurs in CD_3OD, in which both the CD_3 rocking frequencies would be expected to be near 860 cm^{-1} by analogy with the CD_3OH bands at 877 cm^{-1} and 858 cm^{-1}, and the OD in-plane bending frequency would be expected to be near 867 cm^{-1}, the frequency in CH_3OD. In fact, a strong band occurs at 776 cm^{-1} and this must be due to coupled a' OD bending and a' CD_3 rocking modes. The a'' CD_3 rocking mode is at 856 cm^{-1}, relatively unshifted from CD_3OH. The other band due to the coupled a' OD bending and a' CD_3 rocking vibrations is presumably increased in frequency to near 1024 cm^{-1}, a value which fits well with the product rule (see below). This whole region, both in the vapor and in condensed phases, contains considerable structure due to the CD_3 bending modes, and the exact position of the CD_3 rocking band is uncertain. However, the increased absorption of CD_3OD as compared to CD_3OH in the region 1000 to 1100 cm^{-1} confirms the presence of an additional band there. The two coupled vibrations at 776 and 1024 cm^{-1} are not displaced equally from their unperturbed frequency expected near 860 cm^{-1}. Coupling with other vibrations therefore occurs.

The above approximate description of the coupling of group vibrations in methanol accounts partly for the irregular isotope shifts, and disposes of the main objection of previous authors[2,8,11,12] to the assignment of the 1346-cm^{-1} band in CH_3OH vapor to the a' OH bending mode.

In Table VI our assignments of the fundamental frequencies for the four methanol molecules are listed and the observed and calculated product-rule ratios are compared. The moments of inertia used in the calculation were derived from the microwave values of Venkateswarlu and Gordy.[31] The average deviation between the theoretical and experimental ratios is 2.5%, a reasonable value in view of the uncertainties of 1% in several of the frequencies. It is likely therefore that our assignments of the CH_3 bending and rocking modes are essentially correct.

Several combination bands were observed, and tentative assignments are advanced in Tables I–IV.

[31] P. Venkateswarlu and W. Gordy, J. Chem. Phys. **23**, 1200 (1955).

TABLE VII. Vapor and crystal frequencies in cm^{-1} of CH_3OH and CH_3OD.

	CH_3OH			CH_3OD		
	vapor	crystal	shift	vapor	crystal	shift
a' fundamentals:						
OH stretching	3687	3261[a], 3173[a]	−470[b]	2720	2420[a], 2366[a]	−327[b]
CH_3 asym. stretching	2973	2955	−18	2965	2962	−3
CH_3 sym. stretching	2845	2829	−16	2840	2838	−2
CH_3 asym. bending	1477	1468	−9	1500	1476	−24
CH_3 sym. bending	1455	1445	−10	1458	1465	+7
OH bending	1346	1514[a], 1492[a]	+146[b]	867	998[a], 949[a]	+107[b]
CO stretching	1034	1029	−5	1041	1027	−14
CH_3 rocking	1116	1142	+26	1160	1163	+3
a'' fundamentals:						
CH_3 stretching	2973	2955	−18	2965	2962	−3
CH_3 bending	1415	1426	+11	1427	1443	+16
CH_3 rocking	1233	1256	+23	1228	1240	+12
crystal fundamentals:						
OH bending		824[a], 698[a]			593[a], 502[a]	
translation frequency (?)		520[a]			...	
translation frequency		372[a]			359[a]	

[a] Frequencies extrapolated to 0°K.
[b] Shifts calculated using averages of the two components in the crystal.

3.2 Liquid Spectra

The frequencies of the liquid bands are listed in Tables I–IV. Assignments were made mainly by comparison with vapor spectra.

The infrared spectra of all four liquids are as expected, and there is little difference between the infrared and Raman liquid frequencies. The infrared bands are mostly fairly broad, and those due to OH stretching and bending motions are, as is common with hydrogen-bonded substances, very broad. The usual shifts from the vapor frequencies occur, i.e., CH_3 stretching and bending and CO stretching modes are little affected, and the OH stretching frequency decreases and the OH bending frequency increases. A very broad band, which is not present in the vapor, occurs in the range 450 to 850 cm^{-1} in CH_3OH and CD_3OH and in the range 350 to 630 cm^{-1} in CH_3OD and CD_3OD, which is clearly due to the out-of-plane bending mode of the hydrogen-bonded OH, and was already so assigned in liquid CH_3OH and CH_3OD by Stuart and Sutherland.[6,32].

3.3 Solid Spectra

Solid films condensed at liquid-nitrogen temperature were visibly transparent and their spectra consisted of broad bands resembling those of liquids. Only relatively small shifts from the liquid frequencies occurred, the largest shifts being observed for the OH and OD out-of-plane bending modes. One new band of moderate intensity appeared near 300 cm^{-1}. The solids were presumably glasses.

Upon warming, the films became snowy-white at about −140°C, their spectra became sharper, all fundamental bands that involve mainly motions of the O-hydrogen atom split into two components of comparable intensity, some weak bands in the region 2100 to 2600 cm^{-1} sharpened and resolved into several components, a few other bands appeared to split into two closely separated components of unequal intensity, and the band near 300 cm^{-1} sharpened. The transformation was irreversible, and evidently the films had crystallized.

Further sharpening of the spectrum and some additional splitting into two components of unequal intensity occurred when the crystalline films were cooled to −180°C. Some bands were sensitive to temperature, those involving OH motion generally broadening and shifting towards the vapor frequencies as the temperature increased. These changes were completely reversible.

In both CH_3OH and CH_3OD there is a first-order solid-solid phase transition, at −113.5°C in CH_3OH and at −109.9°C in CH_3OD[33,34] and this presumably also occurs in CD_3OH and CD_3OD, perhaps at somewhat higher temperatures. An attempt was made to observe a change of spectrum when the phase changed. Films of all four methanols were held near −120°C and −108°C for two hours. By comparison with observations on bulk specimens[35,36] this should be long enough for the phase change to be complete. There was no essential

[32] A. V. Stuart and G. B. B. M. Sutherland, J. Chem. Phys. **20,** 1977 (1952).

[33] D. W. Davidson, Can. J. Chem. **34,** 1243 (1956).
[34] D. W. Davidson, Can. J. Chem. **35,** 458 (1957).
[35] L. A. K. Staveley and A. K. Gupta, Trans. Faraday Soc. **45,** 50 (1949).
[36] L. A. K. Staveley and M. A. P. Hogg, J. Chem. Soc. 1013 (1954).

difference between the spectra, the small changes in frequency and breadth of bands being consistent with the temperature variation of the bands in the low-temperature phase.

The assignment of the bands was made mainly by comparison with the vapor spectra, and is given in Tables I–IV. However, the coupling that occurs in the vapor is modified in the solid, and the identification of some of the bands is uncertain. Bands due to dilute CH_3OH in CH_3OD and to dilute CD_3OH in CD_3OD occur. These are listed in Tables II and IV and discussed in Sec. 4.4. In CH_3OH and CD_3OH there is a band near 500 cm^{-1}, and in all four there is a band near 320 cm^{-1}. They are discussed in Sec. 4.3. For a later paper we shall need the frequencies of CH_3OH and CH_3OD at 0°K. Those that shift with temperature have been extrapolated linearly to 0°K using the data of Tables I–IV and some data at intermediate temperatures which we have not reported. The results are in Table VII.

The sum of the frequency shifts from vapor to crystal for CH_3OH is 1.49 times that for CH_3OD, and that for CD_3OH is 1.44 times that for CD_3OD. The factor expected if the force constants for the four methanols are the same in the vapor and are the same in the solid is 1.41, in rough agreement with the experiment.

The two CH_3 internally asymmetrical stretching modes of species a' and a'' are not resolved in the vapor. In the crystalline solid the bands are much narrower and several peaks occur. The two modes appear to be separated in all four methanols by about 20 to 30 cm^{-1}. This is readily accounted for by the occurrence of Fermi resonance between one of the internally asymmetrical CH_3 stretching modes and the first overtone of one of the CH_3 bending modes, resulting in a shift of both the overtone and the stretching mode.

Bands occur in the spectrum of CH_3OH and CD_3OH at 1370 and 1354 cm^{-1} at −180°C. The intensity of these bands decreases very markedly as the temperature is increased and small shifts of frequency downwards occur. The downward shifts are consistent with the bands' being first overtones of the OH out-of-plane bending mode at 685 cm^{-1} in both CH_3OH and CD_3OH, and the intensity is possibly due to Fermi resonance with the OH in-plane bending mode that is symmetrical relative to the chain. The resonance decreases as the frequency of the out-of-plane bending mode shifts downward with rising temperature.

4. DISCUSSION OF SPECTRA OF CRYSTALLINE SOLIDS

4.1 β-Phase

The high temperature (β) phase of methanol belongs to the centro-symmetrical space group D_{2h}^{17}-$Cmcm$.[37] The molecules are arranged in hydrogen-bonded zig-zag chains and two chains, each containing two molecules,

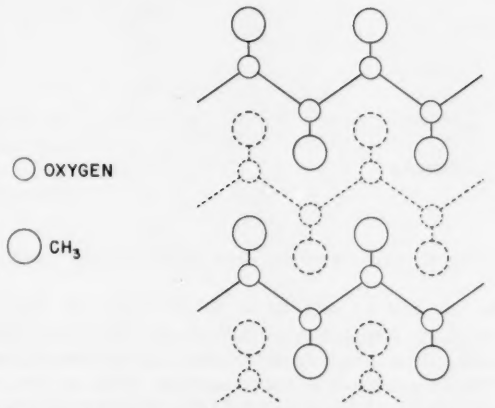

FIG. 7. Diagrammatic sketch of the crystal of methanol. Atoms represented by solid lines are in the plane of the paper, and those represented by broken lines are below the plane of the paper.

pass through the unit cell. The structure is shown diagrammatically in Fig. 7. The full symmetry of the x-ray diffraction pattern implies that the methyl group (treated as one atom) and the oxygen and hydrogen atoms of one chain lie in one plane, and that the hydrogen atoms are midway between the oxygens. The rather large thermal amplitude of approximately 0.32 A rms perpendicular to the chain[37] and the high dielectric constant of the β-phase[34,38,39] were interpreted[37] to indicate that the apparent x-ray symmetry might be the mean of two forms in which the methyl groups are off the plane of the oxygen atoms in the same chain.

The only infrared-active fundamental modes of a crystal are those which are totally symmetrical with respect to translation, i.e., those in which all unit cells vibrate in phase.[40,41] If the crystal is anharmonic then combinations of forbidden fundamentals with lattice modes may be active, and their intensity will probably be quite strongly temperature-dependent. In none of the bands that we observed does the intensity increase markedly as the temperature increases from −180°C to −108°C, and so we will assume that only allowed fundamentals are seen.

There are four molecules in the unit cell, and consequently each internal mode of the isolated methanol molecule gives four modes in the crystal that may be active, and so some splitting of the frequencies of the isolated molecule is expected.

Experimentally, each of the three bands that are due to the motions of the O-hydrogen atoms have two components of comparable intensity, usually about 50 to 100 cm^{-1} apart. The other bands are either not split

[37] K. J. Tauer and W. N. Lipscomb, Acta Cryst. **5,** 606 (1952).

[38] C. P. Smyth and C. S. Hitchcock, J. Am. Chem. Soc. **56,** 1084 (1934).

[39] C. P. Smyth and S. A. McNeight, J. Am. Chem. Soc. **58,** 1597 (1936).

[40] S. Bhagavantam and T. Venkatarayudu, *Group Theory and its Applications to Physical Problems* (Andhra University, Waltair, India, 1951).

[41] D. F. Hornig, J. Chem. Phys. **16,** 1063 (1948).

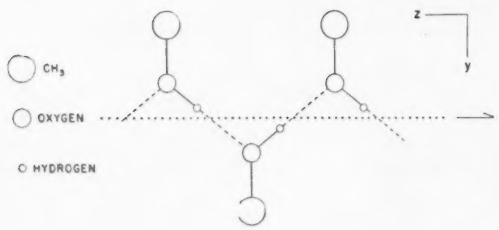

FIG. 8. Symmetry of one chain in the methanol crystal.

or are split by only 10 to 20 cm^{-1}, and the higher-frequency component is usually far less intense than the lower. It seems very likely that the splitting of the O-hydrogen bands is due to coupling of the motions of molecules in the same unit cell. The splitting of the other bands is referred to below.

We consider first the spectrum of the whole unit cell.

Space-Group Analysis

For analyzing the crystal spectrum, the analysis based on the factor group of the space group[40,42] is appropriate. The factor group of the space group D_{2h}[17] is isomorphous with the point group D_{2h}. We call the a, b, and c axes of the unit cell the x, y, and z directions, so that the x axis is perpendicular to the plane of the chains, the z axis is parallel to the chain axis, and the y axis is the remaining axis. Under the symmetry D_{2h} both the OH stretching and OH in-plane bending modes split into four components in the crystal, two, of species b_{1u} and b_{2u}, being infrared-active, and two, of species b_{1g} and b_{2g}, being Raman-active. The OH out-of-plane bending vibration gives four components in the crystal, one of which, of species b_{3u}, is infrared-active, two, of species a_g and b_{1g}, are Raman-active, and one, a_u, is forbidden in both Raman and infrared spectra. We find experimentally that the OH stretching and in-plane bending modes give two infrared-active modes, as expected, but the OH out-of-plane bending mode also gives two components, which disagrees with the above predictions. The possibility that the splitting occurs because of Fermi resonance with an overtone is very unlikely because similar bands occur in all four methanols. It follows, therefore, that the symmetry of the unit cell is lower than the apparent x-ray symmetry.

There are two possible causes of the high apparent x-ray symmetry. Either the hydrogen atoms are not observed, or the chains are of lower symmetry, but they are irregularly oriented in such a way as to give this apparent x-ray symmetry. It seems likely, therefore, that either the O-hydrogen atoms are not at the midpoint of the line joining the oxygen atoms, or the methyl groups are not coplanar with the oxygen atoms, or both these dissymmetries occur. Whichever occur, each chain has two possible orientations, and it is likely that these orientations are irregularly distributed, so giving the apparent x-ray symmetry. If this occurs, then there are no rigorous selection rules. However, as only a limited number of bands occurs, approximate selection rules must hold, and these are almost certainly those appropriate for an isolated chain. The isolated-chain approximation has frequently been used for discussing the spectrum of polymer molecules,[43–46] in which, however, the covalent bonding along the chains is much stronger than the hydrogen-bonding in the methanol chains. Accordingly, we now discuss the spectrum expected for an isolated chain.

Line-Group Analysis

A possible structure of the isolated chain that is consistent with the observed x-ray symmetry and with the arguments of the foregoing paragraphs is a chain in which the carbon, oxygen, and hydrogen atoms are coplanar and the hydrogen atom is not midway between the two oxygen atoms. The spectrum of the chain is best considered in terms of the one-dimensional space group (or line group)[44] that describes the symmetry of the chain. The symmetry elements of the chain (Fig. 8) are an infinite number of translations along the z axis, one C_2 screw axis along the z axis, one reflection plane yz, and one glide plane xz. The only modes that are potentially active in infrared or Raman spectra are those that are in phase in all unit segments of the chain,[43,44] and consequently the factor group of the line group is appropriate for analyzing the spectrum. It is isomorphous with the point group C_{2v}. Under this symmetry both the OH stretching and OH in-plane bending modes give two components, of species a_1 and b_2, both of which are infrared-active, as observed. The two components of the OH out-of-plane bending mode are of species a_2 and b_1, of which only the b_1 mode is infrared-active. Since two infrared modes are observed, then the planar chain with the hydrogen not midway between the two oxygen atoms is not consistent with the infrared spectrum. It follows that further relaxation of the symmetry is necessary, and hence that either the carbon or the hydrogen or both are out of the plane of the oxygen atoms.

We now inquire whether the spectrum is consistent with the methyl group's being out of the plane of the oxygen atoms and the hydrogen atom's being midway between the oxygen atoms. The assumed structure of the chain is that of the low-temperature form (see below) in which the methyl groups on one side of the chain are above the plane of the oxygen atoms and those in the other side are below the plane. There are two possible chains consistent with this structure according

[42] H. Winston and R. S. Halford, J. Chem. Phys. **17**, 607 (1949).

[43] C. Y. Liang, S. Krimm, and G. B. B. M. Sutherland, J. Chem. Phys. **25**, 543 (1956).

[44] M. C. Tobin, J. Chem. Phys. **23**, 891 (1955).

[45] R. E. Moynihan, J. Am. Chem. Soc. **81**, 1045 (1958).

[46] A. Novak and E. Whalley, Trans. Faraday Soc. **55**, 1484 (1959).

as the methyl groups on a particular side of the chain are above or below the plane of the chain. They are assumed to be irregularly distributed so as to give the x-ray symmetry. We assume, as we assumed above, that, although rigorous selection rules do not hold, the observed spectrum is closely related to the spectrum of an isolated chain. The corresponding point group is C_{2h}. The hydrogen atom is at the center of symmetry, and so all motions of the hydrogen atom destroy the center of symmetry. Their species are therefore either a_u or b_u and they are allowed in the infrared spectrum.

The infrared spectrum thus strongly confirms Tauer and Lipscomb's somewhat tentative suggestion that the chains in methanol are puckered. It does not prove that the O-hydrogen atom is not midway between the oxygen atoms, though this seems likely by analogy with other compounds.

We now discuss briefly the splitting of the vibrations that do not involve mainly O-hydrogen atoms. If the symmetry of the chain is C_{2h}, then in the isolated-chain approximation only one active vibration occurs for each of these vibrations in the vapor. If the symmetry C_{2h} is destroyed by moving the O-hydrogen atom, it is likely that the intensity of bands that were forbidden and that now become active will be rather low. This agrees with experiment. Another explanation of the experimental results is that the low-intensity component is due to a combination of the main vibration with a low-frequency lattice vibration. It is not possible at present to decide between these two explanations and so the chain symmetry C_{2h} cannot be rigorously eliminated.

4.2 α-Phase

According to Tauer and Lipscomb the low-temperature (α) phase has probably the space symmetry $C_{2h}^2-P2_1/m$.[37] The molecules are arranged in hydrogen-bonded zig-zag chains, the methyl groups on one side being above the plane of the oxygen atoms and the methyl groups on the other side being below. Weak superlattice reflections suggested that the unit cell may be twice that proposed and that perhaps the methyl groups are alternately staggered relative to their neighbors in the chain. Such small changes in symmetry should make no detectable difference in the infrared spectrum and are neglected in this discussion.

No significant change in spectrum is observed in passing from the β to the α phase. The heat of transition is only 170 cal mole^{-1} [35] so only very small shifts of frequency are expected. The number of fundamental bands does not alter, and hence the selection rules are not significantly altered, as expected for the structure of the α-phase proposed by Tauer and Lipscomb. If we neglect a possible superlattice, there are only two molecules in the unit cell. If the hydrogen atoms are midway between the oxygen atoms then the point group isomorphous with the factor group is C_{2h}, and as discussed above each of the three O-hydrogen motions should give two infrared-active components. Any reduction in symmetry will not affect the number of infrared-active bands due to the motions of the O-hydrogen atom.

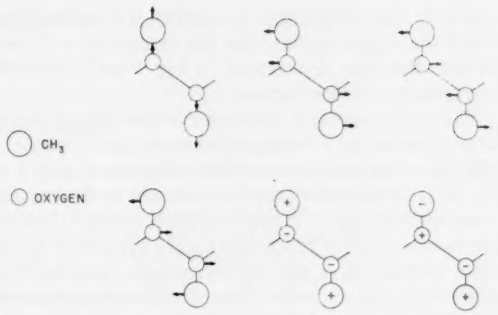

FIG. 9. Expected infrared-active fundamentals of a methanol chain that involve motion of the whole molecules.

4.3 Lattice Modes

A weak, moderately broad band occurs in the spectrum of CH_3OH at $-180°C$ at 520 cm^{-1} and in CD_3OH at $\sim$510 cm^{-1}. The OD out-of-plane bending bands obscure any band of similar frequency that may occur in CH_3OD and CD_3OD. A moderate, sharp band occurs in the spectra of all the methanols at the following frequencies at $-180°C$: CH_3OH, 357 cm^{-1}, CH_3OD, 344 cm^{-1}; CD_3OH, 339 cm^{-1}; CD_3OD, 331.5 cm^{-1}. The frequency of all these bands decreases on warming, and the bands are not observed in the liquids. In the spectra of the vitreous films the band near 500 cm^{-1} is not observed, and the bands near 340 cm^{-1} are considerably broader and at a lower frequency than in the crystalline films. The isotope shifts for both bands are small, and so they cannot be connected with the CH_3 internal rotation. Neither is it possible to explain them as difference bands involving the internal fundamentals. They must, therefore, be due to external modes of the molecules. The 500-cm ^{1} band is quite weak and it might be an overtone.

Since there are two molecules in the unit cell in the α phase, neglecting the possible superlattice, there are six nonzero fundamentals in which the whole molecules move that are potentially active in the infrared. These are roughly represented in Fig. 9. Modes 1 and 2 are closely related to translational modes of the isolated molecules. The four other modes that are derived from the translations of isolated molecules are three translations of the chain and one rotation about the chain axis, which are of zero frequency in the isolated chain. If the symmetry of the chain is C_{2h}, and the O-hydrogen atoms are midway between the oxygen atoms then vibrations 1, 2, 3, and 6 of Fig. 9 preserve the center of symmetry and should be infrared-inactive. Vibrations 4 and 5, which destroy the center of symmetry should be infrared-active. The first overtones of all these vibrations are fully symmetrical and should be infrared-in-

active. If the O-hydrogen atoms are not midway between the oxygen atoms then the symmetry is C_2 and all the vibrations represented in Fig. 9 and their first overtones are infrared-active.

The isotope shifts for both observed bands are roughly those expected for a translational mode, and it would be difficult to reconcile them with vibrations 4 and 5 of Fig. 9. It seems likely that they are due to the translational modes 1 and 2. If this is so, then whether they are due to overtones or fundamentals the symmetry of the chain cannot be C_{2h}, and the O-hydrogen atom must be off the midpoint of the O–O line. This is not unexpected, the O–O distance being much longer than usually required for symmetrical hydrogen bonds.

4.4 Bands Due to Dilute Isotopic Molecules

Bands that we ascribe to CH_3OH and CD_3OH occur in crystalline CH_3OD and CD_3OD, respectively; they are included in Tables I–IV. The OH stretching, in-plane bending, and out-of-plane bending are observed for CD_3OH in CD_3OD. The OH stretching and out-of-plane bending bands are observed for CH_3OH in CH_3OD, the OH in-plane bending being hidden by CH_3OD absorption. Unlike the corresponding bands in the pure crystals, the bands of the isotopically diluted species show no splitting. This is to be expected, since no coupling can occur with vibrations of neighboring molecules, which now have too different frequencies.

The uncoupled frequency should fall between the two observed frequencies of the coupled molecules for the following reason. During a vibration the lone-pair electrons that take part in hydrogen-bonding will move in phase with the nuclei. The two observed bands correspond to motion of adjacent molecules in phase and out of phase. In one of these vibrations the lone-pair electrons will move in step with the hydrogen atom of the adjacent molecule and in the other vibration they will move π radians out of step. Consequently, the coupling will cause one frequency to be higher than in a molecule whose neighbors do not move and will cause the other frequency to be lower. The frequencies of dilute CH_3OH in CH_3OD and of dilute CD_3OH in CD_3OD are probably close to the values they would have if the neighboring molecules did not vibrate. It follows therefore, that the frequency, of a dilute molecule should fall between the two observed frequencies of the coupled molecules. This is indeed observed.

In all the other vibrations of a crystal that correspond to a given vibration of the isolated molecule, adjacent unit cells vibrate out of phase. It follows that the lone-pair electrons of one molecule will be out of step by between 0 and π radians with the O-hydrogen atom of the neighboring molecule. It seems likely that these frequencies will be between those corresponding to a phase difference of 0 and π radians and so that the two observed frequencies are the extremes of the set of crystal frequencies corresponding to a given mode of the isolated molecule.

ACKNOWLEDGMENTS

We should like to thank Dr. R. N. Jones for the use of his Raman spectrophotometer, Dr. K. Noack for the assistance in recording the Raman spectra, and M. E. Bednas for the gas-chromatographic analysis of our methanol samples.

Difference of Intermolecular Potentials of CH_3OH and CH_3OD†

E. WHALLEY AND M. FALK*

Division of Applied Chemistry, National Research Council, Ottawa, Canada

(Received September 2, 1960)

The intermolecular potentials of CH_3OH and CH_3OD have been examined using the difference of the heats of vaporization at 0°K obtained from thermal data, and the vibrational frequencies obtained from the preceding paper. They do not differ within the accuracy of the measurements. The intermolecular potential due to the change of the intramolecular zero-point energy is greater for CH_3OH than for CH_3OD, and so the other contributions to the intermolecular potential, viz., repulsive, dispersion, electrostatic, etc., energies, are greater by $459\pm\sim260$ joule mole^{-1} for the deuterium bond than for the hydrogen bond. This might be due mainly to a higher polarity of CH_3OD than of CH_3OH.

1. INTRODUCTION

IN this paper we shall attempt to determine whether there is any difference in the intermolecular potentials of the hydrogen bond in methanol and methanol-d_1 from the difference of the heats of vaporization at 0°K. In order to do this we must define the relation between the heats of vaporization and intermolecular potentials. It is generally accepted that the zero-point energy of the rotational and translational vibrations shall be added to the heat of vaporization at 0°K in order to obtain a quantity related to the intermolecular potential. If internal rotation occurs in the free molecules then coupling of vibrations in the crystal may inextricably mix the internal rotation and an external rotation. In this case, the intermolecular potentials must be related to the heat of vaporization plus the zero-point energy of the internal and external rotations and the translations less the zero-point energy of the internal rotation in the vapor. Similar considerations apply to the relation between heats of dissociation and intermolecular potentials in gaseous clusters of molecules.

Of course an intermolecular potential as defined above is only useful if the internal (excluding internal rotational) vibrations are clearly distinguishable from the internal rotational and external vibrations.

2. DIFFERENCE IN THE HEATS OF VAPORIZATION OF CH_3OH AND CH_3OD AT 0°K

The heat capacities from 90°K upwards, heats of transition, heats of melting, and heats of vaporization at 0°C to their saturated vapors at pressures of 30.4 (CH_3OH) and 28.3 (CH_3OD) mm Hg, have been measured by Staveley and Gupta.[1] The difference in the heats of expansion from the saturated vapor to zero pressure, assuming that CH_3OH and CH_3OD have the same virial coefficients, is negligibly small. The heat capacities of solid CH_3OH and CH_3OD rapidly approach one another at low temperatures. Thus at 110, 100, and 90°K the differences are 0.16, 0.12, and 0.08 cal deg^{-1} mole^{-1}. Hence, an extrapolation of the difference of the heat capacities to 0°K can be made without large error if we assume that no phase transitions occur between 90 and 0°K. From these data we find by graphical methods, that

$$\{H^\circ_{273.15}(g)-H^\circ_0(c)\}_{CH_3OH}-\{H^\circ_{273.15}(g)-H^\circ_0(c)\}_{CH_3OD}=-1125\pm\sim120 \text{ joule mole}^{-1}, \quad (2.1)$$

the error being the best estimate remembering that because the measurements were made in the same calorimeter, some errors will partly cancel.

The vibrational contribution to $\{H^\circ_{273.15}(g)-H^\circ_0(g)\}$, calculated from the frequencies given in the preceding paper and assuming harmonic vibrations, is 152 joule mole^{-1} for CH_3OH and 233 joule mole^{-1} for CH_3OD. The contribution of the internal rotation for CH_3OH is 1105 joule mole^{-1}.[2] For CH_3OD, assuming the same potential function and barrier to internal rotation as for CH_3OH,[3] and using Venkateswarlu and Gordy's[4] values of the moments of inertia, the contribution was calculated from Pitzer and Gwinn's[5] tables to be 1255 joule mole^{-1}. Thus we find

$$\{H^\circ_{273.15}(g)-H^\circ_0(g)\}_{CH_3OH}-\{H^\circ_{273.15}(g)-H^\circ_0(g)\}_{CH_3OD}=152-233+1105-1255 \text{ joule mole}^{-1}=-231 \text{ joule mole}^{-1} \quad (2.2)$$

† N.R.C. No. 6181.

* N.R.C. Post-doctorate Fellow 1958–60. Present address: Spectroscopy Laboratory, Massachusetts Institute of Technology, Cambridge, Massachusetts.

[1] A. K. Staveley and A. K. Gupta, Trans. Faraday Soc. **45**, 50 (1949).

[2] E. V. Ivash, J. C. M. Li, and K. S. Pitzer, J. Chem. Phys. **23**, 1814 (1956).

[3] E. V. Ivash and D. M. Dennison, J. Chem. Phys. **21**, 1804 (1953).

[4] P. Venkateswarlu and W. Gordy, J. Chem. Phys. **23**, 1200 (1955).

[5] K. S. Pitzer and W. D. Gwinn, J. Chem. Phys. **10**, 428 (1942).

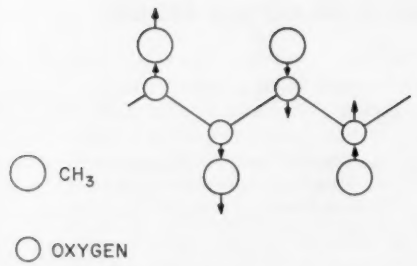

FIG. 1. A vibration of a methanol chain in which adjacent unit cells vibrate π radians out of phase.

with little error. From Eqs. (2.1) and (2.2) the difference in heats of vaporization at 0°K is

$$\{H^\circ_0(g)-H^\circ_0(c)\}_{CH_3OH}-\{H^\circ_0(g)-H^\circ_0(c)\}_{CH_3OD}$$

$$=-894\pm\sim 120 \text{ joule mole}^{-1}.$$

3. DIFFERENCE IN ENERGY OF LATTICE VIBRATIONS AND INTERNAL ROTATION

In order to know whether an intermolecular potential as defined in Sec. 1 is useful for crystalline methanol, it is necessary to inquire whether the internal vibrations of the molecules in the crystal are reasonably distinct from the external vibrations and the internal rotation. It is evident from the infrared spectra of crystalline CH_3OH, CH_3OD, CD_3OH, and CD_3OD, which are discussed in the preceding paper, that they are. The vibrations of the gaseous molecules can be correlated well with vibrations in the solid and there seems to be little perturbation by interaction with external vibrations or the internal rotation in the solid. The most likely of the vibrations of the solid to interact with internal vibrations is the OH out-of-plane bending vibration. This contains two components in each of the methanols, and for CH_3OH and CH_3OD the isotope shifts for both the high-frequency and the low-frequency component is 1.39. For CD_3OH and CD_3OD the corresponding shifts at -180°C are 1.34 and 1.38. For CH_3OH and CD_3OH the high-frequency components have frequencies at -180°C of 790 and 776 cm^{-1}, and both the low-frequency components have frequencies of 685 cm^{-1}. From this it is evident that the motions that cause these bands are almost entirely motions of the O-hydrogen atom, and so that there is no detectable coupling with internal motions.

The next problem is to determine the difference between the zero-point energies of the internal rotational plus the external vibrations for crystalline CH_3OH and CH_3OD, and the difference between the zero-point energy of the internal rotational vibration for the two gases. The frequency of the internal rotational vibration of CH_3OH is 270 cm^{-1}.[6] It has not been observed in CH_3OD, but from the value for CH_3OH and the moments of inertia for internal rotation[4] its frequency is calculated to be 213 cm^{-1}. The difference of zero-point energy is then 57 cm^{-1} or 341 joule $mole^{-1}$ assuming the vibration is harmonic, CH_3OH having the higher energy.

The rough forms of vibration of the optically active lattice vibrations are depicted in Fig. 9 of the preceding paper. The internal rotational vibration of the CH_3 group is not shown. Because the methyl group seems to play no part in the out-of-plane bending vibrations, it is expected that the O-hydrogen atom will play no part in the internal rotation of the methyl group, although it can in principle do so because there is a one-to-one correspondence between the symmetry species, relative to the full crystal symmetry, of the N(=Avogadro's number) OH out-of-plane and the N CH_3 internal rotational vibrations that occur in one mole of methanol. The frequencies appear to be far enough apart that little or no resonance occurs between them. Consequently, the frequencies of the CH_3 internal rotation in crystalline CH_3OH and CH_3OD can be taken to be the same, and so they cancel when differences in zero-point energies are required.

In Sec. 4.4 of the preceding paper arguments were advanced that indicate that the two observed OH out-of-plane bending frequencies are the extremes of the N similar frequencies that occur in one mole of methanol. Therefore, the best estimate of the zero-point energy of these vibrations is that of N vibrations each with the mean frequency of the observed vibrations. Nothing is known about the anharmonicity of the vibrations, and so they are assumed to be harmonic. Because the anharmonicities are neglected in the gas, there will be at least a partial cancellation of error, and there will be a further cancellation when the difference between CH_3OH and CH_3OD is calculated. The difference of zero-point energy associated with the OH out-of-plane modes is therefore $\frac{1}{2}Nhc\delta\nu$ with $\delta\nu=214$ cm^{-1}, or 1280 joule $mole^{-1}$, CH_3OH having the higher energy. The best estimate of the error of this is about 10% or 130 joule $mole^{-1}$.

One of the infrared-active lattice translational frequencies or an overtone is about 500 cm^{-1}, but we have no firm evidence of a difference between its values in CH_3OH and CD_3OH, so it is taken to be the same for CH_3OH and CH_3OD. It does not therefore enter into the calculations. The other observed infrared-active translational frequency extrapolated to 0°K is 350 cm^{-1} in CH_3OH and 327 cm^{-1} in CH_3OD. It is likely that the observed frequency is the maximum of a set of N frequencies. The reason for this is that in the vibration that gives rise to the observed band all unit cells move in phase, so that all O—H···O bands within a single chain are stretched by the same amount. In vibrations in which adjacent unit cells in the same chain are not in phase some at least of the O—H···O bonds are less stretched than in the optically active vibration, as can

[6] J. S. Koehler and D. M. Dennison, Phys. Rev. **57**, 1006 (1940).

be seen in Fig. 1 for one mode showing two unit cells in the same chain. Similar arguments apply to vibrations that are not in phase in two unit cells that are not in the same chain. The lowest frequency corresponding to this motion is a zero frequency that is a translation of the crystal. A Debye distribution therefore seems the most appropriate simple distribution of frequencies. Accordingly, the difference of zero-point energy due to this set of vibrations is $\frac{3}{8}Nhc\delta\nu$ with $\delta\nu = 359-327 = 32$ cm^{-1}, or $85\pm\sim 20$ joule mole^{-1}.

There are $3N$ lattice vibrations still to be accounted for. These are very likely to have low frequencies, and, since the isotope shifts are expected to be small, the difference of zero-point energies will be small. This is confirmed by the rapid decrease in the relative difference of specific heats[1] as the temperature decreases towards 80°K. It is, however, certain that the frequency, and hence the zero-point energy, of these vibrations in CH_3OH will be greater than in CH_3OD, and so an allowance should be made. We put it arbitrarily as the same as that of the translational vibrations discussed above, i.e., 85 joule mole^{-1}, with an error of ~ 40 joule mole^{-1}. The difference of the changes, when vaporization occurs, of zero-point energy due to the translational, rotational, and internal rotational vibrations is therefore $85+85+1280-341 = 1109\pm\sim 200$ joule mole^{-1}, that for CH_3OD being the greater.

The contribution of the difference of intermolecular potentials to the difference of heats of vaporization is therefore $-894+1109 = 215\pm\sim 220$ joule mole^{-1}. This is consistent with what is found for water,[7,8] where the intermolecular potential of the hydrogen bond, as defined in this paper, is greater than that of the deuterium bond by enough to contribute $610\pm\sim 300$ joule mole^{-1} to the difference of the heats of vaporization of H_2O and D_2O at 0°K. As there are two hydrogen bonds per molecule of water, the hydrogen bond in water is stronger by $305\pm\sim 150$ joule mole^{-1}.

[7] E. Whalley, Trans. Faraday Soc. **53**, 1578 (1957).
[8] E. Whalley, Trans. Faraday Soc. **54**, 1613 (1958).

4. DIFFERENCE OF INTERMOLECULAR POTENTIALS OF CH_3OH AND CH_3OD

If all the interactions between CH_3OH molecules that are not classed as hydrogen-bond interactions are the same as those in CH_3OD, then the hydrogen bond in CH_3OH has about the same strength as or is a little stronger than the deuterium bond in CH_3OD. The contribution of the change of intramolecular zero-point energy[8] on vaporization will be different for CH_3OH and CH_3OD, and this effect will now be allowed for.

The intramolecular vibrations in the crystal are coupled, and the OH stretching and bending vibrations are strongly coupled. Each of the OH vibrations gives rise to two infrared bands, and reasons were advanced in Sec. 4.4 of the preceding paper for thinking that the observed frequencies are the extreme frequencies of the coupled oscillators. Consequently, the best value for the zero-point energy of these vibrations is obtained by assuming a uniform distribution over the range between the observed frequencies. If only one band is observed in the infrared spectrum, it is assumed that the frequency distribution is sharp. Then, from the frequencies given in the preceding paper and assuming that the vibrations are harmonic, we find that the difference of the change of intramolecular zero-point energy upon vaporization is $674\pm\sim 100$ joule mole^{-1}, the error being estimated, taking account of the partial cancellation of errors. It might be noted that the change of intramolecular zero-point energy for CH_3OH is about 2 kj mole^{-1}, or about 4% of the heat of vaporization. It follows that for the remaining contributions to the intermolecular potential the difference between CH_3OH and CH_3OD is $674-215 = 459\pm\sim 260$ joule mole^{-1}, the deuterium bond being the stronger. The corresponding contributions for the hydrogen bond in water are $640\pm\sim 300$ joule mole^{-1} weaker than those for the deuterium bond in D_2O.[8] It seems rather likely, as it seemed with water, that the main reason that these contributions are stronger for the deuterium bond is a higher electrostatic moment for O—H than for O—D.

Condensation of Atomic and Molecular Hydrogen at Low Temperatures*

R. T. BRACKMANN AND WADE L. FITE

John Jay Hopkins Laboratory for Pure and Applied Science, General Atomic Division of General Dynamics Corporation, San Diego, California

(Received November 18, 1960)

With the use of reflected modulated atomic-beam techniques, the reflection of hydrogen atoms and molecules at cold surfaces has been examined. It was found that at low temperatures (~4°K) hydrogen atoms reflect as atoms with a very high probability. The reflection of hydrogen molecules is strongly dependent upon the amount of water vapor condensed on the target previously to or simultaneously with the H_2. The fact that condensation of stable gases can be affected by simultaneous condensation of water vapor at temperatures exceeding the gases' normal boiling points leads to an application in the form of an extraordinarily inexpensive way to produce vacuums in the 10^{-6} mm Hg range.

I. INTRODUCTION

FOLLOWING observation of the green glow emitted by the low-temperature condensate of nitrogen gas which had passed through an electric discharge and spectroscopic studies indicating that this light arose from nitrogen atoms trapped in the condensate,[1] free-radical stabilization became a very active field of research. Of particular practical interest was the possibility that free radicals, stabilized at liquid helium temperatures, could be used as ultra-energy propellants for rockets, if sufficiently high concentrations of free radicals could be achieved.

Perhaps the most interesting of the free radicals for application to rocket propulsion is the free hydrogen atom. Although the dissociation energy of molecular hydrogen is only moderate (~100 kcal/mole), the light mass of the hydrogen atom accords it a unique position among free radicals for the production of high specific impulse. Further, the work of Jen, Foner, Cochran, and Bowers[2] on electron spin resonance established in 1956, that when partially dissociated hydrogen gas is condensed on a liquid-helium-cooled surface, the condensate contains free hydrogen atoms in small quantities.

Following that discovery, it became desirable to find methods by which concentrations of atoms in the condensate could be increased to values of practical interest, and a number of laboratories undertook studies aimed at learning how large concentrations of atoms could be stabilized. In the early experimental studies at General Atomic, attempts to form atomic hydrogen solids centered about the condensation at liquid-helium temperatures of beams containing hydrogen atoms; detection was made by warming the surface and observing energy releases associated with reassociation of atoms into molecules, using low-temperature calorimetric techniques. Experimentation with various degrees of dissociation (in beams of H and H_2), various incident-beam temperatures, various mixtures of gases, and with spin-aligned atoms failed to yield energy releases ascribable to stabilized hydrogen atoms. From these experiments, which have been discussed elsewhere,[3] it was concluded that the probability that a hydrogen atom condenses and stabilizes at a liquid-helium-cooled surface is less than 10^{-3} for all conditions used in these experiments.

Experiments of this kind, in which one seeks to determine the probability that an atom in the gas phase will become an atom in the solid phase, may be envisaged as comprising two processes, so that the actual probability is the product of two other probabilities. The first is the probability that an atom in the gas phase will condense at the surface, irrespective of the atom's subsequent history. The second is the probability that condensed atoms will not reassociate with other atoms to form molecules but will remain for long times in the condensate as free atoms. Finding a very small value for the product of these two probabilities leads one naturally to question their relative magnitudes; that is, to question whether the difficulty in freezing atoms is in condensing the atoms or in keeping them separated after condensation.

Among the most pertinent information on the condensation process alone is that which comes from a study of the reflection of atomic beams by cold surfaces. The present paper summarizes a series of experiments of this kind which were performed on the General Atomic modulated beam apparatus, GAMBA I.

II. EXPERIMENTAL APPROACH

In order to study the reflection of normally gaseous particles by a cold surface, the basic technique was to direct a beam in high vacuum at the surface and to use mass spectrometric detection of the particles reflecting from the surface. While such an experiment is extremely simple in concept, the experimental implementation of this approach is beset with a basic signal-to-noise difficulty. The problem is to discern the beam above the background gas even in a good high vacuum.

* This research was supported by the United States Air Force through the Air Force Office of Scientific Research of the Air Research and Development Command.

[1] H. P. Broida and J. R. Pellam, Phys. Rev. **95**, 845 (1954).

[2] C. K. Jen, S. N. Foner, E. L. Cochran, and J. A. Bowers, Phys. Rev. **104**, 856 (1956); **112**, 1169 (1958).

[3] R. T. Brackmann and W. L. Fite, Fourth Symposium on Free Radical Stabilization, Washington, D. C., 1959.

Mass spectrometric detection of neutral particles requires, first, the ionization of the particles, which is usually done by electron-impact ionization. In this process, the ion currents are proportional to the number density (particles per unit volume) of the neutral particles to be detected. In typical atomic and molecular beam experiments the number density of particles in the beam is of the order of 10^9 particles/cm^3, which is adequate to provide amply large signals from electron-impact ionization; the difficulty arises from the fact that this density corresponds to a vacuum of about 2.5×10^{-8} mm Hg. The usual laboratory vacuum system simply will not provide vacuums at pressures in this range and below when gas is being purposely admitted, as is the case in gaseous molecular beam experiments. It would appear that in any normal dc experiment, the presence of the beam would be difficult to detect above the presence of the background gas in the vacuum.

While in principle the pressure of the background gas should be sufficiently stable that its contributions to the mass spectrometer signal could be subtracted, in practice the irregular pumping of diffusion pumps and other effects give rise to quite serious pressure drifts and low-frequency fluctuations which make subtractive procedures quite unattractive.

However, one may take advantage of the fact that each vacuum system has a characteristic pressure-time constant, given by the vacuum chamber volume divided by the speed of its vacuum pumps, and fluctuations are integrated in a manner analogous to the integration provided by an electrical *RC* circuit. Thus, the mean amplitude of pressure fluctuations decays with increasing frequency, and when one uses a pressure-time constant of the order of one second, the amplitudes of pressure fluctuations in the audio-frequency range are quite small.

These considerations indicate that great advantages accrue in conducting an ac or modulated-beam experiment for the study of reflection of particles from surfaces. If the neutral beam is mechanically interrupted at an audio-frequency and the ionizing electron beam is dc, then the presence of the neutral beam may be readily discerned above the background gas. Signals associated with the neutral beam occur at the modulation frequency and in a definite phase, while signals arising from ionization of the background gas are dc. Thus, the two signals may be separated by nothing more complicated than a condenser. Of course, the dc signal contains some noise, principally the unexcludable shot noise associated with the dc ion current, but the pressure integration by the vacuum system itself removes the very serious pressure fluctuation effects.

Figure 1 is a schematic representation of the experiments which used modulated atomic-beam techniques for the study of reflection of particles by cold surfaces. The source of hydrogen atoms and molecules was a radio-frequency electrodeless discharge located in the first of two differentially pumped vacuum chambers. The beam, after leaving a small aperture on the axis of the source tube, passed to the wall separating the two chambers where it was collimated by a slit located in this wall. After entering the second chamber, the neutral beam was interrupted at a frequency of 100 cps by a rotating chopper wheel. The modulated beam next traversed a pair of ion sweep plates between which an electrostatic field was established and whose purpose was to remove all ions and electrons accompanying the neutral particles in the beam. The beam then struck the cold surface from which it was diffusely reflected. The reflected particles were detected by a small magnetic-sector mass spectrometer located inside the vacuum chamber.

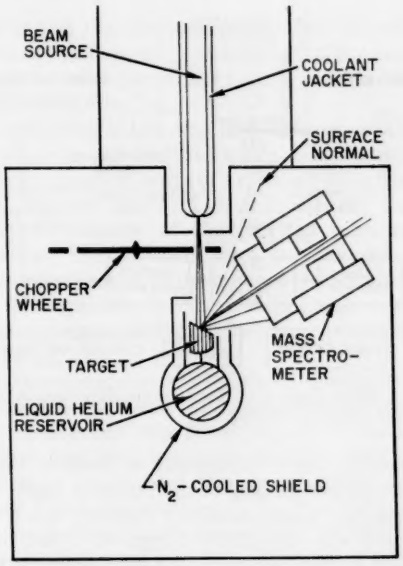

FIG. 1. Diagram of general experimental arrangement.

Figure 2 is a schematic representation showing the circuitry of the experiment. The voltage signal arising from the ions at the mass spectrometer collector, generated by passing the ion current through a 10^{10}-ohm resistor, was the input to a plate-follower preamplifier (also in the vacuum chamber). The preamplifier had the dual task of blocking the dc ion signal while passing the ac ion signal and of changing the impedance of the voltage signal to a sufficiently low value that it could be taken outside the vacuum system without excessive losses due to distributed capacity. The ac ion signals were then amplified in a narrow-band tuned amplifier, the output of which was fed into a phase-sensitive detector. The reference signal for the phase-sensitive detector was derived from a light and photocell device which monitors the passing of each tooth of the chopper wheel. The reference signal was electronically phased before entering the phase-sensi-

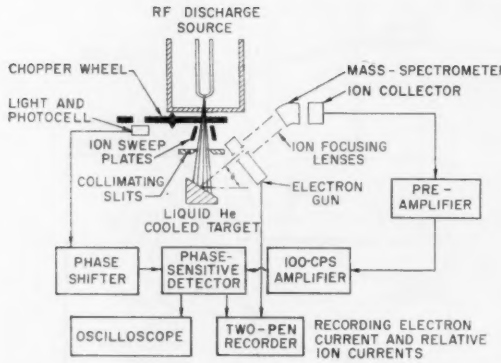

FIG. 2. Block diagram of electronic circuitry used in reflected modulated-beam experiments.

tive detector, and a cathode-ray oscilloscope was used to verify proper phasing of the reference signal. After detection, the phase-sensitively detected and rectified ion signal was electrically integrated before it was displayed by one pen of a two-pen recording potentiometer. The second pen recorded the current of the mass-spectrometer electron gun.

Atom Beam Source

The source of atoms in the present experiments was a radio-frequency electrodeless discharge operating at a frequency of 13 Mc. The discharge tube, a Pyrex tube of about 6 mm o.d., was enclosed by a cooling jacket having an o.d. of about 1 in. In the majority of the experiments described here a rather low-temperature beam was desired, and the coolant was normally liquid nitrogen. Some experiments were conducted using CCl_4 as a coolant when room-temperature beams were desired. The fact that the discharge tube was excited through capacitive coupling, where the electrodes were attached to the outside of the cooling jacket, limited the choice of coolants to liquids of high dielectric constant. An axial aperture of 0.025 in. diam (at the end of the discharge tube) served as the neutral-beam source. The coupling jacket terminated just before the aperture end of the discharge tube. The entire discharge tube and its cooling jacket were located within the first vacuum chamber where the pressure was normally of the order of 1×10^{-5} mm Hg.

The discharge tube normally operated at pressures in the range from 0.1–1 mm Hg at radio-frequency power levels of the order of 10 w. Under normal operating conditions with the liquid-nitrogen-cooled source, by varying the rf power and the discharge pressure, beams could be readily produced which ranged up to 80% dissociated, and for short running times even higher dissociation could be achieved. This was readily shown experimentally by removing the cold surface indicated in Fig. 1 and positioning the mass spectrometer so that it would sample the beam incident into the second vacuum chamber. Since the electron-impact ionization cross sections for both atomic and molecular hydrogen are known,[4] a comparison of the mass 1 and 2 peaks in the mass spectrometer immediately yielded the degree of dissociation at any time.

Targets

The targets against which the atom beam was directed were solid cylinders of copper. The target end of the cylinder was bevelled so that the surface normal was about 30° off the cylinder axis. A copper rod, of diam ~1 mm and length ~2 cm, provided both thermal and mechanical connection between the perpendicular end of the target and a liquid-helium reservoir, as is shown in Fig. 1. A liquid-helium-cooled radiation shield enclosed the target except at its bevelled end, and a liquid-nitrogen-cooled shield protected the liquid-helium-cooled shield.

Embedded into the copper of the target were carbon composition resistors, which were sealed into the body of the copper using Formvar enamel, thus providing good thermal connection and electrical insulation; these resistors were used as thermometers for the target in the manner described by Clement and Quinnell.[5] Two resistors were normally used, one for measuring in the neighborhood of 20°K and the other near 4°K. Heating coils were wrapped around the body of the target cylinders. By use of these coils and the rather poor thermal short between the target and the helium reservoir, the target temperature could be increased up to about 100°K without excessive loss of helium.

The helium reservoir itself, as well as its liquid-nitrogen-cooled shield (see Fig. 1), were lowered into the path of the atomic beam through the top of the beam apparatus.

Mass Spectrometer Detector

The mass spectrometer used in these experiments was a small magnetic-sector instrument of 35° deflection. A neutral beam approaching this instrument was first collimated by an aperture in the repeller of the spectrometer and then crossed at right angles by the ionizing electron beam. There was no further collimation or slitting of the ion beam after ionization; the exit side of the ionizer was left open and the acceleration lenses were of quite large diameter (1 in.). This was done to ensure that particles from the beam would not be trapped inside the ionizer, but would have only a single pass through the electron beam. Were trapping to occur, recombination of atoms could occur at the walls of the ionizer, in which case the ions would not be representative of the neutral gas beam entering the ionizer. Further, having an ionizer exit slit was not re-

[4] W. L. Fite and R. T. Brackmann, Phys. Rev. **112**, 1141 (1958).
[5] J. R. Clement and E. H. Quinnell, Rev. Sci. Instr. **23**, 213 (1952).

quired for adequate resolution, since the ac ion signal could arise only from ionization of the neutral gas beam which was already suitably collimated before it was ionized.

The mass spectrometer used in these experiments had another unusual feature. Rather than using the normal magnetic-sector focusing condition, which takes a real point object and focuses it into a real line image, the real "point" image was first electrostatically focused to a virtual "point" image behind the magnet, and the magnet then completed the focusing to the real detector slit. This permits the ionizer and the detector slit to be much closer to the magnet than in the normal focusing condition and thus reduces the mass spectrometer to a compact size that permits readily mounting the entire unit on a rotating table within the vacuum system. Although using this "post-focusing" ion optical system greatly reduces the dispersion of the spectrometer, when working with low masses both resolution and dispersion are more than adequate. In addition, the ion collection efficiency is greatly improved with post-focusing, since the ion beam is actually converging when it enters the magnet. Ion losses are thus substantially reduced.

Origin of Mass Spectrometer Signals

In using a mass spectrometer to detect particles in a gas beam which has but a single pass through the ionizing electron beam, it is important to note that the signals are proportional to the *number density* n of the gas species detected. Since the current density J of neutral particles in the beam is related to the number density by $J=n\bar{v}$, where $\bar{v}$ is the mean speed of the neutral beam particles, the mass-spectrometer signal S, is proportional to $J/\bar{v}$. When the neutral beam has a Maxwellian velocity distribution $\bar{v}=(8kT/\pi m)^{\frac{1}{2}}$, and the mass-spectrometer signal is given by

$$S \propto JT^{-\frac{1}{2}}, \tag{1}$$

where T is the absolute temperature, k is Boltzmann's constant, and m is the mass of the neutral particles.

This dependence of a mass-spectrometer signal upon both J and $\bar{v}$ (or T) leads to some equivocation in interpretation of results of reflected-beam experiments where mass-spectrometric detection alone is used. For example, as a target temperature is varied using a constant incident beam, $\bar{v}$ will be changed by thermal accommodation effects and J will vary when condensation can occur. The concern that J might also vary when a fixed mass-spectrometer detection angle is used, due to variation of the angular distribution of the reflected particles, was in the present experiments shown to be of no consequence from actual measurements of the reflected angular distributions under a wide range of conditions. In all cases the angular distribution maps for both reflected atoms and molecules were independent of the beam and target conditions and closely approximated the distribution expected for reflection by a rough surface, i.e., proportional to the cosine of the angle between the surface normal and the direction of observation.

In considering the mass-spectrometer signals associated with reflected neutral beams, it is convenient to express the signals in terms of a reflected-beam temperature T_r, so that $S \propto JT_r^{-\frac{1}{2}}$. Were it assured that the velocity distribution of the reflected particles was Maxwellian, then T_r would be a true temperature in the theoretical sense; in the absence of such assurance, using this expression for the mass-spectrometer signal defines a thermometer and, hence, a practical temperature.

The convenience of relating signal to reflected temperature T_r is that a thermal accommodation coefficient may be introduced, thus permitting some inferences to be drawn regarding limits of reflection probabilities. Introducing the reflected temperature in terms of the incident beam temperature T_i (a true temperature, since the incident beam comes from an equilibrated source) and the usual definition of thermal accommodation coefficient α, the mass-spectrometer signal is given by

$$S \propto JT_r^{-\frac{1}{2}}=J[T_i+\alpha(T_s-T_i)]^{-\frac{1}{2}}, \tag{2}$$

where T_s is the temperature of the surface.

In the present experiments, where T_i was generally kept constant at about 80°K and T_s was varied, it was convenient to obtain a reflected-beam reference signal S_0 which was that detected when the surface temperature was the same as that of the incident beam. Under these conditions thermal accommodation effects were nonexistent. Then for temperatures $T_s \neq T_i$,

$$[S(T_s)/S_0]=\{\beta(T_s)/[1-\alpha(1-T_s/T_i)]^{\frac{1}{2}}\}, \tag{3}$$

where $\beta(T_s)=J(T_s)/J_0$, and J_0 is the reflected current density when $T_s=T_i$.

Since the angular distribution of reflected particles was found to be independent of the experimental variables, $\beta(T_s)$ may also be equated to $P(T_s)/P_0$, where $P(T_s)$ is the probability that a particle will be reflected at the surface and $P_0=P(T_i)$.

Although in the case of chemically stable gases one can select T_i sufficiently high that no condensation can occur, so that P_0 may be taken as unity, in the case of hydrogen atoms P_0 always has a smaller value. For in addition to losses of reflected atoms by condensation, reassociation of atoms into molecules at the surface provides a sink for atoms. Additional experiments have shown that the reflection probability P_0 of hydrogen atoms from a liquid-nitrogen-cooled source impinging upon a liquid-nitrogen-cooled copper surface is only about 0.78, the atom loss being accounted for by recombination at the surface into molecules. These measurements were made by comparison of the dissociation fraction of the incident and reflected beams, using mass-spectrometric detection and the known ionization

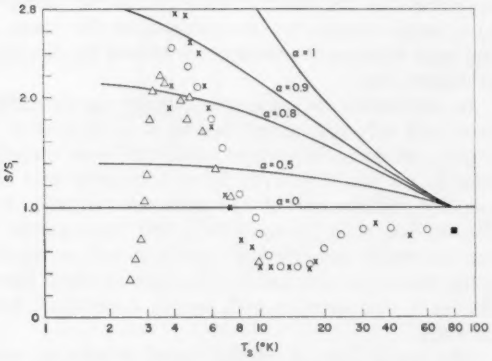

FIG. 3. Reflected hydrogen atom signals for a liquid-nitrogen-cooled incident beam as a function of surface temperature. The different symbols represent data from different runs and indicate the reproducibility of the data. For comparison, curves appropriate to the assumption of complete reflection with various thermal accommodation coefficients (α) are shown.

cross sections of hydrogen atoms and molecules.[4] Using this value for P_0, substitution in Eq. (3) yields

$$[S(T_s)/S_1]=[S(T_s)/1.28S_0]$$
$$=\{P(T_s)/[1-\alpha(1-T_s/T_i)]^{\frac{1}{2}}\}, \quad (4)$$

where $S_1(=S_0/P_0)$ is the mass-spectrometer signal which would be expected if the reflection probability of atoms at $T_s=T_i$ were unity. Equation (4), indicating the dependence of the mass-spectrometer signal on both the thermal accommodation coefficient and the reflection probability, is that with which it is most instructive to compare data.

III. RESULTS. ATOMIC HYDROGEN

Figure 3 shows experimental points for the quantity S/S_1 taken from three runs and several theoretical curves for this quantity assuming $P=1$ and calculated for various values of α. While the scatter of the points is considerable, it may be noted that a rather smooth curve could be drawn through the set of points for any given run, and that curves so drawn would display very similar behavior. At the higher temperatures, where it might be expected that P would be rather temperature-insensitive, the slowly changing values of the mass-spectrometer signal suggest rather low values of α. As the temperature is reduced to about 30°K, a loss of atoms begins to occur and this loss continues to increase until a temperature of about 12°K is reached. At that temperature, the reflected-atom signal increases with decreasing temperature, with a very large maximum atom-current signal being found at about 4°K. At lower temperatures, the reflected-atom signal falls rapidly to very low values.

Similar data using atomic deuterium exhibits the same general features except that the maximum is shifted to a temperature of about 6.5°K.

There is no question that the dip in this curve in the neighborhood of 15°K occurs because of increased surface recombination of the atoms, for accompanying this dip in reflected-atom signal was always an enhancement in H_2 signal. While it is difficult, for reasons to be discussed later in this paper, to make a perfect correlation, it appears that the large majority of the atoms lost appear as molecules in the gas phase for surface temperatures near 15°K.

The most interesting feature of the data shown in Fig. 3 is the peak near 4°K. It clearly indicates a high probability of reflection of atoms by the surface at this temperature, and perhaps helps to explain the failure of those experiments which seek to condense large concentrations of atomic hydrogen. Irrespective of the problems of stabilizing condensed hydrogen atoms, the problem of condensing hydrogen atoms in the first place is evidently rather severe. And it appears that the worst temperature for attempted condensation and stabilization of hydrogen atoms is precisely that temperature at which most experiments have been conducted, namely at the boiling point of helium.

Some semi-quantitative arguments about the maximum atom reflection probability in the neighborhood of 4°K can be made. Referring to Fig. 3, it is seen that the values for S/S_1 range between 1.9 and 2.8 at 4°K. If we assume a value of 2.4 as the "best value" for S/S_1 at this temperature, then Eq. (4) may be used to find pairs of parameters P and α, some of which are shown in Table I.

Table I presents two limits. First, since the thermal accommodation coefficient cannot exceed one, it appears that the probability of reflection of 80°K hydrogen atoms at a 4°K surface cannot be less than about 50%, and second, since the reflection probability cannot exceed one, it seems that the thermal accommodation coefficient cannot be very much less than 0.9. These same general conclusions hold even if the value of S/S_1 at 4°K is taken to be 2.2, the lowest maximum value shown in Fig. 3. This table also indicates the sharp increase of reflection probability which is associated with very small deviations from perfect thermal accommodation. It seems likely that perfect thermal accommodation does not occur and that the reflection probability is considerably more than the lower limit of about 50%.

In speculating about the reason for the structure of the curve which would be drawn through the experimental points of Fig. 3, it is pertinent to note that in a 10^{-6} mm Hg vacuum the actual surface seen by the atoms changes with temperature. At temperatures near

TABLE I. Values of thermal accommodation coefficient α and reflection probability P at 4°K, assuming $S/S_1=2.4$.

α	1	0.98	0.95	0.90	0.87
P	0.54	0.64	0.75	0.91	1

77°K, condensing water vapor in the vacuum would produce a surface of ice rather than copper and as the surface temperature is lowered the principal surface material would become frozen air. Thermodynamical considerations suggest that this would occur at about 25°K. The fact that a decrease in atom reflection is observed beginning at this temperature suggests that frozen air might be a good catalytic surface for recombination of hydrogen atoms. As the temperature is reduced yet further, molecular hydrogen in the background gas and in the partially dissociated incident beam would freeze out, giving a surface of frozen hydrogen. The fact that high atom reflection is observed at temperatures where a frozen molecular hydrogen surface can exist would suggest that the reflection probability of H by frozen H_2 is unexpectedly high.

While this explanation has considerable qualitative appeal, it encounters a quantitative difficulty. Although frozen H_2 surfaces can exist in the neighborhood of 4°K, the enhancement of atom reflection apparently extends up to almost 10°K; extrapolation of hydrogen vapor pressure data[5] down into the liquid-helium temperature range indicates that under the conditions of these experiments the sublimation rate of H_2 exceeds the rate of arrival of gaseous H_2 at the surface at temperatures above about 5°K. A stable frozen H_2 surface could presumably not exist at the higher temperatures covered by the peak in the data shown in Fig. 3. Another explanation of the enhanced atom reflection has to be evoked, unless some unknown mechanism for binding molecular hydrogen at the surface at unusually high temperature were operative.

The latter possibility provided incentive for experimentation on the reflection of hydrogen molecules and other chemically stable gases by cold surfaces.

IV. RESULTS. MOLECULAR HYDROGEN AND OTHER GASES

In studying the reflection of H_2 and other chemically stable gases by cold surfaces, the experimental procedure was exactly that previously described. The only experimental difference was that radio-frequency power was not applied to the gas-discharge neutral-beam source. The data taken was, again, S/S_1 as given in Eq. (4). In the case of the chemically stable gases, however, a simplification in interpretation of the experiments arises, for the only loss mechanism of reflected particles is condensation at the surface (whereas with H, recombination is also a loss mechanism). Also, since it may be assumed that no condensation of 80°K H_2 molecules can occur at a liquid-nitrogen-cooled surface $P_0=1, \beta(T_s)=P(T_s)$ and S_1 of Eq. (4) may be equated to S_0 of Eq. (3). As to interpreting the mass spectrometer signal loss as indicating condensation, it is pertinent to remark that because beams modulated at 100 cps were used in these experiments, reflected molecules could be observed only if their residence time at the surface were short compared to the period of the modulation. Molecules remaining at the surface for times appreciably longer than a few milliseconds before re-evaporating could not be detected by the ac mass spectrometer because their phase sense was lost.

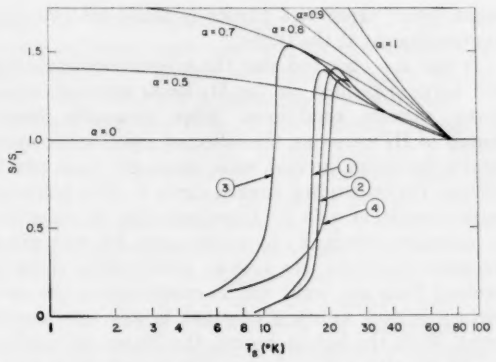

FIG. 4. Reflected hydrogen molecule signals for a liquid-nitrogen-cooled incident H_2 beam as a function of surface temperature. Curves 1 and 2 are representative of data taken under usual vacuum conditions; i.e., where the frozen gas on the surface is the residual gas in the vacuum. Curve 3 was obtained when a dc beam or dry nitrogen was directed at the surface simultaneously with the modulated H_2 beam. Curve 4 is representative of data taken when water vapor was condensed at the target surface during the measurement of the reflected H_2.

Molecular Hydrogen

Figure 4 shows four representative experimental curves of S/S_1 taken under different experimental conditions. All the curves show a rise of signal as the surface temperature is reduced from 77°K, with a clear indication that the thermal accommodation coefficient increases from something less than 0.5 to about 0.7 around 25°K. Then, as the temperature is further decreased, all curves show a rather sudden drop of signal, followed by a more gradual decrease as the temperature moves into the liquid-helium range.

The first interesting point about the curves in Fig. 4 is that the temperature at which the sudden drop occurs is strongly dependent upon the nature of the background gas in the vacuum chamber, indicating that the nature of the frozen gas surface on the target and/or the gas striking on the target simultaneously with the beam is the principal determinant for this behavior. Curves 1 and 2 are representative of the large majority of data taken with the beam machine operating at its normal pressures (from 3×10^{-7} to 2×10^{-6} mm Hg), and where the principal background gases were H_2, H_2O, N_2, and O_2 in relative amounts, determined mass spectrometrically, of about 3, 1, 3.5, and 1, respectively. Curve 3 is representative of data taken when dry air or argon, either admitted to the background gas or directed onto the target from a dc beam source, was the principal gas striking the target concurrently with the H_2 beam. A shift of the curve to the higher temperatures, as indicated by curve 4, occurred

when water vapor was purposely made the principal condensing gas at the target.

It was also observed that the reflected-molecule signal curve depended on the H_2 beam strength under given vacuum conditions. When unusually heavy beams of H_2 were run, the reflected signal curve more nearly resembled curve 3, while unusually weak beams yielded curves tending toward curve 4. This behavior seems consistent with the hypothesis that H_2 reflection is controlled principally by water vapor, for, with given vacuum conditions, the rate at which water vapor is evolved from the walls and is condensed at the cold surface is very nearly a constant in any one experiment. With the lighter beams, the frozen-gas surface would contain a relatively large fraction of water, while the use of heavier beams would reduce the role played by water vapor to a relatively less important position.

The second remarkable feature of the curves shown in Fig. 4 is the high temperatures at which the sudden drops occur. Only in curve 3 does the drop in signal begin at a temperature appreciably less than the boiling point of hydrogen, and curve 4 indicates considerable loss of molecules at the hydrogen boiling point. The most obvious difference of experimental conditions corresponding to the various curves is the nature of the frozen gas at the surface, with a surface consisting in large part of water ice being particularly capable of condensing the H_2, and with dry-gas surfaces showing the least tendency toward condensing H_2 at unusually high temperatures.

To investigate the possibility that appreciable thermal gradients were present across the layers of frozen gases on the target surface, and that water's principal role was to alter the temperature of the outermost layer of the frozen-gas surface, experiments were performed in which water vapor and hydrogen were leaked into the background alternately several times. Examination of the temperature at which attenuation of the reflected signal took place showed that this temperature depended only on the gas which had last been added to the background and was not noticeably affected by accumulation of previously condensed layers of gas.

After ruling out thermal gradient effects as a principal cause of the observed gas-reflection characteristics of frozen-gas surfaces, it seems appropriate to suggest that the experimental results indicate either a true adsorption of H_2 to frozen-water surfaces or a trapping of H_2 by simultaneously condensing water vapor, or perhaps both.

In view of the inability in these experiments to completely exclude water vapor from the residual gas in the vacuum chamber (and therefore water vapor being one of the condensed gases), and in view of water vapor's large influence on the condensation of H_2, we feel that these experiments yield no reliable information on the condensation of dry molecular hydrogen onto a dry frozen-H_2 surface.

However, with respect to the possibility of molecular hydrogen trapped on the surface at 10°K being responsible for the enhanced atom reflection observed beginning at this temperature, the experiments on molecule reflection suggest an affirmation.

Other Gases

The observed loss of reflected-molecule signal at unusually high temperatures and associated with condensed and condensing water vapor at the target, naturally raises the question whether hydrogen is unique in its being trapped by water. To answer this question, some additional experiments were performed using other stable gases, particularly helium, oxygen, and water vapor itself, in the modulated beam. In all cases it was found that the shape of the reflected beam signal was similar to that given in Fig. 4. The temperatures at which the sudden drop in the curve commenced, as the temperature was lowered, varied of course with the gas under study and with the amount of water vapor and other gases either previously condensed or simultaneously condensing on the surface. In the case of helium, this temperature ranged from 7°K to as high as 14°K, and for oxygen this temperature was in the 60°–90°K range. As in the case of hydrogen, the higher temperatures for condensation onset could be associated with the presence of water vapor. Water vapor was observed to reflect from a copper target down to temperatures of about 150°K, with an unusually abrupt drop of reflected signal below this temperature.

It was also of interest to examine the effect of water vapor on the reflection of atomic hydrogen. It was found that, as with the chemically stable gases, the reflected-beam signal was strongly dependent on water vapor condensing and condensed on the target. In a typical experiment, with an incident beam of approximately equal amounts of atomic and molecular hydrogen directed against targets at temperatures between 4° and 10°K, the simultaneous condensation of water vapor greatly reduced both the H and H_2 reflected signals below the values found when no water was admitted. When a freshly condensed water surface was laid down prior to the admission of the beam but water was not simultaneously condensing, the atomic hydrogen signal was diminished but the loss of atoms was accompanied by an increase of the molecular signal, presumably due to reassociation of the adsorbed H and evaporation. This situation was only a transient effect however, for after a minute or so (depending on the incident beam strength), the reflected-molecule signal diminished and the atom signal increased to steady state values.

This type of experiment suggests that adsorption to an already deposited layer of ice was responsible for at least part of the attenuation of the reflected-gas beam, but also permits the inclusion of a mechanism wherein the condensing water vapor traps gas molecules which

arrive at the surface simultaneously with the water vapor.

V. ICE PUMPING[6]

In the reflected modulated beam experiments, it was clear that water vapor is capable of trapping gases at their boiling points and above, and that among these gases is air itself. However, recognizing that a loss of reflected beam signal indicated only that the gas was being held at the surface for mean times long compared with the period of the modulation, it was natural to raise the question of the duration of the entrapment. Clearly, if the entrapment persisted for mean times of the order of minutes, water condensation could provide the basis for a uniquely simple and inexpensive vacuum pump.

Since the atomic-beam machine used in these experiments is not a variable-frequency instrument, the most straightforward approach to determine the entrapment time was not to use the beam at all, but to try to use water condensation to produce the vacuum in the beam machine.

To this end a series of experiments of the following type were run. With the diffusion pumps isolated, the 300-liter main vacuum chamber of the atomic beam machine was first roughed down to pressures in the range from 100–1000 μ mercury. One of the liquid-nitrogen cold traps which insert into the main chamber and which have a cold surface area of about 1200 cm^2 was then filled. After the very small pressure drop associated with trapping of the condensible gases in the air in the chamber occurred, a burst of water vapor was purposely admitted to the chamber from an external reservoir of liquid water. It was always observed that, with the admission of the water vapor, the pressure underwent a sudden drop and the resulting pressure would hold for periods of the order of an hour with only a slight upward drift.

Experiments of this type, in which the original pressure of the air in the chamber was varied and different amounts of water vapor added, revealed (1) the best vacuum which can be produced and held for long times is about 2×10^{-5} mm Hg, as measured on both thermionic and Philips ionization gauges, (2) the principal pumping action appears to be simultaneous condensation of the water and the air at the surface, and (3) during the condensation phase it requires about 50 condensing water molecules to trap one nitrogen or oxygen molecule. Helium and hydrogen gases are, of course, not pumped at liquid-nitrogen temperature.

This last figure is of concern in considering the pumping speed of an "ice pump" of this type. For a fixed rate of water condensation, the pumping speed as usually defined (in terms of volume per unit time) increases with decreasing pressure. As an index of the pumping speed one can consider effusive flow of water at a pressure of 10^{-5} mm Hg pumping air at a pressure of 10^{-4} mm Hg. In this case, the pumping speed is estimated to be about 15 liters/sec per square foot of cold surface. The experiments qualitatively confirmed this figure. While this is quite low compared to a diffusion pump of comparable throat area, it appears likely that the use of directed jets of water vapor and folded surfaces can give ice pumping speeds quite comparable to those of diffusion pumps of comparable size.

An additional demonstration of ice pumping of particular interest dispenses with the mechanical vacuum pump to provide the forepressure and uses (1) an aspirator at a sink, (2) short rubber hose and hose clamp, (3) a commercial, inexpensive-glass liquid-nitrogen trap, (4) a side thimble of 2 or 3 cc of water, and (5) a small chamber to be evacuated. While the measured pressure produced by the aspirator is poor, the 20 mm Hg or so of gas left in the vacuum chamber is almost entirely water. This being the case, when the aspirator is isolated from the remainder of the system and when the liquid-nitrogen trap is cooled, this residual water vapor joins with that from the side thimble to pump the air remaining in the system, dropping the pressure, again, to the value of about 2×10^{-5} mm Hg.

This demonstration is not entirely reliable, unfortunately. A noticeable diurnal effect has been apparent which is presumed to indicate a variation in the amount of air dissolved in the San Diego city water used in the aspirator. However, it represents probably the world's least expensive method of producing a vacuum, for the total cost of the equipment is something less than ten dollars.

Experiments with other vapors than water in ice-pumping experiments have revealed nothing as effective as water, and we cannot offer at present a satisfactory theory as to the manner in which water vapor influences the condensation of gases at cold surfaces.

[6] Patent pending. General Dynamics Corporation, General Atomic Division, San Diego, California.

Second-Order Effects in Low-Field NMR for Ammonium Ion Solutions

ROBERT J. S. BROWN AND DON D. THOMPSON

California Research Corporation, La Habra, California

(Received November 18, 1960)

Low-field free-precession signals from aqueous ammonium nitrate solutions show a complex beat pattern containing the 52.55 cps first-order spin-spin splitting observed at high fields and also a 1.35 cps second-order splitting when the proton precession frequency is 2137 cps. The T_1 is slightly longer for the ammonium hydrogen than for the water hydrogen; T_2 is shorter than T_1 for the ammonium hydrogen and is shorter for the outer lines than for the central line.

INTRODUCTION

PROTON free-precession signals at low fields can exhibit beat patterns due to spin-spin interaction between the protons and nuclei of other species. Such beats, corresponding to known first-order splitting of NMR lines, were previously observed at low fields in fluorobenzene.[1]

Several authors[2] have published comprehensive theories containing calculations to describe in detail the NMR spectra of compounds, the calculations including second- and higher-order perturbation corrections to the transition energies. The general theory was first presented by Anderson[3] and extended by others.[4] If a molecule contains two groups of like nuclei that are nonequivalent because of chemical shifts, the observed second-order frequency shift is of the order $J_{AB}^2/(\nu_A-\nu_B)$, where J_{AB} is the spin-spin coupling constant and ν_A and ν_B are the two precission frequencies. For like nuclei (such as protons), this observed correction is significant at fields where NMR work is usually done, i.e., 2 to 14 kgauss. At low fields, however, this effect becomes unobservable, because ν_A and ν_B approach the same value. For different nuclei, whose magnetogyric ratios are widely different, the second-order terms may be quite significant, but only at low fields. In general, signals from different nuclei are so widely separated in the NMR spectrum that perturbation treatment of the spin-spin splitting is very accurate. Anderson presented a perturbation theory for nonequivalent nuclei for which the coupling between any two sets of nuclei is the same.

Consider a molecule containing two sets of nuclei, A and B, containing n_A and n_B nuclei, respectively. The Hamiltonian may be written

$$\mathcal{H}=\mathcal{H}^{(0)}+\mathcal{H}^{(1)} \tag{1}$$

$$\mathcal{H}^{(0)}=\nu_A F_z(A)+\nu_B F_z(B) \tag{2}$$

$$\mathcal{H}^{(1)}=J_{AB}\mathbf{F}(A)\cdot\mathbf{F}(B), \tag{3}$$

where $\mathbf{F}(A)$ or $\mathbf{F}(B)$ is the total spin in each set. The calculation which gives the first-order spectra is very simple. The higher-order corrections are explicitly given by Anderson. Each set of nuclei is labeled by quantum numbers F_A and m_A, where $F_A(F_A+1)$ is the eigenvalue of $F(A)^2$ and m_A the eigenvalue of $F_z(A)$. The B nuclei are labeled similarly.

The application of this treatment to first order yields an energy in frequency units,

$$\mathcal{E}(F_A, m_A; F_B, m_B)=\nu_A m_A+\nu_B m_B+J_{AB}m_A m_B, \tag{4}$$

and to second order, the additional energy

$$\mathcal{E}^{(2)}(F_A, m_A; F_B, m_B)=(\tfrac{1}{2})[J_{AB}^2/(\nu_A-\nu_B)]\{m_A[F_B(F_B+1)-m_B^2]-m_B[F_A(F_A+1)-m_A^2]\}. \tag{5}$$

The general third-order result also was given by Anderson and will not be given here. It suffices to say that it is of the order

$$(\tfrac{1}{2})\,J_{AB}^3/(\nu_A-\nu_B)^2. \tag{6}$$

Application to Ammonium Ion Solution

These energy levels for nonexchanging ammonium ions are shown in Fig. 1. The frequency associated with transitions between states $(F_A, m_A-1; F_B, m_B)$ and $(F_A, m_A; F_B, m_B)$ is

$$\nu=\nu_A+J_{AB}m_B+(\tfrac{1}{2})\delta' F_B(F_B+1)-m_B(m_B+1)+2m_A m_B, \tag{7}$$

where $\delta'=J_{AB}^2/(\nu_A-\nu_B)$, with J given in frequency units. The selection rules are $\Delta m_A=\pm 1$, $\Delta m_B=0$. The relative transition intensity is, to the same order,

$$(F_A-m_A+1)(F_A+m_A)[1-2J_{AB}m_B/(\nu_A-\nu_B)]. \tag{8}$$

The calculated spectral lines are shown in Fig. 2. The calculated free-precession signal $s(t)$ correspond-

[1] D. F. Elliot and R. J. Schumacher, J. Chem. Phys. **26**, 1350 (1957).

[2] J. A. Pople, W. G. Schneider, and H. J. Bernstein, *High Resolution Nuclear Magnetic Resonance* (McGraw-Hill Book Company, Inc., New York, 1959).

[3] W. A. Anderson, Phys. Rev. **102**, 151 (1956).

[4] H. M. McConnell, A. D. McLean, and C. A. Reilly, J. Chem. Phys. **23**, 1152 (1955).

ing to the spectrum of Fig. 2 is computed by adding together cosine terms starting at zero phase angle and having the amplitudes and frequencies indicated in Fig. 2,

$$s(t) = \cos\omega t\{(1-a)+(a/12)\cos Jt(3+4\cos\delta' t + \cos 2\delta' t)+(a/3)\cos\delta' t\}$$
$$+(a/12)\sin\omega t\{\cos Jt(2\sin\delta' t+\sin 2\delta' t)+4\sin\delta' t\}, \quad (9)$$

where a is the proton fraction for the ammonium ions and is about 0.48 in our experiments at room temperature.

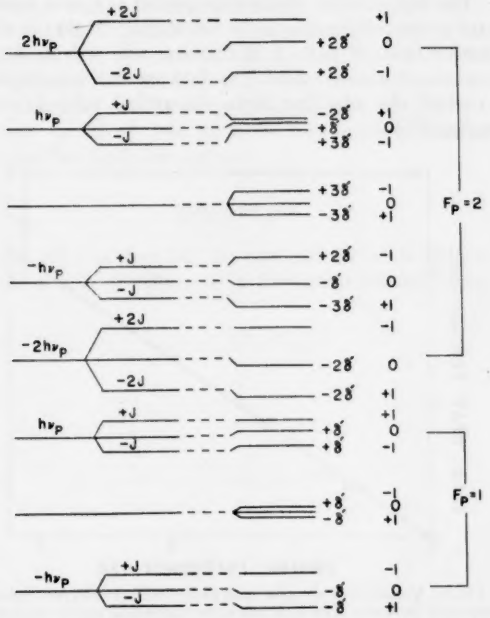

FIG. 1. Energy level diagram for the ammonium ion showing the necessary second-order corrections at low field. The column of digits gives the N^{14} nuclear spin orientation I_z.

EXPERIMENTAL

In the work being presented, nearly saturated samples of aqueous NH_4NO_3, treated with HNO_3 to stop exchange, were placed in the coil of an earth's field free-precession apparatus,[5] and the resulting signal was displayed on the face of an oscilloscope and photographed. Typical signals are shown in Fig. 3. The beat pattern shown in Fig. 3 is used in the calibration of the free-precession apparatus to show accurately at what time precession has begun. The proton precession frequency ν_P and the first-order splitting frequency J were measured with the aid of a Hewlett-Packard timer and found to be 2137 cps (in the earth's field) and 52.55±0.25 cps (in any field), respectively. This

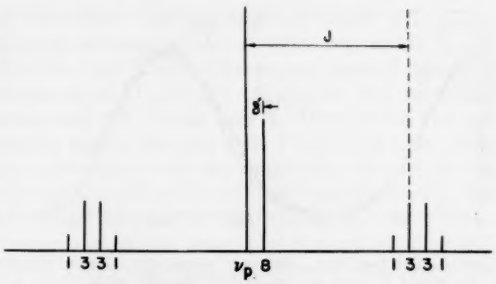

FIG. 2. Low-field spectrum for aqueous ammonium ion solution. The high central line is for the water and is not to scale.

value of J is in agreement with values measured previously at both high[5] and low[6] fields.

The Fast Beats

The fast beats shown in Fig. 3 can unambiguously be assigned ordinal numbers n despite the intervals where the fast beats do not appear. The above value of J was obtained by superimposing 10-msec timing pips from the timer on photographs such as those in Figs. 3(b) and 3(d). In the case of Fig. 3(b), about 35 cycles of the fast beat can be timed accurately, because in the original photographs, dark lines from the off-scale minima at the left are clearly visible.

As can be seen in Fig. 3(a), the 52.55 cycle beat, or fast beat, is modulated, with the fast beats appearing in three groups in the figure. With increased gain, even a fourth group can be seen. In order to check the

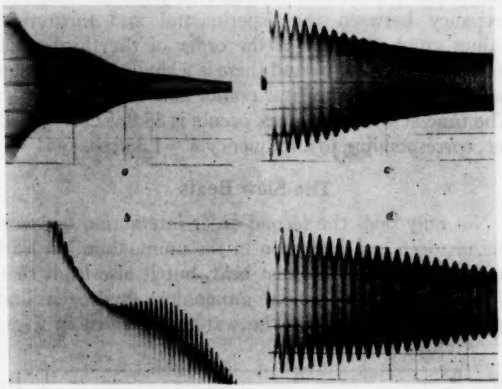

FIG. 3. Oscilloscope traces of free precession signals from aqueous ammonium ion solutions. All except (d) are for precession in the earth's field. (a) shows the signal for 2 sec, with three distinct groups of fast beats and also clearly showing the slow beats. In (b), the baseline is off scale and the second set of fast beats is shown on a 1-sec (end-to-end) sweep. The presence of the slow beat is also clearly seen; (c) and (d) both show the fast beats on a half-second sweep; (c) is at 2137 cps for the water proton frequency, and (d) is for a water proton frequency of 6250 cps.

[5] R. J. S. Brown, Bull. Am. Phys. Soc. Ser. II **5**, 298 (1960).

[6] H. Benoit and H. Ottavi, Compt. rend. **15**, 2708 (1960).

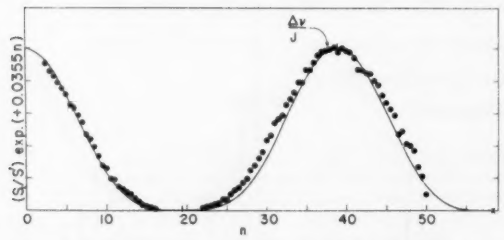

FIG. 4. The fast beats, fast beat amplitudes S_1 were divided by the signal S' from an unacidified (rapidly exchanging) ammonium sample to compensate for instrumental effects and thermal relaxation; (S_1/S') was multiplied by an exponential factor to bring the second peak up to the same amplitude as that of the first peak. The abscissa n is the time in units of the fast beat period.

coefficient of $\cos Jt$ in the first bracket of Eq. (9), the beat amplitude $S_1(t)$ was divided by the signal $S'(t)$ from an unacidified sample of NH_4NO_3 to compensate for instrumental signal decay (from inhomogeneous fields), and thermal relaxation. This ratio was then multiplied by $\exp(0.0355n)$ in order to compensate for the additional transverse relaxation, that is, to bring the second peak up to the initial amplitude. These data are shown in Fig. 4. The solid line is the factor $(3+4\cos\delta' t+\cos 2\delta' t)$ of Eq. (9) with the scale adjusted to make the second peak coincide with the experimental points in the vicinity of the peak. The beat number n is used for the time scale because the fast beats themselves provide an accurate time scale. The second peak comes at $n=38.9\pm0.5$. The calculated value is $\Delta\nu/J=37.8$, where $\Delta\nu$ is the difference between the proton and nitrogen frequencies. The discrepancy between the experimental and theoretical values given above is of the order of the third-order term given in Eq. (6) and there is a similar discrepancy between the experimental points and the solid curve. The time at which the peak occurs is $38.9/52.55=0.740$ sec, corresponding to a frequency $\delta'=1.35$ cps.

The Slow Beats

Not only does the second-order interaction between the nitrogen and hydrogen in the ammonium ion lead to a modulation of the fast beat, but it also leads to a slow beat of the central ammonium hydrogen line against the signal from the water, as shown in Figs. 2 and 3 and in Eq. (9). This slow beat is plotted in Fig. 5, where S_2 is the signal measured to a point midway between the peaks and valleys of the fast beats. As before, instrumental effects are compensated by dividing by S'. Note that the slow beat period is slightly shorter than the calculated value $\Delta\nu/J^2$, rather than slightly longer as was noted for the fast beats. In the case of the slow beats, however, the experimental uncertainty is about equal to the discrepancy, which is in turn of the order of the third-order terms indicated in Eq. (6).

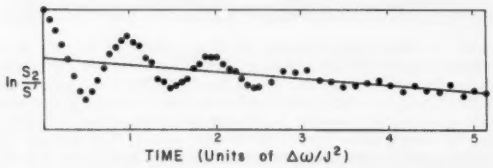

FIG. 5. The slow beats, the signal amplitude S_2 excluding the fast beats is divided by S' and plotted on semilog paper. The straight line indicates the water signal. The difference between the experimental points and the water line represents the central ammonium line beating against the water line with frequency δ'.

Frequency Dependence

The second-order interaction period $1/\delta'$ was measured at several frequencies in the vicinity of that in the earth's field. A pair of Helmholtz coils was used to augment the earth's field. The data are shown in Fig. 6, in which the solid line is the theoretical value $[(\nu_P-\nu_N/(\nu_P J^2)]\nu_P$.

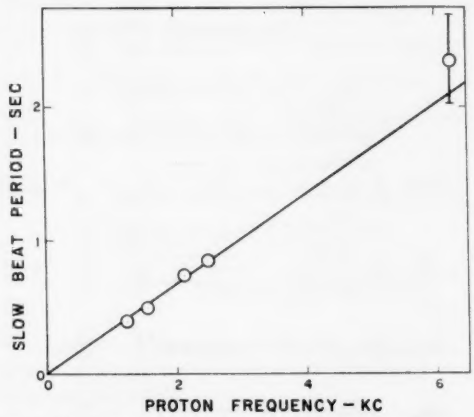

FIG. 6. Variation of the slow beat period with proton precession frequency for water. The solid line is the theoretical curve (second-order perturbation).

Thermal Relaxation

Rough thermal relaxation measurements at room temperature at fields from 2 gauss to 6000 gauss showed no field dependence of thermal relaxation times for either the water or ammonium hydrogens. Accurate measurements at 24.5°C showed the relaxation rates (reciprocal times) r_1 (water hydrogens) $=0.376$ sec^{-1} and r_1 (ammonium hydrogens) $=2.297$ sec^{-1}. Thus the difference in relaxation rates at room temperature is only about 0.08 sec^{-1}. An accurate measurement of the ammonium hydrogen thermal relaxation rate at -11°C was made, giving r_1 (ammonium) $=0.543$ sec^{-1}, or $T_1=1.84$ sec. The time for water at this temperature was much shorter.

Transverse Relaxation

To plot Fig. 4, it was necessary to multiply S_1/S' by an exponential factor which corresponds to a trans-

verse relaxation rate of 1.9 sec^{-1} in excess of the thermal relaxation rate, that is $r_2-r_1=1.9$ sec^{-1}. At $-11°C$, it was found that $r_2-r_1=2.8$ sec^{-1} for the fast beats. However, at 60°C, it was found that the fast beats died out very rapidly, indicating rapid transverse relaxation, probably due to chemical exchange of hydrogen nuclei between ammonium ions.

A plot of the slow beat amplitude as shown in Fig. 5 shows that the additional transverse relaxation rate $r_2-r_1=1.0$ sec^{-1}, only half that for the fast beats. If this difference is due to chemical exchange of hydrogen between ammonium ions, one might expect more rapid decay of the fast beats than of the slow beats, because exchange among the four left hand (or four right hand) lines of Fig. 2 would lead to decay of the fast beats, while there is no corresponding effect for the central ammonium line producing the slow beats. However, it is hard to see that this effect should give the observed factor of two between transverse relaxation rates of fast and slow beats.

Effect of *p*H

For *p*H less than 1.0, the acid concentration did not make a striking difference in the signals obtained from the ammonium ion solutions. At higher *p*H values, chemical exchange occurs at significant rates. To observe the effect of this exchange, we observed signals for samples of *p*H 1.0, 2.0, 3.0, 4.0, and 5.0. The unacidified sample has *p*H a little over 5. At *p*H=2.0, the ammonium signals died out with T_2 about 25 msec, while the water signal was not drastically affected by the exchange. At *p*H=3.0, no beats were observable, but the signal decay was nonexponential. After about 20 msec, the semilog decay plot is a straight line with $T_2=64$ msec, indicating exchange for both water and ammonium hydrogen but still showing partially separated ammonium lines. At *p*H=4.0 and at 5.0, simple exponentially decaying signals were observed. The ratio of the two signals decayed with a time constant of 0.28 sec at room temperature, and the signal for *p*H=5.0 has T_2 greater than 1.0 sec. Thus exchange is slow enough at *p*H=1.0 to give several sharp lines, and exchange is fast enough at *p*H=5.0 to give one sharp line.

The above data on *p*H dependence are in agreement with the measurements on the exchange rates made by McConnell and Thompson.[7]

[7] H. M. McConnell and D. D. Thompson, J. Chem. Phys. **31**, 85 (1959).

Spin-Lattice Relaxation Time of F^{19} Nuclei in Ag_2F

Q. WON CHOI* AND W. GILBERT CLARK†

Baker Laboratory, Cornell University, Ithaca, New York

(Received November 25, 1960)

The spin-lattice relaxation time of F^{19} nuclei in Ag_2F crystals has been measured at several temperatures. From the inverse proportionality constant of the relaxation time with respect to temperature in conjunction with the Korringa's theory, it is concluded that the relatively large paramagnetic shift observed is not due to the second-order paramagnetism but to the hyperfine interaction between conduction electrons and F^{19} nuclei.

IT has been observed that the fluorine nuclear magnetic resonance in Ag_2F is shifted by 0.023% to a lower magnetic field relative to AgF.[1] The purpose of the present note is to see if this shift can be interpreted as a Knight shift.[2]

The spin-lattice relaxation time T_1 for the F^{19} nuclei has been measured at several temperatures using pulsed magnetic resonance techniques. The apparatus and detailed principles are described elsewhere.[3]

Since the skin depth is small compared to the size of the particles of our sample, the rf magnetic field H_1 is not uniform throughout the volume of a particle. It is, therefore, necessary to consider the magnetization M of small volume elements. Starting with the spin system at thermal equilibrium with the magnetization M_0 when two rf pulses are applied to the sample at an interval t_w the magnetization at a point $\hat{r}$ at the beginning of the second pulse will be[4]

$$M(\hat{r}, t_w)=M_0[1-1+\cos\gamma H(\hat{r})\tau_1 \exp(-t_w/T_1)], \quad (1)$$

where τ_i is the duration of the ith pulse and γ is the magnetogyric ratio of the nucleus concerned. After the second pulse, the signal picked up by the receiving coil from the volume element dv will be proportional to $M(\hat{r}, t_w)\sin\gamma H_1(\hat{r})\tau_2 \cdot dv$,[4] when $T_1 \gg T_2 \gg \tau_i$ is assumed. The time constant of the free induction decay is T_2. If a function of $\hat{r}$, $\phi(\hat{r})$, which depends on the filling factor, attenuation, and phase shift of the signal generated inside the conducting sample, is introduced, the signal S from all such volume elements can be written as

$$S(t_w)=M_0\left\{\int \phi(\hat{r})\cdot \sin\gamma H_1(\hat{r})\tau_2 \cdot dv - \exp(-t_w/T_1) \times \int [1+\cos\gamma H_1(\hat{r})\tau_1]\phi(\hat{r}) \sin\gamma H_1(\hat{r})\tau_2 \cdot dv\right\}. \quad (2)$$

For a given system, with fixed τ_1 and τ_2, Eq. (2) has the form

$$S(t_w)=M_0[A-B\exp(-t_w/T_1)], \quad (3)$$

where A and B are constants. Noting $S(\infty)=AM_0$, Eq. (3) can be written as

$$S(\infty)-S(t_w)=[B/S(\infty)]\ \exp(-t_w/T_1). \quad (4)$$

Therefore, it is possible to compute T_1 from a log $[S(\infty)-S(t_w)]$ vs t_w plot, which is a straight line with the slope $-1/T_1$. To perform an experiment, no special values of τ_1 and τ_2 are necessary. They must, however, be kept constant for any set of measurements. For the present work, $\tau_1=\tau_2$ was adjusted to give no free induction signal after the second pulse, when $T_1 \gg t_w \gg T_2$.

The experimental results obtained at 9 Mc are given in Table I. A graph of T_1 vs inverse absolute temperature gives a straight line, for which $T_1=7.35/T$ sec.

The inverse proportionality of T_1 with respect to absolute temperature indicates that the relaxation is caused by the hyperfine interaction of F^{19} nuclei with the conduction electrons in Ag_2F. Furthermore, the magnitude of T_1 is much shorter than the reported values for F^{19} resonance in ionic crystals. Assuming that the relaxation is solely caused by the hyperfine interaction, the Knight shift is calculated to be 0.020% by means of the Korringa equation.[5] This is very close to the observed shift.

It has been pointed out[6] that the Korringa equation is correct only when the interaction between free electrons can be neglected. At present, it is impossible to make such a correction. Nevertheless, one can conclude that the observed shift is not caused primarily by the second-order paramagnetism.[7]

TABLE I. T_1 of F^{19} resonance.

Temperature (°K)	298	221	165	77
T_1, msec	27.6±0.6	33±6	59±4	98±4

[a] Errors in temperature were at most ±3° except for the liquid nitrogen temperature.

* Present address: Department of Chemistry, College of Liberal Arts and Sciences, Seoul University, Seoul, Korea.

† Present address: Physics Department, University of California, LaJolla, California.

[1] Q. Won Choi, J. Am. Chem. Soc. **82**, 2686 (1960).

[2] W. D. Knight, Phys. Rev. **76**, 1259 (1949).

[3] W. Gilbert Clark, Ph.D. thesis, Cornell University, 1961.

[4] This equation is based on the simple vector model described, for example, by E. L. Hahn, Phys. Today **6**, 4 (November, 1953).

[5] J. Korringa, Physica **16**, 601 (1950).

[6] D. Pines, *Solid State Physics*, edited by F. Seitz and D. Turnbull (Academic Press, Inc., New York, 1955), Vol. 1, p. 367.

[7] F. N. Ramsey, Phys. Rev. **78**, 699 (1950).

Application of a Theory of Nonideal Solutions to Results of Ultrasonic Absorption Measurements

F. O. GOODMAN*

Queen Mary College, University of London, London

(Received October 4, 1960)

It is shown that results of ultrasonic absorption measurements on solutions can sometimes be explained by application of a theory of nonideal solutions when the corresponding ideal-solution theory is inadequate. The results of ultrasonic absorption in tertiary butanol solutions in cyclohexane reported recently by R. Musa and M. Eisner are studied using a theory of nonideal solutions. This differs from the corresponding ideal-solution theory by the appearance of terms proportional to the derivatives of the ratio (k/l) of the relevant rate constants with respect to the concentration of the solute. In ideal solutions, these derivatives are zero. It is assumed that monomers and dimers are the only complexes present and it is concluded that a perturbation of the monomer-dimer equilibrium is responsible for the measured "excess absorption." The nonideality of the solutions is discussed, and a "nonideality coefficient" is introduced. A comparison with the imperfect gas theory of Tabuchi is made.

INTRODUCTION

RECENTLY, R. Musa and M. Eisner[1] reported measurements of the "excess absorption" associated with tertiary butanol solutions in cyclohexane between 0.005 and 0.02 mole %. They concluded that a perturbation of a monomer-tetramer ($T \rightleftharpoons 4M$) equilibrium in ideal solution expalined the measured "excess absorption." It is thought that a perturbation of such a complicated mechanism is rarely likely to occur. It will be shown in this paper how a simpler and more likely mechanism (a monomer-dimer equilibrium perturbation) is adequate for an explanation of the results, provided that the solution is not restricted to ideality.

BASIC EQUATIONS FOR THE ANALYSIS

Let the number of moles of monomer, dimer, and solvent in the solution be, respectively, N_1, N_2, and N_s.

Let $(\mu \text{ max})$ be the maximum value of the absorption per wavelength and let β be a solution property of the system given by

$$\beta=\frac{(N_1+2N_2+N_s)}{RT}\sum_i\sum_j \nu_i\nu_j(\partial\mu_i/\partial N_j)_{p,T}, \quad \begin{cases}(gr\beta)\\(gr\mu)\\(gr\nu)\end{cases} \quad (1)$$

where ν is the matrix of stoichiometric coefficients; μ_i is the chemical potential per mole of the ith component. For the monomer-dimer reaction, the summations are over $i, j=1,2$ with $\nu_1=+2$ and $\nu_2=-1$. It should be noted that the factor $(N_1+2N_2+N_s)$ is a constant during any one reaction. It may be shown[2] that $(\mu \text{ max})$ and β are related as follows:

$$(\mu \text{ max})\beta=\tfrac{1}{2}\pi(\gamma-1)(1/C_pRT^2) \times[\Delta H-(C_p/\alpha)(\Delta V/V)]^2. \quad (gr\gamma) \quad (2)$$

If we consider just one mole of solution with the number of moles of solute based on the molecular weight of the monomer, then in (1), $(N_1+2N_2+N_s)=1$ mole, and in (2) γ = the heat capacity ratio Cp/Cv, Cp, Cv = the heat capacities per mole of solution at constant pressure, volume, α = the thermal coefficient of volume expansion, $\Delta H=(\partial H/\partial Z)_{eq}$ = the derivative of the enthalpy *w.r.t.* the "molar degree of reaction" Z, evaluated at the equilibrium point. Similarly, $\Delta V=(\partial V/\partial Z)_{eq}$ and V is the volume of one mole of solution. Here ΔH and ΔV may be called the molar enthalpy of reaction and the molar volume of reaction, respectively. Both of these "reaction coefficients" are in fact, functions of concentration in nonideal solutions. We shall assume, however, that at the concentrations we are considering, the reaction coefficients are effectively constant. We now introduce a set of "reaction constants" which are independent of concentration. These reaction constants are ΔH^0, ΔV^0, and ΔG^0. The affices^0 indicate that the reaction constants are referred to the pure solute. For example, ΔH^0 is the enthalpy change due to one mole of pure dimer changing over to two moles of pure monomer. In ideal solutions, the reaction constants ΔH^0 and ΔV^0 are identical, respectively, with the reaction coefficients ΔH and ΔV. In nonideal solutions this is not so. For all types of solutions, of course, the reaction coefficient ΔG is zero. Roughly speaking, we may say that the percentage difference between the reaction coefficients ΔH and ΔV and the corresponding reaction constants ΔH^0 and ΔG^0 will be of the order of the "percentage nonideality" of the solution. The term "percentage nonideality" will be given clearer meaning later.

Define x = mole fraction of dimer $= N_2/N$ (3a)

y = mole fraction of monomer $= N_1/N$, (3b)

where

$$N=N_1+N_2+N_s. \quad (4)$$

* Present address: Royal Aircraft Establishment, Farnborough, Hants, England.

[1] R. Musa and M. Eisner, J. Chem. Phys. **30**, 227 (1959).

[2] F. O. Goodman, Ph.D. thesis, to be published, 1961.

TABLE I. Some results of the analysis.

T°K	$\xi, 10^3$	$x, 10^3$	$y, 10^3$	$y, 10^3$ [a]	$a(T)$	$Q, 10^3$	$\beta=\beta^1+\Delta\beta$	β^1	$-I=-\Delta\beta/\beta^1$	$(\mu\ \max), 10^3$ [b]	$(\mu\ \max)\beta$	Mean values of $(\mu\ \max)\beta$
	5	0.797	3.41	...		14.6	2180	2420	0.10	2.79	6.1	
	10	2.61	4.80	...		8.82	1070	1220	0.12	6.01	6.4	
279	15	4.86	5.35	...	0.377	5.88	859	960	0.11	7.42	6.4	6.3
	20	7.26	5.62	...		4.34	780	855	0.088	8.17	6.4	
	5	0.612	3.78	...		23.2	2440	2690	0.092	2.02	4.9	
	10	2.22	5.58	...		14.0	1020	1170	0.13	5.04	5.1	
288	15	4.35	6.37	...	0.598	9.33	760	861	0.12	6.78	5.1	5.0
	20	6.68	6.78	...		6.88	669	744	0.10	7.1	4.7	
	5	0.436	4.13	4.13		38.8	3010	3260	0.076	0.85	2.6	
	10	1.78	6.45	6.45		23.4	1030	1180	0.13	2.7	2.8	
300	15	3.72	7.62	7.62	1.000	15.6	695	796	0.13	4.2	2.9	2.8
	20	5.93	8.26	8.26		11.5	581	656	0.11	4.8	2.8	

[a] From Prigogine and Desmyter, see work cited in footnote 4.
[b] From Musa and Eisner, see work cited in footnote 1.

Then if ξ is the total concentration of the solute based on the molecular weight of the monomer, ξ is the same as Musa and Eisner's[1] N_0. We assume that no trimers or higher complexes are present and we obtain

$$\xi=(N_1+2N_2)/(N_1+2N_2+N_s)$$
$$=(2x+y)/(1+x)\,(gr\xi). \tag{5}$$

We define rate constants k and l such that at equilibrium:

number of transitions (2 monomers→1 dimer)/sec
$$=Ny^2l, \tag{6a}$$

number of transitions (1 dimer→2 monomers)/sec
$$=Nxk. \tag{6b}$$

When defined in this way, the rate constants k and l are $[1/(1+x)]$ times those used normally by the chemists [for example, $(1+x)k$ corresponds to the $A_{n1}{}^0$ of Musa and Eisner[1]].

For nonideal solutions, the chemical potentials μ_i may be written

$$\mu_i=\mu_i{}^0(p,\ T)+RT\ \ln\gamma_i+RT\ \ln x_i,\quad (gr\gamma) \tag{7}$$

where γ_i = the activity coefficient of component i. The first and last terms on the right-hand side of (7) would be the only terms appearing if we had an ideal solution. Thus, the chemical potentials may be written as the sum of two parts, an "ideal" part, which we denote by $\mu_i{}^1$ where

$$\mu_i{}^1=\mu_i{}^0(p,\ T)+RT\ \ln x_i, \tag{8}$$

and a "nonideal" part, which we denote by $\Delta\mu_i$ where

$$\Delta\mu_i=RT\ \ln\gamma_i. \tag{9}$$

Thus

$$\mu_i=\mu_i{}^1+\Delta\mu_i. \tag{10}$$

Hence the solution property β given by (1) may be written in the case of a nonideal solution as the sum of two parts, an ideal part which we denote by β^1, and a nonideal part which we denote by $\Delta\beta$,

$$\beta=\beta^1+\Delta\beta. \tag{11}$$

It is evident from (1), (9), and (10) that $\Delta\beta$ consists of terms containing derivatives of the activity coefficients with respect to the concentrations of the monomer and dimer parts of the solute. These derivatives vanish in ideal solutions.

It may be shown by a method similar to that used for other reacting mechanisms by R. O. Davies[3] that these derivatives may be related directly to the derivatives of the ratio (k/l) with respect to concentration. For a complete analysis, see work cited in footnote 2. It may in fact be shown[2] that for the monomer-dimer reaction in nonideal solution, β is given by

$$\beta=(1+x)^2\{(1/x)+(4-2\xi)/y-[(\partial/\partial x)\ \ln(l/k)]_\xi\}, \tag{12}$$

and the corresponding inverse relaxation time is given by

$$W=\tau^{-1}=(1+x)\{k+yl(4-2\xi)-xk[(\partial/\partial x)\ \ln(l/k)]_\xi\}. \tag{13}$$

The corresponding ideal-solution theory yields[2]

$$\beta^1=(1+x)^2[(1/x)+(4-2\xi)/y] \tag{14}$$

and

$$W^1=(1+x)[k+yl(4-2\xi)]. \tag{15}$$

Thus

$$\Delta\beta=-(1+x)^2[(\partial/\partial x)\ \ln(l/k)]_\xi, \tag{16}$$

and the difference between ideal and nonideal solutions is the appearance of the derivative terms in (12) and (13). For ideal solutions it may be shown[2] that in fact

$$\text{(ideal solution)}\quad [(\partial/\partial x)\ \ln(l/k)]_\xi=0. \tag{17}$$

[3] R. O. Davies, Proc. Roy. Soc. (London) **A257**, 541 (1960).

Evidently $[(\beta-\beta^1)/\beta^1]$ is a measure of the nonideality of the solution. A "nonideality coefficient" I is introduced such that

$$I=\Delta\beta/\beta^1=(\beta-\beta^1)/\beta^1. \tag{18}$$

We define an "equilibrium coefficient" Q given by

$$Q=y^2/x=k/l \tag{19}$$

at equilibrium. It must be remembered that Q is not the "equilibrium constant," which we denote by E where

$$E=\exp[-(\Delta G^0/RT)] \tag{20}$$

and ΔG^0 is the free-energy reaction constant. This is because we have a nonideal solution. In fact

$$E=\Gamma Q, \tag{21}$$

where

$$\Gamma=(\gamma_2)^2/\gamma_2, \tag{22}$$

and the γ's are the activity coefficients.

We shall assume that the temperature variation of $\ln\Gamma$ is much less than that of $\ln Q$. That is, we shall assume that, even though we have a nonideal solution,

$$\Delta H^0/R=-T^2(\partial/\partial T)(\Delta G^0/RT)=T^2(\partial/\partial T)(\ln Q). \tag{23}$$

EXPERIMENTAL DATA

The values of (μ max) and $W/2\pi[=(2\pi\tau)^{-1}]$ reported by Musa and Eisner[1] will be used in the analysis. (For the method of calculating these parameters from actual experimental measurements, see the original paper.[1]) In order to evaluate β and W from Eqs. (13) to (16), we need the equilibrium values of x and y (and hence Q) for each ξ and T. As a basis for the evaluation of these, we shall use the values of $N_1^0(=y)$ at 300°K quoted by Musa and Eisner[1] and based on data by Prigogine and Desmyter.[4] These data are in Table I.

ANALYSIS OF THE EXPERIMENTAL DATA

In order to estimate the derivatives in (12) and (13), we must make some guess as to the variation of (l/k) with x at constant ξ. This guess must be consistent with the experimental equilibrium values of y at 300°K referred to above. [The equilibrium value of (l/k), which we may denote by $(l/k)_{eq}$ at any one (T, ξ) is of course $Q^{-1}(T, \xi)$.]

ESTIMATION OF THE DERIVATIVES

The data of Prigogine and Desmyter in Table I give us the equilibrium values of y, $\bar{y}$ [and hence $\bar{x}$, $(l/k)_{eq}$, and Q] at four different values of at 300°K. We assume that (l/k) can be expressed as a linear function of and y as follows,

$$(l/k)=A+Bx+Cy. \tag{24}$$

[4] I. Prigogine and A. Desmyter, Trans. Faraday Soc. **47**, 1137 (1951).

TABLE II. Values of the derivative $[(\partial/\partial x)\ln(l/k)]_\xi$.

ξ, 10^3	$[(\partial/\partial x)\ln(l/k)]_\xi$
5	249
10	150
15	100
20	74

We assume that (24) is valid both at equilibrium, and for reasonably small deviations away from equilibrium. For equilibrium values (24) becomes

$$Q^{-1}=(l/k)_{eq}=A+B\bar{x}+C\bar{y}. \tag{25}$$

Equation (25) was fitted to the equilibrium data referred to above. It was found that although we have four values of $(l/k)_{eq}$ as a function of $\bar{x}$ and $\bar{y}$, all four could be fitted by suitable choice of our three constants A, B, and C. This is, of course, very fortunate. The values of A, B, and C chosen were

$$A=14.0$$
$$B=1{,}740$$
$$C=9{,}890. \tag{26}$$

Putting these values into Eq. (24), we obtain as a basis for estimating the derivatives, that

$$(l/k)=14.0+1{,}740x+9{,}890y. \tag{27}$$

To facilitate this estimate, we may substitute for y as a function of x and ξ in (27) from (5) to obtain

$$(l/k)(300°\text{K})=14.0+1{,}740\xi(1+x)+6{,}410x. \tag{28}$$

CONSTANCY OF (μ MAX)β

A test of the theory is the constancy of (μ max)β at any one temperature from (2). Here β was calculated at 300°K from the values of x and y in Table I substituted into (12). The derivative in (12) was evaluated directly using (28). The results of the evaluation of the derivative are in Table II; (μ max)β at 300°K was calculated from (2) and the resulting values are in Table I. It is seen that (μ max)β is indeed a constant within possible experimental error.

Next, values of Q at 288°K and 279°K were found. This was done by writing

$$Q(\xi, T)=a(T)Q(\xi, 300°\text{K}), \tag{29}$$

and finding a (288°K) and a (279°K) so that (μ max)β was made constant at these two temperatures. [From a given Q and ξ, x and y may be found by trial and error, using the relations (5) and (19). The derivative terms may be evaluated at the new temperature by noting that it is evident from (29) that the results in Table II are in fact independent of T.] A small amount of latitude was found in the choice of the two a's, still keeping

TABLE III. Data on Cyclohexane.

T°K	279	288	300
C_p (cal/mole deg)[a]	41.85	42.15	42.8
$\alpha\times10^3$ deg^{-1}[a]	1.221	1.208	1.190
γ[b]	1.363	1.331	1.285

[a] J. Timmermans, *Physico-chemical Constants* (Elsevier Publishing Company, Inc., New York, 1950).
[b] See work cited in footnote 1.

(μ max)β constant. Values of a, and hence of Q, were chosen in these ranges to give acceptable values of ΔH^0 from (23). The chosen a's, together with the resulting values of Q, (μ max)β, etc., at the two new temperatures are shown in Table I. It is seen that (μ max)β is constant at any one temperature.

VALUES OF ΔV, ΔH, AND ΔH^0

A mean value of (μ max)β was found at each temperature (see Table I), and from these values and the data in Table III, a value of $[\Delta H-(C_p/\alpha)(\Delta V/V)]$ was calculated at each temperature from (2). The resulting values are in Table IV.

An estimation of ΔH^0 may be made making use of the variation of $\ln Q$ with T via (23). Using the three values of $Q(T)$ at $\xi=5.10^{-3}$, we find that they are consistent with the following assumptions:

$$Q(279°\text{K})=14.6\times10^{-3} \tag{30a}$$

$$[(\partial/\partial T)\ln Q]_{279°\text{K}}=55\times10^{-3}\text{ deg}^{-1} \tag{30b}$$

$$[(\partial^2/\partial T^2)\ln Q]_{279°\text{K}}=-0.81\times10^{-3}\text{ deg}^{-2}, \tag{30c}$$

and

$$[(\partial^n/\partial T^n)\ln Q]_{279°\text{K}}=0 \quad \text{for} \quad n>2. \tag{30d}$$

From (23) and (30) it follows that

$$\Delta H^0=RT^2[(\partial/\partial T)\ln Q] \tag{31a}$$

$$[(\partial/\partial T)\Delta H^0]=2RT[(\partial/\partial T)\ln Q]+RT^2[(\partial^2/\partial T^2)\ln Q] \tag{31b}$$

$$[(\partial^2/\partial T^2)\Delta H^0]=2R[(\partial/\partial T)\ln Q]+4RT[(\partial^2/\partial T^2)\ln Q] \tag{31c}$$

$$[(\partial^3/\partial T^3)\Delta H^0]=6R[(\partial^2/\partial T^2)\ln Q] \tag{31d}$$

and

$$[(\partial^n/\partial T^n)\Delta H^0]=0 \text{ for } n>3. \tag{31e}$$

Thus we may calculate from (30) and (31) that at 279°K

$$\Delta H^0=8.52\text{ kcal/mole}^{-1}. \tag{32a}$$

$$[(\partial/\partial T)\Delta H^0]=-6.43\times10^{-3}\text{ kcal/mole}^{-1}\text{ deg}^{-1} \tag{32b}$$

$$[(\partial^2/\partial T^2)\Delta H^0]=-1.58\times10^{-3}\text{ kcal/mole}^{-1}\text{ deg}^{-2} \tag{32c}$$

and

$$[(\partial^3/\partial T^3)\Delta H^0]=-9.67\times10^{-6}\text{ kcal/mole}^{-1}\text{ deg}^{-3}. \tag{32d}$$

The values of ΔH^0 at the three temperatures calculated from (32) are shown in Table IV.

Now, as has already been discussed, it is to be expected that ΔH and ΔH^0 may differ by a percentage equivalent to the percentage nonideality of the solution. This percentage nonideality is in fact found to be of the order of 10%. (See Table I for values of the nonideality coefficient I, defined by Eq. (18).] Thus we may expect ΔH and ΔH^0 to differ by about 10%. From Table IV, it is clear that the positive signs in row 1 are the correct ones. From this Table and what has been said above concerning ΔH and ΔH^0, we may in fact conclude that $|(C_p/\alpha)(\Delta V/V)|$ is of the order of, or less than, 10% of ΔH. This is an important result, as it shows that to an accuracy of about 10%, it is valid to neglect the $[(C_p/\alpha)(\Delta V/V)]$ term with respect to the ΔH term in Eq. (2). This is usually done in the literature but is rarely justified. We may make an estimate of $|\Delta V/V|$ from Table IV and we find that

$$|\Delta V/V|<3\%. \tag{33}$$

THE RATE CONSTANTS k AND l

It is evident from (6b) that the number of transitions (1 dimer→2 monomers)/sec is given by N_2k. Thus k is a sort of "transition probability". Here l is a measure of the probability that (2 monomers→1 dimer) given that the monomers collide. In order to calculate k and l we rewrite (13) as follows,

$$W/k=\tau^{-1}/k=(1+x)\{1+(y/Q)(4-2\xi)-x\times[(\partial/\partial x)\ln(l/k)]_\xi\}. \tag{34}$$

From (34) values of W/k were calculated at each experimental point. Then, using the measured[1] values of W it was possible to calculate k and $l=k/Q$. The results are in Table V. It appears from Table V that k may well be a constant at any one temperature, although the results at the lower temperatures indicate that k may decrease with increasing concentration. (The range of this decrease, however, is probably within the range of possible experimental error.) Assuming that at each temperature k *is* a constant, its mean values are tabulated in Table V.

TABLE IV. Values of $[\Delta H-(C_p/\alpha)(\Delta V/V)]$ and ΔH^0.

T°K	279	288	300
$[\Delta H-(C_p/\alpha)(\Delta V/V)]$ kcal/mole from mean values of (μ max)β and Eq. (2)	±8.5	±8.2	±6.9
ΔH^0 kcal/mole from Eq. (32)	8.5	7.9	6.8
(C_p/α) kcal/mole from Table III.	34.3	34.9	36.0

TABLE V. Rate constant data.

T°K	ξ, 10^3	From Musa and Eisner $10^{-6}W=10^{-6}\tau^{-1}$ sec^{-1}	$10^{-6}k$ sec^{-1}	$10^{-9}l$ sec^{-1}	Mean value of k, 10^{-6} $10^{-6}\bar{k}$ sec^{-1}
	5	104	60	4.1	
	10	163	59	6.6	
279	15	226	55	9.3	56
	20	283	50	12	
	5	116	77	3.3	
	10	180	80	5.7	
288	15	242	74	7.9	75
	20	314	71	10	
	5	145	110	2.8	
	10	236	130	5.5	
300	15	315	120	7.9	120
	20	368	110	9.3	

DISCUSSION OF THE RESULTS AND CONCLUSIONS

The resulting constancy of (μ max)β from Table I and the reasonable values of ΔH, ΔH^0, and $\Delta V/V$ found from Table IV indicate that a perturbation of an equilibrium monomer-dimer reaction is the correct mechanism. From Table V, k, a sort of "transition probability," increases with increasing temperature, a result which is to be expected; l decreases with increasing temperature. In view of what has been said above about l, this is also to be expected.

The "nonideality coefficient" $I=\Delta\beta/\beta^1$ is of interest. It is tabulated in Table I. It is of course a measure of the departure from ideality of the solutions (ideal solutions yield $I=0$). There are three observations which we can make concerning I:

(*i*) In the limit of $\xi\rightarrow 0$ we may show that

$$\text{(a)}\quad \lim_{\xi\rightarrow 0}\Delta\beta=-458 \tag{29}$$

and

$$\text{(b)}\quad \beta^1\rightarrow\infty \quad \text{as} \quad \xi\rightarrow 0. \tag{30}$$

Thus

$$\text{(c)}\quad \lim_{\xi\rightarrow 0} I=0. \tag{31}$$

This is the result we expect, i.e., in the limit of small concentrations, the solution becomes ideal.

(*ii*) Comparing (16) and Table II we see that $\Delta\beta$ at any one ξ is effectively independent of T.

(*iii*) From Table I we find that for lower ξ,

$$(\partial\beta/\partial T)_\xi>0, \tag{32a}$$

for higher ξ,

$$(\partial\beta/\partial T)_\xi<0. \tag{32b}$$

Combining (ii) and (iii) we obtain the result that for lower ξ,

$$(\partial|I|/\partial T)_\xi<0, \tag{33a}$$

for higher ξ,

$$(\partial|I|/\partial T)_\xi>0. \tag{33b}$$

Thus for lower ξ, the solution gets more ideal, and for higher ξ, it gets less ideal as the temperature is increased.

COMPARISON WITH THE IMPERFECT GAS THEORY OF TABUCHI

D. Tabuchi[5] has developed a theory of chemical reactions in imperfect gases. In this theory, as in most other theories of this type, the derivative terms are neglected. For example, no derivative terms appear in Tabuchi's Eq. (2.23) for the inverse relaxation time. It may be shown that Tabuchi's rate constants for the forward and backward reactions, k_f and k_b, respectively, are related to k and l by the equations

$$k=k_f[\gamma_2/(1+x)] \tag{34a}$$

$$l=k_B(N/\mathrm{V})[(\gamma_1)^2/(1+x)]. \tag{34b}$$

Putting these values of k and l into our expression (13) for the inverse relaxation time we obtain for $\xi=0$

$$W=k_f\gamma_2[1+4(N_2/N_1)]+(\text{derivative term}). \tag{35}$$

Tabuchi's Eq. (2.23) becomes, after the relevant substitutions,

$$W=k_f\gamma_2N_2[(1/N_2)+(4/N_1)]. \tag{36}$$

Equation (35) without the derivative term is identical with (36). It is evident that in any exact theory of simple relaxation mechanisms, these derivative terms must be considered.

ACKNOWLEDGMENT

The author wishes to acknowledge several helpful discussions on the subject of this paper with Dr. R. O. Davies.

[5] D. Tabuchi, J. Chem. Phys. **23**, 2033 (1955).

Mass Spectrometer Investigation of Ionization of N_2O by Electron Impact

R. K. Curran and R. E. Fox

Westinghouse Research Laboratories, Pittsburgh, Pennsylvania

(Received August 12, 1960)

The N_2O molecule has been studied with a nearly monoenergetic electron beam. A result of the positive ion data is a value for $D(N_2-O) \leq 1.34 \pm 0.2$ ev and a value of $D(N-NO) \leq 4.50+0.10$ ev. Measurements were made of the kinetic energies of the ions formed. N^+ and N_2^+ are found to have zero kinetic energy at threshold. The production of an O^- ion is observed with an appearance potential in the range 0 to 0.05 ev.

I. INTRODUCTION

PREVIOUS work[1–3] on positive-ion formation in N_2O has been done with electron beams having wide energy spreads, without kinetic-energy analysis of the ions formed, and without accompanying data on the formation of negative ions. The present experiment utilizes electrons with narrow energy spread to form the ions, and measures the kinetic energy of the ions. This has resulted in a new upper limit for $D(N_2-O)$, the dissociation energy of the bond between N_2 and O in N_2O.

II. EXPERIMENTAL PROCEDURE

The mass spectrometer used was a 90° deflection type. The ion source was equipped for the RPD method.[4] Pulsing techniques were not used, since ions with kinetic energy were being studied. The dc ion-repeller voltage necessary to extract the ions in the experiment influenced the electron energy distribution with the result that typical electron energy distributions obtained by the RPD method ranged from 0.2 ev to 0.3 ev in width.

Ion detection for the positive ions was made with an electron multiplier with a stable gain of about 2000. The multiplier was used only during appearance potential measurements. Ion detection for negative ions and kinetic energy measurements of negative and positive ions was accomplished with a Faraday cage and a vibrating-reed electrometer.

Kinetic-energy measurement was accomplished by running the mass spectrometer analyzer at the ion acceleration voltage and the ion collector at zero potential; then, as the entire ion source is raised or lowered with respect to zero potential, the ion kinetic energy retarding curve is traced out by plotting the ion current at the collector vs the ion source potential. A comparison of such a curve with that obtained for an ion formed with zero kinetic energy then yields the maximum kinetic energy of the ion in question. On account of discrimination in the ion source, however, the true distribution in energy is not obtainable, and hence the relative magnitudes of such ions may be in considerable error. For positive ions the electron energy and the ion kinetic energy scales are calibrated with neon and argon. The zero of the energy scale for negative ion formation is determined from the electron retarding curve. Zero electron energy is taken to be the onset of this curve and thus is determined by the fastest electrons in the distribution. All figures are representative data with corrected energy scales. Numerical values in the text are averages over several unweighted measurements. Errors quoted are estimated absolute errors and do not represent reproducibility of data which in all measurements was less than 0.1 ev.

III. RESULTS

1. N_2O^+

The ionization efficiency near threshold for N_2O^+ is shown in Fig. 1. The appearance potential (AP) is 12.63 ± 0.05 ev as compared with the spectroscopically determined value[5] of 12.72 ev. Breaks were observed in the ionization efficiency at 13.1 ± 0.1 ev, 13.6 ± 0.1 ev, 14.1 ± 0.3 ev, 15.5 ± 0.3 ev, and 16.8 ± 0.3 ev. These breaks presumably indicate ionization to various excited electronic states of N_2O^+. A break is located by linear extrapolation from linear regions on either side of the break.

2. NO^+

Figure 2 shows the ionization efficiency for NO^+ from N_2O near threshold. There is an NO^+ background due to an NO impurity either introduced with the N_2O sample or generated by pyrolysis on the filament. Also shown in Fig. 2 is the ionization efficiency of NO^+ from NO in the neighborhood of the appearance potential of NO^+ from N_2O, demonstrating that the process onsetting near 13.75 ev is NO^+ from N_2O. Note that the ionization efficiency for NO^+ from N_2O near threshold (13.75 ev) has a shape characteristic of pre-ionization.[6] This type of structure near threshold is usually interpreted as arising from a pair-formation process. In the present case, however, this would necessitate postulating the existence of a stable N^- ion. There is no evi-

[1] H. D. Smyth, Revs. Modern Phys. **3**, 347 (1931).
[2] E. C. G. Stueckelberg and H. D. Smyth, Phys. Rev. **36**, 478 (1930).
[3] J. Collin and F. P. Lossing, J. Chem. Phys. **28**, 900 (1958).
[4] R. E. Fox, W. M. Hickam, D. J. Grove, and T. Kjeldaas, Rev. Sci. Instr. **26**, 1101 (1955).
[5] A. B. F. Duncan, J. Chem. Phys. **4**, 638 (1936).
[6] W. M. Hickam, Phys. Rev. **95**, 703 (1954).

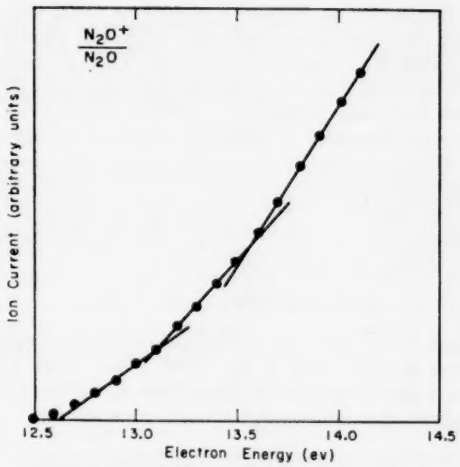

FIG. 1. Ionization efficiency of N_2O^+/N_2O near threshold. Breaks in the linearity of the curve represent the onset of ionization to excited states of N_2O^+.

dence in the present experiment to support this interpretation. The appearance potential of NO^+ from N_2O is 13.75 ± 0.10 ev. This ion was observed to have zero kinetic energy in a range about 3 ev above threshold. Now, since

$$D(\mathrm{N-NO}) \leq \mathrm{AP}(\mathrm{NO}^+) - I(\mathrm{NO}),$$

and using $I(\mathrm{NO}) = 9.25\pm0.02$ ev, the ionization potential[7] of NO spectroscopically determined, one obtains $D(\mathrm{N-NO}) \leq 4.50\pm0.1$ ev. Note that the inequality is used here and in what follows, since internal energies of fragments are omitted. A break occurs in the NO^+ ionization efficiency at 17.0 ± 0.3 ev.

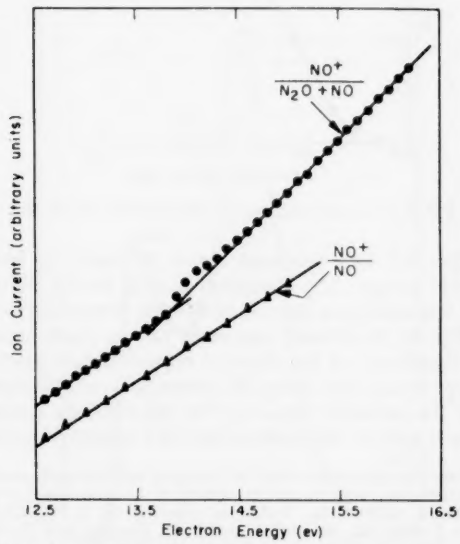

FIG. 2. Ionization efficiency of NO^+. The upper curve is the ionization efficiency of NO^+ from a mixture of N_2O and NO. The NO presumably arises from pyrolysis of N_2O on the filament. The ionization efficiency of NO^+ from NO is given by the lower curve. The absence of a break in NO^+/NO efficiency demonstrates that the break observed in the NO^+/N_2O+NO efficiency is due to the onset of NO^+/N_2O.

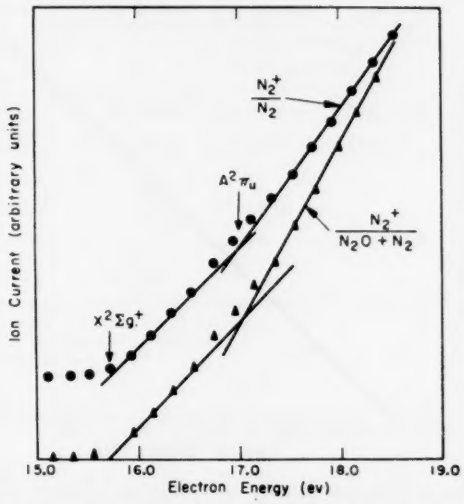

FIG. 3. Ionization efficiency of N_2^+. The lower curve is the ionization efficiency of N_2^+ from a mixture of N_2O and N_2. The N_2 impurity arises from pyrolysis of N_2O on the filament. The ionization efficiency of N_2^+ from N_2 is given in the upper curve. The increase in slope in the N_2^+/N_2O+N_2 near 17 ev being greater than that in the N_2^+/N_2 is interpreted as indicating the onset of N_2^+/N_2O at an energy close to the onset of the $A^2\pi_u$ state of N_2^+/N_2.

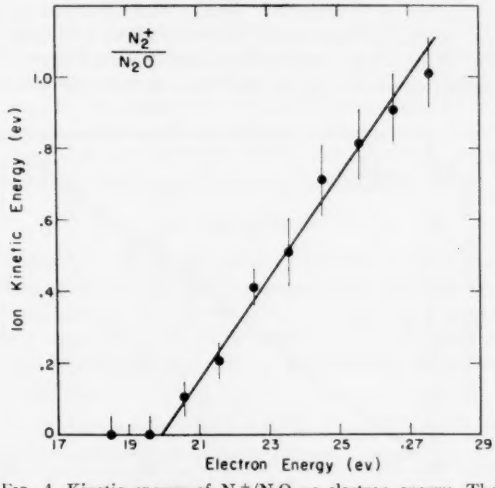

FIG. 4. Kinetic energy of N_2^+/N_2O vs electron energy. The intercept at $20.0+0.1$ ev agrees with the observed position of a break in the N_2^+ ionization efficiency at $20.2+0.2$ ev and demonstrates that the N_2^+ made in this process has zero kinetic energy at onset.

[7] K. Watanabe, F. Marmo, and E. C. Y. Inn, Phys. Rev. **91**, 436 (1953).

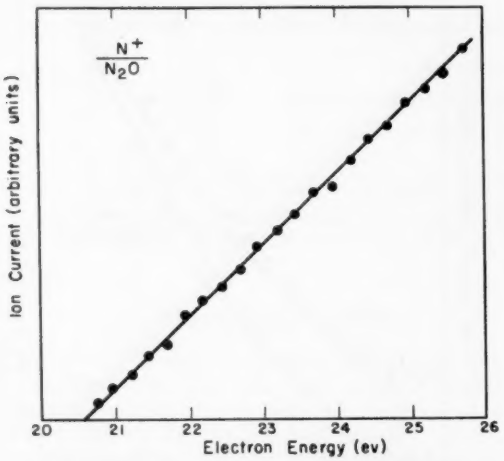

FIG. 5. Ionization efficiency of N^+/N_2O near threshold. Data were not taken below the point where the difference current signal was equal to background noise.

3. N_2^+

Breaks in the ionization efficiency of N_2^+ from N_2O could not be measured with precision because of a background of N_2^+ from N_2. This background N_2 did not appear to be introduced with the N_2O sample, since several attempts at purifying the N_2O sample by repeated freezing at liquid nitrogen temperatures and pumping out the residual gas produced no sensible change in the relative N_2 concentration. Thus, it was concluded that pyrolysis of N_2O on the filament was the cause of N_2 impurity. Breaks were observed in the N_2^+ from N_2O ionization efficiency curve at 17.0±0.2 ev, 18.3±0.2 ev, and 20.2±0.2 ev. Figure 3 shows the ionization efficiency for N_2^+ from N_2O in the vicinity of the breaks[8] at 17.0 ev. It should be noted that the ratio of slopes above and below 17.0 ev is greater for N_2^+ from N_2O than for N_2^+ from N_2. This can be interpreted as implying a process for the production of N_2^+ from N_2O near 17.0±0.2 ev which is close to the appearance potential of the $A^2\Pi_u$ state[9] of N_2^+ from N_2 at 16.89±0.04 ev. Now, if one assigns the observed breaks at 17.0±0.2 ev, 18.3±0.2 ev, and 20.2±0.2 ev in the N_2^+ from N_2O ionization efficiency to the breakup of N_2O into $O(^3P)$ and N_2^+ in the states $X\ ^2\Sigma_g$, $A\ ^2\Pi_u$, and $B\ ^2\Sigma_u^+$, then one has

$$D(N_2-O) \leq AO(N_2^+) - I(N_2),$$

where $I(N_2)$ has the following values[9] for the indicated states of N_2^+: 15.60 $X\ ^2\Sigma_g$, 16.93 $A\ ^2\Pi_u$, 18.84 $B\ ^2\Sigma_u$. These give values for an upper limit for $D(N_2-O)$ as 1.4±0.2, 1.37±0.2, and 1.36±0.2, respectively.

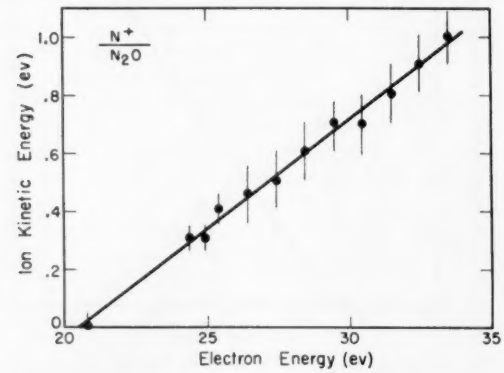

FIG. 6. Kinetic energy of N^+/N_2O vs electron energy. The point on the electron energy axis is the measured appearance potential. The agreement between this and the intercept of the line through the points obtained from kinetic energy measurement implies that the N^+ ions have zero kinetic energy at threshold.

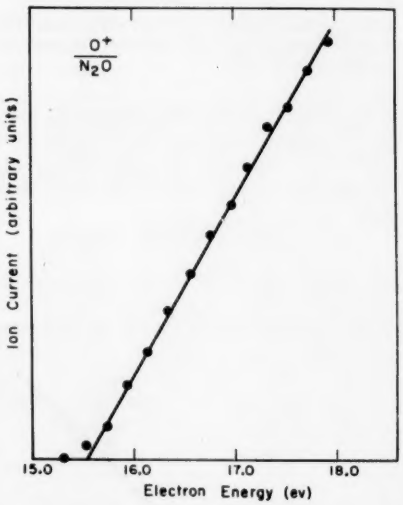

FIG. 7. Ionization efficiency of O^+/N_2O near threshold.

The N_2^+ ions produced above 20.2±0.2 ev have kinetic energy. The maximum kinetic energy of the N_2^+ measured as a function of electron energy is shown in Fig. 4. No definite statement can be made about the significance of the observed slope of the ion kinetic energy vs electron energy. However, it should be noted that the observed slope may be less than the proper slope if some of the incident electron's energy is carried

[8] Note that the shape of the N_2^+ curves in both instances shows deviation from linearity in the vicinity of 17.0 ev, which is in agreement with similar deviations observed by E. M. Clark [Can. J. Phys. **32**, 764 (1954)] and F. H. Dorman *et al.* [F. H. Dorman, J. D. Morrison, and A. J. C. Nicholson, J. Chem. Phys. **32**, 378 (1960)] and attributed by Dorman *et al.* to a preionization process. That this was not observed in the work cited in footnote 9 is due partly to the fact that data points were not taken at sufficiently small intervals. Smaller energy intervals were not justifiable at that time due to the electron energy spread and reproducibility of the data.

[9] R. E. Fox and W. M. Hickam, J. Chem. Phys. **22**, 2059 (1954).

off by the outgoing electrons. The agreement between the intercept at 20.0±0.1 ev and the break at 20.2±0.2 ev indicates that the N_2^+ is formed in the $B\,^2\Sigma_u$ state with zero kinetic energy.

4. N^+

The ionization efficiency near threshold for N^+ from N_2O is shown in Fig. 5. This ion carries kinetic energy, and a plot of ion kinetic energy vs appearance potential is shown in Fig. 6. The intercept of the kinetic-energy plot agrees with the measured appearance potential of N^+ and so the N^+ is formed with zero kinetic energy at onset. The result for the appearance potential of N^+ from N_2O is AP = 20.81±0.1 ev. Now, since

$$D(N-NO) \leq AP(N^+) - I(N),$$

then with $I(N) = 14.54$ ev, the spectroscopic value[10] for the ionization potential of nitrogen, the dissociation energy for the N—NO bond $D(N-NO) \leq 6.27$ ev if the NO fragment carries no internal energy. The fact that the NO fragment does have internal energy is shown later. The N_2 and NO impurities do not contribute N^+ since $AP(N^+/N_2)$ is about 24 ev and $AP(N^+/NO)$ is about 22 ev, and the mean free path of electrons for these processes is large.

5. O^+

The ionization efficiency for O^+ is shown in Fig. 7. The appearance potential $AP(O^+) = 15.49 \pm 0.10$ ev,

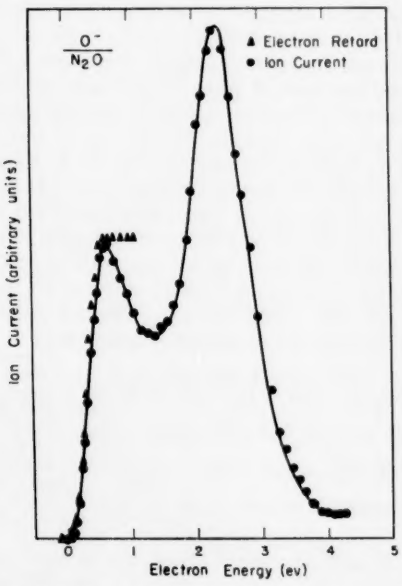

FIG. 8. Ionization efficiency of O^-/N_2O. An electron retarding curve is shown which is used to locate the zero of the electron energy. Zero energy is taken as the intercept of the retarding curve with the electron energy axis.

[10] C. E. Moore, Natl. Bur. Standards U.S. Circ. No. **467** (1949).

TABLE I. Appearance potentials of ions from N_2O.

	Present	Previous work		
N_2O^+	12.63±0.05	12.9±0.5[a]	13.09±0.05[b]	12.72[c]
NO^+	13.75±0.10	15.3±0.5[a]	15–16.9[b]	
N_2^+	17.0 ±0.2			
N^+	20.81±0.10	21.4±0.5[a]		
O^+	15.49±0.10	16.3±1[a]	15.33±0.02[b]	
O^-	0–0.05			

[a] See the work cited in footnotes 1 and 2.
[b] See the work cited in footnote 3.
[c] See footnote 5.

and since

$$D(N_2-O) \leq AP(O^+) - I(O)$$

with $I(O) = 13.61$ ev, the spectroscopic value,[10] then $D(N_2-O) \leq 1.88$ ev. This ion was observed to have zero kinetic energy. The presence of an O^+ from the NO impurity is not observed, since $AP(O^+/NO)$ is about 19 ev.

6. O^-

An O^- ion was observed with an onset in the range 0 ev to 0.05 ev. The negative ion efficiency curve is shown in Fig. 8 along with an electron retarding curve which is used to calibrate the energy scale. Now,

$$D(N_2-O) \leq AP(O^-) + EA(O),$$

where $EA(O)$ is the electron affinity of oxygen, and AP(O) = 0+0.05 ev. With the electron affinity of oxygen[11] $EA(O) = 1.465 \pm 0.005$ ev, then $D(N_2-O) \leq 1.47$ ev. Kinetic-energy measurements near threshold for this ion were not possible because of low intensity of the O^-. Measurements of kinetic energy above 1 ev were not inconsistent with those of Schulz.[12] The onset in the range of 0 to 0.05 ev is in good agreement with Schulz's measurements using a total-ionization tube.

IV. DISCUSSION

Table I compares the present determination of appearance potentials with previous values. For the determination of the N_2—O bond strength, five upper limits were obtained as described above. Further, if $D(N-NO) = 4.50 \pm 0.1$ ev, as determined from the $AP(NO^+)$,

$$D(N_2-O) = D(N-NO) + D(N-O) - D(N-N),$$

with the values[13] $D(N-O) = 6.49 \pm 0.05$ ev and $D(N-N) = 9.76$ ev gives $D(N_2-O) \leq 1.23 \pm 0.15$ in agreement with the values of $D(N_2-O)$ obtained from

[11] L. M. Branscomb, J. Chem. Phys. **29,** 452 (1958).
[12] G. J. Schulz (to be published).
[13] A. G. Gaydon, *Dissociation Energies* (Chapman and Hall, Ltd., London, 1953).

$AP(O^-)$ and $AP(N^+)$. It is suggested that the high value 1.88 ev for $D(N_2-O)$ obtained from $AP(O^+)$ results from vibrational excitation of the N_2 fragment molecule formed in the dissociation. This would require $v=2$ in the $X\,^1\Sigma_g$ state of N_2. Also, since the derived value for $D(N_2-O)\leq 1.23\pm 0.15$ from $D(N-NO)=4.50+0.1$ ev is in agreement with the values obtained from $AP(O^-)$ and $AP(N^+)$, it is suggested that the value $D(N-NO)=6.27$ ev obtained from the $AP(N^+)$ is high as a result of vibrational excitation of the NO fragment molecule. This would, however, require excitation to $v=5$ in the $X\,^3\Pi$ state. It is concluded that $D(N-NO)\leq 4.50\pm 0.1$ ev. The values 1.40 ± 0.2 ev, 1.37 ± 0.2 ev, 1.36 ± 0.2 ev, and 1.23 ± 0.15 ev have been obtained for upper bounds on $D(N_2-O)$ from $AP(N_2^+)$ and $AP(NO^+)$ and give an average value of $D(N_2-O)\leq 1.34+0.2$ ev. The value of $D(N_2-O)$ obtained from $AP(O^-)$ is not included in the average, since information was not obtained on the kinetic energy of O^- at threshold and thus the value of $D(N_2-O)\leq 1.47$ ev may not be a lowest upper bound. Thermochemical data[14] give the heat of formation of N_2O as $\Delta Hf°=20.31$ kcal/mole at 0°K. Combining this with the value[15] $D(O-O)=5.114+0.002$ ev, one has $D(N_2-O)=1.67$ ev. The discrepancy of 0.33 ± 0.2 ev, if significant, cannot be given a satisfactory explanation.

Finally, it should be emphasized that the values of $D(N_2-O)$ and $D(N-NO)$ presented are least upper bounds for the dissociation energies and would be revised only downward in the event that there were more internal energy carried off by neutral fragments than has been allowed for here.

ACKNOWLEDGMENTS

We wish to thank G. J. Schulz and A. V. Phelps for stimulating discussion of the work reported here. We are indebted to J. Kearney for technical assistance.

[14] F. D. Rossini, D. D. Wagman, W. H. Evans, S. Levine, and I. Jaffe, Natl. Bur. Standards U.S. Circ. No. **500** (1952).
[15] P. Brix and G. Herzberg, J. Chem. Phys. **21**, 2240 (1953).

Ionization Processes in CCl_4 and SF_6 by Electron Beams

R. E. Fox and R. K. Curran

Westinghouse Research Laboratories, Pittsburgh, Pennsylvania

(Received October 26, 1960)

The ionization processes in CCl_4 and SF_6 have been studied for both positive and negative ions in a mass spectrometer, and in a total ionization tube. The appearance potential of Cl^- is 0+0.05 ev with a very sharp energy dependence. A second process with an onset at about 0.4 ev and a maximum at about 0.7 ev, exhibits a much broader energy dependence. The relative intensities of these two processes are found to be extremely sensitive to the energy distribution of the electron beam, but do not appear to exhibit a temperature dependence. From the appearance potentials and kinetic energy measurements of Cl^- a value of 3.30±0.07 ev is obtained for $D(CCl_3-Cl)$. The appearance potential curves for CCl_3^+ and SF_5^+ near threshold indicate structure which may be associated with energy states of these ions.

I. INTRODUCTION

IONIZATION by electron impact in CCl_4 vapor has been studied by a number of investigators.[1–8] Most of the investigations have dealt with the formation of negative ions. Warren and Craggs[8] studied the positive ion formation, while Baker and Tate[1] studied both positive and negative ions. Reese *et al.*,[5] in studying the ion formation with a mass spectrometer, showed that the predominant ion was Cl^- and was formed at about zero energy. Cl_2^- was found to be about 45 times less abundant, while the CCl_3^- ion was found to be about 450 times less abundant than the Cl^- ion.

Studies of the Cl^- ion current as a function of electron energy, resulting presumably from the process $CCl_4+e\rightarrow Cl^-+CCl_3$, have resulted in quite different shapes observed by different investigators. For example, Baker and Tate[1] observed a single peak, as did Craggs *et al.*[2] and Reese *et al.*,[5] while a double peak was observed by Marriott *et al.*[4] as well as by Hickam and Berg[6] and by Buchel'nikova.[7] Although the relative intensities of these two peaks differed in each case, the energy separation of the two maxima agrees reasonably well. Hickam and Berg[6] reported that the relative intensities of the two peaks varied with the ion-source temperature, and proposed the possibility that the effect might be due to electron capture by molecules in differently excited states. This effect was reported for several molecules. Buchel'nikova concluded that the differences in peak shape were due to the electron energy distribution used to form the negative ions. The present experiments were undertaken in an effort to establish if the temperature effect was real or whether the effect could be explained entirely by the electron energy distribution.

II. EXPERIMENTAL PROCEDURE

The present experiments were performed with two separate instruments. The ionization probabilities for different ionization processes were studied with a 90° sectored field mass spectrometer.[9,10] The total ionization as a function of electron energy was studied with a so-called total ionization tube.[10,11] Both instruments were equipped with an electron gun which enabled the use of the retarding potential difference method[12] for obtaining ionization due to essentially monoenergetic electrons.

In both the total ionization tube and the mass spectrometer considerable difficulty was encountered due to chemical reactions of CCl_4, and to a much lesser extent of SF_6, with the tungsten filament and the gold-plated electrodes. Thoriated iridium and rhenium filaments were tried in an effort to minimize the chemical attack on the hot filaments. A study of Cl^+ ions in the mass spectrometer indicates the presence of free chlorine. It is presumed that the hot filaments dissociate the CCl_4, thus producing free chlorine, some of which reacts with the tungsten to form tungsten chloride which volatilizes at the filament temperature. Neither thoriated iridium nor rhenium showed any appreciable improvement over tungsten in this respect. Tungsten chloride is undoubtedly deposited on the adjacent electrode surfaces. In addition, some of the liberated chlorine apparently also reacts with the gold-plated electrodes to form insulating gold chloride surfaces. This is evidenced by a considerable degeneration

[1] R. Baker and J. Tate, Phys. Rev. **53**, 683 (1938).
[2] J. Craggs, C. M. McDowell, and J. Warren, Trans. Faraday Soc. **48**, 1093 (1952).
[3] J. Marriott and J. Craggs, Electrical Research Associates Rept L/T 308 (1954).
[4] J. Marriott, R. Thorburn, and J. Craggs, Proc. Phys. Soc. (London) **B67**, 437 (1954).
[5] R. Reese, V. Dibeler, and F. Mohler, J. Research Natl. Bur. Standards **57**, 367 (1956).
[6] W. M. Hickam and D. Berg, in *Advances in Mass Spectrometry*, edited by J. D. Waldron (Pergamon Press, New York, 1959), p. 458.
[7] I. S. Buchel'nikova, J. Exptl. Theoret. Phys. (U.S.S.R.) **35**, 1119 (1958).
[8] J. W. Warren and J. D. Craggs, *Mass Spectrometry* (Institute of Petroleum, London, 1952), p. 36.
[9] R. E. Fox, *Advances in Mass Spectrometry*, edited by J. D. Waldron (Pergamon Press, New York, 1959), p. 397.
[10] R. E. Fox, *Positive and Negative Ion Formation by Electron Beams*, Westinghouse Research Laboratories Rept. 10-0302-1-R2.
[11] G. J. Schulz and R. E. Fox, Phys. Rev. **106**, 1179 (1957).
[12] R. E. Fox, W. M. Hickam, D. J. Grove, and T. Kjeldaas, Rev. Sci. Instr. **26**, 1101 (1955).

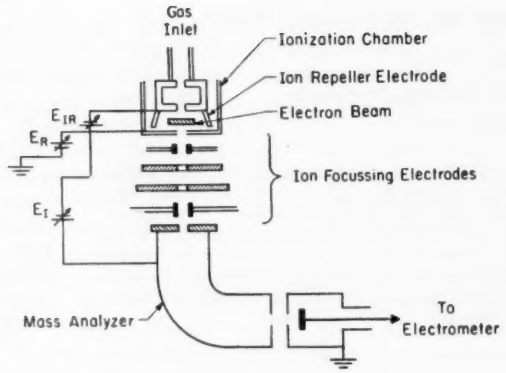

FIG. 1. A schematic representation of the mass spectrometer ion slit system and accelerating voltages.

in the performance of the electron gun resulting in a broadening of the electron energy distribution as well as in a shift in electrode contact potentials. In an effort to minimize these effects, the electrode surfaces of the total ionization tube were coated with colloidal graphite suspended in alcohol by means of a spray gun (artist's air brush). It was possible to obtain a smooth coating which could withstand temperatures up to 450°C without deterioration. It was reasoned that any chemical reaction would result in a volatile compound which would prevent insulating surfaces from forming. Although there was some slight improvement, the deterioration of the energy distribution was still marked.

The total ionization tube was wrapped with a Nichrome wire-asbestos furnace with which the tube could be operated at temperatures up to 325°C. Higher temperatures were not feasible due to excessive electrical leakage. The total ionization tube was connected to an ultra-high vacuum system which could be baked at temperatures up to 450°C. After bakeout for several hours at this temperature and upon subsequent cooling to room temperature the base pressure was of the order of 10^{-10} Torr. At temperatures up to 300°C the base pressure did not exceed 10^{-8} Torr. There was no evidence that contaminants due to degassing at these elevated temperatures were producing any extraneous effects.

The mass spectrometer was operated with the ion source at ground potential and the analyzer section at elevated voltages in a manner similar to that previously reported.[13] A schematic of the mass spectrometer is shown in Fig. 1. Electrons from a hot filament are collimated by a small auxiliary magnet and pass through a series of slits which form an electron gun capable of using the retarding potential difference method. This gun is essentially the same as previously reported.[12] The gas is admitted from the gas handling system through the inlet directly into the ionization chamber through a slit in the ion-repeller electrode just above the electron beam. The *u*-shaped ion-repeller electrode affords some focusing for extracting the ions from the bottom of the ion source through the first ion slit. The ions are then focused and accelerated through a series of electrodes which are arranged essentially as originally employed by Nier.[14]

The arrangement shown allows the maximum kinetic energy of the ions to be determined. By varying the ion source potential with respect to ground, a retarding curve can be obtained for each ion. An ion known to be formed with zero kinetic energy is used to establish the zero of the kinetic-energy scale. A comparison of the vanishing currents of the ion retarding curves is then a measure of the maximum kinetic energy.

The electron energy is calibrated from electron retarding measurements.[15] A retarding curve for the electron beam serves to determine the zero of the electron-energy scale and to indicate the energy distribution. Since the electron beam has a finite energy spread, two choices are available for determining appearance potentials. One can compare the point of maximum slope of the retarding curve (which corresponds to the maximum of the electron energy distribution) to the ion peak maximum, or one can compare the points of initial onset. The distribution maximum may be used only if the energy function for electron capture is narrow compared to the electron energy spread. Since for most ions, especially those formed by dissociative capture, this does not hold true, the use of this method can result in error.

The comparison of the high-energy onset of the electron retarding curve to the high-energy onset of the ion peak will always be correct if they can be determined accurately. The disadvantage lies in that it is not always easy to determine this initial onset. This is especially true for a normal electron distribution which has a long exponential high-energy tail. However, with the RPD method this high-energy tail is essentially eliminated and, if the electron gun is operating properly, the energy distribution is narrow and hence the retarding curve approaches the axis rather steeply with a finite slope at onset. This allows the initial onset to be determined with good accuracy.

III. EXPERIMENTAL RESULTS

A. Mass Spectrometer

1. *Appearance Potentials. Negative Ions*

A mixture of CCl_4 and SF_6 gas is introduced into the mass spectrometer to a total pressure of about 1×10^{-5} Torr. At this pressure the mean free path is sufficiently long to ensure that only primary collision processes take place in the ionization chamber. Figure 2(a) shows the Cl^- ion current (open circles) as a function of electron accelerating voltage and the electron current (solid points) recorded simultaneously. The onset of

[13] R. E. Fox and J. A. Hipple, Rev. Sci. Instr. **19**, 462 (1948).

[14] A. O. Nier, Rev. Sci. Instr. **18**, 398 (1947).

[15] W. M. Hickam and R. E. Fox, J. Chem. Phys. **25**, 642 (1956).

the retarding curve for the electron beam is used to determine zero energy and the shape is an indication of the energy distribution. From Fig. 2(a) it is seen that the electron current and ion current appear at the same energy. From this, one can conclude that Cl^- from CCl_4 is formed at zero electron energy. Shown in Fig. 2(b) are the SF_6^- ion current and electron current similarly recorded as a function of electron accelerating voltage. These data show that the SF_6^- onset is at zero energy in agreement with previous work.[15] The shape of the SF_6^- peak may be used as a measure of the electron energy distribution[15] as well as a differentiation of the electron retarding curve. In this experiment the maximum energy spread is about 0.3 ev with a width at half maximum of about 0.1 ev.

The Cl^- current plotted as a function of electron energy exhibits two peaks within the first 1.5 ev. There is a large sharp peak near zero energy, with a second smaller peak at about 0.75 ev. The width at half-maximum for the Cl^- peak is only about 0.1 ev indicating that this process has an extremely sharp energy dependence. The shape of this peak reflects largely the electron energy distribution.

The onset of the second peak apparently occurs at about 0.4 ev and maximizes at about 0.75 ev above zero. The second peak exhibits a measurable cross section for electron energies up to 1.4 ev. Thus, this peak would not be nearly as sensitive to the electron-energy distribution as the first peak. This undoubtedly accounts for the large discrepancies which may be found in the literature concerning the shape of the Cl^- peak from CCl_4.

From Fig. 2(a) it is seen that the ratio of the first peak to the second peak is about 9.6. Buchel'nikova[7] obtained a ratio of about 1.0, Marriott, Thorburn, and Craggs[4] obtained a ratio of 0.9, Hickam and Berg[6] obtained a ratio of 2.0 at room temperature and showed that this ratio could be varied considerably by changing the temperature of the ion source (0.7 at 250°C). Other experiments observed a single broad peak instead of two peaks.

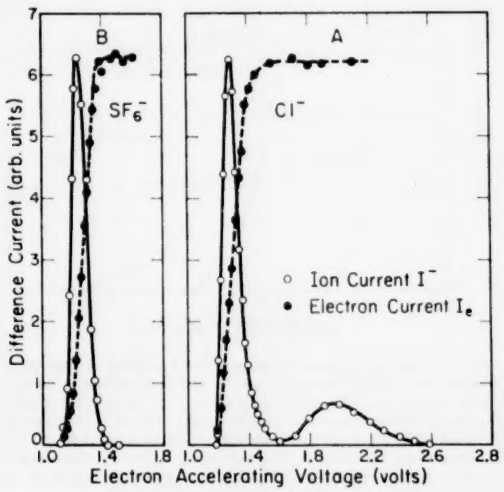

FIG. 2. SF_6^- and Cl^-/CCl_4 as a function of electron energy spread. Open circles show ion current, closed circles show electron current. Onset of I_e curve determines zero energy, and the shape indicates the electron energy distribution.

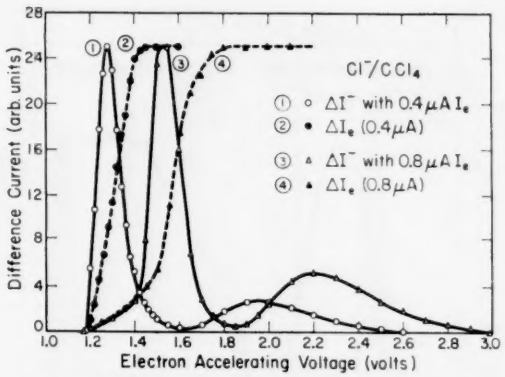
Cl^-/CCl_4
① ○ ΔI^- with 0.4 μA I_e
② ● ΔI_e (0.4 μA)
③ △ ΔI^- with 0.8 μA I_e
④ ▲ ΔI_e (0.8 μA)
Difference Current (arb. units)
Electron Accelerating Voltage (volts)

FIG. 3. Cl^-/CCl_4 and I_e as a function of electron accelerating voltage for two values of electron current. Differences in electron energy distribution are reflected in differences in shapes of Cl^- ion current as a function of electron energy. Onset of I_e curves indicate zero energy.

The separation between the two maxima of 0.7 ev compares to 0.6 ev obtained by Buchel'nikova,[7] 0.75 ev obtained by Marriott *et al.*[4] and 1.0 ev obtained by Hickam and Berg.[6]

The influence of the electron energy distribution on the relative peak heights is illustrated in Figs. 3 and 4. In Fig. 3, curve 1 is the peak shape obtained with the RPD method in which 0.4 μa is used as the difference electron current. Curve 2 is the electron retarding curve from which one can obtain the electron-energy distribution. The difference electron current was increased to 0.8 μa by increasing the filament current, but without increasing the ΔV_R which determines the energy "slice" of the electron-energy distribution. As has been previously shown,[12,15] this increases the electron-energy distribution, due presumably to space-charge effects in the vicinity of the retarding slit. The effect of this increased electron distribution is shown in Curve 3. The first maxima have been normalized to the same height in both cases. It is seen that the second maximum is now approximately twice as large with respect to the first maximum. One also notes that the first peak has been considerably broadened. The increased electron-energy distribution is reflected in the electron retarding curve 4. In Fig. 4 the electron distribution has been broadened by increasing the retarding potential difference (ΔV_R) as well as the electron current. The electron-retarding curve (solid points) indicates a wide energy distribution which is not Maxwellian. The relative intensities of the two peaks have been considerably altered. The

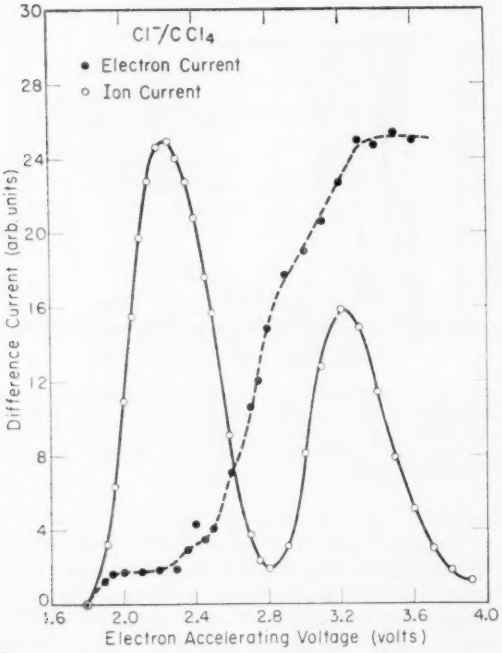

FIG. 4. Cl^-/CCl_4 and I_e for a greatly increased electron energy distribution. Note that not only are the two maxima broadened but that the higher energy peak is greatly increased in intensity relative to the low energy peak.

ratio of the first peak to the second peak is less than 2:1 compared to a ratio of 9.6:1 shown in Fig. 2(a) for a narrow energy distribution.

These data show the importance of knowing the electron-energy distribution in interpreting the peak shapes of ions obtained by electron capture. It is not clear why the peak shape obtained by Buchel'nikova[7] does not exhibit a larger relative intensity for the low-energy peak since she claims to have an electron-energy distribution of only 0.2–0.3 ev. From the shape of the curve for the total negative ion current for SF_6 shown in the same article, the typically sharp peak due to SF_6^- is considerably decreased in amplitude compared to that portion of the curve attributed to SF_5^-. The curve shown would seem to indicate a larger electron energy distribution than that claimed in the studies of the formation of negative ions in SF_6 and CCl_4.

2. *Kinetic-Energy Measurements*

The kinetic energy of the ions was determined by a retardation at the collector end discussed above, by two methods. (*a*) *Constant electron energy.* With the electron energy adjusted to yield the first peak (0.12 ev), the ion retarding potential E_R was increased and the difference ion current as a function of retarding voltage was recorded. The electron energy was increased to the second maximum (0.75 ev) and a similar curve taken. A similar curve was taken for the SF_6^- ion. These results are shown in Fig. 5. The amount of kinetic energy is determined by a comparison with SF_6^- which is formed with essentially zero (thermal) kinetic energy. Only the high E_R portions of the Cl^- and SF_6^- curves are shown. The difference in maximum kinetic energy of the ions is given by the difference in the vanishing points of the Cl^- curves with respect to the SF_6^- curves. The Cl^- curve for ions produced at the first maximum (0.12 ev) shows a maximum kinetic energy of 0.4 ev while the Cl^- ions produced at the second maximum (0.75 ev) possess a maximum kinetic energy of 0.70 ± 0.05 ev. Since the sensitivity of collection for kinetic-energy ions is dependent on the ion repeller voltage E_{IR}, curves were obtained using several ion-repeller voltages.[16] The results showed that the measured kinetic-energy difference between SF_6^- and Cl^-/CCl_4 was not dependent on the ion-repeller voltage.

(*b*) *Constant retarding voltage.* A second method for determining the kinetic energy involved a study of the appearance potential as a function of the ion retarding voltage. In this case the ion retarding voltage is set at a series of values, and at each value the electron energy was changed to produce the ion current as a function

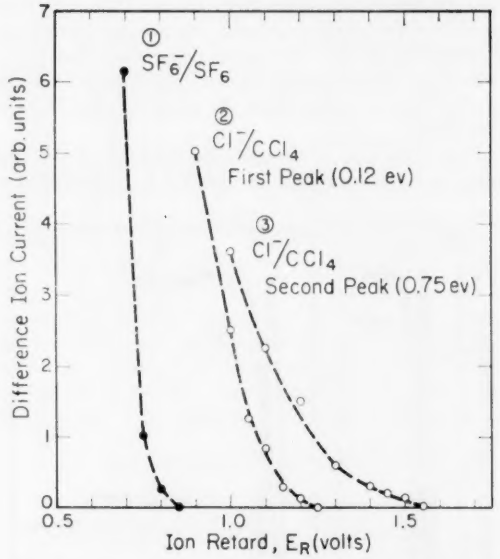

FIG. 5. Ion current as a function of ion retarding voltage to determine ion kinetic energy. Curve 1 is taken with the electron energy set to yield the maximum current of SF_6^-. The onset of this curve determines zero kinetic energy. Curve 2 is taken for Cl^- ions at the low energy maximum. Curve 3 is taken for ions at the second maximum. The difference between the onset of the SF_6^- curve and each of the Cl^- curves is a measure of the kinetic energy of Cl^-/CCl_4 formed by each process.

[16] Since the ion repeller voltage influences the electron energy, the electron energy was adjusted in each case to yield the maximum ion current.

of electron energy. The data for SF_6^- are shown in Fig. 6(a) while that for the low-energy (large-peak) process to form Cl^- is shown in Fig. 6(b). In neither case is there a shift in appearance potential indicating that both ions are formed with zero-energy electrons. This method results in a difference in kinetic energy between the two ions of 0.3 ± 0.1 ev in good agreement with the result of the first method. It should be emphasized that the absence of a shift in the appearance potential shows that all Cl^- ions formed in the low-energy process have the same kinetic energy and thus the value 0.40 ± 0.05 ev obtained by the first method can be taken as the more accurate value for the kinetic energy of these ions.

3. *Appearance Potentials. Positive Ions*

The appearance potential curve for Cl^+ was studied near the threshold. A value of 12.83 ± 0.1 ev is obtained for $A(Cl^+)$. These data exhibit a linear behavior with a break in the curve at 16.10 ± 0.2 ev. The initial onset at 12.83 ev is in reasonably good agreement with the spectroscopic value of 13.01 ev for the ionization potential[17] of $Cl[I(Cl^+/Cl)]$. The break at 16.19 ev may then be attributed to $A(Cl^+/CCl_4)$.

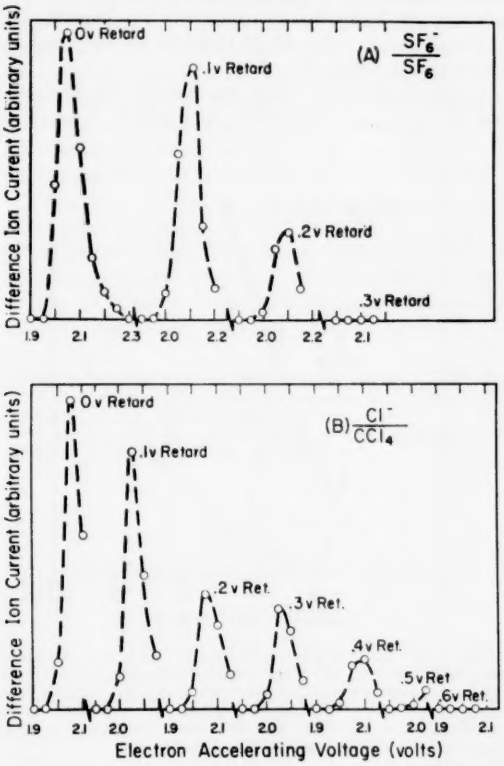

FIG. 6. (a) Appearance potential curves for SF_6^- for different ion retarding voltages. (b) Appearance potential curves for Cl^-/CCl_4 for different ion retarding voltages. Retarding voltage differences at which SF_6^- and Cl^- disappear is a measure of kinetic energy of Cl^-/CCl_4.

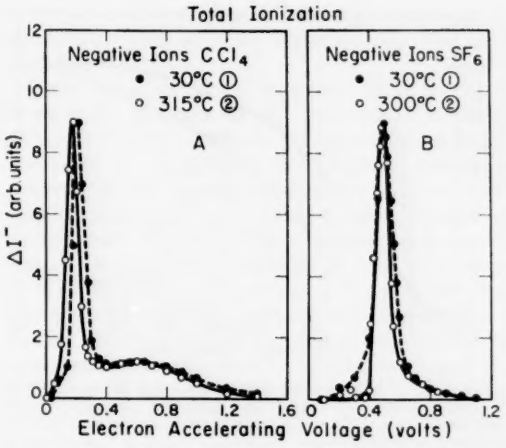

FIG. 7. Total negative ions of SF_6 and CCl_4 as a function of electron energy with the gases at room temperature, and at an elevated temperature. Minor differences in shape can be attributed to differences in electron energy distribution in each case.

B. Total Ionization Tube Measurements

1. *Temperature Effects on Peak Shape*

The earlier work by Hickam and Berg[6] indicated a large change in peak shape of several ions as a function of the ion source temperature.

In the present experiment it was not possible to change the mass spectrometer ion source temperature, so the effect was studied with the total ionization tube[10,11] described above. Either SF_6 or CCl_4 was admitted to the system at the desired pressure and the ion current measured as a function of electron energy. The RPD method was employed to obtain a narrow energy distribution. The electron-energy distribution was monitored by obtaining electron retarding curves. As mentioned in Sec. II, considerable difficulty was encountered due to pyrolysis effects at the hot filament. For this reason the purity of the CCl_4 in the system was not known even though CCl_4 vapor flowed through the system at an appreciable rate. From a comparison of the data taken with the mass spectrometer, however, any contaminants were probably too small to produce appreciable effects.

The peak shapes of the total negative ions from CCl_4 are shown in Fig. 7(a), with the tube at essentially room temperature (30°C) and at 315°C. In Fig. 7(b) are shown curves for negative ions of SF_6 also obtained at these two temperatures. It is seen from these curves, which have been normalized to the same

[17] C. E. Moore, *Atomic Energy Levels*, National Bureau of Standards Circular No. 467 (U. S. Government Printing Office, Washington, D. C., 1952).

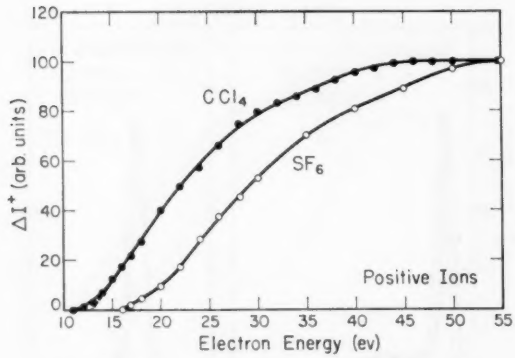

FIG. 8. Total positive ionization for CCl_4 and SF_6 as a function of electron energy. The two curves have been normalized to the same amplitude at 55 ev. Energy scale is determined from an electron retarding curve.

maximum height, that there is very little change in the peak shape.

From electron retarding curves (not shown) there were small changes in the electron-energy distribution also as a function of temperature. After the tube had been in use for some time the electron-energy distribution became very poor, especially at room temperature, but it could be greatly improved by heating the tube to temperatures above 275°C. Apparently, the halogens create insulating surface films on the electrodes which greatly disturb the electron beam. These insulating films became more conducting at elevated temperatures and hence the electron beam behaves in a more normal manner. These changes in electron-energy distribution produce large changes in the shapes of the observed ion currents.

When the tube temperature is varied between 30° and 300°C there are no observed changes in the peak shapes which cannot be accounted for by changes in the electron-energy distribution within the accuracy of the experiment.

2. *Positive Ions*

The positive ions formed in CCl_4 and SF_6 were observed with the total ionization tube using the RPD method for a narrow electron-energy distribution. These results are shown in Fig. 8 for electron energies up to 55 ev where the two curves have been normalized to the same maximum value. It was not possible to obtain accurate measurements of cross-section values since the pyrolysis at the filament resulted in an uncertainty in gas composition and density.

The appearance potential curves of the positive ions near threshold are shown in Fig. 9. Curve 1 is the appearance potential of positive CCl_4 ions. The energy scale has been corrected by using the electron retarding curve to determine zero energy.

It has been shown[8] that CCl_4^+ is not observed by normal electron impact, and that the lowest appearance potential is due to CCl_3^+. In the present experiment 11.65±0.10 ev is obtained as a value of the appearance potential of CCl_3^+. This compares favorably with a value of 11.83±0.05 ev obtained by Warren and Craggs,[8] and a value of 11.47 obtained by Watanabe[18] by photoionization.

The curve exhibits a break at 12.6 and 13.5 ev. These cannot be due to the formation of other ions since Warren and Craggs[8] obtain a value of 16.1 ev for the formation of CCl_2^+ and the other ions at even higher energies. It is, therefore, presumed that the breaks exhibited in curve 1 are due to excited states of CCl_3^+. There is a slight possibility that the break at 12.6 ev could be due to Cl^+ from Cl produced by pyrolysis at the filament since the ionization potential of Cl is 13.01 ev, although the agreement is not very good. The first excited state of Cl^+ is 1.5 ev above the ground state and hence the break at 13.5 ev does not fit with this energy separation. From these considerations it is not likely that this portion of the curve is due to Cl^+ ions.

The appearance potential of positive ions from SF_6 shown in curve 2 is due to SF_5^+ since SF_6^+ is not produced. A value of 15.85±0.15 ev is obtained in the present experiment, which is in good agreement with a value of 15.9±0.2 ev obtained by Dibeler and Mohler[19] and a value of 15.77±0.05 ev obtained by Marriott and Craggs.[20]

Breaks in the SF_5^+ curve are observed at 17.0±0.2 and 18.0±0.2 ev. Since SF_4^+ is observed to have an

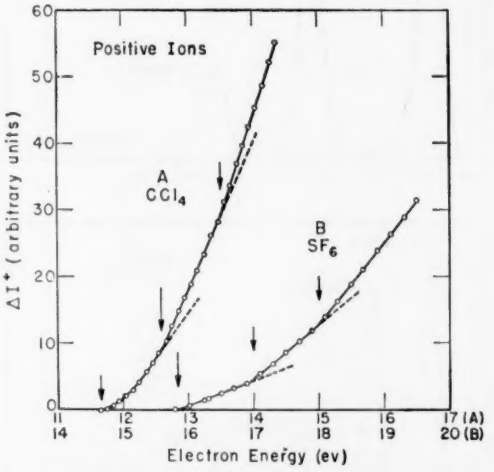

FIG. 9. (a) Total positive ionization for CCl_4 near threshold using RPD method. (b) Total positive ionization for SF_6 near threshold. Labels on energy scales refer to the ions. Arrows indicating onsets of new ionization processes are presumed to be excited states of the CCl_3^+ and SF_5^+ ions. The energy scale is determined by an electron retarding curve.

[18] K. Watanabe, J. Chem. Phys. **26**, 342 (1957).
[19] V. H. Dibeler and F. L. Mohler, J. Research Natl. Bur. Standards **40**, 25 (1948), Washington, D. C.
[20] J. W. Marriott and J. D. Craggs, Electrical Research Associates Technical Rept. L/T 301 (1953).

onset[19,20] at about 18.8 ev, it is concluded that these breaks are due to excited states of the SF_5^+ ion.

IV. DISCUSSION

A. $D(CCl_3—Cl)$

The dissociation of CCl_3—Cl bond can be obtained from the appearance potential (AP) of the Cl^- ion and a measure of its kinetic energy (KE) if one assumes the published value of the electron affinity (EA) of chlorine to be correct and the internal energy (E_i) of the CCl_3 fragment to be zero,

$$AP(Cl^-) = D(CCl_3-Cl) - EA(Cl) + KE + E_i.$$

The measured kinetic energy of Cl^- is 0.40 ± 0.05 ev. This represents 117/152 or 0.77 of the total kinetic energy. Therefore, the total kinetic energy of the dissociation process is 0.52 ± 0.05 ev. If E_i is assumed to be zero and the electron affinity (EA) is 3.82 ± 0.06 ev,[21] then $D(CCl_3-Cl) = 3.82-0.52 = 3.30\pm0.07$. This is in excellent agreement with the thermochemical value[22] of 3.39 ev, but does not agree with the electron impact value of 2.89 ev obtained by Farmer[23] *et al.*

From the appearance potential curve for Cl^+ discussed above, $I(Cl^+/Cl)$ is 12.83 ± 0.1 ev while $AP(Cl^+/CCl_4)$ is 16.10 ± 0.2 ev. This leads to a difference in energy of 3.27 ± 0.3 ev for $D(CCl_3-Cl)$, assuming no kinetic energy of the fragments, or no internal energy of the CCl_3 radical. This is in reasonably good agreement with the value obtained from the study of the negative ions.

The value obtained by Farmer *et al.*[23] is based on the appearance potential of CCl_3^+ from CCl_4 and on the ionization potential of the free radical CCl_3. They obtained a value of 8.78 ev for $I(CCl_3^+)$, and 11.67 ± 0.05 ev for $AP(CCl_3^+)$ from CCl_4. Since the latter is in excellent agreement with the value of 11.65 ± 0.1 ev obtained in this experiment, it would appear that the discrepancy must lie in the ionization potential of the CCl_3 free radical.

From the shape of the ionization curve in Fig. 10 there is no evidence of the pair-formation process $CCl_4+e=CCl_3^++Cl^-+e$, to any measurable extent.

A small Cl^- signal is observed with the mass spectrometer in the energy range above 12.5 ev which may be attributed to the pair-formation process but which is not sufficiently intense to enable a determination of the appearance potential. If this Cl^- ion arises from the pair-formation process, it is not a very probable one. This is in agreement with the findings of Farmer *et al.*[23] Baker and Tate,[1] however, reported the appearance potential of CCl_3^+ at 12.2 ev as well as a fairly intense Cl^- ion whose appearance potential was 12.4 ev. They concluded that the pair-formation process was a fairly probable one. They also report a small CCl_4^+ ion with an appearance potential of 11.0 ev. This ion has not been reported by any other investigator.

B. Low-Energy Formation of Cl^-

From the shape of the curve obtained for Cl^- as a function of electron energy it appears that there is a capture process which has an onset at $0+0.05$ ev with an extremely sharp dependence that is essentially as sharp as the SF_6^- process.

The second process at 0.4 ev is assumed to arise from an excited state of CCl_4^- and since the kinetic energy of 0.7 ev for these ions is only slightly larger than those of the lower energy process, it would suggest that this energy may be dissipated either as radiation or an internal energy of the CCl_3 fragment.

There is no evidence for a gas temperature dependence in the formation of either Cl^- or SF_6^-. Large changes in observed shapes of the energy dependence curves can in all cases be explained by changes in the energy distribution of the electron beam which undoubtedly are due largely to changes in electrical conductivity of insulating deposits on the source electrodes.

---

[21] H. O. Pritchard, Chem. Revs. **52**, 529 (1953).
[22] T. L. Cottrell, *The Strength of Chemical Bonds* (Butterworth Publications, Ltd., London, 1958), 2nd ed.
[23] J. B. Farmer, I. H. S. Henderson, F. P. Lossing, and D. G. H. Marsden, J. Chem. Phys. **24**, 348 (1956).

The State of the Nd^{3+} Ion as Derived from the Absorption and Fluorescence Spectra of $NdCl_3$ and Their Zeeman Effects*

E. H. Carlson and G. H. Dieke

The Johns Hopkins University, Baltimore, Maryland

(Received October 3, 1960)

The absorption and fluorescence spectra of Nd^{3+} in $NdCl_3$ diluted by $LaCl_3$ have been examined with their Zeeman effect at 4.2° and less completely also at 77°K. The empirical energy-level diagram is complete up to 28 000 cm^{-1} except for the location of the ^2K term. Crystal Stark splittings, magnetic properties, and intensities are compared to calculated values obtained from an intermediate coupling calculation of the $4f^3$ configuration.

I. INTRODUCTION

SEVERAL investigators in the past have obtained absorption spectra of Nd^{3+} salts at low temperatures.[1–3] A comparison of these data with calculations made in various stages of approximation[2,4–8] has given considerable insight into the structure of the energy levels of the Nd^{3+} ion and energy-level splitting in the crystalline electric field.

The anhydrous chlorides of the rare earths diluted with $LaCl_3$ give, in general, considerably sharper lines than other salts and are largely free from superposed molecular and lattice vibrations. Furthermore, because of the fact that they give strong fluorescence,[9] they make it possible to obtain the important low-lying levels and, because of the high symmetry (C_{3h}) of the crystalline field, the Stark and Zeeman effect calculations are relatively easy.

The present paper gives the results of a study of the absorption and fluorescence spectra of anhydrous $NdCl_3$ including the Zeeman effect at 4.2° and 77°K. The data were analyzed with the help of intermediate coupling calculations of the energy levels of the $4f^3$ configuration[10] for various values of the spin-orbit coupling parameter. Similar calculations by Wybourne[8] appeared in the literature after ours were completed.

As the original data are very bulky and the reasoning for assigning quantum numbers is generally the same, only the final results will be presented here, and a discussion will be given only of doubtful or newly made assignments.

Greater details can be found in a report[11] issued at a time when the empirical data were completed but the analysis not quite as far advanced as in the present paper.

II. EXPERIMENTAL PROCEDURE

The crystals used for this study contained 2% or 0.2%, respectively, $NdCl_3$ in $LaCl_3$. We are indebted for them to Dr. Hutchison and Dr. Wong[12] of the University of Chicago.

The experimental technique was essentially the same as that used previously in this Laboratory.[3] Because of the hygroscopic properties of the crystals, they were mounted in glass tubes containing several centimeters of helium for heat conduction. The mounting was such as to allow the symmetry axis to be placed parallel or perpendicular to the magnetic field, and the light beam was always perpendicular to the symmetry axis. The fluorescence spectra were photographed on an $f/20$ Wadsworth mounting spectrograph at 5A/mm. The strongest lines come in over the scattered background in a 5-min exposure. With complementary filters on the H-6 source and spectrograph slit, exposures of up to 10^h were made. Experiments with bandpass filters were made to identify the originating state for some of the stronger lines.

At 77°, the lines of the fluorescence and absorption spectra become much broader and weaker, and many lines disappear. However, some new lines appear and are useful in establishing otherwise unidentified levels. The Zeeman effect at 77°K was not studied.

III. THE GROUND (^4I) MULTIPLET

Figure 1, which gives in the center the empirically found energy levels, indicates by a semicircle those levels from which fluorescence is observed. The lower states of the fluorescent radiation are in many cases the Stark components of the ground multiplet which thus

* This work was carried out with the support of the U. S. Atomic Energy Commission.

[1] H. Ewald, Ann. Phys. **34,** 209 (1939).
[2] R. A. Satten, J. Chem. Phys. **21,** 637 (1953).
[3] G. H. Dieke and L. Heroux, Phys. Rev. **103,** 1227 (1956).
[4] C. K. Jørgenson, Kgl. Danske Videnskab Selskab, Mat.-fys. Medd. **29,** No. 11 (1955).
[5] B. R. Judd, Proc. Roy. Soc. (London) **A250,** 562 (1959).
[6] B. R. Judd and E. Wong, J. Chem. Phys. **28,** 1097 (1958).
[7] B. R. Judd, Proc. Roy. Soc. (London) **A251,** 134 (1959).
[8] B. G. Wybourne, J. Chem. Phys **32,** 639 (1960).
[9] E. Carlson and G. H. Dieke, J. Chem. Phys. **29,** 229 (1958).
[10] E. H. Carlson, Levels of the $4f^3$ configuration in intermediate coupling, Johns Hopkins Spectroscopic Report, No. 19 (1960).
[11] E. H. Carlson, "Absorption and fluorescence spectra of $NdCl_3$ and states of the neodymium ion," Johns Hopkins Spectroscopic Report No. 18 (1960). Limited numbers of this report, and also Report No. 19, are available to interested persons. Report No. 18 has been deposited as Document No. 6658 with the ADI Auxiliary Publications Project, Photoduplication Service, Library of Congress, Washington 25, D. C. A copy may be secured by citing the document number and by remitting $17.50 for photoprints or $5.50 for 35-mm microfilm. Advance payment is required. Make checks payable to Chief, Photoduplication Service, Library of Congress.
[12] C. A. Hutchison and E. Wong, J. Chem. Phys. **29,** 754 (1958).

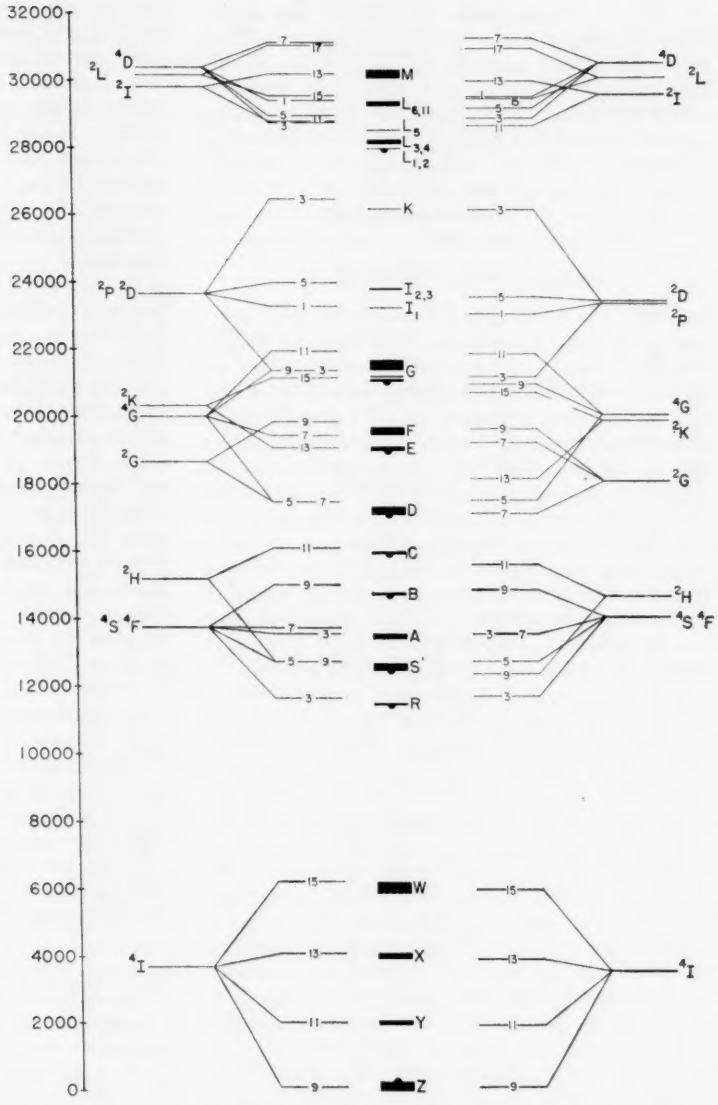

FIG. 1. Energy levels of the Nd^{+3} ion. Units are in cm^{-1}. The calculated levels on the left are Wybourne's calculations. Those on the right are those of footnote 11. The values $2J$ are written on the energy levels. The pendent semicircles indicate fluorescent levels.

can be determined from the frequencies of the emission lines. The results are listed in Table I. The values of the crystal quantum number μ are obtained by comparing the empirical levels with those calculated by Judd,[7] and verifying the results by Zeeman effects and the selection rules (Fig. 2). The last column gives the number of different lines from which a particular level is determined. The error in the penultimate column is approximately half the difference between the extreme values found. Weak and diffuse lines are the reason for some of the relatively large errors. As all levels are based on at least four lines, the chances that accidental coincidences have given spurious levels are very slight.

Transitions to the $^4I_{15/2}$ level in fluorescence are so weak that its components could not be identified from the fluorescence spectrum. Its position in Fig. 1 is taken from infrared absorption lines obtained by Varsanyi.[13]

IV. ABSORPTION DATA. ASSIGNMENT OF EXCITED LEVELS

Previously published work[2,3,5,6,9] demonstrates that the four levels of the ^4F term lie in groups R S A and

[13] F. Varsanyi and G. H. Dieke, J. Chem. Phys. **33**, 1616 (1960). The approximate position of this level was determined by Satten, footnote 2, from absorption at 1.7 μ of a solution of neodymium bromate in D_2O.

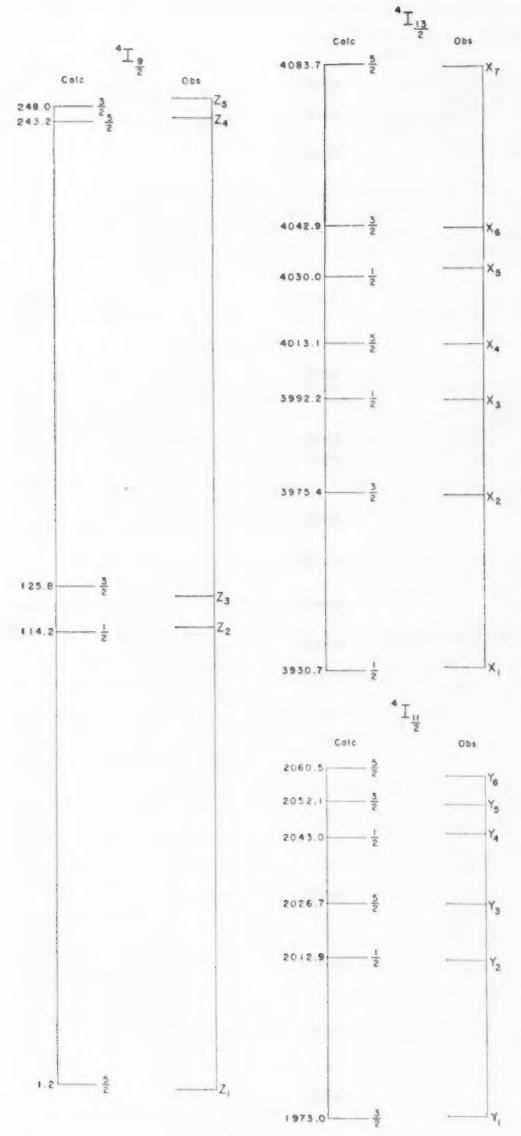

FIG. 2. Stark splitting in the ^4I levels. On the left are given the splittings calculated by Judd (footnote 7) and adjusted so that the center of gravity fits the observed pattern given on the right. The values of the crystal quantum number μ of the calculated levels are given in the center.

B, respectively, ^4S in A, and ^2H in S and C; further that I contains $^2P_{1/2}$ and $^2D_{5/2}$, and K is one component of the levels resulting from the spin orbit interaction of $^2P_{3/2}$ and $^2D_{3/2}$. Our work supports these assignments, in several cases giving much more convincing evidence, through the Zeeman effect 1st-order Stark calculations, than was previously available. The observed absorption spectrum is presented in Table II, together with the Zeeman effect and polarization data. Absorption at 77°K and fluorescence helped establish three levels which are not linked with the ground state by absorption. Estimated intensities are given in column 3; d means diffuse, and S means the line is probably a satellite. In the polarization column for zero field, the unpolarized lines are marked $\sigma\pi$. In the polarization columns for the Zeeman effect, o and i are the polarizations of the outside and inside components of the symmetric four-line patterns. The Zeeman splittings are those of the upper state. For two-line patterns, one of the two possible upper-state splittings is chosen on the basis of either the best fit with the theory, or that the forbidden components of the Zeeman pattern were faintly observed. The entry in the polarization column then has a dash for the supposed position of the missing components. The splittings of the ground state agree within experimental error with the more accurate values of $s_1=-3.996$, $s_2=1.863$ obtained by Hutchison and Wong[12] by paramagnetic resonance. A negative value for s_1 means the component with the negative value of μ is the higher. The entries under "Level" give the LSJ and μ quantum numbers in the usual notation. The predicted Zeeman splitting s_1 and s_2 are those of the RSS coupling approximation of the free ion (Landé g values) with the assumption that there is no M or J mixing either through the crystal field or the magnetic field.

In several groups, notably the B and C group, the Stark components lie so close together that a crystal Paschen-Back effect causes considerable mixing of neighboring Stark components in high magnetic fields. The Zeeman data for groups B and C were also taken at low fields and are included in the report.[11]

For the remaining empirical levels an attempt was made to identify them with expected free-ion levels. For this purpose use was made of the number of lines

TABLE I. Crystal energy levels of ^4I.

Level		μ	Energy (cm^{-1})	Error	Lines
$^4I_{9/2}$	Z_1	5/2	0	...	...
	Z_2	1/2	115.39	±0.2	15
	Z_3	3/2	123.21	±0.1	21
	Z_4	5/2	244.40	±0.5	4
	Z_5	3/2	249.35	±1	4
$^4I_{11/2}$	Y_1	3/2	1973.85	±0.2	7
	Y_2	1/2	2012.58	±0.2	7
	Y_3	5/2	2026.90	±0.3	10
	Y_4	1/2	2044.19	±0.2	5
	Y_5	3/2	2051.60	±0.2	7
	Y_6	5/2	2058.90	±0.2	6
$^4I_{13/2}$	X_1	1/2	3931.84	±1	5
	X_2	3/2	3974.88	±0.2	6
	X_3	1/2	3998.89	±0.2	5
	X_4	5/2	4012.92	±0.2	6
	X_5	1/2	4031.86	±0.2	6
	X_6	3/2	4042.08	±0.2	7
	X_7	5/2	4083	±2	4

in each group, the selection rules, the calculated position of the level, and the first-order calculations of the crystal-field splittings.[14] Especially useful were the Zeeman effect data.

The E group is certainly $^4G_{7/2}$ based on Zeeman effects and first-order Stark effects. The F group and lines G_1 and G_2 which form group $G(I)$ are assigned to the two $J=\frac{9}{2}$ levels resulting from the strong spin-orbit mixing of ^4G and ^2G. Because of this mixing, the Zeeman effect and Stark calculations were not conclusive, but together with line counts and selection rules were sufficient to rule out the ^2K levels. The lines G_7 to G_{14} comprise group $G(\mathrm{III})$. Lines G_7 to G_{10} belong to $^4G_{11/2}$, as both Zeeman and first-order Stark effects show clearly. The remaining lines are assigned as vibration-electronic transitions. Lines G_5 and G_6 comprise group $G(\mathrm{II})$ and are assigned to the lower level resulting from the $^2P_{3/2}$-$^2D_{3/2}$ spin-orbit interaction. The levels F' previously assigned[8,15] to this level are probably due to Pr^{3+} impurity. Wybourne[8] has made the same assignments to groups E, F, $G(\mathrm{I})$, and $G(\mathrm{III})$.

Satten[2] has assigned two strong close lines near 28 000 cm^{-1} to $^4D_{3/2}$. These are L_1 and L_2 in $NdCl_3$ and our data confirm his assignment. The Zeeman effects were not analyzed completely because of satellite structure, but do not contradict this assignment. In addition, the L_5 line is identified with $^4D_{1/2}$. There are other levels which could not yet be identified.

The D group has caused considerable difficulty in past attempts at assignment.[6] The intermediate coupling calculations show that $^4G_{5/2}$ and $^2G_{7/2}$ lie close together here.[8,10] Line D_1 is a strong transition to a $\mu=\frac{1}{2}$ level with parallel splitting $s_1=1.34$ and perpendicular splitting $s_2=0.72$. The μ assignment is well established by $\sigma\pi$ polarization in absorption and by transitions in fluorescence. No Paschen-Back shifts are observed, although two faint σ polarized lines D_2 and D_3 with unobservable Zeeman effects lie close by, representing transitions to $\mu=\frac{3}{2}$ levels. Starting about 65 cm^{-1} above are three strong, very broad and structured absorption bands. Unfortunately, the observed Zeeman effects do not at all fit either $^4G_{5/2}$ or $^2G_{7/2}\mu=\frac{1}{2}$ levels for D_1. In each case, s_1 is too large and s_2 much too small. In intermediate coupling $^4G_{5/2}$ is nearly pure, while $^2G_{7/2}$ becomes[10]

$$-0.0369\,|^4F\rangle+0.0743\,|(10)^2F\rangle+0.0731\,|(21)^2F\rangle$$
$$+0.5516\,|^4F\rangle+0.5413\,|(20)^2G\rangle-0.4486\,|(21)^2G\rangle$$
$$+0.4349\,|^4G\rangle$$

for $\chi=2.60$. The resulting g values are still in complete disagreement. The Stark effect will mix these $J=\frac{5}{2}$ and $\frac{7}{2}$ levels. A calculation of s_1 and s_2 based on such a mixture and including the off-diagonal in J terms between $^4G_{5/2}$ and $^4G_{7/2}$ still could not explain the small value of s_2. Finally, the effects of mixing $^2K_{13/2}$ into the above two levels through the Stark effect were considered. It is then possible to choose the mixing coefficients such as to reproduce the observed Zeeman splittings. It is possible that part of the absorption observed in the bands D_4, and D_5, and D_6 is due to $^2K_{13/2}$ levels. Further experimental data on the D levels are needed to elucidate their origin completely.

V. INTERMEDIATE COUPLING

For many of the above assignments the calculations[16] of EJR to obtain a Russel-Saunders coupling approximation energy-level diagram for f^3 were sufficient. Better results can be achieved when interactions between different LS levels because of spin-orbit coupling are taken into account (intermediate coupling). For this reason calculations were made[10] which take into account completely the electrostatic and spin-orbit interactions within the $4f^3$ configuration. These were based on the values of the matrix elements given by Judd and Louden[15] and hydrogenic wave functions which makes it possible to express all results in terms of two parameters, the Slater integral F_2, and the spin-orbit interaction constant ζ for one $4f$ electron. The energies were obtained as a function of $\chi=\zeta/F_2$ for $-6.8<\chi<+10.00$.

The results of these calculations are equivalent to those of Wybourne[8] but are not identical with them. Wybourne took the constants F_2, F_4, and F_6 as well as ζ as independent parameters to be adjusted to fit the empirical levels best, whereas in our calculations, based on those of Judd,[16] F_4 and F_6 are expressed in terms of F_2. This produces small, not very significant differences in the energy levels calculated by the two procedures, which are seen in the difference between the left and right sides of Fig. 1. Naturally with more adjustable parameters one can expect somewhat better agreement between calculated and empirical levels with Wybourne's calculations, but the differences are not sufficient to say, in view of other neglected interactions, that the nonhydrogenic wave functions implied in Wybourne's values are necessarily superior. Until more levels of the $4f^3$ configuration are found and the shift of the center of gravity of Stark groups from their free-ion position are taken into account, it is unlikely that the Slater integrals F_n calculated by Judd can be much improved. Empirical values of the free-ion levels would be of great help for this, and investigations are now under way in this Laboratory to obtain such levels from the emission spectrum of Nd vapor.

The calculations also gave the wave functions from the eigenvectors of the problem. These, for $F_2=337$ cm^{-1} and $\zeta=2.60$, may be used to calculate a number of quantities and to compare them with observed values.

[14] The following values of the crystal field parameters determined by Judd, footnote 7, were used. $A_2^0=103.7$ cm^{-1}; $A_4^0=-36.0$ cm^{-1}; $A_6^0=-44.5$ cm^{-1}; $A_6^6=426.2$ cm^{-1}.

[15] B. R. Judd and R. Louden, Proc. Roy. Soc. (London) **A251**, 127 (1959).

[16] J. P. Elliott, B. R. Judd, and W. A. Runciman, Proc. Roy. Soc. (London) **A240**, 509 (1957).

TABLE II. Absorption spectrum data.

			Zeeman effect							
				$H \| A_3$		$H \perp A_3$				
				s_1	Pol.	s_2	Pol.	Upper level	Predicted[a]	
Line	ν(cm^{-1})	I	Pol.	L.U.	o i	L.U.	o i	$2s+^1L_J(\mu)$	s_1	s_2
R_1	11 423.90	15d	σ π	+0.40	σ π	0.80	σ π	$^4F_{3/2}(1/2)$	0.40	0.80
R_2	453.91	15d	σ	+1.26	— σ	0	σ	$^4F_{3/2}(3/2)$	1.20	0
S_1	12 458.37	15	σ π	+1.22	σ π	2.90	σ π	$^4F_{5/2}(1/2)$	1.03	3.09
S_2	480.65	15	σ	+2.81	— σ	0	σ	$^4F_{5/2}(3/2)$	3.09	0
S_3	487.47	1	σ			0	σ	$^4F_{5/2}(5/2)$	5.14	0
S_4	536.14	1	σ π					$^2H_{9/2}(5/2)$		
S_5	555.73	12	σ	−0.04	σ —			$^2H_{9/2}(3/2)$		
S_6	643.52	1dd	σ π							
S_7		1ddd	σ π							
S_8	662.91	8ddd	σ π							
A_1	13 396.05	12	σ π	+1.06	σ π	4.64	σ π	$^4F_{7/2}(1/2)$	1.24	4.95
A_2	400.02	2	σ π					$^4F_{7/2}(5/2)$		
A_3	474.53	15ddd	σ					$^4F_{7/2}(3/2)$	3.71	0
A_3'	488.08		b					$^4F_{7/2}(5/2)$		
A_4	527.22	15	σ π	+2.10	c	2.96	c	$^2S_{3/2}(1/2)$	2.00	4.00
A_5	529.37	8S	σ					sat.		
A_6	531.23	12	σ	+5.97	c	0.92	c	$^2S_{3/2}(3/2)$	6.00	0
A_7	533.33	1S	σ					sat.		
B_1	14 705.73	1	σ π	−5.91	σ π	0.08	c	$^4F_{9/2}(5/2)$		
B_2	710.70	2	σ		σ	0.52	c	$^4F_{9/2}(5/2)$		
B_3	715.30	7d	σ	+3.70	— σ	1.36	c	$^4F_{9/2}(3/2)$		
B_4	721.87	5	σ π	+1.33	σ π	4.38	c	$^4F_{9/2}(1/2)$	1.33	6.67
B_5	579.24	5dd	σ	−10.91	σ —	0	σ	$^4F_{9/2}(3/2)$		0
C_3	15 907.08	5d	σ	−9.11	σ —	0.23	σ	$^2H_{11/2}(3/2)$		
C_4	923.91	b				2.59	c	$^2H_{11/2}(5/2)$		
C_5	948.12	5d	σ π	+0.65[c]	σ π	3.98	σ π	$^2H_{11/2}(1/2)$		
C_6	953	1	σ			3.75	c	$^2H_{11/2}(3/2)$		
C_7	960.77	5d	σ π	−11.35	π σ	0.17	σ π	$^2H_{11/2}(1/2)$		
D_{1a}	17 093.77	1S						sat.		
D_1	095.12	15	σ π	+1.34	σ π	0.72	π σ			
D_{1a}	097.25	1S						sat.		
D_2	098.94	2								
D_3	099.92	2								
D_4	165.17	12dd	σ							
D_5	228.75	9ddd	σ							
D_6	297.44	9ddd	π							
E_4	18 993.59	7	σ	+2.95	— σ	0	σ	$^4G_{7/2}(3/2)$	2.95	0
E_5	19 012.88	b				2.47		$^4G_{7/2}(5/2)$		
E_6	042.34	12	σ π	+0.92	σ π	3.46	σ π	$^4G_{7/2}(1/2)$	0.98	3.94
E_7	078.02	b						$^4G_{7/2}(5/2)$		
F_1	19 430.93	12	σ π	+0.64[d]	σ π	5.01	π σ	$^2G_{9/2}(1/2)$	1.11	5.56
F_2	434.75	12	σ	−9.96	σ —	0	σ	$^2G_{9/2}(3/2)$		0
F_3	454.60	3	σ	+2.19		0.84		$^2G_{9/2}(3/2)$		0
F_4	458.72	b						$^2G_{9/2}(5/2)$		
F_5	546.65	8dd	σ π							
F_6	556.10	8ddd	π							
F_7	653.67	6ddd	σ							

TABLE II.—*Continued.*

Line	ν(cm^{-1})	I	Pol.	Zeeman effect $H\|\|A_3$ s_1 L.U.	Pol. o i	Zeeman effect $H\perp A_3$ s_2 L.U.	Pol. o i	Upper level $2s+^1L_J(\mu)$	Predicted[a] s_1	Predicted[a] s_2
G_1	21 029.08	4	σ π	+1.19	σ π	4.40	π σ	$^4G_{9/2}(1/2)$	1.27	6.36
G_2	042.33	2	σ	+1.02	— σ			$^4G_{9/2}(3/2)$		0
G_5	161.71	5dd	σ π	+1.13	σ π	1.54	σ π	$^2(P, D)_{3/2}(1/2)$	1.07	2.14
G_6	187.72	3dd	σ		σ			$^2(P, D)_{3/2}(3/2)$	3.21	0
G_7	21 369.56	8d	σ π	−1.40	π σ	5.81	σ π	$^4G_{11/2}(1/2)$		
G_8	393.35	2d	σ	−5.75	σ —	0.29	σ π	$^4G_{11/2}(3/2)$		
G_9	407.90	4d	σ π	−11.25	π σ	1.03	σ π	$^4G_{11/2}(1/2)$		
G_{10}	465.95	0ddd	σ					$^4G_{11/2}(3/2)$		
G_{11}	527.55	5ddd	π	5.19	π	1.23	π			
G_{12}	554.38	5ddd	σ π	−12.13	π σ					
G_{13}	572.64	2ddd	σ							
G_{14}	651.16	3ddd								
I_1	23 214.93	8	σ π	+0.59	σ π	0.60	π σ	$^2P_{1/2}(1/2)$	0.67	0.67
I_{1s}	223.33	2S	π					sat.		
I_2	759.73	8	σ π	+1.17	σ π	3.41	π σ	$^2D_{5/2}(1/2)$	1.20	3.60
I_3	778.42	5	σ	+3.42	— σ	0	σ	$^2D_{5/2}(3/2)$	3.60	0
K_1	26 134.85	5	σ π	+1.07	σ π	2.14	σ π	$^2(P, D)_{3/2}(1/2)$	1.07	2.14
K_2								$^2(P, D)_{3/2}(3/2)$	3.21	0
L_1	27 972.88	6d	σ					$^4D_{3/2}(3/2)$	3.60	0
L_2	975.68	8d	σ π					$^4D_{3/2}(1/2)$	1.20	2.40
L_{2s}	978.04	4S								
L_3	28 105.10	3d	f							
L_4	210.06	7dd	f							
L_5	514.52	9ddd	σ π	0.11	σ π			$^4D_{1/2}(1/2)$	0	0
L_6	29 216.58	4S	σ							
L_7	218.34	6d	σ	−2.30	σ —	0				
L_8	221.12	3S	σ							
L_9	314.53	8	σ π	+1.00	σ π	4.49	σ π			
L_{10}	320.19	2d	σ							
L_{11}	327.76	4d	σ	+3.47	— σ					
M_1	30 042.85	4	σ							
M_2	110.82	2d	σ							
M_3	289.90	3d	σ π							

[a] Based on *LS* coupling (Landé g factors) in the free ion and no magnetic or crystal field interaction between different levels.
[b] This level observed by indirect methods.
[c] Polarization is special due to Paschen-Back effect.
[d] Measurement on another plate gives 0.75_6.
[e] Poor measurement.
[f] An absorption band with considerable structure extends from L_3 to L_4.

TABLE III. Stark splittings of $J=\frac{3}{2}$ levels.

Level	Absorption lines	Observed (cm^{-1})	L-S (cm^{-1})	Im C (cm^{-1})
^4S	A_4, A_6	4.01	0	2.97
^2P	K_1, K_2	32	66.0[a]	51.01
$20\,^2D$	G_5, G_6	26.01	11.8[a]	14.70
$21\,^2D$				
^4D	L_1, L_2	−2.80	0	−12.91
^4F	R_1, R_2	30.01	33.2	32.05

[a] Assuming the states[18] as $2^{-\frac{1}{2}}(|^2P\rangle \pm |^2D\rangle)$ with the ^2D a pure $U=20$.

Table III gives as an example of the crystal field splittings for all the $J=\frac{3}{2}$ levels, with parameters obtained by Judd. The agreement with the observed levels is not very good, although the observed nonzero splittings of $^4S_{3/2}$ and $^4D_{3/2}$ are correctly predicted and the changes through intermediate coupling are all in the right direction.

The reason that discrepancies are greatest for the higher levels is probably to be found in the fact that the levels are fairly crowded and therefore interactions in this region linking different levels become much more important. Also, a larger deviation from LS coupling makes these levels more sensitive to the approximations present in our intermediate coupling calculation.

The free ion g factors in intermediate coupling were also calculated. The results did not usually agree with observed splittings better than the LS coupling values, so that they have not been included here.

In the crystal field the Zeeman effect may be greatly modified by the interaction between levels with different J (J mixing). That this is not negligible may be seen from the Zeeman splitting of levels that would consist purely of one value of M in the first order. For instance, for pure $M=\frac{1}{2}$ states the ratio of s_2/s_1 should be equal to $J+\frac{1}{2}$. For the levels S_1, A_1, E_6, which have $M=\frac{1}{2}$ the observed ratios are 2.37, 4.38, and 3.77 against the expected values 3, 4, and 4, respectively.

Some predictions can be made about the intensities, especially of the doublet-quartet transitions. For Russel-Saunders coupling the electric-dipole transition rule is $\Delta L=0, \pm 1$ and $\Delta S=0$. Intermediate coupling which mixes different values of L and of S causes the breakdown of this rule in the free ion. The crystal Stark effect causes further mixing of L and J but does not mix states with different S. The absence of a center of symmetry allows mixing of odd and even states and thus makes electric-dipole transitions possible.

The mixing of even states into the $4f^3$ ground configuration takes place from even configurations rather far removed from $4f^3$. Therefore, the magnitude of even quartet nature of the $4f^3$ doublets should be rather closely proportional to the $4f^3$ quartet fraction in the free-ion states. The intensities of the doublet-quartet transitions are then given by the square of the amplitudes of the quartet admixtures of the doublet states of the free ion. In Table IV the sum of the amplitude squares are given and therefore the intensity of the doublet-quartet line in comparison to some average quartet-quartet transition.

The doublet admixture of the ground state is only about 0.0040 and must be taken into account for nearly pure excited doublet states. In general the observed intensities are in agreement with Table IV. In particular we note that transitions to ^2K, ^2I, and ^2L should be very weak, of the order of magnitude 10 times weaker than transitions to the $^2H_{11/2}$ level which has been identified with the C group.

VI. POLARIZATION RULE

A rule concerning polarization in the perpendicular Zeeman effect has been noticed. The four-component Zeeman patterns of absorption transitions to $\mu=\frac{1}{2}$ levels are well polarized in the perpendicular effect if the level is isolated so that no crystal Paschen-Back effect occurs. If $J=\frac{1}{2}(\text{mod}2)$ the π components are outside; if $J=\frac{3}{2}$ (mod2) they are inside. We hope to come back to the theoretical significance of this rule in a later communication.

VII. CONCLUSIONS

The results of the present paper show that the theoretical treatment of the properties of the Nd^{3+} ion

TABLE IV. Expected doublet intensities.

J	L, S	Energy	Quartet component	Absorption group
1/2	^2P	22 940	0.0481	I_1
3/2	^2P	26 020	0.0580	K
	$20\,^2D$	21 080	0.0887	G(II)
	$21\,^2D$	33 680	0.1782	
5/2	$20\,^2D$	23 430	0.0223	I_2, I_3
	$21\,^2D$	35 000	0.2003	
	$10\,^2F$	69 750	0.0003	
	$21\,^2F$	39 470	0.0136	
7/2	$10\,^2F$	68 550	0.0016	
	$21\,^2F$	40 930	0.0169	
	$20\,^2G$	17 030	0.2941	D?
	$21\,^2G$	49 190	0.0004	
9/2	$20\,^2G$	20 870	0.5179	G(I)[a]
	$21\,^2G$	48 300	0.0007	
	$11\,^2H$	32 750	0.0043	
	$21\,^2H$	12 260	0.1311	S
11/2	$11\,^2H$	34 090	0.0150	
	$21\,^2H$	15 480	0.0523	C
	^2I	28 550	0.0057	
13/2	^2I	29 840	0.0003	
	^2K	18 600	0.0044	
15/2	^2K	20 600	0.0136	
	^2L	29 340	0.0002	
17/2	^2L	30 810	0	

[a] As $\chi \to 0$ this level actually becomes pure $^4G_{9/2}$ and is so named in our energy-level diagrams.

in $NdCl_3$ gives a good account of the observed properties in some cases, less good in others. The approximations made in the calculations (neglect of all interactions with levels outside of the $4f^3$ configuration, hydrogenic wave functions for the $4f$ electron, first-order crystal Stark effect only) should be most satisfactory for the lowest states which is in agreement with the experimental facts. For the higher states the calculations are in general sufficient to identify the levels but do not express quantitatively the observed properties.

In order to go beyond the results given here, the calculations must be perfected to take care of some of the omitted interactions; in particular J mixing must be taken into account for calculations of Zeeman and crystal Stark effects. It would also be desirable to obtain experimentally the higher levels beyond the present limit at about 30 000 cm^{-1}. Also work with more concentrated samples is required in order to obtain the weak transitions to the missing ^2I, ^2K, and ^2L levels. Finally an exact empirical knowledge of the free-ion levels through an analysis of the emission spectrum of the vapor would be of fundamental importance. Work on some of these phases is at present under way in this Laboratory.

ACKNOWLEDGMENTS

We wish to thank Professor C. A. Hutchison and Dr. E. Wong for the samples used in this investigation. On several occasions Dr. B. R. Judd has kindly communicated to us results of calculations that have proved very helpful.

THE JOURNAL OF CHEMICAL PHYSICS VOLUME 34, NUMBER 5 MAY, 1961

Crystal Spectra of Metal Coordination Compounds. IV. *Bis*-Acetylacetonato-Copper (II)

J. FERGUSON

Division of Chemical Physics, C.S.I.R.O. Chemical Research Laboratories, Melbourne, Australia

(Received November 15, 1960)

The polarized crystal absorption spectrum of *bis*-acetylacetonato-copper (II) has been measured with light incident on three different crystal faces. Four absorption bands have been found and a consistent analysis made in terms of a strong rhombic (D_{2h}) field from the ligands. The symmetries of the ground and excited states are not those predicted on the basis of simple crystal field theory and it has been suggested that strong metal-ligand π bonding will account for the observed order of states. The slight differences between the positions of the bands in the crystal and in chloroform are accounted for by weak intermolecular interactions between adjacent molecules in the crystal.

INTRODUCTION

THE theory which has had most success in explaining the physical properties of transition metal complexes is the simple electrostatic crystal field model in which the ligands are replaced by point charges or point dipoles. Although it is known that electron spin resonance spectra and electron-transfer bands require molecular orbital formulation, it is generally believed that the crystal field approach is a good one when only the weak metal ion absorption spectra are considered. The basis for this view rests mainly on the fitting of the observed bands to the theoretical energy levels with reasonable values of the parameters involved since, as yet, few attempts have been made to test the theoretical assignments on symmetry grounds. Recently it was shown[1] that the simple crystal field model breaks down for some nickel chelate compounds. The theory, of course, remains valid only so far as the assumption that the ligands can be replaced by point charges or point dipoles holds good. While this may be true for unidentate ligands it does seem that the model is unrealistic for multidentate ligands, judging from the spectra of the nickel compounds, and it is therefore of considerable interest to extend the measurements to other systems and metal ions. The present paper gives an analysis of the polarized single crystal absorption spectrum of *bis*-acetylacetonato-copper (II). The crystal spectrum has been reported previously,[2] but not in detail and not in relation to current theories of the bonding in metal coordination compounds.

CRYSTAL STRUCTURE

The crystal lattice[3] is monoclinic, space group $P2_1/n$ with cell dimensions $a=11.40$, $b=4.75$, $c=10.33$, and $\beta=92.2°$. There are two molecules in the unit cell. The crystals grow as lathes elongated along the b axis, the well-developed face being either (101) or ($10\bar{1}$). Initially the face was identified by x-ray methods using

[1] J. Ferguson, J. Chem. Phys. **34**, 611 (1961).

[2] S. Yamada and R. Tsuchida, Bull. Chem. Soc. Japan **29**, 694 (1956).

[3] H. Koyama, Y. Saito, and H. Kuroya, J. Inst. Polytech. Osaka City Univ. **C4**, 43 (1953).

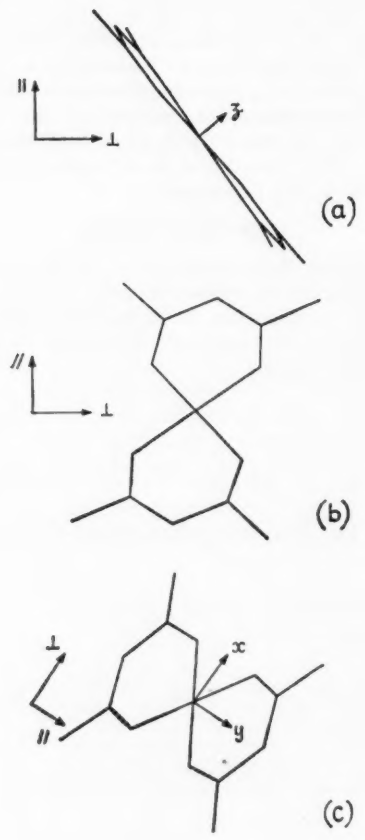

FIG. 1. Projections of the molecule on (a) $(10\bar{1})$, (b) (101), and (c) (010). The optical extinction directions are indicated by || and ⊥ in an arbitrary way. The choice of coordinate axes (x, y, z) is indicated in (a) and (c).

a moving film goniometer,[4] but once defined the two can be easily distinguished with the aid of a polarizing microscope. The (101) face shows marked dichroism with transmitted light, appearing blue for light polarized along the needle axis and green perpendicular to it. There is little dichroism observed with the $(10\bar{1})$ face and the color is deep blue along both extinction directions. One other face was used for the measurement of the absorption spectra, the (010), and this was obtained by sectioning crystals normal to the needle axis.

The projections of the molecule on the three faces are shown in Fig. 1.

EXPERIMENTAL

The spectra were measured with a reflecting microscope and a Hilger constant-deviation spectrometer.[1] One set of spectra was taken using a Beckman DK2 spectrophotometer in conjunction with the microscope.

The (010) sections (about 10 μ thick) were cut with the aid of a rotary microtome, the crystals being embedded in paraffin wax.

Two methods of preparation of the complex were used. The first, described by Jones,[5] gave crystals with the (101) face well developed. The second method involved the reaction between stoichiometric amounts of acetylacetone, anhydrous sodium acetate, and copper acetate monohydrate, in 50% aqueous-alcohol. Most of these crystals had the $(10\bar{1})$ face well developed.

RESULTS

The visible and near infrared spectrum of the complex in various solvents has been extensively studied by Belford, Calvin, and Belford.[6] However, these authors did not report measurements in the near-ultraviolet region where there is another weak absorption band.[7] Figure 2 shows the spectrum in chloroform and pyridine throughout the spectral range relevant to the present work.

The polarized absorption spectra obtained for light incident on the $(10\bar{1})$, (101), and (010) faces are shown in Figs. 3(a), (b), and (c), respectively. It is necessary to know the projections that molecular transition moments make on the two optical extinction directions of each face. These optical extinction directions have in each case been arbitrarily labelled || and ⊥: their relation to the molecular orientation is shown in Fig. 1. The squares of the projections of unit transition moments (x, y, and z) on the two extinction directions of each face are collected in Table I.

Examination of the spectra in Fig. 3 shows evidence for three bands at 18 000, 15 600, and 14 500 cm^{-1}, respectively. Of these, the first and the last carry the majority of the intensity; the other band is seen clearly only in the ⊥ polarization of the two faces (010) and (101). Belford, Calvin, and Belford[6] analyzed the bands in chloroform solution by means of two Gaussian bands centered at 18 800 and 15 200 cm^{-1}, respectively, and their measurements were reproduced in the present work. The bands in the crystal thus occur at slightly different energies from those in chloroform; in addition, there is clear evidence for three bands in the crystal.

The polarization of the three bands can be deduced with the aid of Fig. 1 and Table I. The x molecular axis makes zero projection in all cases except for the (101) and (010) faces and their ⊥ extinction directions. From Fig. 3(b) and (c) it can be deduced that the band at 15 600 cm^{-1} is the only one which is active for light polarized in the x molecular direction. The shoulder in the ⊥ direction near 18 000 cm^{-1} in Fig. 3(b) is assumed to result from the fact that the light incident on

[4] The identification was kindly carried out by Dr. A. McL. Mathieson of these Laboratories.

[5] M. M. Jones, J. Am. Chem. Soc. **81**, 3188 (1959).

[6] R. L. Belford, M. Calvin, and G. Belford, J. Chem. Phys. **26**, 1165 (1957).

[7] D. P. Graddon [J. Inorg. & Nuclear Chem. **14**, 161 (1960)] has also recently noted the existence of this band.

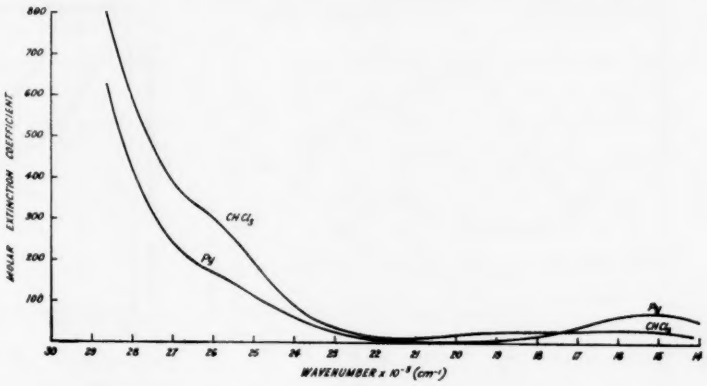

FIG. 2. Absorption spectrum of *bis*-acetylacetonato-copper (II) in chloroform and pyridine.

the crystal face is necessarily convergent and the values in Table I are strictly correct only for parallel light.

The other two bands are seen to be polarized in the yz plane from Fig. 3(a) and Table I. If the bands were solely y polarized, then a $\|/\perp$ ratio of about 1.7:1 would be expected. The addition of a z component would lower this value to about 1.3:1, which is close to the observed quantity. The spectrum of this face also suggests that the weak band at 15 600 cm^{-1} also has a y polarized component because the $\|/\perp$ ratio is a little higher than 1.3:1 in this region. The evidence for this, however, is not so clear.

It is deduced, therefore, that the band at 18 000 cm^{-1} is polarized in the yz plane and is inactive along the x direction; the band at 15 600 cm^{-1} is polarized in the xy plane, and the band at 14 500 cm^{-1} is polarized in the yz plane.

Unfortunately the band around 26 000 cm^{-1} could not be clearly observed because it is strongly overlapped by increasing absorption from a more intense band in the ultraviolet. Figure 4 shows the spectrum of a crystal with the (101) face well developed. It is clear that the band must be polarized along the x direction as well as in one or both of the y and z directions. The polarizations of all the bands are summarized in Table II.

DISCUSSION

The electronic transitions are again assumed to depend on the perturbing effect of u vibrations in the usual way.[8] The combination of electronic and vibrational motions leads to a resultant vibronic state and it is necessary to determine its symmetry properties. The marked spectral dichroism in the plane of the molecule shows that the vibronic symmetry is not tetragonal (D_{4h}) but must be rhombic (D_{2h}). The absorption spectra also indicate that the in-plane twofold axes do not lie along the copper-oxygen directions but lie between these and coincident with the axes of the point group of the molecule (D_{2h}).

[8] A. D. Liehr and C. J. Ballhousen, Phys. Rev. **106**, 1161 (1957).

There remains the possibility that the electric field at the copper ion has tetragonal symmetry. In this case, one of the states is orbitally degenerate and three absorption bands are predicted. Belford, Calvin, and Belford[6] have examined the visible absorption spectrum in a number of different solvents and their analysis of the band contours strongly suggests the presence of three bands. However, when the absorption spectrum is extended to the near ultraviolet region (Fig. 2), it is seen that there is another weak absorption band in the region of 26 000 cm^{-1} which is overlapped by stronger absorption further into the ultraviolet. There is thus evidence, even from solution spectra, for four electronic absorption bands and this shows that the electronic field cannot be tetragonal but must be rhombic, coincident with the molecular point group.

It is now necessary to establish from the polarization of the bands in the spectrum the symmetry representations of the ground and excited states on the assumption that the point group is D_{2h}. The coordinate axes are taken in the way shown in Fig. 1 and the ^2D ground state of Cu^{++} splits into the following five levels: $^2B_{3g}$, $^2B_{2g}$, $^2B_{1g}$, ^2A_g, and ^2A_g. The possible vibronic combinations are shown in Table III.

A transition is allowed between two states when the vibronic symmetry representation is B_{3u}, B_{2u}, or B_{1u}, corresponding to transition moments in the x, y, or z directions, respectively. It was shown above that the three bands at 18 000, 15 600, and 14 500 cm^{-1} have vibronic symmetry $B_{2u}+B_{1u}$, $B_{2u}+B_{3u}$, and $B_{2u}+B_{1u}$,

TABLE I. Squares of the projections (absorption intensities) of unit molecular transition moments (x, y, and z) on the two extinction directions of each crystal face.

Crystal face	$\|$ extinction direction			$\perp$ extinction direction		
	x	y	z	x	y	z
$(10\bar{1})$	0	0.63	0.53	0	0.38	0.53
(101)	0	0.65	0.49	0.95	0.01	0.02
(010)	0	0.34	0.48	1.0	0	0

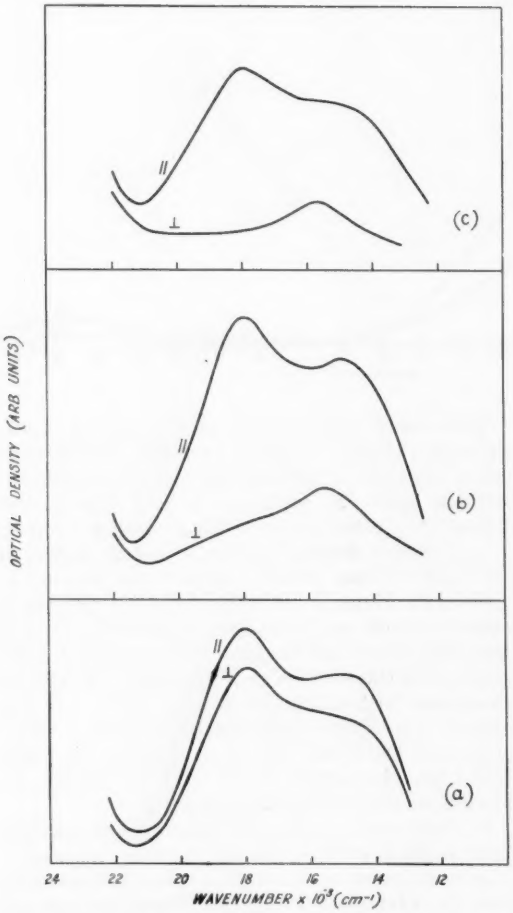

FIG. 3. Polarized absorption spectrum for light incident on the (a) (10$\bar{1}$), (b) (101), and (c) (010) faces.

respectively. It follows, from Table III, that the symmetries of the product of ground and excited wave functions belong to the representations B_{3g}, B_{1g}, and B_{3g}, respectively. The ground state is therefore $^2B_{3g}$ and the excited states in increasing energy are ^2A_g, $^2B_{2g}$, ^2A_g, and $^2B_{1g}$, as shown in Fig. 5. The $^2B_{1g}$ state was arrived at by elimination since the polarization of the transition from the ground state to it could not be uniquely determined from the spectrum. However, the predicted polarization agrees with one of the three possible combinations (Table II).

Now that the symmetries of the electronic states have been determined from an analysis of the polarized absorption spectrum, it remains to relate these to the 3*d* orbitals of the copper ion. The five 3*d* orbitals belong to four representations of D_{2h} in the following way: d_{z^2}, $d_{x^2-y^2}(A_g)$, $d_{xy}(B_{1g})$, $d_{xz}(B_{2g})$, and $d_{yz}(B_{3g})$. The relative energies of the orbitals as deduced from the polarization measurements are shown in Fig. 5.

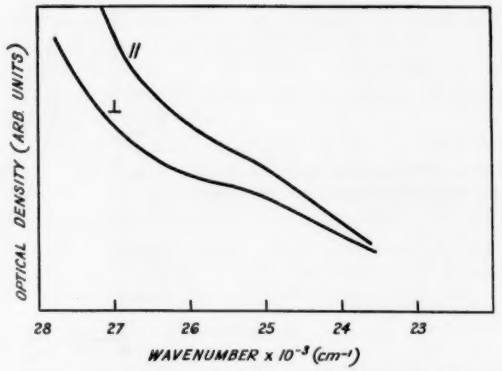

FIG. 4. Polarized absorption spectrum for light incident on the (101) face in the near ultraviolet.

It is interesting to make a comparison between the crystal spectrum and that in solution. Belford, Calvin, and Belford[6] showed that in chloroform the spectrum could be analyzed into two Gaussian curves, centered at 18 800 and 15 200 cm^{-1}, but they suggested that the band at 15 200 cm^{-1} represents two overlapping bands because in other solvents two bands were found to move to lower energy while a third remained in the region of 15 000 cm^{-1}. The absorption bands in the crystal are centered at 18 000, 15 600, and 14 500 cm^{-1}, which suggests that two of the bands have moved to lower energy. The difference between the chloroform solution spectrum and the crystal spectrum most probably arises through an axial perturbation by neighboring molecules in the crystal. The crystal structure shows that each copper atom has two CH groups from adjacent molecules at a distance of 2.84 A forming a distorted octahedron. The weak interaction between the copper atom and these CH groups therefore appears to be responsible for the difference between the two spectra.

The effect of solvent on the absorption spectrum is satisfactorily explained by the energy level scheme in Fig. 5. Only two of the four bands in the solution spectrum shift strongly on solvation and these correspond to the bands at 18 000 and 14 500 cm^{-1} in the crystal. Both of these have been shown to involve electron jumps from the two a_g orbitals to the b_{3g} orbital. The A_g representation contains the $d_{x^2-y^2}$ and d_{z^2} orbitals and the latter points towards the approach-

TABLE II. Positions and polarizations of the bands.

Band	Polarization (molecular axis)	Representation in D_{2h}
26 000 cm^{-1}	x; y and/or z	B_{3u}; B_{2u} and/or B_{1u}
18 000	y and z	B_{2u} and B_{1u}
15 600	y and x	B_{2u} and B_{3u}
14 500	y and z	B_{2u} and B_{1u}

TABLE III. Vibronic representations in D_{2h} (product of ground electronic state, excited electronic state, and perturbing vibration).

Symmetry representation of perturbing vibration	Symmetry representation of the product of ground and excited electronic wave functions			
	A_g	B_{1g}	B_{2g}	B_{3g}
$b_{1u}(z)$	B_{1u}	A_u	B_{3u}	B_{2u}
$b_{2u}(y)$	B_{2u}	B_{3u}	A_u	B_{1u}
$b_{3u}(x)$	B_{3u}	B_{2u}	B_{1u}	A_u

ing solvent molecule. Because the two orbitals have similar energies and belong to the same symmetry representation, there will be considerable interaction between them and solvation should affect the energy of both levels. However, the other three orbitals are not directed to the solvent molecule and their energies will not change in the first approximation. Since one of these orbitals is vacant in the ground state, the other two bands in the spectrum should not vary greatly from solvent to solvent. This is observed.

The most disturbing feature of the analysis is the complete failure of the simple crystal field model, which predicts that the d_{yz} and d_{xz} orbitals will be the most stable and the d_{xy} the least stable. A large number of copper coordination compounds has been examined by the author[9] and in every case, where an analysis of the band polarization has been made, the least stable orbital appears to be the one directed to the ligands in the plane (d_{xy}). The assigned order of energy levels therefore appears to be peculiar to copper acetylacetonate and it seems unlikely that it arises as a result of unjustified assumptions made in the analysis of the bands. The complex is, of course, noted for its great stability and resonance has been freely invoked to explain this.[10] This stability is reflected in the very large splitting of the d orbital energy levels (about 26 000 cm^{-1}), more than in any other monomeric copper complex. Unlike most other chelates only one bonding orbital of the ligand is fixed by the nuclear framework, the σ bond between the oxygen, and the neighboring carbon atom. It has been established that the remaining orbitals of the ligand cannot be replaced by a point dipole directed toward the copper atom and a molecular

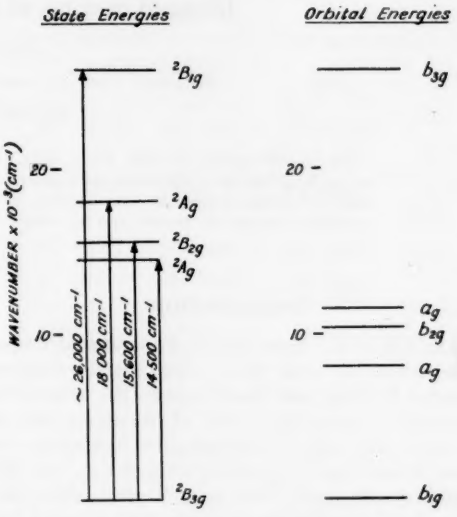

FIG. 5. State energies and orbital energies for *bis*-acetylacetonato-copper (II).

orbital approach appears more fruitful. It is also clear that ligand p_z and sp^2 hybrid orbitals would not represent good basis orbitals, because one of the sp^2 hybrids must be directed toward the copper thereby raising the energy of the d_{xy} orbital. Inclusion of more p character would reduce the extent of σ bonding between metal and ligand and increase the amount of π bonding. Reasonably strong π bonding is compatible with the polarization results because the metal b_{3g} and b_{2g} orbitals have the correct symmetry for formation of π bonds. It is beyond the scope of the present work to proceed with a complete molecular orbital analysis of the problem, but it is felt that such an approach could be very fruitful. It should be noted that Maki and McGarvey[11] obtained evidence for π bonding from an analysis of the electron spin resonance spectrum, but unfortunately their analysis is dependent on an assignment of the absorption bands which conflicts with that presented here.

ACKNOWLEDGMENTS

The author thanks Dr. A. L. G. Rees and Dr. N. S. Ham for valuable discussions, and Dr. A. McL. Mathieson for his continued help and advice on problems associated with the crystal structure.

[9] J. Ferguson (unpublished).

[10] A. E. Martell and M. Calvin, *Chemistry of the Metal Chelate Compounds* (Prentice-Hall, Inc., Englewood Cliffs, New Jersey, 1952), p. 160.

[11] A. H. Maki and B. R. McGarvey, J. Chem. Phys. **29**, 35 (1958).

Infrared Spectra of Alkali Metal Azide Crystals

HAROLD A. PAPAZIAN

Convair Scientific Research Laboratory, San Diego, California

(Received September 22, 1960)

The infrared spectra of CsN_3, RbN_3, KN_3, and NaN_3 crystals have been recorded at room temperature and at liquid-nitrogen temperature. Considerable anharmonicity in the fundamentals of N_3^- and combinations with lattice modes has been observed. Splitting of the doubly degenerate ν_2 has been observed. Discrepancies between the several reported values of ν_3 are discussed.

INTRODUCTION

RECENTLY, values for the fundamental frequencies of the azide ion in alkali metal azides were reported by Gray and Waddington[1]; the spectra were obtained by preparing a mull of the appropriate salt in Nujol, and only the fundamental frequencies were given. Moore[2] has taken the spectra of KN_3 and NaN_3 single crystals from 7000 to 500 cm^{-1}. His values of the bending vibration ν_2 agree with those of Gray and Waddington but values for ν_3 the asymmetric stretch, do not. We have measured the spectra of CsN_3 and RbN_3 as well as those of KN_3 and NaN_3. Our values of ν_3 do not check with those of either of these authors. A possible reason for the discrepancies is discussed below.

We have also measured the spectra at liquid-nitrogen temperature. Considerable anharmonicity of the azide-ion vibrations is found in the tetragonal lattice of CsN_3, RbN_3, and KN_3. The azide ion in the rhombohedral lattice of NaN_3 appears to be much less anharmonic.

EXPERIMENTAL

The spectra were studied with a Perkin-Elmer model 13 spectrophotometer using interchangeable NaCl and KBr prisms. The NaCl prism was calibrated against NH_3, CO_2, HBr, CO, CH_4, H_2O vapors, and a Hg arc. The KBr prism was calibrated against CO_2 and H_2O vapor.

The azide crystals were grown from saturated aqueous solutions of the appropriate azide salts. Saturated solutions were made in distilled water at room temperature, and the solutions were placed in desiccators using $CaSO_4$ as desiccant. In two or three days crystals approximately 40 mm^2 in area were obtained. By covering the beaker with aluminum foil with a small hole in it, in order to slow down evaporation, we grew one KN_3 crystal 20 mm on an edge and about 3 mm thick. Crystals could be grown equally well in glass or polyethylene beakers. (The large KN_3 was grown in a polyethylene beaker.) The CsN_3 crystals grew in a maze of thin sheets which could easily be separated from each other. The RbN_3 and KN_3 were thicker and had well-developed crystal faces and angles.[3] NaN_3 grew on the surface of the solution in a very thin and fragile sheet; the entire surface of the solution was essentially one large crystal which broke easily into smaller pieces.

The spectra of RbN_3 and KN_3 were taken along the c axis of the platelike crystals. The similarity of the CsN_3 spectrum suggests that it too is taken along the c axis. We did not make a crystal orientation determination of NaN_3.

The sample holder was the usual type Dewar with NaCl windows and a Cu-glass seal for thermal contact to the Cu-crystal holder. The Dewar was evacuated and the temperature measured with an iron-constantan thermocouple.

RESULTS

Figure 1 shows the spectra recorded at room temperature and at -196°C. The frequencies obtained at room temperature are listed in Table I. Several crystals of each azide were studied, and the NaCl and KBr regions shown are not necessarily of the same crystal. Overlap of the regions is shown in order that some comparison of the fundamental band intensities may be made. It is apparent that ν_3 the asymmetric stretch is much more intense than the bending vibration ν_2.

Our spectra for KN_3 and NaN_3 are very similar to those found by Moore.[2] The spectrum of NaN_3 agrees quite closely (in some cases to 1 cm^{-1}) except for the fundamental ν_3; the KN_3 spectra are similar but with greater discrepancy in the values of all the observed frequencies. Table II lists the fundamentals ν_2 and ν_3 found in the works cited in footnotes 1 and 3 and this work.[4]

For CsN_3, RbN_3, and KN_3, at low temperatures there is a decrease in intensity for the bands around 3300 cm^{-1} and 2200 cm^{-1}. The band on the low-frequency side of ν_3 disappears completely along with the bands close to 694 cm^{-1} and 625 cm^{-1}. The frequency near 640 cm^{-1} decreases by approximately $\frac{1}{3}$ in peak height with no change in bandwidth. The asymmetric stretch ν_3 decreases in peak height and also appears to become

[1] P. Gray and T. C. Waddington, Trans. Faraday Soc. **53,** 901 (1957).

[2] P. W. M. Moore (private communication).

[3] R. W. Dreyfus and P. W. Levy, Proc. Royal Soc. (London) **A246,** 233 (1958), have described KN_3 and NaN_3.

[4] As a check on our calibration, the value for ν_2 of NaN_3 was checked independently on another Perkin-Elmer model 13 spectrophotometer.

TABLE I. Infrared spectral data for N_3^- at room temperature.

Possible assignment	Observed frequencies (cm^{-1})[a] CsN_3	RbN_3	KN_3	NaN_3
ν_{2a}	621.7±0.5	624.5±0.5	624.0±0.5	628.0±0.5
ν_{2b}	640.0±0.5	643.5±0.5	646.0±0.5	643.5±0.5
	667.0±0.5	661.7±0.5	663.5±0.5	662.5±0.5
$\nu_1-\nu_{2a}$	692.7±0.5	694.4±0.5	694.5±0.5	709.5±0.5 718.5±0.5
Lattice combinations with ν_1	1293±1	1280±1 1407±1	1255±1 1441±1	1567±1
ν_1	1365±1			
$3\nu_{2a}$	1876±2	1876±2	1882±2	1860±2
Lattice combinations with ν_3	2173±2	2200±2	2114±2 2217±2	1924±2 2009±2
ν_3	2015±2	2008±2	2002±2	2189±2
	3285±5			3187±5
	3355±5	3330±5	3380±5	3355±5
		3405±5	3430±5	3455±5
Fundamental combinations				3537±5
				3755±5
				4202±5
	4914±5	4950±5	4985±5	
	4988±5	5015±5	5050±5	

[a] The accuracies are estimates of our ability to read our calibration curves.

narrower but because of its great intensity and the behavior of the bands close by it is difficult to estimate the effects. There is no shift in frequency.

For NaN_3 there is somewhat different behavior in that a band is split off on the high-frequency side of ν_3 (at 2290 cm^{-1}), the band at 700 cm^{-1} disappears, the band at 628 cm^{-1} is reduced by approximately 40% and there is no change in the peak height of the band at 643 cm^{-1}. There is no apparent change in the intensity for the asymmetric stretch ν_3.

DISCUSSION

There is no simple explanation for the discrepancies of the various values of ν_3 found by the several investigators. It is not a mull vs single crystal effect since Moore used single crystals as we did, and our results do not resemble his.

It may be that ν_3 is extremely sensitive to small amounts of impurity in the crystals. However, we should like to suggest an alternative which seems more reasonable to us. Dreyfus and Levy[3] have shown that by deforming KN_3 and NaN_3 very slightly by heating, brightly colored birefringent bands are produced in these crystals. Associated with these bands are planes in the crystal which for NaN_3 are (110) and for KN_3 are the (112) planes. We suggest that the variation in ν_3 may be caused by the degree of strain and perfection of the lattice depending upon the crystal-growing method. Because of the anisotropy of forces around the azide ion in these crystals, one would expect different values for ν_3 depending on crystal orientation with respect to the electric vector of the impinging radiation. Thus, the frequency observed should be sensitive to crystal history. Further speculation into the details of this suggestion must await a better understanding of the spectra of solids.

The crystal structure[5] for CsN_3, RbN_3, and KN_3 is the body-centered tetragonal with the linear azide ions lying in parallel planes; NaN_3 is rhombohedral with the linear azide ion lying on a body diagonal. For the azide ion on a D_{2h} site in the tetragonal lattice the forces within the planes are considerably different from those perpendicular to the planes. For the azide ion on a D_{3d} site in the rhombohedral lattice these large differences in forces around the body diagonal might not be expected. Indeed from the temperature behavior of the fundamentals, it is apparent that the azide ion is much

[5] B. L. Evans, A. D. Yoffe, and P. Gray, Chem. Revs. **59**, 515 (1959) have compiled physical and chemical data of inorganic azides.

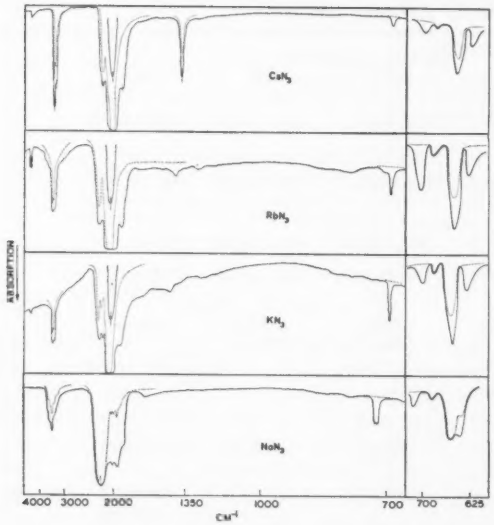

FIG. 1. Observed spectra of the several azides. Solid line at room temperature, broken line at liquid-nitrogen temperature.

more anharmonic in the tetragonal lattice than in the rhombohedral lattice.

From the strong temperature dependence of the bands around 625 cm^{-1} we might assign these to difference bands such as $2\nu_2-\nu_2$. However, with the very strong anharmonicity present in the tetragonal lattice it is not unreasonable to assume that one bending mode (for example, in the plane) is more temperature sensitive than the other, so that its intensity is much more reduced at low temperatures. We prefer to consider the band at 625 cm^{-1} as ν_{2a}. If we can extend the comparison to gaseous CO_2 we would expect $2\nu_2-\nu_2$ to be on the longer wavelength side of the fundamental ν_2 by as much as 50 cm^{-1} whereas our band at 625 cm^{-1} is split by only 20 cm^{-1}.

In NaN_3 the picture is more difficult. Hornig[6] has shown that degenerate vibrations on a D_{3d} site may combine with a rotational mode of the lattice and be split. It is not clear why in NaN_3 only one mode of ν_2 should be much more temperature sensitive than the other, but by analogy with the other azides we assign this also to ν_{2a}. It should be noted that the average values of our bending frequencies agree reasonably well with the one value for ν_2 reported by Gray and Waddington (see Table II).

The other extremely temperature-sensitive bands are at approximately 1870 cm^{-1} and 700 cm^{-1}. Both of these bands behave very much like ν_{2a} at 625 cm^{-1}, in that all bands go essentially to zero intensity in our crystals whereas the other temperature-sensitive bands

[6] D. F. Hornig, J. Chem. Phys. **16**, 1063 (1948).

TABLE II. Reported values of ν_2 and ν_3 for N_3^-.

	CsN_3	RbN_3	KN_3	NaN_3	Reference
	2015 cm^{-1}	2008 cm^{-1}	2002 cm^{-1}	2189 cm^{-1}	(this work)
ν_3			2063	2160	b
	2062	2024	2041	2128	c
ν_{2a}	621.7	624.5	624.0	628.0	(this work)
			621.2[a]	628.0[a]	b
ν_{2b}	640.0	643.5	646.0	643.5	(this work)
			647.7	639.3	b
ν_2	635	642	645	639	c

[a] Moore assigns this to $2\nu_3-\nu_2$.
[b] See work cited in footnote 3.
[c] See work cited in footnote 1.

decrease but still retain considerable intensity. We might expect then that the bands at 625 cm^{-1}, 1870 cm^{-1}, and 700 cm^{-1} are related. A simple assignment for 1870 cm^{-1} is $3\nu_{2a}$. Usually anharmonicity constants are negative[7] so that one would expect $3\nu_{2a}$ to lie at smaller wave numbers. There is, however, no *a priori* reason that anharmonicity constants should be negative, and they may well not be in these crystals. The argument is strengthened if we consider the "best values" for ν_2 and $2\nu_2$ compiled[6] by Evans *et al.* For LiN_3 they give $\nu_2=635$ cm^{-1} and $2\nu_2=1277$ cm^{-1} and for CsN_3, $\nu_2=635$ cm^{-1} and $2\nu_2=1267$ cm^{-1}. The first pair indicates positive anharmonicity constants and the second pair indicates vanishingly small negative constants or positive and negative constants of comparable value.

Although the symmetric stretch ν_1 is "forbidden," its combination with another fundamental is allowed. We can assign the bands at approximately 700 cm^{-1} to $\nu_1-\nu_{2a}$. The doublet at 700 cm^{-1} for NaN_3 is difficult to explain.

The relative intensity of the band at 1365 cm^{-1} in CsN_3 varies from crystal to crystal so that one might be tempted to assign it to an impurity. However, our CsN_3 crystals were physically very different from RbN_3 and KN_3 in that the CsN_3 crystals were plastic. It may be that the symmetric stretch ν_1 in CsN_3 is sufficiently perturbed to become infrared active. The Raman value is given[6] as 1329 cm^{-1} which is considerably different, but in view of the large differences reported for ν_3 this may not be too surprising.

Possible assignments of the other bands are listed in Table I.

It may be of considerable value to prepare azide crystals under the mildest possible conditions and to study their spectra as a function of strain introduced into the crystal.

[7] G. Herzberg, *Infrared and Raman Spectra of Polyatomic Molecules* (D. Van Nostrand Company, Inc., New York, 1947).

THE JOURNAL OF CHEMICAL PHYSICS VOLUME 34, NUMBER 5 MAY, 1961

Photolysis of Nitrous Oxide. I. 1236 A

JOHN P. DOERING AND BRUCE H. MAHAN

Department of Chemistry, University of California, Berkeley, California

(Received November 3, 1960)

The photolysis of nitrous oxide containing an N^{15} atom in the external position has been investigated using 1236-A light. The products include N_2^{29}, $N^{15}O$, $N^{14}O$, and small amounts of N_2^{30}. The appearance of N_2^{30} shows that there are two primary processes occurring at this wavelength, one of which is dissociation to a nitrogen atom and a nitric oxide molecule, the other dissociation to an oxygen atom and a nitrogen molecule. The latter process is approximately 10 times as important as the former. The quantum yield of nitrogen is 1.34 ± 0.04.

THE photolysis of nitrous oxide by light of 1236-A wavelength has been investigated by Zelikoff and Aschenbrand.[1] These workers have suggested that the decomposition proceeds by two primary photochemical processes, one involving dissociation to an oxygen atom and an electronically excited nitrogen molecule, the other producing a nitrogen atom and an electronically excited nitric oxide molecule. Their evidence for participation of both primary processes was the qualitative behavior of product ratios as a function of pressure. Because of the intrinsic insensitivity of this method to the actual mechanism of the reaction, Zelikoff and Aschenbrand were unable to estimate the relative importance of the two primary processes. The very existence of a nitrogen atom primary process has been questioned by Kistiakowsky and Volpi[2] who point out that because of the great speed of the reaction between nitrogen atoms and nitric oxide, it is unlikely that any nitric oxide would be found in the products of the photolysis of nitrous oxide even if any nitrogen atoms were actually produced. The possibility of the existence of two primary processes in such a simple molecule is intrinsically interesting; furthermore, the photolysis of nitrous oxide by the hydrogen atom Lyman α line might serve as a source of nitrogen atoms and nitric oxide in the upper atmosphere. The purpose of this work was to ascertain the existence and relative importance of the two primary processes by photolysing nitrous oxide which had an isotopically labeled external nitrogen atom.

EXPERIMENTAL

A microwave discharge through krypton together with a lithium fluoride window provided monochromatic radiation of 1236-A wavelength. The details of this lamp have been published previously.[3] The reaction vessel was a Pyrex cylinder of 25 mm diameter divided into two separate chambers by a Pyrex plate. One of the chambers was used to contain the reaction mixture while the other was filled with either N_2O or CO_2 and served as a relative actinometer. This arrangement was necessary since over the period of many experiments the lamp intensity might change by as much as a factor of three.

The products of the photolysis were separated by passing them through a trap at -210°C. This served to retain all the NO and N_2O, and allowed the isotopic composition of the nitrogen to be ascertained without their interference. Naturally this treatment resulted in a reaction between NO and O_2 and consequently the absolute amounts of these products are not reliable. The relative amounts of $N^{15}O$ and $N^{14}O$ should have some qualitative significance, however, so nitric oxide was separated from nitrous oxide at -183°C, and also analysed by mass spectrometry. In the runs in which carbon monoxide was added, the noncondensible fraction of the products was passed over hot copper oxide until all the CO had been removed as CO_2. This precaution avoided any interference from the heavier isotopic forms of CO in the N_2^{29} and N_2^{30} analyses. In a few runs it was desirable to have nearly complete recovery of the nitric oxide. In these cases the trap at -210°C was not used, and nitrous oxide was separated from the products at -183°C.

The isotopically labeled nitrous oxide was prepared from commercially available 95% enriched $N^{15}H_4N^{14}O_3$ by gentle heating. The nitrous oxide was then purified by bulb-to-bulb distillation. The final product contained 5% $N^{14}N^{14}O$ and 0.5% $N^{15}N^{15}O$. All other gases were obtained commercially, and mass spectrometric analysis showed them to be of satisfactory purity.

RESULTS AND DISCUSSION

Table I shows that small, but significant, amounts of $N^{15}N^{15}$ are formed in every photolysis of pure $N^{15}N^{14}O$. This fact in itself strongly suggests the existence of a primary photochemical process which produces nitrogen atoms. The formation of doubly labeled nitrogen molecules would surely seem to involve nitrogen atoms either reacting with themselves or with some molecule containing a labeled nitrogen atom. No reaction between oxygen atoms and nitrous or nitric oxide is known in which nitrogen atoms are produced. Furthermore, the photolyses were carried out to a limited percentage

[1] M. Zelikoff and L. Aschenbrand, J. Chem. Phys. **27**, 123 (1957).
[2] G. B. Kistiakowsky and G. G. Volpi, J. Chem. Phys. **27**, 1141 (1957).
[3] B. H. Mahan, J. Chem. Phys. **33**, 959 (1960).

TABLE I.[a]

Run	N_2^{29}	N_2^{30}	NO^{30}	NO^{31}	P_{CO}(mm)	P_{NO}(mm)	P_{total}(mm)
82	440	25	5.2	...			
83	420	24	4.8	...			
84	380	23	4.5	...			
85	272	6.2	9.1	6.6			
90	345	3.5	18.7	13.3			
91	296	3.8	19.8	12.6			
CO Additions							
85	272	6.2	9.1	6.6	0		
86	201	1.7	1.8	0	247		
87	187	1.3	2.9	0.6	546		
88	225	2.2	2.9	1.5	115		
89	226	3.7	5.9	2.9	44		
NO Additions							
90	345	3.5	18.7	13.3		0	6.0
91	296	3.8	19.8	12.6		0	6.0
92	256	0.4	...	30.3		2.5	9.1
93	217	0.3	...	29.5		2.9	10.8
105	417	...	...	81.3		2.4	47.6
106	410	...	...	71.0		1.8	20.0

[a] Unless otherwise indicated the amounts are in units of μmoles$\times 10^9$, produced in 300-sec photolysis time. The pressure of N_2O in each run was 7±1 mm, which completely absorbs all incident radiation.

decomposition so that the nitrogen atoms are not the result of the photolysis of nitric oxide. The only reasonable alternative is that nitrogen atoms are produced in the primary photochemical decomposition of nitrous oxide.

The nitrogen atom primary process is also indicated by the fact that, in every experiment, the amount of the lighter isotope of nitric oxide significantly exceeds that of the heavier isotope, after the appropriate correction is made for the amount of labeling in the parent nitrous oxide. This fact shows that the two varieties of the nitric oxide molecule are not produced exclusively in the same reaction, as is required by a mechanism involving only an oxygen atom primary process.

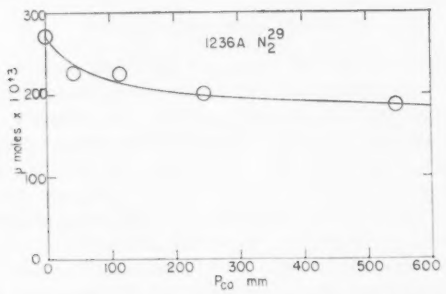

FIG. 1. The dependence of yield of N_2^{29} on the pressure of carbon monoxide.

Now that the existence of two primary processes is accepted we must ascertain the detailed path by which doubly labeled nitrogen molecules are formed. As a basis for discussion we take some of the steps proposed by Zelikoff and Aschenbrand:

$$N^{15}NO+h\nu \rightarrow N_2(B^3\pi)+O(^3P) \quad (1)$$

$$N_2(B^3\pi)+N_2O \rightarrow 2N_2+O(^1S) \quad (2)$$

$$O(^1S)+N_2O \rightarrow N^{15}O+N^{14}O \quad (3)$$

$$O(^1S)+N_2O \rightarrow N_2+O_2 \quad (4)$$

$$N_2(B^3\pi) \rightarrow N_2+h\nu \quad (5)$$

$$N^{15}NO+h\nu \rightarrow N^{15}+N^{14}O(^2\pi) \quad (6)$$

$$N^{14}O(^2\pi) \rightarrow NO+h\nu. \quad (7)$$

In the above mechanism the isotopic labeling is indicated only in those cases where some ambiguity is likely to arise. The details of the primary processes were deduced by Zelikoff from the nature of the absorption spectrum of nitrous oxide and from considerations of reaction energy. Reactions (2) and (4) have the un-

attractive feature that they do not conserve electron spin, but they are necessary to explain the existence of appreciable quantities of nitric oxide in the reaction products. Several workers[2,4,5] have demonstrated that ground-state oxygen atoms and nitrogen atoms do not react with nitrous oxide at room temperature. Since most of the nitric oxide produced in reaction (6) will be consumed by the reverse reaction (*vide infra*), some type of attack of oxygen atoms on nitrous oxide must be admitted.

One set of reactions which must obviously be added to the above mechanism is

$$N^{15}+N^{14}O\rightarrow N^{15}N^{14}+O(^3P) \qquad (8a)$$

$$N^{15}+N^{15}O\rightarrow N^{15}N^{15}+O(^3P). \qquad (8b)$$

Zelikoff[1] has suggested that nitrogen atoms might recombine on the walls of the reaction vessel, or recombination might occur by a homogeneous mechanism. However, reactions (8a) and (8b) are fast[2,6] enough to exclude any appreciable amount of atomic combination reaction. If one makes the extreme assumption that $[N]\cong[NO]$, then, by using the published values of the rate constants for reaction (8) and for the combination nitrogen atoms,[7] one can calculate that nitrogen atoms will disappear by reactions (8) 1000 times as fast as by recombination in the pressure range of our experiments. Without doubt, reaction (8b) provides a better explanation of the production of doubly labeled nitrogen than does atomic recombination.

In a further effort to test the above mechanism, several experiments were performed in which carbon monoxide or nitric oxide were added to the reaction mixture. Since the formation of $N^{15}O$ proceeds through reaction (2), the amount of $N^{15}O$ produced should decrease in the presence of a gas which quenches the electronic excitation of $N_2(B^3\pi)$ and/or reacts with ^1S oxygen atoms. Carbon monoxide possesses energy levels which are nearly coincident with the energy of $N_2(B^3\pi)$; it also reacts with ^1S oxygen atoms.[8] Table I shows that the rate of $N^{15}O$ production does noticeably decrease upon addition of carbon monoxide. Furthermore, Figs. 1 and 2 show that the yields of N_2^{29} and of N_2^{30} steadily decrease with increasing carbon monoxide concentration. This behavior is completely consistent with the mechanism which has been proposed. It cannot be expected that $N^{15}N^{15}$ will disappear entirely, since at the highest pressures used here atom-nitrogen-atom recombination may become a source of $N^{15}N^{15}$. An extreme upper limit of the rate of atom recombination may be estimated from the rate constants by again

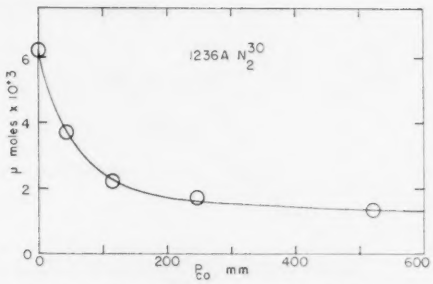

FIG. 2. The variation of the yield of N_2^{30} with carbon monoxide pressure.

assuming that $[N^{15}]\cong[NO]$. This leads to the conclusion that no more than one-third of the nitrogen atoms produced will recombine even at the highest pressure of carbon monoxide used in these experiments.

The addition of nitric oxide to the reaction mixture should produce results similar to those obtained with carbon monoxide addition. Nitric oxide may quench the $N_2(B^3\pi)$ molecule either by dissociating or becoming electronically excited; the possibility also exists that if nitric oxide does not quench the excited nitrogen molecules it will react with ^1S oxygen atoms. If either or both of these reactions occur, the yield of $N^{15}O$ should decrease. As a consequence of this, and also because the added nitric oxide will tend to react with nitrogen atoms to give $N^{15}N^{14}$, we expect $N^{15}N^{15}$ production to cease. Table I shows that the amount $N^{15}N^{15}$ is actually reduced by a factor of 10 when relatively small amounts of added nitric oxide are present. This is further proof that nitrogen atoms do exist in this system, and do produce doubly labeled nitrogen though a reaction involving labeled nitric oxide. The unexpected feature of the data is that $N^{15}O$ increases as nitric oxide is added. This increase is in great excess of the contribution due to the naturally occurring heavy nitrogen isotope in the added nitric oxide, so the addition of nitric oxide must provide a new path for the production of $N^{15}O$. We can also conclude that the addition of small amounts of nitric oxide do not seriously inhibit the production of $N^{15}O$ by reactions (1), (2), and (3). With the low concentrations of nitric oxide used here, electronically excited nitrogen molecules will collide more often with nitrous oxide than with nitric oxide, and ^1S oxygen atoms will continue to be produced by reaction (2). Therefore the reaction of ^1S oxygen atoms with nitrous oxide must be rapid compared with their reaction with nitric oxide at these pressures. The data in Table I also indicate that when the amount of added nitric oxide is held approximately constant the amount of $N^{15}O$ produced increases with the total pressure. This suggests that the additional $N^{15}O$ is formed by the reaction of N^{15} atoms with an intermediate whose concentration increases with total pressure. Nitrogen dioxide, formed from nitric oxide and ^3P oxygen atoms in the presence of a third body, is likely to be this inter-

[4] F. Henriques, A. B. F. Duncan, and W. A. Noyes, Jr., J. Chem. Phys. **6,** 518 (1938).
[5] E. J. R. Willey and E. K. Rideal, J. Chem. Soc. **130,** 699 (1927).
[6] G. B. Kistiakowsky and G. G. Volpi, J. Chem. Phys. **28,** 665 (1958).
[7] P. Harteck, A. Reeves, and G. Mannella, J. Chem. Phys. **28,** 608 (1958).
[8] B. H. Mahan (unpublished results).

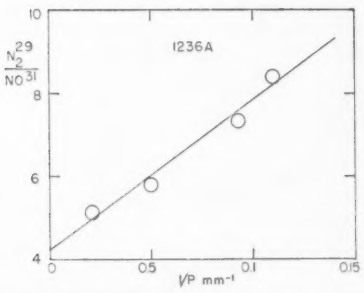

FIG. 3. The dependence of $N_2^{29}/N^{15}O$ on the reciprocal of the total pressure when nitric oxide is added. The two runs at higher pressure were made in the presence of added helium.

mediate. In order to test this idea, small amounts ($\sim 10^{-3}$ μ moles/cc) of NO_2 were added to the nitrous oxide and the mixture was photolysed. In each such experiment there was an increase in the amount of $N^{15}O$ produced. A steady-state treatment of the reaction mechanism further confirms this interpretation. Let us assume that, in the experiments in which nitric oxide is added, the concentration of nitrogen dioxide will be determined primarily by the reactions

$$O(^3P)+NO+M\rightarrow NO_2+M \qquad (9)$$

$$O^3P+NO_2\rightarrow NO+O_2, \qquad (10)$$

and to a lesser degree by

$$N^{15}+NO_2\rightarrow N^{15}O+NO, \qquad (11)$$

where M is any molecule. Then the approximate steady-state concentration of NO_2 will be

$$[NO_2]=k_9(NO)(M)(O)/[k_{10}(O)+k_{11}(N^{15})]$$
$$\cong[k_9(NO)(M)/k_{10}].$$

This approximation is valid if reaction (6) occurs infrequently compared with reaction (1), and if the nitrogen atoms react rapidly by reactions (8). The steady-state concentration of N^{15} is given by

$$[N^{15}]=k_6/[k_{11}(NO_2)+k_8(NO)].$$

The rate of formation of $N^{15}O$ due to nitrogen-atom-nitrogen-dioxide reaction alone is

$$d(N^{15}O)/dt=\frac{k_6}{1+[k_8k_{10}/k_9k_{11}(M)]}.$$

This equation predicts an increase in the $N^{15}O$ production with total pressure, providing the reaction sequence (1) through (5) is unaffected. This would seem to be satisfied in the series of experiments in which the concentration of added nitric oxide was kept constant, and the total pressure was varied by helium addition. The equation further predicts that $1/(N^{15}O)$ should be a linear function of $1/(M)$. Figure 3 shows that $(N_2^{29})/(N^{15}O)$ is very nearly a linear function of the reciprocal of the total pressure. The ratio is plotted in order to minimize the effect of variation in light intensity from run to run. If the absolute value of the rate of production of nitrogen atoms in this system were known, then the slope of the line in Fig. 3 would provide a measure of k_{11} relative to the better known constants k_8, k_9, and k_{10}. In order to calculate k_{11} we must determine the relative importance of the two primary processes and the absolute quantum yield of nitrogen. The quantum yield of nitrogen was determined by measuring the incident light intensity by CO_2 actinometry.[3] This led to a value of 1.34 ± 0.04 for the quantum yield of nitrogen. In order to calculate the relative rates of (6) and (1), the two primary processes, we make the assumption that all the nitrogen atoms produced by (6) react according to reactions (8a) or (8b). Therefore, since the concentrations of the two varieties of nitric oxide are approximately equal, the number of nitrogen atoms produced should be just twice the amount of N_2^{30}. If we assume that the primary quantum yield of nitrogen from all sources is unity, then we have for the ratio of the primary processes

$$k_6/k_1=\frac{2\,N_2^{30}}{(N_2^{29}/1.34)-N_2^{30}}=0.08/(0.72-0.04)=0.12,$$

where we have chosen N_2^{30}/N_2^{29} equal to its average value of 0.04.

Now that the ratio of the rates of the primary processes have been determined, we can calculate k_{11} from the slope of Fig. 3. However, since the exact value of k_8 seems uncertain,[6] we will first determine the ratio of k_{11} to k_8. The slope of the line in Fig. 3 is determined by the equation

$$(N_2^{29}/k_6t)[1+(k_8k_{10}/k_9k_{11})(1/M)]=N_2^{29}/N^{15}O,$$

and has the numerical value 2.1×10^{-6} moles/cc. For the value of N_2^{29}/k_6t we take $N_2^{29}/2\times N_2^{30}=1/0.08$. These values give $k_{11}/k_8=6\times10^2$, if $k_9=2.0\times10^{16}$ cc^2/mole^2 sec, and $k_{10}=2\times10^{12}$ cc/mole sec. This would seem to be a rather large ratio for two rate constants which are very near the collision frequency. However, if k_8 is as low as 4×10^{11} cc/mole sec, which is Kistiakowsky's[2] first estimate, then k_{11} still has a reasonable value.

ACKNOWLEDGMENTS

We would like to thank Professor George Pimentel for supplying the labeled ammonium nitrate. One of us (J.P.D.) wishes to acknowledge the support received from a Woodrow Wilson Fellowship and a National Science Foundation Fellowship.

The Second Law of Thermodynamics

BRYCE CRAWFORD, JR.

Chemistry Department, University of Minnesota, Minneapolis, Minnesota

AND

I. OPPENHEIM

Physics Section, Convair, San Diego, California

(Received October 3, 1960)

Derivations of the mathematical statement of the second law of thermodynamics from the physical statements of Kelvin and Clausius are presented. Caratheodory's principle is obtained as a direct consequence of either Kelvin's or Clausius's statement.

PERHAPS the most satisfying treatment[1] of the second law begins from Caratheodory's principle: that from an arbitrary point (state) there is a finite region (set of states of finite measure), arbitrarily near to the initial point, which cannot be reached by an adiabatic process, reversible or irreversible. Usually, the physical statements of the second law formulated by Kelvin and Clausius are presented, but no direct connection between their statements and Caratheodory's rather abstract principle is presented. We shall here present derivations filling this gap. Once Caratheodory's principle has been proved, it is an easy task to derive the equilibrium form of the second law.[1] We shall not present the details of this proof. However, we shall show how the same techniques can be used to demonstrate that the entropy change in an isolated system must be greater than zero in an irreversible process.

I. DERIVATION OF CARATHEODORY'S PRINCIPLE FROM KELVIN'S STATEMENT

Kelvin's statement of the second law is as follows: In a cycle of processes, it is impossible to transfer heat from a heat reservoir and convert it all into work without at the same time transferring a certain amount of heat from a hotter to a colder body. The system under consideration is one in which all parts are at the same temperature. We assume that no phase transitions occur during the processes discussed so that we may make assumptions concerning the continuity of the heat absorbed or liberated during these processes as a function of the variables of state. This restriction is easily removed.

We first consider a system whose states are functions of the empirical temperature t and one parameter x, for example, the volume. (See Fig. 1.) We assume that the heat absorbed in any process is a continuous function of x along the isotherms. We consider state 1 at t_1 and x_1. To it we connect a series of states, 1′, 1″, etc., along the isotherm at temperature t_1 by a reversible process. Through 1′, 1″, etc., we draw paths representing reversible adiabatic processes which intersect the isotherm at arbitrary temperature t_2 at the points 2′, 2″, etc., respectively. Adiabatic processes are those in which no heat is absorbed or liberated by the system. We now make the assertion that no points along these adiabatics are accessible from 1 by an adiabatic path reversible or irreversible. If such a path existed, we could, for example, go around the cycle 1, 2′, 1′, 1. The net heat absorbed by the system in this cycle would be $Q_{1'1}=-Q_{11'}$ which is assumed to be greater than zero. (If $Q_{1'1}$ decreases as x_1 increases, we may choose the points 1′, 1″, etc., to the right of 1 on the isotherm.) The work done by the system in the cycle would be

$$W=Q_{1'1}, \tag{1}$$

which follows from the first law. Thus, the net result of such a cycle would be the conversion of heat into work without transferring any heat from a higher to a lower temperature. This is contrary to Kelvin's principle.

Thus, no adiabatic paths through 1 can intercept the isotherm t_2 at the points 2′, 2″, etc. The points 2′, 2″⋯, cannot coincide since the argument above implies that reversible adiabatics cannot cross. Because of the continuity properties assumed, all points on the isotherm t_2 that are to the left of 2 can be reached by

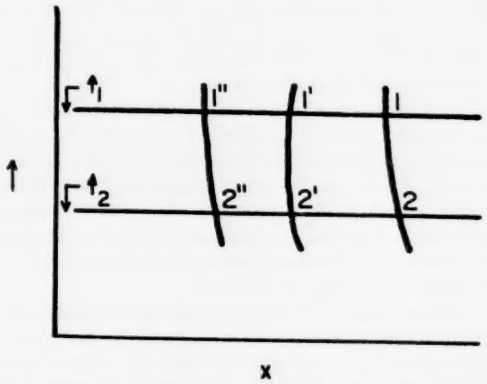

FIG. 1. Isothermal and adiabatic paths in the $t-x$ plane.

[1] See, for example, S. Chandrasekhar, *Introduction to the Study of Stellar Structure* (Dover Publications, New York, 1957), Chap. 1.

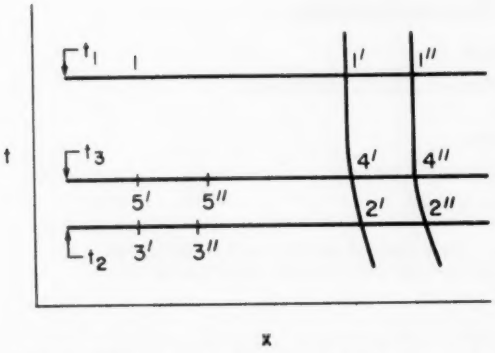

FIG. 2. Isothermal and adiabatic paths in the $t-x$ plane

reversible adiabatics from points on the isotherm t_1 which are to the left of 1. Since the temperature t_2 is arbitrary, and since the system has the proper continuity properties, similar conclusions hold for all isotherms. In this manner, we find that all points in the $t-x$ plane lying to the left of the reversible adiabatic through 1 are inaccessible from 1 along an adiabatic from 1. We have also proved that reversible adiabatics cannot cross and must be monotonic as a function of t.

If the states of the system are functions of t, and more than one other parameter, we note that the conclusions drawn from Fig. 1 hold for any plane in the space of the variables characterizing the system that contains the t axis. Thus, the region around 1 that is inaccessible adiabatically from 1 may be rotated about 1, thereby sweeping out a finite volume inaccessible adiabatically from 1. This volume includes points that are arbitrarily close to 1. We note that reversible adiabatic paths through 1 are restricted to lie on a surface through 1.

Thus, we have proved Caratheodory's principle.

II. DERIVATION OF CARATHEODORY'S PRINCIPLE FROM CLAUSIUS'S POSTULATE

Clausius's postulated form of the second law is as follows: It is impossible that, at the end of a cycle of changes, heat has been transferred from a colder to a hotter body without at the same time converting a certain amount of work into heat.

The system considered is identical to that in Proof I. We consider state 1 specified by temperature t_1 and parameter x_1. (See Fig. 2.) To it, we connect a series of state 1′, 1″, $\cdots$, at the same temperature t_1, differing in parameters x, by a reversible process. We assume that heat is absorbed as x increases (otherwise we could let x decrease). We also assume that Q is a continuous function of x along the isotherm.

Through 1′ and 1″ we draw paths representing reversible adiabatic processes which intersect the isotherm at temperature t_2, at the points 2′ and 2″, respectively. The temperature t_2 is arbitrary subject to the restriction that $t_2<t_1$. The heat absorbed by the system proceeding from 1 to 1′ is $Q_{11'}>0$. We now connect the points along the isotherm at temperature t_2 by a reversible process, and locate the state 3′ on this isotherm, such that $Q_{3'2'}=Q_{11'}$.

We now assert that no adiabatic path, reversible or irreversible, connects states 1 and 3′. If such a path existed, we could go around the cycle $1\rightarrow 3'\rightarrow 2'\rightarrow 1'\rightarrow 1$. The net heat absorbed by the system around the cycle would be 0 since $Q_{3'2'}=Q_{11'}=-Q_{1'1}$. The work done by the system around the cycle would also be 0 by the first law. Thus, the net result would be a transfer of heat, in amount $Q_{11'}$, from the reservoir at t_2 to the higher temperature t_1. This is contary to the physical postulate.

We now locate the state 3″ such that the heat absorbed by the system in the reversible process from 3″ to 2″, $Q_{3''2''}$, is equal to the heat absorbed by the system in the reversible process from 1 to 1″, $Q_{11''}$. We assert that 3″ does not coincide with 3′. For, by the argument of the preceding paragraph, $Q_{1'1''}$ cannot be equal to $Q_{2'2''}$ since the paths 1′—2′ and 1″—2″ are both adiabatic. We may then write

$$\begin{aligned} Q_{3''2''}-Q_{3'2''}&=Q_{11''}-Q_{3'2''}\\ &=(Q_{11'}+Q_{1'1''})-(Q_{3'2'}+Q_{2'2''})\\ &=Q_{1'1''}-Q_{2'2''}\neq 0. \end{aligned}$$

Since the heat absorbed by the system when it proceeds from 3″ to 2″ is not equal to the heat absorbed from 3′ to 2″ along the same path, the states 3′ and 3″ do not coincide.

Clearly any points along the line 3′—3″ on the isotherm at temperature t_2 are adiabatically inaccessible from state 1. Since the temperature t_2 is arbitrary, we may carry through the argument presented above for any isotherm at temperature $t<t_1$. We consider, for example, the isotherm at temperature, t_3. The points of intersection of the adiabatics through 1′ and 1″ with the isotherm at temperature t_3 are 4′ and 4″, respectively. The points 5′ and 5″ on the isotherm at temperature t_3 are chosen such that, $Q_{5'4'}=Q_{11'}$ and $Q_{5''4''}=Q_{11''}$. We consider the region included between the paths along the isotherms between 3′ and 3″ and 5′ and 5″,

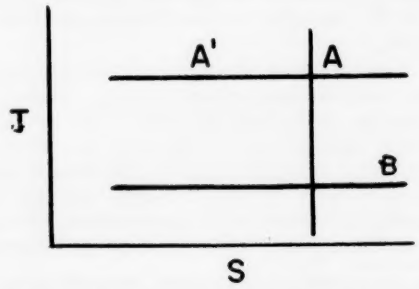

FIG. 3. Reversible isothermal and adiabatic paths in the $T-S$ plane.

and the paths which determine the locus of points along the isotherms between t_2 and t_3 which have the property that the heat absorbed in the reversible process from one of the points, along the isotherm, to the intersection of the reversible adiabatic through 1′ and the isotherm is equal to $Q_{11'}$, and that the heat absorbed in the reversible process from the other point, along the isotherm, to the intersection of the reversible adiabatic through 1″ and the isotherm is equal to $Q_{11''}$. (It is clear that the paths 3′–5′ and 3″–5″ cannot be adiabatic.) The entire area 3′, 3″, 5″, 5′, 3′ is inaccessible by adiabatics from 1. This area can be extended arbitrarily close to 1.

Thus, we have again proved Caratheodory's principle.

III. DERIVATION OF THE RESULT $\Delta S>0$ FOR IRREVERSIBLE PROCESSES IN ISOLATED SYSTEMS

The well-known procedure of Caratheodory applies a restricted Caratheodory's principle (there exists a set of states of finite measure neighboring a given one which are inaccessible along reversible adiabatics) to a treatment of the geometry of solutions of Pfaffian expressions. This attack leads to the following results. There exists a function $T(t)$ such that the differential of the heat dQ for a reversible process, when divided by T, is a perfect differential dS of the entropy function which is a function of state

$$dS=dQ/T. \tag{2}$$

The quantity T, the thermodynamic temperature, is identical with the absolute temperature. This is a proof of the second law of thermodynamics for reversible processes. We shall now present a derivation of the fact that ΔS is greater than zero for irreversible processes in isolated systems.

We consider a system whose states are defined by the variables T, S, and x, where x represents a set of parameters and we assume that a reversible path exists between any two states. We investigate necessary conditions for the existence of an adiabatic process from the state A to the state B. In Fig. 3 we have drawn a representation of the various processes undergone by the system in the $T-S$ plane. We have drawn a line through the states A and A' to represent a reversible isothermal path between the states. The heat absorbed by the system in a given reversible isothermal process increases from left to right since

$$dQ=TdS. \tag{3}$$

We have drawn the line through state A which represents a reversible adiabatic process. Since

$$dQ=TdS=0, \tag{4}$$

in the reversible adiabatic process, this line must be perpendicular to the S axis. We have established in the proof of Caratheodory's principle that the state A cannot be connected by an adiabatic process to any state to the left of the reversible adiabatic through A. Thus, for a natural adiabatic process to exist between the state A and the state B, B must lie to the right of the reversible adiabatic through A. Thus, we have proved that

$$\Delta S=S_B-S_A>0, \tag{5}$$

in a natural adiabatic process. This completes our derivation of the mathematical statement of the second law of thermodynamics from the physical statements.

Proton Resonance Shifts in Alkali Halide Solutions*†

BURTON P. FABRICAND AND SIGMUND GOLDBERG

Columbia University, Hudson Laboratories, Dobbs Ferry, New York

(Received October 24, 1960)

Proton magnetic resonance shifts in alkali halide solutions with respect to distilled water have been measured as a function of ionic charge, radius, and concentration. The shifts are linear with concentration up to a certain concentration depending on the salt. In this linear range, the shifts due to each ion are independent of one another and can be obtained by arbitrarily assuming the shift of the chloride ion to be zero. The ionic shifts so obtained are linear with the ionic crystal radius for anions and cations at a given salt concentration. Results are presented showing that the time-averaged packing of the ions is closer than if they were arranged on a cubic lattice and that the ionic effects on the proton shielding do not extend past nearest-neighbor water molecules.

INTRODUCTION

THE high-resolution nuclear magnetic resonance technique is utilized here to investigate ion-solvent interactions in aqueous alkali halide solutions by measuring the chemical shifts of the protons relative to distilled water. This investigation forms part of a general program designed to measure the proton chemical shifts as a function of ionic charge, size, and concentration. Previous work along these lines was performed by Shoolery and Alder.[1] However, since that time, there has been great improvement in instrumental resolution, allowing new and more accurate results. Also, the coaxial glass-cylinder sample holder[2] now in use enables a correction to the field for the bulk diamagnetic susceptibility of the solution to be applied. This is particularly important here since the correction is of the same order of magnitude as the proton resonance shifts. Unfortunately, the values available for the diamagnetic susceptibilities of alkali halide solutions vary widely so that there is some doubt about the corrections. A discussion of this point will be given below.

The results will be interpreted using the model put forth by Shoolery and Alder in which the proton magnetic shielding by the electrons in the water molecule is changed by the presence of an ion. This change may come about in two ways: (1) the ion disrupts water structure and breaks hydrogen bonds; (2) the ionic electric field distorts the electronic structure of the water molecule. In the first case, the results below, in agreement with most other work,[3] show that the breaking of hydrogen bonds leads to greater apparent shielding of the proton (to higher applied field for resonance). The second case is assumed to lead to lower apparent shielding of the proton. An additional feature presented below is that small ions like lithium actually enhance water structure by causing more hydrogen bonds to be formed in the water near the ion.

Although there are three distinct sites for a water molecule—near an anion, near a cation, and near other water molecules away from any ion—only one resonance line is observed in all cases. This line represents an average of the shifts arising from the three different environments since the exchange rate of the protons is much greater than the observed shifts. The dependence of the shifts on salt concentration should be linear until water molecules are shared among ions. The points of departure from linearity yield information on the packing of ions in solution and also on the maximum distance at which an ion affects the proton shielding.

EXPERIMENTAL

A Varian 56.4-Mc fixed-frequency high-resolution spectrometer was used to measure the shifts. The principal experimental difficulties involved the elimination of air and cooling water temperature fluctuations that affected the stability of the magnetic field. Air conditioning a small house built around the magnet solved the first difficulty. The water problem was solved by feeding the water from an underground stream, which surfaces near the laboratory, into a heat exchanger which cooled the magnet water flowing in a closed system. Since the water temperature of the stream remains nearly constant the year round, excellent stabilization is achieved.

All shifts were measured at 21°C using the side-band technique. The shifts are defined by $\delta = 10^7(H_{H_2O} - H)/H_{H_2O}$, where H is the magnetic field at resonance. Observed shifts were corrected for the bulk diamagnetic susceptibility contribution arising from the ions in solution according to

$$\delta = \delta(\text{obs}) + (2\pi/3)\chi_v,$$

where χ_v is the volume susceptibility of the sample times 10^7.

RESULTS

In terms of the dimensionless parameter δ, both positive and negative proton shifts are obtained. These are shown in Figs. 1 and 2, respectively, which show

* This work was sponsored by the Office of Naval Research.
† Hudson Laboratories Contribution No. 95.

[1] J. N. Shoolery and B. J. Alder, J. Chem. Phys. **23**, 805 (1955).
[2] J. R. Zimmerman and M. R. Foster, J. Phys. Chem. **61**, 282 (1957).
[3] W. G. Schneider, *Hydrogen Bonding* (Pergamon Press, New York, 1959), p. 55.

the concentration dependence of the shifts uncorrected for the bulk diamagnetic susceptibilities of the solutions. It can be seen that all the curves are linear up to a certain concentration, depending on the salt, after which there are deviations from linearity. The concentrations in moles/liter at which these breaks occur are given in column 7 of Table I. For those cases where no break is listed, sufficient points for determining the breaks of interest (which are expected to occur about 3 moles/liter) could not be obtained because of insufficient instrumental resolution. Column 1 lists the salts, column 2 the shifts at a salt concentration of 1 mole/1000 g water (obtained by fitting the best straight lines to the linear portions of the curves). Column 3 lists the bulk diamagnetic susceptibility corrections using the ionic molar susceptibilities obtained theoretically by Pauling,[4] column 5 the susceptibility corrections using experimental values for salt solutions summarized by Myers,[5] and columns 4 and 6, respectively, the corrected shifts using these two sets of corrections. Two sets of corrections have been included to indicate the rather large spread in existing values of the molar diamagnetic susceptibility and their effect on the results.

At a salt concentration of 1 mole/1000 g water where all the shift vs concentration curves are linear, the proton shifts can be looked upon as a sum of independent contributions from water molecules near anions and near cations. If the shift caused by one of the ions, say Cl^-, is arbitrarily taken to be zero, the relative shifts caused by the other ions can be obtained from Table I, columns 4 and 6. Table II lists these relative ionic proton shifts at 1 mole ion/1000 g water. These are the values which best reproduce the observed solution shifts when combined in the proper way. It is immediately apparent that the relative shifts decrease with increasing ionic size except for rubidium and cesium when using the experimental susceptibility correction. Figure 3 shows the dependence of the shift on the ionic crystal radii[6] using Pauling's susceptibilities. The relationship is linear for both anions and cations when using the theoretical correction and for the anions when using the experimental correction. For reasons given below, Pauling's susceptibilities yield the truer values for the shifts.

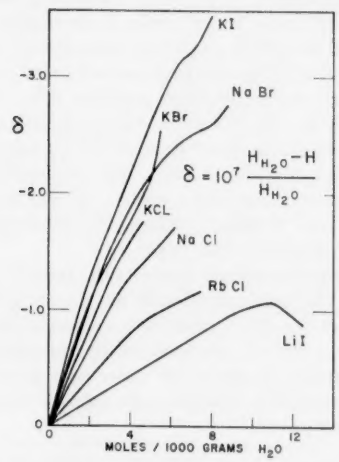

FIG. 1. Negative proton resonance shifts (uncorrected) in solutions relative to distilled water as a function of salt concentration.

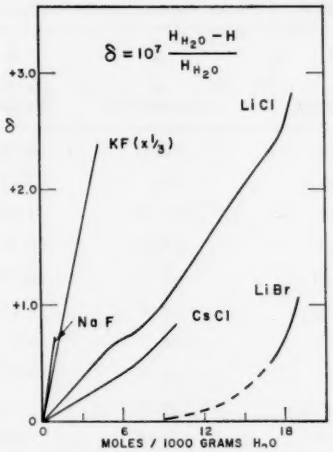

FIG. 2. Positive proton resonance shifts (uncorrected) in solutions relative to distilled water as a function of salt concentration.

The points at which the shift vs concentration curves (see Figs. 1 and 2) depart from linearity indicate the concentrations for the various solutions at which more than one ion starts to affect the proton shielding in a water molecule. From these breaks (see Table I) can be obtained an idea of the time-averaged packing of the ions and the distances from the ions at which ionic effects are observable by NMR. Let r^+ and r^- be the crystal radii of the cations and anions, respectively, and a^+ and a^- the distances from the ions to the points where ionic effects on the shielding can no longer be observed. Then, if the interionic distances at the breaks, $r^+ + a^+ + r^- + a^-$, are plotted against the inverse cube roots of the concentration in moles/liter at which the breaks occur, a straight line will result if the sum of a^+ and a^- is a constant for the molecules included and the coefficient of the inverse cube root of the concentration is a constant for all solutions,

$$r^+ + r^- = kc^{-\frac{1}{3}} - (a^+ + a^-).$$

Figure 4 shows a plot of this equation giving a straight line with the best values of the parameters being $k = 7.9$ and $(a^+ + a^-) = 2.6$ A.

[4] L. Pauling, Proc. Roy. Soc. (London) **A114**, 181 (1927).
[5] W. R. Myers, Revs. Modern Phys. **24**, 15 (1952).
[6] L. Pauling, *The Nature of the Chemical Bond* (Cornell University Press, Ithaca, New York, 1948), p. 346.

TABLE I. Proton resonance shifts in solutions at 1 mole salt/1000 g water; χ_v is volume susceptibility times 10^7.

1	2	3	4	5	6	7
Solution	δ (uncorrected)	$(2\pi/3)\chi_v$ (Pauling)	δ (corrected)	$(2\pi/3)\chi_v$ (experimental)	δ (corrected)	Breaks (moles/liter)
LiCl	+0.12	0.61	−0.49	0.52	−0.40	4.1
LiBr	0	1.12	−1.12	0.71	−0.71	...
LiI	−0.11	1.65	−1.76	1.01	−1.12	...
NaF	+0.71	0.25	+0.46	0.25	+0.46	...
NaCl	−0.34	0.69	−1.03	0.61	−0.95	3.3
NaBr	−0.49	1.18	−1.67	0.82	−1.51	3.0
KF	+0.57	0.52	+0.05	0.49	+0.08	...
KCl	−0.39	0.94	−1.33	0.79	−1.17	2.75
KBr	−0.53	1.43	−1.96	0.99	−1.52	2.5
KI	−0.61	1.90	−2.51	1.26	−1.87	2.2
RbCl	−0.20	1.27	−1.47	0.92	−1.12	...
RbBr	−0.32	1.73	−2.05	1.10	−1.42	...
RbI	−0.43	2.12	−2.55	1.24	−1.67	...
CsCl	+0.07	1.66	−1.59	1.22	−1.15	...

DISCUSSION

The fact that the bulk diamagnetic susceptibilities of the salt solutions are of the same order of magnitude and often larger than the proton resonance shifts, places a serious limitation on the accuracy of the results. Two sets of susceptibilities have been used in presenting the results to show that the estimates of various authors can be quite different. The experimental values themselves vary widely and represent an average over the results of many people.

The whole subject has been reviewed by Myers.[5] Suffice it to be said here that the use of Pauling's theoretical values for the ionic susceptibilities seems to give the most reasonable results in this work for two reasons. First, the least scatter occurs when the observed shifts (columns 4 and 6, Table I) are obtained by the addition of the relative ionic proton shifts (Table II). The second reason is concerned with the shift dependence on the ionic radii. As the radius increases, the proton resonance shift becomes more negative except in the cases of rubidium and cesium when any set of ionic susceptibilities other than Pauling's is used. Now, when the ionic radius increases, the partial molal entropy of solution[7] increases, indicating that water structure is increasingly disrupted and that more hydrogen bonds are being broken. Also, with increasing radius, the electric field at the water proton is decreasing, causing less distortion of the electronic structure of the water molecule. Both these occurrences lead to greater shielding, and, consequently, more negative shifts. It is seen from Table II that the anions do satisfy this argument and, indeed, give a linear dependence no matter which set of susceptibilities is used. But the rubidium and cesium discrepancies make suspect all sets of susceptibilities except Pauling's. Therefore, Pauling's values are the ones used in this paper.

TABLE II. Relative proton shifts for each ion at 1 mole ion/1000 g water, $\delta_{Cl^-}=0$. Column 2 was calculated using Pauling's susceptibilities, and column 3 using experimental susceptibilities.

Ion	δ	δ
Li^+	−0.52	−0.32
Na^+	−1.00	−0.97
K^+	−1.34	−1.17
Rb^+	−1.42	−1.07
Cs^+	−1.60	−1.15
F^-	+1.44	+1.33
Cl^-	0	0
Br^-	−0.63	−0.38
I^-	−1.18	−0.66

The linear dependence between the proton resonance shifts and the ionic crystal radii has a number of implications. Let the shift caused by an anion be the sum of two shifts, a shift δ_B proportional to the average number of hydrogen bonds in the water near an ion, and a polarization shift δ_E dependent on the ionic electric field at the water proton,

$$\delta_{\text{ion}}=\delta_B+\delta_E.$$

Since the sum of the two terms is linearly related to the

[7] W. M. Latimer, K. S. Pitzer, and W. V. Smith, J. Am. Chem. Soc. **60**, 1829 (1938).

ionic crystal radius, each term separately must be so related, unless there occurs a fortuitous cancellation of higher order terms. This implies that the average number of bonds in water near an ion is proportional to the ionic radius and that the number decreases with increasing radius. This result is confirmed by the fact that the ionic entropy of solution, which is a measure of the degree of disorder and, therefore, related to the number of bonds, increases with increasing ionic radius, and, indeed, is directly proportional to the ionic radius for both cations and anions.

The linear relation between the ionic entropy of solution and δ_B (both are proportional to the ionic radius) implies that the lower entropy associated with the smaller ions as compared to larger ions arises because of the greater number of hydrogen bonds near the ion and not because there exists around the ion a region of immobilized water molecules oriented in the spherically symmetric ionic field. Frank and Wen[8] have used entropy data as the basis for assigning an orderly gradation of net structure-altering influence to ions. According to this, cations smaller than potassium are net structure-formers while potassium is slightly structure breaking on balance in comparison to pure water. Therefore, in accord with Gurney,[9] the number of hydrogen bonds in water near sodium and lithium ions is greater than in pure water. The traditional concept of a large, compact "hydrated ion" seems unlikely in these cases.

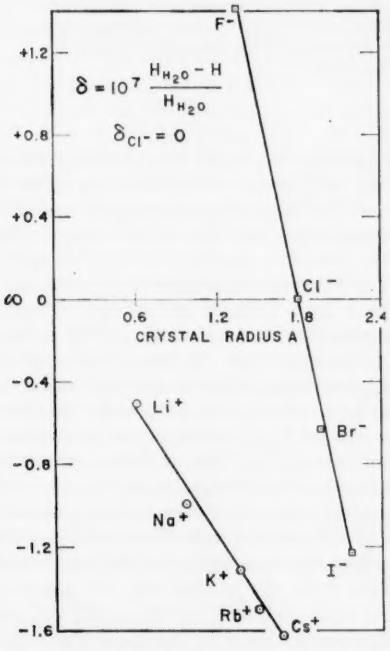

FIG. 3. Relative proton shifts as a function of the ionic crystal radius at a concentration of 1 mole salt/1000 g water.

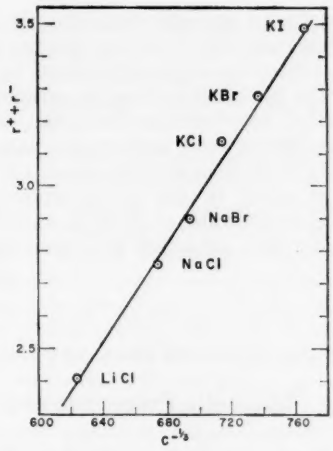

FIG. 4. Plot of the sum of the ionic crystal radii in angstroms for various solutions vs the cube root of the concentration in moles/liter.

The difference in the chemical shifts between anions and cations arises from the polarization term δ_E, since the water proton is closer on the average to an anion and therefore experiences a larger electric field. It is assumed that δ_B is the same for an ion of given radius regardless of the sign of the charge. If this is so, a subtraction of the values of δ for an anion and cation of given ionic radius will yield the difference in the polarization terms for those ions. Thus, the difference for potassium and fluorine ions is 2.78. This difference decreases with increasing ionic radius. A theoretical calculation of this term would involve knowing the magnetic shielding dependence on the electric field at the proton and a distribution function for the proton position. Again, the term δ_E, like δ_B, must be linearly related to the ionic radius, or possibly, a constant.

The points at which the proton shift vs concentration curves depart from linearity designate the concentration at which water molecules become shared between ions. The straight line resulting from the plot of the interionic distance vs the inverse cube of the concentration indicates that the packing of the ions is greater than if they were on the average arranged on a cubic lattice. For the latter case the value of the proportionality constant is 9.4 rather than the observed 7.9. The distance between the ions at the breaks is just enough, about 2.6 A, to position a water molecule. Thus ionic effects on the proton shielding do not extend much beyond nearest-neighbor water molecules.

Some features of the proton resonance shift at high salt concentrations (Figs. 1 and 2) will now be given, although any attempt to explain these at the present

[8] H. S. Frank and W. Y. Wen, Discussions Faraday Soc. **24**, 133 (1957).

[9] R. W. Gurney, *Ionic Processes in Solution* (McGraw-Hill Book Company, Inc., New York, 1953), p. 195.

time does not seem advisable because of the inability to disentangle many effects such as bulk susceptibility changes and many-ion interactions arising from space crowding. The KF curve is linear to saturation. The slope of the LiCl curve changes three times, decreasing at 4.5 moles/1000 g water, increasing at about 8 to a value slightly larger than its initial value, and increasing again at about 18 just before saturation. The LiBr curve is unobservable to about 17, at which point it rises rapidly until saturation. At a point just about 1 mole/1000 g water before saturation, the curves for KI, NaBr, and KBr show increases in the slope. For LiI, the slope actually changes sign just before saturation.

ACKNOWLEDGMENTS

We wish to acknowledge the help of Dr. J. R. Johnson during the early phases of this work, Dr. F. Pollock for interesting discussions, and Mrs. Irene Fiore for the figures.

THE JOURNAL OF CHEMICAL PHYSICS VOLUME 34, NUMBER 5 MAY, 1961

Magnetic Properties and Optical Absorption Spectrum of K_2ReCl_6

J. C. EISENSTEIN

National Bureau of Standards, Washington, D. C.

(Received November 7, 1960)

A phenomenological theory of certain physical properties of the $(ReCl_6)^{2-}$ complex ion is presented here. The ion can be described in terms of a set of parameters which includes the strength of the octahedral ligand field, the Coulomb integrals, the spin-orbit coupling constant and the orbital reduction factors. The interaction matrices for the three-electron system are given in algebraic form. With an appropriate choice of the parameters the eigenvalues of these matrices are in fair agreement with the observed energy levels of the system. The effect of a departure from strict octahedral symmetry is discussed. The matrix elements of the magnetic moment operator are also given in algebraic form and then used in a calculation of the susceptibility. The discrepancy between theory and experiment is attributed to a superexchange interaction which leads, at sufficiently low temperatures, to antiferromagnetism of the compound. Finally, the results of paramagnetic resonance experiments on K_2ReCl_6 are considered.

1. INTRODUCTION

THE compounds A_2BX_6 where A is an alkali metal ion [or NH_4 or $C(NH_3)_4$], B is a metal ion of the $4d$ or $5d$ groups and X is a halogen ion, form a series closely related in many physical properties. Their structures[1–4] and magnetic properties[5–10] have been extensively investigated. Some data on their absorption spectra are also available.[11–16]

These A_2BX_6 compounds differ in important respects from the well-known octahedrally coordinated compounds of the iron group elements such as the alums, the Tutton salts, and the fluosilicates. In the first place, the spin-orbit coupling constant is larger and the Racah[17] parameters are smaller for the $4d$ and $5d$ elements than for the $3d$ (or iron group) elements. As a consequence the sequence of the energy levels differs for corresponding ions of the different groups. In addition, the large value of the spin-orbit coupling constant for the $4d$ and $5d$ compounds makes it necessary to consider the coupling of configurations by the spin-orbit interaction. This coupling can usually be ignored for the iron group compounds.

Second, the $4d$ or $5d$ electrons have orbitals which overlap the halogen orbitals. This overlap makes possible a superexchange interaction between neighboring metal ions. Both the overlap and the superexchange effects must be considered in discussing the magnetic and optical properties of the A_2BX_6 compounds.

The first attempt to interpret theoretically the magnetic data on octahedrally coordinated $4d$ and $5d$ compounds was made by Stevens[18] who extended earlier

[1] R. Hoppe and W. Klemm, Z. anorg. u. allgem. Chem. **268**, 364 (1952).
[2] A. G. Sharpe, J. Chem. Soc. **1953**, 197.
[3] B. Cox and A. G. Sharpe, J. Chem. Soc. **1953**, 1783.
[4] R. D. Peacock, J. Chem. Soc. **1956**, 1291.
[5] D. P. Mellor, Proc. Roy. Soc. New South Wales **77**, 145 (1944).
[6] R. S. Nyholm and A. G. Sharpe, J. Chem. Soc. **1952**, 3579.
[7] E. Weise, Z. anorg. u. allgem. Chem. **283**, 377 (1956).
[8] E. Weise and W. Klemm, Z. anorg. u. allgem. Chem. **272**, 211 (1953).
[9] E. N. Sloth and C. S. Garner, J. Chem. Phys. **22**, 2064 (1954).
[10] V. Norman and J. C. Morrow, J. Chem. Phys. **31**, 455 (1959).
[11] C. K. Jørgensen, Acta Chem. Scand. **9**, 710 (1955).
[12] R. H. Busey and Q. V. Larson, Oak Ridge National Laboratory Unclassified Rept. ORNL–2584 (September, 1958).
[13] G. E. Boyd, J. Chem. Educ. **36**, 3 (1959).
[14] E. K. Maun and N. Davidson, J. Am. Chem. Soc. **72**, 2254 (1950).
[15] C. L. Rulfs and R. J. Meyer, J. Am. Chem. Soc. **77**, 4505 (1955).
[16] D. R. Stephens and H. G. Drickamer, J. Chem. Phys. **30**, 1364, 1518 (1959).
[17] G. Racah, Phys. Rev. **62**, 438 (1942).
[18] K. W. H. Stevens, Proc. Roy. Soc. (London) **A219**, 542 (1953).

theories due to Van Vleck[19] and Kotani.[20] He assumed that in successive compounds (such as WF_6, ReF_6, OsF_6, IrF_6, and PtF_6) the d electrons fill first the available $\epsilon(t_2)$ orbitals and only when the ϵ orbitals are completely filled do electrons go into the $\gamma(e)$ orbitals. Thus, of the five d electrons outside the Ir^{6+} core in K_2IrCl_6 four are paired; the magnetic properties of K_2IrCl_6 are due to a single unpaired electron (or hole).

The compound $(NH_4)_2IrCl_6$ is quite interesting for historical reasons. The discovery[21] of chlorine hyperfine structure in its paramagnetic resonance spectrum led Stevens to postulate that the Ir d electrons can be found on the Cl^- ions about 30% of the time. The existence of this wandering effect now seems firmly established. The magnetic properties of K_2IrCl_6 and $(NH_4)_2IrCl_6$ have recently been thoroughly investigated by an Oxford group.[22–24] They have demonstrated the existence in these compounds of the superexchange interaction mentioned above.

The remainder of this paper will be devoted to the compound K_2ReCl_6 in solid form and in aqueous solution.

2. STRUCTURE AND BONDING

According to Aminoff[25] (and also according to Boyd,[13] who quotes unpublished work by Zachariasen and by Nelson) K_2ReCl_6 is cubic and has the K_2PtCl_6 or fluorite structure. The K^+ and $(ReCl_6)^{2-}$ ions occupy the F^- and Ca^{2+} positions in the fluorite lattice. The unit cell dimension is given as 9.861 A by Aminoff and as 9.82 A by Dalziel, Gill, Nyholm, and Peacock.[26] The $(ReCl_6)^{2-}$ ion is octahedral, or nearly so. Aminoff states that the Re—Cl distance is 2.37 A. Throughout most of this paper it is assumed that in K_2ReCl_6 the Re^{4+} ion is surrounded by a regular octahedraon of Cl^- ions. Effects of departure from octahedral symmetry are discussed in Sec. 4.

For our purposes we can assume that the primary bonds in the complex ion $(ReCl_6)^{2-}$ are either ionic or covalent. In the former case four electrons from neutral Re, whose electron configuration is $5d^56s^2$, migrate to the chlorine atoms. In the latter case one can assume that the four electrons, plus the two electrons acquired by the complex from the K atoms, are in a $5d^26s6p^3$ configuration on the Re^{4+} core. The corresponding orbitals can be hybridized to form six equivalent bonding orbitals which point in the directions of the Cl atoms. These orbitals will overlap hybridized Cl $3p4s$ orbitals thus giving rise to the primary σ bonds. Some support for the covalent-bonding model comes from the nonexistence of K_2WF_6 and K_2WCl_6. One can argue that the nuclear charge of W is too small to stabilize the equivalent bonding orbitals on the central ion.

In either the ionic- or the covalent-bonding approximation the electron configuration is such that the bonding electrons give rise to an electrostatic field of octahedral symmetry at the location of the central ion. This octahedral ligand field has an important perturbing effect on the free-ion energy levels.

If one adopts the covalent-bonding model it follows that the bonding orbitals which use the Re $5d$ functions are fully occupied. The antibonding $5d$ orbitals, however, are available for occupation by the three Re electrons which remain unpaired outside the Re^{4+} core. The Re σ bonding and antibonding orbitals involve d wave functions which span the $\Gamma_3(E)$ representation of the cubic group. Therefore if there is a nonzero amount of covalent σ bonding the (antibonding) $d\gamma$ orbitals will not be pure Re $5d$ functions but will involve admixtures of Cl $3p$ and $4s$ functions.

The work of Stevens has made it clear that π-bonding effects are important in the chloroiridates and therefore also for the structurally similar compound K_2ReCl_6. Linear combinations of Cl p orbitals can be formed which transform in the same way under the operations of the cubic group as the Re d orbitals which span the $\Gamma_5(T_2)$ representation of the cubic group. The correct wave functions for the $(ReCl_6)^{2-}$ complex are therefore mixtures of Re and Cl orbitals. In other words, the overlap of the Re and Cl orbitals leads to a certain amount of π bonding.

Numerous observable effects are consequences of this overlap. First of all, the orbital angular momentum and the spin-orbit coupling constant are effectively reduced from their free-ion values.[27] Second, the Racah parameters are altered. Third, hyperfine structure due to the chlorine nuclei appears in the paramagnetic resonance absorption spectrum.[28] Finally, a superexchange interaction can occur which couples Re ions via Cl intermediaries. This interaction is responsible for the known antiferromagnetic transitions in K_2IrCl_6 and $(NH_4)_2IrCl_6$ at 3.08° and 2.16°K, respectively. There is undoubtedly a similar antiferromagnetic transition in K_2ReCl_6 but it has not yet been observed.

3. INTERACTION MATRICES

It is rather difficult to treat the problem of the $(ReCl_6)^{2-}$ complex in its full generality. Consequently a number of simplifying approximations have been made so that the calculations are tractable. First of all, the wave functions are assumed to be hydrogenic d functions localized on the Re^{4+} core. In order to take

[19] J. H. Van Vleck, J. Chem. Phys. **3,** 807 (1935).
[20] M. Kotani, J. Phys. Soc. Japan **4,** 293 (1949).
[21] J. Owen and K. W. H. Stevens, Nature **171,** 836 (1953).
[22] J. H. E. Griffiths, J. Owen, J. G. Park, and M. F. Partridge, Proc. Roy. Soc. (London) **A250,** 84 (1959).
[23] A. H. Cooke, R. Lazenby, F. R. McKim, J. Owen, and W. P. Wolf, Proc. Roy. Soc. (London) **A250,** 97 (1959).
[24] B. R. Judd, Proc. Roy. Soc. (London) **A250,** 110 (1959).
[25] B. Aminoff, Z. Krist. **A94,** 246 (1936).
[26] J. Dalziel, N. S. Gill, R. S. Nyholm, and R. D. Peacock, J. Chem. Soc. **1958,** 4012.
[27] J. Owen, Proc. Roy. Soc. (London) **A227,** 183 (1955); Discussions Faraday Soc. **19,** 127 (1955).
[28] J. H. E. Griffiths and J. Owen, Proc. Roy. Soc. (London) **A226,** 96 (1954).

TABLE I. Matrix elements of the ligand field, the spin-orbit interaction, and the Coulomb interaction. Over-all representation Γ_6.

	$\lvert {}^2T_1\gamma\epsilon^2\rangle$	$\lvert {}^2T_1\epsilon^3\rangle$	$\lvert {}^2T_1\gamma\epsilon^2\rangle$	$\lvert {}^2T_1\gamma\epsilon^2\rangle$	$\lvert {}^2T_1\gamma^2\epsilon\rangle$	$\lvert {}^2T_1\gamma^2\epsilon\rangle$	$\lvert {}^4T_1\gamma\epsilon^2\rangle$	$\lvert {}^4T_1\gamma^2\epsilon\rangle$	$\lvert {}^4T_2\gamma\epsilon^2\rangle$
$\langle {}^2A_1\gamma\epsilon^2 \rvert$	$V+2A_2+A_0$ $-12B_2+B_0+C_2$ $+2C_0$	$\frac{1}{2}(6)^{\frac{1}{2}}\zeta'$	$-\frac{1}{6}(6)^{\frac{1}{2}}\zeta$	0	$-\frac{1}{6}(6)^{\frac{1}{2}}\zeta'$	$\frac{1}{2}\sqrt{2}\zeta'$	$\frac{1}{3}\sqrt{3}\zeta$	$-\frac{7}{3}\sqrt{3}\zeta'$	0
$\langle {}^2T_1\epsilon^3 \rvert$		$3A_0-6B_0+3C_0$	$3B_1-\frac{1}{2}\zeta'$	$-3B_1+\frac{1}{2}\zeta'$	0	$2\sqrt{3}B_2$	$\frac{1}{2}\sqrt{2}\zeta'$	0	$-\frac{1}{2}\sqrt{2}\zeta'$
$\langle {}^2T_1\gamma\epsilon^2 \rvert$			$V+2A_2+A_0$ $+5B_2-5B_0$ $+3C_2-\frac{1}{3}\zeta$	$-3B_2-\frac{1}{3}\zeta$	$-3B_1+\frac{5}{6}\zeta'$	$3\sqrt{3}B_1+\frac{1}{3}\sqrt{3}\zeta'$	$\sqrt{2}\zeta/12$	$\frac{1}{6}\sqrt{2}\zeta'$	$-\frac{1}{4}\sqrt{2}\zeta$
$\langle {}^2T_1\gamma\epsilon^2 \rvert$				$V+2A_2+A_0$ $-7B_2+B_0$ $+C_2+2C_0$	$3B_1+\frac{1}{2}\zeta'$	$-\sqrt{3}B_1$	$-\frac{1}{4}\sqrt{2}\zeta$	$-\frac{1}{2}\sqrt{2}\zeta'$	$-\frac{1}{4}\sqrt{2}\zeta$
$\langle {}^2T_1\gamma^2\epsilon \rvert$					$2V+A_4+2A_2$ $-8B_4+2B_2$ $+3C_2-\frac{1}{3}\zeta$	$-2\sqrt{3}B_2$	$\frac{1}{6}\sqrt{2}\zeta'$	$\frac{1}{3}\sqrt{2}\zeta$	$\frac{1}{2}\sqrt{2}\zeta'$
$\langle {}^2T_1\gamma^2\epsilon \rvert$						$2V+A_4+2A_2$ $-2B_2+2C_4$ $+C_2-\frac{1}{3}\zeta$	$-\frac{1}{3}(6)^{\frac{1}{2}}\zeta'$	0	0
$\langle {}^4T_1\gamma\epsilon^2 \rvert$							$V+2A_2+A_0$ $+2B_2-5B_0$ $-5\zeta/12$	$6B_1-\frac{5}{6}\zeta'$	$-\frac{1}{4}\zeta$
$\langle {}^4T_1\gamma^2\epsilon \rvert$								$2V+A_4+2A_2$ $-8B_4-4B_2+\frac{5}{6}\zeta$	$\frac{1}{2}\zeta'$
$\langle {}^4T_2\gamma\epsilon^2 \rvert$									$V+2A_2+A_0$ $-10B_2-5B_0+\frac{1}{4}\zeta$

TABLE II. Matrix elements of the ligand field, the spin-orbit interaction, and the Coulomb interaction. Over-all representation Γ_7.

	$\lvert {}^2A_2\gamma\epsilon^2\rangle$	$\lvert {}^4T_1\gamma\epsilon^2\rangle$	$\lvert {}^4T_1\gamma^2\epsilon\rangle$	$\lvert {}^2T_2\epsilon^3\rangle$	$\lvert {}^2T_2\gamma\epsilon^2\rangle$	$\lvert {}^2T_2\gamma\epsilon^2\rangle$	$\lvert {}^2T_2\gamma^2\epsilon\rangle$	$\lvert {}^2T_2\gamma^2\epsilon\rangle$	$\lvert {}^4T_2\gamma\epsilon^2\rangle$
$\langle {}^2A_2\gamma\epsilon^2 \rvert$	$V+2A_2+A_0$ $+8B_2+B_0+C_2$ $+2C_0$	0	0	$\frac{1}{2}\sqrt{2}\zeta'$	$-\frac{1}{6}(6)^{\frac{1}{2}}\zeta$	0	$-\frac{1}{2}\sqrt{2}\zeta'$	$\frac{1}{2}\sqrt{2}\zeta'$	$\frac{1}{3}\sqrt{3}\zeta$
$\langle {}^4T_1\gamma\epsilon^2 \rvert$		$V+2A_2+A_0$ $+2B_2-5B_0+\frac{1}{4}\zeta$	$6B_1+\frac{1}{2}\zeta'$	$-\frac{1}{2}(6)^{\frac{1}{2}}\zeta'$	$\frac{1}{4}\sqrt{2}\zeta$	$-\frac{1}{4}\sqrt{2}\zeta$	$\frac{1}{2}(6)^{\frac{1}{2}}\zeta'$	0	$\frac{1}{4}\zeta$
$\langle {}^4T_1\gamma^2\epsilon \rvert$			$2V+A_4+2A_2$ $-8B_4-4B_2-\frac{1}{2}\zeta$	0	$-\frac{1}{2}\sqrt{2}\zeta'$	$\frac{1}{2}\sqrt{2}\zeta'$	0	0	$-\frac{1}{2}\zeta'$
$\langle {}^2T_2\epsilon^3 \rvert$				$3A_0+5C_0$	$3\sqrt{3}B_1-\frac{1}{6}\sqrt{3}\zeta'$	$-5\sqrt{3}B_1+\frac{1}{2}\sqrt{3}\zeta'$	$-4B_2-2C_2$	$2B_2$	$\frac{1}{6}(6)^{\frac{1}{2}}\zeta'$
$\langle {}^2T_2\gamma\epsilon^2 \rvert$					$V+2A_2+A_0$ $-B_2-5B_0$ $+3C_2-\frac{1}{3}\zeta$	$-3B_2+\frac{1}{2}\zeta$	$-3\sqrt{3}B_1$ $+\frac{1}{6}\sqrt{3}\zeta'$	$3\sqrt{3}B_1+\frac{1}{2}\sqrt{3}\zeta'$	$\sqrt{2}\zeta/12$
$\langle {}^2T_2\gamma\epsilon^2 \rvert$						$V+2A_2+A_0$ $+3B_2+B_0+C_2$ $+2C_0$	$\sqrt{3}B_1-\frac{1}{2}\sqrt{3}\zeta'$	$\sqrt{3}B_1$	$\frac{1}{4}\sqrt{2}\zeta$
$\langle {}^2T_2\gamma^2\epsilon \rvert$							$2V+A_4+2A_2$ $+8B_4-2B_2$ $+4C_4+C_2+\zeta$	$-10B_2$	$-\frac{1}{6}(6)^{\frac{1}{2}}\zeta'$
$\langle {}^2T_2\gamma^2\epsilon \rvert$								$2V+A_4+2A_2$ $-2B_2+2C_4+C_2$ $-\frac{1}{2}\zeta$	$-\frac{1}{3}(6)^{\frac{1}{2}}\zeta'$
$\langle {}^4T_2\gamma\epsilon^2 \rvert$									$V+2A_2+A_0$ $-10B_2-5B_0$ $-5\zeta/12$

TABLE III. Matrix elements of the ligand field, the spin-orbit

	$\lvert {}^4A_2\epsilon^3\rangle$	$\lvert {}^2E\epsilon^3\rangle$	$\lvert {}^2E\gamma\epsilon^2\rangle$	$\lvert {}^2E\gamma\epsilon^2\rangle$	$\lvert {}^2E\gamma^3\rangle$	$\lvert {}^2T_1\epsilon^3\rangle$	$\lvert {}^2T_1\gamma\epsilon^2\rangle$	$\lvert {}^2T_1\gamma\epsilon^2\rangle$	$\lvert {}^2T_1\gamma^2\epsilon\rangle$	$\lvert {}^2T_1\gamma^2\epsilon\rangle$
$\langle {}^4A_2\epsilon^3 \rvert$	$3A_0$ $-15B_0$	0	0	0	0	0	0	0	0	0
$\langle {}^2E\epsilon^3 \rvert$		$3A_0-6B_0$ $+3C_0$	$-6\sqrt{2}B_1$	$3\sqrt{2}B_1$	0	0	0	$-\frac{1}{2}(6)^{\frac{1}{2}}\zeta'$	0	0
$\langle {}^2E\gamma\epsilon^2 \rvert$			$V+2A_2$ $+A_0-2B_2$ $+10B_0+C_2$ $+5C_0$	$-10B_2$	$\sqrt{3}(2B_2+C_2)$	0	$-\frac{1}{3}\sqrt{3}\zeta$	0	$\frac{1}{6}\sqrt{3}\zeta'$	$-\frac{1}{2}\zeta'$
$\langle {}^2E\gamma\epsilon^2 \rvert$				$V+2A_2$ $+A_0-2B_2$ $+B_0+C_2$ $+2C_0$	$-2\sqrt{3}B_2$	$\frac{1}{2}\sqrt{3}\zeta'$	$\frac{1}{6}\sqrt{3}\zeta$	0	$\frac{1}{6}\sqrt{3}\zeta'$	$-\frac{1}{2}\zeta'$
$\langle {}^2E\gamma^3 \rvert$					$3V+3A_4$ $-8B_4+4C_4$	0	0	0	$\frac{1}{2}\zeta'$	$-\frac{1}{2}\sqrt{3}\zeta'$
$\langle {}^2T_1\epsilon^3 \rvert$						$3A_0-6B_0$ $+3C_0$	$3B_1+\frac{1}{4}\zeta'$	$-3B_1-\frac{1}{4}\zeta'$	0	$2\sqrt{3}B_2$
$\langle {}^2T_1\gamma\epsilon^2 \rvert$							$V+2A_2$ $+A_0+5B_2$ $-5B_0+3C_2$ $+\frac{1}{6}\zeta$	$-3B_2+\frac{1}{4}\zeta$	$-3B_1$ $-5\zeta'/12$	$3\sqrt{3}B_1$ $-\frac{1}{6}\sqrt{3}\zeta'$
$\langle {}^2T_1\gamma\epsilon^2 \rvert$								$V+2A_2$ $+A_0-7B_2$ $+B_0+C_2$ $+2C_0$	$3B_1-\frac{1}{4}\zeta'$	$-\sqrt{3}B_1$
$\langle {}^2T_1\gamma^2\epsilon \rvert$									$2V+A_4$ $+2A_2-8B_4$ $+2B_2+3C_2$ $+\frac{1}{6}\zeta$	$-2\sqrt{3}B_2$
$\langle {}^2T_1\gamma^2\epsilon \rvert$										$2V+A_4$ $+2A_2-2B_2$ $+2C_4+C_2$ $+\frac{1}{4}\zeta$
$\langle {}^4T_1\gamma\epsilon^2 \rvert$										
$\langle {}^4T_1\gamma^2\epsilon \rvert$										

interaction, and the Coulomb interaction. Over-all representation Γ_8.

$\vert {}^4T_1\gamma\epsilon^3\rangle$	$\vert {}^4T_1\gamma^3\epsilon\rangle$	$\vert {}^4T_1\gamma\epsilon^3\rangle$	$\vert {}^4T_1\gamma^3\epsilon\rangle$	$\vert {}^2T_2\epsilon^3\rangle$	$\vert {}^2T_2\gamma\epsilon^3\rangle$	$\vert {}^2T_2\gamma\epsilon^3\rangle$	$\vert {}^2T_2\gamma^3\epsilon\rangle$	$\vert {}^2T_2\gamma^3\epsilon\rangle$	$\vert {}^4T_2\gamma\epsilon^3\rangle$	$\vert {}^4T_2\gamma\epsilon^3\rangle$
0	0	0	0	$-\zeta$	$\frac{2}{3}\sqrt{3}\zeta'$	0	0	0	$-\frac{1}{3}\sqrt{3}\zeta'$	$-\frac{2}{3}\sqrt{3}\zeta'$
0	0	0	0	$\frac{1}{2}\sqrt{2}\zeta$	$\frac{1}{6}(6)^{\frac{1}{2}}\zeta'$	0	0	0	$-\frac{1}{3}(6)^{\frac{1}{2}}\zeta'$	$\frac{1}{3}(6)^{\frac{1}{2}}\zeta'$
$-\frac{1}{3}\sqrt{3}\zeta$	$-\frac{1}{3}\sqrt{3}\zeta'$	$\frac{1}{3}\sqrt{3}\zeta$	$\frac{1}{3}\sqrt{3}\zeta'$	ζ'	$-\frac{1}{3}\sqrt{3}\zeta$	0	$\frac{1}{2\sqrt{5}}\zeta'$	$-\frac{1}{2\sqrt{5}}\zeta'$	$-\frac{1}{3}\sqrt{3}\zeta$	$\frac{1}{3}\sqrt{3}\zeta$
$\frac{1}{3}\sqrt{3}\zeta$	$-\frac{1}{3}\sqrt{3}\zeta'$	$-\frac{1}{6}\sqrt{3}\zeta$	$\frac{1}{3}\sqrt{3}\zeta'$	$\frac{1}{2\sqrt{5}}\zeta'$	$-\frac{1}{6}\sqrt{3}\zeta$	0	$-\frac{1}{2\sqrt{5}}\zeta'$	$\frac{1}{2\sqrt{5}}\zeta'$	$-\frac{1}{6}\sqrt{3}\zeta$	$\frac{1}{6}\sqrt{3}\zeta$
0	$-\zeta'$	0	ζ'	0	0	0	$-\frac{1}{2}\sqrt{3}\zeta'$	$-\frac{1}{2}\sqrt{3}\zeta'$	0	0
$-\frac{1}{2\sqrt{5}}\zeta'$	0	$-\zeta'$	0	$-\frac{1}{2}\sqrt{3}\zeta$	$\frac{1}{4\sqrt{5}}\zeta'$	$-\frac{3}{4\sqrt{5}}\zeta'$	0	0	$\frac{1}{2\sqrt{5}}\zeta'$	0
$-\zeta/12$	$-\frac{1}{6\sqrt{5}}\zeta'$	$-\frac{1}{6}\zeta$	$-\frac{1}{2\sqrt{5}}\zeta'$	$-\frac{1}{4}\sqrt{3}\zeta'$	$\frac{1}{2\sqrt{5}}\zeta$	$\frac{1}{4}\zeta$	$\frac{1}{4}\sqrt{3}\zeta'$	0	$\frac{1}{4}\zeta$	0
$\frac{1}{4}\zeta$	$\frac{1}{2\sqrt{5}}\zeta'$	$\frac{1}{4}\zeta$	ζ'	$\frac{1}{4}\sqrt{3}\zeta'$	$-\frac{1}{4}\zeta$	0	$-\frac{1}{4}\sqrt{3}\zeta'$	$-\frac{1}{4}\sqrt{3}\zeta'$	$\frac{1}{4}\zeta$	0
$-\frac{1}{6\sqrt{5}}\zeta'$	$-\frac{1}{2\sqrt{5}}\zeta$	$-\frac{1}{2\sqrt{5}}\zeta'$	$-\frac{2}{\sqrt{5}}\zeta$	0	$5\zeta'/4$	$\frac{1}{4\sqrt{5}}\zeta'$	0	0	$-\frac{1}{2\sqrt{5}}\zeta'$	0
$\frac{1}{3}\sqrt{3}\zeta'$	0	$\frac{2}{3}\sqrt{3}\zeta'$	0	0	0	$\frac{1}{2}\sqrt{3}\zeta'$	0	$-\frac{3}{4}\zeta$	0	0
$V+2A_2$ $+A_0+2B_2$ $-5B_0+\frac{1}{6\sqrt{5}}\zeta$	$6B_1+\frac{1}{2\sqrt{5}}\zeta'$	$-\frac{1}{6\sqrt{5}}\zeta$	$-\frac{1}{2\sqrt{5}}\zeta'$	$-\frac{1}{2}\sqrt{3}\zeta'$	$\frac{1}{4\sqrt{5}}\zeta$	$-\frac{1}{4\sqrt{5}}\zeta$	$\frac{1}{2}\sqrt{3}\zeta'$	0	0	$-\frac{1}{2\sqrt{5}}\zeta$
	$2V+A_1$ $+2A_2-8B_4$ $-4B_2-\frac{1}{2\sqrt{5}}\zeta$	$-\frac{1}{2\sqrt{5}}\zeta'$	$\frac{1}{2\sqrt{5}}\zeta$	0	$-\frac{1}{2\sqrt{5}}\zeta'$	$\frac{1}{2\sqrt{5}}\zeta'$	0	0	0	ζ'

TABLE III.—

	$\lvert {}^4A_2\epsilon^3\rangle$	$\lvert {}^2E\epsilon^3\rangle$	$\lvert {}^2E\gamma\epsilon^2\rangle$	$\lvert {}^2E\gamma\epsilon^2\rangle$	$\lvert {}^2E\gamma^3\rangle$	$\lvert {}^2T_1\epsilon^3\rangle$	$\lvert {}^2T_1\gamma\epsilon^2\rangle$	$\lvert {}^2T_1\gamma\epsilon^2\rangle$	$\lvert {}^2T_1\gamma^2\epsilon\rangle$	$\lvert {}^2T_1\gamma^2\epsilon\rangle$
$\langle {}^4T_1\gamma\epsilon^2 \rvert$										
$\langle {}^4T_1\gamma^2\epsilon \rvert$										
$\langle {}^2T_2\epsilon^3 \rvert$										
$\langle {}^2T_2\gamma\epsilon^2 \rvert$										
$\langle {}^2T_2\gamma\epsilon^2 \rvert$										
$\langle {}^2T_2\gamma^2\epsilon \rvert$										
$\langle {}^2T_2\gamma^2\epsilon \rvert$										
$\langle {}^4T_2\gamma\epsilon^2 \rvert$										
$\langle {}^4T_2\gamma\epsilon^2 \rvert$										

Continued.

$\|^4T_1\gamma\epsilon^3\rangle$	$\|^4T_1\gamma^2\epsilon\rangle$	$\|^4T_1\gamma\epsilon^2\rangle$	$\|^4T_1\gamma^2\epsilon\rangle$	$\|^2T_2\epsilon^3\rangle$	$\|^2T_2\gamma\epsilon^2\rangle$	$\|^2T_2\gamma\epsilon^3\rangle$	$\|^2T_2\gamma^2\epsilon\rangle$	$\|^2T_2\gamma^2\epsilon\rangle$	$\|^4T_2\gamma\epsilon^2\rangle$	$\|^4T_2\gamma\epsilon^2\rangle$
		$V+2A_2$ $+A_0+2B_2$ $-5B_0-\zeta/12$	$6B_1-\frac{1}{6}\zeta'$	0	0	0	0	0	$-\frac{1}{2}\zeta$	$\frac{1}{4}\zeta$
			$2V+A_4$ $+2A_2-8B_4$ $-4B_2+\frac{1}{6}\zeta$	0	0	0	0	0	ζ'	$-\frac{1}{2}\zeta'$
				$3A_0+5C_0$	$3\sqrt{3}B_1$ $+\sqrt{3}\zeta'/12$	$-5\sqrt{3}B_1$ $-\frac{1}{4}\sqrt{3}\zeta'$	$-4B_2-2C_2$	$2B_2$	$-\frac{1}{6}\sqrt{3}\zeta'$	$-\frac{1}{3}\sqrt{3}\zeta'$
					$V+2A_2$ $+A_0-B_2$ $-5B_0+3C_2$ $+\frac{1}{6}\zeta$	$-3B_2-\frac{1}{4}\zeta$	$-3\sqrt{3}B_1$ $-\sqrt{3}\zeta'/12$	$3\sqrt{3}B_1$ $-\frac{1}{6}\sqrt{3}\zeta'$	$-\zeta/12$	$-\frac{1}{6}\zeta$
						$V+2A_2$ $+A_0+3B_2$ $+B_0+C_2$ $+2C_0$	$\sqrt{3}B_1+\frac{1}{4}\sqrt{3}\zeta'$	$\sqrt{3}B_1$	$-\frac{1}{4}\zeta$	$-\frac{1}{12}\zeta$
							$2V+A_4$ $+2A_2+8B_4$ $-2B_2+4C_4$ $+C_2-\frac{1}{2}\zeta$	$-10B_2$	$\frac{1}{6}\sqrt{3}\zeta'$	$\frac{1}{3}\sqrt{3}\zeta'$
								$2V+A_4$ $+2A_2-2B_2$ $+2C_4+C_2$ $+\frac{1}{4}\zeta$	$\frac{1}{3}\sqrt{3}\zeta'$	$\frac{2}{3}\sqrt{3}\zeta'$
									$V+2A_2$ $+A_0-10B_2$ $-5B_0+\frac{1}{6}\zeta$	$-\frac{1}{6}\zeta$
										$V+2A_2$ $+A_0-10B_2$ $-5B_0$ $-\zeta/12$

TABLE IV. Matrix elements of the magnetic moment operator

	$\lvert {}^4A_2\epsilon^3\rangle$	$\lvert {}^2E\epsilon^3\rangle$	$\lvert {}^2E\gamma\epsilon^2\rangle$	$\lvert {}^2E\gamma\epsilon^2\rangle$	$\lvert {}^2E\gamma^3\rangle$	$\lvert {}^2T_1\epsilon^3\rangle$	$\lvert {}^2T_1\gamma\epsilon^2\rangle$	$\lvert {}^2T_1\gamma\epsilon^2\rangle$	$\lvert {}^2T_1\gamma^2\epsilon\rangle$	$\lvert {}^2T_1\gamma^2\epsilon\rangle$
$\langle {}^4A_2\epsilon^3 \rvert$	-3	0	0	0	0	0	0	0	0	0
$\langle {}^2E\epsilon^3 \rvert$		1	0	0	0	$-\frac{2}{3}(6)^{\frac{1}{2}}k$	0	$-\frac{2}{3}(6)^{\frac{1}{2}}\alpha$	0	0
$\langle {}^2E\gamma\epsilon^2 \rvert$			1	0	0	0	0	0	$\frac{2}{3}\sqrt{3}\alpha$	$\frac{2}{3}\alpha$
$\langle {}^2E\gamma\epsilon^2 \rvert$				1	0	$\frac{2}{3}\sqrt{3}\alpha$	0	$\frac{2}{3}\sqrt{3}k$	$\frac{2}{3}\sqrt{3}\alpha$	$\frac{2}{3}\alpha$
$\langle {}^2E\gamma^3 \rvert$					1	0	0	0	-2α	$-\frac{2}{3}\sqrt{3}\alpha$
$\langle {}^2T_1\epsilon^3 \rvert$						$\frac{1}{3}+\frac{1}{3}k$	$-\frac{1}{2}\alpha$	$-\frac{1}{6}\alpha$	0	0
$\langle {}^2T_1\gamma\epsilon^2 \rvert$							$\frac{1}{3}+\frac{1}{6}k$	0	$-\frac{1}{6}\alpha$	$-\frac{1}{3}\sqrt{3}\alpha$
$\langle {}^2T_1\gamma\epsilon^2 \rvert$								$\frac{1}{3}-\frac{1}{6}k$	$-\frac{1}{2}\alpha$	0
$\langle {}^2T_1\gamma^2\epsilon \rvert$									$\frac{1}{3}-\frac{1}{3}k$	0
$\langle {}^2T_1\gamma^2\epsilon \rvert$										$\frac{1}{3}+\frac{1}{6}k$
$\langle {}^4T_1\gamma\epsilon^2 \rvert$										
$\langle {}^4T_1\gamma^2\epsilon \rvert$										
$\langle {}^1T_1\gamma\epsilon^2 \rvert$										
$\langle {}^1T_1\gamma^2\epsilon \rvert$										
$\langle {}^2T_2\epsilon^3 \rvert$										
$\langle {}^2T_2\gamma\epsilon^2 \rvert$										
$\langle {}^2T_2\gamma\epsilon^2 \rvert$										
$\langle {}^2T_2\gamma^2\epsilon \rvert$										
$\langle {}^2T_2\gamma^2\epsilon \rvert$										
$\langle {}^4T_2\gamma\epsilon^2 \rvert$										
$\langle {}^4T_2\gamma\epsilon^2 \rvert$										

account of covalent effects the matrix elements calculated from the hydrogenic functions are altered by the introduction of a number of parameters. For example, the value of the spin-orbit coupling constant depends principally on the amplitude of the radial $5d$ wave function near the nucleus of the central ion. The altered normalization of the $5d$ function due to its hybridization with Cl $3p$ and $4s$ functions results in a reduction of the amplitude of this $5d$ function near the nucleus. The extent of the reduction depends on whether it is the $5d\gamma$ or $5d\epsilon$ function which is being hybridized. Therefore in calculating the matrix elements of the spin-orbit interaction between two ϵ states the spin-orbit coupling constant is taken to be ζ. When an ϵ and a γ state are connected by the spin-orbit interaction, the spin-orbit coupling constant is taken to be ζ'. The spin-orbit interaction has no nonvanishing matrix elements between two γ states. Both ζ and ζ' may be smaller than the free-ion value. By proceeding in this manner we are, in reality, placing foremost the transformation properties of the wave functions rather than their localization on the central ion.

The matrix elements of the Coulomb interaction involve numerous radial integrals which cannot be evaluated unless good radial wave functions are available. Since these functions for the case of octahedral

between the $\Gamma_8 B$ and the $\Gamma_8 B$ states. Here $\alpha=(k_\gamma k_\epsilon)^{\frac{1}{2}}$, $k=k_\epsilon$.

$\lvert {}^4T_1\gamma\epsilon^2\rangle$	$\lvert {}^4T_1\gamma^2\epsilon\rangle$	$\lvert {}^4T_1\gamma\epsilon^2\rangle$	$\lvert {}^4T_1\gamma^2\epsilon\rangle$	$\lvert {}^2T_2\epsilon^3\rangle$	$\lvert {}^2T_2\gamma\epsilon^2\rangle$	$\lvert {}^2T_2\gamma\epsilon^2\rangle$	$\lvert {}^2T_2\gamma^2\epsilon\rangle$	$\lvert {}^2T_2\gamma^2\epsilon\rangle$	$\lvert {}^4T_2\gamma\epsilon^2\rangle$	$\lvert {}^4T_2\gamma\epsilon^2\rangle$
0	0	0	0	0	0	0	0	0	$\frac{2}{3}\sqrt{3}\alpha$	$\frac{2}{3}\sqrt{3}\alpha$
0	0	0	0	0	0	0	0	0	0	0
0	0	0	0	0	0	0	0	0	0	0
0	0	0	0	0	0	0	0	0	0	0
0	0	0	0	0	0	0	0	0	0	0
0	0	0	0	0	$\frac{1}{2}\alpha$	$\frac{1}{2}\alpha$	0	0	0	0
0	0	0	0	$-\frac{1}{2}\sqrt{3}\alpha$	$-\frac{1}{2}k$	0	$-\frac{1}{2}\sqrt{3}\alpha$	0	0	0
0	0	0	0	$-\frac{1}{6}\sqrt{3}\alpha$	0	$-\frac{1}{2}k$	$-\frac{1}{6}\sqrt{3}\alpha$	$-\frac{1}{3}\sqrt{3}\alpha$	0	0
0	0	0	0	0	$-\frac{1}{2}\alpha$	$-\frac{1}{2}\alpha$	0	0	0	0
0	0	0	0	0	0	$\frac{1}{3}\sqrt{3}\alpha$	0	$\frac{1}{2}k$	0	0
$-\frac{1}{3}+\frac{1}{2}k$	$\frac{2}{3}\alpha$	$-\frac{2}{3}+\frac{1}{6}k$	$\frac{1}{3}\alpha$	0	0	0	0	0	0	$\frac{1}{2}k$
	$-\frac{1}{3}-\frac{2}{3}k$	$\frac{1}{3}\alpha$	$-\frac{2}{3}-\frac{1}{3}k$	0	0	0	0	0	0	$-\alpha$
		$5/3-\frac{1}{6}k$	$-\frac{1}{3}\alpha$	0	0	0	0	0	$-\frac{1}{2}k$	$\frac{1}{2}k$
			$5/3+\frac{1}{3}k$	0	0	0	0	0	α	$-\alpha$
				$-1+k$	$\frac{1}{2}\sqrt{3}\alpha$	$\frac{1}{2}\sqrt{3}\alpha$	0	0	0	0
					$-1-\frac{1}{2}k$	0	$\frac{1}{2}\sqrt{3}\alpha$	$\sqrt{3}\alpha$	0	0
						$-1+\frac{1}{2}k$	$\frac{1}{2}\sqrt{3}\alpha$	0	0	0
							$-1+k$	0	0	0
								$-1-\frac{1}{2}k$	0	0
									$1+\frac{1}{2}k$	$-2-\frac{1}{6}k$
										$-1-\frac{1}{6}k$

symmetry have not been evaluated it is necessary to treat the radial integrals as parameters and to determine their values by analysis of the optical absorption spectrum. It is slightly more convenient to express the matrix elements of the Coulomb interaction in terms of the Racah parameters than in terms of the Condon and Shortley F integrals. In view of the inequivalence of the $5d\gamma$ and the $5d\epsilon$ orbitals mentioned above several different sets of Racah parameters are required. They will be written as A_i, B_i, and C_i, where i refers to the number of times (0 to 4) that the $5d\gamma$ radial function occurs in the Coulomb integrals. Since we are allowing these parameters to be determined by experiment we are, in a sense, including the effects of covalent bonding in the calculation of the energy levels.

Another assumption which is made throughout most of this paper is that the ligand field has octahedral symmetry. In this field the electrons in $\epsilon(t_2)$ orbitals will have the lowest energy since these orbitals have their maximum amplitudes away from the directions of the σ bonds (or the ionically bound Cl^- ions). The separation of the $\gamma(e)$ and the $\epsilon(t_2)$ states in the ligand field is taken to be V.

The magnetic and spectroscopic properties of K_2ReCl_6 can be ascribed to the three electrons outside the Re^{4+} core. The ligand field is large in comparison with the

TABLE V. Matrix elements of the magnetic moment operator

	$\|{}^4A_2\epsilon^3\rangle$	$\|{}^2E\epsilon^3\rangle$	$\|{}^2E\gamma\epsilon^2\rangle$	$\|{}^2E\gamma\epsilon^2\rangle$	$\|{}^2E\gamma^3\rangle$	$\|{}^2T_1\epsilon^3\rangle$	$\|{}^2T_1\gamma\epsilon^2\rangle$	$\|{}^2T_1\gamma^2\epsilon\rangle$	$\|{}^2T_1\gamma^2\epsilon\rangle$
$\langle{}^2A_1\gamma\epsilon^2\|$	0	0	0	0	0	$\frac{2}{3}\alpha$	0	$\frac{2}{3}k$	$-\frac{2}{3}\sqrt{3}\alpha$	$-\frac{2}{3}\alpha$
$\langle{}^2T_1\epsilon^3\|$	0	$-\frac{2}{3}\sqrt{3}k$	0	$\frac{1}{3}(6)^{\frac{1}{2}}\alpha$	0	$\sqrt{2}(\frac{2}{3}-\frac{1}{3}k)$	$\frac{1}{2}\sqrt{2}\alpha$	$\frac{1}{6}\sqrt{2}\alpha$	0	0
$\langle{}^2T_1\gamma\epsilon^2\|$	0	0	0	0	0	$\frac{1}{2}\sqrt{2}\alpha$	$\sqrt{2}(\frac{2}{3}-\frac{1}{6}k)$	0	$\frac{1}{6}\sqrt{2}\alpha$	$\frac{1}{3}(6)^{\frac{1}{2}}\alpha$
$\langle{}^2T_1\gamma\epsilon^2\|$	0	$-\frac{2}{3}\sqrt{3}\alpha$	0	$\frac{1}{3}(6)^{\frac{1}{2}}k$	0	$\frac{1}{6}\sqrt{2}\alpha$	0	$\sqrt{2}(\frac{2}{3}+\frac{1}{6}k)$	$\frac{1}{2}\sqrt{2}\alpha$	0
$\langle{}^2T_1\gamma^2\epsilon\|$	0	0	$\frac{1}{3}(6)^{\frac{1}{2}}\alpha$	$\frac{1}{3}(6)^{\frac{1}{2}}\alpha$	$-\sqrt{2}\alpha$	0	$\frac{1}{6}\sqrt{2}\alpha$	$\frac{1}{2}\sqrt{2}\alpha$	$\sqrt{2}(\frac{2}{3}+\frac{1}{3}k)$	0
$\langle{}^2T_1\gamma^2\epsilon\|$	0	0	$\frac{1}{3}\sqrt{2}\alpha$	$\frac{1}{3}\sqrt{2}\alpha$	$-\frac{1}{3}(6)^{\frac{1}{2}}\alpha$	0	$\frac{1}{3}(6)^{\frac{1}{2}}\alpha$	0	0	$\sqrt{2}(\frac{2}{3}-\frac{1}{6}k)$
$\langle{}^4T_1\gamma\epsilon^2\|$	0	0	0	0	0	0	0	0	0	0
$\langle{}^4T_1\gamma^2\epsilon\|$	0	0	0	0	0	0	0	0	0	0
$\langle{}^4T_2\gamma\epsilon^2\|$	$\frac{2}{3}\sqrt{3}\alpha$	0	0	0	0	0	0	0	0	0

spin-orbit coupling constant which in turn is larger than the relevant Racah parameters. In the past the different orders of magnitude of various perturbations have been made the basis for approximate schemes of calculating energy levels. Now, however, large computing machines can be used to find the eigenvalues and eigenvectors of large secular determinants. Consequently there is no reason to make the simplifying assumption that some parts of the Hamiltonian can be neglected in comparison with other parts.

The wave functions for the three-electron system can be constructed by forming appropriately symmetrized linear combinations of products of one electron functions. The orbital wave functions span the following representations: ${}^2A_1(1)$, ${}^2A_2(1)$, ${}^4A_2(1)$, ${}^2E(4)$, ${}^2T_1(5)$, ${}^4T_1(2)$, ${}^2T_2(5)$ and ${}^4T_2(1)$. The superscript refers to the spin multiplicity, $A_1\cdots T_2$ to the orbital representation, and the figure in parentheses is the number of occurrences of each representation of given multiplicity. The complete wave functions span the representations Γ_6, Γ_7, and Γ_8 of the cubic double group. When the ligand field, Coulomb and spin-orbit interactions are all included the secular determinants corresponding to these representations are 9×9, 9×9, and 21×21, respectively. The interaction matrices are given in Tables I–III.

When calculating the matrix elements of the magnetic-moment operator one must again consider the effects of covalence on the wave functions. Here we shall represent the effect phenomenologically by using $k\mathbf{L}+2\mathbf{S}$ as the magnetic moment operator, $\boldsymbol{\mu}$; k will be given the value $(k_\gamma k_\epsilon)^{\frac{1}{2}}$ when $\boldsymbol{\mu}$ has nonvanishing matrix elements between a γ orbital and an ϵ orbital and the value k_ϵ when $\boldsymbol{\mu}$ has nonvanishing matrix elements between two ϵ orbitals; k_γ and k_ϵ are closely related to the parameters which Owen calls α^2 and β^2, respectively.

Let us denote by $\Gamma_6\alpha$ and $\Gamma_6\beta$ a pair of functions which span the representation Γ_6, by $\Gamma_7\phi$ and $\Gamma_7\theta$ a pair of functions which span the representation Γ_7, and by Γ_8A, Γ_8B, Γ_8C, and Γ_8D four functions which span the representation Γ_8. Then, provided the functions are suitably correlated with the designations, μ_z will have nonvanishing matrix elements between the following pairs of states $(\Gamma_8D,\ \Gamma_8D)$, $(\Gamma_8D,\ \Gamma_7\phi)$, $(\Gamma_8B,\ \Gamma_8B)$, $(\Gamma_8B,\ \Gamma_6\alpha)$. Matrix elements of μ_x between other pairs of states are either zero, the negative of elements already mentioned, or irrelevant for the calculation of the magnetic properties of K_2ReCl_6. Because of the octahedral symmetry the matrix elements of μ_x and μ_y are not needed.

The matrix elements of kL_z+2S_z between the above mentioned pairs of states are given in Tables IV–VII.

4. SPECTRUM

The absorption spectrum[29] between 7700 and 17 000 cm^{-1} of a $0.05M$ solution of K_2ReCl_6 in $1M$ HCl is given in Fig. 1. The absorption spectrum[13] between 25 000 and 50 000 cm^{-1} is given in Fig. 2. These spectra are in good agreement in overlapping regions with spectra obtained by Maun and Davidson,[14] Rulfs and Meyer[15] and Stephens and Drickamer.[16]

In drawing the figures the data, which were originally in terms of optical density as a function of wavelength,

[29] This spectrum was obtained by Dr. R. H. Busey and kindly made available to me, prior to publication, by Dr. G. E. Boyd (private communication).

between the $\Gamma_8 B$ and the $\Gamma_6\alpha$ states. Here $\alpha=(k_\gamma k_\epsilon)^{\frac{1}{2}}$, $k=k_\epsilon$.

$\lvert {}^4T_1\gamma\epsilon^3\rangle$	$\lvert {}^4T_1\gamma^2\epsilon\rangle$	$\lvert {}^4T_1\gamma\epsilon^3\rangle$	$\lvert {}^4T_1\gamma^2\epsilon\rangle$	$\lvert {}^2T_2\epsilon^3\rangle$	$\lvert {}^2T_2\gamma\epsilon^2\rangle$	$\lvert {}^2T_2\gamma\epsilon^2\rangle$	$\lvert {}^2T_2\gamma^2\epsilon\rangle$	$\lvert {}^2T_2\gamma^2\epsilon\rangle$	$\lvert {}^4T_2\gamma\epsilon^2\rangle$	$\lvert {}^4T_2\gamma\epsilon^2\rangle$
0	0	0	0	0	0	0	0	0	0	0
0	0	0	0	0	$-\frac{1}{2}\sqrt{2}\alpha$	$-\frac{1}{2}\sqrt{2}\alpha$	0	0	0	0
0	0	0	0	$\frac{1}{2}(6)^{\frac{1}{2}}\alpha$	$\frac{1}{2}\sqrt{2}k$	0	$\frac{1}{2}(6)^{\frac{1}{2}}\alpha$	0	0	0
0	0	0	0	$\frac{1}{6}(6)^{\frac{1}{2}}\alpha$	0	$\frac{1}{2}\sqrt{2}k$	$\frac{1}{6}(6)^{\frac{1}{2}}\alpha$	$\frac{1}{3}(6)^{\frac{1}{2}}\alpha$	0	0
0	0	0	0	0	$\frac{1}{2}\sqrt{2}\alpha$	$\frac{1}{2}\sqrt{2}\alpha$	0	0	0	0
0	0	0	0	0	0	$-\frac{1}{3}(6)^{\frac{1}{2}}\alpha$	0	$-\frac{1}{2}\sqrt{2}k$	0	0
$-\frac{2}{3}+\frac{1}{6}k$	$\frac{1}{3}\alpha$	$-4/3+\frac{1}{3}k$	$\frac{2}{3}\alpha$	0	0	0	0	0	$\frac{1}{2}k$	0
$\frac{1}{3}\alpha$	$-\frac{2}{3}-\frac{1}{3}k$	$\frac{2}{3}\alpha$	$-4/3-\frac{2}{3}k$	0	0	0	0	0	$-\alpha$	0
$-\frac{1}{2}k$	α	0	0	0	0	0	0	0	$-2-\frac{1}{6}k$	$\frac{1}{3}k$

have been re-expressed as $\lambda\epsilon$ vs $\bar{\nu}$. Here ϵ is the molar extinction coefficient. This latter method of representation of the data is more physically significant since $\lambda\epsilon$ is proportional to the transition probability.

The ground state of the $(ReCl_6)^{2-}$ complex has, to a good approximation, the electron configuration ϵ^3. The wave function is predominantly ${}^4A_2(\Gamma_8)$. Here, and subsequently, the quantity in parentheses designates the over-all representation to which the complete wave function belongs.

The first excited state, which lies somewhere below 7700 cm^{-1}, (and, indeed, all the states up to 20 000 cm^{-1}) also has the configuration ϵ^3. Its wave function can be designated by ${}^2T_1(\Gamma_8)$. The next two states are ${}^2E(\Gamma_8)$ at 9105 cm^{-1} and ${}^2T_1(\Gamma_6)$ at 9574 cm^{-1}. Because of the extensive vibrational fine structure, and the lack of rigorous calculations of the vibronic transition probabilities one should probably not assert categorically that a given peak corresponds to a pure electronic transition. The absorption curve from 8500 to 10 500 cm^{-1} can be expressed as a sum of Gaussian functions with good accuracy. The full width at half-maximum of the peaks whose maxima lie at 9279, 9430, 9574 and 9721 cm^{-1} is about 130 cm^{-1}. The width at half-maximum of the peak at 9105 cm^{-1} and the unresolved peaks at lower energies is slightly greater than 130 cm^{-1}.

The separation of the vibrational fine structure peaks in this energy region seems to be nearly constant and to have an average value of about 147 cm^{-1}. The lowest vibrational frequency of the ReF_6 molecule is 170 cm^{-1} according to Claassen.[30] Since the Re—Cl and the Re—F bond lengths are quite different in $(ReCl_6)^{2-}$ and ReF_6, respectively, 147 cm^{-1} seems to be a reasonable value for a vibrational frequency in the former complex. It may not even be the smallest vibrational frequency.

The next excited state at 14 180 cm^{-1} can be designated by ${}^2T_2(\Gamma_7)$. The vibrational fine structure is again apparent. The separations of the peaks have an average value of about 153 cm^{-1}. The peaks do not seem to be as uniformly spaced as the peaks in the 9000 cm^{-1} region. Their approximate width at half-maximum is 140 cm^{-1}.

The peak at 15 385 cm^{-1} is due to transitions to the ${}^2T_2(\Gamma_8)$ state. Casual inspection reveals that this peak is, in reality, (at least) two unresolved peaks. Their centers are about 500 cm^{-1} apart and their full widths at half-maximum are about 600 cm^{-1}. Since the more intense peak is at a lower energy the appearance of two peaks, rather than one, can hardly be ascribed to ground-state vibrations. Furthermore Stephens and Drickamer[16] have found that when a K_2ReCl_6 crystal is subjected to pressure these two peaks become resolved. This fact led the author[31] to identify the 15 385 cm^{-1} peak with transitions to ${}^2T_2(\Gamma_8)$, and to conjecture that the splitting is due to small fields which deviate from octahedral symmetry.

As a simple approximation to a more complicated situation let us assume that the states whose configuration is ϵ^3 are not coupled to other states, and that the field of "low" symmetry has the form

$$V_2V_2^0(\theta,\phi)+V_4V_4^0(\theta,\phi).$$

[30] H. H. Claassen, J. Chem. Phys. **30**, 968 (1959).

[31] J. C. Eisenstein, J. Chem. Phys. **32**, 1887 (1960).

TABLE VI. Matrix elements of the magnetic moment operator

	$\lvert {}^4A_2\epsilon^3\rangle$	$\lvert {}^2E\epsilon^3\rangle$	$\lvert {}^2E\gamma\epsilon^2\rangle$	$\lvert {}^2E\gamma\epsilon^2\rangle$	$\lvert {}^2E\gamma^3\rangle$	$\lvert {}^2T_1\epsilon^3\rangle$	$\lvert {}^2T_1\gamma\epsilon^2\rangle$	$\lvert {}^2T_1\gamma\epsilon^2\rangle$	$\lvert {}^2T_1\gamma^2\epsilon\rangle$	$\lvert {}^2T_1\gamma^2\epsilon\rangle$
$\langle {}^4A_2\epsilon^3 \rvert$	1	0	0	0	0	0	0	0	0	0
$\langle {}^2E\epsilon^3 \rvert$		1	0	0	0	0	0	0	0	0
$\langle {}^2E\gamma\epsilon^2 \rvert$			1	0	0	0	0	0	0	0
$\langle {}^2E\gamma\epsilon^2 \rvert$				1	0	0	0	0	0	0
$\langle {}^2E\gamma^3 \rvert$					1	0	0	0	0	0
$\langle {}^2T_1\epsilon^3 \rvert$						$-1-k$	$\frac{3}{2}\alpha$	$\frac{1}{2}\alpha$	0	0
$\langle {}^2T_1\gamma\epsilon^2 \rvert$							$-1-\frac{1}{2}k$	0	$\frac{1}{2}\alpha$	$\sqrt{3}\alpha$
$\langle {}^2T_1\gamma\epsilon^2 \rvert$								$-1+\frac{1}{2}k$	$\frac{3}{2}\alpha$	0
$\langle {}^2T_1\gamma^2\epsilon \rvert$									$-1+k$	0
$\langle {}^2T_1\gamma^2\epsilon \rvert$										$-1-\frac{1}{2}k$
$\langle {}^4T_1\gamma\epsilon^2 \rvert$										
$\langle {}^4T_1\gamma^2\epsilon \rvert$										
$\langle {}^4T_1\gamma\epsilon^2 \rvert$										
$\langle {}^4T_1\gamma^2\epsilon \rvert$										
$\langle {}^2T_2\epsilon^3 \rvert$										
$\langle {}^2T_2\gamma\epsilon^2 \rvert$										
$\langle {}^2T_2\gamma\epsilon^2 \rvert$										
$\langle {}^2T_2\gamma^2\epsilon \rvert$										
$\langle {}^2T_2\gamma^2\epsilon \rvert$										
$\langle {}^4T_2\gamma\epsilon^2 \rvert$										
$\langle {}^4T_2\gamma\epsilon^2 \rvert$										

between the $\Gamma_8 D$ and the $\Gamma_8 D$ states. Here $\alpha=(k,k_\epsilon)^{\frac{1}{2}}$, $k=k_\epsilon$.

$\lvert {}^4T_1\gamma\epsilon^3\rangle$	$\lvert {}^4T_1\gamma^2\epsilon\rangle$	$\lvert {}^4T_1\gamma\epsilon^3\rangle$	$\lvert {}^4T_1\gamma^3\epsilon\rangle$	$\lvert {}^2T_2\epsilon^3\rangle$	$\lvert {}^2T_2\gamma\epsilon^2\rangle$	$\lvert {}^2T_2\gamma\epsilon^3\rangle$	$\lvert {}^2T_2\gamma^2\epsilon\rangle$	$\lvert {}^2T_2\gamma^3\epsilon\rangle$	$\lvert {}^4T_2\gamma\epsilon^2\rangle$	$\lvert {}^4T_2\gamma\epsilon^3\rangle$
0	0	0	0	0	0	0	0	0	$\frac{2}{5}\sqrt{3}\alpha$	$-\frac{2}{5}\sqrt{3}\alpha$
0	0	0	0	0	$-\frac{2}{5}(6)^{\frac{1}{2}}\alpha$	0	0	0	0	0
0	0	0	0	$\frac{4}{5}\alpha$	0	0	$-\frac{2}{5}\alpha$	$\frac{2}{5}\alpha$	0	0
0	0	0	0	$\frac{2}{5}\alpha$	0	$\frac{2}{5}\sqrt{3}k$	$\frac{2}{5}\alpha$	$-\frac{2}{5}\alpha$	0	0
0	0	0	0	0	0	0	$-\frac{2}{5}\sqrt{3}\alpha$	$-\frac{2}{5}\sqrt{3}\alpha$	0	0
0	0	0	0	0	$\frac{1}{2}\alpha$	$\frac{1}{2}\alpha$	0	0	0	0
0	0	0	0	$-\frac{1}{2}\sqrt{3}\alpha$	$-\frac{1}{2}k$	0	$-\frac{1}{2}\sqrt{3}\alpha$	0	0	0
0	0	0	0	$-\frac{1}{6}\sqrt{3}\alpha$	0	$-\frac{1}{2}k$	$-\frac{1}{6}\sqrt{3}\alpha$	$-\frac{1}{2}\sqrt{3}\alpha$	0	0
0	0	0	0	0	$-\frac{1}{2}\alpha$	$-\frac{1}{2}\alpha$	0	0	0	0
0	0	0	0	0	0	$\frac{1}{2}\sqrt{3}\alpha$	0	$\frac{1}{2}k$	0	0
$1+\frac{1}{3}k$	$\frac{2}{3}\alpha$	$-2-\frac{1}{6}k$	$-\frac{1}{3}\alpha$	0	0	0	0	0	0	$-\frac{1}{2}k$
	$1-\frac{2}{3}k$	$-\frac{1}{3}\alpha$	$-2+\frac{1}{3}k$	0	0	0	0	0	0	α
		$-1-\frac{1}{6}k$	$-\frac{1}{3}\alpha$	0	0	0	0	0	$\frac{1}{2}k$	$\frac{1}{2}k$
			$-1+\frac{1}{3}k$	0	0	0	0	0	$-\alpha$	$-\alpha$
				$\frac{1}{3}-\frac{1}{3}k$	$-\frac{1}{6}\sqrt{3}\alpha$	$-\frac{1}{6}\sqrt{3}\alpha$	0	0	0	0
					$\frac{1}{3}+\frac{1}{6}k$	0	$-\frac{1}{6}\sqrt{3}\alpha$	$-\frac{1}{3}\sqrt{3}\alpha$	0	0
						$\frac{1}{3}-\frac{1}{6}k$	$-\frac{1}{6}\sqrt{3}\alpha$	0	0	0
							$\frac{1}{3}-\frac{1}{3}k$	0	0	0
								$\frac{1}{3}+\frac{1}{6}k$	0	0
									$-\frac{1}{3}+\frac{1}{3}k$	$-\frac{2}{3}+\frac{1}{6}k$
										$5/3-\frac{1}{6}k$

TABLE VII. Matrix elements of the magnetic moment operator

	$\lvert {}^4A_2\epsilon^3\rangle$	$\lvert {}^2E\epsilon^3\rangle$	$\lvert {}^2E\gamma\epsilon^2\rangle$	$\lvert {}^2E\gamma\epsilon^2\rangle$	$\lvert {}^2E\gamma^3\rangle$	$\lvert {}^2T_1\epsilon^3\rangle$	$\lvert {}^2T_1\gamma\epsilon^2\rangle$	$\lvert {}^2T_1\gamma\epsilon^2\rangle$	$\lvert {}^2T_1\gamma^2\epsilon\rangle$	$\lvert {}^2T_1\gamma^2\epsilon\rangle$
$\langle {}^2A_2\gamma\epsilon^2 \rvert$	0	0	0	0	0	0	0	0	0	0
$\langle {}^4T_1\gamma\epsilon^2 \rvert$	0	0	0	0	0	0	0	0	0	0
$\langle {}^4T_1\gamma^2\epsilon \rvert$	0	0	0	0	0	0	0	0	0	0
$\langle {}^2T_2\epsilon^3 \rvert$	0	0	$\frac{2}{3}\sqrt{2}\alpha$	$\frac{1}{3}\sqrt{2}\alpha$	0	0	$\frac{1}{2}(6)^{\frac{1}{2}}\alpha$	$\frac{1}{6}(6)^{\frac{1}{2}}\alpha$	0	0
$\langle {}^2T_2\gamma\epsilon^2 \rvert$	0	$-\frac{2}{3}\sqrt{3}\alpha$	0	0	0	$-\frac{1}{2}\sqrt{2}\alpha$	$\frac{1}{2}\sqrt{2}k$	0	$\frac{1}{2}\sqrt{2}\alpha$	0
$\langle {}^2T_2\gamma\epsilon^2 \rvert$	0	0	0	$\frac{1}{3}(6)^{\frac{1}{2}}k$	0	$-\frac{1}{2}\sqrt{2}\alpha$	0	$\frac{1}{2}\sqrt{2}k$	$\frac{1}{2}\sqrt{2}\alpha$	$-\frac{1}{3}(6)^{\frac{1}{2}}\alpha$
$\langle {}^2T_2\gamma^2\epsilon \rvert$	0	0	$-\frac{1}{3}\sqrt{2}\alpha$	$\frac{1}{3}\sqrt{2}\alpha$	$-\frac{1}{3}(6)^{\frac{1}{2}}\alpha$	0	$\frac{1}{3}(6)^{\frac{1}{2}}\alpha$	$\frac{1}{6}(6)^{\frac{1}{2}}\alpha$	0	0
$\langle {}^2T_2\gamma^2\epsilon \rvert$	0	0	$\frac{1}{3}\sqrt{2}\alpha$	$-\frac{1}{3}\sqrt{2}\alpha$	$-\frac{1}{3}(6)^{\frac{1}{2}}\alpha$	0	0	$\frac{1}{3}(6)^{\frac{1}{2}}\alpha$	0	$-\frac{1}{2}\sqrt{2}k$
$\langle {}^4T_2\gamma\epsilon^2 \rvert$	$-\frac{2}{3}\sqrt{3}\alpha$	0	0	0	0	0	0	0	0	0

That is, we assume the existence of a field which has axial symmetry along a fourfold axis of the octahedron. There will then be a tetragonal distortion. The matrix elements of this perturbing field within the manifold of ϵ^3 states are as follows:

$$\begin{array}{c|ccc} & \lvert {}^2T_1\Gamma_8 D\rangle & \lvert {}^2T_2\Gamma_8 D\rangle & \lvert {}^2T_2\Gamma_7\phi\rangle \\ \langle {}^2T_1\Gamma_8 D \rvert & F & G & -\sqrt{2}G \\ \langle {}^2T_2\Gamma_8 D \rvert & & F & 0 \\ \langle {}^2T_2\Gamma_7\phi \rvert & & & F \end{array}$$

$$\begin{array}{c|ccc} & \lvert {}^2T_1\Gamma_8 B\rangle & \lvert {}^2T_2\Gamma_8 B\rangle & \lvert {}^2T_1\Gamma_6\alpha\rangle \\ \langle {}^2T_1\Gamma_8 B \rvert & F & -G & 0 \\ \langle {}^2T_2\Gamma_8 B \rvert & & F & \sqrt{2}G \\ \langle {}^2T_1\Gamma_6\alpha \rvert & & & F \end{array};$$

F and G are radial integrals which involve linear combinations of V_2 and V_4.

It is clear that the effect of the tetragonal perturbation is to split the ${}^2T_1\Gamma_8$ and ${}^2T_2\Gamma_8$ levels, and to raise the ${}^2T_1\Gamma_6$ and ${}^2T_2\Gamma_7$ levels. The ${}^4A_2(\Gamma_8)$ and ${}^2E(\Gamma_8)$ states are not connected to other states by the perturbation.

One of the interesting results of this calculation is that the ${}^2T_1(\Gamma_8)$ level should be split. No data are at present available on the spectrum below 7700 cm^{-1}. There is a ripple in the absorption curve at 7950 cm^{-1} which indicates that the low-frequency peak may be two unresolved peaks, but the evidence is not conclusive.

The strong peaks in the K_2ReCl_6 spectrum at about 35 000 and 48 000 cm^{-1} cannot be identified with certainty. It is possible that the peaks near 35 000 cm^{-1} correspond to, or mask, transitions to the ${}^4T_2$ and ${}^4T_1$ states. These transitions, which involve a transfer of one electron from an ϵ to a γ orbital, are forbidden. One might therefore expect that they would have about the same probability as the ϵ to ϵ transitions discussed heretofore, which are also forbidden.

Another possibility is that the high-energy peaks correspond to charge-transfer transitions, in which an electron migrates from a Cl orbital to a Re orbital, or vice versa.

In order to fix the value of the ligand field splitting of the ϵ and γ orbitals we have assumed that the peaks at 35 000 cm^{-1} correspond to transitions to ${}^4T_2$ and ${}^4T_1$ states. At worst this assumption gives us a value of V which is too small and an incorrect interpretation of the high-energy peaks. The alternative possibility, regardless of its superior plausibility, does not help in the interpretation of the spectrum in any way.

All the peaks below 20 000 cm^{-1} are due to transitions between configurations which are predominantly ϵ^3. Table VIII gives the configurations calculated from the wave functions corresponding to a particular set of parameters used to fit the observed energy levels.

It has frequently been suggested in the literature[32] that when a transition does not involve a change in configuration the corresponding absorption peak should be narrow; when there is a change in configuration (for example $\epsilon \rightarrow \gamma$) the corresponding absorption peak should be broad. One sees from Table VIII that the changes in

[32] L. E. Orgel, J. Chem. Phys. **23**, 1824 (1955); M. H. L. Pryce, Discussions Faraday Soc. **26**, 21 (1958).

between the $\Gamma_8 D$ and $\Gamma_7\phi$ states. Here $\alpha=(k_7k_8)^{\frac{1}{2}}$, $k=k_8$.

$\lvert {}^4T_1\gamma\epsilon^2\rangle$	$\lvert {}^4T_1\gamma^2\epsilon\rangle$	$\lvert {}^4T_1\gamma\epsilon^2\rangle$	$\lvert {}^4T_1\gamma^2\epsilon\rangle$	$\lvert {}^2T_2\epsilon^3\rangle$	$\lvert {}^2T_2\gamma\epsilon^2\rangle$	$\lvert {}^2T_2\gamma\epsilon^2\rangle$	$\lvert {}^2T_2\gamma^2\epsilon\rangle$	$\lvert {}^2T_2\gamma^2\epsilon\rangle$	$\lvert {}^4T_2\gamma\epsilon^2\rangle$	$\lvert {}^4T_2\gamma\epsilon^2\rangle$
0	0	0	0	$\frac{2}{3}\alpha$	0	$-\frac{2}{3}\sqrt{3}k$	$\frac{2}{3}\alpha$	$-\frac{2}{3}\alpha$	0	0
$2+\frac{1}{6}k$	$\frac{1}{3}\alpha$	$-\frac{1}{3}k$	$-\frac{2}{3}\alpha$	0	0	0	0	0	$\frac{1}{2}k$	0
$\frac{1}{3}\alpha$	$2-\frac{1}{3}k$	$-\frac{2}{3}\alpha$	$\frac{2}{3}k$	0	0	0	0	0	$-\alpha$	0
0	0	0	0	$\sqrt{2}(\frac{2}{3}+\frac{1}{3}k)$	$\frac{1}{6}(6)^{\frac{1}{2}}\alpha$	$\frac{1}{6}(6)^{\frac{1}{2}}\alpha$	0	0	0	0
0	0	0	0	$\frac{1}{6}(6)^{\frac{1}{2}}\alpha$	$\sqrt{2}(\frac{2}{3}-\frac{1}{6}k)$	0	$\frac{1}{6}(6)^{\frac{1}{2}}\alpha$	$\frac{1}{3}(6)^{\frac{1}{2}}\alpha$	0	0
0	0	0	0	$\frac{1}{6}(6)^{\frac{1}{2}}\alpha$	0	$\sqrt{2}(\frac{2}{3}+\frac{1}{6}k)$	$\frac{1}{6}(6)^{\frac{1}{2}}\alpha$	0	0	0
0	0	0	0	0	$\frac{1}{6}(6)^{\frac{1}{2}}\alpha$	$\frac{1}{6}(6)^{\frac{1}{2}}\alpha$	$\sqrt{2}(\frac{2}{3}+\frac{1}{3}k)$	0	0	0
0	0	0	0	0	$\frac{1}{3}(6)^{\frac{1}{2}}\alpha$	0	0	$\sqrt{2}(\frac{2}{3}-\frac{1}{6}k)$	0	0
$\frac{1}{2}k$	$-\alpha$	0	0	0	0	0	0	0	$-\frac{2}{3}+\frac{1}{6}k$	$-\frac{4}{3}+\frac{1}{3}k$

configuration for the levels below 20 000 cm^{-1} are not very great. If Table VIII is taken seriously it follows that the narrowest peaks should be $^2T_1(\Gamma_6)$ and $^2E(\Gamma_8)$; they are, in fact, observed to be the narrowest. Similarly the broadest peak should be $^2T_2(\Gamma_8)$; of all the peaks whose width can be estimated it is, in fact, $^2T_2(\Gamma_8)$ which is the broadest.

Although these qualitative conclusions seem quite satisfactory, the quantitative conclusions one can draw from Table VIII seem rather unsatisfactory. For example, according to the Table the $^2T_2(\Gamma_7)$ and $^2T_2(\Gamma_8)$ peaks should have nearly the same width. It was mentioned above, however, that the widths are approximately 140 and 600 cm^{-1}, respectively. It seems possible that the quantitative conclusions really are correct; that is, the true width of the $^2T_2(\Gamma_8)$ peak may be just large enough so that the vibrational structure is not resolved and the peak appears much broader than it really is. A similar remark applies to the $^2T_1(\Gamma_8)$ peak.

It is somewhat more likely that the excess width of the $^2T_1(\Gamma_8)$ and $^2T_2(\Gamma_8)$ peaks is due to the same factor that causes their splitting, a ligand field of low symmetry with random amplitude at the position of the paramagnetic ion. Absorption measurements on K_2ReCl_6 at several temperatures would enable one to decide between the two possibilities.

Since the configurational changes are small the curves of potential energy as a function of internuclear distance should be approximately the same for all the states below 20 000 cm^{-1}. It follows that the vibrational frequencies of the $(ReCl_6)^{2-}$ should be nearly the same in all the excited electronic states (below 20 000 cm^{-1}) as in the ground state. As nearly as one can tell from observations on different peaks and on both sides of the maxima of the various peaks at least one of the vibrational frequencies is constant.

5. PARAMETERS

In the preceding section the following locations for the energy levels were deduced from the experimental spectrum

$^4A_2(\Gamma_8)$	0	cm^{-1}
$^2T_1(\Gamma_8)$	<7700	
$^2E(\Gamma_8)$	9105	
$^2T_1(\Gamma_6)$	9574	
$^2T_2(\Gamma_7)$	14 180	
$^2T_2(\Gamma_8)$	15 385.	

In addition we shall very tentatively locate the $^4T_2$ and $^4T_1$ levels at 35 900 and 39 000 cm^{-1}, respectively. Each of these levels is, in reality, four levels. The splitting, in a zero-order approximation, is due to the spin-orbit coupling and amounts to $2\zeta/3$. The different levels are not resolved.

To calculate the energy levels values were chosen for the numerous parameters, substituted in the matrices given in Tables I–III, and the eigenvalue problems were solved on a large digital computer. Calculated eigenvalues were compared with experimental positions of the peaks as given above. An attempt was then made to find new parameters which would lead to better agreement between calculated and experimental positions of the energy levels. Some of the results of the calculations are given in Fig. 3.

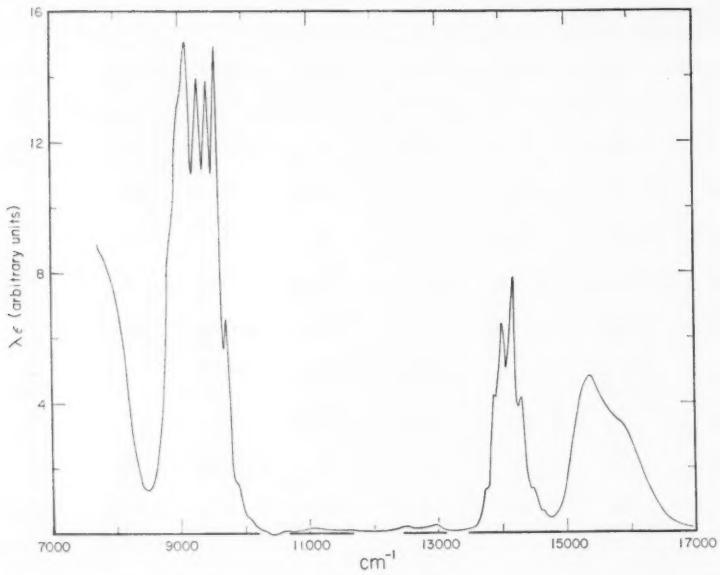

FIG. 1. Absorption spectrum of K_2ReCl_6 from 7000 to 17 000 cm^{-1}.

All of the numerical results of calculations quoted in Table VIII, in this section and in subsequent sections are based on the following choice of parameters:

$$V=33\,500\ \text{cm}^{-1}$$
$$A_0=A_2=A_4=0$$
$$B_0=380\ \text{cm}^{-1}$$
$$B_1=335$$
$$B_2=305$$
$$B_4=260$$
$$C_0=1760$$
$$C_2=1520$$
$$C_4=1300$$
$$\zeta=\zeta'=2300.$$

The calculated positions of the energy levels are as follows:

$^4A_2(\Gamma_8)$	0	cm^{-1}
$^2T_1(\Gamma_8)$	7895	
$^2E(\Gamma_8)$	8798	
$^2T_1(\Gamma_6)$	9167	
$^2T_2(\Gamma_7)$	14 653	
$^2T_2(\Gamma_8)$	15 723	
$^4T_2(\text{Av})$	34 458	
$^4T_1(\text{Av})$	38 546.	

Without doubt the agreement between theory and experiment can be improved by careful adjustment of the parameters. This improvement will not be attempted here for several reasons. In the first place, it has already been mentioned in the previous section that a small ligand field of lower than octahedral symmetry is probably present. The symmetry and magnitude of this field are not known, but they will certainly have an effect on the calculated energy levels. Second, the experimental positions of the $^4T_2$ and $^4T_1$ levels are not known with certainty. Consequently, only a lower limit can be set for the value of the ligand field splitting V. Due to second-order perturbations there is therefore some uncertainty concerning the calculated position of the lower levels which have the ϵ^3 configuration. Finally, the calculated magnetic properties are quite insensitive to small changes in the values of the parameters.

For the sake of completeness the approximate changes in the energy levels which occur when the various parameters are changed have been calculated and are given in Table IX. This table was prepared by changing the parameters, one at a time, from the values given above; for each change the roots of the corresponding secular equations were calculated.

6. SUSCEPTIBILITY

Once one has the matrix elements of the magnetic-moment operator and the eigenfunctions one can readily calculate the susceptibility. The appropriate formula to use is

$$\chi=(N\beta^2/4kT)\sum_i |\langle {}^4A_2, i\,|\mu_z|\,{}^4A_2, i\rangle|^2$$
$$+2N\beta^2\sum_{i,j}\frac{|\langle\psi_j\,|\mu_z|\,{}^4A_2, i\rangle|^2}{E_j}.$$

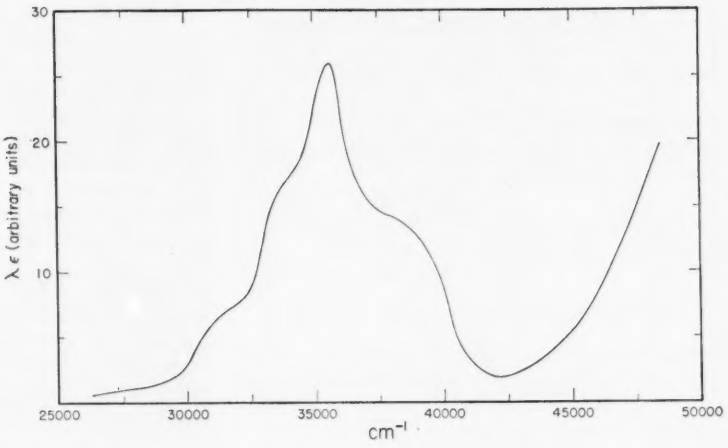

FIG. 2. Absorption spectrum of K_2ReCl_6 from 26 000 to 48 500 cm^{-1}.

TABLE VIII. Calculated configurations $\epsilon^x\gamma^y$ for the lowest energy levels of K_2ReCl_6.

Level	$^4A_2(\Gamma_8)$	$^2T_1(\Gamma_8)$	$^2E(\Gamma_8)$	$^2T_1(\Gamma_6)$	$^2T_2(\Gamma_7)$	$^2T_2(\Gamma_8)$
x	2.9857	2.9748	2.9776	2.9862	2.9720	2.9697
y	0.0143	0.0252	0.0224	0.0138	0.0280	0.0303

TABLE IX. Effect of changes in the parameters on the energy levels of K_2ReCl_6.

Level	Energy (cm^{-1})	ΔV	ΔB_0	ΔB_1	ΔB_2	ΔB_4	ΔC_0	ΔC_2	ΔC_4	$\Delta\zeta$	$\Delta\zeta'$
$^4T_1$(Av)	38 546	0.988	9.751	−0.393	0.649	−0.020	−0.026	0.171	0.014	0.232	0.410
$^4T_2$(Av)	34 458	0.988	9.557	−0.049	−8.707	−0.042	−0.088	0.029	0.009	−0.110	0.345
$^2T_2(\Gamma_8)$	15 723	0.015	13.053	−1.862	−0.298	0.019	4.302	−0.171	0.010	1.475	0.140
$^2T_2(\Gamma_7)$	14 653	0.011	14.265	−0.988	−0.339	0.023	4.720	−0.224	0.012	0.399	0.162
$^2T_1(\Gamma_6)$	9167	0.000	8.400	0.223	−0.134	0.000	2.803	−0.003	0.000	0.411	0.064
$^2E(\Gamma_8)$	8798	0.008	8.469	−1.235	0.017	0.000	2.798	0.008	0.000	0.413	−0.048
$^2T_1(\Gamma_8)$	7895	0.011	9.102	−0.781	−0.155	0.002	2.999	−0.026	0.002	−0.253	−0.112

The first sum is over the index i required to distinguish the four degenerate ground-state wave functions. The second sum is over i and also over all excited states, j; E_j is the excitation energy for the state whose wave function is ψ_j. One finds

$$\chi=(0.37523/2T)\{9.34913-1.71919(k_\gamma k_\epsilon)^{\frac{1}{2}}-0.21451k_\epsilon$$
$$+0.08037k_\gamma k_\epsilon+0.01986(k_\gamma k_\epsilon)^{\frac{1}{2}}k_\epsilon+0.00124k_\epsilon^2\}$$
$$+1.04332\times10^{-4}\{0.2439+0.0118(k_\gamma k_\epsilon)^{\frac{1}{2}}+0.1772k_\epsilon$$
$$+0.1154k_\gamma k_\epsilon+0.0295(k_\gamma k_\epsilon)^{\frac{1}{2}}k_\epsilon+0.0450k_\epsilon^2\}.$$

Both the Curie constant C and the temperature-independent paramagnetism α_p are functions of the orbital reduction factors. Values of C and a for selected values of k_γ and k_ϵ are given in Table X.

According to Griffiths and Owen[28] k_ϵ for the $(IrCl_6)^{2-}$ complex is about 0.7. If this value applies to K_2ReCl_6 as well the value of the Curie constant for the latter can hardly be larger than about 1.52.

The most extensive of the published susceptibility measurements on K_2ReCl_6 have been made by Schüth and Klemm[33] and by Nelson, Boyd, and Smith.[34] Let us take α_p to be 45×10^{-6} emu/mole. Then the

[33] W. Schüth and W. Klemm, Z. anorg. u. allgem. Chem. **220**, 193 (1934).

[34] C. M. Nelson, G. E. Boyd, and W. T. Smith, Jr., J. Am. Chem. Soc. **76**, 348 (1954).

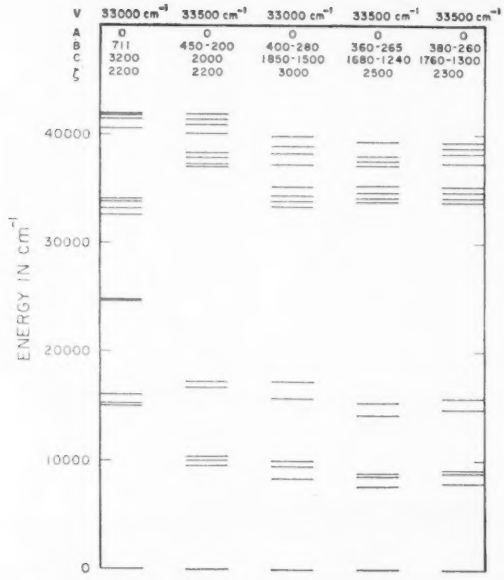

FIG. 3. Calculated energy levels of K_2ReCl_6 for various choices of the parameters. In each case the values of B and C fall within the indicated limits for B and C.

measured susceptibility can be fitted to a formula of the Curie-Weiss type

$$\chi=[C/(T+\theta)]+\alpha_p.$$

The values of C and θ which minimize the mean-square deviation of the calculated values of $1/\chi$ from the experimental values are 1.79 and 90°, respectively. The nonzero value of θ indicates the presence of exchange interaction between the Re ions and an incipient antiferromagnetic transition. The value of the susceptibility calculated from the eigenfunctions thus applies only to a magnetically dilute substance; for example, to K_2ReCl_6 in K_2PtCl_6. No measurements on such a system are available. Some measurements on aqueous solutions of K_2ReCl_6 have been made by Figgis, Lewis, Nyholm, and Peacock[35] but they have reported only the effective moment at 300°K. (For concentrated K_2ReCl_6 their values of C and θ are 1.70 and 80°.)

One can use the formula

$$\chi=(C_{\text{eff}}/T)+\alpha_p=(N\beta^2/3kT)\mu_{\text{eff}}{}^2+\alpha_p,$$

to calculate the effective Curie constant or the effective moment (in units of the Bohr magneton) at any temperature. The values of C_{eff} calculated from the data range from 0.833 at 78° to 1.449 at 403°K, while the values of μ_{eff} lie between 2.58 and 3.40.

[35] B. Figgis, J. Lewis, R. S. Nyholm, and R. D. Peacock, Discussions Faraday Soc. **26,** 103 (1958).

A plot of χT vs T indicates that the asymptotic value of C_{eff} at high temperatures is near 1.5. Such a value would be in very satisfactory agreement with the calculated value if k_ϵ is 0.6–0.7.

It may be worth pointing out here that Cooke[23] *et al.* took the value of the diamagnetic susceptibility for the chloroiridates to be -1.9×10^{-4} emu/mole. They then obtained from their measurements that the temperature-independent paramagnetic susceptibility α_p was 2.9×10^{-4} emu/mole. It then follows, since the latter quantity is inversely proportional to ζ, that $\zeta\sim2000$ cm^{-1}. The diamagnetic susceptibility was obtained from old measurements by Feytis.[36] If it is too large (in absolute value) then Cooke *et al.* have overestimated α_p and underestimated ζ. A larger value of ζ for the chloroiridates is indicated if ζ for the chlororhenates is 2300 cm^{-1}, as found here.

7. MAGNETIC RESONANCE

The diagonal matrix elements of the magnetic-moment operator in the ground manifold can readily be found from Tables IV and VI. If one uses the parameters of Sec. 5 one finds that

$$\langle {}^4A_2D\,|\mu_z|\,{}^4A_2D\rangle=0.96858-0.12374\,(k_\gamma k_\epsilon)^{\frac{1}{2}}-0.01288k_\epsilon$$

$$\langle {}^4A_2C\,|\mu_z|\,{}^4A_2C\rangle=2.90017-0.25507\,(k_\gamma k_\epsilon)^{\frac{1}{2}}-0.03268k_\epsilon.$$

One can express these results in terms of a spin Hamiltonian[37] for effective spin $\frac{3}{2}$

$$\mathcal{H}_M=g\beta(H_xS_x+H_yS_y+H_zS_z+f\beta(H_xS_x{}^3+H_yS_y{}^3+H_zS_z{}^3).$$

One has

$$g=1.9376-0.2572\,(k_\gamma k_\epsilon)^{\frac{1}{2}}-0.0263k_\epsilon$$

$$f=-0.0019-0.0387\,(k_\gamma k_\epsilon)^{\frac{1}{2}}-0.0020k_\epsilon.$$

These values will, of course, apply only in the case of a dilute K_2ReCl_6 crystal.

The ground quartet will probably be split into two doublets by small fields of low symmetry combined with

TABLE X. Values of the Curie constant and the temperature-independent paramagnetic susceptibility of K_2ReCl_6 for selected values of the orbital reduction factors.

k_γ	1.000	0.800	0.600	1.000	1.000
k_ϵ	1.000	0.800	0.600	0.640	0.490
C	1.410	1.476	1.543	1.482	1.517
$10^4\alpha_p$	0.650	0.539	0.444	0.494	0.434

[36] F. Feytis, Compt. rend. **152,** 708 (1911).

[37] B. Bleaney, Proc. Phys. Soc. (London) **73,** 939 (1959); **74,** 493 (1959).

the spin-orbit interaction. This splitting is probably too small to affect the relative occupations of the $m_s=\pm\frac{3}{2}$ and $m_s=\pm\frac{1}{2}$ levels at the temperatures of interest in connection with the available susceptibility measurements. However it has to be considered in connection with paramagnetic resonance experiments. The splitting can be represented by a term

$$\mathcal{H}_C=DS_z^2$$

in the spin-Hamiltonian. The splitting will probably be larger than in the comparable case of the chromium alums, where it is about 0.15 cm^{-1}.

A rather complicated hyperfine structure may be observable in the spin resonance spectrum. The two naturally occurring Re isotopes have nuclear spin $\frac{5}{2}$. The magnetic interaction of the nuclear spin with the electron effective spin gives rise to a dozen hyperfine levels. In addition the spectrum is complicated by the chlorine hyperfine structure.

Griffiths[22] *et al.* have shown that the electron spin resonance spectrum of the dilute chloroiridates contains an intense isotropic line due to isolated $(IrCl_6)^{2-}$ complexes, and fainter anisotropic lines due to Ir—Ir pairs. Similar results can be expected for the chlororhenates, except that the intense part of the spectrum will probably not be isotropic because of the zero-field splitting.

Following Griffiths *et al.* let us assume that the exchange interaction between the two effective spins $s'=s''=\frac{3}{2}$ has the form

$$\mathcal{H}_{ex}=Js'\cdot s''+J_xs_x's_x''+J_ys_y's_y''+J_zs_z's_z'',$$

where $J_x+J_y+J_z=0$. The isotropic part of the exchange interaction splits the spin levels into a singlet, a triplet, a quintet, and a septet at $-15J/4$, $-11J/4$, $-3J/4$, and $9J/4$, respectively. The anisotropic part removes the remaining degeneracy of the spin levels.

The secular equations for the energy levels are as follows:

$$\begin{vmatrix} 4D+\frac{9}{4}(J+J_z)-E & 0 & \frac{3}{4}(J_x-J_y) & 0 \\ 0 & 2D-\frac{3}{4}(J+J_z)-E & \sqrt{3}(J-\frac{1}{2}J_z) & \frac{3}{4}(J_x-J_y) \\ \frac{3}{4}(J_x-J_y) & \sqrt{3}(J-\frac{1}{2}J_z) & \frac{1}{4}(J+J_z)\pm(J_x-J_y)-E & \pm\sqrt{3}(J-\frac{1}{2}J_z) \\ 0 & \frac{3}{4}(J_x-J_y) & \pm\sqrt{3}(J-\frac{1}{2}J_z) & 2D-\frac{3}{4}(J+J_z)-E \end{vmatrix}=0$$

$$\begin{vmatrix} 2D+\frac{3}{4}(J+J_z)-E & 0 & \frac{3}{2}(J-\frac{1}{2}J_z) & \frac{1}{2}\sqrt{3}(J_x-J_y) \\ 0 & 4D-\frac{9}{4}(J+J_z)-E & 0 & \frac{3}{2}(J-\frac{1}{2}J_z) \\ \frac{3}{2}(J-\frac{1}{2}J_z) & 0 & 2D+\frac{3}{4}(J+J_z)-E & \pm\frac{1}{2}\sqrt{3}(J_x-J_y) \\ \frac{1}{2}\sqrt{3}(J_x-J_y) & \frac{3}{2}(J-\frac{1}{2}J_z) & \pm\frac{1}{2}\sqrt{3}(J_x-J_y) & -\frac{1}{4}(J+J_z)\pm 2(J-\frac{1}{2}J_z)-E \end{vmatrix}=0.$$

The zero-field splitting of the $m_s=\pm\frac{3}{2}$ and $\pm\frac{1}{2}$ levels has been included in writing these equations. The equations can be solved explicitly in the special case $J_x=J_y$. In other cases a perturbation solution is possibly the most useful.

The pair spectrum will clearly be very complicated since transitions can be induced between the components of the triplet, of the quintet, and of the septet. There may be some simplification of the spectrum at low temperatures due to depopulation of the quintet and septet. It seems premature to attempt to discuss either the hyperfine structure or the pair spectrum in more detail at the present time.

8. CONCLUSION

It has been shown in this paper that almost all magnetic and spectroscopic data now available on K_2ReCl_6 can be correlated or understood on the basis of a ligand field theory of the $(ReCl_6)^{2-}$ octahedral complex. The absorption peaks below 20 000 cm^{-1} can be unambiguously identified with the lowest energy levels of a d^3 system in a cubic electrostatic field. The calculated susceptibility agrees with the measured susceptibility at high temperatures and would probably agree at all temperatures if data on a magnetically dilute system were available. The value of the ligand field splitting has been estimated to be 33 500 cm^{-1} and the value of the spin-orbit coupling constant to be 2300 cm^{-1}. Also values for the Racah parameters have been given.

A number of experiments remain to be done which will provide useful information about K_2ReCl_6. The optical absorption measurements need to be extended to longer wavelengths in order to determine more fully the width and structure of the $^2T_1(\Gamma_8)$ peak, and to lower temperatures in order to eliminate the "hot" peaks from the spectrum. Susceptibility measurements should be made on a dilute solution of K_2ReCl_6 in K_2PtCl_6 in

order to check the theoretical predictions, and should also be extended to lower temperatures in order to locate the antiferromagnetic transition. This transition could also be located by means of specific heat measurements. Finally, electron spin resonance should be observable in K_2ReCl_6 but the interpretation of the resonance spectrum may be rather difficult.

Some questions, the answers to which depend partly on the acquisition of new data, must be left open for the present. For example, the parameters introduced in Sec. 5 were chosen by trial and error. Until additional spectroscopic data become available there seems to be little point in attempting to "improve" these parameters. Perhaps eventually one can obtain values of B_0, B_1, B_2, and C_0 which are correct to within 10%. It is unlikely that such precise values of the A's, B_4, C_2, and C_4 will ever be obtained from analysis of the K_2ReCl_6 spectrum. The value of V given here is also subject to considerable error if the transitions to the $^4T_2$ and $^4T_1$ states are masked by charge-transfer transitions.

Another open question is the nature of the distortion of the octahedral complex. For convenience it was assumed in this paper that the distortion is tetragonal, but there is no evidence for this symmetry.

Finally, the effect of the superexchange interaction on the resonance spectrum of Re—Re pairs has been treated very briefly. Because of the complicated nature of the system the energy levels of the pairs in a magnetic field must be obtained numerically rather than analytically. It seems advisable to wait with these calculations until some experimental information is available on the values of the exchange integrals.

ACKNOWLEDGMENTS

I should like to thank Dr. G. E. Boyd for sending me the K_2ReCl_6 spectrum and for correspondence about it. I am indebted to Professor M. H. L. Pryce for frequent talks and correspondence about closely related problems. The eigenvalue problems were coded for machine calculation by Miss Irene Stegun and Miss Ruth Zucker.

Near-Infrared Absorption Spectrum of Solid Methane at the λ Point

JAY ARTHUR GLASEL

*University of California, School of Science and Engineering, La Jolla, California**

(Received November 4, 1960)

Observations on the near-infrared absorption spectrum of solid methane in the region of $\nu_1+\nu_4$ and $\nu_3+\nu_4$ over a temperature range of 6° to 33°K are presented and discussed. There is no evidence of molecular rotation, and the observations are shown to lead to an interpretation involving an order-disorder transition. Approximate f numbers for the transitions are measured.

I. INTRODUCTION

In recent years there has been considerable discussion concerning the origin of the λ-phase transition which takes place in solid methane at 20.44°K. The original thermal measurements were done by Clusius *et al.*[1] Pauling[2] has furnished an interpretation depending upon a transition between oscillation and free rotation for the molecules in the solid. More recently, several papers have appeared giving observations on the proton spin resonance of solid methane at its λ point.[3] However, these observations have yielded somewhat ambiguous results with regard to the existence of rotational motion. The most recent theoretical work has been done by Nagamiya[4] and Tomita.[5] The conclusions reached by Tomita are, briefly, that solid methane at the λ point changes from a lattice consisting of molecules oscillating about a stable configuration, to one of molecules singularly or cooperatively rotating.

Subsequently, an example of a molecule rotating in a lattice at low temperatures has been observed using its rotation-vibration spectrum,[6] and since the infrared spectrum of solid methane has never been studied it seemed worthwhile to make some observations of this nature.

II. EXPERIMENTAL

The apparatus used was the usual optical low-temperature Dewar. It was fitted into a Beckman DK-1 double-beam spectrophotometer. Phillips research-grade, or Matheson CP methane was condensed, unpurified, onto a special target suspended in the instrument. Observations on mixtures of methane with argon were done at matrix to gas ratios of 20:1 using analyzed reagent-grade argon.

The copper target is shown in Fig. 1. Contact between the window and the block was achieved by a paste of aluminum powder and stopcock grease. The thermal conductivity of sapphire is higher than copper throughout the temperature region studied. Approximate calculations show that the thermal gradient and rise time between the window and the resistance thermometer were very small. The spectra to be described below, which were taken at temperatures higher than the equilibrium value of the target temperature (about 6°K when cooled with liquid helium), were obtained as follows. The liquid helium was allowed to boil off, and the temperature of the target began to rise. The conductivity of the thermal barrier represented by the copper rod was chosen such that the temperature rise was small in the time it took to scan the observed spectral region. It is assumed that the conductivity of the condensed film was high enough so that there was no observable thermal gradient between the film temperature and the temperature that the resistor measured. The thermometer was a 47-ohm, ¼-w resistor baked into the target with Formvar in the normal fashion. It was calibrated at room temperature, immersed in boiling nitrogen, and immersed in boiling helium. However, it was cycled from room temperature to 4.2°K many times, and so an absolute accuracy of more than ±0.05°K cannot be assigned to the temperature values obtained.

III. OBSERVATIONS

Figures 2–4 display the main points of the observations. The region studied was that of $\nu_1+\nu_4$ (called

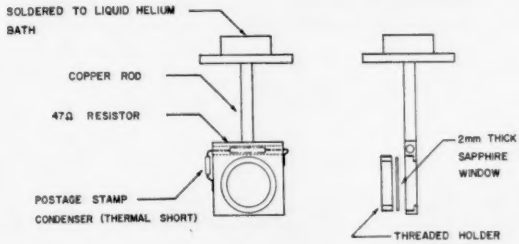

FIG. 1. Target, showing sapphire window and resistance thermometer element, machined from a solid piece of OFHC copper, gold plated.

* Present address: Imperial College of Science and Engineering, Department of Chemistry, London, S.W. 7, England.

[1] K. Clusius, Z. physik Chem. (Leipzig) **B23,** 213 (1933); K. Clusius and A. Perlick, *ibid.* **B24,** 313 (1934); A. Eucken and H. Veith, *ibid.* **34,** 275 (1936); A. Frank and K. Clusius, *ibid.* **36,** 291 (1937); L. Popp and K. Clusius, Z. Elektrochem. **43,** 664 (1937).

[2] L. Pauling, Phys. Rev. **36,** 430 (1930).

[3] F. Bitter, N. L. Albert, H. L. Poss, C. G. Lehr, and S. T. Lin, Phys. Rev. **71,** 738 (1947); N. L. Albert, *ibid.* **75,** 398 (1949); J. T. Thomas, N. L. Albert, and H. C. Torrey, J. Chem. Phys. **18,** 1511 (1950).

[4] T. Nagamiya, Progr. Theoret. Phys. (Kyoto) **6,** 702 (1951).

[5] K. Tomita, Phys. Rev. **89,** 429 (1953).

[6] J. A. Glasel, J. Chem. Phys. **33,** 252 (1960).

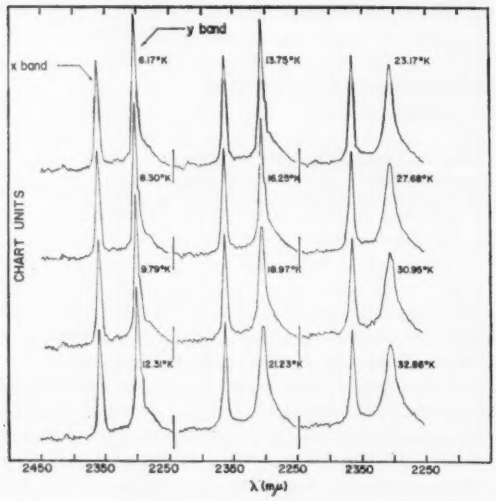

FIG. 2. Spectrum of pure solid methane at various temperatures. Spectrophotometer on I/I_0 scale with transmission decreasing upwards, showing x and y bands.

hereafter the "x" band in the solid-state spectrum), and $\nu_3+\nu_4$ (called hereafter the "y" band). By utilizing the method of reflection interference fringes, a value for the film thickness was measured using an arbitrary value of 1.50 for the index of refraction of the solid. From this, and the density of 0.517 g/cc for solid methane,[7] an f number was obtained for the x and y bands of the solid-state spectrum of 6°K. The values obtained were: $f_{x,6°K}=1.2\pm0.3\times10^{-4}$ and $f_{y,6°K}=2.7\pm0.5\times10^{-4}$. These values assume all molecules to be active in the transitions (see below). They may be compared to a measured value for the $Q(\Delta J=0)$ band of $\nu_1+\nu_4$ in the gas at 300°K, 1 atm, of $f=1.3\times10^{-4}$. Changes in the integrated absorption coefficients in the solid are $\alpha_{x,6°K}<\alpha_{x,30°K}$, and $\alpha_{y,30°K}=1.2\alpha_{y,6°K}$. When a film at 30°K was recooled to 6°K by refilling the Dewar with liquid helium, the spectrum obtained from the recooled film was in every way identical to the original film.

TABLE I. Connection table for molecular vibrations to vibrations active in the crystalline absorption spectrum (tetrahedral field).[a]

Molecular vibration and upper state symmetry species	Site group T_d	Crystal group $T_d^2(F\bar{4}3m)$
	A_1	A_1
	A_2	A_2
	E	E
	F_1	F_1
$\nu_1+\nu_4=(F_2)$		
$\nu_3+\nu_4=(F_2)+A+E+F_1$ ———	F_2 ←——→	F_2

[a] F_2 infrared active.

[7] H. H. Mooy, Proc. Koninkl. Alad. Wetenschap. Amsterdam **34,** 550 (1931).

IV. DISCUSSION

The crystal structure of solid methane has been observed at temperatures extending through the λ point by x-ray diffraction techniques.[8,9] These indicate a fcc lattice above and below the λ point. At the λ point some extraneous lines appear,[9] but their origin has never been cleared up.

In the discussion to follow, the nomenclature of Halford[10] and Hornig[11] will be used to describe the crystal-molecular interaction. Thus, the *site* symmetry of the molecules in the fcc lattice is either T_d ($F\bar{4}3m$ crystal space group), or C_3 ($P2_13$ space group) depending upon the orientation of the molecules in the unit cell. Incidental to the present work, Nagamiya[4] concludes that the configuration is T_d on stability grounds. The molecular symmetry is tetrahedral in the ground state. The relationship between the vibrations of the present interest in the free molecule, and the vibrations active in the spectrum of the solid are shown in Tables I and II.

TABLE II. Connection table for molecular vibrations to vibrations active in the crystalline absorption spectrum (trigonal field).[a]

Molecular vibration and upper state symmetry species	Site group C_3	Crystal group T^4
	A	A
	E	E
$\nu_3+\nu_4=(A+E)+F_1+F_2$ ———	$A+E$ ←——→	F

[a] F infrared active.

The methane molecule exists as three modifications: A (para), E (meta), and F (ortho) because of the spin of the hydrogens. In the absence of paramagnetic perturbations E and F will not convert to the A modification rapidly at low temperatures, and it is expected that at 6°K there will be three kinds of molecules. If rotation is allowed at 6°K there will be E and F molecules undergoing rotation while the A molecules will be mostly in the $J=0$ ground state. The allowable transitions for the free molecule are shown in Fig. 5.[12] This shows that in the absence of rotation the Q ($\Delta J=0$) branch for an A to F vibrational transition will be totally absent since there is no such transition for the A molecules. The rotational constant for methane is $B=5.25$ cm^{-1},[13] and this is to be compared to $kT=2.8$ cm^{-1} at 4°K and 12 cm^{-1} at 20°K.

[8] A. W. Maue, Ann. Physik **30,** 555 (1937).
[9] A. Schallamach, Proc. Roy. Soc. (London) **171,** 569 (1939).
[10] R. S. Halford, J. Chem. Phys. **14,** 8 (1946).
[11] D. F. Hornig, J. Chem. Phys. **16,** 1063 (1948).
[12] G. Herzberg, *Infrared and Raman Spectra* (D. Van Nostrand Company, Inc., Princeton, New Jersey, 1945), p. 450.
[13] M. Childs, Proc. Roy. Soc. (London) **153,** 555 (1936).

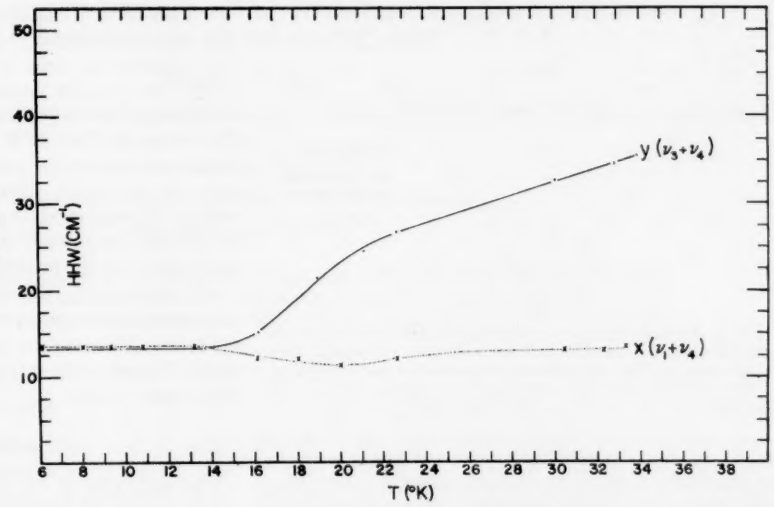

FIG. 3. Half-height width of the x and y bands vs temperature from several experiments. Slit width of instrument is about 2 cm^{-1}.

V. INTERPRETATION

(1) At temperatures less than about 15°K, molecular rotation is not present in the solid, and therefore the only kind of molecules contributing to the spectra are those of the A modification. The spectrum in this range consists of bands representing the A molecules going from $v=0$, $J=0$, to $v=1$, $J=1$ in a crystal field of tetrahedral symmetry (T_d *site* group). As is intuitively clear, the theory of Halford and Hornig shows that in a field of this symmetry all transitions infrared active in the free molecule are active in the crystal. The broadness of the bands, of the order 13 cm^{-1}, results from the fact that the lifetime of a molecule in a rotational state is very short (about 10^{-12} sec or 10 rotations) so that any rotation returns to the $J=0$ ground state very rapidly.

(2) Starting at about 15°K increasing numbers of the molecules flop over, cooperatively, to the $P2_13$ configuration of the fcc lattice structure. This places them in a field of trigonal symmetry. The crystal spectra theory now says that the allowed transition is from the ground state to an upper state of vibrational symmetry species $A+E$. The vibration $\nu_3+\nu_4$ has an upper state of species $A+E+F_1+F_2$. In the tetrahedral field this state is ninefold degenerate (each of the F's are threefold degenerate, and the E twofold) with the F_2 being the infrared-active species. In the trigonal field the $A+E$ is the active state so far as observing the transition in the crystal is concerned. Reference to Fig. 6 shows that if rotation is not allowed the transition will represent the A molecules undergoing a $\Delta J=0$ transition. This will be shifted to the low-frequency side of the $\Delta J=+1$ band by 10.5 cm^{-1} (5.5 $m\mu$). Furthermore, if the degeneracy is lifted, as it can be in the trigonal field, the transition is shifted further from the transition in a tetrahedral field.

Thus, the spectrum in this region consists of two parts superimposed upon one another. First, the spectrum of A molecules which have remained in the T_d field, and second, the spectrum of A molecules in the C_3 field. This latter consists of the single band of the $\nu_3+\nu_4$ vibration (upper state $A+E$ shifted from the tetrahedral transition by 10.5 cm^{-1} plus any degeneracy split shifting). This leads to the fact that the y band broadens suddenly starting at 15°K while the x band remains at constant width. Furthermore, the x band begins to lose intensity slightly at the same time the other band broadens and gains intensity. This is due to the fact that the molecules in the trigonal field cannot be seen directly in the solid undergoing the $\nu_1+\nu_4$

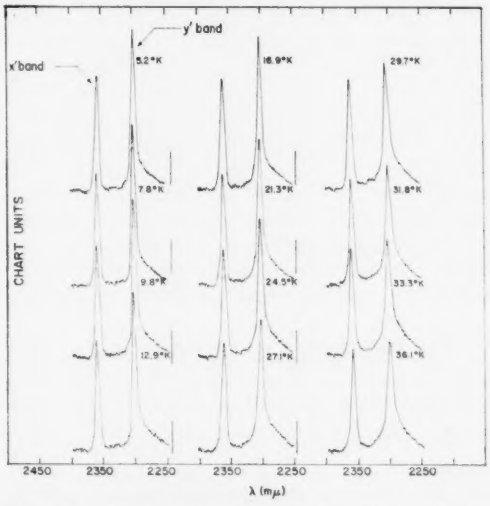

FIG. 4. Spectrum of methane suspended in solid argon (matrix/gas=20) at various temperatures. Spectrophotometer on I/I_0 scale with transmission decreasing upwards, showing modified x and y bands.

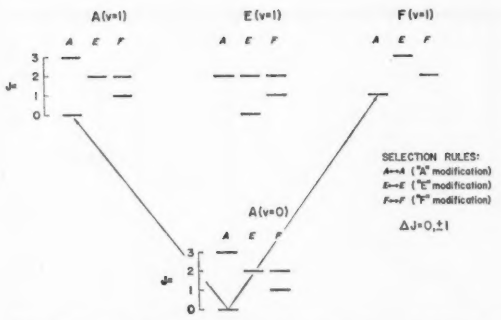

FIG. 5. Allowed states for the various modifications in the free molecule case. The ground state for $v=0$ is of vibrational symmetry species A. The transition in the tetrahedral field is indicated by the solid line, and the transition in a trigonal field by the broken line.

transition. The noticeable narrowing of the x band in the transition range must then represent a longer lifetime for rotation in the range when the molecules start to flop over into the C_3 configuration. This is consistent with the suddenly enlarged lattice constant in this region.[9]

(3) In addition, the y band has a tail on the high-frequency side caused by combinations of this vibration with the lattice vibrations.[11] This is evidently due to the fact that $\nu_3+\nu_4$ couples with the lattice much more tightly than $\nu_1+\nu_4$. It is expected that studies done at higher resolution would indicate that the tail is actually an unresolved side peak such as seen in the spectrum of solid hydrogen.[14,15]

[14] E. J. Allin, H. P. Gush, H. L. Hare, and W. F. J. Welsh, Nuovo cimento Suppl. **9**, 77 (1958).
[15] W. F. J. Hare and H. L. Welsh, Can. J. Phys. **36**, 88 (1958).

) In none of the spectra is there any evidence of any sort of molecular rotation in the ground state. In the experiments done with matrix isolation in solid argon, the y peak broadens slightly but retains its asymmetry, indicating more lattice-molecular coupling. The value of kT at 20°K is much larger than the rotational separation between $J=0$ and $J=1$, and the $\Delta J=-1$ transition should make itself visible if the rotation were allowed. In particular, any rotation should be seen in the x band since the separations are large compared with the resolution of the spectrophotometer.

(5) It is not clear why the f numbers are so high. The A modification represents only $5/5+9+2=0.31$ of the molecules. However, in view of the lack of knowledge about f numbers in solids the figure should be taken with some caution.

VI. CONCLUSIONS

The molecules of methane exist in a field of tetrahedral symmetry below 15°K with any rotation being of a very short duration. In the transition region some of them undergo an order-disorder transition by flopping over into a fcc configuration of trigonal symmetry where rotation is still forbidden. In addition the $\nu_3+\nu_4$ vibration combines with the lattice vibrations.

ACKNOWLEDGMENTS

The author wishes to acknowledge several stimulating discussions with Professor J. E. Mayer. This work was done under a grant from the Atomic Energy Commission and a post-doctoral fellowship from the National Science Foundation.

THE JOURNAL OF CHEMICAL PHYSICS VOLUME 34, NUMBER 5 MAY, 1961

Protection against Radiation Damage in Polymethylmethacrylate by High-Energy Electrons and by Ultraviolet Light*

DONALD G. GARDNER

Department of Chemistry, University of Arkansas, Fayetteville, Arkansas, and Westinghouse Electric Corporation, Pittsburgh, Pennsylvania†

AND

LAWRENCE M. EPSTEIN

Westinghouse Electric Corporation, Pittsburgh, Pennsylvania

(Received August 18, 1960)

The protection against damage caused by ultraviolet light and 2-Mev electrons afforded polymethylmethacrylate by small amounts of such additives as pyrene, *p*-terphenyl, xylene, benzene, and lead stearate is examined. The results are discussed in terms of a model involving energy transport by both excited and ionized states.

I. INTRODUCTION

WHEN ionizing radiation interacts with a solid such as polymethylmethacrylate (Lucite), the energy introduced into the plastic is dissipated in a number of different ways. Part of the energy is used up producing chemical and physical changes, while the rest appears as heat. The primary chemical effects involve the production of free radicals, excited and ionized atoms and molecules, and electrons. The end result is main-chain scission of the polymer together with the production of a considerable quantity of such gases as CH_4, H_2, CO, and CO_2. Physically, the plastic tends to assume the inferior bulk properties of a low molecular weight polymer.[1] At sufficiently high doses (of the order of megarads) a sufficient number of light absorption centers are introduced so that the plastic becomes visibly discolored, although much of the discoloration is transient and tends to disappear in a matter of hours.

The problem of inhibiting radiation damage in organic and biological systems through the use of small amounts of additives has been studied fairly extensively in the past.[1–3] A great deal of work has also been devoted to the development of solid solutions of scintillators in plastics for use as radiation detectors.[4] However, the deliberate use of scintillators as low-concentration additives to reduce radiation damage in solids has not been studied extensively, although the idea was suggested by Maddock[5] in 1952.

We are interested here in true protection of the plastic, in the sense of Burton and Lipsky,[6] rather than with the inhibition of *further* damage from chemical species produced by an initial radiation-induced chemical change in the plastic. The basis for the use of small amounts of additives is the fact that energy is known to be able to migrate for relatively large distances in organic liquids and solids.[7–12] The point is to try to intercept the energy during its migration and to quench it before it has a chance to damage the host material.

It is not likely that the additives function by combining with two broken chain ends and thereby repairing the chain. Alexander and Toms[3] checked this point using tagged additives and found that they did not appear in the polymer chain after irradiation. Furthermore, in our electron work the small amount of additives would have been used up soon after the start of the bombardment. In this work the relative efficiencies for preventing damage of two scintillators, *p*-terphenyl and pyrene, will be compared with typical nonluminescent energy sinks such as benzene and xylene, and with certain inorganic ions such as Pb(II) and Mn(II). Both ultraviolet and 2-Mev electron radiation were used since it appeared reasonable that the electronically excited states, produced along with ionization by electron irradiation, would rapidly convert to the same lower excited state that is accessible through ultraviolet irradiation at 2537 A. Lucite was chosen for this work primarily because it undergoes almost solely chain scission with essentially no cross-linking.[13] Other reasons for the choice of Lucite include: the specific

* Presented at the American Physical Society Meeting, Detroit, March, 1960.

† Supported in part by the U. S. Atomic Energy Commission while at present address of the University of Arkansas.

[1] F. A. Bovey, *The Effects of Ionizing Radiation on Natural and Synthetic High Polymers* (Interscience Publishers, Inc., New York, 1958).

[2] J. W. Born, WADC Tech. Rept. 55–58 (Pt. I, 1954 and Pt. II, 1955).

[3] P. Alexander and D. J. Toms, Radiation Research **9,** 509 (1958).

[4] J. B. Birks, *Scintillation Counters* (McGraw-Hill Book Company, Inc., New York, 1953).

[5] A. G. Maddock, in general discussions, Discussions Faraday Soc. **12,** 124 (1952).

[6] M. Burton and S. Lipsky, J. Phys. Chem. **61,** 1461 (1957).

[7] H. Kallmann and M. Furst, Phys. Rev. **79,** 857 (1950).

[8] H. Kallmann and M. Furst, *Liquid Scintillation Counting*, edited by C. G. Bell and F. N. Hayes (Pergamon Press, New York, 1958), Chap. I.

[9] H. B. Rosenstock and J. H. Schulman, J. Chem. Phys. **30,** 116 (1959).

[10] S. Lipsky and M. Burton, J. Chem. Phys. **31,** 1221 (1959).

[11] M. Burton and H. Dreeskamp, Discussions Faraday Soc. **27,** 64 (1959).

[12] J. Weiss, J. Polymer Sci. **29,** 425 (1958).

[13] A. R. Shultz, J. Polymer Soc. **35,** 369 (1959).

rate of chain scission is high so that it is sensitive to protective agents, the polymer is nearly perfectly linear and random in its molecular weight distribution and remains so after irradiation, the viscosity-molecular weight relationship is very well documented,[14] the polymer is fairly readily soluble at room temperature in a variety of solvents, and the polymer is relatively transparent to 2537-A light so that photolytic breakdown can also be studied.

II. EXPERIMENTAL

A. Materials

The monomer, methylmethacrylate, was purified by distillation. Pyrene was recrystallized twice from ethyl acetate. Reagent grade *p*-terphenyl and benzene were used as received. Lead and manganous acetates were precipitated and recrystallized once.

The sample materials were prepared by either dissolving the additive in the monomer before polymerization, or else by dissolving the additive in an acetone solution of the polymer and slowly evaporating the solution to dryness. Samples were polymerized thermally at about 100°C in the absence of any initiator, the polymerization being carried to completion. Samples to be irradiated with electrons were molded on a laboratory press at 350°F into pieces 0.16 cm in thickness. These were then irradiated, examined with respect to optical absorption with a Beckman DU spectrophotometer, and finally dissolved in benzene to determine the molecular weight. Several samples of Rohm & Haas Plexiglas $\frac{1}{8}$-in. sheet were also irradiated with electrons. For the ultraviolet studies films were cast from acetone onto aluminum foil, and when dried averaged about 1 mg/cm^2. This corresponds to a thickness of about 10^{-3} cm. The films were irradiated on the foil. After irradiation the foils were boiled in benzene to remove all of the polymer for molecular weight determinations.[15]

Since the films were irradiated with ultraviolet light while on a bright aluminum foil a correcton was made for the reflected light. It is assumed here that at 2537 A 100% of the light reaching the aluminum surface is reflected. While this is an approximation, the error introduced is not likely to be large for the following reasons. The reflectance at 2500 A from a freshly evaporated aluminum surface is given as 92.1%.[16] However, in our case all of the incident light was not normal to the surface of the plastic. In addition, the surfaces of the films themselves were not completely smooth. Therefore the path length of the light will exceed two film thicknesses slightly. The values for the absolute amount of light absorbed will be somewhat in error but the values for the various films relative to pure Lucite should not be greatly affected.

In the case of pure Lucite we estimate, using an index of refraction of 1.49, that about 4% of the light will be reflected when normal to the surface.[16] At an angle of 60° about 9% is reflected. Of the light entering normal to the surface 38% will be absorbed during its passage through two film thickness (2×10^{-3} cm). We therefore estimate that about 35% of the incident light will be absorbed.

B. Electron Irradiation

Samples were placed on a cooled aluminum plate and passed beneath the swept electron beam from the 2-Mev Van de Graaff generator. The dose per pass was limited to about 0.5 megarad to minimize heating, and was determined using a blue cellophane dosimeter. The variation of dose with depth plus the backscattering effect was checked experimentally with cellophane and corrected for. The dosimetry was further verified by the good agreement between our radiation yields on the pure polymer and the literature values.

C. Ultraviolet Irradiations

Four Westinghouse Sterilamps were arranged to give uniform intensity over an area of at least 4 in.$\times$12 in. The intensity was determined using uranyl oxalate actinometry. This was done with and without a Pyrex shield to determine the intensity in the 2537-A region, which is presumed here to be the active light.

D. Molecular Weight Determinations

The irradiated polymers were dissolved in benzene, and boiled to ensure complete dissolution and the breakage of any peroxide cross-links.[15] Solutions were filtered and the viscosity η was measured in a Cannon-Fenske viscometer at 30°C as a function of concentration. Extrapolation of η_{sp}/c to infinite dilution with the aid of the usual Huggins constant of 0.35 yielded $[\eta]$, the intrinsic viscosity.[17] The number average molecular weight M_n was obtained using the empirical expression[14]

$$M_n = 2.0\times10^5[\eta]^{1.46}. \quad (1)$$

Use of Eq. (1) is based on the assumption of a fixed ratio of M_n to the viscosity average molecular weight, which closely follows the weight average molecular weight M_w. In the case of the ultraviolet irradiations of optically dense films the distribution of molecular weights is altered by the fact that the dose diminishes with depth. The consequent alteration in the ratio M_w/M_n can be calculated and used as an approximate correction to M_n as determined by viscometry. A correction formula of this type was published by Flynn[18]

[14] J. Baxendale, S. Bywater, and M. G. Evans, J. Polymer Sci. **1**, 237 (1946).
[15] L. A. Wall and D. W. Brown, J. Phys. Chem. **61**, 129 (1957).
[16] *American Institute of Physics Handbook*, edited by D. E. Gray (McGraw-Hill Book Company, Inc., New York, 1957).
[17] P. Flory, *Principles of Polymer Chemistry* (Cornell University Press, Ithaca, New York, 1953).
[18] J. Flynn, J. Polymer Sci. **27**, 83 (1958).

and indicates a dependence on dose. However it can be shown that the correction is independent of dose at high doses and takes the form

$$M_w/M_n = 8([\sinh(D'/2)]/D')^2, \qquad (2)$$

where D' is the optical density to the base e. This form was derived independently by us in a somewhat different manner. Calculations using both Flynn's formula and Eq. (2) showed that the latter was applicable at the lowest doses employed in this work. It is significant to note that a plot of degradation versus dose uncorrected for the above effect still appears essentially linear for the range of doses used here. Hence, the linearity of degradation with dose does *not* necessarily imply a uniform degradation with depth if the initial molecular weight is very high.

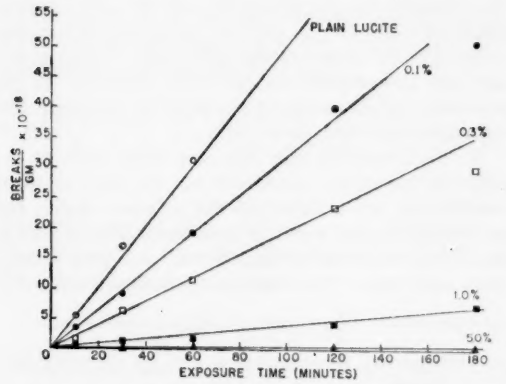

FIG. 1. Damage versus dose curves for Lucite films containing pyrene exposed to ultraviolet light.

III. RESULTS

A. Ultraviolet Irradiation

The intensity of the 2537-A radiation was 6.1×10^{-4} w/cm^2. The quantum yield for main-chain scission with pure Lucite was calculated to be 0.032 breaks/quantum. At 2537 A this corresponds to 154 ev/break. For comparison, the quantum yield for main-chain scission of polymethacrylic acid solutions aerated and de-aerated, respectively, are given as 0.023 and 0.045 by Baxendale and Thomas,[19] although the absolute values are considered somewhat uncertain due to the presence of initiator impurities.

The plots of bond breaks versus exposure time for the Lucite films containing various amounts of additives were essentially linear in nature. An example for the case of pyrene as an additive is shown in Fig. 1. The data have not been corrected for molecular weight variation with depth. In Table I we list the slopes of the various curves relative to that for pure Lucite.

[19] J. H. Baxendale and J. K. Thomas, Trans. Faraday Soc. **54**, 1515 (1958).

TABLE I. Values for the slopes of the damage versus dose plots of loaded Lucite films exposed to ultraviolet light.

Additive	Concentration (percent by weight)	Slope relative to pure Lucite[a]
Pyrene	0.1	0.671
	0.3	0.476
	1.0	0.201
p-Terphenyl	0.3	0.451
	1.0	0.261
Xylene	0.18	0.865
	0.9	0.616
Benzene	0.1	0.849
	1.0	0.650
Pb acetate	1.0	0.495

[a] Corrected for molecular weight variation with depth.

The value for the case of 5% pyrene was not included in Table I because the molecular weight correction becomes so large here as to introduce considerable uncertainty into the final result.

B. Electron Irradiation

The 2-Mev electron bombardment results, plotted as bond breaks versus dose, resemble the ultraviolet results in form, but the effect of the additives in reducing the damage is less. Also, these curves seemed to exhibit a slight upward curvature at high doses, as if some of the additive were being destroyed.

For pure Lucite we find that the slope of the damage curve is 9.8×10^{17} main chain break/g megarad. This corresponds to a G value of 1.56 main chain scissions/100 ev, as compared to literature values of 1.64 and 1.69 (1). Figure 2 shows some results for pyrene and *p*-terphenyl additives. Table II lists the slopes of the various damage curves relative to that for pure Lucite.

Electron bombardment produces broad optical absorptions centered about 410 mμ and 580 mμ, together with intense absorption below 350 mμ. Even for short bombardments ($\sim$0.5 megarads) the latter absorption was too intense in our thick samples to be analyzed. The visible color was not all permanent and decay curves at various wavelengths indicated three principle half-lives: $\sim$7 min, $\sim$2 hr, and "permanent," i.e.,

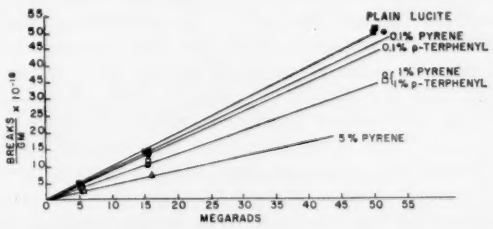

FIG. 2. Damage versus dose curves for Lucite samples containing pyrene and *p*-terphenyl exposed to 2-Mev electrons.

TABLE II. Values for the slopes of the damage versus dose plots of loaded Lucite samples exposed to 2-Mev electron radiation.

Additive	Concentration (percent by weight)	Slope relative to pure Lucite
Pyrene	0.1	0.928
	1.0	0.694
	5.0	0.439
p-Terphenyl	0.1	0.887
	1.0	0.694
Benzene	0.1	0.980
	1.0	0.886
Pb stearate	0.1	0.948

greater than one week. The extent of coloration appeared to saturate between 0.5 and 5 megarads. Some ratios of the initial color intensities are given in Table III. Generally the samples containing Pyrene exhibited little coloration, temporary or "permanent," around 580 mμ. The "permanent" color, integrated over the visible range, increased rapidly initially, but after 5 to 10 megarads increased only slowly with dose.

Several samples of commercial Lucite were irradiated to a dose of about 1 megarad. One was dissolved at once, one was allowed to decay (colorwise) several hours before dissolving, and another was heated before dissolving. No differences in the viscosities were observed, indicating no significant potential chemical effects attributable to the temporary color centers. Samples of Lucite containing different additives were irradiated and then allowed to stand for about half a year before dissolving. In this case the amount of damage increased by about $\frac{1}{3}$ over the anticipated amount. In another experiment, after 50 megarads one sample was heated until it foamed from the trapped radiolysis gas. Still its viscosity was the same as an unheated sample. It may be that the increased damage found in the samples allowed to stand about six months, and that did not appear in the samples heated soon after irradiation, may depend on oxygen diffusion into the sample.

IV. MODEL FOR THE DAMAGE PROCESS

A. Ultraviolet Irradiation

One would immediately suspect that the ultraviolet protection afforded by the pyrene, as shown in Fig. 1, is due to its effectiveness as a light filter. This implies that each photon absorbed by the scintillator cannot produce any damage in the Lucite (here the photolysis of the scintillator is considered insignificant). When a correction is made for this effect it is found that the pyrene still exerts a strong protective effect above and beyond merely acting as a filter. For example, in the case of 1.0% pyrene the rate of chain scission is still reduced by a factor of about 1.7 even after the correction for filtering has been made. In the following discussion we will not consider a filter effect as such, since we would like to suggest the possibility of a two-way transfer of energy between the Lucite and the scintillator. Furthermore, in the electron bombardment case there is obviously no filtering.

In Fig. 3 we show the major courses of action open to the excited species after absorption of a quantum of ultraviolet light.[19a] We will call this energy of excitation an exciton. If the exciton is associated with a Lucite monomer unit, indicated as L^*, it might transfer to another monomer unit, be quenched by a radiationless transition to the ground state, or produce a main chain break. The Lucite is considered here to emit negligible fluorescence.[4] (We will not be concerned here with the actual mechanism of the main-chain scission process, although the diradical process involving a side chain suggested by Schultz[13] seems reasonable to us.) Another possibility is that it might transfer to an adjacent additive molecule. The excited additive S^* might then transfer the energy back to a Lucite unit, or else it might be quenched by internal conversion or luminescence. The p_i values are the probability of each event, and are proportional to the rate constants of the processes and inversely proportional to the mean lifetime associated with each event.

We shall consider only the case where none of the additive molecules, considered for the present to be scintillators, are attached to the polymer chains, but are merely in solid solution. A constant illumination of the film is considered so that we may deal with steady-state conditions. The following symbols are defined:

π_1^e = probability that exciton breaks a main chain.

π_2^e = probability that exciton is lost by all other processes.

E_L = fraction of excitons on Lucite monomer units.

E_S = fraction of excitons on scintillators.

First

$$\pi_1^e+\pi_2^e=1, \tag{3}$$

and

$$E_L+E_S=1. \tag{4}$$

Now

$$\pi_1^e=E_L p_2, \tag{5}$$

TABLE III. Optical properties of absorption bands introduced in Lucite samples by 2-Mev electron bombardment.

Sample	Wavelength mμ	Density Ratio Permanent	: 2 hr	: 7 min
0.1% Pyrene	410	2	1	0.5
1.0% Pyrene	410	2.5	1	0.6
Commercial Plexiglas	410	1.7	1	0.8
Commercial Plexiglas	580	1.7	1	4.4

[19a] At the suggestion of the reviewer we give in the Appendix a list of the reactions involved here so that the order of the reactions can more easily be seen.

and

$$\pi_2^e = E_L p_3 + E_S p_7 + E_S p_8. \quad (6)$$

But

$$\pi_1^e/\pi_2^e = \pi_1^e/(1-\pi_1^e) = E_L p_2/[E_L p_3 + E_S(p_7+p_8)]. \quad (7)$$

Hence

$$\pi_1^e = \{[(p_2+p_3)/p_2] + (E_S/E_L)([p_7+p_8]/p_2)\}^{-1}. \quad (8)$$

If the concentration of the scintillator, c, is expressed as a ratio of the number of scintillator molecules to the number of monomer units in the Lucite chain, and assuming steady-state conditions, the ratio E_S/E_L can be expressed as:

$$E_S/E_L = [p_5 c + P_S(p_2+p_3)]/[p_6(1-c) + P_L(p_7+p_8)], \quad (9)$$

where P_S and P_L are, respectively, the probability that a scintillator or a Lucite unit will absorb a photon. Substituting (9) into (8) we obtain

$$\pi_1^e = \left\{\frac{p_2+p_3}{p_2} + \left[\frac{p_5 c + P_S(p_2+p_3)}{p_6(1-c) + P_L(p_7+p_8)}\right]\frac{(p_7+p_8)}{p_2}\right\}^{-1}. \quad (10)$$

We shall now try to simplify Eq. (10) by considering two possibilities regarding the relative magnitude of the probabilities p_6 and (p_7+p_8).

Case 1. $p_6 \ll (p_7+p_8)$

This means that there is very little chance that an exciton on a scintillator will transfer back to a Lucite unit. It will be shown later that $(p_2+p_3)/p_2 = 31$. Hence $p_3 \gg p_2$. Now $P_S = ck_S/(ck_S+k_L)$ and $P_L = k_L/(ck_S+k_L)$ where the k_i's are the extinction coefficients. As an approximation we obtain:

$$\pi_1^e \approx \left\{\frac{p_2+p_3}{p_2} + c\left[\frac{p_5}{p_2}\left(\frac{ck_S}{k_L}+1\right) + \frac{p_3 k_S}{p_2 k_L}\right]\right\}^{-1}. \quad (11)$$

At this point we can go no further in the simplification. It is expected that $p_5 \gg p_3$, but it is not obvious that $p_5 c \gg p_3$.

Case 2. $p_6 \gg (p_7+p_8)$

This assumption means that it is quite likely that the scintillator can transfer energy back to the Lucite. This implies that the transfer process is rapid enough that the molecules do not relax before the transfer takes place. Considering the term $(1-c)$ as being equal to 1, we obtain:

$$\pi_1^e \approx \left\{\frac{p_2+p_3}{p_2} + \frac{c p_5(p_7+p_8)}{p_6 p_2}\left[1 + \frac{p_3}{p_5(c+k_L/k_S)}\right]\right\}^{-1}. \quad (12)$$

Again we must stop because the size of the term $(p_3/p_5)(c+k_L/k_S)^{-1}$ as compared to 1 is not known *a priori*.

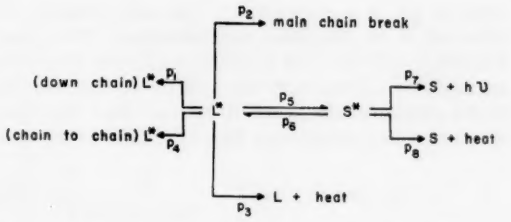

FIG. 3. Fate of exciton produced by ultraviolet light in Lucite containing additive molecules.

We will now attempt to decide if either Eq. (11) or Eq. (12) fits the data. When no scintillator is present $(c=0)$:

$$\pi_1^e = p_2/(p_2+p_3) \equiv \pi_1^e(0) \equiv 1/A. \quad (13)$$

This is just the probability that an exciton will break a main chain divided by the sum of the ways in which an exciton can be lost. As a first approximation we can write either (11) or (12) in the form:

$$\pi_1^e = 1/(A+cF). \quad (14)$$

The number of bond breaks per unit dose, or the slope of the damage curves, is given by:

$$B = \pi_1^e \phi(1-10^{D_{L+S}}). \quad (15)$$

Here ϕ is the photon flux and D_{L+S} is the optical density of the material. When no scintillator is present we have

$$B(0) = \pi_1^e(0)\phi(1-10^{D_L}). \quad (16)$$

Hence

$$B(0)/B = [\pi_1^e(0)(1-10^{D_L})]/[\pi_1^e(1-10^{D_{L+S}})] = \pi_1^e(0)/\pi_1^e K(c). \quad (17)$$

Then F can be determined from the relation

$$F = [AK(c)/c][B(0)/B - 1/K(c)]. \quad (18)$$

Knowing the intensity of the incident light we have determined $A=31$ excitons per main chain break. Some values of F for pyrene are as follows:

c	% by weight	F
0.0005	0.1	70 600
0.0015	0.3	65 100
0.0050	1.0	72 100
		av 69 300±4%

It is clear that F is constant to within about 4%. Furthermore there is no trend with concentration. Note Eq. (11). Here

$$F = (p_5/p_2)(ck_S/k_L+1) + p_3 k_S/p_2 k_L = p_5/p_2(1200c+1) + 36\,000. \quad (19)$$

If $F \approx 69\,300$, as an approximation, then p_5/p_2 evaluated at $c=0.0005$ becomes about 2×10^4. Since the

ratio of p's is a constant, we can now estimate the value of F at the other concentrations. This gives: $F(0.0015)\approx 92\,000$ and $F(0.005)\approx 176\,000$. Since the calculated F values vary by a factor of 2.5 over the above concentration range it is clear that Eq. (11) does not represent our data. From Eq. (12) we see that

$$F=[p_5(p_7+p_8)/p_6p_2]\left[1+\frac{p_3}{p_5(c+k_L/k_S)}\right]. \quad (20)$$

In order for F to remain about constant, $p_5(c+k_L/k_S)\gg p_3$. But this is just what we have found from Eq. (11), except at the lowest concentration used here. (Actually the ratio p_5/p_2 must be considerably larger than that estimated above.) Therefore Eqs. (11) and (12) can be rewritten as

$$\pi_1^e\approx(A+C_1c^2+C_2c)^{-1}, \quad (11')$$

$$\pi_1^e\approx(A+C_3c)^{-1}. \quad (12')$$

Here the C_i's are constants. Our results fit (12') and definitely do not fit (11'). In general, we can say that Eq. (14)

$$\pi_1^e=(A+cF)^{-1}, \quad (14)$$

gives the probability that an exciton will break a main chain. We are then led to believe that the exciton may transfer from a scintillator back to a Lucite unit. The constant F in Eq. (14) is a measure of this transfer ability, and its value depends in part on the scintillator used. The parameter A depends only on the plastic chosen.

B. Electron Irradiation

It is proposed that the general situation is as expressed in the next equation

$$S=X_1\pi_1^e+X_2\pi_1^v. \quad (21)$$

Here we say that the over-all rate of production of chain breaks with respect to dose, S, is composed of two factors, the effect due to excitons and the effect due to ions. π_1^e is the probability that an exciton will break a chain, and it is assumed to be the same as was found in the ultraviolet case; π_1^v is the probability that an ion will cause a chain to break when it recombines with an electron. X_1 and X_2 are, respectively, the number of excitons and ions produced per unit dose. Using the form for π_1^e derived above we can form Eqs. (22) and (23)

$$S(0)=X_1/A+X_2\pi_1^v(0) \quad (22)$$

$$S=X_1/(A+cF)+X_2\pi_1^v. \quad (23)$$

Equation (22) represents the case where the concentration of additive is zero.

A consideration of the data shows that several possible relationships between $\pi_1^v(0)$ and π_1^v can be immediately dismissed. For example, it could be that $\pi_1^v(0)=\pi_1^v$, i.e., the scintillator cannot protect the plastic from damage due to ionization. As it turns out our data indicates that they are the same order of magnitude but not identical. Other possibilities that were eliminated are (a) $(\pi_1^v(0)/\pi_1^v)=(\pi_1^e(0)/\pi_1^e)$, and (b) $\pi_1^v(0)=\pi_1^v=0$.

Two more possibilities may be considered, both of which say that the additive can, in some way, inhibit the damage due to ions. The neutralization of the ion might take place on a Lucite unit and a neighboring additive molecule could then quench the energy released. On the other hand, the positive charge may be transferred to a nearby additive molecule by a charge exchange process where it becomes trapped due to a lower ionization potential, forcing the additive to be the place where the neutralization occurs. The exact mechanism is not clear, although at this time we tend to favor the charge-transfer process. There is, however, one aspect that may be considered, and that is whether or not a mobile exciton is produced during the neutralization involving the additive that may wander off through the plastic as another potential source of damage.

Case 1. No Mobile Exciton Produced

We define the following probabilities[19b]:

p_{2c} = probability that Lucite ion transfers to another Lucite unit.

p_{21} = probability that Lucite ion transfers to additive.

p_{22} = probability that Lucite ion recombines and breaks main chain.

p_{23} = probability that Lucite ion recombines and quenches without breaking.

In a similar manner to the ultraviolet case we can write

$$\pi_1^v=p_{22}, \quad (24)$$

and

$$\pi_2^v=p_{21}c+p_{23}; \quad (25)$$

$$\pi_1^v=[1+(p_{21}c+p_{23})/p_{22}]^{-1}=[(p_{22}+p_{23})/p_{22}+p_{21}c/p_{22}]^{-1}. \quad (26)$$

In general then

$$\pi_1^v=(M+cN)^{-1}. \quad (27)$$

This gives the equations:

$$S(0)=(X_1/A)+(X_2/M), \quad (28)$$

$$S=[X_1/(A+cF)]+[X_2/(M+cN)]. \quad (29)$$

Case 2. Mobile Exciton Produced

Here we say that an exciton may be produced during the neutralization process involving the additive which

[19b] At the suggestion of the reviewer we give in the Appendix a list of the reactions involved here so that the order of the reactions can more easily be seen.

can diffuse away and add to the exciton population produced by direct means. If we assume that one exciton is produced for each neutralization and that the positive charge can transfer to the additive but not back again, it can be shown that S takes the form:

$$S \approx (X_1+X_2Dc)/(A+cF)+(X_2/M)[1-Dc]. \quad (30)$$

The presence of the additive, according to Eq. (30), lowers X_2 and increases X_1 slightly.

The experimental data do not fit Eq. (30) but do fit Eq. (29).[19c] Equation (29) is restated in Eq. (31) to indicate that we can obtain numerical values only for the ratios X_2/M and N/M;

$$S=X_1/(A+cF)+(X_2/M)[1+(cN/M)]^{-1}. \quad (31)$$

V. INTERPRETATION OF RESULTS ACCORDING TO DAMAGE MODEL

In Table IV we list some of our results.

The value of X_1 is quite close to the value of about 5×10^{18} estimated by Burton.[20] The values for F and N/M for the two scintillators are quite similar and much larger than the values obtained for xylene and benzene which are poor scintillators but still good energy sinks. The reason for the great similarity between the two scintillators is not clear. According to Sangster and Irvine[21] the scintillation decay times, scintillation efficiencies, and emission regions are appreciably different. Only their extinction coefficients at 2537 A are almost the same. It is of interest that the inorganic lead ion Pb(II) shows a strong protective effect with the ultraviolet light. This is to be expected from its absorption and emission properties. Experiments with Mn(II) and combinations of Pb(II) and Mn(II) showed that the addition of manganese had little if any protective effect with ultraviolet light.

TABLE IV. Evaluation of the parameters of Eq. (31) for Lucite. The damage equation:

$$S=[X_1/(A+cF)]+(X_2/M)[1+c(N/M)]^{-1}$$

$A=31$ excitons per main chain scission.
$X_1=6.0\times10^{18}$ excitons per g megarad.
$X_2/M=7.88\times10^{17}$ breaks due to ionized states per g megarad.

Additive	Percent by weight	F	N/M
Pyrene	0.1	70 600	
	0.3	65 100	
	1.0	72 100	
		av 69 300±4%	35
p-Terphenyl	0.3	76 400	
	1.0	60 800	
		av 68 400±11%	35
Xylene	0.18	3420	
	0.9	3170	
		av 3300±4%	
Benzene	0.1	3100	
	1.0	2100	
		av 2600±20%	~0.5[a]
Pb acetate	1.0	~22 200	
Pb stearate	0.1	[b]	~170

[a] The F value for xylene was used to calculate this N/M value.
[b] The F value for lead acetate was used here. For some undetermined reason the lead stearate samples produced scattered results under ultraviolet irradiation.

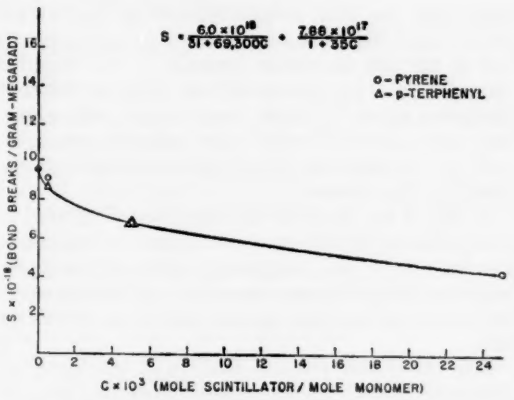
S = 6.0×10^18 / (51+69,300C) + 7.88×10^17 / (1+35C)
o - PYRENE
Δ - p-TERPHENYL
S × 10^-18 (BOND BREAKS / GRAM-MEGARAD)
C × 10^3 (MOLE SCINTILLATOR / MOLE MONOMER)

FIG. 4. Plot of Eq. (31), the damage equation.

The ratios F/A and N/M are the number of Lucite monomer units per additive molecule at which concentration the damage due to excitons or to ions, respectively, is reduced by one half. Thus one molecule of pyrene for every 2200 monomer units will cut the exciton damage in half. But the concentration of pyrene must be increased to one molecule in 35 monomer units to cut the ion damage in half. In the case of benzene and xylene one must increase the concentration by about a factor of 20 to get the same effect for excitons, and even moreso with respect to the ions. Thus it would appear that scintillators that can convert excitons to a lower energy emission possess a real advantage over simple energy sinks such as benzene. The trend in the values of the ratio N/M is also of interest. While the actual values for benzene and lead stearate are somewhat uncertain the trend seems to be real. This trend is consistent with the trend in ionization potentials for benzene and pyrene.[22] We assume that the ionization potential for p-terphenyl is about the same as the meta isomer, which would place it about half way between benzene and pyrene. Clearly the

[19c] Actually this limiting case does not prove that mobile excitons are never produced during the neutralization process, but only that this is not the dominant process.

[20] M. Burton, *Effects of Radiation on Materials*, edited by Harwood *et al.* (Reinhold Publishing Corporation, New York, 1958), Chap. 9.

[21] R. C. Sangster and J. W. Irvine, J. Chem. Phys. **24**, 670 (1956).

[22] R. M. Hedges and F. A. Matson, J. Chem. Phys. **28**, 950 (1958).

large ratio for lead stearate cannot be due to the Pb(II) ion.[23] We assume here that this large value is due to the low ionization potential of the negative stearate ion. Thus one would say that an excellent protective agent for Lucite would consist of a scintillator and a material with a low-ionization potential, such as a negative ion, that would be relatively stable after loss of an electron.

In Fig. 4 we illustrate the behavior of the rate of chain scission per unit dose as a function of concentration for pyrene and *p*-terphenyl under electron bombardment. The solid curve was calculated from the equation at the top, and fits the experimental points fairly well.

The curve also predicts fairly well the result of Alexander[3] that 4.1% pyrene yields a protection factor of 56%. This is close to the value of 51% obtained from Fig. 4.

If we take the reasonable assumption of Burton,[20] there are about twice as many excitons produced as there are ions, we can estimate the value of M. This turns out to be about 3.8. Thus about one out of every four ions will cause a main chain break when no additive is present. Hence it is about eight times more likely that an ion will cause a chain break in plain Lucite than it is for an exciton.

ACKNOWLEDGMENT

The authors wish to acknowledge the assistance of James Kwiecinski in the determination of many of the viscosity measurements.

[23] W. M. Latimer, *The Oxidation States of the Elements and their Potentials in Aqueous Solutions* (Prentice-Hall, Inc., Englewood Cliffs, New Jersey, 1938).

APPENDIX

I. Reactions in Ultraviolet Case

$L^* + L \rightarrow L + L^*$ (down chain)

$L^* \rightarrow$ chain break

$L^* \rightarrow L +$ heat

$L^* + L \rightarrow L + L^*$ (chain to chain)

$L^* + S \rightarrow L + S^*$

$S^* + L \rightarrow S + L^*$

$S^* \rightarrow S + h\nu$

$S^* \rightarrow S +$ heat

$S + h\nu \rightarrow S^*$

$L + h\nu \rightarrow L^*$.

II. Reactions in Electron Case

$L \overset{\text{radiation}}{\rightsquigarrow} L^+ +$ negative fragment (usually electron)

$L^+ + L \rightarrow L + L^+$ (down chain or chain to chain)

$L^+ + S \rightarrow L + S^+$

$L^+ +$ negative fragment $\rightarrow$ chain break

$L^+ +$ negative fragment $\rightarrow L +$ heat

$S^+ +$ negative fragment $\rightarrow S +$ heat and/or $h\nu$

$S^+ +$ negative fragment $\rightarrow S +$ mobile exciton.

THE JOURNAL OF CHEMICAL PHYSICS VOLUME 34, NUMBER 5 MAY, 1961

Extraordinary Basic Functions in Valence Theory* †

LAWRENCE C. SNYDER‡ AND ROBERT G. PARR§

Department of Chemistry, Carnegie Institute of Technology, Pittsburgh, Pennsylvania

(Received November 7, 1960)

It is pointed out that, provided kinetic energies are properly computed, one may use functions which are continuous with piecewise continuous first derivatives as trial variation functions in quantum-mechanical calculations of molecular electronic wave functions. As a simple example, a function of the type

$$A \exp[-(Z_< r_< + Z_> r_>)]$$

is shown to be a good alternative to the conventional Eckart function for the helium atom. A rather more detailed study of helium is carried out to illustrate the use of *individual lobes of real hydrogenlike atomic orbitals* as an extended basic set of functions for molecular calculations. Implications for the general problem of correlation energies in atoms and molecules are discussed, and it is shown that a rationalization of the lowered electronic repulsions employed in modern pi-electron theory is provided by the supposition that pi electrons tend to move in opposite rather than the same lobes of pi orbitals.

I. INTRODUCTION

ACCURATE molecular electronic wave functions are very difficult to obtain. The method that works for two-electron atoms and molecules, use of trial variational functions explicitly including the interelectronic distances, is virtually impossible to extend to polyelectronic systems,[1] and the method in which one-electron atomic orbitals are used as a basis is slowly convergent and requires evaluation of many extraordinarily difficult integrals.[2] The present study concerns the possibility of employing as basic functions a class of functions more general than apparently has heretofore been tried for molecules,[3] functions which have discontinuous derivatives, or *extraordinary functions*.[4] Just possibly, extraordinary functions may provide faster enough convergence in the variation-iteration procedure to make worthwhile the extra trouble of handling them.

A fairly close examination of the problem of correlation of pi electrons in unsaturated organic molecules[5] has already revealed that resolution of a real $2p$ atomic orbital into its two separate lobes is a helpful device.[4,6,7] This is one example of the use of extraordinary functions.

In the following, extraordinary functions first are defined, and their fundamental properties established. Then are given one simple and one more complex example of their use in the problem of the ground state of the helium atom. Next the pi-correlation problem is discussed from the viewpoint of extraordinary functions. Finally, the various numerical results that have been obtained are discussed, other possible applications are indicated, and a possible further generalization is briefly considered.

II. DEFINITION AND PROPERTIES OF EXTRAORDINARY FUNCTIONS

An *extraordinary function* is defined[4] as an electronic wave function which is *continuous* in the electronic coordinates but which has only *piecewise continuous derivatives* with respect to one or more of these coordinates. The function Φ is extraordinary if Φ is continuous but $\nabla_i\Phi$ is piecewise continuous for one or more electrons i.

That such functions are admissible as trial variational functions can be seen as follows. For the exact wave function Ψ for a system, which is not extraordinary, one has

$$E=\int\Psi^*[-\tfrac{1}{2}\sum_i\nabla_i^2+V]\Psi dv \Big/ \int\Psi^*\Psi dv. \qquad (1)$$

By integrations by parts this can be converted to the

* Based on part of a thesis submitted by Lawrence C. Snyder in partial fulfillment of the requirements for the degree of Ph.D., Carnegie Institute of Technology, 1959.

† Supported in part by research grants from the National Science Foundation, the Petroleum Research Fund of the American Chemical Society, and the Alfred P. Sloan Foundation.

‡ National Science Foundation Predoctoral Fellow, 1953–1954, 1956–1958. Present address: Bell Telephone Laboratories, Murray Hill, New Jersey.

§ Alfred P. Sloan Fellow, 1956–1960.

[1] For recent work, see, for example, W. Kolos and C. C. J. Roothaan, Revs. Modern Phys. **32**, 219 (1960), C. C. J. Roothaan and A. W. Weiss, *ibid.* **32**, 194 (1960).

[2] For the current status, see, for example, S. F. Boys and G. B. Cook, Revs. Modern Phys. **32**, 285 (1960).

[3] A possible exception is some of the unpublished work of G. E. Kimball and collaborators, for example, G. F. Neumark, Ph.D. thesis, Columbia University, New York, 1951.

[4] L. C. Snyder and R. G. Parr, J. Chem. Phys. **28**, 1250 (1958). One of the numerical results quoted in this preliminary communication was wrong: The energy given by the wave function of Eq. (2) is −2.895915 a.u., not −2.89700 a.u.

[5] R. Pariser and R. G. Parr, J. Chem. Phys. **21**, 466, 767 (1953).

[6] The idea that pi electrons might prefer to move in opposite lobes of pi orbitals (opposite sides of the molecular plane for planar unsaturated molecules) was suggested to R.G.P. by Dr. Rudolph Pariser in 1953.

[7] M. J. S. Dewar and C. Wulfman, J. Chem. Phys. **29**, 158 (1958).

alternative form,[8]

$$E=\int[\tfrac{1}{2}\sum_i \nabla_i\Psi^*\cdot\nabla_i\Psi+\Psi^*V\Psi]dv \Big/ \int\Psi^*\Psi dv. \quad (2)$$

The quantity E is a functional $E(\Psi)$, and variational minimization of $E(\Psi)$ with respect to the form of Ψ can be carried out with either Eq. (1) or (2). Equation (2) is mathematically preferable, however, since it involves the lower derivatives of Ψ; if one uses it, one automatically admits a larger class of trial functions.[8,9] For a trial function Φ which is extraordinary, Eq. (1) gives trouble. One avoids this simply by using Eq. (2), in which piecewise discontinuities in $\nabla_i\Phi$ are allowable.

The prescription for handling extraordinary functions then is: if Φ is normalized and extraordinary, the expectation value for the kinetic energy $T=-\frac{1}{2}\sum_i\nabla_i^2$ associated with Φ must be computed from the formula

$$T=\tfrac{1}{2}\sum_i\int\nabla_i\Phi^*\cdot\nabla_i\Phi dv. \quad (3)$$

More generally, integrals $T_{fg}=-\frac{1}{2}\int f\nabla^2 g dv$ must be computed from the formula,[10,11]

$$T_{fg}=\tfrac{1}{2}\int\nabla f\cdot\nabla g dv, \quad (4)$$

in which the function g may or may not be extraordinary.

Equation (3) is well known in mathematical physics. From it one immediately has $T\geqq 0$,[12] which does not follow so directly from the more familiar formula involving the ∇_i^2.

Substitute formulas also must be employed for expectation values of other operators involving second derivatives. Thus for the total angular momentum operator,

$$\mathbf{M}^2=-[(\partial^2/\partial\theta^2)+\cot\theta(\partial/\partial\theta)+\csc^2\theta(\partial^2/\partial\phi^2)],$$

one has matrix elements $(\mathbf{M}^2)_{fg}=\int f\mathbf{M}^2 g dv$, which must be computed from the formula

$$(\mathbf{M}^2)_{fg}=\int[(\partial f/\partial\theta)(\partial g/\partial\theta) + \csc^2\theta(\partial f/\partial\phi)(\partial g/\partial\phi)]dv. \quad (5)$$

This may be verified by an integration by parts of $\int f\mathbf{M}^2 g dv$, or by picking out relevant terms in Eq. (4).

An alternative proof of these equations can be obtained by treating each extraordinary function g as the limit of an analytic function g'. In the limit, delta functions are created in $\nabla_i^2 g'$ at points of discontinuity in $\nabla_i g$, and contributions to T_{fg} result which make Eq. (4) correct.[11–13]

III. A MODIFIED ECKART-TYPE WAVE FUNCTION FOR HELIUM

A classic approximate description of the ground state of the helium atom is provided by the wave function of Eckart,[14]

$$\Psi(\text{Eckart})=(2+2S^2)^{-\frac{1}{2}}[1s(1)1s'(2)+1s'(1)1s(2)], \quad (6)$$

where $1s$ and $1s'$ are hydrogenlike orbitals of effective charges Z and Z', respectively, and S is the overlap integral between them. The best wave function of this form gives, for $Z=2.183171$, $Z'=1.188530$, an energy -2.8757 a.u.,[15] much closer to the true nonrelativisitic limit, -2.9037 a.u.,[16] than is for example the Hartree-Fock result -2.8617 a.u.[17] Physically, the picture provided by this wave function is (approximately) that when one electron is in the orbital $1s$, the other is in the orbital $1s'$. That is to say that, in order to provide in some measure for the detailed repulsion between the electrons, instead of both being placed in the same orbital, which is the Hartree-Fock description, one is put in an inner orbital, one in an outer one—the $(1s)^2$ shell is "split" into an inner $1s$ component and an outer $1s'$ component. An "in-out" or "radial" correlation is thereby included in the wave function.[18]

Now the function of Eq. (6) does not place the *inner electron* always in the *inner orbital* $1s$ and the *outer electron* in the *outer orbital* $1s'$. A function that will do precisely this is

$$\Psi(\text{modified Eckart})=\begin{cases}1s(1)1s'(2) & \text{if } r_1\leqq r_2\\ 1s'(1)1s(2) & \text{if } r_1\geqq r_2\end{cases}. \quad (7)$$

The simplicity of this mathematical expression may be noted; it would appear to be a purer embodiment of the in-out correlation idea than is the function of Eq. (6). In a more compact notation,

$$\Psi(\text{modified Eckart})=A\exp(-Z_<r_<-Z_>r_>), \quad (8)$$

[8] R. Courant and D. Hilbert, *Methods of Mathematical Physics* (Interscience Publishers, Inc., New York, 1953) Vol. I, p. 176. See also Lord Rayleigh, *Theory of Sound* (Dover Publications, New York, 1945).

[9] The authors are indebted to Professor R. J. Duffin for calling this derivation of Eq. (2) to their attention.

[10] It is assumed that all functions vanish strongly at the boundaries of v.

[11] The difference $\int f\nabla^2 g dv$ minus $-\int\nabla f\cdot\nabla g dv$ can be identified with the surface integral $\int f(\nabla g^+-\nabla g^-)dS$, where ∇g^+ and ∇g^- are right and left normal derivatives of g at a surface S of discontinuity in ∇g. It may be noted that if S is a nodal surface for f, this difference vanishes.

[12] For example, F. Seitz, *Modern Theory of Solids* (McGraw-Hill Book Company, Inc., New York, 1940), p. 229.

[13] This argument is written out in detail in J. O. Hirschfelder and G. V. Nazaroff, Theoretical Chemistry Laboratory, University of Wisconsin, Rept. WIS-AEC-27 (August 15, 1960), and J. Chem. Phys. **34,** 1666 (1961).

[14] C. Eckart, Phys. Rev. **36,** 878 (1930).

[15] J. N. Silverman, O. Platas, and F. A. Matsen, J. Chem. Phys. **32,** 1402 (1960).

[16] C. L. Pekeris, Phys. Rev. **112,** 1649 (1958); **115,** 1216 (1959).

[17] L. C. Green, M. M. Mulder, M. N. Lewis, and J. W. Woll, Jr., Phys. Rev. **93,** 757 (1954).

[18] G. R. Taylor and R. G. Parr, Proc. Natl. Acad. Sci. (U.S.) **38,** 154 (1952).

where $Z_>$ and $Z_<$ have been written in place of Z' and Z.

Equation (8) is an *extraordinary function* in the sense of Sec. II, and so to use it as a trial variational function requires the grad·grad formula for the kinetic energy, Eq. (3). The final energy formula is, in terms of the parameters $\bar{Z}=\frac{1}{2}(Z_<+Z_>)$ and $\tau=(Z_<-Z_>)/\bar{Z}$,

$$E=\bar{Z}^2(1+\tau^2)-\bar{Z}(27-28\tau+9\tau^2)/(8-9\tau+3\tau^2). \quad (9)$$

The best energy value is obtained for $Z_>=1.5103$ and $Z_<=1.8465$; it is -2.8727 a.u., a shade less good than the Eckart value.[19]

IV. INDIVIDUAL LOBES OF REAL HYDROGENLIKE ATOMIC ORBITALS AS BASIC FUNCTIONS. CALCULATION ON HELIUM

The feasibility of working with trial variation functions which have discontinuous derivatives creates the possibility of breaking traditional atomic orbitals into pieces corresponding to parts of them between nodal surfaces—their individual *lobes*. This section explores this idea.

As an illustration, consider a normalized $2p$ hydrogenlike atomic orbital for electron 1, $2p_z(1)$. It may be written

$$p_z(1)=2^{-\frac{1}{2}}[Z_+(1)-Z_-(1)], \quad (10)$$

where Z_+ and Z_- are the normalized extraordinary functions

$$Z_+(1)=\begin{cases} 2^{\frac{1}{2}}p_z(1) & \text{if } z\geqq 0 \\ 0 & \text{if } z<0 \end{cases},$$

$$Z_-(1)=\begin{cases} 0 & \text{if } z>0 \\ -2^{\frac{1}{2}}p_z(1) & \text{if } z\leqq 0 \end{cases}. \quad (11)$$

It will be noted that Z_+ and Z_-, which are the individual lobes of p_z, are functions which are everywhere nonnegative. They are not eigenfunctions of M^2, and they are not orthogonal to s orbitals.

Any utility as basic functions for molecular calculations of functions like these in Eq. (11) probably resides in their application to the correlation problem. An electron configuration of the conventional type p_z^2 can be expanded,

$$p_z(1)p_z(2)=2^{-1}\{2^{-\frac{1}{2}}[Z_+(1)Z_+(2)+Z_-(1)Z_-(2)] -2^{-\frac{1}{2}}[Z_+(1)Z_-(2)+Z_-(1)Z_+(2)]\}, \quad (12)$$

or, if one defines

$$p_z^2(\text{together})=2^{-\frac{1}{2}}[Z_+(1)Z_+(2)+Z_-(1)Z_-(2)],$$

$$p_z^2(\text{away})=2^{-\frac{1}{2}}[Z_+(1)Z_-(2)+Z_-(1)Z_+(2)], \quad (13)$$

one has

$$p_z^2=2^{-\frac{1}{2}}[p_z^2(\text{together})-p_z^2(\text{away})]. \quad (14)$$

The p_z^2 is composed of equal portions of together and away functions; the electrons are as likely to be in the same lobe as in opposite lobes.

Electrons, other things being equal, like to be away from each other because of their Coulomb repulsion. This suggests that there may be problems in which the optimum weighting of away and together components is not equal. This can be brought into the variational scheme in a straightforward way if the individual lobes are regarded as the basic entities. This brings into play, in addition to p_z^2 of Eq. (14), for example, the function

$$|p_z|^2=2^{-\frac{1}{2}}[p_z^2(\text{together})+p_z^2(\text{away})]. \quad (15)$$

By a mixing of this with p_z^2, one can achieve an arbitrary ratio of together and away character.

In dealing with individual lobes such as Z_+ and Z_- it is useful to recognize that their kinetic and potential energies are the same as those of the complete orbital from which they come. Their extraordinary character does not enter in integrals like $\int Z_+TZ_+dv$,[11] but does in integrals like $\int sTZ_+dv$, where the grad·grad formula of Eq. (3) must be applied.

The problem of determining the various elementary integrals for individual lobes of atomic orbitals will be treated in a separate communication by one of the authors (L.C.S.). Here an application to the ground state of helium will be described.

The conventional configuration interaction treatment of helium[18,20] involves mixing the Eckart (ss') function of Eq. (6) with terms of the form,

$$(p)^2=3^{-\frac{1}{2}}[(p_x)^2+(p_y)^2+(p_z)^2],$$

$$(d)^2=5^{-\frac{1}{2}}[(d_{xy})^2+\text{four other terms}],$$

$$(f)^2=7^{-\frac{1}{2}}[(f_{xyz})^2+\text{six other terms}], \text{ etc.} \quad (16)$$

Results are summarized in Table I. In the first calculation[18] principal quantum numbers n were taken to be integral: 1 for s, 2 for p, 3 for d and 4 for f orbitals; the calculation recently has been redone[21] with non-

[19] This result provides an interesting paradox. If one at the outset were satisfied to seek the best wave function for helium of the restricted from $\Psi=\Psi(r_1, r_2)$, one could immediately replace $(1/r_{12})$ in the Hamiltonian operator with $(1/r_>)$. The Schrödinger equation then would take the form

$$[-\tfrac{1}{2}\nabla_<^2-\tfrac{1}{2}\nabla_>^2-(2/r_<)-(1/r_>)]\Psi=E\Psi. \quad (A)$$

This equation is *apparently* separable in $r_<$ and $r_>$, and has the *apparent* lowest-energy eigenfunction

$$\Psi=A\exp(-2r_<-r_>) \quad (B)$$

and the *apparent* lowest eigenvalue $-\frac{1}{2}(1+4)=-2.50$ a.u. These results contradict those obtained above. They are wrong because they do not properly account for the $r_1=r_2$ part of space, where one must be careful about the kinetic energy, as has been seen already. An investigation of the differential Eq. (A) would be of some interest in this connection; if it could be solved one would have an absolute determination of the radial correlation energy of helium (in the absence of angular factors).

[20] R. K. Nesbet, Phys. Rev. **110**, 1073 (1958).

[21] L. C. Snyder, J. Chem. Phys. **33**, 1711 (1960).

TABLE I. Wave functions for the helium atom.

Functional Form[a]	Reference	Energy (a.u.)[b]
(ss')	14, 22	−2.87566
$(ss')+(p)^2$	18, 15	−2.89523
$(ss')+(p)^2+(d)^2+(f)^2$	18, 21	−2.89742
$(ss')+(P_T)+(P_A)$	This work[c]	−2.89592
$(ss')+(P_T)+(P_A)+(P_N)$	This work[d]	−2.89595
$(ss')+(P_T)+(P_A)+(d)^2+(f)^2$	This work[e]	−2.89774

[a] See text for description of wave functions.
[b] All energies are for wave functions with integral principal quantum numbers: $n_s=n_{s'}=1$, $n_p=2$, $n_d=3$, $n_f=4$. Compare work cited in footnote 21.
[c] Parameter values are as follows: $\zeta_s=1.2085774$, $\zeta_{s'}=2.1471983$, $\zeta_p=2.5021301$, which minimize the energy of this function.
[d] Parameter values (not quite the best) are as in footnote c.
[e] Parameter values (not quite the best) are as follows: $\zeta_s=1.2091169$, $\zeta_{s'}=2.1583259$, $\zeta_p=2.4756866$, $\zeta_d=4.0978811$, $\zeta_f=4.7053604$.

integral values of n.[22] Convergence of the expansion

$$\Psi=A_1(ss')+A_2(p)^2+\cdots \tag{17}$$

is seen to be quite good.

As an alternative to Eq. (19), one may examine the trick of treating the together and away pieces of $(p)^2$ as separate entities. If one defines [cf. Eq. (13)]

$$P_T=3^{-\frac{1}{2}}[p_x^2(\text{together})+p_y^2(\text{together})+p_z^2(\text{together})],$$

$$P_A=3^{-\frac{1}{2}}[p_x^2(\text{away})+p_y^2(\text{away})+p_z^2(\text{away})], \tag{18}$$

one has

$$(p)^2=2^{-\frac{1}{2}}(P_T-P_A), \tag{19}$$

so that an expansion

$$\Psi=C_1(ss')+C_2(P_T)+C_3(P_A)+\cdots \tag{20}$$

is more general than Eq. (17), and includes Eq. (17) as a special case.

Table I gives some results of calculations with Eq. (20) at various levels of approximation. The separate introduction of P_T and P_A is seen to indeed improve the energy. For example, while the two-term function

$$\Psi=0.998098(ss')-0.061638(p)^2$$

$$=0.998098(ss')-0.043585(P_T)+0.043585(P_A) \tag{21}$$

gives an energy of −2.89523 a.u., the function

$$\Psi=1.016963(ss')-0.053895(P_T)+0.032086(P_A), \tag{22}$$

gives a better result, −2.89592 a.u. Comparison of Eqs. (21) and (22) shows that in fact the situation in which the electrons are in opposite lobes is favored over the situation in which they are in the same lobe. The Eckart function is improved by the addition of P_A and the subtraction of P_T.

[22] R. G. Parr and H. W. Joy, J. Chem. Phys. **26**, 424 (1957).

The function

$$6^{-\frac{1}{2}}[p_x(1)p_y(2)+p_y(1)p_x(2)$$
$$+p_x(1)p_z(2)+p_z(1)p_x(2)+p_y(1)p_z(2)+p_z(1)p_y(2)]$$

does not mix with (ss') and $(p)^2$. When individual lobes are introduced, however, there is a function of this general type that does so mix, the function which puts electrons symmetrically into adjacent lobes, as one in X_+ and one in Y_+. This is

$$P_N=24^{-\frac{1}{2}}[X_+(1)Y_+(2)+Y_+(1)X_+(2)+X_-(1)Y_+(2)$$
$$+Y_+(1)X_-(2)+20\text{ other terms}]. \tag{23}$$

The effectiveness of this function in lowering the energy is not great; the function

$$\Psi=1.014261(ss')-0.055229(P_T)+0.030705(P_A)$$
$$+0.001193(P_N) \tag{24}$$

has an energy −2.89595 a.u., very little better than the energy associated with Eq. (22).

In Table I is included the result obtained if the usual $(d)^2$ and $(f)^2$ terms are added to Eq. (22). The energy increment due to the presence of P_T and P_A is lessened as the higher terms are added; it falls from 0.00069 to 0.00032. This is what would be expected, since P_T and P_A are not orthogonal to $(d)^2$ and $(f)^2$.

One could resolve d, f, $\cdots$ orbitals themselves into their individual lobes. Only a few preliminary calculations have been carried out with this much enlarged basis however.[23]

The mean-square angular momentum associated with the exact ground-state function for helium is zero, as is that associated with the approximate functions of Eqs. (20) and (21). For the function of Eq. (22), on the other hand, $\langle M^2\rangle_{Av}=0.000564\hbar^2$. Quite generally,

TABLE II. Coulomb repulsion integrals between pi orbitals.[a]

R	Theoretical[b] $(pp\mid qq)$	Semiempirical[c] $(pp\mid qq)$	Computed $(p_up_u\mid q_lq_l)$	Computed $(p_up_u\mid q_uq_u)$
0.00A	16.930	10.959	10.978[d] (9.955)[e]	22.889[d] (23.902)[e]
1.39	9.027	6.895	7.181[e]	10.360[e]
2.41	5.668	5.682	5.121[e]	5.973[e]

[a] Values, in ev, of integrals $(ab\mid cd)=\int a(1)b(1)(e^2/r_{12})c(2)d(2)\,d\tau$, where p and q are carbon $2p\pi$ orbitals a distance R apart. Subscripts u and l denote normalized individual upper and lower lobes, as defined in Eq. (11) of the text.
[b] See work cited in footnote 25.
[c] See work cited in footnote 24.
[d] Accurately computed for Slater orbitals.
[e] Computed using uniformly charged sphere approximation, see R. G. Parr, J. Chem. Phys. **20**, 1499 (1952).

[23] If one went to very high l values, and simultaneously to high radial quantum numbers, the individual lobes would become numerous and small, spanning a great many little cells in space. It is possible that the individual lobes in this limit would be useful for the correlation problem.

an *approximate* eigenfunction of H need not be an *exact* eigenfunction of every operator which commutes with H; not requiring it to be may be advantageous in special cases.

V. PI-ELECTRON CORRELATION PROBLEM

A vital and novel feature in modern semiempirical theories of the spectra of unsaturated molecules[5] is the lowering from their theoretical values of Coulomb repulsion integrals, the repulsion between one pi electron and another on the same atom $(pp|pp)$ and the repulsions between pi electrons on different atoms $(pp|qq)$. In Table II are listed semiempirical and theoretical values for some of these integrals, for carbon atom pi systems. The semiempirical values were obtained by Pariser from a treatment of polyacene spectra[24]; the theoretical values are for $2p\pi$ Slater atomic orbitals with effective charge 3.18.[25]

It has been suggested by Pariser,[6] and independently by Dewar and Wulfman,[7] that the lowered values for these integrals may reflect a tendency of the electrons in a pi system to stay on opposite sides of the pi nodal plane.[4]

This idea is readily tested, by breaking repulsions between full pi orbitals into repulsions between individual lobes of pi orbitals. Results of doing this are displayed in Table II. The theoretical $(pp|pp)$ for carbon, 16.93 ev, is the mean of the theoretical $(p_up_u|p_lp_l)$, 10.98 ev, and the theoretical $(p_up_u|p_up_u)=$ 22.89 ev. (Here subscripts u and l denote upper and lower lobes, respectively.) The fact that the first of these is close to the empirical value of 10.96 ev is encouraging evidence supporting the idea that two electrons are seldom in the same $2p\pi$ lobe in an actual unsaturated system.

The values of $(p_up_u|q_uq_u)$ and $(p_up_u|q_lq_l)$, for $p\neq q$, could be accurately calculated for Slater orbitals, although this has not yet been done. Instead, the uniformly charged sphere approximation has been employed, calibrated so as to give the correct $(pp|pp)$ value at zero distance. The values of $(p_up_u|q_lq_l)$ are surprisingly close to the empirical $(pp|qq)$ values, again supporting the idea that indeed there is an "up-down" correlation present for pi electrons.

One might set out to do purely theoretical calculations on pi systems using individual lobes of pi orbitals as the basic variational entities. One could represent thereby, by suitable combinations of functions of the type P_T and P_A, any degree of correlation across the nodal plane. This device might be particularly useful for handling polarizations of pi systems, as in the interaction of an aromatic molecule with another charged fragment.

Dewar and Hojvat have begun calculations of just this kind.[26] They point out, in accordance with the foregoing discussion, that no kinetic-energy peculiarity occurs in the use of the individual lobes in a purely pi-electron problem. This is due to the fact that the pi orbitals themselves have nodes at the surfaces of discontinuity in the derivatives of the orbitals.[11]

There is a difficulty in the individual use of p_z^2 (together) and p_z^2 (away) type functions in the pi problem (Dewar and Hojvat in fact use solely the away type). These are not individually orthogonal to wave functions for the sigma electrons, and such an orthogonality is basic for justification of the pi-electron approximation itself.[27] One could orthogonalize p_z^2 (away) functions to sigma-electron functions; probably one should think of this as implicitly having been carried out in the Dewar-Hojvat method.

VI. DISCUSSION

It has been demonstrated that trial functions with discontinuous derivatives, called extraordinary functions, are acceptable in the variational method. The illustrative calculations that have been carried out on the helium atom do not show great improvement over the use of ordinary functions, but one should remain alert for places where extraordinary functions may be more substantially beneficial.

One might well ask whether functions which are discontinuous could be employed as well. The answer to this question is negative, for in this case the kinetic energy becomes infinite.[13]

Individual lobes of atomic orbitals are everywhere positive functions, so that if a (nodeless) ground-state function could be built by adding up pieces formed as products of individual lobes one would have a method for building up a wave function from nodeless bits. This would circumvent (at the cost of some nonorthogonality difficulties) an essential problem in conventional expansions in orthogonal functions: the introduction of nodes at early stages which must be removed at later stages.[28]

A straightforward simple application of these ideas would be to atoms containing closed p shells, as the $(1s)^2(2s)^1(2p)^6$ configuration of neon, or to molecules for which such united-atom configurations are important, as in CH_4.[29] Possibilities for further work with pi-electron systems already have been mentioned. More novel from the fundamental viewpoint could be the use of extraordinary functions to improve wave functions in a particular region in a molecule, which should be specially effective for calculations of certain molecular properties.

[24] R. Pariser, J. Chem. Phys. **24**, 250 (1956).
[25] H. J. Kopineck, Z. Naturforsch. **5a**, 420 (1950).
[26] M. J. S. Dewar and N. L. Hojvat, J. Chem. Phys. (to be published).
[27] P. G. Lykos and R. G. Parr, J. Chem. Phys. **24**, 1166, **25**, 1301 (1956).
[28] G. E. Kimball, talk presented at Molecular Quantum Mechanics Conference, The University of Texas, Austin, Texas, December 7–9, 1955.
[29] A. F. Saturno and R. G. Parr, J. Chem. Phys. **33**, 22 (1960).

Applicability of Approximate Quantum-Mechanical Wave Functions Having Discontinuities in Their First Derivatives*

JOSEPH O. HIRSCHFELDER AND GEORGE V. NAZAROFF
University of Wisconsin Theoretical Chemistry Laboratory, Madison, Wisconsin

(Received November 7, 1960)

The method of convolutions is used to form smoothed functions from approximate wave functions which are discontinuous or have discontinuous first derivatives. As a parameter ϵ in the smoothed function decreases, the smoothed function approaches the approximate wave function. The expectation values for physical properties corresponding to the approximate wave function are defined to be the limit as ϵ approaches zero of the expectation values corresponding to the smoothed function. It is found that if the approximate wave function is discontinuous, the corresponding expectation value for the kinetic energy is infinite. Therefore, it seems unlikely that discontinuous approximate wave functions can ever be useful. However, if the approximate wave function is continuous but has a discontinuity in its first derivative, then, as a result of the discontinuity, there is a contribution $\delta\bar{T}_{12}$ to the expectation value of the kinetic energy. For a one-dimensional problem

$$\delta\bar{T}_{12}=-(\hbar^2/2m)\psi^*(0)\,[\psi_2'(0)-\psi_1'(0)\,].$$

Here $\psi(0)$ is the value of the approximate wave function at the point zero where the discontinuity in its first derivative occurs, and $\psi_1'(0)$ and $\psi_2'(0)$ are the first derivatives of ψ taken from the left and from the right, respectively, at this point. Similarly, for an N-dimensional problem having a surface $S_{12}=0$ over which the first derivatives of the approximate wave function are discontinuous,

$$\delta\bar{T}_{12}=\int_{\text{surface}}\psi^*[\,(\partial/\partial n)\,(\psi_2-\psi_1)\,]\,dS_{12}.$$

Here the $\partial/\partial n$ is the normal derivative with the normal pointed from region 1 towards region 2.

IN order for a function to be interpretable and physically acceptable as the wave function of a Schrödinger equation, the function and its first derivatives must satisfy the following conditions[1]:

(1) The function must be single-valued and analytic in all of its variables at every point in configurational space where the potential energy is analytic.

(2) The function and its first derivatives must be absolutely and quadratically integrable over the whole of configuration space.

(3) The function must vanish at infinity faster than any negative power of the Cartesian coordinates.

Unfortunately, we do not know the true wave functions for most quantum-mechanical problems and therefore we consider various types of approximate wave functions. As Snyder and Parr[2] have shown, it may be expedient to construct approximate wave functions whose derivatives are piece-wise continuous. Thus, all of configuration space might be divided into a set of domains: 1, 2, $\cdots$, n. The approximate wave function ψ is composed of a set of distinct functions ψ_i such that $\psi=\psi_i$ in the ith domain. At all interior points of its domain, ψ_i is single-valued and analytic. Furthermore, ψ_i and all[3] of its derivatives are absolutely and quadratically integrable over the interior points of the domain. According to the continuity conditions, which apply to all true wave functions, the approximate wave function should have the same value on both sides of a domain boundary, and the first and second derivatives of the approximate wave function (normal to the domain boundary) should have the same value on both sides of the domain boundary. However, let us inquire as to the expectation values of various physical properties in case the approximate wave function, or one of its derivatives, is not continuous across the domain boundaries.

In order to discuss expectation values, it is necessary to define an approximate wave function χ_ϵ which is everywhere continuous and has continuous first and second derivatives, but differs very slightly from the approximate wave function ψ. Clearly, if $\mathcal{O}$ is the operator corresponding to the physical property P, then the expectation value of P resulting from the approximate wave function χ_ϵ is

$$\bar{P}_\epsilon=\int\chi_\epsilon^*\mathcal{O}\chi_\epsilon d\tau\Big/\int\chi_\epsilon^*\chi_\epsilon d\tau. \tag{1}$$

Now, if χ_ϵ everywhere approaches the value of ψ as a parameter ϵ approaches zero, then we shall define the expectation value of P corresponding to the approximate wave function ψ as

$$\lim_{\epsilon\to 0}\bar{P}_\epsilon=\bar{P}. \tag{2}$$

Furthermore, let us express $\bar{P}$ in the form

$$\bar{P}=\left[\sum_i\int_{(i)}\psi_i^*\mathcal{O}\psi_i d\tau+\sum_{i<j}\delta\bar{P}_{ij}\right]\Big/\left[\sum_i\int_{(i)}\psi_i^*\psi_i d\tau\right]. \tag{3}$$

Here the $\delta\bar{P}_{ij}$ are the contributions to the expectation value resulting from the discontinuity of the first

* This research is being reported under contract with the U. S. Atomic Energy Commission.

[1] E. C. Kemble, *Fundamental Principles of Quantum Mechanics* (McGraw-Hill Book Company, Inc., New York, 1937), Sec. 32 gives an excellent discussion of the conditions required for physical acceptability of a wave function.

[2] L. C. Snyder and R. G. Parr, J. Chem. Phys. **34**, 1661 (1961); **28**, 1250 (1958); see also L. C. Snyder, doctoral dissertation, Carnegie Institute of Technology, Pittsburgh, Pennsylvania (1959).

[3] A singular point in the potential energy should coincide with a domain boundary. Except at a singular point in the potential, the higher derivatives of a true wave function never become infinite. Therefore, it is reasonable to impose this strong condition on the integrability of the higher derivatives of an approximate wave function.

derivatives of ψ at the boundary between the ith and jth domains. As we shall presently show, it is essential that ψ itself should be everywhere continuous. Otherwise, the expectation value of the kinetic energy would be infinite. It is the purpose of the present paper to determine the $\delta\bar{P}_{ij}$.

Let us suppose that the configurational space of the problem under consideration is N dimensional and is spanned by the Cartesian coordinates $x_1, x_2, \cdots, x_N$. Then, in accordance with the method of convolutions, we may define

$$\chi_\epsilon(x_1, \cdots, x_N) = \int_{-1}^{1}\cdots\int_{-1}^{1} w(u_1)\cdots w(u_N)\psi(x_1-\epsilon u_1, \cdots, x_N-\epsilon u_N)\, du_1\cdots du_N. \quad (4)$$

Here $w(u)$ may be taken to be any even single-valued analytic function throughout the range $-1\leq u\leq 1$ which is normalized so that

$$\int_{-1}^{1} w(u)\,du=1. \quad (5)$$

Furthermore, the values of $w(u)$ and its first and second derivatives are zero at $u=1$ and -1. For convenience of notation, let

$$\int_{-1}^{1} u^2 w(u)\,du=a. \quad (6)$$

One possible function which would satisfy the above requirements is

$$w(u)=(35/32)\,(1-u^2)^3. \quad (7)$$

However, the functional form given by Eq. (7) is in no sense unique. There are, indeed, an infinite variety of functional forms which might be used. One of the most elegant features of the method of convolutions is that the end results are independent of the functional form of $w(u)$.

First, let us consider the set of expectation values $\bar{P}$ for one-dimensional quantum-mechanical problems. Then, we generalize the results to N dimensions.

I. ONE-DIMENSIONAL QUANTUM-MECHANICAL PROBLEMS

Let us consider a one-dimensional approximate wave function ψ which consists of the function ψ_1 in the coordinate range $-\infty<x<0$ and the function ψ_2 in the range $0<x<\infty$. Within their respective ranges of applicability, the functions ψ_1 and ψ_2 are single-valued and analytic (except at the point infinity), both the functions and all of their derivatives are absolutely and quadratically integrable over their half-space, and the functions fall off at infinity faster than any negative power of x. However, at the point $x=0$, where the two functions join, ψ may be discontinuous or its first derivative may be discontinuous. We ask the question, how does the presence of this discontinuity affect the expectation values for various physical properties.

In accordance with Eq. (4), let

$$\chi_\epsilon(x)=\int_{-1}^{1} w(u)\psi(x-\epsilon u)\,du. \quad (8)$$

Then $\chi_\epsilon(x)$ is everywhere continuous and has continuous first and second derivatives. However, the functional form of $\chi_\epsilon(x)$ depends on which of three zones contains the value of x:

(1) In the left zone, $-\infty<x\leq-\epsilon$

$$\chi_\epsilon^{(i)}(x)=\int_{-1}^{1} w(u)\psi_1^{(i)}(x-\epsilon u)\,du, \qquad i=0, 1, 2\cdots. \quad (9)$$

Throughout this paper the superscript, index or primes, denotes the order of the derivative, with the superscript zero (or no superscript) corresponding to the function itself.

The $\psi_1^{(i)}(x-\epsilon u)$ can be expanded in a Taylor's series about the point x. Then as a result of the assumed properties of $w(u)$, Eq. (9) becomes

$$\chi_\epsilon^{(i)}(x)=\psi_1^{(i)}(x)+(\epsilon^2 a/2)\psi_1^{(i+2)}(x)+\cdots. \quad (10)$$

Clearly, in the limit as ϵ approaches zero, the smoothing of the approximate wave function outside of the discontinuity zone does not affect the expectation values. Thus, in the N-dimensional problems, the smoothing of the wave functions is only carried out in the discontinuity zones.

(2) In the discontinuity zone, $-\epsilon\leq x\leq\epsilon$,

$$\chi_\epsilon(x)=\int_{x/\epsilon}^{1} w(u)\psi_1(x-\epsilon u)\,du+\int_{-1}^{x/\epsilon} w(u)\psi_2(x-\epsilon u)\,du \quad (11)$$

$$\chi_\epsilon'(x)=\int_{x/\epsilon}^{1} w(u)\psi_1'(x-\epsilon u)\,du+\int_{-1}^{x/\epsilon} w(u)\psi_2'(x-\epsilon u)\,du+\epsilon^{-1}w(x/\epsilon)[\psi_2(0)-\psi_1(0)] \quad (12)$$

$$\chi_\epsilon''(x)=\int_{x/\epsilon}^{1} w(u)\psi_1''(x-\epsilon u)\,du+\int_{-1}^{x/\epsilon} w(u)\psi_2''(x-\epsilon u)\,du+\epsilon^{-1}w(x/\epsilon)[\psi_2'(0)-\psi_1'(0)]+\epsilon^{-2}w'(x/\epsilon)[\psi_2(0)-\psi_1(0)]. \quad (13)$$

The $\psi_1(x-\epsilon u)$, $\psi_2(x-\epsilon u)$, and their derivatives can be expanded in Taylor's series about the point 0. These expansions are useful in performing the integrations required to obtain the expectation values.

(3) In the right zone, $\epsilon\leq x<\infty$, the expressions for $\chi_\epsilon(x)$ and its derivatives are the same as for the left zone with the exception that now ψ_2 replaces ψ_1.

It is easy to use Eqs. (10) and (11) and the Taylor's series about the origin to show that the normalization

integral has the form

$$\int_{-\infty}^{\infty}\chi_\epsilon^*(x)\chi_\epsilon(x)dx=\int_{-\infty}^{0}\psi_1^*(x)\psi_1(x)dx+\int_{0}^{\infty}\psi_2^*(x)\psi_2(x)dx+O(\epsilon). \quad (14)$$

Here and throughout this paper, $O(\epsilon)$ denotes terms of the order of ϵ plus terms in higher orders of ϵ. In the limit as ϵ approaches zero, the $O(\epsilon)$ becomes zero.

The kinetic-energy integral is somewhat more difficult to express. Using Eqs. (10), (11), and (13); performing a considerable number of integrations by parts; and making use of the properties of $w(u)$, we obtain

$$\int_{-\infty}^{\infty}\chi_\epsilon^*(x)\chi_\epsilon''(x)dx=\int_{-\infty}^{0}\psi_1^*(x)\psi_1''(x)dx+\int_{0}^{\infty}\psi_2^*(x)\psi_2''(x)dx+\tfrac{1}{2}[\psi_1^*(0)+\psi_2^*(0)][\psi_2'(0)-\psi_1'(0)]-\tfrac{1}{2}[\psi_1'^*(0)+\psi_2'^*(0)][\psi_2(0)-\psi_1(0)]-\epsilon^{-1}[\psi_2^*(0)-\psi_1^*(0)][\psi_2(0)-\psi_1(0)]\int_{-1}^{1}[w(u)]^2du+O(\epsilon). \quad (15)$$

If $\psi_2(0)$ is not equal to $\psi_1(0)$, then, because of the term which is proportional to ϵ^{-1}, the kinetic energy integral becomes infinite as ϵ approaches zero. Since the kinetic energy cannot be infinite for any physically reasonable problem, *we must limit our consideration to approximate wave functions which are everywhere continuous but may have discontinuous first and higher derivatives.* Thus, we require

$$\psi_1(0)=\psi_2(0)=\psi(0). \quad (16)$$

The operator for kinetic energy is

$$\mathfrak{I}=-(\hbar^2/2m)d^2/dx^2, \quad (17)$$

where m is the mass of the particle. As a result of Eq. (15), taking into account Eq. (16), the boundary between domains 1 and 2 contributes to the expectation value for the kinetic energy

$$\delta\bar{T}_{12}=-(\hbar^2/2m)\psi^*(0)[\psi_2'(0)-\psi_1'(0)]. \quad (18)$$

A very important special case corresponds to the wave function which has a discontinuity in its first derivative at a nodal point where $\psi^*(0)=0$, in which case $\delta\bar{T}_{12}=0$.

It is easy to show that for a physical property $Q(x)$,

$$\delta\bar{Q}_{12}=\lim_{\epsilon\to 0}\psi^*(0)\psi(0)\int_{-\epsilon}^{\epsilon}Q(x)dx. \quad (19)$$

Thus, if $Q(x)$ is continuous and nonsingular in the vicinity of $x=0$, then $\delta\bar{Q}_{12}=0$. If $Q(x)=|x|^{-n}$, then $\delta\bar{Q}_{12}=0$ if $n<1$ and infinite if $n\geq 1$. Also, $\delta\bar{Q}_{12}=0$ if $Q(x)=\log(x^2)/2$.

From Eqs. (10), (11), and (12), it is easy to see that if $U(x)$ is continuous and nonsingular in the vicinity of $x=0$, then the expectation values for an operator of the form

$$\mathfrak{g}=U(x)d/dx,$$

will have zero contribution from the boundary between domains 1 and 2, so that $\delta\bar{J}_{12}=0$.

For one-dimensional quantum-mechanical problems in which the approximate wave function has a discontinuous first derivative at more than one point, the resulting contributions to the expectation values are similar to those at the boundary which we have discussed in detail.

II. *N*-DIMENSIONAL QUANTUM-MECHANICAL PROBLEMS

The N-dimensional problems are generalizations of the one-dimensional problem which we have already examined. Let us consider the contribution to the expectation values which results from the surface, $S_{12}(x_1, x_2, \cdots, x_N)=0$, separating domains 1 and 2. In domain 1, the approximate wave function is ψ_1 and in domain 2 it is ψ_2. Along the boundary surface $\psi_1=\psi_2$, as otherwise the expectation value of the kinetic energy would be infinite (as we saw in the one-dimensional case). However, along the boundary surface, the normal derivative of ψ_1 is not necessarily equal to the normal derivative of ψ_2,

$$(\partial\psi_1/\partial n)_{S_{12}}\neq(\partial\psi_2/\partial n)_{S_{12}}. \quad (20)$$

Let us define $\mathbf{n}$ as the unit vector normal to the surface S_{12} pointed from domain 1 towards domain 2. The components of $\mathbf{n}$ (or direction cosines) with respect to the $x_1, x_2, \cdots, x_N$ coordinate axes are $n_1, n_2, \cdots, n_N$, respectively. The n_i are given by

$$n_i=\pm(\partial S_{12}/\partial x_i)/[\sum_{j=1}^{N}(\partial S_{12}/\partial x_j)^2]^{\frac{1}{2}}, \qquad i=1, 2, \cdots, N. \quad (21)$$

The choice of the plus or the minus sign depends upon which set of relations is consistent with the requirement that $\mathbf{n}$ points from domain 1 towards domain 2. Also, to simplify notation, let $\mathbf{x}$ be the vector whose components are $x_1, x_2, \cdots, x_N$, respectively. Points on the surface are designated by $\mathbf{x}_s$.

In the following analysis, we assume that the radius of curvature of S_{12} is everywhere greater than a small parameter ϵ. As in the one-dimensional case, we use the method of convolutions to form from the approximate wave function a smoothed approximate wave function χ_ϵ which is everywhere continuous and has continuous

derivatives. As in the one-dimensional case, the smoothing of the approximate wave function outside of the discontinuity zone does not affect the expectation values. Thus, we may concentrate on those points which lie at a distance t from S_{12}, where $-\epsilon \leq t \leq \epsilon$. Points having negative values of t lie in domain 1 and points having positive values of t lie in domain 2. Clearly,

$$\partial t/\partial x_i = n_i, \qquad i=1, 2, \cdots, N. \tag{22}$$

Also, a point on the surface is given by

$$\mathbf{x}_s = \mathbf{x} - t\mathbf{n}. \tag{23}$$

Within this discontinuity zone, an acceptable form for the smoothed approximate wave function is

$$\chi_\epsilon(\mathbf{x}) = \int_{t/\epsilon}^{1} w(u)\psi_1(\mathbf{x}-\epsilon u\mathbf{n})du + \int_{-1}^{t/\epsilon} w(u)\psi_2(\mathbf{x}-\epsilon u\mathbf{n})du. \tag{24}$$

Taking the derivative of $\chi_\epsilon(\mathbf{x})$, making use of Eq. (22), and assuming that $\psi_1(\mathbf{x}_s) = \psi_2(\mathbf{x}_s)$,

$$\partial\chi_\epsilon/\partial x_i = \int_{t/\epsilon}^{1} w(u)\,(\partial\psi_1/\partial x_i)_{\mathbf{x}-\epsilon u\mathbf{n}}du + \int_{-1}^{t/\epsilon} w(u)\,(\partial\psi_2/\partial x_i)_{\mathbf{x}-\epsilon u\mathbf{n}}du. \tag{25}$$

And taking the derivative of Eq. (25),

$$\partial^2\chi_\epsilon/\partial x_i^2 = \int_{t/\epsilon}^{1} w(u)\,(\partial^2\psi_1/\partial x_i^2)_{\mathbf{x}-\epsilon u\mathbf{n}}du + \int_{-1}^{t/\epsilon} w(u)\,(\partial^2\psi_2/\partial x_i^2)_{\mathbf{x}-\epsilon u\mathbf{n}}du + (n_i/\epsilon)w(t/\epsilon)\left[(\partial\psi_2/\partial x_i)_{\mathbf{x}_s} - (\partial\psi_1/\partial x_i)_{\mathbf{x}_s}\right]. \tag{26}$$

But since the derivatives of ψ_2 and ψ_1 parallel to the surface are equal,

$$(\partial\psi_2/\partial x_i)_{\mathbf{x}_s} - (\partial\psi_1/\partial x_i)_{\mathbf{x}_s} = n_i(\partial/\partial n)(\psi_2-\psi_1). \tag{27}$$

Here the $\partial/\partial n$ is the derivative in the direction of $\mathbf{n}$. If Δ is the generalized Laplacian,

$$\Delta = \sum_{i=1}^{N} \partial^2/\partial x_i^2, \tag{28}$$

then, since

$$\sum_{i=1}^{N} n_i^2 = 1,$$

it follows from Eq. (26) that

$$\Delta\chi_\epsilon = \int_{t/\epsilon}^{1} w(u)\,(\Delta\psi_1)_{\mathbf{x}-\epsilon u\mathbf{n}}du + \int_{-1}^{t/\epsilon} w(u)\,(\Delta\psi_2)_{\mathbf{x}-\epsilon u\mathbf{n}}du + \epsilon^{-1}w(t/\epsilon)\left[(\partial/\partial n)(\psi_2-\psi_1)\right]. \tag{29}$$

The contribution of the discontinuity zone to the normalization integral is

$$\lim_{\epsilon\to 0}\int_{\text{surface}} dS_{12}\int_{-\epsilon}^{\epsilon} dt\,\chi_\epsilon^*(\mathbf{x})\chi_\epsilon(\mathbf{x}) = 0. \tag{30}$$

The kinetic energy operator is

$$\mathfrak{I} = -(\hbar^2/2m)\Delta,$$

provided that the scale of the coordinates is properly adjusted. Thus, the contribution of the discontinuity zone to the expectation value for the kinetic energy is

$$\delta\bar{T}_{12} = \lim_{\epsilon\to 0}\int_{\text{surface}} dS_{12}\int_{-\epsilon}^{\epsilon} dt\,\chi_\epsilon^*(x)\,(-\hbar^2/2m)\Delta\chi_\epsilon(\mathbf{x}) = \int_{\text{surface}} \psi^*\left[(\partial/\partial n)(\psi_2-\psi_1)\right]dS_{12}. \tag{31}$$

Special analysis shows that no additional terms are required to add to the expectation value of the kinetic energy if the boundary surface has sharp corners.

Also, it is easy to show that if ψ is a function of the spherical coordinates r, θ, ϕ, with a finite value at $r=0$ and a finite derivative $\partial\psi/\partial r$ at $r=0$, there is no additional term required to add to the expectation value of the kinetic energy on account of the discontinuity in the Cartesian derivatives of ψ at the origin.

ACKNOWLEDGMENTS

The authors wish to thank Professor E. H. Zarontello (of the Universidad Nacional de Cuyo, San Juan, Argentina and the U.S. Army Mathematics Research Center at the University of Wisconsin) for suggesting the use of the method of convolutions.

APPENDIX

An alternative procedure for calculating $\delta\bar{T}_{12}$ results from expanding $\psi(x)$ in a Fourier series $F(x)$ in the range $=-\epsilon<x<\epsilon$. Then

$$\delta\bar{T}_{12} = -(\hbar^2/2m)\left[\int_{-\epsilon/2}^{\epsilon/2} F''(x)\,F(x)dx - \int_{-\epsilon/2}^{0} \psi_1''(x)\psi_1(x)dx - \int_{0}^{\epsilon/2} \psi_2''(x)\psi_2(x)dx\right]. \tag{A1}$$

For example, suppose that

$$\psi_1(x) = 1+x \qquad -\epsilon<x<0 \tag{A2}$$

$$\psi_2(x) = 1-x \qquad 0<x<\epsilon. \tag{A3}$$

The Fourier expansion of $\psi(x)$ is then

$$F(x)=(1-\tfrac{1}{2}\epsilon)+(4\epsilon/\pi^2)\sum_{m=0}^{\infty}\frac{\cos[(2m+1)\pi x/\epsilon]}{(2m+1)^2}. \quad \text{(A4)}$$

After two termwise differentiations,

$$F''(x)=-(4/\epsilon)\sum_{m=0}^{\infty}\cos[(2m+1)\pi x/\epsilon]. \quad \text{(A5)}$$

Integrating termwise,

$$F''(x)F(x)dx=-2. \quad \text{(A6)}$$

Thus, for this example, Eq. (A1) gives

$$\delta\bar{T}_{12}=\hbar^2/m, \quad \text{(A7)}$$

which agrees with Eq. (18), obtained by the method of convolutions.

THE JOURNAL OF CHEMICAL PHYSICS VOLUME 34, NUMBER 5 MAY, 1961

Application of Ligand Field Theory to the Electronic Spectra of Gaseous $CuCl_2$, $NiCl_2$, and $CoCl_2$

JON T. HOUGEN,* GEORGE E. LEROI,† AND THOMAS C. JAMES‡

Mallinckrodt Chemical Laboratories, Harvard University, Cambridge, Massachusetts

(Received November 7, 1960)

The absorption spectra of $CuCl_2$, $NiCl_2$, and $CoCl_2$ in the gas phase at 1000°C have been obtained under low resolution in the visible, near-infrared, and near-ultraviolet regions. The observed absorptions have extinction coefficients of the order of 100 liter/mole·cm, suggesting that they correspond to "forbidden" intraconfigurational $d^n \leftarrow d^n$ transitions analogous to those found in solutions and crystals containing these metal ions. The observed spectra are rather well described by the two ligand field parameters appropriate to a molecule of symmetry $D_{\infty h}$.

INTRODUCTION

THE success of ligand field theory in describing the positions of the low-lying energy levels for a great number of compounds and complexes of the rare earth and transition metal elements is well known.[1,2] This theory is concerned with calculating the energies of the states arising from metal ion configurations of the form [closed shells] f^n and [closed shells] d^n, when these configurations are perturbed by the electrostatic ("stark") field of the surrounding anions. The principal contribution to the nonzero intensities of transitions among these ligand field energy levels for molecules with a center of symmetry arises from the coupling of vibrational motions with electronic motions, i.e., from vibronic interactions. Our understanding of such vibronic interactions is not yet complete, a fact attributable in part to the lack of experimental knowledge concerning the vibrational structure of ligand field transitions. Ligand field transitions of complexes in solution are broadened to an extent which makes the resolution of overlapping vibrational bands difficult. On the other hand, in solids, where rather sharp absorption and fluorescence lines are observed, the analysis of the spectrum is complicated by the necessity of treating the coupling of the lattice modes with the electronic motions of the metal ion. These remarks indicate the desirability of studying gaseous systems, where one can hope eventually to observe the detailed vibrational structure, and where the complications which arise in solid spectra are largely eliminated. Recently, several gaseous metal hexafluorides have been studied.[3–6] These compounds, however, possess 15 vibrational degrees of freedom, which makes a vibronic analysis of the spectrum difficult.

The present authors have turned their attention to the first-row transition metal dihalides in the hope that these simpler systems might eventually lend themselves to a complete vibronic analysis. The isolated gaseous molecules, possessing only four vibrational degrees of freedom, appear to be ideal d electron systems for a study of the coupling of electronic and vibrational motions. In this work we have assigned the observed absorptions of the dichlorides of copper, nickel, and cobalt to electronic transitions between levels of the $3d^9$, $3d^8$, and $3d^7$ metal ion configurations as perturbed by an axial ligand field. Assignments were made using

* Present address: Division of Pure Physics, National Research Council, Ottawa, Canada.

† Present address: Department of Chemistry, University of California, Berkeley, California.

‡ Present address: Department of Chemistry, Northwestern University, Evanston, Illinois.

[1] W. Moffitt and C. J. Ballhausen, Ann. Rev. Phys. Chem. **7**, 107 (1956).

[2] D. S. McClure, Solid State Phys. **9**, 399 (1959).

[3] W. Moffitt, G. L. Goodman, M. Fred, and B. Weinstock, Mol. Phys. **2**, 109 (1959).

[4] G. L. Goodman, Ph.D. dissertation, Harvard University, Cambridge, Massachusetts, 1959.

[5] G. L. Goodman and M. Fred, J. Chem. Phys. **30**, 849 (1959).

[6] J. C. Eisenstein and M. H. L. Pryce, Proc. Roy. Soc. (London) **A255**, 181 (1960).

low-resolution spectra. The vibrational structure brought out by higher resolution is purposely ignored in this report.

EXPERIMENTAL

The low-resolution absorption spectra of gaseous $CuCl_2$, $NiCl_2$, and $CoCl_2$ were obtained between 3500 cm^{-1} and 38 000 cm^{-1} with a modified Perkin-Elmer model 98 monochromator using either a quartz or a sodium chloride prism. The samples, which had been prepared as described below, were heated to the desired temperatures in a Kanthal-wound resistance furnace which was placed in the optical path of the monochromator. Different light sources were employed for each region of the spectrum: a high-pressure xenon arc for the ultraviolet, a tungsten ribbon filament lamp for the visible, and a Nernst glower for the infrared. Absorption in the region 14 000 cm^{-1} to 40 000 cm^{-1} was also photographed using a Bausch & Lomb medium

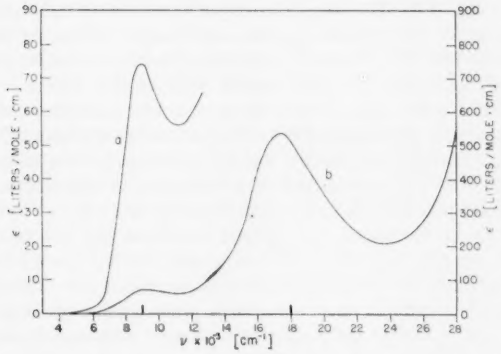

FIG. 1. The absorption spectrum of $CuCl_2(g)$. (a) left-hand scale; (b) right-hand scale.

dispersion quartz prism spectrograph. Optical densities, i.e., $\log I_0/I$, were computed point by point from a background spectrum (I_0) and from a spectrum of the sample cell (I), both taken on the single beam Perkin-Elmer instrument. The extinction coefficients determined from these optical densities, which are shown in Figs. 1–3, have been corrected for the absorption and scattering of the cell windows. The uncertainty associated with the cell window corrections and the uncertainty in the moisture content of the samples during weighing suggest that our absolute extinction coefficients may be in error by as much as a factor of two. Nevertheless, the coarse features of the spectrum are easily discernible.

Reagent-grade anhydrous cupric chloride (Fisher) was dried by heating in the presence of chlorine. Weighed samples of $CuCl_2$ were placed in Vycor cylinders 20 cm long and 4.5 cm in diam, to which quartz windows were fused. The sample was again heated under Cl_2, the cells evacuated, and several mm of chlorine gas readmitted before the cell was sealed off.

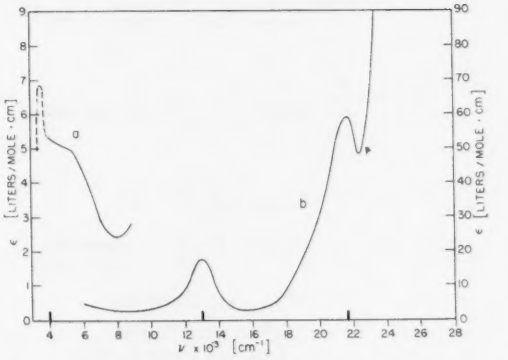

FIG. 2. The absorption spectrum of $NiCl_2(g)$. (a) left-hand scale; (b) right-hand scale.

Sufficient chlorine[7–9] was added to each sample cell to suppress decomposition of the $CuCl_2$ according to the equation

$$CuCl_2 \rightleftharpoons CuCl + \tfrac{1}{2}Cl_2 \qquad (1)$$

at the temperatures used to vaporize the sample. The spectrum of $CuCl_2$ is presented in Fig. 1. Anhydrous $NiCl_2$ and $CoCl_2$ were prepared by heating $NiCl_2 \cdot 6H_2O$ (Mallinckrodt) and $CoCl_2 \cdot 6H_2O$ (Baker) in a stream of hydrogen chloride gas. Weighed samples were placed in the Vycor cells described above, the samples reheated in the presence of HCl, and the cells evacuated and sealed off while the sample was still hot.

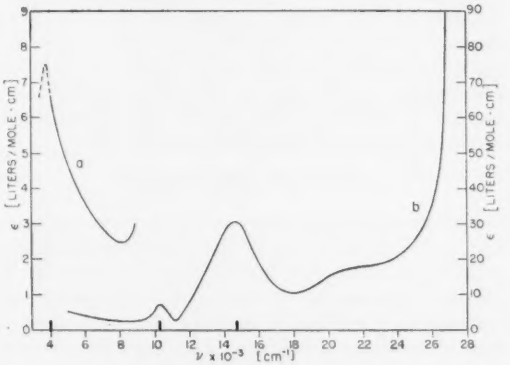

FIG. 3. The absorption spectrum of $CoCl_2(g)$. (a) left-hand scale; (b) right-hand scale.

[7] L. Brewer, in *The Chemistry and Metallurgy of Miscellaneous Materials: Thermodynamics*, edited by L. L. Quill (McGraw-Hill Book Company, Inc., New York, 1950), p. 235.

[8] The spectrum through a cell containing 3 mg of $CuCl_2$, but no Cl_2, showed bands in the region of 23 000 cm^{-1} which were not present in the spectra of sample cells containing Cl_2. Since CuCl is known to have band systems throughout the visible (see footnote 9), the authors took the presence or absence of these new bands as an empirical indication of the presence or absence of CuCl.

[9] G. Herzberg, *Molecular Spectra and Molecular Structure* I: *Spectra of Diatomic Molecules* (D. Van Nostrand Company, Inc., Princeton, New Jersey, 1950), 2nd ed., p. 525.

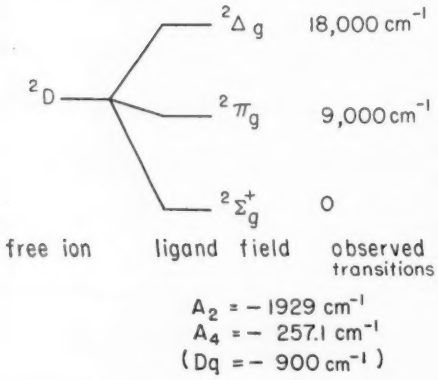

FIG. 4. Energy levels of $CuCl_2$ ($3d^9$).

The spectra of $NiCl_2$ and $CoCl_2$ are presented in Figs. 2 and 3. Vaporization of all three materials took place at temperatures between 700 and 1100°C.

Photographs of the charge transfer spectra in the ultraviolet have been obtained. $CuCl_2$ and $NiCl_2$ absorb strongly from 2800 to 3600 A; $CoCl_2$ absorbs strongly between 2600 and 3200 A. These results agree with earlier photographic observations[10] on $NiCl_2$ and $CoCl_2$.

The spectra were recorded at temperatures above that at which all of the sample present was vaporized. Under these conditions, where the vapor is not in equilibrium with the solid phase, one may infer from the results of Porter and co-workers,[11] who studied the composition of these vapors using mass spectrometric techniques, that for the temperature range employed in our experiments, any observed absorption may safely be ascribed to monomeric molecules. This was also justified empirically by the observation that the spectra of sufficiently hot samples were insensitive to further temperature increases exceeding 150°C.

SPECTRAL ASSIGNMENTS

The molecular symmetry of the gaseous molecules $CuCl_2$, $NiCl_2$, and $CoCl_2$ has not been experimentally established, but their similarity to the group II dihalides suggests that it is $D_{\infty h}$.[12] Furthermore, estimates of the contributions to the bending force constant from interactions of the unfilled d shell with the ligand field suggest that these are insufficient to lead to a bent molecule in either the ground or excited states. Therefore the molecules studied in this work will be considered to be linear symmetric triatomic molecules.

The ligand field theory formalism for molecules of symmetry $D_{\infty h}$ has been utilized elsewhere.[13,14] Nevertheless its development will be sketched here again. We shall first carry through a simple *crystal field* treatment, i.e., a treatment in which only $3d$ electronic wave functions are considered. The generalization to a molecular orbital, *ligand field* treatment is presented in the discussion section. Let the origin of a coordinate system lie at the metal ion M, and let one M—Cl bond define the direction of the polar axis. Let θ be the polar angle and ϕ be the azimuthal angle. Then the Hamiltonian for n d electrons in the field of the M^{+n+2} ion and the two negative ligands can be written[15]

$$H = H_{\text{free ion}} + H_{\text{crystal field}} \tag{2}$$

$$= \sum_{i=1}^{n} [T_i + V(r_i)] + \sum_{i>j=1}^{n} e^2/r_{ij}$$

$$+ 2\sum_{i=1}^{n} [\bar{A}_0(r_i)\, Y_{00} + \bar{A}_2(r_i)\, Y_{20}(\theta_i) + \bar{A}_4(r_i)\, Y_{40}(\theta_i)], \tag{3}$$

where T_i is the kinetic energy, $V(r_i)$ the free-ion potential energy, and $\mathbf{r}_i$ the coordinates of the "i"th electron. The first sum represents the interaction of the n electrons with the central field of the metal ion M^{+n+2}; the second sum represents the interelectronic coulomb repulsions. These two terms together comprise the Hamiltonian for the n d electrons in the free metal ion M^{+2}. The potential of an electron in the electrostatic field of the two symmetrically placed Cl^- ions can be expanded as a power series in the spherical harmonics $Y_{lm}(\theta, \phi)$, with expansion coefficients which are functions of r. The third sum represents this crystal field potential. For molecules with symmetry $D_{\infty h}$, only spherical harmonics of even l, with $m=0$ can occur in the expansion. Because matrix elements between d electron wave functions vanish for spherical harmonics with $l \geq 5$, the expansion has been truncated at $l=4$.

One Electron Formalism. $3d^1$ and $3d^9$

A free ion containing one $3d$ electron outside of closed shells has one fivefold orbitally degenerate Russell-Saunders term: ^2D. The axial crystal field partially removes this fivefold degeneracy and splits the ^2D term into states characterized by the irreducible representations of the point group $D_{\infty h}$. The $3d$ orbital wave functions, labeled by the irreducible representation of $D_{\infty h}$ to which they belong, are

$$\sigma_g^+ = r^{-1} R_{3d}(r)\, Y_{20}(\theta)$$

$$\pi_g = r^{-1} R_{3d}(r)\, Y_{2\pm1}(\theta, \phi)$$

$$\delta_g = r^{-1} R_{3d}(r)\, Y_{2\pm2}(\theta, \phi). \tag{4}$$

[10] E. Miescher, Helv. Phys. Acta **11**, 463 (1938).
[11] R. C. Schoonmaker, A. H. Friedman, and R. F. Porter, J. Chem. Phys. **31**, 1586 (1959) and references cited therein.
[12] P. A. Akishin and V. P. Spiridonov, Kristallographiya **2**, 475 (1957); Chem. Abstracts **51**, 17297i (1957).
[13] R. E. Robertson and H. M. McConnell, J. Phys. Chem. **64**, 70 (1960).
[14] R. A. Berg and O. Sinanoglu, J. Chem. Phys. **32**, 1082 (1960).

[15] In this Hamiltonian spin orbit coupling has been neglected (as well as all interactions involving still smaller amounts of energy). The effects of spin orbit interaction are not apparent in the broad absorption bands observed under low resolution in this work. See discussion section.

The complete Hamiltonian (3) is diagonal in this representation and yields energy levels given (except for a constant factor) by

$$E_\sigma = 4A_2 + 12A_4$$
$$E_\pi = 2A_2 - 8A_4$$
$$E_\delta = -4A_2 + 2A_4, \qquad (5)$$

where,

$$A_2 = [(5/4\pi)^{\frac{1}{2}}/7]\int_0^\infty \bar{A}_2(r)\, R_{3d}^2(r)\, dr$$

and

$$A_4 = [(9/4\pi)^{\frac{1}{2}}/21]\int_0^\infty \bar{A}_4(r)\, R_{3d}^2(r)\, dr \qquad (6)$$

are the two crystal field parameters needed to describe the splitting.

The sign and relative importance of these two parameters can be estimated from a point charge model. We find that for a $3d^1$ configuration A_2 and A_4 are positive, corresponding to a repulsive potential between the chloride ions and the electron. For a $3d^9$ configuration treated by the hole formalism, A_2 and A_4 are negative, corresponding to an attractive potential between the chloride ions and the hole. In addition, if we set $R_{3d}(r) = \delta(r, r_0)$ and place the two point charges at $\pm a$ on the polar axis, then the ratio A_2/A_4 is given by $3a^2/r_0^2$. Taking the ratio of the effective radius of the $3d$ shell r_0 to the M—Cl distance a to be $\frac{1}{2}$, we conclude that $|A_2|$ is perhaps an order of magnitude larger than $|A_4|$.

The spectrum of $CuCl_2$ exhibits two transitions located at 9000 and 18 000 cm^{-1}, as shown by the markers on Fig. 1. There are six possible ways of assigning the three labels $^2\Sigma_g^+$, $^2\Pi_g$, and $^2\Delta_g$ to three energy levels, but only one of these yields negative A_2 and A_4 with $A_2/A_4 > 1$. The spectrum of $CuCl_2$ can thus be uniquely assigned, leading to the empirically determined parameters

$$A_2 = -1929 \text{ cm}^{-1}$$
$$A_4 = -257.1 \text{ cm}^{-1} \qquad (7)$$

and to the energy level diagram presented in Fig. 4.

Many-Electron Formalism

If there is more than one $3d$ electron or more than one $3d$ hole, then the electronic spins can couple to give Russell-Saunders terms of different multiplicity. Since the Hamiltonian given in Eq. (3) does not contain spin dependent terms and cannot mix terms of different multiplicity, we observe that its energy matrix in a Russell-Saunders basis immediately factors into blocks characterized by the total spin angular momentum S. To the extent that S is a good quantum number, only transitions to states with the same multiplicity as the ground state will be observed in the absorption spectrum. Because the complexes of chloride ions with the first-row transition metal ions fall into the "weak field" case, the ground states of $NiCl_2$ and $CoCl_2$ would be expected to have the same multiplicity as the ground states of the free Ni^{++} ion (two d holes; $S=1$) and the free Co^{++} ion (three d holes; $S=\frac{3}{2}$), respectively.

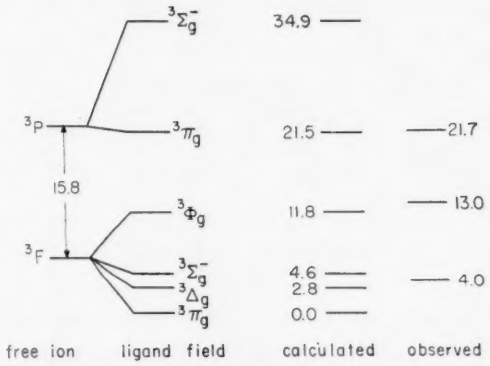

FIG. 5. Energy levels of $NiCl_2$ ($3d^8$) in thousands of cm^{-1}. (For value of 15.8, see C. E. Moore, Natl. Bur. Standards Circ. No. **467**, Vol. II.)

In addition to a coupling of the spins, the several $3d$ electrons or $3d$ holes will experience a mutual coulombic repulsion within the molecule. Because of this two additional parameters F_2 and F_4 are necessary to specify the energy level diagram for systems containing more than one d electron outside of closed shells.[16] However, for compounds and complexes of ligands such as the chloride ion, which lie towards the "ionic" or "weak field" portion of the spectrochemical series, electronic repulsion energies within the molecule can be approximated by the free ion electronic repulsion energies. These latter are responsible for the observed Russell-Saunders term separations in the free ion spectrum. The Russell-Saunders terms for the $3d^8$ configuration of the Ni^{++} ion are: ^1S, D, G and ^3P, F. Those for the $3d^7$ configuration of the Co^{++} ion are: ^2P, D, D, F, G, H, and ^4P, F.

The triplet energy levels of $NiCl_2$ and the quartet energy levels of $CoCl_2$ were calculated by noting that in the Russell-Saunders basis, the free ion portion of the Hamiltonian is diagonal and possesses matrix elements equal to the free ion energy levels.[17] The effect of the crystal field portion of the Hamiltonian in splitting these free ion energy levels into states characterized by the projection of the electronic angular momentum along the internuclear axis and in mixing states of the same symmetry arising from the two different free ion terms was completely specified by using for the parameters A_2 and A_4, *the values determined from the assignment of the $CuCl_2$ spectrum.* The

[16] E. U. Condon and G. H. Shortley, *The Theory of Atomic Spectra* (Cambridge University Press, Cambridge, England, 1935), Chap. 7.

[17] C. Moore, Natl. Bur. Standards (U. S.) Circ. No. **467**, Vol. II (1952).

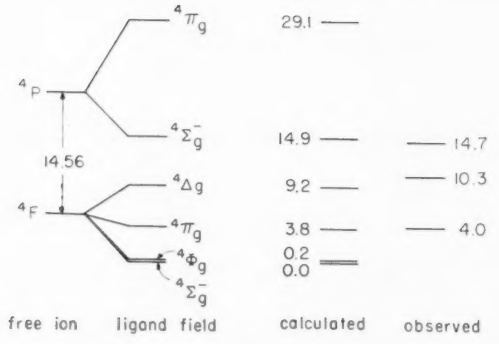

FIG. 6. Energy levels of $CoCl_2$ ($3d^7$) in thousands of cm^{-1}. (For value of 14.56, see C. E. Moore, Natl. Bur. Standards Circ. No. **467**, Vol. II.)

observed transitions indicated by the markers on Figs. 2 and 3 are compared in Figs. 5 and 6 with the energy levels calculated in this manner. The very low-lying infrared transitions could not be observed because the quartz windows were opaque below 3500 cm^{-1}; the very high-lying transitions could not be seen because they were buried in the strong charge transfer spectrum lying in the near ultraviolet.

To substantiate the correctness of the choice of a triplet ground state for $NiCl_2$, the lowest singlet state of $NiCl_2$ was calculated. This state would approximate the $^1\Sigma_g^+$ state $(\sigma_g^+)^2$. The observed[18] singlet terms of the $3d^8$ configuration of the Ni^{++} ion are the ^1D at 13 036 cm^{-1} and the ^1G at 22 115 cm^{-1} above the center of gravity of the ^3F ground state. The unobserved ^1S term was placed at 28 200 cm^{-1} by analogy to the term values in the $3d^2$ isoelectronic series.[16] These energies together with the crystal field parameters determined from the $CuCl_2$ assignment place the lowest singlet state some 4700 cm^{-1} above the $^3\Pi_g$ ground state of $NiCl_2$. A semi-quantitative argument against a doublet ground state for $CoCl_2$ can be presented as follows: The lowest doublet term[19] in the free Co^{++} ion spectrum, the ^2G term, lies 16 510 cm^{-1} above the center of gravity of the ^4F ground state. If the state of this ^2G term with $M_L=1$ were the pure $(\sigma_g^+)^2(\pi_g)^1$ state, the state with the lowest possible crystal field energy, then it would be depressed by the crystal field approximately 22 200 cm^{-1} to a position some 5700 cm^{-1} below the free ion ^4F level. Since the lowest quartet state of the $CoCl_2$ molecule, a $^4\Sigma_g^-$ state, has been depressed only 5560 cm^{-1} below the free ion ^4F term value, this $^2\Pi_g$ state would appear to be the ground state of the molecule. However, the $^2G{:}M_L=1$ state contains only 4.3% of the $(\sigma_g^+)^2(\pi_g)^1$ state. Since the next two lowest doublet terms lie 3100 and 5700 cm^{-1} above the $^2G{:}M_L=1$ state, the energy of the lowest $^2\Pi_g$ state will be significantly higher than the figure given above, probably some thousands of wave numbers above the lowest $^4\Sigma_g^-$ state.

[18] A. G. Shenstone, J. Opt. Soc. Am. **44**, 749 (1954).
[19] A. G. Shenstone, Can. J. Phys. **38**, 677 (1960).

DISCUSSION

The arguments presented in the previous section can be given in a more general fashion. The orbital wave functions of a $3d^1$ configuration transform according to the irreducible representations σ_g^+, π_g, and δ_g of the point group $D_{\infty h}$. However, in a molecule of symmetry $D_{\infty h}$ with the metal ion at the center of symmetry the actual lowest lying orbitals of the above symmetry will not be derived strictly from free metal ion $3d$ orbitals, but will contain admixtures of many other orbitals having the same transformation properties. It is here that the distinction between ligand field theory and crystal field theory is drawn. In crystal field theory one considers molecular orbitals derived solely from metal ion $3d$ orbitals, which are of the form given in (4). These five *crystal field* orbitals, taken by themselves, span a representation of the full rotational group. In ligand field theory the σ_g^+, π_g, and δ_g orbitals each acquire different admixtures of other orbitals of their own symmetry. Consequently, the five *ligand field* orbitals no longer span a representation of the full rotation group. The σ_g^+, π_g, and δ_g orbitals no longer have the same radial charge distribution, for example. Nevertheless, there will still be only two ligand field parameters: $E_1=E_\delta-E_\pi$ and $E_2=E_\pi-E_\sigma$ describing the separations of the three orbitals in the one electron case. We shall consider E_1 and E_2 to be the fundamental ligand field parameters. These are determined empirically from the $CuCl_2$ spectrum to be: $E_1=E_2=9000$ cm^{-1}. A_2 and A_4 may simply be considered as secondary parameters defined by forming appropriate differences among Eqs. (5).

The treatment of the coupling of electronic spins in the many electron case is not changed in passing from crystal field to ligand field theory. The treatment of Coulombic repulsions is drastically altered. Since the orbitals no longer all have a $3d$ radial dependence in ligand field theory, the Coulombic repulsion can no longer be described by only two parameters. To avoid a large increase in the number of parameters, we again express the hope that the Coulombic repulsions in these "ionic" molecules will be well approximated by those in the free metal ion. The effect of the ligand field portion of the Hamiltonian can now be specified completely by using the E_1 and E_2 determined empirically from the $CuCl_2$ spectrum, since all matrix elements among the states under consideration can be expressed as linear combinations of the molecular orbital energy differences $E_\delta-E_\pi$, $E_\pi-E_\sigma$, and the free ion Russell-Saunders splittings. These conceptual changes do not alter the results of the calculations. They simply show that a great deal of covalent bonding can be absorbed in the empirical ligand field parameters E_1 and E_2 (or A_2 and A_4).

The parameters A_2 and A_4 were determined in the

previous section by assigning the observed absorptions to transitions in a linear molecule. Two plausible assignments of the absorptions to transitions in a bent molecule are illustrated in Fig. 7. In this diagram the parameters A_2 and A_4 determined from the spectral assignment for a linear molecule of $CuCl_2$ were used to calculate the energies for a molecule in which the Cl–Cu–Cl angle ranges from 180° to 90°. It is apparent that if the transitions indicated by arrows, corresponding to Cl–Cu–Cl angles of 136° and 90°, respectively, were assigned to the observed absorptions, A_2 and A_4 would be increased or decreased by some factor without changing their ratio. Clearly, if the ratio of A_2 to A_4 is also varied, many sets of values for the angle and ligand field parameters will provide a description of the observed spectrum of $CuCl_2$. Some of these sets of values would undoubtedly also give reasonably good descriptions of the $NiCl_2$ and $CoCl_2$ spectra. Thus, this work cannot be construed as evidence of the linearity of these three molecules, although certainly a linear model satisfactorily fits the observed energies.

The neglect of spin orbit coupling introduces qualitatively different errors in the one electron and in the many electron cases. The ligand field transitions of $CuCl_2$ can only occur between levels of spin $\frac{1}{2}$, since there is only one hole. Hence, the only first-order consequence of introducing spin orbit coupling is to split the $^2\Pi$ and the $^2\Delta$ states and to mix the $^2\Pi_{1/2}$ with the $^2\Sigma_{1/2}$ and the $^2\Pi_{3/2}$ with the $^2\Delta_{3/2}$. For the free Cu^{++} ion the spin orbit coupling constant ζ_{3d} is[20] about 830 cm^{-1}. Since the separations of the $^2\Sigma_g^+$, $^2\Pi_g$, and $^2\Delta_g$ states are 10 times this large, the component of electronic orbital angular momentum along the internuclear axis is a rather good quantum number. Because the spin orbit coupling constant is often lower in complexes than in the free ion, an upper bound for the splitting can be set;

$$^2\Pi_{1/2}-{}^2\Pi_{3/2}\leq 830\ cm^{-1}$$
$$^2\Delta_{3/2}-{}^2\Delta_{5/2}\leq 1660\ cm^{-1}. \quad (8)$$

Such splittings are comparable with the observed low-resolution half-widths, and their neglect does not affect the spectral assignments.

The spin orbit interaction in $NiCl_2$ and $CoCl_2$ can, in addition to splitting the spin multiplets, destroy the good quantum number S by mixing states of different multiplicity. The free ion one electron spin orbit constant for Ni^{++} is 644 cm^{-1} and will therefore be rather ineffective in mixing singlet character into the $NiCl_2$ triplet ground state because the lowest singlet state lies 4700 cm^{-1} above the ground state. The one electron spin orbit constant for Co^{++} is 528 cm^{-1}, which might also be expected to be ineffective in mixing doublet character into the quartet ground state. Transitions from the high multiplicity ground state to many of the lower multiplicity states lie in the visible and near infrared. These transitions, however, are spin forbidden, and would be very weak unless the separation between levels of different multiplicity were comparable to the spin orbit coupling constant. In that case, the two levels would be intermixed and transitions from the ground state would occur to both. Under low resolution, however, the spectrum would still appear to have only a single broad absorption in this region, which would be assigned solely to the transition within the system of higher multiplicity. For these reasons only levels of the ground state multiplicity have been considered in the spectral assignments.

[20] The three one electron spin orbit coupling constants ζ_{3d} have been taken from the convenient Table VIII of footnote 2. They can, of course, also be obtained from the term values given in footnote 17.

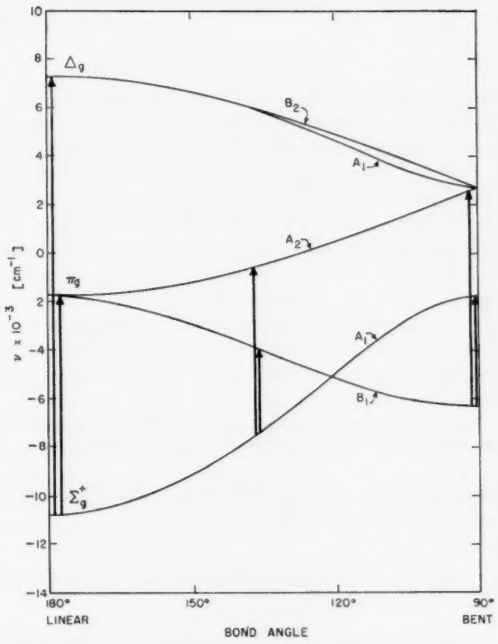

FIG. 7. The ligand field splittings for $CuCl_2$ as a function of bond angle.

The possibility of assigning the $CuCl_2$ spectrum in any of six different ways has been mentioned in the preceding section. One of these six assignments was chosen as the correct one because it led to A_2 and A_4 parameters with the sign and approximate ratio predicted by the point charge model. We shall now qualitatively examine the relative energies of metal ion $3d$ orbitals in MX_2 molecules, to determine if other plausible assignments can be made. The electron density at any point in space of a system containing one electron in a $3d$ orbital is given by

$$|r^{-1}R_{3d}(r)\Theta_{2m}(\theta)\Phi_m(\phi)\,|^2. \quad (9)$$

Only the directional properties of these orbitals as a function of θ are of interest here, and these are il-

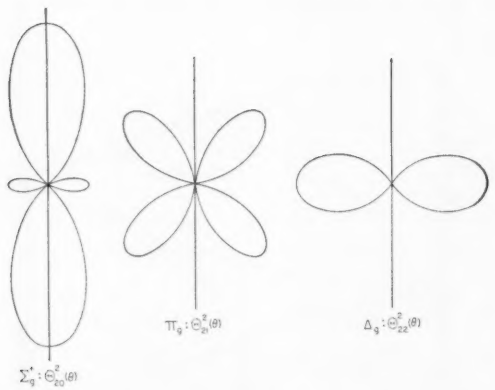

FIG. 8. Variation with polar angle θ of the electron density of the orbitals arising from metal ion $3d^1$ wave functions.

lustrated by a plot against θ of the function (9) averaged over r and ϕ. Thus in Fig. 8

$$\Theta_{2m}^2(\theta)=\int_{r=0}^{\infty}\int_{\phi=0}^{2\pi}R_{3d}^2(r)\Theta_{2m}^2(\theta)\,|\Phi_m(\phi)\,|^2drd\phi \qquad (10)$$

is plotted against θ. Here the vertical axis is the axis of the molecule and the orbitals can be qualitatively visualized as volumes of revolution about this axis. Clearly the σ_g^+ orbital brings the electron closest to the chloride ions, the π_g orbital brings it less close, while the δ_g orbital allows the electron to remain farthest from the negative ligands. These qualitative considerations lead to the order of levels already chosen.

In addition, it can be rigorously shown for any non-vanishing distribution of negative charge along an axis through the central metal ion, that the energy for electrons of the metal ion $3d\sigma$ orbital is greater than that of the $3d\pi$ orbital, which is greater than that of the $3d\delta$ orbital, i.e.,

$$\int V(\mathbf{r})\,|\sigma_g^+(\mathbf{r})\,|^2d\tau>\int V(\mathbf{r})\,|\pi_g(\mathbf{r})\,|^2d\tau$$

$$>\int V(\mathbf{r})\,|\delta_g(\mathbf{r})\,|^2d\tau, \quad (11)$$

where $V(\mathbf{r})$ is the potential due to the negative charge along the axis. As long as there is a σ bond between the M and X atoms in MX_2, or any other bond in which most of the displaced charge density lies on or near the internuclear axis of the bonded atoms, then the order of the orbitals will be that given above. If, on the other hand, the displaced charge is distributed along a ring whose axis is coincident with the internuclear axis, then by varying the radius of the ring and its distance from the metal ion, either the π_g or the δ_g orbital can be raised in energy to a point above the σ_g^+ orbital (see footnote 13). Since such a ring-like charge distribution in the copper-chlorine bond is unlikely, the authors feel quite confident that the assignment of the $CuCl_2$ spectrum is the correct one. This assignment, of course, depends upon the energy for holes rather than for electrons of the $3d\sigma$, $3d\pi$, and $3d\delta$ orgitals. For this case, the inequalities given in (11) must be reversed.

The assignments of $NiCl_2$ and $CoCl_2$ are less certain. For these compounds there are five possible transitions, of which but three have been seen. Since the only test for the correctness of an assignment is an examination of the agreement of observed and calculated energies, there are several plausible ways of assigning these spectra. The fact that the parameters determined from the $CuCl_2$ spectrum do describe the other two spectra simply *suggests* that the assignment given is the correct one.

It is possible by means of crystal field formalism to make a naive comparison between dihalide molecules MX_2 and the hexahalo complex ions MX_6^{-4}. For this comparison we assume that the crystal field potential due to each individual chloride ion in both systems is the same, and that, if the Cu—Cl bond in question is taken as the polar axis, the potential can be expanded in the power series

$$V(\mathbf{r})=\bar{A}_0Y_{00}+\bar{A}_1Y_{10}+\bar{A}_2Y_{20}+\bar{A}_3Y_{30}+\bar{A}_4Y_{40}+\cdots, \qquad (12)$$

where the A_i are functions of r and the Y_{l0} are functions of θ. The present work has determined the average over the radial wave functions of $\bar{A}_2(r)$ and $\bar{A}_4(r)$; the parameters A_2 and A_4 are constants times these averages. Studies on octahedral complexes, because of the higher symmetry involved, determine the average over the radial wave functions only of $\bar{A}_4(r)$; Dq is a constant times this average. Since the expansion (12) is the same for each chloride ion, Dq and A_4 obey the relation

$$Dq=(\tfrac{7}{2})A_4. \qquad (13)$$

The value of A_4 determined in this work leads to a Dq of -900 cm^{-1} for the three hexachloro complexes: MCl_6^{-4}. The observed[2] Dq for the complex $CuCl_6^{-4}$, for example, is -650 cm^{-1}. In any case, the A_4 parameter determined in this work is not unreasonably different from that expected on the basis of octahedral complex studies.

All of the absorptions described above are forbidden for a molecule fixed in a linear, symmetrical configuration, since they violate the Laporte rule for electric dipole radiation, $g\leftrightarrow g$. In addition, many of them violate the selection rule on electronic orbital angular momentum $\Delta\Lambda=\pm1, 0$. The absorptions occur for the most part because these electronic selection rules are relaxed through vibronic interactions. The metal dichlorides have four vibrations; a symmetric stretch, an antisymmetric stretch, and a doubly degenerate bend. Stretching the molecule symmetrically does not

lower the symmetry of the molecule; this vibration cannot couple with the electronic motions to make any of the observed transitions allowed. Stretching the molecule antisymmetrically destroys the center of symmetry, but does not destroy the good quantum number Λ; this vibration can interact with the electronic motions to make allowed any transitions $g \leftrightarrow g$, which violate the Laporte rule, providing the selection rule $\Delta\Lambda = \pm 1, 0$ is still obeyed. Bending the molecule destroys the center of symmetry and the good quantum number Λ; this vibration can interact with the electronic motions to make any of the observed transitions allowed. It is not clear, however, in precisely what manner the antisymmetric stretch and the bend are cooperating to give these transitions finite intensities.

Several points not mentioned in the preceding text mar the impression of the apparently good agreement between the observed and calculated spectra. Because the intensities of some transitions are considerably less than those of others in the same spectrum, there is danger that portions of the vibrational and multiplet structure of given transitions may be mistaken for separate electronic band systems and vice versa. Second, since the absorptions are extremely wide, their centers, which were the experimentally determined quantities, may differ from the band system origins, which were to be the calculated quantities, by several thousand wave numbers. And finally, while the A_2 and A_4 parameters might be expected to change monotonically across the periodic table, one does not expect the dichlorides of three adjacent metals to have identical crystal field parameters. It is important to note that these criticisms are *within* the framework of the simple ligand field model.

CONCLUSIONS

The triatomic molecules $CuCl_2$, $NiCl_2$, and $CoCl_2$ can be considered to be d electron systems, i.e., to contain $3d$ electrons, more or less localized on the central metal ion. The ligand field formalism appropriate to such d electron systems describes the observed spectra rather well by means of a single set of two ligand field parameters. Alternatively, a set of crystal field parameters can be calculated, one of which can be converted to a Dq of -900 cm^{-1}, which is in agreement with observations on octahedral complexes. The ratio of the two crystal field parameters is consistent with a simple point charge model. These molecules, or the corresponding fluorides, may well be favorable cases in which to attempt a detailed vibronic spectral analysis. Such a detailed investigation will presumably not alter the general interpretation presented here, nor significantly change the parameters, but it will unambiguously determine the labels of the states between which the observed transitions take place, and should provide some insight into the vibronic couplings involved.

ACKNOWLEDGMENTS

The authors wish to thank Professor William Klemperer and Dr. Gordon Goodman for many helpful discussions, and to thank Professor Klemperer for the use of his laboratory. The financial support of the National Science Foundation is gratefully acknowledged.

Polarity of the C—H Bonds in Acetylene and Its Molecular Quadrupole Moment

H. HAMANO

Chemical Laboratory, Tokyo Gakugei University, Tokyo, Japan

(Received May 2, 1960)

By using the molecular quadrupole moment data of acetylene, the polarity and the dipole moment of the CH bonds have been investigated. The semiempirical LCBO MO method was applied to this problem. The results obtained show that the CH bonds in this molecule are almost homopolar, but hydrogen is slightly positive in polarity. From this, the so-called bond moment and the infrared bond moment have been discussed. The sign of the molecular quadrupole moment of acetylene which cannot be given by the experimental data was determined as positive in the present work.

INTRODUCTION

THE polarity of CH bonds is of great interest together with their dipole moments. In fact, the CH bond moment is most fundamental to any account of the moments of organic molecules. This problem has hitherto been discussed by many authors.[1-4] In theoretical investigation, however, these quantities depend greatly upon the molecular wave function and our knowledge of wave functions is very little in the present problem. Accordingly, satisfactory theoretical calculations are very few.

An electronic charge distribution in a molecule has frequently been estimated empirically from the experimental dipole moment. Unfortunately the dipole moments have not been observed for most hydrocarbons because of their symmetry. Therefore, the CH bond polarity may be estimated only from the other experimental data, for example, the infrared intensity of vibration, the molecular quadrupole moment, and the chemical shift in the nuclear magnetic resonance spectra of these compounds. From the first point of view, this problem was studied by Coulson and Stephen.[4] On the other hand, the third quantity is difficult to be theoretically interpreted.

In the present work, the CH bond polarity and its dipole moment are discussed by using the second quantity, i.e., the molecular quadrupole moment which was obtained from the data of the breadths of microwave spectral lines. These data have been obtained for acetylene, ethylene, and ethane.[5] Above all, the acetylene molecule is the simplest in a theoretical treatment and the semiempirical MO method is rather easily applied to this molecule.

For an axially symmetric molecule,[5a] the molecular quadrupole moment is defined as

$$Q=\iiint q_i r_i^2(3\cos^2\theta_i-1)d\tau, \qquad (1)$$

where q_i is an element of charge (electron or nucleus), r_i is the distance from the origin, θ_i is the angle between the symmetry axis and r_i. In general, it is rather convenient to choose the mass center of the molecule as the origin, that is, in acetylene, the midpoint of the C—C axis. The quadrupole moment of this molecule[5] obtained from the experimental data is[5b]

$$|Q(C_2H_2)|=1.1\times10^{-16}\ \text{cm}^2,$$

but the sign of Q cannot be determined. Hence, the theoretical treatment is quite necessary to determine this quantity.

THEORETICAL METHOD

Equation (1) may be expanded to

$$Q=Q_N+Q_e,$$

$$Q_N=e\sum_n Z_n r_n^2(3\cos^2\theta_n-1)=\text{nuclear contribution},$$

$$Q_e=-e\int\Psi\sum_e r_e^2(3\cos^2\theta_e-1)\Psi^*d\tau$$

$$=\text{electronic contribution}, \qquad (2)$$

where e is the magnitude of the electronic charge. The term in Eq. (2) which is of interest in interpreting molecular properties is the electronic contribution to the quadrupole moment. If an orthogonalized molecular orbital ψ_{MO} is chosen as a basis for a calculation, Q_e is given by a sum of contributions from each doubly occupied MO in the ground state as follows:

$$Q_e=-2e\sum_{MO}\int\psi_{MO}r_e^2(3\cos^2\theta_e-1)\psi_{MO}^*d\tau. \qquad (3)$$

In general, these MO's are obtained from the condition that the electronic energy should be a minimum. In the present calculation, however, these MO's will be

[1] C. A. Coulson, Trans. Faraday Soc. **38**, 433 (1942).
[2] W. L. G. Gent, Quart. Revs. (London) **2**, 383 (1948).
[3] S. Maeda, J. Chem. Soc. Japan, Pure Chem. Sect. **75**, 36 (1954); **75**, 854 (1954).
[4] C. A. Coulson and M. J. Stephen, Trans. Faraday Soc. **53**, 272 (1957).
[5] R. M. Hill and W. V. Smith, Phys. Rev. **82**, 451 (1951). (a) It is sufficient to have at least a threefold axis of symmetry. (b) Previously, the molecular quadrupole moment Q defined in Eq. (1) was multiplied by $\frac{1}{2}$, since it was interpreted as being averaged over molecular rotation by W. V. Smith and R. Howard [Phys. Rev. **19**, 132 (1950)]. Later, Smith [J. Chem. Phys. **25**, 510 (1956)] however, showed that the previous Q values should be multiplied by 2.40/2.09 with the omission of the factor of $\frac{1}{2}$ and interpreted as applying to the nonrotating molecules. Therefore, this value should be recomputed according to his interpretation. In the present calculation, the corrected value was used.

obtained only from the molecular quadrupole moment data, although this procedure cannot be carried out without some assumptions. That is, the parameters required here were determined in the following way.

Lennard-Jones and his collaborators[6] showed that in a σ system the usual occupied delocalized MO's in the ground state can be replaced by an equivalent set of orbitals each essentially localized in a single bond, in other words, the localized equivalent orbitals can be derived by a unitary transformation of the occupied MO's. This suggests that the MO's can be formed as linear combinations of the localized bond orbitals in a good approximation, instead of atomic orbitals centered on each atom in the system. Based on this suggestion, the basis of the MO's are taken as a set of the following bond orbitals (BO), except for the inner shells.

$$B_{CC}=N_{CC}(\chi_C+\chi_{C'}),$$
$$B_{CH}=N_{CH}(\tilde{\chi}_C+\lambda_1 h),$$
$$B_{CH'}=N_{CH'}(\tilde{\chi}_{C'}+\lambda_1 h'),$$
$$B_{\pi\pi}=N_{\pi\pi}(\pi_+ +\pi_-),$$

where N_{ii} is the normalizing factor of each BO, λ_1 is the unknown parameter, χ_C, $\chi_{C'}$, $\tilde{\chi}_C$, and $\tilde{\chi}_{C'}$ are the hybridized AO's of two carbon atoms in each bond as shown below; they are assumed to be the following typical sp hybridized orbitals:

$$\chi_C=1/\sqrt{2}s+1/\sqrt{2}\sigma,$$
$$\tilde{\chi}_C=1/\sqrt{2}s-1/\sqrt{2}\sigma,$$
$$\chi_{C'}=1/\sqrt{2}s'+1/\sqrt{2}\sigma';$$
$$\tilde{\chi}_{C'}=1/\sqrt{2}s'-1/\sqrt{2}\sigma';$$

where h, h', s, s', σ, σ', π_+, π_+', π_-, and π_-' stand for $1s$ orbitals of two hydrogen atoms and $2s$, $2p\sigma$, $2p\pi_+$, and $2p\pi_-$ orbitals[7] of two carbon atoms, respectively. The primed notations indicate the corresponding quantities related to another atom or bond. Throughout this paper, these notations will be used in the same way.

Then, the MO's are made up as linear combinations of these BO's (LCBO) so that they belong in sets to irreducible representations of the symmetry group $D_{\infty h}$ of acetylene. In the present calculation, acetylene is treated as a 14-electron problem, in which all the electrons are assigned to the MO's, that is, $(K\sigma_g)^2$ $(K\sigma_u)^2$ $(1\sigma_g)^2$ $(2\sigma_g)^2$ $(1\sigma_u)^2$ $(1\pi_u)^4$ $^1\Sigma_g^+$, where the $1s$ electrons of two carbon atoms are regarded as the inner shells $(K\sigma_g)$ and $(K\sigma_u)$ of this molecule, because of the very small mixing with the valence shells.

Now, because of the slight delocalization of bonds and the symmetry of this molecule, it is convenient to introduce the LCBO type semilocalized orbitals (LCBO SLO)[8] in the form

$$\phi_1=N_1[B_{CC}+\lambda_2(B_{CH}+B_{CH'})],$$
$$\phi_2=N_2[B_{CH}+\lambda_3 B_{CC}],$$
$$\phi_2'=N_2'[B_{CH'}+\lambda_3 B_{CC}],$$

where each N_i is a normalizing factor, λ_2, λ_3 are the parameters to be determined with smaller magnitudes than unity, that is, ϕ_1, ϕ_2, and ϕ_2' are mainly localized in B_{CC}, B_{CH}, and $B_{CH'}$, respectively.

Then, using these LCBO SLO's,the occupied MO's are written as

$$K\sigma_g=2^{-\frac{1}{2}}(c+c'), \qquad K\sigma_u=2^{-\frac{1}{2}}(c-c'),$$
$$1\sigma_g=\phi_1,$$
$$2\sigma_g=N_g(\phi_2+\phi_2'),$$
$$1\sigma_u=N_u(\phi_2-\phi_2'),$$
$$1\pi_u=B_{\pi\pi},$$

where c, c' are the $1s$ orbitals of two carbon atoms, respectively, and N_g, N_u are normalizing factors.

The aforementioned LCBO SLO's are not assured to be mutually orthogonal. The orthogonality between $1\sigma_g$ and $2\sigma_g$, however, confirms that between ϕ_1 and ϕ_2 or ϕ_2', because ϕ_2 and ϕ_2' are equivalent to each other for ϕ_1. Although ϕ_2 and ϕ_2' are not exactly orthogonal, an orthogonality is assumed. This assumption may be accepted to be reasonable, because the overlap integral $S(\phi_2, \phi_2')$ can be estimated as $S(B_{CH}, B_{CH'})$ in the first-order approximation in its expansion, and $S(B_{CH}, B_{CH'})$ is very small; even if the second-order quantities as $\lambda_3 S(B_{CC}, B_{CH})$ and λ_3^2 are great, $S(\phi_2, \phi_2')$ is very small, since λ_3 is negative[9] and $S(B_{CC}, B_{CH})$ is positive and these terms largely cancel out. Furthermore, this assumption has no effect on the λ_1 values which will be obtained as a result, because the total molecular quadrupole moment Q which will be given as a sum of the contributions from each MO in Eq. (4) below is unrelated to this orthogonality condition, and consequently the parameters λ_1 contained in the BO's which are the basis of the SLO's and MO's are also quite insensible to this in the present method. On the other hand, the λ_2 and λ_3 values are affected by this condition (the λ_2 value, however, indirectly through the orthogonality condition between ϕ_1 and ϕ_2 or ϕ_2'). Accordingly, the uncertainty on the electronic distribu-

[6] J. E. Lennard-Jones, Proc. Roy. Soc. (London) **A198,** 1, 14 (1949); G. G. Hall and J. E. Lennard-Jones, *ibid.* **A202,** 155 (1950); J. E. Lennard-Jones and J. Pople, *ibid.* **A202,** 166 (1950); G. G. Hall, *ibid.* **A202,** 336 (1950).

[7] The $2p\sigma$ and $2p\sigma'$ orbitals are taken to be pointed toward each other along the molecular axis.

[8] The definition of "semilocalized orbital" used here differs from that by Müller and Eyring. [C. R. Müller and H. Eyring, J. Chem. Phys. **19,** 1495 (1951); C. R. Müller, *ibid.* **19,** 1498 (1951).]

[9] The MO $1\sigma_g$ is the lowest energy one, except the inner shells, so λ_2 is considered to be positive. Hence, from the orthogonality condition between ϕ_1 and ϕ_2 or ϕ_2', λ_3 should be negative.

TABLE I. Bond orbitals and semilocalized orbitals.

$$B_{CC}=0.522(\chi_C+\chi_{C'})=0.369[(s+s')+(\sigma+\sigma')]$$

$$B_{CH}=0.545\bar{\chi}_C+0.514h=0.386s-0.386\sigma+0.514h$$

$$B_{CH'}=0.545\bar{\chi}_{C'}+0.514h'=0.386s'-0.386\sigma'+0.514h'$$

$$B_{\pi\pi}=0.593(\pi_{\pm}+\pi_{\pm}')$$

$$\phi_1=0.871B_{CC}+0.270(B_{CH}+B_{CH'})$$
$$=0.426(s+s')+0.218(\sigma+\sigma')+0.139(h+h')$$

$$\phi_2=0.972B_{CH}-0.365B_{CC}$$
$$=0.240s-0.240\sigma+0.500h-0.135(s'+\sigma')$$

$$\phi_2'=0.972B_{CH'}-0.365B_{CC}$$
$$=0.240s'-0.240\sigma'+0.500h'-0.135(s+\sigma)$$

tion in this molecule obtained cannot be avoided, but this effect may be very small as described above.

By using these MO's, the molecular quadrupole moment Q is obtained from Eqs. (2) and (3) as follows:

$$2[Q(K\sigma_g)+Q(K\sigma_u)+Q(1\sigma_g)+Q(2\sigma_g)+Q(1\sigma_u)+2Q(1\pi_u)]+Q_N=Q, \quad (4)$$

where $Q(\psi_i)=-e\int\psi_i|r_i^2(3\cos^2\theta_i-1)|\psi_i^*d\tau$. Hence, we can determine the unknown parameters λ_1, λ_2, and λ_3, from the orthogonality conditions among ϕ_1, ϕ_2, and ϕ_2', and the molecular quadrupole moment Q in Eq. (4), and subsequently the MO's can also be obtained.

NUMERICAL EVALUATIONS AND RESULTS

In the previous section, the integrals which are required to be evaluated are the overlap and quadrupole integrals. In the calculation, the atomic orbitals used are the analytical SCF AO's which were obtained by Löwdin[10,11] as follows:

H: $h=(1s)_{\delta=1}$,

C: $2s=-0.37659(1s)_{\delta=3.9471}+0.84123(2s)_{\delta=1.4784}+0.32990(2s)_{\delta=2.8493}+0.02329(2s)_{\delta=7.7990}$,

$2p=0.62966(2p)_{\delta=1.0780}+0.42857(2p)_{\delta=2.1444}+0.02154(2p)_{\delta=5.9216}$,

where $(nl)_\delta$ is the nl simple Slater-type AO with orbital exponent δ. All the integrals were exactly calculated. The atomic distances[12] adopted here are $R_{CC}=1.210$ A and $R_{CH}=1.055$ A. For the reason described above, the positive and negative Q values for acetylene should be assigned to the present calculations. The result for the former λ_1 value is $\lambda_1=0.943$, for the latter, $\lambda_1=1.958$. The latter result, however, may be unlikely, because this means the great polarity C^+H^-, which is difficult to be interpreted, considering the small difference between the electronegativity of carbon and that of hydrogen. In fact, this value could not give a reasonable result. Hence, the former value ($\lambda_1=0.943$) was adopted in the present calculation. The sign of the Q value for acetylene, therefore, is determined as positive. In this case, the values of λ_2 and λ_3 are $\lambda_2=0.310$, and $\lambda_3=-0.376$, respectively.

The BO's, SLO's, and MO's thus obtained are shown in Tables I and II, respectively. For convenience, these are listed both in the LCBO and LCAO forms. In Table II, the LCBO MO's obtained here are compared with the SCF LCAO MO's obtained by Maeda.[3] The agreement between them is quite excellent, allowing for the difference of each AO used. (The Slater AO's were used in his work.) The equivalent orbitals (EO's) obtained by a unitary transformation of the above MO's are given in Table III, where the suffixes indicate the corresponding localized bonds. These EO's have the semilocalized feature similar to the SLO's, as shown in Tables I and III. This is due to the small overlapping among the BO's and the approximation used here. The result that E_{CC} is quite equivalent to B_{CC} is also due to the approximation based on the previous assumption.

DISCUSSIONS

In the present paper, the molecular wave function of acetylene was derived from the observed quadrupole moment. Usually a quadrupole moment is very sensitive to the wave function, especially to the outer parts of it. Therefore, such a process seems to be unreliable. But in acetylene this is not the case. The reasons are as follows: The exchange quadrupole moments[13] are generally quite smaller than the one-center ones, though the ones far from the origin are considerably great. On the other hand, the quadrupole moments, especially one-center ones, are greatly sensitive to the forms of the AO's, except to the s orbitals. As the electronic configuration of each carbon atom in acetylene is considered to be $(2s)(2p\sigma)(2p\pi)^2$ and $Q(p\pi)=-\frac{1}{2}Q(p\sigma)$, the contributions of the p electrons of the carbon atoms are largely canceled out. Thus the molecular quadrupole moment of acetylene depends greatly on the CH bond polarity. Next, the single configuration MO type wave function was used and the CI was neglected in the present calculation. This assumption, however, is supported by the extensive work of Ross,[14] in which it was shown that the contributions of the excited configurations to the ground state of acetylene are very small. The calculation for the CH radical by Higuchi[15] also showed the same conclusion. Thus, in spite of some assumptions, the results obtained here are considered to be acceptable.

[10] P. O. Löwdin, Phys. Rev. **90**, 120 (1953).
[11] The explicit form of the 1s orbitals of carbons is not required to be given in the present calculations.
[12] H. C. Allen, E. D. Tidwell, and E. K. Plyler, J. Am. Chem. Soc. **78**, 3034 (1956).
[13] C. Greenhow and W. V. Smith, J. Chem. Phys. **19**, 1298 (1951).
[14] I. G. Ross, Trans. Faraday Soc. **48**, 973 (1952).
[15] J. Higuchi, J. Chem. Phys. **22**, 1339 (1954); also J. Higuchi S. Aono, *ibid.* **32**, 52 (1960), footnote 23.

TABLE II. LCBO MO's occupied for the ground state of C_2H_2.

LCBO MO	SCF LCAO MO[a]
$K\sigma_g=2^{-\frac{1}{2}}(c+c')$, $K\sigma_u=2^{-\frac{1}{2}}(c-c')$	...
$1\sigma_g=0.871B_{CC}+0.270(B_{CH}+B_{CH}')$ $=0.426(s+s')+0.218(\sigma+\sigma')+0.139(h+h')$	$1\sigma_g=0.440(s+s')+0.234(\sigma+\sigma')+0.071(h+h')$
$2\sigma_g=0.687(B_{CH}+B_{CH}')-0.517B_{CC}$ $=0.074(s+s')-0.456(\sigma+\sigma')+0.353(h+h')$	$2\sigma_g=0.052(s+s')-0.372(\sigma+\sigma')+0.436(h+h')$
$1\sigma_u=0.687(B_{CH}-B_{CH}')$ $=0.265(s-s')-0.265(\sigma-\sigma')+0.353(h-h')$	$1\sigma_u=0.268(s-s')-0.339(\sigma-\sigma')+0.310(h-h')$
$1\pi_u=0.593(\pi_\pm+\pi_\pm')$	$1\pi_u=0.612(\pi_\pm+\pi_\pm')$

[a] The notations used by Maeda (see footnote 3 in text) are modified as they fit the present ones.

As can be seen from the property of B_{CH} obtained here, the CH bonds in acetylene are regarded to be almost homopolar ($\lambda_1=0.943$) though hydrogen is slightly positive. In fact, the charge distribution of the CH bond is formulated as $C^{-0.033e}H^{+0.033e}$, using Mulliken's approximation.[16] This agrees well with the result ($\lambda_1=0.92$) obtained from the infrared absorption intensity study by Coulson and Stephen.[4] The magnitude of the molecular quadrupole moment Q used here may, however, be in considerable error, because of necessary theoretical approximations in deriving quadrupole moments from the observed data of microwave linewidths. Now, if the value used here were in errors by as much as $\pm 30\%$, it follows that the λ_1 value has the range $0.86\sim1.05$. Accordingly, the present results should not be taken as final, but the qualitative conclusions obtained here shall not be modified. On the other hand, the result obtained from the MO's indicates that the charge densities of the acetylene molecule may be formulated as $H^{+0.037e}$ $C^{-0.037e}$ $C^{-0.037e}$ $H^{+0.037e}$, using the same approximation as above. This result also gives the same conclusion as that from the localized bonds. It has hitherto been said that the CH bond is almost homopolar. The present results confirm that this argument is reasonable, apart from the problem concerning the discrepancies of the polarity among the $C(sp^3)$—H, $C(sp^2)$—H, and $C(sp)$-H bonds.

The problem of the CH bond moment is closely related to its polarity. A "bond moment" is, however, greatly affected by the localization feature of a "bond." This problem will be examined for the acetylene molecule. The CH bond moment in acetylene was calculated in the following different four ways: $\mu(B_{CH})$, $\mu(E_{CH})$, $\mu(\delta_1R)$, $\mu(\delta_2R)$, where

$$\mu(\psi_i)=e(2\bar{Z}-R_{CH}),\ \bar{Z}=\int\psi_i Z\psi_i^* d\tau,\ \mu(\delta_iR)=\delta_iR_{CH}.$$

The z axis is taken along the molecular axis with the carbon atom at the origin, R_{CH} is the internuclear distance between carbon and hydrogen, and δ_1, δ_2 are the formal charges on the carbon or hydrogen atom obtained from the BO's and MO's, respectively ($\delta_1=0.033e$, $\delta_2=0.037e$). The AO's used in the calculation of the moment integrals $\bar{Z}$ are the same as in the previous section. These obtained values are as follows: $\mu(B_{CH})=2.46D$ (C^+H^-), $\mu(E_{CH})=2.48D$ (C^+H^-), $\mu(\delta_1R)=0.17D$ (C^-H^+), and $\mu(\delta_2R)=0.19D$ (C^-H^+), respectively. The great magnitudes of the values of the former two are due to the atomic dipole term arising from the hybridized carbon orbital. The latter two are rather interpreted as the classical dipole moment based on the formal charge distribution.

A so-called "bond moment" has hitherto been defined in many ways. In any case, however, it is required that this moment is localized in the corresponding bond and the vector sum gives a molecular dipole moment. These two conditions are incompatible with each other because if the perfectly localized BO's were chosen as the basis of evaluations, the overlap moment comes into question and the vector sum does not exactly give a molecular dipole moment; on the other hand, if the orthogonalized EO's were chosen, the vector sum rule is exactly satisfied, but the semilocalization of the EO's breaks the property of localized bonds. In the present case, $\mu(B_{CH})$ and $\mu(\delta_1R)$ are accorded with the former, and $\mu(E_{CH})$ and $\mu(\delta_2R)$ the latter, though, in both cases, the vector sum is zero, because of the symmetry of this molecule.

The closeness between $\mu(B_{CH})$ and $\mu(E_{CH})$ or between $\mu(\delta_1R)$ and $\mu(\delta_2R)$ is due to the fact that the overlap effect (between BO's) cancels the effect based on the semilocalization of E_{CH}, and it does not always mean that the overlap effect is negligibly small. Nevertheless, this effect is often neglected. The reason for this is that the concept "bond" which is perfectly localized in a molecule is convenient to chemical problems and

TABLE III. Equivalent orbitals.

$E_{CC}=B_{CC}=0.369(s+s')+0.369(\sigma+\sigma')$
$E_{CH}=1.006B_{CH}-0.111B_{CC}$ $=0.347s-0.429\sigma+0.517h-0.041(s'+\sigma')$
$E_{CH}'=1.006B_{CH}'-0.111B_{CC}$ $=0.347s'-0.429\sigma'+0.517h'-0.041(s+\sigma)$

[16] R. S. Mulliken, J. Chim. Phys. **46**, 500, 521 (1949).

the contribution of the overlap effect can be included in that of each bond, using Mulliken's approximation.[16] Thus the molecular dipole moment can be divided into each bond. A so-called bond moment, therefore, does not exactly have the localization feature. But the differences of this delocalization effect among many molecules are usually not very great.

In this case, the atomic dipole terms are rather more important than the moment based on the delocalization effect because these terms have generally great values. The hybrid moments of central carbon atoms, however, largely cancel each other, when they contribute to the bonds in opposite directions. In the present case, the hybrid moments of carbon orbitals in the CC and CH bonds fairly cancel out. Such a circumstance is often found in many molecules. (For the lone-pair dipole, this is not always correct, but its effect can be included in the corresponding bond moment.) Hence, roughly speaking, a so-called bond moment need not include the hybrid moment. This problem was previously discussed in detail by Hamilton.[17] The conclusions obtained here are consistent with his. According to this definition, $\mu_0(B_{CH}) = 1.76D\cdot(C^+H^-) = \mu_0(E_{CH})$ is obtained, where $\mu_0(\psi_i)$ is defined as the corresponding bond moment in which the carbon hybrid moment is omitted. Similarly $\mu(\delta_1 R)$ and $\mu(\delta_2 R)$ are also assigned to the CH bond moment, though they are based on the formal charge distribution, since they do not include the carbon hybrid moment. The CH bond moment has hitherto been taken as 0.3 or $0.4D(C^-H^+)$ which is not based on the rigid evidence. Though the latter two moments are close to this empirical value, the former two which are based on the quantum-mechanical calculations are considered to be reasonable. Thus a bond moment is difficult to define because it cannot be directly compared with the experimental data.

From this viewpoint, the bond moments obtained from bending vibrational modes in infrared intensity studies are of great interest. The CH bond moment obtained for acetylene is $\pm 1.00D$[18] or $\pm 1.05D$.[19] This bond moment is not directly associated with a so-called "bond moment," because the infrared bond moment contains the change in the electronic charge distribution following a bending vibration. This, therefore, cannot be explained by a static model. If a bending vibration is, however, regarded as a small perturbation, this value can be inferred from the static charge distribution. Based on this suggestion, the following model is adopted here. The acetylene molecule is divided into two equivalent parts which are essentially localized in the CH bonds. The dipole moment of each part is regarded as the infrared CH bond moment and calculated by using the above MO's, including the overlap moment between two parts, as follows:

$$\mu_\sigma = 2e\sum_i\Big[\sum_{p,q} C_{ip}C_{iq}\bar{Z}_{pq} + \tfrac{1}{2}\sum_{p,p'} C_{ip}C_{ip'}\bar{Z}_{pp'}\Big] - eR_{CH},$$

$$p, q = s, \sigma, h,$$

$$p' = s', \sigma', h',$$

$$\mu_\pi = 4e\big[C_{\pi\pi}^2 Z_{\pi\pi} + C_{\pi\pi}C_{\pi\pi'}\bar{Z}_{\pi\pi'},$$

where the C's are the coefficients of AO's in LCAO MO's; the first suffixes i number the σ MO's; the second p, q and p' AO's as shown above; $C_{\pi\pi}$ and $C_{\pi\pi'}$ are the coefficients of π and π' in the $1\pi_u$ MO, respectively; $\bar{Z}$ used in the same way as described above in the present section, and μ_σ and μ_π the contributions from the σ system and π system, respectively. The CH bond moment μ_{CH} is given as $\mu_{CH} = \mu_\sigma + \mu_\pi$. This calculated value is $1.49D$ (C^-H^+), which contains $\mu_\sigma = 0.23D$ (C^+H^-) and $\mu_\pi = 1.72D$ (C^-H^+). It is considered that, during the bending vibration, the changes of the electronic charge distribution in the C≡C bond contribute to the CH bond moment, especially the π electrons in this bond make a significant contribution. The present model qualitatively confirms this interpretation. In fact, μ_π mainly dominates the magnitude and direction of μ_{CH}. The small value of μ_σ is based on the fact that the moments of the CC σ bond and of the CH bond have opposite directions. From this, it is concluded that the high value of the infrared CH bond moment in acetylene is explained by the great contributions of the π electrons and that the direction of this moment may be C^-H^+. This conclusion agrees well with the guess by Hyde and Hornig.[20] Also, in connection with the discussion of Hornig and McKean,[21] the present result is very interesting. The conclusion obtained here shows that the C≡C bond electrons follow to a considerable extent the bending vibration and thus the infrared CH bond moment is not equivalent to the static one which is localized in the CH bond. Besides, the infrared CH bond moment obtained for HCN is $1.14D$,[20] which is close to that of acetylene. This high value is also considered to be due to the π electrons in the C≡N bond in the similar way as in acetylene. It may, therefore, be considered that the smaller values of the infrared CH bond moments $0.52D$,[22,23] for C_2H_4 and $0.31D$[24] for C_2H_6 are based on the smaller contributions of the π bond electrons, and not on the smaller polarity of the CH bonds in these molecules. This conclusion also supports that of Hornig and McKean.[21] Consequently, the property of a permanent bond moment is

[16] W. C. Hamilton, J. Chem. Phys. **26**, 345 (1957).
[17] E. C. Wingfield and J. W. Straley, J. Chem. Phys. **23**, 731 (1955).
[18] R. L. Kelley, R. Rollefson, and B. S. Schurin, J. Chem. Phys. **19**, 1595 (1951); D. F. Eggers, I. C. Hisatsune, and L. Van Alten, J. Phys. Chem. **59**, 1124 (1955).
[19] G. E. Hyde and D. F. Hornig, J. Chem. Phys. **20**, 647 (1952).
[20] D. F. Hornig and D. C. McKean, J. Phys. Chem. **59**, 1133 (1955).
[21] This value was obtained from the intensity of the out-of-plane vibration (B_{1u}). From the other modes of vibrations, $0.77D$ and $0.37D$ have been obtained. The value from the B_{1u} vibrational mode is, however, suitable to this problem, considering the contributions of the π electrons.
[22] A. M. Thorndike, E. B. Wilson, and A. J. Wells, J. Chem. Phys. **15**, 157 (1947).
[23] A. M. Thorndike, J. Chem. Phys. **15**, 868 (1947).

difficult to be estimated from that of the infrared bond moment, especially the small bond moment for the CH bond.

In view of the present results, the following conclusions are obtained:

(1) The sign of the molecular quadrupole moment of acetylene is positive.

(2) The CH bonds in acetylene are almost homopolar with the polarity C^-H^+.

(3) The direction of the infrared moments of the CH bonds in acetylene is probably C^-H^+.

ACKNOWLEDGMENTS

The author wishes to thank Dr. J. Higuchi and Dr. T. Yoshino for their helpful advice and discussion.

THE JOURNAL OF CHEMICAL PHYSICS VOLUME 34, NUMBER 5 MAY, 1961

Theory of Localized Contributions to the Chemical Shift. Application to Fluorobenzenes*

M. KARPLUS†

Department of Chemistry and Watson Scientific Computing Laboratory, Columbia University, New York, New York

AND

T. P. DAS‡

Department of Chemistry, Columbia University, New York, New York

(Received November 7, 1960)

An expression for the magnetic shielding tensor is obtained by the use of single-determinant Hartree-Fock molecular wave functions. For nuclei of atoms in which the change in the second-order (paramagnetic) contribution is dominant, LCAO theory is employed to express the shielding in terms of localized bond parameters (ionic character, hybridization, and double bonding) and to compare it with the related treatments of the quadrupole coupling constant. Application of the formulation to the multifluorobenzenes provides an explanation of the available experimental chemical shift data and permits the prediction of shift values for other compounds. Of particular interest is the demonstration that double bonding in the C—F bond plays an important role in the fluorobenzenes. Also, the presence of an "ortho" effect in the shift is isolated by a comparison of experimental and theoretical results and tentatively explained in terms of charge repulsions.

I. INTRODUCTION

THE interactions between nuclear moments and the electrons of an atom or molecule afford the opportunity for an increased understanding of chemical bonds. Because of their small magnitude and localized character, these interactions are effective probes for a detailed examination of the stationary-state electron distribution. The magnetic shielding observed by nuclear magnetic resonance spectroscopy arises from one such interaction. Of particular importance is the variation (chemical shift) in the shielding of a nucleus when present in different molecules. The general theory of the chemical shift was developed by Ramsey.[1] For systems that do not have spherical symmetry he showed that, in addition to the first-order diamagnetic shielding of Lamb,[2] one has to include a second-order term, which is often called the paramagnetic or high-frequency contribution.

Since the work of Ramsey, a number of attempts have been made to employ his theory to obtain relationships between chemical shifts and changes in the electron distribution. Most of the studies have been concerned with protons, for which the interpretation is rather complicated because of the primarily *s*-orbital nature of the hydrogen wave function. Both first- and second-order terms are found to be important, with comparable contributions deriving from the immediate electronic environment of the proton and the electrons in the remainder of the molecule. Although accurate calculations have been made for the shielding in the hydrogen molecule,[3] it has not been possible to find precise general relationships between the proton shift and the properties of the bond in which the hydrogen is involved.[4] Nevertheless, some useful correlations with the molecular electronic structure have been obtained.[5]

* Much of the work reported in this paper was done while the authors were at the Departments of Physics (T.P.D.) and Chemistry (M.K.) of the University of Illinois, Urbana, Illinois.

† Alfred P. Sloan Foundation Fellow.

‡ Present address: Government of India Atomic Energy Establishment, Trombay, Apollo Pier Road, Bombay 1, India.

[1] N. F. Ramsey, Phys. Rev. **77**, 567 (1950); **78**, 699 (1950).

[2] W. Lamb, Phys. Rev. **60**, 817 (1941).

[3] T. P. Das and R. Bersohn, Phys. Rev. **104**, 849 (1956); M. J. Stephen, Proc. Roy. Soc. (London) **A243**, 264 (1957).

[4] J. A. Pople, Proc. Roy. Soc. (London) **A239**, 541, 550 (1957); H. M. McConnell, J. Chem. Phys. **27**, 226 (1957); T. P. Das and T. Ghose, *ibid.* **31**, 42 (1959).

[5] L. H. Meyer and H. S. Gutowsky, J. Phys. Chem. **57**, 481 (1953); H. J. Bernstein, W. G. Schneider, and J. A. Pople, Proc. Roy. Soc. (London) **A236**, 515 (1956); P. L. Corio and B. P. Dailey, J. Am. Chem. Soc. **73**, 3043 (1956); J. S. Waugh and R. W. Fessenden, *ibid.* **79**, 846 (1957).

For many atoms other than hydrogen, the valence electrons occupy orbitals with nonzero intrinsic angular momentum ($p, d, f, \cdots$orbitals). These may give rise to large deviation from spherical symmetry on molecule formation. When this occurs, the chemical shift is usually dominated by the second-order contribution, which can be interpreted in terms of localized bond properties. For F^{19}, in an unhybridized single bond, Saika and Slichter[6] have used the valence-bond method and perturbation theory to obtain a very useful correlation between the ionic character and the fluorine resonance shift. Similar arguments have been applied to the chemical shift of phosphorous.[7]

In this paper we employ a molecular orbital wave function and perturbation theory to obtain a formula for the first- and second-order contributions to the magnetic shieldings tensor. By the introduction of suitable approximations, the shielding is expressed in terms of localized bond properties (ionic character, hybridization, and double-bonding). Specializing to F^{19}, we apply the formulation in a semiempirical fashion to chemical shifts measured in some fluorobenzenes. Sec. II is concerned with the development of a molecular-orbital expression for the magnetic shielding tensor. In Sec. III the general expression is reformulated in terms of localized bond parameters and compared with the corresponding theory for the quadrupole coupling constant. The resulting equations are applied in Sec. IV to an analysis of the F^{19} shielding in fluorobenzenes and contrasted with the quadrupole coupling in chlorobenzenes and bromobenzenes.

II. GENERAL FORMULATION FOR MAGNETIC SHIELDING TENSOR

For a nucleus of magnetic moment $\boldsymbol{\mu}$ in a uniform magnetic field $\mathbf{H}$, the shielding tensor $\boldsymbol{\sigma}$ is defined by the relation

$$\Delta E(\mu, H) = -\boldsymbol{\mu}\cdot(\mathbf{I}-\boldsymbol{\sigma})\cdot\mathbf{H}, \tag{1}$$

where $\Delta E(\mu, H)$ is the energy contributed to the molecule by the coupling of $\boldsymbol{\mu}$ and $\mathbf{H}$, and $\mathbf{I}$ is the unit dyadic. In a $^1\Sigma$ molecule, Ramsey[1] has shown that the significant part of the Hamiltonian $\mathcal{H}$ for the system can be written in the form

$$\mathcal{H}=\mathcal{H}_0+\mathcal{H}_1+\mathcal{H}_2+\mathcal{H}_3, \tag{2}$$

where

$$\mathcal{H}_0=-\sum_k(\hbar^2/2m)\nabla_k^2+V \tag{3}$$

$$\mathcal{H}_1=(e/2mc)\sum_k\mathbf{H}\cdot\mathbf{l}_k \tag{4}$$

$$\mathcal{H}_2=(e/mc)\sum_k(\boldsymbol{\mu}\cdot\mathbf{l}_k/r_k^3) \tag{5}$$

and

$$\mathcal{H}_3=\frac{e^2}{2mc^2}\left[\boldsymbol{\mu}\cdot\left(\sum_k\frac{r_k^2\mathbf{I}-\mathbf{r}_k\mathbf{r}_k}{r_k^3}\right)\cdot\mathbf{H}\right]. \tag{6}$$

The function V is the potential energy of the electrons, $\mathbf{l}_k$ is the orbital angular momentum of electron k, and r_k is the vector from the magnetic nucleus to electron k. Implicit in Eqs. (3)–(6) is the choice of the magnetic nucleus as the origin for the vector potential.

To use the Hamiltonian of Eq. (2) in a calculation of magnetic shielding, we assume that the molecular wave function Ψ_0 for the unperturbed system with Hamiltonian $\mathcal{H}_0$ and energy eigenvalue E_0 can be written as a single determinant of the form

$$\Psi_0=[(2n)!]^{-\frac{1}{2}}\times|\psi_1(1)\beta(1)\psi_1(2)\alpha(2)\psi_2(3)\beta(3)\cdots\psi_n(2n)\alpha(2n)|, \tag{7}$$

where each of the doubly filled molecular orbitals $\psi(k)$ is an eigenfunction of the Hartree-Fock operator[8] $h_0(k)$ with orbital energy ϵ_j, that is,

$$h_0(k)\psi_j(k)=\epsilon_j\psi_j(k). \tag{8}$$

The first-order contribution $\boldsymbol{\sigma}^{(1)}$ to the shielding tensor of Eq. (1) is obtained directly from the expectation value of the perturbation Hamiltonian $\mathcal{H}_3$ with the wave function Ψ_0. On utilizing the orthogonality property of the $\psi_j(k)$, we have

$$\boldsymbol{\sigma}^{(1)}=\frac{e^2}{2mc^2}\sum_j\left\langle\psi_j(k)\left|\frac{r_k^2\mathbf{I}-\mathbf{r}_k\mathbf{r}_k}{r_k^3}\right|\psi_j(k)\right\rangle. \tag{9}$$

For complex molecules, each of the molecular orbitals is often approximated by a sum over atomic orbitals $\phi_\nu(k)$ (LCAO-MO) in the form[8]

$$\psi_j(k)=\sum_\nu a_{\nu j}\phi_\nu(k), \tag{10}$$

where $a_{\nu j}$ is the appropriate expansion coefficient. On substituting into Eq. (9), we have

$$\boldsymbol{\sigma}^{(1)}=\frac{e^2}{2mc^2}\sum_j\sum_{\nu,\mu}2a_{\nu j}^*a_{\mu j}\times\langle\phi_\nu(k)\,|\,(r_k^2\mathbf{I}-\mathbf{r}_k\mathbf{r}_k)/r_k^3\,|\,\phi_\mu(k)\rangle \tag{11}$$

or

$$\boldsymbol{\sigma}^{(1)}=\frac{e^2}{2mc^2}\sum_{\nu,\mu}p_{\mu\nu}\langle\phi_\nu(k)\,|\,(r_k^2\mathbf{I}-\mathbf{r}_k\mathbf{r}_k)/r_k^3\,|\,\phi_\mu(k)\rangle. \tag{12}$$

Here the quantity $p_{\mu\nu}$ is an element of the usual charge-bond order matrix,[9]

$$p_{\mu\nu}=\sum_j 2a_{\nu j}^*a_{\mu j}=\sum_j 2a_{\mu j}a_{j\nu}^\dagger. \tag{13}$$

[6] A. Saika and C. P. Slichter, J. Chem. Phys. **22**, 26 (1954).
[7] N. Muller, P. C. Lauterbur, and J. Goldenson, J. Am. Chem. Soc. **78**, 3557 (1956); J. R. Parks, *ibid.* **79**, 757 (1957).
[8] C. C. J. Roothaan, Revs. Modern Phys. **23**, 69 (1951).
[9] C. A. Coulson and H. C. Longuet-Higgins, Proc. Roy. Soc. (London) **A191**, 16 (1947); **193**, 447, 456; **195**, 188 (1948).

For the second-order contribution $\sigma^{(2)}$ we write the perturbation theory expression

$$\sigma^{(2)}=\frac{e^2}{2m^2c^2}\sum_m (E_0-E_m)^{-1}\{\langle\Psi_0|\sum_k \mathbf{l}_k|\Psi_m\rangle\langle\Psi_m|\sum_k (\mathbf{l}_k/r_k^3)|\Psi_0\rangle+\langle\Psi_0|\sum_k (\mathbf{l}_k/r_k^3)\Psi_m\rangle\langle\Psi_m|\sum_k \mathbf{l}_k|\Psi_0\rangle\}, \quad (14)$$

where the functions Ψ_m with energies E_m are unperturbed excited-state wave functions for the system. Each of the Ψ_m that yields nonzero integrals in Eq. (14) is a singlet function with one of the occupied orbitals $\psi_j(k)$ of Ψ_0 excited to an unoccupied orbital $\psi_j'(k)$. With the energy denominator for this excitation written in the form $-\Delta E_{jj'}$, Eq. (14) becomes

$$\sigma^{(2)}=-\frac{e^2}{2m^2c^2}\sum_{jj'}\frac{2}{\Delta E_{jj'}}\{\langle\psi_j(k)|\mathbf{l}_k|\psi_{j'}(k)\rangle\langle\psi_{j'}(k)|(\mathbf{l}_k/r_k^3)|\psi_j(k)\rangle+\langle\psi_j(k)|(\mathbf{l}_k/r_k^3)|\psi_{j'}(k)\rangle\langle\psi_{j'}(k)|\mathbf{l}_k|\psi_j(k)\rangle\}, \quad (15)$$

where a factor of 2 is introduced by the normalization of the excited-state functions and the sum over α and β spins. The index j ranges over the orbitals that are occupied in the ground state and j' over those that are unoccupied. Expansion of the $\psi_j(k)$ and $\psi_j'(k)$ in terms of the atomic orbitals $\phi_\nu(k)$ [Eq. (10)] yields

$$\sigma^{(2)}=-\frac{e^2}{2m^2c^2}\sum_{jj'}\sum_{\nu,\mu}\sum_{\lambda,\rho}\frac{2a_{\nu j'}^*a_{\mu j'}a_{\lambda j'}^*a_{\rho j}}{\Delta E_{jj'}}\{\langle\phi_\nu(k)|\mathbf{l}_k|\phi_\mu(k)\rangle\langle\phi_\lambda(k)|\mathbf{l}_k/r_k^3|\phi_\rho(k)\rangle$$
$$+\langle\phi_\nu(k)|\mathbf{l}_k/r_k^3|\phi_\mu(k)\rangle\langle\phi_\lambda(k)|\mathbf{l}_k|\phi_\rho(k)\rangle\} \quad (16)$$

or

$$\sigma^{(2)}=-\frac{e^2}{2m^2c^2}\sum_{\nu,\mu}\sum_{\lambda,\rho}2\pi_{\mu\nu,\rho\lambda}\,\mathrm{Re}\{\langle\phi_\nu(k)|\mathbf{l}_k|\phi_\mu(k)\rangle\langle\phi_\lambda(k)|\mathbf{l}_k/r_k^3|\phi_\rho(k)\rangle\}, \quad (17)$$

where

$$\pi_{\mu\nu,\rho\lambda}=\sum_{jj'}\frac{2a_{\nu j}^*a_{\mu j'}a_{\lambda j'}^*a_{\rho j}}{\Delta E_{jj'}} \quad (18)$$

is a generalization of the Coulson and Longuet-Higgins polarizability[9] to antisymmetrized wave functions.[10]

Equations (12) and (17) are expressions that can be used for calculating both the first- and second-order contributions to the magnetic shielding from a knowledge of the $p_{\mu\nu}$ and $\pi_{\mu\nu,\rho\lambda}$.[11] Although the $p_{\mu\nu}$ can be obtained directly from the ground-state wave function for a molecule, the $\pi_{\mu\nu,\rho\lambda}$ require a knowledge of the excited states. Since we are concerned primarily with the study of the ground-state function, it is useful to recast $\sigma^{(2)}$ in a form that is independent of the excited states. An approach, which has been useful for semiquantitative arguments and small perturbations, is based on the introduction of an average excitation energy.[12,13] Substitution of this average energy could be made directly into Eq. (18) to simplify the expression for $\pi_{\mu\nu,\rho\lambda}$. However, a clearer picture of the procedure is obtained by referring back to Eq. (14). We introduce Δ for the average energy denominator and obtain

$$\sigma^{(2)}=-\frac{e^2}{\Delta m^2c^2}\left\langle\Psi_0\left|\sum_{k,k'}\frac{\mathbf{l}_k\mathbf{l}_{k'}}{r_k^3}\right|\Psi_0\right\rangle. \quad (19)$$

On expanding Ψ_0 in terms of the molecular orbitals $\psi_j(k)$, we find

$$\sigma^{(2)}=-\frac{e^2}{\Delta m^2c^2}\sum_j 2\{\langle\psi_j(k)|\mathbf{l}_k\mathbf{l}_k/r_k^3|\psi_j(k)\rangle+2\sum_{j'}\langle\psi_j(k)\psi_{j'}(k')|\mathbf{l}_k\mathbf{l}_{k'}/r_k^3|\psi_j(k)\psi_{j'}(k')\rangle$$
$$-\sum_{j'}\langle\psi_j(k)\psi_{j'}(k')|\mathbf{l}_k\mathbf{l}_{k'}/r_k^3|\psi_j(k')\psi_j(k)\rangle\}. \quad (20)$$

[10] P. O. Löwdin, J. Chem. Phys. **21**, 496 (1953).

[11] R. McWeeny [Mol. Phys. **1**, 311 (1948)] has obtained related expressions for Hückel-type molecular orbital functions in aromatic systems.

[12] M. Karplus, Revs. Modern Phys. **32**, 455 (1960).

[13] For more exact calculations, a direct solution of the first-order Schrödinger equation for the perturbed function can be used [e.g., R. M. Sternheimer and H. M. Foley, Phys. Rev. **102**, 731 (1956)]. A formulation of this procedure for the shielding problem is given in the Appendix.

This expression immediately reduces to

$$\mathfrak{d}^{(2)}=-\frac{e^2}{\Delta m^2c^2}\sum_j 2\{\langle\psi_j(k)\,|\mathbf{l}_k\mathbf{l}_k/r_k^3\,|\psi_j(k)\rangle-\sum_{j'}\langle\psi_j(k)\,|\mathbf{l}_k/r_k^3\,|\psi_{j'}(k)\rangle\langle\psi_{j'}(k)\,|\mathbf{l}_k\,|\psi_j(k)\rangle\}. \tag{21}$$

since the second summation of Eq. (20) is equal to zero for the systems of interest here. It should be noted that, in contrast to Eq. (15), the indices j and j' both range over the occupied molecular orbitals. On introducing the atomic orbitals $\phi_\nu(k)$ into Eq. (21), we obtain

$$\mathfrak{d}^{(2)}=-\frac{e^2}{\Delta m^2c^2}\sum_j 2\{\sum_{\nu,\mu}a_{\nu j}{}^*a_{\mu j}\langle\phi_\nu(k)\,|\mathbf{l}_k\mathbf{l}_k/r_k^3\,|\phi_\mu(k)\rangle-\sum_{j'}\sum_{\nu,\mu}\sum_{\lambda,\rho}a_{\nu j}{}^*a_{\mu j}a_{\lambda j'}{}^*a_{\rho j'}$$
$$\times\langle\phi_\nu(k)\,|\mathbf{l}_k/r_k^3\,|\phi_\rho(k)\rangle\langle\phi_\lambda(k)\,|\mathbf{l}_k\,|\phi_\mu(k)\rangle\}. \tag{22}$$

By use of the charge-bond order matrix elements $p_{\mu\nu}$ [Eq. (13)], $\mathfrak{d}^{(2)}$ can be expressed in the form

$$\mathfrak{d}^{(2)}=-\frac{e^2}{\Delta m^2c^2}\sum_{\nu,\mu}p_{\mu\nu}\{\langle\phi_\nu(k)\,|\mathbf{l}_k\mathbf{l}_k/r_k^3\,|\phi_\mu(k)\rangle-\sum_{\lambda,\rho}\tfrac{1}{2}p_{\rho\lambda}\langle\phi_\nu(k)\,|\mathbf{l}_k/r_k^3\,|\phi_\rho(k)\rangle\langle\phi_\lambda(k)\,|\mathbf{l}_k\,|\phi_\mu(k)\rangle\}. \tag{23}$$

On combining Eqs. (12) and (23), we obtain the desired expression for the magnetic shielding tensor $\mathfrak{d}$,

$$\mathfrak{d}=\frac{e^2}{2mc^2}\sum_{\nu,\mu}p_{\mu\nu}\left\{\left\langle\phi_\nu(k)\,\middle|\,\frac{r_k{}^2\mathbf{I}-\mathbf{r}_k\mathbf{r}_k+(2/\Delta m)\mathbf{l}_k\mathbf{l}_k}{r_k{}^3}\,\middle|\,\phi_\mu(k)\right\rangle\right.$$
$$\left.-(\Delta m)^{-1}\sum_{\lambda,\rho}p_{\rho\lambda}\langle\phi_\nu(k)\,|\mathbf{l}_k/r_k^3\,|\phi_\rho(k)\rangle\langle\phi_\lambda(k)\,|\mathbf{l}_k\,|\phi_\mu(k)\rangle\right\}. \tag{24}$$

In this form, the evaluation of $\mathfrak{d}$ requires a knowledge of the charges $p_{\mu\mu}$, the bond orders $p_{\mu\nu}$, matrix elements over the atomic orbitals $\phi_\nu(k)$, and the average excitation energy Δ. If molecular orbital wave functions are available, Eq. (24) can be used directly to calculate the magnetic shielding. In the following section, we employ the equation to obtain a simplified expression for $\mathfrak{d}$ in terms of parameters related to bond properties.

III. RELATION BETWEEN SHIELDING AND BOND PARAMETERS

We consider an atom, such as F^{19}, which has an unbalanced p-electron valence shell. For this type of atom, the dominant contribution to the chemical shift arises from the second-order term. Consequently, we restrict most of the discussion to $\mathfrak{d}^{(2)}$, as given by Eq. (23), although an expression for the entire shielding tension is finally obtained from Eq. (24). To simplify the treatment we neglect all orbitals on atoms other than the one being considered. This approximation[6] is partly justified by the $1/r_k^3$ term present in the perturbation Hamiltonian. Also, some of the errors introduced by the approximation are compensated by the semiempirical character of the approach. Since s orbitals do not contribute, we have to sum in Eq. (23) over only the p orbitals (ϕ_x, ϕ_y, and ϕ_z) on the atom. If these orbitals all have the same radial function, operating on one by a component of $\mathbf{l}_k$ gives zero or transforms it into another; for example,

$$\mathbf{l}_{zk}\phi_x(k)=0,\qquad \mathbf{l}_{zk}\phi_y(k)=-(\hbar/i)\phi_x(k),$$
$$\mathbf{l}_{xk}\phi_z(k)=(\hbar/i)\phi_y(k). \tag{25}$$

With Eqs. (23) and (25), the principal components of $\mathfrak{d}^{(2)}$, namely, $\sigma_{xx}{}^{(2)}$, $\sigma_{yy}{}^{(2)}$, and $\sigma_{zz}{}^{(2)}$, are given by

$$\sigma_{xx}{}^{(2)}=-(e^2\hbar^2/\Delta m^2c^2)\langle 1/r^3\rangle\{p_{yy}+p_{zz}-p_{yy}p_{zz}+p_{yz}p_{zy}\} \tag{26}$$

with corresponding expressions for $\sigma_{yy}{}^{(2)}$ and $\sigma_{zz}{}^{(2)}$. Here the quantity $\langle 1/r^3\rangle$ is the expectation value of $1/r^3$ for the normalized p-orbital radial function.

Since most measurements of shielding are made in solution, only the average of $\mathfrak{d}$ over rotation is obtained. On writing $\sigma^{(2)}$ for the rotational average of the second-order term, we have

$$\sigma^{(2)}=\tfrac{1}{3}(\sigma_{xx}{}^{(2)}+\sigma_{yy}{}^{(2)}+\sigma_{zz}{}^{(2)})=\sigma_0\{(p_{xx}+p_{yy}+p_{zz})$$
$$-\tfrac{1}{2}(p_{xx}p_{yy}+p_{yy}p_{zz}+p_{zz}p_{xx})$$
$$+\tfrac{1}{2}(p_{xy}p_{yx}+p_{yz}p_{zy}+p_{zx}p_{xz}\}, \tag{27}$$

where

$$\sigma_0=-(2e^2\hbar^2/3\Delta m^2c^2)\langle 1/r^3\rangle \tag{28}$$

and the p_{xx}, p_{yy}, and p_{zz} are orbital populations. An expression analogous to Eq. (27) has been used by Pople[4] for estimating the neighboring atom contributions to proton shielding. As he suggests, the p_{ii} are most meaningful if identified with the gross orbital populations of Mulliken[14] [$N(r_k)$ of his Eq. (7)]. For a closed-shell atom, we would have $p_{ii}=2$, $p_{ij}=0$, and $\sigma^{(2)}=0$, as expected.

Although Eq. (27) can be used to calculate $\sigma^{(2)}$ as a function of the p_{ii} and p_{ij} for molecules with known

[14] R. S. Mulliken, J. Chem. Phys. **23**, 1833 (1955).

LCAO-MO wave functions, it is useful to recast the result in a form involving bond parameters. We specialize to an atom that is directly bonded to only one other atom in the molecule (e.g., F^{19} in a F—C bond) and choose the bond line as the z axis. If the symmetry of the system is such as to cause no mixing of ϕ_x, ϕ_y, and ϕ_z orbitals, $\sigma^{(2)}$ reduces to

$$\sigma^{(2)}=\sigma_0\{(p_{xx}+p_{yy}+p_{zz})-\tfrac{1}{2}(p_{xx}p_{yy}+p_{yy}p_{zz}+p_{zz}p_{xx})\}. \tag{29}$$

The quantities p_{xx} and p_{yy} can be related to the double-bond characters ρ_x and ρ_y by the expressions

$$p_{xx}=2-\rho_x, \qquad p_{yy}=2-\rho_y. \tag{30}$$

Similarly, the quantity p_{zz} is determined by the extent of (sp) hybridization s of the bond orbital and its ionic character I. If we write the molecular orbital ψ_z and the lone-pair orbital ψ_{lp} in the form

$$\psi_z=(1+1/2)^{\frac{1}{2}}\{(1-s)^{\frac{1}{2}}\phi_z+s^{\frac{1}{2}}\phi_s\}+\cdots,$$
$$\psi_{lp}=(1-s)^{\frac{1}{2}}\phi_s+s^{\frac{1}{2}}\phi_z,$$

where ϕ_z and ϕ_s are p_z and s orbitals on the atom under consideration, we have

$$p_{zz}=1+s+I-Is, \tag{31}$$

since there are two electrons in the lone-pair orbital. On substituting from Eqs. (30) and (31) into Eq. (29), we find that

$$\sigma^{(2)}=\sigma_0\{[1-s-I+\tfrac{1}{2}(\rho_x+\rho_y)]$$
$$+\tfrac{1}{2}[2Is+(\rho_x+\rho_y)(I+s-Is)-\rho_x\rho_y]\}. \tag{32}$$

For s, I, ρ_x, ρ_y small, only the terms in the first set of parentheses are important, and we can write

$$\sigma^{(2)}\cong\sigma_0[1-s-I+\tfrac{1}{2}(\rho_x+\rho_y)]. \tag{33}$$

Equation (33) is derived also in the Appendix by a perturbation procedure that avoids the need for an average excitation energy.

It is of interest to compare these results with the expression for the quadrupole coupling constant in a comparable system. From the studies of Townes and Dailey,[15] we have for the quadrupole coupling constant

$$q=q_0\{[(p_{xx}+p_{yy})/2]-p_{zz}\}, \tag{34}$$

and for small I and s,

$$q=q_0[1-s-I-\tfrac{1}{2}(\rho_x+\rho_y)], \tag{35}$$

where

$$q_0=\tfrac{4}{5}e\langle 1/r^3\rangle. \tag{36}$$

Comparison of Eqs. (33) and (35) shows the relationship between chemical shift and quadrupole coupling constant. Although $\sigma^{(2)}$ and q are both decreased in magnitude by increasing hybridization (s) and ionic character (I), there is an important difference in their dependence on double-bond character. The observed value of q is expected to *decrease* with *increasing* ρ_x and ρ_y, while the observed value of $\sigma^{(2)}$ is expected to *increase* in magnitude ($\sigma_0<0$) with *increasing* ρ_x and ρ_y. Although no measurements of q and $\sigma^{(2)}$ are available for the same nucleus, an illuminating comparison can be made for different halogens (F, Cl, and Br) in the halobenzenes (see Sec. IV).

A particularly simple and interesting form of Eqs. (29) and (34) occurs if the shielded atom X is conjugated with an aromatic ring. For the ring in the yz plane, ρ_y can be set equal to zero and we find from Eq. (29) that

$$\sigma^{(2)}=\sigma_0\{2-\tfrac{1}{2}p_{zz}p_{xx}\}. \tag{37}$$

Without any restriction on the magnitudes of I, s, or ρ_x, Eq. (37) yields the convenient result[16]

$$\sigma^{(2)}=\sigma_0\{1-s-I+Is(\rho_x/2)+(\rho_x/2)(s+I)\}. \tag{38}$$

The expression for the quadrupole coupling constant in this type of system is

$$q=q_0\{1-s-I+Is-(\rho_x/2)\}. \tag{39}$$

It is useful to introduce the anisotropy η_σ of the second-order shielding, defined by the expression

$$\eta_\sigma=(\sigma_{xx}^{(2)}-\sigma_{yy}^{(2)})/\sigma_{zz}^{(2)}. \tag{40}$$

From Eq. (26) for $\sigma_{xx}^{(2)}$ and the corresponding results for $\sigma_{yy}^{(2)}$ and $\sigma_{zz}^{(2)}$, we have

$$\eta_\sigma=\frac{(p_{yy}-p_{xx})(1-p_{zz})+(_{yz}p_{zy}-p_{xz}p_{xz})}{p_{xx}+p_{yy}-p_{xx}p_{yy}+p_{xy}p_{yx}}. \tag{41}$$

If the cross terms (p_{ij}, $i\neq j$) are zero and $p_{yy}=2$, η_σ reduces to

$$\eta_\sigma=(1-p_{xx})=-s-I+Is. \tag{42}$$

Thus, the anisotropy in the shielding measures the hybridization and ionic character of the bond. This result supplements the anisotropy of the quadrupole coupling constant, which is determined by the double-bonding parameter ρ_x in corresponding systems. Unfortunately, no experimental values of η_σ are available. Measurements should be attempted in oriented solids or with molecular beams.

IV. DISCUSSION OF HALOBENZENES

In standard NMR measurements of magnetic shielding, the chemical shift δ between some reference system and the compound of interest is determined. We introduce the quantity $\Delta\sigma$,

$$\Delta\sigma=\sigma_r-\sigma_c=[(H_r-H_c)/H_r]=-\delta, \tag{43}$$

[15] C. H. Townes and B. P. Dailey, J. Chem. Phys. **17**, 782 (1949).

[16] A valence-bond treatment which neglects hybridization and cross terms between different structures leads to the equation

$$\sigma^{(2)}=\sigma_0[1-I+\rho/2].$$

where σ_r and σ_c are the rotational average of the shielding tensor in the reference system and the compound, respectively.

We can write $\Delta\sigma$ in the form

$$\Delta\sigma=\Delta\sigma^{(1)}+\Delta\sigma^{(2)}. \tag{44}$$

From Eq. (12), we have for atoms conjugated with aromatic rings

$$\Delta\sigma^{(1)}=(e^2/3mc^2)\langle 1/r\rangle\{\Delta I-\Delta\rho\}, \tag{45}$$

with neglect of terms arising from orbitals on neighboring atoms and ρ used instead of ρ_z to simplify the writing. Similarly, Eq. (38) yields

$$\begin{aligned}\Delta\sigma^{(2)}&=\sigma_0\{-\Delta I+(\Delta\rho/2)-\Delta s+(I_r-\Delta I+s_r-\Delta s)(\Delta\rho/2)\\&\quad+[(2s_r+\rho_r)/2]\Delta I+[(\rho_r/2)+I_r]\Delta s-\Delta I\Delta s\},\end{aligned} \tag{46}$$

where

$$\Delta I=I_r-I_c,\qquad \Delta\rho=\rho_r-\rho_c,\qquad \Delta s=s_r-s_c,$$

and again ρ is used instead of ρ_z. Implicit in these equations for $\Delta\sigma^{(1)}$ and $\Delta\sigma^{(2)}$ is the assumption that $\langle 1/r\rangle$ and σ_0 are not changed in going from one compound to another.

Direct calculation[17] shows that $\Delta\sigma^{(1)}$ is negligible in comparison with $\Delta\sigma^{(2)}$, so that $\Delta\sigma$ can be approximated by $\Delta\sigma^{(2)}$.[18]

Equation (46) can here be simplified by the neglect of all terms quadratic in ΔI, Δs, and $\Delta\rho$, since the changes in I, s, and ρ are small in going from one fluorobenzene to another. Further, from a knowledge of the small magnitude of s (~ 0.05),[19] we can ignore Δs terms and obtain the expression

$$\begin{aligned}\Delta\sigma\cong\Delta\sigma^{(2)}\cong\sigma_0\{&-[1-(\rho_r/2)-s_r]\Delta I\\&+(1+I_r+s_r)(\Delta\rho/2)\}.\end{aligned} \tag{47}$$

To employ Eq. (47) we need a value for σ_0, as well as a knowledge of ρ_r, I_r, and s_r. On choosing fluorobenzene as the reference compound, we set $s_r=0.05$ (see above). The ionic character I_r equal to 0.75 is obtained from the ionic character vs electronegativity curves of Dailey and Townes[20] and of Gordy,[21] which are based on quadrupole coupling constant measurements. We use their relationship rather than that of Pauling[22] because the chemical shift involves a radial operator which is of the same form as that required for the quadrupole coupling constant; that is, both the chemical shift and quadrupole coupling emphasize the wave function in the neighborhood of the nucleus. The double-bond character was determined by the Hückel theory,[23] which makes use of one-electron orbitals and the assumed parameters $\alpha_F=1.5\ \beta_{CC}$ and $\beta_{CF}=\beta_{CC}$. A complete solution of the appropriate secular determinant yielded $\rho=\rho_z=0.126$.

The evaluation of σ_0 can be performed theoretically or by reference to experiment. A theoretical evaluation would best be done by use of a variation-perturbation approach (see Appendix). Consistent with the semiempirical nature of the present application, we chose to determine an effective σ_0 by means of an experimental comparison. The chemical shift between the fluorine molecule (F_2) and fluorobenzene (ϕF) has been found to be[24]

$$\Delta\sigma=\sigma_{\phi F}-\sigma_{F_2}=+0.543\times 10^{-3}. \tag{48}$$

From Eq. (46), we can express σ_0 in terms of the ΔI, $\Delta\rho$, and Δs parameters. Since we listed I, ρ, and s for fluorobenzene in the previous paragraph, we only require the corresponding values for the F_2 molecule to make use of Eqs. (46) and (48). The ionic character I and double-bond character ρ can be set equal to zero in F_2. For the degree of hybridization s we use the value of 0.02 obtained by Ransil in his SCF-LCAO-MO calculation.[25] Substitution of these numbers into Eq. (46), and comparison with Eq. (48) yields

$$\sigma_0=-0.863\times 10^{-3}. \tag{49}$$

This value is different from that obtained by Saika and Slichter,[6] but gives better agreement with the measured F_2, HF shift which was discussed in their papers.[26] The exact value of σ_0, however, is not important for the treatment that follows because an alteration in σ_0 would not affect the trends which are of primary significance.

Subsituting the σ_0 value of Eq. (49) and the other fluorobenzene parameters into Eq. (47), we obtain

$$\Delta\sigma=0.765\Delta I-0.777\Delta\rho. \tag{50}$$

For ΔI positive ($I_r>I_c$), we have a positive contribution to $\Delta\sigma$, which corresponds to less shielding (*more antishielding*) in c than in r; for $\Delta\rho$ positive ($\rho_r>\rho_c$), we have a negative contribution in $\Delta\sigma$, which corresponds to more shielding (*less antishielding*) in c than in r.

[17] The quantity $(e^2/3mc^2)\langle 1/r\rangle$ is approximately 3×10^{-5} for a fluorine $2s$ or $2p$ electron.

[18] The neglect of contributions from other atoms implies that ring current effects are not included. Although these effects are assumed to be of major importance for aromatic protons, they do not contribute significantly to the fluorine shifts.

[19] D. H. Anderson, P. J. Frank, and H. S. Gutowsky, J. Chem. Phys. **32,** 196 (1960).

[20] B. P. Dailey and C. H. Townes, J. Chem. Phys. **23,** 118 (1955).

[21] W. Gordy, J. Chem. Phys. **19,** 792 (1951); **22,** 1470 (1954).

[22] L. Pauling, *The Nature of the Chemical Bond* (Cornell University Press, Ithaca, New York, 1960).

[23] C. A. Coulson, *Valence* (Oxford University Press, New York, 1953). For more quantitative calculations than the exploratory work reported here, self-consistent field orbitals should be used.

[24] H. S. Gutowsky, D. W. McCall, B. R. McGarvey, and L. H. Meyer, J. Am. Chem. Soc. **74,** 4809 (1952). The shift used by Gutowsky *et al.* is the *negative* of the usual δ and agrees in sign with the $\Delta\sigma$ convention.

[25] B. J. Ransil, Revs. Modern Phys. **32,** 245 (1960).

[26] The value of σ_0 is also in good agreement with that estimated by us from the spin-rotational constant of HF measured by Ramsey and his co-workers (private communication).

The form of Eq. (50) provides a qualitative theoretical justification for Taft's empirical studies of substituted fluorobenzenes,[27] in which he correlated the observed shift for para-substituents with separate inductive and resonance parameters.

Dihalo Compounds

We now consider ortho (o), meta (m), and para (p) difluorobenzene. In Table I, the first column gives $\Delta\rho$ as calculated by Hückel theory. Substitution of these $\Delta\rho$ values into Eq. (50) yields the quantity $\Delta\sigma(\rho)$, the contribution of the change in double-bond character to $\Delta\sigma$ (column 2 of Table I). The difference between $\Delta\sigma(\rho)$ and $\Delta\sigma$(exptl) can be used with Eq. (50) to obtain $\Delta\sigma(I)$, the ionic contribution to $\Delta\sigma$ (column 4) and ΔI itself (column 5). The results for the m- and p-fluorobenzenes appear very reasonable, with the decrease in ΔI from m to p corresponding to the expected attenuation in inductive effect.[28] However, the ortho shift, which could be fitted by an unlikely large and negative $\Delta I(-0.0246)$ is puzzling and requires further discussion (see below).

It is of interest to compare the fluorobenzene shifts with the quadrupole coupling constants in the corresponding chlorobenzenes and bromobenzenes. To use Eq. (35), we determine q_0 from atomic beam experiments[29] (q_0(Cl)=109.6 Mc, q_0(Br)=643 Mc) and assume that ρ and s are small and unchanged by substitution ($\rho\cong 0.03$ in chlorobenzenes from asymmetry parameter measurements).[30] With these assumptions, we have the simplified equations

$$\Delta q(\mathrm{Cl}) = -109.6\Delta I, \qquad \Delta q(\mathrm{Br}) = -643\Delta I, \qquad (51)$$

from which the results given in Table II are obtained. Comparison of the quadrupole coupling measurements with the shielding in Table I shows certain differences between the two. Considering only the meta and para results, we find that $\Delta\sigma(m)$ is of opposite sign to $\Delta\sigma(p)$ while $\Delta q(m)$ and $\Delta q(p)$ have the same sign. This difference substantiates the important conclusion that double bonding contributes significantly to $\Delta\sigma$ in the fluorobenzenes, while consistent Δq values can be obtained without double bonding in the chlorobenzenes and bromobenzenes. Although the quantitative results are of less importance, the ΔI values found from $\Delta\sigma$ and Δq for the meta and para substitution do not appear unreasonable. Unfortunately, there are no reliable independent criteria available at present for checking these values.

TABLE I. Difluorobenzenes.

Compound	$\Delta\rho$	$\Delta\sigma(\rho)$ $\times 10^6$	$\Delta\sigma$(exptl) $\times 10^6$	$\Delta\sigma(I)$ $\times 10^6$	ΔI
Ortho	0.0093	−0.72	−2.60[a]	...	...
Meta	0.0003	−0.02	+0.30[b]	+0.32	+0.0042
Para	0.0115	−0.89	−0.65[b]	+0.24	+0.0031

[a] See work cited in footnote 24.
[b] Average of values reported in the work cited in footnote 24 and by R. W. Taft, S. Ehrenson, I. C. Lavis, and R. E. Glick, J. Am. Chem. Soc. **81**, 5352 (1959).

TABLE II. Dichloro- and dibromobenzenes.

Compound	Δq(Cl) (exptl)[a]	ΔI(Cl)	Δq(Br) (exptl)[b]	ΔI(Br)
Ortho	−2.214	(0.020)	−11.41	(0.035)
Meta	−0.628	0.0057	−4.62[c]	0.0145
Para	−0.314	0.0029	−1.88	0.0058

[a] P. J. Bray, R. G. Barnes, and R. Bersohn, J. Chem. Phys. **25**, 813 (1956).
[b] P. A. Cassabella, P. J. Bray, S. L. Segel, and R. Barnes, J. Chem. Phys. **25**, 1280 (1956).
[c] Estimated from values given in the work cited in footnote b.

Other Nonortho Fluorobenzenes

We now consider the three multifluorobenzenes (1,3,5; 1,3,4; 1,3,4,5) which have a fluorine (1) without any ortho neighbors. The change in double-bond character is calculated by the Hückel procedure used above. Further, because of the small ΔI values, the assumption is made that ΔI values are additive.[31] This is the result that would be obtained by a first-order perturbation theory approach and seems reasonable as an initial approximation. On using the calculated $\Delta\rho$ values and the appropriate ΔI contributions based on the difluorobenzenes, we obtain the results presented in Table III. Comparison of the $\Delta\sigma$ (calc) with the available $\Delta\sigma$ (exptl) shows good agreement.

Ortho Multifluorobenzenes

The remaining fluorines in the multifluorobenzenes have one or two ortho neighbors. Since we have already determined in the 1,2 compound that there is an "ortho effect," we proceed empirically. Table IV lists all the compounds for which measured values are available. The $\Delta\rho$ values and $\Delta\sigma(\rho)$ values were calculated for each case. It is seen that approximate additivity exists for $\Delta\rho$ as a function of the number of ortho and para neighbors.[31] By evaluating ΔI and $\Delta\sigma(I)$ for meta and para neighbors on the basis of additivity as before and subtracting $\Delta\sigma(\rho)+\Delta\sigma(I)$ from $\Delta\sigma$(exptl), the ortho

[27] R. W. Taft, Jr., J. Am. Chem. Soc. **79**, 1045 (1957).
[28] See the article by R. W. Taft in *Steric Effects in Organic Chemistry*, edited by M. S. Newman (John Wiley & Sons, Inc., New York, 1956).
[29] V. Jaccarino and J. G. King, Phys. Rev. **83**, 471 (1951), **94**, 1610 (1954).
[30] R. Bersohn, J. Chem. Phys. **22**, 2078 (1954); H. C. Meal, *ibid.* **24**, 1011 (1956).
[31] It is of interest that the calculated contributions to $\Delta\rho$ from the various substituents are approximately additive; i.e., $\Delta\rho$ ($1m$ or $2m$)$\sim$0, $\Delta\rho$($1o$ or 1ρ)$\sim$0.01, $\Delta\rho$($2o$ or $1o+1\rho$)$\sim$0.02, $\Delta\rho(2o+1\rho)\sim$0.03. This provides an additional justification for the assumed additivity of ΔI, which might be expected to behave similarly.

TABLE III. Nonortho multifluorobenzenes.

Compounds[a]	No. and types of neighbors	$\Delta\rho$	$\Delta\sigma(\rho)\times10^6$	ΔI	$\Delta\sigma(I)\times10^6$	$\Delta\sigma$(calc)$\times10^6$	$\Delta\sigma$(exptl)[b]$\times10^6$
1, 3, 5	$2m$	0.0006	−0.04	0.0084	+0.64	+0.60	+0.53
1, 3, 4	$1m+1p$	0.0103	−0.80	0.0073	+0.56	−0.24	−0.25
1, 3, 4, 5	$2m+1p$	0.0109	−0.85	0.0115	+0.88	+0.03	...

[a] The fluorine whose shift is being considered is italicized.
[b] See work cited in footnote 24; there is no published value for the *1*, 3, 4, 5 compound.

TABLE IV. Measured ortho fluorobenzenes.

Compound[a]	No. and types of neighbors	$\Delta\rho$	$\Delta\sigma(\rho)\times10^6$	ΔI[b]	$\Delta\sigma(I)\times10^6$	$\Delta\sigma$(exptl)$\times10^6$	$\Delta\sigma(o)\times10^6$
1, 2	$1o$	0.0093	−0.72	...	...	−2.60	−1.88
1, *2*, 4	$1o+1m$	0.0088	−0.68	0.0042	+0.32	−2.04	−1.68
1, 2, 4	$1o+1p$	0.0204	−1.59	0.0031	+0.24	−3.03	−1.68
1, 2, 4, 5	$1o+1m+1p$	0.0200	−1.55	0.0073	+0.56	−2.65	−1.66

[a] The fluorine whose shift is being considered is italicized.
[b] Only the ΔI contributions from meta and para neighbors are included.
[c] See work cited in footnote 24.

TABLE V. Predicted mono-ortho fluorobenzene shifts.

Compound[a]	No. and types of neighbors	$\Delta\rho$	$\Delta\sigma(\rho)\times10^6$	ΔI	$\Delta\sigma(I)\times10^6$	$\Delta\sigma(o)\times10^6$	$\Delta\sigma\times10^6$
1, 2, 3	$1o+1m$	0.0117	−0.91	0.0042	+0.32	−1.67	−2.23
1, 2, 3, 5	$1o+2m$	0.0109	−0.85	0.0084	+0.64	−1.67	−1.88
1, 2, 3, 4	$1o+1m+1p$	0.0210	−1.63	0.0073	+0.56	−1.67	−2.74
1, 2, 3, 4, 5	$1o+2m+1p$	0.0204	−1.59	0.0115	+0.88	−1.67	−2.38

[a] The fluorine whose shift is being considered is italicized.

contribution $\Delta\sigma(o)$, to shielding is obtained. It is evident from the results that the "ortho effect" is relatively independent of the number and types of nonortho neighbors. From the experimental values, the ortho effect is somewhat larger in magnitude (-1.88×10^{-5}) in the ortho difluoride than in the compounds which also have meta and para substituents [average of $\Delta\sigma(o)$ is -1.67×10^{-5}]. Setting $\Delta\sigma(o)=-1.67\times10^{-5}$ and calculating $\Delta\sigma(\rho)$ and $\Delta\sigma(I)$ as before, we can predict the $\Delta\sigma$ values for the remaining mono-ortho multifluorobenzenes. The theoretical results are given in Table V.

Comparing the sign and magnitude of $\Delta\sigma(o)$ with Eq. (50), we see that a negative $\Delta I(o)$, a positive $\Delta\rho(o)$, or both are required to explain the observed effect. A sufficiently large negative ΔI seems most unlikely since it would mean that two fluorines next to each other have larger negative charges than the fluorine in fluorobenzene itself. Also arguing against this is the evidence that the large ortho effect in the quadrupole coupling of the 1,2-chloro- and bromobenzenes can most easily be understood in terms of a positive ΔI, which corresponds to the result expected from the competition for electrons between neighboring substituents.[32] To explain $\Delta\sigma(o)$ in terms of $\Delta\rho$, a minimum value of $\Delta\rho(o)$ equal to approximately 0.023 is required.[33] Such a change in ρ could result from steric effects which reduced β_{CF} to 0.92. For fluorines in which the van der Waals repulsion should be negligible, the dominent interaction is electrostatic. This could lead to both bending and stretching of the CF bond. To obtain the change of β_{CF} from 1.00 to 0.92, an increase in the CF bond length of approximately 0.03 A is needed.[34] Although such a change is reasonable in terms of order-of-magnitude calculations, experimental stud-

[32] E. Scrocco, P. Bucci, and M. Maestro, J. chim. phys. **56**, 623 (1959).
[33] This minimum value is obtained for $\Delta I(o)=0$.
[34] Estimated with the exponential dependence of β on bond length suggested by H. C. Longuet-Higgins and L. Salem for CC bonds [Proc. Roy. Soc. (London) **A251, 172** (1959)].

ies of fluorobenzene structures are necessary to confirm the suggestion. At the present time, the theoretical and experimental evidence on the distortions of multihalobenzenes is unfortunately not sufficiently clear to warrant any conclusions.[35]

It should also be mentioned that some possible causes for the ortho shifts (e.g., distortion of the electron cloud by the charge on the neighboring fluorine, contribution of the magnetic anisotropy of the neighboring atom) appear to be too small by one or two orders of magnitude.[36]

V. CONCLUSIONS

By an analysis of the contributions to the magnetic shielding, a relatively simple, approximate expression for its variation with bond parameters has been developed for systems with s and p electrons in the valence shell. The formula obtained relates the chemical shift to orbital populations, which can be expressed in terms of ionic character, hybridization, and double bonding. Because of the approximations involved in the derivation, the most fruitful applications of the equations arise in the discussions of series of closely related systems. For one such series provided by the F^{19} chemical shifts in the multifluorobenzenes, the available experimental data have been interpreted in terms of differences in double bonding and ionic character. The analysis demonstrates that the changes caused by substitution in the fluorine atomic charge must be very small, on the order of 5% or less. Also, it follows from comparison of theory and experiment that double bonding in the CF bond is significant in the compounds studied. Finally, an ortho effect in the chemical shift is clearly isolated and tentatively explained in terms of charge repulsions.

The extension of the formulation to the chemical shifts in a variety of fluorine-containing compounds, as well as to other magnetic nuclei, is straightforward. It is to be hoped that these will lead to an increase in our understanding of the chemical bond.

ACKNOWLEDGMENTS

We wish to acknowledge some conversations with Dr. H. S. Gutowsky concerning the material in this paper. Also, we wish to thank the Illiac Computer Staff at the University of Illinois for providing the eigenvalue-eigenvector program used in the machine solution of the Hückel theory secular equation for the fluorobenzenes.

APPENDIX

To derive expressions analogous to Eqs. (29), (32), and (38) without the introduction of an average excitation energy, we consider the first-order perturbation function Ψ_2 obtained by applying the perturbation operator $\mathcal{H}_2$ [Eq. (5)] to the ground-state function Ψ_0[Eq. (7)]. In terms of Ψ_2, the second-order energies $\Delta E(\mu, \mu)$ and $\Delta E(\mu, H)$ have the form

$$\Delta E(\mu,\mu)=\langle\Psi_0|\mathcal{H}_2|\Psi_2\rangle+\langle\Psi_2|\mathcal{H}_2|\Psi_0\rangle+\langle\Psi_0|\mathcal{H}_0-E_0|\Psi_0\rangle \tag{A1}$$

and

$$\Delta E(\mu,H)=\langle\Psi_0|\mathcal{H}_1|\Psi_2\rangle+\langle\Psi_2|\mathcal{H}_1|\Psi_0\rangle. \tag{A2}$$

On writing $\delta\psi_j$ for the perturbation of the occupied one-electron molecular orbital ψ_j due to $\mathcal{H}_2$, we can express $\Delta E(\mu, \mu)$ as

$$\Delta E(\mu,\mu)=2\sum_j[\langle\delta\psi_j|h_0-\epsilon_j|\delta\psi_j\rangle+\sum_k(\epsilon_j-\epsilon_k)\{|\langle\psi_k|\delta\psi_j\rangle|^2+|\langle\psi_j|\delta\psi_k\rangle|^2\}$$

$$+\{\langle\psi_j|\mathcal{H}_2|\delta\psi_j\rangle+\delta\psi_j|\mathcal{H}_2|\psi_j\rangle-\sum_k\langle\psi_j|\mathcal{H}_2|\psi_k\rangle\{\langle\psi_k|\delta\psi_j\rangle+\langle\psi_j|\delta\psi_k\rangle]\}. \tag{A3}$$

By minimizing this expression with respect to variations in the ψ_j, we obtain the integral equations

$$\delta\psi_j=[1/(h_0-\epsilon_j)]\{\mathcal{H}_2\psi_j-\sum_k\langle\psi_k|\mathcal{H}_2|\psi_j\rangle\psi_k+\sum_k(\epsilon_j-\epsilon_k)\psi_k\}. \tag{A4}$$

Substitution into Eq. (A2) of the $\delta\psi_j$ determined by Eqs. (A4) yields the second-order energy required for the magnetic shielding.

For the CF bond of interest here, we have to consider four orbitals ψ_j, which correspond to the two nonbonded pairs (ψ_2 and ψ_4), the σ-bond orbital (ψ_3), and the π-bond orbital (ψ_1). The unperturbed functions for these occupied orbitals can be approximated by the expressions

$$\psi_1=a_x\phi_x^{\mathrm{F}}+(1-a_x^2)^{\frac{1}{2}}\phi_x^{\mathrm{C}}$$

$$\psi_2=\phi_y^{\mathrm{F}}$$

$$\psi_3=s_1\phi_s^{\mathrm{F}}+a_{z1}\phi_z^{\mathrm{F}}+b_{z1}\phi_z^{\mathrm{C}}$$

$$\psi_4=s_2\phi_s^{\mathrm{F}}-a_{z2}\phi_z^{\mathrm{F}} \tag{A5}$$

where ϕ_s^{F}, ϕ_x^{F}, ϕ_y^{F}, and ϕ_z^{F} represent the $2s$, $2p_x$, $2p_y$, and $2p_z$ orbitals of fluorine, and ϕ_x^{C} and ϕ_z^{C}, the

[35] C. A. Coulson and D. Stocker, Mol. Phys. **2**, 397 (1960).

[36] A perturbation calculation of the polarization of F^{19} atom electrons by the charge on an ortho neighbor yields a chemical shift which is 50 times smaller than the observed ortho effect and in the wrong direction.

$2p_x$ and $2p_z$ orbitals of carbon. From Eqs. (A4) and (A5) with neglect of carbon orbital contributions, and the assumption of equal energies ϵ for the occupied orbitals, we find

$$\delta\psi_1 = -(e\hbar/2mci)\{\mu_y a_x(h_0-\epsilon)^{-1}[(1/r^3)-(a_{z1}^2+a_{z2}^2)\langle 1/r^3\rangle]\phi_z^F - \mu_z a_z(h_0-\epsilon)^{-1}[(1/r^3)-\langle 1/r^3\rangle]\phi_y^F\}$$

$$\delta\psi_2 = -(e\hbar/2mci)\{\mu_x(h_0-\epsilon)^{-1}[(1/r^3)-(a_{z1}^2+a_{z2}^2)\langle 1/r^3\rangle]\phi_z^F - \mu_z(h_0-\epsilon)^{-1}[(1/r^3)-a_x^2\langle 1/r^3\rangle]\phi_x^F\}$$

$$\delta\psi_3 = -(e\hbar/2mci)\{\mu_y a_{z1}(h_0-\epsilon)^{-1}[(1/r^3)-a_x^2\langle 1/r^3\rangle]\phi_x^F - \mu_x a_{z1}(h_0-\epsilon)^{-1}[(1/r^3)-\langle 1/r^3\rangle]\phi_y^F\}$$

$$\delta\psi_4 = -(e\hbar/2mci)\{\mu_y a_{z2}(h_0-\epsilon)^{-1}[(1/r^3)-a_x^2\langle 1/r^3\rangle]\phi_x^F - \mu_x a_{z2}(h_0-\epsilon)^{-1}[(1/r^3)-\langle 1/r^3\rangle]\phi_y^F\}. \quad \text{(A6)}$$

On substituting these perturbation functions into Eq. (A2), we have, in terms of the definition of $\sigma^{(2)}$ given in Eqs. (1) and (27),

$$\sigma^{(2)} = \sigma_0\{(1+a_x^2)(1-a_{z1}^2-a_{z2}^2)+(1+a_{z1}^2+a_{z2}^2)(1-a_x^2)\}+(\sigma_{ex}/2)\{(1-a_{z1}^2-a_{z2}^2)(1+a_x^2)(\tfrac{1}{2}-a_{z1}^2-a_{z2}^2)$$
$$+(1-a_x^2)(1+a_{z1}^2+a_{z2}^2)(\tfrac{1}{2}-a_x^2)\}, \quad \text{(A7)}$$

where

$$\sigma_0 = -\{\sigma_d-(\sigma_{ex}/2)\}$$
$$\sigma_d = \tfrac{2}{3}(e\hbar^2/mc)\langle(h_0-\epsilon)^{-1}(1/r^3)\rangle$$
$$\sigma_{ex} = \tfrac{2}{3}(e\hbar^2/mc)\langle(h_0-\epsilon)^{-1}\rangle\langle 1/r^3\rangle. \quad \text{(A8)}$$

By using Eqs. (30) and (31), we obtain

$$\sigma^{(2)} = \sigma_0\{1-I-s+Is+\tfrac{1}{2}\rho_x+\tfrac{1}{2}(I+s-Is)\rho_x\}$$
$$+(\sigma_{ex}/16)\{-[(I+s-Is)(1-I-s+Is)](1-\rho_x)-\rho_x(1-\rho_x)(3+I+s-Is)\}. \quad \text{(A9)}$$

Equation (A9) is to be compared with Eq. (38), with the "constant" now given by Eqs. (A8) and the solutions of the appropriate integral equations. No semi-empirical average energy parameter is required. The set of terms involving $\sigma_{ex}/2$ that appear in Eq. (A9) may be regarded as corrections that would be present in Eq. (38) if Δ varied with I, s, and ρ_x. The corrections are unimportant for ρ_x small and $I \cong 0$ or $\cong 1$.

Isotropic and Anisotropic Hyperfine Interactions in Hydrazyl and Carbazyl*

N. W. LORD† AND S. M. BLINDER

Applied Physics Laboratory, The Johns Hopkins University, Silver Spring, Maryland

(Received October 12, 1960)

This paper describes a detailed experimental and theoretical study of the hyperfine structure of diphenylpicrylhydrazyl (hydrazyl) and picrylaminocarbazyl (carbazyl). Both isotropic and anisotropic hyperfine interactions involving the α and β nitrogen atoms are considered. Experimentally, electron spin resonance spectra are observed for dilute solutions of each radical in both fluid and solid media. Concentrations of the order of 0.001 M are employed so as to minimize dipolar and exchange interactions among radicals. The fluid spectra yield, in straightforward fashion, the absolute values of the isotropic coupling constants $|A_1|$ and $|A_2|$. These splitting parameters are chosen such that a synthesized line shape composed of Gaussians gives optimal reproduction of the observed resonance profile. For the solid solutions, Duco cement (with hydrazyl) and Lucite (with carbazyl) provide glassy trapping matrices. It is assumed that the radicals are frozen in an ensemble of random orientations in these solids. Appropriate theoretical line shapes, considering interactions with two magnetic nuclei, are derived, and values assigned to the anisotropic parameters B_1 and B_2 from comparison of experimental and theoretical resonance patterns. The isotropic constants are assumed to be unchanged in the transition from liquid to solid solution. It is found moreover that the inherent Gaussian half-width σ is approximately the same in both states. The parameters assigned through our analysis are Hydrazyl—$A_1=9.35\pm0.20$ gauss; $A_2=7.85\pm0.20$ gauss; $B_1=6.6\pm0.5$ gauss; $B_2=5.8\pm0.5$ gauss; $\sigma=3.36\pm0.20$ gauss. Carbazyl—$A_1=10.2\pm0.5$ gauss; $A_2=5.8\pm0.5$ gauss; $B_1=7.7\pm1.0$ gauss; $B_2=4.1\pm1.0$ gauss; $\sigma=3.4\pm0.5$ gauss. Resonance of the hydrazyl-Duco solution during incipient solidification was also observed. In this intermediate medium the anisotropic hyperfine interactions are only partially averaged out by molecular motions. It was found possible to characterize the rigidity of the medium by a parameter λ $(0\leq\lambda\leq1)$ such that each anisotropic parameter is exhibited in the spectrum as if it were λ times its full value. Various implications of our results on the structure of hydrazyl and carbazyl are considered. One conclusion drawn is that both radicals are largely planar in configuration.

I. INTRODUCTION

THE parameters which characterize the hyperfine coupling in a free radical are of considerable chemical interest since these relate to the distribution of the change and spin in the radical. These parameters may be assigned from detailed analysis of the orientation-dependent electron spin resonance (ESR) spectrum of a single crystal containing the radical. Some very thorough studies along these lines have recently been reported by three groups of workers.[1] In single-crystal studies, however, some rather formidable difficulties are often encountered. These may include preparation of the crystalline sample and its crystallographic characterization as well as analysis and interpretation of complex spectra, particularly when there is more than one molecular orientation corresponding to one crystal orientation.

We propose and illustrate in this paper an alternative to single crystal analysis. Our method is capable of yielding almost as much useful information while requiring somewhat less experimental work. The only condition for its applicability is that it be possible to observe ESR spectra of a free radical dispersed in both fluid and solid media. This holding, at least two of the three hyperfine coupling parameters can be assigned. Our procedure should be applicable to a large class of stable polyatomic free radicals.[2]

The basis of the method is the following. The hyperfine coupling consists of two parts: an isotropic part (A term) containing a single scalar parameter A, and an anisotropic part (B term) characterized by any two of the principal values of the traceless tensor $\mathfrak{B}$. In fluid medium, where the molecules are subjected to high-frequency reorientations, the tensor term is effectively averaged to zero.[3] In the solid, however, the B term combines with the A term to produce orientation-dependent ESR spectra.[4] In single crystals the resonances generally remain sharp but their frequencies become dependent on the orientation of the molecule with respect to the magnetic field. In polycrystalline media, a superposition of single-crystal resonances results and broad, widely spaced ESR lines are observed. From the positions of the peaks in the latter (and secondarily from the line shape) a second hyperfine coupling parameter may be determined. In cases of local cylindrical symmetry (*vide infra*), two parameters suffice to characterize the hyperfine interaction

* Work supported by Bureau of Naval Weapons, Department of the Navy.

† Present address: Hudson Laboratories, Columbia University, Dobbs Ferry, New York.

[1] D. K. Ghosh and D. H. Whiffen, Mol. Phys. **2,** 285 (1959); I. Miyagawa and W. Gordy, J. Chem. Phys. **30,** 1590 (1959); **32,** 255 (1960); H. M. McConnell, C. Heller, T. Cole, and R. W. Fessenden, J. Am. Chem. Soc. **82,** 766 (1960); C. Heller and H. M. McConnell, J. Chem. Phys. **32,** 1535 (1960).

[2] Extension to include unstable radicals might also be possible. This could be accomplished by observation of (a) the fluid ESR spectrum by the new steady-state technique [L. H. Piette and W. C. Landgraf, J. Chem. Phys. **32,** 1107 (1960)] and (b) the spectrum of the free radical trapped in an inert matrix [C. K. Jen, S. N. Foner, E. L. Cochran, and V. A. Bowers, Phys. Rev. **112,** 1169 (1958)].

[3] S. I. Weissman, J. Chem. Phys. **22,** 1378 (1954).

[4] We presume that the molecule is not free to rotate (or tunnel with high frequency) in the solid. Small radicals, e.g., NH_2, CH_3, may exhibit such behavior. See H. M. McConnell, J. Chem. Phys. **29,** 1422 (1958); C. K. Jen in *Formation and Trapping of Free Radicals*, edited by A. M. Bass and H. P. Broida (Academic Press, Inc., New York, 1960), pp. 237–238.

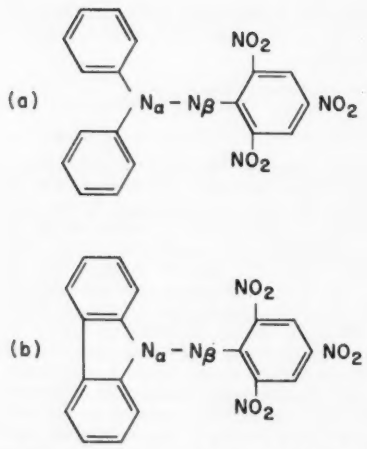

FIG. 1. Structural formulas; (a) hydrazyl, (b) carbazyl. The central nitrogen atoms are labeled by the subscripts α and β.

completely. These may unambiguously be assigned (except perhaps for sign) from correlation of the fluid and solid spectra. It is necessary that the free radicals be dispersed in a diamagnetic matrix in order to minimize dipolar and exchange interactions.

In this paper we shall apply our method to two stable organic free radicals, α, α-diphenyl-β-picrylhydrazyl (DPPH), hereafter referred to as hydrazyl, and N-picryl-9-aminocarbazyl, hereafter referred to as carbazyl (see Fig. 1).

II. GENERAL THEORY

The theoretical basis underlying this paper has been given in detail by one of the authors.[5] To be applicable to the present work, these results must be extended to the case of two magnetic nuclei interacting with an electron spin. The necessary generalization is outlined in this section.

We begin with the spin Hamiltonian for Zeeman and magnetic hyperfine interactions involving one unpaired electron and one magnetic nucleus

$$\mathcal{H}(\mathbf{S}, \mathbf{I}) = -g\mu_0 \mathbf{H}\cdot\mathbf{S} + A\mathbf{S}\cdot\mathbf{I} + \mathbf{S}\cdot\mathfrak{B}'\cdot\mathbf{I}, \quad (1)$$

with

$$A\mathbf{S} = -gg_I\mu_0\mu_N(8\pi/3)\left\langle\sum_k \delta(\mathbf{r}_k)\mathbf{S}_k\right\rangle \quad (2)$$

and

$$'\mathfrak{B}' = -gg_I\mu_0\mu_N\langle 3\mathbf{r}\mathbf{r}r^{-5} - \Im r^{-3}\rangle. \quad (3)$$

Here $\mathbf{r}_k$ is the position vector of electron k in a space-fixed coordinate system with origin at the magnetic nucleus. The three parts of (1) represent, respectively, the electron Zeeman energy, the isotropic hyperfine interaction, and the tensor hyperfine coupling. In a large magnetic field the first term is the dominant contribution to the magnetic energy of the system. We shall neglect the analogous nuclear Zeeman term.[5a] Implicit in the Hamiltonian (1) is the assumption that the electron magnetic moment is due entirely to spin. In the polyatomic free radicals under consideration in this paper, orbital momenta are almost totally "quenched" by asymmetric molecular or crystal fields. Consequently, the anisotropy in the g tensor should be rather small. We shall assume that g is effectively a scalar with value very close to that of the free electron. Experimental evidence bearing on this point will be discussed in Sec. III. Such additional complications as quadrupole coupling and spin-rotational interactions will not be considered. The expectation value brackets in (2) and (3) denote averages over the complete molecular wave function. In the B part (3), the bracket is effectively an integral over the orbital of the unpaired electron. The A term (2), however, will, in general, include contributions from other orbitals as a consequence of spin polarization (see Sec. IX).

Following footnote 5, the tensor $\mathfrak{B}'$ is transformed to its molecule-fixed principal axis system by an orthogonal transformation involving the Eulerian angles

$$\mathfrak{B}' = Q^{-1}(\theta, \phi, \chi)\mathfrak{B}Q(\theta, \phi, \chi). \quad (4)$$

The principal values of $\mathfrak{B}$ are then the diagonal elements of its matrix representation

$$\mathfrak{B} = \begin{bmatrix} B_{xx} & 0 & 0 \\ 0 & B_{yy} & 0 \\ 0 & 0 & B_{zz} \end{bmatrix}, \quad (5)$$

where

$$B_{xx} + B_{yy} + B_{zz} = 0. \quad (6)$$

The angular coordinates are defined as shown in Fig. 2.

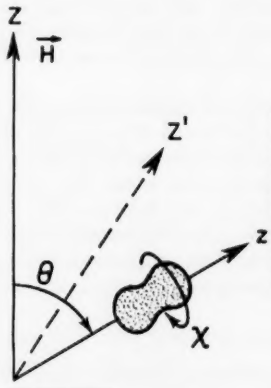

FIG. 2. Coordinate system for spin Hamiltonian. Z is the direction of the static magnetic field, z is the figure axis of the molecule, and Z', the direction of the electron spin's magnetic field at the nucleus. θ, ϕ, χ are the Eulerian angles connecting the molecule-fixed xyz axes with the space-fixed XYZ axes.

[5] S. M. Blinder, J. Chem. Phys. **33**, 748 (1960).

[5a] A N^{14} nucleus at X-band frequency (3300-gauss field) has a maximum Zeeman energy corresponding to 0.36 gauss. This may be neglected for our purposes. For protons, however, this quantity is 2.5 gauss and may no longer be negligible. In particular, satellite lines may result under such circumstances. See G. T. Trammell, H. Zeldes, and R. Livingston, Phys. Rev. **110**, 630 (1958).

The hyperfine coupling of a nucleus is characterized by three parameters: A, and two of the principal values of $\mathfrak{B}$. It is convenient for what follows to define two auxiliary parameters

$$\left.\begin{aligned} B &\equiv \tfrac{1}{2}B_{zz} = -\tfrac{1}{2}(B_{xx}+B_{yy}) \\ C &\equiv \tfrac{1}{2}(B_{xx}-B_{yy}) \end{aligned}\right\}. \tag{7}$$

In terms of the molecular wave function, these are given by

$$\left.\begin{aligned} B &= -\tfrac{1}{2}gg_I\mu_0\mu_N\langle(3z^2-r^2)/r^5\rangle \\ C &= -\tfrac{3}{2}gg_I\mu_0\mu_N\langle(x^2-y^2)/r^5\rangle \end{aligned}\right\}. \tag{8}$$

With the odd-electron charge distribution about a nucleus has at least a threefold axis of symmetry, in particular, for cylindrical symmetry, two of the principal values of $\mathfrak{B}$ become degenerate. Choosing z as the symmetry axis, C vanishes and the hyperfine interaction is now characterized by just two constants, A and B; C is evidently a measure of deviation from axial symmetry. The hyperfine coupling with some particular magnetic nucleus exhibits cylindrical symmetry if the singly occupied orbital partakes only of s and p character with reference to that nucleus. Significant admixture of higher-orbital character, for example, d or f, would, of course, introduce nonaxial contributions. If there are more than one hyperfine-coupled nuclei in the molecule, there can no longer be rigorous cylindrical symmetry about any one. However, should the unpaired electron's orbital still contain principally s and p character about some nucleus, we would ascribe to that nucleus "local cylindrical symmetry." In most cases, we might expect the deviation from rigorous cylindrical symmetry to be quite small whenever local cylindrical symmetry prevails. It is important to note that for a prolate charge distribution, $B>0$. This too will obtain whenever the orbital contains predominantly s and p character. As we shall subsequently show, hydrazyl and carbazyl exhibit, to good approximation, local cylindrical symmetry about both central nitrogen nuclei. Hence, we shall be particularly concerned with results pertaining to this special case.

We wish now to compute the orientation-dependent eigenvalues of the spin Hamiltonian. This is most conveniently approached by perturbation theory, the electronic Zeeman coupling serving as the unperturbed Hamiltonian, the hyperfine terms as perturbation operators. Carrying the perturbation expansion to first order we obtain

$$E(M_S, M_I') = -g\mu_0 HM_S + K(\theta,\chi)M_SM_I', \tag{9}$$

where

$$\begin{aligned} K^2 = {} & A^2+2AB(3\cos^2\theta-1)+B^2(3\cos^2\theta+1) \\ & +C^2\sin^2\theta+2C(A-B)\sin^2\theta(\cos^2\chi-\sin^2\chi). \end{aligned} \tag{10}$$

Physically speaking, the electron spin is coupled strongly to the external field $\mathbf{H}$. Thus only the Z component of $\mathbf{S}$ is stationary. Presuming, as before, that hyperfine terms are much larger than nuclear Zeeman terms, the nuclear spin is most strongly coupled to the electron's tensor field. Consequently, the two spins have, in general, different axes of quantization. The first-order perturbation treatment turns out to be equivalent to finding an effective axis of quantization for the nuclear spin. This axis, denoted by Z' in Fig. 2, represents the direction of the electron spin's magnetic field at the nucleus. M_I' in Eq. (9) is then the quantized component of $\mathbf{I}$ along Z'.

If the odd-electron charge density has axial symmetry in the locality of the magnetic nucleus, then $C=0$ and the lower line of the expression for K [Eq. (10)] vanishes. All dependence on the angle χ is thereby removed to accuracy of first order. It is not necessary for our purposes to carry the perturbation expansion beyond first order. For X-band spectroscopy, transitions arising from second-order mechanisms are of considerably reduced intensity.[6]

In first order, the selection rules for ESR transitions are $\Delta M_S=\pm1$, $\Delta M_I'=0$. The observed hyperfine frequency shifts for cylindrical symmetry are given by

$$\nu = [A^2+2AB(3\cos^2\theta-1)+B^2(3\cos^2\theta+1)]^{\frac{1}{2}}M_I'. \tag{11}$$

When $|A|\gg|B|$, the root may be expanded to yield the familiar $(3\cos^2\theta-1)$-angular dependence. Equation (11) applies to an oriented single crystal. In a polycrystalline sample we would observe the ensemble distribution of single crystal resonances. The range of resonance absorption is then bracketed by the frequencies $|A-B|M_I'$ and $|A+2B|M_I'$.

We denote the theoretical shape of the powder spectrum by $g(\nu)$. This is a sum of $2I+1$ component line-shape functions, one for each M_I',

$$g(\nu) = \sum_{M=-I}^{I} g_M(\nu). \tag{12}$$

If each component is normalized to unity [with $g_0(\nu)=\delta(\nu)$], $g(\nu)$ is normalized to $2I+1$. The fraction of molecules (or crystallites) having polar angle between θ and $\theta+d\theta$ is $\frac{1}{2}\sin\theta d\theta$. The corresponding resonance frequencies are denoted by ν and $\nu+d\nu$. We have thus

$$g_M(\nu)d\nu = \tfrac{1}{2}\sin\theta d\theta, \tag{13}$$

ν being implicitly dependent on θ through (11). Consequently,

$$g_M(\nu) = -\tfrac{1}{2}(d\cos\theta)/d\mu = -\tfrac{1}{2}[d\nu/(d\cos\theta)]^{-1}. \tag{14}$$

For convenience, we may label the high-frequency ($\nu>0$) part of the spectrum with $M>0$, the low-

[6] In higher frequency ranges, say the K band, second-order transitions may become important. See I. Miyagawa and W. Gordy, J. Chem. Phys. **32**, 255 (1960).

frequency part ($\nu<0$) with $M<0$. Accordingly, a normalized hyperfine component line shape is given by

$$g_M(\nu)=\frac{\nu(\theta)}{(6AB+3B^2)M^2\cos\theta}. \tag{15}$$

It is necessary now to derive a corresponding expression for two magnetic nuclei. In general, the $\mathfrak{G}$ tensor will have a different set of principal axes about each nucleus, depending upon the local electron spin distribution. Consequently, the angular specification of molecular orientation will be different for each nucleus. The dependence of the composite hyperfine structure on the orientation of the molecule will be thus a rather complicated function of the various θ's and χ's. The composite line shape does, however, assume a simple form if for both nuclei there is cylindrical symmetry *with the two z axes parallel*. Then the same angle θ pertains to either nucleus and may be ascribed to the molecule as a whole. Composite hyperfine frequency shifts are sums (or differences) of those for the individual nuclei, i.e.,

$$\nu_{M_1M_2}=\nu_{M_1O}+\nu_{OM_2}. \tag{16}$$

Denoting by $g_{M_1O}(\nu)$ and $g_{OM_2}(\nu)$ the powder line shape associated with nucleus 1 and 2, we may write, analogous to (14)

$$\left.\begin{aligned}\frac{1}{g_{M_1O}(\nu)}&=-2\frac{d\nu_{M_1O}}{d\cos\theta_1},\\ \frac{1}{g_{OM_2}(\nu)}&=-2\frac{d\nu_{OM_2}}{d\cos\theta_2}\end{aligned}\right\}. \tag{17}$$

Also,

$$\frac{1}{g_{M_1M_2}(\nu)}=-2\frac{d\nu_{M_1M_2}}{d\cos\theta}, \tag{18}$$

where $g_{M_1M_2}(\nu)$ is the composite line shape. Since $\theta_1=\theta_2=\theta$, it follows that

$$\frac{1}{g_{M_1M_2}(\nu)}=\frac{1}{g_{M_1O}(\nu)}+\frac{1}{g_{OM_2}(\nu)}, \tag{19}$$

the equality holding for each value of θ. The $g_{M_1M_2}(\nu)$ is suitably normalized to unity. The over-all composite line shape is then

$$g(\nu)=\sum_{M_1=-I_1}^{I_1}\sum_{M_2=-I_2}^{I_2}g_{M_1M_2}(\nu) \tag{20}$$

and is normalized to $(2I_1+1)(2I_2+1)$.

In discussing line shape we have, thus far, neglected the influence of other factors. The latter might include dipolar broadening, exchange interaction, anisotropy in g, unresolved hyperfine structure associated with other magnetic nuclei, as well as various factors inherent in the experimental procedure, e.g., field homogeneity, power saturation, and field modulation. Additional broadening of the two-nucleus line shape would also occur should there be any deviation from parallelism of the principal axis systems. The line shape from all factors excluding hyperfine angular dependence may generally be represented by either a Gaussian or a Lorentzian distribution function. The observed line shape might then be approximated by an integral transformation of $g(\nu)$

$$g_{\exp}(\nu)=\int d\nu' g(\nu')G(\nu-\nu'), \tag{21}$$

where the kernel $G(\nu-\nu')$ specifies the inherent broadening. In this paper we shall use Gaussians for the $G(\nu-\nu')$ with parameters inferred from the corresponding spectra in fluid media.

Usually it is the derivative of $g_{\exp}(\nu)$ which is observed directly. Since the functions $g_M(\nu)$ are discontinuous at the frequencies $|A-B|M$ and $|A+2B|M$, we might expect maxima and minima in $g_{\exp}'(\nu)$ to occur close to these frequencies (and the corresponding ones for the composite lines). These provide important clues in the assignment of the B parameters from the solid spectra.

III. HYDRAZYL AND CARBAZYL

Several tri-aryl-substituted hydrazyl free radicals have been found to be stable at room temperature. The most extensively studied of these, diphenylpicrylhydrazyl, was first prepared in 1922.[7] During the past ten years, the technique of electron spin resonance has stimulated renewed interest in this class of free radicals.

Resonance absorption by crystalline hydrazyl was first reported by Holden, *et al.*,[8] and by Townes and Turkevich.[9] The sharpness of the resonance was attributed by the latter authors to strong exchange interactions between radicals.[10] Hutchison, Pastor, and Kowalsky[11] resolved hyperfine structure for hydrazyl dissolved in benzene. Dilution to approximately 0.001 M was found necessary in order to minimize dipolar and exchange interactions which would otherwise obscure the hyperfine structure. They observed five equally spaced components (10-gauss intervals, five-gauss half-widths) which they attributed to equal interactions with the two central nitrogen nuclei. Schneider[12] studied the resonance of hydrazyl dispersed in solidified plastics (1% solutions in perspex

[7] S. Goldschmidt and K. Renn, Ber. deut. chem. Ges. **55,** 628 (1922).

[8] A. N. Holden, C. Kittel, F. R. Merritt, and W. A. Yager, Phys. Rev. **77,** 147 (1950).

[9] C. H. Townes and J. Turkevich, Phys. Rev. **77,** 148 (1950).

[10] J. H. Van Vleck, Phys. Rev. **74,** 1168 (1948); M. H. L. Pryce and K. W. H. Stevens, Proc. Phys. Soc. (London) **A63,** 36 (1950).

[11] C. A. Hutchison, R. C. Pastor, and A. G. Kowalsky, J. Chem. Phys. **20,** 534 (1952). Similar results for hydrazyl were reported later by Jarrett (see footnote 17) and by Kikuchi and Cohen (see footnote 18).

[12] E. E. Schneider, Discussions Faraday Soc. **19,** 158 (1955).

and in polystyrene) as well as in liquid solvents. He observed quintets in both liquid and solid solutions with spacings of 10 and 20 gauss, respectively. The increased splitting in the solid was attributed to the appearance of the anisotropic terms. Van Roggen, *et al.*[12a] have also studied dilute solutions of hydrazyl in liquid and frozen benzene.

Most recently, Holmberg, Livingston, and Smith[13] have observed the resonance of small concentrations of hydrazyl in oriented crystals of the parent hydrazine. They have thereby assigned values to both the isotropic and anisotropic hyperfine parameters. However, since these assignments are based on measurement of integrated ESR absorption, rather than on its derivative, we do not believe them to be as reliable quantitatively as ours. This conclusion is further supported by the fact that the isotropic constants assigned to the solid are completely different from those in solution—a result which we consider inadmissible.

Evidence for hyperfine coupling with the protons in hydrazyl was found by Beljers, *et al.*[14] They observed enhancement of the proton resonance when the electron spin resonance was saturated (Overhauser effect). Resolution of the proton hyperfine structure has recently been achieved by Deguchi[15] by using oxygen-free solvents.[15a]

Carbazyl was first synthesized by Turkevich; its resonance in the crystalline state was observed by Cohen, Kikuchi, and Turkevich.[16] Jarrett[17] and Kikuchi and Cohen[18] studied its resonance in dilute solution and obtained seven resolved peaks. This pattern was shown to be consistent with the supposition that the hyperfine coupling constants of the two nitrogen atoms are in approximately 2:1 ratio.

Of considerable pertinence to our work are the papers of Weissman and co-workers[19-21] on the paramagnetic ion peroxylamine disulfonate $(SO_3)_2NO^{--}$. The hyperfine structure of this ion is due entirely to the nitrogen nucleus. This we might regard as the isolation of one of the interactions present in the hydrazyl radicals. In liquid solution a triplet with 13-gauss interval is observed.[19] At concentrations of 0.001 M in chloroform the individual linewidth is reduced to less than 0.5 gauss (full width).[20] Weissman and Banfill[21] have also observed the resonance of a single crystal of diamagnetic potassium hydroxylamine disulfonate containing a small concentration (0.25 mole %) of dispersed $(SO_3)_2NO^{--}$. A highly anisotropic spectrum was reported with triplet interval varying between the limits of 6 and 27 gauss.

On the basis of our theory (Sec. II), these results may be very easily explained. If we assign the parameters $|A|=13$ gauss, $|B|=7$ gauss with the same sign as A, $C\approx 0$, then the single crystal resonances will always fall in the field range $|A-B|M=6$ gauss to $|A+2B|M=27$ gauss. A particularly gratifying feature is the fact that the spectrum is consistent with $C\approx 0$.[22] Thus the distribution of the unpaired electron in the neighborhood of the nitrogen nucleus is very nearly cylindrically symmetrical. We shall assume that this holds true also around the two central nitrogen nuclei in hydrazyl and carbazyl. Thus the specializations of the theory for local cylindrical symmetry shall pertain. We shall also suppose, initially for convenience in computation, that the symmetry axes for the two charge distributions are more or less parallel. The essential consistency of the observed spectra with this hypothesis (see Secs. VI, VIII) does indeed justify its validity. We note further that, since orbitals containing principally s and p character are prolate, then $B>0$ for nitrogen hyperfine couplings. For peroxylamine disulfonate we have consequently $A>0$. Our analysis shall establish also, for hydrazyl and carbazyl, that both isotropic coupling constants are positive (presuming both B's are positive). It has been established experimentally that the isotropic coupling constants are positive for atomic nitrogen[23] and for nitric oxide.[24] Thus a rather consistent pattern emerges with regard to the signs of nitrogen coupling constants. We shall return to this discussion on a more quantitative level in Sec. IX.

It was assumed in Sec. II that anisotropy in the g tensor could be neglected. We shall now see how closely this idealization is realized. Kikuchi and Cohen,[18] using single crystals, found that the range of variation in g with orientation amounts to 2.4 gauss in carbazyl and $\sim$1 gauss in hydrazyl (both at 9400 Mc). Livingston and Zeldes[24a] report 1.2 gauss for the latter. Figures 14 and 15 of footnote 18 indicate very clearly how the anisotropy in g affects polycrystalline spectra. Principally, it contributes an additional source of broaden-

[12a] A. von Roggen, L. van Roggen, and W. Gordy, Phys. Rev. **105,** 50 (1957).
[13] R. W. Holmberg, R. Livingston, and W. T. Smith, J. Chem. Phys. **33,** 541 (1960).
[14] H. G. Beljers, L. Van der Kint, and J. S. Van Wieringen, Phys. Rev. **95,** 1683 (1954).
[15] Y. Deguchi, J. Chem. Phys. **32,** 1584 (1960).
[15a] Our hydrazyl line shapes accordingly represent envelopes of the fully resolved proton hyperfine structures.
[16] V. W. Cohen, C. Kikuchi, and J. Turkevich, Phys. Rev. **85,** 379 (1952).
[17] H. S. Jarrett, J. Chem. Phys. **21,** 761 (1953).
[18] C. Kikuchi and V. W. Cohen, Phys. Rev. **93,** 394 (1954).
[19] G. E. Pake, J. Townsend, and S. I. Weissman, Phys. Rev. **85,** 682 (1952); **89,** 606 (1953).
[20] T. L. Chu, G. E. Pake, D. E. Paul, J. Townsend, and S. E. Weissman, J. Phys. Chem. **57,** 504 (1953).
[21] S. I. Weissman and D. Banfill, J. Am. Chem. Soc. **75,** 2534 (1953).

[22] When $C\neq 0$, the range of resonance contains the three field values $|A+2B|M$, $|A-B+C|M$, and $|A-B-C|M$. This set contains both the largest and the smallest field value of the theoretical line shape, as may be deduced from Eq. (10). Given that the two extremes are 6 and 27 gauss and that $|A|=13$ gauss, it is impossible to choose a consistent set A, B, C unless $C=0$.
[23] L. W. Anderson, F. M. Pipkin, and J. C. Baird, Phys. Rev. **116,** 87 (1959).
[24] R. Beringer and J. G. Castle, Phys. Rev. **78,** 581 (1950); R. Beringer, E. B. Rawson, and A. F. Henry, *ibid.* **94,** 343 (1954).
[24a] R. Livingston and H. Zeldes, J. Chem. Phys. **24,** 170 (1956).

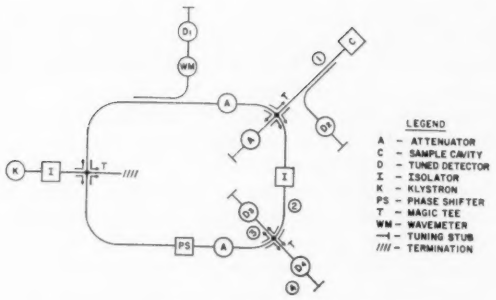

FIG. 3. Balanced bolometer detection system.

ing with half-width 1–2 gauss. In pure polycrystalline samples of these radicals the g anisotropy determines the line shape. The lines are then somewhat asymmetric, the peak being as much as 1 gauss removed from the centroid. However, in dilute solid solutions, where exchange interactions are eliminated and gaussian broadening mechanisms come into play, the symmetry of the polycrystalline profiles is effectively restored. For hydrazyl at least, no asymmetry can be detected in our solid line shapes (see Figs. 7 and 8). In fluid media, of course, the g anisotropy averages out in the same way as the hyperfine anisotropy.

It is not known with certainty which coupling constant is associated with which nitrogen in either hydrazyl or carbazyl. There is some theoretical justification for one particular choice, as will be seen in Sec. IX. An unambiguous assignment could be made through isotopic substitution with N^{15}, as suggested by Hutchison[11] and others. In this paper we shall arbitrarily label the larger coupling constants with the subscript 1, the smaller with the subscript 2.

IV. EXPERIMENTAL

Preparation of the Free Radicals[25]

The precursor substances, diphenylpicrylhydrazine (mp 176°C) and picrylaminocarbazole (mp 238°C), were oxidized with finely divided PbO_2 to the corresponding free radicals. The reactions were carried out immediately before each resonance measurement. Benzene or chloroform was generally used as the solvent. It was also found possible to use silicone fluid for low concentrations of radical. The solid solutions were prepared by initially dissolving the crystalline radicals in polymerizing fluids (Duco cement or Lucite). Hydrazyl was recrystallized from benzene-hexane solution and gave an mp of 129°C. Carbazyl was obtained by evaporation of the solvent and had an mp range of 205–215°C.

[25] All samples of hydrazyl and carbazyl were synthesized by Martin L. Peller and Monica R. Nees in this laboratory.

Microwave Detection

To observe ESR absorption we used a balanced-bolometer homodyne system[26] operating at around 9300 Mc. This system is shown schematically in Fig. 3. The klystron frequency could be stabilized to either the sample cavity resonance or that of the reference wave meter using D_1 or D_2. For the present set of experiments the sample cavity resonance was used. Microwave energy at levels between 1 and 10 mw is sent through arm 1 to the sample through the cavity iris. The latter is small enough to keep the cavity slightly undercoupled. The reflected signal goes back through Magic Ree A; the isolation arm 2 is superposed on the reflection from the tuned arm of the bridge. The bridge is balanced in order to give in arm 2 a small signal proportional to the change in cavity absorption due to magnetic resonance. The signal in arm 2 is now split equally at Magic Tee B and goes to arms 3 and 4 where it is mixed with about 16 mw of coherent microwave energy from the klystron. Thus the original signal from arm 2 is amplified. The bolometers present a signal proportional to $V\Delta V$, V being the signal voltage in arms 3 and 4 and ΔV, the voltage change caused by the change in sample cavity absorption during resonance. The phase of the large coherent signal V is adjusted to match that of ΔV, the signal in arm 2. The dc bias power on the bolometers is also 16 mw in accordance with the conditions for optimum sensitivity (bias power equal to rf power, their sum as high as bolometers will take without burning out). The two elements in what is effectively a tunable balanced mixer operate in push-pull into a transformer circuit which matches their impedance to that of a hushed transistor amplifier (noise figure 3 db). The signal is finally amplified, rectified and recorded using conventional apparatus.

Magnetic Field and ESR Recording

The sample cavity, operating in the TE_{102} mode, is placed between the poles of a Varian 4012-3B magnet with the broad face parallel to the pole face. The sample pole is the center of the short face with the sample in a 4-mm quartz tube lying in the nodal plane of the E field. By means of small coils rigidly attached onto the broad faces of the cavity, the magnetic field is sinusoidally modulated at a frequency of 100 cps with amplitude in the range 2.5–10 gauss. The detection amplifiers are tuned to 100 cps and thus present a signal proportional to the field derivative of the magnetic resonance absorption. Phase demodulation to a recorded dc voltage is effected in a special self-balanced diode circuit[27] with an output filter network

[26] G. Feher, Bell System Tech. J. **36**, 449 (1957).

[27] R. E. Gorozdos and R. L. Konigsberg, The Johns Hopkins University Applied Physics Laboratory, Technical Rept. CM–913, September, 1957.

limiting the signal bandwidth to 0.1–10 cps. The steady magnetic field is swept triangularly back and forth at 1 cps. This reversal eliminates errors due to response lags in the train of detection circuits. Precise measurements of the field were obtained by means of a proton resonance probe a few centimeters from the sample.

V. HYDRAZYL IN FLUID

Dilute solutions (approximately 0.001 M) of hydrazyl in benzene, chloroform, and silicone fluid exhibited practically identical spectra. No influence of anisotropic hyperfine interaction was apparent. Figure 4 shows a typical spectrum in benzene solution. The

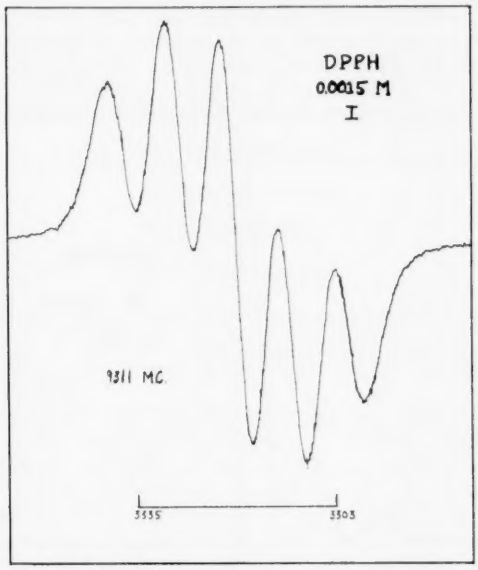

FIG. 4. Resonance of hydrazyl in benzene solution.

five-peak pattern is in qualitative agreement with earlier work on dilute solutions of hydrazyl.[11,16,17] Hutchison, Pastor, and Kowalsky[11] had attributed this spectrum to approximately equal isotropic interactions with the two nitrogens, estimating that

$$|A_1| \approx |A_2| \approx 10 \text{ gauss}.$$

By a more detailed analysis of the spectrum, outlined below, we have been able to make more exact assignments of the isotropic coupling constants. The underlying pattern for the isotropic hyperfine splitting is shown in Fig. 5. It is apparent that the intervals between centroids of the fine line clusters are equal even when the two constants $|A_1|$, $|A_2|$ are different. The width of each cluster does, however, depend on $|A_1|-|A_2|$. We denote by σ^* the second moment of a line cluster and by σ the Gaussian half-width of each component line (presumed all equal). It may be shown that

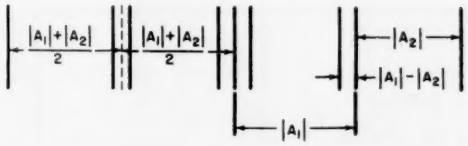

FIG. 5. Basic pattern for isotropic hyperfine interaction in hydrazyl.

$$\sigma_2^* = [\sigma^2 + \tfrac{1}{4}(|A_1| - |A_2|)^2]^{\frac{1}{2}} \tag{22}$$

for a two-component cluster and

$$\sigma_3^* = [\sigma^2 + \tfrac{2}{3}(|A_1| - |A_2|)^2]^{\frac{1}{2}} \tag{23}$$

for a three-component cluster. Furthermore, in both cases, σ^* is very nearly equal to the distance from centroid to point of maximum slope in a line cluster, indicating that the cluster shape is also essentially gaussian.

The over-all line shape was accordingly represented by a superposition of five equally-spaced Gaussians in intensity ratio 1:2:3:2:1 with half-widths σ, σ_2^*, σ_3^*, σ_2^*, σ, respectively. The following choice of parameters was found to best reproduce the experimental line shape:

$$|A_1| = 9.35 \pm 0.20 \text{ gauss},$$
$$|A_2| = 7.85 \pm 0.20 \text{ gauss},$$
$$\sigma = 3.36 \pm 0.20 \text{ gauss}.$$

The synthesized resonance spectrum with these parameters is drawn in Fig. 6. Here, and in what follows, the limits of error are estimated by constructing curves for neighboring values of the parameters. The cluster approximation agrees very closely with the rigorous nine-Gaussian line shape corresponding to the same constants (the latter used for Fig. 6).

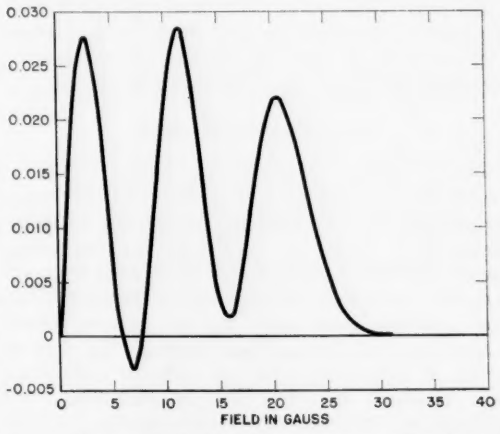

FIG. 6. Hydrazyl in liquid: theoretical resonance line shape.

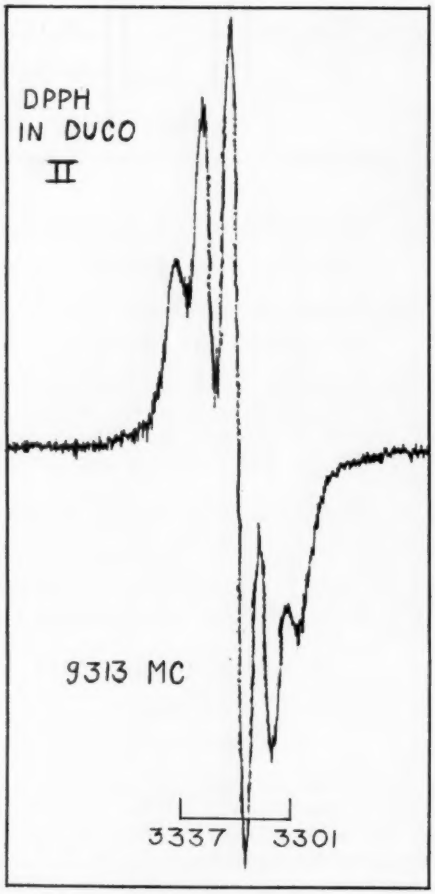

FIG. 7. Resonance of hydrazyl in semifluid Duco cement. (The observation was made one day after the solution was prepared.)

Recently, Deal and Koski[28] have reported a determination of the ratio $|A_2/A_1|=0.82$ in close accord with our value of 0.84. No estimates of the coupling constants themselves are given by these authors.

VI. HYDRAZYL IN SOLID

Figure 7 shows the spectrum of hydrazyl dispersed in semi-fluid Duco cement. Here the anisotropic hyperfine terms begin to manifest themselves, indicating hindrance to molecular motions in the increasingly viscous medium. A detailed discussion of the fluid-solid transition is given in the next section. Eventually, the Duco hardens completely (as the acetone solvent evaporates) and the spectrum shown in Fig. 8 is observed. It is assumed that the hydrazyl radicals are here completely frozen in random orientations. The resonance line shape should thereby be governed by the theory of Sec. II. The solid spectrum is considerably more difficult to analyze than the liquid spectrum. Relative signs as well as magnitudes of the four interaction constants are now significant. We note that the spectrum retains its five-peak structure, the components being, however, broadened and their spacing increased to about 21 gauss. It was originally supposed that these peaks corresponded to the maxima in the solid spectra, i.e., to the frequencies $|A-B|M$, etc. This would lead to values for B in the neighborhood of 12 gauss with opposite signs from the A's.[29] These constants, in addition to being rather implausible on theoretical grounds, do not provide an accurate fit of the experimental derivative spectrum, particularly as concerns the widths of the individual lines. If, on the other hand, the solid peaks (exclusive of the central one) are presumed to correspond to the $|A+2B|M$ ends of the component lines, then an excellent fit of the experimental spectrum may be obtained. The optimal

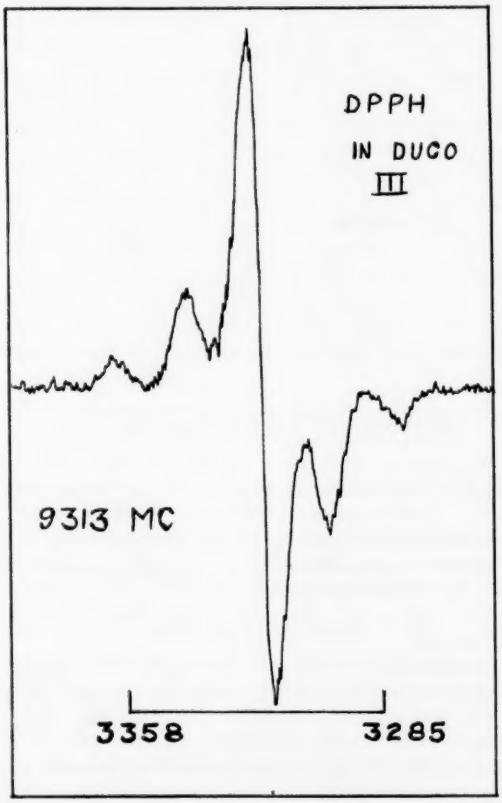

FIG. 8. Resonance of hydrazyl in hardened Duco cement.

[28] R. M. Deal and W. S. Koski, J. Chem. Phys. **31,** 1138 (1959).

[29] Such an assignment was reported by us during a preliminary stage of this work: N. W. Lord and S. M. Blinder, Bull. Am. Phys. Soc. **5,** 72 (1960).

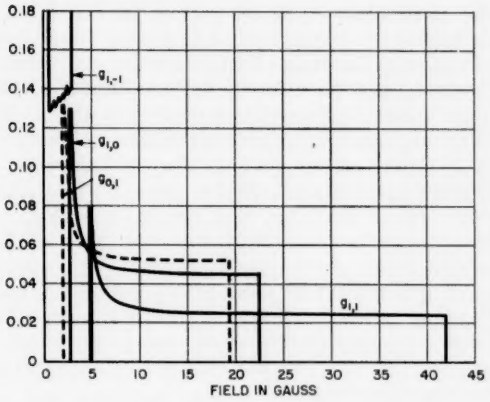

FIG. 9. Hydrazyl in solid: components of theoretical line shape.

set of constants determined in this fashion is:

$$A_1=9.35\pm0.20 \text{ gauss};$$

$$A_2=7.85\pm0.20 \text{ gauss};$$

$$B_1=6.6\pm0.5 \text{ gauss};$$

$$B_2=5.8\pm0.5 \text{ gauss}.$$

The uncertainty in the anisotropic parameters is larger since, in addition to the solid analysis being more tedious, any error in the isotropic parameters is compounded.

Each isotropic parameter has the same sign as its corresponding anisotropic parameter. Since it is highly probable that both B's are positive (see Sec. III), all four hyperfine coupling constants are almost certainly positive. The ambiguity in the signs of the isotropic parameters is thereby removed. The components of the theoretical line shape (with no Gaussian broadening)

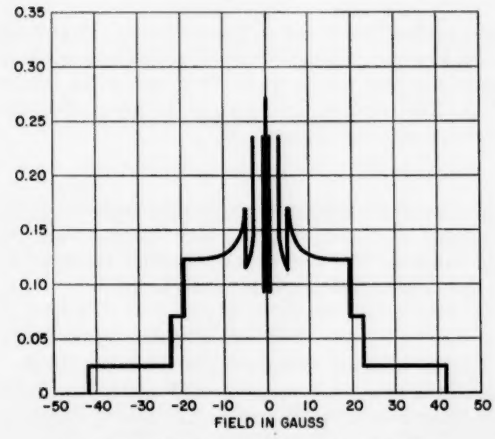

FIG. 10. Hydrazyl in solid: theoretical line shape.

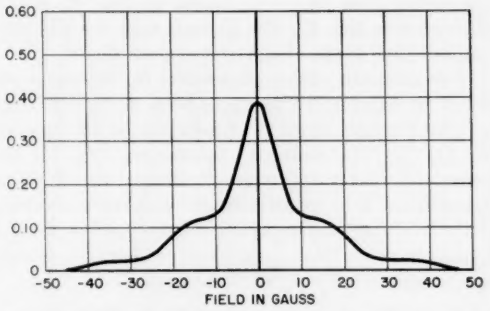

FIG. 11. Hydrazyl in solid: theoretical line shape with Gaussian broadening.

are drawn in Fig. 9. Figure 10 shows the complete theoretical profile. The outer edges of the g_{01} and g_{10} component functions are quite close together, which accounts for the five-line structure of the solid spectrum. The solid line shape is also critically dependent on the Gaussian broadening parameter. It is noteworthy that an excellent fit can be obtained by using the liquid value, $\sigma=3.36$ gauss, for each component line in the solid. This would indicate that the principal source of line broadening is the same in both phases, presumably unresolved hyperfine interaction with the other magnetic nuclei. The Gaussian transform of the

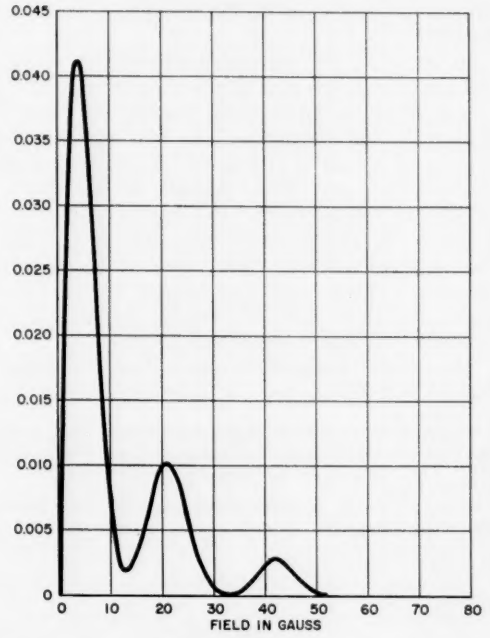

FIG. 12. Hydrazyl in solid: derivative of theoretical line shape. (This is the theoretical construction of the spectrum shown in Fig. 8.)

theoretical line shape is shown in Fig. 11 and its derivative in Fig. 12. The latter is then the theoretical construction of the observed spectrum Fig. 8.

To summarize, three parameters B_1, B_2, and σ were fitted to theoretical line shapes such as Eq. (19) so as to give the best possible reproduction of the spectrum in Fig. 8. The isotropic parameters, A_1, A_2 were presumed to remain constant during the fluid-solid transition. The quantitatively excellent agreement between theory and experiment constitutes *a posteriori* verification for the hypotheses of local cylindrical symmetry and near parallelism of axes.

VII. HYDRAZYL. INTERMEDIATE STATE

We shall now discuss in greater detail the hyperfine structure of the resonance during the transition from liquid to solid solution. The nature of the medium manifests itself in spin-resonance experiments in the mode of averaging the spin Hamiltonian over its orientation variables. Presuming that such molecular motions are governed by the theory of random processes,[30] the medium may be characterized by a correlation time τ_c. This parameter represents some effective average time during which a molecular orientation persists, or alternatively, the average time between reorienting collisions. A well-known application of this concept was made by Debye[31] in his study of dielectric dispersion in polar liquids. The importance of the correlation time in magnetic resonance was made evident by the work of Bloembergen, Purcell, and Pound.[32]

In our case, the orientation-dependent features of the spectra are governed by the relative magnitude of τ_c and h/A, the latter being roughly the period of nuclear Larmor precession. The two extreme cases, $h/A \gg \tau_c$ and $\tau_c \gg h/A$ characterize the liquid and solid states respectively. These present no difficulties in analysis or interpretation. The intermediate case, in which τ_c and h/A become comparable, is a different matter entirely. A very viscous fluid would fall in this category.[33] Theory must now account for the exceedingly complex interplay of hyperfine interactions and molecular motions of comparable frequency.

McConnell,[34] following the approach of Bloembergen, Purcell, and Pound, gave an approximate analysis of the intermediate state as applied to line breadth. Analogous procedures applied to explicit computation of resonance line shapes for intermediate states would, however, prove prohibitively difficult. Moreover, there arises a more fundamental question as to whether it is valid to regard molecular orientations as being instantaneously determinate in the classical sense. A rigorous quantum-mechanical approach[35] would necessitate extension of the Hamiltonian to include the effects of molecular reorientations and collisions. The random nature of the latter interactions might then be taken into account by some quantum-statistical technique. In the absence of any full treatment, along either classical or quantum-mechanical lines, we are forced to seek some less exact model to account for the effects of random molecular motion.

To facilitate our treatment, we rewrite the hyperfine interaction terms of the spin Hamiltonian (1) in the form

$$\mathcal{U}(M_S, \mathbf{I}) = M_S\{\alpha(\Omega) I_X + \beta(\Omega) I_Y + [A + \gamma(\Omega)] I_Z\}, \tag{24}$$

where $\alpha(\Omega)$, $\beta(\Omega)$ and $\gamma(\Omega)$ are functions of molecular orientation and of the anisotropic parameters B and C. The explicit forms of α, β and γ are given in footnote 5. For the present, we need only know that

$$\int d\Omega\alpha(\Omega) = \int d\Omega\beta(\Omega) = \int d\Omega\gamma(\Omega) = 0, \tag{25}$$

and that α, β, and γ are linear and homogeneous in B and C. The averages of these functions for some particular mode of molecular motion are denoted by $\langle\alpha\rangle_{Av}$, $\langle\beta\rangle_{Av}$, and $\langle\gamma\rangle_{Av}$. Representing the relative probability of an orientation Ω during a time h/A by the distribution function $\rho(\Omega)$, we have

$$\langle\alpha(\Omega)\rangle_{Av} = (1/4\pi)\int d\Omega\rho(\Omega)\alpha(\Omega), \tag{26}$$

and similarly for β and γ. When $h/A \gg \tau_c$, all elements of solid angle are available to the molecule many times over and with equal probability during an interval h/A. The distribution function is spherically symmetrical and when normalized,

$$\rho_0(\Omega) = 1,$$

the subscript 0 being used to label the liquid state. The averages $\langle\alpha(\Omega)_0\rangle_{Av}$, $\langle\beta(\Omega)_0\rangle_{Av}$, and $\langle\gamma(\Omega)_0\rangle_{Av}$ are just the integrals (25) and all vanish. Thus the hyperfine operator in liquids assumes the simple form

$$\langle\mathcal{U}_0\rangle_{Av} = AM_S I_Z. \tag{27}$$

In the opposite extreme $\tau_c \gg h/A$ each molecule is restricted to a small range of solid angle. We idealize the latter as a single orientation Ω_k, differing, in general,

[30] Excellent reviews of physical applications of random function theory are given by S. Chandrasekhar, Revs. Modern Phys. **15**, 1 (1943) and by M. C. Wang and G. E. Uhlenbeck, *ibid.* **17**, 323 (1945).

[31] See, for example, P. Debye, *Polar Molecules* (Dover Publications, New York, 1945), Chap. V.

[32] N. Bloembergen, E. M. Purcell, and R. V. Pound, Phys. Rev. **73**, 679 (1948).

[33] According to Bloembergen, Purcell, and Pound, the viscosity is related to the correlation time by

$$\tau_c \approx 4\pi\eta a^3/3kT,$$

where a is the effective Stokes' law radius. When $\tau_c \sim h/A$, the viscosity of our hydrazyl-Duco solution is thus of the order of 100 cp.

[34] H. M. McConnell, J. Chem. Phys. **25**, 709 (1956).

[35] Probably beyond the scope of present theoretical understanding of the liquid state.

for each molecule k, and write

$$\rho_1(\Omega)=\delta(\Omega-\Omega_k),$$

the subscript 1 denoting the solid state. We find then that

$$\langle\alpha(\Omega)_1\rangle_{Av}=\alpha(\Omega_k), \quad \text{etc.} \tag{28}$$

By superposition of the ensemble distribution of hyperfine interactions (for all orientations Ω_k) we arrive at the polycrystalline spectra of Sec. II.

We are faced now with a choice of some parametric representation of the continuum of intermediate states. To this end, we postulate that there exists a parameter $\lambda(0\leq\lambda\leq 1)$ which characterizes the degree of transition from the liquid to the solid state. More concretely, we assume that the distribution function for the intermediate state depends linearly on λ. Accordingly, we have

$$\begin{aligned}\rho_\lambda(\Omega)&=(1-\lambda)\rho_0(\Omega)+\lambda\rho_1(\Omega)\\&=1-\lambda+\lambda\delta(\Omega-\Omega_k).\end{aligned} \tag{29}$$

Integration over Ω yields the averages

$$\langle\alpha(\Omega)_\lambda\rangle_{Av}=\lambda\alpha(\Omega_k), \quad \text{etc.} \tag{30}$$

The term in A remains unchanged. Recalling that α, β, γ are linear and homogeneous in B and C, it follows that

$$\lambda\alpha_{B,C}(\Omega_k)=\alpha_{\lambda B,\lambda C}(\Omega_k), \quad \text{etc.} \tag{31}$$

We obtain thereby the key result that the polycrystalline solid line-shape formulas apply as well to the intermediate state provided that we make the substitutions

$$B\rightarrow\lambda B$$

$$C\rightarrow\lambda C.$$

Thus, in the case of cylindrical symmetry, for interaction with a single magnetic nucleus, the normalized line shape is given by

$$g_{M,\lambda}(\nu)=\frac{1}{M\left|6A\lambda B+3\lambda^2B^2\right|^{\frac{1}{2}}}\frac{\nu/M}{\left|(\nu/M)^2-(A-\lambda B)^2\right|^{\frac{1}{2}}}, \tag{32}$$

the range of resonance being

$$|A-\lambda B|M \quad \text{to} \quad |A+2\lambda B|M.$$

For interactions with more than one nucleus, one would expect the corresponding λ coefficients to be the same.

A possible physical interpretation of our parametrization is that $1-\lambda$ represents the fraction of solid angle accessible to some representative molecule during some typical time interval h/A.

It was found possible to fit the resonance line shape for hydrazyl in partially hardened Duco (Fig. 7) to a theoretical curve (Fig. 13) corresponding to $\lambda=0.25\pm 0.02$. Apparently, the hydrazyl sample has made roughly one-fourth the transition from liquid to solid, insofar as magnetic resonance constitutes a gauge. The impressive concordance between the experimental and the fitted resonance line shapes lends weighty support to our model for the intermediate state. Secondarily, further verification is provided for our assignment of hyperfine coupling constants, as will be seen more explicitly in the following paragraph.

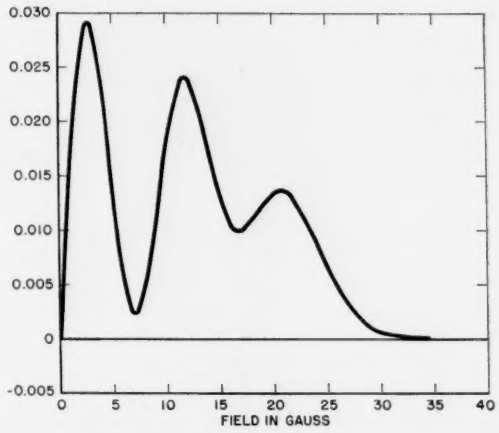

FIG. 13. Hydrazyl intermediate state: theoretical resonance line shape $\lambda=0.25$. (This is the theoretical synthesis of the spectrum Fig. 7.)

The shape of a single hyperfine component undergoing incipient broadening remains practically gaussian until the line breadth (from angular dependence of hyperfine structure) becomes comparable with the gaussian σ. The second moment of the line is closely approximated, for small λ, by $[\sigma^2+\frac{3}{4}\lambda^2B^2M^2]^{\frac{1}{2}}$. The centroid of the component line shifts from AM in the liquid to $[A^2-\frac{1}{2}A\lambda B+\frac{7}{4}\lambda^2B^2]^{\frac{1}{2}}M$. *If A and B are of the same sign, this initial shift is inward* (towards the center of the resonance). In our intermediate spectrum the peaks shift inward precisely as predicted thus providing independent proof that both pairs A_i, B_i have the same sign.

For the spectrum Fig. 7 the approximation that the broadened lines remain Gaussian was found quite adequate despite the rather large value of λ. The synthesized spectrum (Fig. 13) was nevertheless computed rigorously, as were the solid state curves (Sec. VI). As λ increases further we should expect each peak to split into two, corresponding to the two frequencies $|A-\lambda B|M$ and $|A+2\lambda B|M$. Naturally, not all of these would be observable because of overlapping. As shown in Sec. VI, only peaks corresponding to the $|A+2\lambda B|M$ survive after complete solidification of the matrix containing hydrazyl.

VIII. CARBAZYL IN FLUID AND SOLID MEDIA

A procedure analogous to that of Secs. V and VI was followed with carbazyl. Resonance of a dilute solution of carbazyl in benzene is illustrated in Fig. 14. An

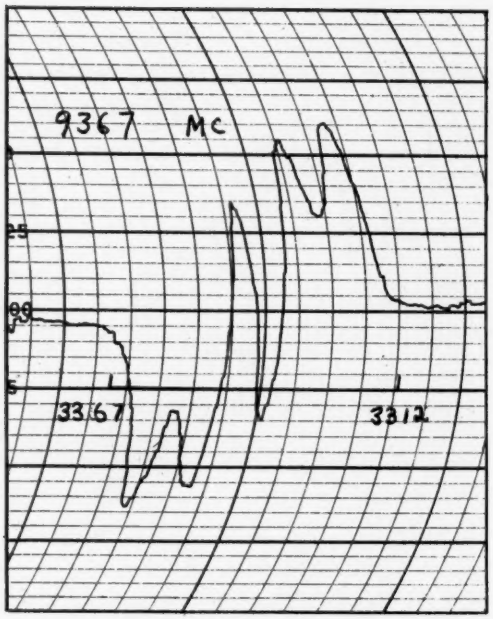

FIG. 14. Resonance of carbazyl in benzene solution.

identical spectrum was obtained in chloroform solution. Again, there is no evidence of any anisotropic interaction. Consistent with earlier studies[17,18] a seven-line pattern is observed. This had been attributed to isotropic hyperfine interaction with $|A_1| \approx 2|A_2|$. Jarrett[17] gives the value 37.3 Mc (13.3 gauss) for the larger constant.[36] Kikuchi and Cohen[18] estimate that the interval is $\frac{5}{8}$ that of hydrazyl, which is equivalent to $|A_1| = 10.8$ gauss using our hydrazyl data.

Figure 15 shows the basic pattern for the isotropic hyperfine structure of carbazyl. The relationships among the various spacings are evident from the diagram. Representing the line shape by a sum of nine gaussians, we obtain the best fit with the parameters:

$$|A_1| = 10.2 \pm 0.5 \text{ gauss};$$
$$|A_2| = 5.8 \pm 0.5 \text{ gauss};$$
$$\sigma = 3.4 \pm 0.5 \text{ gauss}.$$

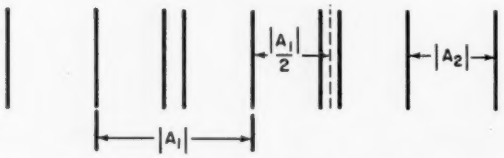

FIG. 15. Isotropic hyperfine structure of carbazyl.

[36] The resonance spectrum for carbazyl shown in Fig. 1(b) of Jarrett's paper (see footnote 17) is very similar to ours. Hence, our assignment of parameters is more in accord with his data than are the values quoted by him: $A_1 = 37.3$ Mc (13.3 gauss), $A_2 = 18.6$ Mc (6.6 gauss).

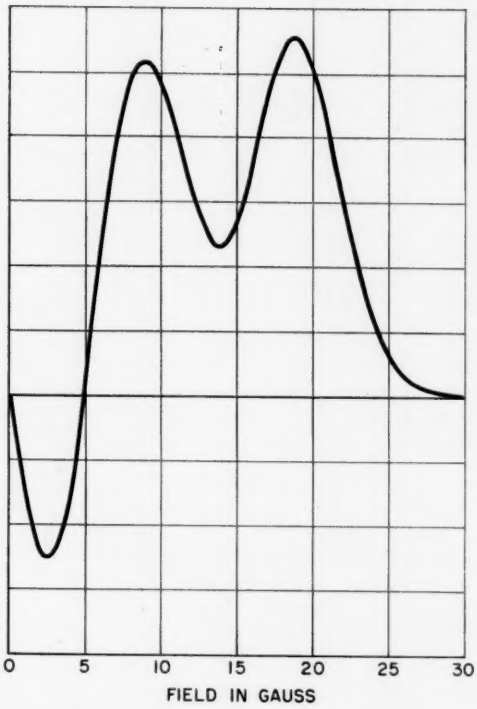

FIG. 16. Carbazyl in liquid: theoretical resonance line shape.

FIG. 17. Resonance of carbazyl in Lucite.

The synthesized derivative is drawn in Fig. 16. Our ratio $|A_2/A_1|$ is 0.57 in contrast with the idealized value of $\frac{1}{2}$.

A trace of the ESR of carbazyl dispersed in the solid is shown in Fig. 17. Methyl methacrylate (Lucite) was used as the trapping matrix. Duco cement is not suitable here since carbazyl is destroyed by reaction with acetone. The asymmetry of the spectrum, Fig. 17, is attributed to the presence of another paramagnetic species in the solid. As shown in Fig. 18, the asymmetric spectrum may be resolved into a sum of two symmetric components with slightly different g factors. The second species has, evidently, an over-all line shape very similar to that of the principal species. The former may be carbazyl which has segregated into small crystallites. The narrowing and g shift would thereby be consequences of enhanced exchange interaction.

We must now construct a theoretical representation of the absorption derivative (solid curve of Fig. 18). As before, the isotropic hyperfine parameters from the liquid are presumed to carry over to the solid. In fitting the two anisotropic parameters to the solid spectra (in hydrazyl as well) it was found possible to employ a two-step procedure with only one variant at a time. First the sum of B_1 and B_2 is fitted to the outermost peak of the resonance, then their ratio is adjusted to best reproduce the other features of the spectrum. The outer peak remains relatively insensitive to variations in the ratio. The parameters chosen in this manner are:

$$A_1 = 10.2 \pm 0.5 \text{ gauss};$$

$$A_2 = 5.8 \pm 0.5 \text{ gauss};$$

$$B_1 = 7.7 \pm 1.0 \text{ gauss};$$

$$B_2 = 4.1 \pm 1.0 \text{ gauss};$$

$$\sigma = 3.4 \pm 0.5 \text{ gauss}.$$

Again, all the parameters are positive, and again the gaussian σ for the liquid applies for the solid.

The steps in the synthesis of the carbazyl line shape, analogous to Figs. 9–12, are drawn in Figs. 19–22. Comparing Figs. 17 and 22, we see that the principal features of the spectrum are reproduced and that the positions of maxima and minima are predicted very closely. The agreement is, however, not so impressive visually as in the case of solid hydrazyl. In rationalization we should note that the carbazyl resonance is more complex than that of hydrazyl. It is also considerably weaker and is thus subjected to a relatively higher noise level. Moreover, an additional step, viz., subtraction of the superposed signal, was necessary to isolate the physically meaningful absorption derivative. Notwithstanding these operational difficulties, there is the possibility that our idealizations, i.e., isotropic g tensor, axial symmetry, and parallel orbitals, are not as closely realized in carbazyl.

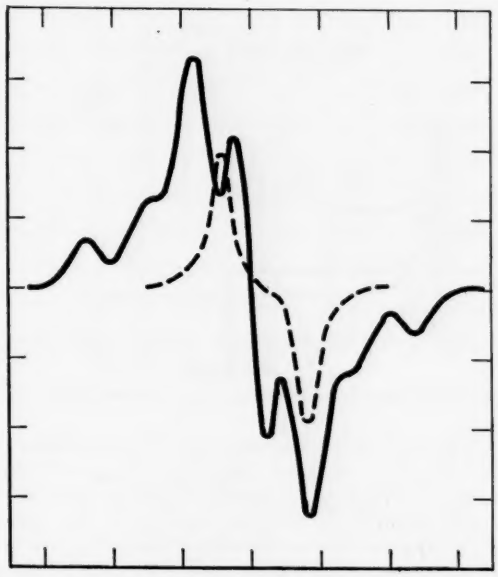

FIG. 18. Synthesis of the asymmetric spectrum of carbazyl in solid.

The implications of the hydrazyl and carbazyl hyperfine spectra with regard to the electronic structure of these radicals will be discussed next.

IX. DISCUSSION

Isotropic and anisotropic hyperfine coupling constants may be represented as integrals over a molecular wave function (see Sec. II). Hence, these parameters contain certain information about the wave function, particularly that part of it describing the unpaired electron. In this section we shall attempt to extract such information as we can from calculated and observed features of the hyperfine structure in hydrazyl and carbazyl.

The essential validity of our model of local cylindrical symmetry (see Sec. III) is borne out by its consistency with the observed spectra (Secs. V–VIII). We conclude that the unpaired spin, in the vicinity of the α and β nitrogen atoms, resides in orbitals having at least approximate cylindrical symmetry (or three-fold axial symmetry). An obvious limitation on cylindrical symmetry is the fact that the proximity of the second spin distribution perturbs the symmetry of the first. For a spin density ρ_i on atom i, a distance 1.46 A from atom j (see footnote 39), we calculate that $C_j = 0.67\rho_i$ gauss. Thus we have been neglecting individual off-axial contributions of 0.2–0.5 gauss, probably within the uncertainty of the corresponding B parameters.[37]

We can deduce further that the singly-occupied orbital has principally p character. For an atomic nitrogen $2p$ orbital, the integral (8) yields the value

[37] Small deviations from axial symmetry, <1 gauss say, will not radically affect the polycrystalline line shapes.

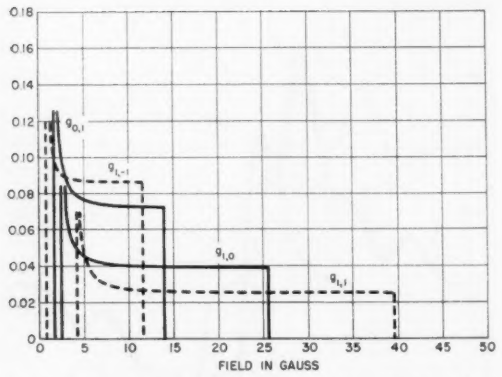

FIG. 19. Carbazyl in solid: components of theoretical line shape.

10.2 gauss for B_N.[38] The sum B_1+B_2 is comparable to this for both hydrazyl ($B_1+B_2=12.4$ gauss) and carbazyl ($B_1+B_2=11.8$ gauss).[39] The fact that $B_1+B_2>B_N$ might be attributed to two factors: (i) decrease in the effective nuclear shielding σ when the atom becomes bonded, a consequence of the outward diffusion of charge,[40] and (ii) the possibility that the sum of the spin densities on N_α and N_β is greater than unity, which could arise from introduction of negative spin densities into other parts of the molecule.[41]

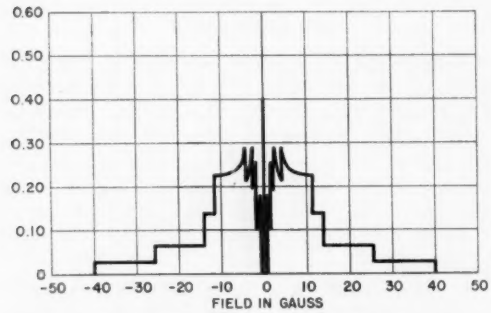

FIG. 20. Carbazyl in solid: theoretical line shape.

[38] Using in the integral (8) a hydrogen-like $2p_z$ orbital,

$$\psi(r,\theta)=[4(2\pi)^{\frac{1}{2}}]^{-1}(Z-\sigma)^{5/2}r\cos\theta\exp[-(Z-\sigma)r/2],$$

where σ is the effective electron shielding parameter, we find

$$B=0.229(Z-\sigma)^3, \text{ in gauss.}$$

For the $2p$ shell of atomic nitrogen, Hartree gives $\sigma=3.46$ [D. R. Hartree, *The Calculation of Atomic Structures* (John Wiley & Sons, Inc., New York, 1957), p. 167]. Hence $B_N=10.2$ gauss.

[39] These sums include the effect of interatomic interaction, whereas the corresponding quantities for isolated atoms would be more meaningful for our purposes. A spin density ρ_i on nitrogen atom i decreases B_j by 0.16 ρ_i gauss, presuming that the $N-N$ distance is 1.46 A, its value in hydrazine. [See T. Moeller, *Inorganic Chemistry* (John Wiley & Sons, Inc., New York, 1952), p. 582]. This contribution is within the uncertainty in the sums, hence is not considered further.

[40] This effect may be complicated by introduction of net positive or negative charges on these atoms. See resonance structures, Fig. 23.

[41] H. M. McConnell and D. B. Chesnut, J. Chem. Phys. **27**, 984 (1957).

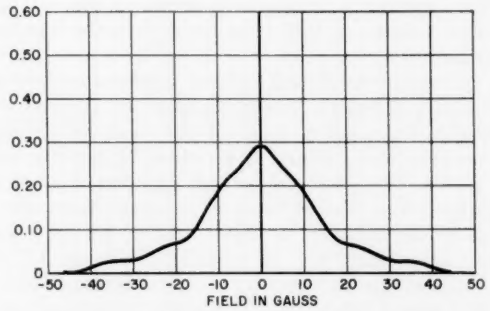

FIG. 21. Carbazyl in solid: theoretical line shape with Gaussian broadening.

The isotropic hyperfine interactions are more difficult to analyze quantitatively since these are due to a combination of two effects: (i) direct contact interaction from admixture of s character into the orbital containing the odd electron, and (ii) spin polarization, resulting in contributions from doubly-occupied orbitals. A prototype of the first effect might be the hyperfine interaction in atomic hydrogen, of the second, that in atomic nitrogen.[42] The resolution into (i) and (ii) is not unique but depends on the choice of ground state molecular orbital configuration. A single configuration, no matter how expediently chosen, will always have a residual effect (ii) (excepting cases of fortuitous cancellation). Thereby is manifest the fact that a many-electron system cannot rigorously be described by a single MO configuration.

The origin of spin polarization, as pointed out by McConnell and Chesnut,[43] may be discussed from three complementary points of view. In the language of molecular orbital theory one would ascribe the effect to configuration interaction with excited molecular states of the same symmetry. Accordingly, the unpaired spin

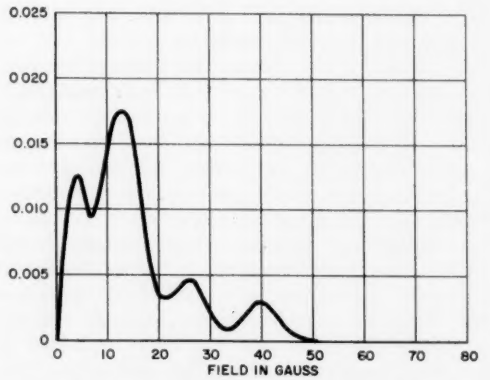

FIG. 22. Carbazyl in solid: derivative of theoretical line shape.

[42] S. M. Blinder, Bull. Am. Phys. Soc. **5**, 14 (1960).

[43] H. M. McConnell and D. B. Chesnut, J. Chem. Phys. **28**, 107 (1958).

would not reside totally in one particular molecular orbital but would be transmitted partially to other orbitals. Alternately, one might choose to remain within the formalism of a single configuration and attribute the transference of spin to "exchange polarization." Such is the result of the application of the unrestricted Hartree-Fock method[44] to systems having net spin. Physically, spin polarization is a manifestation of the Exclusion Principle, whereby electrons of the same spin experience mutual repulsions over and above their ordinary electrostatic repulsions. The third mode of description is provided by valence bond theory. Delocalization of spin is here a consequence of resonance among alternative electron pairing schemes. For example, we could write for either of our radicals a set of structures having an unpaired electron localized on the α nitrogen, and another set with one on the β nitrogen. There are, of course, still other structures in which the odd electron is drawn into the ring systems. It is, in fact, the last, which to a large degree enhance the stability of these radicals. We indicate in Fig. 23 representations of the three types of canonical valence-bond structures.

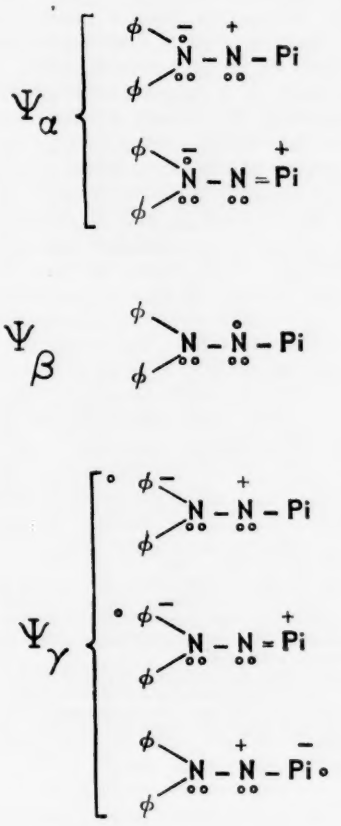

FIG. 23. Some valence bond structures for substituted hydrazyl free radicals.

It is clear that the direct contact interaction is rather small in hydrazyl and carbazyl, for an unpaired electron in a pure $2s$ orbital would give a value for A in excess of 600 gauss.[45] The observed values (6–10 gauss) indicate that the hybridization of the p orbitals can be no greater than 1–2%. Three N_α bond orbitals must then be constructed out of the $2s$ orbital and the remaining two $2p$ orbitals. Such bonds must necessarily lie in the plane perpendicular to the unpaired p orbital. We deduce thereby an important fact about the structure of our two radicals, namely that the three bonds to the α nitrogen lie very nearly in a plane and are, on the average, sp^2 hybrids. In contrast, the corresponding bonds in hydrazine (likewise in ammonia) form a trigonal pyramid.[46]

It is similarly evident that the two bonds to the β nitrogen lie in the same plane, but it is not unambiguously clear whether they are sp^2 hybrids (along with the unshared pair) or colinear sp hybrids, leaving the unshared pair in a p orbital. The latter is favored in view of the several double-bonded resonance structures (Fig. 23).

We know then that the two nitrogen atoms and the three carbon atoms bonded to them all lie in a plane. The well-known criterion for maximum stability in π electron systems suggests further that (neglecting steric effects) the two radicals are planar in their entirety. Therefore, the structural formulas (Fig. 1) as drawn are probably good representations of the actual geometric configurations of hydrazyl and carbazyl.

Thus far we have established an upper limit on s admixture into the unpaired electron's orbital (1–2%). We consider even this small percentage to be too large for two reasons: (i) From simple energetic considerations, it would be more feasible here that all available s character be used in the bond orbitals so as to maximize their overlap with neighboring atoms.[47] For instance, in the free radicals CH_3 and NH_2, isoelectronic with the α and β nitrogen atoms, respectively, the odd electron has pure p character.[48] (ii) The approximate proportionality of pairs A_i, B_i[49] suggests that spin polarization is the dominant mechanism for the isotropic interactions. We note first that the B constants are probably the best measure we have of spin density

[44] R. K. Nesbet, Proc. Roy. Soc. (London) **A230,** 312 (1955); G. W. Pratt, Phys. Rev. **102,** 1303 (1956).

[45] This value is calculated from Hartree's SCF wave function for the $2s$ atomic orbital in the nitrogen atom [D. R. Hartree and W. Hartree, Proc. Roy. Soc. (London) **A193,** 299 (1948)].

[46] T. Moeller, *Inorganic Chemistry* (John Wiley & Sons, Inc., New York, 1952), p. 582.

[47] See, for example, L. Pauling, *The Nature of the Chemical Bond* (Cornell University Press, Ithaca, New York, 1948), 2nd ed., pp. 86–89; C. A. Coulson, *Valence* (Oxford University Press, London, 1952), Chap. VIII.

[48] R. S. Mulliken, J. Chem. Phys. **1,** 492 (1933).

[49] For hydrazyl, $A_1/B_1=1.42$, $A_2/B_2=1.35$; for carbazyl, $A_1/B_1=1.32$, $A_2/B_2=1.41$.

since they involve no indirect interactions. (This presumes that the effective shielding constants σ for the two nitrogens are not overly disparate). It follows then that each A is approximately proportional to its corresponding spin density, which evokes associations with McConnell's rule[50] ($A_i = Q\rho_i$) for indirect proton hyperfine coupling in π-electron systems.[51]

We return finally to the unanswered question of associating the assigned A and B parameters with particular nitrogen atoms. Bersohn[52] has calculated by simple molecular orbital theory the spin densities in hydrazyl and carbazyl. He finds for hydrazyl, densities of 0.1416 and 0.1518 on α and β, respectively; for carbazyl 0.1064 and 0.2061. The magnitudes of these densities are too small by a factor of at least two to account for the observed anisotropic coupling constants.[53] We suggest that extension of the calculation to include configuration interaction could possibly remove this disparity, for introduction of negative spin densities into some parts of the molecule would necessarily enhance the positive densities of other parts, very likely including the central nitrogens. Notwithstanding the omission of configuration interaction in the Bersohn calculation, it is quite probable that the *relative* densities on the α and β atoms are essentially correct. We would then have ρ_α/ρ_β equal to 0.93 in hydrazyl, 0.52 in carbazyl. The corresponding ratios B_2/B_1 are 0.88 and 0.53. These figures suggest that the larger constants should be associated with the β nitrogen in both hydrazyl and carbazyl.

Note added in proof. Chen, Sane, Walter, and Weil[54] have recently studied N^{15}-labeled hydrazyl and have concluded that the larger isotropic coupling constant belongs to the β(picryl) nitrogen. Using carefully deoxygenated solvents, they find: $A_\alpha = 7.63 \pm 0.20$ gauss, $A_\beta = 9.90 \pm 0.20$ gauss.

ACKNOWLEDGMENTS

The authors wish to thank their colleagues at the Applied Physics Laboratory for many fruitful discussions on several phases of this work. In particular, the collaboration of Martin L. Peller and Monica R. Nees on the chemical aspects of the work was indispensable. Mrs. Sylvia Ellsworth aided in some of the line-shape computations. Dr. John A. Weil of Argonne National Laboratory communicated to us his results on hydrazyl and contributed several valuable suggestions on our work.

[50] H. M. McConnell, J. Chem. Phys. **24,** 632, 764 (1956).

[51] We have neglected the possibility that the degree of hybridization is the same in the four nitrogen atoms in question. Also, we do not intend to imply that the same proportionality extends to nitrogen atoms in other radicals.

[52] R. Bersohn, Arch. sci. (Geneva) **11,** 177 (1958).

[53] If both these densities and the B constants were correct, the effective shielding parameters would necessarily have average values of 1.30 and 1.52 in hydrazyl and carbazyl, respectively. See footnote 38.

[54] M. M. Chen, K. V. Sane, R. I. Walter, and J. A. Well, J. Phys. Chem. (to be published).

THE JOURNAL OF CHEMICAL PHYSICS VOLUME 34, NUMBER 5 MAY, 1961

Effect of Molecular Oxygen on the Emission Spectra of Atomic Oxygen-Acetylene Flames

S. L. N. G. KRISHNAMACHARI* AND H. P. BROIDA

National Bureau of Standards, Washington, D. C.

(Received December 6, 1960)

Studies have been made of the emission spectra (3000 to 6000 A) obtained from low-pressure atomic oxygen-acetylene flames diluted with varying amounts of molecular oxygen and molecular nitrogen. Added molecular oxygen greatly increased the OH emission while reducing CH and C_2 emission. It also had an effect on the rotational intensity distribution of OH and on the vibrational intensity distribution of C_2. Nitrogen addition greatly reduced the rotational and vibrational "temperatures" and decreased C_2 emission relative to the other emitters.

INTRODUCTION

PREVIOUS studies[1] have shown that much of the radiation emitted from acetylene flames by the radicals CH, C_2, and OH is due to chemiluminescence as a result of the formation of the radicals directly in excited electronic states during the chemical reactions. To some extent studies of atomic flames (electric discharge products of oxygen mixed with acetylene) have been disappointing in that the radiation is not greatly different from premixed flames of acetylene and oxygen.[2,3] One possible reason for this is that a large amount of molecular oxygen accompanies the atomic oxygen from discharges (few discharges dissociate more than 20% of the oxygen). Thus a source of oxygen atoms without molecular oxygen would provide a means for studying the effects of molecular oxygen on the emission spectra.[4]

The atomic titration technique[5,6] provides a method of obtaining atomic oxygen in the presence of chemically inert molecular nitrogen instead of molecular oxygen. This titration technique is based upon the fact that nitrogen atoms react rapidly with nitric oxide to produce oxygen atoms and molecular nitrogen, according to the reaction,

$$N+NO \rightarrow O+N_2. \qquad (1)$$

Nitrogen molecules can be dissociated in an electrical discharge; the discharge products, which contain nitrogen atoms, are mixed with nitric oxide to just replace the atomic nitrogen with atomic oxygen (titration point), and then the atomic oxygen-molecular nitrogen stream can be mixed with acetylene. This technique also is adaptable to the study of the effect of the addition of different amounts of molecular oxygen to the atomic oxygen-molecular nitrogen stream.

The present paper describes a spectrometric examination of the emission of CH ($A\,^2\Delta - X\,^2\Pi$ and $B\,^2\Sigma^- - X\,^2\Pi$), OH ($A\,^2\Sigma^+ - X\,^2\Pi_i$), C_2 ($A\,^3\Pi_g - X\,^3\Pi_u$), and CN ($B\,^2\Sigma^+ - X\,^2\Sigma^+$) in flames from acetylene reacting with mixtures of atomic oxygen, molecular nitrogen, and molecular oxygen. Relative intensities, rotational "temperatures" and vibrational "temperatures" were measured and compared for three types of flames at pressures near 2 mm Hg: (a) atomic oxygen, molecular nitrogen, and acetylene, (b) atomic oxygen, molecular oxygen, molecular nitrogen, and acetylene, and (c) atomic oxygen, molecular oxygen, and acetylene.

Changes of pressure, small additions of atomic nitrogen, or addition of excess nitric oxide were found to have minor effects on the relative intensities and temperatures. The most striking effect of the addition of molecular oxygen was the large increase of OH emission accompanied by decrease of C_2 and CH emission. This effect strongly supports the previously suggested mechanism[1] for the production of excited hydroxyl radicals

$$CH+O_2 \rightarrow OH^*+CO. \qquad (2)$$

There was also an effect of molecular oxygen on the rotational intensity distribution of OH and on the vibrational intensity distribution of C_2.

EXPERIMENTAL

The gas flow system comprising a 2450-Mc electrodeless discharge and a reaction cell for mixing the products from the discharge with acetylene was similar to that described by Kiess and Broida.[7] Nitric oxide could be added to the gas stream about 20 cm after the discharge and 20 cm before the reaction cell. Molecular oxygen

* On deputation from the Atomic Energy Establishment, Bombay, India.

[1] A. G. Gaydon, *The Spectroscopy of Flames* (Chapman and Hall Ltd., London, 1957).

[2] R. E. Ferguson and H. P. Broida, in the *Fifth Symposium on Combustion* (Reinhold Publishing Corporation, New York, 1955), p. 754.

[3] D. F. Heath and H. P. Broida, J. Chem. Phys. **26**, 223 (1957).

[4] J. E. Morgan, L. Elias and H. I. Schiff, J. Chem. Phys. **31**, 930 (1961).

[5] G. B. Kistiakowsky and G. G. Volpi, J. Chem. Phys. **27**, 1141 (1957).

[6] F. Kaufman and J. Kelso, in the *Seventh Symposium on Combustion* (Butterworths Scientific Publications, Ltd., London, 1959), p. 53.

[7] N. H. Kiess and H. P. Broida, in the *Seventh Symposium on Combustion* (Butterworths Scientific Publications, Ltd., London, 1959), p. 207.

TABLE I. Relative band intensities.

Emitter	Electronic transition	λ, A	Intensity[a] a	b	c
CH	$A^2\Delta - X^2\Pi$	4315	1.00 (1.00)	1.00 (0.11)	1.00 (0.14)
CH	$B^2\Sigma^- - X^2\Pi$	3889	0.055	0.06	0.07
OH	$A^2\Sigma^+ - X^2\Pi_i$	3090	0.004	0.28	0.18
C_2	$A^3\Pi_g - X^3\Pi_g$	5165	0.20	0.20	0.71
CN	$B^2\Sigma^+ - X^2\Sigma^+$	3883	0.44	0.40	...

[a] (a) O, N_2, and C_2H_2; (b) O, O_2, N_2, and C_2H_2; (c) O, O_2, and C_2H_2.

either was added downstream from the nitric oxide inlet or was mixed with the acetylene. Acetylene flows were adjusted to give the brightest flames. At such flows the acetylene concentration is close to the atom concentration.[7] It is known from previous work that about 1% nitrogen atoms are produced in the discharges through nitrogen and about 10% oxygen atoms in the discharges through oxygen. Commercial, high-purity cylinder gases were used in all experiments.

Spectra were obtained both photographically and photoelectrically. The photographic instrument was an $F/2$ grating spectrograph with a dispersion of 20 A/mm and was used between 3000 and 4500 A. Photoelectric tracings were obtained with a grating monochromator[8] using slits of 200 μ (1.0 A) and of 40 μ (0.2 A).

RESULTS

The effects of molecular oxygen on the measured intensities of the band heads of CH, OH, C_2, and CN in "atomic" flames with acetylene are illustrated in Table I. Case (a) is a mixture of atomic oxygen and molecular nitrogen formed by reacting nitric oxide with products of a discharge through nitrogen [Eq. (1)] at a pressure of 2 mm Hg and a nitrogen flow rate of 3.5 cm^3/sec (NTP). Case (b) is the same mixture to which 0.6 cm^3/sec of molecular oxygen has been added downstream of the discharge, raising the pressure to 2.5 mm Hg. For comparison, case (c) is the product of a discharge through oxygen at a flow rate of 0.6 cm^3/sec and a pressure of 0.75 mm Hg. In each case the intensities are normalized, with the intensity of the 4315 A band of CH taken as unity and the intensities of the other bands expressed as fractions thereof. In order to give an idea of changes in intensity in the three cases, the relative intensities of the 4315-A CH band are shown in brackets. Since the instrument response varies by a factor of about four over the wavelength range of the five band heads, these relative intensities are only for the purpose of comparison to determine the relative effects of the addition of molecular oxygen.

[8] W. G. Fastie, J. Opt. Soc. Am. **42**, 641 (1952).

It can be seen by comparison of case (a) with case (b) that oxygen addition caused the OH emission to increase by more than seven fold while the CH, C_2, and CN decreased by nearly a factor of ten. Smaller additions of molecular oxygen caused smaller but similar effects, i.e., with decreasing amounts of oxygen, OH intensity decreased while the intensities of the other radicals increased.

Changes in total pressure caused changes in over-all intensity but did not cause large changes in the relative intensities of the various emitters. Since pressure changes cause changes in atom concentration and in the size of the flame, it does not appear useful to include variations due to this cause.

Small changes in the amount of nitric oxide did not greatly change the emission except for that of CN. The CN intensity was very sensitive to the amount of added nitric oxide, decreasing tenfold with very small additions near the titration point. Surprisingly, CN was still observed even when more nitric oxide was added than needed for titration as judged by visual observation.

The vibrational and rotational "temperatures" determined by conventional methods[9] from the observed, resolved rotational lines and vibrational band heads are given in Table II. The absolute values of the rotational "temperatures" are good to about 10% except that for C_2 which is far less precise but is indicative of the trends. Vibrational "temperatures" are not as well calibrated and are given to show the relative intensities of vibrational bands. The values obtained for case (c) in the present investigation agree closely with those

TABLE II. Rotational "temperatures" measured from the 0, 0 bands.[a]

Emitter	Temperature, °K a	b	c	Remarks
CH	1900	2000	2600	$A^2\Delta - X^2\Pi$
OH	500	600	2400	Low quantum numbers
	7200	8100	10 600	High quantum numbers
C_2	3300	3400	4300	
CN	400	400	...	
	Vibrational temperatures			
CH	1500	1500	1900	0, 0 and 1, 1
OH	1100	1100	2600	0, 0 and 2, 2
C_2	8500	7300	4400	0, 0 and 1, 1
C_2	8600	7700	6200	0, 0 and 2, 2

[a] See work cited in footnote 9.

[9] H. P. Broida, in *Temperature, Its Management and Control in Science and Industry* (Reinhold Publishing Corporation, New York, 1955), Vol. 2, p. 265.

reported earlier[2] for similar flames. Comparison of cases (c) and (b) shows that on the addition of molecular oxygen, there is a slight tendency for the "temperatures" to change toward case (c). This is most noticeable for OH and C_2. It seems likely that the CN and OH (low quantum numbers) rotational "temperatures" indicate the translational temperatures of the flames.

Molecular nitrogen has a large effect on the rotational and vibrational intensity distributions. With the exception of the C_2 vibrational "temperature," all "temperatures" were reduced by the addition of nitrogen. A similar effect was observed when the discharge products of oxygen in an excess of argon were reacted with acetylene.

THE JOURNAL OF CHEMICAL PHYSICS VOLUME 34, NUMBER 5 MAY, 1961

Studies of Rates of Conversion and Populations of Conformations in Saturated Ring Compounds. III.* *NN'* Dimethyl Piperazine

L. W. REEVES AND K. O. STRØMME†

Chemistry Department, University of British Columbia, Vancouver 8, British Columbia

(Received September 15, 1960)

At room temperature the two proton resonance signals observed in *NN'*-dimethyl piperazine are not of equal half-width. The signal caused by the ring methylene protons broadens as the temperature is lowered and below −40°C the spectrum is typical of an A_2B_2 case. These observations are indicative of fast interconversion relative to the axial-equatorial chemical shift between two identical chair forms of this molecule at +40°C and slow interconversion below −40°C. The A_2B_2 spectrum is partially analyzed, showing reasonable values for $J_{e_1a_1}$, $J_{e_1e_2}$, $J_{e_1a_2}$, and the axial-equatorial chemical shift assuming only that the value of $J_{a_1a_2}$ is known. The energy barrier for interconversion is computed from the coalescence temperature and the exchange broadened single peak near the fast exchange limit. It is found to be 13.3±0.3 kcal. A comparison with earlier measurements in similar compounds is made. The *N*-methyl axial-equatorial motion is discussed.

INTRODUCTION

In two previous papers[1,2] we have shown that six-membered alycyclic ring compounds which are not locked, by the substitution of large groups into one conformation, are resolved into two possible chair forms by their proton resonance spectra at low temperature. At room temperature the spectra of these conformers are rapidly averaged.[3]

Four halogen-substituted cyclohexanes which show a chemically shifted –CHX– proton were cooled in appropriate solvents, and at −30 to −60°C the "adjacent" proton resonance splits into two signals. The relative areas under these proton resonance signals give an analysis of the equilibrium mixture of the two chair forms.[1,2] The effect of solvent and concentration on the conformational equilibrium has been investigated. The "coalescence temperature"[4,5] may be used to indicate an average lifetime for the species in equilibrium at this temperature. The assumption that frequency factors are normal enables an estimate of the energy barrier for conversion to be made. In the present study, we shall confine our attention to a heteroalycyclic ring compound. An attempt will be made to estimate an energy barrier by observation of linewidths near the fast exchange limit.[6]

EXPERIMENTAL

A Varian 40-Mc spectrometer equipped with flux stabilizer was used to take NMR spectra. Techniques for taking NMR spectra at low temperatures have already been described.[7] The stability of temperature is ±0.5°C down to −80°C.[8] *NN'*-dimethyl piperazine available commercially showed no impurity peaks in its proton resonance spectrum and was, therefore, used without further purification. A 30 mole % solution in dichloromethane with 1% tetramethyl silane as internal standard was used in a sealed evacuated 5-mm o.d. tube.

RESULTS

Figure 1 shows spectra of the solution at various temperatures. The low-field signal (I) is assigned to the

* Contribution from the Chemistry Department, University of British Columbia, Vancouver 8, British Columbia.

† Permanent address: Chemistry Department, University of Oslo, Blindern, Norway.

[1] L. W. Reeves and K. O. Strømme, Can. J. Chem. **38**, 1241 (1960).

[2] L. W. Reeves and K. O. Strømme, Trans. Faraday Soc. (to be published).

[3] J. A. Pople, W. G. Schneider, and H. J. Bernstein, *High Resolution Nuclear Magnetic Resonance* (McGraw-Hill Book Company, Inc., New York, 1959).

[4] H. S. Gutowsky and A. Saika, J. Chem. Phys. **21**, 1688 (1953).

[5] H. S. Gutowsky and C. H. Holm, J. Chem. Phys. **25**, 1228 (1956).

[6] I. Solomon and N. Bloembergen, J. Chem. Phys. **25**, 261 (1956).

[7] H. J. Bernstein, W. G. Schneider, and J. A. Pople, J. Chem. Phys. **28**, 601 (1958).

[8] P. Gray and L. W. Reeves, J. Chem. Phys. **32**, 1878 (1960).

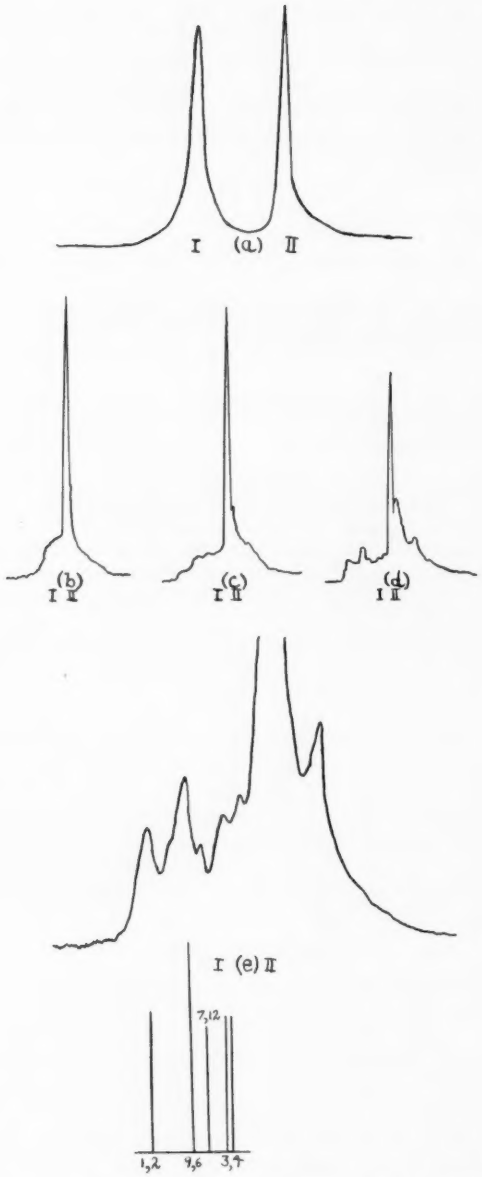

FIG. 1. Appearance of proton resonance signals in NN'-dimethyl piperazine at various temperatures. (a) 28°C, (b) −11.5°C, (c) −27.5°C, (d) −56°C, (e) −48°C. This spectrum is taken under high gain conditions and the signals in the A_2B_2 spectrum are assigned according to P.S.B.

ring methylene protons, and the high-field signal (II) to the right is assigned to the six N-methyl protons. The methylene protons have a smaller value of T_2 compared to the N-methyl peaks at 28°C. [Fig. 1(a)]. As the temperature is lowered, the low-field peak broadens rapidly and at −27.5°C develops fine structure. The chemical shift of the low field peak compared to the sharp N-methyl resonance is −7.2±0.7 cps at 40 Mc and −88.4 cps at 40 Mc compared to tetramethyl silane.

Figure 1(b)–(d) show the sharp methyl resonance and the broadening and final development of fine structure, on signal I for the methylene protons, as the temperature is lowered. The spectrum in Fig. (e) shows more detail of the fine structure of the methylene proton resonance at −48°C. The high-field side of the methylene proton resonance at −48°C. The high-field side of the methylene signal is marred by overlap with the methyl resonance, but somewhat over half the lines in signal I can be accurately determined relative to the tetramethyl silane peak at high field.

The average chemical shift of signal I at low temperatures can be determined by averaging the position of the two outer lines. The chemical shift so obtained is −7.1 cps at −48°C relative to the N-methyl peak compared to −7.2 cps obtained for the single line at 28°C.

DISCUSSION

General Considerations

The signal broadening of the $-CH_2-$ peak as the temperature is lowered is interpreted as resulting from slowing of interconversion in the equilibrium between two identical chair forms of NN'-dimethyl piperazine. This can be represented as the position of the nitrogen

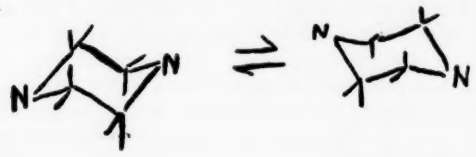

methyl group being ignored for the moment. At a temperature of +45°C, the interconversion rate between these two forms is rapid enough to allow observation of an average shielding for the methylene protons[4] rather than resolving separate chemical shifts for the axial and equatorial protons.[1,2,9] At room temperature the lifetime of the individual forms becomes long enough to cause exchange broadening[4–6] of the single methylene peaks, and this broadening continues to a temperature at which individual chemical shifts and coupling constants are resolved (e.g., −40°C).

At low temperatures, the spectrum of these identical forms is not averaged in the ring methylene protons and this we expect two superimposed A_2B_2 spectra.[10] The sharp methyl resonance at all temperatures warrants some discussion.

It is reasonable that the N-methyl groups have dis-

[9] R. N. Lemieux, R. K. Kullnig, H. J. Bernstein, and W. G. Schneider, J. Am. Chem. Soc. **80**, 6098 (1958).

[10] J. A. Pople, W. G. Schneider, and H. J. Bernstein, Can. J. Chem. **35**, 1063 (1957).

tinct chemical shifts in the axial and equatorial position, since they are oriented at different angles to the various bonds in the molecule in these two positions. The diamagnetic anisotropy of the σ bonds in the molecule will produce, therefore, different secondary fields at the N-methyl protons. The nitrogen atom is surrounded by four approximately tetrahedrally-arranged groups, two σ bonds to the adjacent ring methylene groups, a σ bond to the N-methyl group, and a nonbonding or lone pair orbital.

The N-methyl axial-equatorial motion is related to the problem of nitrogen inversion in ring systems.[11,12] Kincaid and Henriques[12] suggested that the nitrogen in a three-membered ring might undergo quite slow inversion and this was confirmed by Bottini and Roberts.[11] The nitrogen in a six-membered ring probably has an inversion frequency similar to the microwave absorption found for the normal breathing mode of ammonia.[12] This rules out the resolution of N-methyl into an axial and equatorial chemical shift, even if there in in fact any reasonable amount of axial methyl groups in view of the steric hindrance in this position.

Partial Analysis of the Low-Temperature Spectrum

The problem of the A_2B_2 case is set up with the precise notation of Pople, Schneider, and Bernstein[10] (hereafter P.S.B.).

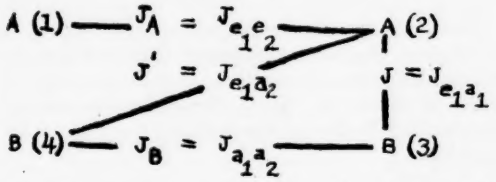

The four nuclei are represented as $A(1)$, $A(2)$, $B(3)$, and $B(4)$. In order to satisfy the conditions for A_2B_2 case in Fig. 4 of footnote 10, we relate the coupling constants and nuclei represented above as $A(1)$ and $A(2)$ equatorial protons on adjacent methylene groups, and $B(3)$ and $B(4)$ axial protons on adjacent methylene groups. Then, since we know $J_{e_1a_1}=J\gg J_{e_1a_2}=J'>0$, and $J_{a_1a_2}=J_B\gg J_A=J_{e_1e_2}>0$ from many other conformational studies,[3,9] we can assign principal lines of spectrum 4 (P.S.B.) to the present low-temperature spectrum directly. The assignments of various lines in the low temperature spectrum are related to those of Bernstein, Schneider, and Pople in Fig. 2(e).

We have, therefore,

$$N=E_1-E_3=15.6 \text{ cps} \quad (1)$$

$$(M^2+L^2)^{\frac{1}{2}}=E_9-E_{11}=12.1 \text{ cps} \quad (2)$$

$$[(\nu_0\delta)^2+N^2]^{\frac{1}{2}}=E_1+E_3=19.0 \text{ cps} \quad (3)$$

$$[(\nu_0\delta+M)^2+L^2]^{\frac{1}{2}}=E_9+E_{11}=12.1 \text{ cps}, \quad (4)$$

using the exact notation of P.S.B. and inserting the experimental numbers from the spectrum Fig. 1(e). The value of $K=J_{e_1e_2}+J_{a_1a_2}$ is needed for a complete analysis and cannot be determined directly. The assumption is made that $J_{a_1a_2}=7.43$ cps. This is an average value of 10 $J_{a_1a_2}$ coupling constants in saturated six-membered ring compounds.[3] The other parameters can then be obtained (P.S.B.) from Eqs. (1)–(4):

$$M=-5.3 \text{ cps}=J_{e_1e_2}-J_{a_1a_2}$$

$$N=15.6 \text{ cps}=J_{a_1e_1}+J_{e_1a_2}$$

$$L=10.8 \text{ cps}=J_{a_1e_1}-J_{e_1a_2}$$

$$J_{a_1a_2}=7.41 \text{ cps (assumed)}.$$

Thus,

$$J_{a_1e_1}=13.2 \text{ cps}, \quad J_{e_1a_2}=2.4 \text{ cps}, \quad \text{and} \quad J_{e_1e_2}=2.1 \text{ cps}$$

$$\nu_0\delta=10.8 \text{ cps}.$$

All these are reasonable values from comparison with similar compounds.[3]

Energy Barrier for Conversion between Two Chair Forms

In previous papers, the energy barriers for interconversion have been obtained from the so-called "coalescence temperature."[4,5] The two chemical shifts which coalesce were associated with many splittings caused by J coupling with other chemically shifted protons in the molecule.[1,2] These splittings remain on averaging the two chemical shifts, but change their individual values since, in general, *aa* coupling is large compared to *ae* and *ee*. The over-all halfwidth of the average signal is some function of the position of the equilibrium and the individual values $J_{a_1a_2}$, $J_{e_1e_2}$, and $J_{e_1a_2}$.

In the molecule studied here, the energy barrier can be estimated both from coalescence and from measurements on the single signal at higher temperatures near the exchange limit.[6,13–16] The simple case of two chemically shifted uncoupled nuclei of spin $\frac{1}{2}$ near the exchange limit has been treated adequately,[13,15] and from experimental measurements τ, the average nuclear lifetime, can be obtained at various temperatures. The present molecule satisfies the conditions of these equations approximately since there are two sets of two protons chemically shifted by 10.8 cps. There is, however, coupling between these spins at low temperatures which averages to zero when all nuclei become identical in the limit of fast exchange. The splittings resulting from the A_2B_2 case at low temperatures defines a shorter critical lifetime τ_c for collapse, and thus,

[11] A. T. Bottini and J. D. Roberts, J. Am. Chem. Soc. **78**, 5126 (1956).

[12] J. F. Kincaid and F. C. Henriques, Jr., J. Am. Chem. Soc. **62**, 1474 (1940).

[13] S. Meiboom, Z. Luz, and D. Gill, J. Chem. Phys. **27**, 1411 (1957).

[14] J. Kaplan, J. Chem. Phys. **28**, 27 (1958).

[15] L. H. Piette and W. A. Anderson, J. Chem. Phys. **30**, 899 (1959).

[16] H. M. McConnell, J. Chem. Phys. **28**, 430 (1958).

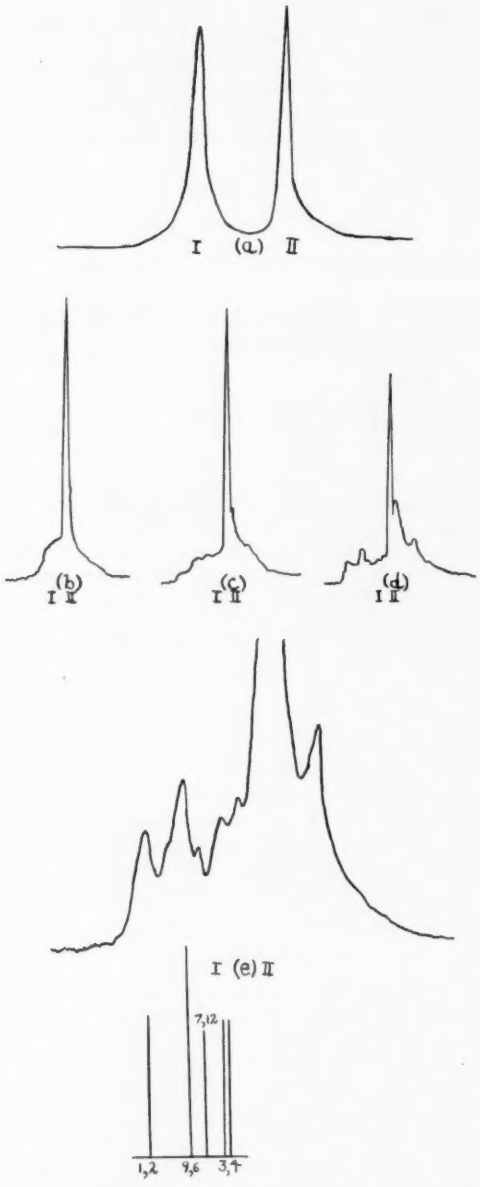

FIG. 1. Appearance of proton resonance signals in *NN'*-dimethyl piperazine at various temperatures. (a) 28°C, (b) −11.5°C, (c) −27.5°C, (d) −56°C, (e) −48°C. This spectrum is taken under high gain conditions and the signals in the A_2B_2 spectrum are assigned according to P.S.B.

ring methylene protons, and the high-field signal (II) to the right is assigned to the six N-methyl protons. The methylene protons have a smaller value of T_2 compared to the *N*-methyl peaks at 28°C. [Fig. 1(a)]. As the temperature is lowered, the low-field peak broadens rapidly and at −27.5°C develops fine structure. The chemical shift of the low field peak compared to the sharp *N*-methyl resonance is −7.2±0.7 cps at 40 Mc and −88.4 cps at 40 Mc compared to tetramethyl silane.

Figure 1(b)–(d) show the sharp methyl resonance and the broadening and final development of fine structure, on signal I for the methylene protons, as the temperature is lowered. The spectrum in Fig. (e) shows more detail of the fine structure of the methylene proton resonance at −48°C. The high-field side of the methylene proton resonance at −48°C. The high-field side of the methylene signal is marred by overlap with the methyl resonance, but somewhat over half the lines in signal I can be accurately determined relative to the tetramethyl silane peak at high field.

The average chemical shift of signal I at low temperatures can be determined by averaging the position of the two outer lines. The chemical shift so obtained is −7.1 cps at −48°C relative to the *N*-methyl peak compared to −7.2 cps obtained for the single line at 28°C.

DISCUSSION

General Considerations

The signal broadening of the $-CH_2-$ peak as the temperature is lowered is interpreted as resulting from slowing of interconversion in the equilibrium between two identical chair forms of *NN'*-dimethyl piperazine. This can be represented as the position of the nitrogen

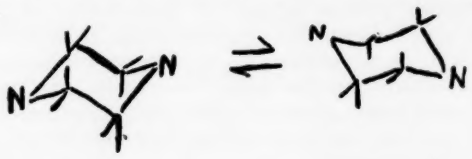

methyl group being ignored for the moment. At a temperature of +45°C, the interconversion rate between these two forms is rapid enough to allow observation of an average shielding for the methylene protons[4] rather than resolving separate chemical shifts for the axial and equatorial protons.[1,2,9] At room temperature the lifetime of the individual forms becomes long enough to cause exchange broadening[4–6] of the single methylene peaks, and this broadening continues to a temperature at which individual chemical shifts and coupling constants are resolved (e.g., −40°C).

At low temperatures, the spectrum of these identical forms is not averaged in the ring methylene protons and this we expect two superimposed A_2B_2 spectra.[10] The sharp methyl resonance at all temperatures warrants some discussion.

It is reasonable that the *N*-methyl groups have dis-

[9] R. N. Lemieux, R. K. Kullnig, H. J. Bernstein, and W. G. Schneider, J. Am. Chem. Soc. **80**, 6098 (1958).

[10] J. A. Pople, W. G. Schneider, and H. J. Bernstein, Can. J. Chem. **35**, 1063 (1957).

tinct chemical shifts in the axial and equatorial position, since they are oriented at different angles to the various bonds in the molecule in these two positions. The diamagnetic anisotropy of the σ bonds in the molecule will produce, therefore, different secondary fields at the N-methyl protons. The nitrogen atom is surrounded by four approximately tetrahedrally-arranged groups, two σ bonds to the adjacent ring methylene groups, a σ bond to the N-methyl group, and a nonbonding or lone pair orbital.

The N-methyl axial-equatorial motion is related to the problem of nitrogen inversion in ring systems.[11,12] Kincaid and Henriques[12] suggested that the nitrogen in a three-membered ring might undergo quite slow inversion and this was confirmed by Bottini and Roberts.[11] The nitrogen in a six-membered ring probably has an inversion frequency similar to the microwave absorption found for the normal breathing mode of ammonia.[12] This rules out the resolution of N-methyl into an axial and equatorial chemical shift, even if there in in fact any reasonable amount of axial methyl groups in view of the steric hindrance in this position.

Partial Analysis of the Low-Temperature Spectrum

The problem of the A_2B_2 case is set up with the precise notation of Pople, Schneider, and Bernstein[10] (hereafter P.S.B.).

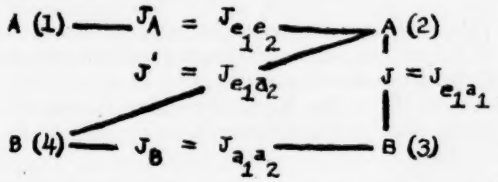

The four nuclei are represented as $A(1)$, $A(2)$, $B(3)$, and $B(4)$. In order to satisfy the conditions for A_2B_2 case in Fig. 4 of footnote 10, we relate the coupling constants and nuclei represented above as $A(1)$ and $A(2)$ equatorial protons on adjacent methylene groups, and $B(3)$ and $B(4)$ axial protons on adjacent methylene groups. Then, since we know $J_{e_1a_1}=J\gg J_{e_1a_2}=J'>0$, and $J_{a_1a_2}=J_B\gg J_A=J_{e_1e_2}>0$ from many other conformational studies,[3,9] we can assign principal lines of spectrum 4 (P.S.B.) to the present low-temperature spectrum directly. The assignments of various lines in the low temperature spectrum are related to those of Bernstein, Schneider, and Pople in Fig. 2(e).

We have, therefore,

$$N=E_1-E_3=15.6 \text{ cps} \quad (1)$$

$$(M^2+L^2)^{\frac{1}{2}}=E_9-E_{11}=12.1 \text{ cps} \quad (2)$$

$$[(\nu_0\delta)^2+N^2]^{\frac{1}{2}}=E_1+E_3=19.0 \text{ cps} \quad (3)$$

$$[(\nu_0\delta+M)^2+L^2]^{\frac{1}{2}}=E_9+E_{11}=12.1 \text{ cps}, \quad (4)$$

using the exact notation of P.S.B. and inserting the experimental numbers from the spectrum Fig. 1(e). The value of $K=J_{e_1e_2}+J_{a_1a_2}$ is needed for a complete analysis and cannot be determined directly. The assumption is made that $J_{a_1a_2}=7.43$ cps. This is an average value of $10\,J_{a_1a_2}$ coupling constants in saturated six-membered ring compounds.[3] The other parameters can then be obtained (P.S.B.) from Eqs. (1)–(4):

$$M=-5.3 \text{ cps}=J_{e_1e_2}-J_{a_1a_2}$$

$$N=15.6 \text{ cps}=J_{a_1e_1}+J_{e_1a_2}$$

$$L=10.8 \text{ cps}=J_{a_1e_1}-J_{e_1a_2}$$

$$J_{a_1a_2}=7.41 \text{ cps (assumed)}.$$

Thus,

$$J_{a_1e_1}=13.2 \text{ cps}, \quad J_{e_1a_2}=2.4 \text{ cps}, \quad \text{and} \quad J_{e_1e_2}=2.1 \text{ cps}$$

$$\nu_0\delta=10.8 \text{ cps}.$$

All these are reasonable values from comparison with similar compounds.[3]

Energy Barrier for Conversion between Two Chair Forms

In previous papers, the energy barriers for interconversion have been obtained from the so-called "coalescence temperature."[4,5] The two chemical shifts which coalesce were associated with many splittings caused by J coupling with other chemically shifted protons in the molecule.[1,2] These splittings remain on averaging the two chemical shifts, but change their individual values since, in general, *aa* coupling is large compared to *ae* and *ee*. The over-all halfwidth of the average signal is some function of the position of the equilibrium and the individual values $J_{a_1a_2}$, $J_{e_1e_2}$, and $J_{e_1a_2}$.

In the molecule studied here, the energy barrier can be estimated both from coalescence and from measurements on the single signal at higher temperatures near the exchange limit.[6,13–16] The simple case of two chemically shifted uncoupled nuclei of spin $\frac{1}{2}$ near the exchange limit has been treated adequately,[13,15] and from experimental measurements τ, the average nuclear lifetime, can be obtained at various temperatures. The present molecule satisfies the conditions of these equations approximately since there are two sets of two protons chemically shifted by 10.8 cps. There is, however, coupling between these spins at low temperatures which averages to zero when all nuclei become identical in the limit of fast exchange. The splittings resulting from the A_2B_2 case at low temperatures defines a shorter critical lifetime τ_c for collapse, and thus,

[11] A. T. Bottini and J. D. Roberts, J. Am. Chem. Soc. **78**, 5126 (1956).

[12] J. F. Kincaid and F. C. Henriques, Jr., J. Am. Chem. Soc. **62**, 1474 (1940).

[13] S. Meiboom, Z. Luz, and D. Gill, J. Chem. Phys. **27**, 1411 (1957).

[14] J. Kaplan, J. Chem. Phys. **28**, 27 (1958).

[15] L. H. Piette and W. A. Anderson, J. Chem. Phys. **30**, 899 (1959).

[16] H. M. McConnell, J. Chem. Phys. **28**, 430 (1958).

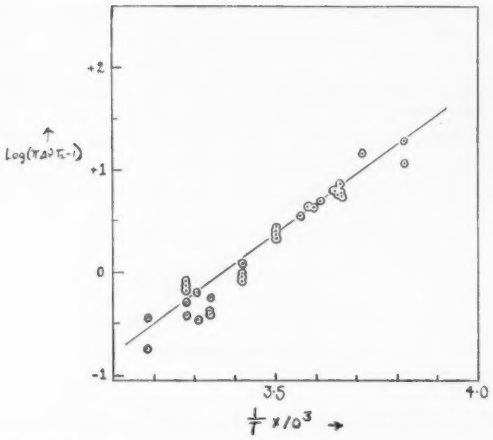

FIG. 2. Energy barrier for interconversion obtained from plot of $\log(\pi\cdot\Delta\nu\cdot T_2-1)$ vs $1/T$.

and thus, the fine structure collapses to two broad chemically shifted lines before the two chemical shifted lines collapse. At temperatures near the exchange-narrowing limit, the equations for two uncoupled protons will apply[13,15]; we use, therefore,

$$\log_{10}(\pi\Delta\nu\cdot T_2-1)=\log_{10}(\nabla T_2/2V_0)+\frac{E_a}{2.303RT}, \qquad (5)$$

where

$$k=\exp(-E_a/RT), \qquad (6)$$

$\Delta\nu$=signal half-width at temperature T°K near exchange-narrowing limit, T_2=transverse relaxation time in fast exchange limit, ∇=second moment of line at temperature T°K, V_0=frequency factor for interconversion process, E_a=energy barrier for conversion between two chair forms, k=rate constant at temperature T°K for conversion, R=gas constant.

Figure 2 shows a plot of $\log_{10}(\pi\Delta\nu\cdot T_2-1)$ vs $1/T$. At the high temperatures, near to the natural linewidths defined by T_2, there is a large error in the term $(\pi\Delta\nu\cdot T_2-1)$, but at lower temperatures -10°C to 20°C the points fall on a straight line. The maximum and minimum slopes of this line define the limits 13.65 and 13.03 kcal for the energy barrier to conversion $'E_a'$.

The energy barrier $'E_a'$ obtained from the coalescence temperature 248.2°K where one broad line occurs is 13.04 kcal, assuming a chemical shift between axial and equatorial positions of 10.8 cps. The agreement between these two independent measurements is satisfactory, and the value of E_a obtained is more reliable than that obtained in earlier studies on cyclohexane rings.[1,2]

It is nevertheless interesting to note a significant increase in the energy barrier per mole in the series; cyclohexane~9.7 kcal,[17] chloro- and bromo-cyclohexane~10.85 kcal, 1.2 *trans*-dichloro and 1.2 *trans*-dibromo~11.8 kcal, and *NN'*-dimethyl piperazine 13.3±0.3 kcal. This may be caused by the increasing bulk of substituted groups.

ACKNOWLEDGMENTS

This work was supported by research grants to L.W.R. from the National Research Council of Canada and the Research Corporation. One of us (K.O.S.) wishes to thank the Royal Norwegian Council for Scientific and Technical Research for the award of a fellowship.

[17] F. R. Jensen, S. Noyce, C. H. Sederholm, and A. J. Berlin, J. Am. Chem. Soc. **82**, 1256 (1960).

THE JOURNAL OF CHEMICAL PHYSICS VOLUME 34, NUMBER 5 MAY, 1961

Dissociation Processes in Electronically Excited Molecules. Linear Chain Model*

JOHN L. MAGEE AND KOICHI FUNABASHI

Department of Chemistry, University of Notre Dame, Notre Dame, Indiana

(Received October 17, 1960)

Dissociation mechanisms in a chain of coupled molecules have been considered. The attempt has been made to look at general features of the influence of electronic coupling on such processes. Actual calculations have only been made for the special case of a chain of H_2^+ ions. The weak-coupling and strong-coupling cases have been discussed explicitly, and various criteria for applicability of the special cases have been presented in terms of the physical constants of the system.

1. INTRODUCTION

RECENT theoretical and experimental studies have made clear that electronic excitation of molecules in condensed systems differs from that of isolated molecules.[1-7] Chemical effects which result from electronic excitation usually depend upon dissociation processes. In this paper we are interested in the mechanism of dissociation of electronically excited molecules in condensed systems. For this purpose, we present the study of a model: a linear chain of identical molecules in an excited electronic state of such a type that is clearly dissociative in the case of very weak coupling. The study of such a definite model has the advantage that detailed calculations can be made, whereas any real case of interest is too complicated for rigorous treatment. On the other hand, there is reason to believe that the influence of coupling on dissociation observed in the model may have a general validity.

Two extreme cases of coupling have been recognized.[2,4,7] In weak coupling the collective system is essentially composed of separate molecules, each of which has its complete wave function, including electronic, vibrational, and rotational parts. In strong coupling, the collective system behaves as one giant molecule with a single electronic wave function, and a single vibrational wave function.

In this paper we consider examples of potentially dissociative systems in both weak and strong coupling. We have attempted to consider these problems in a very general manner. Some calculations have been made and for this purpose it was found that the system $(H_2^+)_N$ was very useful.

2. EXCITATION TRANSFER

2.1. Propagation of Excitation

In the limit of very weak coupling, the probability of excitation transfer to neighboring molecules is so small that a dissociative electronic state initially localized in a molecule remains localized and eventually dissociates the molecule. In this section, we shall show that in weak coupling the dissociative excitation migrates from the initial locale to a finite distance. A dissociation is always produced. On the other hand, in strong coupling, the excitation can migrate throughout the system. In this case the probability of a dissociation occurring at all is very small.

Let $\Psi_n(t)$ be the zeroth-order wave function of the chain of N molecules in which the nth molecule is excited to a repulsive state. The first-order wave function at time t for the chain may be written as

$$\Psi(t)=\sum_{n=1}^{N}a_n(t)\Psi_n(t), \tag{2.1}$$

where the $a_n(t)$'s are to be determined by the Schrödinger equation

$$H\Psi(t)=i\hbar(\partial/\partial t)\Psi(t). \tag{2.2}$$

Throughout this paper we shall be primarily interested in solutions for the following initial conditions:

$$a_p(0)=1, \qquad a_n(0)=0 \qquad \text{for } n\neq p; \tag{2.3}$$

Ψ_n can be written as a product of electronic and nuclear wave functions,

$$\Psi_n=\Phi_n\cdot X_n, \tag{2.4}$$

where Φ_n is an electronic wave function and X_n is a nuclear wave function for the chain. The Φ_n can be written in turn as a product of individual molecular electronic wave functions,

$$\Phi_n=\phi_1\cdots\phi_{n-1}\phi_n'\phi_{n+1}\cdots\phi_N, \tag{2.5}$$

where the unprimed ϕ_j is the electronic wave function for the ground state of the jth molecule and ϕ_n' is the electronic wave function for the excited repulsive state

* Contribution from the Radiation Laboratory operated by the University of Notre Dame and supported in part by the U. S. Atomic Energy Commission.

[1] U. Fano, Phys. Rev. **118,** 451 (1960).
[2] W. T. Simpson and D. L. Peterson, J. Chem. Phys. **26,** 588 (1957).
[3] E. G. McRae and M. Kasha, J. Chem. Phys. **28,** 721 (1958).
[4] J. Franck and E. Teller, J. Chem. Phys. **6,** 861 (1938).
[5] U. Fano, Phys. Rev. **103,** 1202 (1956).
[6] B. G. Anex and W. T. Simpson, Revs. Modern Phys. **32,** 466 (1960).
[7] A. Witkowski and W. Moffitt, J. Chem. Phys. **33,** 872 (1960).

of the nth molecule. We shall assume that the product form for Φ_n is valid both for weak and strong coupling.

In the case of weak coupling, X_n can be written as a product of molecular nuclear wave functions,

$$X_n=\chi_1\cdots\chi_{n-1}\cdot\xi_n\cdot\chi_{n+1}\cdots\chi_n, \tag{2.6}$$

where χ_j is the vibrational wave function for the ground state of the jth molecule and ξ_n is the nuclear wave function for the repulsive state of the nth molecule.

In the case of strong coupling, all X_n's can be made to have the common form X, because all the nuclei in the chain share common potential hypersurfaces which are determined by the relevant electronic wave functions for the chain.

For the Φ_n we use the wave function without the customary time factor $\exp(-i/\hbar\epsilon_n t)$. This procedure amounts to taking ϵ_n as zero. For ξ_n we take a wave packet [see Eqs. (2.28)–(2.30)]. The only time-dependent part of $\Psi_n(t)$ is $\xi_n(t)$, and we can write

$$(\partial/\partial t)\Psi_n(t)=\Phi_n\chi_1\cdots\chi_{n-1}\chi_{n+1}\cdots\chi_N(\partial\xi_n/\partial t). \tag{2.7}$$

Equation (2.2) becomes

$$\sum_{n=1}^{N}\dot{a}_n(t)\Psi_n(t)+\sum_{n=1}^{N}a_n(\partial/\partial t)\Psi_n=-(i/\hbar)\sum_{n=1}^{N}a_nH\Psi_n. \tag{2.8}$$

Multiplication of 2.8 by Ψ_q^* and integration over all electronic and nuclear coordinates gives

$$\dot{a}_q+a_q[\xi_q^*(\partial/\partial t)\xi_q]=-(i/\hbar)\sum_j a_{q\pm j}(\Psi_q^*H\Psi_{q\pm j}), \tag{2.9}$$

where all other terms vanish because of orthogonality. We chose ξ_q to be a wave packet which satisfies the equation

$$(\partial/\partial t)\xi_q=-(i/\hbar)H_q\xi_q, \tag{2.10}$$

where H_q is the Hamiltonian of the qth molecule. Thus,

$$[\xi_q^*(\partial/\partial t)\xi_q]=-(i/\hbar)\langle\xi_q\rangle \tag{2.11}$$

since the wave packet has a well-defined average energy $\langle\epsilon_q\rangle$.

The substitution

$$b_q=a_q\exp(-i/\hbar\langle\epsilon_q\rangle t) \tag{2.12}$$

allows Eq. (2.9) to be written as

$$db_q/dt=-(i/\hbar)\sum_j b_{q\pm j}\int\Psi_q^*H\Psi_{q\pm j}d\tau. \tag{2.13}$$

In order to obtain a solution for (2.13), we assume that

$$\int\Psi_q^*H\Psi_{q\pm j}d\tau=0, \qquad \text{except for } j=1, \tag{2.14}$$

and

$$\int\Psi_q^*H\Psi_{q-1}d\tau=\int\Psi_q^*H\Psi_{q+1}d\tau\equiv M(t). \tag{2.15}$$

The assumption (2.15) involves the use of a common time dependences for all Ψ_q's, and thus for all ξ_q's.

Equation (2.13) can now be written as

$$db_q(t)/dt=(-i/\hbar)M(t)[b_{q+1}(t)+b_{q-1}(t)], \qquad q=1, 2, \cdots, N. \tag{2.16}$$

Equations (2.16) constitute a set of linear difference differential equations. The solution for (2.16) can be obtained from the well-known recurrence formula for Bessel functions,

$$dJ_n(x)/dx=\tfrac{1}{2}[J_{n-1}(x)-J_{n+1}(x)]. \tag{2.17}$$

Comparison of (2.16) and (2.17) together with the initial condition (2.3) yields the solutions

$$b_{p+n}(t)=\exp(-in\pi/2)\,J_n(\gamma), \quad n=0, 1, 2, \cdots, \tag{2.18}$$

where

$$\gamma=(2/\hbar)\int_0^t M(t)dt. \tag{2.19}$$

From Eq. (2.18), the probability of finding excitation at the $(p+n)$th molecule is

$$a_{p+n}^*\cdot a_{p+n}=[J_n(\gamma)]^2. \tag{2.20}$$

The same result was obtained by one of us[8] for the special case of a time-independent M. The most useful measure of the spread of excitation from the initially excited pth molecule in a long chain can be given by

$$\langle n^2\rangle^{\frac{1}{2}}=\{2\sum_{n=0}^{\infty}n^2[J_n(\gamma)]^2\}^{\frac{1}{2}}. \tag{2.21}$$

The right-hand side of (2.21) can be evaluated using the following well-known equations:

$$2n/x=J_n(x)=J_{n-1}(x)+J_{n+1}(x),$$

$$\int_0^x x[J_n(x)]^2dx=(x^2/2)\{[J_n(x)]^2-J_{n-1}(x)\,J_{n+1}(x)\}. \tag{2.22}$$

The result is

$$\langle n^2\rangle^{\frac{1}{2}}=\gamma/\sqrt{2}. \tag{2.23}$$

It can be seen that the spread of excitation is a linear function of γ which is a function of time as defined in (2.19). As we shall see in the next section, in the case of weak coupling the function $M(t)$ of (2.19) becomes vanishingly small within a time of the order of 10^{-14} sec, and in the meanwhile γ approaches an asymptotic value, whereas in the case of strong coupling, $M(t)$ is almost a constant and γ becomes a linear function of time. In other words, in the case of weak coupling, the spread of dissociative excitation does not increase indefinitely with time, but is a characteristic constant of the system. On the other hand, in the case of strong coupling, the excitation does travel throughout the entire system. It is interesting to note that the value of $\langle n^2\rangle$ varies as the *square* of the time for this system. If

[8] J. L. Magee, *Comparative Effects of Radiation* (John Wiley & Sons, Inc., New York, 1960), Chap. VII, p. 130.

the excitation migrated by a diffusion mechanism $\langle n^2 \rangle$ would vary as the *first* power of the time.

In the comparison of the extent of spreading of excitation for weak and strong coupling, it should be remembered that there is another important difference between these cases. In weak coupling, dissociation always occurs within the region involved, whereas in strong coupling, dissociation is improbable.

2.2. Evaluation of Matrix Element

In this section we shall evaluate the matrix element $M(t)$ defined in (2.15) for a typical dissociative potential curve as shown in Fig. 1(a).

In the case of weak coupling, $M(t)$ can be expressed in terms of wave functions defined in (2.5) and (2.6) as

$$M(t) = \int \beta (\xi_n \cdot \chi_{n+1})^* (\chi_n \cdot \xi_{n+1}) d\tau_n, \qquad (2.24)$$

where the integration is over the nuclear coordinates and β is an integral over the electron coordinates

$$\beta \equiv \int (\phi_n' \cdot \phi_{n+1})^* H \phi_n \cdot \phi_{n+1}' d\tau_e. \qquad (2.25)$$

Although β in (2.25) is an explicit function of nuclear coordinates, it is much less sensitive to variation of nuclear coordinates (see Sec. 3.3) than the overlap integrals of nuclear wave functions. It is, therefore, natural to make the following approximation:

$$M(t) = \beta \int (\xi_n \chi_{n+1})^* \chi_n \xi_{n+1} d\tau_n, \qquad (2.26)$$

where β is to be evaluated at the normal internuclear separation, and χ_n and χ_{n+1} are taken in the form

$$\chi = (\alpha^2/\pi^{1/4}) \exp(-\alpha^2 \delta^2/2), \qquad (2.27)$$

where δ is the displacement from the equilibrium internuclear separation. For ξ_n and ξ_{n+1} we assume that the initial wave functions are of the form of a wave packet

$$\xi(\delta, 0) = (\alpha^2/\pi^{1/4}) \exp(-\alpha^2 \delta^2/2). \qquad (2.28)$$

This initial form for the wave function of the dissociative state seems reasonable because of the Franck-Condon principle. It is possible to show that this state would actually result from certain types of excitation. For a given form of potential curve, the form of the wave packet at time t, $\xi(\delta, t)$, can be found by a suitable Fourier transform. It has been shown that a wave packet of the type (2.28) moving in an harmonic potential does not change its form, and the center of gravity of the wave packet moves with the classical velocity.[9] Since we are interested in the time-dependent behavior of the wave packet only for a limited part of the potential curve, any such curve can be approximated as a potential curve for a harmonic oscillator with a suitable choice of parameters. In this case, the center of gravity of the wave packet moves with the classical velocity Ft/μ from P [see Fig. 1(a)] where F is the common tangent at P, μ is the reduced mass of the diatomic molecule, and t is the time. Thus, at least for the immediate vicinity of the point P, the time-

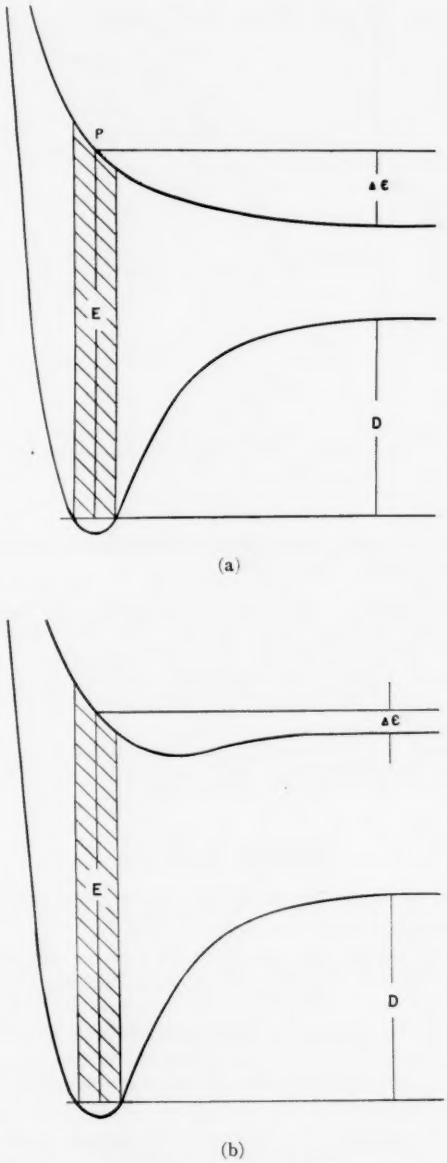

FIG. 1. (a) and 1(b) Schematic potential curves for diatomic molecule with dissociative excited state. D is the dissociation energy of the ground state; E is the excitation energy; $\Delta\epsilon$ is the kinetic energy of dissociated molecule. The potential curve for (b) has a minimum.

[9] L. Schiff, *Quantum Mechanics* (McGraw-Hill Book Company, Inc., New York, 1955), 2nd ed., p. 67.

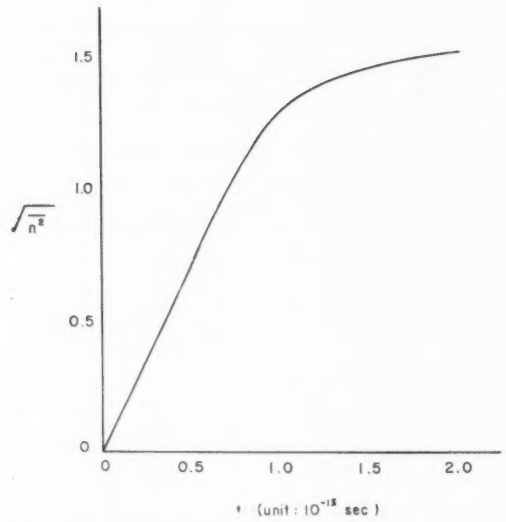

FIG. 2. Spread of excitation as a function of time for weak coupling [Eqs. (2.21) and (2.23).]

dependent form of the wave function packet can be given as

$$\xi(\delta, t)=\frac{\alpha^{1/2}}{\pi^{1/4}}\exp\left[\frac{-\alpha^2}{2}\left(\delta-\frac{Ft^2}{2\mu}\right)^2+i\theta\right], \quad (2.29)$$

where θ is a phase factor which is a function of time alone. Substitution of (2.27) and (2.29) into (2.26) gives

$$M(t)=\beta\exp\left(\frac{-\alpha^2F^2}{8\mu^2}t^4\right). \quad (2.30)$$

From (2.19), (2.23), and (2.30), the spread of excitation can be found as a function of time.

A calculation has been made for a model consisting of a chain of hydrogen molecule ions. The axis of each molecule is perpendicular to the long axis of the chain and the intermolecular separations are kept constant. The repulsive state is taken to be the first excited state of H_2^+, Σ_u^+. The parameters involved in the calculation are the following:

$$F=2.96\cdot10^{-3}\text{ erg cm}^{-1} \qquad \alpha=3.434\cdot10^{17}\text{ cm}^{-2}$$

$$\mu=0.83625\cdot10^{-24}\text{ g} \qquad \beta=0.1\text{ ev}.$$

The result of this calculation is given in Fig. 2.

For strong coupling, the parallel calculation leads to $M(t)=\beta$ because the nuclear overlap integral is unity. Therefore, the spread of excitation is

$$\langle n^2\rangle^{\frac{1}{2}}=\beta t/\sqrt{2}. \quad (2.31)$$

The strong-coupling assumption that the wave function for the chain can be separated into an electronic part and a nuclear part actually includes the assumption that the nuclear motion is adiabatic. Dissociation mechanisms can only be ascertained from the potential energy surfaces of the chain.

3. ELECTRONIC ENERGY

3.1. Stationary States Solution

In the case of a strongly coupled chain of molecules, the electronic wave function for the chain can be given adequately as

$$U_k=\sum_{p=1}^{N}C_{kp}\Phi_p, \quad (3.1)$$

where Φ_p's are defined in (2.4) and (2.5), and C_{kp}'s are constants to be determined by solution of the secular determinant which has the form

$$\begin{vmatrix} x & \beta & & & & & \\ \beta & x & \beta & & & & \\ & \beta & x & \beta & & & \\ & & \cdot & \cdot & \cdot & & \\ & & & & \beta & x & \beta \\ & & & & & \beta & x \end{vmatrix}=0, \quad (3.2)$$

where

$$x=E-\int\Phi_p^*H\Phi_p d\tau.$$

Here β is given by Eq (2.25) and we have taken all resonance integrals as zero if the excitation is on non-adjacent molecules in the two states involved.

Eq. (3.2) has the well-known solutions

$$x_k=2\beta\cos[k\pi/(N+1)], \qquad k=1, 2, 3, \cdots, N. \quad (3.3)$$

Equation (3.2) applies to the case in which all β's are

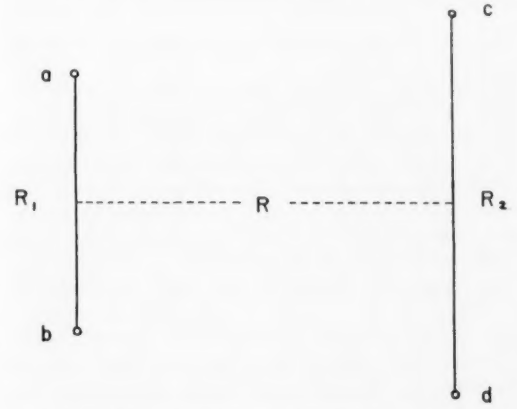

FIG. 3. Nuclear configuration for hydrogen molecule-ions used in calculation of β'.

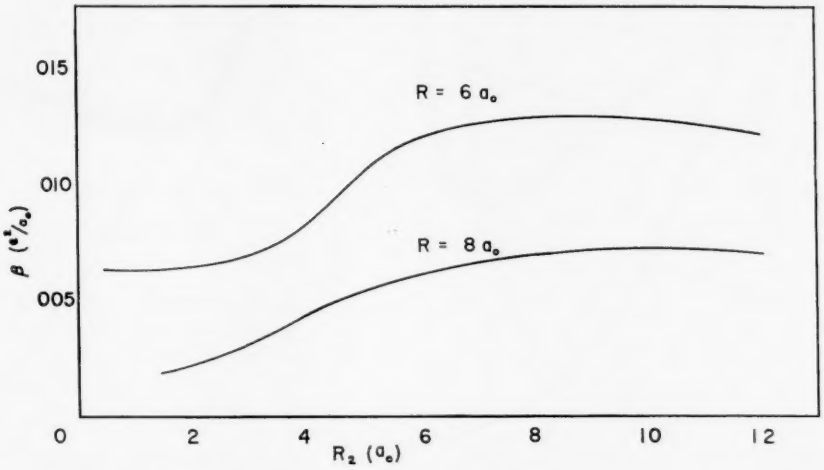

FIG. 4. Matrix element β' as a function of internuclear separations (see Fig. 3). R_1 is constant at $2a_0$.

equal. Thus, all molecules have the same internuclear separation and have the same orientation with respect to the chain. In order to investigate dissociation processes, it is necessary to consider the solutions, (i.e., x_k's) of this equation for cases in which the internuclear separation of one or more of the molecules are different from the others. If the qth has a different separation from the others, the secular equation becomes

$$\begin{array}{l} \\ \\ \\ \\ \\ q\text{th row} \\ \\ \\ \\ \\ \end{array} \begin{vmatrix} x & \beta & & & & & & & \\ \beta & x & \beta & & & \cdot & & & \\ \beta & x & \beta & & \cdot & & & & \\ & \cdot & \cdot & \cdot & \cdot & & & & \\ & & \beta & x & \beta' & & & & \\ \cdot & \cdot & \cdot & \cdot & \beta' & x' & \beta' & & \\ & & & & \beta' & x & \beta & & \\ & & & & & \cdot & \cdot & \cdot & \\ & & & & & & \beta & x & \beta \\ & & & & & & & \beta & x \end{vmatrix} = 0, \qquad (3.4)$$

qth column

since it is clear that the matrix element x' for this molecule is different and the integral β' with its neighbors are different. We indicate these altered matrix elements with primes.

The secular equation (3.4) can be solved approximately by methods discussed in the Appendix.

3.2. Potential Energy Curves for Isolated Molecule

In an isolated diatomic molecule there are two possible types of dissociative states as shown in Figs. 1(a) and 1(b). The Franck-Condon region is indicated by cross-hatching. The important parameters of these curves are the excitation energy E, the binding energy D, and the exothermicity $\Delta\epsilon$. The ratio E/D gives the upper limit for the number of possible dissociations in the chain of interacting molecules following excitation. The effect of $\Delta\epsilon$ depends upon how it compares with the matrix element β.

3.3. Matrix Element β

In the absence of exchange effects, the matrix element β can be written as

$$\beta = \int \phi_{p\pm1}'(1)\phi_{p\pm1}(1) H \phi_p'(2)\phi_p(2) d\tau_1 d\tau_2, \qquad (3.5)$$

where we have taken the wave function to be real. Since the direct evaluation of (3.5) is difficult except for certain simple cases, the integrand of β is usually expanded in terms of multipoles and β is expressed as a sum of multipole interactions. If only the dipole interaction is important, β has the form

$$\beta = (e^2/R^3)\{|X|^2 + |Y|^2 - 2|Z|^2\}, \qquad (3.6)$$

where X, Y, and Z are the components of the dipole transition matrix between the ground state and the excited state of an isolated molecule, and Z is the direction of the long axis of the chain. From Eq. (3.6), it can be seen that β can be positive or negative depending upon the relative orientation of the two dipoles. In this particular case the matrix element is called a "resonance integral."[10]

[10] H. Margenau, Revs. Modern Phys. **11**, 1 (1939).

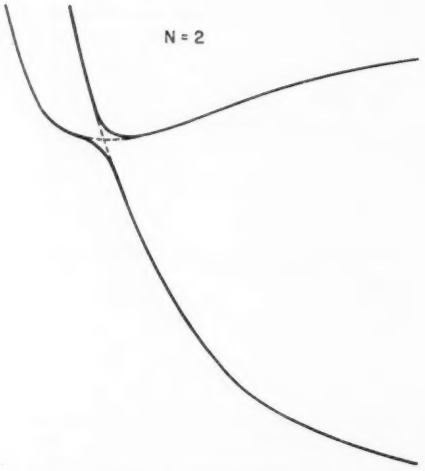

FIG. 5. Cross section of hypersurface for pair of hydrogen molecule ions in excited state. The ordinate is energy and the abscissa is the separation of one of the molecules. The other molecule has its normal separation $2a_0$. The behavior of the diagonal matrix elements is indicated by the dashed line.

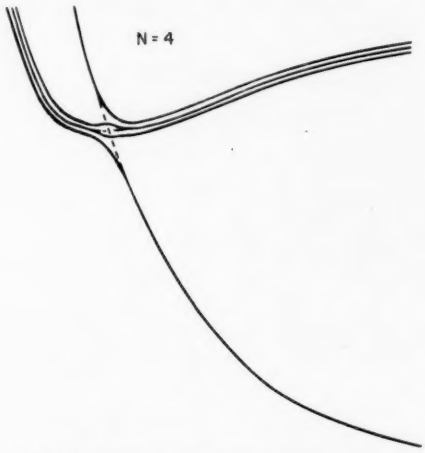

FIG. 7. Cross section of hypersurface for excited state of linear chain $(H_2^+)_N$ with $N=4$. The ordinate is energy and the abscissa is the internuclear separation of one of the central molecules. The other three molecules have normal internuclear separation $2a_0$. The dashed curves give the behavior of two of the diagonal matrix elements.

Whereas β is a matrix element between neighboring molecules with the same internuclear separation, in Eq. (3.4) β' is a matrix element between neighboring molecules with different internuclear separations. Let R_1 and R_2 be the internuclear separations of the two molecules and R the intermolecular separation (Fig. 3). For this case β' can be written as

$$\beta' = (e^2/R^3)\{|X_{R_1}|\cdot|X_{R_2}| + |Y_{R_1}|\cdot|Y_{R_2}| - 2|Z_{R_1}|\cdot|Z_{R2}|\}, \quad (3.7)$$

where X_{R_1}, for example, stands for the X component of the dipole transition matrix at internuclear separation R_1. The dipole approximation for the resonance integral has been discussed at length by Margenau,[10] Förster,[11] and others. Experimental data can be utilized since the transition dipole is related to the oscillator strength of the transition.

The integrals β and β' are difficult to obtain for general cases. In order to have an example which can be

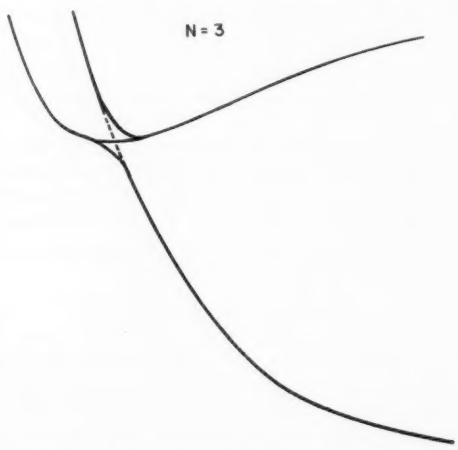

FIG. 6. Cross section of hypersurface for excited state of linear chain $(H_2^+)_N$ with $N=3$. The ordinate is energy and the abscissa is the internuclear separation of the central molecule. The other two molecules have their normal separation $2a_0$. The curve at the extreme left is doubly degenerate and the upper curve at the right is doubly degenerate. The dashed curve gives the behavior of one of the diagonal matrix elements.

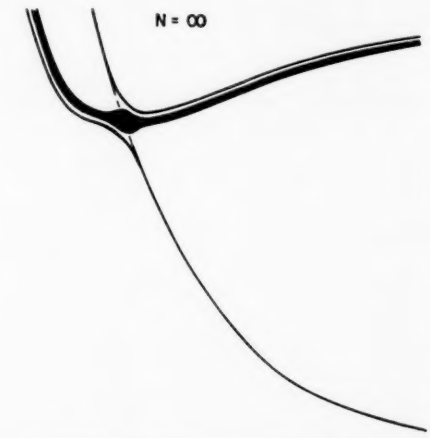

FIG. 8. Cross section of hypersurface for excited state of linear chain $(H_2^+)_N$ for N approaching infinity. The ordinate is energy and the abscissa is the internuclear separation of one of the central molecules. The other $N-1$ molecules have normal internuclear separation $2a$. The heavy curve is a band of $N-2$ closely spaced curves. The light curves are nondegenerate.

[11] Th. Förster, *Fluoreszenz organischer verbindung* (Vandenhoeck and Ruprecht, Göttingen, Germany, 1951).

worked out completely, we have again considered the case of interaction of a chain of H_2^+ ions, one of which is in the first excited state Σ_u^+. For this example the integral can be obtained without use of the multipole expansion of the integrand. In terms of the LCAO scheme, the ground state of the left molecule in Fig. 3 has the molecular orbital

$$\phi_{R_1}=\{2+2S_{R_1}\}^{-\frac{1}{2}}\{(1s)_a+(1s)_b\}, \qquad (3.8)$$

and its excited state has the molecular orbital

$$\phi_{R_1}'=\{2-2S_{R_1}\}^{-\frac{1}{2}}\{(1s)_a-(1s)_b\}, \qquad (3.9)$$

where $(1s)_a$ and $(1s)_b$ are the $(1s)$ atomic orbitals of hydrogen at a and b, and S_{R_1} is the overlap integral at the separation R_1. Similar expressions can be written for ϕ_{R_2}' and ϕ_{R_3}. By using these wave functions and Eq. (3.5), β' was calculated for $R=6a_0$ and $8a_0$. The Hamiltonian in Eq. (3.5) has just one term, $1/r_{12}$ in this case. In Fig. 4, β' is plotted against R_2 with R_1 fixed at the equilibrium separation $2a_0$. For the H_2^+ case it is clear that the integral β' does not depend sensitively upon the internuclear separation R_2. It should be noted here that the magnitude of β' in this case is too small for the strong-coupling classification. Nevertheless, we proceed to calculate the potential curves for the chain, because the qualitative features of these curves are applicable in general both to weak and strong coupling.

3.4. Potential Curves for Chain

A complete description of the potential energy of the linear model of N diatomic molecules, even with fixed intermolecular separation and orientation, would require an $(N+1)$ dimensional hypersurface. If only one molecule of the chain changes its internuclear separation, keeping the other $(N-1)$ molecules at, say, the equilibrium separation of the ground state, potential energies can be described by two-dimensional curves, which represent cross sections of the $(N+1)$ dimensional hypersurface along certain directions.

FIG. 9. Cross section of hypersurface for excited state of linear chain $(H_2^+)_N$ for $N\to\infty$. The ordinate is energy and the abscissa is the common internuclear separation of a pair of two central molecules. The other $N-2$ molecules have normal internuclear separation $2a_0$. The heavy curve is a band of $N-4$ closely spaced curves. The upper and lower curves are doubly degenerate. The curves of this figure are essentially independent of the choice of the two molecules whose internuclear separation is varied.

FIG. 10. Cross section of hypersurface for excited state of linear chain $(H_2^+)_N$ with $N\to\infty$. The ordinate is energy and the abscissa is the common internuclear separation of a set of three of the central molecules. The other $N-3$ molecules have normal internuclear separation $2a_0$. The heavy curve is a band of $N-6$ closely spaced curves. The upper and lower curves are triply degenerate. The curves of this figure are essentially independent of the choice of the three molecules whose separation is varied.

The results of such two-dimensional potential curves are shown in Figs. 5–8 for $N=2$, 3, 4, and ∞.

Similar cross sections of the $(N+1)$-dimensional hypersurface, in which particular sets of 2, 3, 4, and 5 molecules in the chain for $N=\infty$ change their internuclear separation equally while the other molecules are fixed at the equilibrium separation of the ground state, are shown in Figs. 9–12.

In all cases, the diatomic molecules are hydrogen molecule ions, and are arranged in such a way that all the molecular axes are perpendicular to the long axis of the chain and intermolecular separations between every pair of neighboring molecules are the same.

It can be seen from these figures that in the case of H_2^+, the excitation energy $(\Sigma_g^+\to\Sigma_u^+)$ is large enough to dissociate four molecules in the chain. Strictly speaking, potential curves shown in Figs. 5–12 depend somewhat on positions of the molecules which are chosen for change of internuclear separation. Each interior molecule interacts with two neighboring molecules while the end molecules have just one neighbor. Since the electrostatic interaction is smaller than the matrix element β in the range of intermolecular separation with which we are concerned, all the molecules in the chain are approximately equivalent; thus, all diagonal elements x in Eq. (3.2) are taken to be equal.

FIG. 11. Cross section of hypersurface for excited state of linear chain $(H_2^+)_N$ with $N\to\infty$. The ordinate is energy and the abscissa is the common internuclear separation of four of the central molecules. The other $N-4$ molecules have normal internuclear separation $2a_0$. The heavy curve is a band of $N-8$ closely spaced curves. The upper and lower curves are fourfold degenerate.

3.5. Application to Other Systems

The curves of Figs. 5–8 are very nearly made up of sections of the potential curves for the isolated molecule. For example, the band of $(N-2)$ closely spaced states in Fig. 8 is the same shape as the potential curve of the ground state of H_2^+; the single states which are split off above and below are composed partly of the excited dissociative state and partly of the ground state. This situation results from the relative unimportance of β in shifting the energy. The same situation is expected to obtain whenever β is considerably smaller than the molecular binding energy.

In the case of general diatomic molecules, potential curves for ground and excited states can be quite varied. Typical cases of dissociative excited states are shown in Figs. 1(a) and 1(b). It is clear that cross sections of the hypersurface for linear systems composed of molecules with such potential curves will be similar to those for H_2^+. In particular, for large N a band of closely spaced states of width 4β will have the shape of the ground state. The single state, which at the left of the figure is the upper state and at the right of the figure is the lower state, will have the general shape of the repulsive upper state.

Let us now consider possible effects on dissociation processes introduced by the presence of foreign entities in the neighborhood of the chain. When the chain has free ends, there is no qualitative difference in potential curves for molecules in the middle and at the ends. However, the situation is different if the end molecule, for example, is associated with some other kind of molecule or ion which introduces an additional electrostatic energy ΔE. If ΔE is very small, there is again no marked difference in the potential curves for molecules in the middle and at the ends. However, if ΔE is not small compared to the magnitude of β, there is a stabilizing effect for the central molecules or the end molecules depending upon the sign of ΔE. The relevant secular equation has the form

$$\begin{vmatrix} x\pm\Delta E & \beta & & & & & \\ \beta & x & \beta & & & & \\ & \beta & x & \beta & & & \\ & & \cdot & \cdot & \cdot & & \\ & & & \cdot & \cdot & \cdot & \\ & & & & \beta & x & \beta \\ & & & & & \beta & x \end{vmatrix} = 0. \qquad (3.10)$$

Let us take the potential curves for the isolated molecule to be of the form given in Fig. 1(a). The zeroth-order solution [ignoring all of β's of Eq. (3.10)] are shown in Figs. 13(a) and 14(a) for positive and negative ΔE, respectively. In both cases, the abscissa is the internuclear separation of the end molecule. When β's are introduced into the solution, these curves change as shown in Figs. 13(b) and 14(b), respectively. It can be seen from these figures that when $\Delta E>0$, or the end molecule repels the foreign entity, its dissociation, when the system is in the lowest state, is prevented by an energy barrier γ whereas if $\Delta E<0$, or the end molecule attracts the foreign entity, there is no barrier for dissociation of the lowest state.

FIG. 12. Cross section of hypersurface for excited state of linear chain $(H_2^+)_N$ with $N\to\infty$. The ordinate is energy and the abscissa is the common internuclear separation of five molecules. The other $N-5$ molecules have normal internuclear separation $2a_0$. The heavy curve is $N-10$ closely spaced curves and the upper and lower curves are fivefold degenerate.

The situation is exactly reversed for potential curves of the central molecules. If $\Delta E>0$, the lowest state is completely dissociative, whereas if $\Delta E<0$, an energy barrier prevents dissociation of the lowest state.

The magnitude of the energy barrier γ depends not only upon the magnitude of ΔE, but very sensitively upon the slope of the repulsive curve and the curvature of the potential curve for the ground state at the equilibrium internuclear separation; that is, the steeper the repulsive curve and the smaller the curvature of the potential curve for the ground state, the smaller the energy barrier and vice versa.

It should be noted that in all of these cases it is only the lowest state of the system which can dissociate adiabatically.

4. DISCUSSION

No progress has been made in the treatment of systems in intermediate coupling. This void in our theoretical knowledge is particularly unfortunate because many systems of interest fall into this category. Presumably it would be possible to consider this case from the strong-coupling or weak-coupling side. In this paper only potentially dissociative states have been considered, and it is very apparent that our treatment is not uniform in estimation of deviation from the extreme cases of coupling. Whereas for weak coupling we have estimated the extent of excitation migration before dissociation occurs, for strong coupling we have not made the corresponding estimate of the probability for dissociation. Presumably dissociation in strong coupling would occur because of vibronic interaction. A feature of the strong-coupling case is the possibility of multiple dissociation occurring from one excitation if the system can reach the lowest electronic state.

An estimate of the limit of the region of weak coupling can be made as follows. It has been shown that the average increase in internuclear separation in

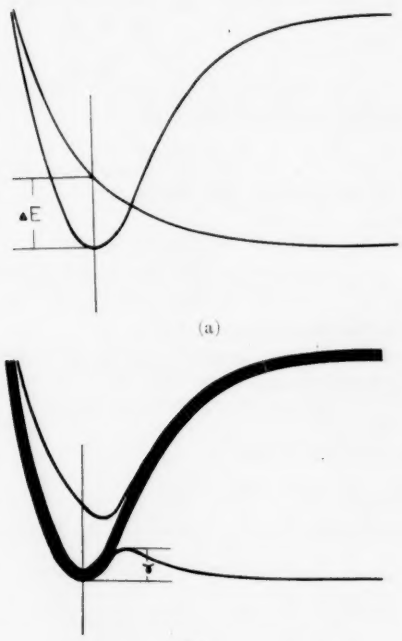

FIG. 13. Cross section of hypersurface for excited state of linear chain of diatomic molecules (large N). The abscissa is the internuclear separation of one of the end molecules which has its zeroth-order energy raised by a perturbation. In (a) the zeroth-order curves are given, i.e., all β's in Eq. (3.10) are taken as zero. In (b) the approximate solution of (3.10) is given with β taken as constant (see Sec. 4). The heavy curve is a band of $N-2$ closely spaced curves and the light curves are nondegenerate. A potential barrier for dissociation of the lowest state of magnitude γ results from the perturbation.

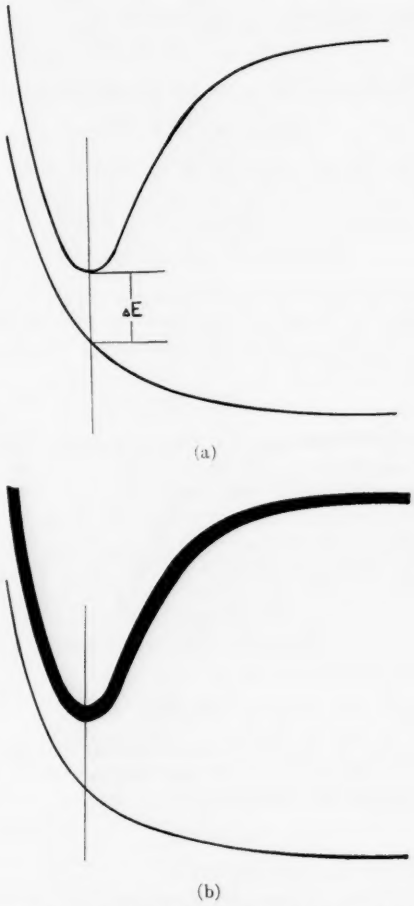

FIG. 14. Cross section of hypersurface for excited states of linear chain of diatomic molecules (large N). The abscissa is the internuclear separation of one of the end molecules which has its zeroth-order energy lowered by a perturbation. In (a) the zeroth-order curves are given, i.e., all β's in Eq. (3.10) are taken as zero. In (b) the approximate solution of (3.10) is given with β taken as constant. The heavy curve is a band of $N-1$ closely spaced curves and the light curve is nondegenerate.

a dissociating molecule can be given as

$$\bar{\delta}=\tfrac{1}{2}[-\mu^{-1}(\partial V/\partial\delta)]t^2.$$

The wave packet for δ has the exponential term

$$\exp[(-\alpha^2/2)(\delta-\bar{\delta})^2],$$

so that the molecule can be considered as intact for $\bar{\delta}<1/\alpha$. Whereas it can be considered as dissociated for $\bar{\delta}>1/\alpha$. The time of dissociation is, therefore,

$$\tau_w\approx\{(2/\alpha)[-\mu^{-1}(\partial V/\partial\delta)]^{-1}\}^{\frac{1}{2}}.$$

This time must be shorter than the required time for transfer of electronic excitation to the neighboring molecules $\hbar/2\beta$. Thus, we have as the condition for weak coupling

$$\tau_w\ll(\hbar/2\beta).$$

In the particular case of the coupled chain of H_2^+ ions, $\tau_w=1.2\times10^{-14}$ sec, and we find that β must be much less than 0.16 ev for weak coupling.

The corresponding estimate of the limit of strong coupling cannot be made with the same confidence, but a rough estimate would be useful. The limiting time which must be compared with $\hbar/2\beta$ is the time required for an internal conversion between electronic states with excitation of vibrations. The rate constant for this process can be given as

$$1/\tau_s=(2\pi/\hbar)\,|H_{if}'|^2\rho_E,$$

where H_{if}' is the perturbation operator and ρ_E is the density of final states. It is clear that $\rho_E\approx4\beta/N$. Thus, the condition for strong coupling is that

$$\tau_s\gg\hbar/2\beta,$$

which gives the condition on β

$$\beta\gg|H_{if}'|\,(\pi N/2)^{\frac{1}{2}}.$$

In the treatment of Secs. 2 and 3 it has been assumed (implicitly) that H_{if}' is zero. It is clear that in real systems H_{if}' will have a finite value. Several estimates of this quantity have actually been made.[12,13] In any case, it is clear that finite H_{if}' introduces a qualitative difference to be expected in systems with moderately strong coupling. Such systems would dissociate in a finite time as a result of transitions to the lowest surface by means of internal conversions.

Furthermore, as we have noted earlier, on this surface it is sometimes possible for several dissociations to occur as a result of one excitation. At this time it is impossible to say anything at all about the relative locations of such multiple dissociations.

The initial condition used throughout the paper is location of the excitation on a single molecule. It is clear from general considerations that such a situation could not result directly from excitation by electromagnetic radiation (since the wavelength is very long compared with molecular dimensions) or from very fast particle impacts. Such states can be excited by slow particle impacts or by the conversion of very high electronic excitation into lower excited states. In the latter case, one is always interested in more than one excitation and perhaps a more important problem is the correlation of their behavior. We believe that this problem can be approximately solved using single excitations of the type discussed here.

[12] H. Sponer and E. Teller, Revs. Modern Phys. **13**, 75 (1941).
[13] J. O. Hirschfelder, C. F. Curtiss, and R. B. Bird, *Molecular Theory of Gases and Liquids* (John Wiley & Sons, Inc., New York, 1954), p. 928.

APPENDIX. APPROXIMATE SOLUTIONS OF SECULAR DETERMINANTS

Define the determinant $D_n(x,\beta)$ as

$$D_n(x,\beta)\equiv\begin{vmatrix} x & \beta & & & & & \\ \beta & x & \beta & & & & \\ & \beta & x & \beta & & & \\ & & \cdot & \cdot & \cdot & & \\ & & & \cdot & \cdot & \cdot & \\ & & & & \beta & x & \beta \\ & & & & & \beta & x \end{vmatrix}=0. \quad \text{(A1)}$$

A secular equation of the type

$$D_n(x,\beta)=0 \quad \text{(A2)}$$

can be factored in the following form:

$$D_n(x,\beta)\equiv\prod_{k=1}^{n}(x-x_k^n)=0,$$
$$x_k^n=2\beta\cos[k\pi/(n+1)], \quad \text{(A3)}$$

where x_k^n is the kth root of (A2).

We shall seek approximate solutions of the following type of secular determinant:

$$D_n^m(x,\beta;\gamma,\beta')\equiv\begin{vmatrix} x & \beta & & & & & \\ \beta & x & \beta & & & & \\ & \cdot & \cdot & \cdot & & & \\ & & \beta & x & \beta' & & \\ & & & \beta' & (x-\gamma) & \beta' & \\ & & & & \beta' & x & \beta \\ & & & & & \cdot & \cdot & \cdot \\ & & & & & & \beta & x & \beta \\ & & & & & & & \beta & x \end{vmatrix}=0, \quad \text{(A4)}$$

where $(x-\gamma)$ and β' replace x and β of the mth row and column in (A1).

We shall be concerned only with the correction to the zeroth-order root $x-\gamma$ of (A4) in this Appendix. A more detailed treatment of such a determinant can be found in footnote 14.

In order to solve (A4), let us first consider the special case $\beta'=\beta$; that is,

$$D_n^m(x, \beta; \gamma, \beta)=0. \tag{A5}$$

(i) $\gamma>\beta$

$D_n^m(x, \beta; \gamma, \beta)$ can be expanded as

$$D_n^m(x, \beta; \gamma, \beta)=(x-\gamma)D_{m-1}(x, \beta)\cdot D_{n-m}(x, \beta)-\beta^2[D_{m-2}(x, \beta)\cdot D_{n-m}(x, \beta)+D_{m-1}(x, \beta)\cdot D_{n-m-1}(x, \beta)]=0. \tag{A6}$$

The zeroth-order solution is given by dropping the second term of (A6),

$$(x-\gamma)D_{m-1}(x, \beta)D_{n-m}(x, \beta)=0. \tag{A7}$$

The correction to the zeroth-order root, $x=\gamma$, can be given by

$$\begin{aligned} x-\gamma&=\frac{\beta^2[D_{m-2}(x_1, \beta)\cdot D_{n-m}(x_1, \beta)+D_{m-1}(x_1, \beta)\cdot D_{n-m-1}(x_1, \beta)]}{D_{m-1}(x_1, \beta)D_{n-m}(x_1, \beta)} \\ &=\beta^2\left[\frac{D_{m-2}(x_1, \beta)}{D_{m-1}(x_1, \beta)}+\frac{D_{n-m-1}(x_1, \beta)}{D_{n-m}(x_1, \beta)}\right], \end{aligned} \tag{A8}$$

where x_1 is the corrected value for the zeroth-order root $x=\gamma$. Obviously, if x_1 is the exact root of (A5), the right-hand side of (A8) is equal to $x_1-\gamma$. If x_1 is not the exact root, the equality does not hold and an iterative procedure is needed. However, if $\gamma\gg\beta$, $x_1=\gamma$ is already a good approximation.

(ii) $\gamma\leqq\beta$

It is more convenient to expand $D_n^m(x, \beta; \gamma, \beta)$ in the following form:

$$D_n^m(x, \beta; \gamma, \beta)=D_n(x, \beta)-\gamma D_{m-1}(x, \beta)\cdot D_{n-m}(x, \beta). \tag{A9}$$

The zeroth-order solution is given by

$$D_n(x, \beta)=\prod_{k=1}^{n}(x-x_n^k)=0. \tag{A10}$$

The correction to $x=x_n^n$ can be given by

$$x-x_n^n=\gamma D_{m-1}(x_1, \beta)D_{n-m}(x_1, \beta)\Big/\prod_{k=1}^{n-1}(x_1-x_n^k). \tag{A11}$$

An obvious choice for the starting value of x_1 in the iterative procedure is $x_1=x_n^n$.

After obtaining an approximate solution for (A5), we proceed to the original secular equation (A4), which can be expanded as

$$\begin{aligned} D_n^m(x, \beta; \gamma, \beta')&=D_n^m(x, \beta; \gamma, \beta)\{(\Delta\beta)+2(\Delta\beta)\} \\ &\{D_{m-2}(x, \beta)D_{n-m}(x, \beta)+D_{m-1}(x, \beta)D_{n-m-1}(x, \beta)\}, \end{aligned} \tag{A12}$$

where $\Delta\beta=\beta'-\beta$. The zeroth-order solution, $D_n^m(x, \beta; \gamma, \beta)=0$, can be corrected by the similar procedure.

[14] J. D. Swalen and L. Pierce (to be published).

Radiolysis of Cyclohexane. III. Vapor Phase*

J. M. RAMARADHYA AND G. R. FREEMAN

Department of Chemistry, University of Alberta, Edmonton, Alberta, Canada

(Received September 12, 1960)

The radiolysis of cyclohexane vapor by Po^{210} α particles was investigated. The Po^{210} source was calibrated by ferrous-sulfate dosimetry, using $G(Fe^{+++})=5.5$. The product yields were studied as a function of dose. The initial yield for hydrogen was $G(H_2)_i=8.0$. The fraction volatile at $-112°C$, consisting of C_2, C_3, and C_4 hydrocarbons, had an initial G value of 4.9 ± 0.5. The poor agreement in material balance is tentatively ascribed to ion-molecule reactions, since ions formed during radiolysis have a life-time of the order of 10^{-3} sec. The value of the ratio $G(\text{cyclohexene})/(\text{dicyclohexyl})=1.67$ is similar to that found in liquid cyclohexane radiolysis. The G values for various types of cyclohexane fragmentation are also given.

I. INTRODUCTION

THE passage of high-energy particles or ionizing radiations through matter results in the production of ions and excited molecules. Subsequent to this ionization and excitation, a number of secondary processes occur to give the final products of chemical change. The probability that a particular secondary process will occur might depend on whether the medium is a gas or a liquid.

In a gas, the molecular mean free path and average time between collisions are longer than in a liquid and there are no cage effects. Two radicals formed by the dissociation of a molecule in the gas phase have negligible chance of immediate recombination. Differences in the processes occurring in the two states might be revealed in the amount and nature of the products obtained by irradiating a compound in both the liquid and gas phases.

The radiolysis of liquid cyclohexane has been investigated by using electrons,[1–8a] deuterons,[8b] helium ions,[8a,b] γ rays[5,9–16] and x rays.[17,18] Hydrogen appears to be the major single product in the liquid-phase radiolysis. However, there have been very few investigations of the radiolysis of cyclohexane vapor.[2,19] This paper deals with the α radiolysis of cyclohexane vapor.

II. EXPERIMENTAL

(a) Apparatus

A conventional vacuum apparatus was used in this investigation. The reaction chamber consisted of a 1-liter bulb fitted with an outer B_{19} ground-glass joint at one end and a high-vacuum stopcock at the other.

An inner B_{19} joint was made into a test tube and a glass tube with a tungsten seal was fused into the B_{19} by a condenser seal. The Po^{210} probe was cemented to the glass tube by araldite cement. A copper wire, soldered to the stem of the polonium probe, was attached to the tungsten wire in the inner glass tube. The tungsten wire was grounded to ensure that a negative charge did not build up on the polonium source. Such a charge might have increased the tendency for polymer to form on the polonium probe. The B_{19} joint with the Po^{210} source was fitted into the outer B_{19} of the liter bulb. This junction was covered with an improved type of Dekhotinsky cement. A furnace was constructed around the reaction vessel, using nichrome wire and asbestos. This enabled the vessel to be heated, thereby keeping the reactants in the vapor phase during irradiation. A copper-constantan thermocouple buried in the asbestos against the wall of the reaction chamber was used in conjunction with a potentiometer to measure the temperature of the liter bulb (108°C in all experiments).

(b) Materials

Eastman-Kodak Spectrograde cyclohexane was used. The same product yields were obtained whether the cyclohexane was further purified by distillation or not.

(c) Techniques

(*i*) *Standardization of Po^{210} Source*

All the glassware that was used in these calibrations was thoroughly cleaned by keeping it immersed in hot

* This research was supported by the National Research Council of Canada.

[1] M. Burton and W. N. Patrick, J. Phys. Chem. **58**, 421 (1954).
[2] J. P. Manion and M. Burton, J. Phys. Chem. **56**, 560 (1952).
[3] C. S. Schoepfle and C. H. Fellows, Ind. Eng. Chem. **23**, 1396 (1931).
[4] H. A. Dewhurst, J. Chem. Phys. **24**, 1254 (1956).
[5] R. W. Fessenden and R. H. Schuler, J. Am. Chem. Soc. **79**, 273 (1957).
[6] N. S. Guentner, R. J. Hardwick, and R. P. Nejak, J. Chem. Phys. **30**, 601 (1959).
[7] H. A. Dewhurst, J. Phys. Chem. **63**, 813 (1959).
[8a] R. H. Schuler and A. O. Allen, J. Am. Chem. Soc. **77**, 507 (1955).
[8b] H. A. Dewhurst and R. H. Schuler, J. Am. Chem. Soc. **81**, 3210 (1959).
[9] G. R. Freeman, J. Chem. Phys. **33**, 71 (1960).
[10] G. R. Freeman, Can. J. Chem. **38**, 1043 (1960).
[11] M. Burton and G. Meshitsuka, Radiation Research **9**, 152 (1958).
[12] A. C. Nixon and R. E. Thorpe, J. Chem. Phys. **28**, 1004 (1958).
[13] M. Hamashima, M. P. Reddy, and M. Burton, J. Phys. Chem. **62**, 246 (1958).
[14] M. Burton, J. Chang, S. Lipsky, and M. P. Reddy, J. Chem. Phys. **26**, 1337 (1957).
[15] G. E. Adams, J. H. Baxendale, and R. D. Sedgwick, J. Phys. Chem. **63**, 854 (1959).
[16] R. H. Schuler, J. Phys. Chem. **61**, 1472 (1957).
[17] C. C. Schubert and R. H. Schuler, J. Chem. Phys. **20**, 518 (1952).
[18] E. N. Weber, P. F. Forsyth, and R. H. Schuler, Radiation Research **3**, 68 (1955).
[19] V. P. Henri, C. R. Maxwell, W. C. White, and D. C. Peterson, J. Phys. Chem. **56**, 1953 (1952).

sulfo-nitric acid for about 20 min, washed several times with tap water, followed by washing twice with doubly distilled water (once distilled over alkaline potassium permanganate and redistilled) and dried in an oven. Two sets of ferrous ammonium sulfate solutions were prepared in 0.8 N sulphuric acid: (1) 1 mM sodium chloride+1 mM ferrous ammonium sulfate; (2) 1 mM sodium chloride+3 mM ferrous ammonium sulfate. Three ml aliquots of each of these solutions were pipetted into 5-ml beakers and the Po^{210} source was positioned about 2 mm above the surface of the solution. The solutions were thus irradiated for periods of 5, 10, 15, and 20 min and the extent of oxidation was measured with a Cary spectrophotometer. The molar extinction coefficient used for ferric ion in these calculations was 2225 at 25°C. The rate of production of Fe^{3+} was the same in solution 1 as in 2. Special care was taken to exclude impurities including dust from the atmosphere.

The previously obtained values of $G(Fe^{3+})$ in 0.8 N sulphuric acid and 1 mM Fe^{++} for Po^{210} α particles are tabulated in Table I. The energy emission rate of the nominally 100-Mc Po^{210} source was computed assuming $G(Fe^{3+})=5.5$. No correction was applied for the loss of energy (about 7%) of the α particles in the 2-mm air gap between the source and the surface of the solution. The rate of oxidation of Fe^{++} was found to be independent of the distance between the source and the surface of the solution, in the range from about 1 to 4 mm. Miller[20] suggested that ozone formed in the air gap might dissolve in the solution and oxidize Fe^{++}. This would tend to compensate for the energy loss of the α particles.

TABLE I. $G(Fe^{3+})$ by α-particle oxidation of Fe^{++}.

$G(Fe^{3+})$	Reference
5.9	a, b
6.2	c
5.6	d
5.2	e
5.5	f
5.1	g
4.7	h
5.5±0.4 average	

[a] See work cited in reference 20.
[b] M. Haissinski and M. C. Anta, Compt. rend. **236**, 1161 (1953).
[c] R. McDonnel and E. J. Hart, J. Am. Chem. Soc. **76**, 2121 (1954).
[d] M. Lefort, Compt. rend. **245**, 1623 (1957).
[e] C. N. Trumbore, J. Am. Chem. Soc. **80**, 1772 (1958).
[f] M. Lefort and X. Tarrago, J. Phys. Chem. **63**, 833 (1959).
[g] C. N. Trumbore and E. J. Hart, J. Phys. Chem. **63**, 867 (1959).
[h] N. Miller, Radiation Research **9**, 633 (1958).

[20] N. Miller, Trans. Faraday Soc. **50**, 690 (1954).

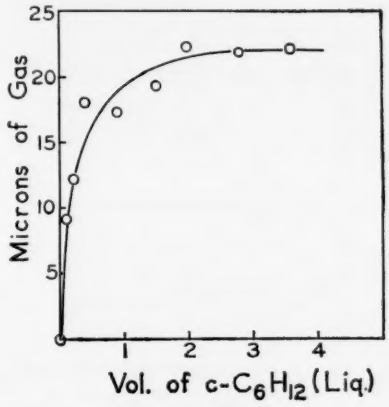

FIG. 1. Yield of gas at (−196°C) as a function of the volume of cyclohexane liquid vaporized. 1 ml of liquid corresponds to 180-mm pressure of vapor at 108°C.

The rate of energy absorption in the irradiated organic vapor was about 3×10^{12} ev/cc sec in most of the experiments.

(*ii*) *Preparing Samples for Irradiation*

The cyclohexane was degassed by the usual thawing-freezing-pumping technique and then volatilized into the reaction chamber.

(*iii*) *Analytical techniques*

The gaseous products obtained during the vapor phase radiolysis of cyclohexane were fractionated at (−196°C) and (−112°C). The (−196°C) fraction consisted of hydrogen and methane only. The (−112°C) fraction contained C_2, C_3, and C_4 hydrocarbons. These two fractions were each measured in a McLeod gauge-Toepler pump combination and analyzed by gas chromatography. The liquid products were then removed from the vacuum apparatus and analyzed gas chromatographically. One-meter charcoal, 2.5-m Silica gel, and both Silical gel and 1-m Apiezon L columns were used to analyze the (−196°C) fraction, (−112°C) fraction, and the liquid products, respectively.

III. RESULTS

(a) To determine the pressure of cyclohexane vapor which would absorb all the alpha particles emitted by the source, different amounts of cyclohexane were each irradiated for a period of 4 hr. The total yield of gas noncondensible at −196°C was measured and is presented in Fig. 1. The amount of cyclohexane is expressed in milliliters of liquid at room temperature (≈23°C).

The yield of gas increases with increasing amount of cyclohexane and approaches a constant value at about 2 ml of cyclohexane. Thus it may be assumed that all

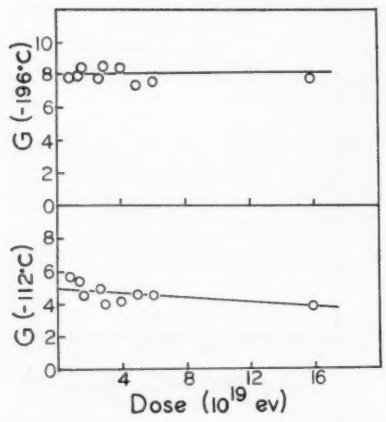

FIG. 2. $G(-196°C)$ and $G(-112°C)$ as a function of dose.

the energy was absorbed from the α particles when two or more ml of cyclohexane were vaporized into the reaction vessel. The size of the sample of cyclohexane employed in all subsequent experiments was 2 ml (360-mm pressure in the reaction vessel).

(b) Cyclohexane vapor was irradiated and the product yield was studied as a function of dose. The yields of the $-196°C$, and $-112°C$ fractions are shown in Fig. 2. The amount of methane was so small that it could only be detected and measured at the highest dose by the present analytical system. The product yields, expressed as G values, are presented in Fig. 3. The yields of other products obtained in the highest dose experiment are $G(CH_4)=0.13$, $G(C_8$ hydrocarbon$)=0.06$, $G(C_9$ hydrocarbon$)=0.07$, and $G(C_{10}$ hydrocarbon$)=0.17$. If it is assumed that $G(CH_4)=0.13$ at all the doses in these experiments, then $G(H_2)=8.0$.

IV. DISCUSSION

It appears from a general survey that hydrogen is the major single product that is obtained during the radiolysis of cyclohexane in both the liquid and the gas phases. The $G(H_2)$ values obtained for liquid cyclohexane are mostly around 5.4.[9] The two values previously reported for $G(H_2)$ for the vapor phase radiolysis of cyclohexane are at variance. The $G(H_2)$ for electron radiolysis of cyclohexane vapor reported by Manion and Burton[2] is 1.4 and that reported by Henri and coworkers[19] for α radiolysis is 3.6. Both these values are far lower than the corresponding values of $G(H_2)$ obtained from the radiolysis of liquid cyclohexane and this does not seem reasonable by comparison with *n*-pentane and *n*-hexane.[21,22]

The gaseous yield at $-196°C$ is a linear function of dose. It therefore appears that the primary decomposition of cyclohexane vapor is a linear function of dose over the range studied. The decrease in the yields of some of the products is probably due to secondary reactions. The initial yields G_i of the products were obtained by extrapolating the curves in Fig. 3 to zero dose.

If the decomposition of cyclohexane is represented as

$$c\text{-}C_6H_{12} \rightarrow H_2 + X,$$

then the total hydrogen deficiency in the products X should be equal to $G(H_2)_i=8.0$. A material balance of all the identified products obtained during radiolysis of cyclohexane is given in Table II. The C_8, C_9, and C_{10} hydrocarbons may be secondary products and perhaps should not have been included in the table. Since no G_i values were available for these compounds, G values obtained in the highest dose run are given and are in parenthesis.

It can be easily seen, by comparing the total hydrogen equivalent with $G(H_2)_i=8.0$, that the hydrogen equivalent of about 7 G units of hydrocarbon products have been missed. A similar deficiency of over one G unit in material balance has been reported by Freeman[9] in liquid phase radiolysis of cyclohexane.

From the investigation of the α radiolysis of cyclohexane vapor, Henri and co-workers[19] have given the following G values of the products: $H_2=3.6$; $CH_4=0.53$; $C_2H_6=1.2$; $C_3H_8=0.33$; $C_4H_{10}=0.34$. No yields for liquid products were reported. However, it is evident that there is a very poor material balance, since the products reported use up hydrogen during their formation.

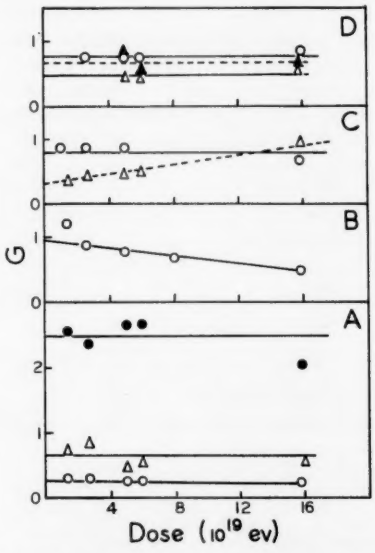

FIG. 3. Product yields as a function of dose. (A) ○ ethane, △ acetylene, ● ethylene. (B) ○ propane. (C) △ C_4 olefin (probably C_4H_8), ○ propylene. (D) ○ cylcohexene, △ dyciclo hexyl, ▲ total C_{12} hydrocarbons.

[21] H. A. Dewhurst, J. Phys. Chem. **61**, 1466 (1957).
[22] R. A. Back and N. Miller, Trans. Faraday Soc. **55**, 911 (1959).

The material balance is much worse in the vapor phase than in the liquid phase. It is believed that the lifetime of a positive ion in an irradiated liquid is of the order of 10^{-13} sec.[23] Under the present conditions of gas phase irradiation [10^{13} ev absorbed per ml per sec, k (ion-electron recombination) $\approx 10^{-6}$ cc/ion sec[24]] the lifetime of the positive ion is of the order of 10^{-3} sec. Thus one possible explanation of the carbon deficiency in the measured products is that polymers are formed by ion-molecule reactions. Hydrocarbons with carbon number higher than 12 (i.e., larger than dimers of cyclohexane) would not have been detected by the present analytical system. The much longer lifetime of the ions in the gas phase than in the liquid phase might permit a larger amount of some such polymerization reaction to occur in the gas phase.

The formation of hydrogen involves the cleavage of C—H bonds in the cyclohexane molecule. The products obtained in the −112°C fraction, viz., C_2, C_3, and C_4 hydrocarbons, involve the rupture of the ring. The yields of the latter products were over ten times greater in the gas phase than they were in the liquid phase irradiations.[9] This large difference might be due to the rapid recombination of hydrocarbon radical fragments in the liquid cages. It might also be partly due to the formation of different excited states in the two phases.

If hydrogen is formed by the decomposition of excited cyclohexane molecules, it is probably formed by the reactions,

$$c\text{-}C_6H_{12}^* \rightarrow c\text{-}C_6H_{11} + H \quad (1)$$

$$H + C\text{-}C_6H_{12} \rightarrow H_2 + c\text{-}C_6H_{11}, \quad (2)$$

and possibly

$$c\text{-}C_6H_{12}^* \rightarrow c\text{-}C_6H_{10} + H_2. \quad (3)$$

If hydrogen is produced via ion-molecule reactions, these might be

$$c\text{-}C_6H_{12}^+ + c\text{-}C_6H_{12} \rightarrow c\text{-}C_6H_{13}^+ + c\text{-}C_6H_{11} \quad (4)$$

$$c\text{-}C_6H_{13}^+ + e \rightarrow c\text{-}C_6H_{11} + H_2. \quad (5)$$

Reaction (5) represents the dissociative combination of an electron e with the $c\text{-}C_6H_{13}^+$ ion. Reactions (4) and (5) generate cyclohexyl radicals, so they are the ionic analogues of reactions (1) and (2). The cyclohexyl radicals would combine or disproportionate:

$$2c\text{-}C_6H_{11} \rightarrow C_{12}H_{22} \quad (6)$$

$$\rightarrow c\text{-}C_6H_{10} + c\text{-}C_6H_{12}. \quad (7)$$

[23] A. H. Samuel and J. L. Magee, J. Chem. Phys. **21**, 1085 (1953).

[24] M. A. Biondi and S. C. Brown, Phys. Rev. **76**, 1697 (1949).

TABLE II. Material balance of products from irradiation of cyclohexane vapor. The hydrogen equivalent of a product corresponds to the amount of hydrogen that was formed when that product was formed from cyclohexane.

Product	G_i	H_2 equivalent
C_2H_6	0.28	−0.28
C_2H_4	2.48	0.00
C_2H_2	0.65	+0.65
C_3H_8	0.95	−0.95
C_3H_6	0.78	0.00
C_4H_{10}	0.04	−0.04
C_4H_8	0.30	0.00
Cyclohexene	0.77	+0.77
C_8 hydrocarbons	(0.06)	+(0.06?)
C_9 hydrocarbons	(0.07)	+(0.07?)
C_{10} hydrocarbons	(0.17)	+(0.17?)
Total C_{12} hydrocarbons	0.69	≈+0.69
		Total ≈+1.14

The value of the ratio of the initial yields of cyclohexene and dicyclohexyl is $G(c\text{-}C_6H_{10})_i/G(C_{12}H_{22})_i = 0.77/0.46 = 1.67$, which is similar to the value 1.84 observed in the liquid phase.[9] This might be taken as an additional argument that only a small portion of the cyclohexene is formed by reaction (3) and that the value of the ratio k_7/k_6 is greater than unity in both the liquid and gas phases.[25]

Ring fragmentation appears to occur in three types:

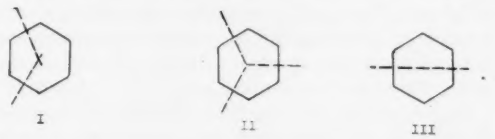

Type II might simply be a continuation of type I. From the yields of ethylene, propylene, and butene, the G values for cyclohexane fragmentation of types I, II, and III were calculated to be 0.3, 0.7, and 0.4, respectively. The total G value of cyclohexane molecules that underwent fragmentation was about 2.1.

The yield of propane is surprisingly high and the mechanism of its formation is not evident. The relative yields of propane and propylene indicate that the former was probably not entirely produced by hydrogenation of the latter.

[25] G. R. Freeman, J. Phys. Chem. **64**, 1576 (1960).

Temperature Dependence of NMR Absorption in Solid Acetic Acid and in Some of Its Chloro and Acid Chloride Derivatives

A. PETERLIN

*Department of Physics, University, Ljubljana, Yugoslavia**

AND

M. PINTAR

J. Stefan Institute, Ljubljana, Yugoslavia

(Received June 13, 1960)

Acetic acid and some of its chloro and acid chloride derivatives with increased substitution of protons by chlorine in the CH_3-group were studied by NMR from $-175°$–$0°$C in order to elucidate the temperature dependence of molecular and CH_nCl_{3-n} group mobility and association in the solid state. While CH_3 is free to rotate around the C—C bond, the substitution of one proton by chlorine already results in fixed CH_2Cl group. In order to obtain dimeric association, however, one has to substitute two or all protons by chlorine. The rotational freedom of single molecules of such associates reappears upon heating to temperatures far below the melting point.

1. INTRODUCTION

IN a previous work,[1] NMR was applied to acetic acid, and to some of its chloro acid derivatives, in order to study the mobility of methyl and chloride groups, and the arrangement of molecules into dimer or polymer structure. In the case of polymer arrangement, the acidic proton is isolated, yielding a simple one-peak absorption curve, the width being mainly determined by the intensity of the lattice field. In dimers, however, the acidic protons occur in pairs; the interprotonic distance in the pair is substantially smaller than that from other protons in the same molecule. As a consequence, the absorption envelope has two maxima. The difference in NMR spectrum is so marked that, in the case investigated here, the distinction between the two cases is rather easy. Because the conclusions may obtain a better foundation by measuring the temperature dependence of NMR absorption spectra, we extended the investigation in the whole temperature range from $-170°$C–$0°$C.

Measurements were made on dichloroacetic, monochloroacetic, and acetic acid and the chlorides of monochloroacetic and acetic acid.

2. EXPERIMENTAL ARRANGEMENT

The experimental arrangement used for observation of broad proton lines in solids was of the usual PKW type.[2] The field strength of the stabilized electromagnet was 3600 G, with an inhomogeneity of the field over the sample a little less than 0.4 G. The cryostat for low temperature work was described by Pirkmajer.[3] The accuracy of temperature measurement was about 2°C.

The substances investigated were either obtained commercially or synthetized by Schara. After purification they were put into thin walled glass tubes of 7 mm diam, the tubes sealed up, and the substances frozen by liquid nitrogen and held at so low temperature that the samples remained solid during the whole experiment.

In order to shorten the relaxation time T_1, some samples had to be irradiated by a 300 Curie ^{60}Co source. All irradiations were performed at liquid nitrogen temperature.

3. EXPERIMENTAL RESULTS

Dichloroacetic Acid ($CHCl_2COOH$)

Dichloroacetic acid melts at $+5°$C. Its crystal structure is unknown. The NMR spectrum, easily observable without previous irradiation, shows a characteristic structure at $-175°$C, rather unambiguously demonstrating the existence of dimers in the solid sample. The absorption lines corresponding to the two peaks at $\Delta H = 3.4$ and $7.4G$, respectively, have nearly equal area, i.e., the corresponding first moments of the derivatives have the ratio 1:1, so that they may be assigned to the methyl and acid proton, respectively. The acid proton of every molecule is paired with that of the adjacent molecule of the same dimeric association unit. The methyl proton, however, yields a Gaussian line (inner peak) as a result of the broadening by surrounding protons. This assignment is supported by subtracting the line shape of CCl_3COOH, which also shows dimer

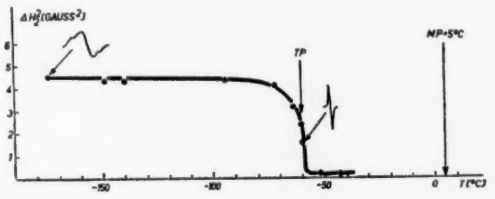

FIG. 1. Temperature dependence of ΔH_2^2 of $CHCl_2COOH$.

* Present address: Physikalisches Institut, Technische Hochschule, München, Germany.

[1] M. Pintar, *Proceedings of the 4th International Meeting on Molecular Spectroscopy*, 1959.

[2] R. V. Pound, Progr. in Nuclear Phys. **2**, 21 (1952).

[3] E. Pirkmajer, Eng. D. thesis, University, Ljubljana, Yugoslavia, 1959.

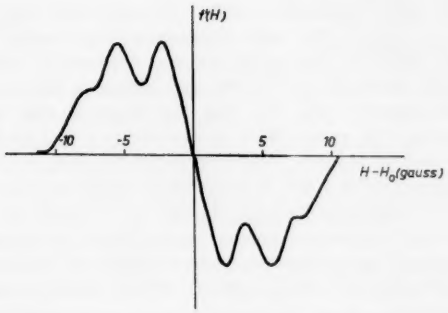

FIG. 2. Absorption spectrum derivative of $CH_2ClCOOH$ at $-175°C$.

association,[1,4,5] from the $CHCl_2COOH$ line shape which results in a single proton Gaussian line. This subtraction procedure, although neglecting the differences in intermolecular proton interaction in both cases, is quite reasonable because the proton pair absorption spectrum is rather insensitive to the lattice field and, moreover, the next methyl proton is rather far away. The same applies to the case of monochloroacetic acid.

With rising temperature, the linewidths and also the second moments ($\Delta H_2^2=4.5G^2$), shown in Fig. 1, remain nearly unchanged up to the transition point at nearly $-60°C$. Above this temperature the absorption spectrum is narrow; its width is determined solely by the magnetic field inhomogeneity over the sample. Hence, the molecules, formerly arranged in dimers with fixed proton pairs, reach a fairly high degree of rotational and translational freedom in the still-persisting crystal lattice far below the melting point. As a result of impurities, the temperature of transition is not very accurate. The impurities positively did not include water which, when present, would markedly influence the absorption spectrum.

Monochloroacetic Acid (CH_2ClOOH)

Monochloroacetic acid melts between 52° and 63°C according to the orientation of the substituted methyl group in the lattice.[6] We did not pay attention to this point. The NMR absorption spectrum became observable after 3 Mr of gamma ray irradiation. It has a fine structure (Fig. 2) which may be explained by superposition of methyl spin pair to the Gaussian broadening line of the isolated acidic proton. The separation of both contributions can be obtained by subtracting the $CH_2ClCOCl$ absorption line from that of $CH_2ClCOOH$. The difference is a single proton line. The ratio of the corresponding first moments of the derivatives is 2:1 in agreement with the assignment. This rough analysis shows that $CH_2ClCOOH$ in solid state does not form dimers, but most probably arranges in polymeric chains. A dimeric structure would yield two superimposed pair spectra, a result markedly differing from the spectrum observed.

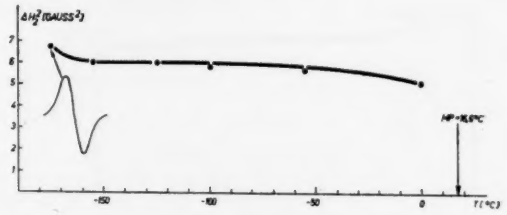

FIG. 4. Temperature dependence of ΔH_2^2 of CH_3COOH.

The second moment is $2.7G^2$ at $-175°C$ and does not change appreciably with rising temperature up to 0°C, the highest temperature investigated (Fig. 3). In this whole range, the CH_2Cl group is fixed and it would be worthwhile to see whether it starts rotating already below the melting point.

Acetic Acid (CH_3COOH)

Acetic acid melts at 16.6°C. The molecules in the solid are claimed to be polymerized.[7] The single broad line can be explained by superposition of the rotating CH_3 group line[8] to that of the isolated acid proton.[1] Neither the width, $\delta H=4G$, nor the second moment, $\Delta H_2^2=6,\ 7G^2$, change appreciably with temperature in the range investigated (Fig. 4). An approximate calculation of the second moment on the basis of the polymeric structure[1] yields a second moment of $6.6G^2$, in good agreement with the measured value.

FIG. 3. Temperature dependence of ΔH_2^2 of $CH_2ClCOOH$.

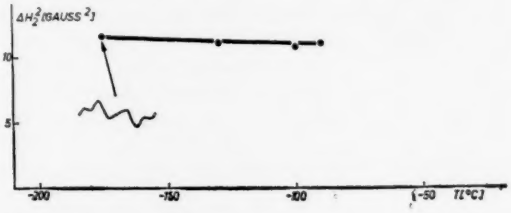

FIG. 5. Temperature dependence of ΔH_2^2 of $CH_2ClCOCl$.

[4] M. Goldman, J. Phys. Chem. Solids **7**, 165 (1951).
[5] M. Yagi and U. Ueta, J. Phys. Soc. Japan **14**, 377 (1959).
[6] E. H. Huntress, *Organic Chlorine Compounds* (John Wiley & Sons, Inc., New York, 1948), p. 173.
[7] R. E. Jones, University of California (1956) W9405.
[8] E. R. Andrew and R. Bersohn, J. Chem. Phys. **18**, 159 (1950).

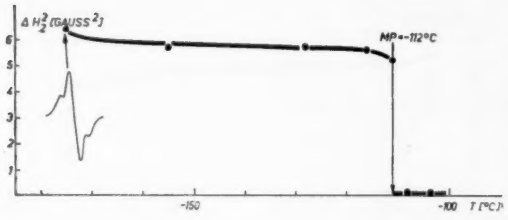

FIG. 6. Temperature dependence of ΔH_2^2 of CH_3COCl.

Monochloroacetyl Chloride ($CH_2ClCOCl$)

Neither the melting point nor the crystal structure are known. The sample had to be irradiated by 6 Mr of gamma rays in order to obtain an easily observable absorption spectrum. At -175°C, the linewidth $\delta H = 6.7G \pm 10\%$ yields 1.84 ± 0.06 A for the interprotonic distance in the fixed CH_2Cl group, a little more than the electron diffraction and IR value, 1.79 A, the difference being still within the experimental error. From the second moment $\Delta H_2^2 = 11.7G^2$, at -175°C the intermolecular contribution β^2 turns out to be $0.3G^2$, in fairly good agreement with observations on similar systems.

The temperature dependence shows no change in the second moment from -175°C up to -90°C (Fig. 5). The shape of the spectrum and the magnitude of the second moment unambiguously require a fixed CH_2Cl group in this temperature range. The same follows from the relatively long relaxation time T_1.

Acetylchloride (CH_3COCl)

Acetylchloride melts at -112°C; unit cell structure is unknown. The NMR spectrum may be observed without previous irradiation. The inner and outer peaks with their respective widths, 2.5 and $8.2G$, do not change appreciably with temperature and nearly the same applies to the second moment $\Delta H_2^2 = 6.4G^2$, which slowly increases at -175°C and decreases before the melting point (Fig. 6). The line shape is that of a rotating CH_3 group. With its contribution of $5.45G^2$ to the second moment, the intermolecular parameter β^2 turns out to be $1.3G^2$. It is definitely larger than in the case of monochloroacetyl chloride as a result of the increased number of protons and of the consequently decreased interproton distances of adjacent molecules.

Although the results obtained on such a small number of samples cannot be expected to be representative of the effect of chlorine substitution, one is tempted to summarize the observations in the following way. The substitution of one hydrogen by chlorine in the methyl group blocks rotation in the temperature range observed. The unsubstituted methyl group, however, rotates rather freely already far below the melting point. Some rotational restriction may be suspected from the nonnegligible slope of the second moment curve which shows a steeper increase below -170°C. The fixed CH_2Cl group also results in a rather long relaxation time, so that NMR spectrum becomes easily observable only after γ-ray irradiation. Dimer formation was observed only in the case of $CHCl_2COOH$, so that one has the impression that, at least with chlorine derivatives of acetic acid, two or three hydrogens of the methyl group have to be substituted in order to obtain paired hydrogen bonds in the temperature range of our investigation. However, already far below melting point the characteristic pair structure of NMR spectrum completely disappears, and the linewidth drastically decreases, indicating considerable rotational freedom of single molecules. In the other two cases with one or no chlorine in the methyl group, the acid hydrogen is always unpaired, yielding a single broad line.

Infrared Optical Constants of NaCl†

JACOB NEUBERGER*‡ AND ROBERT D. HATCHER

Washington Square College, New York University, New York

(Received August 25, 1960)

The infrared optical constants of NaCl are calculated by applying an extended form of the Born and Blackman anharmonic potential theory to the Kellerman model of the NaCl crystal. A damping factor is derived which depends on the amplitudes and frequencies of the characteristic modes as well as on the frequency of the incident radiation. By a numerical sampling of wave vector space, this damping factor and the resultant optical constants are calculated in the range 25μ–500μ. The theory predicts a subsidiary absorption maximum near 100μ which agrees with recent experimental measurements. The frequency distribution function of NaCl is also given here.

I. INTRODUCTION

THE methods of lattice dynamics as developed by Born and von Karman[1–3] have been successfully applied to studies in specific heats of crystals and to the relationships between elastic constants and infrared resonance frequencies. For the prediction of the dispersive behavior of crystals in the infrared, the theory has been less successful. This is mainly because of the fact that simple harmonic lattice theory predicts a line absorption at the resonant frequency, whereas a broad absorption maximum and some subsidiary structure has been observed for even the simple ionic crystals.[4,5] The introduction of a constant damping factor was shown by Czerny[4] to be useless in correlating the theory with the experimental observations. Several approaches have been suggested to obviate this difficulty. Born and Blackman[6,7] (to be abbreviated B.B.) introduced anharmonic potential terms and by treating these as a perturbation, they were able to predict for a one-dimensional model the existence of a subsidiary maximum in the absorption spectrum of NaCl. The method was also sketched for a special three-dimensional model, but because of insufficient data concerning the interaction constants, no definite conclusions were drawn. Physically, the anharmonic forces provide a mechanism whereby the resonant mode is able to excite nearby modes of vibration resulting in a broad absorption region. Lax and Burstein[8] suggested that a deformation of the ionic charge distribution during vibration can be used to explain the appearance of the secondary maxima in the infrared absorption spectrum. This deformation was shown to lead to a second-order electric moment and a modification of the first-order moment. As applied to a one-dimensional model, the theory yielded the approximate position of the secondary maxima. The broadening of the main absorption maximum was, however, left to an anharmonic theory. Rosenstock[9] proposed that the broadening of the main maximum could be accounted for in part by setting up correct boundary conditions rather than the cyclic Born-von Karman conditions. He pointed out that whereas in the application to statistical problems the latter are adequate, this may not be the case for optical problems. Since each mode of vibration contributes to the net electric moment, a small change in each mode may have large cumulative effects. As applied to a one-dimensional model, Rosenstock obtains a small but finite contribution to the electric moment at all frequencies. No comparison with experiment was attempted. Born and Huang[10] developed the quantum-mechanical analog of the B.B. anharmonic theory and obtained a dispersion formula in terms of three damping constants. It is pointed out that the B.B. theory bears a close relationship to the quantum-mechanical treatment provided that the temperature is not high compared to the Debye temperature θ_D of the crystal. Since for NaCl, $\theta_D = 281°K$, the room temperature absorption spectrum can be adequately discussed by a classical anharmonic theory.

The present study is an extension of the B.B. method to a realistic three-dimensional model of ionic crystals. We have adopted the Kellerman[11] model for the NaCl crystal. In Sec. II, the harmonic approximation as applied to a regular lattice is discussed. The derivation of the dispersion formula including a special damping term resulting from the anharmonic potential is given in Sec. III. The Kellerman model of the NaCl crystal is summarized in Sec. IV. The numerical calculation of

† The research reported in this paper has been sponsored by the Electronics Research Directorate of the Air Force Cambridge Research Center, Air Research and Development Command.

* Now at Queens College, Flushing, New York.

‡ Much of the material included in this paper was used in a Ph.D. dissertation at New York University (1958).

[1] M. Born and T. von Karman, Physik Z. **13,** 297 (1912); **14,** 15 (1913).

[2] M. Born, Enc. d. Mat. Wiss. V**3,** 529 (1926).

[3] M. Born and M. Goeppert Mayer, *Handbuch der Physik* (Springer-Verlag, Berlin, Germany, 1933), XXII, p. 623.

[4] M. Czerny, Z. Physik. **65,** 600 (1930).

[5] M. Czerny and W. Barnes, Z. Physik. **72,** 447 (1931).

[6] M. Born and M. Blackman, Z. Physik. **82,** 551 (1933).

[7] M. Blackman, Z. Physik. **86,** 421 (1933).

[8] M. Lax and E. Burstein, Phys. Rev. **97,** 39 (1955).

[9] H. Rosenstock, Phys. Rev. **99,** 656 (1955).

[10] M. Born and K. Huang, *Dynamical Theory of Crystal Lattices* (Oxford University Press, New York, 1954).

[11] E. Kellerman, Phil. Trans. Roy. Soc. (London) **A238,** 513 (1940).

the damping factor with the resultant optical constants of NaCl and a frequency distribution curve based on a more dense wave vector subdivision is presented in Sec. V.

II. HARMONIC APPROXIMATION

The potential energy of a lattice in its equilibrium configuration under the assumption of central forces is given by

$$\Phi_0=\tfrac{1}{2}\sum_{k,k'=1}^{s}\sum_{l,l'=0}^{N-1}\phi_{kk'}(|\mathbf{r}_{kk'}{}^{l-l'}|), \tag{1}$$

where $l=(l_1, l_2, l_3)$ denotes the cell index, k, k' the basis index each extending from 1 to s, and $\phi_{kk'}(|\mathbf{r}_{kk'}{}^{l-l'}|)$ is the interaction potential between particles k and k' in cells l and l', respectively; $\mathbf{r}^l=l_1\mathbf{a}_1+l_2\mathbf{a}_2+l_3\mathbf{a}_3$ with the $\mathbf{a}_i$'s being the basic vectors and $\mathbf{r}_{kk'}{}^{l-l'}=\mathbf{r}_k{}^l-\mathbf{r}_{k'}{}^{l'}=\mathbf{r}^l+\mathbf{r}_k-\mathbf{r}^{l'}-\mathbf{r}_{k'}$, with $\mathbf{r}_k$ being the position vector of particle k in the basic cell. Following the Born notation,[2] we let $u_{kx}{}^l$ represent the x component of the displacement from equilibrium of particle k in cell l. The equations of motion then become

$$m_k\ddot{u}_{kx}{}^l-\sum_{k',l',y}(\phi_{kk'}{}^{l-l'})_{xy}u_{k'y}{}^{l'}=0, \tag{2}$$

there being $3sN^3$ equations of this type and $\sum_x$ means a summation over the three coordinates x, y, z. Also m_k is the mass of the kth particle, $\ddot{u}$ represents the second derivative with respect to time, and N is the number of cells along each coordinate axis. With the assumption of plane wave solutions of the form

$$u_{kx}{}^l=U_{kx}(m_k)^{-\frac{1}{2}}\exp(-i\omega T)\exp[2\pi i\boldsymbol{\delta}\cdot\mathbf{r}_k{}^l], \tag{3}$$

where ω is the circular frequency of one of the normal modes of amplitude U_{kx}, T is the time, and $\boldsymbol{\delta}$ the wave vector, Eq. (2) becomes

$$\omega^2U_{kx}+\sum_{k'y}\begin{bmatrix}kk'\\xy\end{bmatrix}U_{k'y}(m_km_{k'})^{-\frac{1}{2}}=0, \tag{4}$$

where

$$\begin{bmatrix}kk'\\xy\end{bmatrix}=\sum_l(\phi_{kk'}{}^l)_{xy}\exp(2\pi i\boldsymbol{\delta}\cdot\mathbf{r}_{k'k}{}^l). \tag{5}$$

The set of $3s$ simultaneous homogeneous equations of type (4) can be represented as a square matrix with the U's and ω^2's being eigenvectors and eigenvalues, respectively. Since $(\phi_{kk'}{}^l)_{xy}=(\phi_{k'k}{}^{-l})_{xy}$ it follows that

$$\begin{bmatrix}kk'\\xy\end{bmatrix}^*=\begin{bmatrix}k'k\\yx\end{bmatrix}$$

with $[\ \ ]^*$ being the complex conjugate of $[\ \ ]$ and thus the matrix is Hermitian. Hence, all eigenvalues are real and the U's are orthogonal such that they may be normalized with

$$\sum_{k,x}U_{kxt}(\sigma)\,U_{kxt'}{}^*(\sigma)=\delta_{tt'}, \tag{6}$$

where t refers to one of the $3s$ eigenvalues associated with a particular σ and $U_{kxt}(\sigma)$ is the corresponding amplitude. Furthermore, since $U_{kxt}{}^*(\sigma)$ satisfies the same equation as $U_{kxt}(-\sigma)$, one can choose

$$U_{kxt}(-\sigma)=U_{kxt}{}^*(\sigma) \tag{7}$$

and

$$\omega_t(-\sigma)=\omega_t(\sigma). \tag{8}$$

The Born-von Karman boundary conditions $u_{kx}{}^{l+N}$ etc., show that

$$\boldsymbol{\delta}=(h_1/N)\mathbf{b}_1+(h_2/N)\mathbf{b}_2+(h_3/N)\mathbf{b}_3, \tag{9}$$

with h_i an integer such that $-N/2<h_i\leq N/2$, and $\mathbf{b}_1$, $\mathbf{b}_2$, $\mathbf{b}_3$ are the basic vectors of the reciprocal lattice. This restriction on $\boldsymbol{\delta}$ leads directly to a vanishing of the electric dipole moment of the vibrating lattice for all $\boldsymbol{\delta}$ except $\boldsymbol{\delta}=0$. For if we let p_{kx} be the x component of the electric dipole moment of particle k having charge e_k, then the total dipole moment P_x in the x direction is

$$P_x=\sum_k p_{kx}=\sum_{k,l}e_ku_{kx}{}^l, \tag{10}$$

or

$$P_x=\sum_k e_kU_{kx}\exp(-i\omega T)\times\exp(2\pi i\boldsymbol{\delta}\cdot\mathbf{r}_k)\Big[\sum_l\exp(2\pi i\boldsymbol{\delta}\cdot\mathbf{r}^l)\Big] \tag{11}$$

on using Eq. (3). But the sum over l vanishes for all nonzero values of $\boldsymbol{\delta}$, since a typical term has the form

$$\sum_{l=0}^{N-1}\exp(2\pi ihl/N)=N\delta_{h,0},$$

or more generally

$$\sum_{l=0}^{N-1}\exp(2\pi i\boldsymbol{\delta}\cdot\mathbf{r}_k{}^l)=N^3\delta_{\sigma,0}. \tag{12}$$

The infrared resonance frequency corresponds to wave vector $\boldsymbol{\delta}=0$ and thus, we conclude that as far as optical phenomena are concerned, the crystal behaves like an oscillator of a single frequency. This disagrees with experimental observations as already mentioned in Sec. I.

III. ANHARMONIC POTENTIAL AND DERIVATION OF DAMPING FACTOR

We follow here in principle the B.B. anharmonic potential perturbation theory. Suppose that polarized radiation is incident on a crystal with its electric field vector in the x direction. Then, as a first-order approximation, we assume that only the x component of the displacement of each ion has to be included in the anharmonic terms. For an fcc crystal like NaCl, with two particles per cell, the anharmonic potential V_A,

confined to nearest neighbor interactions takes the form

$$V_A=\beta/6\sum_l[(u_{kx}{}^l-u_{k'x}{}^{l'})^3-(u_{kx}{}^l-u_{k'x}{}^{l''})^3]. \quad (13)$$

Here β is a constant and l', l'' are related to l by

$$\mathbf{r}_{k'k}{}^{l'l}=\mathbf{i}r_0; \qquad \mathbf{r}_{k'k}{}^{l''l}=-\mathbf{i}r_0, \quad (14)$$

with r_0 the nearest distance between particles k and k'. The unperturbed Hamiltonian H_0 of the vibrating crystal is

$$H_0=\tfrac{1}{2}\sum_{k,l}m_k(\dot{\mathbf{u}}_k{}^l)^2-\tfrac{1}{2}\sum_{\substack{l,l',k\\k',x,y}}(\phi_{kk'}{}^{l-l'})_{xy}u_{kx}{}^l u_{k'y}{}^{l'}. \quad (15)$$

Consider now the normal coordinate transformation from $\mathbf{u}_k{}^l$ to $a_t(\sigma)$ defined by

$$u_{kx}{}^l=\sum_{t,\sigma}\frac{U_{kxt}(\sigma)}{(m_kN^3)^{\frac{1}{2}}}a_t(\sigma)\exp(2\pi i\boldsymbol{\sigma}\cdot\mathbf{r}_k{}^l), \quad (16)$$

where t ranges from 1 to $3s$ (i.e., 1–6 for NaCl) and

$$\sum_{\sigma} \text{ implies } \sum_{h_1,h_2,h_3}.$$

We note that since $u_{kx}{}^l$ is real and $U(\sigma)^*=U(-\sigma)$, that

$$a_t{}^*(\sigma)=a_t(-\sigma). \quad (17)$$

Substituting Eq. (16) into Eq. (15) and making use of Eq's. (6), (7), (12), and (17) yields after some simplification

$$H_0=\tfrac{1}{2}\sum_{t,\sigma}[\dot{a}_t(\sigma)\dot{a}_t(-\sigma)+\omega_t{}^2(\sigma)a_t(\sigma)a_t(-\sigma)]. \quad (18)$$

The $a_t(\sigma)$'s are thus the complex normal modes for the vibrating crystal. Applying transformation (16) to V_A in Eq. (13) yields with the help of Eq. (14)

$$V_A=\frac{\beta}{6N^{9/2}}\sum_{\substack{\sigma,\sigma',\sigma''\\t,t',t''}}a_t(\sigma)a_{t'}(\sigma')a_{t''}(\sigma'')$$
$$\times[A_t(\sigma)A_{t'}(\sigma')A_{t''}(\sigma'')-A_t{}^*(\sigma)A_{t'}{}^*(\sigma')A_{t''}{}^*(\sigma'')]$$
$$\times\sum_l\exp 2\pi i[(\boldsymbol{\sigma}+\boldsymbol{\sigma}'+\boldsymbol{\sigma}'')\cdot\mathbf{r}_k{}^l], \quad (19)$$

where

$$A_t(\sigma)=U_{kxt}(\sigma)(m_k)^{-\frac{1}{2}}-U_{k'xt}(\sigma)(m_{k'})^{-\frac{1}{2}}$$
$$\times\exp(2\pi i\sigma_x r_0). \quad (20)$$

Since $\boldsymbol{\sigma}$ is in the range $-\mathbf{b}/2<\boldsymbol{\sigma}\leqslant\mathbf{b}/2$, condition (12) needs a slight modification when applied to Eq. (19). Using the same reasoning as in Eq. (12) and choosing the origin of the basis at the site of the kth particle, we obtain

$$\sum_l\exp[2\pi i(\boldsymbol{\sigma}+\boldsymbol{\sigma}'+\boldsymbol{\sigma}'')\cdot\mathbf{r}_k{}^l]$$
$$=\begin{cases}N^3 & \text{for } \boldsymbol{\sigma}+\boldsymbol{\sigma}'+\boldsymbol{\sigma}''=0 \text{ or } \pm\mathbf{b}\\ 0 & \text{otherwise}\end{cases}. \quad (21)$$

Thus, Eq. (19) becomes

$$V_A=\frac{\beta}{6N^{\frac{3}{2}}}\sum_{\substack{\sigma,\sigma',\sigma''\\t,t',t''}}{}'F_{tt't''}(\sigma,\sigma',\sigma'')a_t(\sigma)a_{t'}(\sigma')a_{t''}(\sigma''), \quad (22)$$

with

$$F_{tt't''}(\sigma,\sigma',\sigma'')=A_t(\sigma)A_{t'}(\sigma')A_{t''}(\sigma'')$$
$$-\text{complex conj.} \quad (23)$$

and $\sum'$ indicates that the sum is subject to the condition $\boldsymbol{\sigma}+\boldsymbol{\sigma}'+\boldsymbol{\sigma}''=0$ or $\pm\mathbf{b}$. The Hamiltonian of the lattice will contain an additional term due to the interaction of the lattice with the incident radiation. The polarized radiation is characterized by

$$E=E_0\exp(i\omega T), \quad (24)$$

with ω the circular frequency of the incident radiation, and E_0 the amplitude of the electric field E. For diatomic ionic crystals of the NaCl type, let us identify atoms k and k' as the positive and negative ions, respectively. The contribution V_E to the Hamiltonian thus becomes

$$V_E=-eE\sum_l(2u_{kx}{}^l-u_{k'x}{}^{l'}-u_{kx}{}^{l''})/2, \quad (25)$$

where l' and l'' are related to l as in Eq. (14) and e is the magnitude of the electronic charge. Application of Eq. (16) gives

$$V_E=-eE\sum_t a_t(0)N^{\frac{3}{2}}A_t(0). \quad (26)$$

The total Hamiltonian of the lattice thus consists of the sum of Eqs. (18), (22), and (26).

We assume as solutions for $a_t(\sigma)$ the form

$$a_t(\sigma)=\sum_{j=1,-1}c_{tj}(\sigma)e^{i\omega_{tj}(\sigma)T}, \quad (27)$$

where we define $\omega_{t-j}(\sigma)=-\omega_{tj}(\sigma)$ and $c_{tj}(\sigma)$ is a complex amplitude. From Eq. (17), it follows that

$$c_{tj}{}^*(\sigma)=c_{t-j}(-\sigma). \quad (28)$$

The functions $c_{tj}(\sigma)$ represent constant amplitudes for the unperturbed Hamiltonian (Eq. 18). As a result of the perturbing potentials V_A and V_E they will depend on T. By regarding Eq. (27) as a canonical transformation, it is shown in Appendix A that the momenta conjugates of $c_{tl}(\sigma)$, $p_{c_{tl}}(\sigma)$, are given by

$$p_{c_{tl}}(\sigma)=-2i\omega_{tl}(\sigma)c_{t-1}(-\sigma), \quad (29)$$

and that the transformed Hamiltonian K takes the

form

$$K=(\beta/6N^{\frac{1}{2}})\sum_{\substack{\sigma,\sigma',\sigma''\\ t,t',t''\\ j,j',j''}} F_{tt't''}(\sigma,\sigma',\sigma'')c_{tj}(\sigma)c_{t'j'}(\sigma')c_{t''j''}(\sigma'')\exp\{i[\omega_{tj}(\sigma)+\omega_{t'j'}(\sigma')+\omega_{t''j''}(\sigma'')]T\}$$

$$-eEN^{\frac{1}{2}}\sum_{t,j}A_t(0)c_{tj}(0)e^{i\omega_{tj}(0)T}. \quad (30)$$

The Hamilton canonical equations yield

$$\dot{c}_{tj}(\sigma)=-\frac{1}{2i\omega_{tj}(\sigma)}\frac{\partial K}{\partial c_{t-j}(-\sigma)} \quad (31)$$

or

$$\dot{c}_{tj}(\sigma)=-\frac{3\beta}{4i\omega_{tj}(\sigma)N^{\frac{1}{2}}}\sum_{\substack{\sigma',t',j'\\ t'',j''}} F_{tt't''}(-\sigma,\sigma',\sigma-\sigma')$$

$$\times c_{t'j'}(\sigma')c_{t''j''}(\sigma-\sigma')\exp\{i[\omega_{t'j'}(\sigma')+\omega_{t''j''}(\sigma-\sigma')-\omega_{tj}(\sigma)]T\} \quad (32)$$

for $\sigma\neq 0$, and

$$\dot{c}_{tj}(0)=-\frac{3\beta}{4i\omega_{tj}(0)N^{\frac{1}{2}}}\sum_{\substack{\sigma',t',j'\\ t'',j''}} F_{tt't''}(0,\sigma',-\sigma')c_{t'j'}(\sigma')c_{t''j''}(-\sigma')\exp\{i[\omega_{t'j'}(\sigma')+\omega_{t''j''}(\sigma')-\omega_{tj}(0)]T\}$$

$$+[eEN^{\frac{1}{2}}/2i\omega_{tj}(0)]A_t(0)e^{-i\omega_{tj}(0)T} \quad (33)$$

for $\sigma=0$. Here we have made use of the relation $c_{tj}(\mathfrak{d}\pm\mathbf{b})=c_{tj}(\mathfrak{d})$ which follows from the fact that the motion is a periodic function in reciprocal lattice space. Since the time dependence of $c_{tj}(\sigma)$ for $\sigma\neq 0$ is caused solely by the anharmonic potential which by hypothesis is small, let us write

$$c_{tj}(\sigma)=c_{tj}^{(0)}(\sigma)+c_{tj}^{(1)}(\sigma) \quad (34)$$

for $\sigma\neq 0$, where $c_{tj}^{(0)}(\sigma)$ is constant in time, and thus $c_{tj}^{(0)}(\sigma)\gg c_{tj}^{(1)}(\sigma)$. For $c_{tj}(0)$, which is time dependent even for vanishing V_A, as a result of V_E we introduce

$$c_{tj}(0)=\eta_{tj}(0)\exp\{i[\omega-\omega_{tj}(0)]T\}. \quad (35)$$

To first order, Eq. (32) thus becomes

$$\dot{c}_{tj}^{(1)}(\sigma)=-\frac{3\beta}{4i\omega_{tj}(\sigma)N^{\frac{1}{2}}}\sum_{\substack{\sigma',t',j'\\ t'',j''}}'' F_{tt't''}(-\sigma,\sigma',\sigma-\sigma')c_{t'j'}^{(0)}(\sigma')c_{t''j''}^{(0)}(\sigma-\sigma')$$

$$\times\exp\{i[\omega_{t'j'}(\sigma')+\omega_{t''j''}(\sigma-\sigma')-\omega_{tj}(\sigma)]T\}-\frac{3\beta}{2i\omega_{tj}(\sigma)N^{\frac{1}{2}}}\sum_{\substack{t',t''\\ j',j''}} F_{tt't''}(-\sigma,0,\sigma)\eta_{t'j'}(0)c_{t''j''}^{(0)}(\sigma)$$

$$\times\exp\{i[\omega+\omega_{t''j''}(\sigma)-\omega_{tj}(\sigma)]T\}. \quad (36)$$

Here $\sum''$ denotes that $\sigma'\neq\sigma$ or 0. Integration of Eq. (36) yields

$$c_{tj}^{(1)}(\sigma)=\frac{3\beta}{4\omega_{tj}(\sigma)N^{\frac{1}{2}}}\sum_{\substack{\sigma',t',j'\\ t'',j''}} F_{tt't''}(-\sigma,\sigma',\sigma-\sigma')c_{t'j'}^{(0)}(\sigma')c_{t''j''}^{(0)}(\sigma-\sigma')\left[\frac{\exp(ixT)-1}{x}\right]$$

$$+\frac{3\beta}{2\omega_{tj}(\sigma)N^{\frac{1}{2}}}\sum_{\substack{\sigma',t',j'\\ t'',j''}} F_{tt't''}(0,\sigma',-\sigma')\eta_{t'j'}(0)c_{t''j''}^{(0)}(\sigma)\left[\frac{\exp(iyT)-1}{y}\right], \quad (37)$$

with

$$x=\omega_{t'j'}(\sigma')+\omega_{t''j''}(\sigma-\sigma')-\omega_{tj}(\sigma)$$

and

$$y=\omega+\omega_{t''j''}(\sigma)-\omega_{tj}(\sigma).$$

In order to solve Eq. (33) for $c_{tj}(0)$, one must include first-order terms on the right side of that equation. The zero-order terms give no contribution to the first factor of Eq. (33). To prove this, note that this factor contains a sum involving $c_{t'j'}(\sigma')c_{t''j''}(-\sigma')$. The phases associated with the complex amplitudes are arbitrary so that

on the average a sum of this sort vanishes unless $t''=t'$ and $j''=-j'$ when it takes the form $c_{t'j'}{}^{(0)}(\sigma')c_{t'-j'}{}^{(0)}(-\sigma')=|c_{t'j'}{}^{(0)}(\sigma')|^2$ as a result of Eq. (28). But $F_{tt't'}(0,\sigma',-\sigma')$ vanishes since

$$F_{tt't'}(0,\sigma',-\sigma')=A_t(0)A_{t'}(\sigma')A_{t'}(-\sigma')-A_t{}^*(0)A_{t'}{}^*(\sigma')A_{t'}{}^*(-\sigma')$$

and $A_t{}^*(\sigma)=A_t(-\sigma)$. Thus Eq. (33) becomes

$$\dot{c}_{tj}(0)=-\frac{3\beta}{4i\omega_{tj}(0)N^{\frac{1}{2}}}\sum_{\substack{\sigma',j',t'',j''\\ [t''\neq t']}}F_{tt't''}(0,\sigma',-\sigma')[c_{t'j'}{}^{(1)}(\sigma')c_{t''j''}{}^{(0)}(-\sigma')+c_{t'j'}{}^{(0)}(\sigma')c_{t''j''}{}^{(1)}(-\sigma')]\exp(iqT)$$
$$+[eEN^{\frac{1}{2}}/2i\omega_{tj}(0)]A_t(0)e^{-i\omega_{tj}(0)T}, \quad (38)$$

where $q=\omega_{t'j'}(\sigma')+\omega_{t''j''}(\sigma')-\omega_{tj}(0)$. On inserting the value of $c_{tj}{}^{(1)}(\sigma)$ from Eq. (34) and $\dot{c}_{tj}(0)$ from Eq. (35) with $\eta_{tj}(0)$ constant (i.e., first-order term), Eq. (38) reduces to

$$i[\omega-\omega_{tj}(0)]\eta_{tj}(0)=-\frac{9\beta^2}{8iN^2\omega_{tj}(0)}\sum_{\substack{\sigma',t',j',t'',j''\\ [t''\neq t']}}[\eta_{t''j''}(0)F_{tt't''}(0,\sigma',-\sigma')F_{t't''t}(-\sigma',0,\sigma')]$$
$$\times\left[\frac{1-\exp(-i\rho T)}{\rho}\right]\left[\frac{|c_{t''j''}(-\sigma')|^2}{\omega_{t'j'}(\sigma')}+\frac{|c_{t'j'}(\sigma')|^2}{\omega_{t''j''}(\sigma')}\right]+\frac{eE_0}{2i\omega_{tj}(0)}A_t(0)N^{\frac{1}{2}}, \quad (39)$$

where $\rho=\omega-\omega_{t'j'}(\sigma')-\omega_{t''j''}(\sigma'')$. Here again we have used the fact that a sum over σ involving an odd number of the amplitudes $c_{tj}(\sigma)$ will vanish.

For simple ionic crystals such as NaCl, there exists only one transverse mode of oscillation for $\sigma=0$. This implies that $t'''=t$ in Eq. (39). Furthermore, the functions $U_{kxt}(\sigma)$ are real for the NaCl structure. Thus,

$$F_{tt't''}(0,\sigma',-\sigma')F_{t't''t}(-\sigma',0,\sigma')=-[A_t(0)]^2[A_{t'}(\sigma')A_{t''}(-\sigma')-A_{t'}(-\sigma')A_{t''}(\sigma')]^2. \quad (40)$$

On inserting the value of $A_t(\sigma)$ from Eq. (20), this becomes

$$F_{tt't''}(0,\sigma',-\sigma')F_{t't''t}(-\sigma',0,\sigma')=(4/m_km_{k'})[\sin(2\pi\sigma_x r_0)]^2\left[\frac{U_{kxt}(0)}{(m_k)^{\frac{1}{2}}}-\frac{U_{k'xt}(0)}{(m_{k'})^{\frac{1}{2}}}\right]^2$$
$$\times[U_{kxt'}(\sigma')U_{k'xt''}(\sigma')-U_{kxt''}(\sigma')U_{k'xt'}(\sigma')]^2. \quad (41)$$

Thus Eq. (39) can be written in the form

$$[\omega-\omega_{tj}(0)-\gamma_j]\eta_{tj}+\eta_{t-j}\gamma_{-j}=-\frac{eE_0A_t(0)N^{\frac{1}{2}}}{2\omega_{tj}(0)}, \quad (42)$$

with γ_j given by

$$\gamma_j=\frac{9\beta^2}{2m_km_{k'}N^3\omega_{tj}(0)}\left[\frac{U_{kxt}(0)}{m_k{}^{-\frac{1}{2}}}-\frac{U_{k'xt}(0)}{m_{k'}{}^{-\frac{1}{2}}}\right]^2\sum_{\sigma,t',j',j''}[\sin(2\pi\sigma_x r_0)]^2[U_{kxt'}(\sigma)U_{k'xt''}(\sigma)-U_{kxt''}(\sigma)U_{k'xt'}(\sigma)]^2$$
$$\times\left[\frac{|c_{t''j''}(\sigma)|^2}{\omega_{t'j'}(\sigma)}+\frac{|c_{t'j'}(-\sigma)|^2}{\omega_{t''j''}(\sigma)}\right]\frac{\exp(-izT)-1}{z}, \quad (43)$$

and $z=\omega+\omega_{t'j'}(\sigma)+\omega_{t''j''}(\sigma)$. If V_A were absent, γ_j would be zero, since for that case Eq. (33) reduces to

$$\dot{c}_{tj}(0)=\frac{eE}{2i\omega_{tj}(0)}A_t(0)e^{-i\omega_{tj}(0)T}, \quad (44)$$

and with the help of Eq. (35) this would reduce to

$$i\eta_{tj}(0)[\omega-\omega_{tj}(0)]=\frac{eE_0N^{\frac{1}{2}}A_t(0)}{2i\omega_{tj}(0)}, \quad (45)$$

which is the same as Eq. (42) with $\gamma_j=0$.

The real part of γ_j causes a slight shift in the position of the resonant frequency. This will be ignored here. The imaginary part, however, leads to a coupling between the different modes and gives rise to a damping factor. Letting $\gamma_j=\epsilon_j+i\Gamma_j$, Γ_j may readily be obtained from Eq. (43). For $|c_{tj}(\sigma)|^2$, we will take its time average. The

average potential energy associated with mode t, σ is

$$\left.\frac{\omega_t^2 |a_t(\sigma)|^2}{2}\right|_{Av}$$

and will be taken to be $\frac{1}{2}K\theta$ with K the Boltzmann constant and θ the absolute temperature. Equation (27) shows that

$$|a_t(\sigma)|^2_{Av}=2|c_{tj}(\sigma)|^2_{Av}.$$

Hence,

$$|c_{tj}(\sigma)|^2_{Av}=\frac{K\theta}{2[\omega_{tj}(\sigma)]^2}. \tag{46}$$

With these substitutions, Eq. (42) becomes

$$[\omega-\omega_{tj}(0)-i\Gamma_j]\eta_{tj}+i\Gamma_{-j}\eta_{t-j}=-\frac{eE_0A_t(0)N^{\frac{1}{2}}}{2\omega_{tj}(0)}, \tag{47}$$

and Γ_j takes the form

$$\Gamma_j=-\frac{9\beta^2K\theta}{4N^3m_km_{k'}\omega_{tj}(0)}\left[\frac{U_{kzt}(0)}{m_k^{\frac{1}{2}}}-\frac{U_{k'zt}(0)}{m_{k'}^{\frac{1}{2}}}\right]^2\sum_{\substack{\sigma,t',t''\\ j',j''}}[\sin(2\pi\sigma_z\gamma_0)]^2[U_{kzt'}(\sigma)U_{k'zt''}(\sigma)-U_{kzt''}(\sigma)U_{k'zt'}(\sigma)]^2$$
$$\times\frac{[\omega_{t'j'}(\sigma)+\omega_{t''j''}(\sigma)]}{[\omega_{t'j'}(\sigma)\omega_{t''j''}(\sigma)]^2}\frac{\sin zT}{z}. \tag{48}$$

The electric dipole moment of the lattice can be expressed in the form

$$P_x=B(e_k/2)\sum_l[2u_{kx}{}^l-u_{k'x}{}^{l'}-u_{k'x}{}^{l''}], \tag{49}$$

where l' and l'' refer to cells to the right and left of cell l, respectively [see Eq. (14) for relation to l] and B is constant. The normal coordinate transformation yields

$$P_x=B\sum_t A_t(0)a_t(0). \tag{50}$$

As a result of the existence of only one transverse mode at $\sigma=0$, we can remove the sum over t. From Eqs. (27) and (35), we have that

$$a(0)=(\eta_1+\eta_{-1})e^{i\omega T}. \tag{51}$$

Noting that $\Gamma_{-j}=-\Gamma_j$, Eq. (47) gives rise to simultaneous equations in η_1 and η_{-1} which yield

$$\eta_1+\eta_{-1}=-\frac{G}{\omega^2-\omega_1^2-2i\Gamma\omega_1}, \tag{52}$$

where $G=eE_0A(0)N^{\frac{1}{2}}$, ω_1 is written for $\omega_1(0)$ and Γ represents Γ_1. Thus,

$$P_x=\frac{A(0)GB}{E_0}\frac{E}{\omega_1^2-\omega^2+2i\Gamma\omega_1}. \tag{53}$$

This dispersion relation leads to a complex index of refraction $\mathbf{n}=\eta+i\kappa$ in the usual manner:

$$\eta^2-\kappa^2=1+\frac{D[\omega_1^2-\omega^2]}{[\omega_1^2-\omega^2]^2+4\Gamma^2\omega_1^2} \tag{54}$$

and

$$2\eta\kappa=\frac{2\omega_1\Gamma D}{[\omega_1^2-\omega^2]^2+4\Gamma^2\omega_1^2} \tag{55}$$

with D a constant.

These formulas differ from usual dispersion theory in two respects. Firstly, an interchange of ω_1 and ω in both Eqs. (54) and (55) is required to yield the expressions for η and κ in normal dispersion theory. Secondly, the damping factor Γ is not a constant but frequency dependent according to Eq. (48). Thus, to find the optical constants, the series for Γ needs to be evaluated for different values of ω, the frequency of the impinging radiation. The expression for the electric dipole moment [Eq. (53)] is in agreement with a corrected formula given by Blackman.[12] The damping factor as given by Eq. (48) is somewhat more complicated than the corresponding B.B. relation. This is because B.B. confine the discussion to at most next-nearest neighbor interactions in the harmonic potential, whereas here no restriction is placed on the range of interaction. The dependence of Γ on $\sin zT/T$ appears in the B.B. model, whereas the $U_{kzt}(\sigma)$ terms in the sum of Eq. (48) are absent. No attempt was made by B.B. to find Γ as a function of ω except to locate the frequencies which cause Γ to be a maximum, because of the artificial nature of their model. The expression here can be applied to any model provided that the frequencies and amplitudes of the normal modes are known.

[12] M. Blackman, Phil. Trans. Roy. Soc. (London) **A236**, 103 (1937).

IV. MATRIX EQUATION FOR NaCl

For the NaCl structure, each ion is a center of symmetry such that the coupling coefficients

$$\begin{bmatrix} kk' \\ xy \end{bmatrix}$$

defined by Eq. (5) are real or

$$\begin{bmatrix} kk' \\ xy \end{bmatrix} = \sum_l (\phi_{kk'}{}^l)_{xy} \cos(2\pi \mathfrak{d} \cdot \mathbf{r}_{kk'}{}^l). \tag{56}$$

Following Kellerman,[11] the coupling coefficients are split up into a Coulomb contribution and a repulsive term caused by nearest neighbor only. Expressions for the Coulomb terms were obtained by Kellerman with the help of the Theta Function Transformation. The repulsive terms are given as function of the compressibility and the Madelung constant. Since we are adopting the Kellerman model for the harmonic potential, these relationships were taken directly from Kellerman's work. The wave vector $\mathfrak{d}$ has rectangular components.

$$\mathfrak{d} = (1/2r_0)(q_x, q_y, q_z), \tag{57}$$

with the q's subject to the condition

$$q_x \pm q_y + q_z \leq \pm\tfrac{3}{2}; \qquad q_x, q_y, q_z \leq 1. \tag{58}$$

As a result of the symmetry of the coupling coefficients, the characteristic frequencies can be further restricted inside the first Brillouin zone by the relations

$$1 \geq q_x \geq q_y \geq q_z \geq 0; \qquad q_x + q_y + q_z \leq \tfrac{3}{2}. \tag{59}$$

For the calculation of the frequency distribution function $f(\nu)$, the calculated frequencies must be weighed so as to include all wave vectors belonging to the first Brillouin zone. For the calculation of the damping factor Γ, the eigenvectors U_{1x} and U_{2x} are also needed. As a consequence of the symmetry properties of the coupling coefficients, the matrix equation has the form

$$\begin{vmatrix} a_{11}-\lambda & a_{12} & a_{13} & a_{14} & a_{15} & a_{16} \\ a_{12} & a_{22}-\lambda & a_{14} & a_{24} & a_{16} & a_{26} \\ a_{13} & a_{14} & a_{33}-\lambda & a_{34} & a_{35} & a_{36} \\ a_{14} & a_{24} & a_{34} & a_{44}-\lambda & a_{36} & a_{46} \\ a_{15} & a_{16} & a_{34} & a_{36} & a_{55}-\lambda & a_{56} \\ a_{16} & a_{26} & a_{36} & a_{46} & a_{56} & a_{66}-\lambda \end{vmatrix} \begin{vmatrix} U_{1x} \\ U_{2x} \\ U_{1y} \\ U_{2y} \\ U_{1z} \\ U_{2z} \end{vmatrix} = 0, \tag{60}$$

with $\lambda = \omega^2$.

Interchange of q_x with q_y gives

$$\begin{vmatrix} a_{33}-\lambda & a_{3}{}^{4} & a_{13} & a_{14} & a_{35} & a_{36} \\ a_{34} & a_{44}-\lambda & a_{14} & a_{24} & a_{36} & a_{46} \\ a_{13} & a_{14} & a_{11}-\lambda & a_{12} & a_{15} & a_{16} \\ a_{14} & a_{24} & a_{12} & a_{22}-\lambda & a_{16} & a_{26} \\ a_{35} & a_{36} & a_{15} & a_{16} & a_{55}-\lambda & a_{5}{}^{6} \\ a_{26} & a_{46} & a_{16} & a_{26} & a_{56} & a_{66}-\lambda \end{vmatrix} \begin{vmatrix} U'_{1x} \\ U'_{2x} \\ U'_{1y} \\ U'_{2y} \\ U'_{1z} \\ U'_{2z} \end{vmatrix} = 0. \tag{61}$$

The λ's are unchanged since both matrices have identical determinants (interchange rows 3 and 4 with rows 1 and 2 and then columns 1 and 2 with 3 and 4) and it is also readily seen that $U_{1x}' = U_{1y}$; $U_{2x}' = U_{2y}$; $U_{1y}' = U_{1x}$; $U_{2y}' = U_{2x}$; $U_{1z}' = U_{1z}$; $U_{2z}' = U_{2z}$. A change in the sign of q_x will result in $U_{1x}' = -U_{1x}$; $U_{2x}' = -U_{2x}$, the other amplitudes remaining the same. Since Γ depends only on the product $U_{1x}U_{2x}$, no change will occur. Thus, Eq. (59) is an adequate wave vector scanning for both $f(\nu)$ and Γ when multiplicities are properly included.

V. EVALUATION OF FREQUENCY DISTRIBUTION AND THE OPTICAL CONSTANTS OF NaCl

The calculation of the damping factor requires a knowledge of both the eigenvectors and eigenvalues for a fairly dense set of wave vectors. Since Kellerman obtained eigenvalues only, it was decided to repeat

TABLE I. The circular frequencies ω of NaCl as a function of the wave vector $\mathbf{d}$ with $\mathbf{p}=24r_0\mathbf{d}$. The components of $\mathbf{p}$ are either all odd or all even subject to the conditions $12\geq p_x\geq p_y\geq p_z\geq 0$ and $p_x+p_y+p_z\leq 18$. The ω's are scaled by 10^{-10} and the six ω's belonging to each choice of $\mathbf{p}$ are given.

p_x	p_y	p_z	ω_1	ω_2	ω_3	ω_4	ω_5	ω_6
12	6	0	3385	2723	2872	2312	3385	2723
12	4	2	3659	3306	2893	2814	2637	1946
12	4	0	3751	2933	2929	2160	3154	2341
12	2	2	3953	3143	2991	2916	2271	1799
12	2	0	4066	3019	3001	1897	3052	1944
12	0	0	4186	3046	3022	1772	3022	1772
11	5	1	3621	3262	2901	2800	2575	2170
11	3	3	3793	3237	2944	2786	2592	1825
11	3	1	3951	3116	2981	2903	2250	1910
11	1	1	4161	3052	3008	2991	1901	1763
10	8	0	3306	2814	2637	1946	3659	2893
10	6	2	3773	3229	2992	2748	2414	2087
10	6	0	3611	2880	2671	2163	3330	2667
10	4	4	3928	3248	3004	2615	2462	1857
10	4	2	3935	3114	2974	2767	2459	1901
10	4	0	3961	2958	2758	2087	3127	2273
10	2	2	4140	3061	2933	2901	2184	1745
10	2	0	4220	2996	2910	1834	3033	1878
10	0	0	4315	2970	3005	1709	3005	1709
9	7	1	3728	3321	2950	2700	2559	1969
9	5	3	4079	3250	2903	2625	2279	1906
9	5	1	4027	3141	2926	2630	2366	2046
9	3	3	4215	2993	2927	2761	2323	1740
9	3	1	4296	3024	2906	2773	2091	1799
9	1	1	4435	2987	2960	2857	1769	1643
8	8	2	3928	3248	3004	2615	2462	1857
8	8	0	3657	2848	2625	1887	3432	2763
8	6	4	4281	3464	2657	2472	2056	1904
8	6	2	4144	3199	2947	2527	2240	1961
8	6	0	4085	2850	2481	1988	3203	2482
8	4	4	4352	3270	2679	2590	2166	1771
8	4	2	4418	2958	2892	2620	2167	1774
8	4	0	4427	2795	2577	1906	3060	2072
8	2	2	4576	2881	2861	2758	1947	1590
8	2	0	4618	2859	2711	1653	2984	1688
8	0	0	4673	2707	2960	1525	2960	1525
7	7	3	4244	3386	2782	2439	2142	1895
7	7	1	4133	3187	2924	2450	2417	1925
7	5	5	4457	3521	2441	2423	1967	1839
7	5	3	4527	3183	2729	2439	2020	1801
7	5	1	4535	3033	2782	2429	2101	1877
7	3	3	4726	2845	2721	2668	1974	1583
7	3	1	4791	2943	2684	2592	1807	1595
7	1	1	4886	2907	2895	2516	1519	1415
6	6	6	4493	2341	3618	1885	2341	1885
6	6	4	4548	3412	2544	2346	1882	1870
6	6	2	4584	3025	2856	2355	1990	1876
6	6	0	4573	2689	2360	1874	3076	2160
6	4	4	4804	3086	2560	2465	1844	1646
6	4	2	4920	2834	2676	2487	1797	1590
6	4	0	4935	2505	2447	1662	2980	1757
6	2	2	5079	2808	2736	2405	1601	1354
6	2	0	5109	2754	2298	1380	2921	1393
6	0	0	5142	2240	2900	1237	2900	1237
5	5	5	4748	3303	2412	1769	2412	1769
5	5	3	4938	2903	2667	2407	1705	1651
5	5	1	4987	2939	2503	2406	1734	1667
5	3	3	5192	2676	2568	2506	1560	1383
5	3	1	5272	2872	2589	2186	1438	1327
5	1	1	5362	2847	2816	1987	1180	1102
4	4	4	5151	2721	2533	1513	2533	1513
4	4	2	5314	2767	2515	2300	1409	1360
4	4	0	5341	2509	2071	1370	2909	1379
4	2	2	5513	2671	1908	1194	2756	1074
4	2	0	5547	2693	1728	1050	2860	1028
4	0	0	5579	1600	2842	868	2842	868
3	3	3	5504	2640	2070	1188	2640	1188
3	3	1	5614	2817	2620	1694	1062	1016
3	1	1	5741	2761	1329	789	2797	741
2	2	2	5769	2719	1390	818	2719	818
2	2	0	5823	2706	1124	703	2816	653
2	0	0	5880	833	2800	447	2800	447
1	1	1	5946	2753	699	416	2753.	416
0	0	0	5985	0	2782	0	2782	0

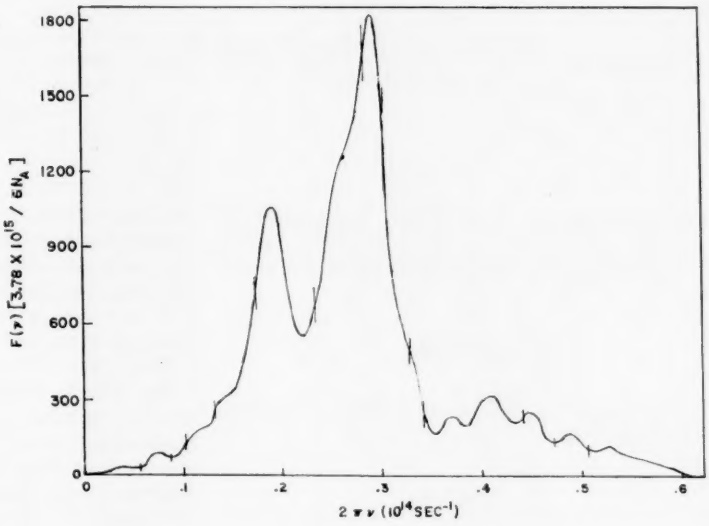

FIG. 1. Frequency distribution function $F(\nu)$ for NaCl. The vertical lines indicate the error associated with the calculations.

the calculations with a more dense distribution in wave vector space. We chose $q_x=p_x/12$, etc. with p_x, p_y, p_z either all even or all odd and subject to the condition $p_x+p_y+p_z\leq 18$; $12\geq p_x\geq p_y\geq p_z\geq 0$. There are 74 σ's of this type. This compares with Kellerman's choice of $q_x=p_x/10$, etc. or 48 choices of σ. The Coulomb coupling coefficients were calculated with the help of UNIVAC according to the series given by Kellerman for 73 choices of σ. For the wave vector (0, 0, 0) we used Kellerman's expression

$$\begin{bmatrix} k & k' \\ x & y \end{bmatrix}^C = \frac{4\pi}{3}\frac{e_k e_{k'}}{v_a}\delta_{xy}.$$

The eigenvectors and eigenvalues of the resultant 73 matrices were again computed by UNIVAC with orthonormality for each set serving as check point. The traces of the matrices for different σ's are all constant according to the Kellerman model, and this was verified to at least four significant digits. The constants were taken from room temperature data. Table I gives the list of frequencies.

In order to calculate $f(\nu)$, the number of frequencies falling into intervals $\Delta\omega=2\pi\Delta\nu=2\times 10^{12}$ rad/sec were counted. Four types of step curves were plotted, each shifted against the other by 0.5×10^{12} rad/sec in the ω scale. The distribution curve, Fig. 1, is the approximation of these graphs by a smooth curve. The normalizing factor was taken to be $6N_A$, N_A being Avogadro's number, i.e.,

$$\int_0^{\nu\ \max} f(\nu)d\nu=6N_A.$$

This distribution function is very similar to Kellerman's original curve and a more recent study by Karo.[13] The presence of minor fluctuations in $f(\nu)$ in the high-frequency region which were not obtained by Kellerman and Karo is most probably a result of the denser spacing in σ space chosen here. Specific heat curves were not calculated by us, since our major concern was the evaluation of the optical constants. (See, however, E. Arase[14] on low-temperature specific heats based on the frequency spectrum as calculated here.)

For the damping factor Γ (see Eq. 48), we can only obtain its relative value since β, the anharmonic potential coefficient, is not specified and furthermore, the $\sum_\sigma$ is based on a small sampling of σ. Thus, dropping constant terms, Eq. (48) becomes

$$\Gamma\sim\sum_{\substack{\sigma tt' \\ jj'}}[\sin(2\pi\sigma_z r_0)]^2[U_{kzt}(\sigma)U_{k'zt'}(\sigma)-U_{kzt'}(\sigma)U_{k'zt}(\sigma)]^2\frac{\omega_{tj}(\sigma)+\omega_{t'j'}(\sigma)}{[\omega_{tj}(\sigma)\omega_{t'j'}(\sigma)]^2}\frac{\sin\{[\omega+\omega_{tj}(\sigma)+\omega_{t'j'}(\sigma)]T\}}{\omega+\omega_{tj}(\sigma)+\omega_{t'j'}(\sigma)}. \quad (62)$$

An inspection of Eq. (62) shows that the major contribution to the sum comes from the choice of j and j' which cause $\omega+\omega_{tj}(\sigma)+\omega_{t'j'}(\sigma)$ to be as small as possible. Thus, for the case when $\omega_t(\sigma)\geq\omega_{t'}(\sigma)$, this implies that we

[13] A. Karo, J. Chem. Phys. **31,** 1489 (1959).
[14] E. Arase and R. Hatcher, J. Chem. Phys. **33,** 1704 (1960).

TABLE I. The circular frequencies ω of NaCl as a function of the wave vector $\mathbf{\delta}$ with $\mathbf{p}=24r_0\mathbf{\delta}$. The components of $\mathbf{p}$ are either all odd or all even subject to the conditions $12\geq p_x\geq p_y\geq p_z\geq 0$ and $p_x+p_y+p_z\leq 18$. The ω's are scaled by 10^{-10} and the six ω's belonging to each choice of $\mathbf{p}$ are given.

p_x	p_y	p_z	ω_1	ω_2	ω_3	ω_4	ω_5	ω_6
12	6	0	3385	2723	2872	2312	3385	2723
12	4	2	3659	3306	2893	2814	2637	1946
12	4	0	3751	2933	2929	2160	3154	2341
12	2	2	3953	3143	2991	2916	2271	1799
12	2	0	4066	3019	3001	1897	3052	1944
12	0	0	4186	3046	3022	1772	3022	1772
11	5	1	3621	3262	2901	2800	2575	2170
11	3	3	3793	3237	2944	2786	2592	1825
11	3	1	3951	3116	2981	2903	2250	1910
11	1	1	4161	3052	3008	2991	1901	1763
10	8	0	3306	2814	2637	1946	3659	2893
10	6	2	3773	3229	2992	2748	2414	2087
10	6	0	3611	2880	2671	2163	3330	2667
10	4	4	3928	3248	3004	2615	2462	1857
10	4	2	3935	3114	2974	2767	2459	1901
10	4	0	3961	2958	2758	2087	3127	2273
10	2	2	4140	3061	2933	2901	2184	1745
10	2	0	4220	2996	2910	1834	3033	1878
10	0	0	4315	2970	3005	1709	3005	1709
9	7	1	3728	3321	2950	2700	2559	1969
9	5	3	4079	3250	2903	2625	2279	1906
9	5	1	4027	3141	2926	2630	2366	2046
9	3	3	4215	2993	2927	2761	2323	1740
9	3	1	4296	3024	2906	2773	2091	1799
9	1	1	4435	2987	2960	2857	1769	1643
8	8	2	3928	3248	3004	2615	2462	1857
8	8	0	3657	2848	2625	1887	3432	2763
8	6	4	4281	3464	2657	2472	2056	1904
8	6	2	4144	3199	2947	2527	2240	1961
8	6	0	4085	2850	2481	1988	3203	2482
8	4	4	4352	3270	2679	2590	2166	1771
8	4	2	4418	2958	2892	2620	2167	1774
8	4	0	4427	2795	2577	1906	3060	2072
8	2	2	4576	2881	2861	2758	1947	1590
8	2	0	4618	2859	2711	1653	2984	1688
8	0	0	4673	2707	2960	1525	2960	1525
7	7	3	4244	3386	2782	2439	2142	1895
7	7	1	4133	3187	2924	2450	2417	1925
7	5	5	4457	3521	2441	2423	1967	1839
7	5	3	4527	3183	2729	2439	2020	1801
7	5	1	4535	3033	2782	2429	2101	1877
7	3	3	4726	2845	2721	2668	1974	1583
7	3	1	4791	2943	2684	2592	1807	1595
7	1	1	4886	2907	2895	2516	1519	1415
6	6	6	4493	2341	3618	1885	2341	1885
6	6	4	4548	3412	2544	2346	1882	1870
6	6	2	4584	3025	2856	2355	1990	1876
6	6	0	4573	2689	2360	1874	3076	2160
6	4	4	4804	3086	2560	2465	1844	1646
6	4	2	4920	2834	2676	2487	1797	1590
6	4	0	4935	2505	2447	1662	2980	1757
6	2	2	5079	2808	2736	2405	1601	1354
6	2	0	5109	2754	2298	1380	2921	1393
6	0	0	5142	2240	2900	1237	2900	1237
5	5	5	4748	3303	2412	1769	2412	1769
5	5	3	4938	2903	2667	2407	1705	1651
5	5	1	4987	2939	2503	2406	1734	1667
5	3	3	5192	2676	2568	2506	1560	1383
5	3	1	5272	2872	2589	2186	1438	1327
5	1	1	5362	2847	2816	1987	1180	1102
4	4	4	5151	2721	2533	1513	2533	1513
4	4	2	5314	2767	2515	2300	1409	1360
4	4	0	5341	2509	2071	1370	2909	1379
4	2	2	5513	2671	1908	1194	2756	1074
4	2	0	5547	2693	1728	1050	2860	1028
4	0	0	5579	1600	2842	868	2842	868
3	3	3	5504	2640	2070	1188	2640	1188
3	3	1	5614	2817	2620	1694	1062	1016
3	1	1	5741	2761	1329	789	2797	741
2	2	2	5769	2719	1390	818	2719	818
2	2	0	5823	2706	1124	703	2816	653
2	0	0	5880	833	2800	447	2800	447
1	1	1	5946	2753	699	416	2753	416
0	0	0	5985	0	2782	0	2782	0

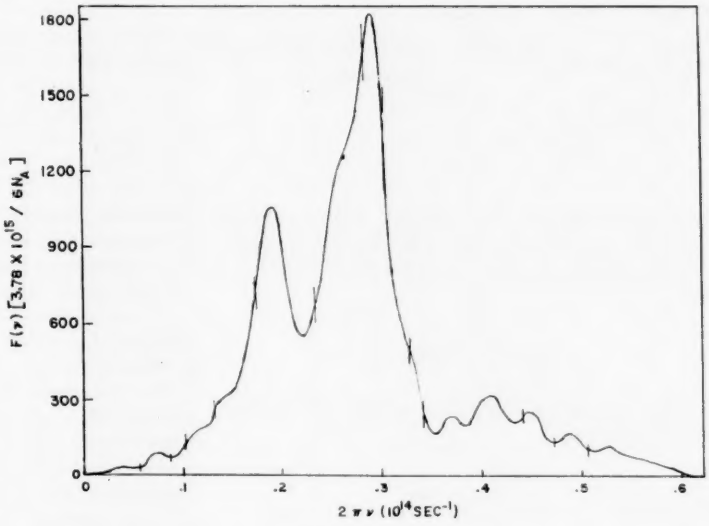

FIG. 1. Frequency distribution function $F(\nu)$ for NaCl. The vertical lines indicate the error associated with the calculations.

the calculations with a more dense distribution in wave vector space. We chose $q_x=p_x/12$, etc. with p_x, p_y, p_z either all even or all odd and subject to the condition $p_x+p_y+p_z\leq 18$; $12\geq p_x\geq p_y\geq p_z\geq 0$. There are 74 σ's of this type. This compares with Kellerman's choice of $q_x=p_x/10$, etc. or 48 choices of σ. The Coulomb coupling coefficients were calculated with the help of UNIVAC according to the series given by Kellerman for 73 choices of σ. For the wave vector (0, 0, 0) we used Kellerman's expression

$$\begin{bmatrix} k & k' \\ x & y \end{bmatrix}^C = \frac{4\pi}{3}\frac{e_k e_{k'}}{v_a}\delta_{xy}.$$

The eigenvectors and eigenvalues of the resultant 73 matrices were again computed by UNIVAC with orthonormality for each set serving as check point. The traces of the matrices for different σ's are all constant according to the Kellerman model, and this was verified to at least four significant digits. The constants were taken from room temperature data. Table I gives the list of frequencies.

In order to calculate $f(\nu)$, the number of frequencies falling into intervals $\Delta\omega=2\pi\Delta\nu=2\times 10^{12}$ rad/sec were counted. Four types of step curves were plotted, each shifted against the other by 0.5×10^{12} rad/sec in the ω scale. The distribution curve, Fig. 1, is the approximation of these graphs by a smooth curve. The normalizing factor was taken to be $6N_A$, N_A being Avogadro's number, i.e.,

$$\int_0^{\nu\ \max} f(\nu)d\nu=6N_A.$$

This distribution function is very similar to Kellerman's original curve and a more recent study by Karo.[13] The presence of minor fluctuations in $f(\nu)$ in the high-frequency region which were not obtained by Kellerman and Karo is most probably a result of the denser spacing in σ space chosen here. Specific heat curves were not calculated by us, since our major concern was the evaluation of the optical constants. (See, however, E. Arase[14] on low-temperature specific heats based on the frequency spectrum as calculated here.)

For the damping factor Γ (see Eq. 48), we can only obtain its relative value since β, the anharmonic potential coefficient, is not specified and furthermore, the $\sum_\sigma$ is based on a small sampling of σ. Thus, dropping constant terms, Eq. (48) becomes

$$\Gamma\sim\sum_{\substack{\sigma tt'\\ jj'}}[\sin(2\pi\sigma_z r_0)]^2[U_{kzt}(\sigma)U_{k'zt'}(\sigma)-U_{kzt'}(\sigma)U_{k'zt}(\sigma)]^2\frac{\omega_{tj}(\sigma)+\omega_{t'j'}(\sigma)}{[\omega_{tj}(\sigma)\omega_{t'j'}(\sigma)]^2}\frac{\sin\{[\omega+\omega_{tj}(\sigma)+\omega_{t'j'}(\sigma)]T\}}{\omega+\omega_{tj}(\sigma)+\omega_{t'j'}(\sigma)}. \quad (62)$$

An inspection of Eq. (62) shows that the major contribution to the sum comes from the choice of j and j' which cause $\omega+\omega_{tj}(\sigma)+\omega_{t'j'}(\sigma)$ to be as small as possible. Thus, for the case when $\omega_t(\sigma)\geq\omega_{t'}(\sigma)$, this implies that we

[13] A. Karo, J. Chem. Phys. **31,** 1489 (1959).
[14] E. Arase and R. Hatcher, J. Chem. Phys. **33,** 1704 (1960).

choose $j=-1$ and $j'=\pm 1$. Thus,

$$\Gamma\sim\sum_{\sigma tt'}[\sin(2\pi\sigma_x x_0)]^2\frac{[U_{kxt}(\sigma)U_{k'xt'}(\sigma)-U_{kxt'}(\sigma)U_{k'xt}(\sigma)]^2}{[\omega_t(\sigma)\omega_{t'}(\sigma)]^2}\Big\{[\omega_t(\sigma)+\omega_{t'}(\sigma)]\frac{\sin([\omega-\omega_t(\sigma)-\omega_{t'}(\sigma)]T)}{\omega-\omega_t(\sigma)-\omega_{t'}(\sigma)}$$
$$+|\omega_t(\sigma)-\omega_{t'}(\sigma)|\frac{\sin([\omega-|\omega_t(\sigma)-\omega_{t'}(\sigma)|]T)}{\omega-|\omega_t(\sigma)-\omega_{t'}(\sigma)|}\Big\}. \quad (63)$$

This expression for Γ is actually independent of T, the time, provided that $\omega T>10$. For if we replace $\sum_\sigma$ by an integral, the major contribution will be of the form

$$\int_0^y(\sin xT/x)dx$$

with $x=\omega-\omega_t(\sigma)-\omega_{t'}(\sigma)$ and y of order ω. Letting $z=xT$, this becomes

$$\int_0^{yT}(\sin z/z)dz$$

or the $Si(z)$ function which rapidly converges to its limiting value $\pi/2$. For $yT>10$, $Si(z)$ differs by less than 5% from $\pi/2$. As a check, Γ was calculated for a particular choice of ω, the frequency of the impinging radiation, using several values of T. Reasonable agreement was found. In order to sample the value of Γ over a fairly wide range of frequencies, we chose 19 values of ω with $T=10\pi\times10^{-14}$ sec. For each σ, 15 different combinations of amplitudes and lattice frequencies were summed corresponding to t and t' ranging from 1 to 6 with $t\neq t'$. The amplitude factors and multiplicities were included as outlined in part IV. The resultant values of $\Gamma_{\text{rel}}=\Gamma/F$ where F is a constant are shown in Table II.

TABLE II. The calculated values of the damping coefficient.

λ in μ	$\omega=2\pi c/\lambda$	$\Gamma_{\text{rel}}=\Gamma/F$
25.0	7.53×10^{13} rad/sec	217
32.5	5.79	410
38.0	4.96	1539
40.0	4.71	1888
42.0	4.48	2025
47.5	3.96	1531
55.0	3.42	434
62.5	3.01	52
66.0	2.85	99
70.0	2.69	75
77.5	2.43	56
82.0	2.30	141
85.0	2.21	194
92.5	2.04	290
100.0	1.88	349
200.0	.942	318
300.0	.628	280
400.0	.471	259
500.0	.377	244

The optical constants η and κ, as given by Eq. (54) and Eq. (55), may be obtained as a function of frequency from a knowledge of η and κ at a single frequency, thus fixing the constants F and D. Calculations were made based on either of two choices for η and κ as given by Czerny.[4] (a) $\lambda=94\mu$, $\eta=2.94$ and $\kappa=0.10$ or (b) $\lambda=38\mu$, $\eta=0.4$ and $\kappa=0.5$. The resonant frequency $\omega_1(0)$ was taken as 3.09×10^{13} rad/sec. Figures 2 and 3 give the behavior of η and κ based on either of these two reference points. We estimate that the error associated with those calculations is no larger

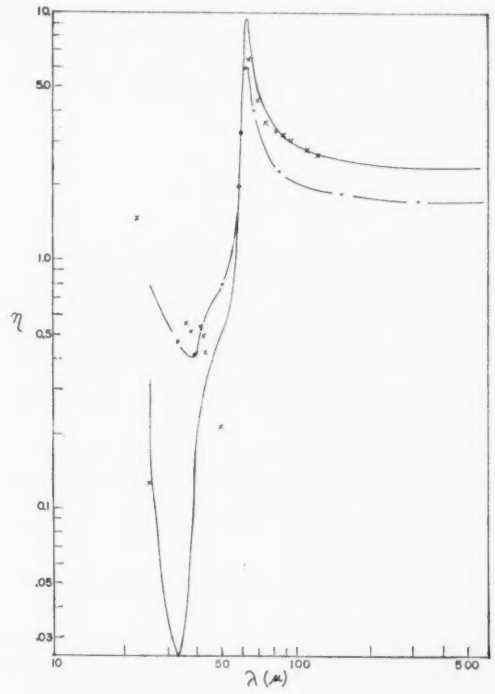

FIG. 2. Index of refraction of NaCl, η vs wavelength λ. — fitted at 94μ, —·—· fitted at 38μ. Experimental values[15] are indicated by crosses.

than 5%. Recent experiments[15] covering the wavelength region under consideration are also included. It will be noted that whereas the absolute calculated values of η and κ differ somewhat, the shape of the curves remains the same. Especially interesting is the appearance of a subsidiary maximum of κ at about 120μ which had not been known previously. The experimental results confirm the presence of this maximum. The complexity of the anharmonic theory does not permit us to make any definite conclusion as to the position of this subsidiary absorption maximum for other alkali halides. However, we can expect that they will be present and will apply the anharmonic theory to other ionic crystals in the near future.

The temperature dependence of the optical constants cannot be deduced completely from this theory. This is due to the fact that the absolute values of η and κ cannot be obtained because of the arbitrary anharmonic interaction constant β. We have assumed sufficiently high temperatures where equipartition is valid (see Eq. 46) and this gives rise to a damping term proportional to the absolute temperature. For the calculation of η and κ, however, all the eigenfrequencies and eigenvectors are required and these will depend on temperature also. Hence, we cannot make any definite conclusions regarding temperature dependence, and a $T^{\frac{1}{2}}$ dependence experimentally found by Haas[16] may be possible with the theory presented here.

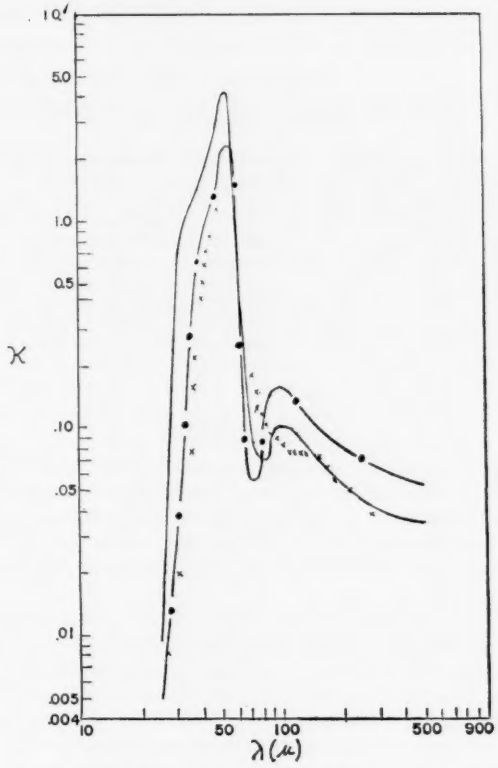

FIG. 3. Extinction coefficient of NaCl, κ vs wavelength λ. — fitted at 94μ, —·—· fitted at 38μ. Experimental values[15] are indicated by crosses.

APPENDIX A

In order to prove that $\dot{p}_{c_{tl}(\sigma)}=-2i\omega_{tl}(\sigma)c_{t-1}(-\sigma)$ (Eq. 29), consider the unperturbed Hamiltonian

$$H_0=\tfrac{1}{2}\sum_{t,\sigma}[\dot{p}_{a_t(\sigma)}\dot{p}_{a_t(-\sigma)}+\omega_t^2(\sigma)a_t(\sigma)a_t(-\sigma)], \qquad (A.1)$$

with $\dot{p}_{a_t(\sigma)}=\dot{a}_t(-\sigma)$. Transformation (27)

$$a_t(\sigma)=\sum_i c_{ti}(\sigma)\,\exp[i\omega_{ti}(\sigma)\,T]$$

implies that

$$\dot{p}_{a_t(\sigma)}=\sum_i i\omega_{ti}(\sigma)c_{ti}(-\sigma)\,\exp[i\omega_{ti}(\sigma)\,T]. \qquad (A.2)$$

We now regard $c_{tl}(\sigma)$ and $c_{tl}(-\sigma)$ as the new coordinates and seek a generating function of the form

$$F_1[a_t(\sigma), a_t(-\sigma), c_{tl}(\sigma), c_{tl}(-\sigma), T]$$

involving the old and the new coordinates and the time such that the transformed Hamiltonian K should vanish. This implies that[17]

$$\dot{p}_{a_t}(\sigma)=\frac{\partial F_1}{\partial a_t(\sigma)}, \qquad (A.3)$$

$$\dot{p}_{c_{tl}}(\sigma)=-\frac{\partial F_1}{\partial c_{tl}(\sigma)}, \qquad (A.4)$$

and

$$K=H+(\partial F_1/\partial T). \qquad (A.5)$$

By writing H_0 and $\dot{p}_{a_t}(\sigma)$ as a function of the old and new coordinates, it is readily verified that F_1 takes the form

$$F_1=\sum_{\sigma,t}\{i\omega_{tl}(\sigma)\}\Big\{2a_t(\sigma)c_{tl}(-\sigma)\,\exp[i\omega_{tl}(\sigma)\,T]$$

$$-c_{tl}(\sigma)c_{tl}(-\sigma)\,\exp[2i\omega_{tl}(\sigma)\,T]-\frac{a_t(\sigma)a_t(-\sigma)}{2}\Big\}. \qquad (A.6)$$

Thus Eq. (A.4) yields

$$\dot{p}_{c_{tl}}(\sigma)=-\{i\omega_{tl}(\sigma)\}\{2a_t(-\sigma)\,\exp[i\omega_{tl}(\sigma)\,T]$$

$$-2c_{tl}(-\sigma)\,\exp[2i\omega_{tl}(\sigma)\,T]\}. \qquad (A.7)$$

With the help of Eq. (A.2) this becomes

$$\dot{p}_{c_{tl}(\sigma)}=-2i\omega_{tl}(\sigma)c_{t-1}(-\sigma). \qquad (A.8)$$

[15] L. Genzel, H. Happ, and R. Weber, Z. Physik. **154,** 15 (1959).
[16] M. Haas, Phys. Rev. **117,** 1497 (1960).
[17] H. Goldstein, *Classical Mechanics* (Addison-Wesley Publishing Company, Reading, Massachusetts, 1953).

THE JOURNAL OF CHEMICAL PHYSICS VOLUME 34, NUMBER 5 MAY, 1961

Inelastic Scattering of Atoms. I. Intermultiplet Transitions

WALTER R. THORSON

Department of Chemistry, Massachusetts Institute of Technology, Cambridge, Massachusetts

(Received December 7, 1960)

Electronic-translational energy transfer processes have minute cross sections for atoms with thermally attainable kinetic energies, unless the amount of energy converted from electronic to translational form (or vice versa if the threshold permits) is rather less than 1 ev. The transfer processes of interest to chemical kinetics, therefore, involve highly restricted sets of energy levels. Two situations are commonly encountered: (1) The "two-state" case, in which two energy levels of the diatomic system cross or approach closely in energy, so that a respectable probability of resonance transfer is achieved; cases of this type almost always involve transfer of most of the excitation from one atom to the other. (2) Transitions among the multiplet levels of a given Russell-Saunders term of an atom, induced by collision with an "inert" atom. Spin-orbit coupling is the electronic interaction splitting the levels. The present work is concerned with the latter case. The "high-energy approximation," a necessary modification of the Born approximation, and various "modified adiabatic approximations," which take account of the details of angular momentum coupling during collision, are described, and practical methods of calculation considered.

I. INTRODUCTION

INELASTIC collisions between atoms may be categorized as involving ionization of electrons, rearrangement of electrons, or electronic transitions. This work is concerned with the last, and in particular with rather restricted classes of them, to be outlined shortly.

General features of the problem of inelastic scattering have been discussed by Mott and Massey,[1] and Bates, Massey, and Stewart,[2] although a number of other workers have contributed to the subject. The application of the formal scattering theory to the problem has been made in one approximation by Mittleman and Watson.[3] (The formal theory indicates procedure and steps for systematic improvement when higher-order perturbation theory is desired.) All of these workers have been concerned with the most general class of electronic transitions and in practice have restricted any applications to the simplest prototypes, usually scattering of protons and hydrogen atoms at very high relative translational energies.

The physical interactions which establish energy differences between electronic states vary greatly in strength. Associated with each type of interaction there is a critical period, which one may think of as the time necessary to establish or resolve the energy separation. This "period of electronic motion" is defined by the quantity $\tau_e=(h/\Delta E_{ij})$, where ΔE_{ij} is the energy difference between i, j of the electronic system in some nuclear configuration. Often this period may be given an intuitive physical significance on a semiclassical basis; for example, when the interaction being considered is the electrostatic interaction of electrons with the self-consistent field in an atom, one may think of the period τ_e as that associated with motion in a "Bohr orbit"; or, when the interaction is spin-orbit coupling, the relevant period is that for the precession of the vectors **L** and **S** about their resultant, **J**.

When the effective time of collision interaction τ_c, as measured by the quotient a/V, where a is an effective interaction distance, and V is the relative velocity in collision, is very long compared with τ_e, then one has what is termed adiabatic behavior; the electronic motion adjusts itself to each change in the slowly varying nuclear configuration without undergoing transitions. Only small nonadiabatic coupling terms in the Hamiltonian lead to transitions; the most important of these is proportional to V, and leads to resonant effects in the transition probability only when $(\tau_e/\tau_c)\sim 1$. For energy transfers of 1 ev or more, this condition of nonadiabatic resonance is not achieved until kinetic energies far greater than the threshold energy are attained. It is easy to show that if the energy transfer exceeds $\sim$0.5 ev, the transition probabilities are easily calculable by first order perturbation theory in an adiabatic approximation, and are exceedingly small, so small as to be of no practical interest, for any thermally attainable kinetic energies, even for de-excitation processes where no threshold requirements exist. The implication of this fact is that inelastic scattering processes of chemical interest are those in which the amount of energy converted to translation is less than 1 ev, in most cases far less.

When $\tau_e \gg \tau_c$, the interaction associated with τ_e does not have time to adjust adiabatically to the nuclear motion. An appropriate description is to regard the zero-order states as *adiabatic eigenfunctions* of all those interactions whose periods τ_e' are still shorter than τ_c, and to treat as transition-producing perturbations those whose periods, like τ_e, are much longer than τ_c. The potential for elastic scattering of the atoms is a well-defined "adiabatic" surface, with solutions which deviate far from the free-particle description afforded by the first Born approximation. Only in the case that

[1] N. F. Mott and H. S. W. Massey, *The Theory of Atomic Collisions* (Oxford University Press, New York, 1949), 2nd ed., Chap. VIII.

[2] D. R. Bates, H. S. W. Massey, and A. L. Stewart, Proc. Roy. Soc. (London) **A216**, 437 (1953); D. R. Bates, *ibid.* **A240**, 437 (1957); **A243**, 15 (1958).

[3] M. Mittelman and K. F. Watson, Phys. Rev. **113**, 198 (1959).

τ_e is greater than all periods τ_e' associated with interactions of the atoms, is it legitimate to employ the first Born approximation; in general, the collision is "fast" with respect to some interactions, "slow" with respect to others. More special approximations treating such situations need to be developed.

In practice, cases in which ΔE_{ij} is substantially less than 1 ev arise in two ways. (1) In a diatomic collision, energy levels of one or both atoms may be close enough that under the influence of interaction they cross or nearly cross. Resonant transfer of most of the electronic energy from one excited state to another may then occur, with little or no conversion to translational energy. The probability of transfer depends on the closeness of approach in energy of the two states involved. We may refer to this general problem as the "two-state" problem. (2) A given Russell-Saunders term of an atom is split by spin-orbit coupling into multiplet levels. Characteristically, the multiplet separations are less than 1 ev. Under the influence of a perturbing collision with an "inert" atom, transitions between levels may occur.

As a rule of thumb, $\Delta E_{ij}(R)$ may sometimes be estimated by the value at infinite separation, $\Delta E_{ij}(\infty)$, for case (2), though obviously not for case (1), where most transition occurs at the crossing region, when $\Delta E_{ij}(R) \approx 0$.

When $(\tau_e/\tau_c) \sim 1$ for a given interaction, the coupling between the electronic and nuclear motions is at resonance. The inelastic scattering cross section may then become large, and the concept of motion on a single effective surface is not strictly valid since such motion leads only to elastic scattering. Motion for the heavy-particle system is inevitably complex, involving at least two effective "elastic potentials" and a "transition potential" as well. The estimates of the inelastic cross section afforded by either the high energy approximation or the adiabatic approximation in this resonance range are too high because the repeated strong interaction of the transition-causing perturbation causes scatterings that to first order are virtually inelastic, but are elastic in second and higher orders. It would be desirable to develop an approximation which gives a better first-order perturbation estimate of the cross section, near the resonance maximum. Physically, such an approximation would represent the electrons as moving in the field of moving nuclei, in which the nuclear motion is crudely approximated, say by a classical estimate. We hope to devote some further work to such an approximation in the case of two states.

The two-state problem has been treated phenomenologically by Landau[4] and Zener,[5] and the most thorough study has been made by Stueckelberg,[6] who developed a WKB type of approximation which is valid when the motion is semiclassical, the crossing point being far from the classical turning points. A cruder solution is obtained by him for the near-resonance transfer problem.

[4] L. D. Landau, Physik. Z. Sowjetunion **2**, 46 (1932).
[5] C. Zener, Proc. Roy. Soc. (London) **A137**, 696 (1932).
[6] E. C. G. Stueckelberg, Helv. Phys. Acta **5**, 369 (1932).

II. RELATION OF APPROXIMATIONS TO FORMAL SCATTERING THEORY

Mittleman and Watson[3] developed the formal theory of scattering for atomic systems, using as the basis for treatment the compound states made up of products of electronic wave functions for isolated atoms and free particle functions for nuclear motion. They deduced formal expressions for an "elastic" scattering potential and for the inelastic transition matrix elements, and exhibited the possibility of variational expressions for these quantities which improve on the first-order theory. Their method is practical and yields improved results over the Born approximation at very high energies. They also deduce formal expressions for the adiabatic limit, but when these are examined from the standpoint of practical calculation, they prove to be at least equivalent in the amount of labor required to the solution of the adiabatic electronic problem by nth-order perturbation theory.

It is not difficult to prove that one may use any desirable alternative set of basis functions, provided they can be uniquely correlated with the solutions for the isolated atoms as $R \to \infty$. That is, one may arbitrarily divide the Hamiltonian into a part H_E, which has as solutions the desired basis set, and an interaction part H_I, which appears in the numerator of the formal theory prescription for the propagation-with-interaction operator. The first-order estimate of the transition probability then involves the matrix element $(\Psi_f^0, H_I \Psi_i^0)$, where Ψ_i^0 and Ψ_f^0 are the initial and final states, eigenfunctions of H_E.

The formal theory gives the method for higher-order estimates of scattering cross sections, but these always involve extensive iterations of integral equations, and for systems with many partial waves to consider, as is the case in atomic scattering, such a process is not practical at present. Therefore, it is of considerable value to choose, if possible, a judicious form of the elastic Hamiltonian H_E so that a good first-order estimate of the cross section may be obtained. This is the consideration which has guided our thinking on the special problems we consider.

It is worth pointing out also that inelastic cross sections, when correctly computed in any approximation, are always larger than the true values.

III. INTERMULTIPLET TRANSITIONS IN AN ATOM

Let us assume that one atom A, say, is in a given Russell-Saunders term state, and that collisions with "inert" B (i.e., the internal electronic structure of B is not considered except for its effect as a potential; all excitations in B require very high energies) cause transitions among the multiplet levels of A. Experimentally, for example, we might consider collisional

transfer among the multiplet levels in the excited ^2P term of an alkali atom in the presence of an inert gas, or the effect of an inert gas in the deactivation transition $^2P_{1/2} \rightarrow {}^2P_{3/2}$ in a halogen (iodine is of interest in connection with kinetic studies of the recombination of iodine atoms after photodissociation). When specific reference to an example is necessary, we shall have in mind a $^2P_{3/2} \leftrightarrow {}^2P_{1/2}$ transition.

At this point, it is necessary to define for clarity's sake the names for the various kinds of angular momenta appearing in the problem. Some definitions depart from the usual notation, but as the reader will appreciate, this is unavoidable without annoying defection to the use of subscripts of subscripts.

L is electronic orbital angular momentum; it has component M_L in the space-fixed axis system, component Λ on the molecule axis if separately quantized.

S is the electron spin angular momentum, M_s and Σ its components in space and molecule-fixed axes..

J is the total electronic angular momentum, M_J and Ω its space- and molecule-fixed axis components.

N is the nuclear rotational angular momentum, M_N its space-fixed component.

K=N+L is a partial sum of electronic and nuclear rotational angular momentum which is of use in Hund's case (b) coupling in diatomic molecules, and finds similar employment here. M_K is its space-fixed axis component.

P=N+J is the total angular momentum, M_p its component in the space-fixed axis system, and Ω (necessarily) its component on the molecule axis.

Electron coordinates in space-fixed axes are (x, y, z). Those in molecule-fixed axes are (ξ, η, ζ). The nuclear coordinates we measure by R, the internuclear distance; θ, ψ, the Eulerian angles, defined, respectively, in the same way as Edmonds[7] defines the Eulerian angles β, α. With this definition, the following transformation exists between (ξ, η, ζ) and (x, y, z) for an electron:

$$\begin{aligned}\xi_i &= x_i \cos\theta \cos\psi + y_i \cos\theta \sin\psi - z_i \sin\theta \\ \eta_i &= -x_i \sin\psi + y_i \cos\psi \\ \zeta_i &= x_i \sin\theta \cos\psi + y_i \sin\theta \sin\psi + z_i \cos\theta. \end{aligned} \tag{1}$$

The Hamiltonian is

$$H = -(\hbar^2/2M)\nabla_R^2 - (\hbar^2/2m)\sum_i \nabla_i^2 + V(\mathbf{r}, \mathbf{R}). \tag{2}$$

Here V is the interaction potential of all particles, including the spin-orbit coupling interactions; ∇_i^2 is the Laplacian with respect to the ith electron coordinates; and ∇_R^2 the Laplacian with respect to nuclear coordinates, with electron coordinates implied fixed in the space-fixed system. M is the reduced mass of the diatomic system for relative motion. Here it is implicitly assumed that the motion of the center of mass of the system has been separately treated, and that the centers of mass of the atoms coincide with their respective nuclei. Small corrections to the treatment of the problem, arising out of the fact of finite electronic mass and related complexity in the definition of the center of mass of the system, have been considered by Jepsen and Hirschfelder.[8] We have not concerned ourselves with their inclusion because they are small.

Physically, the limiting approximations may be roughly categorized as follows:

(1) High-energy approximation. The collision occurs in a time $\tau_c \ll \tau_s$ (spin-orbit-axial field). The collision is, however, adiabatic with respect to all other interactions except those associated with axial field perturbations and the spin-orbit-interaction. The axial perturbation introduces transitions among the zero-order eigenfunctions of J^2, M_J. The nuclear motion occurs on an effective elastic scattering surface determined by the interaction energy of the filled shells of A and B. This approximation is identical to the "distorted wave" approximation of Mott and Massey.

(2) Adiabatic approximations. The collision is slow, so that electronic states of the diatomic system for fixed nuclei make an appropriate basis set. Transitions occur from the action of nonadiabatic coupling terms involving derivatives of electronic functions with respect to nuclear coordinates. As will be seen, some of these coupling terms must be handled carefully, and modify the form of the adiabatic approximations.

IV. HIGH-ENERGY APPROXIMATION

When the atoms A and B are well isolated, we may treat them as separate systems. We shall suppose that A has n_A electrons, n_v valence electrons, and B has n_B electrons in a filled shell structure or at least a spherically symmetric electron distribution with no low-lying energy levels near the ground level. We assume B to be in its ground state $\phi_B{}^0(\mathbf{r})$. We shall assume a one-electron Hartree-Fock form for the atomic wave functions, and that no transition occurs in the filled shell configurations of either atom. In the theory of atomic structure, all the multiplet states $(n\Gamma LSJM_J)$, (where $n\Gamma$ specify principal features of the atomic terms in question) are constructed out of the orbitals of a given configuration $\{n_i l_i\}$, where $i = 1 \ldots n_v$. The eigenfunctions $\phi_A(n\Gamma JM_J)$ are specified linear combinations of the Russell-Saunders eigenfunctions $\phi_A'(n\Gamma LSM_LM_S)$, themselves again linear combinations of the basic antisymmetrized determinants $\phi_A''(\mu\{n_i l_i m_{l_i} m_{s_i}\})$. The last notation means that the subscript μ here implies assignment of n_v orbitals as occupied, specifying the whole ordered set of numbers $\{n_i l_i m_{l_i} m_{s_i}\}$. We may summarize the foregoing by the expression

$$\phi_A(n\Gamma JM_J) = \sum_\mu (LSM_J|\mu)\phi_A''(n\Gamma\mu). \tag{3}$$

[7] A. R. Edmonds, *Angular Momentum in Quantum Mechanics* (Princeton University Press, Princeton, New Jersey, 1957), p. 7.

[8] D. W. Jepsen and J. O. Hirschfelder, J. Chem. Phys. **32**, 1323 (1960).

The coefficients in the expansion are determined in the theory of atomic structure.

Small differences in the calculation can arise depending on whether electronic functions for the entire system are antisymmetrized with respect to all possible electron interchanges, or only with respect to the interchanges of electrons in individual atoms. Strictly speaking, the former procedure is correct, including the exchange interactions between A and B. In the development given here, we ignore the complete antisymmetrization. It may be included in an obvious but tedious extension. When final results are given, we shall modify them to include the results of exchange.

Accordingly, we represent the electronic states for the system as

$$\phi_{AB}(n\Gamma JM_J)=\phi_A(n\Gamma JM_J)\phi_B{}^0. \tag{4}$$

When A and B interact at a finite distance R, there is a self-consistent field interaction energy $V_{core}{}^{AB}(R)$, which is spherically symmetric and independent of the values J, M_J. We may evaluate it as the average of the SCF interaction energy of A and B in states J, M_J, over all angles θ, ψ, and the possible values of J, M_J. This interaction energy is not small. It is diagonal in J, M_J, and, therefore, leads to elastic scattering. Because it involves the filled-shell interactions, it is usually considerably larger than the remaining "elastic" interactions, which are specifically angle dependent and J, M_J dependent, though diagonal in J. In addition, the interaction between A and B has matrix elements which are nondiagonal in J and M_J, and it is these which can lead to inelastic scattering.

The potential $V_{core}{}^{AB}(R)$ represents mutual polarizations of the atoms, and it is of course true that the one-electron orbitals are polarized as well, having a different self-consistent field from that in the free atom. However, the conditions of the approximation are, that the wave functions to be used are the zero-order functions, unperturbed by the axial field. If perturbations on the functions by the axial field are considered, this amounts to moving toward an adiabatic approximation. It is essential to the high energy approximation that the electronic functions are the zero-order functions of the isolated atoms, and that $V_{core}{}^{AB}(R)$ is the average first-order perturbation energy of the A-B interaction, diagonal in J, M_J, and averaged over J, M_J and space orientations θ, ψ; the nondiagonal elements of the interaction energy lead to inelastic scattering if they are nondiagonal in J. Additional elastic scattering arises from terms diagonal in J but not in M_J, but we do not consider these here.

The basic difference between this approximation and the first Born approximation is that the size of $V_{core}{}^{AB}(R)$ is taken into account, and the radial functions for the nuclear motion are solutions to the problem of motion in the potential $V_{core}{}^{AB}$.

The expression for $V_{core}{}^{AB}(R)$, then, is

$$V_{core}{}^{AB}(R)=[1/4\pi\sum_J(2J+1)]\sum_{J,M_J}\int_0^{\pi}\int_0^{2\pi}V_{AB}(n\Gamma JM_J;\,R,\theta,\psi)\,\sin\theta d\theta d\psi, \tag{5}$$

where $V_{AB}(n\Gamma JM_J;\,R,\theta,\psi)$ is the interaction energy of A and B at R,θ,ψ in $(n\Gamma JM_J)$:

$$V_{AB}(n\Gamma JM_J)=(n\Gamma JM_J\,|\,H_e-\epsilon_A{}^0(n\Gamma JM_J)-\epsilon_B{}^0\,|\,n\Gamma JM_J),$$

$$=\sum_\mu(n\Gamma JM_J/\mu)\{(Z_AZ_Be^2/R)-\sum_{i=1}^{\eta_A}[\phi_{i\mu}(1)\,|\,Z_Be^2/r_{B1}\,|\,\phi_{i\mu}(1)]$$

$$-\sum_{j=1}^{\eta_B}[\phi_j(1)\,|\,Z_Ae^2/r_{A1}\,|\,\phi_j(1)]+\sum_{i=1}^{\eta_A}\sum_{j=1}^{\eta_B}[\phi_{i\mu}(1)\phi_j(2)\,|\,e^2/r_{12}\,|\,\phi_{i\mu}(1)\phi_j(2)]$$

$$-\sum_{\substack{i=1\\(\text{same spin})}}^{n_A}\sum^{n_B}[\phi_{i\mu}(1)\phi_j(2)\,|\,e^2/r_{12}\,|\,\phi_j(1)\phi_{i\mu}(2)]\}.^{8a} \tag{6}$$

This expression already contains the results of exchange, as may readily be seen in the presence of the exchange integrals with orbitals of the same spin. Derivation following the simple product function quoted in Eq. (4) would lead to a result without the exchange integrals. In the above expressions, H_e is the electronic Hamiltonian, $\epsilon_A{}^0(n\Gamma JM_J)+\epsilon_B{}^0$ the energy of the isolated atoms; $\varphi_{i\mu}$ is the ith one-electron orbital in the μth antisymmetrized determinant $\phi_A{}''(\mu)$; φ_j is the jth one-electron orbital in $\phi_B{}^0$.

An alternative way to obtain $V_{core}{}^{AB}(R)$ could be to employ experimental values obtained, say, from accurate elastic scattering. Such information is not presently available in the region of interest. High-

[8a] Equation (6) is not correct because it neglects overlap of orbitals on different atoms; it is necessary to include the overlap to get reliable results for $V_{core}{}^{AB}$.

energy molecular beam data deal with portions of the curve too high in energy for the kinetic energies we are considering, in the thermally accessible range. Second, even if such potentials were available, they actually include adiabatic effects in the polarization. Some preliminary computed results show that an accurate correlation between the magnitude of $V_{\text{core}}^{AB}(R)$ and the magnitude of the interaction matrix element, to be discussed shortly, is vital to the calculations; variations of 5% to 10% in the location of the classical turning point on $V_{\text{core}}^{AB}(R)$, with the same value for the interaction matrix element as a function of R, can produce as much as 200 to 300% variation in the inelastic scattering cross section. Therefore, it seems desirable to use the same approximation to calculate both $V_{\text{core}}^{AB}(R)$ and the interaction matrix elements, rather than two unrelated calculations, or estimates.

The interaction matrix elements are

$$V_{\text{int}}^{AB}(J'M_J'JM_J;\, R,\theta,\psi) = (n\Gamma J'M_J'|H_e|n\Gamma JM_J). \quad (7)$$

There are, of course, other perturbations, leading in first order to elastic scattering, arising from matrix elements diagonal in J:

$$V_{\text{int}}^{AB}(JM_J'M_J;\, R,\theta,\psi) = (n\Gamma JM_J'|H_e|n\Gamma JM_J); \quad (8a)$$

$$V_{\text{int}}^{AB}(JM_J;\, R,\theta,\psi) = V_{AB}(n\Gamma JM_J;\, R,\theta,\psi) - V_{\text{core}}^{AB}(R); \quad (8b)$$

but, since we are not interested in the detailed elastic scattering, we neglect them.

We now treat the nuclear motion. The total Hamiltonian appears as a second-order differential operator in the nuclear coordinates R,θ,ψ, and as a matrix in the electronic eigenfunction vector space, with the basis $\{\phi_{AB}(n\Gamma JM_J)\}$:

$$H = [-(\hbar^2/2M)\nabla_R^2 + V_{\text{core}}^{AB}(R)]\mathbf{1} + \boldsymbol{\epsilon}^0 + \mathbf{V}_{\text{int}}^{AB}(R,\theta,\psi). \quad (9)$$

Here $\mathbf{1}$ is the unit matrix, $\mathbf{V}_{\text{int}}^{AB}$ is a matrix with the elements quoted in Eqs. (7) and (8), and $\boldsymbol{\epsilon}^0$ is the diagonal matrix with the elements $\epsilon^0(n\Gamma J) = \epsilon_A{}^0(n\Gamma J) + \epsilon_B{}^0$. If the general solution Ψ is written as a vector in the electronic basis set,

$$\Psi = \sum_{JM_J} \phi_{AB}(n\Gamma JM_J) \{ \sum_{NM_N} a(n\Gamma JM_JNM_N) F(n\Gamma JN;\, R)\, P_N^{M_N}(\cos\theta)\, \exp(iM_N\psi/R) \}, \quad (10)$$

a set of coupled differential equations for the functions F results. This approximation is the same as the "distorted wave" approximation of Mott and Massey[1] and Bates, Massey, and Stewart.[2] For the purpose of clarity we prefer, however, to use the formal theory of scattering as the framework for calculating the cross section.

In the formal theory, initial and final states are presumed eigenfunctions of a zero-order Hamiltonian H_E, which in our case is the matrix operator

$$H_E = [-(\hbar^2/2M)\nabla_R^2 + V_{\text{core}}^{AB}(R)]\mathbf{1} + \boldsymbol{\epsilon}^0. \quad (11)$$

The cross section for scattering into any final state is proportional to the absolute square of the transition matrix element T_{fi} defined as

$$T_{fi} = (\Psi_f, H_I\Psi_i^{(+)}), \quad (12)$$

where Ψ_f is the properly normalized final state, and H_I is the interaction Hamiltonian, which in our case is

$$H_I = \mathbf{V}_{\text{int}}^{AB}(R,\theta,\psi). \quad (13)$$

The $\Psi_i^{(+)}$ is a state prepared from the initial state Ψ_i by summing up the results of all orders of interactions with H_I, separated by propagation with H_E between interactions. An integral equation exists for $\Psi_i^{(+)}$; it is

$$\Psi_i^{(+)} = \Psi_i + (1/E + i\epsilon - H_E)H_I\Psi_i^{(+)}. \quad (14)$$

The meaning of this formal expression is explained in the paper by Lippmann and Schwinger,[9] for example. The first approximation to the scattering is given, then, by the substitution of Ψ_i for $\Psi_i^{(+)}$,

$$T_{fi} = (\Psi_f, H_I\Psi_i); \quad (15)$$

Ψ_i is properly normalized (the normalization will be given later) and its detailed form is determined by boundary conditions in the elastic scattering problem.

Eigenfunctions to the equation

$$H_E\Psi = E\Psi \quad (16)$$

are composed of linear combinations of solutions of the form

$$\chi(n\Gamma JM_JNM_N) = (C/R)\phi_{AB}(n\Gamma JM_J)\, E(n\Gamma JN;\, R)\, P_N^{M_N}(\cos\theta) \times \exp(iM_N\psi). \quad (17)$$

The value of the constant C will be discussed later; F satisfies the equation

$$-(\hbar^2/2M)(d^2F/dR^2) + [V_{\text{core}}^{AB}(R) + N(N+1)\hbar^2/2MR^2]F = [E - \epsilon^0(n\Gamma J)]F, \quad (18)$$

and it has the property of being everywhere finite. Asymptotically, as $R\to\infty$, we take it to be

$$\lim_{R\to\infty} F = [\sin(kR - \tfrac{1}{2}N\pi + \delta_N)]/k, \quad (19)$$

[9] B. Lippmann and J. Schwinger, Phys. Rev. **79**, 469 (1950).

where k satisfies the relation

$$(\hbar^2/2M)k^2 = E - \epsilon^0(n\Gamma J). \tag{20}$$

The final states we consider are eigenfunctions χ. The initial state will be a specified linear combination of them. It may be found by solving the elastic scattering problem in the usual fashion. The result is

$$\Psi_i = (1/\mathcal{V}^{\frac{1}{2}}R)\phi_{AB}(n\Gamma JM_J)\left[\sum_N (2N+1)F(n\Gamma JN;\, R)\, P_N^0\,(\cos\theta)\, \exp i(N\pi/2+\delta_N)\right]. \tag{21}$$

It will be found that this function has the following asymptotic behavior for $R\to\infty$,

$$\lim_{R\to\infty}\Psi_i = (1/\mathcal{V}^{\frac{1}{2}})\phi_{AB}(n\Gamma JM_J)\left[\exp(ikR\cos\theta) + \exp(ikR)\left[f(\theta)/R\right]\right], \tag{22}$$

and, therefore, it has the property of being normalized in volume $\mathcal{V}$. A properly normalized final state is so defined that the constant C takes the value

$$C = (1/\mathcal{V})^{\frac{1}{2}}\left[(2N'+1)\,(N'-M_N')!/4\pi(N'+M_N')!\right]. \tag{23}$$

It should be noted that this formulation for the final state is for use only in connection with evaluating the matrix element T_{fi}; the asymptotic form for inelastically scattered waves must of course contain only the outgoing wave e^{ikR}/R, and a calculation of the propagated state $\Psi_i^{(+)}$ will show such behavior.

The cross section for scattering from J, M_J to the partial wave final state $(n\Gamma J'M_J'N'M_N')$ is given by

$$\sigma(n\Gamma,\, JM_J J'M_J'N'M_N') = (M^2k_f\mathcal{V}^2/4\pi^2\hbar^4k_i)\,|T_{fi}(n\Gamma JM_J J'M_J'N'M_N')\,|^2. \tag{24}$$

We may obtain the total cross section by evaluating the sum over all values of N' and M_J', and averaging over all M_J:

$$\sigma(n\Gamma,\, J\to J') = (1/2J+1)\sum_{M_J}\sum_{M_J'}\sum_{N'}\sigma(n\Gamma,\, JM_J,\, J'M_J'N'M_N'). \tag{25}$$

The selection rules, are in general,

$$M_J' - M_J = 0, \pm 1, \pm 2; \qquad M_N' + M_J' = M_J;$$
$$N' = N,\ N\pm 2. \tag{26}$$

As an example, we shall work out in somewhat greater detail the expression for $\sigma(1^2P, \frac{1}{2}\to\frac{3}{2})$ in an alkali atom, say, colliding with a rare gas atom. (We assume the configuration $2p$ for the outer electron.) The electronic matrix elements may all be expressed in terms of two simple interaction integrals; Let $p\pi$ be a real $2p$ orbital perpendicular to the internuclear axis, and let $p\sigma$ be the $2p$ orbital along it. Define

$$V_\pi(R) = \int p\pi(1)\, H_{\text{int}}\, p\pi(1)\, d\tau_1; \tag{27a}$$

$$V_\sigma(R) = \int p\sigma(1)\, H_{\text{int}}\, p\sigma(1)\, d\tau_1. \tag{27b}$$

The H_{int} includes the exchange interaction if exchange is desired. The matrix elements $V_{\text{int}}^{AB}(R, \theta, \psi)$ then turn out to be

$$\left(\tfrac{3}{2}\ \tfrac{3}{2}\middle|V_{\text{int}}^{AB}\middle|\tfrac{1}{2}\ \tfrac{1}{2}\right) = \left[(V_\sigma - V_\pi)\,(6)^{\frac{1}{2}}\right]P_2'\,(\cos\theta)\,\exp(-i\psi) = \left(\tfrac{1}{2}\ \bar{\tfrac{1}{2}}\middle|V_{\text{int}}^{AB}\middle|\tfrac{3}{2}\ \bar{\tfrac{3}{2}}\right)$$

$$\left(\tfrac{3}{2}\ \tfrac{1}{2}\middle|V_{\text{int}}^{AB}\middle|\tfrac{1}{2}\ \bar{\tfrac{1}{2}}\right) = \left[-(V_\sigma - V_\pi)/\sqrt{2}\right]P_2'\,(\cos\theta)\,\exp(-i\psi) = \left(\tfrac{1}{2}\ \tfrac{1}{2}\middle|V_{\text{int}}^{AB}\middle|\tfrac{3}{2}\ \bar{\tfrac{1}{2}}\right)$$

$$\left(\tfrac{3}{2}\ \tfrac{3}{2}\middle|V_{\text{int}}^{AB}\middle|\tfrac{1}{2}\ \bar{\tfrac{1}{2}}\right) = \left[(V_\sigma - V_\pi)\,(6)^{\frac{1}{2}}\right]P_2^2\,(\cos\theta)\,\exp(-2i\psi) = -\left(\tfrac{1}{2}\ \tfrac{1}{2}\middle|V_{\text{int}}^{AB}\middle|\tfrac{3}{2}\ \bar{\tfrac{3}{2}}\right) \tag{28}$$

$$\left(\tfrac{3}{2}\ \tfrac{1}{2}\middle|V_{\text{int}}^{AB}\middle|\tfrac{1}{2}\ \tfrac{1}{2}\right) = \left[-2(V_\sigma - V_\pi)/3\sqrt{2}\right]P_2^0\,(\cos)\theta = -\left(\tfrac{3}{2}\ \bar{\tfrac{1}{2}}\middle|V_{\text{int}}^{AB}\middle|\tfrac{1}{2}\ \bar{\tfrac{1}{2}}\right).$$

These matrix elements lead to nonvanishing integrals for $N'=N$, $N\pm2$. It is easily seen that the final result will contain the elastic phase shifts in the initial state, but not those of the final state. The necessary radial integrals are all of the form

$$\int_0^\infty F(n\Gamma J'N';R)[V_\sigma(R)-V_\pi(R)]F(n\Gamma JN;R)dR. \tag{29}$$

We shall defer until later a discussion of practical calculations in this approximation.

V. ADIABATIC APPROXIMATIONS

A. Approximation (A)

The electronic basis vectors for the first adiabatic approximation are eigenfunctions of the complete electronic Hamiltonian $H_e(\mathbf{r},\mathbf{R})$ in the molecule-fixed coordinate system. Perturbations resulting from nuclear motion, both radial and angular, couple the states. Angular momentum couplings have both elastic and inelastic effects; the elastic parts dominate as $R\to\infty$ and rotational angular momentum increases, and represent the physical fact that adiabatic "following" of the diatomic axis does not occur for distant collisions. The modified adiabatic approximation presented here takes account of this partial following, and brings the approximation to a form which gives a valid description for "slow" collisions.

The Hamiltonian for electron motion in the space-fixed axis system and the relative nuclear motion is

$$H=-(\hbar^2/2M)\nabla_R{}^2-(\hbar^2/2m)\sum_i\nabla_i{}^2+V(\mathbf{r},R). \tag{30}$$

Derivatives with respect to the nuclear coordinates are to be performed holding the space-fixed electron coordinates (x_i, y_i, z_i) fixed, and supposing their spins quantized with respect to the Z axis. If the electronic Hamiltonian is to be written in molecule-fixed coordinates (ξ_i, η_i, ζ_i) and spins are quantized with respect to the diatomic axis, and derivatives with respect to nuclear coordinates R, θ, ψ are taken holding electrons fixed in the molecule-fixed system, the Hamiltonian must be appropriately transformed. The general lines of the transformation are given, for example, by Kronig.[10] The resulting transformed Hamiltonian is

$$\begin{aligned}H'=&H_e(\xi_i,\eta_i,\zeta_i,R)-(\hbar^2/2MR^2)(\partial/\partial R)[R^2(\partial/\partial R)]\\&-(\hbar^2/2MR^2)\{(1/\sin\theta)(\partial/\partial\theta)[\sin\theta(\partial/\partial\theta)]\\&+(1/\sin^2\theta)[(\partial/\partial\psi)-(i\cos\theta/\hbar)J_\zeta]^2\}\\&+(1/2MR^2)[J_\xi{}^2+J_\eta{}^2-J_+Q_+-J_-Q_-],\end{aligned} \tag{31}$$

where

$$J_\pm=J_\xi\pm iJ_\eta;$$

$$Q_\pm=\hbar[\mp(\partial/\partial\theta)+(i/\sin\theta)(\partial/\partial\psi)+(\cot\theta/\hbar)J_\zeta], \tag{32}$$

and $H_e(\mathbf{r},R)$ expressed in the coordinates (ξ,η,ζ) is only a parametric function of R. Let us now define the functions $\phi(n\Gamma\Omega;\mathbf{r},R)$, eigenfunctions of H_e and J_ζ:

$$H_e(\mathbf{r},R)\phi(n\Gamma\Omega;\mathbf{r},R)=\epsilon(n\Gamma\Omega;R)\phi(n\Gamma\Omega;\mathbf{r},R); \tag{33}$$

$$J_\zeta\phi(n\Gamma\Omega;\mathbf{r},R)=\Omega\hbar\phi(n\Gamma\Omega;\mathbf{r},R); \tag{34}$$

$H_e(\mathbf{r},R)$ includes the spin-orbit interaction. Let $\mathfrak{R}(PM_P\Omega;\theta,\psi)$ be functions which satisfy the equations

$$\begin{aligned}\{(1/\sin\theta)(\partial/\partial\theta)[\sin\theta(\partial/\partial\theta)]&\\+(1/\sin^2\theta)[(\partial/\partial\psi)-i\Omega\cos\theta]^2\}\mathfrak{R}&\\=-[P(P+1)-\Omega^2]\mathfrak{R}.&\end{aligned} \tag{35}$$

Kronig[10] discusses these functions. They are normalized to unity when integrated over θ, ψ, and have the property

$$\mathfrak{R}(P,M_p,-\Omega;\theta,\psi)=(-1)^{P-\Omega}\mathfrak{R}(PM_p\Omega;\theta-\pi,\psi); \tag{36}$$

they are Jacobi polynomials in $\cos\theta$ with appropriate phases, multiplied by $\exp(iM_P\psi)$. We wish to use the representations of finite rotations defined in Edmonds[11] and having the symbol $d_{M_P\Omega}{}^P(\theta)$; the connecting definition is

$$\begin{aligned}&\mathfrak{R}(pM_p\Omega;\theta,\psi)\\&\quad=[(2P+1)/4\pi]^{\frac{1}{2}}d_{M_P\Omega}{}^P(\theta)\exp(iM_P\psi).\end{aligned} \tag{37}$$

The angular matrix elements of $Q_\pm$ are of interest; the only nonvanishing elements are

$$\begin{aligned}&(PM_p\Omega\pm1\,|\,Q\pm\,|\,PM_p\Omega)\\&\quad=\hbar[(P\pm\Omega+1)(P\pm\Omega)]^{\frac{1}{2}}.\end{aligned} \tag{38}$$

The simple adiabatic approximation (called the "perturbed stationary states" approximation by Mott and Massey[1] and Bates, Massey, and Stewart[2]) consists of using as the zero-order eigenfunctions the products

$$\psi=(1/R)\phi(n\Gamma\Omega;\mathbf{r},R)\mathfrak{R}(PM_p\Omega;\theta,\psi)f(n\Gamma P\Omega;R) \tag{39}$$

and in neglecting the terms in $d\phi/dR$ and those arising from the last term in the Hamiltonian of Eq. (31). f satisfies the equation

$$\begin{aligned}&-(\hbar^2/2M)(d^2f/dR^2)\\&+[\epsilon(n\Gamma\Omega;R)+(\hbar^2/2MR^2)(P(P+1)-\Omega^2)]f=Ef.\end{aligned} \tag{40}$$

The neglected terms lead to coupling between different states. The validity of approximation depends on their magnitude. At very large distances, the simple adiabatic electronic states tend to unperturbed atomic eigenfunctions, but they are rotating with the diatomic

[10] R. de L. Kronig, *Band Spectra and Molecular Structure* (Cambridge University Press, New York, 1930), pp. 6–16, 40–44.

[11] A. R. Edmonds, see footnote 7, Secs. 4.2–4.7.

axis. Obviously, such a basis set is an unrealistic one as $R\to\infty$. Intuitively, one expects that physically appropriate states are the "uncoupled" functions which form the basis of the high energy approximation; certainly the initial state must be so described, and a correct treatment of the collision should give an account of the onset of angular momentum coupling, with its resultant "following" of the diatomic axis by the electron cloud. The simple adiabatic approximation is, therefore, not suitable as $R\to\infty$, this fact seems to have been the reason for its rejection in the more recent work of Bates.[12] However, the adiabatic approximation may be revised in a manner which takes account of the partial "following."

Before and after collision, atom A has a definite electronic angular momentum quantum number J and a space-fixed z-component M_J. We are not concerned with the final value of M_J, but that of J. The collision is elastic if $J_{\text{final}}=J_{\text{initial}}$, inelastic otherwise. What are of interest are the "intermanifold" transitions, in which not merely M_J, but J, is finally altered.

The perturbation in the last square brackets of Eq. (31) has both *inter-* and *intra*manifold coupling effects. In fact, as $R\to\infty$, since J then becomes a good quantum number, it is obvious that the *inter*manifold effects tend to zero, while the *intra*manifold effects remain and couple the adiabatic states for large R and P. From a physical point of view, we may expect that this perturbation will be diagonal in an "uncoupled" representation.

As $R\to\infty$, the adiabatic functions may be correlated uniquely with limiting values of J. We shall designate each manifold by its limiting J value

$$\lim_{R\to\infty}\phi(n\Gamma(J)\Omega;\,\mathbf{r},\,R)=\phi^{(\infty)}(n\Gamma J\Omega;\,\mathbf{r}). \tag{41}$$

In the "coupled" description, the basis states as $R\to\infty$ are the products

$$\phi^{(\infty)}(n\Gamma J\Omega;\,\mathbf{r})\mathfrak{D}(PM_P\Omega;\theta,\psi), \tag{42}$$

but in an "uncoupled" description they are

$$\phi^{(\infty)}(n\Gamma JM_J;\,\mathbf{r})\,Y(NM_N;\theta,\psi), \tag{43}$$

where $Y(NM_N;\theta,\psi)$ is the properly defined spherical harmonic. The relation between these basis sets is obtained by using the properties of the representations of finite rotation:

$$\phi(n\Gamma JM_J;\,\mathbf{r})\,Y(NM_N;\theta,\psi)=(-1)^{M_N}\sum_{\Omega}\sum_{P}\left[\left(\frac{2N+1}{2P+1}\right)^{\frac{1}{2}}(NM_NJM_J\,|\,NJPM_P)\,(NJP\Omega\,|\,N0J\Omega)\right]\phi(n\Gamma J\Omega;\,\mathbf{r})$$
$$\times\mathfrak{D}(PM_P\Omega;\theta,\psi); \tag{44}$$

$$\phi(n\Gamma J\Omega;\,\mathbf{r})\mathfrak{D}(PM_P\Omega;\theta,\psi)$$
$$=\sum_{M_J}\sum_{N}(-1)^{M_N}\left[\left(\frac{2N+1}{2P+1}\right)^{\frac{1}{2}}(NJPM_P\,|\,NM_NJM_J)\,(N0J\Omega\,|\,NJP\Omega)\right]\phi(n\Gamma JM_J;\,\mathbf{r})\,Y(NM_N;\theta,\psi). \tag{45}$$

The Hamiltonian is diagonal in P, M_P, and, therefore, whether or not the uncoupling of states succeeds in diagonalizing the perturbing terms of the simple adiabatic approximation as $R\to\infty$, depends on the accomplishment of that diagonalization by the transformation

$$\sum_{\Omega=-J}^{J}(NJP\Omega\,|\,N0J\Omega)\phi(n\Gamma J\Omega;\,\mathbf{r})\mathfrak{D}(PM_P\Omega;\theta,\psi). \tag{46}$$

There are $2J+1$ such combinations for each J, P, one for each of the possible consistent values of N such that $N+J=P$. It is easily shown directly that the Hamiltonian is indeed diagonalized by such transformations, and for given J, P, there are $2J+1$ eigenvalues,

$$\epsilon\to\epsilon^0(n\Gamma J)+[N(N+1)\hbar^2/2MR^2]. \tag{47}$$

This transformation indicates a procedure for treating the coupling at finite R. The states $\phi[n\Gamma(J)\Omega;\,\mathbf{r},\,R]$ all have the energy $\epsilon^0(n\Gamma J)$ as $R\to\infty$. For a given J, P, the $(2J+1)$-dimensional space spanned by the products

$$\phi[n\Gamma(J)\Omega;\,\mathbf{r},\,R]\mathfrak{D}(PM_P\Omega;\theta,\psi) \tag{48}$$

is called the *manifold* of J for the given total angular momentum P. For general values of R, P we elect to use as the zero-order basis the "electronic-rotational" functions $Z[n\Gamma(J)P\mu;\,\mathbf{r},\,R,\,\theta,\,\psi]$, defined by the transformation which diagnalizes the electronic-rotational Hamiltonian H_A *within a given manifold*;

$$H_A=H_e(\mathbf{r},\,R)-(\hbar^2/2MR^2)$$
$$\times\left[(1/\sin\theta)\frac{\partial}{\partial\theta}\left(\sin\theta\frac{\partial}{\partial\theta}\right)+(1/\sin^2\theta)\left(\frac{\partial}{\partial\psi}-(i/\hbar)\cos\theta J_\zeta\right)^2\right]$$
$$+(1/2MR^2)[J_\xi^2+J_\eta^2-J_+Q_--J_-Q_+]. \tag{49}$$

It is evident that the functions Z_μ are identical with the linear combinations of Eq. (46) as $R\to\infty$, and are, therefore, also then related to the uncoupled eigen-

[12] D. R. Bates, Proc. Roy. Soc. (London) **A245,** 299 (1958); Proc. Phys. Soc. (London) **A73,** 227 (1959).

functions as follows:

$$\phi(n\Gamma M_J;\mathbf{r})\,Y(NM_N;\theta,\psi)$$
$$=(-1)^{M_N}\sum_P(NM_NJM_J\,|\,NJPM_P)\left(\frac{2N+1}{2P+1}\right)^{\frac{1}{2}}$$
$$\times Z[n\Gamma P(J)\mu(N_\mu)]. \quad (50)$$

At arbitrary R the functions Z_μ which form this new basis are thus defined by a separate matrix diagonalization for each manifold $(n\Gamma JP)$. The limiting behavior at $R\to\infty$ links each Z_μ within the manifold with a value of N, (N_μ), and at strong coupling with a value of Ω. Over the whole range neither quantum number is valid and we merely use the index μ. The associated energy eigenvalues are $\lambda[n\Gamma P(J)\mu;R]$.

Transitions $(n\Gamma JP\to n\Gamma J'P)$ take place by virtue of the remaining perturbations (H_I):

(1) the electrorotational Hamiltonian H_A has *inter*manifold matrix elements which genuinely represent inelastic scattering due to angular "drag effects."

(2) There are intermanifold terms in $(\partial\phi/\partial R)$.

(3) There are intramanifold terms in $(\partial Z_\mu/\partial R)$ which arise from the fact that the coefficients of transformation to the Z_μ representation are functions of R.

The general solution Ψ to a scattering problem may be expanded in the products

$$\chi=(1/R)Z[n\Gamma P(J)\mu;\mathbf{r},R,\theta,\psi]F[n\Gamma P(J)\mu;R], \quad (51)$$

where $F_\mu(R)$ satisfies the equation

$$-(\hbar^2/2M)(d^2F_\mu/dR^2)+\lambda_\mu(R)F_\mu=EF_\mu; \quad (52)$$

in the limit of weak coupling,

$$\lambda_\mu\to\epsilon^0(n\Gamma J)+[N_\mu(N_\mu+1)\hbar^2/2MR^2], \quad (53)$$

and for strong coupling,

$$\lambda_\mu\to\epsilon(n\Gamma\Omega;R)+[P(P+1)-\Omega^2]\hbar^2/2MR^2. \quad (54)$$

The functions F_μ are those solutions of (52) which are everywhere finite, and in the limit of large R have the asymptotic behavior

$$\lim_{R\to\infty}F_\mu(R)=(1/k_s)\sin(k_JR+N_\mu\pi/2+\delta_\mu). \quad (55)$$

The basis eigenvectors Z_μ may be expressed as normalized linear combinations,

$$Z[n\Gamma P(J)\mu]=\sum_\Omega A[n\Gamma P(J)\mu\Omega;R]$$
$$\times\phi[n\Gamma(J)\Omega;\mathbf{r},R]\mathfrak{D}(PM_J\Omega;\theta,\psi). \quad (56)$$

Expressions for the eigenvalues λ_μ and coefficients $A_{\mu\Omega}$ are readily obtained by rapid diagonalization of matrices of small dimensions; for machine computation this problem does not complicate the calculation, since other features of a scattering calculation require detailed results for each value of the total angular momentum in any case (i.e., the functions F_μ). In the basis set of the simple adiabatic approximation, the intramanifold matrix elements of H_A are

$$[n\Gamma(J)P\Omega|H_A|n\Gamma(J)P\Omega]=\epsilon(n\Gamma\Omega;R)$$
$$+[P(P+1)-\Omega^2]\hbar^2/2MR^2$$
$$+(1/2MR^2)\{\phi[n\Gamma(J)\Omega]|J^2|\phi[n\Gamma(J)\Omega]\}; \quad (57a)$$
$$[n\Gamma(J)P\Omega\pm1|H_A|n\Gamma(J)P\Omega]$$
$$=-(\hbar/2MR^2)[(P\pm\Omega+1)(P\mp\Omega)]^{\frac{1}{2}}$$
$$\times\{\phi[n\Gamma(J)\Omega\pm1]|J\pm|\phi[n\Gamma(J)\Omega]\}. \quad (57b)$$

All inelastic transitions are *inter*manifold transitions. These can arise only from perturbations of types (1) and (2) mentioned earlier; those of type (3) vanish because of the orthogonality of functions $\phi[n\Gamma(J)\Omega]$ of different manifolds.

There remains only the problem of nuclear motion in the initial and final states. The initial state is to represent the elastic scattering, and asymptotically has the form

$$\Psi_i\to\phi(n\Gamma JM_J)\exp(ik_iR\cos\theta)$$
$$+[\exp(ik_iR)/R]\sum_{M_J'}\phi(n\Gamma JM_J')f(JM_J';\theta,\psi). \quad (58)$$

The plane wave may be expanded under asymptotic conditions in the functions Z_μ:

$$\lim_{R\to\infty}\phi(n\Gamma JM_J)\exp(ik_iR\cos\theta)$$
$$=(1/k_iR)\sum_N\sum_P(4\pi/2P+1)^{\frac{1}{2}}(2N_\mu+1)$$
$$\times\exp(iN_\mu\pi/2)(N_\mu0JM_J\,|\,N_\mu JPM_J)$$
$$\times Z[n\Gamma P(J)\mu(N_\mu)]\sin(k_iR+N_\mu\pi/2). \quad (59)$$

The general elastic scattering solution Ψ_i may be expanded at any value of R, as

$$\Psi_i=(1/R)\sum_P\sum_\mu\alpha[n\Gamma P(J)\mu]F_\mu(R)Z_\mu(\mathbf{r},R,\theta,\psi). \quad (60)$$

Comparing coefficients in the asymptotic limit $R\to\infty$, and applying the condition of outgoing waves only in the scattered waves, one obtains

$$\alpha[n\Gamma P(J)\mu]=(4\pi/2P+1)^{\frac{1}{2}}(2N_\mu+1)$$
$$\times(N_\mu0JM_J\,|\,N_\mu JPM_J)\exp(i\delta_\mu+iN_\mu\pi/2). \quad (61)$$

A normalizing factor $(\mathcal{V})^{-\frac{1}{2}}$ is included in the initial state to normalize it to unity in a box of volume $\mathcal{V}$. The properly normalized final states are

$$\Psi_f=(1/\mathcal{V}^{\frac{1}{2}}R)Z_\mu(\mathbf{r},R,\theta,\psi)F_\mu(R). \quad (62)$$

The transition matrix elements for $(n\Gamma;JM_J\to PJ'\mu')$ are

$$T(n\Gamma;JM_J\to PJ'\mu')=(1/\mathcal{V})[\Psi_f(\mu',PJ'),H_I\Psi_i], \quad (63)$$

and the cross section for that transition is

$$\sigma(n\Gamma;\, JM_J\rightarrow PJ'\mu')$$
$$=(M^2k_{J'}/4\pi^2\hbar^4k_J)\,|\,T(n\Gamma;\, JM_J\rightarrow PJ'\mu')\,|^2. \quad (64)$$

The total cross section is obtained by summing over all μ' within the manifold of J', P, summing over P, and averaging over M_J,

$$\sigma(J\rightarrow J')=(1/2J+1)\sum_{M_J}\sum_{P}\sum_{\mu'}\sigma(n\Gamma;\, JM_J\rightarrow J'P\mu'). \quad (65)$$

B. Approximation (B)

In approximation A, it was implicitly assumed that spin-orbit interaction is strong enough to couple the electron spin to the diatomic axis if the axial field is able to couple the orbital momentum. However, many cases arise in which the spin-orbit coupling is not large, and one should consider a "Hund's case (b)" approximation in which the electronic polarization by the axial field occurs adiabatically, but spins remain quantized in a space-fixed axis system. As will be seen, development of the zero-order Hamiltonian in such an approximation leads not only to elastic scattering, but to inelastic scattering as well, because the spin-orbit interaction is not a part of the zero-order Hamiltonian, and is to be treated as a perturbation.

A brief physical description of a collision will be helpful in understanding the mathematical analysis and in approximation (C). When a collision commences, axial fields are substantially weaker than the spin-orbit interactions, and the slight partial following of the diatomic axis by the orbital angular momentum which occurs is accompanied by strong coupling of spin and orbital momenta. As the axial field increases, however, for rapid passage and strong axial fields and orbital angular momentum is wrenched free from the spin and reoriented. Only at the end of collision is the spin-orbit interaction again able to restore the separation into eigenstates of J and its z component.

A discussion of the role of the zero-order Hamiltonian in producing inelastic scattering is only appropriate after it has been defined. The Hamiltonian for approximation (B) is obtained by a transformation of the electron coordinates to molecule-fixed axes, as in Sec. A, but the spin transformation is omitted and the electronic states have characteristic values of M_s. The Hamiltonian is, then,

$$H''=H_e^0(\xi,\eta,\zeta;\, R)+H_{s.o.}(\xi,\eta,\zeta,\, m_s;\, R,\theta,\psi)$$
$$-(\hbar^2/2MR^2)\,(\partial/\partial R)\big[R^2(\partial/\partial R)\big]$$
$$-(\hbar^2/2MR^2)\{(1/\sin\theta)\,(\partial/\partial\theta)\big[\sin\theta(\partial/\partial\theta)\big]$$
$$+(1/\sin^2\theta)\big[(\partial/\partial\psi)-(i/\hbar)\,\cos\theta L_\zeta\big]^2\}$$
$$+(1/2MR^2)\big[L_\xi^2+L_\eta^2-L_+U_+-L_-U_-\big], \quad (66)$$

where

$$L_\pm=L_\xi\pm iL_\eta;$$
$$U_\pm=\hbar\big[\mp(\partial/\partial\theta)+(i/\sin\theta)\,(\partial/\partial\psi)+(\cot\theta/\hbar)\,L_\zeta\big], \quad (67)$$

H_e^0 is the electronic Hamiltonian exclusive of spin-orbit interaction, and $H_{s.o.}$ is the spin-orbit interaction itself. Derivatives with respect to R, θ, ψ, are understood to be taken with ξ, η, ζ fixed.

We now define an operator H_B, analogous in this approximation to H_A of approximation (A):

$$H_B=H_e^0-(\hbar^2/2MR^2)\{(1/\sin\theta)\,(\partial/\partial\theta)\big[\sin\theta(\partial/\partial\theta)\big]$$
$$+(1/\sin^2\theta)\big[(\partial/\partial\psi)-(i/\hbar)\,\cos\theta L_\zeta\big]^2\}$$
$$+(1/2MR^2)\big[L_\xi^2+L_\eta^2-L_+U_+-L_-U_-\big]. \quad (68)$$

The matrix elements of H_B are readily defined in the representation provided by the vectors

$$\phi\big[n\Gamma M_s(L)\,\Lambda;\, \mathbf{r},\, R\big]\mathfrak{IC}(KM_k\Lambda;\theta,\psi), \quad (69)$$

where ϕ is an eigenfunction of H_e^0, L_ζ, S, and M_s:

$$H_e^0\phi(n\Gamma M_s\Lambda;\, \mathbf{r},\, R)=\epsilon'(n\Gamma\Lambda;\, R)\phi(n\Gamma M_s\Lambda); \quad (70)$$
$$L_\zeta\phi=\Lambda\hbar\phi. \quad (71)$$

The $\mathfrak{IC}(KM_k\Lambda;\theta,\psi)$, entirely analogous to $\mathfrak{IC}\,(PM_p\Omega;\,\theta,\psi)$ in approximation (A), satisfies the equation

$$\{(1/\sin\theta)\,(\partial/\partial\theta)\big[\sin\theta(\partial/\partial\theta)\big]$$
$$+(1/\sin^2\theta)\big[(\partial/\partial\psi)-i\Lambda\,\cos\theta\big]^2\}\mathfrak{IC}$$
$$=-\big[K(K+1)-\Lambda^2\big]\mathfrak{IC}. \quad (72)$$

The matrix elements of $U_\pm$ between the functions $\mathfrak{IC}$ are

$$(KM_k\Lambda\pm1\,|\,U_\pm\,|\,KM_k\Lambda)=\hbar\big[(K\pm\Lambda+1)\,(K\mp\Lambda)\big]^{\frac{1}{2}}. \quad (73)$$

Just as in approximation (A), a relation exists between the "uncoupled" electronic-rotational basis set and this "coupled" set, as $R\rightarrow\infty$:

$$\phi^{(\infty)}(n\Gamma M_sM_L;\, \mathbf{r})\,Y(NM_N;\theta,\psi)$$
$$=(-1)^{M_N}\sum_K\sum_\Lambda\left(\frac{2N+1}{2K+1}\right)^{\frac{1}{2}}(NM_NLM_L\,|\,NLKM_k)$$
$$\times(NLK\Lambda\,|\,N0L\Lambda)\phi^{(\infty)}(n\Gamma M_s\Lambda;\, \mathbf{r})\mathfrak{IC}(KM_k\Lambda;\theta,\psi). \quad (74)$$

Furthermore, it is easily shown that the transformation

$$\sum_\Lambda(NLK\Lambda\,|\,N0L\Lambda)\phi^{(\infty)}(n\Gamma\Lambda;\, \mathbf{r})\mathfrak{IC}(KM_k\Lambda;\theta,\psi) \quad (75)$$

diagonalizes H_B as $R\rightarrow\infty$. The eigenvalues are asymptotically

$$\epsilon\rightarrow\epsilon^0(n\Gamma LS)+N(N+1)\hbar^2/2MR^2, \quad (76)$$

where N takes on the $2L+1$ possible values consistent with given K, and $\epsilon^0(n\Gamma LS)$ is the Russell-Saunders

atomic term value (omitting spin-orbit interaction energies).

At finite R, we now define the zero-order basis set for this approximation as the set of eigenfunctions $X(n\Gamma K\mu)$ which diagonalize the matrix H_B. Since H_B is diagonal in K, S, M_s this basis set is obtained by the diagonalization of the noninteracting $(2L+1)$-dimensional matrices for each K value, and the given values of S, M_s. The eigenvalues we shall define by the symbol $\omega(n\Gamma K\mu; R)$.

The solution to the scattering problem is chosen to be expanded using X_μ as a basis:

$$\Psi=(1/R)\sum C(n\Gamma K\mu)X(n\Gamma K\mu;\mathbf{r},R,\theta,\psi)F(n\Gamma K\mu;R); \tag{77}$$

the functions F are chosen to satisfy the equation,

$$-(\hbar^2/2M)d^2F/dR^2+\omega_\mu(R)F=EF, \tag{78}$$

and to be finite everywhere with the asymptotic property

$$\lim_{R\to\infty} F(n\Gamma K\mu;R)=(1/k)\sin(kR+N_\mu\pi/2+\delta_\mu). \tag{79}$$

Because the spin-orbit coupling is not included in H_B, the electronic states of the system are all degenerate as $R\to\infty$. Splitting between states of distinct J is only introduced by the spin-orbit interaction.

The spin-orbit interaction, and the matrix elements arising from the terms in $(dX_\mu/dK)\cdot(dF_\mu/dk)$, lead to perturbations of the zero-order states. The effect of these will be considered later, after the results of the zero-order scattering are treated.

In this approximation, the collision is assumed to be "fast" with respect to spin-orbit interaction. The initial state of the system is an eigenfunction of the entire electronic Hamiltonian H_e, including spin-orbit coupling. In the treatment of this approximation, it is imagined that the spin-orbit interaction is suddenly "turned off," and the eigenstate is expanded in eigenstates $\phi'(n\Gamma M_J M_L;\mathbf{r})$. This expansion is the "initial state" for the formal theory treatment, and propagates itself under the zero-order Hamiltonian in terms of the basis set X_μ. Neglecting the perturbations, no transitions in the X_μ occur, and the final amplitude at each θ, ψ solid angle for scattering into various values of M_L is determined by the boundary conditions and phase shifts. These "final states" are then re-expanded in terms of eigenfunctions of H_e; i.e., the spin-orbit interaction is suddenly "turned on" again. Therefore, because of the sudden approximation treatment of the spin-orbit interaction at the beginning and end of a collision, "elastic" scattering in terms of the zero-order Hamiltonian is inelastic scattering in actuality.

The initial electronic state is $\phi(n\Gamma JM_J;\mathbf{r})$; it may be written as a linear combination of the Russell-Saunders eigenfunctions:

$$\phi(n\Gamma JM_J;\mathbf{r})=\sum_{M_s}(LSJM_J\,|\,LM_LSM_s)\phi'(n\Gamma M_LM_s). \tag{80}$$

Since the spin-orbit interaction is neglected, the value of M_s may not change, and the solution to the scattering problem must have the asymptotic form

$$\Psi\to\sum_{M_s}(LSJM_J\mid LM_LSM_s)\{\phi'(n\Gamma M_LM_s)\exp(ikR\cos\theta)+(\exp ikR/R)\sum_{M_L'}f(M_L',\theta,\psi)\phi'(n\Gamma M_L'M_s)\}. \tag{81}$$

For each value of M_s, we shall consider the problem separately $(M_L=M_J-M_s)$. The plane wave may be expanded for each M_L in the basis $\mathbf{X}_\mu$ as $R\to\infty$:

$$\lim_{R\to\infty}\phi'(n\Gamma M_LM_s)\exp(ikR\cos\theta)$$

$$=\sum_N\sum_K(4\pi/2K+1)^{\frac{1}{2}}(2N_\mu+1)\exp(iN_\mu\pi/2)(N_\mu 0LM_L\,|\,N_\mu LKM_L)\mathbf{X}(n\Gamma K\mu)\sin(kR+N_\mu\pi/2)/R. \tag{82}$$

Comparing the coefficients of the general solution with the required asymptotic behavior, one readily obtains the result

$$C(n\Gamma K\mu)=(4\pi/2K+1)^{\frac{1}{2}}(2N_\mu+1)(N_\mu 0LM_L\mid N_\mu LKM_L)\exp(iN_\mu\pi/2+i\delta_\mu). \tag{83}$$

The scattered wave may now be readily written in the basis X_μ as $R\to\infty$; it is,

$$[\exp(ikR)/R]\sum_{M_L'}f(M_L';\theta,\psi)\phi'(n\Gamma M_L'M_s)$$

$$=\sum_N\sum_K[\exp(ikR)/kR](-1)^N(4\pi/2K+1)^{\frac{1}{2}}(2N+1)(N0LM_L\,|\,NLKM_L)[(e^{2i\delta_\mu}-1)/2i]\mathbf{X}_\mu(n\Gamma K\mu). \tag{84}$$

The right-hand side of Eq. (81) is now expanded in appropriate functions; the scattered wave is

$$[\exp(ikR)/2ikR]\sum_{N_\mu}\sum_K(-1)^{N_\mu+M_N}(4\pi/2K+1)^{\frac{1}{2}}(2N_\mu+1)(e^{2i\delta_\mu}-1)(N_\mu 0LM_L\,|\,N_\mu LKM_L)$$

$$\times(N_\mu LKM_L\,|\,N_\mu M_N LM_L')\phi'(n\Gamma M_L'M_s)Y(NM_N;\theta,\psi). \tag{85}$$

The next step is to suddenly turn the spin-orbit interaction "on" again; wave functions $\phi'(n\Gamma M_L' M_s)$ are to be expanded in the eigenfunctions $\phi(n\Gamma J' M_J')$. The scattered wave then becomes

$$[\exp(ikR)/2ikR]\sum_{M_s}\sum_{N_\mu}\sum_{K}\sum_{J'}(LSJM_J|LM_LSM_s)(N_\mu 0LM_L|N_\mu LKM_L)(N_\mu LKM_L|N_\mu N_N LM_L')$$

$$\times(LM_L'SM_s|LSJ'M_J')(-1)^{N_\mu+M_N}(4\pi/2K+1)^{\frac{1}{2}}(2N_\mu+1)(e^{2i\delta_\mu}-1)\phi(n\Gamma J'M_J')Y(NM_N;\theta,\psi), \quad (86)$$

(note that the phase shift δ_μ depends on K as well as N_μ). This expression is set equal to the general expression for a final scattered wave:

$$[\exp(ikR)/R]\sum_{J',M_J'} f'(J'M_J';\theta,\psi)\phi(n\Gamma J'M_J'); \qquad M_J'+M_N=M_J. \quad (87)$$

Such a definition of f' yields the cross section for scattering as

$$\sigma(JM_J\rightarrow J'M_J') = \int_0^\pi\int_0^{2\pi}\sin\theta d\theta d\psi\,|f'(J'M_J';\theta,\psi)|^2, \quad (88)$$

and the total inelastic cross section is

$$\sigma(J\rightarrow J') = (\tfrac{1}{2}J+1)\sum_{M_J}\sum_{M_J'}\sigma(JM_J\rightarrow J'M_J'). \quad (89)$$

C. Approximation (C)

This approximation is an obvious extension of approximations (A) and (B), and is an attempt to treat the case of slow passage through a region of competition between axial fields and spin-orbit interaction. Diagonalization of all perturbation terms, except those caused by radial motion, determines the electronic-rotational basis set.

The procedure followed is the same as that of approximation (A), up to the development of the complete electronic-rotational Hamiltonian H_A. However, the *manifold* for approximation (C) is the direct sum of the manifolds of all possible J values and a fixed value of P for approximation (A). That is, a (C) manifold is designated only by the associated total angular momentum; it is of dimensionality $(2L+1)(2S+1)$ and is spanned by the complete set of electronic states for the Russell-Saunders term, multiplied by appropriate functions for angle dependence with total angular momentum P.

The zero-order electronic-rotational basis set for approximation (C) is obtained by diagonalizing H_A within each manifold. The resulting eigenfunctions we shall call $W(n\Gamma P\mu)$. They may be expressed in terms of the simple adiabatic functions:

$$W(n\Gamma P\mu;\mathbf{r},R,\theta,\psi) = \sum_J\sum_\Omega C(n\Gamma P\mu;J\Omega;R)\phi[n\Gamma(J)\Omega;\mathbf{r},R] \times\mathfrak{K}(PM_p\Omega;\theta,\psi). \quad (90)$$

The eigenvalues are called $\rho(n\Gamma P\mu;R)$; the limiting values are, for large R, weak axial fields,

$$\lim_{R\rightarrow\infty}\rho(n\Gamma P\mu;R) = \epsilon^0(n\Gamma J_\mu) + [N_\mu(N_\mu+1)\hbar^2/2MR^2], \quad (91)$$

while for strong axial fields the energy is

$$\rho(n\Gamma P_\mu;R)\rightarrow\epsilon[n\Gamma(J_\mu)\Omega_\mu;R] + [P(P+1)-\Omega^2]\hbar^2/2MR^2. \quad (92)$$

The coefficients $C(n\Gamma P\mu;J\Omega;R)$ satisfy the unitary relations

$$\sum_{J,\Omega}C^*(n\Gamma P\mu',J\Omega;R)C(n\Gamma P\mu;J\Omega;R)=0, \qquad \mu'\neq\mu;\ 1,\ \mu'=\mu. \quad (93)$$

The basic zero-order eigenfunctions χ are of the form

$$\chi=(1/R)W_\mu(\mathbf{r},R,\theta,\psi)F_\mu(R), \quad (94)$$

where F_μ satisfies the equation

$$-(\hbar^2/2M)(d^2F_\mu/dR^2)+\rho_\mu(R)F_\mu(R)=EF_\mu, \quad (95)$$

is everywhere finite, and has the asymptotic property

$$\lim_{R\rightarrow\infty}F_\mu(R)=(1/k_\mu)\sin(k_\mu R+N_\mu\pi/2+\gamma_\mu). \quad (96)$$

When the Hamiltonian acts on a wave function composed of this zero-order set, the most significant perturbations arise from the terms

$$-(\hbar^2/M)[(dW_\mu/dR)\cdot(dF_\mu/dR)];$$

other terms come from $F_\mu(d^2W_\mu/dR^2)$, but we ignore these. The interaction integrals will all be of the form

$$H_I(\mu',\mu) = (-\hbar^2/M)\iiiint dRF_{\mu'}{}^*W_{\mu'}{}^*(dW_\mu/dR)\cdot(dF_\mu/dR)d\tau_e \times\sin\theta d\theta d\psi. \quad (97)$$

These elements are diagonal in P, M_p. We now find the explicit expressions for the electronic-rotational integrals:

$$\iiint W_{\mu'}{}^*(dW_\mu/dR)d\tau_e d(\cos\theta)d\psi = \sum_{\Omega,J}C^*(n\Gamma P\mu';J\Omega)(d/dR)C(n\Gamma P\mu;J\Omega) + \sum_{\Omega,J'\neq J}C^*(n\Gamma P\mu;J'\Omega)C(n\Gamma P\mu;J\Omega)A(J'J\Omega;R), \quad (98)$$

where

$$A(J'J\Omega;\, R) = \int d\tau_e \phi^* [n\Gamma(J')\Omega](d/dR)\phi[n\Gamma(J)\Omega]. \tag{99}$$

The initial state of the system is, by analogy with approximation (A),

$$\Psi_i = (1/R)\sum_{N_\mu}\sum_{P}(4\pi/2P+1)^{\frac{1}{2}}(2N_\mu+1)$$
$$\times(N_\mu 0 JM_J|N_\mu JPM_J)\exp(iN_\mu\pi/2+i\gamma_\mu)W_\mu F_\mu. \tag{100}$$

The transition matrix element is T_{fi},

$$T_{fi}(JM_J\rightarrow P\mu') = [\chi(P\mu'), H_I\Psi_i], \tag{101}$$

and the cross section is computed in a manner fully analogous to that of approximation (A), but with the new matrix elements $H_I(\mu', \mu)$ and phase shifts γ_μ, as well as new radial functions F_μ.

IV. METHODS OF CALCULATION

As was indicated in earlier discussion, the use of variational expressions based on the formal scattering theory, or of the explicit perturbation theory it provides, involves too much labor to be practical at present beyond the first approximation; therefore, we have devoted our attention to the development of useful electronic basis sets whose first or even zero-order approximations to inelastic scattering may be computed with no more labor than is common to all such calculations. This labor may be categorized into the following components:

(1) Determination of the effective "elastic scattering potential surfaces" for the approximation in question.

(2) Determination of the electronic-rotational basis associated with the eigenvalue surfaces [if a first-order theory with transition matrices be involved; in adiabatic approximation (B), for example, this is not necessary].

(3) Computation of the electronic-rotational parts of the transition matrix elements.

(4) Solutions for the radial functions $F_\mu(R)$, describing nuclear motion on each elastic surface, and the associated phase shifts, and computation of radial parts of the transition matrix elements.

(5) Summation of partial-wave cross sections. The present status of practical calculation on any of these component problems is rudimentary in the extreme. For example, most actual calculations on problem (4) have been based on the Born approximation or semiclassical approximations for the nuclear motion. Consequently, a large part of the necessary work is survey, concerned with merely studying the effect of assumptions or further approximations in the above five areas. Here we shall give only brief discussions of the situation in each at present, and of programs for further investigation. We hope to devote most of our future effort to pursuit of these programs.

(1) Effective "elastic scattering potential." Part of this problem, in fact the major part, is concerned with the classic problem of calculating or otherwise obtaining an accurate description of the interaction energy and wave function for the diatomic system. In the case of the high energy approximation, this problem is perhaps the simplest since there the elastic potential is defined in terms of the isolated atom wave functions, and one may hope that the Hartree-Fock wave functions for these will be sufficiently good to use for the most refined calculations. At present, our calculations employ a cruder estimate obtained with the simple "best atom exponent" Slater-type orbitals (STO) for the high energy approximation. In the adiabatic approximations, one must solve for the molecular electronic energies and wave functions, and we need not elaborate our commentary here by lamentation over conditions. One does the best he can, and perhaps should devote his energies to studying the effects of variation in the absolute value of the energy as a function of R, rather than of its shape, or investigate the perturbation splitting of spin-orbit interaction as a function of axial field strength. The other part of the eigenvalue problem, the diagonalization of the manifold matrices, we do not consider a real difficulty, since they are always of small dimensionality.

It might be proposed that experimental data be used to obtain the adiabatic potential energy curves. This data is nonexistent because present scattering measurements are all at far too high energies, and transport property measurements weight the attractive van der Waals region in a crude way, together with the repulsive region, while the only region of interest to us in most cases is the immediate vicinity of the classical turning point for given energy.

(2), (3) Electronic-rotational eigenfunctions and their transition matrix elements. The major part of this problem has already been discussed, i.e., the determination of adiabatic wave functions. The determination of the manifold eigenvectors is merely a computational operation, though perhaps a slightly tedious one.

One topic that is of interest here is whether it is a good idea to use independent procedures for elastic energy surfaces and for the associated electronic functions used to compute the transition matrix elements. This question has come into prominence because it is found that the transition matrix elements are almost always functions which decrease exponentially as R increases, in the interaction region, and mild displacements of the matrix element curve with respect to the potential energy curves lead to huge variations in the cross section. Our present feeling is that the two calculations should be strongly coupled, and further study will be made on the best way to do this.

(4) Solution of the radial equations for nuclear motion. The practical problem in this area is the question of machine time. Even the best methods of solving

the differential equations are time consuming when one considers that there are up to $(2L+1)(2S+1)$ radial equations for each partial wave, and as many as fifty of these may be needed.

Because, as has been stated, the major contribution to transition always comes from the classical turning point region, the WKB approximation is not very useful. On the other hand, a tremendous simplification is tempting, namely to use hard-sphere wave functions with hard-sphere radius equal to R_0, the classical turning point. This appears at present to be a good standard approximation, although its validity needs to be investigated later. Phase shifts are also easy to calculate in such a case, without an expensive additional integration.

(5) The last component problem does not appear difficult, except for the handling, generation, and processing of the large numbers of vector coupling coefficients, matrix elements, phase shifts, etc., needed for the final summations.

ACKNOWLEDGMENTS

The author is grateful to the National Science Foundation for support during the summer of 1960 when some of this research was done. He also wishes to thank J. W. Moskowitz for useful preliminary information on practical calculation problems.

THE JOURNAL OF CHEMICAL PHYSICS VOLUME 34, NUMBER 5 MAY, 1961

Phase Transitions in the Ammonium Halides*

RICHARD STEVENSON

Eaton Electronics Research Laboratory, McGill University, Montreal, Canada

(Received November 11, 1960)

High-pressure experiments, using the piston displacement technique have been performed at temperatures down to that of liquid nitrogen on NH_4I, NH_4Br, ND_4Br, and NH_4Cl. For the iodide two new phase transitions under pressure and a new triple point were observed. A new transition and a new triple point were observed in both the bromides; the existence of another transition was confirmed. The role of multipole interactions in causing the transitions is discussed, and on the basis of structural data and the present experiments a generalized phase diagram is presented which describes the gross behavior of the transitions in these substances.

I. INTRODUCTION

AMMONIUM chloride, bromide, and iodide exhibit at atmospheric pressure a number of phase transitions from one cubic structure to another. It is known from neutron diffraction studies (as will be discussed later) that in the various substances analagous phases appear. These modifications, labeled for convenience α, β, γ, and δ, involve some orientation or reorientation of the ammonium tetrahedron with respect to the halide ion. The temperatures at which the transitions occur under atmospheric pressure are given in Table I. Although identical structures appear from substance to substance, there is no evident correlation among the transition temperatures or any indication of why a particular phase should appear at the temperature it does. The purpose of the investigation reported here was to study the effect of pressure on the transitions, and to obtain some correlation among the phase diagrams.

II. EXPERIMENTAL TECHNIQUE

The method of the experiments is similar to that of Bridgman.[1] The polycrystalline substance to be studied is compressed into a coherent cylindrical mass, and wrapped in a 0.005-in.-thick sheet of indium metal. The indium acts as a lubricating agent and materially reduces friction in the apparatus. The wrapped sample is inserted into a thick-walled cylinder of hardened beryllium-copper. Beveled brass washers fit into each end of the cylinder to prevent extrusion of indium into the space between the compressing pistons and the cylinder walls. The cylinders used in these experiments had inner diameters of $\frac{1}{4}$ in. or $\frac{1}{2}$ in.; the former allowing a maximum pressure of 10 000 atm, the latter 2500 atm. The assembly of pistons and cylinder is placed in a hydraulic press similar to that of Stewart.[2]

The whole apparatus is set into a variable temperature cryostat which is of the design of Swenson and Stahl.[3] With liquid nitrogen in the cryostat, any temperatue between that and room temperature can be chosen and controlled to within about a tenth of a degree. The cryostat temperature is fixed and data accumulated as a series of readings of the piston displacement while the force on the piston is increased to a maximum and then decreased. In experiments with highly incompressible substances such as the ammonium

* Supported by the Office of Naval Research and in part by the Defence Research Board (Canada).

[1] P. W. Bridgman, Proc. Am. Acad. Arts. Sci. **76**, 9 (1945).

[2] J. W. Stewart, Phys. Rev. **97**, 578 (1955).

[3] C A. Swenson and R. H. Stahl, Rev. Sci. Instr. **25**, 608 (1954).

TABLE I. Atmospheric pressure transition temperatures of the ammonium halides. (Three dots in the table mean that the transition does not occur at atmospheric pressure.)

	$\alpha-\beta$	$\beta-\gamma$	$\beta-\delta$	$\gamma-\delta$
NH_4Cl	458°K[a]	...	243[b]	...
ND_4Cl		...	249[c]	...
NH_4Br	411[d]	235[e]	...	100[f] (approx.)
ND_4Br	398[g]	215[g]	...	169[f]
NH_4I	257[h]	231[h]	...	...
ND_4I	254[i]	227[i]	...	...

[a] F. E. C. Scheffer, Proc. Akad. Wetenschapper **18,** 446 (1915); 1498 (1916).
[b] A. Smits, G. J. Muller, and F. A. Kroger, Z physik Chem. **B38,** 177 (1937).
[c] A. Smits and G. J. Muller, Nature **13,** 804 (1937).
[d] A. Smith and H. E. Eastlach, J. Am. Chem. Soc. **38,** 1261 (1916).
[e] F. Simon, C. von Simson, and M. Ruhemann, Z. physik Chem. **129,** 339 (1927).
[f] C. C. Stephenson, R. W. Blue, and J. W. Stout, J. Chem. Phys. **20,** 1658 (1952).
[g] H. A. Levy and S. W. Peterson, Phys. Rev. **83,** 1270 (1951).
[h] C. C. Stephenson, L. A. Landers, and A. G. Cole, J. Chem. Phys **20,** 1044 (1952).
[i] A. Smits and D. Tollenaar, Z. physik Chem. **B52,** 222 (1942).

halides, the "background stretch" of the apparatus may account for over half of the nominal compression. Thus, at the end of a series of experiments the sample is removed from the cylinder and stripped of its indium jacket. The indium is put back into the cylinder and a blank run made. When this correction is substracted from the experimental results, the force-displacement curves can be converted into pressure-volume isotherms. When a comparison has been possible between results from this apparatus and data arrived at by other methods, the agreement has been at least within 5%.

A phase transition is seen as a break in the pressure-volume isotherm, as has been explained previously.[4] This experimental method produces only an approximate hydrostatic pressure; thus, the transition appears at a higher pressure with the pressure increasing than with pressure decreasing. In the ammonium halides this tendency is aggravated by a natural hysteresis which accompanies some of the transitions. The hysteresis or "region of indifference" is shown on the phase diagram by bars extending above and below the mean pressure.

A break in the experimental isotherm is accepted as a phase transition only if it appears in a consistent pattern at a number of temperatures. Large phase changes (i.e., 3% or more of the zero-pressure volume) are easily observed. However, the interpretation of small phase changes is often problematical; this is a basic and unremovable defect of this type of experiment.

TABLE II. Compressions of the ammonium halides. This table gives $-\Delta V/V_0$ at 77°K. The data for NH_4I contain the $\gamma-\delta$ transition and are shown in more detail in Fig. 7.

Pressure atm	NH_4Cl	NH_4Br	NH_4I
0	0	0	0
2500	0.015	0.017	0.013
5000	0.030	0.033	0.029
7500	0.044	0.043	0.038
10 000	0.052	0.049	0.048

[4] R. Stevenson, J. Chem. Phys. **27,** 147, 656, 673 (1957).

III. EXPERIMENTAL RESULTS

The compression of the three halides at 77°K are given in Table II. The data for ammonium iodide contain the $\gamma-\delta$ transition, and are shown in more detail by Fig. 7.

A. Ammonium Chloride

The higher temperature transition ($\alpha-\beta$) has been studied previously by Bridgman.[5] Two points of the $\beta-\delta$ transition were observed in the present work, and are shown as bars on Fig. 1. Bridgman[6] had earlier obtained two other points which are shown as dots on the curve. The volume changes associated with the transition are given in Bridgman's paper.

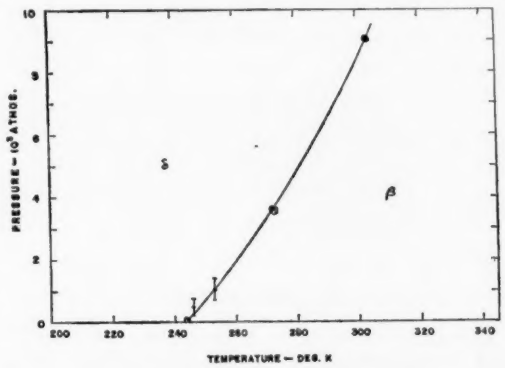

FIG. 1. Phase diagram for NH_4Cl. The circles represent earlier work by Bridgman; the bars the present research.

B. Ammonium Bromide

The observed phase diagram for NH_4Br is shown in Fig. 2. The volume changes associated with the $\gamma-\beta$ and $\gamma-\delta$ transitions were approximately equal, thus the position of the triple point is uncertain, as is the slope of the $\beta-\delta$ transition line. Figure 2 gives the best choice from the available information. One point on the $\gamma-\beta$ transition line had been observed previously by Bridgman.[6]

[5] P. W. Bridgman, Proc. Am. Acad. Arts. Sci. **52,** 91 (1916).
[6] P. W. Bridgman, Phys. Rev. **38,** 182 (1931).

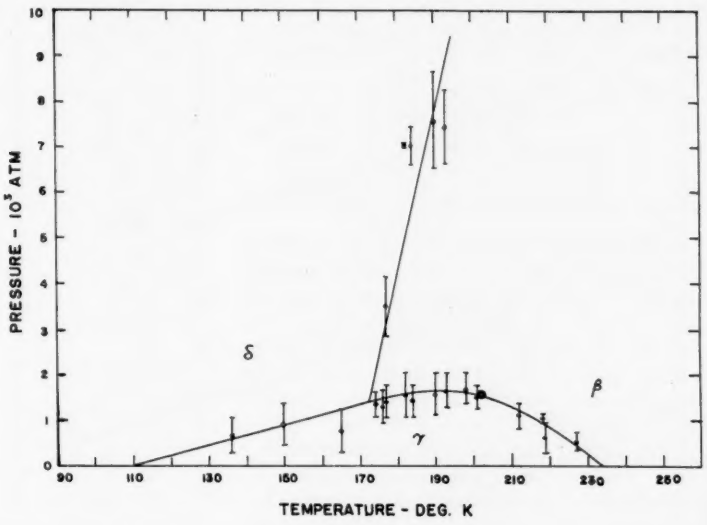

FIG. 2. Phase diagram for NH_4Br. The circle on the $\gamma-\beta$ line represents a point observed earlier by Bridgman.

C. Deuterated Ammonium Bromide

The sample obtained had been used previously for specific heat studies.[7] The size of the $\beta-\delta$ transition for this substance was enough larger (than that in NH_4Br) to make the determination of the transition line much easier. The phase diagram is given in Fig. 3 and typical experimental isotherms in Fig. 4.

Both of the bromides show similar phase diagrams, with the triple point on the low-temperature side of the $\beta-\gamma$ "hump." The $\gamma-\delta$ transition is not always observed in specific heat studies.[7] The present experiments which show the transition and its associated large volume change definitely establish its existence.

D. Ammonium Iodide

The phase diagram for ammonium iodide is given by Fig. 5. A new phase, which we shall postulate is the δ phase, appears under pressure. Figure 6 shows a typical experimental isotherm through the $\gamma-\delta$ transition at liquid nitrogen temperature, and Fig. 7 is the idealized $p-V$ isotherm constructed from it.

The low-pressure points on Fig. 5 are from calorimetric experiments.[8] The "hump" characteristic of the

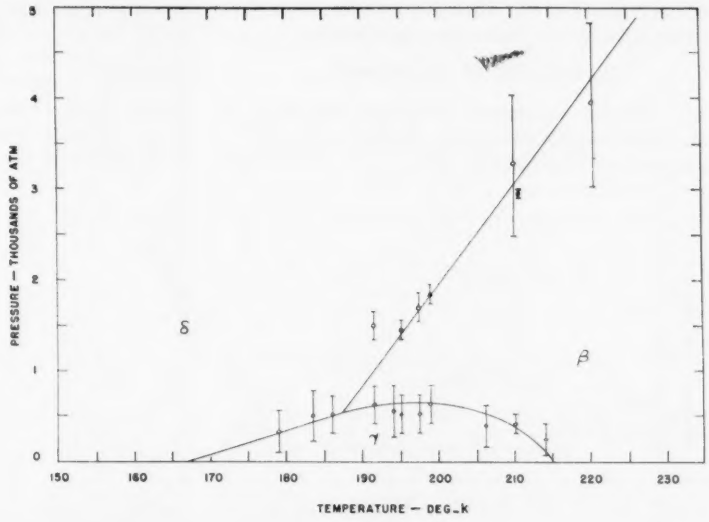

FIG. 3. Phase diagram for ND_4Br.

[7] C. C. Stephenson and H. E. Adams, J. Chem. Phys. **20**, 1658 (1952).
[8] S. A. Zlunitsyn, J. Exptl. Theoret. Phys. (U.S.S.R.) **8**, 724 (1938); **9**, 72 (1939).

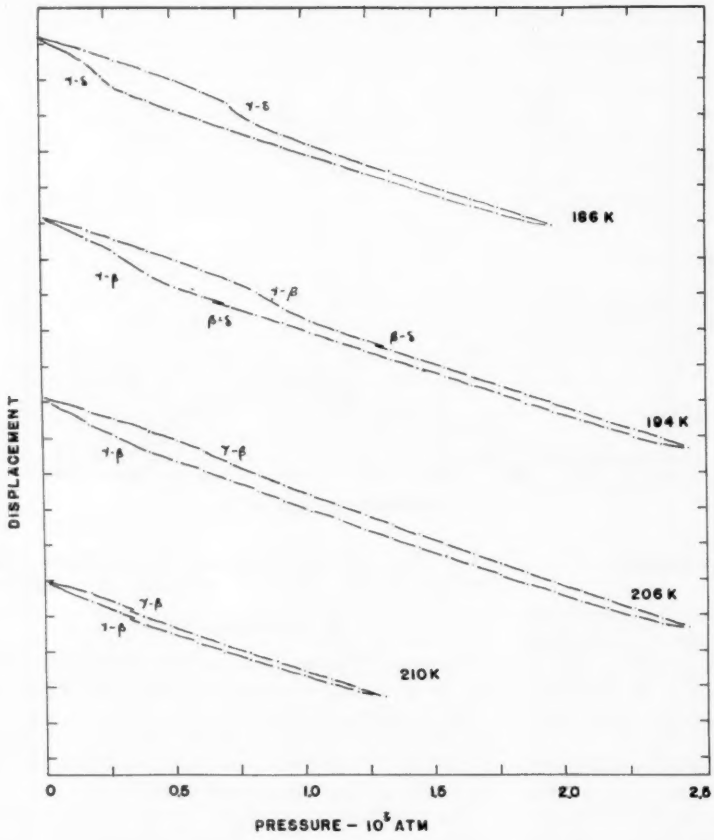

FIG. 4. Experimental isotherms for ND_4Br.

bromide transitions was observed, and the triple point appears to be on the higher temperature side.

IV. DISCUSSION OF RESULTS

The different occurrences of phase transitions in these various substances are due mainly to the relative importance of electrostatic interactions between the ions and the disorienting effects of thermal vibration. In all the phases the halide ions are located on cube corners associated with the structural unit cells, thus producing an electrostatic field of octahedral symmetry at the center of the cube. The ammonium tetrahedra are placed on the face of the cube as in the α phase, or at the center of the cube for all the other phases. The

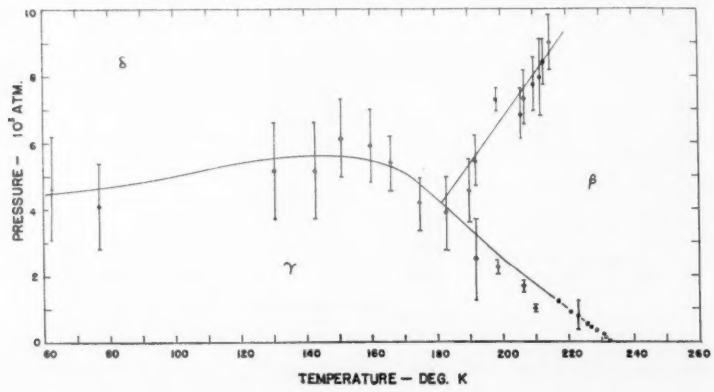

FIG. 5. Phase diagram for NH_4I. The low pressure points are from calorimetric measurements of Zlunitsyn.

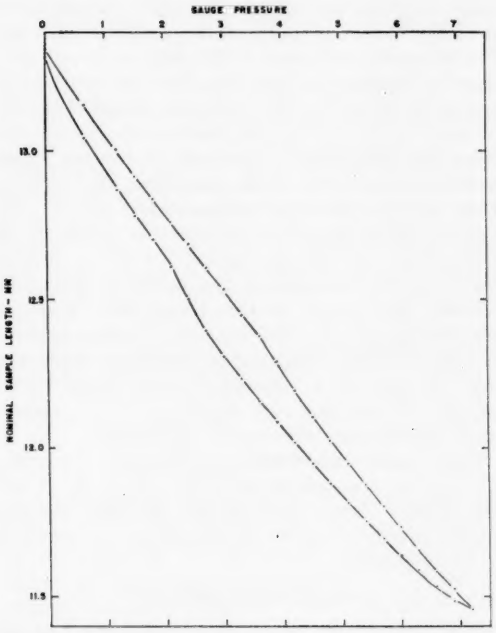

FIG. 6. Experimental isotherm through the $\gamma-\beta$ phase transition of NH_4I 77°K.

field due to the ammonium ions, which is of tetrahedral symmetry, is superimposed on the field due to the halide ions. Thus the electrostatic interactions of interest are associated with the possible orientations of the hydrogens attached to the ammonium tetrahedron

The main structural information about the ammonium halides is gathered from the neutron diffraction

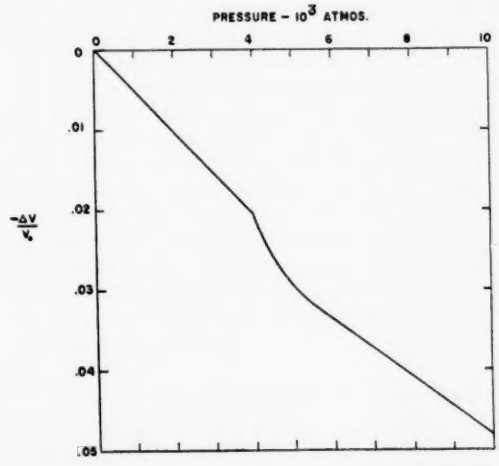

FIG. 7. Idealized pressure-volume isotherm formed from the data of Fig. 6 (77°K).

TABLE III. The correlation of transition temperatures (β–δ) on the basis of an octupole-octupole interaction $T\alpha a_0^{-7}$.

	a_0	T_{exp}	T_{calc}
NH_4Cl	3.85	243	(243)
NH_4Br	4.02	170 extrapol.	169
NH_4I	4.25	150 extrapol.	125

studies of Levy and Peterson[9] which is conveniently reviewed by Shull and Wollan.[10] In the β, γ, and δ phases the ammonium tetrahedra are located at the center of the cube formed by the halide ions. For the δ phase the tetrahedra are oriented in a parallel sense from cell to cell, in the γ phase, antiparallel, and in the β phase, randomly. A tetragonal unit cell is necessary for the descriptions of the γ phase, but it is important to notice that the nitrogens are in the same relative position with respect to the halide ion as in the δ phase.

The theory of the phase changes in NH_4Cl and NH_4Br has been studied by Nagamiya.[11] His calculations indicate that the long-range ordering of ammonium tetrahedra brought about by a $\beta-\delta$ transition is due to the interaction of the octupole moments. The transition temperature is proportional to the ordering energy, which for octupole-octupole interactions varies as a_0^{-7}, where a_0 is the lattice constant. The present experiments indicate the existence of a $\beta-\delta$ transition for each of the halides. In Table III is shown a correlation of the transition temperatures (extrapolated to zero pressure) on the basis of an octupole-octupole interaction. The agreement is quite satisfactory, which gives further support to Nagamiya's theory.

The occurrence of the γ phase is ascribed by Nagamiya to the finite polarization of the halide ion,

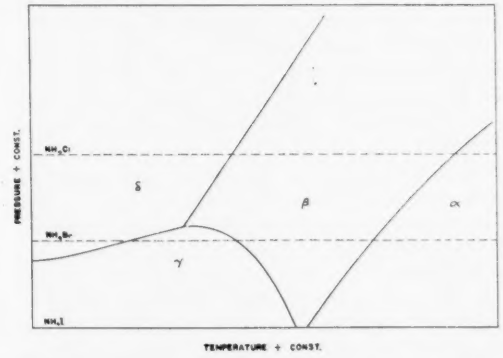

FIG. 8. Schematic generalized phase diagram. This diagram shows in outline the general type of correlation which is found among the phases of the ammonium halides.

[9] H. A. Levy and S. W. Peterson, Phys. Rev. **83,** 1270 (1951); **86,** 766 (1952); J. Chem. Phys. **21,** 366 (1953); J. Am. Chem. Soc. **75,** 1536 (1953).

[10] C. G. Shull and E. O. Wollan, Solid State Phys. **3,** 154 (1956).

[11] T. Nagamiya, *Changements de Phase* (Societé de Chimie Physique, Paris, 1952), p. 251.

which makes an antiparallel orientation of the ammonium tetrahedra energetically more favorable. A decrease of the ionic separation reverses the situation eventually, and gives rise to the appearance of the parallel orientation. This is seen in the present experiments by the disappearance of the γ phase in NH_4I under pressure.

The present experiments are of interest because they indicate what appears to be a rather more general behavior of the substances. The correlation among the $\beta-\delta$ transition lines and the appearance of the δ phase in NH_4I are particularly significant. (That the δ phase in the iodide has the same structure as those of the other halides is assumed on the basis that the lower temperature phase at any pressure will have the higher symmetry. Since the higher temperature phase is known to be the β, it appears eminently reasonable that the lower is actually a δ phase.) It is known that the appearance of the phases is due by and large to the electrostatic interactions, and this will depend on the separation of the ions. Then from the point of view of a high-pressure experiment the only difference among the halides is in the magnitude of the molecular volume. As pressure is applied the volume is decreased, and eventually the behavior of the substance should be similar to that of another halide with an initially smaller molecular volume. This is just what happens.

Thus if pressure and temperature affect these substances only indirectly by causing a change in the ionic separation, it is possible to think of a hypothetical ammonium halide, for which a schematic phase diagram is shown in Fig. 8. To obtain the phase diagram of any particular halide we need only consider that part of the phase diagram above a pressure which corresponds to the initial molecular volume of the particular substance. The schematic usefulness of this diagram is very great since it presents at once the observed relationships among all transitions. However even though it is possible to correlate the transition lines for one type of transition from substance to substance, it does not appear possible to correlate all the transition lines at once. That is, if we place the γ lines on top of each other (which can be done with considerable accuracy) the $\alpha-\beta$ lines are thrown askew; which is perhaps not surprising considering the profound differences between the causes of the transitions. None the less the experiments indicate almost total similarity in behavior from substance to substance, suggesting that the key for a theoretical study would be the influence of changing ionic separation on the electrostatic interactions and thermal vibrations.

Even ammonium fluoride, which has a wurtzite structure at atmospheric pressure appears to fit into this pattern. Under pressure the structure collapses into what appears to be a cubic structure,[12] probably of a δ orientation.

ACKNOWLEDGMENTS

Parts of this work were done during stays at the Massachusetts Institute of Technology and the University of Western Ontario. Dr. S. C. Collins very generously gave the apparatus used. Dr. W. H. Stockmayer made many useful suggestions. The ND_4Br was obtained from Dr. C. C. Stephenson.

[12] R. Stevenson, J. Chem. Phys. **34,** 346 (1961).

Effect of Several Light Molecules on the Vibrational Relaxation Time of Oxygen*

J. G. PARKER

Applied Physics Laboratory, The Johns Hopkins University, Silver Spring, Maryland

(Received October 12, 1960)

Measurements of vibrational relaxation times of O_2-H_2, O_2-D_2, and O_2-He mixtures have been carried out by means of an acoustic resonance tube. It was found that all these light elements shorten the vibrational relaxation time of oxygen with H_2 being by far the most effective. Surprisingly, D_2 and He produced almost identical effects, indicating that molecular mass is the dominating factor in the ability of these gases to excite vibration in O_2. Results of these measurements show that an O_2-H_2 collision is 2.96×10^3, an O_2-D_2 collision 2.96×10^2, and an O_2-He collision is 3.53×10^2 more effective than an O_2-O_2 collision. Most extensively studied was O_2-H_2, for which relaxation times were measured in eight different mixtures, the maximum concentration of H_2 being 2.64% and the minimum 0.072%. Variation of the relaxation frequency with H_2 concentration was linear, indicating that binary collisions alone are important. Extrapolation of this data to zero concentration gives a relaxation time for pure O_2 of approximately 1.8×10^{-2} sec which is considerably longer than that obtained by other investigators. Comparison of the experimental data with theory suggests that the variation of intermolecular forces in the interaction of light elements with oxygen is much less steep than one would predict from a knowledge of the interaction forces in the separate similar interactions.

I. INTRODUCTION

A CONSIDERABLE amount of experimental data pertaining to the effect of gases and vapors of various types on the vibrational relaxation time of oxygen has appeared in the literature in the last few decades. One of the first observations of this sort was that of Knudsen[1] on anomalous sound absorption in air, an anomaly which was removed by Kneser[2] who traced the discrepancy to the extreme effectiveness of small amounts of water vapor in exciting vibration in atmospheric oxygen. Shortly thereafter Kneser and Knudsen,[3] using a reverberation chamber, studied the effect of large number of gases and vapors. They found, in general, that hydrogen and hydrogen-bearing substances which combine actively with oxygen have a strong effect in shortening the relaxation time. Water vapor also was found to be very effective, a fact which supported the earlier findings. A series of measurements on mixtures of water vapor and oxygen and ammonia and oxygen showed that the relaxation frequency (directly proportional to the inverse relaxation time) varied quadratically with the water vapor concentration, as was previously known, and varied linearly with the ammonia concentration. This was interpreted as being a result of the fact that for water vapor, a three-body collision involving two H_2O molecules and one O_2 molecule was most important, while for ammonia, binary collisions were most effective. All of these measurements, however, were devoted to determining the *relative* effect of gases of various types, and not much was known about the relaxation frequency of pure oxygen except that it was very low and that gas purity was of great importance.

A good portion of this early work reached its culmination in an excellent paper by H. and L. Knötzel.[4] In this work, both ammonia and water vapor were employed as agents to vary the relaxation frequency of oxygen. These measurements were carried out by means of an acoustic resonance tube which had an advantage over the reverberation technique in that the sound frequency could be easily varied, thus enabling the gas composition to be held fixed. Results of this work were qualitatively in agreement with those of Kneser and Knudsen, but were of considerably higher accuracy so that now an estimate could be made as to the relaxation frequency of pure oxygen. From the series of measurements using ammonia, the value obtained from an extrapolation to zero concentration of a least-squares fit to the data was 60 cps. A similar extrapolation for water vapor on the other hand gave 40 cps. The average of these two is 50 cps, corresponding to a relaxation time of 3.2 msec.

The present investigation was undertaken in an effort to see whether or not one would obtain the same results as Knötzel and Knötzel for the relaxation time of pure oxygen by using as catalyzing agents gases of fairly simple structure, thus allowing interpretation of the data to be more direct and straightforward. One difficulty with vapors such as H_2O and NH_3 is their ability to be adsorbed on solid surfaces, thus making it difficult to accurately determine amounts present at low concentration. Furthermore, these molecules structurally are rather complex and are, therefore, capable of being excited in many different internal modes. Another difficulty presents itself when one tries to establish a model of the intermolecular forces between oxygen and these molecules in order to relate experimental data to theory.

From the investigations of Kneser and Knudsen,[3] it is known that molecules such as hydrogen and helium can, by virtue of their small mass, bring about a

* This work is supported by the Bureau of Ordnance, Department of the Navy, under contract.

[1] V. O. Knudsen, J. Acoust. Soc. Am. **3**, 126 (1931).

[2] H. O. Kneser, J. Acoust. Soc. Am. **5**, 122 (1933).

[3] H. O. Kneser and V. O. Knudsen, Ann. Phys. **21**, 682 (1934/35).

[4] H. and L. Knötzel, Ann. Phys. **2**, 393 (1948).

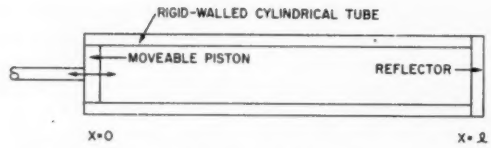

FIG. 1. Simplified diagram of the resonance tube.

shortening of relaxation times of heavier molecules. Both H_2 and He are simply constituted and, furthermore, cannot be excited internally at ordinary temperatures, thus making them ideal tools to use in the investigation of collisional excitation of vibration in O_2. Also, the problems associated with the condensation of vapors is avoided, thus making concentration measurements direct and simple.

Since the acoustic resonance tube as used by Knötzel and Knötzel is fairly uncomplicated and proved itself a reliable means of making relaxation time measurements, it was decided to follow their method. Several modifications, however, have been introduced and they will be pointed out in the next section.

II. APPARATUS

A. Theory of Operation

Ideally, an acoustic resonance tube consists of a hollow cylinder, circular in cross section, having infinitely rigid walls with an inflexible, movable piston closing one end and a perfect reflector the other (see Fig. 1). The piston is driven sinusoidally to and fro in the direction of the tube axis, and the plane sound waves thus generated travel down the tube, strike the reflector, reverse direction, and finally return to the piston. If the phase of the wave when it returns is equal to that at initiation, then energy may be fed from the piston into the gas and a system of standing waves or so-called "organ pipe oscillations" generated. The condition to be satisfied for the production of these standing waves is that an integral number of half wavelengths be contained in the tube length, i.e.,

$$\lambda_n = 2l/n; \qquad n=1, 2, 3, \cdots, \tag{1}$$

or, in terms of frequency,

$$f_n = n(c/2l) = nf_a, \tag{2}$$

where f_a is the fundamental frequency and c is the velocity of sound in the gas contained by the tube.

More specifically, it can be shown that if U is the amplitude of the velocity with which the piston is driven, then the sound pressure within the tube is

$$p(x, t) = -j\rho_0 cU\frac{\cos k(l-x)}{\sin kl}e^{j\omega t} = -jPe^{j\omega t}, \tag{3}$$

where $\omega=2\pi f$ and $k=\omega/c$.

We note from Eq. (3) that, under conditions of frequency for which $\sin kl$ vanishes, P becomes infinite, corresponding to the situation already noted in Eqs. (1) and (2). This, however, holds only for a dissipationless medium, which, needless to say, is an idealization; nevertheless, it happens under certain circumstances that the dissipation is rather small and in these cases the sound field within the tube can become very large indeed.

For the sound pressure at the reflector, we have from Eq. (3),

$$P_e = \rho_0 cU \sin^{-1} kl, \tag{4}$$

which, if we allow k to be complex, i.e.,

$$k=\beta-j\sigma, \tag{5}$$

to account for dissipation, may be written

$$|P_e| = \rho_0 cU[\sin^2\beta l + \sinh^2\sigma l]^{-\frac{1}{2}}. \tag{6}$$

Confining ourselves to the vicinity of the nth resonance,

$$\beta l = (2\pi f/c)l = (2\pi l/c)(f-f_n)+n\pi, \tag{7}$$

and imposing the restriction $\sigma l \ll 1$ (i.e., small absorption) along with

$$(2\pi l/c)(f-f_n) \ll 1, \tag{8}$$

we have

$$|P_{en}| = (\rho_0 c^2 U/2\pi l)[(f-f_n)^2+(\sigma c/2\pi)^2]^{-\frac{1}{2}}. \tag{9}$$

This is a bell-shaped curve disposed symmetrically about the resonant frequency with a width varying directly as the magnitude of σ. Equation (9) may be further written as

$$|P_{en}|/|P_{en}|_{\max} = \{[(2\pi/\sigma c)(f-f_n)]^2+1\}^{-\frac{1}{2}}. \tag{10}$$

The two frequencies for which this ratio falls to $1/\sqrt{2}$ are called the "half-power points" and lie at equal distances above and below the point of resonance. From Eq. (10), we see that the frequency separation of these power points is

$$\delta = \sigma c/\pi. \tag{11}$$

Thus, the sound absorption in the gas may be directly determined from a measurement of δ.

Before proceeding further, it might be well to examine the approximations leading to Eq. (11). Within the half-power frequencies, the inequality (8) is satisfied as long as $\sigma l \ll 1$ or, conversely, $\sigma l \ll 1$ as long as

$$(2l/c)\delta \ll 2/\pi,$$

which from Eq. (2) means that

$$\delta/f_a \ll 2/\pi.$$

Thus, we can vouch for the validity of Eq. (11) as long as the width of the resonance curve in cps is much smaller than the fundamental frequency.

Sound absorption within the tube may arise in three different ways. The first is a result of the effects of viscosity and heat conductivity in the interaction of the plane sound waves with the walls of the tube. Viscosity

causes the walls to exert a frictional drag on the sound wave, with a consequent loss in momentum; heat conductivity, on the other hand, gives rise to a loss in thermal energy. The theory generally accepted as correctly accounting for these losses is that of Helmholtz and Kirchhoff,[5] which gives for the sound absorption coefficient

$$\sigma_w=[(\eta\pi)^{\frac{1}{2}}/R]\{1/\gamma^{\frac{1}{2}}+(\kappa/\eta c_v)^{\frac{1}{2}}[(\gamma-1)/\gamma]\}(f/p_0)^{\frac{1}{2}}, \tag{12}$$

where η is the coefficient of viscosity, κ is the coefficient of heat conductivity, γ is the ratio of specific heats, c_v is the specific heat at a constant volume per gram, R is the tube radius, and p_0 is the equilibrium pressure. This formula, it should be pointed out, takes into account only losses arising at the cylindrical surfaces of the tube and does not include end effects. An approximate calculation indicates that, upon reflection, the amplitude of the wave is diminished by a factor

$$\Omega=\exp\{-2(\pi\kappa/c_v)^{\frac{1}{2}}[(\gamma-1)/\gamma](f/p_0)^{\frac{1}{2}}\}=\exp(-\theta). \tag{13}$$

This is to be compared with the factor $e^{-\sigma wl}$ giving the diminution caused by the lateral surfaces. The ratio $\theta/\sigma wl$ turns out to be R/l, approximately, which for the tube used here is about 3%.

Viscosity and heat conduction also may cause a loss in the body of the gas quite independently of the existence of any boundaries. For this type of loss, the resultant coefficient of absorption is, according to Stokes and Kirchhoff,[6]

$$\sigma_b=(2\pi^2\eta/\gamma c)\{\tfrac{4}{3}+[(\gamma-1)/\gamma](\kappa/\eta c_v)\}(f^2/p_0). \tag{14}$$

In general, the volume effects of viscosity and heat conductivity are small unless one goes to rather high frequencies. At the highest frequency used here (i.e., $\sim$3200 cps) we have

$$\sigma_b/\sigma_w\simeq 2\times 10^{-3},$$

so that this type of loss may be completely ignored.

Thirdly, absorption of energy may take place due to a difference in the rate of approach to equilibrium of the internal degrees of freedom compared to the translational degrees whenever the state of the gas is changed. In general, the rotational degrees of freedom reach equilibrium very quickly (i.e., in less than 10 collisions), however, vibration may require under certain conditions as many as 10^6 or more collisions. Thus vibration, in general, exhibits a very large dynamic separation from the other degrees of freedom.

The absorption occurring in such a process may be written[6]

$$\sigma_v=(\pi c/c_0^2)(RC_i/C_p^{\infty}C_v^0)[f_0f^2(f_0^2+f^2)]. \tag{15}$$

Here c_0 is the limiting sound velocity for frequencies sufficiently low that the internal degree of freedom under consideration participates fully, C_i is the specific heat of the internal degree of freedom, C_v^0 is the specific heat at constant volume including C_i, i.e.,

$$C_v^0=C_v^{\infty}+C_i,$$

and $C_p^{\infty}=C_v^{\infty}+R$ is the specific heat at constant pressure excluding C_i. The quantity f_0 is called the relaxation frequency and is related to the relaxation time τ by the relation

$$f_0=(1/2\pi\tau)(C_p^0/C_p^{\infty}). \tag{16}$$

For oxygen at room temperature, $C_i\ll C_v^{\infty}$, and Eqs. (15), (16) may be written

$$\sigma_v=(\pi/c)(RC_i/C_p^{\infty}C_v^{\infty})[f_0f^2/(f_0^2+f^2)], \tag{17}$$

and also

$$f_0=(1/2\pi\tau). \tag{18}$$

Since here we are dealing with relatively low frequencies and thus small absorptions, we assume that the total absorption may be written merely as the sum of the individual contributions, i.e.,

$$\sigma=\sigma_w+\sigma_v. \tag{19}$$

Thus, by Eq. (11)

$$\delta=c\sigma/\pi=\delta_w+\delta_v, \tag{20}$$

and

$$\delta_v=(RC_i/C_p^{\infty}C_v^{\infty})[f_0f^2/(f_0^2+f^2)]. \tag{21}$$

We shall use this last expression in determining relaxation times from measurements of the width of resonances.

B. Mechanical Details

The apparatus used is essentially that of Knötzel.[7] One of the main differences, however, is that the tube used here did not have to be placed inside a second container to make it vacuum tight and was therefore much more accessible than the arrangement used by Knötzel.

The central component of the resonance tube was a precisionbore Pyrex glass cylinder having an inner diameter of 2.005±0.002 in., a wall thickness of $\frac{1}{4}$ in., and a length of $29\frac{5}{8}$ in. Both ends of the tube were ground and polished to make smooth seats for two neoprene gaskets, sealing heavy brass flanges to either end. These flanges were held in position by four tension rods which pulled one flange against the other and thus against the two gaskets. The tension rods were acoustically isolated from the flanges by thick rubber bushings, thus minimizing any sound transmission via this

[5] Lord Rayleigh, *Theory of Sound* (Dover Publications, New York, 1945), Chap. XIX.

[6] K. F. Herzfeld, *Thermodynamics and the Physics of Matter*, (Princeton University Press, Princeton, New Jersey, 1955), Vol. 1, Sec. H.

[7] H. Knötzel, Akust. Z. **5**, 245 (1940).

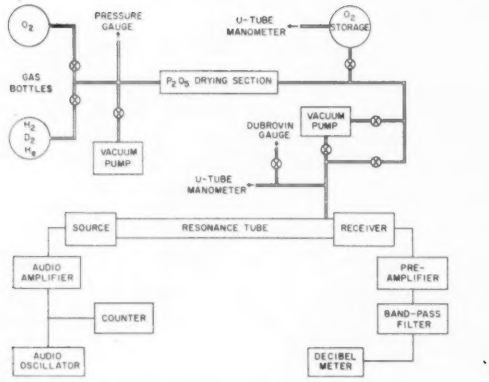

FIG. 2. Arrangement of the electronic and gas handling system.

path. Because of the flanges, the over-all length of the tube was increased to $31\frac{1}{2}$ in.

To one of the flanges was bolted the sound source and to the other the receiver. The sound source consisted of a cylindrical brass piston $1\frac{1}{2}$ in. in diam and 1 in. long, suspended $\frac{1}{4}$ in. from either end by two 0.010-in. thick circular brass membranes. The piston-suspension assembly was built as an integral part of a vacuum-tight housing containing the piston. Acoustic excitation was supplied to the piston through a bellows by an externally situated Goodmans VR-II electromagnetic shaker.

An Altec 21-BR 180–1 condenser microphone was used as the receiving element. A vacuum-tight system was obtained by flush mounting the condenser microphone in a $\frac{1}{4}$-in. thick circular reflector plate which, in turn, was securely fastened to one end of a thick-walled brass housing. Electrical leads to the preamplifier, built as an integral part of the microphone, were introduced into the housing through kovar seals. The microphone housing was then securely fastened to one of the flanges, a flat neoprene gasket insuring a good seal. A valve, externally actuated through a bellows to permit evacuation and filling of the tube, was also built into the receiving end. Since the valve opening was in the reflector plate, it was necessary, in order to achieve an acoustically-tight system, to seat the valve stem against the back side of the reflector by means of a neoprene O ring.

After carefully assembling the apparatus and outgassing for a day or two, a pressure of a few tenths of a micron could be achieved. The leak rate was 8–9 μ/hr, which was more than sufficient for the measurements carried out here.

C. Electronic

A General Radio Interpolation Oscillator was used as a signal generator. This gave good frequency stability and had the advantage that frequency increments of up to 10 cycles either side of a central frequency could be ready directly from a vernier scale. Accuracy of an individual reading was 0.05 cycles with a maximum error of twice this in reading the width of a resonance. Signals from the oscillator were amplified by a McIntosh audio amplifier and then fed to the electromagnetic driver. The output of the condenser microphone was fed into a General Radio 1551-P1 preamplifier and then through a Krohn-Hite band-pass filter into a Ballantine RMS voltmeter.

In making a measurement, the frequency was varied until a resonance was obtained and then the gain of the driving amplifier adjusted to give a microphone output sufficient to produce a fullscale reading of 10 db on the Ballantine meter. The frequency was then varied either side of resonance by means of the oscillator vernier control until the reading dropped to 7 db, these frequency increments being recorded along with the resonant frequency. A Berkeley counter was used to measure the central frequency.

The combined noise level and level caused by signals transmitted along paths other than the gas column was 30 db or more below the value at resonance. Furthermore, the structure of the resonance curve was investigated by changing the frequency either side of resonance in increments of 0.5 cycles up to a total change of 10 cycles and simultaneously recording the meter output. The results were found to be in good agreement with the predictions of Eq. (10).

A block diagram of the electronic and other apparatus is shown in Fig. 2.

D. Gas Handling System

All gases admitted to the resonance tube were first dried by passing them through two 4-ft long columns containing phosphorus pentoxide. In preparing the tube for a run, the hydrogen, deuterium, or helium gas was first let into the tube until the desired pressure was attained. This pressure was in all cases less than 20 mm and was measured by means of a Dubrovin gauge for pressures greater than 1 mm and by means of a McLeod gauge for smaller pressures. The resonance tube was then closed off and the supply lines and drying columns evacuated. Oxygen was then flushed through the system for several minutes and finally admitted to a pre-evacuated storage vessel. After the pressure in this vessel reached atmospheric, a stopcock was opened to allow the oxygen to flow into the resonance tube. In this manner, the possibility of any back diffusion of the hydrogen or any of the other light gases into the supply lines was strictly reduced. The total pressure of the mixture was measured by means of a mercury U tube manometer and was on all runs 750 ± 3 mm.

Purity and sources of the gases used are as follows:

1. Oxygen—Obtained from liquified air so as to have a minimum hydrogen content. Water vapor content was less than 26 ppm. Stated purity was $>99.5\%$ with

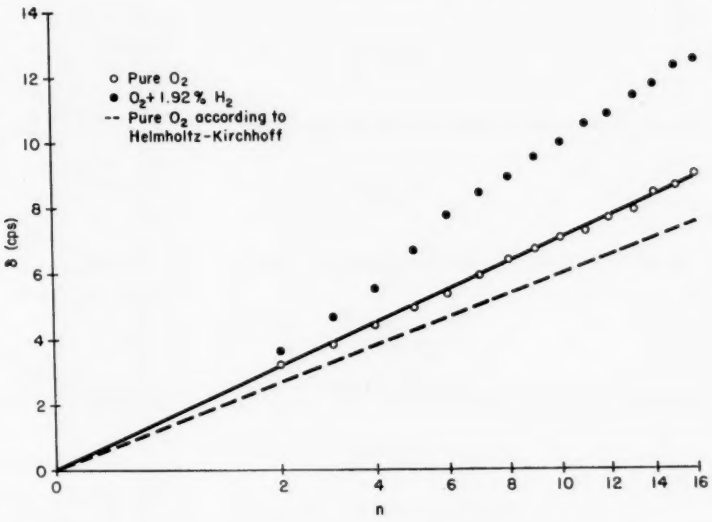

FIG. 3. Absorption in pure oxygen and the effect of adding a small amount of hydrogen.

main impurities being nitrogen and argon. Supplied by Southern Oxygen Company.

2. Hydrogen—Electrolytic with a purity >99.8%. Supplied by The Matheson Company.

3. Deuterium—Purity >99.5%. Obtained from General Dynamics Corp., Liquid Carbonic Division.

4. Helium—Purity >99.9%. Furnished by U.S. Navy.

E. Temperature

The temperature was fixed by the surrounding thermostatically-controlled air temperature. This was on all runs set to 23°C with a fluctuation of no more than ±0.2°C during any particular run.

III. RESULTS

A. Pure Oxygen

The first set of runs was devoted to a determination of absorption in pure oxygen. A typical set of data obtained is shown in Fig. 3. Here we have plotted δ, the resonance width, vs the mode number n on a $\sqrt{n}$ scale. As can be seen from the figure, the variation of δ with $\sqrt{n}$ is linear, indicating that for pure oxygen, only absorption resulting from boundary effects is important [see Eq. (12)]. Quantitatively, we have

$$\delta = 2.23\sqrt{n}.$$

Three such runs were made prior to commencing the series of experiments with mixtures and one after their conclusion. These four runs all gave straight lines, their slopes agreeing to within a fraction of a percent.

Substitution of the appropriate data[8] into Eq. (12) gives

$$\delta_{\text{th}} = 1.87\sqrt{n}.$$

Thus, the experimental values of δ exceed the theoretical by 19%. An explanation of just why there should be a discrepancy of this magnitude is not readily available. In an effort to obtain an insight into the difficulty, a series of measurements was made using, in addition to oxygen, three monatomic (He, Ne, Ar) and three diatomic (H_2, CO, N_2) gases. Results of these experiments show that:

1. In all cases the variation of δ with $\sqrt{n}$ is linear; however, experimental values always exceed the theoretical, with discrepancies ranging from a minimum of 6.5% for He to a maximum of 30% for Ar.

2. The discrepancy is a monotonically increasing function of the molecular weight, or, since the pressure was the same in all cases, the density.

A discrepancy somewhat over 14% appeared in the measurements of Knötzel and Knötzel. Mariens[9] reports an excess of 13% for air using a tube of similar dimensions to that used here. Other investigators working at pressures near atmospheric and using tubes several inches in diameter have also measured excesses.[10] Lagemann and Shields,[11] however, report values agreeing very well with Eq. (12). It is to be noted, however, that they worked at lower pressures and with a tube of fairly small diameter.

In any case, the data appearing in Fig. 3 serve to establish a base to which all other absorption measurements can be referred when effects of relaxation are present.

[8] "Tables of Thermal Properties of Gases," Natl. Bur. Standards Circ. No. **564**, 1955.

[9] P. Mariens, J. Acoust. Soc. Am. **29**, 442 (1957).

[10] H. Oberst, Akust. Z. **2**, 76 (1937).

[11] F. D. Shields and R. T. Lagemann, J. Acoust. Soc. Am. **29**, 470 (1957).

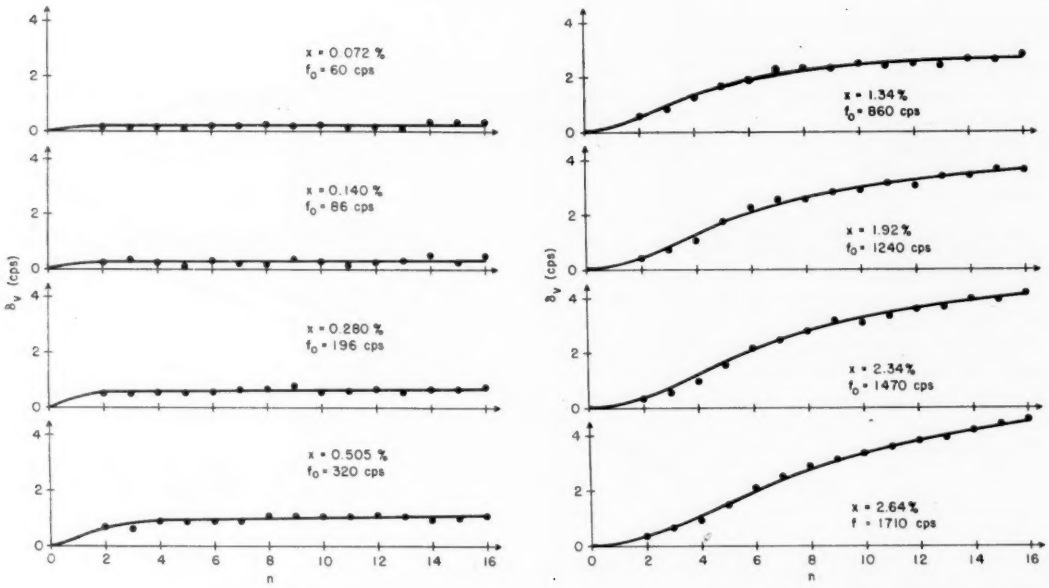

FIG. 4. Absorption due to vibrational effects in various mixtures of oxygen and hydrogen.

The frequency of the fundamental resonance was 203.0 cycles for pure oxygen. This frequency rose slightly with the addition of light gases, the maximum being 205.6 cycles for a hydrogen concentration of 2.64%.

B. Oxygen-Hydrogen

In accordance with the earlier work of Kneser and Knudsen, it was found that small amounts of H_2 can cause considerable shortening of the vibrational relaxation time of oxygen. Referring once again to Fig. 3, we see the effect of adding approximately 2% H_2 to oxygen. By subtracting the already determined wall loss component, we obtain the absorption due to vibrational relaxation effects alone. This was done for eight different concentrations x of H_2 and the results appear in Figs. 4(a,) and (b). The quantities C_i and f_0 used in fitting theoretical curves to the data were determined by plotting f^2/δ_v vs f^2, which from Eq. (21) should be a straight line with a slope

$$S=(C_p^\infty C_v^\infty/RC_i)(1/f_0), \tag{22}$$

and a zero intercept

$$I=(C_p^\infty C_v^\infty/RC_i)f_0. \tag{23}$$

Combining Eqs. (22) and (23), we find that

$$f_0=(I/S)^{\frac{1}{2}}, \tag{24}$$

and that

$$C_i/R=[1/(IS)^{\frac{1}{2}}](C_p^\infty/R)(C_v^\infty/R). \tag{25}$$

The data when plotted in this fashion actually did give straight lines, and the resultant values of I and S for the four highest concentrations were determined by a least-squares fit. For lower concentrations, where measurement error becomes a larger percent of the measured values, this method was rather ineffective; hence, an asymptotic fit was used, since in these cases the relaxation frequencies are lower than the lowest frequency used, and δ_v has reached its limiting value for the higher modal numbers. This limiting value is

$$\delta_{v\infty}=(RC_i/C_p^\infty C_v^\infty)f_0. \tag{26}$$

Using the values of $RC_i/C_p^\infty C_v^\infty$ obtained from measurements at the higher concentrations, f_0 may be determined immediately. Values of C_i/R obtained are presented in Table I.

The average value is 2.90×10^{-2} and agrees quite well with the value 2.97×10^{-2} calculated from the Planck-Einstein formula.[12] In Fig. 5 appears a plot of the relaxation frequency vs hydrogen concentration. Clearly, the experimental values indicate a linear dependence of f_0 on x, showing that binary collisions control the excitation process. The line appearing in the figure is a least-squares fit. Extrapolation of this curve to zero concentration, corresponding to the case of pure O_2, gives a relaxation frequency of 8.8 cycles or

[12] It should be pointed out that this value was obtained by using $\Theta=hc\omega/k=2239°K$ and not the generally quoted value $\Theta=2228°K$. The latter value is obtained by using the pre-1937 values of the physical constants which give $hc/k=1.432$ while the post-1937 values give 1.439. In both cases, ω is taken to be 1556 cm^{-1}.

a relaxation time $\tau_v(0, 0) = 1.8 \times 10^{-2}$ sec. However, it should rapidly be pointed out that the rms deviation is approximately equal to this value so that this figure is not to be taken as exact. In any case, one can say with certainty that the relaxation frequency is less than 20 cycles, i.e., $\tau_v(0, 0) > 8 \times 10^{-3}$ sec. Thus, the relaxation time of pure oxygen as determined by these measurements is substantially larger than the 3.2×10^{-3} sec obtained by Knötzel and Knötzel. If we assume for pure O_2 that f_0 is 8.8 cycles, we find from the slope of this curve that H_2 is 7200 times more effective in exciting vibration in oxygen than oxygen itself. This effectiveness of H_2 in shortening the relaxation time is partly a result of the fact that the hydrogen raises the collision rate, and also because an O_2–H_2 collision, on the average, produces greater excitation of vibration than an O_2–O_2 collision.

Oxygen-Deuterium and Oxygen-Helium

Measurements were made using a mixture of oxygen and 2.64% deuterium, and also oxygen and 2.63% helium. The results are shown in Fig. 6. It is quite clear from this figure that both helium and deuterium shorten the relaxation time of oxygen, but that the shortening is much smaller than with hydrogen. It is further evident that both these gases have almost exactly the same effect, the relaxation frequency for the D_2–O_2 mixture being 124 cycles and that of the He–O_2 mixture, 130 cycles. Referring these numbers to the value 8.8 cycles for pure oxygen and assuming a linear dependence of the relaxation frequency on concentration, we find that (1) deuterium is 530 times as effective as oxygen and that (2) helium is 560 times as effective. Comparing these values with the results of part B, we see that H_2 is about ten times as effective as either D_2 or He.

TABLE I. Vibrational specific heat of oxygen at 23°C.

Percentage of H_2 added	$C_v/R \times 10^2$
1.34	2.89
1.92	2.88
2.34	2.92
2.64	2.92

IV. DISCUSSION

One rather significant result of this investigation is the fact that both helium and deuterium have about the same effect in exciting vibration in oxygen. This suggests that the effectiveness of these gases is determined, to a large extent, by their mass. Thus, the reason hydrogen is much more effective is because of its small mass. In making a supposition of this sort, it is of course, implied that the intermolecular force fields between oxygen and each of these gases is essentially the same, an assumption which would not seem unreasonable.

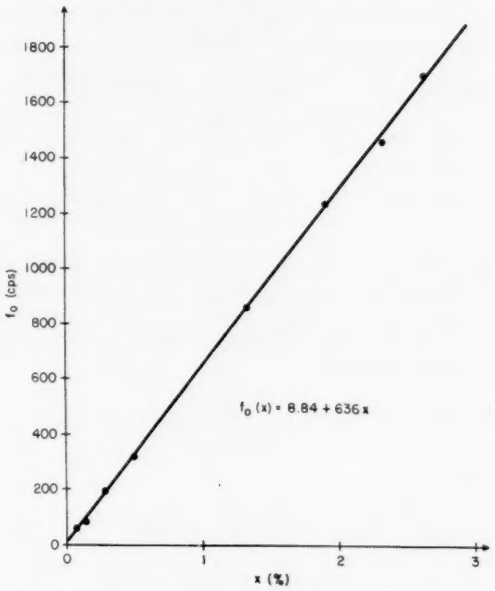

FIG. 5. Variation of the relaxation frequency with hydrogen concentration.

The equivalence of deuterium and helium clearly rules out the possibility of attributing the rather large effect of hydrogen to forces of a chemical nature. It also eliminates the rotational degrees of freedom of hydrogen or deuterium as being the responsible mechanism. This might otherwise be a possibility since in hydrogen there is a rather large spacing of the rotational levels which could bring about a significant energy exchange between vibration and rotation.

In interpreting the experimental results obtained here, we shall make use of a theoretical study published recently by the author.[13] Although said paper deals only with collisions of like molecules, the results

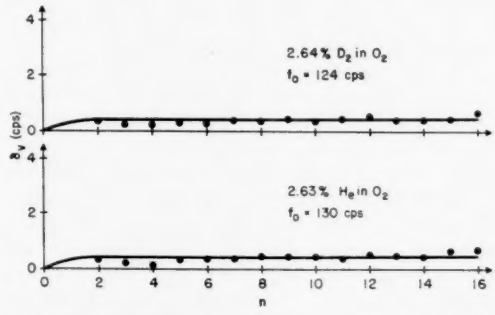

FIG. 6. Absorption resulting from vibrational effects in deuterium-oxygen and helium-oxygen mixtures.

[13] J. G. Parker, Phys. Fluids **2**, 449 (1959).

TABLE II. Relative collision rates and vibrational collision efficiencies.

Molecular pair	Relative collision rate	Relative vibrational collision efficiency
O_2-H_2	2.43	2.96×10^{3}
O_2-D_2	1.79	2.96×10^{3}
O_2-He	1.58	3.53×10^{3}

obtained may be extended without difficulty to binary gas mixtures. Denoting the components of the mixture as O and X, we have analogously to Eq. (68) of footnote 13, for the time rate of excitation of vibrational energy per oxygen molecule

$$dE_v/dt=(192/m)kT\{[\Gamma_{0,0}{}^2/\tau_c(o,o)]\kappa_{0,0}+[\Gamma_{0,x}{}^2/\tau_c(o,x)]\kappa_{0,x}\}, \quad (27)$$

where

$$\kappa_{0,x}=\mu_{0,x}\int_0^{\pi/2}F(\beta_{0,x}/\cos\Theta)\cos^3\Theta\sin\Theta d\Theta; \quad (28)$$

$$F(y)=(\pi y)^2\int_0^{\infty}\left[\frac{\cosh(2\zeta y/x)}{\cosh(\pi y/x)}\right]^2\operatorname{csch}^2(\pi y/x)\times\exp(-x^2)x^3dx, \quad (29)$$

in which

$$\zeta=\pi/2+\tan^{-1}(y/\beta^*x);$$

$$\beta_{0,x}=(\mu_{0,x}/2kT)^{\frac{1}{2}}(\omega_0/\alpha_{0,x}); \quad (30)$$

and finally

$$\Gamma_{0,x}=\left(\frac{2}{\alpha_{0,x}d^*}\right)\frac{I_2(\alpha_{0,x}d^*/2)}{I_0(\alpha_{0,x}d^*/2)}, \quad (31)$$

where the I's are modified Bessel functions. The quantity m is the atomic mass of oxygen, $\mu_{0,x}$ is the reduced molecular mass of the two component gas, T is the temperature, k Boltzmann's constant, and ω_0 the angular vibration frequency of the oxygen molecule.

Before proceeding further, it might be well to make a few remarks about the model of the intermolecular forces used in establishing the above equations. Each molecule is endowed with two centers of repulsion and one center of attraction. The center of attraction is assumed to be at the geometric center of the molecule; the centers of repulsion, on the other hand, are located on the nuclear axis, each a distance $d^*/2$ from the molecular center. It is then assumed that the force of repulsion exerted by repulsive centers of one molecule on those of another varies exponentially as the separation of these centers, with the constant α giving the rate of this variation. The attractive centers are assumed to behave similarly with respect to each other; however, in this case the constant is $\alpha/2$. Thus, the intermolecular potential used may be referred to as a generalized Morse potential. If we denote the energy giving the depth of the potential well caused by the attractive forces as E^*, we have

$$T^*=E^*/k,$$

and, referring to Eq. (30),

$$\beta^*=\beta(T^*).$$

In the light of the above discussion, it is then clear that the $\alpha_{0,0}$ gives the rate of variation of the molecular forces for an O_2–O_2 interaction and $\alpha_{0,x}$ that for an O_2–X interaction. Furthermore, the quantity d^*, being the separation of repulsive centers in the oxygen molecule itself, is independent of the interaction partner.

The quantities $\tau_c(0,0)$ and $\tau_c(0,x)$ are the mean collision times for an oxygen molecule colliding with other oxygen molecules and for an oxygen molecule colliding with a molecule of species X, respectively. For the ratio $\tau_c(0,0)/\tau_c(0,x)$, we have

$$\tau_c(0,0)/\tau_c(0,x)=\chi_{0,x}(p_x/p_0), \quad (32)$$

where p_0 and p_x are the partial pressures of oxygen and X, respectively, and χ, a quantity depending only on molecular parameters, measures the rate of collisions of the type $(0,x)$ relative to that of the type $(0,0)$. Using this equation, we may write Eq. (27) as

$$dE_v/dt=(192/m)[\Gamma_{0,0}{}^2/\tau_c(0,0)]\kappa_{0,0}\times[1+\chi_{0,x}(p_x/p_0)(\Gamma_{0,x}/\Gamma_{0,0})^2(\kappa_{0,x}/\kappa_{0,0})]. \quad (33)$$

The relaxation time of the mixture is thus

$$\tau_v(0,x)=\frac{\tau_v(0,0)}{[1+\chi_{0,x}(p_x/p_0)(\Gamma_{0,x}/\Gamma_{0,0})^2(\kappa_{0,x}/\kappa_{0,0})]}, \quad (34)$$

where $\tau_v(0,0)$ is the relaxation time for pure oxygen, i.e.,

$$\tau_v(0,0)=(m/192)[\tau_c(0,0)/\Gamma_{0,0}{}^2]\times\left(\frac{h\nu/kT}{[\exp(h\nu/kT)-1]}\right)(1/\kappa_{0,0}). \quad (35)$$

In terms of the relaxation frequency, Eq. (34) becomes

$$f_0(0,x)=f_0(0,0)[1+\chi_{0,x}(p_x/p_0)(\Gamma_{0,x}/\Gamma_{0,0})^2(\kappa_{0,x}/\kappa_{0,0})]. \quad (36)$$

Hence, if J is the slope of the curve of relaxation frequency vs concentration, we have from Eq. (36) that

$$J_{0,x}=\chi_{0,x}(\Gamma_{0,x}/\Gamma_{0,0})^2(\kappa_{0,x}/\kappa_{0,0}). \quad (37)$$

As an approximation to $\chi_{0,x}$, we take[14]

$$\chi_{0,x}=(D_{0,x}/D_{0,0})^2(\mu_{0,0}/\mu_{0,x})^{\frac{1}{2}}, \quad (38)$$

where the μ's are the reduced masses and the D's the molecular diameters. Using the combining law

$$D_{0,x}=\tfrac{1}{2}(D_{0,0}+D_{x,x}), \quad (39)$$

[14] R. H. Fowler, *Statistical Mechanics* (Cambridge University Press, New York, 1955), 2nd ed., p. 665.

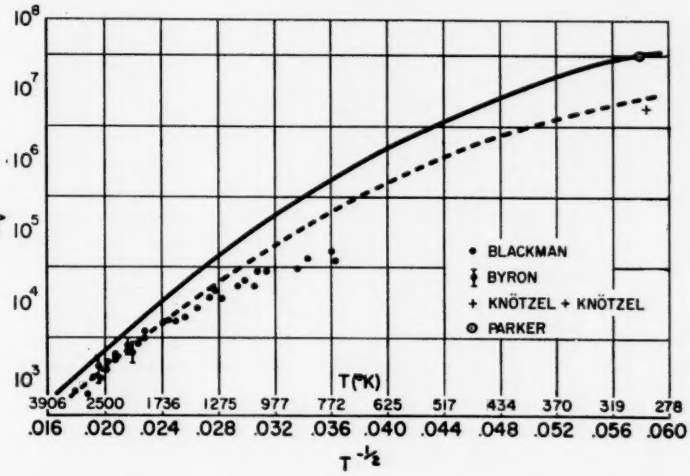

FIG. 7. Variation of experimental and theoretical values of the vibrational collision number with temperature.

and making use of experimental data on intermolecular interaction potentials,[15] we arrive at the values for the relative collision rate $\chi_{0,x}$ shown in Table II. Also in Table II have been included values of the relative vibrational collision efficiency $J_{0,x}/\chi_{0,x}$.

It has been possible to reduce the rather complex expression for $\kappa_{0,x}$ as it appears in Eq. (28) to a fairly straightforward approximate expression, which, within the limits of its validity, agrees very well with numerical calculations. This approximation gives

$$\kappa_{0,x}=(4\pi/3)^{\frac{1}{2}}\mu_{0,x}\{1+[1/2(\pi\beta)^{2/3}]\}(1-\tfrac{3}{2}q)(\pi\beta)^{7/3} \times\exp[-3(\pi\beta)^{2/3}(1-q)], \quad (40)$$

where

$$q=(4/3\pi)(T^*/T)^{\frac{1}{2}}(\pi\beta)^{-1/3},$$

for which the condition

$$\pi\beta^*>(\pi\beta)^{2/3}>1$$

must be satisfied. It is interesting to note in Eq. (40) that the dependence of $\kappa_{0,x}$ on the potential well depth is given essentially by the factor

$$\exp[3(\pi\beta)^{2/3}q]=\exp[(4/\pi)(T^*/T)^{\frac{1}{2}}(\pi\beta)^{1/3}].$$

In Fig. 7 is presented a plot of the number of collisions $Z_v=\tau_v/\tau_c$ to establish vibrational equilibrium in pure oxygen vs $T^{-\frac{1}{2}}$, where T is the temperature in degrees Kelvin. Data in the temperature range 700–3000°K was obtained by means of the shock tube.[16,17] The dotted curve was calculated from Eq. (35) by choosing values of α and d^* which when substituted into this equation give agreement with experimental data in the limit of high temperature where this data would be expected to be most reliable. However, as pointed out in footnote 13, these values of α and d^* must also predict the correct rotational relaxation time. Subject to these conditions, we find the best choice of α and d^* to be

$$\alpha=4.10\ \text{A}^{-1}$$

and

$$d^*=0.605\ \text{A}.$$

Surprisingly enough, when this curve is extended to room temperature, it is in good agreement with the value given by Knötzel and Knötzel.

The measurements presented in this paper, as mentioned above, differ considerably with Knötzel and Knötzel, giving a higher value for the vibrational collision number. The solid curve in Fig. 7 was obtained by readjusting α and d^* to agree with the present results, but keeping the rotational relaxation time the same as that given in footnote 12 (i.e., $Z_r^\infty=14.4$ coll.). Values of α and d^* used were

$$\alpha=3.85\ \text{A}^{-1}$$

and

$$d^*=0.623\ \text{A},$$

being only slightly different from the above; however, α is now smaller, thus suggesting that the repulsive core of the oxygen molecule is somewhat softer than before. From these values, we obtain for ϵ, the quantity measuring the departure of the repulsive field from spherical,

$$\epsilon=0.290.$$

Thus, the length to width ratio of the repulsive core is

$$(1+\epsilon/1-\epsilon)=1.82.$$

As may be seen from Fig. 7, the solid curve gives values of Z_v at high temperatures which are consistently higher than the shock tube measurements, however, approaching these values asymptotically.

[15] J. O. Hirschfelder, C. F. Curtiss, and R. B. Bird, *Molecular Theory of Gases and Liquids* (John Wiley & Sons, Inc., New York, 1954), pp. 1110–1111.
[16] V. Blackman, J. Fluid Mech. **1**, 61 (1956).
[17] S. Byron, J. Chem. Phys. **30**, 1380 (1959).

TABLE III. Values of $\alpha_{0,x}$ derived from experimental data.

Molecular pair	T^*(°K)	$\alpha_{0,x}$(A^{-1})
O_2-O_2	90	3.85
O_2-H_2	56	2.58
O_2-D_2	56	2.88
O_2-He	30	2.94

The fact that the shock tube data falls far below both of these curves at lower temperatures indicates that some sort of difficulty is present. Extrapolation of this data to room temperature, for example, gives values which disagree very strongly with both the Knötzels' data and that obtained here.

Using values of $\Gamma_{0,0}$ and $\kappa_{0,0}$ calculated by taking for $\alpha_{0,0}$ and d^* the above revised numbers, we may determine values of $\alpha_{0,x}$ required to bring the theoretical and experimental vibrational collisional efficiencies into agreement. To do this, it is necessary to make an assumption as to the value of T^* for a dissimilar interaction. Here we shall use the conventional combining law

$$T^*(0, x) = [T^*(0, 0)\, T^*(x, x)]^{\frac{1}{2}},$$

with values of T^* for similar interactions obtained from footnote 15. Values of $\alpha_{0,x}$ obtained appear in Table III along with those of $T^*(0, x)$.

As is readily apparent, values of α for dissimilar collision partners are substantially smaller than the O_2–O_2 value. This suggests that the interaction of oxygen with the light elements is relatively soft. Just why this should be is not obvious since values of α for interaction of similar light molecules are approximately the same as that for the O_2–O_2 interaction. This being the case, one might well suppose that for the dissimilar interaction, α should be something like the arithmetic mean of the values for the separate similar interactions. It is possible, however that the relatively large disparity in electronic charge might in some way be responsible. For a collision of given relative kinetic energy between, say, hydrogen and oxygen, the disturbance of the electronic configuration of the hydrogen molecule is bound to be much more severe than that of oxygen since the latter has many more electrons among which to distribute the interaction. If the orbital electrons of hydrogen are sufficiently disturbed, an attraction between hydrogen nuclei and orbital electrons of oxygen could take place with a consequent softening of the interaction.

ACKNOWLEDGMENT

The author would like to express his appreciation to all members of the Fluid Mechanics Laboratory who aided in this work, particularly Dr. H. J. Unger.

Delineation of the Problem of Soret Diffusion

R. A. ORIANI

Edgar C. Bain Laboratory for Fundamental Research, U. S. Steel Corporation Research Center, Monroeville, Pennsylvania

(Received October 12, 1960)

The phenomenological heat of transport is analyzed for the simple cases of self-diffusion via a vacancy mechanism and of diffusion of solutes in interstitial solid solutions. The heat of transport is shown to be equal to the sum of an energy-conversion term and an energy-transport term. The latter is a function of the details of the mechanism and is of kinetic character; a positive contribution is made to it by the localized normal modes about a solute atom. The energy-conversion term has a thermodynamic character once the diffusion mechanism is specified, and by its use one can decompose energies of solution or of vaporization into a part associated with the solute atom and another part associated with the solvent lattice.

IF a temperature gradient is imposed upon an initially homogeneous solid or liquid solution, an unmixing will be observed such that the hotter portion of the specimen will become enriched in one of the components. This phenomenon, the analog of thermal diffusion in gases, is known as the Ludwig-Soret effect. It cannot be understood from equilibrium considerations, but rather depends upon the mechanism of the unit step in diffusion; as such, investigation of the Soret effect would appear to furnish a valuable means toward the elucidation of the details of the diffusion process.

The thermodynamics of irreversible phenomena[1] shows that the magnitude and sign of the Soret effect at steady state can be expressed in terms of the phenomenological quantity, the heat of transport Q^*_i. This is the total energy transported less the enthalpy. This quantity is the amount of heat $\mathbf{J}_q$ transported across a reference plane as a consequence of unit material flux $\mathbf{J}_i$ for the ith species at $\nabla T=0$; thus, $\mathbf{J}_q=Q^*_i\mathbf{J}_i$. A complementary and more operational definition of Q^*_i is[1] that it is the heat that must be furnished to the region of origin of the jumping atom in order to maintain that region at constant temperature. For simplicity, we will restrict our considerations to cases where only one component diffuses, i.e., either self-diffusion or interstitial solute diffusion in interstitial solid solutions. Following Alexander,[2] the material fluxes may be referred to frames of reference fixed in the immediate surroundings of the jumping atom, so that the Q^*_i are independent of each other. Physically, one can see why the sign of the heat of transport controls the sign of the enrichment of that component in the temperature gradient by considering the extended LeChatelier principle. If $Q^*_i>0$, that is, if the jumping atom takes heat along with it, then its jump will be statistically biased towards the lower-temperature side where the excess heat can be more easily dissipated away. The converse statement holds for $Q^*_i<0$.

In atomistic terms, it seems clear that the basic problem of Soret diffusion is that of the momentum transfer between the asymmetric phonon distribution and the mobile atoms. Because this problem seems unapproachable at present, the Soret phenomenon has been qualitatively considered in terms of a distribution of the activation energy for diffusion between the jumping atom and the lattice.[3] More recently, the writer[4] has discussed the role of localized normal modes in the Soret phenomenon. Shewmon,[5] utilizing a kinetic treatment due to Wirtz,[6] has stressed the role of activation energy in preparing the lattice at the site into which the atom jumps. Allnatt and Rice[7] have analyzed thermal diffusion on the basis of the effect of a temperature gradient upon the mean displacement of a particle undergoing a random walk. Their clear result is that for the operation of the vacancy mechanism Q^* for the jumping atom equals the energy for migration of a vacancy, and that for diffusion of an interstitial solute, Q^* equals the heat of activation for its diffusion. Their result does not admit the possibility of a negative value of Q^* for an interstitial, which is what in fact has been experimentally observed for carbon[3,5] and nitrogen[3] in alpha-iron. It is clear that consideration of minor factors, such as correlation effects, leading to deviations from the assumption of a random walk, cannot change the inability of the calculation to agree, even as to sign, with these experimental results. In what follows, a qualitative analysis of the energetics entailed in the jumping of an atom is presented, the purpose of which is simply to delineate the problem clearly. An incidental result is that it proves possible to define energy changes for the lattice and for the dissolved atom separately, as well as to show how to obtain approximate values for such "part quantities" from the data of Soret diffusion and ordinary thermodynamics.

[1] S. R. deGroot, *Thermodynamics of Irreversible Processes* (Interscience Publishers, Inc., New York, 1951).
[2] K. F. Alexander, J. Appl. Phys. **21**, 446 (1955); Z. physik. Chem. (Leipzig) **203**, 181, 203, 213, 228 (1954).
[3] L. S. Darken and R. A. Oriani, Acta. Met. **2**, 841 (1954).
[4] R. A. Oriani in *Thermodynamic and Transport Properties of Gases, Liquids, and Solids*, ASME (McGraw-Hill Book Company, Inc., New York, 1959), p. 123.
[5] P. G. Shewmon, Acta Met. **8**, 605 (1960).
[6] K. Wirtz and J. W. Hiby, Physik Z. **44**, 369 (1943).
[7] A. R. Allnatt and S. A. Rice, J. Chem. Phys. **33**, 573 (1960).

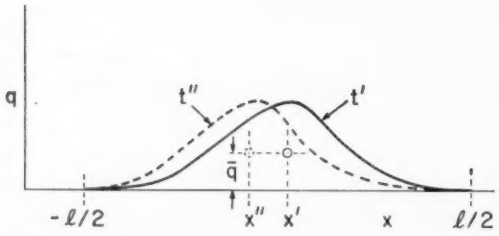

FIG. 1. Representations of the excess thermal energy q as a function of distance within the coordination sphere at the instant t' just before and at the instant t'' just after the last atom-vacancy interchange.

APPLICATION OF DYNAMICAL THEORY OF DIFFUSION TO SORET EFFECT

Rice[8] has modified the unimolecular dissociation model of Slater[9] to form the basis for the calculation of the diffusivity via a vacancy mechanism if the normal mode distribution can be specified. In Rice's development, the frequency of atom-vacancy interchange is equal to the frequency of occurrence of a configuration such that the atom in question has a sufficiently large amplitude of vibration properly oriented towards an adjacent vacancy and such that there is concomitantly an out-of-phase motion of the intervening atoms. Such a dynamic configuration is achieved by the chance contributions from many different normal modes so that, whereas the energy per normal mode does not change, the energy of any particular trajectory in the dynamic configuration does change. The large vibrational amplitude of an atom relative to an adjacent vacancy will be composed largely of the highest-frequency normal modes, but these, while necessary to accomplish a diffusive jump, are not sufficient. Also necessary are concomitant motions of the surrounding atoms in order to make space available to the central atoms, and such motions will be composed of normal modes of lower frequencies. The resulting wave packet, necessary to effect a diffusive jump, will sweep past a given volume element, and the time during which any one atom is affected by a wave packet will be much larger than the time during which that atom takes part in a half-wave of the highest-frequency vibration necessary for an atom-vacancy interchange. This can be seen by considering the phenomenon of beats between two waves having a frequency difference $\delta\omega$. The duration of a half-wave of the envelope of the constructive interference is $\pi/(\delta\omega)$, whereas the duration of a half-wave of the individual oscillation is π/ω. Hence, if one were to measure as a function of time the vibrational energy content of some local unit such as an atom or a bond between atoms, one would observe fluctuations, above and below the mean of $3kT$ per atom, the relaxation of which would be characterized on the average by a time τ much larger than the mean time of one atomic jump.

We now draw a sphere about one atom-vacancy pair such that the sphere contains all the atoms, the motions of which sensibly affect the motion of the atom-vacancy pair in question. We will call this the coordination sphere, and the rest of the lattice will serve only as a heat bath for this zone. Using as axis the sphere diameter that contains the atom-vacancy pair, we slice up the coordination sphere into slabs normal to that axis and of thickness Δx. Now we follow the vibrational energy content of each slab in the times before and after an atom-vacancy interchange within that coordination sphere. We do this repeatedly for many such diffusive jumps, and use the average results to construct a graph of the vibrational energy per slab less the mean thermal energy as a function of distance along the diffusion axis. Figure 1 represents such a plot for two instants, just before (t') the atom-vacancy interchange, and just afterwards (t''). Because this plot represents the statistical average situation, the sphere diameter l has a definite value; for the same reason, the curves will have unique shapes. During the duration of the inflow and outflow of excess vibrational energy, the atom-vacancy pair may change places many times, but only the last forward jump of the atom is effective; hence, the instants t' and t'' must be those that bound the last jump of the atom in the arbitrarily chosen forward direction.

It is now possible to define Q^* in terms of this diagram. Let $(\bar{q}',x')$ be the coordinates of the centroid of the $q(x)$ curve at t', and $(\bar{q}'', x'')$ those for the centroid of the $q(x)$ curve for t''. We note that $(t''-t')$ is of the order of 10^{-12}–10^{-13} sec, and is therefore $\ll\tau$. Consequently, the atom-vacancy interchange may be regarded as adiabatic as far as the coordination sphere is concerned, so that the area under the t' curve equals that under the t'' curve. Hence $\bar{q}'l=\bar{q}''l$, showing that the centroid, on the average, moves along a line parallel to the path of the jumping atom. Now, $\bar{q}'(x''-x')$ represents the thermal energy transported concomitantly with one atom-vacancy interchange, with reference to any plane normal to the diffusive jump; hence, $\bar{q}'(x''-x')=\mathbf{J}_q/\mathbf{J}$ where $\mathbf{J}_q$ and $\mathbf{J}$ are, respectively, the heat flux and the atom flux, both on a per sec per cm^2 basis. Consequently, $\bar{q}'(x''-x')=Q^*$.

We have noted that the definition of Q^* does not depend upon the specification of any one plane of reference; any plane will do as long as it is parallel to the plane across which $\mathbf{J}$ is measured. However, simple considerations lead to a natural specification of a plane of reference which simplifies subsequent discussion. We note, first of all, that because of the adiabatic nature of the processes within the coordination sphere, whatever energy changes take place as the atom leaves its initial site must be reversed as the atom arrives at its final site. We note also that this inversion-mirror symmetry is associated with the inversion of the atom-vacancy pair.

[8] S. A. Rice, Phys. Rev. **112,** 804 (1958).
[9] N. B. Slater, Proc. Roy. Soc. (London) **A194,** 112 (1948); Proc. Roy. Soc. (Edinburgh) **A164,** 161 (1955).

It seems physically reasonable, therefore, to specify the plane which bisects $(x''-x')$ as the plane to which the heat flux is to be referred. We will use this plane to divide the lattice into two semi-infinite systems, one labeled L which the jumping atom leaves, and the other labeled R at which the jumping atom arrives. The advantage of this device is that it permits a complementary definition of Q^* which is quite instructive.

We now inquire into the reasons why the $q(x)$ curves at the instants t' and t'' differ from one another. One must realize that the $q(x, t')$ curve in the L region represents the excess thermal energy as it exists just prior to the atom jump, and that all of this excess energy would get back into the heat bath in L if the atom jump were not to occur. However, for the jump to occur some thermal energy may have to be converted at L into the chemical (e.g., electronic) energy, represented for example by the hole created by the departing atom. Whatever the mechanism by which some excess thermal energy thus becomes converted, the heat bath at L does not receive back all the thermal energy that entered the coordination zone at L. Hence, in order to maintain L isothermal, an amount of thermal energy equal to this deficiency must be supplied to L. But this last sentence is the complementary definition[1] of Q^*. Consequently, letting E_c^L stand for the amount of the excess vibrational energy that becomes converted into chemical (electronic) energy, E_c^L constitutes a contribution to Q^*.

But in addition to the existence of sinks for the excess thermal energy, there is another reason why the $q^L(x, t')$ need not coincide with the $q^L(x, t'')$. This is that the change in atomic configuration of both L and R entailed by the atom jump from L to R will, in the general case, necessitate a different manner of sharing of the total excess vibrational energy between L and R. Thus, even if there were no energy-conversion phenomenon, there would still be a finite contribution to Q^* from the outright transfer out of, or into, L of excess vibrational energy. We will let E_v represent the amount of vibrational energy transferred, positive if from L to R, per atomic jump.

It is difficult to make definite statements concerning E_v; it clearly demands extremely detailed knowledge of the atomic vibrations at conditions such that the deviations from harmonic behavior are large. However, one aspect of E_v may be partially appreciated from a consideration of the localized normal mode analysis of Montroll and Potts.[10] The presence of a chemical impurity in an otherwise pure lattice will produce normal modes of vibration, the effect of which sensibly affects only the neighborhood of the impurity, and the frequency of which is higher than the highest frequency of the unperturbed lattice. The smaller the ratio of the mass of the impurity to that of the normal atom, and the larger the ratio of the effective force constant between the impurity and host atoms to that between two host atoms, the greater will be the localization of the out-of-phase normal modes produced and the higher will be their discrete frequencies. It follows then that when these conditions obtain an appreciable portion of the excess vibrational energy, the aggregation of which is a prerequisite for the atom-vacancy interchange, will be contained in such localized normal modes centered about the impurity. Consequently, when the impurity changes places, it takes with it these singular localized normal modes.[4] There is, as a result, a positive contribution to E_v, and hence to Q^*, which must go through qualitatively unchanged by the presence of large anharmonicities.

The full statement for the heat of transport is then $Q^*=E_c^L+E_v$, and since this is the thermal energy abstracted from L by the atom-vacancy interchange, it is also the amount that must be furnished L in order to keep it isothermal. This energy transfer is a necessary concomitant of the unit step in diffusion, but it is of no experimental consequence save when the diffusion occurs in a temperature gradient; then, the dissimilarity between the in and out flow of activation energy can make itself felt. It should be noted that Q^* might equally well have been defined in terms of R. Since what happens at R is the negative of what happens at L, the choice between the two bases of definition is purely arbitrary.

Perhaps a few additional words are needed in order better to elucidate the division of Q^* into two terms. The chemical term E_c^L would be the only contribution to Q^* at 0°K, were the process able to proceed at that temperature. The vibrational energy transfer term E_v can contribute only at finite temperatures. Furthermore, it should be realized that a process the lifetime of which is less than τ cannot contribute to E_c^L. An example may make this clear. Suppose that in order to jump, an atom finds it energetically advantageous first to ionize, i.e., to contribute its electrons temporarily to the conduction band of the metal (since then only a smaller opening is needed between itself and the adjacent vacancy.) The energy of ionization represents a conversion from thermal energy to electronic energy, but does not contribute to E_c^L because the relaxation of the electrons back to the jumping atom will undoubtedly occur in much less time than τ, so that there will be a reconversion back to thermal energy at L. The net contribution to E_c^L will simply be that of the energy of creating a vacancy at L, whether or not an ionization step occurred. A corollary of this time limitation is that E_c^L must signify the energy for the formation of an equilibrium vacancy (as an example), and not the energy for forming a vacancy in a highly active lattice characterized by having a large excess vibrational energy.

APPLICATION TO SELF-DIFFUSION VIA VACANCY MECHANISM

When an atom at L exchanges with a vacancy at R, what has happened as far as the L region is concerned

[10] E. W. Montroll and R. B. Potts, Phys. Rev. **100**, 525 (1955).

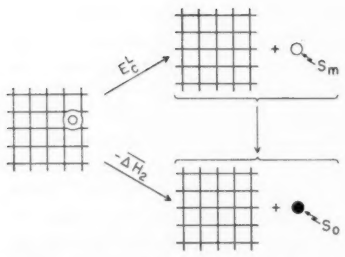

FIG. 2. Schematic representation of the relationship between the energetics of the alloying process and that of the energy conversion term E_c^L in diffusion.

is that a vacancy is created in L at the expense of some of the excess vibrational energy. In other words, thermal energy has been used to "boil out" an atom, and this conversion of thermal energy at L implies a positive E_c^L. It should be noted that E_c^L is not quite equal to h_{vac}, the energy for forming a vacancy as ordinarily defined, because the vacancy to be created at L is at a position adjacent to the already existing vacancy at R. Crudely, on a nearest-neighbor basis one may estimate that for this reason E_c^L is smaller than h_{vac} by (h_{vac}/Z), where Z is the coordination number of the lattice. The net result is that one may expect E_c^L to be about 10% smaller than h_{vac} for the case of self-diffusion via a vacancy mechanism.

Shewmon[11] and Brammer[12] were unable to perceive any marker motion in zinc and copper, respectively, by holding the metals in a temperature gradient. Taking the experiments at face value, one can conclude[4] that $Q^* \approx h_{\text{vac}}$, where Q^* refers to the atom. Because of our considerations above, $E_c^L \approx h_{\text{vac}}$, so that $E_v \approx 0$, or at most, $E_v \approx 0.1 h_{\text{vac}}$. The smallness of the vibrational transfer contribution is what one might have expected in view of the absence of a localized normal mode effect. Another semiquantitative deduction that one can draw from these experiments depends on the inequality $|Q^*| \leqslant E_m$, in which E_m is the activation energy for moving the vacancy; this inequality clearly follows from our discussion of the nature of the heat of transport. Since the experiments show that $Q^* \approx h_{\text{vac}}$, it follows that $E_m \gg h_{\text{vac}}$ for zinc and for copper. This conclusion is corroborated by recent measurements[13] of $h_{\text{vac}} = 1.0 \pm 0.1$ ev and $E_m = 1.3$ ev for copper. However, Brammer's experiment[12] with bcc iron, with similar negative results, cannot be similarly interpreted in view of Meecham's recent finding[14] that casts serious doubt upon the existence of a vacancy mechanism for self-diffusion in bcc iron. If, as Meecham suggests, self-diffusion proceeds by a ring mechanism, one would expect $Q^* = 0$ because of the identity of configuration in L before and after the unit step in diffusion, and hence a temperature gradient could not bias the self-diffusion. However, because of the absence of net mass transport with the ring mechanism, the Shewmon-Brammer type of experiment cannot be used as a criterion for mechanism.

[11] P. G. Shewmon, J. Chem. Phys. **29**, 1032 (1958).
[12] W. A. Brammer, Bull. Am. Phys. Soc. **2**, 388 (1957).
[13] G. Airoldi, G. L. Baechella, and E. Germagnoli, Phys. Rev. Letters **2**, 145 (1959).
[14] C. J. Meecham, Phys. Rev. Letters **4**, 284 (1960).

APPLICATION TO DIFFUSION OF INTERSTITIAL SOLUTES

Dissolved nitrogen and carbon in α-Fe increase in concentration at the hotter side of an initially homogeneous solid solution.[3] Since at these temperatures only the interstitial solutes are mobile, one can deduce that $Q^* < 0$ for these solutes in α-Fe. Now, as discussed previously, the E_v has a positive contribution from the localized normal-mode effect so that E_v is either positive or a small negative quantity. Consequently, one can assert that $E_c^L < 0$ for these cases. This means that the removal of these solutes from their sites at L liberates thermal energy. In other words, the solute-lattice configuration is an energy-rich situation in the sense that the lattice "cage" would like to be emptied of the solute atom, and only the activation barrier prevents this. Of course, the transfer of the solute to the adjacent interstitial site at R raises the energy content at R by a similar amount. Thus, E_c^L (or Q^* if E_v is negligible) is a measure of the energy change produced in one region of a lattice by the removal of the solute species to another portion of the lattice.

It is possible to be more specific about the referent of E_c^L by realizing that the solute atom at L goes from the as-dissolved state to the as-dissolved state at R, so that it is unchanged by the transit. Except for a detail that will be referred to below, it is immaterial to the region L whether the solute terminates its transit at an adjacent site in R, far away in R, or indeed, in any other piece of metal of the same species, as long as the solute species is unaltered in detail. Hence, E_c^L is the energy change of the lattice only, as it changes from occupation to nonoccupation by a solute atom. The energy relations are illustrated in Fig. 2, in which the solute in its

TABLE I. $E_{\text{met}} \approx (\Delta H)_2 + E_c^L$ = energy for metallizing solute from reference state; $-E_c^L \approx -Q^*$ = energy for perturbing lattice cage.

System	E_{act}	(ΔH_2)	Q^*	E_{met}
α Fe (C)	24 kcal[a]	25.7 kcal (graphite)	−24 kcal[b]	~0 kcal
γ Fe (C)	36	10.0 (graphite)	−2[b]	~8
α Fe (H)	3	−44.8 [H(g)]	+[c]	~−43
α Zr (H)	7	−68.0 [H(g)]	3.5[d]	~−65
α Fe (N)	~18	−79 [N(g)]	~−18[e]	~−97

[a] R. P. Smith, (to be published).
[b] See work cited in footnote 5.
[c] O. D. Gonzalez (private communication).
[d] J. M. Markowitz (private communication).
[e] See work cited in footnote 3.

as-dissolved state is symbolized by S_m. Figure 2 also displays the process underlying the thermodynamic partial molar heat of solution. An atom in its pure solid state S_0 is added to the unperturbed lattice of the solvent, and the resulting enthalpy change is the partial thermodynamic heat of solution $(\Delta H)_2$ which cannot be broken down into a portion referring to the modification of the lattice and another relating to the modification of the solute. One can complete the cycle, as shown in Fig. 2, finding that the energy change $[(\Delta H)_2+E_c{}^L]$ for the third leg of the triangle must relate only to the modification undergone by the solute species in going from S_0, the pure solid state, to S_m, the as-dissolved state, since the lattice remains unperturbed in this step. If, instead, the state S_0 is taken as that of the discrete atom in the gas phase, the combination $[\Delta H_{\text{vap}}+E_c{}^L]$ represents the energy for modifying the atom alone from its gaseous state to the as-dissolved state in the lattice (ΔH_{vap} is the energy of vaporization of the dissolved species from the solution). Table I presents the relevant energy quantities, as well as an estimate of the energy E_{met} for "metallizing" the solute species from its arbitrary reference state. The estimate depends upon the assumption that $Q^*\approx E_c{}^L$, i.e., that E_v is negligible. Therefore, the numbers for E_{met} can be regarded only as indications, but they may be of use to theoreticians concerned with the energies associated with electronic modifications of atoms.

It remains to point out that the process characterized by the energy $E_c{}^L$ indicated in Fig. 2 is not completely represented by that diagram. What has been consciously neglected so far is the fact that because the species S_m in R actually occupies a position immediately adjacent to the region L, the lattice at L is not the perfectly unperturbed lattice but is modified to a small extent by S_m near it. Consequently, $[(\Delta H)_2+E_c{}^L]$ contains in it a small contribution arising from the modification of the lattice by the nearness of the solute. However, the work of Powers[15] on the interaction between oxygen atoms dissolved in tantalum, and the calculations of Fisher[16] on the interaction between carbon atoms dissolved in α-Fe show that this effect is small. Therefore, it is a good first approximation to decompose the partial molar heat of solution into $[(\Delta H)_2+E_c{}^L]$, the part associated only with the solute, and $-E_c{}^L$, the part associated only with the lattice.

CONCLUSIONS

The present analysis shows that the heat of transport and hence Soret diffusion for the case of a single mobile component, may be understood in terms of a thermodynamic contribution and of a kinetic contribution. The former $(E_c{}^L)$ is the energy for the formation of a pseudovacancy (in the case of self-diffusion), or the thermal energy absorbed or released upon the removal of a solute atom (in the case of interstitial diffusion). The kinetic contribution (E_v) arises from the redistribution of vibrational energy between the L and R regions due to the change of place of the atom-vacancy pair; a portion of the kinetic contribution, that due to the singular localized normal-mode distribution, must be a positive contribution to E_v, and can be important only for low ratio of solute-atom mass to solvent-atom mass and/or large ratio of effective force constants. It is also shown that $E_c{}^L$ is an energy change suffered only by the lattice since the displaced atom finds itself in identical states after as before its jump. Consequently, it becomes possible to decompose a thermodynamic quantity such as the partial molar heat of solution, or of vaporization, into a portion due to changes undergone by the lattice and another due to changes undergone only by the solute species.

The theoretical problems which must be solved to render the present analysis quantitative are formidable. These are: the calculation of τ, the time of regression of the activation energy; the calculation of the energy for the removal of an atom from a lattice site adjacent to a substitutional vacancy, or of an interstitial solute from a normal site, keeping the solute atom in its as-dissolved state; and finally and most difficult, E_v must be calculated from the fine details of the atomic vibrations as affected by chemical or structural singularities represented by solute atoms or substitutional vacancies and as affected by the probably large deviations from harmonic vibrational character in the neighborhood of the saddle-point configuration. In this connection, a basic assumption of the present analysis must be investigated, namely, that after the instant t'' there is no "leakage" of thermal energy between L and R. Probably this assumption departs more widely from reality the larger is the departure of the lattice vibrations from harmonic character, so that more energy can be transmitted between quasi-normal modes.

Energy transfer such as discussed in this paper must occur in every kind of diffusion, except in the case of self-diffusion by the ring mechanism; however, unless a temperature gradient is present, there cannot be a direct experimental consequence from this phenomenon. Possible exceptions are correlation effects in isothermal diffusion. It is conceivable that the direction and magnitude of the energy transfer will influence the probability of the next jump of a vacancy.

ACKNOWLEDGMENTS

The benefit of stimulating conversations with Dr. James C. M. Li and Dr. Howard Reiss are gratefully acknowledged.

[15] R. W. Powers and M. V. Doyle, Trans. AIME **215**, 655 (1959).
[16] J. C. Fisher, Acta Met. **6**, 13 (1958).

Study of the N_2O Molecule Using Electron Beams*

G. J. SCHULZ

Westinghouse Research Laboratories, Pittsburgh 35, Pennsylvania

(Received October 18, 1960)

Inelastic processes and negative ion formation in N_2O are measured using the trapped-electron method and conventional techniques, respectively. A large inelastic process is observed at 2.2 ev and is interpreted as the formation of vibrationally excited N_2O via the formation of a temporary negative ion state. Negative ions O^- are observed beginning at zero ev with peaks of the negative ion current occurring at 0.7 and 2.2 ev. The latter peak is attributed to the formation of the temporary negative ion with subsequent decay into a stable O^- plus N_2 in various states of vibrational excitation. Measurements of the kinetic energy of the negative ions confirm this hypothesis. A value of the dissociation energy of the N_2—O bond in N_2O is found from the appearance potential of O^- extrapolated to zero kinetic energy. This value, $D(N_2-O) = 1.2\pm0.2$ ev, agrees within experimental error with the value of 1.3 ± 0.2 found independently by Curran and Fox, but disagrees with the thermochemical value of 1.66 ev.

THE formation of stable negative ions by electron impact on diatomic molecules has been the subject of extensive investigations for many years. Although precise values of onset energies, shape of the cross section and its magnitude, and the kinetic energies of the products are far from settled, the basic processes are well understood. The detailed processes involved in stable negative ion formation from triatomic and more complex molecules has received much less attention. In this paper, excitation and negative ion formation in N_2O are discussed.

The methods used in this study are identical to those recently discussed in connection with a study of the H_2O molecule.[1] The interpretation of a portion of the data parallels the considerations invoked in connection with a study of N_2 and CO.[2] In the case of N_2, it has been found that a large cross section for an energy loss process exists below the dissociation energy of N_2, namely in the region 1.5 to 4 ev, with a peak at 2.3 ev. This energy loss process has been discussed in terms of the formation of a temporary negative ion which subsequently decays into various vibrational states of the nitrogen molecule, plus a free electron. A similar process is discussed below for the N_2O molecule.

I. EXPERIMENT

The experimental arrangement and the tube used for this study are identical to that used in connection with a study of the H_2O molecule, and the reader is referred to footnote 1 for a description of the experimental arrangement and the calibration of the energy scale. Briefly, an electron beam, monoenergetic within about 0.1 ev, is aligned by a magnetic field and traverses the collision chamber. Positive or negative ions can be drawn to a cylindrical collector by the application of suitable potentials. Also, the kinetic energy of the negative ions can be studied by retarding them near the cylindrical collector.

The "trapped electron" mode of operation can be achieved by establishing a potential well at the axis of the tube. All of the beam electrons which have lost energy in an inelastic collision and whose residual energy is smaller than the well depth are trapped and eventually reach the outer cylinder. A plot of the trapped electron current vs electron energy shows peaks resulting from electronic excitation or vibrational excitation. Stable negative ions also reach the collector in the "trapped-electron" mode of operation, but these can be subtracted from the curve. In the N_2O molecule, the cross section for production of stable negative ions is found to be small compared to any of the inelastic peaks, and thus no correction is needed.

II. EXCITATION SPECTRUM

Figure 1 shows a plot of the trapped-electron current against electron energy using a well depth of 0.3 ev. For comparison, the absorption regions in the vacuum ultraviolet[3] and near ultraviolet[4] are indicated in Fig. 1. These absorption peaks have been discussed in detail by Zelikoff, Watanabe, and Inn[3] and by Sponer and Bonner.[4] There is generally good agreement between the absorption spectrum and the trapped-electron peaks except that the trapped-electron method indicates a peak about 5.6 ev which has not been detected in absorption. Its significance is not understood. The large peak at 2.2 ev has not been seen in any absorption experiment and it is the only feature of Fig. 1 which will be considered further in this paper (Sec. IV).

III. NEGATIVE IONS

Figure 2 shows the negative ion current as a function of electron accelerating voltage. The energy scale is

* This work was supported by the Advanced Research Projects Agency, and the Office of Naval Research.

[1] G. J. Schulz, J. Chem. Phys. **33,** 1661 (1960).

[2] G. J. Schulz, Phys. Rev. **116,** 1141 (1959).

[3] M. Zelikoff, K. Watanabe, and E. C. Y. Inn, J. Chem. Phys. **21,** 1643 (1953).

[4] H. Sponer and L. G. Bonner, J. Chem. Phys. **8,** 33 (1940).

established by retarding the electron beam (with N_2O in the tube) in front of the collision chamber and collecting the unretarded portion of the electron beam on the electron collector which is kept a few volts positive with respect to the collision chamber. Such a retarding curve is shown dashed in Fig. 2. Further proof that the energy scale thus established is correct can be obtained from the positive ion onset which is found to occur at the appropriate spectroscopic value.[5] The peaks of the negative ion current occur at 0.7 ± 0.1 ev and 2.23 ± 0.1 ev, which is the average of six determinations. Mass spectrometer studies by Curran and Fox[6] show that the ion involved over the whole range of Fig. 2 is O^-.

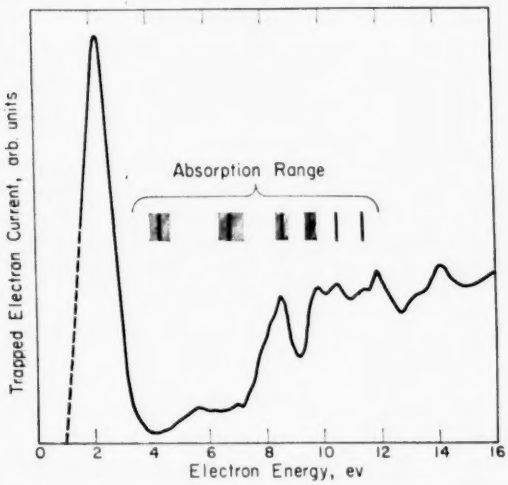

FIG. 1. Excitation spectrum of N_2O. The trapped-electron current is plotted against electron energy. The well depth is approximately 0.3 v. The curve is taken with an x–y recorder

It is interesting to note that the onset of the negative ion current occurs between zero and 0.1 ev. The structure of the curve at low electron energies is reproducible and is not believed to be instrumental. A possible interpretation of the negative ion curve is given in Sec. IV.

The kinetic energy of the negative ions can be measured by retarding them at the cylindrical collector. Typical retarding curves are shown in Fig. 3. The procedure employed to find the kinetic energy is explained in the caption. It is the same as that employed successfully in previous work.[7] The contact potential involved in the scale for kinetic energies is found to be less than 0.1 v from positive ion retarding curves. A plot of the kinetic energy vs electron energy is shown

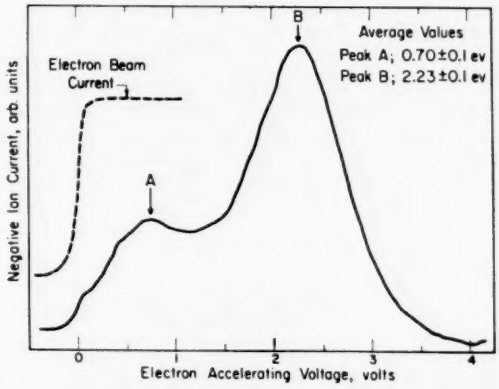

FIG. 2. Negative ion production in N_2O The negative ion involved is O^- in the whole energy range shown. A retarding curve for the electron beam, on the same voltage scale, determines the energy scale. The structure near the onset of the negative ion current is reproducible. The curve is taken with an x–y recorder.

in Fig. 4. Our studies of simple negative ion production processes (such as the production of O^- from O_2; H^- from H_2;[7] H^- from H_2O[1]) using the present apparatus show that the curve of kinetic energy vs electron energy for the processes enumerated above agree with the theoretical slope (0.5 for O^-/O_2, 0.5 for H^-/H_2, 17/18 for H^-/H_2O).[8] The intercept of these curves leads to the proper values of $D-A$, the difference between the dissociation energy and the electron

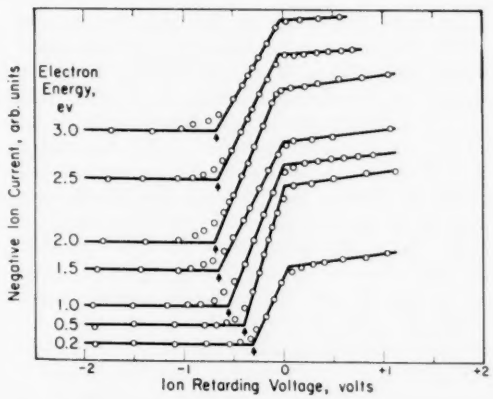

FIG. 3. Ion retarding curves in N_2O. Negative ions produced by "monoenergetic" electrons (the electron energy is indicated) are retarded at the cylindrical collector. A linear extrapolation is used to find the kinetic energy of the ions. The arrows show the ion kinetic energy at each electron energy. The individual curves are displaced on the ordinate for clarity. The vertical scale is arbitrary and is different for each curve.

[5] A. B. F. Duncan, J. Chem. Phys. **4,** 638 (1939).
[6] R. K. Curran and R. E. Fox (to be published). Curran and Fox find the onset of O^- at 0 ± 0.05 ev. They find the peaks of the O^- current at 0.5 ± 0.2 and 2.0 ± 0.2 ev, respectively (R. K. Curran, private communication).
[7] G. J. Schulz Phys. Rev. **113,** 816 (1959).

[8] The retarding potential difference method is used in all these experiments for obtaining essentially monoenergetic electrons. The fact that the proper slope of the kinetic energy vs electron energy curve can be obtained with the retarding potential difference method, is worth noting.

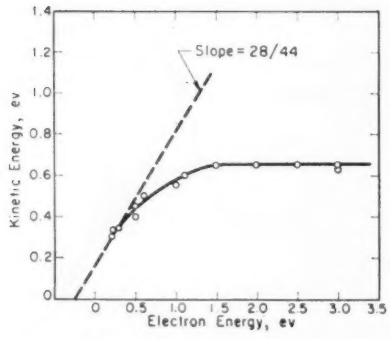

FIG. 4. Negative ion kinetic energy vs electron energy. The data for this curve are obtained from curves similar to those shown in Fig. 3. The unusual shape of the curve is discussed in the text.

affinity, except in the case of O^-/O_2.[9] An examination of Fig. 4 shows that if there is a linear region of kinetic energy vs electron energy, it is not evident from the figure. Nevertheless, a line with the theoretical slope (assuming that there are no excited states of the fragments) is drawn through the lowest points. This procedure will be justified in the next section. The saturation of the curve is an indication that unusual processes are involved, especially in the range of energies 1 to 3 ev, i.e., in the range of the second peak in Fig. 2.

IV. DISCUSSION

A. Dissociation Energy

The zero-energy onset of the negative ion current (see Fig. 2) places an upper limit of 1.47 ev (equal to the electron affinity of oxygen) on the dissociation energy of the N_2—O bond in N_2O. In fact, the straight line drawn through the lowest points in Fig. 4 intercepts the abscissa at a value $D(N_2-O)-A(O)=-0.25$ ev (for a justification of the straight-line extrapolation, see Sec. IV C). From this one obtains, on using the accepted value of 1.47 ev for the electron affinity, $A(O)$, the value for $D(N_2-O)=1.2\pm0.2$ ev. This value must be compared with the value obtained from the heat of formation of N_2O[10] (0.88 ev), and the dissociation energy of O_2[11] (5.11 ev), i.e., $D(N_2-O)=1.67$ ev. Recently, Curran and Fox[6] determined $D(N_2-O)$ from a mass spectrometer study of positive ion formation to be 1.34 ± 0.2 ev, in fair agreement with the present value.

[9] For the dissociative attachment in O_2, i.e., the formation of O^- from O_2, presently accepted, the value of $D-A$ is $5.11-1.47$, equal to 3.64 where the value of the electron affinity is taken from L. M. Branscomb, D. S. Burch, S. J. Smith, and S. Geltman, Phys. Rev. **111,** 504 (1958). Despite repeated experiments the value found by the author is $D-A$ equal to 3.0 ± 0.1 ev. This low value is, however, in agreement with many other beam experiments, such as Lozier (2.6 ev) and Marriot (3.1 ev). The significance of this discrepancy is not understood.

[10] F. D. Rossini, D. D. Wagman, W. H. Evans, S. Levine, and I. Jaffe, Natl. Bur. Standards (U. S.) Circ. No. **500** (1952).

[11] P. Brix and G. Herzberg, Can. J. Phys. **32,** 110 (1954).

B. Inelastic Process

Figure 5 shows a possible potential energy diagram applied to the lowest states of N_2O. The shape of the curves has been discussed by Stearn and Eyring.[12] The state $N_2(^1\Sigma)+O(^3P)$ is drawn 1.2 ev above the ground state of the N_2O molecule. This puts the $N_2(^1\Sigma)+O^-(^2P)$ state approximately 0.2 ev below the ground state of N_2O.

It is unlikely that the large inelastic peak of Fig. 1, starting below 1.5 ev (extrapolated onset at 1.0 ev) with a peak at 2.2 ev and extending past 3 ev, can be explained by a potential curve resulting from the state $N_2(^1\Sigma)+O(^3P)$ for the following reasons. The height of the peak at 2.2 ev is larger than any of the other peaks; the extrapolated appearance potential is below the energy of the state at infinite separation, which would contradict the repulsive nature of this state[12]; the coincidence in energy of the peaks in the inelastic and negative ion processes points to an alternate interpretation advanced below.

It should be noted that the peak of the inelastic process occurs within 0.1 ev of the peak found previously in the N_2 molecule and being interpreted in terms of a temporary negative ion state of the nitrogen molecule.[13] In view of the known linear asymmetrical

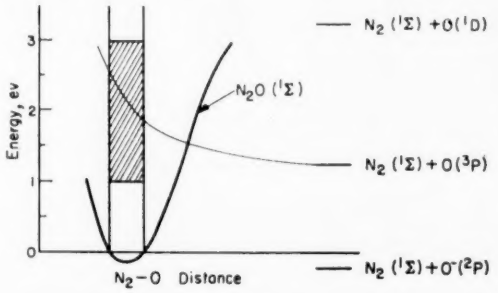

FIG. 5. Hypothetical potential diagram of the lowest states of the N_2O molecule. The shaded area is the extent of the temporary negative ion state. The incident electron excites this state, and the system decays either into a vibrationally excited N_2O plus an electron, or into O^- plus nitrogen in either the ground or a vibrationally excited state. The values used in constructing the diagram are $D(N_2-O)=1.2$ ev, $A(O)=1.48$ ev.

[12] A. E. Stearn and H. Eyring, J. Chem. Phys. **3,** 778 (1935).

[13] The question naturally arises whether any N_2 is present in the apparatus so that the peak at 2.2 ev would be caused by N_2 instead of N_2O. A number of precautions are taken to minimize this possibility. The use of ultrahigh vacuum techniques and baking at 400°C enables us to attain residual gas pressures of the order of 10^{-10} mm Hg. The N_2O is admitted to the vacuum system from a high-pressure lecture bottle to a pressure of about 10^{-3} mm Hg. The ion gauge is turned off during the experiment because it has been found that the ion gauge filament enhances chemical reactions which may alter the gas composition. Comparing the excitation spectrum of N_2O (Fig. 1) with the excitation spectrum of N_2 (Fig. 5 of footnote 2), one finds that the sharp peak at 11 ev, characteristic of N_2 and caused by the excitation of the $C^3\pi_u$ state, is not present in the excitation spectrum of N_2O; this constitutes an experimental indication that the concentration of N_2 in the tube is low and, thus, it is unlikely that the peak around 2.2 ev (Fig. 1) results from the N_2 impurity.

structure of N_2O(N—N—O), it is reasonable to postulate that the 2.2-ev inelastic peak of Fig. 1 results from the excitation of a temporary negative ion state.

Figure 5 shows schematically the extent of the temporary negative ion state by the shaded region. The incident electron excites the temporary negative ion, and the system subsequently decays into various vibrational states of the neutral N_2O. The departing electron carries away the energy difference between the incident electron and the vibrational state in which the N_2O molecule remains. There is a competing process by which the temporary negative ion can decay; it can form O^- and N_2 in an excited vibrational state.

C. Negative Ions

The first negative ion peak of Fig. 2 is interpreted, on the basis of the potential diagram of Fig. 5, as resulting from the excitation of N_2O to form O^- and a nitrogen molecule in the first few vibrational states. This explains the ragged structure of the negative ion current near its onset (if a better energy resolution could be obtained, one should see the contribution of the various vibrational levels). A plot of kinetic energy vs electron energy will have a linear portion of the proper slope only in the energy range where the zeroth vibrational state is excited. Thus, a straight line is drawn through the lowest points of Fig. 4, and the value of $D(N_2-O)-A(O)$ is obtained from the intercept of this line with the axis.

The second negative ion peak of Fig. 2 results from the excitation of a higher state of the N_2O^- molecule (temporary negative ion) with subsequent dissociation into a vibrationally excited nitrogen molecule and O^-. The higher the energy of the incident electron, the higher the vibrational state of N_2; therefore, the kinetic energy of the products tends to remain constant, explaining the "saturation" of the curve of Fig. 4. It is now evident that both the inelastic cross section (first peak of Fig. 1) and the negative ion cross section (second peak of Fig. 2) should have the same shape (both peak at 2.2 ev) since both these processes have the same intermediate state.

It should be noted that a sharp peak at 2.2 ev in the total collision cross section has been observed using a Ramsauer-type experiment.[14] This is in agreement with the present observations, since one expects that both the elastic and inelastic cross sections are enhanced at 2.2 ev.

V. CONCLUSIONS

The formation of temporary negative ions in molecules seems to have an important role in determining many collision processes. Thus, N_2 and CO have large cross sections for vibrational excitation with peaks at 2.3 and 1.7 ev, respectively, which proceed via the formation of a temporary negative ion. A similar process occurs in N_2O. In addition, a part of the O^- formation from N_2O is postulated to proceed via the temporary negative ion. Various other molecules studied to date (H_2, O_2, CH_4, C_2H_6, H_2O) do not exhibit a striking behavior which can be explained by temporary negative ion formation.

The dissociation energy of the N_2—O bond in N_2O can be found from the appearance potential of O^- extrapolated to zero kinetic energy. This value is $D(N_2-O)=1.2\pm0.2$, and it agrees within experimental error with the value found by Curran and Fox ($1.34\pm$ 0.2 ev), but disagrees with the value derived from thermochemical data (1.66 ev).

ACKNOWLEDGMENTS

The author is indebted to R. E. Fox and R. K. Curran for discussion of the mass spectrometer experiments in N_2O, to A. V. Phelps for valuable comments, and to W. Uhlig for construction of the tube. Also, the technical assistance of J. Kearney is acknowledged.

[14] H. S. W. Massey and E. H. S. Burhop, *Electronic and Ionic Impact Phenomena* (Clarendon Press, Oxford, England, 1952), p. 208.

Irradiation Yields of Radicals in Gamma-Irradiated Ice at 4.2° and 77°K*

SEYMOUR SIEGEL, JOHN M. FLOURNOY, AND LILLIAN H. BAUM

Aerojet-General Corporation, Chemical Division, Azusa, California

(Received August 8, 1960)

The EPR spectra of both ice and deuterated ice which have been subjected to γ irradiation at 4.2°K are presented and discussed. Experimental radical irradiation yields at 4.2°K are reported for the H_2O system as a function of sustained irradiation dosage. A comparison between the irradiation yields at 4.2° and 77°K is given and the resulting similarities discussed in terms of intra-spur reactions. Finally, preliminary evidence is presented for the existence of an appreciable isotope effect for the irradiation yields in a mixture of H_2O and D_2O.

I. INTRODUCTION

THE basic purpose of the investigations being undertaken at this laboratory is to add to the understanding of the nature of the stabilizing forces which trapped radicals experience in solid matrices at low temperatures. Toward this goal a study was initiated to observe the stabilization and decay reactions of trapped radicals in kinetic detail. Taking advantage of the inherent paramagnetism of free radicals, the stabilization build-up and the decay reactions are being examined by following the corresponding growth and decay of the EPR spectrum of radicals produced by γ irradiation and by other methods. The use of EPR techniques has the additional advantage, besides causing negligible perturbation of the system under study and permitting continuous observation, of yielding information on the spatial distribution and matrix perturbations of the radicals by the analysis of line shapes, g-factors, and power saturation studies. This paper will be concerned primarily with the build-up of stabilized radicals in γ-irradiated ice at 4.2°K and the relationship of this buildup with the irradiation yields at 77°K. Subsequent papers will deal with a detailed study of the kinetics of H atom reactions between 4.2° and 77°K and with the spatial distribution of radicals in ice as determined by line shape studies on the EPR absorption lines.

In a previous paper[1] the authors discussed the build-up of OH radicals in ice at 77°K under sustained γ irradiation, as well as the thermal behavior of the radicals (the spectrum of ice irradiated at 77°K is shown in Figs. 1 and 2). It was found that the OH radicals decayed according to a diffusion controlled $\frac{3}{2}$-order rate law with an activation energy of 60 kcal/mole. The $\frac{3}{2}$-order concentration dependence can be explained in terms of an acid-base dissociation equilibrium involving the OH radical (a more complete discussion of this point will be published shortly). However, the OH build-up curve as a function of radiation dosage was found to be only slightly dependent upon the observed stabilized radical concentration and could be empirically described by a buildup law of the following form,

$$d(\mathrm{OH})/dI = a - k(\mathrm{OH})^{\frac{1}{2}}, \tag{1}$$

where a and k are constants. In view of the fact that the H_2O_2, H_2, and O_2 concentrations found after warming the sample were relatively small, it was postulated that the most probable reaction taking place *during* irradiation must be the recombination reaction,

$$\mathrm{H} + \mathrm{OH} \rightarrow \mathrm{H_2O}. \tag{2}$$

For an isotropic (homogeneous) reaction mechanism involving the recombination reaction given in Eq. (2) as the primary destruction reaction occurring during irradiation at 77°K, the rate of stabilization of OH radicals with sustained irradiation can be written as,

$$d(\mathrm{OH})/dI = a - k'(\mathrm{H})(\mathrm{OH}), \tag{3}$$

where a is the rate of OH radical production with constant irradiation. However, the ratio of stabilized hydrogen atom to OH concentrations is estimated to be less than 10^{-3} in all cases, since no hydrogen atom spectrum was observed. Therefore, the hydrogen atom concentration can be considered as a steady state concentration and the rate law given in Eq. (3) predicts a greater dependence upon stabilized OH concentration than was observed [see Eq. (1)]. Thus the possibility of a nonisotropic reaction distribution corresponding to preferred reaction coordinates or preferential reaction between radicals within a given electron spur seems a likely explanation for the observed $(\mathrm{OH})^{\frac{1}{2}}$ concentration dependence. Another explanation which suggests itself (although a less likely one) is that the lifetime of the H atoms might be of the order of several seconds but that the concentration decayed to an immeasurably small value in the time required to move the sample from the irradiation source to the EPR spectrometer.

* This research is being supported by a contract with the Air Force Office of Scientific Research.

[1] S. Siegel, L. H. Baum, S. Skolnik, and J. M. Flournoy, J. Chem. Phys. **32,** 1249 (1960).

[2] L. Pauling, *The Nature of the Chemical Bond* (Cornell University Press, Ithaca, New York, 1960), p. 464.

In order to investigate these possibilities more fully and to help elucidate the nature of the radical production process in ice, studies of radical stabilization at 4.2°K were undertaken.

II. EXPERIMENTAL

The experimental techniques employed in this study were essentially the same as those reported previously,[1] therefore, they will not be described in detail here. Spectra were obtained with a Varian Associates V-4500 EPR spectrometer equipped with a 12-in. magnet system and low-temperature accessories. The microwave frequency was approximately 9.5 kMc. Samples of distilled water were degassed under vacuum, frozen, and then transferred to the precooled cavity with only slight melting on the surface. An 800-C cobalt-60 source was used for the irradiations. The maximum dose rate was approximately 8.0×10^4 rep/hr.

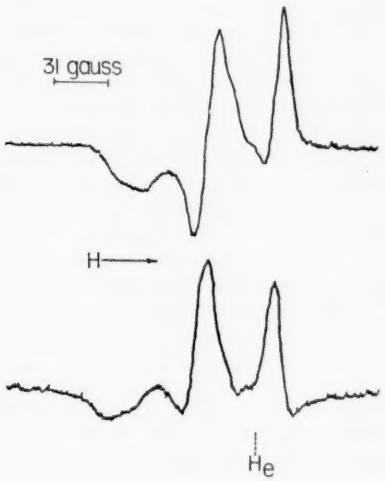

FIG. 1. Paramagnetic resonance spectrum of ice γ-irradiated and observed at 77°K. The upper and lower spectra are the absorption and dispersion signals, respectively. In this and the following figures H_e represents the free electron resonance as given by the equation $h\nu = g_e\mu_0 H_e$.

Absolute concentration assays were made using the spectral intensity of a known quantity of Wurster's blue perchlorate (WBP) as a standard. The WBP was dispersed in ice samples whose size and geometry were very similar to those of the ice samples used for irradiation purposes. Relative spectral intensities were estimated by double integrations of the observed derivative curves, as well as by first moment calculations. For the most favorable cases the error is estimated to be less than $\pm 50\%$.

FIG. 2. Paramagnetic resonance spectrum of D_2O γ-irradiated and observed at 77°K. The upper and lower spectra are the absorption and dispersion signals, respectively.

III. RESULTS

Description of Observed Spectra

The EPR spectrum of degassed ice irradiated and observed at 4.2°K is shown in Fig. 3. The 500-gauss doublet is obviously the spectrum expected for trapped H atoms.[3–5] Analysis of the middle section of the observed trace is much more difficult; however, by comparison with the spectrum obtained by irradiation and observation at 77°K it can be seen that the essential doublet structure present at 77°K can also be discerned at 4.2°K. In the work cited in footnote 1 this doublet was identified by the effect of isotopic substitution on the spectrum (see Figs. 1 and 2), as well as by other arguments, as being due to trapped OH radicals involved in the hydrogen bonded network of the ice lattice. Unfortunately, the remaining absorption cannot be unambiguously assigned, but such species as trapped electrons, H_2O^-, or OH radicals not involved in the

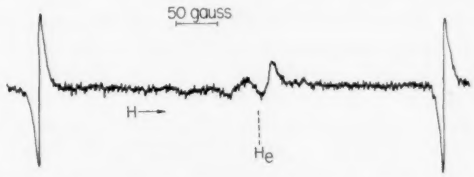

FIG. 3. Paramagnetic resonance absorption spectrum of ice γ-irradiated and observed at 4.2°K.

[3] L. H. Piette, R. C. Rempel, H. E. Weaver, and J. M. Flournoy, J. Chem. Phys. **30**, 1623 (1959).
[4] R. Livingston, H. Zeldes, and E. H. Taylor, Discussions Faraday Soc. **19**, 166 (1955); Phys. Rev. **94**, 725 (1954).
[5] C. K. Jen, S. N. Foner, E. L. Cochran, and V. A. Bowers, Phys. Rev. **112**, 1169 (1958).

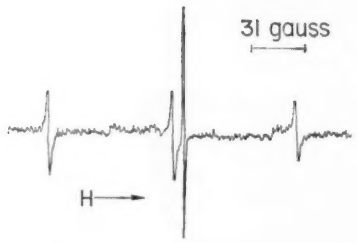

FIG. 4. Paramagnetic resonance absorption spectrum of D_2O γ-irradiated and observed at 4.2°K.

hydrogen bonded network might be responsible. If an ice sample irradiated at 77°K is observed at 4.2°K, the middle spectrum shown in Fig. 3 is accurately reproduced, except for part of the broad underlying base line. It should also be pointed out that there are marked differences in the power saturation parameters of the various lines with the H atom spectrum saturating the most easily. The H atoms are saturated at the lowest power levels available in this study ($<0.1\mu$ w). The weak broad line on the low-field side of the OH doublet and a broad underlying base absorption are the least easily saturated. The thermal stabilities of the radicals responsible for the observed spectrum are considerably different; however, most of the radicals decay rapidly above 110°K. Stabilization of hydrogen atoms occurs in a variety of sites with varying stabilization energies; there are stabilized hydrogen atoms which react very slowly at 60°K, as well as atoms which react rapidly at 15°K.

Irradiation of D_2O at 4.2°K yields the EPR spectrum shown in Fig. 4. The triplet spectrum of the deuterium atoms is easily distinguished from the background. However, the spectrum of the OD radicals is badly obscured due to the perturbing influence of the middle *D* line and the presence of the spectra of unidentified radicals which are produced by the ionizing radiation. If the sample is warmed to 77°K to destroy the stabilized deuterium atoms and some of the other radicals, essentially the same, slightly resolved, triplet hyperfine structure of the OD spectrum shown in Fig. 2 is observed at both 77° and 4.2°K. It should be pointed out that the spectra shown in Figs. 3 and 4 were taken at very low power levels ($\sim 0.1\mu$ w). At higher power levels the spectra of the OD radicals and other unidentified radicals become more pronounced since they saturate at higher power levels than the spectrum of the deuterium atoms. The very sharp intense line at $g=2.0$ in Fig. 4 is not present in the corresponding spectrum of irradiated H_2O (Fig. 3). This line disappears permanently if the sample is warmed slightly above 4.2°K (<10°K).

On account of the partially resolved physiognomy of the OH spectrum at 77° and 4.2°K it has been suggested that the identification of this spectrum as a doublet was fortuitous and that the spectrum in fact consists of a series of unresolved lines broadened by anisotropic matrix and hyperfine interactions. The substitution of D_2O for H_2O and the resultant transformation of the doublet into a triplet serves as strong evidence that the identification of the OH spectrum was correct. However, it was decided to test further the identification by irradiating a mixture of D_2O and H_2O. The spectrum of 20% H_2O in D_2O is shown in Fig. 5. It is apparent that two lines (labeled *A* and *B*) separated by approximately 40 gauss are present flanking the OD triplet spectrum. It is also apparent that the OH spectrum is considerably narrowed due to the decreased nuclear perturbations an OH radical experiences in a D_2O matrix as compared to an H_2O matrix; the corresponding broadening of the OD spectrum in a 20% D_2O in H_2O mixture has also been observed. The persistence of the doublet character of the OH spectrum despite the narrowing of the spectrum is conclusive evidence that the spectrum observed in H_2O irradiated at 77°K, or below, does contain a unique doublet which is due to a hyperfine interaction of an unpaired electron with a single proton. It should be pointed out that the considerable narrowing of the OH spectrum indicates that the linewidth is determined largely by the inter-molecular nuclear spin-electron spin coupling, rather than being dominantly caused by anisotropy of the intra-molecular hyperfine interaction.

Irradiation Yields

The stabilization curve of H atoms with sustained irradiation dosage at 4.2°K is given in Fig. 6. The curve was constructed by irradiating the sample for a period of time at a constant dose rate and then transferring the sample to the EPR spectrometer for a measurement of spectral intensity; the sample was then put back into the Co-60 source for further irradiation. The intermittent nature of the irradiation treatment was shown in separate experiments to have no measurable effect upon the irradiation yield. The H atom concentration was determined from the observed line intensities in the manner described above; however, since the H spectral lines are saturated at the lowest rf powers available in this study, corrections were approximated by plotting a power saturation curve for the hydrogen

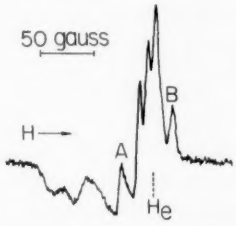

FIG. 5. Paramagnetic resonance absorption spectrum of a 20% H_2O in D_2O mixture irradiated and observed at 77°K. The peaks labeled *A* and *B* are believed to be due to the OH radical.

atom spectrum and extrapolating to unsaturated conditions. The errors inherent in the latter approximation would tend to give a low value for the concentration determination; the errors from this source are estimated to be less than 15%. As can be seen from Fig. 6 the stabilization yield of H atoms is linear with irradiation dosage over a considerable range and then the yield begins to decrease slowly with further irradiation. Unfortunately, because of a decision as to the best utilization of the available liquid helium, the curve could not be followed far enough to determine the maximum concentration, or radical saturation concentration.[6] The initial slope corresponds to an irradiation yield of 0.9 H atoms/100 ev. The yield is somewhat insensitive to the concentration of the other radicals present.

The determination of radiation yields for the radicals responsible for the middle section of the observed spectrum is complicated by the fact that the dependence of concentration on dosage is not the same for the different radicals that are responsible for the various components of the observed overlapping absorption spectrum. A comparison between the spectrum in Fig. 3 and that of ice irradiated by 40-Mev electrons from a linear accelerator[3] shows that the radicals responsible for the broad underlying base line absorption and the species producing the low-field line saturate with respect to concentration at much higher dosages than do the hydrogen atoms or OH radicals. From the limited data available it cannot be unambiguously determined if this behavior is due to differences in the stability of the various radicals present, to differences

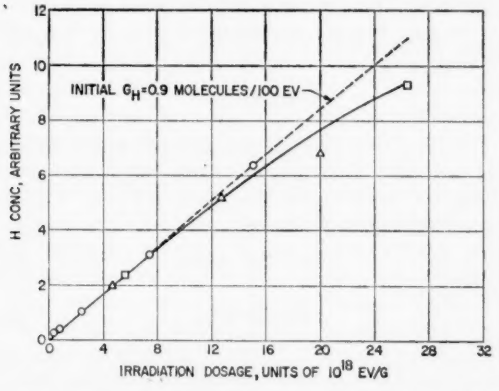

FIG. 6. Stabilization of H atoms in γ-irradiated ice at 4.2°K as a function of cumulative dosage. A constant dose rate of 4.8×10^{18} ev/g hr was used. One arbitrary unit is approximately equal to 3.6×10^{-5} m/1. The irradiation treatment was extended over three successive days; the symbols ○, ▽, □ denote the first, second and third day's irradiation, respectively.

[6] L. Piette *et al.* in the work cited in footnote 3 using dose rates one to two orders of magnitude larger than the dose rate used in this study found a maximum of 8×10^{-3}m/1 for the stabilized hydrogen atom concentration at 4.2°K. However, Piette's work was carried out with a linear accelerator and heating effects due to the high dose rate might be important.

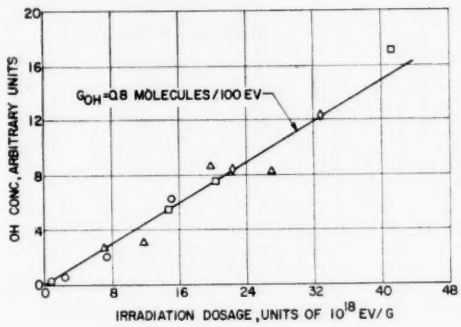

FIG. 7. Stabilization of OH radicals in γ-irradiated ice at 4.2°K. A constant dose rate of 4.8×10^{18} ev/g hr was used. One arbitrary unit is approximately equal to 3.6×10^{-5} m/1. The irradiation treatment was extended over four successive days; the symbols ○, ▽, □, ◇ denote the first, second, third, and fourth days' irradiation, respectively.

in the irradiation yields, or to the large difference in the dose rate used in the two investigations. Also, the extensive overlapping of the several lines in the spectrum makes quantitative assays of a particular set of lines difficult. However, the high-field peak of the OH spectrum is relatively unperturbed and can be used as an index for determining the OH irradiation yield at 4.2°K.

The stabilization curve of OH radicals produced by γ irradiation at 4.2°K is given in Fig. 7. This curve was synthesized in a somewhat complicated manner due to experimental problems. The irradiation treatment was extended over several days (because of reasons external to the experiment) with intervals of storage of the ice sample at 77°K; therefore, the OH production was not a continuous process, since warmup to 77°K destroyed all of the H atoms and part of the OH radical concentration (see below). Consequently, the stabilization curve was constructed by first plotting the points which were run continuously at 4.2°K in the same manner as described above for the H atom curve, the sample was then warmed to 77°K and left overnight. No appreciable reaction takes place during storage overnight at 77°K. The next day the sample was cooled again to 4.2°K, a spectrum was taken, and the reduced height of the high-field line at 4.2°K was used to determine an effective dosage value as a starting point from which the curve was extended by continued irradiation and observation. This procedure resulted in a certain amount of overlap for successive portions of the curve, as seen in Fig. 7.

Concentrations of the OH radicals at 4.2°K were determined essentially by a comparison technique. A spectrum of an ice sample irradiated and observed at 77°K was used to determine the OH concentration at this temperature. The sample was then cooled to 4.2°K and the height of the high-field OH line calibrated for this concentration; the errors inherent in determining *relative* concentrations are of the order of 10% (which

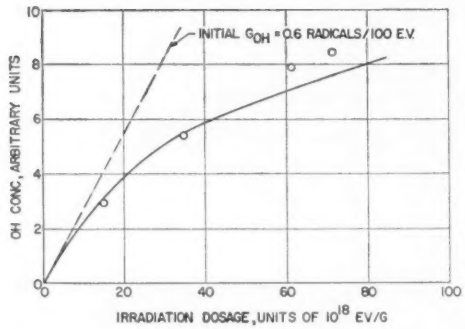

FIG. 8. A comparison between the OH yield in ice irradiated at 77°K (solid curve) and the OH yield obtained by irradiation at 4.2°K and observation at 77°K (circles). The estimated uncertainty of the points is ±10%. One arbitrary unit is approximately equal to 3.6×10^{-5} m/1.

is the reproducibility found for the heights of OH spectra in different samples irradiated to similar dosages). The concentrations obtained in this manner were checked by taking the first moment of the entire middle section of the 4.2°K spectrum and then subtracting out the contributions from the low-field unresolved lines. The resultant values were then compared to the first moments of the hydrogen lines and to the WBP line. The agreement between the two methods of concentration determination was better than 20%, even though either method alone probably does not have accuracy better than 50%. The resultant build-up curve is, within experimental error, linear with radiation dosage up to the highest effective dosage administered, 4×10^{19} ev/g. The slope of the estimated straight line corresponds to an irradiation yield of approximately 0.8 radicals/100 ev. An initial irradiation yield of approximately 0.6 radicals/100 ev was found for irradiation at 77°K.[7] The experimentally obtained value for the ratio of the initial yield at 77°K and the yield at 4.2°K can only be regarded as a lower limit to the true value despite the relatively high accuracy (~10%) estimated for determining relative concentrations at the two temperatures. The reason for this uncertainty is that the linear portion of the buildup curve at 77°K is very small (see Fig. 8), and thus the estimation of a slope for this portion is quite difficult. However, the most likely errors lie in the direction of giving too small a value for the slope. Therefore, the true value for the above mentioned ratio probably lies between unity and 0.67.

It should be noted that the H and OH yields at 4.2°K are essentially the same, to well within the estimated 50% experimental error in concentration determination; refinements in the concentration measurement would be exceedingly difficult. The fact that the OH buildup curve is still linear at the highest dosage used while the H atom curve is beginning to exhibit some curvature is probably due to either experimental error or to the perturbation of the OH peak by the spectra of the other radicals formed during the irradiation. However, the possibility that there is a difference in the stabilization of H atoms and OH radicals at higher dosages cannot be discounted. It should be pointed out that the maximum observed OH concentration given in Fig. 7 is of the order of 0.6×10^{-3} m/1 and the curve is still approximately linear with irradiation dosage; however, the saturation concentration of OH radicals found at 77°K was also of the order of 0.6×10^{-3} m/1. It is obvious that a considerably larger concentration of radicals can be stabilized at 4.2°K than can be stabilized at 77°K (the maximum ratio is felt to be no greater than 10). As a matter of general interest, the energy storage, on the basis of recombination reactions, corresponding to a concentration of 0.6×10^{-3} m/1 of OH and H, is approximately 5% of the absorbed gamma energy.

Since one of the main reasons for undertaking this study was to elucidate the nature of the recombination reactions taking place *during* irradiation at 77°K, a comparison was made between the stabilization curve obtained by irradiation and observation at 77°K and the stabilization curve obtained by irradiating at 4.2°K, warming the sample and observing the spectrum at 77°K and then cooling the sample to 4.2°K for further irradiation. This comparison is illustrated in Fig. 8. As can be seen, the two stabilization curves are strikingly similar.

IV. DISCUSSION

If it is assumed that the primary reactions, involving OH radicals and hydrogen atoms, which take place during the warming period between 4.2° and 77°K are the recombination reactions[8]

$$H+OH\rightarrow H_2O \quad (4)$$

and

$$H+H\rightarrow H_2, \quad (5)$$

[7] The value of the initial yield at 77°K reported here is approximately a factor of 3 smaller than the value reported in the previous publication on this subject (see the work cited in footnote 1). The reason for the discrepancy in the two values is that a calculational error was made in footnote 1 and all OH radical concentration values given in that paper should be reduced by a factor of 3.

[8] The H_2O_2 and O_2 concentrations in a sample of H_2O which had been subjected to prolonged irradiation at 4.2°K and then warmed to room temperature for a colorimetric analysis was at least an order of magnitude lower than the value predicted on the basis of the OH+OH recombination reaction. This observation together with the fact that OH is stable at 77°K leads to the assumption that the OH recombination reaction is not important between 4.2° and 77°K. Also, the so-called back reactions, Eqs. (a) and (b),

$$H+H_2O_2\rightarrow H_2O+OH \quad (a)$$

$$OH+H_2\rightarrow H_2O+H, \quad (b)$$

can be neglected because, up to 77°K, it is very probable that the stabilized OH radicals are not mobile and no H_2O_2 is produced until the temperature is raised above 77°K.

TABLE I. Comparison between calculated and experimental yields at 77°K.

Dosage[a] ev/g×10⁻¹⁸	$(H)_{4.2°}$ Exptl[b]	$(OH)_{4.2°}$ Calc[b,c]	$(OH)_{77°}$ Calc[b,d]	$(OH)_{77°}$ Exptl[b,e]	Deviation %
15.0	1	1	0.5	0.53	+6.0
35.0	1.33	1.83	1.06	0.99	−6.6
61.5	1.75	2.81	1.73	1.44	−16.7
71.8	0.71	2.44	1.88	1.53	−18.6

[a] The irradiation dosages are cumulative.
[b] Concentrations are given in arbitrary units and equal H and OH yields at 4.2°K per unit dosage are assumed. One arbitrary unit is approximately equal to 2×10^{-4} m/l.
[c] The OH concentration at 4.2°K is calculated by adding the yield from the new irradiation at 4.2°K to that concentration calculated for $(OH)_{77°}$ in the fourth column.
[d] Calculated on the basis of Eq. (8) with β equal to unity.
[e] The relative values reported here are estimated to be good to ±10%.

the rate laws describing these reactions can be written as,

$$d(\mathrm{H})/dt=-k[2\beta(\mathrm{H})^2+(\mathrm{H})(\mathrm{OH})] \quad (6)$$

$$d(\mathrm{OH})/dt=-k(\mathrm{H})(\mathrm{OH}), \quad (7)$$

where β is the relative probability of Eq. (5) to Eq. (4) distinct from normal concentration effects. Since in this study we are interested only in the final stabilized OH concentration at 77°K Eqs. (6) and (7) can be combined to eliminate time as a variable. If we make the rather strong assumption that β is independent of temperature, then the resulting expression can be integrated, after the simple substitution $X=\mathrm{H/OH}$, to give

$$[1+X(2\beta-1)]^{1/(2\beta-1)} = [(\mathrm{OH})/(\mathrm{OH}_{4.2°})][1+(2\beta-1)X_{4.2°}]^{1/(2\beta-1)}, \quad (8)$$

where $X_{4.2°}$ is the ratio of the hydrogen atom and hydroxyl concentrations at 4.2°K. Taking the limit as $X\to0$, since $\mathrm{H/OH}<10^{-3}$ at 77°K, it is easily shown that Eq. (8) predicts an OH radical concentration at 77°K given by the following expression

$$\mathrm{OH}_{77°}=\mathrm{OH}_{4.2°}[1+(2\beta-1)(\mathrm{H/OH})_{4.2°}]^{1/(1-2\beta)}. \quad (9)$$

Admittedly the model implied by Eqs. (6) and (7) is a simple one and the situation is undoubtedly more complex. Nevertheless, a comparison over a limited dosage range between the hydroxyl radical concentrations at 77°K calculated from Eq. (9) assuming β equal to unity and the experimental values given in Table I shows remarkably good agreement to within ±20%. It can be seen, however, that there is a systematic increase in the disagreement shown in Table I. There was no one value of β which could fit all the available data, including the observed ratio of approximately $\frac{2}{3}$ for the initial OH yields at 77° and 4.2°K. Considering all the experimental data it becomes obvious that the data could be approximated by Eq. (9) only by assuming a continually decreasing value of β with increasing dosage. A decreasing value of β corresponds to an increased relative probability of Eq. (4). The magnitude of β varies from approximately 2 at very small irradiation dosages to about unity at a dosage of 4.0×10^{19} ev/g. As the irradiation dosage increases the value of β decreases further.

The concept of a decreasing value of β with increasing irradiation is inconsistent with a random, isotropic, diffusion controlled reaction. Even if the necessity of a changing value of β were neglected, the dependence of the stabilized OH concentration at 77°K upon the hydrogen atom concentration that was present before warming from 4.2°K (as shown in Table I) is still inconsistent with an isotropic reaction mechanism, in view of the OH buildup similarity illustrated in Fig. 8. The latter conclusion is based on the fact that the stabilized hydrogen atom concentration is several orders of magnitude larger[9] at 4.2°K than at 77°K. Therefore, an obvious inference that can be drawn from Fig. 8 is that the radical destruction paths which are traversed in the reactions taking place between 4.2°K and 77°K are the same reaction coordinates which are effective during irradiation at 77°K. A hydrogen atom produced by γ irradiation at 77°K must have the same relative probability of reacting with another H atom or with an OH radical as an atom produced at 4.2°K. This type of kinetic behavior can be invoked to explain both the slight concentration dependence on stabilized OH concentration that was found for the OH stabilization curve at 77°K [see Eq. (1)] and the decreasing values of β found for increasing irradiation dosages.

Since the H atoms are very reactive at 77°K and the reactions probably take place along the irradiation damage paths which were created coincident with the formation of the radicals, the majority of the individual recombination reactions take place in a limited volume of space, i.e., an H atom created in one part of the ice sample will probably never travel more than a couple of hundred angstrom units from the point of initial thermalization. Therefore, considering the fact that the stabilization concentration of the OH radicals per unit volume is never very large, the majority of the initial reactions

[9] There was no hydrogen atom spectrum observable at 77°K.

take place between radicals created within the same electron spur and thus are essentially independent of the total stabilized radical concentration. However, as the irradiation dosage is increased the stabilized OH radical concentration becomes larger and the intra-spur model becomes increasingly perturbed by inter-spur reactions. The overlapping of the spatial distribution of the radicals in a newly created electron spur by the previously stabilized radical concentration results in an "effective" increase in the OH concentration. Therefore, considered from the point of view of the isotropic model described by Eqs. (6) and (7), the perturbation of the intra-spur reactions by the inter-spur reactions corresponds to a decreasing value for β as the irradiation dosage is increased.

The model of preferred reaction coordinates and intra-spur reactions described above is undeniably naive but refinements must await more detailed information on the spatial distribution of the radicals and on the matrix damage created by the ionizing radiation. However, the validity of the general concepts involved is demonstrated by the relatively small values of the H_2 and H_2O_2 concentrations found after warming ice samples which have been subjected to considerable irradiation dosage. Additional evidence supporting this model was obtained from a detailed study of the decay reactions of the stabilized H atoms between 4.2°K and 77°K. It was found that most of the stabilized H atoms react following a rate law with a first-order concentration dependence essentially independent of impurities; this observation can be explained on the basis of intra-spur reactions.

V. CONCLUDING REMARKS

The yields reported in this paper for the radicals produced by the γ irradiation of ice at 77° and 4.2°K are believed to be good to $\pm 50\%$. However, by consideration of the width of the lines, the observed multiplicity of the H trapping sites, and the unresolved nature of the middle spectrum it seems quite probable that a considerable amount of the spectral intensity lies in the wings of the absorption lines and that its effect is minimized in the derivative curve. Therefore, the concentration values reported here are best considered as good lower limits to the actual irradiation yields.

An interesting comparison which can be made is to compare the experimentally determined value $G_{H_2}=0.1$, reported by Livingston and Weinberger[10] and Ghormley and Stewart,[11] for the molecular hydrogen yield found in ice which had been subjected to γ irradiation at 77°K and then warmed to room temperature, with the yield predicted by the model discussed in this paper. The experimental atomic hydrogen yield, $G_{H_2}=0.9$, would predict a molecular yield of 0.45 on the basis of a direct recombination reaction. However, if the reaction given in Eq. (4) is also considered, then the discussion presented above indicates that the molecular hydrogen yield present after warming an irradiated ice sample is equal to $\frac{1}{2}$ the stabilized OH yield at 77°K. The irradiation dosage used in the works cited in footnotes 10 and 11 was approximately equal to 3.4×10^{19} ev/g. The stabilized OH yield at 77°K found in this study after subjecting an ice sample to a similar dosage was $G_{OH}=0.3$. Therefore, the predicted molecular hydrogen yield at this dosage is $G_{H_2}=0.15$, which is in relatively good agreement with the experimentally determined values.

The stabilization build-up of D and OD radicals was also studied. However, the unresolved nature of the spectrum of irradiated D_2O made quantitative correlations somewhat difficult. Construction of the same type of curves reported above for the H atoms gave results which were very similar to the H_2O system. The existence of an observable isotope effect on the irradiation yields was indicated by the analysis of the spectrum of a 20% H_2O in D_2O mixture which had been irradiated at 4.2°K. The ratio of the spectral intensities of the D lines and the H absorption spectrum should be a factor of 4 if there were no isotope effect present; however, the estimated relative intensity is approximately 1.5. This result can be interpreted as strong evidence for the preferential breaking of a DO—H bond in the primary process.[12] It should be emphasized that these are only preliminary observations and very careful quantitative analyses must be performed before the magnitude of the isotope effect can be separated from experimental error. Such careful concentration assays are planned in the near future.

ACKNOWLEDGMENT

The authors are indebted to Dr. Sol Skolnik for his advice and the interest he has shown in this investigation.

[10] R. Livingston and A. J. Weinberger, J. Chem. Phys. **33,** 499 (1960).

[11] J. A. Ghormley and A. C. Stewart, J. Am. Chem. Soc. **78,** 2934 (1956).

[12] J. H. Baxendale and G. Hughes, Z. Physik Chem. (Frankfurt) **14,** 306 (1958).

Theoretical Investigations on the Light Scattering of Colloidal Spheres. XI. Determination of Size Distribution Curves from Spectra of the Scattering Ratio or from Depolarization Spectra*

ARTHUR F. STEVENSON

Department of Physics, Wayne State University, Detroit, Michigan

AND

WILFRIED HELLER AND MORTON L. WALLACH†

Department of Chemistry, Wayne State University, Detroit, Michigan

(Received August 24, 1960)

The theory of a method is developed by means of which size distributions in heterodisperse systems of colloidal and small microscopic spheres can be determined from spectra of the scattering ratio or depolarization. The method is applicable whenever the distribution is unimodal, positively skewed, and of the type most commonly found in emulsions. It makes use of the Mie-scattering functions and encompasses α values up to 25.2 (diameters up to 3.3 μ if the vacuum wavelength is 5460.73 A) and the relative refractive indices $m=1.05$ (0.05) 1.30. The method yields the mean number or weight average diameter, modal diameter, half-width, and "half-spread" of a distribution and, in addition, the diameter of the smallest particles present in consequential numbers. For those instances where the assumed type of distribution does not apply, an extension of the theory is provided which is based upon a linear combination of two distribution functions of the same type. It allows one, in principle, to consider also negatively skewed and bimodal distributions. Use of the linear combination is indicated only when failure to obtain a satisfactory fit between theoretical and experimental spectra shows nonvalidity, in a particular system, of the simple one-term distribution function.

I. INTRODUCTION

THE most straightforward method for determining size distribution curves in dispersed systems consists of measuring directly the size of a sufficiently large number of individual particles. For colloidal dispersions where a considerable percentage of the particles are below the resolving power of the light microscope, only electron microscopy has been used successfully for this purpose if the particles are solid and undeformable and not subject to shrinkage due to desolvation during specimen preparation. In all other instances, and particularly with emulsions, indirect methods must be considered. The outstanding classical method is sedimentation, either by gravity or centrifugation or ultracentrifugation. The present paper is concerned with the theoretical principles of a method based upon light scattering measurements in resting dispersed systems.

Factors which make the light scattering method promising are (1) the generally extensive variation of light-scattering quantities with particle size; (2) the fact that the actual distribution of particles in a system is not interfered with or affected by the measurement and (3) the fact that by proper experimentation a record of the size distribution can be obtained which pertains to a definite time. This is of particular importance in systems where particle size and particle size distribution are subject to changes with time, such as in emulsions or in coagulating systems. With sedimentation, centrifugation, or ultracentrifugation, such an "instantaneous" record is not obtainable.

II. PREVIOUS WORK ON LIGHT SCATTERING IN HETERODISPERSE SYSTEMS

Early exploratory work by LaMer and collaborators[1] showed that light scattering measurements are, in principle, applicable for the purpose stated. They found that the scattered intensity and the turbidity observed on mixing two or three very dilute monodisperse sulphur sols were additive. They also explored the effect of heterodispersity in sulfur aerosols upon the angular variation of the "polarization ratio," upon the sharpness of the orders in the "higher order Tyndall spectra," and upon the degree of ellipticity of the scattered light. The assumption was made that the particle size distribution is "rectangular" (the number or weight of the particles is constant within an arbitrary range of particle size and is zero above and below the limiting sizes). Dandliker[2] investigated the effect of the spread of a rectangular distribution upon the angular variation of light scattering near the first angular intensity minimum. Arrington[3] also concentrated on this minimum and proposed an interesting semiempirical method

* This work was supported by the Office of Naval Research. A preliminary account has been given at the 134th meeting of the American Chemical Society in Chicago, Illinois, September, 1958.

† Present address: Film Department, E. I. duPont de Nemours & Company, Wilmington, Delaware.

[1] I. Johnson and V. K. LaMer, J. Am. Chem. Soc. **69**, 1184 (1947); M. Kerker and V. K. LaMer, J. Am. Chem. Soc. **72**, 3516 (1950).

[2] W. B. Dandliker, J. Am. Chem. Soc. **72**, 5110 (1950). See also F. Bueche, J. Am. Chem. Soc. **74**, 2373 (1952).

[3] C. H. Arrington, Jr., Abstract from 125th meeting of Am. Chem. Soc., Kansas City, Kansas, March, 1954.

applied subsequently by Sloan,[4] by means of which qualitative information on size distribution can be obtained from the angular variation of scattering without making an assumption about the nature of the distribution curve. Gumprecht and Sliepcevich[5] attempted to determine size distribution curves in a settling suspension by studying the variation, with time, in the attenuation of the transmitted light. Kerker, Cox, and Shoenburg[6] subsequently proceeded in an analogous fashion except for using the variation, with time, in the intensity of scattering at an angle of 130° with respect to the reverse direction of the incident beam. Significant also are the turbidity and dissymmetry calculations and experiments of Atherton and Peters[7] for Gaussian distributions of spheres, and the calculations of Ellison[8] and Evva[9] on the theoretical effect of different types of distributions upon light scattering.[10] The most elegant method developed thus far, but restricted to particles of microscopic dimensions, is that of Chin, Sliepcevich, and Tribus.[11] Here, the angular variation of scattering is measured at small angles with respect to the direction of the primary beam.

III. PRINCIPLES OF THE THEORY AND METHOD USED IN THIS INVESTIGATION

1. The General Type of Distribution Curve Considered

In order to obtain a size distribution curve without introducing any restrictive assumption into the analysis, it is necessary to have available a very large number of characteristically different experimental data. This is possible with sedimentation, centrifugation, or ultracentrifugation methods where one can study the variation of particle concentration with the height in the settling system and the variation of this function with time. Similarly, one could study the variation of several light-scattering quantities with both the angle of observation and with wavelength. A very considerable computational labor would be involved in an analysis of this type due to the complicated variation of angular light scattering functions with particle size. This is a deterrent unless one can rely exclusively upon electronic computation. A simpler labor-saving alternative is to assume a basic type of distribution function. Unless the systems to be investigated differ radically in their method of preparation, such an assumption is safe.

A priori, several types of distribution may be considered. We disregard the unrealistic rectangular distribution referred to, the Gaussian (i.e., normal) distribution, found very rarely in colloidal systems and bimodal distributions, which almost never occur in nature unless mixtures are considered or unless two independent mechanisms are operating during the formation of a heterodisperse system. A useful possibility is the gamma distribution function. This was considered by Arrington.[12] A Maxwellian distribution has been used by Hosemann and co-workers[13] who treated the problem of determining size distribution curves in heterodisperse systems by means of small angle x-ray scattering.[14] The log-normal type of distribution function, another useful function, has been used recently by Meehan and Beattie[15] in investigating silver bromide sols by transmission measurements at two wavelengths.

The gamma function, the Maxwellian, or the log-normal distribution appear, in principle, suitable since in general they give nonsymmetrical positively skewed distribution curves. This is the distribution most often found in colloidal and microscopic dispersions.[16] These distribution functions extend down to infinitely small particle sizes. Most actual distribution curves seem to decline asymptotically towards the origin (see, e.g., footnote 17) so that a consequential number of particles are found only above a certain particle size.[16a] Selecting a distribution curve which does not trail off in particle numbers towards the origin has the advantage that it introduces an additional parameter by defining the particle size below which the relative contribution of the dispersed material to the distribution is negligible. It should also be noted that the portion of the distribution curve near the origin is not accessible to evaluation since both the spectral and angular variation of light scattering are insensitive to particle size within the Rayleigh range. The low particle size section of distribution curves obtained by the functions mentioned above is, therefore, meaningless.

Since the present work is intended primarily for the study of emulsions, it was necessary that the model distribution function selected coincide as closely as

[4] C. K. Sloan, J. Phys. Chem. **59**, 834 (1955).

[5] R. O. Gumprecht and C. M. Sliepcevich, J. Phys. Chem. **57**, 95 (1953). See also D. Sinclair and V. K. LaMer, Chem. Rev. **44**, 245 (1949).

[6] M. Kerker, A. L. Cox, and M. D. Shoenberg, J. Colloid Sci. **10**, 413 (1955).

[7] E. Atherton and R. H. Peters, Brit. J. Appl. Phys. **4**, 344, 366 (1953).

[8] J. McK. Ellison, Brit. J. Appl. Phys. **5**, 38 (1954).

[9] F. Evva, Z. Physik. Chem. **202**, 208 (1953); **203**, 86 (1954).

[10] Noteworthy also is the work of Benoit on the asymptotic behavior in the angular variation of light scattering by polydisperse Gaussian coils. [H. Benoît, J. Polymer Sci. **11**, 507 (1953).]

[11] J. H. Chin, C. M. Sliepcevich, and M. Tribus, J. Phys. Chem. **59**, 841, 845 (1955).

[12] C. H. Arrington, Jr. (private communication).

[13] R. Hosemann, Z. Physik **113**, 751 (1939), **114**, 133 (1939); Kolloid-Z. **117**, 13 (1950); F. Motzkus and R. Hosemann, I.U.P.A.C. Symposium on Macromolecules in Wiesbaden, Germany, Sec. II Macromolecular Substances in Solution, Vol. II C 8, October 12–17, 1959.

[14] Shull and Roess employed the same technique assuming rectangular, Gaussian, and Maxwellian functions, testing their results against the theoretical curves obtained for all these types of distribution. [J. Appl. Phys. **18**, 308 (1947).]

[15] E. J. Meehan and W. H. Beattie, J. Phys. Chem. **64**, 1006 (1960).

[16] C. Orr and J. M. Dallavale, *Fine Particle Measurement* (The Macmillan Company, New York, 1959), pp. 10, 29. [16a] In some instances, the distribution curves actually seem to start at a given particle size (e.g., E. O. Kraemer and A. J. Stamm, footnote 17).

possible with that found empirically for emulsions, except for the restriction just mentioned. A number of size distribution curves found in the literature[17] were, therefore, analyzed. In addition, very careful microscopic determinations of size distribution curves in emulsions carried out by Dr. H. Oppenheimer[18] were considered. All turned out to exhibit the same general type of distribution. Curve I in Fig. 1 is representative of it. It reproduces the results obtained on an ethylbenzene-water emulsion containing 1% of potassium myristate as a stabilizer. Curve II in Fig. 1 represents a plot of the theoretical model distribution selected and discussed in detail below.

2. Light-Scattering Theory and Light-Scattering Quantities Considered

In the quoted earlier attempts at using light scattering for the determination of size distribution curves, either the Rayleigh-Gans or Debye theory[2–4,7,8] was used or it was assumed that the diffraction theory was applicable.[5,8,11] The former theories are applicable if the relative refractive index m approaches unity and the latter if the sizes of the particles are throughout in the upper microscopic range. Both assumptions introduce severe restrictions on the practical application of the light scattering method. In the present work (as in the earlier exploratory investigations of LaMer,[1] Kerker,[6] and Evva[9]), the Mie theory was taken as a basis, which requires that the particles are spheres. This applies strictly in emulsions and in lattices.

The experimental variables that one may use for the present purpose are the variation of light scattering, or of some special feature of light scattering, with wavelength or with the angle of observation. The former was selected for the present work. The choice as to the light-scattering quantity and the angle of observation was made in favor of the spectra of the scattering ratio (depolarization) observed at an angle of 90° with respect to the incident beam. This ratio, which has been discussed elsewhere for monodisperse systems, both with regard to theory[19] and experiment,[20] has the practically important advantage in that the instrument constant is eliminated. Results are, therefore, directly comparable to theory.[20a] The application of other light-scattering quantities for the present purpose will be discussed in subsequent papers.

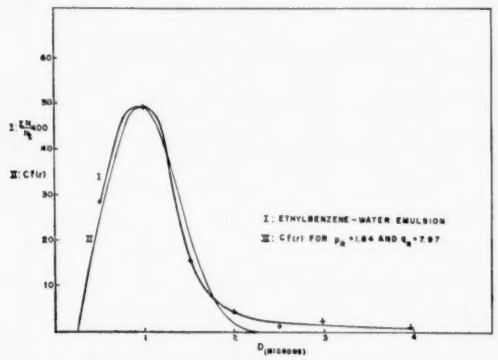

FIG. 1. Typical experimental (I) and assumed standard theoretical (II) distribution curve in emulsions.

3. Outline of the Theory

The distribution function adopted is defined by

$$f(r)=(r-r_0)\exp\{-[(r-r_0)/s]^3\}, \qquad r\geq r_0 \qquad (1)$$
$$=0, \qquad r<r_0,$$

where $Cf(r)\,dr$ is the number of particles per unit volume with radii between r and $r+dr$, C is a normalization constant, and r_0, s are parameters characterizing the distribution; of these, r_0 is the radius of the smallest particle present in consequential numbers, while s determines the modal radius, r_m, the half-width w,[20b] and the "halfspread" (r_m-r_0) through the relations

$$w=0.9015s \qquad (2)$$

$$r_m-r_0=3^{-\frac{1}{3}}s. \qquad (2a)$$

The scattering ratio σ has been defined[19] as

$$\sigma=I_{||}/I_{\perp}, \qquad (3)$$

where $I_{||}$ and $I_{\perp}$ are the intensities, per unit solid angle, of the light scattered at 90° by unit volume of the scattering system, when the incident beam is of unit intensity and polarized with the electric vector parallel or perpendicular, respectively, to the plane of observation. The intensities per unit solid angle for a *single* particle of radius r are

$$J_{||}=(\lambda^2/4\pi^2)i_{||}(\alpha); \qquad J_{\perp}=(\lambda^2/4\pi^2)i_{\perp}(\alpha) \qquad (4)$$

where $\alpha=2r\pi/\lambda$, λ is the wavelength in the medium, and $i_{||}$, $i_{\perp}$ are the basic Mie functions for scattering at 90°.[19] (Their dependence on the relative refractive

[17] P. Finkle, H. D. Draper, and J. H. Hildebrand, Colloid Symposium Monograph **I**, 203 (1923); W. D. Harkins and N. Beeman, J. Am. Chem. Soc. **51**, 1674 (1929); E. O. Kraemer and A. J. Stamm, *ibid.* **46**, 2709 (1924); J. O. Sibree, Trans. Faraday Soc. **27**, 172 (1931); A. I. Yurzhenko, J. Phys. Chem. U.S.S.R. **19**, 152 (1945).

[18] Unpublished work by W. Heller and H. Oppenheimer carried out from 1943–45 at the University of Chicago in connection with an Office of Rubber Reserve project on emulsion polymerization.

[19] W. Heller, W. J. Pangonis, and N. Economou, J. Chem. Phys. **34**, 971 (1961).

[20] W. Heller and R. Tabibian (to be published elsewhere).

[20a] In order to be comparable, it is of course necessary in addition that the experimental data are extrapolated to zero concentration. Otherwise, complications arise due to multiple scattering. These experimental matters are discussed in detail elsewhere (footnotes 20 and 27).

[20b] It may be recalled that the modal radius is the radius at the peak of the distribution curve and the half-width is the distance between the two points of the curve at which the frequency of particle numbers is one-half the peak frequency.

[20c] The factor $1/q^2$ is inserted in Eqs. (7) and (8) in order to make $F_{||}$ and $F_{\perp}$ finite as $q\to 0$.

index m is not expressed here explicitly.) Hence,

$$I_{||}=\int_0^\infty J_{||}Cf(r)dr; \qquad I_\perp=\int_0^\infty J_\perp Cf(r)dr; \tag{5}$$

From Eqs. (3)–(5), we then have, on changing the variable of integration from r to α,

$$\sigma=F_{||}(p,q)/F_\perp(p,q), \tag{6}$$

where[20e]

$$F_{||}(p,q)=(q^2)^{-1}\int_p^\infty i_{||}(\alpha)(\alpha-p) \times \exp\{-[(\alpha-p)/q]^3\}d\alpha, \tag{7}$$

$$F_\perp(p,q)=(q^2)^{-1}\int_p^\infty i_\perp(\alpha)(\alpha-p) \times \exp\{-[(\alpha-p)/q]^3\}d\alpha. \tag{8}$$

The quantities p and q are defined by

$$p=2\pi r_0/\lambda, \tag{9}$$

$$q=2\pi s/\lambda. \tag{9a}$$

They are the two primary parameters by means of which a distribution curve can be defined. The former is proportional to the radius of the smallest particles present in consequential numbers, the latter defines the degree of heterodispersion. It is seen that $w=0$ if $q=0$, i.e., $q=0$ corresponds to a monodisperse system and increasing q to increasing heterodispersity. Equations (6)–(8) give σ, at constant m, as a function of the two dimensionless quantities p and q. Electronic computations of $F_{||}(p,q)$, $F_\perp(p,q)$ and σ have been made for the following ranges of m, q and p[21]:

$m=1.05(0.05)1.30,$

$q=0.0(0.2)12.8,$

$p=0.0(0.2)25.2$ for $q=0.2,$

$p=0.0(0.2)24.8$ for $q=0.4,$

.....

$p=0.0$ for $q=12.8.$

It was found convenient to normalize all data by using as a reference the wavelength

$$\lambda_R=4093.57A\ (\lambda_0=5460.73A),$$

which is the wavelength of the green Hg line *in water* at 25°C, and to define

$$p_R=2\pi r_0/\lambda_R, \tag{10}$$

$$q_R=2\pi s/\lambda_R. \tag{10a}$$

The relations between p, p_R and q, q_R are, for any given heterodisperse system,

$$p\lambda=p_R\lambda_R, \tag{11}$$

$$q\lambda=q_R\lambda_R. \tag{11a}$$

From Eqs. (2), (2a), (10), and (10a) we deduce, *in microns*:

$$w=0.05873q_R, \tag{12}$$

$$r_m-r_0=0.04517q_R, \tag{12a}$$

$$r_m=0.04517q_R+0.06515p_R, \tag{12b}$$

$$r_0=0.06515p_R. \tag{12c}$$

Thus, once p_R and q_R have been found, the distribution function, half-width, halfspread, modal radius, and radius of the smallest particles present in consequential numbers can be determined.

In addition to these quantities, the mean diameter $\bar{D}$, is also of interest. It is defined by

$$\bar{D}_n=2\int_0^\infty rf(r)dr \Big/ \int_0^\infty f(r)dr. \tag{13}$$

The subscript n indicates the number average. After substitution of Eq. (1) and subsequent integration,

$$\bar{D}_n=[4s/3\Gamma(5/3)]+D_0, \tag{14}$$

where

$$D_0=2r_0.$$

On replacing the gamma function by the proper numerical value, one finally obtains, in microns,

$$\bar{D}_n=1.476s+D_0, \tag{15}$$

or, on considering the parameters q_R and p_R,

$$\bar{D}_n=0.06515(1.476q_R+2p_R). \tag{16}$$

The weight average diameter $\bar{D}_w$ and the "surface

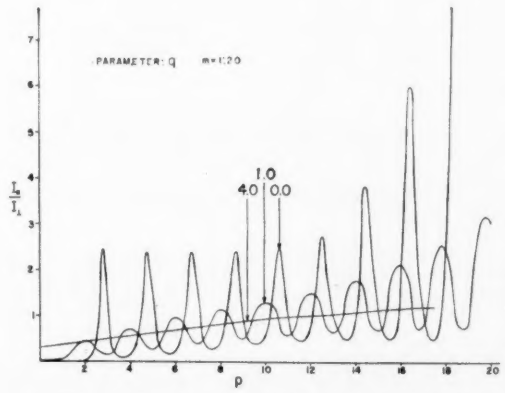

FIG. 2. Variation of scattering ratio (depolarization) with p.

[21] The results, too lengthy to be reproduced here, have been collected in book form: A. F. Stevenson and W. Heller, *Scattering Functions for Heterodisperse Systems* (Wayne State University Press, Wayne State University, Detroit, Michigan, 1961).

average" diameter $\bar{D}_s$ are also of interest:

$$\bar{D}_w = 2.214s + D_0 = 0.06515(2.214q_R + 2p_R), \quad (17)$$

$$\bar{D}_s = 2.022s + D_0 = 0.06515(2.022q_R + 2p_R). \quad (18)$$

IV. SIZE DISTRIBUTION CURVES FROM THE SCATTERING RATIO

1. Theoretical Variation of the Scattering Ratio with p and q

The scattering ratio σ traverses a series of successive numerically different maxima and minima as p increases. With increasing heterodispersity the amplitude of these oscillations becomes progressively smaller, as shown in Fig. 2 for $m=1.20$. The amplitudes are maximal at $q=0$ (p is then identical with α). At $q=2.0$, the maxima and minima have already nearly vanished particularly if p is small. The multivaluedness of p to be associated with σ at a given q disappears, of course, at these higher q values. It will be noted (a) that the peaks shift towards smaller p values as q increases, and (b) that σ is not zero for $p \to 0$ provided $q \neq 0$. Once q is sufficiently large ($q \geq 2$), σ increases almost linearly with p up to at least $p=10$, i.e., at constant q,

$$\sigma_q \cong hp + b(q), \quad (19)$$

the slope h decreasing only very slightly with a further increase of q.

Figure 3 shows that σ is, at lower q values, very sensitive to q but q is a bi-valued function of σ if $p \geq 2$. If q is small, σ approaches zero asymptotically, provided $p \leq 1$. ($p \to 0$ and $q \to 0$ characterize Rayleigh scattering where $I_{\perp} = 0$.) At moderate or high q values, on the other hand, σ increases linearly with q at any p, viz.,

$$\sigma_p \cong h'(q-3) + b'(p), \qquad q \geq 3, \quad (20)$$

the slope h' decreasing very slightly as p increases. [The behavior of the $\sigma_q(p)$ and $\sigma_p(q)$ curves has been discussed here for the particular case where the relative refractive index $m=1.20$. For other m values, the numerical values of the $\sigma_p(q)$ and $\sigma_q(p)$ curves will (in most p and q ranges) differ appreciably from those given in Figs. 2 and 3 but their general shape is the same.]

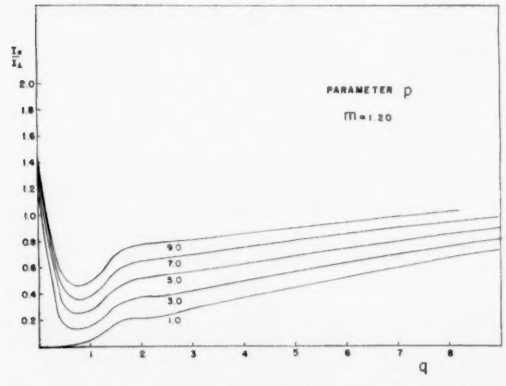

FIG. 3. Variation of scattering ratio (depolarization) with q.

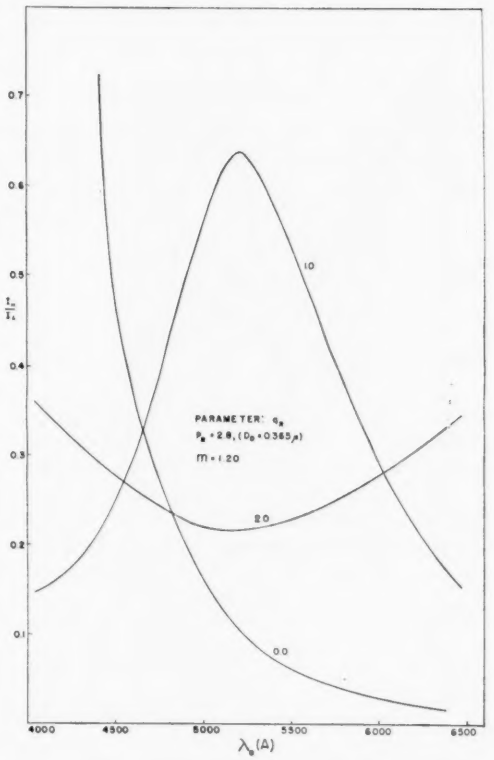

FIG. 4. Theoretical spectra of scattering ratio (depolarization) and their variation with the degree of heterodispersion. I. The number of particles with a diameter $<0.365\ \mu$ is negligible.

In view of Eqs. (9), and (9a), Fig. 2 would also represent the variation of σ with $1/\lambda$ if, in first approximation, the parameter q were replaced by q_R. Corresponding considerations apply to Fig. 3 where one would replace the parameter p by p_R. This shows the relationship between the data illustrated in these figures and theoretical σ spectra.[22]

2. Theoretical Variation of σ Spectra with p_R and q_R

The last problem is the actual derivation of p_R and q_R values for a given heterodisperse system, from the experimental spectral record of σ. To do this, one has a choice between several procedures. (1) One may derive from the experimental data normalized $\sigma_{qR}(p_R)$ or $\sigma_{pR}(q_R)$ curve sections and then search for a graphical fit with normalized theoretical curves of these func-

[22] The introduction of p_R and q_R entails additional work in the practical application of the data. If the spectral range covered is small, one may operate with p and q directly unless optimum accuracy is desirable.

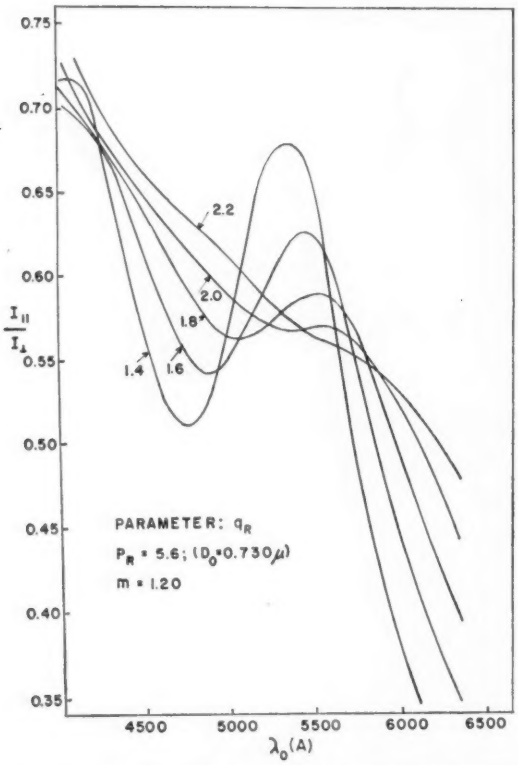

FIG. 5. Theoretical spectra of scattering ratio (depolarization) and their variation with the degree of heterodispersion. II. The number of particles with a diameter $<0.730\ \mu$ is negligible.

tions.[23] (2) One can establish a series of theoretical curves on the variation of σ with λ, within the λ range to be used experimentally, varying systematically q_R and p_R.[24] The actually observed spectra are then compared graphically with the theoretical spectra. (3) One may, by successive numerical approximation, arrive at the p_R and q_R values which satisfy any experimental spectrum best.[25] The second method was found to be by far the most advantageous both from the point of view of conclusiveness of the result and time required for a complete analysis.[26] It was therefore used for the practical application of the theoretical method described in this paper.

Examples of the numerous theoretical σ spectra used in the practical application of this method to the determination of size distribution curves in polystyrene latices,[27] where $m=1.20$, are given in Figs. 4–6 for the three D values 0.365, 0.730, and 1.069 μ and for various degrees of heterodispersion. The curves are, therefore, representative of the spectra which one may encounter with heterodisperse systems which encompass the colloidal or the lower microscopic range or both. It is seen that an increase in heterodispersity follows the qualitatively well-known pattern of a gradual decrease in height of the maxima accompanied by a relatively smaller increase in height of the minima. In addition, the wavelengths at which the maxima and minima occur shift, at the same time, gradually towards the red. A comparison of the three figures suggests that the experimental data may, at any one q_R, be more sensitive to changes in heterodispersity the larger r_0. This is likely because the number and height of the maxima and minima which enter into a given spectral range increases with r_0 irrespective of q_R. However, it is apparent from Fig. 4 that even at relatively small

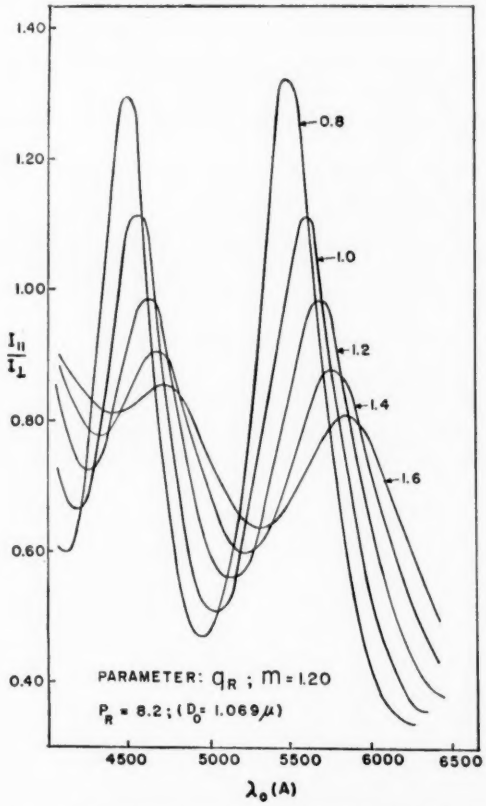

FIG. 6. Theoretical spectra of scattering ratio (depolarization) and their variation with the degree of heterodispersion. III. The number of particles with a diameter $<1.069\ \mu$ is negligible.

[23] For sufficiently heterodisperse systems this procedure may be combined with the use of analytical expressions (Eqs. 19 and 20).

[24] The $\sigma(\lambda)$ curve may be derived from the $\sigma(p, q)$ values by means of Eqs. (11) and (11a).

[25] This numerical equivalent to the graphical method would be most promising if electronic computation is available. Such an electronic fitting procedure, which is under preparation, could allow one to obtain size distribution curves from spectra within a few minutes after completion of the experiments.

[26] There are still other possible methods, most of which were tried. They are not discussed here since they proved to be less attractive from the practical point of view.

[27] Those results will be published elsewhere.

r_0 values, the effect of increasing heterodispersity is very striking.

On applying these theoretical spectra, it must be borne in mind that the relative refractive index m varies with wavelength. In the systems investigated[27] the dispersion was relatively small, and therefore the error resulting from a disregard of the dispersion of m was less than the over-all experimental error. It is necessary, however, to be aware of this potential source of disagreement between theoretical and experimental σ spectra in cases where Eq. (1) applies. It may be necessary in the case of strong dispersion differences between medium and colloidal material to eliminate this potential error by allowing for the dependence of m on λ in the calculation of σ spectra.

In some instances it may be desirable to have an additional argument besides the spectra of the scattering ratio. The turbidity spectra, to be discussed in a following paper, may serve this purpose.

3. Determination of Distribution Curves not Satisfied by the Distribution Function Assumed

The practical application of the scattering functions derived is limited, as stated, to systems which satisfy the distribution function assumed by Eq. (1). It is, therefore, important to know whether or not in doubtful cases the method outlined is applicable. Systematic experiments, carried out with lattices prepared so as to give distributions radically different from that assumed, showed that a satisfactory fit between experimental data and theoretical data cannot be obtained under any circumstances. Whenever a fit is obtained for a spectral range of about 1000 A, one has, therefore, an implicit assurance that the distribution curve is reasonably similar to that assumed by Eq. (1). This excludes the risk of deriving fictitious distribution curves.

For systems which do not obey Eq. (1), one has, *a priori*, three possible methods of approach: (1) One may increase the number of experimental parameters, by the inclusion of other light scattering quantities, so that a more general theoretical treatment not requiring any assumption may become possible; (2) one may limit the experimental data to the spectra of one scattering quantity as done here but repeat the theoretical treatment for other basic distribution functions such as log normal, Gaussian, or Maxwellian. In that case, electronic matching of theoretical and experimental spectra would involve the successive application of several distribution functions until an optimum fit is obtained; (3) one may simply modify Eq. (1) in order to provide it with more flexibility. Possibility (3) has been taken advantage of in the present investigation. To that effect a linear combination of distribution functions of the same form was used.

Denoting the distribution function given by Eq. (1) more precisely by $f(r, r_0, s)$, consider the distribution

$$g(r)=C_1 f(r, r_0, s)+C_2 f(r, r_0', s'). \tag{21}$$

There are five parameters in this equation, r_0, r_0', s, s', and C_2/C_1. In order to calculate σ from this equation, it is necessary to know the individual values of $F_{\parallel}$ and $F_{\perp}$,[28] since now

$$\sigma=\frac{F_{\parallel}(p, q)+(C_2/C_1)F_{\parallel}(p', q')}{F_{\perp}(p, q)+(C_2/C_1)F_{\perp}(p', q')}, \tag{22}$$

where

$$p_R'\lambda_R=p'\lambda, \qquad p'=2\pi r_0'/\lambda,$$

$$q_R'\lambda_R=q'\lambda, \qquad q'=2\pi s'/\lambda.$$

The introduction of the second term makes it possible to consider distributions which are negatively skewed or bimodal. For the practical application of the second term, it was found best to construct a plot or carry out a numerical analysis of the mean square deviations between the experimental σ spectrum and the theoretical σ spectrum obtained with the p_R and q_R parameter pair which allowed one to come nearest to a fit. The trend of the deviations allows one to decide as to whether the parameters p_R' and q_R' are larger or smaller than p_R and q_R. One then fixes tentatively the values of p_R' and q_R' assuming at first that $C_1=C_2$ and one varies the ratio C_2/C_1 until the sum of the mean square deviations over the entire spectral range is minimal. This yields the first approximation value of C_2/C_1. This entire procedure is repeated until by successive approximations, p_R', q_R', and C_2/C_1 values are obtained which lead to a satisfactory fit between theoretical and experimental data. Practical application of this method has shown that, in general, a few successive trials are sufficient in order to approach an acceptable fit and to lead to a distribution curve which is in acceptable agreement with distribution curves determined by the electron microscope. Tests limited to a negatively skewed distribution were successful. The one-term equation was tested successfully on a distribution obeying Eq. (1) and also on a Gaussian distribution.

ACKNOWLEDGMENTS

The electronic computations were obtained with the efficient cooperation of Dr. A. Jacobson, former Director of the Wayne State University Computation Laboratory and H. James McCarty. The electronic computations were kindly financed by the Research Laboratories of the United States Rubber Company, Wayne, New Jersey.

[28] The values of $F_{\perp}$ which, together with σ, are sufficient for an application of Eq. (21) are given in the collection of scattering functions referred to in footnote 21.

Theoretical Investigations on the Light Scattering of Colloidal Spheres. XII. The Determination of Size Distribution Curves from Turbidity Spectra*

MORTON L. WALLACH† AND WILFRIED HELLER

Department of Chemistry, Wayne State University, Detroit 2, Michigan

AND

ARTHUR F. STEVENSON

Department of Physics, Wayne State University, Detroit 2, Michigan

(Received August 26, 1960)

The theory of a method is outlined which gives size distribution curves in heterodisperse systems of non-absorbing colloidal and small microscopic spheres from measurements of turbidity spectra. The assumption is made that the distribution follows a function previously given which closely approximates that commonly found in emulsions. All the numerical data necessary for practical application of the method are provided for the relative refractive indices $m=1.05$ (0.05) 1.30. They were obtained from the Mie theory. The method may be used independently, but is particularly useful in conjunction with an alternate method described in a previous publication (XI).

A PRECEDING paper[1] dealt with the theory of a method for determining size distribution curves in colloidal suspensions of spheres from the spectra of the scattering ratio or depolarization. The present paper is concerned with an extension of this theory to an alternate method in which use is made of turbidity spectra obtained from transmission measurements. This alternate method is attractive for two reasons: (a) the measurements necessary are relatively simple and high precision is possible; (b) far less computational work is necessary because the theoretical functions are monotonic over wide ranges of particle size. In many instances, turbidity spectra alone will allow one to obtain a conclusive answer on size distribution curves; in others, they will be a welcome supplemental argument in an analysis based on the use of spectra of the scattering ratio.

I. PRINCIPLES OF THE THEORY

The basic assumption made here as in the preceding paper[1] is that the size distribution curve to be determined can be approximated by the function

$$Cf(r)=(r-r_0)\exp\{-[(r-r_0)/s]^3\},\ r\geq r_0$$
$$=0,\qquad r<r_0, \tag{1}$$

where $Cf(r)dr$ is the number of particles, per unit volume of dispersed system, which have radii between r and $(r+dr)$, C is a normalization factor, r_0 is the radius of the smallest particles present in consequential numbers, and s is a parameter proportional to the width of the distribution curve.[2a] Equation (1) is applicable if the distribution curve is positively skewed and it is especially suitable for emulsions.

The total radiation scattered by a single sphere from an incident beam of unit intensity (scattering cross section)[2b]

$$R=(\lambda^2/2\pi)\sum(\alpha, m), \tag{2}$$

where

$$\sum=\sum_1^\infty[(|a_n|^2+|b_n|^2)/(2n+1)],$$

and the turbidity of the entire system at a given m

$$\tau=(\lambda^2/2\pi)C\int_{r_0}^\infty\sum(\alpha)f(r)dr. \tag{3}$$

Since the volume fraction of the scattering material is given by

$$\phi=C\int_{r_0}^\infty(4\pi r^3/3)f(r)dr, \tag{4}$$

one obtains for the convenient dimensionless quantity

$$\lambda\tau/\phi=(3\lambda^3/8\pi^2)\int_{r_0}^\infty\sum(\alpha)f(r)dr/\int_{r_0}^\infty r^3f(r)dr, \tag{5}$$

where λ is the wavelength in the scattering system. On using the concentration c expressed in terms of g of scattering material per 100 g of dispersed system

$$\lambda\tau/c=(0.01\lambda\tau/\phi)(\rho_{12}/\rho_2), \tag{6}$$

where ρ_2 and ρ_{12} are the densities of the scattering spheres and of the entire system, respectively. The

* This work was supported by the Office of Naval Research; a preliminary account of this work was given at the 134th meeting of the American Chemical Society, September, 1958.

† Present address: Film Department, E. I. duPont de Nemours & Company, Wilmington, Delaware.

[1] A. F. Stevenson, W. Heller, and M. L. Wallach, J. Chem. Phys. **34**, 1789 (1961).

[2] (a) For all symbols not specifically defined here as far as they pertain to the development and use of Eq. (1), the preceding paper should be consulted. (b) For the definition of other symbols see W. Heller and W. J. Pangonis, J. Chem. Phys. **26**, 498 (1957).

quantity $\lambda\tau/c$ is, at a fixed wavelength, proportional to the specific turbidity investigated before in detail for monodisperse systems.[2b] Introducing the quantities

$$p=2r_0\pi/\lambda; \qquad q=2s\pi/\lambda \tag{7}$$

previously[1] defined, one finally obtains, remembering that $r=\alpha\lambda/2\pi$ and $dr=(\lambda/2\pi)d\alpha$:

$$\lambda\tau/\phi=3\pi\int_p^\infty \sum(\alpha)(\alpha-p)\,\exp\{-[(\alpha-p)/q]^3\}d\alpha/\int_p^\infty \cdot\alpha^2(\alpha-p)\,\exp\{-[(\alpha-p)/q]^3\}d\alpha. \tag{8}$$

Table I gives the electronically computed theoretical values of $(\lambda\tau/\phi)$ for a wide range of p and q values and for the relative refractive indices $m=1.05$ (0.05) 1.30.[3] It contains all the information needed for an application of the method.[4]

The variation of $\lambda\tau/\phi$ with p is shown in Fig. 1 for various values of q if $m=1.20$. If $q=0$, p is identical with α (monodispersed system). The variation of the intercepts ($p=0$) with q represents at constant λ the variation of $\lambda\tau/\phi$ with the degree of heterodispersion if $r_0=0$. A progressive increase in the degree of heterodispersion in a system containing particles in consequential numbers down to $r=0$ is, therefore, accompanied by an increase in specific turbidity up to a maximum and a subsequent decrease. This qualitatively well-known phenomenon now follows directly from theory. The maximal specific turbidity in such a system is, however, distinctly smaller than in a monodisperse system. The exclusively negative slope of the curves at sufficiently high heterodispersion ($q\geq 8$) indicates that the specific turbidity is then dominated by those particles whose individual contributions are pertinent to α values beyond the turbidity maximum.

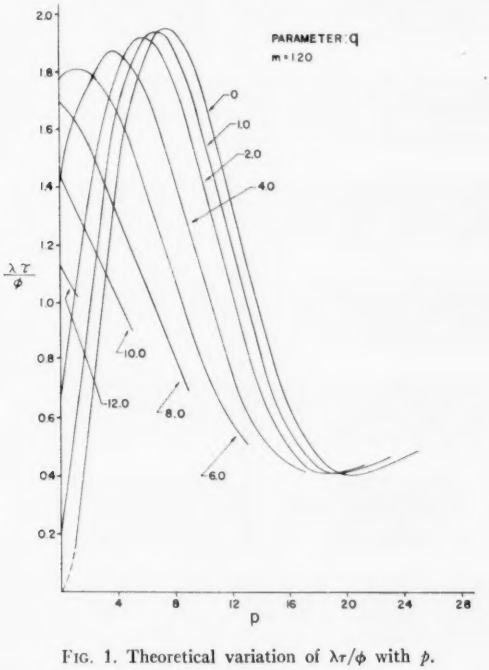

FIG. 1. Theoretical variation of $\lambda\tau/\phi$ with p.

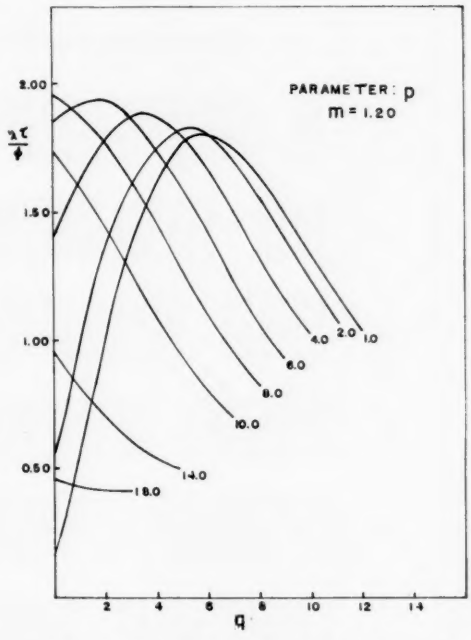

FIG. 2. Theoretical variation of $\lambda\tau/\phi$ with q.

Figure 2 shows the variation of $\lambda\tau/\phi$ with q for various values of the parameter p. Here, the intercepts give the variation of $\lambda\tau/\phi$ with α in a monodisperse system.

It is clear from Figs. 1 and 2 that a given $\lambda\tau/\phi$ value is associated with an infinite number of pairs of p and q values. Consequently, turbidity spectra are needed in order to arrive at a decision about particle size distribution. It is convenient to introduce again, as in the case of σ spectra,[1] a reference wavelength λ_R and with it the quantities q_R and p_R previously defined.[1] The wavelength 5460.73 A was selected for λ_R.

II. THEORETICAL TURBIDITY SPECTRA

Table I allows one by means of the equations given to construct theoretical turbidity spectra on fixing p_R and q_R. In order to compare them with experimental turbidity spectra, it was found advantageous to normalize both theoretical and experimental $\lambda\tau/\phi$ values with

[3] The integral in the denominator was evaluated explicitly. The $\Sigma(\alpha)$-values were taken from: W. J. Pangonis, W. Heller, and A. Jacobson, *Tables of Light Scattering Functions for Spherical Particles* (Wayne State University Press, Detroit, Michigan, 1957).

[4] The relatively wide spacing of the p and q values is warranted on account of the relatively simple nature of $(\lambda\tau/\phi)$ curves.

TABLE I. The variation of $(\lambda\tau/\phi)\times 10^2$ with the parameters p and q.

$m=1.05$

q \ p	0	1	2	3	4	5	6	7	8	9	10	11	12	
0	...	0.01252	0.03906	0.06780	0.09382	0.12363	0.15019	0.17570	0.19899	0.22352	0.24566	0.26663	0.28402	
1	0.00968	0.03174	0.05924	0.08745	0.11263	0.14173	0.16755	0.19233	0.21489	0.23865	0.25999	0.28013	0.29670	
2	0.03318	0.05588	0.08202	0.10864	0.13254	0.16061	0.18548	0.20936	0.23104	0.25389	0.27433	0.29355		
3	0.05986	0.08133	0.10561	0.13058	0.15311	0.17999	0.20376	0.22661	0.24730	0.26915	0.28860	0.30682		
4	0.08569	0.10657	0.12925	0.15273	0.17392	0.19956	0.22217	0.24390	0.26352	0.28429	0.30268		0.58968	25
5	0.11141	0.13114	0.15260	0.17476	0.19468	0.21907	0.24049	0.26106	0.27956	0.29918	0.31647		0.63738	24
6	0.13622	0.15512	0.17550	0.19645	0.21517	0.23832	0.25854	0.27792	0.29527	0.31372		0.64895	0.68449	23
7	0.16016	0.17848	0.19784	0.21764	0.23524	0.25716	0.27618	0.29435	0.31054	0.32777		0.69568	0.73004	22
8	0.18355	0.20108	0.21951	0.23824	0.25473	0.27545	0.29328	0.31023	0.32524		0.70522	0.74057	0.77294	21
9	0.20614	0.22292	0.24045	0.25813	0.27356	0.29308	0.30972	0.32546	0.33929		0.74931	0.78260	0.81214	20
10	0.22785	0.24397	0.26059	0.27724	0.29163	0.30995	0.32542	0.33994		0.75556	0.79030	0.82070	0.84670	19
11	0.24879	0.26415	0.27988	0.29550	0.30887	0.32600	0.34029	0.35361		0.79542	0.82718	0.85386	0.87560	18
12	0.26884	0.28341	0.29825	0.31286	0.32520	0.34116	0.35429		0.79704	0.83101	0.85893	0.88112	0.89779	17
13	0.28791	0.30173	0.31566	0.32925	0.34059	0.35536	0.36734		0.83089	0.86136	0.88461	0.90152	0.91242	16
14	0.30603	0.31905	0.33206	0.34463	0.35497	0.36857		0.83357	0.85941	0.88555	0.90330	0.91420	0.91883	15
15	0.32315	0.33533	0.34741	0.35896	0.36830	0.38074		0.86127	0.88173	0.90272	0.91420	0.91842	0.91630	14
16	0.33919	0.35054	0.36168	0.37221	0.38056		0.85823	0.88286	0.89704	0.91212	0.91661	0.91360	0.90411	13
17	0.35415	0.36464	0.37484	0.38435	0.39171		0.87877	0.89760	0.90465	0.91309	0.90995	0.89919	0.88204	12
18	0.36803	0.37761	0.38686	0.39535		0.87274	0.89268	0.90486	0.90400	0.90513	0.89379	0.87482	0.85001	11
19	0.38073	0.38942	0.39772	0.40520		0.88613	0.89939	0.90415	0.89467	0.88788	0.86784	0.84036	0.80770	10
20	0.39226	0.40007	0.40741		0.87678	0.89270	0.89852	0.85913	0.87639	0.86115	0.83202	0.79584	0.75499	9
21	0.40264	0.40953	0.41592		0.88324	0.89213	0.88980	0.87763	0.84909	0.82494	0.78637	0.74130	0.69254	8
22	0.41181	0.41780		0.87765	0.88308	0.88427	0.87317	0.85168	0.81290	0.77944	0.73115	0.67700	0.62091	7
23	0.41978	0.42488		0.87873	0.87622	0.86914	0.84877	0.81752	0.76816	0.72506	0.66683	0.60356	0.53983	6
24	0.42658		0.87151	0.87374	0.86277	0.84696	0.81696	0.77564	0.71549	0.66245	0.59405	0.52159	0.44960	5
25	0.43219		0.86837	0.86281	0.84303	0.81819	0.77836	0.72682	0.65579	0.59258	0.51370	0.43147	0.35230	4
		0.86290	0.85994	0.84628	0.81747	0.78350	0.73384	0.67213	0.59034	0.51680	0.42707	0.33418	0.24870	3
		0.85705	0.84649	0.82458	0.78677	0.74377	0.68454	0.61299	0.52087	0.43707	0.33619	0.23214	0.13562	2
	0.84823	0.84669	0.82842	0.79832	0.75172	0.70003	0.63181	0.55115	0.44967	0.35634	0.24486	0.13038	0.03930	1
	0.84043	0.83213	0.80619	0.76809	0.71313	0.65337	0.57704	0.48847	0.37940	0.27877	0.16145	0.05120	...	0
	12	11	10	9	8	7	6	5	4	3	2	1	0	p \ q

$m=1.10$

$m = 1.15$

p \ q	0	1	2	3	4	5	6	7	8	9	10	11	12	
0	...	0.11691	0.37330	0.63407	0.83816	1.03834	1.17202	1.25921	1.29629	1.30807	1.28067	1.22831	1.15163	
1	0.08944	0.30079	0.56233	0.79732	0.97221	1.14113	1.24440	1.30275	1.31427	1.30282	1.25711	1.19090	1.10577	
2	0.31178	0.53654	0.75948	0.95670	1.09673	1.23037	1.30141	1.33052	1.31728	1.28415	1.22228	1.14465		
3	0.57193	0.75841	0.94260	1.10040	1.20414	1.30113	1.33994	1.34077	1.30458	1.25214	1.17678	1.09047		
4	0.79767	0.95417	1.10112	1.22040	1.28863	1.34960	1.35772	1.33246	1.27605	1.20735	1.12161		0.48737	25
5	0.98962	1.11839	1.22946	1.31188	1.34657	1.37359	1.35376	1.30556	1.23236	1.15093	1.05816		0.47043	24
6	1.14851	1.24771	1.32462	1.37239	1.37632	1.37250	1.32833	1.26104	1.17495	1.08459		0.46766	0.44703	23
7	1.27215	1.34072	1.38551	1.40139	1.37799	1.34723	1.28292	1.20082	1.10594	1.01054		0.44850	0.42481	22
8	1.35839	1.39760	1.41258	1.39992	1.35312	1.29987	1.21999	1.12756	1.02799		0.44389	0.42789	0.40990	21
9	1.40738	1.41966	1.40764	1.37031	1.30443	1.23350	1.14276	1.04446	0.94411		0.42488	0.41256	0.40824	20
10	1.42158	1.40918	1.37367	1.31596	1.23558	1.15193	1.05496	0.95501		0.42409	0.41303	0.41033	0.42570	19
11	1.40418	1.36954	1.31460	1.24113	1.15086	1.05939	0.96058	0.86283		0.41677	0.41622	0.42941	0.46754	18
12	1.35862	1.30510	1.23511	1.15059	1.05495	0.96031	0.86363		0.42243	0.42552	0.44199	0.47697	0.53849	17
13	1.28900	1.22096	1.14034	1.04941	0.95264	0.85907	0.76791		0.43728	0.45743	0.49671	0.55800	0.64266	16
14	1.20049	1.12247	1.03563	0.94268	0.84857	0.75975		0.45364	0.47529	0.51823	0.58472	0.67456	0.78191	15
15	1.09880	1.01505	0.92623	0.83522	0.74703	0.66593		0.49593	0.54126	0.61138	0.70732	0.82517	0.95365	14
16	0.98948	0.90400	0.81707	0.73141	0.65174		0.51653	0.56473	0.63773	0.73731	0.86210	1.00426	1.14991	13
17	0.87757	0.79430	0.71256	0.63499	0.56571		0.58684	0.66190	0.76432	0.89297	1.04275	1.20218	1.35759	12
18	0.76787	0.69029	0.61638	0.54891		0.60612	0.68277	0.78660	0.91731	1.07158	1.23913	1.40572	1.55959	11
19	0.66483	0.59553	0.53138	0.47526		0.69889	0.80305	0.93494	1.08960	1.26282	1.43780	1.59894	1.73658	10
20	0.57211	0.51264	0.45950		0.71081	0.81280	0.94378	1.10006	1.27103	1.45346	1.62284	1.76418	1.86921	9
21	0.49228	0.44339	0.40176		0.81672	0.94415	1.09851	1.27249	1.44905	1.62829	1.77713	1.88347	1.94037	8
22	0.42679	0.38862		0.81619	0.93716	1.08715	1.25870	1.44083	1.60969	1.77145	1.88384	1.94010	1.93651	7
23	0.37621	0.34826		0.92594	1.06718	1.23444	1.41441	1.59276	1.73892	1.86784	1.92796	1.92024	1.84790	6
24	0.34022		0.90928	1.04405	1.20070	1.37766	1.55522	1.71628	1.82401	1.90476	1.89789	1.81440	1.66816	5
25	0.31752		1.01547	1.16569	1.33098	1.50834	1.67136	1.80102	1.85514	1.87345	1.78687	1.61836	1.39372	4
		0.98455	1.12537	1.28565	1.45141	1.61878	1.75481	1.83959	1.82683	1.77070	1.59433	1.33362	1.02413	3
		1.08374	1.23504	1.39883	1.55609	1.70292	1.80035	1.82882	1.73939	1.60047	1.32778	0.96846	0.56768	2
	1.03823	1.18402	1.34058	1.50063	1.64034	1.75688	1.80619	1.77042	1.59987	1.37588	1.00735	0.54786	0.16046	1
	1.12884	1.28235	1.43832	1.58718	1.70093	1.77905	1.77371	1.67047	1.42142	1.12033	0.67777	0.21016	...	0
	12	11	10	9	8	7	6	5	4	3	2	1	0	p \ q

$m = 1.20$

TABLE I.—*Continued.*

$m = 1.25$

p \ q	0	1	2	3	4	5	6	7	8	9	10	11	12	
0	...	0.33105	1.07421	1.71041	2.06002	2.26801	2.23792	2.07535	1.83606	1.59421	1.36461	1.17266	1.01778	
1	0.25242	0.87608	1.56521	2.03724	2.23172	2.29741	2.16662	1.94301	1.68011	1.43806	1.22620	1.05841	0.92814	
2	0.91239	1.51870	1.99787	2.27705	2.31526	2.25005	2.03908	1.77670	1.50939	1.28145	1.09539	0.95494		
3	1.59738	2.01958	2.29807	2.39611	2.29806	2.12728	1.86366	1.58698	1.33350	1.13145	0.97638	0.86408		
4	2.09777	2.33947	2.44027	2.38504	2.18290	1.94032	1.65431	1.38690	1.16245	0.99437	0.87230		0.39011	25
5	2.39861	2.47508	2.42742	2.25536	1.98681	1.70886	1.42915	1.19062	1.00560	0.87527	0.78503		0.36435	24
6	2.50482	2.44247	2.28155	2.03341	1.73652	1.45733	1.20750	1.01141	0.87051	0.77733		0.37687	0.39061	23
7	2.43655	2.27261	2.03747	1.75400	1.46312	1.21070	1.00680	0.85967	0.76203	0.70160		0.40078	0.44604	22
8	2.22969	2.00647	1.73660	1.45446	1.19673	0.99055	0.84022	0.74157	0.68165		0.41151	0.44795	0.50452	21
9	1.93294	1.68914	1.42060	1.16919	0.96241	0.81215	0.71496	0.65855	0.62754		0.46563	0.51991	0.58560	20
10	1.60010	1.36436	1.12584	0.92490	0.77713	0.68309	0.63182	0.60746		0.48444	0.54234	0.60962	0.64664	19
11	1.27993	1.06927	0.87986	0.73817	0.64815	0.60312	0.58606	0.58162		0.55517	0.62109	0.68393	0.72272	18
12	1.00661	0.82980	0.69851	0.61508	0.57373	0.56508	0.56867		0.56945	0.63387	0.69534	0.73767	0.76585	17
13	0.79354	0.65933	0.58490	0.55112	0.54490	0.55749	0.56841		0.63294	0.69177	0.73353	0.74655	0.75550	16
14	0.63991	0.55973	0.53236	0.53371	0.54726	0.56680		0.63444	0.68701	0.72749	0.73888	0.72019	0.69045	15
15	0.54499	0.52120	0.52695	0.54683	0.56506	0.57963		0.67577	0.71039	0.72561	0.70943	0.67343	0.60830	14
16	0.50619	0.52565	0.54890	0.57272	0.58420		0.66506	0.70056	0.70957	0.69862	0.66488	0.63311	0.60737	13
17	0.51400	0.55419	0.57921	0.59478	0.59283		0.68507	0.70167	0.68966	0.66701	0.64194	0.64745	0.71440	12
18	0.55460	0.58793	0.60350	0.60308		0.67405	0.69415	0.69292	0.67102	0.65846	0.67424	0.75155	0.93791	11
19	0.60519	0.60939	0.60962	0.59211		0.68848	0.69756	0.69203	0.68494	0.71387	0.80353	0.97679	1.25814	10
20	0.62864	0.61140	0.59319		0.68629	0.70476	0.71172	0.72047	0.75659	0.85886	1.04875	1.32732	1.65634	9
21	0.61823	0.59180	0.55794		0.71233	0.73299	0.75608	0.80491	0.91212	1.11009	1.40585	1.77226	2.12259	8
22	0.58011	0.54966		0.72223	0.75097	0.78641	0.84550	0.95901	1.15792	1.45976	1.84413	2.25364	2.59112	7
23	0.52513	0.49569		0.76707	0.81050	0.87816	0.99363	1.18887	1.48195	1.87191	2.30059	2.68571	2.94802	6
24	0.47028		0.77633	0.82856	0.89825	1.01356	1.20009	1.48241	1.85250	2.29069	2.69452	2.97105	3.06989	5
25	0.43044		0.83677	0.91141	1.01998	1.19449	1.45567	1.81186	2.12893	2.64428	2.93926	3.01894	2.86314	4
		0.83722	0.91270	1.01813	1.17433	1.41260	1.73990	2.13979	2.52514	2.86179	2.95944	2.76122	2.28768	3
		0.90641	1.00661	1.15046	1.35794	1.65462	2.02520	2.42401	2.72026	1.89107	2.71269	2.17008	1.35824	2
	0.89069	0.98905	1.11936	1.30570	1.56198	1.90310	2.28402	2.62972	2.77255	2.71533	2.21145	1.28845	0.36514	1
	0.96367	1.08675	1.25157	1.48049	1.77605	2.13892	2.49175	2.73535	2.67870	2.36634	1.55767	0.47967	...	0
	12	11	10	9	8	7	6	5	4	3	2	1	0	p \ q

$m = 1.30$

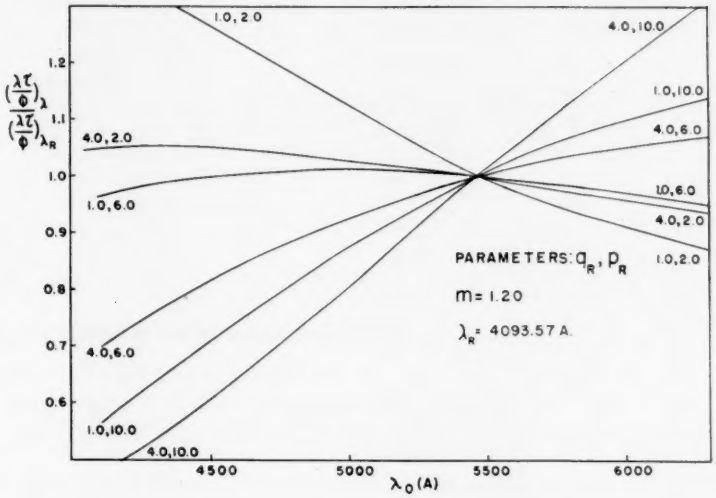

FIG. 3. Normalized theoretical spectra of $\lambda\tau/\phi$.

respect to those at λ_R. The important advantage of normalization is that the influence of uncertainties in ϕ determinations—which do not affect the shape of the experimental spectra, but the numerical values—is automatically excluded. The same applies to the solid angle corrections which have been discussed in detail previously.[5] They affect the shape of the spectra very little, but can have a major effect upon the numerical values. An additional practical advantage of normalization is that a large number of theoretical turbidity spectra can be assembled in a single graph which facilitates the comparison between theoretical and experimental spectra.

Typical normalized $\lambda\tau/\phi$ spectra are given in Fig. 3. It is seen that the normalized spectra are quite sensitive to changes in heterodispersion at any of the p_R values considered (2.0, 6.0, 10.0). In the case of the examples given, the sensitivity is highest within the range of short wavelengths, unless p_R is very large (i.e., the smallest particles present in consequential numbers are already in the microscopic range). An increase in either the width of the distribution or in the size of the smallest particles present in consequential numbers, reduces the numerical values in the blue and raises them in the red. Either increase also leads to a shift of the maximum towards larger wavelengths.

Practical application of the method to a determination of size distribution curves in synthetic latices[6] has shown that a graphical comparison of an experimental normalized $\lambda\tau/\phi$ spectrum with a set of theoretical normalized $\lambda\tau/\phi$ spectra may in performance be equivalent to the method described previously.[1] While the σ spectra are, in general, more profoundly altered by changes in p_R and q_R, the precision of turbidity measurements is higher, which is a compensating factor. Particularly inviting is the use of both σ spectra and turbidity spectra for a determination of size distribution curves. A concordant answer obtained in a given case by both methods is a reassuring check of the reliability of the result. Electronic matching of theoretical and experimental spectra should allow one to obtain a distribution curve in a short time by simultaneous application of both methods.

On applying the method outlined here, it must be borne in mind that the relative refractive index m varies with wavelength. This has not been taken into account for the theoretical model spectra in Fig. 3. In many instances, such as for the systems on which the method has been tested thus far, corrections for the dispersion are not important enough to be applied. In those cases, where the dispersion should be taken into account, Table I contains all the information necessary for secure interpolations.

In conclusion, it may be pointed out that a more elaborate distribution function which is a linear combination of two terms of the form (1), with different parameters r_0, s, may be used in connection with the present method in a manner entirely analogous to the one employed in scattering ratio measurements.[1] The numerator and denominator of Eq. (8) now appear in place of the functions $F_{||}$, $F_\perp$ considered in the preceding paper.[1] It is then necessary to have available tabulated values of both the numerator and denominator of Eq. (8) (and not merely of their ratio). Such

[5] W. Heller and R. Tabibian, J. Colloid Sci. **12**, 25 (1957).
[6] Results to be described elsewhere.

tables were computed in connection with the construction of Table I, but are not included here.

ACKNOWLEDGMENTS

The electronic computations which led to the data given in Table I were obtained with the efficient cooperation of Dr. A. Jacobson, former Director of the Wayne State University Computation Laboratory and H. James McCarty. The electronic computations were kindly financed by the Research Laboratories of the United States Rubber Company, Wayne, New Jersey.

THE JOURNAL OF CHEMICAL PHYSICS VOLUME 34, NUMBER 5 MAY, 1961

Field Emission from Whiskers*

A. J. MELMED† AND R. GOMER‡

Institute for the Study of Metals, University of Chicago, Chicago, Illinois

(Received November 7, 1960)

A method for obtaining field emission from whiskers grown *in situ* from the vapor under high-vacuum conditions has been developed and is described. It is possible to fabricate clean and strong emitters from almost any conducting material, so that the range of substances that can be used for field emission has been considerably expanded. Electrical methods for following the growth kinetics and determining whisker length and radius are described and applied to Au. Growth is found to be positively exponential with time, which supports a mechanism of growth by diffusion of impinging atoms over the whisker sides and incorporation at the growing end. Cessation of growth is diffusion limited in these experiments. It was possible to estimate the activation energy for the surface diffusion of Au on Au as 23 ± 5 kcal from the variation of terminal length with temperature. Some adsorption and oxidation experiments indicate that the method can also be used for the study of these phenomena. It was found for instance that H_2 is not adsorbed on Au and that Al is oxidized with severe surface rearrangement even at 77°K.

THE development of field and ion microscopy[1] has permitted the study of a variety of surface phenomena in previously undreamed-of detail. Unfortunately these methods have been restricted to a small number of high melting metals of great strength, because emitters are subject to very high-electrostatic stresses (5×10^8 d/cm² in electron and 5×10^{10} d/cm² in ion emission) and must be outgassed at high temperatures if clean surfaces are to be obtained. With most low-melting metals excessive blunting occurs during this process. If the impurities are less volatile than the substrate, conventional methods fail entirely unless field desorption[2] can be used; however this involves high stresses and thus requires great strength.

It was found in a previous investigation[3,4] that Hg whiskers grown *in situ* from the vapor could be used as field emitters, having adequate strength and adhesion to a variety of substrates. It seemed worthwhile to apply an analogous method to other materials in the hope of extending the range of field and ion emission. It turned out that clean whiskers, sufficiently strong to be used as field electron emitters, could be grown *in situ* under high-vacuum conditions from a large variety of materials. The application to ion emission turned out to be less promising than hoped for, primarily because of inadequate adhesion to the substrate. It is likely, however, that this problem can be overcome.

This paper describes the techniques for growing field emitters *in situ* and presents preliminary results of a number of applications. Some of this work has been briefly reported.[5]

PRINCIPLE OF THE METHOD

It was found by Sears[6] that Hg whiskers rather than a solid film were nucleated on glass surfaces from the vapor at low supersaturations and that these grew to considerable lengths without thickening. He was able to show by an ingenious method utilizing the Brownian motion of the whiskers that their radii were of the order of 100 A. Sears explained these results by assuming

* This work was supported in part by a contract with the U. S. Atomic Energy Commission.

† Present address: Engineering Research Laboratory, Du Pont Experimental Station, E. I. Du Pont de Nemours and Company, Inc., Wilmington, Delaware.

‡ Alfred P. Sloan Fellow.

[1] R. H. Good and E. W. Müller, *Handbuch der Physik* (Springer-Verlag, Berlin, 1956), Vol. 21, p. 176.

[2] E. C. Cooper and E. W. Müller, Rev. Sci. Instr. **29**, 309 (1958).

[3] R. Gomer, J. Chem. Phys. **28**, 457 (1958).

[4] R. Gomer in *Growth and Perfection of Crystals* (John Wiley & Sons, Inc., New York, 1959), p. 126.

[5] A. J. Melmed and R. Gomer, J. Chem. Phys. **30**, 586 (1959).

[6] G. W. Sears, Acta Met. **3**, 361 (1955).

that nucleation occurred only on specially favorable sites and postulated the presence of a screw dislocation in those nuclei which grew into whiskers. His mechanism consists of the diffusion of impinging atoms over the whisker sides and their incorporation into the crystal at the emerging screw dislocation, which provides a nonvanishing anchorage for loose atoms.

Growth also occurs on a variety of conductors so that it was possible to grow and obtain field emission patterns from Hg whiskers.[3,4] It was found that these are single crystals of great strength and adhere strongly to substrates which provide microcrevices.[4] In the present work the technique was modified by using a heated evaporator to simulate a vapor pressure and a heated wire substrate to adjust the supersaturation.

EXPERIMENTAL

Tube Design

A typical growth and emission tube is shown in Fig. 1. For general work it proved most convenient to use spherical tubes completely coated with phosphor, except for pyrometer sighting windows, so that all growth directions could be observed. The inner surface of tubes was made conducting by the stannous chloride method[7]; care was taken to provide a good electrical contact[8] to the external power source, since currents of the order of 0.5 ma were sometimes drawn.

The substrate usually consisted of a heatable tungsten wire loop, provided with potential leads when accurate temperature measurements were required. A conducting shield, equipotential with the substrate, was sometimes used to shield portions of the latter from the source. It was found with Hg[4] and confirmed here that growth, or at least sufficient adhesion for field emission, requires a rough substrate. In the case of materials growing at moderate temperatures this is adequately provided by the oxide coating on electrolytically polished tungsten, if this has not been heated above 1000°C. When higher growth temperatures were required, or when it was desired to outgas the substrate very thoroughly, growth could be achieved only after prolonged evaporation from the source. Apparently this created the required topography, possibly by alloying, or merely by the random piling up of crystallites. A more satisfactory substrate for these cases consisted of a rope of 40 strands of 0.0005-in. diam tungsten wire, twisted to moderate tightness. This substrate could be outgassed above 2000°C and then provided exceptionally good adhesion, presumably because the growth sites consisted of the contacts between rope strands and thus combined crevices with clean metal to metal adhesion. The diameter of the strands was small to minimize the electrical shadow zone between them, where the field is low.

[7] R. Gomer, Rev. Sci. Instr. **24**, 993 (1953).
[8] R. Gomer, Rev. Sci. Instr. **27**, 544 (1956).

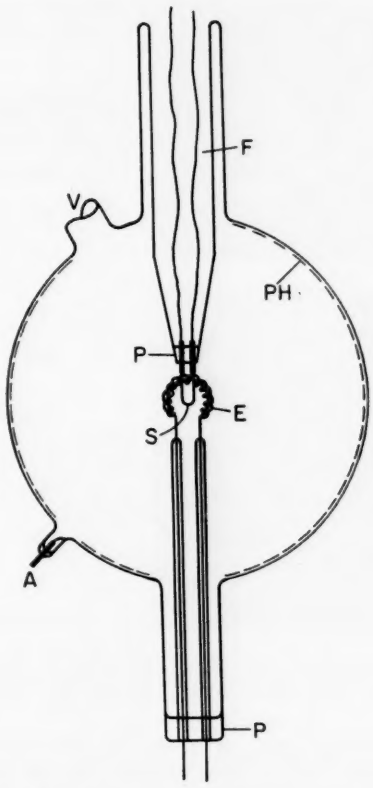

FIG. 1. Schematic diagram of F.E. tube for whisker growth and observation. *P*, pressed seals; *S*, substrate (potential leads not shown); *E*, source; *V*, vacuum lead; *A*, electrical lead in; *PH*, phosphor; *F*, cold finger for cooling substrate; magnetically operated shield not shown.

Substrates other than tungsten were also used. It was found that Pt wire, W covered with aquadag, and substrates consisting of the whisker material itself (for high-melting substances) were satisfactory for field electron emission.

The lines of force originating on the whisker tips are compressed anisotropically by cylindrical substrates, so that the patterns appear elongated normal to the substrate axis, when the whiskers are very short. While this may be annoying in some instances, it has the advantage of making it possible to identify the section of the substrate from which the whiskers grow. This is useful for the rapid determination of correct growth conditions on a nonuniformly heated substrate.

Uniform pattern compression could be achieved by using a spherical substrate, welded to a heating loop. In most cases a number of patterns appears simultaneously on the screen. There is usually very little overlap because the images are fairly small. In some cases it was possible by careful temperature control to grow

TABLE I. Summary of whisker growth conditions.

Material	$T_{substrate}$ °C	T_{source} Pyrometer reading °C	T_{source} Corrected °C	T_{sub}/T_{melt}	Observed orientations
Ni	(700)–900	1000–1200	1049–1271	0.66	110, 111, 100
Cu	(600–700)	(900)		0.68	110
Fe	661–753	1100	1198	0.54	fcc–100 bcc–100, 111, 110
Pt	750–(960)	1480	1616	0.53	110
Ti	765	1200	1247	0.53	hex–1000 bcc–100, 110
Au	557–630	935–990	1092–1111	0.65	110
Al	500–630	*		0.88	110, 111, 100
Ba	(550–600)	*		0.86	111
Ge	(750–800)	(900)		0.83	111
Va	(800–850)	*		0.48	100, 110
Ag	(600–650)	(800–950)		0.70	110

* Not measured accurately. Values in parentheses estimated visually.

whiskers one at a time on the tip of a 3000 A tungsten field emitter. In these cases there is very little pattern compression or field reduction, so that large images could be obtained at voltages too low to cause emission from the substrate.

Sources generally consisted of electrically heatable tungsten wire loops, wrapped with the material to be evaporated. In emission these were made equipotential with the screen. Single beads, formed by melting *in situ*, were used when the source geometry had to be known accurately. High-melting materials in wire form were directly heated electrically. Where wire was not available, small slabs of the material were wrapped by electrically heatable coils of tungsten wire.

In many cases the formation of an evaporated film on the tube walls was permissible and acted as a getter. In some cases the walls were protected by a magnetically operated shield.

Vacuum Techniques

Bakeable systems with Hg or oil diffusion pumps were used. Copper-filled traps were used in some but not in all cases. In addition to an ion gauge, systems included a field emission monitor tube, which could be used as an integrating pressure gauge and for rough qualitative analysis of the residual gas. Whiskers were grown at pressures of $<10^{-9}$ mm Hg after thorough outgassing of all heatable parts. In some cases the entire source assembly was subjected to preliminary outgassing in an auxiliary system before incorporation in the tube.

Gas sources for adsorption experiments consisted of electrically heatable Pt foil crucibles containing ZrH_2 for H_2 and CuO for O_2 generation prepared *in situ* and connected to the system via breakoff valves. High pressures of O_2 were obtained from Airco Spectroscopic grade O_2 without further purification and admitted via stopcocks or bakeable metal valves.

Temperature Measurements

Temperatures were measured pyrometrically and/or from resistance values. In the former case corrections for emissivity and adsorption by the conducting coating on the tube walls were made. In some instances temperatures were estimated only roughly.

Growth Conditions

Growth by the Sears mechanism requires relatively low supersaturation, mobility of atoms on the whisker side, and a flux sufficient for some nucleation. These conditions are met over a moderate range of source and substrate temperatures, as indicated by Table I. The data are somewhat arbitrary in that they were chosen for growth times of 5–10 min. Nevertheless they can be roughly summarized by stating that substrate temper-

FIG. 2. F.E. pattern from Al, at 77°K, 110 oriented.

FIG. 3. F.E. pattern from Ag, at 77°K, 110 oriented.

FIG. 4. F.E. pattern from Ba at 300°K, 111 oriented, field build-up noticeable.

FIG. 5. F.E. pattern from Au, 300°K, 110 oriented.

atures vary from 0.5 to 0.7 T_{melting}(°K), while source temperatures correspond to equilibrium vapor pressures of 10^{-5} to 10^{-6} mm Hg. In most experiments sources consisted of loops 1 cm in diam, 1–3 mm in front of the substrate.

In a typical experiment the substrate was brought to temperature before the source was heated. After growth both were allowed to cool, the former frequently to 77°K, before high voltage was applied. As the latter was increased, patterns became visible and finally the

FIG. 6. F.E. pattern from Cu, 300°K, 110 oriented.

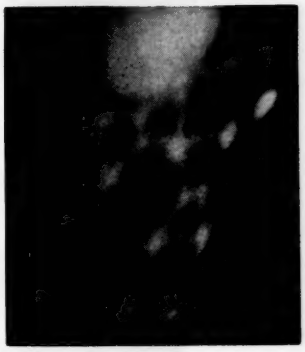

FIG. 7. F.E. pattern from Ge, 300°K, 111 oriented.

whiskers were torn off, while new patterns appeared. This behavior corresponds to the spectrum in whisker lengths and radii first observed with Hg.[3]

RESULTS AND DISCUSSION

Table I lists most of the materials investigated. The corresponding patterns are shown in Figs. 2–16. No attempt was made to include particularly good ones in these figures. In many instances considerably better looking patterns have been observed repeatedly. In addition to the substances listed, very preliminary experiments were carried out for Mo and Si which yielded normal images and for C which gave only irregular patterns.

Orientation

Table I indicates the observed whisker orientations, determined from the symmetry of the emission patterns. These are limited to a few low index directions among

FIG. 8. F.E. pattern from Ge, 800°K, 111 oriented, build-up marked.

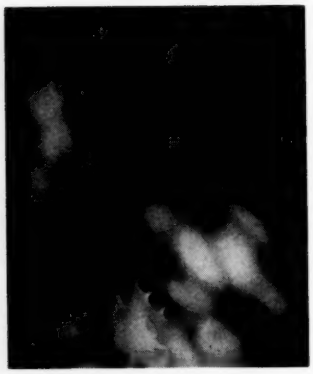

FIG. 9. F.E. pattern from Ni, at 300°K, 110 oriented.

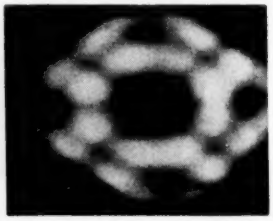

FIG. 10. F.E. pattern from Fe, at 300°K, fcc, 100 oriented.

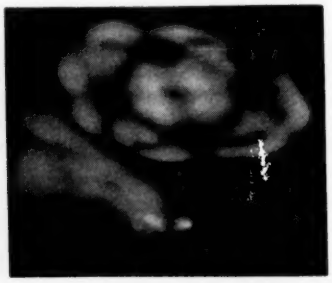

FIG. 11. F.E. pattern from Fe at 300°K, bcc, 100 oriented.

FIG. 12. F.E. pattern from Pt at 300°K, 110 oriented.

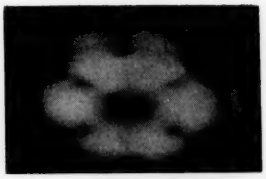

FIG. 13. F.E. pattern from Ti at 300°K, bcc, 110 oriented.

FIG. 14. F.E. pattern from Ti at 300°K, bcc, 110 oriented.

which 110 predominates for fcc and 100 for bcc materials.

In the case of Hg it was established that the predominant 110 orientation is independent of the substrate.[4] There is insufficient evidence on this point for other materials, but it is reasonable to assume that orientation is mainly determined by the crystal structure of the whisker, as discussed in the work cited in footnote 4.

Structure

It is possible to determine crystal structure as well as orientation from clean emission patterns, since work function anisotropies depend on the former. Thus, the close-packed (and hence high work function) faces are, in order of decreasing work function, 111, 100, 110, for fcc, and 110, 211, 100, for bcc crystals, so that structure can be determined once a pattern has been indexed from symmetry.

It was found in this way that the high-temperature phases of Fe and Ti (Figs. 10, 13, and 14) could exist

FIG. 15. F.E. pattern from Ti at 300°K, hex 1000 oriented, built up purposely to show symmetry.

FIG. 16. F.E. pattern for *V*, 300°K, 112 oriented.

at 300°K as well as the structures normally stable at room temperature (Figs. 11 and 15). When the latter were heated above the respective transition temperatures, transformation to the high-temperature forms took place, but too rapidly for the observation of details.

In the presence of certain residual gases at pressures of about $10^{-6}-10^{-7}$ mm Hg, several fcc metals grow predominantly as whiskers having fivefold rotational symmetry (Fig. 17). It was pointed out in a previous communication[9] that the anomalous form is most probably a penta-crystal with five 111 twin boundaries arranged about a common longitudinal 110 axis.

The various structural anomalies encountered with whiskers are undoubtedly traceable to surface energy effects. It will be shown that many of the whiskers investigated were 50–200 A thick so that surface to volume ratios were unusually high, thus making the surface contribution to the total energy sufficient to affect not only shape but structure. For instance the fivefold symmetric whiskers, whose internal boundries are of low energy, probably represent the lowest energy configuration when surface energies have been modified by adsorption.

Surface Condition

The presence of crystal faces inclined to the whisker axis and the absence of localized regions of high emission indicate that the whisker ends are approximately hemispheroidal in shape. This is to be expected from surface tension and from the probable growth mechanism. In the case of some whiskers, e.g., Au, and also Hg, the patterns are often polygonal, suggesting polyhedral whisker tips. This can be the result either of very small radius, so that the lattice cannot approximate a spheroidal shape, or of field induced buildup at temperatures high enough to permit surface mobility (Figs. 8 and 15). Visual evidence of surface agitation could be seen on low melting materials even at pressures of 10^{-10} mm, and could be arrested by cooling.

The simplicity of the patterns and their close resemblance to those obtained from conventional uncontaminated emitters show that the present method can produce clean field emitters from materials impossible or difficult to utilize conventionally, such as Ba, Al, or Ge. The pattern found in the latter case (Fig. 7) shows more structure than those of metals. Recent work by Dyke and co-workers[10] and by Allen[11] indicates that this seems to be the case for semiconductors. The pattern shown in Fig. 7 is identical to those obtained by Allen from annealed field desorbed Ge tips, prepared conventionally.[11]

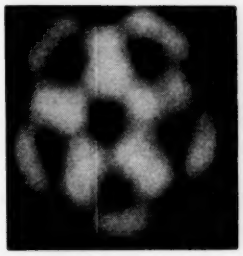

FIG. 17. F.E. pattern for Ni whisker grown at 10^{-6} mm O_2. Note fivefold symmetry.

Strength and Adhesion

The applied stress over the (assumed) circular cross section of a whisker σ_{app} is balanced by bulk and surface tension forces

$$\sigma_{app}=(1/8\pi)(E/300)^2=\gamma_s/r_w+\sigma_{bulk}, \qquad (1)$$

where γ_s is the surface tension, E the applied field in v/cm and r_w the whisker radius. If $\gamma_s=1000$ ergs/cm^2, a whisker of 100 A radius can support an applied stress of 10^9 d/cm^2 by surface tension forces alone. Thus, the fact that very thin whiskers can support high stresses is no guanantee of their perfection unless the value of the surface tension is known to be low.

In the case of weak materials like Hg the whiskers often rupture before they are torn from the substrate, as indicated by re-emerging patterns at higher voltage.[3] In the case of relatively strong materials like Pt this was not observed, so that the maximum supportable stress is probably limited by adhesion.

Nevertheless, the present experiments provide a means of putting lower bounds on tensile strength where surface tension can be ruled out. Thus, Ni whiskers withstood $>10^{10}$ d/cm^2 before being torn off and Al whiskers withstood $\sim 4\times 10^9$ d/cm^2. These values are based on field strengths of $\sim 3\times 10^7$ v/cm for electron emission, computed from the Fowler-Nordheim equation and the estimated emission currents and approximate work functions of the whiskers.

Reversible rotations of the patterns were often observed when the stresses were changed by adjusting the field. As in the case of Hg, where this was first noted,[3] the angles can vary from 0 to $>360°$. The phenomenon is probably connected with the presence of a screw dislocation in the whiskers, although the simple analysis presented previously[3] has been shown by Eshelby[12] to be quantitatively inadequate.

Rotation with heating at constant field was also occasionally observed. It seems unlikely that changes in length due to expansion could account for the rotation. At present we do not have a very good explanation of the phenomenon.

[9] A. J. Melmed and D. O. Hayward, J. Chem. Phys. **31**, 545 (1959).
[10] W. P. Dyke (private communication).
[11] F. G. Allen (private communication).

[12] J. D. Eshelby in *Growth and Perfection of Crystals* (John Wiley & Sons, Inc., New York, 1959), p. 130.

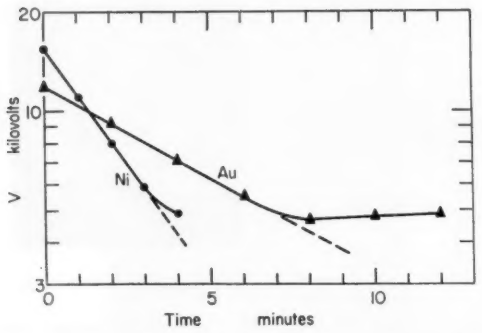

FIG. 18. Semilogarithmic plot of appearance voltage vs time for an Au and an Ni whisker. Note increase in V beyond 7 min for Au.

Emission Current

No attempt was made to obtain accurate Fowler-Nordheim plots for single whiskers. It was noted however that currents of several microamperes could be drawn from whiskers in most cases. At high-current densities some buildup due to resistive heating was noted. It can easily be shown from Eq. (34) of the work cited in footnote 3 that heating from this cause is very slight in all cases if currents are limited to 10^{-8} amp from whiskers with radii $\geqslant 50$ A.

Kinetics of Whisker Growth

During the study of Hg whiskers it was found that growth led to increases in pattern size and decreases in the emission voltage. This was interpreted as the result of a decompression of the lines of force at the tip as the whisker grew. It was possible to find a quantitative relation between length and field at the tip.

In the present case the substrate-anode geometry can be approximated by a coaxial cylindrical condenser, so that considerations entirely analogous to those previously described[3] lead to

$$E/E_{\text{free}} = \ln(1+h/rs)/\ln(L/r_s), \tag{2}$$

where E is the field at the top of a whisker of length h, E_{free} the field at that voltage if the whisker were semi-infinite, and r_s and L the radii of substrate and anode, respectively; E_{free} is given by

$$E_{\text{free}} = V/5r_w, \tag{3}$$

where r_w is the whisker radius and V the applied voltage. Consequently

$$V = 5r_wE[\ln(L/r_s)/\ln(1+h/r_s)] \tag{4}$$

$$= 5r_wr_sE\ln(L/r_s)/h \quad \text{if} \quad h \ll r_s. \tag{5}$$

In the cases investigated here $r_s = 0.0217$ cm and $h \leqq 0.001$ cm, so that Eq. (5) can be used throughout the subsequent discussion. Whisker growth at constant r_w can then be followed from the relation

$$h(t) = h(0)[V(0)/V(t)], \tag{6}$$

where the quantities in parentheses refer to the growth time measured from an arbitrary starting point $t=0$, and the voltages are those corresponding to constant emission and hence field.

Attempts to measure h as a function of time were made for Ni and Au whiskers. In the latter case the substrate was cooled to 77°K before high voltage was applied to prevent buildup. The experiments consisted of periodic determinations of the visual appearance voltage of individual whiskers as a function of time. Since the emission current varies exponentially with field and hence voltage, even moderate errors in i correspond to negligible ones in E and V.

Figure 18 shows typical plots of $\log V$ vs time for Au and Ni whiskers. These are linear over a considerable range indicating that growth is exponential, as in the case of Hg.[4] This suggests very strongly that the growth mechanism consists of the diffusion of impinging metal atoms over the whisker sides, followed by incorporation at the growing end. As long as all atoms impinging on the whiskers are able to reach its end, the growth rate will be proportional to the impinging flux and hence to the whisker area, which is proportional to its length. The growth law is then

$$h(t) = h(0)\exp(\gamma t), \tag{7}$$

where γ is a constant.

Although quantitative measurements were made only with Hg, Au, and Ni, nonlinear decreases with time in appearance voltage were noted in all cases, so that it is probably safe to conclude that the mechanism outlined holds initially for all the whiskers grown by us.

Whisker Radii

It is possible to estimate whisker thickness from the growth constants, i.e., from the slope of $\ln V$ vs time curves. For the case of uniform isotropic pressure γ takes the form[3]

$$\gamma = P(2m/\pi kT_e\rho^2)^{\frac{1}{2}}(\alpha/r_w)\ \text{sec}^{-1}, \tag{8}$$

where P is the pressure in d/cm^2, ρ the whisker density, T_e the vapor temperature, and α the sticking coefficient on the whisker. Equation (8) must be modified slightly for the present conditions. For a flux impinging from a spherical source of radius r_e the pressure must be replaced by $P(r_e/x)^2\alpha\sin\theta$, where x is the source to whisker distance and θ the angle between the whisker axis and the source-substrate line of separation. The effective impingement area is $2r_wh$ in the present case, rather than $2\pi r_wh$, so that Eq. (8) takes the form

$$\gamma = P(r_e/x)^2\sin\theta(m/2\pi kT_e)^{\frac{1}{2}}(\bar{\alpha}^2/r_w)/2\pi\rho\ \text{sec}^{-1},$$

$$= cP\sin\theta(\bar{\alpha}^2/r_w), \tag{9}$$

TABLE II. Growth of Au whiskers.

Whisker no.	$\sin\theta$	T_{substr} °K	T_{source} °K	γ exptl. sec^{-1}	V_c kv	$r_w/\bar{\alpha}^2$ A°	$r_w^2\gamma/\bar{\alpha}^4V_c^2$	$D/\bar{\alpha}^4$ $cm^2\ sec^{-1}$
32	0.81	903	1384	18.6×10^{-4}	5.1	88	5.47×10^{-23}	20.6×10^{-9}
36	0.59	903	1384	18.6×10^{-4}	5.3	64	2.72×10^{-23}	10.3×10^{-9}
59	0.59	879	1369	19.0×10^{-4}	6.0	45	1.07×10^{-23}	4.0×10^{-9}
63	0.52	879	1369	22.0×10^{-4}	4.6	34	1.20×10^{-23}	4.5×10^{-9}
66	0.59	830	1369	6.6×10^{-4}	10.3	130	1.05×10^{-23}	4.0×10^{-9}
67	0.707	830	1369	6.8×10^{-4}	9.0	150	1.89×10^{-23}	7.1×10^{-9}
70	0.59	879	1365	11.7×10^{-4}	7.1	69	1.10×10^{-23}	4.2×10^{-9}
79	0.52	859	1365	3.0×10^{-4}	9.3	237	1.95×10^{-23}	7.4×10^{-9}
84	0.76	859	1365	9.3×10^{-4}	6.8	111	2.48×10^{-23}	9.4×10^{-9}

where $\bar{\alpha}^2$ represents $\alpha(T_w)\alpha(T_e)$, T_w being the temperature of the whisker and T_e that of the source.

In the case of Au the following geometry was used: $r_s=0.9127$ cm; $r_e=0.064$ cm; $x=0.30$ cm; θ was estimated in each case from the position of the image on the screen. Pressures were estimated from the relation

$$\log_{10}P_{mm}=(-18047/T)+8.815 \qquad (10)$$

found by Edwards[13] and Brodsky for Au in the liquid range. Table II gives the resultant values of $r_w/\bar{\alpha}^2$ and θ for a number of whiskers. The latter never exceeded 90° and lie close to 36° in most cases. The values of r_w are small even if $\bar{\alpha}$ is close to unity. Since it would be impossible to obtain emission patterns showing definite crystal faces if r_w were much less than $r_w/\bar{\alpha}^2$, it must be concluded that $\bar{\alpha}$ is close to unity in the temperature range of the experiments. Further evidence for this conclusion will be presented later.

The measurements of r_w reported here are relatively crude, since the errors introduced by even slight variations in source temperature are magnified exponentially, while errors in geometry appear quadratically. A glass shield was used which may have acted as reflector, raising the source temperature slightly above the measured value. This would tend to make the actual radii higher than those calculated. The magnitudes found, however, are similar to those of Hg whiskers, where these uncertainties are much smaller.

An entirely different method was also employed for the estimation of radii and applied to Ni. This is based on the fact that the local magnification M' of a small surface asperity of radius r_b depends on the radius r of the main emitter. It was shown by Rose[14] that

$$M'/M=1.1\,(r_b/r)^{\frac{1}{2}}, \qquad (11)$$

where M is the magnification of the main image. It was possible to adsorb Cu phthalocyanine molecules on Ni whiskers and to find the relative angular size of the molecule patterns relative to the main image. This value of M'/M was then compared with that for Ptcy adsorbed on a tungsten emitter of known radius, so that r_w could be found. Values of 50–65 A were obtained in this way. These estimates do not depend on the absolute value of the effective Ptcy radius and assume only that it is the same on Ni as on W. Since it is known that there are slight variations in the effective r_b of molecules adsorbed on a given emitter, depending on their positioning, this method is also open to uncertainties.

Whisker lengths and thicknesses could be estimated very qualitatively from the relation of image size to appearance voltage. Large patterns, indicating little compression and hence relatively long whiskers coupled with high-appearance voltages, indicated long but thick whiskers. Small patterns and low voltages indicated short but thin whiskers, and so on.

Usually emission with fcc metals could be obtained only from thin (50–200 A radius) whiskers, while emitters from bcc metals could be grown much thicker. Nevertheless thick whiskers certainly grew also from fcc metals, as Fig. 19 shows. The explanation may be

[13] R. Edwards (private communication).

[14] D. J. Rose, J. Appl. Phys. **27**, 215 (1956).

FIG. 19. Microphotograph of W wire with vapor grown Au whiskers. 375×.

connected with the greater adhesion of bcc whiskers on W. If it is assumed that whiskers originally grow out of microcrevices 30–100 A in radius and thicken in most cases during later stages of growth, strong adhesion would be limited to the "root" while the total force on the whisker is proportional to its cross section at the tip. Consequently thickened whiskers must have very strong "roots" in order to withstand emission stresses.

Whisker Length

Equation (5) can be used to obtain whisker lengths if r_w has been determined and if E is known. The latter can be computed from the Fowler-Nordheim equation, the whisker work function, and the known or estimated emission current. For most metals fields of the order of 3×10^7 v/cm may be assumed for emission. In this way the lengths of Au whiskers just before cessation of exponential growth were estimated to be ~0.0015 cm. These small values are clearly responsible for high voltages required to obtain emission from very thin emitters.

Surface Diffusion on Whiskers

It was found in all cases that emission voltages either leveled off or actually increased beyond a certain point. This behavior is illustrated by the Au curve in Fig. 18. Similar observations were also made with Hg,[3] and interpreted as the cessation of exponential growth, followed by thickening. Exponential growth ceases when atoms impinging at the base of the whisker fail to reach the growing end, either because they evaporate before reaching it, or because they cannot catch up with it. In the latter case the concentration of loose atoms on the whisker shank increases, so that new layers may be nucleated. The latter, being monatomic, will grow very rapidly, compared to the bulk of the whisker, and will compete successfully with the sink at the tip for most impinging atoms. Axial growth will cease almost entirely and thickening will result until new layers can no longer be nucleated. The occurrence of thickening can, therefore, be taken as evidence of diffusion rather than evaporation limited exponential growth.

It can be shown[3] that the critical length for exponential growth under these conditions is given by

$$h_c=(D/5.44\gamma)^{\frac{1}{2}}, \tag{12}$$

where D is the surface diffusion coefficient of atoms on the whisker sides. Combination of Eqs. (5) and (12) yields

$$D=25r_w^2r_s^2E^2(\ln L/r_s)^2 5.44\gamma/V_c^2, \tag{13}$$

so that

$$\ln D=\ln \text{const}+\ln[(r_w/\bar{\alpha}^2)^2\gamma/V_c^2], \tag{14}$$

where V_c is the emission voltage corresponding to h_c. Equation (13) permits a rough estimate of surface diffusion coefficients (Table II). Their exponential part can be obtained somewhat more accurately from a plot of $\ln(D/\bar{\alpha}^4)$ vs $1/T_s$, as shown in Fig. 20 for Au. Despite the scatter of the data it is possible to estimate the activation energy for surface diffusion of Au on Au as 23∓5 kcal. If D can be represented by

$$D=a^2\nu \exp(-E_{\text{diff}})/kT_s, \tag{15}$$

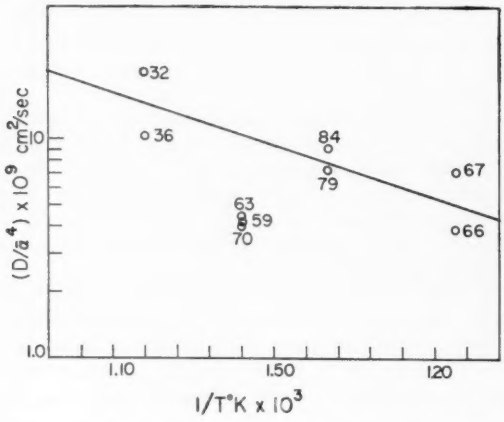

FIG. 20. Plot of log$D$ vs $1/T_{\text{substr}}$ for Au whiskers. Numbers refer to whisker numbers in Table II.

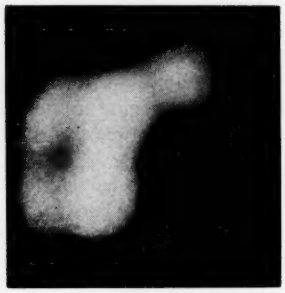

FIG. 21. Clean Al whisker at 300°K, showing dark 111 face and smaller 100 face. $V=6$ kv.

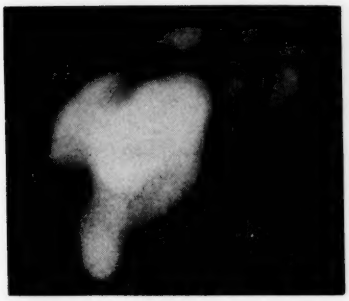

FIG. 22. Same whisker at 300°C after exposure to 6 mm O_2 for 10 min. Photograph at $p\sim10^{-7}$ mm. $V=10$ kv.

where a is a jump length (~3.3 A) and ν a frequency, $\nu\leqq4\times10^{12}\bar{\alpha}^4$ sec^{-1}. Since values of $\nu\sim10^{11}$–10^{12} sec^{-1} are normal for surface diffusion,[15] it can be concluded that $\bar{\alpha}\geq0.5$, so that the radii are given within a factor of 2 by the values of $r_w/\bar{\alpha}^2$ listed in Table II.

Adsorption on Au

Some preliminary attempts to look for chemisorption on Au were made. In these experiments Au whiskers were grown in high vacuum, and it was shown by means of a monitor field emission tube that appreciable adsorption could not have occurred during growth.

It was found that 10^{-5} mm H_2 produced no pattern or work function changes, while leading to typical chemisorption patterns on the monitor tip. It could also be shown by heating the latter that the H_2 was free from impurities like O_2, N_2, or CO.

Exposure to O_2 was carried out similarly. No changes resulted at 10^{-5} mm. Pressures of 1 mm produced no pattern changes but decreased emission by 40%. If it is assumed that no changes in the pre-exponential term of the Fowler-Nordheim equation occurred (usually a rather bad assumption), this would correspond to a work function increase of ~0.2 ev.

These experiments were carried out mainly to test the usefulness of the method for the study of adsorption. It should be quite possible to adapt it to a number of applications, such as surface diffusion of adsorbates, and even contact potential measurements.

Oxidation of Aluminum

Some attempts were made to follow the oxidation of Al whiskers. The latter were grown from "five-nine" Al at pressures of 10^{-9} to 10^{-10} mm Hg and then exposed to varying oxygen pressures. Experiments were carried out both at 300°K and 77°K. In most cases viewing was done at 77°K.

The first effect of exposure to O_2 was a decrease in emission, most notably on the vicinals of 100. This was rapidly followed by the changes indicated in Figs. 21–27. It will be seen that even low pressures (10^{-5} mm) cause marked surface rearrangement, presumably because of oxidation. This is most pronounced on and near the cube faces and least so on the most closely packed face, 111. This result is also interesting in connection with the finding that fivefold whiskers expose mainly 100 faces.[9]

Concomitant with oxidation the emission voltage increased, probably because of increases in work function and decreases in the effective microscopic emitting area, as found[16] even with O_2 on W.

The oxide exhibited no regular structure itself, nor did it seem to form a cohesive film in the earlier stages

FIG. 23. Clean Al whisker, 77°K.

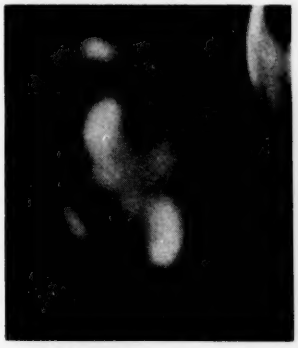

FIG. 24. Whisker of Fig. 23 after exposure to 10^{-6} mm O_2 at 300°K. Photograph at 77°K. Note surface rearrangement.

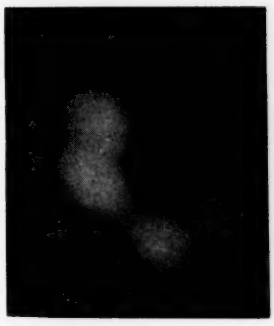

FIG. 25. Clean Al whisker at 77°K. $V=6.5$ kv.

[15] R. Gomer, Discussions Faraday Soc. **28**, 23 (1959).
[16] R. Gomer and J. K. Hulm, J. Chem. Phys. **27**, 1363 (1957).

FIG. 26. Whisker of Fig. 25 after 1 min exposure to 3×10^{-7} mm O_2 $V=9.5$ kv at 77°K. Note surface rearrangement.

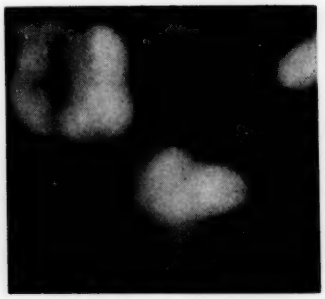

FIG. 27. Whisker of Fig. 25 after 60 min exposure to 3×10^{-7} mm O_2 at 77°K. $V=12$ kv.

of oxidation. In the later ones it was sometimes noted that the patterns became less irregular, almost as if a cohesive and smooth film were forming. However, this point is not definitely established.

NMR Measurement of Gas Compressibility*

M. LIPSICAS, M. BLOOM, AND B. H. MULLER†

Department of Physics, University of British Columbia, Vancouver, British Columbia, Canada

(Received October 26, 1960)

The nuclear magnetic resonance technique has been applied to measurement of the compressibility factors of gases. Some results are given for CH_4 and compared with data available in the literature.

WE wish to report a novel method for determining the relative compressibility of gases using nuclear magnetic resonance. This method can be applied over a wide range of temperatures and pressures to all gases with nuclei of nonzero spin. The measurements take a relatively short time and involve few instrumental corrections. We restrict ourselves here to molecules containing protons, but the method could be generalized to compare molecules with nonidentical nuclei.

Using a spin-echo spectrometer[1] originally designed to measure the spin-lattice relaxation time T_1 of protons in hydrogen and other hydrocarbon gases, an accuracy of a few percent has been obtained in compressibility factors. Greater accuracy could be obtained using nuclear magnetic resonance (NMR) apparatus explicitly designed to measure compressibility factors, but the principle usefulness of the NMR technique over standard methods will be in systems where speed of measurement is very important and where extreme accuracy is not necessary.

If a nuclear spin system is allowed to come into thermal equilibrium with its environment (in this case, a gas) the application of a short pulse of rf, of frequency close to the Larmor frequency of the nuclei in an externally applied magnetic field, results in a nuclear-induction signal of magnitude

$$S_x = Kn\rho_x\delta_x = Kn[(1/Z_x)(P_x/RT_x)]\delta_x, \qquad (1)$$

where K is a constant of the system, which includes the "effective volume" of the sample and the sensitivity of the system, n is the number of protons per molecule, ρ_x is the number of molecules per cc, δ_x is the fractional excess population of protons in the lower energy state which is equal to $2\mu H/kT_x$, Z_x is the compressibility of the gas defined as equal to P_xV/RT_x at the temperature T_x and pressure P_x, and R is the gas constant per mole. Therefore, if the signal S_x is measured as a function of the pressure P_x at a constant temperature T_x the relative compressibilities Z_x, as a function of pressure may be computed from the ratio of P_x to S_x. Alternatively, the relative densities can be exhibited on a plot of S_x vs P_x.

In order to measure the absolute compressibility of any gas, it is necessary to measure K, which can be done by measuring the induction signal from a gas of known compressibility in the same apparatus. We have found it convenient to use hydrogen for this purpose, especially since it is a gas over the entire temperature range of all other gases (except helium) and accurate values for its compressibility are readily available.[2] From Eq. (1), the ratio of the signal from gas x to that from hydrogen will be

$$S_x/S_{H_2} = (n/2)(P_x/P_{H_2})(Z_{H_2}/Z_x)(T_{H_2}/T_x)^2. \qquad (2)$$

From this equation it is clear how the absolute compressibility of any gas at temperature T_x and pressure P_x may be determined from the known compressibility of hydrogen, Z_{H_2} at temperature T_{H_2} and pressure P_{H_2} and from the ratio of the two pulsed signals.

Table I gives a comparison of values of compressibility factors for CH_4 at several temperatures and pressures with values of Z measured by conventional methods.[3]

A linear interpolation has been made between the values given in the tables.[3] The estimated maximum error in this interpolation was considerably less than 1%. The values given in the table have been rounded off to the last decimal place. The agreement is within a few percent in all cases. Similar measurements were carried out in C_2H_4 and similar agreement with published values of Z was obtained.

TABLE I.

Pressure atm	Temp. °K	CH_4 compressibility	
		Tables	Measured
58.4	208.5	0.56	0.56
49.0	209.5	0.66	0.63
41.1	210.5	0.73	0.74
34.0	212	0.80	0.78
27.3	213.5	0.84	0.86

* Research supported in part by the National Research Council of Canada.

† Holder of National Science Foundation fellowship on leave of absence from University of Wyoming. Present address: Department of Physics, University of Wyoming, Laramie, Wyoming.

[1] E. L. Hahn, Phys. Rev. **80**, 980 (1950).

[2] H. W. Woolley, R. B. Scott, and F. G. Brickwedde, J. Research Natl. Bur. Standards **41**, 379 (1948).

[3] American Petroleum Institute, Project 44, *Selected Values of Properties of Hydrocarbon and Related Compounds*, Vol. III, Table I.

Each measurement took a very short time (the rf pulses were about 10 μsec in length and the induction tail decayed in a few hundred microseconds), but the time between measurements had to be much longer than T_1 (say $\gtrsim 10T_1$) in order to allow the magnetization of the proton-spin system to return to its equilibrium value after being disturbed by the preceding measurement. Here T_1 for CH_4 gas in the temperature and pressure range reported in Table I is of the order of several seconds and is roughly proportional to density.[4]

Several experimental precautions must be taken if one is to obtain results of reasonable accuracy. In order to ensure that K is indeed a constant for a given gas, the gain of the system must be constant during the time of measurement. Since we inspected the detected signal, it was necessary for us to correct for the nonlinearity of the detecting diode. If one were to observe the rf signal directly on an oscilloscope or with phase-sensitive detection, there would be no need for this correction. The "effective volume" of the sample is determined completely by the dimensions of the chamber (the sample "bomb") and the rf coil configuration, and neither of these is varied.

Finally, it should be remarked that the technique reported here is closely related to that previously used to study deviations of the He^3 nuclear susceptibility from Curie's Law.[5] One can interpret the results of Table I to indicate that the nuclear susceptibility in CH_4 does obey Curie's Law over the range studied, as we have assumed. There may be a point to searching for departures from Curie's Law using this technique for H_2 gas at very high pressures and low temperatures, though a search in solid HD has given negative results.[6]

[4] M. Bloom, M. Lipsicas, and B. H. Muller, Can. J. Phys. (to be published).

[5] W. M. Fairbank and G. K. Walters, *Symposium on Liquid and Solid* He^3 (Ohio State University Press, Columbus, Ohio, 1957), p. 205.

[6] D. C. Freeman, Jr., Proceedings of the VIIth International Conference on Low Temperature Physics, 1960.

THE JOURNAL OF CHEMICAL PHYSICS VOLUME 34, NUMBER 5 MAY, 1961

Relaxation of Laminar Flow with Reference to Streaming Birefringence Decay

C. A. HOLLINGSWORTH AND W. T. GRANQUIST*

Department of Chemistry, University of Pittsburgh, Pittsburgh, Pennsylvania

(Received October 31, 1960)

Equations are obtained which express the decay of motion of fluids between concentric cylinders, parallel plates, and in tubes. Numerical examples are given which indicate that the time required for the flow to decay may not always be short compared to the streaming birefringence relaxation times.

I. INTRODUCTION

VARIOUS studies of streaming birefringence relaxation in colloidal solutions have been reported.[1–4] In these studies the time required for the flow to cease has been considered negligible compared to the optical relaxation time. One might wonder about the validity of this assumption when the optical relaxation times are of the order of a second or less and when the viscosity of the solution is low. It is, therefore, of interest to have an estimate of the rate of flow relaxation in these systems.

Although some problems dealing with flow relaxation have been treated,[5,6] the particular problem which is involved in the study of flowing birefringence decay apparently has not been treated, and it is the purpose of this paper to consider some aspects of this problem.

The various flow relaxation times discussed in the following sections refer to the relaxation of the flow after the stress, or motion, which caused the flow has been reduced to zero. The time required for the mechanical motion or stress to be released is neglected. End effects are also neglected in all of the examples treated in this paper. For example, concentric cylinders are assumed to have lengths which are very large compared to thickness of the annulus.

II. GENERAL THEORY

The differential equation[7] for the velocity of an incompressible Newtonian fluid can be expressed

$$\rho(\partial \mathbf{V}/\partial t)+\rho\mathbf{V}\cdot\nabla\mathbf{V}=\rho\mathbf{F}-\nabla p+\eta\nabla\cdot\nabla\mathbf{V}, \qquad (1)$$

* National Lead Fellow, Mellon Institute, Pittsburgh, Pennsylvania.

[1] I. Langmuir, J. Chem. Phys. **6**, 873 (1938).

[2] V. E. Gonsalves, Proc. Intern. Rheol. Congr. 1st Congr. 1948, II–239 (1949).

[3] W. P. Conner and P. I. Donnelly, Ind. Eng. Chem. **43**, 1136 (1951).

[4] W. T. Foreman, J. Chem. Phys. **32**, 277 (1960).

[5] H. Stearn, Quart. J. Math. **17**, 90 (1881).

[6] H. Bateman, Phys. Rev. **35**, 177 (1930).

[7] For example, see L. Page, *Introduction to Theoretical Physics* (D. Van Nostrand Company, Inc., Princeton, New Jersey, 1952), p. 276.

where $\mathbf{V}$ is the velocity, ρ is the density, F is the external body force, p is the pressure, and η is the coefficient of viscosity.

In the problems we consider in the following sections, the body forces (gravitational) are neglected, and the pressure gradient is zero. For these examples it can be shown rigorously that the term $\mathbf{V}\cdot\nabla\mathbf{V}$ is zero because of the geometry of the flow. Equation (1) then becomes

$$\rho(\partial\mathbf{V}/\partial t)=\eta\nabla\cdot\nabla\mathbf{V} \tag{2}$$

and the solution which satisfies the appropriate boundary and initial conditions can be expressed in the infinite series form

$$\mathbf{V}(\mathbf{r},t)=\sum_{n=1}^{\infty}A_n\exp(-t/\tau_n)\mathbf{V}_n(\mathbf{r}), \tag{3}$$

where $\tau_n(n=1,2,3,\cdots)$ is a relaxation time spectrum, $\mathbf{r}$ is the position vector of the point in space at which the velocity is being considered, and A_n are constants. The relaxation times τ_n depend upon the boundary conditions but are independent of the initial condition.

Sometimes Eq. (3) can be operated on term by term to obtain a function of $\mathbf{V}$ and the relaxation time spectrum of that function. In other cases term by term operation produces a divergent series. The velocity gradient which is considered in Sec. IV cannot be obtained from term-by-term differentiation. Some examples of permissible term-by-term operations are the following.

(a) When the series in Eq. (3) is uniformly convergent, then term-by-term integration over space is possible, and this leads to the result that the average velocity, defined by

$$\langle\mathbf{V}\rangle_{\text{Av}}=\int\mathbf{V}(\mathbf{r})d\mathbf{r}\Big/\int d\mathbf{r}, \tag{4}$$

has the same relaxation time spectrum as $\mathbf{V}$.

(b) When the series in Eq. (3) is absolutely convergent, then $V^2(=\mathbf{V}\cdot\mathbf{V})$ can be obtained by multiplication of the series by itself as though it were a finite sum. This leads to the following relaxation time spectrum for V^2,

$$(\tau_1/2),\quad[\tau_1\tau_2/(\tau_1+\tau_2)],\quad(\tau_2/2),\quad[\tau_1\tau_3/(\tau_1+\tau_3)],$$
$$[\tau_2\tau_3/(\tau_2+\tau_3)],\quad(\tau_3/2),\quad\text{etc.}\cdots, \tag{5}$$

where τ_1, τ_2, etc., are the relaxation times for $\mathbf{V}$, and where in Eq. (5) the order may deviate somewhat from descending order, but $\tau_1/2$ is always the longest time.

(c) When the series for V^2 is uniformly convergent the integration of V^2 can be carried out term by term, and the average value, given by

$$\bar{V}^2=\int V^2(\mathbf{r})d\mathbf{r}\Big/\int d\mathbf{r}, \tag{6}$$

is seen to have the spectrum (5). Therefore, the average kinetic energy has the spectrum (5).

It should be noted that if the series for a function of $\mathbf{V}$ converges so slowly that the leading term is not dominant, then the decay may be very different from exponential decay. In such cases the relaxation time spectrum alone does not give a good picture of the decay, and one must then know the sign and magnitude of the amplitudes A_n.

A one-parameter estimate of the decay time for a function of the velocity $F[\mathbf{V}]$ is the "apparent relaxation time" τ defined by

$$\{F[\mathbf{V}(\mathbf{r},\tau)]/F[\mathbf{V}(\mathbf{r},0)]\}=e^{-1}. \tag{7}$$

If the decay of $F[\mathbf{V}]$ is greatly different from exponential, the apparent relaxation time will be only a crude description of the decay.

III. SPECIAL CASES. VELOCITY AND ITS RELAXATION TIME SPECTRUM

Concentric Cylinders

Consider a fluid between two concentric cylinders of radii a and $b(a<b)$. During the steady-state flow one cylinder is rotating with a uniform velocity, and the other one is stationary. We assume that the rotating cylinder is then stopped slowly enough to prevent slipping of the fluid, but quickly enough so that the stopping time is negligible compared to the time required for the subsequent decay of the motion of the fluid.

In cylindrical coordinates the differential equation for the velocity and the boundary and initial conditions for motion between the cylinders are

$$\partial V/\partial t=(\eta/\rho)[(\partial^2V/\partial r^2)+(1/r)(\partial V/\partial r)-(V/r^2)],$$
$$V(a,t)=0,$$
$$V(r,0)=f(r),$$
$$V(b,t)=0,\quad t>0, \tag{8}$$

where V is the magnitude of the velocity. The solution to (8) can be expressed in terms of the Bessel functions of order one of the first and second kind, $J_1(\alpha r)$ and $Y_1(\alpha r)$, as follows,

$$V(r,t)=\sum_{n=1}^{\infty}A_n\exp(-\alpha_n^2(\eta/\rho)t]U_1(\alpha_n r), \tag{9}$$

where

$$U_1(\alpha r)=J_1(\alpha r)\,Y_1(\alpha b)-J_1(\alpha b)\,Y_1(\alpha r), \tag{10}$$

and $\alpha_n(n=1,2,3,\cdots)$ are the roots of

$$U_1(\alpha a)=J_1(\alpha a)\,Y_1(\alpha b)-J_1(\alpha b)\,Y_1(\alpha a)=0. \tag{11}$$

The relaxation times are given by

$$\tau_n=\rho/\alpha_n^2\eta. \tag{12}$$

The roots α_n are given in tables.[8] Thus, from a knowledge of the values of a, b, ρ, and η, one can calculate the

[8] E. Jahnke and F. Emde, *Tables of Functions* (Dover Publications, New York, 1945), pp. 204–206.

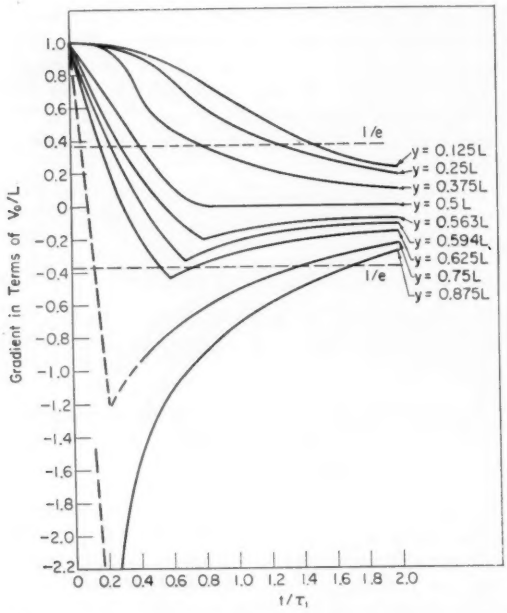

FIG. 1. Relaxation of the velocity gradient at various positions between parallel plates.

velocity relaxation time spectrum. In order to calculate the values of the amplitudes A_n we must know $f(r)$. These functions are in this case,

$$f(r)=[a^2b^2\Omega/(b^2-a^2)][(r/a^2)-(1/r)] \quad \text{(outer cylinder rotating)}, \tag{13}$$

$$f(r)=[-a^2b^2\Omega/(b^2-a^2)][(r/b^2)-(1/r)] \quad \text{(inner cylinder rotating)}, \tag{14}$$

where Ω is the constant angular velocity of the cylinder during the steady motion. The amplitudes are given by

$$A_n=\frac{\pi^2\alpha_n^2 J_1^2(\alpha_n a)}{2\{J_1^2(\alpha_n a)-J_1^2(\alpha_n b)\}}\int_a^b rf(r)\,U_1(\alpha_n r)\,dr. \tag{15}$$

With Eq. (13) this becomes for the outer cylinder rotating

$$A_n=a_n\{Y_1(\alpha_n b)[J_0(\alpha_n b)-J_0(\alpha_n a)+(b^2/a^2)J_2(\alpha_n b)-J_2(\alpha_n a)]-J_1(\alpha_n b)[Y_0(\alpha_n b)-Y_0(\alpha_n a)+(b^2/a^2)Y_2(\alpha_n b)-Y_2(\alpha_n a)]\}, \tag{16}$$

and with Eq. (14), Eq. (15) gives

$$A_n=a_n\{Y_1(\alpha_n b)\times[J_0(\alpha_n a)-J_0(\alpha_n b)-J_2(\alpha_n b)+(a^2/b^2)J_2(\alpha_n a)]-J_1(\alpha_n b)[Y_0(\alpha_n a)-Y_0(\alpha_n b)-Y_2(\alpha_n b)+(a^2/b^2)Y_2(\alpha_n a)]\} \tag{17}$$

for the inner cylinder rotating. The constant a_n is in both cases given by

$$a_n=\frac{\pi^2\alpha_n J_1^2(\alpha_n a)\,a^2b^2\Omega}{2\{J_1^2(\alpha_n a)-J_1^2(\alpha_n b)\}(b^2-a^2)}. \tag{18}$$

Circular Tube

Suppose that the flow is in a tube of radius b. The flow is produced by a pressure along the axis of the tube. After steady flow the pressure is released over a time period assumed negligible, and the fluid comes to a stop. When the pressure gradient has become zero the boundary value problem for the fluid velocity is

$$\partial V/\partial t=(\eta/\rho)[(\partial^2V/\partial r^2)+(1/r)(\partial V/\partial r)],$$
$$V(b,t)=0,$$
$$V(r,0)=f(r). \tag{19}$$

The solution is

$$V(r,t)=\sum_{n=1}^{\infty}A_n\exp[-\beta_n^2(\eta/\rho)t]J_0(\beta_n r), \tag{20}$$

where β_n are the roots of

$$J_0(\beta b)=0. \tag{21}$$

Here τ_n is given by

$$\tau_n=\rho/\beta_n^2\eta. \tag{22}$$

In this case

$$f(r)=(\Delta p/4\eta l)(r^2-b^2), \tag{23}$$

and

$$A_n=[2/b^2J_1^2(\beta_n b)]\int_0^b rf(r)\,J_0(\beta_n r)\,dr$$
$$=\frac{-J_2(\beta_n b)\,\Delta p}{\eta l\beta_n^2J_1^2(\beta_n b)}=\frac{-2\Delta p}{\eta l\beta_n^3 bJ_1(\beta_n b)}. \tag{24}$$

Plane Parallel Plates

Flow between parallel plates produced by the motion of one plate relative to the other can be treated as the limiting case as $[(a-b)/a]\to 0$ of the concentric cylinders. However, it is easier to start with the boundary value problem for this case, which is

$$\partial V/\partial t=(\eta/\rho)(\partial^2V/\partial y^2),$$
$$V(0,t)=0,$$
$$V(y,0)=f(y),$$
$$V(L,t)=0, \qquad t>0, \tag{25}$$

where y is the coordinate perpendicular to the plates. A Fourier series solution to (25) is

$$V(y,t)=\sum_{n=1}^{\infty}A_n\exp[-(n\pi/L)^2(\eta/\rho)t]\sin(n\pi y/L), \tag{26}$$

where L is the distance between the plates. The relaxation times are, therefore, given by

$$\tau_n=(L/n\pi)^2(\rho/\eta). \tag{27}$$

The initial condition is

$$f(y)=y(V_0/L), \tag{28}$$

where V_0 is the velocity of the moving plate during the steady motion. The amplitudes are given by

$$A_n=(1/L)\int_{-L}^{L}f(y)\,\sin(n\pi y/L)dy=(-1)^{n+1}(2V_0/n\pi). \tag{29}$$

IV. SOME APPARENT RELAXATION TIMES FOR THE PARALLEL PLATE CASE

Velocity

Equation (26) with Eq. (29) can be written

$$V[(y/L),\,(t/\tau_1)]=2V_0/\pi)\sum_{n=1}^{\infty}[(-1)^{n+1}/n]\times\exp(-n^2t/\tau_1)\,\sin(n\pi y/L), \tag{30}$$

where τ_1 is the first relaxation time for parallel plates (Eq. 27).

The apparent relaxation time [see Eq. (7)] for the velocity at any given value of y/L can be calculated in terms of τ_1 by use of Eq. (30). Thus the apparent relaxation time at $y/L=\frac{1}{2}$ is found by numerical calculation to be

$$\tau\simeq 1.22\tau_1 \qquad (y=L/2). \tag{31}$$

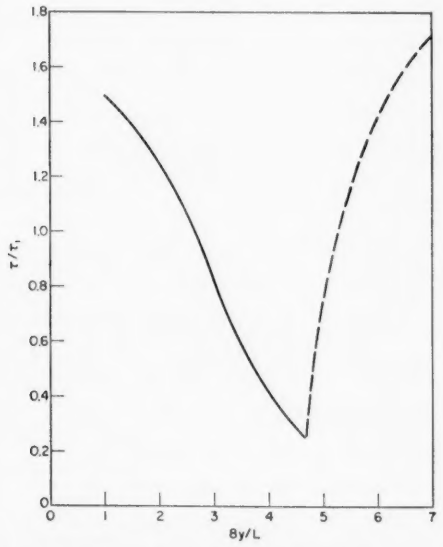

FIG. 2. Apparent relaxation times for the velocity gradient as a function of position between parallel plates.

TABLE I. First three flow velocity relaxation times for water in various types of apparatus with dimensions as shown.

Apparatus and dimensions, cm	τ_1 (sec)	τ_2 (sec)	τ_3 (sec)
Concentric cylinder, radii 1.5, 1.3	0.38	0.10	0.04
Single tube, radius 0.2	0.69	0.13	0.05
Parallel plates, $L=0.2$	0.40	0.10	0.04

Average Velocity

Integration of Eq. (30) according to Eq. (4) gives

$$\bar{V}/\bar{V}_0=(8/\pi^2)\sum_{n\ \text{odd}}\exp(-n^2t/\tau_1)$$

$$=(4/\pi^2)\sum_{n=1}^{\infty}\frac{[1-(-1)^{n+1}]}{n^2}\exp(-n^2t/\tau_1). \tag{32}$$

Numerical evaluation gives for the apparent relaxation time of the average velocity

$$\tau\simeq 0.8\tau_1. \tag{33}$$

Average Kinetic Energy

The average of the square of the velocity can be evaluated by use of the Hurwitz-Liapounoff theorem.[9] This gives

$$\bar{E}/\bar{E}_0=(6/\pi^2)\sum_{n=1}^{\infty}[\exp(-2n^2t/\tau_1)/n^2], \tag{34}$$

where $\bar{E}_0$ is the average kinetic energy at zero time. By numerical evaluation it was found that the apparent relaxation time of $\bar{E}$ is given by

$$\tau\simeq 0.5\tau_1. \tag{35}$$

Velocity Gradient

The velocity gradient is the quantity that is of interest in connection with flow birefringence. The gradient cannot be calculated by differentiation of Eq. (30) term by term, because the resulting series is divergent. The curves in Fig. 1 have been obtained by numerical differentiation of Eq. (30). The change in sign of the gradient with time when $y>L/2$ is a complicating feature of the gradient decay. If we assume that, when $y>L/2$, the relaxation which is of interest is the second one (i.e., the one following the minimum) then the ratio of the apparent relaxation time to τ_1 is shown as a function of y/L in Fig. 2.

NUMERICAL EXAMPLES

Table I shows the values of τ_1, τ_2, and τ_3 for water ($\eta=0.01$ poise) in various types of apparatus with the dimensions indicated. Table II shows how τ_1 for water

[9] E. T. Whittaker and G. N. Watson, *Modern Analysis* (The Macmillan Company, New York, 1946), p. 180.

TABLE II. The first flow relaxation time (sec) for water between concentric cylinders of the indicated radii.

b/a	$a=1.0$ cm	1.5 cm	2.0 cm
1.05	0.025	0.057	0.102
1.10	0.101	0.226	0.406
1.15	0.228	0.510	0.910
1.20	0.408	0.910	1.62
1.25	0.633	1.42	2.52
1.50	2.51	5.61	10.00

between concentric cylinders depends upon the dimensions of the cylinders.

As an example in which we can compare a theoretical flow relaxation time with some measured optical relaxation times, we consider some results for V_2O_5 sols reported by Foreman.[4] These optical relaxation times vary from 0.254 to 2.47 sec. The apparatus consisted of two coaxial disks, one stationary and one rotatable, and viewing was perpendicular to the stream lines of flow and parallel to the flow gradient. We assume that our parallel plate solution applied to this case. For these solutions η/ρ is essentially that for water. Since the light path was perpendicular to the plates, the beam passed through all values of y from $y=0$ to $y=L$. The minimum relaxation shown in Fig. 2 is $0.25\tau_1$ sec. The plates were $\frac{1}{16}$ in. apart, corresponding to τ_1 of 0.26 sec. and thus a minimum relaxation time of 0.07 sec. This minimum time is probably several times smaller than the actual effective relaxation time across the length L. If, as was assumed to obtain the results in Fig. 2, the reversal of the gradient in the region $y>L/2$ does not have some effect which we have not yet considered, the flow relaxation time may not in this case be negligible compared to some of the optical relaxation times.

ACKNOWLEDGMENTS

Very helpful discussions of the subject matter with Dr. Hershel Markovitz, Dr. Neill Weber, and L. J. Kroko, all of Mellon Institute, are gratefully acknowledged. We are indebted to Professor I. M. Krieger, Case Institute of Technology, for suggesting the Hurwitz-Liapounoff approach to the average kinetic energy.

Infrared and Raman Spectra of Fluorinated Ethanes. XIV. $CF_2Cl—CHF_2$ and $CF_2Br—CHF_2$†

PETER KLABOE* AND J. RUD NIELSEN

Department of Physics, University of Oklahoma, Norman, Oklahoma

(Received September 6, 1960)

The infrared absorption spectra of gaseous CF_2Cl-CHF_2 and CF_2Br-CHF_2 at five temperatures between 30° and 180°C were obtained in the region 300–6000 cm^{-1} with a Perkin-Elmer double-pass spectrometer equipped with CsBr, NaCl, and LiF prisms. In addition, infrared spectra of the solids at −170°C were recorded in the region 350–5000 cm^{-1}. The Raman spectra of the liquids at 30°, −30°, and −80°C were photographed with a three-prism glass spectrograph of reciprocal linear dispersion 15 A/mm at 4358 A, and polarization measurements were made. In all three states of aggregation both compounds exist as mixtures of rotational isomers. For each compound, the two isomeric forms (*trans* and *gauche*) are about equally stable, both in the gaseous and the liquid state. Tentative assignments have been made of the fundamentals of both compounds.

INTRODUCTION

THE vibrational spectra of a number of halogenated ethanes with asymmetrical end groups have been studied with special reference to rotational isomerism, and this work has been reviewed by Mizushima[1] and Sheppard.[2] A number of fluorinated ethanes of the general form CX_2Y–CX_2Y[3–6] have been studied, and they are all reported to exist as equilibrium mixtures of rotational isomers of symmetries C_{2h} (*trans*) and C_2 (*gauche*). The compounds CF_2Cl–CHF_2 and CF_2Br–CHF_2 have a less symmetrical form, and only a few fluorinated ethanes of this type have been studied.[7] The Raman[8] and infrared[9] spectra of liquid CF_2Cl–CHF_2 have been obtained previously, but no data have been reported for CF_2Br–CHF_2. In the present paper infrared and Raman spectral data are reported for CF_2Cl–CHF_2 and CF_2Br–CHF_2. The vibrational spectra of these compounds show striking similarities, and both exhibit rotational isomerism in all three states of aggregation. However, for both compounds, the enthalpy difference $\Delta H°$ between the two rotational isomers is approximately equal to zero. Partly because of this fact, no quite reliable way was found to distinguish between the vibrational fundamentals of the rotational isomers.

EXPERIMENTAL RESULTS

The samples of CF_2Cl–CHF_2 (bp −15°C at 746 mm pressure) and CF_2Br–CHF_2 (bp 12°–13°C at 746 mm pressure), hereafter called (C) and (B), respectively, were prepared and purified in the laboratory of Professor A. L. Henne at Ohio State University. The spectra indicate that the purity of both samples is high, except that the sample of (C) contains a considerable amount of carbon dioxide. The infrared spectra of the gaseous and solid states and the Raman spectra of the liquids were obtained as described previously.[6] The infrared spectrum of (C) in the gaseous state is shown in Figs. 1–3, the spectrum of (B) in Figs. 4–6. The Raman spectral data for (C) and (B) are listed in Tables I and II. Certain discrepancies exist between the Raman bands observed by Glockler and Sage[8] for CF_2Cl–CHF_2 and those observed here. A very weak band at 910.2 cm^{-1} and an uncertain band at 93.0 cm^{-1} reported by these authors were not observed in the present work. On the other hand, eight bands, most of them weak and diffuse, were observed in the present study, but were not reported by Glockler and Sage.

INTERPRETATION

The large amount of information available about halogenated ethanes[1,2] indicates that these molecules exist in staggered configurations only. The large number of strong infrared and Raman bands observed for CF_2Cl–CHF_2 and CF_2Br–CHF_2 shows that these compounds consist of rotational isomers. The probable isomeric configurations of (C) and (B) are a *trans*-form having the symmetry C_s and two enantiomorphic *gauche*-forms obtained from the *trans*-form by rotating one of the end-groups a certain angle, probably not far from 120°. The *gauche*-form has no symmetry.

The 18 normal vibrations of the molecules of symmetry C_s divide into 11 a' and 7 a''. The former should be polarized in the Raman spectrum, while the latter should be depolarized. All vibrations of the *gauche*-

* Present address: Department of Chemistry, University of Oslo, Blindern, Oslo, Norway.

† This work has been supported by the U. S. Atomic Energy Commission.

[1] S.-I. Mizushima, *Structure of Molecules and Internal Rotation* (Academic Press, Inc., New York, 1954).

[2] N. Sheppard, Advances in Spectroscopy **1,** 288 (1959).

[3] R. E. Kagarise and L. W. Daasch, J. Chem. Phys. **23,** 113, 130(1955).

[4] R. E. Kagarise, J. Chem. Phys. **23,** 207 (1955); **24,** 300, 1264 (1956); **26,** 380 (1957).

[5] M. Iwasaki, S. Nagase, and R. Kojima, Bull. Chem. Soc. Japan **30,** 230 (1957).

[6] P. Klaboe and J. Rud Nielsen, J. Chem. Phys. **32,** 899 (1960); **33,** 1765 (1960).

[7] R. E. Kagarise, J. Chem. Phys. **26,** 380 (1957); **29,** 680 (1958).

[8] G. Glockler and C. Sage, J. Chem. Phys. **9,** 387 (1941).

[9] Naval Research Lab. Rept. 3924 (1952).

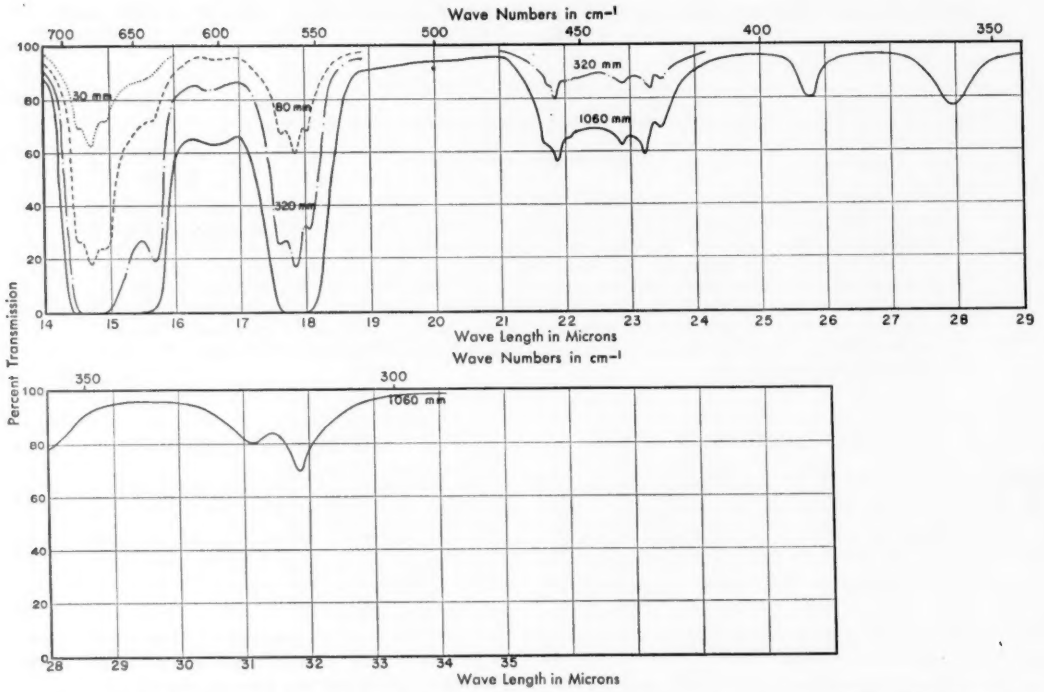
Wave Numbers in cm⁻¹
700 650 600 550 500 450 400 350
30 mm
80 mm
320 mm
1060 mm
Percent Transmission
Wave Length in Microns
14 15 16 17 18 19 20 21 22 23 24 25 26 27 28 29
Wave Numbers in cm⁻¹
350 300
1060 mm
Wave Length in Microns
28 29 30 31 32 33 34 35

FIG. 1. Infrared absorption spectrum of CF_2Cl-CHF_2. Cesium bromide prism; state: gas; temperature: 25°C; cell length: 6 cm.

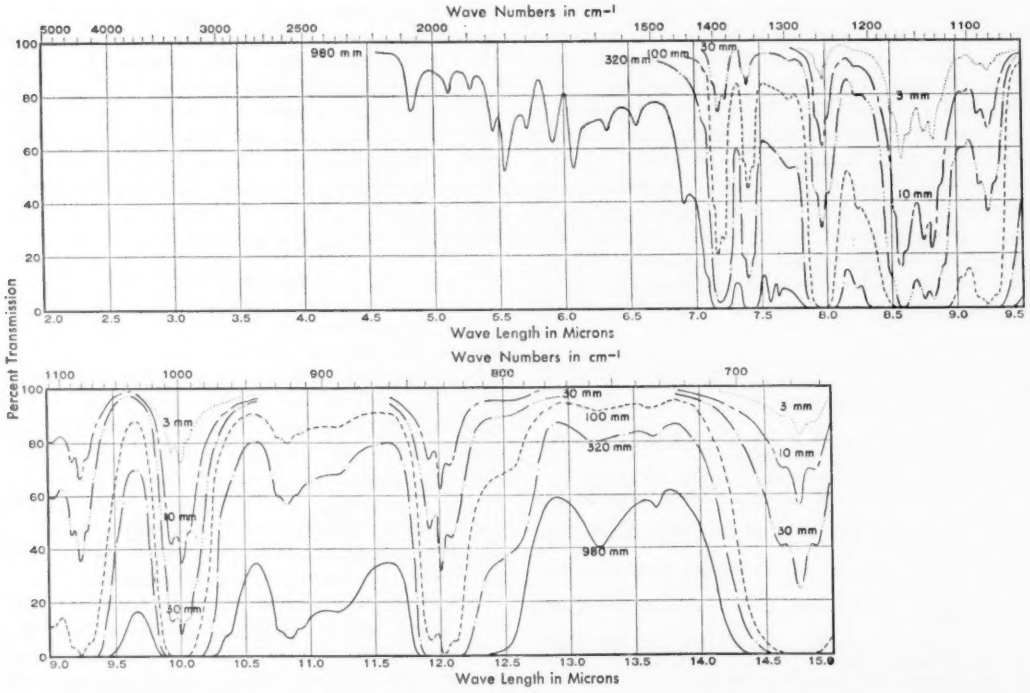

FIG. 2. Infrared absorption spectrum of CF_2Cl-CHF_2. Sodium chloride prism; state: gas; temperature: 25°C; cell length: 10 cm.

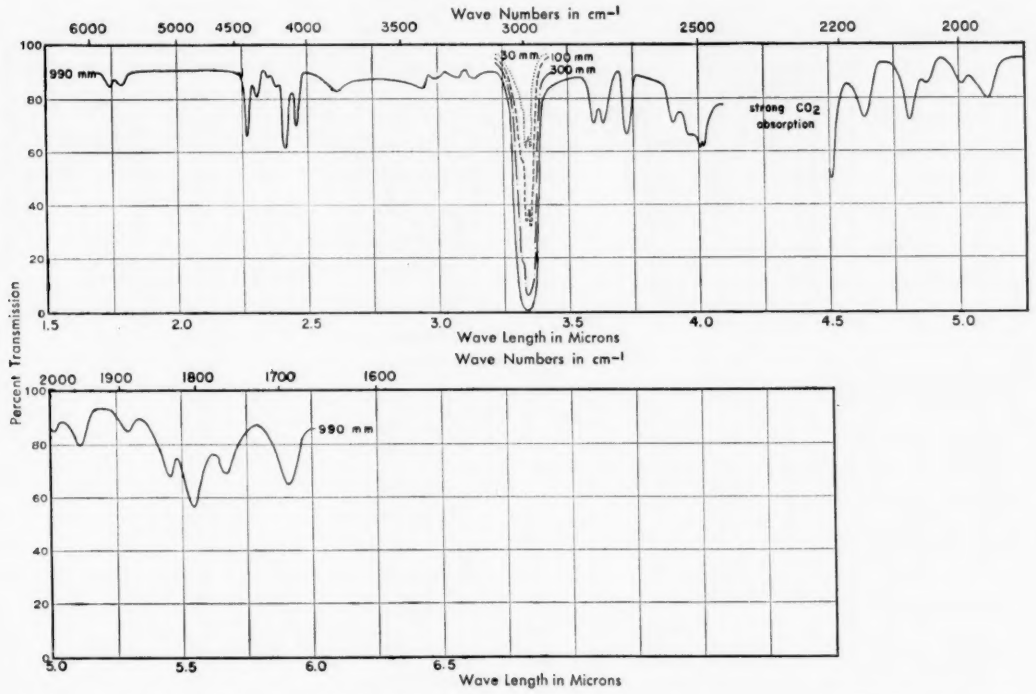

FIG. 3. Infrared absorption spectrum of CF_2Cl-CHF_2. Lithium fluoride prism; state: gas; temperature: 25°C; cell length: 10 cm.

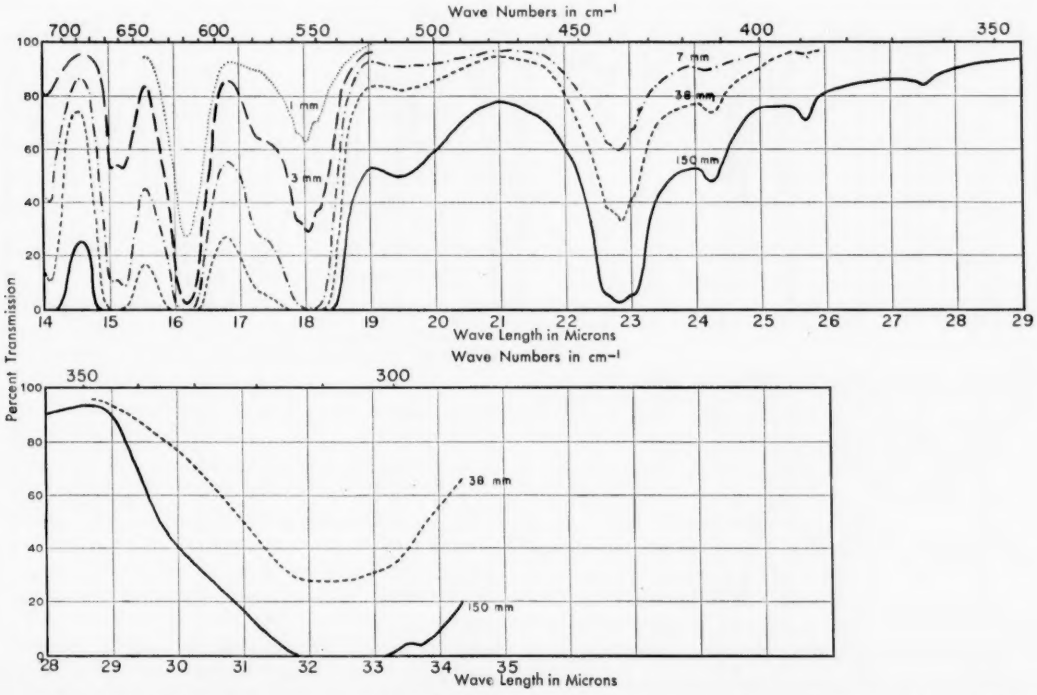
Wave Numbers in cm⁻¹
700 650 600 550 500 450 400 350
1 mm
3 mm
7 mm
38 mm
150 mm
Percent Transmission
14 15 16 17 18 19 20 21 22 23 24 25 26 27 28 29
Wave Length in Microns
Wave Numbers in cm⁻¹
350 300
38 mm
150 mm
28 29 30 31 32 33 34 35
Wave Length in Microns

FIG. 4. Infrared absorption spectrum of CF_2Br-CHF_2. Cesium bromide prism; state: gas; temperature: 25°C; cell length: 1 m.

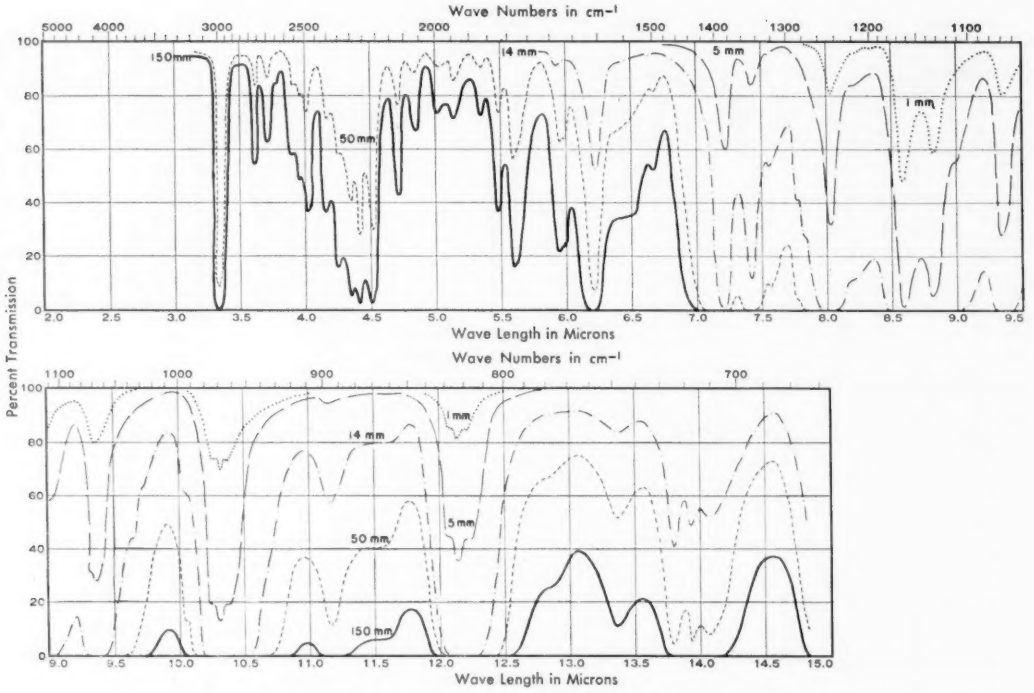

FIG. 5. Infrared absorption spectrum of CF_2Br-CHF_2. Sodium chloride prism; state: gas; temperature: 25°C; cell length: 1 m.

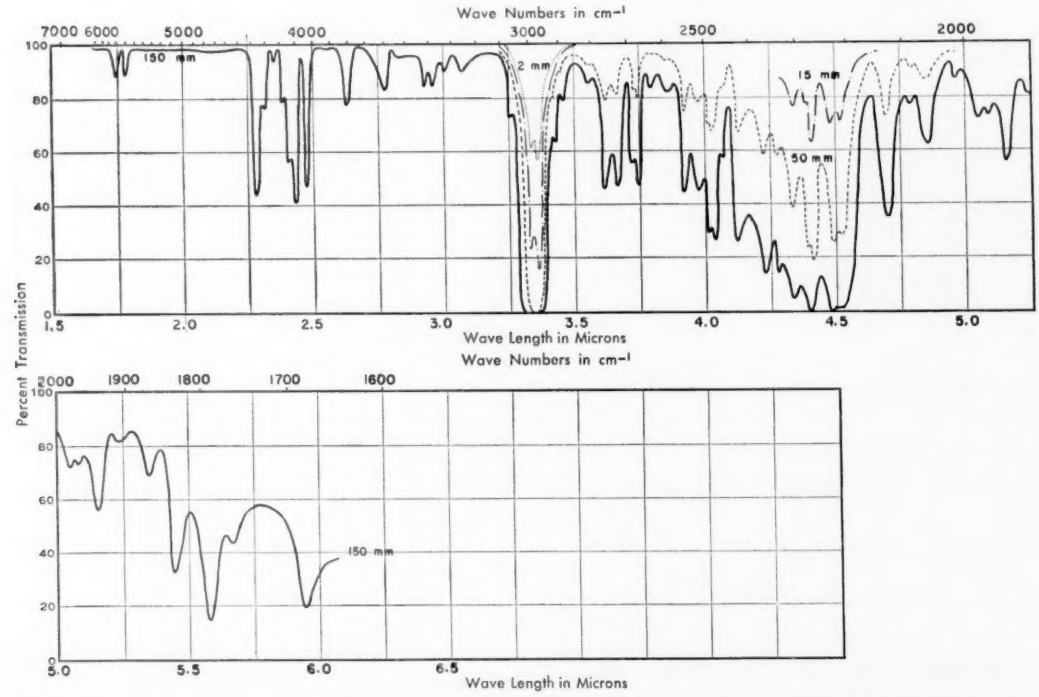

FIG. 6. Infrared absorption spectrum of CF_2Br-CHF_2. Lithium fluoride prism; state: gas; temperature: 25°C; cell length: 1 m.

TABLE I. Raman spectral data for liquid $CF_2Cl-CHF_2$.

Wave number	Description[c]	Depolarization[d]	Exciting Hg lines[e]	Interpretation[f]
[93.0?][a]				
approx 138[b]	vw		±*e*	Fundamental I, II
approx 196	w		±*e*	Fundamental I, II
231[b]	vvw		*e*	Fundamental I
253	w		*e*, *k*	Fundamental II
321	s, sh	0.5	±*e*, *k*, *i*	Fundamental I
340	m	0.7	±*e*, *k*	Fundamental II
361	s, sh	0.6	±*e*, *k*	Fundamental I, II
432	vs, b	0.3	±*e*, *k*, *i*	Fundamental I, II
458	s	0.5	*e*, *k*	Fundamental I, II
496[b]	w, d	0.8	*e*	138+361=499; 2×253=506
514	w, d	0.8	*e*	196+321=517
560	m, sh	0.5	*e*, *k*	Fundamental II
638	vs, sh	0.1	*e*, *k*	Fundamental I, II
672	vs, b	0.1	*e*, *k*	Fundamental I, II
699	w		*e*	340+361=701
720[b]	vw		*e*	2×361=722
828	s	0.2	*e*, *k*	Fundamental I, II
863[b]	vw		*e*	2×432=864
[910.2]				
995	w, d	0.9	*e*	Fundamental II
1072	m, d	0.6	*e*, *k*	Fundamental I
1115	m	0.5	*e*	Fundamental I
1145	m	0.5	*e*	Fundamental II
1214	m		*e*	Fundamental I
1249[b]	w, d		*e*	Fundamental II
1318[b]	vw		*e*	253+1072=1325
1358	m, d	0.9	*e*	Fundamental I
1399[b]	w, d	0.5	*e*	Fundamental II
2980–3015	vs	0.2	*e*, *k*, *i*	Fundamental I, II

[a] Bands enclosed by brackets were observed by Glockler and Sage[8] but not in the present work.
[b] These bands were not observed by Glockler and Sage.[8]
[c] The following abbreviations have been used: s strong, m medium, w weak, v very, d diffuse, sh sharp, b broad.
[d] Measured depolarization ratios.
[e] The meaning of the Kohlrausch symbols are: *e*=4358 A, *k*=4047 A, and *i*=4078 A; ± indicates that the Raman band has been observed both as a Stokes and an anti-Stokes shift.
[f] Roman numerals I and II refer to different rotational isomers.

TABLE II. Raman spectral data for liquid $CF_2Br-CHF_2$.

Wave number	Description[a]	Depolarization[b]	Exciting Hg lines[c]	Interpretation[d]
approx 165	w		±*e*	Fundamental I, II
approx 182	w	*p*	±*e*	Fundamental I, II
299	s, sh	0.8	±*e*, *k*, *i*	Fundamental I
312	s, sh	0.3	±*e*, *k*, *i*	Fundamental II
331	vs, b	0.3	±*e*, *k*, *i*	Fundamental I, II
365	s, sh	0.1	±*e*, *k*	Fundamental I, II
439	w	0.5	*e*, *k*	Fundamental I, II
504	w, d	0.8	*e*	182+331=513
554	s	0.2	*e*, *k*	Fundamental II
600	vvw		*e*	165+439=604
614	vs	0.1	*e*, *k*	Fundamental I
623	vs	0.1	*e*, *k*	Fundamental II
665	s, sh	0.15	*e*, *k*	Fundamental I, II
711	w		*e*	Fundamental I, II
770	vvw		*e*	331+439=770
819	s	0.12	*e*, *k*, *i*	Fundamental I, II
861	vw		*e*	312+554=866
906	w	0.5	*e*	299+614=913
955	w	0.3	*e*	299+665=964
967	m		*e*, *k*	Fundamental II
1061	s	0.3	*e*, *k*	Fundamental I
1104	m, d	0.3	*e*, *k*	Fundamental I
1134	m, d	0.3	*e*, *k*	Fundamental II
1205	m		*e*, *k*	Fundamental I
1238	w, d		*e*	Fundamental II
1279	vw		*e*	182+1104=1286
1349	s	0.8	*e*, *k*	Fundamental I
1386	m	0.3	*e*, *k*	Fundamental II
1422	w, d		*e*	2×711=1422
1775	vw, d		*e*	439+1349=1788; 711+1061=1772
2970–3010	s	0.19	*e*, *k*, *i*	Fundamental I, II

[a] For abbreviations used see footnote c in Table III.
[b] Numbers indicate the measured depolarization ratios: *p* polarized, *d* depolarized.
[c] See footnote b, Table III for the meaning of the Kohlrausch symbols.
[d] Roman numerals I and II refer to different rotational isomers.

molecules belong to the same species. Assuming the internuclear distances C−C=1.54, C−H=1.093, C−F=1.37, C−Cl=1.78, and C−Br=1.98 A, and tetrahedral angles, one finds the principal moments of inertia 335.4, 455.4, and 474.4 gcm², for the *trans*-form of (C) and 394.4, 606.1, and 684.8 gcm², for the *trans*-form of (B). From Badger and Zumwalt's curves[10] the *PR* separations of types *A*, *B*, and *C* contours are found to be 10, 11, and 14 cm⁻¹, respectively, for (C) and 10, 12, and 14 cm⁻¹ for (B). Infrared bands of species *a''* should have type *C* contours in the gaseous state, while bands of species *a'* should have contours that are hy-

[10] R. M. Badger and L. R. Zumwalt, J. Chem. Phys. **6**, 711 (1938).

TABLE III. Fundamental vibrational frequencies for $CF_2Cl-CHF_2$ and $CF_2Br-CHF_2$.

$CF_2Cl-CHF_2$			$CF_2Br-CHF_2$			
Infrared		Raman	Infrared		Raman	
Gas	Solid[a]	Liquid	Gas	Solid[a]	Liquid	Approximate motion[c]
		138w[b]				Torsional I, II
		196w			165w	Rocking I, II
		231vw				Rocking I
					182w	Rocking I, II
		253w				Rocking II
321m		321s			299s	Rocking I
		340m	307s		312s	Rocking II
	353m					
358w		361m	332m		331vs	Rocking I, II
	360m					
431s	431s	432vs	363vw		365s	CF_2 Hal bend I, II
457m	459m	458s	438s	440w	439m	CF_2 Hal bend I, II
		514w	513m		504m	CHF_2 bend I
561vs	554s	560m	554vs	553vs	554m	CHF_2 bend II
637m	634m	638s				CF_2 Hal bend I, II
			618vs	614vs	614vs	CF_2 Hal bend I
					623vs	CF_2 Hal bend II
			656s	657s		
678vs	672s	672s			665vs	C−Hal stretch I, II
			665s	664s		
801m	800m		718vs	710s	711vw	CH_2F bend I, II
833vs	828vs	828vs	824vs	819vs	819s	C−C stretch I, II
922s	919w		870m	862w	861w	C−F stretch I, II
999vs	996vs	995w	969vs	967vs	967m	C−F stretch II
1082vs	1070vs	1072w	1069vs	1056vs	1061s	C−F stretch I
1138vs	1116vs	1115m	1135vs	1115vs	1104s	C−F stretch I
1169vs	1153vs	1145m	1164vs	1152vs	1134s	C−F stretch II
1214vw	1212s	1214m	1207vw	1203s	1205m	CHF_2 deform I
1255vs	1245vs	1249m	1245vs	1237vs	1238w	CHF_2 deform II
1352s	1353s	1358m	1348s	1348s	1349s	C−F stretch I
1396vs	1391s	1399vw	1384vs	1384vs	1386m	C−F stretch II
2987vs	2999s	2997vs	2977vs	2987s	2990s	C−H stretch I
3001vs	2999s	2997vs	2998vs	2987s	2990s	C−H stretch II

[a] See footnote c, Table I.
[b] See footnote d, Table I, for abbreviations used.
[c] Roman numerals I and II refer to different rotational isomers.

brids between types *A* and *B*. Since the configuration of the *gauche*-isomers is not accurately known, no predictions are made about the contours of their bands.

Of the observed infrared bands for which the *PR* separation can be estimated, 7 bands of (C) and 4 bands of (B) have separations in the 10-12 cm^{-1} range, while 7 bands of (C) and 2 bands of (B) have *PR* separations close to 14 cm^{-1}.

All the fundamental frequencies except the one connected with C-H stretching are expected to lie below 1450 cm^{-1}. For each compound about 26 observed bands appear to be fundamentals. It is evident, therefore, that in many cases fundamentals belonging to the different isomers overlap to give what appears to be a single band. This may be expected from the very close geometrical similarity between the *trans*- and *gauche*-isomers.

No way has been found to determine without con-

siderable uncertainty whether an observed band belongs to the *trans*-isomer, the *gauche*-isomer or is a superposition of *trans*- and *gauche*-bands. The infrared spectra of the solids at −180°C appear as complex as the spectra of the gas and hence are of limited value for differentiating between the fundamentals of different isomers. Moreover, the equilibria between the rotational isomers in the gaseous or liquid states are not sufficiently displaced with change in temperature to provide a basis for such differentiation. The method of displacing the equilibrium by dissolving the sample in solvents of different polarities could not be utilized, except at low temperatures, due to the volatility of the compounds.

However, in some cases the observation of infrared combinations bands could be used to ascertain that two fundamentals belong to the same isomeric form. Thus, the combination bands appearing above 4000 cm^{-1} gave a clue to the differentiation between the fundamentals of the two isomeric forms of (C) and (B) in the region around 1200 cm^{-1}.

The two very strong infrared bands at 2987 and 3001 cm^{-1} in the spectrum of gaseous CF_2Cl–CHF_2 have somewhat uncertain *PQR* contours with *PR* separations of approximately 15 and 10 cm^{-1}, respectively. They must represent the single C–H stretching mode for each isomer. Similar bands are found at 2977 and 2998 cm^{-1} in the infrared spectrum of CF_2Br–CHF_2. The corresponding Raman bands are very broad, producing a single maximum at 2995 and 2990 cm^{-1} for (C) and (B), respectively. Instead of the terms *trans* and *gauche* the noncommittal designation, I and II will be used to describe the isomers. For (C), I is defined as the isomer having a C–H stretching mode at 2987 cm^{-1} in the infrared spectrum of the gas, while II is defined as the isomer having a C–H stretching mode at 3001 cm^{-1}. Correspondingly, isomers I and II of (B) are defined as those causing the bands at 2977 and 2998 cm^{-1}, respectively.

While none of the strong infrared bands of the gas disappears in the spectrum of the solid, the relative intensities of many of the bands change considerably and by roughly the same amount, unlike what was observed for CH_2F–CH_2F,[6] CF_2Cl–$CFCl_2$, and CF_2Br–CCl_2Br.[11] In the region between 1200 and 1400 cm^{-1}, where the differentiation between the bands belonging to the different rotational isomers can be made with considerable certainty on the basis of observed combinations, it is found that for both compounds the bands ascribed to I are enhanced, while those ascribed to II suffer a decrease in relative intensity on going from gas to solid. It is believed, therefore, that these intensity variations are caused by a shift in the isomeric equilibrium rather than by changes in extinction coefficients brought about by intermolecular interactions.

Tentative fundamentals for both compounds are listed in Table III which shows the close similarity between their spectra. In the region from 650 to 3000 cm^{-1}, the fundamentals of the chloro- and bromo-compounds that are believed to correspond to each other are listed in the same horizontal line. A fundamental of (C) and the corresponding fundamental of (B) lie fairly close together, the fundamental of (B) being displaced somewhat towards smaller wave numbers, and in most cases they have about equal intensities. Furthermore, corresponding fundamentals undergo about the same intensity change upon solidification. With few exceptions, the same combinations bands are observed for (C) and (B). Since it has not been possible to decide which of the isomeric forms I and II is *trans* and which is *gauche*, the fundamentals are not classified into symmetry species.

The uncertainties in the assigned fundamentals are fairly large in the low-frequency region where only Raman data are available. The lowest Raman frequency, 138 cm^{-1}, observed for (C) probably represents overlapping fundamentals of I and II involving mainly torsion. The corresponding fundamentals of (B) have not been observed, probably because of the rather strong background near the exciting mercury line.

In terms of the assigned fundamentals, it has been possible to interpret all of the observed Raman bands and practically all of the infrared bands, not taken as fundamentals, as binary combinations or overtones.

ENTHALPY DIFFERENCE BETWEEN THE ROTATIONAL ISOMERS

No appreciable intensity variation of the infrared bands of either compound in the gaseous state was observed when the temperature was raised from 30° to 180°C. For the C–H stretching bands near 3000 cm^{-1}, and for some of the bands in the 1100–1400 cm^{-1} region, accurate extinction measurements were made at many positions in each band by means of a densitometer, but no temperature variation could be established. It was concluded, therefore, that the enthalpy difference ΔH° (*gas*) between the rotational isomers in the gaseous state is zero within the experimental error, estimated to be ±200 cal/mole.

Identical sets of Raman exposures were made at 30°, −30°, and −80°C. The microphotometer curves showed no observable temperature variation of any band of either compound. It was concluded that ΔH° (*liquid*) = 0±300 cal/mole.

The absence of observable enthalpy differences between the *trans*- and the *gauche*-isomers is not surprising, since the steric repulsion should be nearly the same for both isomers. Moreover, because of the small difference between the dipole moment of the C–F bond, on the one hand, and the C–Cl and C–Br moments on the other, the —CF_2Cl and —CF_2Br end-groups will have resultant dipole moments nearly parallel to the C—C bond. The *trans* and *gauche*-isomers will, therefore, have nearly equal dipole moments and, according

[11] P. Klaboe and J. Rud Nielsen, J. Mol. Spectroscopy (to be published).

to Onsager's theory,[12] should undergo about the same stabilization in the liquid state.

As has been mentioned, both isomers of (C) and (B) are present in the solid at −180°C. This has been found to be the case for some halogenated ethanes, while for others only one isomer is present in the solid.[1,2,6] Some of the former ethanes have been reported to be amorphous in the solid state.[3,13,14] However, there are reasons to believe that (C) and (B) solidify as mixed crystals. In fact, the solids appeared under visual examination as crystalline aggregates. No changes in their spectra were observed when they were made to solidify very slowly or at different temperatures. When the solids were allowed to warm up slowly no change in the spectra was observed close below the melting point.

[12] L. Onsager, J. Am. Chem. Soc. **58,** 1486 (1936).
[13] J. K. Brown and N. Sheppard, Discussions Faraday Soc. **9,** 144 (1950); J. Chem. Phys. **19,** 976 (1951).
[14] F. E. Malherbe and H. J. Bernstein, J. Chem. Phys. **19,** 1607 (1951).

ACKNOWLEDGMENTS

The writers are indebted to Professor A. L. Henne and Dr. Leonard H. Beck of Ohio State University for providing the samples.

High Frequency Factors in Unimolecular Reactions

COLIN STEEL*

Department of Chemistry, Brandeis University, Waltham, Massachusetts

AND

KEITH J. LAIDLER

Department of Chemistry, University of Ottawa, Ottawa, Canada

(Received August 22, 1960)

High frequency factors are associated with two main classes of unimolecular reactions: (1) reactions in which two bonds are ruptured simultaneously, and (2) certain dissociation reactions in which only one bond is broken, such as the decomposition of ethane into two methyl radicals. These high values are related to the entropy increases occurring during the rupture of the bond or bonds, and a discussion is given of the way in which the entropy may change during the process. For the reactions of type (2) the data are consistent with the view that the entropy change occurs well before the bond is completely ruptured. For reactions of both types the rates at low pressures (i.e., the rates of energization) are probably not affected by such entropy increases, so that the pressures at which transition occurs from first to second order will be abnormally high for such reactions; this point of view is supported by detailed calculations for five reactions. The entropy changes during the course of reaction are interpreted as being due to a "softening" of molecular vibrations in the activated state.

INTRODUCTION

CONSIDERABLE attention has recently been devoted to abnormally high ($\gg 10^{13}$ sec^{-1}) frequency factors in unimolecular reactions in the gas phase. The theories of Kassel[1] and of Rice and Ramsperger,[2] on the one hand, and of Slater[3] on the other, although differing in their treatment of the vibrating molecule, lead in their simplest form to the same conclusion: namely that the first-order constants at high pressures are given by

$$k_\infty = A_\infty \exp(-\epsilon_0/kT), \qquad (1)$$

where A_∞ is closely related to the vibrational frequencies of the molecule and normally has a magnitude of about 10^{13} sec^{-1}. The Eyring theory[4] leads to the formal equation

$$k_\infty = (kT/h) \exp(\Delta S^*/R) \exp(-\Delta H^*/RT) \qquad (2)$$

and can account for high frequency factors if there is a large positive entropy of activation. However, this theory has never been properly integrated with the Kassel-Rice-Ramsperger-Slater theories, and there has been difficulty in understanding how a molecule vibrating with a frequency of $\sim 10^{13}$ sec^{-1} can apparently cross over an energy barrier with a frequency that is higher by several powers of ten.

Several of the reactions exhibiting high frequency factors are ones in which more than one critical coordinate or oscillator is involved in the reaction. Slater's theory in its simplest form[5] leads to the conclusion that a reaction involving the critical extension of a single coordinate, or the passage of energy into a single normal mode, must lead to a frequency factor of $\sim 10^{13}$ sec^{-1}. Recently Steel[6] has improved an earlier treatment of Pritchard[7] and has considered the problems of the accumulation of energy in z normal modes (following the Kassel-Rice-Ramsperger procedure), and of the attainment by a coordinate of a critical extension when the energy is distributed between z normal modes (the Slater procedure); in both cases the theory leads to a frequency factor that may be greater than 10^{13} sec^{-1} by several powers of ten. This treatment appears to be formally correct, but there is a difficulty in applying it to actual examples, as will be seen later. The same is true of recent theoretical treatments by Thiele and Wilson,[8] and by Slater.[9]

There is, moreover, an important group of reactions to which this explanation cannot apply. These are the decompositions of certain molecules, by the breaking of a single bond, into two radicals. The kinetic information about these dissociations is largely indirect, but is very reliable; it involves the results for the reverse associations of the radicals, and the calculated dissociation constant. The procedure may be exemplified by

* Present address: Chemistry Department, University of Toronto, Toronto, Canada.

[1] L. S. Kassel, J. Phys. Chem. **32,** 225 (1928); *Kinetics of Homogeneous Gas Reactions* (Reinhold Publishing Corporation, New York, 1932), Chap. 5.

[2] O. K. Rice and H. C. Ramsperger, J. Am. Chem. Soc. **49,** 1617 (1927); **50,** 617 (1928).

[3] N. B. Slater, Proc. Cambridge Phil. Soc. **35,** 36 (1939), and many subsequent papers; see especially N. B. Slater, *Theory of Unimolecular Reactions* (Cornell University Press, Ithaca, New York, 1959).

[4] S. Glasstone, K. J. Laidler, and H. Eyring, *The Theory of Rate Processes* (McGraw-Hill Book Company, Inc., New York, 1941), pp. 281–97.

[5] N. B. Slater, Trans. Faraday Soc. **55,** 5 (1959).

[6] C. Steel, J. Chem. Phys. **31,** 899 (1959).

[7] H. O. Pritchard, J. Chem. Phys. **25,** 267 (1956); D. Clark and H. O. Pritchard, J. Chem. Soc. **1956,** 2136.

[8] E. Thiele and D. J. Wilson, J. Phys. Chem. **64,** 473 (1960).

[9] N. B. Slater, J. Phys. Chem. **64,** 476 (1960).

TABLE I. Thermal decompositions of the type R−R′→R+R′ in the gas phase.

Compound	Log A (sec^{-1})	E (kcal $mole^{-1}$)
CH_3—CH_3	16.5	85
C_2H_5—C_2H_5	17	80
NO_2—NO_2	16	13
NO_2—NO_3	(17.5)	(24.7)
CH_3—NO	15	...
CH_3—$C(CH_3)_3$	17	...

the reaction

$$C_2H_6 \rightleftarrows 2CH_3.$$

Dodd and Steacie[10] have found the reverse recombination of methyl radicals to have a second-order rate constant of 3.7×10^{13} cc $mole^{-1}$ sec^{-1} at 200°C, and to have no activation energy; this implies that recombination occurs at approximately every collision. With a value of 85.0 kcal $mole^{-1}$ for the energy of dissociation of ethane into $2CH_3$, and of 16 eu for the standard entropy of the process (the standard state is 1 mole per cc; the entropy is calculated assuming a planar methyl radical) the equilibrium constant at the same temperature is calculated to be 1.5×10^{-36} mole cc^{-1}. These values lead to 5.6×10^{-23} sec^{-1} for the first-order rate constant for the dissociation, and to a frequency factor of 3×10^{16} sec^{-1}. Similar calculations for other dissociations lead to the results shown in Table I (see Appendix) which is similar to one given by Trotman-Dickenson.[11]

These high frequency factors are clearly related to the positive entropies of the dissociation reaction; the problem is to interpret the values in terms of the vibration of a molecule and the passage over the energy barrier. At first sight one would have expected the reverse reactions to have abnormally low frequency factors (by analogy with CH_3+CH_4 and $CH_3+C_2H_6$, both of which have values of $\sim10^{11}$ cc $mole^{-1}$ sec^{-1}) in which case the frequency factors of the dissociation reactions would have been close to "normal."

ENTROPY VARIATIONS DURING REACTION

All of the reactions having high frequency factors have in common the fact that there is a considerable increase of entropy during the reaction. It will now be shown how such entropy increases may lead to a formal interpretation of the high factors; a more detailed discussion, in terms of vibrational frequencies in the activated state, is given later.

Three ways in which entropy may vary during the course of a reaction are shown in Fig. 1, which relates specifically to the dissociation of C_2H_6 into $2CH_3$. Each curve shows the variation of E, TS, and $F(=E-TS)$ with the carbon-carbon distance. The activated complex corresponds to the top of the free-energy barrier, and in accordance with the Kassel-Rice-Ramsperger-Slater theories the system is to be regarded as crossing the barrier with a frequency of $\sim10^{13}$ sec^{-1}.

In the left-hand figure (case I) the entropy increase is shown as occurring at an early stage in the dissociation process, and the free-energy curve now rises to a limiting value as the bond is broken. The activated complex therefore has a high entropy, and the free energy of activation is $D_0-T\Delta S=85\,000-16T=78.4$ kcal at 200°C. The association reaction has a zero entropy of activation. The reactions in Table I probably conform to this situation.

In the central figure (case II) the entropy increase is shown as occurring after the C—C bond has been broken. The free-energy curve then shows a maximum at a point which corresponds to a broken bond. The free energy of activation corresponding to the dissociation is therefore equal to the energy of dissociation, and the entropy of activation is zero. For the reverse reaction the entropy of activation is negative. This is evidently *not* the situation that exists with the reactions in Table I.

The right-hand figure (case III) represents an intermediate type of situation which gives rise to a special type of behavior. The entropy increase now corresponds to a partial breaking of the bond, and in certain cases this can correspond to a maximum in the free-energy curve at a point at which the bond is not completely broken. The activation energy for the reaction is in this case less than the dissociation energy, and there is in addition a positive entropy of activation. For the reverse reaction, the association, the energy of activation is negative, and there is a negative entropy of activation.

It is not certain whether this third situation has ever been observed. Cases of activation energies which are less than the degree of dissociation and of negative temperature coefficients for radical recombinations have been reported,[12] but these probably occur in the low-pressure region where another explanation applies.[13]

The case I behavior, to which the reactions in Table I apparently conform, is to be interpreted as meaning that the normal modes of vibration should actually be worked out in terms of free energy instead of total energy. The molecule still crosses the barrier with a frequency of $\sim10^{13}$ sec^{-1}, but the barrier is lower since it is actually a free-energy rather than an energy barrier. At low energies the E and F curves are equivalent, but at higher energies the entropy factors become important and the vibration is modified by the fact

[10] R. E. Dodd and E. W. R. Steacie, Proc. Roy. Soc. (London) **A223,** 283 (1954); cf. E. W. R. Steacie, J. Chem. Soc. **1956,** 3986.
[11] A. F. Trotman-Dickenson, *Gas Kinetics* (Butterworths Scientific Publications, Ltd., London), p. 125.
[12] M. Page, H. O. Pritchard, and A. F. Trotman-Dickenson, J. Chem. Soc. **1953,** 3878.
[13] A. F. Trotman-Dickenson, footnote 11, p. 79.

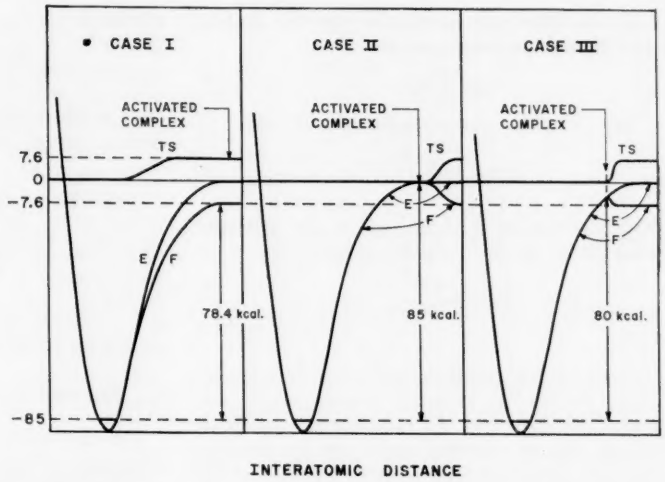

FIG. 1. Hypothetical curves showing the variation of E, TS, and F with interatomic distance for the dissociation of ethane into two methyl radicals; the increase of TS occurs at different separations in the three cases.

that certain configurations are favored because they correspond to states of higher entropy. This point is further considered later.

BEHAVIOR AT LOW PRESSURES

At low pressures, according to all theories of unimolecular reactions, the over-all rate of reaction is equal to the rate of energization, which is a second-order process. According to the Hinshelwood-Kassel-Rice-Ramsperger (HKRR) theories the rate constant k_1 for the energization process is given approximately by

$$k_1 = Z(\epsilon_0/kT)^{s-1}[(s-1)!]\exp^{-1}(-\epsilon_0/kT), \qquad (3)$$

where Z is the collision number and s the number of normal modes of vibration that contribute to energization. Slater's theory gives rise to a rate constant k_1 that is generally lower than the above by several orders of magnitude, since the condition for energization is a more stringent one in that the energy must initially be distributed in a particular way between the normal modes. Gill and Laidler[14] have recently compared the two theories and have concluded that the HKRR theories give a more satisfactory interpretation of the results at least for relatively small molecules such as N_2O, H_2O_2, and C_2H_6.

An important question is whether the low-pressure rate constant is modified when there is an entropy increase during the activation process. The considerations of the previous section lead to the conclusion that no modification will be found; the enhanced rates, in other words, will occur in the process in which the energized molecule becomes an activated one but not in the process of energization. That this is so becomes evident when one considers that the condition for energization is that the energy ϵ_0 must become distributed among the s normal modes, and this is still true when there is an entropy increase during the breaking of the bond. When a number of normal modes are involved a typical energized molecule will have relatively little energy in each mode; with ethane, for example, for which 8 or 9 normal modes appear[14a] to contribute to reaction and in which $E_\infty(=N\epsilon_0)=85$ kcal, most of the energized molecules have only about 10 kcal in each mode. Their vibrations will be approximately harmonic, and the entropy increases discussed above will have little, if any, effect on the vibration. Only when the activated state is approached will these entropy changes make themselves felt, and they will lead to an enhancement of the rate with which an energized molecule becomes an activated one, i.e., to a decrease in the mean life of the energized molecule.

It follows as a general conclusion from the above considerations that, when high-pressure frequency factors are abnormally high owing to entropy effects, the transition pressures will be correspondingly high.

In order to make a further test of this conclusion a theoretical treatment of the transition pressure will now be developed, and will be applied numerically to five reactions for which adequate data are available.

"Average" Rate Constant of the Energized Species

The first-order rate constant at a pressure p is given by the general equation

$$k_p = \sum_i k_i f_i \{\omega(p)/[\omega(p)+k_i]\}, \qquad (4)$$

where k_i is the rate constant for molecules in state i (k_i has the dimensions of time^{-1} and is proportional to the reciprocal of the mean lifetime of molecules in state i); f_i is the equilibrium proportion of molecules in state i; and $\omega(p)$ is the effective collision frequency

[14] (a) E. K. Gill and K. J. Laidler, Proc. Roy. Soc. (London) **A250,** 121 (1959); see also (b) Can. J. Chem. **36,** 1570 (1958); (c) Trans. Faraday Soc. **55,** 753 (1959); (d) Proc. Roy. Soc. (London) **A251,** 66 (1959).

per molecule. The rate constants for the limiting cases at high and low pressures are

$$k_\infty = \sum_i k_i f_i \tag{5}$$

and

$$k_0 = \omega(p) \sum_i f_i. \tag{6}$$

It is natural to define $\sum_i k_i f_i / \sum_i f_i$ as the "average" rate constant k_{Av}, for the energized species. Thus

$$k_\infty = k_{Av} \sum_i f_i \tag{7}$$

and

$$k_\infty / k_0 = k_{Av} / \omega(p). \tag{8}$$

The average rate constant k_{Av} can therefore be determined from the experimental high- and low-pressure rate constants, provided that $\omega(p)$ can be estimated. Both the Kassel[1] and the Slater[3] theories assume (with good experimental justification) that every collision suffered by an energized molecule leads to deactivation. If this is so $\omega(p)$ is given by Zc, where Z is the collision number and c is the concentration of the reacting molecules.

The average rate constant may also be calculated theoretically. For example, the Kassel theory for a system of s loosely coupled oscillators gives

$$\sum_i k_i f_i = \lambda \exp(-\epsilon_0/kT) \tag{9}$$

and

$$\sum_i f_i \approx (\epsilon_0/kT)^{s-1}[1/(s-1)!] \exp(-\epsilon_0/kT) \tag{10}$$

provided that $\epsilon_0 \gg skT$. It thus follows that

$$k_{Av} = \lambda(s-1)!(\epsilon_0/kT)^{1-s}. \tag{11}$$

Slater has emphasized that the constant λ is equal to the frequency of internal energy transfer between the coupled oscillators, and should therefore lie in the range $(10^{12}-10^{14})$ sec^{-1}. However, the calculations presented later show that for agreement with experiment λ must be set equal to the experimental high-pressure frequency factor A_∞.

"Transition" Pressure P

A transition pressure P may be defined by the relationship[15]

$$\omega(P) = k_{Av}. \tag{12}$$

The rate constant at such a pressure P will therefore be given by

$$k_P = \sum_i k_i f_i [k_{Av}/(k_{Av}+k_i)]. \tag{13}$$

Only in the limiting case $s=1$ will $k_i = k_{Av}$ for all values of i so that $k_p = k_\infty/2$. In terms of the Kassel theory

$$\frac{k_P}{k_\infty} = \frac{\int_{\epsilon_0}^{\infty} \frac{(1-\epsilon_0/\epsilon)^{s-1}(\epsilon/kT)^{s-1}\exp(-\epsilon/kT)}{(s-1)!} \frac{d\epsilon}{kT}}{\exp(-\epsilon_0/kT)}. \tag{14}$$

It is to be seen that λ does not enter into this expression so that an anomalous value of λ causes no trouble.

Example 1: Thermal Decomposition of N_2O

The experimental data for this reaction have recently been reviewed critically by Johnston,[16] and a theoretical treatment given by Gill and Laidler,[14b] on whose discussion the following is based. The data are best fitted with s equal to 2. At 880°K $k_\infty = 7.47\times10^{-4}$ sec^{-1}, $E_\infty = 60.0$ kcal mole^{-1}, $A_\infty = 8\times10^{11}$ sec^{-1}, $k_0/c = 14.0$ cc mole^{-1} sec^{-1}, $Z = 2\times10^{14}$ cc mole^{-1} sec^{-1}, $(k_{Av})_{exp} = Zc(k_\infty/k_0) = 1\times10^{10}$ sec^{-1}. If λ is put equal to A_∞, then $(k_{Av})_{calc} = \lambda(s-1)!(\epsilon_0/kT)^{1-s} = 2\times10^{10}$ sec^{-1}. We can therefore set $\omega(P)$ at 2×10^{10} sec^{-1}: this corresponds to a pressure of 5×10^{3} mm. At this pressure Gill and Laidler's analysis shows that the rate constant has fallen off to $\frac{1}{3}$ of its high-pressure value. The value of k_P/k_∞ calculated from Eq. (14) is 1/2.5. The theoretical and experimental results are therefore seen to be in satisfactory agreement provided that $\lambda = A_\infty(8\times10^{11}$ sec$^{-1})$.

This example is of special interest as being the only one in which the frequency factor is abnormally low.

Example 2: Thermal Decomposition of N_2O_5 in the Presence of NO

The thermal decomposition of N_2O_5 has been studied by Mills and Johnston,[17] and by Perrine and Johnston.[18] The former give $k_\infty = 0.29$ sec^{-1} (300°K), $A_\infty = 10^{14.8}$ sec^{-1}, $E_\infty = 21.0$ kcal mole^{-1}, $k_0/c = 2.3\times10^{5}$ cc mole^{-1} sec^{-1} (300°K), $E_0 = 14.5$ kcal mole^{-1}, and $Z = 9\times10^{13}$ cc mole^{-1} sec^{-1}. However, Perrine and Johnston[18] state that the early work was slightly in error due to a contribution from a heterogenous reaction, and they give $k_0/c = 1.3\times10^{5}$ cc mole^{-1} sec^{-1} (300°K) and $E_0 = 19.3$ kcal mole^{-1}; they also found that their data were best fitted by a value of s equal to 10. Further work is clearly needed on the reaction at high pressures, especially since the decomposition of N_2O_5 in solution (which must correspond to an extremely high pressure)

[15] We have

$$k_\infty/k_1 = N_p \sum_i k_i f_i/\omega(P) \sum_i f_i = N_p k_{Av}/\omega(P),$$

where k_1 is the bimolecular rate constant of energization and N_p is the number of molecules per cc at pressure p. Since by definition $\omega(P) = k_{Av}$ it follows that $k_\infty/k_1 = N_p$. The N_p is thus equivalent to the $[A]_{\frac{1}{2}}$ employed by Gill and Laidler.[14]

[16] H. S. Johnston, J. Chem. Phys. **19,** 663 (1951).

[17] R. L. Mills and H. S. Johnston, J. Am. Chem. Soc. **73,** 938 (1951).

[18] R. L. Perrine and H. S. Johnston, J. Am. Chem. Soc. **73,** 4782 (1951).

has been found[19] to have an activation energy of 24.7 kcal mole^{-1}. Indeed, if $E_0=19.3$ kcal mole^{-1} the Kassel theory would predict that the high-pressure activation energy would be $E_\infty=\epsilon_0 N=E_0+(s-\frac{3}{2})RT=24.7$ kcal mole^{-1}. If $E_\infty=24.7$ kcal mole^{-1} then $A_\infty=10^{17.5}$ sec^{-1}; however, if $E_\infty=21.0$ kcal mole^{-1} then $A_\infty=10^{14.8}$ sec^{-1}. Using Eq. (8) it is found that $(k_{Av})_{exp}=2\times10^8$ sec^{-1}. If $E_\infty=24.7$ kcal mole^{-1} and $\lambda=10^{17.5}$ sec^{-1}, then $(k_{Av})_{calc}=3\times10^8$ sec^{-1}. However, if $E_\infty=21.0$ kcal mole^{-1} and $\lambda=10^{14.8}$ sec^{-1}, we get $(k_{Av})_{calc}=3\times10^6$ sec^{-1}, and if λ is set at 10^{13} we get $(k_{Av})_{calc}=4\times10^4$ sec^{-1}. Agreement is therefore only obtained with λ taken equal to $10^{17.5}$ sec^{-1}. A value of $\omega(P)$ equal to 2×10^8 sec^{-1} corresponds to a pressure of 40 mm. At this pressure the rate constant has fallen to $\frac{1}{10}$ of its high-pressure value, and calculation, using Eq. (14) and $E_\infty=24.7$ kcal mole^{-1}, gives k_P/k_∞ as $\frac{1}{20}$.

Example 3: Thermal Decomposition of Ethane

In the case of ethane the same detailed analysis cannot be carried out, since the experimental data[10] are more scanty. We have $A_\infty=3\times10^{16}$ sec^{-1}, $E_\infty=85.0$ kcal mole^{-1}; Gill and Laidler[14a] have estimated that the data are fitted best with a value of $s=9$. A pressure P' may be defined such that $\omega(P')=10k_{Av}$; that is, P' is 10 times the "transition" pressure P already defined. Thus

$$\frac{k_{P'}}{k_\infty}=\frac{\int_{\epsilon_0}^{\infty}\frac{10(1-\epsilon_0/\epsilon)^{s-1}(\epsilon/kT)^{s-1}\exp(-\epsilon/kT)}{10(s-1)!+(\epsilon_0/kT)^{s-1}(1-\epsilon_0/\epsilon)^{s-1}}\frac{d\epsilon}{kT}}{\exp(-\epsilon_0/kT)}$$

$$=1/8.2, \quad \text{at } 200°\text{C}. \qquad (15)$$

From the experimental data it is seen that this corresponds to a pressure of about $\frac{1}{2}$ mm. Thus $Zc=1.4\times10^{14}\times1.7\times10^{-8}=2.4\times10^6$ sec^{-1} and $\omega(P')=2.4\times10^6$ sec^{-1}. Hence $k_{Av}=2.4\times10^5$ sec^{-1}. However, the calculated k_{Av} is given by $(k_{Av})_{calc}=\lambda(s-1)!(\epsilon_0/kT)^{1-s}$ sec^{-1}. If this is set equal to the experimental values for $E_\infty=85.0$ kcal /mole^{-1} and $s=9$ we obtain $\lambda=3\times10^{16}$ sec^{-1} which agrees with the experimental value of 3×10^{16} sec^{-1} for the high-pressure frequency factor.

Example 4: Thermal Decomposition of Azomethane

The thermal decomposition of azomethane has been extensively investigated by several workers,[20–24] and although the reaction has been shown to be slightly complicated by a short chain process, the general shape of the rate-pressure curves is undoubtedly correct. In particular the region in which the falloff in rate occurs is unambiguous. Willbanks[24] has shown that the data are fitted adequately by the Kassel integral when $s=12$.

From the experimental results $E_\infty=51.2$ kcal mole^{-1}, $A_\infty=5\times10^{15}$ sec^{-1}. A pressure P'' may be defined such that $\omega(P'')=10^2k_{Av}$. As before, $k_{P''}/k_\infty=1/4.5$ at 290°C. From the experimental data it is seen that this corresponds to a pressure of 1.7 mm, so that $\omega(P'')=Zc=1.3\times10^7$ sec^{-1} and $k_{Av}=1.3\times10^5$ sec^{-1}. The calculated value of k_{Av} is given by $\lambda(s-1)!(\epsilon_0/kT)^{1-s}=1.0\times10^5$ sec^{-1} provided that $\lambda=5\times10^{15}$ sec^{-1}.

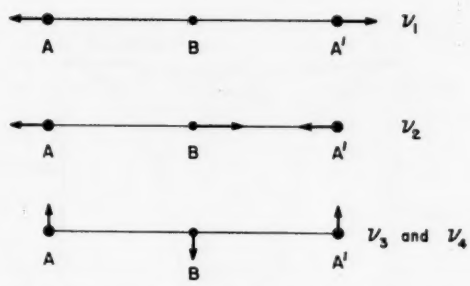

FIG. 2. The normal modes of vibration for a linear triatomic molecule ABA'.

Example 5: Thermal Decomposition of Azoethane

The thermal decomposition of azoethane has been investigated over wide temperature and pressure ranges by Clark.[25] The results lead to $A_\infty=5.9\times10^{15}$ sec^{-1}, $E_\infty=48.5$ kcal mole^{-1}, and $s=18$. A pressure P''' may be defined such that $\omega(P''')=10^4\,k_{Av}$, whence $k_{P'''}/k_\infty=1/2.1$ at 280°C. From the experimental rate-pressure curve at 280°C this is found to correspond to a pressure of 0.5 mm, so that $\omega(P''')=4.3\times10^6$ sec^{-1} and $k_{Av}=4.3\times10^2$ sec^{-1}. Then, if $\lambda=5.9\times10^{15}$ sec^{-1}, $(k_{Av})_{calc}=2.3\times10^2$ sec^{-1}, in good agreement.

Conclusion

The experimental and theoretical values of k_{Av} are seen to be in good agreement in all cases provided that λ is taken to be equal to $(A_\infty)_{exp}$. In other words, high frequency factors are associated with a k_{Av} that is greater than would be expected from formula (14) with λ equal to the expected value of $\sim10^{13}$ sec^{-1}. This results in a shift of the rate-pressure curves toward higher pressures.

VIBRATION OF THE ACTIVATED COMPLEX

The main conclusion of the previous sections has been that for unimolecular reactions having high frequency factors the rates of energization are normal, the high values being associated with the high rate with which

[19] H. Eyring and F. Daniels, J. Am. Chem. Soc. **52,** 1472 (1930).
[20] C. Steel and A. F. Trotman-Dickenson, J. Chem. Soc. **1959,** 975.
[21] R. D. McCoy, Ph.D. dissertation, University of Oregon, Eugene, Oregon (June, 1956).
[22] O. K. Rice and D. V. Sickman, J. Chem. Phys. **4,** 242 (1936).
[23] H. C. Ramsperger, J. Am. Chem. Soc. **49,** 912, 1495 (1927).
[24] E. M. Willbanks, "The Evaluation of the Kassel Integral via IBM 704," Office of Technical Services, U. S. Department of Commerce, Washington, D. C. (1958).
[25] W. D. Clark, Ph.D. dissertation, University of Oregon, Eugene, Oregon, June, 1958.

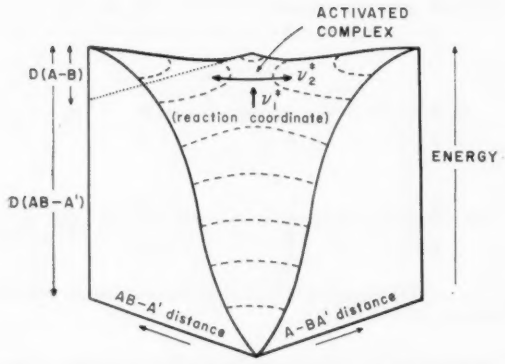

FIG. 3. Schematic potential-energy surface for the dissociation of ABA' into $A+B+A'$. The state $A+B+A'$ is of lower energy than either $AB+A'$ or $A+BA'$.

the energized molecule becomes an activated one. This has been attributed to an unusual type of vibration, a matter which will now be considered in more detail.

Simultaneous Rupture of More than One Bond

The suggestion has been made by Pritchard[7] that when there is simultaneous rupture of more than one bond in a unimolecular process an abnormally high frequency factor can result because the critical energy is localized in more than one oscillator. The theory of this has recently been developed by Steel.[6]

Attempts to apply this type of treatment to particular examples are not, however, successful. This may be seen with reference to the triatomic molecule shown in Fig. 2. Of the four normal modes of vibration only one, ν_1, contributes to the simultaneous rupture of the two bonds; both ν_1 and ν_2, on the other hand, contribute to the rupture of $A-B$ (and of $A-B'$). In general, the number of modes contributing to the simultaneous rupture of two bonds is not greater (indeed it is usually less) than the number contributing to the rupture of one particular bond. It would therefore seem impossible to explain high frequency factors in terms of the contribution of more than one normal mode.

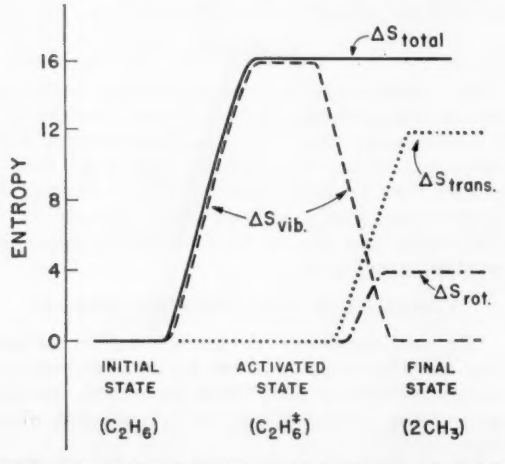

FIG. 4. Variations of the different kinds of entropy during the process $C_2H_6 \rightarrow 2CH_3$.

The only alternative explanation would appear to be that, as in the case of the ethane dissociation discussed above, the activated state corresponds to a state of higher entropy than the initial state. The simultaneous rupture of two bonds will obviously tend to lead to such a situation. Figure 3 shows the potential-energy surface for the system $A-B-A'$ ($A=A'$), derived after the method of Szwarc and Herk[26]; the dissociation energy $D(A-B)$ is less than zero. This is probably the situation in the decomposition of symmetrical azo-compounds, since the decompositions of radicals of the type R–N=N– are known to be exothermic.[12] In the case of azomethane, for example, $A=A=CH_3$ and $B=-N=N-$. The most favorable reaction path is clearly the one involving the simultaneous rupture of the two bonds. The reaction coordinate in this case corresponds to the vibration ν_1, and both the Eyring and Slater theories predict that

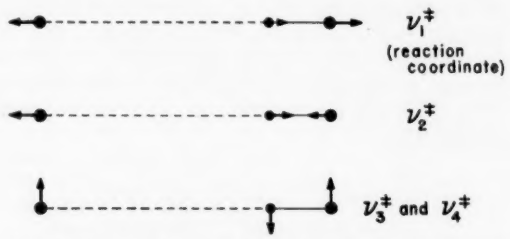

FIG. 5. The normal modes of vibration for an activated complex for the process $ABA' \rightarrow A+BA'$.

$$A=\nu_1\nu_2\nu_3\nu_4/\nu_2^\ddagger\nu_3^\ddagger\nu_4^\ddagger. \qquad (16)$$

The frequencies ν_1, ν_2, ν_3, and ν_4 will usually be close to 10^{13} sec^{-1}, but owing to the shallowness of the potential-energy surface at the activated state the three frequencies $\nu_2^\ddagger$, $\nu_3^\ddagger$, and $\nu_4^\ddagger$ may be considerably reduced or "softened." These three vibrations correspond to vibrations in which there is little resistance to stretching or bending. If, for example, $\nu_2^\ddagger$, $\nu_3^\ddagger$, and $\nu_4^\ddagger$ were reduced to 10^{12} sec^{-1}, the experimental frequency factor A_∞ becomes 10^{16} sec^{-1}.

When $A \neq A'$, as in the case of unsymmetrical azo-compounds and many of the peroxides, the potential-energy surface will be somewhat skewed. When $D(A-B)$ is small but positive the simultaneous rupture of two bonds, although no longer affording the path of lowest energy, will still be the favored route provided that there is a corresponding entropy compensation over the path of lowest energy. This may be the situation in the pyrolysis of mercury alkyls.[27]

[26] M. Szwarc and L. Herk, J. Chem. Phys. **29,** 437 (1958).
[27] H. V. Carter, E. I. Chapell, and E. Warhurst, J. Chem. Soc. **1956** 106.

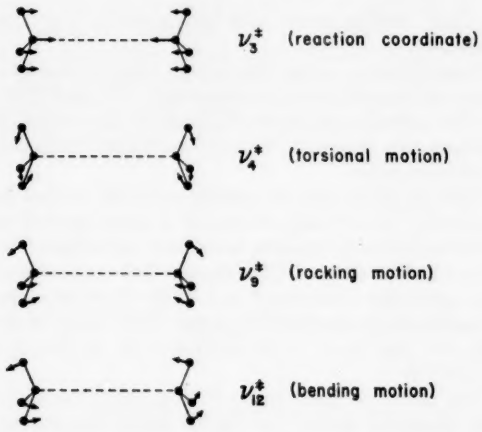

FIG. 6. Some of the normal modes of vibration for the activated complex for a process such as $C_2H_6 \rightarrow 2CH_3$.

Dissociations of the Type R−R′→R+R′

The suggestion has been made[11] that the high frequency factors for reactions such as the decomposition of ethane into two methyl radicals are associated with a high rotational entropy in the activated state. The entropy of activation for this reaction is ∼16 eu, and the increase in rotational entropy corresponding to the process $C_2H_6 \rightarrow 2CH_3$ is about 4 eu; thus even completely free rotation in the activated state does not account for more than a small fraction of the total effect. The bulk of the entropy change in the process $C_2H_6 \rightarrow 2CH_3$ is actually translational entropy (∼12 eu), but this cannot be involved in the activated state. It therefore follows, by elimination, that most of the entropy of activation is vibrational entropy. It is postulated that, as discussed above, there is a softening of certain of the vibrations in the activated state, these loose vibrations ultimately becoming translational and rotational motions. These changes in the case of the ethane dissociation are shown schematically in Fig. 4.

This proposed softening of vibrations in the activated state is illustrated in Figs. 5 and 6. Figure 5 shows a triatomic molecule ABA' dissociating into $A+BA'$, and it is supposed that $\nu_1^\ddagger$ corresponds to the reaction coordinate. The frequency $\nu_2^\ddagger$ is expected to be normal in that it corresponds to the stretching of a bond which is essentially unweakened. The bending frequencies $\nu_3^\ddagger$ and $\nu_4^\ddagger$, on the other hand, are expected to be somewhat softened, since the restoring force will be reduced. The frequency λ of transition from the energized to the activated state will therefore be increased, and A_∞ will be large.

Figure 6 shows the situation for the vibration of an activated ethane-like molecule, the nomenclature being that of Herzberg.[28] The reaction coordinate[29] is assumed to correspond to $\nu_3^\ddagger$. Since the C—C bond is essentially broken in the activated state the torsional vibrational

TABLE II. Pyrolysis of organic mercury compounds in the gas phase.

Compound	Log A (sec^{-1})	Kinetic studies E (kcal $mole^{-1}$)
$HgMe_2$	13.3	51±2
$HgEt_2$	14.1	43±2
$HgPr^n_2$	15.2	46±2
$HgPr^i_2$	16.2	40±2
$HgPh_2$	16.0	68±4
PhHgCl	13.0	59±3
PhHgBr	14.3	63±2
PhHgI	15.7	63±2

TABLE III. Pyrolysis of carbonyl compounds in the gas phase.

Compound	Log A (sec^{-1})	E (kcal $mole^{-1}$)
Me_2CO	14.2	71
$(PhCH_2)_2CO$	17.3	72
$PhCH_2COMe$	15.9	68
PhCOMe	15.7	78
$PhCOCF_3$	15.3	74
PhCOPh	16.3	88
MeCO·OCMe	15.7	66
PhCO·OCPh	16.3	66

TABLE IV. Decomposition of t-butyl peresters in solution.

Compound	log A (sec^{-1})	E (kcal $mole^{-1}$)
$CH_3CO—O—O—C(CH_3)_3$	16.7	38
$C_6H_5CO—O—O—C(CH_3)_3$	14.7	33
$CCl_3CO—O—O—C(CH_3)_3$	15.0	30
$(CH_3)_3C—CO—O—O—C(CH_3)_3$	16.1	31
$X—C_6H_4—CH_2—CO—O—O—C(CH_3)_3$	13.0–14.2	25–30
X=H, m-CH_3O, p-CH_3O, m-Cl, p-Cl, p-CH_3, p-NO_2.		
$R—O—CO—OC—O—O—C(CH_3)_3$	14.0–14.5	25–28
R=$(CH_3)_2CO$, $CH_3OC_6H_4CH_2$, C_2H_5, $C_6H_5CH_2$, $O_2NC_6H_4CH_2$.		

[28] G. Herzberg, *Infrared and Raman Spectra* (D. Van Nostrand Company, Inc., Princeton, New Jersey, 1945), p. 115.

[29] In fact, a reaction coordinate need not correspond to a single normal mode, and will usually be related to several modes. The assumption that $\nu_3\ddagger$ corresponds to the reaction coordinate is made to simplify the argument.

TABLE V. Decomposition of azo-compounds in solution.

Compound	log A (sec^{-1})	E (kcal $mole^{-1}$)
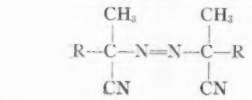	14–17	28–34
R = CH_3, C_2H_5, n-C_3H_7, i-C_3H_7, c-C_3H_5, i-C_4H_9, t-C_4H_9, n-C_5H_{11}, neo-C_5H_{11}, C_2H_4COOH.		
R—N=N—R	14–17	26–35
R = c-C_4H_6CN, c-C_5H_8CN, c-$C_6H_{10}CN$, c-$C_7H_{12}CN$, c-$C_8H_{14}CN$, c-$C_{10}H_{18}CN$.		
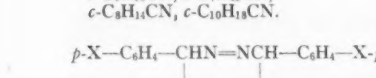	14–17	32–36
X,R = H, CH_3; H, C_2H_5; CH_3, CH_3; H, i-C_4H_9; CH_2O, CH_3.		
p-X—C_6H_4N=N—$C(C_6H_5)_3$ X = H, CH_2O, NO_2, CH_3CONH, OH, Br.	14–17	27–32
m-X—C_6H_4—N=N—$C(C_6H_5)_3$ X = CH_3, H, Br, NO_2.	14–16	26–30

frequency $\nu_4^{\ddagger}$ will be considerably reduced below that for the normal molecule. The same is true, for example, of the bending vibrations $\nu_9^{\ddagger}$ and $\nu_{12}^{\ddagger}$.

In view of these considerations it may be asked why frequency factors are normal for any unimolecular reactions, especially those involving the rupture of a single bond. In the Appendix it is suggested that "normal" frequency factors for unimolecular reactions may be less common than has frequently been supposed. On the other hand, it may be that the frequency factor of a reaction such as $C_6H_5CH_2CH_3 \rightarrow C_6H_5CH_2\cdot + CH_3\cdot$ is indeed close to 10^{13} sec^{-1} because torsional vibrations are unimportant both in the unactivated molecule and in the activated complex, and perhaps because bending modes in the latter remain relatively stiff.

APPENDIX

Survey of Experimental Results

Table I shows frequency factors and activation energies for reactions of the type R—R′→R+R′. The N_2O_5 case was discussed above and the value for CH_3—$C(CH_3)_3$ was given by Pritchard[30] in a recent review of the general problem of high frequency factors. All of the remaining values are calculated from data for the reverse reactions, as shown above for C_2H_6. Similar values have been given by Trotman-Dickerson.[11]

Table II gives similar data for the thermal decompositions of organic mercury compounds,[7,27,31] and Table III for carbonyl compounds.[32] These reactions were for the most part studied in the gas phase using the toluene-carrier technique.

Table IV gives data for organic peresters, studied by Bartlett.[33] The decompositions of a large number of azo-compounds in solution have been investigated by Cohen and co-workers,[34] Overburger and co-workers,[35] and Lewis and Matheson,[36] and Table V shows representative results obtained by them. Table VI gives the data for the same types of reactions in the gas phase.[11,37,38]

The above examples make it clear that abnormally high frequency factors are by no means uncommon. Indeed, it seems that other reactions, now believed to have normal frequency factors, will turn out to have large ones. The reason for this suggestion is that many of the values have been measured using the toluene-carrier technique; the total pressure is usually about 15 mm, and at such pressures the decompositions of molecules of moderate complexity will be in the region of the transition pressure where frequency factors and activation energies are lower than at higher pressures

TABLE VI. Decomposition of azo-compounds in the gas phase.

Compound	log A (sec^{-1})	E (kcal $mole^{-1}$)
CH_3N=NCH_3	15.7	51.2
C_2H_5N=NC_2H_5	15.7	48.5
i-C_4H_9N=Ni-C_4H_9	16.3	42.8

[30] B. G. Gowenlock, Quart. Revs. (London) **14,** 133 (1960).

[31] M. Copperthwaite and E. Warhurst, J. Chem. Soc. **1958,** 2429.

[32] D. Clark and H. O. Pritchard, J. Chem. Soc. **1956,** 2136.

[33] P. D. Bartlett, Experentia Supple. No. **7,** 275 (1957); P. D. Bartlett and J. Hiatt, J. Am. Chem. Soc. **80,** 1398 (1958); P. D. Bartlett and D. M. Simone, *ibid.* **82,** 1753 (1960); P. D. Bartlett and C. Rüchardt, *ibid.* **82,** 1756 (1960); P. D. Bartlett, E. P. Benzing, and R. E. Pincock, *ibid.* **82,** 1762 (1960); P. D. Bartlett and R. E. Pincock, *ibid.* **82,** 1769 (1960).

[34] S. G. Cohen, S. J. Grozzos, and D. B. Sparrow, J. Am. Chem. Soc. **72,** 3947 (1950); S. Solomon, C. H. Wang, and S. G. Cohen, *ibid.* **79,** 4104 (1957); S. G. Cohen and C. H. Wang, *ibid.* **75,** 5504 (1953).

[35] C. G. Overburger, M. T. O'Shaughnessy, and H. Shalit, J. Am. Chem. Soc., **71,** 2661 (1949); C. G. Overburger and M. B. Berenbaum, *ibid.* **73,** 2618 (1951); C. G. Overburger, W. F. Hale, M. B. Berenbaum, and A. B. Finestone, *ibid.* **76,** 6185 (1954); C. G. Overburger and J. C. Lombardino, *ibid.* **80,** 2317 (1958).

[36] F. M. Lewis and M. S. Matheson, J. Am. Chem. Soc. **71,** 747 (1949).

[37] D. Swinehart (private communication, 1959).

[38] J. B. Levy and B. W. Copeland, 137th American Chemical Society Meeting, Cleveland, Ohio (1960).

where the kinetics are first order.[13] An example of this situation is provided by the work of Trotman-Dickenson on the thermal decomposition of azomethane. Using the carrier technique[12] the frequency factor was found to be normal, but at higher pressures in a static system[20] it was $10^{15.7}$ sec^{-1}.

ACKNOWLEDGMENTS

One of us (C.S.) expresses his thanks to Dr. H. Linschitz (Brandeis) in whose laboratory some of this work was carried out; he also thanks the U. S. Atomic Energy Commission for financial support.

THE JOURNAL OF CHEMICAL PHYSICS VOLUME 34, NUMBER 5 MAY, 1961

Ionized States in a One-Dimensional Molecular Crystal*

R. E. MERRIFIELD

Central Research Department, Experimental Station, E. I. du Pont de Nemours and Company, Wilmington, Delaware

(Received October 24, 1960)

Generalization of the theory of excitons in molecular crystals to include ionized states is carried out for an idealized one-dimensional model for which the exact wave functions and energy levels can be derived. The ionized states are found to form a progression of bands corresponding to bound states of the electron and hole. The bound levels converge to a band of free states in which the electron and hole move independently and can carry an electric current. The lowest-lying ionized states may interact significantly with the un-ionized molecular exciton states and give rise to weak charge-transfer absorption bands.

INTRODUCTION

THE theory of excitons in molecular crystals as developed by Frenkel[1] and Davydov[2] successfully accounts for those properties of the low-lying excited states which are manifested in absorption and fluorescence spectra. However, Lyons[3] has pointed out that consideration of the electrical properties of molecular crystals requires extension of the simple exciton theory to include ionized states in which an electron has been removed from one molecule and placed on another in the crystal. As a first step in the development of such a generalized exciton theory, this paper considers a highly idealized crystal model for which most of the details of the structure of the ionized states can be worked out without prohibitive effort.

THE CRYSTAL MODEL

The model consists of an infinite one-dimensional array of equally spaced, identical molecules. Two types of excited states of this crystal will be considered. The first corresponds to an un-ionized excited state of an individual molecule and the second to a charge-transfer state in which an electron has been removed from one molecule and placed on another. The wave functions corresponding to these basis states will be designated $|m, n\rangle$, where m represents the position of the hole (positive ion) and n is the position of the electron.[4] (The unit of length is taken to be the lattice spacing, so m and n are integers.) If $m=n$, the function designates an excited state of molecule n. It is assumed that these basis functions are normalized and mutually orthogonal. The general excited state of the crystal in terms of these functions is then

$$\psi=\sum_{m,n}c(m,n)\,|m,n\rangle. \tag{1}$$

In order to find the stationary states of this system, the matrix elements of the Hamiltonian operator among the various basis functions are required. The diagonal components will be designated

$$\langle m,n|\mathcal{H}|m,n\rangle=V(n-m). \tag{2}$$

It is assumed that Eq. (2) may be idealized as a Coulomb interaction when the electron and hole are on different molecules. Thus, we put

$$\begin{aligned} V(n)&=-A_1|n|^{-1}, && n\neq 0,\\ &=-A_0, && n=0, \end{aligned} \tag{3}$$

* Contribution No. 577.

[1] J. Frenkel, Phys. Rev. **37**, 17, 1276 (1931); Physik. Z. Sowjetunion **13**, 158 (1936).

[2] A. S. Davydov, Zhur. Eksp. i Teoret. Fiz. **18**, 210 (1948).

[3] L. E. Lyons, J. Chem. Soc. **1957**, 5001; Australian J. Chem. **10**, 365 (1957).

[4] The configuration $|m, n\rangle$ actually leads to two states, a singlet and a triplet. The ensuing discussion applies equally to either set of states, although of course, the values of the energy matrix elements will be multiplicity dependent.

where the zero of the energy scale is taken to be the energy of an infinitely separated electron and hole in the crystal; A_1 will then be approximately e^2/D, where D is the dielectric constant of the crystal, and $-A_0$ is the energy of the molecular excited state.

The interaction between two excited states on different molecules is the usual exciton interaction matrix element[1]

$$\langle m, m|\mathcal{H}|n, n\rangle = H(n-m). \tag{4}$$

The other nondiagonal matrix elements which will be considered are those corresponding to the transfer of either an electron or a hole between nearest neighbors. These elements will be designated

$$\langle m, n|\mathcal{H}|m\pm 1, n\rangle = \epsilon_1$$
$$\langle m, n|\mathcal{H}|m, n\pm 1\rangle = \epsilon_2. \tag{5}$$

These correspond to the matrix elements which are considered in the usual band theory, ϵ_1 and ϵ_2 referring to the valence and conduction bands, respectively.

EQUATIONS OF MOTION

From the matrix elements given in the preceding section, a set of difference equations may be derived which must be satisfied by the coefficients in Eq. (1). However, by virtue of the translational symmetry of the crystal, it is possible to separate out the coordinates of the "center of mass" of the electron-hole pair immediately. One need then consider only the equations for the relative motion of the two particles. This separation may be accomplished if the solutions are expressed in terms of the functions

$$\psi_k(n) = N^{-\frac{1}{2}} \sum_m \exp ik(2m+n)\,|m, m+n\rangle. \tag{6}$$

This function describes a state wherein the electron and hole are separated by n units and the pair propagates through the crystal as a plane wave with wave vector k.[5] The values of k are fixed by the requirement that the wave function (6) be invariant under the operation $|m, n\rangle \rightarrow |m+N, n+N\rangle$, i.e., $\exp 2ikN = 1$. If the summation in (6) is taken over N consecutive values of m, these functions then form an orthonormal set. From the argument of the complex exponential, it is seen that it has been assumed that the "center of mass" of the electron and hole is halfway between them. It will be seen below that if $\epsilon_1 \neq \epsilon_2$, this assumption will have to be slightly modified.

Calculation shows that there are no matrix elements between functions (6) having different values of k and that, for functions having the same value of k, the nonvanishing matrix elements are

$$\langle \psi_k(n)|\mathcal{H}|\psi_k(n)\rangle = V(n) + \delta_{n,0} \sum_m \exp 2ikmH(m),$$
$$\equiv V_k(n), \tag{7}$$

and

$$\langle \psi_k(n)|\mathcal{H}|\psi_k(n-1)\rangle = \epsilon_1 \exp(ik) + \epsilon_2 \exp(-ik),$$
$$\langle \psi_k(n)|\mathcal{H}|\psi_k(n+1)\rangle = \epsilon_1 \exp(-ik) + \epsilon_2 \exp(ik). \tag{8}$$

The charge-transfer matrix elements, Eqs. (8), may be expressed in the form

$$\epsilon_1 \exp(ik) + \epsilon_2 \exp(-ik) = \epsilon_k \exp i\delta k, \tag{9}$$

where the quantities on the right-hand side are given by

$$\epsilon_k = (\epsilon_1^2 + \epsilon_2^2 + 2\epsilon_1\epsilon_2 \cos 2k)^{\frac{1}{2}}$$
$$\tan\delta_k = \frac{\epsilon_1 - \epsilon_2}{\epsilon_1 + \epsilon_2} \tan k. \tag{10}$$

If one then defines modified wave functions (corresponding to a relocation of the center of mass) by

$$\psi_k'(n) = \exp in\delta_k \psi_k(n), \tag{11}$$

the matrix elements take on the simple form

$$\langle \psi_k'(n)|\mathcal{H}|\psi_k'(n)\rangle = V_k(n),$$
$$\langle \psi_k'(n)|\mathcal{H}|\psi_k'(n\pm 1)\rangle = \epsilon_k. \tag{12}$$

It is possible to divide the states into two noncombining sets, one of which is unchanged under the transformation $n \rightarrow -n$, while the other changes sign under this operation. This separation is accomplished by putting for the even states

$$\phi_k(n) = 2^{-\frac{1}{2}}[\psi_k'(n) + \psi_k'(-n)], \quad n>0,$$
$$\phi_k(0) = \psi_k'(0),$$

and for the odd states

$$\chi_k(n) = 2^{-\frac{1}{2}}[\psi_k'(n) - \psi_k'(-n)], \qquad n>0. \tag{13}$$

The matrix elements in terms of these functions then become

$$\langle \phi_k(n)|\mathcal{H}|\phi_k(n)\rangle = V_k(n),$$
$$\langle \phi_k(n)|\mathcal{H}|\phi_k(n\pm 1)\rangle = \epsilon_k, \quad n\neq 0, \quad 1,$$
$$\langle \phi_k(0)|\mathcal{H}|\phi_k(1)\rangle = 2^{\frac{1}{2}}\epsilon_k,$$

and

$$\langle \chi_k(n)|\mathcal{H}|\chi_k(n)\rangle = V_k(n),$$
$$\langle \chi_k(n)|\mathcal{H}|\chi_k(n\pm 1)\rangle = \epsilon_k. \tag{14}$$

For the even states of the crystal, the wave functions will be expressed as a linear combination of the first two of functions (13), i.e.,

$$\phi_k = \sum_{n=0}^{\infty} \alpha_k(n)\phi_k(n). \tag{15}$$

[5] Note that for $n=0$, the function (6) becomes the conventional Frenkel exciton wave function and (7) the exciton energy band.

From this wave function and the matrix elements, Eq. (14), the following set of difference equations for the expansion coefficients can be derived,

$$E\alpha_k(n)=V_k(n)\alpha_k(n)+\epsilon_k[\alpha_k(n-1)+\alpha_k(n+1)],$$
$$n>1,$$
$$E\alpha_k(1)=V_k(1)\alpha_k(1)+\epsilon_k[2^{\frac{1}{2}}\alpha_k(0)+\alpha_k(2)],$$
$$E\alpha_k(0)=V_k(0)\alpha_k(0)+2^{\frac{1}{2}}\epsilon_k\alpha_k(1). \quad (16)$$

For subsequent calculations it is convenient to introduce the dimensionless quantities

$$x=E/2\epsilon_k, \quad V_1=-V_k(1)/2\epsilon_k, \quad V_0=-V_k(0)/2\epsilon_k, \quad (17)$$

in terms of which the difference equations for the coefficients become

$$[x+(V_1/n)]\alpha(n)=[\alpha(n-1)+\alpha(n+1)]/2, \quad n>1,$$
$$(x+V_1)\alpha(1)=[2^{\frac{1}{2}}\alpha(0)+\alpha(2)]/2,$$
$$(x+V_0)\alpha(0)=2^{-\frac{1}{2}}\alpha(1). \quad (18)$$

A similar expansion is employed for the odd states;

$$\chi_k=\sum_{n=1}^{\infty}\beta_k(n)\chi_k(n). \quad (19)$$

The resulting difference equations for these expansion coefficients are

$$E\beta_k(n)=V_k(n)\beta_k(n)+\epsilon_k[\beta_k(n-1)+\beta_k(n+1)],$$
$$n>1,$$
$$E\beta_k(1)=V_k(1)\beta_k(1)+\epsilon_k\beta_k(2), \quad (20)$$

or, in terms of the quantities (17),

$$[x+(V_1/n)]\beta(n)=[\beta(n-1)+\beta(n+1)]/2, \quad (21)$$

with the proviso that $\beta(0)=0$.

The solutions of Eqs. (18) and (21) determine the wave functions and energy levels of the electron-hole system.

EIGENVALUES AND WAVE FUNCTIONS

Bound States

The first of Eqs. (18) and (21) are second-order linear difference equations which may be solved by standard methods.[6] The two linearly independent solutions are

$$\gamma_1(n)=z^{-n+1}\{[\Gamma(n-\lambda)]/[\Gamma(n)\Gamma(1-\lambda)]\}$$
$$\times F(1-n, 1+\lambda|1-n+\lambda|z^2),$$
$$\gamma_2(n)=z^n\{[\Gamma(1-\lambda)\Gamma(1+n)]/[\Gamma(1-\lambda+n)]\}$$
$$\times F(n, -\lambda|1+n-\lambda|z^2), \quad |z|\leq 1, \quad (22)$$

where $F(a, b|c|u)$ is the hypergeometric function, and the parameters z and λ are defined implicitly by

$$x=(z+z^{-1})/2, \qquad V_1=\lambda(z-z^{-1})/2. \quad (23)$$

Hence,

$$z=(V_1/\lambda)\pm[1+(V_1/\lambda)^2]^{\frac{1}{2}}$$
$$x=\pm[1+(V_1/\lambda)^2]^{\frac{1}{2}}. \quad (24)$$

The sign in Eqs. (24) is to be chosen such that $|z|<1$.

The two basic solutions of the general difference equation have the following special values,

$$\gamma_1(0)=0, \qquad \gamma_1(1)=1,$$
$$\gamma_2(0)=1. \quad (25)$$

From this one may immediately make the identification

$$\beta(n)=\gamma_1(n). \quad (26)$$

In order to construct a solution of Eqs. (18), we take a linear combination of the two basic solutions of the first of these equations and adjust the constants so that the second two equations are satisfied. It is convenient to normalize the $\alpha(n)$ such that $\alpha(0)=1$. Thus, we have

$$\alpha(n)=c_1\gamma_1(n)+c_2\gamma_2(n), \qquad n>0,$$
$$\alpha(0)=1. \quad (27)$$

Substituting of these expressions into Eqs. (18) yields for the values of the constants

$$c_1=2^{\frac{1}{2}}[x+V_0-\gamma_2(1)],$$
$$c_2=2^{\frac{1}{2}}. \quad (28)$$

The solutions (26) and (27) satisfy the corresponding difference equations for all values of the parameters λ and z consistent with Eq. (23). In order to obtain definite values for these parameters, and thus for the energy, appropriate boundary conditions must be applied to the solutions. These boundary conditions may be of two types. In the first type it is required that the coefficients vanish as $n\to\infty$. Such solutions represent bound states of the electron-hole pair. The other type of boundary condition is that the coefficients become asymptotically plane waves, such solutions corresponding to a free electron and hole.

In view of the foregoing, the next step is to examine the asymptotic behavior of the basic solutions (22). This analysis requires a straightforward application of Stirling's theorem, together with the asymptotic values of $F(a, b|c|u)$ for large values of $|a|$, $|b|$, and $|c|$.[7] The results are the following. For γ_1, if λ is not a positive integer, the asymptotic form is

$$\gamma_1(n)\simeq n^{-\lambda}z^{-n+1}/\Gamma(1-\lambda)(1-z^2)^{\lambda+1}, \quad (29)$$

[6] L. M. Milne-Thomson, *The Calculus of Finite Differences* (Macmillan and Company, Ltd., London, 1933), pp. 478.

[7] G. N. Watson, Trans. Cambridge Phil. Soc. **22**, 277 (1918).

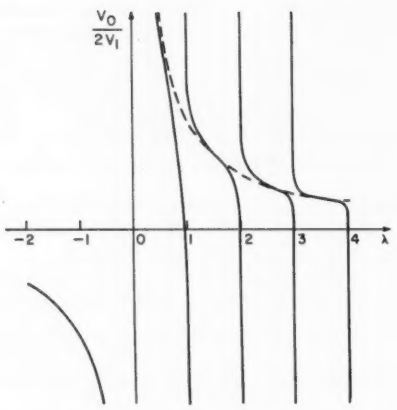

FIG. 1. Graphical determination of λ for even states. Solid curve: right-hand side of Eq. (36). Dashed curve: $(V_0/2V_1)=(1/2\lambda)$.

and, if λ is a positive integer, the asymptotic form is

$$\gamma_1(n)\simeq(z^2-1)^{\lambda-1}n^{\lambda}z^{n-\lambda+1}/\lambda!. \tag{30}$$

Since $|z|<1$, it is seen that γ_1 converges if λ is a positive integer but diverges otherwise.

Since from Eqs. (17), $V_1>0$, the value of z when $\lambda>0$ is

$$z=(V_1/\lambda)-[1+(V_1/\lambda)^2]^{\frac{1}{2}}, \tag{31}$$

and, from Eqs. (17) and (24), the energy becomes

$$E(k,\lambda)=-[4\epsilon_k^2+(A_1/\lambda)^2]^{\frac{1}{2}}. \tag{32}$$

Equation (32) thus gives the spectrum of allowed values of energy for the odd states when λ takes on positive integral values.

The situation is somewhat more complex for the even states. The asymptotic value of γ_2 is given by

$$\gamma_2(n)\simeq\Gamma(1-\lambda)\,(1-z^2)^{\lambda}n^{\lambda}z^{n}. \tag{33}$$

From Eqs. (29), (30), and (33), it is seen that γ_1 and γ_2 never converge for the same value of λ. Since, from Eq. (28) c_2 is a constant, the only alternative is to require that $c_1=0$. If this requirement, regarded as fixing the allowed values of λ, does not lead to integral values, then $\alpha(n)$ will converge.

Explicitly then, the equation determining the allowed values of λ for the even states is

$$x+V_0=\gamma_2(1). \tag{34}$$

From Eq. (22) and the series expression for the hypergeometric function it may be shown that

$$\gamma_2(1)=z^{-1}+2V_1\sum_{n=0}^{\infty}[z^{2n}/(\lambda-n)]. \tag{35}$$

Combining Eqs. (34) and (35), subject to Eqs. (17), leads finally to

$$V_0/2V_1=1/2\lambda+z^2/(\lambda-1)+z^4/(\lambda-2)+\cdots. \tag{36}$$

This equation together with Eq. (31) then determines the values of λ and z and, hence, the allowed energies for the even states. The behavior of the right-hand side of Eq. (36), regarded as a function of γ with z fixed, is shown in Fig. 1. Since the positions of the singularities are independent of z, it follows that there will be one value of λ satisfying Eq. (36) lying between each successive pair of nonnegative integers. Hence, the allowed values of this parameter for the even states are interlaced with those for the odd states. However, it should be noted that, in contrast to the situation for the odd states, the allowed values of λ for the even states depend on k.

Free States

For the free states it is required that the solutions behave asymptotically like plane waves. From Eqs. (23) it is seen that if z is not real, it must be a complex number of unit absolute value and λ must be purely imaginary. Thus, we may put

$$z=\exp i\kappa, \qquad \lambda=-i\nu. \tag{37}$$

In terms of κ and ν, Eqs. (23) may be rewritten

$$x=\cos\kappa, \qquad V_1=\nu\sin\kappa. \tag{38}$$

Under these conditions the asymptotic forms of the basic solutions become

$$\gamma_1(n)\simeq\text{const}\times\exp i(n\kappa+\nu\log n),$$
$$\gamma_2(n)\simeq\text{const}\times\exp i(-n\kappa-\nu\log n). \tag{39}$$

Thus, for all values of κ and ν, both solutions behave asymptotically like plane waves. (The appearance of the term $\nu\log n$ in the argument of the complex exponential is typical of Coulomb potential problems.) Thus, there are solutions for both the even and odd states for every value of κ. The corresponding value of ν is determined by the second of Eqs. (38), and the corresponding energies are

$$E(k,\kappa)=2\epsilon_k\cos\kappa. \tag{40}$$

DISCUSSION

The results of the previous section lead to a fairly complete picture of the rather complex distribution of energy levels for this model. There will be both a singlet and triplet series of levels; however, it is expected that the singlet-triplet splitting will be appreciable only for the molecular excited states. It should be quite small for the charge-separated states since in this case the separation will depend on an intermolecular exchange integral, which will be of order S^2, where S is an intermolecular overlap integral. In contrast the charge-transfer interaction, ϵ_k, will be of order S.

For a given multiplicity the zero-order energies, i.e., those for $\epsilon_k=0$, are determined by the values of A_0 and A_1. Means of estimating these quantities have been discussed by Lyons.[3] The zero-order energies of the charge-transfer states are $-A_1/n$, where n takes on positive integral values, while the energy of the molecular-excited state is $-A_0$. This latter state will be broadened into an exciton band according to Eq. (7). There is no necessary relation between the values of A_0 and A_1, that is, the energy of the nearest-neighbor charge-transfer state may be either above or below that of the molecular-excited state.

As the charge-transfer interaction, ϵ_k, is "turned on," according to Eq. (32), each of the odd bound states broadens into a band which lies entirely below the corresponding zero-order level. For each value of k the odd levels converge with increasing λ to the value $-2\epsilon_k$, which from Eq. (40) is the lower edge of the band of free states corresponding to the same value of k.

The behavior of the even bound states for large values of λ is essentially the same as that of the odd states; however, for the lower-lying even states the interaction with the molecular-excited state may become important. It may be seen by reference to Fig. 1 that only the first charge-transfer state will be appreciably perturbed by this interaction, and this only if its zero-order energy is nearly the same as that of the molecular-excited state. One result of this interaction will be a mixing of the molecular-excited state and the first charge-transfer state so that optical transitions from the ground state of the crystal to the charge-transfer state will become allowed. This possibility has been pointed out by Lyons.[3]

Finally, turning on the charge-transfer interaction will broaden the level corresponding to infinite separation of electron and hole into a free-state band, whose energies are given by Eq. (40). For the levels in this band the electron and hole move independently of each other, while in the bound states their motions are strongly correlated. Thus, it is only in the free states that the crystal will be electrically conducting.

Because of the many approximations inherent in this treatment, the results obtained cannot be expected to apply quantitatively to any real crystal. However, the qualitative picture of the nature of the wave functions and the distribution of energy levels should be valid for molecular crystals. The principal limitation arises from the one-dimensional nature of the model. A second serious approximation is the assumption that the zero-order energies of the charge-transfer states can be represented by a Coulomb potential. While this is doubtless valid for large electron-hole separation, its validity for small distances is open to serious question. The approximations of neglect of nonorthogonality of the various basis functions and the limitation of the charge-transfer interaction to nearest neighbors are probably not seriously in error for most molecular crystals.

Letters to the Editor

THE Letters to the Editor section is subdivided into three parts entitled Communications, Comments and Errata, and Notes. These three sections are all subject to the same limitations on length. The textual material of each Letter is limited to a number of words equal to 950 minus the following; (a) 200 words for each average-sized figure: (b) 50 words for each displayed equation: (c) 7 words for each line of table including headings and horizontal rulings. No proof will be sent to the authors of "Communications" and "Comments and Errata." Proof will be sent to the authors of "Notes." The publication charge for Letters is $30 per page, with a minimum of $30 per Letter. If honored, the Institution will be entitled to 100 reprints without covers. See issues of May–September, 1957, for descriptions of categories.

Communications

Spin and Charge Exchange in Anions of Biphenylyl Ether*

DOLAN H. EARGLE, JR., AND S. I. WEISSMAN

Washington University, Saint Louis, Missouri

(Received February 20, 1961)

IN order to test whether the recently reported[1] slow spin exchange in the substance formed by joining together two triphenylmethyls by an oxygen atom is to be ascribed to an "insulating" property of the oxygen bridge, we have examined the singly and doubly charged anion of biphenylyl ether. Reduction of the ether by sodium or potassium in 1,2-dimethoxyethane or tetrahydrofuran leads first to an orange paramagnetic substance, then to a green diamagnetic one. The latter shows no ESR absorption over a wide range of magnetic fields. Treatment of the completely reduced green substance with an equivalent quantity of the unreduced ether leads to immediate restoration of the orange paramagnetic material. The orange substance is probably the uninegative anion, the green one the dinegative ion.

FIG. 1. Part of the ESR spectrum of $C_6H_5C_6H_4OC_6H_5C_6H_5^-$ in 1,2-dimethoxyethane at 203° K.

The ESR spectrum of the uninegative ion exhibits 179 resolved components in a span of about 15 gauss (Fig. 1). The spectra of the sodium and potassium salts are indistinguishable.

The number of lines indicates that the spin migrates rapidly between the biphenyl groups. If the exchange were slow a maximum of 162 lines could be observed. An odd number of lines could be produced by one accidental degeneracy; only 135 lines could occur in such a case. Thus, the observed spectrum is compatible only with rapid exchange. The dinegative ion is either diamagnetic or has such a broad ESR absorption that it cannot be detected. The sharpness of the spectrum of the residual uninegative ion in the presence of a large concentration of dinegative ion suggests that the latter is in fact diamagnetic. Hence, the coupling between spins in the dinegative ion is not only large compared with the hyperfine splittings, but compared with kT as well.

We are continuing work with singly and doubly charged ions of pairs of biphenyl separated by various groups in order to gather more information on rates of spin exchange in even electron molecules and rates of spin and charge exchange in odd electron molecules.

* This work was supported by the U. S. Air Force Office of Scientific Research of the Air Research and Development Command under contract and by the Office of Naval Research under an equipment loan contract.

[1] D. C. Reitz and S. I. Weissman, J. Chem. Phys. **33**, 700 (1960).

Excitation Transfer Splitting in the $n \rightarrow \pi^*$ Transitions of the Diazines*

M. A. EL-SAYED AND G. W. ROBINSON

Gates and Crellin Laboratories of Chemistry,† California Institute of Technology, Pasadena, California

(Received March 13, 1961)

THE diazines[1] form a set of molecules through which interactions between excited chromophoric groups may be conveniently studied. The electrons in each of the nonbonding nitrogen orbitals can undergo $n \rightarrow \pi^*$ transitions. If the two nitrogens were infinitely far apart, the transitions would occur in degenerate pairs; but at finite distances interelectronic interactions remove the twofold degeneracy of the excited states. Two transitions, one symmetry-allowed and one symmetry-forbidden, occur. These molecules thus present prototype examples of the same kind of interactions which take place betwen molecules in crystals,[2] and between chromophores in complex molecules.[3,4] It therefore is important to know the magnitude of the splitting and to understand its origin for both the singlet (S') and triplet (T) states.

To simplify the analysis, spectra of the diazines trapped in crystalline H_2, Ne, Ar, Kr, and Xe at 4.2°K were obtained.[5] An analysis of the vibronic structure in

the 3200-A transition of pyrazine (para)[6] showed the splitting to be 435±15 cm^{-1}, with the *forbidden* component[7] lying lowest. An enhancement of the intensity of the forbidden (0, 0) band is expected in the pure crystal[1] and in the presence of heavy rare-gas atoms.[5] Although the crystal spectrum is not very sharp, a new band appears 500±100 cm^{-1} to the red of the strong (0, 0) band. The splitting was found to be 450±50 cm^{-1} by the heavy rare-gas perturbation. Thus three independent measurements fix the S' splitting in pyrazine to be near 440 cm^{-1}.

The $T\rightarrow S$ spectrum at 4.2°K and the $T\leftarrow S$ spectrum of a 42-m path[8] of pyrazine vapor showed that the phosphorescence and the strongest absorption features belong to the same transition and that the transition is spatially allowed, with the (0, 0) band in the free molecule lying at 26 818±4 cm^{-1}. The intensity of the absorption spectrum also is consistent with these views.[9] Since the lowest triplet state is expected to be the phosphorescing state, the order of the allowed and forbidden triplet components must be reversed from the order of the singlets; or possibly the two components are essentially degenerate.

It is possible to calculate the splitting by using an *independent systems model* as an approximation.[10] Such an approximation is valid only if the excited π^* orbital in the $n\rightarrow\pi^*$ transition is localized in the vicinity of the nitrogen atom. Localization is physically reasonable because of the strong Coulomb attraction of the excited electron with the remaining nonbonding positive hole. The zero-order eigenfunctions $\Psi_\pm$ are thus taken to be symmetric and antisymmetric combinations of products of ground-state and localized excited-state functions at the two nitrogen centers, A and B. Taking into account electron exchange in the essentially four-electron problem, one finds[11] that the energy splitting $\Delta E_\pm = E_+ - E_-$ is given by $\Delta E_\pm$ (singlet) $= 2J - K$ and $\Delta E_\pm$ (triplet) $= -K$, where

$$J = e^2\langle n_A(1)\, n_B(2)\,|\, r_{12}^{-1}\,|\,\pi_A^*(1)\,\pi_B^*(2)\,\rangle$$

and

$$K = e^2\langle n_A(1)\, n_B(2)\,|\, r_{12}^{-1}\,|\,\pi_A^*(2)\,\pi_B^*(1)\,\rangle.$$

If the effective nuclear charge on nitrogen is assumed[12] to be 3.82 and if 2.74 A is used as the $N\cdots N$ distance in pyrazine,[13] the values of the integrals can be obtained from the literature.[14,15] In all calculations the n orbitals are taken to be nitrogen sp^2 hybrids, and *pure nitrogen 2p orbitals perpendicular to the molecular frame are used as the localized π^* orbitals.* The theoretical splitting in pyrazine is found to be $\Delta E_\pm$(singlet) $= +440$ cm^{-1} and $\Delta E_\pm$(triplet) ≈ -2.4 cm^{-1}. The order of the theoretical components is indeed inverted in the triplet state. However, higher order effects neglected in the calculation may dominate the small triplet splitting. The theoretical splittings in the other diazines are $\Delta E_\pm$(singlet) $= +900$ cm^{-1}, $\Delta E_\pm$(triplet) $= -33$ cm^{-1} for pyrimidine (meta); and $\Delta E_\pm$(singlet) $= +9030$ cm^{-1}, $\Delta E_\pm$(triplet) $= -330$ cm^{-1} for pyridazine (ortho). A full analysis of these spectra has not been made, but the experimental singlet splittings are found to be $(600+\nu_p')$ cm^{-1} in the first case and $(8790+\nu_p')$ cm^{-1} in the second case, where ν_p' is the wave number of the excited-state vibration which makes the forbidden $n\rightarrow\pi^*$ component allowed. In pyrazine $\nu_p' = 240$ cm^{-1}; ν_p' for the other diazines must be within 100 cm^{-1} of this. *The experimental splittings for pyrimidine and pyridazine are then 840±100 cm^{-1} and 9030±100 cm^{-1}, respectively.* The long wavelength extension of the pyridazine spectrum is caused by its large splitting since the center of gravity of the allowed and forbidden (0, 0) bands lies near 30 500 cm^{-1}. This is roughly coincident with the centers of gravity in pyrazine (30 658 cm^{-1}) and in pyrimidine (~30 625 cm^{-1}), a fact which is consistent with the independent systems model.

The agreement between theory and experiment here is seen to be truly remarkable. *The success of the independent systems model gives strong support to the hypothesis of highly localized π^* orbitals for $n\rightarrow\pi^*$ transitions in this kind of molecule. The use of sp^2 nonbonding orbitals for the excited states appears justified.* The extension of these considerations to more complex azines is straightforward.

Using the polarization results of Innes *et al.*,[16] but our assignment, it can be concluded that the forbidden component in pyrazine gains much of its intensity through mixing with a (π, π^*) state. In pyridizine, simple, sharp structure occurs in the vicinity of the assigned origins, but much of the intensity is located between the origins where the structure becomes highly complex. *Pyridazine therefore appears to present a case of of strong vibronic coupling between the two (n, π^*) components while pyrazine looks like a case of weaker coupling.*

* Supported in part by the National Science Foundation.
† Contribution No. 2688.

[1] M. Kasha, in *Light and Life*, edited by W. D. McElroy and B. Glass (Johns Hopkins Press, Baltimore, 1961); see this paper for a recent review of previous work on the diazines.
[2] D. S. McClure, *Solid State Physics* (Academic Press, Inc., New York, 1959), Vol. 8, pp. 1–48.
[3] D. S. McClure, Can. J. Chem. **36,** 59 (1958).
[4] I. Tinoco, J. Am. Chem. Soc. **82,** 4785 (1960).
[5] G. W. Robinson, J. Mol. Spectroscopy **6,** 58 (1961).
[6] M. A. El-Sayed and G. W. Robinson (unpublished).
[7] *Component* here signifies a member of the set of orbitally degenerate $n\rightarrow\pi^*$ states.
[8] By the method of H. Bernstein and G. Herzberg, J. Chem. Phys. **16,** 30 (1948).
[9] This conclusion was reached earlier by L. Goodman and M. Kasha, J. Mol. Spectroscopy **2,** 58 (1958).
[10] We thank Professor W. T. Simpson for pointing out to us the apparent near validity of this approximation in other systems.
[11] This is a special case of the exciton problem. See R. E. Merrifield, J. Chem. Phys. **23,** 402 (1955).
[12] L. Goodman and R. W. Harrell, J. Chem. Phys. **30,** 1131 (1959).
[13] V. Schomaker and L. Pauling, J. Am. Chem. Soc. **61,** 1769 (1936).

[14] C. C. J. Roothaan, *Special Technical Report of the Laboratory of Molecular Structure and Spectra*, (University of Chicago, Chicago, 1955).
[15] M. Kotani, E. Ishiguro, and K. Hijikata, J. Phys. Soc. Japan **9**, 553 (1954).
[16] K. Innes, J. Merritt, W. Tincher, and S. Tilford, Nature **187**, 500 (1960).

Reactive Scattering in Crossed Molecular Beams. K Atoms with CH_3I and C_2H_5I†

D. R. Herschbach, G. H. Kwei, and J. A. Norris

Department of Chemistry and Lawrence Radiation Laboratory, University of California, Berkeley, California

(Received March 6, 1961)

ANGULAR distributions of reactively scattered KI have been measured at the intersection of a K atom beam with beams of CH_3I and C_2H_5I. In these reactions kinematical features[1] are particularly favorable for a study of the recoil spectrum of the product molecules, and an analysis of the data which relies only upon conservation laws has shown: (1) the final relative velocity vector $\mathbf{v}'$ has a quite anisotropic distribution, peaked about the direction of the initial relative velocity vector $\mathbf{v}$; (2) over 80% of the 25 kcal/mole energy of reaction goes into vibrational and rotational excitation of the products.

The beams are formed by thermal effusion from ovens mounted on a turntable which is rotated to sweep the angular distribution past surface ionization detectors. Vertical adjustment of the detector positions allows the scattering to be measured out of the plane as well as in the plane of the incident beams. The KI is distinguished from elastically scattered K by use of two detectors[2]: one a W filament, about equally sensitive to K and KI; the other a Pt-W alloy, more than 50 times as effective for K as for KI. For these reactions, this differential detector was not crucial, however, since the KI distributions are displaced far enough from the K beam to be observable with the W detector alone.

Typical results for $K+CH_3I$ are shown in Fig. 1; under the same conditions C_2H_5I gives similar results except that the KI distribution is shifted to larger θ, by about 7°. For both reactions the collision yield (integrated intensity of KI divided by total K scattered from the parent beam) is found to be about 10^{-4} corresponding to a total reaction cross section[3] of roughly 10 A^2. Measurements at several temperatures of the incident beams indicate that the activation energy is negligibly small, less than 0.3 kcal/mole.

The qualitative features implied by the observed angular distributions may be seen in Fig. 1(c). The recoil velocity which carries the KI away from the center of mass can have any direction but conservation of momentum and energy determine its magnitude as $v_4' = [(M_3/M_4)(2/M)(E+Q)]^{\frac{1}{2}}$, where $M_4 \leftrightarrow KI$ and $M_3 \leftrightarrow CH_3$; E is the initial relative kinetic energy and Q the internal energy converted into translational energy of separation of the products. Thus the possible spectrum of recoil vectors for KI is represented by a set of spheres, one for each value of Q up to a maximum of about 25 kcal/mole (the difference in dissociation energy of the K—I and C—I bonds). It is seen that the broad peak observed near 83° in the laboratory corresponds to scattering in which an observer stationed at

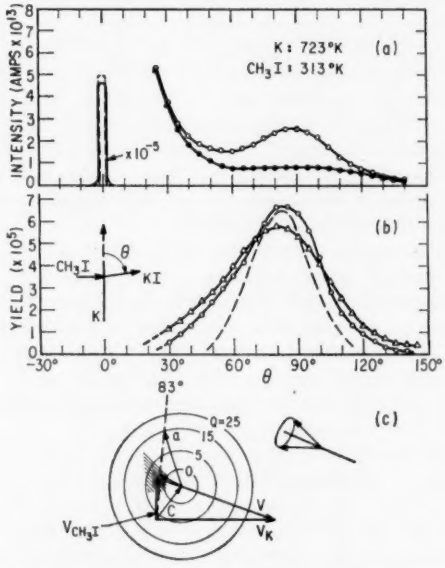

FIG. 1. Typical data and analysis: (a) Parent K beam 0.7° wide attenuated 7% by perpendicularly crossed CH_3I beam. Readings on Pt detector (solid circles) normalized to W (open circles) at parent beam peak. (b) KI distributions; circles derived from (a), triangles from a replicate experiment (four months later) using a parent K beam 2° wide and 40% attenuated. Area under curves gives collision yield. (c) Vector diagram showing most probable velocities of reactants and center of mass vector $\mathbf{c}$; 50% of the KI recoil vectors appear within doubly shaded region, 90% within singly shaded region.

the center of mass would see the KI recoil backward (and the CH_3 forward) with respect to the incoming K beam. Large Q values can contribute to this peak only if the recoil velocity vector deviates considerably from the direction of $\mathbf{v}$, as illustrated by the vector labeled $\mathbf{a}$. The scattering must have cylindrical symmetry about $\mathbf{v}$, since the incident beams contain all possible molecular orientations and impact parameters. Therefore, the angular deviation of $\mathbf{v}_4'$ from $\mathbf{v}$ can be studied directly by measurement of the out-of-plane scattering. The shaded region indicates where end-

points of $\mathbf{v}_4'$ vectors must lie in order to contribute to the observed peak, as derived by combining the in-plane and out-of-plane data and allowing for the influence of the velocity distributions in the reactants. These results demonstrate that the dominant contributions to the recoil spectrum have Q values in the range 0–5 kcal/mole. Velocity selection is essential if the resolution is to be improved. Much of the observed width of the KI peaks is due just to velocity averaging, as shown by the dashed curve in Fig. 1(b), calculated for zero activation energy, $\mathbf{v}_4'$ collinear with $\mathbf{v}$, and $Q=1.6$ kcal/mole.

The observed small shift in the KI distribution for the C_2H_5I reaction is expected from the mass change. Another check of the interpretation has been found in results for the analogous reactions of Rb atoms.[4]

One other reaction, K+HBr→H+KBr, has previously been studied in crossed molecular beams[2,5]; however, because of unfavorable kinematical features, the angular distribution observed has yielded information about only the total reaction cross section.[1,6]

† Support received from the U. S. Atomic Energy Commission and the Alfred P. Sloan Foundation is gratefully acknowledged.

[1] D. R. Herschbach, J. Chem. Phys. **33,** 1870 (1960); further details are given in UCRL Report 9379 (University of California Radiation Laboratory, April, 1960).

[2] E. H. Taylor and S. Datz, J. Chem. Phys. **23,** 1711 (1955); **25,** 395 (1956).

[3] Elastic scattering hides any reactive scattering that might appear in the region $-30°<\theta<30°$.

[4] J. L. Kinsey, G. H. Kwei, and D. R. Herschbach, Bull. Am. Phys. Soc. **6,** 152 (1961).

[5] E. F. Greene, R. W. Roberts, and J. Ross, J. Chem. Phys. **32,** 940 (1960).

[6] The conservation laws confine the KBr recoil spectrum to a very small sphere and the blurring effect of the initial velocity distributions is therefore greatly aggravated. See S. Datz, D. R. Herschbach, and E. H. Taylor, J. Chem. Phys. (to be published).

Electrical Conductance of Solutions of Salts in Liquid Metals. Potassium Iodide in Potassium*

H. R. Bronstein, A. S. Dworkin, and M. A. Bredig

Chemistry Division, Oak Ridge National Laboratory, Oak Ridge, Tennessee

(Received March 9, 1961)

THE high degree of solubility of the alkali halides KX, RbX, and CsX in their corresponding liquid metals,[1] with attainment of complete miscibility in all proportions at or slightly above the melting temperatures of the salts, affords the opportunity to investigate the continuous change in the properties of these solutions from a molten salt to a molten metal. Previous measurements of the electrical conductivity in the salt-rich KX–K solutions[2] exhibited an increasing conductivity with increasing metal content. The increase was interpreted[2] in terms of the gradual establishment of a metallic conduction band by the overlap of the orbitals of the metal atoms or molecules in the salt melt. We report here the first results of a study of the metal-rich mixtures, or solutions of salts in liquid metals. The measurements were carried out in an apparatus essentially similar to that described earlier.[2]

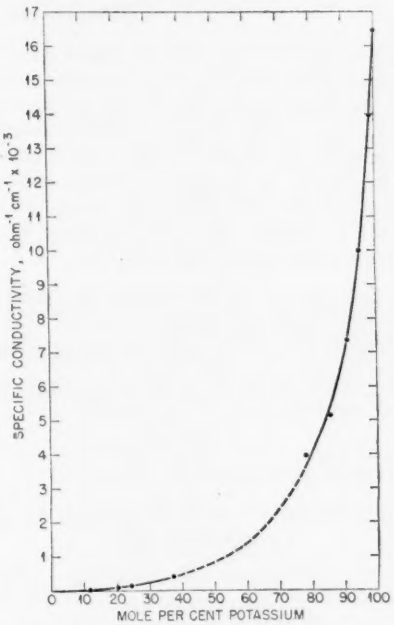

FIG. 1. The electrical conductivity of KI—K solutions at 700°.

The electrode arrangement was modified to be used with a dc circuit and a Mueller bridge for accurately measuring very low resistances in the absence of polarization effects. The electrode inserted in the cup of the capillary dip cell fabricated from synthetic sapphire was a hollow stainless-steel tube welded closed at the bottom. Running axially inside the tube was a ceramic-insulated wire which had been welded to the inner bottom of the tube. The tube and the inner wire are thus two leads. Penetrating into the bottom of the tank to just below the capillary end of the dip cell was the junction of two other lead wires. This arrangement afforded the four terminal leads necessary to accurately measure the resistance of the liquid in the capillary. The cell constant of the sapphire cell was determined as previously.[2] The accuracy of the method was checked by measuring the resistivity of liquid Hg.

Figure 1 shows the rapid decrease in the *specific conductivity* upon dissolution of KI in the liquid K metal at 700°. It also illustrates the manner in which the specific conductivity of the metal-rich solutions approaches the previous measurements at 700° of the

salt-rich solutions.[2] Of significance is the observation that the *resistivity* ρ of the metal-rich solutions increases linearly with increasing salt concentration. With an average deviation of $\pm 2.5\%$, between mole fractions $N_{KI}=0$ and 0.20, the data can be expressed by the equation

$$\rho(\mu\text{ohm cm}) = aN_{KI} + b; \qquad a = 920\ \mu\text{ohm cm},$$
$$b = 58\ \mu\text{ohm cm}.$$

Thus the *resistivity* of the metallic liquid seems to be essentially a linear function of the concentration of the electron scattering centers introduced by the addition of the salt. We are proceeding to investigate the effect of other anions by measuring the electrical conductivity of solutions of KF, KCl, and KBr in potassium metal. Metal-rich solutions of other alkali metals and their halides will be studied. Also of some interest would be an investigation of mixed anion solutions.

* Work performed for the U. S. Atomic Energy Commission at the Oak Ridge National Laboratory, operated by the Union Carbide Corporation, Oak Ridge, Tennessee.

[1] M. A. Bredig and J. W. Johnson, J. Phys. Chem. **64,** 1899 (1960); and earlier papers.

[2] H. R. Bronstein and M. A. Bredig, J. Am. Chem. Soc. **80,** 2077 (1958) and another paper (to be published).

Comments and Errata

Erratum: Diffusion and Exchange of Zn in Crystalline ZnS

[J. Chem. Phys. **29,** 406 (1958)]

E. A. Secco

Chemistry Department, St. Francis Xavier University, Antigonish, Nova Scotia

(Received December 28, 1960)

THE purpose of this communication is to correct the results already reported[1] on the exchange between zinc vapor and single crystals of zinc sulfide. An error was found in the calculation of the solid-phase equilibrium activity which reflected itself in the reaction fraction and hence the diffusion coefficient. The reaction fractions were recalculated and the correct D values evaluated using the solution to the diffusion equation for the case of a thin slab as given by Crank.[2] A few more exchange experiments were done following the same procedure in order to confirm the diffusion-controlled exchange reaction. Figure 1 shows a plot of the nondimensional Dt/a^2 as a function of time with the zero intercept indicating a diffusion process. (See Table I.)

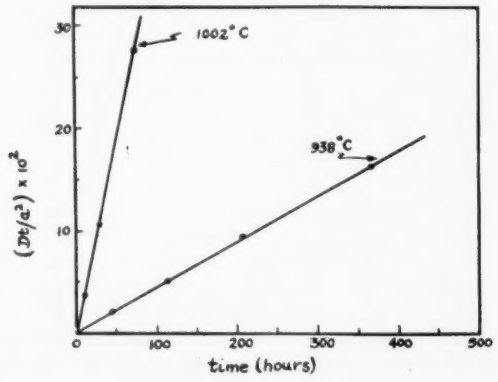

FIG. 1.

TABLE I.

Temperature °C	P_{Zn} atm	r cm	D cm² sec⁻¹
927	1.01	0.035	2.60×10^{-12}
938	1.00	0.030	3.16×10^{-12}
938	1.00	0.010	3.10×10^{-12}
949	1.00	0.040	9.75×10^{-12}
975	1.01	0.040	1.90×10^{-11}
1002	1.00	0.045	4.65×10^{-11}
1002	1.00	0.010	2.60×10^{-11}
1018	1.00	0.035	6.50×10^{-11}
1029	1.00	0.055	1.27×10^{-10}
1029	0.97	0.015	4.47×10^{-11}
1038	1.02	0.025	9.90×10^{-11}
1056	0.99	0.045	2.86×10^{-10}
1073	1.00	0.043	4.62×10^{-10}
1095	1.00	0.020	1.11×10^{-9}
1029	0.14	0.020	3.60×10^{-10}
1029	2.0	0.020	5.22×10^{-11}

[1] E. A. Secco, J. Chem. Phys. **29,** 406 (1958).

[2] J. Crank, *Mathematics of Diffusion* (Clarendon Press, Oxford, England, 1956), p. 55.

Erratum: Thermal-Diffusion-Column Shape Factors for the Lennard-Jones (12-6) Potential

[J. Chem. Phys. **33,** 570 (1960)]

B. B. McInteer and M. J. Reisfeld

Los Alamos Scientific Laboratory, University of California, Los Alamos, New Mexico

(Received February 17, 1961)

WE regret that all values of h contained in the work cited in reference 6 of this article are incorrect. The tables contained therein were photographically reproduced from an early erroneous listing from the IBM 704 computer. The final correct listing was used by us throughout the above paper. We are indebted to S. C. Saxena and S. Raman of the Indian Atomic Energy Establishment and Edward Von Halle of the Oak Ridge National Laboratory for pointing out this error to us. Correct values of the shape factors are now reissued in a new report.[1]

[1] B. B. McInteer and M. J. Reisfeld, Los Alamos Scientific Laboratory Report LAMS-2517, March 1961. Available by writing to Office of Technical Services, Department of Commerce, Washington 25, D. C.

Notes

Vibration Perturbations in Electronically Excited Monosubstituted Benzenes

O. E. WEIGANG, JR., AND A. J. DAHL*

Chemistry Department, Texas Lutheran College, Seguin, Texas

(Received September 22, 1960)

THE effects of solvents on molecular vibration have been observed most often for electronic ground-state vibrators through shifts in the infrared or Raman spectra.[1,2] Recent studies have observed the effect in electronically excited molecules as evidenced by the change in frequency of the relative separations of vibronic peaks on going from vapor to solution.[3]

The observation in the latter studies of shifts to the blue (notably in benzene and naphthalene) suggested further studies to determine the extensiveness of the phenomenon in electronically excited vibrators. Blue vibration-frequency shifts have been observed widely only in highly pressurized solutions for the ground electronic state.[1]

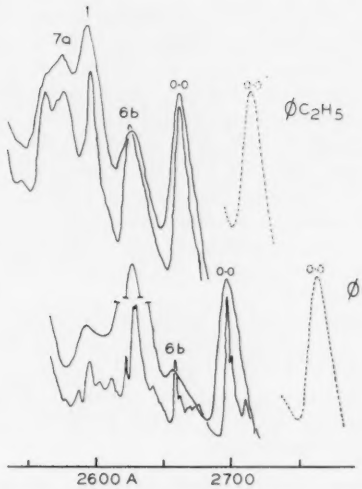

FIG. 1. Solution spectra of ethylbenzene an chlorobenzene placed above the respective vapor spectra. Dashed contours show the actual position in wavelength of the solution spectra. With superposition of the O—O bands, the vibration frequency shifts are qualitatively demonstrated by the displacement of the other vibronic peaks.

Comparisons of the ^1L_b vapor spectra to the methylcyclohexane solution spectra for six monosubstituted benzenes were made. In each case, a number of sharp vibronic peaks can be observed which correspond to single fundamental vibrations that are slight modifications of the well-known benzene modes.[4] The similarity of the spectra makes a complete analysis of only toluene[5] and chlorobenzene[6] suffice for assigning the main bands of all.

Spectrograms were obtained in triplicate with a Beckman DK-1 recording spectrophotometer. The average deviation in band-frequency separations was about ± 5 cm^{-1}. The separations observed in the vapor generally agree with the published values within the same limits.

Table I gives the change in frequency separation of a given band from the O—O band on going from the vapor state to methylcyclohexane solution. A study of Fig. 1 shows that it is unlikely that the apparent shifts of band maxima could be accounted for by broadening and overlap of adjacent bands. The generality of the blue shift is striking, and the change by the 6*b* vibration from red to blue shift on going to halogen substitutents is distinct.

The theoretical approach of Benson and Drickamer to stretching vibration shifts (applicable here to 1 and 7*a*) would predict a shortening of the vibrating bond equilibrium distance on solvation.[1,3] Weiderkehr has calculated that blue shifts in CN vibrations at high pressures are due to the predominant contribution of repulsive interactions with the solvent.[7] But it is conceivable that either repulsive or attractive potentials could bring about shortening, depending on the distribution of solvent matter about a bond. It is not evident why the blue shift is so characteristic of the excited state. The new properties (bond length, force constant, etc.) that can be predicted for the bonds in the excited state[8] fail to give a consistent explanation for such shifts in contrast to red shifts for ground-state vibrators.

It is of interest that the carbon-carbon ring breathing

TABLE I. Vapor to methylcyclohexane solution vibration frequency shifts (cm^{-1}) (average deviation± 5 cm^{-1}).

Vibration number[a]	Chromophores						
	Benzene[b]	Toluene	Ethyl-benzene	*i*-Propyl benzene	*t*-Butyl benzene	Chloro-benzene	Bromo-benzene
1	0	+28	+17	+25	+29	...	...
7*a*	+25	+28	+2	+21	...	...	...
6*b*	0	−31	−21	−20	−28	+31	+28

[a] See work cited in reference 4.
[b] Taken from work cited in reference 3.

vibration 1 displays an approximate 25-cm^{-1} blue shift in the alkyl substituted benzenes, which is essentially absent in benzene. Should the lack of shift in benzene be due to shielding of the C—C bonds, it would not seem unreasonable that the extension of the vibrating carbon system by alkyl substitution would provide a "handle" which alone interacts with the solvent and modifies the whole ring vibration through coupling. Carbon-hydrogen bonds in the same position as the alkyl substituents are apparently subject to interaction with solvents as indicated by the 7*a* C—H shifts for all cases in Table I.

Acknowledgement is made to the donors of The Petroleum Research Fund, administered by the American Chemical Society, for partial support of this research. The research was also supported in part by a grant from the National Science Foundation which is gratefully acknowledged.

* American Chemical Society-Petroleum Research Fund Scholar, 1958–59.

[1] A. M. Benson, Jr., and H. G. Drickamer, J. Chem. Phys. **27**, 1164 (1957); R. R. Weiderkehr and H. G. Drickamer, *ibid.* **28**, 311 (1958).
[2] G. Herzberg, *Infrared and Raman Spectra of Polyatomic Molecules* (D. Van Nostrand Company, Inc., Princeton, New Jersey, 1945), pp. 534–5.
[3] O. E. Weigang, Jr., and W. W. Robertson, J. Chem. Phys. **30**, 1413 (1959).
[4] K. S. Pitzer and D. W. Scott, J. Am. Chem. Soc. **65**, 803 (1942).
[5] N. Ginsburg, W. W. Robertson, and F. A. Matsen, J. Chem. Phys. **14**, 511 (1946).
[6] H. Sponer and S. H. Wollman, J. Chem. Phys. **9**, 816 (1941).
[7] R. R. Weiderkehr, doctoral dissertation, University of Illinois (1957).
[8] F. M. Garforth, C. K. Ingold, and H. G. Poole, J. Chem. Soc. **1948**, 508.

Determination of Relative Signs of Spin Coupling Constants in an AB_2X Nuclear Magnetic Resonance Spectrum

P. Diehl and I. Gränacher

Physics Department, University of Basel, Switzerland

(Received January 16, 1961)

THE simplest systems in which relative signs of spin coupling constants can be determined are systems of three nonequivalent nuclei. Spectra of this type have been analyzed by Gutowsky *et al.*[1] in the *ABX* limit and by Alexander[2] as *ABC* spectra. The *ABX* spectrum depends on the relative signs of J_{AX} and J_{BX} only, whereas the relative signs of all three spin-spin interactions are deducible from *ABC* spectra.

As Diehl and Pople[3] have shown, the simplest systems that can be used to compare couplings between nuclei of different species (AX and BX) with couplings between nuclei of the same species (AB) are AB_2X systems. The energies and intensities of such spectra are explicit analytical expressions.[4] The X spectrum of AB_2X systems shows an asymmetry that is inverted by changing the relative signs of J_{AB} and J_{BX}. As there are X transitions with a separation of $J_{AX}+2J_{BX}$, the relative signs of J_{AX} and J_{BX} can be obtained as well.

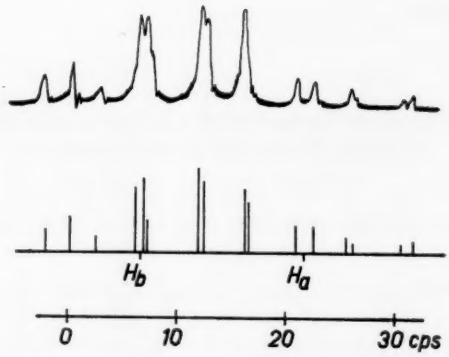

FIG. 1. Experimental and calculated proton spectrum of 1-fluoro-2,6-dichlorobenzene; $\delta_{AB}=-15.0$ cps, $J_{HH,\text{ortho}}=+8.4$ cps, $J_{HF,\text{meta}}=+6.5$ cps, $J_{HF,\text{para}}=-1.7$ cps. Resonance frequency: 56.4 Mc. H is increasing from left to right.

To determine relative signs of couplings in AB_2X spectra compounds with a strongly interacting AB_2 group must be used, i.e., the chemical shift δ_{AB} has to be of the same order of magnitude as the coupling constant J_{AB}. We have analyzed the proton and fluorine resonance spectra of 1-fluoro-2,6-dichlorobenzene and calculated the fluorine spectrum for the four possible combinations of relative signs of the couplings. The results are given in Figs. 1 and 2.

In order to fit the observed spectra $J_{HH,\text{ortho}}$ and $J_{HF,\text{meta}}$ must have the same sign, whereas $J_{HF,\text{meta}}$ and $J_{HF,\text{para}}$ have opposite signs. This confirms the

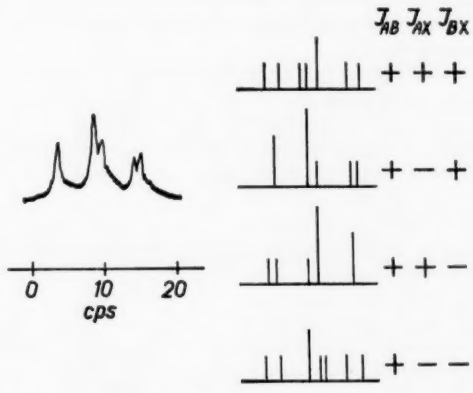

FIG. 2. Experimental fluorine spectrum of 1-fluoro-2,6-dichlorobenzene and calculations for the four possible combinations of relative signs of spin coupling constants. Resonance frequency: 56.4 Mc. H is increasing from left to right.

results obtained by Bak *et al.*[5] from the analysis of an A_2B_2XY system and therefore argues strongly for positive $J_{HH,\,\text{ortho}}$ and $J_{HF,\,\text{meta}}$. Furthermore this confirms that J_{HF} changes sign between meta- and paraposition.[1]

We are indebted to Dr. A. Zenhäusern from the Chemical Laboratory of the Swiss Federal Institute of Technology for the preparation of the sample.

[1] H. S. Gutowsky, A. Holm, A. Saika, and G. A. Williams, J. Am. Chem. Soc. **79**, 4596 (1957).
[2] S. Alexander, J. Chem. Phys. **32**, 1700 (1960).
[3] P. Diehl and J. A. Pople, J. Mol. Phys. (to be published).
[4] R. J. Abraham, E. O. Bishop, and R. E. Richards, J. Mol. Phys. **3**, 485 (1960).
[5] B. Bak, J. N. Shoolery, and G. A. Williams, J. Mol. Spectroscopy **2**, 525 (1958).

Microwave Spectrum of O^{18} Formyl Fluoride and the Structure of Formyl Fluoride*

RONALD F. MILLER AND R. F. CURL, JR.

Department of Chemistry, Rice University, Houston, Texas

(Received January 6, 1961)

PREVIOUS structural determinations of HCOF have been made by Jones, Hedberg, and Schomaker[1] by means of electron diffraction and by Le Blanc, Laurie, and Gwinn[2] by means of microwave spectroscopy. The isotopic species assigned by Le Blanc *et al.*[2] (HCOF, DCOF, $HC^{13}OF$) were not sufficient to determine the structure completely and they incorporated what they felt to be the most reliable electron diffraction data in their results. In the present investigation, the microwave spectrum of $HCO^{18}F$ was assigned and the results combined with the microwave data of Le Blanc *et al.* to give a new set of parameters. In the course of the investigation, a different *b*-type assignment of $HC^{13}OF$ was made.

TABLE I. Rotational constants and frequency of observed transitions.

	Rotational constants (Mc/sec) $HCO^{18}F$	$HC^{13}OF$
A	89 769.5±0.5	88 505.1±0.5
B	11 102.9±0.1	11 755.2[a]
C	9 863.4±0.1	10 357.3[a]

Assignment	Transition frequencies (Mc/sec)[b] Observed	Calculated
$HCO^{18}F$		
$0_{00}\rightarrow1_{01}$	20 966.32	20 966.2
$1_{01}\rightarrow2_{11}$	43 172.2	43 172.0
$1_{11}\rightarrow2_{12}$	40 692.6	40 692.9
$2_{02}\rightarrow1_{11}$	36 748.3	36 748.8
$3_{03}\rightarrow2_{12}$	14 601.9	14 601.7
$3_{13}\rightarrow4_{04}$	8 085.9	8 086.3
$4_{14}\rightarrow5_{05}$	31 267.2	31 267.8
$HC^{13}OF$		
$2_{02}\rightarrow1_{11}$	32 544.1	32 544.1
$3_{13}\rightarrow4_{04}$	14 919.9	14 917.8
$8_{17}\rightarrow7_{26}$	30 947.4	30 958.5

[a] After reference 2.
[b] Estimated error: ±0.2 Mc/sec for frequency less than 40 kMc/sec; ±0.4 Mc/sec for frequency greater than 40 kMc/sec.

Ordinary HCOF was prepared by the method outlined in Morgan, Staats, and Goldstein[3] and $HCO^{18}OH$ was then produced by hydrolysis of HCOF with 30% H_2O^{18}. This $HCO^{18}OH$ was dried over anhydrous $CuSO_4$ and converted to $HCO^{18}F$ by an adaption in small of the method of Morgan *et al.*[3]

A conventional 100-kc Stark-modulated microwave spectrometer was used to determine the transition frequencies. A list of line frequencies and the rotational constants fitted to them is given in Table I.

TABLE II. Structure of HCOF.

	Present investigation	Le Blanc *et al.* Structure II
r_{C-F}	1.338±0.005 A	1.341
r_{C-O}	1.181±0.005 A	1.183
r_{C-H}	1.095±0.008 A	1.098
<FCO	122°46′±30′	122.7°
<HCO	127°20′±3°	129°
<HCF	109°54′±3°	108°

There are two difficulties which prevent the determination of the coordinates of the atoms in HCOF from microwave data by the best method: (1) the absence of any stable isotope of fluorine other than F^{19}; and (2) the proximity of the carbon and the hydrogen atoms to the *b* principle axis of the molecule. As Costain[4] has demonstrated, Kraitchman's equations yield the most consistent coordinates for atoms sufficiently far from the principal axes. Therefore the *b* coordinates of the H, C, and O atoms and the *a* coordinate of the O atom were determined thereby. The first set in conjunction with the first moment equation yielded all the *b* coordinates.

Unfortunately, the C and H atoms are too near the *b* axis for satisfactory use of Kraitchman's equations for determination of their *a* coordinates. Since the first-moment equation and the diagonalization of the inertial tensor give two relations, only one more is needed to obtain the three *a* coordinates. This was obtained from I_b. There is a very slight contribution of the H and C atoms to I_b and the *a* coordinate of the O atom is accurately known. Following the suggestion by Costain,[4] $I_b^0 - I_b^s$ was estimated (as 0.098 amu-A^2) and the *a* coordinate of *F* obtained from I_b^s.

Admittedly there is little justification for the exact estimate used, but an error of 100% [which would

carry one beyond the range of $(I_b^0-I_b^s)/(I_b^0)$ given as extremes by Costain[4] will move the F atom only 0.003 A, so the fluorine position is fairly well fixed. As an added check, $\Delta(I_b^0-I_b^s)$ upon C^{13} substitution was estimated from the corresponding change for a similar molecule, formic acid[5]; and the resultant parameters agreed within the limits of error given.

Table II gives the structural parameters obtained in this investigation. They appear to be a confirmation of "Structure II" of Le Blanc *et al.*[2] and agree well with electron-diffraction data.

* This work supported by grants from the Robert A. Welch Foundation and Monsanto Chemical Company.

[1] M. E. Jones, K. Hedberg, and V. Schomaker, J Am. Chem. Soc. **77**, 5278 (1955).
[2] A. H. Le Blanc, V. H. Laurie, and W. D. Gwinn, J. Chem. Phys. **33**, 598 (1960).
[3] H. W. Morgan, P. A. Staats, and J. W. Goldstein, J. Chem. Phys. **25**, 337 (1956).
[4] C. C. Costain, J. Chem. Phys. **29**, 864 (1958).
[5] G H. Kwei and R. F. Curl, Jr., J. Chem. Phys. **32**, 1592 (1960).

Interaction Energy in the Amaldi-Fermi Theory for a Pair of Simple Negative Ions of the Same Kind with Filled Electronic Shells

T. TIETZ

Department of Theoretical Physics, University of Lodz, Lodz, Poland

(Received July 11, 1960)

WHILE[1] the Thomas-Fermi-Dirac theory yields stable negative ions, an analytic formula for interionic repulsion can hardly be obtained from it. The original Thomas-Fermi theory did not lead to stable negative ions, but the Amaldi-Fermi theory, which does give stable ions, retains its simplicity, and we adopt that theory here. Using the treatment of interaction energy given by Jensen,[2] Lenz,[3] and Gombas,[4] we derive in this paper a simple expression for the interaction energy of two singly ionized atoms of the same kind, comprising filled electronic shells like rare gas atoms. Neglecting the exchange energy as well as the correlation energy, we can write the interaction energy u for a pair of simple negative ions of the same kind with the above structure, $u=u_c+u_n+u_e+u_k$, the sum of four terms,

$$u_c=e^2/\delta, \qquad u_n=2Z\gamma(\delta)e \tag{1}$$

and

$$u_e=-e\left[N\gamma(\delta)+\int\gamma\rho dv\right]$$

$$u_k=\kappa_k\int[(2\rho)^{5/3}-2\rho^{5/3}]dv. \tag{2}$$

These terms were first introduced for a more general case by Jensen and Lenz.[5] Here u_c is the electrostatic interaction energy of a pair of simple negative ions, u_n is the energy arising from the penetration of each nucleus into the electronic cloud of the other ion, u_e is the decrease of the electrostatic energy on account of the overlapping of the electronic clouds, and u_k is the kinetic energy change. Further details can be found in Gombas'[6] excellent article. N and Z denote the number of electrons and the atomic number of each ion, and e is the electron change. The constant κ_k in the last equation is $\kappa_k=2.871\ e^2a_0$ where a_0 is the radius of the first Bohr orbit of the hydrogen atom. The electron density $\rho(r)$ in the Fermi-Amaldi model is

$$\rho(r)=(Z/4\pi\mu^{*3})[N/(N-1)][\phi_0(x)/x]^{3/2},$$

where

$$x=r/\mu^*$$

and

$$\mu^*=(0.88534/Z^{1/3})[N/(N-1)]^{2/3}a_0. \tag{3}$$

For the simple negative ion in the Fermi-Amaldi model, $\phi_0(x)$ denotes the Thomas-Fermi function for free neutral atoms as in the original Thomas-Fermi theory, and for the function $\gamma(r)$ of (1) and (2) above is given in the Fermi-Amaldi theory by

$$V(r)=(Ze/r)\phi_0(r/\mu^*)=[\gamma(r)r/r]. \tag{4}$$

[See Eqs. (7.18) and (18.4) of Gombas' book.[1]]

Using Gombas' treatment[7] of the Jensen-Lenz simplification of the theory it can easily be shown that in our case of simple negative ions of the same kind with filled electron shells, the interaction energy is

$$u=e^2/\delta-2\gamma(\delta)e+(\alpha+2\beta)\rho(\delta), \tag{5}$$

where the constants α and β are

$$\alpha=4\pi e\int_0^\infty\gamma(r)r^2dr$$

$$\beta=(20\pi/3)\kappa_k\int_0^\infty[\rho(r)]^{2/3}r^2dr. \tag{6}$$

Formulas (5) and (6), for a pair of simple negative ions of the same kind with filled electron shells like rare gas atoms, are valid for Z when $N=Z-1$. In our case, with $\rho(r)$ and $\gamma(r)$ given by Eqs. (3) and (4) we can easily calculate that

$$u=(e^2/\delta)-(2Ze^2/\delta)\phi_0(\delta/\mu^*)+\frac{ZN}{4\pi(N-1)}\left(\frac{\phi_0(\delta/\mu^*)}{\delta/\mu^*}\right)^{3/2}$$

$$\times\left[\frac{4\pi Ze^2}{\mu^*}+\frac{40\pi\kappa_k}{3\mu^{*2}}\left(\frac{ZN}{4\pi(N-1)}\right)^{2/3}\right]\int_0^\infty x\phi_0(x)dx. \tag{7}$$

This formula gives the dependence of the interaction energy u on the distance δ, and is convenient for practical use because good tables of the function ϕ_0 exist, while the integral indicated is a pure number.

The author is indebted to Dr. P. Gombas for the opportunity of visiting his Institute at the Academy, and also to Dr. R. Gaspar for his helpful discussions of this problem.

[1] P. Gombas, *Die Statistische Theorie des Atoms und ihre Anwendungen* (Springer-Verlag, Berlin, 1949).
[2] H. Jensen, Z. Physik **77,** 722 (1952).
[3] W. Lenz, Z. Physik **77,** 713 (1952).
[4] P. Gombas, Z. Physik **121,** 523 (1943).
[5] See works cited in footnotes 2 and 3.
[6] P. Gombas, *Encyclopedia of Physics,* edited by S. Flügge (Springer-Verlag, Berlin, 1956), Vol. 36.
[7] P. Gombas, see work cited in footnote 1, Appendix p. 378, and also R. Gaspar, Acta Physiol. Acad. Sci. Hung. **11,** 71 (1960).

Neutralization of Hydroxide Ion in Melt-Grown NaCl Crystals

DUMAS A. OTTERSON

Lewis Research Center,
National Aeronautics and Space Administration, Cleveland, Ohio

(Received January 30, 1961)

MANY recent studies of solid-state phenomena, particularly in the area of crystal imperfections, have involved the use of melt-grown NaCl single crystals. Quite often trace impurities in these materials have had a prominent effect on these phenomena. Trace amounts of hydroxide ion have been found in melt-grown NaCl crystals.[1–4] This paper describes a nondestructive method of neutralizing the hydroxide ion in such crystals. Crystals of similar hydroxide content are maintained at an elevated temperature below the melting point of NaCl in a flowing atmosphere containing dry hydrogen chloride. Heat treatment is continued until an analysis of the test specimens shows no excess hydroxide ion. A colorimetric method previously described[4] is used for this analysis.

The crystals had a cross section of 4×7 mm and a length of 2 to 4 cm. They were rinsed with four or five portions of carbon tetrachloride or chloroform to remove organic impurities from their surfaces. A platinum boat holding these crystals was placed in a quartz tube inside a tube furnace. The boat had a tightly fitting cover and platinum tubes extending from its sides to the cooler portions of the system in order to retard attack of the quartz by the salt vapors. Glass-wool plugs, previously freed from organic substances by heating to 650°C in an airstream, were used as heat shields inside the system. The apparatus was purged for about 3 or 4 hr with argon to remove the oxygen. Dry hydrogen chloride, prepared by adding concentrated hydrochloric acid to concentrated sulfuric acid, was then passed through the system until the atmosphere in contact with the salt was primarily HCl. The portion of the system containing the NaCl was heated to and maintained at 730°C for 48 hr in the slowly moving HCl atmosphere.

Failure to remove oxygen from the system permitted reactions that destroyed the boat and the salt wherever they were in contact, deposited platinum on the hot surfaces of the system, deposited a compound thought to be Na_2PtCl_6 on the cooler parts, and produced considerable amounts of free chlorine. When the glass wool or the crystal was not free from organic material, a thin, black, uneven deposit was found on the treated crystals.

When starting with melt-grown crystals of NaCl having an initial concentration of 20 ppm or less, treatments of 48 hr reduced the NaOH concentration in these crystals to less than 1 ppm. All Optovac OH-free and Harshaw crystals tested at this laboratory initially contained 20 ppm NaOH or less. However, neutralization was incomplete in all crystals containing hydroxide that were treated only 24 hr and in some crystals initially containing more than 20 ppm NaOH even with the 48-hr treatment. The times involved suggest that a solid-state diffusion mechanism is involved in the neutralization.

Additional experiments have also shown that hydroxide ion can be reintroduced into neutral crystals by heating them in an atmosphere of argon and water vapor at 730°C for 2 hr. Furthermore it may be possible to introduce other anion impurities by treatment of crystals containing hydroxide ion in atmospheres of the corresponding acid.

[1] J. Rolfe, Phys. Rev. Letters **1,** 56 (1958).
[2] H. W. Etzel and D. A. Patterson, Phys. Rev. **112,** 1112 (1959)
[3] W. H. Etzel and J. G. Allard, Phys. Rev. Letters **2,** 452 (1959).
[4] D. A. Otterson, J. Chem. Phys. **33,** 227 (1960).

Dielectric Properties of Polyamides

A. J. CURTIS

National Bureau of Standards, Washington 25, D. C.

(Received February 6, 1961)

THE dielectric relaxation phenomena in two polyamides have been studied over a temperature range from −100° to 175°C and a frequency range from 50 cps to 10 Mc/sec. The polyamides were poly(hexamethylene adipamide) and poly(hexamethylene sebacamide).

Four relaxation phenomena have been identified, and are briefly described as follows:

(1) Above about 80°C there is a dipolar relaxation process, as indicated by a maximum in dielectric loss, in both polymers studied. This is the same dielectric process described in detail by Boyd[1] and by McCall and Anderson.[2] It was proposed by these authors that this process was due to dipole orientation in the amorphous regions of these polymers. The present studies show that this process does not occur in the highly ordered

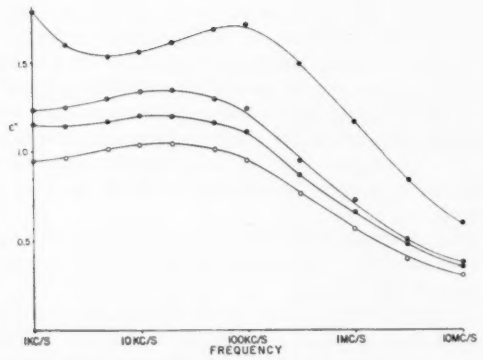

FIG. 1. Dielectric loss index of 610 nylon as a function of frequency at 80°C: ● injection-molded vacuum-dried three days at 110°C, density = 1.0768 g/cc; ◑ injection-molded vacuum-dried five days at 130°C, density = 1.0813 g/cc; ○ injection-molded vacuum-dried one day at 210°C, density = 1.0943 g/cc; ◒ melted in vacuum, molded, and vacuum dried five days at 130°C, density = 1.0892 g/cc.

regions. Figure 1 shows a plot of dielectric loss factor for poly(hexamethylene sebacamide) samples which had different thermal histories resulting in different densities and x-ray diffraction properties, associated with differences in amounts of polymer in the highly ordered state. It is apparent that high-temperature annealing, which produces an increase in the amount of highly ordered material, results in a decrease in the magnitude of this relaxation process.

(2) There is a very low-frequency polarization above 60°C in both polyamides characterized by extremely high loss factor and high dielectric constant. This process, which was also observed by previous authors,[1,2] is undoubtedly due to motions of amide group hydrogens involved in intermolecular hydrogen bonds. This can best be described as motions of bound charges since the observed dc conduction can only account for a fraction of the observed loss factors and cannot account for the enhanced dielectric constants. This polarization has been found to give rise to marked electret-forming capabilities in these polyamides.

(3) There is a relaxation process observed at room temperature as indicated by a maximum in dielectric loss at about 10 kc/sec. This is apparently due to the presence of water and, in one case, was almost completely absent after prolonged drying. (Absolutely dry polyamide can probably only be realized in materials of extremely high molecular weight, since water is a byproduct of the polymerization.) This maximum could be made to reappear on exposure to water, and was again removed on redrying. This has been shown to be the dielectric manifestation of the "β peak" observed in dynamic mechanical measurements by Woodward *et al.*[3] and by Illers and Jenckel.[4]

(4) There is a low-temperature dielectric relaxation process, previously unreported, closely related to the "γ peak" observed in mechanical measurements.[4,5] This phenomenon, observed in both polyamides, necessarily involves dipolar motions and requires modification in the proposal that motions of hydrocarbon segments alone are involved in the "γ peak."

A detailed account of this work will be published shortly in the Journal of Research of the National Bureau of Standards.

[1] R. H. Boyd, J. Chem. Phys. **30**, 1276 (1959).
[2] D. M. McCall and E. W. Anderson, J. Chem. Phys. **32**, 237 (1960).
[3] A. E. Woodward, J. A. Sauer, C. W. Deeley, and D. E. Kline, J. Colloid Sci. **12**, 363 (1957).
[4] K. H. Illers and E. Jenckel, I.U.P.A.C. *Kurzmitteilungen* Sec. 1: "Physik makromolekular Stoffe" (Verlag Chemie, Berlin, 1959); and K. H. Illers (private communication).

Physical Adsorption of Nitrogen on Pyrex at Very Low Pressures

J. P. HOBSON

Radio and Electrical Engineering Division, National Research Council, Ottawa, Canada

(Received December 2, 1960)

PREVIOUS work by the author[1] has been extended to measurements of the adsorption isotherms of nitrogen on Pyrex (Corning 7740) over ranges of temperature, pressure, and surface coverage of $63.3 \leq T \leq 90.2$°K, $5\times10^{-10} \leq P \leq 10^{-3}$ mm Hg, and $10^{-4} \leq \theta \leq 0.3$, respectively. The adsorbing surface used was the interior of a standard ½-liter spherical flask, which was not treated with solvents of any kind but which was subjected to a high-temperature bake (500°C for 12 hr) as part of an ultra-high-vacuum system. The flask was immersed in a Dewar containing liquid nitrogen or liquid oxygen. Pumping on the Dewar, which contained a heater to promote convection, permitted

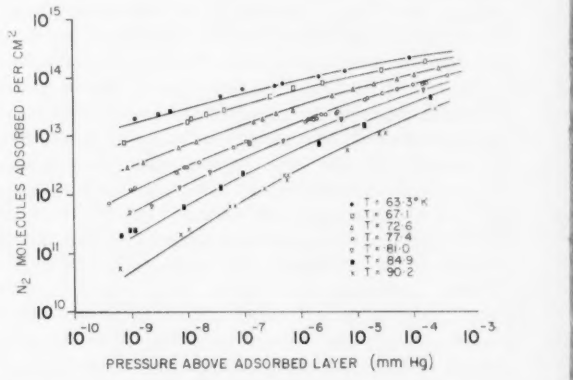

FIG. 1. Adsorption isotherms of nitrogen on Pyrex. Points are experimental. Lines are calculated from Dubinin-Radushkevich equation.

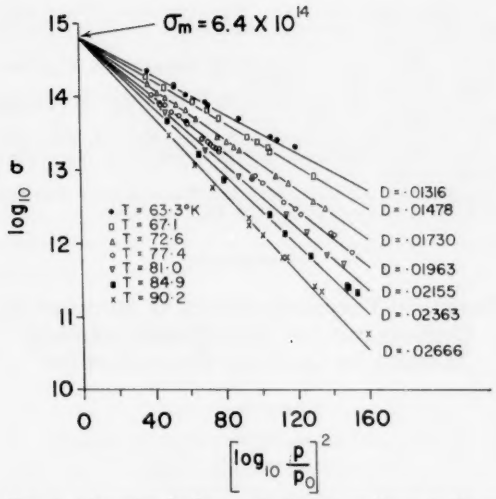

FIG. 2. Adsorption isotherms of nitrogen on Pyrex in the coordinates of the Dubinin-Radushkevich equation.

the temperatures to be held within $\pm 0.1°$, with a maximum difference between top and bottom of the liquid of 0.05°K. The adsorption measurement was volumetric, with the main adsorption volume consisting only of the adsorbing flask, a Bayard-Alpert ionization gauge, and the connecting tubing. In a preliminary experiment at 77.4°K it was established that physical adsorption equilibrium was achieved within 3 min, provided all re-emission and pumping effects in the gauge were kept sufficiently small. The experimental results are plotted in Fig. 1. The ordinate is based on the macroscopic surface area of the cooled glass (311 cm²). Observed pressures have been corrected for thermomolecular pressure effects and for helium background pressure where necessary. It was found useful to plot the data in the coordinates of an adsorption isotherm equation proposed by Dubinin and Radushkevich.[2] This equation is $\log\sigma = \log\sigma_m - D[\log(p/p_0)]^2$, where σ is the amount adsorbed (molecules/cm²), p/p_0 is the relative pressure, σ_m is a constant which Kaganer[3] has identified with the number of molecules/cm² in a monolayer, and $D = AT^2$, where A is a constant. Values of $\sigma_m = 6.4 \times 10^{-14}$ and $A = 3.28 \times 10^{-6}$, which gave a good fit to the experimental data, were found by trial and error. The resulting values of D are shown in Fig. 2. The straight lines of Fig. 2 were then transformed to give the curves of Fig. 1. A somewhat better fit to the experimental points could have been obtained by assigning a small temperature variation to σ_m.

Our conclusions are:

(1) The adsorbing surface is nonporous and nearly flat. This conclusion rests on the absolute magnitude found for $\sigma_m = 6.4 \times 10^{14}$, which is close to 6.2×10^{14} molecules/cm² for nitrogen molecules in a monolayer. The uncertainty in the absolute accuracy of the Bayard-Alpert gauge was about $\pm 10\%$. Examination of the adsorption surface with an electron microscope using platinum-carbon replica techniques showed a rolling surface with an approximate periodicity less than 300 A and a roughness factor less than about 1.4.

(2) The appearance of the Dubinin-Radushkevich equation in the present context is surprising for two reasons. First, it is a particular equation within the Polanyi potential theory, which is a theory of condensation and might not be expected to apply to physical adsorption at very low coverage. Second, most of the adsorbents to which the Dubinin-Radushkevich equation have been applied[3] have been porous, whereas our conclusion (1) above suggests that Pyrex is nonporous for nitrogen. Thus, unless and until a basic derivation for this equation is provided, it can only be considered as a useful empirical relation.

The electron microscope replicas were kindly made by Dr. P. Sewell.

[1] J. P. Hobson, Can. J. Phys. **37**, 1105 (1959).
[2] M. M. Dubinin and L. V. Radushkevich, Proc. Acad. Sci. U.S.S.R. **55**, 331 (1947).
[3] M. G. Kaganer, Proc. Acad. Sci. U.S.S.R. **116**, 603 (1957). (English translation.)

Observed Phosphorescence and Singlet-Triplet Absorption in *s*-Triazine and Trimethyl-*s*-Triazine*

J. P. PARIS,† R. C. HIRT, AND R. G. SCHMITT

Central Research Division, American Cyanamid Company, Stamford, Connecticut

(Received July 18, 1960)

THE phosphorescence spectra of *s*-triazine and its trimethyl derivative were obtained in EPA rigid-glass solutions at 77°K and in the pure solid at that temperature. A phosphoroscope with a rotating cylindrical shutter mounted axially around the Dewar was used. This was unique in its stepwise speed control and the use of four slits on the rotor, permitting a more accurate determination of the mean lifetime from the presentation of the output signal on a long-retention screen oscilloscope. A medium Hilger spectrograph was used with 103a-O plates and an 85-w mercury lamp. The ultraviolet spectral-energy distribution of this source has been described.[1] The details of this phosphoroscope will appear elsewhere.[2] Photodecomposition of the samples necessitated frequent renewal of the material to avoid interference from the photodecomposition products. No luminescence was observed from the Pyrex Dewar and the EPA glass without the sample.

The observed phosphorescence and absorption of *s*-triazine and trimethyl-*s*-triazine are presented in

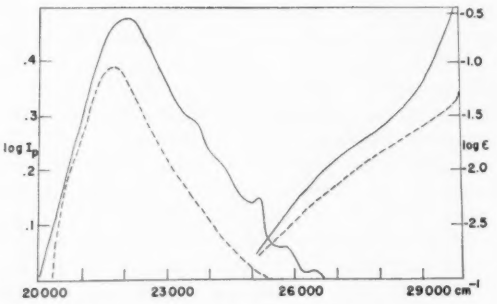

FIG. 1. Phosphorescence (left scale) and absorption (right scale) of *s*-triazine (———) and trimethyl-*s*-triazine (------).

Fig. 1. (The intensity scale for the phosphorescence is arbitrary.) A pronounced blue shift of the absorption on substitution is observed, corresponding to the $n\rightarrow\pi^*$ origin. Mean lifetimes of 0.44 and 0.65 sec were measured for *s*-triazine and its trimethyl derivative, respectively. Brinen and Goodman[3] recently reported the observation of phosphorescence of *s*-triazine "with a lifetime consistent with an orbitally forbidden transition"; our values conform to this observation.

It is interesting to note the suggestion of "structure" in the phosphorescence spectrum of *s*-triazine. The highest wave number band of the *s*-triazine phosphorescence is taken to be 26 400 cm^{-1}, or 3.28 ev. The most prominent feature in the phosphorescence spectrum, however, falls at 25 000 cm^{-1}, or 3.1 ev., which would correspond exactly with the value calculated.[3] Some changes in features of the emission curve between EPA solution and the solid at the same temperature were noted. Trimethyl-*s*-triazine offered no features in its weaker emission, through the singlet-triplet absorption is displaced somewhat to the blue as compared to *s*-triazine.

In an earlier report on the electronic spectra of *s*-triazine,[4] it was stated that no weak absorption bands of a singlet-triplet origin were found between 13 000 and 31 000 cm^{-1} with an $\epsilon>0.02$. A limited supply of highly purified *s*-triazine prevented the search for weaker bands. Following the observation of the phosphorescence and the measurement of mean lifetimes very much longer than that of pyrazine,[5,6] another attempt was made to observe the singlet-triplet absorption in this region at room temperature with an intensity corresponding to the lifetime of the emission. Cells of 10 cm length and 100 g/liter concentration in methanol were used. Attempts to use pure molten samples in a heated cell were unsuccessful, because of escape of the *s*-triazine from the cell. The observed absorption spectra are shown in Fig. 1. (The molar absorptivity scale corresponds to that of the previously published spectra.[4])

* This material was reported in part at the meeting of the Society for Applied Spectroscopy, New York, November 7, 1958.

† Summer employee, 1958. Present address: Polychemicals Department, E. I. duPont de Nemours and Company, Wilmington, Delaware.

[1] R. C. Hirt, R. G. Schmitt, N. D. Searle, and A. P. Sullivan J. Opt. Soc. Am. **50**, 706 (1960).
[2] J. P. Paris, R. G. Schmitt, and R. C. Hirt, Appl. Spectroscopy (to be published).
[3] J. S. Brinen and L. Goodman, J. Chem. Phys. **31**, 482 (1959)
[4] R. C. Hirt, F. Halverson, and R. G. Schmitt, J. Chem. Phys. **22**, 1148 (1954).
[5] L. Goodman and M. Kasha, J. Mol. Spectroscopy **2**, 58 (1958).
[6] R. C. Hirt, Spectrochim. Acta **12**, 114 (1958).

Statistical Thermodynamics of Mixtures. II. Convergence of the Quasi-Chemical Method for the Ising Square Lattice*

STEPHEN G. BRUSH

Lawrence Radiation Laboratory, Livermore, California

(Received February 1, 1960)

THE Ising model, a system of atoms arranged on a lattice with simple nearest-neighbor interactions, provides a more or less realistic description of many physical systems. For convenience we shall use the terminology appropriate to a mixture of two kinds of atoms, A and B, the forces between the atoms being such that a (nearest-neighbor) AB pair has an energy larger by an amount ϵ than the average energy of an AA or BB pair.

A number of approximate methods have been proposed for calculating the thermodynamic properties of such a model system. We discuss here one particular method, the "quasi-chemical" approximation of Guggenheim.[1] This method has been chosen, not because it

TABLE I. Explanation: $x=0.49192$ for a 4×5 rectangle, $x=0.48847$ for a 6×6 square, etc.

	1	2	3	4	5	6
1	0.60653					
2	0.50000	0.48587				
3	0.51186	0.49094	0.49268			
4	0.51454	0.49254	0.49301	0.49278		
5	0.51456	0.49253	0.49243	0.49192	0.49092	
6	0.51377	0.49189	0.49149	0.49081	0.48972	0.48847

it believed to be more accurate than other methods, but because it provides a sequence of approximations which is believed to converge to the exact solution. Each approximation requires the construction and solution of a set of equations in a manner so well defined that practically all the work can be done by an electronic computer.

The basic idea of the quasi-chemical method is to break up the system of N atoms into small groups of r atoms each, these atoms forming some definite figure such as a square or cube of lattice points; one then enumerates the possible configurations of the group,

ignoring interactions with atoms belonging to other groups. Thus, let z be the coordination number of the lattice, p the number of nearest-neighbor pairs in the group of r sites, and m_{ij} the number of ways in which one can place i atoms of type A and $r-i$ of type B on the group of r sites, such that there are j nearest-neighbor AB pairs. By following Guggenheim's method, one can calculate all thermodynamic functions over the whole range of temperatures and in particular it can be shown that the critical solution temperature is determined by the solution of [2,3]

$$\frac{z(1-r)+2p}{rz-2p}\sum_{i,j} m_{ij}x^j+(4/r)\sum_{i,j} m_{ij}x^j(i-(i^2/r)]=0,$$

where $x=\exp(\epsilon/kT_c)$. The problem is thus reduced to finding the coefficients m_{ij} for the group of r sites. As $r\to\infty$ the number of interactions omitted, $(rz/2)-p$, will become negligible compared to the total number of interactions, and therefore one expects x to converge to its correct value for a macroscopic system. On the other hand, the usefulness of the method depends on its accuracy for fairly small values of r, since the amount of work required to obtain thermodynamic functions increases very rapidly with r.

In order to test this approximation we have applied it to the square lattice where the answer is already known[4]: $x=2^{\frac{1}{2}}-1=0.41421$. The coefficients m_{ij} have been computed, and solutions of the above equation obtained, for all the squares and rectangles up to 6×6. The m_{ij} were obtained by adding one site at a time and enumerating the pairs which the new site formed with those already present, thus building up the square row by row; it was therefore possible to compute critical solution temperatures for intermediate figures with little extra work.

The results for rectangles and squares are presented in Table I. It is clear that the convergence of the quasi-chemical method is extremely slow, at least if one is primarily interested in calculating the critical solution temperature. There seems to be no reasonable extraplation procedure by which one could deduce from these numbers the result $x=0.41421$ for an infinite group. Extension of the results to larger groups would require a different code, and this was not considered worthwhile in view of the slight additional information to be gained.

For purposes of comparison, we cite two alternative results for approximations based on a 2×2 square. Kikuchi[5] obtained $x=0.438$ by his method, while the method of Katsura,[6] using periodic boundary conditions, leads to a maximum in the specific heat at $x=0.450$. (Katsura originally obtained the result $x=0.42$ for the 2×2 square; he agrees that the correct result is 0.450.[7]) Methods suitable for machine computation have not yet been developed for extending these two approximations, but it is hoped that some progress can be made in this direction in the future.

I would like to thank Garret Boer for coding this problem for the IBM 709.

* Work performed under the auspices of the Atomic Energy Commission.

[1] E. A. Guggenheim, *Mixtures* (Oxford University Press, New York, 1952).
[2] J. A. Barker, Proc. Roy. Soc. (London) **A216,** 45 (1953).
[3] S. G. Brush, Trans. Faraday Soc. **54,** 1781 (1958).
[4] H. A. Kramers and G. H. Wannier, Phys. Rev. **60,** 252, 263 (1941).
[5] R. Kikuchi, Phys. Rev. **81,** 988 (1951).
[6] S. Katsura, Progr. Theoret Phys. (Kyoto) **11,** 476 (1954).
[7] S. Katsura, Progr. Theoret. Phys. (Kyoto) **23,** 390 (1960).

Tritium as an Internal Source of Radiation in EPR Studies of Organic Materials*

J. Kroh and J. W. T. Spinks

Department of Chemistry, University of Saskatchewan, Saskatoon, Canada

(Received January 13, 1961)

In some recent EPR experiments, tritium has been used as an internal source of radiation for specimens of H_2O and D_2O ice and frozen aqueous solutions.[1] This method of irradiaton has the advantage that the EPR background normally introduced by the simultaneous irradiation of the sample container (usually glass or quartz) is absent. In order to extend the application of tritium in EPR studies, small quantities of aqueous T_2O solution of activity 1 C/ml were introduced into several liquid organic materials. Then the samples were frozen down in liquid nitrogen and their EPR spectra recorded on a Varian V4500, x-band EPR spectrometer.

In the case of substances miscible with water this method is easily feasible. Samples of methyl alcohol, ethyl alcohol, and acetone, with an activity of 0.11 C/ml were prepared. Their EPR spectra, corresponding to a total radiation dose of the order of 4×10^{19} ev/ml are represented by derivative curves shown in Fig. 1. The spectra seem to be identical with those obtained for Co^{60} γ rays[2] and x rays.[3]

The contribution of OH radicals[1] to the formation of the spectrum is negligible because of (1) low concentration of water in sample (about 10%), and (2) low yield of OH production in comparison with yields of organic radicals in the materials under test.

The preliminary estimates of the yields of paramagnetic species produced in methyl alcohol, ethyl alcohol, and acetone give the values 3.5, 5, and 2.8 per hundred ev, respectively.

The above yields, with the exception of that for acetone, are lower than those reported by Alger, Anderson, and Webb for x rays (5.5, 8.3, and 1.6). Nevertheless, the order of succession is the same.

Gases and liquid insufficiently miscible with water may be tritiated by using the technique suggested by

Mitchell,[4] i.e., by rapid condensation of the mixture of tritium oxide and organic vapors at liquid-nitrogen temperature.

The resulting EPR spectra however often appear to be affected by the presence of the OH doublet.[1] This OH "deformation" may be usually removed by warming the sample to about −140°C, at which temperature OH radicals seem to disappear rapidly.

The EPR spectra of chloroform and ethyl ether, tritiated by the vapor condensation method to the activity of the order to 100 mC/ml are shown in Figs. 2 (curve a), 3 (curve a) (before warming) and 2 (curve b), 3 (curve b) (after warming). The appearance of the OH spectrum might probably be completely avoided by using tritium oxide solutions of higher activity and consequently introducing smaller quantities of water into the materials under test.

* This research was supported by the National Research Council of Canada.

[1] J. Kroh, J. W. T. Spinks, and B. C. Green, Nature **189,** 655 (1961).
[2] H. Zelder and R. Livingston, J. Chem. Phys. **30,** 40 (1959).
[3] R. S. Alger, T. H. Anderson, and L. A. Webb, J. Chem. Phys. **30,** 695 (1959).
[4] F. Mitchell (private communication).

CONTE

THE JOURNAL OF CHEMICAL PHYSICS

Thermodynamic Theory of the Pair Correlation Function . . .
On the Theory of Raman Intensities . . .
Statistical Mechanics of Isotope Effects on the Thermodynamic
Competitive Reaction Rates of Hydrogen Atoms with HCl and Cl
. . . . . .
Evidence of Trapped H Atoms in X-Ray Irradiated CaH_2 . . . G.
Nuclear Relaxation Processes of a Nonequivalent Two-Spin Syst
Calculation of Pressure Shifts of Optical Absorption Frequen
Microwave Spectrum of Isobutylene. Dipole Moment . . .
. . . . . .
Half-Crystal Energy Constants . . .
Scattering of High-Velocity Neutral Particles. XI. Further Study of
. . . . . .
Probability of Initial Ring Closure in the Restricted Random
. . . . . .
Statistical Mechanics of Monatomic Systems in an External Field:
Classical Second Virial Coefficient . . .
Statistical Mechanics of Monatomic Systems in an External Field:
Fluids . . . . . .
Infrared Spectra of Methanol and Deuterated Methanols in Ga
Difference of Intermolecular Potentials of CH_3OH and CH_3OD
Condensation of Atomic and Molecular Hydrogen at Low Temp
Second-Order Effects in Low-Field NMR for Asymmetrically Coup
Spin-Lattice Relaxation Time of F^{19} Nuclei in Ag_2F . . .
Application of a Theory of Nonideal Solutions to Reciprocal Ter
Mass Spectrometer Investigation of Ionization of H_2O by Electron
Ionization Processes in CCl_4 and SF_6 by Electron Impact . .
The State of the Nd^{3+} Ion as Derived from the Absorption and Fl
. . . . . .
Crystal Spectra of Metal Coordination Compounds. IV. Bis(dime
Infrared Spectra of Alkali Metal Azide Crystals . . .
Photolysis of Nitrous Oxide. I. 1236 Å . . .
The Second Law of Thermodynamics . . .
Proton Resonance Shifts in Alkali Halide Solutions . . .
Magnetic Properties and Optical Absorption Spectrum of Ni
Near-Infrared Absorption Spectrum of Solid Manganese(II) Ac
Protection against Radiation Damage in Polycrystalline Ice
. . . . . .
Extraordinary Basic Functions in Valence Theory . . .
Applicability of Approximate Quantum-Mechanical Wave Fu
. . . . . .
Application of Ligand Field Theory to the Electronic Spectra of
. . . . . .
Polarity of the C—H Bonds in Acetylene and Its Mixtures with
Theory of Localized Contributions to the Chemical Shift . . .
Isotropic and Anisotropic Hyperfine Interactions in Mn
Effect of Molecular Oxygen on the Emission Spectra of Aro
. . . . . .
Studies of Rates of Conversion and Populations of Conf
Piperazine . . . . . .